NASA Conference Publication 2466

Star Formation in Galaxies

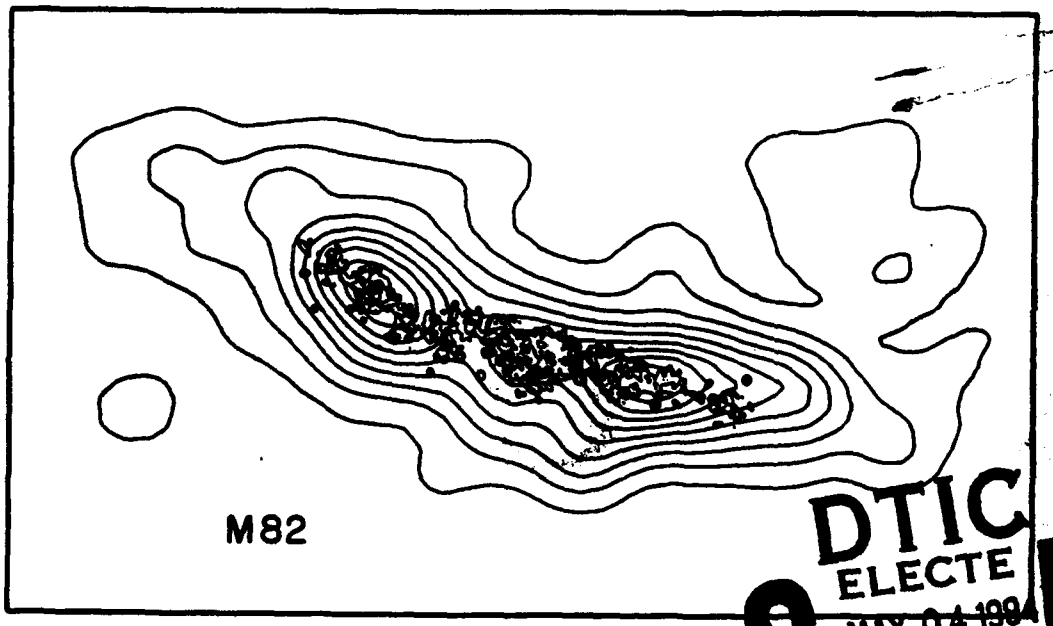

Proceedings of a conference held at the California Institute of Technology Pasadena, California June 16-19, 1986

NASA

NASA Conference Publication 2466

Star Formation in Galaxies

NASA Office of Space Science and Applications
Washington, D.C.

Proceedings of a conference held at
the California Institute of Technology
Pasadena, California
June 16–19, 1986

National Aeronautics
and Space Administration

**Scientific and Technical
Information Branch**

1987

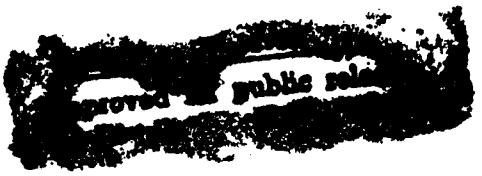

EDITORS' PREFACE

"Star Formation in Galaxies" was a large, international conference, held on June 16-19 1986 in Pasadena, California. There were over 200 attendees from 12 different nations, and together they brought experience and knowledge on many aspects of star formation in normal, starburst and active galaxies. On the observational side there was particular emphasis on the comparison of radio continuum and CO data with the IRAS data, and the nature of the energy source(s) of the most infrared-luminous extragalactic objects, but the discussion and poster papers ranged from the diffuse far-infrared emission in the Galaxy, through the detailed processes and triggers of star formation in disks and starburst nuclei, to the inter-relationship between an active nucleus and a surrounding starburst.

Many people contributed to the success of the Conference. The Local Organizing Committee is especially grateful to Wendy Zhorne for her untiring assistance in the organization and preparation for the Conference. Barbara Bateman and Rosanne Hernandez, were also invaluable. In addition, the assistance of Cynthia Bennett, Ellen Erwin, Linda Fullmer, Helen Hanson, Gaylin Laughlin, Lesley Lloyd, Larry Lloyd and Naomi Theodorou in the running of the oral and poster sessions is greatly appreciated.

For assistance with the preparation of the Proceedings, I am tremendously indebted to Helen Knudsen, who gave up much of her free time for many weeks to correct and organize manuscripts, and construct an excellent set of indices. Thanks are also due to John Fowler, Rosanne Hernandez, Julie Serpa, and Zacqueline Souras for their help in the production of the Proceedings. I would also like to thank those contributing authors who organized and proofed their manuscripts carefully.

Carol J. Lonsdale Persson

Pasadena, November 1986

CONFERENCE PREFACE

As Becklin has remarked in his summary, the IRAS extragalactic discoveries have put infrared astronomy into the big time. This conference, however, was not an IRAS, or even an "infrared" conference. It has been a conference on a scientific subject; we have gone beyond tentative predictions and discussions of data processing. The starburst phenomenon, once thought to be restricted to a very few galaxies, has been shown to be ubiquitous, and has been correlated with the large scale galactic structure and dynamics (bars, spiral arms, galactic collisions) and the smaller scale phenomena such as shocks and cloud collisions which may trigger the star formation. The very luminous infrared galaxies have been shown to be the dominant population of the Universe at the highest luminosities.

We intended this conference to be both a summary and a step forward. We think that the variety and range of papers presented has accomplished these dual goals. We thank the presenters, the local organizing committee and all the others who made this conference a truly pleasant and provocative educational experience.

G. Neugebauer
N. Scoville

Pasadena, November 1986

Scientific Organizing Committee

G. Neugebauer, California Institute of Technology (co-chairman)
N. Scoville, California Institute of Technology (co-chairman)
H. Habing, Sterrewacht Leiden
M. Longair, Royal Observatory Edinburgh
J. Ostriker, Princeton
G. Rieke, Steward Observatory
E. Salpeter, Cornell University
B. Soifer, California Institute of Technology
D. Weedman, Pennsylvania State University
G. Wynn-Williams, University of Hawaii

Local Organizing Committee

C. Beichman, IPAC
G. Helou, IPAC
C. Korkus, IPAC
C. Lonsdale Persson, IPAC
P. McLane, Jet Propulsion Laboratory
S. Molina, IPAC
G. Neugebauer, California Institute of Technology
B. Soifer, California Institute of Technology
Z. Souras, IPAC
G. Squibb, IPAC
R. Von Allmen, IPAC

CONTENTS

A. THE GALAXY

Invited Review: High Mass Star Formation in the Galaxy

N. Z. Scoville and J. C. Good 3 - 20

Diffuse Infrared Emission of the Galaxy:
Large Scale Properties (Abstract)

J. L. Puget, M. Perault, F. Boulanger and E. Falgarone 21

The Origin of the Diffuse Galactic IR/Submm Emission:
Revisited after IRAS

P. Cox and **P. G. Mezger** 23 - 35

Masses, Luminosities, and Dynamics of Galactic Molecular Clouds

P. M. Solomon, A. R. Rivolo T. J. Mooney, J. W. Barrett and L. J. Sage 37 - 59

POSTER PRESENTATIONS:

Regions of Star Formation

IRAS Colors of VLA Identified Objects in the Galaxy

M. Fich and S. Terebey 63 - 66

Star Formation in Carina OB1: Observations of a Giant Molecular
Cloud Associated with the η Carinae Nebula

D.A. Grabelsky, R.S. Cohen and P. Thaddeus 67 - 70

Star Forming Regions of the Southern Galaxy

T.B.H. Kuiper, J.B. Whiteoak and J.W. Fowler 71 - 74

On the Redistribution of OB Star Luminosity and the Warming of Nearby Molecular Clouds

D. Leisawitz 75 - 78

Maps of Millimeter Wave Emission from Three Galactic Star-Forming Regions

M. Barsony 79 - 82

Shock Heated Dust in L1551: L(IR)>20 Solar Luminosities

F.O. Clark, R.J. Laureijs, G. Chlewicki, C.Y. Zhang, W. van Oosterom and D. Kester 83 - 85

Mechanisms for the Circular Polarization of Astrophysical OH Masers in Star-Forming Regions and the Inferred Magnetic Fields

S. Deguchi and W.D. Watson 87 - 90

Diffuse Emission in the Galaxy

Survey of the Galactic Disk from l = -150° to l = 82° in the Submillimeter Range

E. Caux and G. Serra 93 - 96

Diffuse Infrared Emission of the Galaxy: Large Scale Properties (Abstract)

M. Perault, F. Boulanger, E. Falgarone and J.L. Puget 97

The Large Scale Gas and Dust Distribution in the Galaxy: Implications for Star Formation

T.J. Sodroski, E. Dwek, M.G. Hauser and F.J. Kerr 99 - 102

A Correlation Between IRAS Infrared Cirrus at 60 or 100 μm and Neutral Atomic Hydrogen in the Outer Galaxy

S. Terebey and M. Fich 103 - 105

The Arp Ring: Galactic or Extragalactic ?

J.A. Abolins and W.L. Rice 107 - 110

Dust Grains

Infrared Properties of Dust Grains
Derived from IRAS Observations

G. Chlewicki, R. Laureijs, F.O. Clark and P.R. Wesselius 113 - 116

IRAS Observations of the Pleiades

P. Cox and A. Leene 117 - 121

B. NORMAL GALAXIES

Invited Review: Star Formation in Normal Galaxies

C.G. Wynn-Williams 125 - 131

Invited Summary of IRAS Spectral Synthesis Papers:
Models for Infrared Emission from IRAS Galaxies

M. Rowan-Robinson 133 - 152

The Origin of the 40-120 μm Emission of
Galaxy Disks: A Comparison with Hα Fluxes

C.J. Lonsdale Persson and G. Helou 153 - 160

Invited Summary of Magellanic Cloud Papers:
Star Formation in the Magellanic Clouds

J.A. Frogel 161 - 166

Measuring Star Formation Rates in Blue Galaxies*

J.S. Gallagher III and D.A. Hunter 167 - 177

* See also Erratum, page 257

CO Observations of Galaxies
with the Nobeyama 45m Telescope

Y. Sofue, T. Handa, M. Hayashi and N. Nakai 179 - 196

CO Observations of Nearby Galaxies
and the Efficiency of Star Formation

J.S. Young 197 - 215

Submillimeter Observations of IRAS Galaxies (Abstract)

R. Chini, E. Kreysa, **E. Krugel** and P.G. Mezger 217

Stellar Bars and the Spatial
Distribution of Infrared Luminosity

N. Devereux 219 - 226

Star Formation and Spiral Structure in M81

M. Kaufman and F.N. Bash 227 - 233

The HII Regions in M51: Radio
and Optical Observations

J.M. van der Hulst and R.C. Kennicutt Jr. 235 - 238

POSTER PRESENTATIONS

The Magellanic Clouds and Irregular Galaxies

IRAS and Ground-Based Observations of Star
Formation Regions in the Magellanic Clouds

J.H. Elias and J.A. Frogel 241 - 244

Star Formation in the Large Magellanic Cloud

T.J. Jones, A.R. Hyland and P.M. Harvey 245 - 246

Infrared Emission and Excitation in LMC HII Regions

V. Ungerer and F. Viallefond 247 - 251

IRAS Observations of Irregular Galaxies*

D.A. Hunter, W.L. Rice, J.S. Gallagher III and F.C. Gillett 253 - 256

Erratum: IRAS Observations of Irregular Galaxies

D.A. Hunter and J.S. Gallagher III 257

IUE Observations of Luminous Blue Star Associations in Irregular Galaxies

S.A. Lamb, D.A. Hunter and J.S. Gallagher III 259 - 262

Neutral Hydrogen and Star Formation in Irregular Galaxies

E.D. Skillman 263 - 266

Carbon Monoxide Emission from Small Galaxies

H.A. Thronson Jr. and J. Bally 267 - 270

Spirals

Characteristics of UGC Galaxies Detected by IRAS

C.J. Lonsdale Persson, W. Rice and G.D. Bothun 273 - 276

Far-Infrared Properties of Cluster Galaxies

M.D. Bicay and R. Giovanelli 277 - 281

Present Star Formation in Spirals of the Virgo Cluster

B. Guiderdoni 283 - 286

Molecular Gas and Star Formation in HI-Deficient Virgo Cluster Galaxies

J.D. Kenney and J.S. Young 287 - 292

*See also Erratum, page 257

Star Formation Rates as a
Function of Galaxy Mass

W. Romanishin 293 - 296

Global Properties of the Nearby Spiral M101

C. Beichman, F. Boulanger, W. Rice, and C.J. Lonsdale Persson 297 - 302

Efficient Star Formation
in the Bright Bar of M83

S.D. Lord, S.E. Strom and J.S. Young 303 - 307

Large Scale Dissociation of Molecular
Gas in the Spiral Arms of M51

R.P.J. Tilanus and R.J. Allen 309 - 313

Structure and Kinematics of the
Molecular Spiral Arms in M51

G. Rydbeck, A. Hjalmarson, L.E.B.
Johansson, O.E.H. Rydbeck and T. Wiklind 315 - 317

Modelling the IRAS Colors of Galaxies

G. Helou 319 - 322

A Simple Two-Component Model for the
Far-Infrared Emission from Galaxies

T. de Jong and K. Brink 323 - 328

Early – Type Galaxies

Detection of CO (J=1-0) in the Dwarf
Elliptical Galaxy NGC 185

T. Wiklind and G. Rydbeck 331 - 332

Star Forming Regions in Gas-Rich S0 Galaxies

R.W. Pogge and P.B. Eskridge 333 - 336

Models

A Simple Theory of Bimodal Star Formation

R.F.G. Wyse and J. Silk 339 - 342

The History of Gas in Spiral Galaxies

P. Maloney 343 - 347

C. STARBURST AND INTERACTING GALAXIES

Invited Review: Starburst Galaxies

D.W. Weedman 351 - 361

Infrared Spectroscopy of Star Formation in Galaxies

S.C. Beck, **P.T.P. Ho** and J.L. Turner 363 - 366

Molecular Gas in the Starburst Nucleus of M82

K.Y. Lo 367 - 382

Nuclear Star Formation on 100 Parsec Scales: 10 Arcsec Resolution Radio Continuum, HI and CO Observations

J.L. Turner, P.T.P. Ho and R.N. Martin 383 - 386

Extremely Luminous Far-Infrared Sources (ELFs)

M.O. Harwit, J.R. Houck, B.T. Soifer and G.G.C. Palumbo 387 - 393

Star Formation and Dynamics in Starburst Nuclei

C.A. Norman 395 - 400

Induced Star Formation in Interacting Galaxies

R.C. Kennicutt, K.A. Roettiger, W.C. Keel, J.M. van der Hulst and E. Hummel 401 - 408

The Frequency of Enhanced Star Formation in Interacting and Isolated Galaxies (Abstract)

R.M. Cutri 409

Ultraluminous Infrared Galaxies

D.B. Sanders, B.T. Soifer, G. Neugebauer, N.Z. Scoville, B.F. Madore, G.E. Danielson, J.H. Elias, K. Matthews, C.J. Lonsdale Persson and S.E. Persson 411 - 420

Extragalactic Infrared Spectroscopy

R.D. Joseph, G.S. Wright, R. Wade, J.R. Graham, I. Gatley and A.H. Prestwich 421 - 433

Cloud Fluid Models of Gas Dynamics and Star Formation in Galaxies

C. Struck-Marcell, J.M. Scalo and P.N. Appleton 435 - 460

Starburst-Driven Superwinds from Infrared Galaxies

T.M. Heckman, L. Armus, P. McCarthy, W. van Breugel and G.K. Miley 461 - 469

Interferometric CO Observations of the Ultraluminous IRAS Galaxies Arp 220, IC 694/NGC 3690, NGC 6240 and NGC 7469

A.I. Sargent, D.B. Sanders N.Z. Scoville and B.T. Soifer 471 - 475

POSTER PRESENTATIONS

Starburst Galaxies

The Initial Mass Function in HII Galaxies

A.W. Campbell 479 - 482

VLA Continuum Observations of
Barred Spiral Galaxies

J.A. Garcia-Barreto and P. Pismis 483 - 484

A Dust Scattered Halo in the
Starburst Galaxy M82 ?

M. Rohan, P. Morrison and A. Sadun 485 - 489

The Azimuthal and Radial Distributions
of HI and H_2 in NGC 6946

L.J. Tacconi-Garman and J.S. Young 491 - 495

The Infrared Morphology of Galactic Centers

C.M. Telesco, R. Decher, B.D. Ramsey,
R.D. Wolstencroft and S.G. Leggett 497 - 500

Far Infrared Activity and Starburst Galaxies

P. Belfort, R. Mochkovitch and M. Dennefeld 501 - 505

IRAS Observations of Starburst Galaxies

K. Sekiguchi 507 - 511

Interacting and Merging Galaxies

A Near-Infrared Study of the Luminous Merging
Galaxies NGC 2623 and Arp 148 (Abstract)

M. Joy and P.M. Harvey 515

Star Formation in the Merging Galaxy NGC 3256

J.R. Graham, G.S. Wright, R.D. Joseph,
J.A. Frogel, M.M. Phillips and
W.P.S. Meikle 517 - 519

D. SURVEYS

The Luminosity Function of the Brightest Galaxies in the IRAS Survey

B.T. Soifer, D.B. Sanders, B.F. Madore, G. Neugebauer, C.J. Lonsdale Persson, S.E. Persson and W.L. Rice 523 - 530

VLA Observations of a Sample of Galaxies with High Far-Infrared Luminosities

S.A. Eales, C.G. Wynn-Williams and C.A. Beichman 531 - 536

Systematic Identification of IRAS Point Sources

A. Savage, R.G. Clowes, H.T. MacGillivray, R.D. Wolstencroft, S.K. Leggett and P.J. Puxley 537 - 545

A Very Deep IRAS Survey at $l^{II} = 97°$, $b^{II} = +30°$

P. Hacking and J.R. Houck 547 - 552

What are 'Cirrus' Point Sources ?

C. Heiles, P.J. McCarthy W. Reach and M.A. Strauss 553 - 558

Properties of the Unusual Galaxy PSC 09104+4109

S.G. Kleinmann and W. C. Keel 559 - 562

POSTER PRESENTATIONS

Far – Infrared Luminosity Functions

A Redshift Survey of IRAS Galaxies

B.J. Smith, S.G. Kleinmann J.P. Huchra and F.J. Low 565 - 568

Optical and IR Luminosity
Functions of IRAS Galaxies

J.P. Vader and M. Simon 569 - 572

The Radio – Far Infrared Correlation

The Correlation Between Far-IR and Radio
Continuum Emission from Spiral Galaxies

J.M. Dickey, R.W. Garwood and G. Helou 575 - 578

Radio and Infrared Observations of (Almost)
One Hundred Non-Seyfert Markarian Galaxies

L.L. Dressel 579 - 582

The Radio-Far Infrared Correlation: Spiral
and Blue Compact Dwarf Galaxies Opposed

U. Klein and E. Wunderlich 583 - 588

Radio Continuum, Far Infrared and Star Formation

R. Wielebinski, E. Wunderlich,
U. Klein and E. Hummel 589 - 593

The Nature of IR – Luminous Galaxies

Extragalactic OH Megamasers
in Strong IRAS Sources

L. Bottinelli, M. Dennefeld, L. Gouguenheim,
J.M. Martin, G. Paturel and A.M. Le Squeren 597 - 600

Near-Infrared Observations
of IRAS Minisurvey Galaxies

D.P. Carico, B.T. Soifer, J.H. Elias,
K. Matthews, G. Neugebauer, C. Beichman,
C.J. Lonsdale Persson and S.E. Persson 601 - 604

Ground-Based Follow Up of IRAS Galaxies

M. Dennefeld, H. Karoji, P. Bouchet,
L. Bottinelli and L. Gouguenheim 605 - 609

Nuclear Infrared Emission
and the Colors of IRAS Galaxies

G.J. Hill 611 - 617

Enhanced Star Formation - The Importance
of Bars in Spiral Galaxies

P.J. Puxley, T.G. Hawarden
C.M. Mountain and S.K. Leggett 619 - 622

The Properties of Highly Luminous IRAS Galaxies

R.D. Wolstencroft, P.J. Puxley, J.N. Heasley,
S.K. Leggett, A. Savage, H.T. MacGillivray
and R.G. Clowes 623 - 627

Using SIRTF to Study Extragalactic Star Formation

E.L. Wright 629

E. ACTIVE GALACTIC NUCLEI

Invited Review: The Relation Between Star
Formation and Active Nuclei

G.H. Rieke 633 - 641

Ground-Based 1- to 32- μm Observations of
Arp 220: Evidence for a Dust-Embedded 'AGN' ?

E.E. Becklin and C.G. Wynn-Williams 643 - 650

Spatial Deconvolution of IRAS Galaxies at 60 μm

F.J. Low 651 - 660

Star Formation Around Active Galactic Nuclei

W.C. Keel 661 - 667

Star Formation in Seyfert Galaxies

J.M. Rodriguez Espinosa,
R.J. Rudy and B. Jones 669 - 674

Circumnuclear 'Starbursts' in Seyfert Galaxies

A.S. Wilson 675 - 691

IRAS Observations of AGN Candidates
at Low Flux Levels

M.H.K. de Grijp , W.C. Keel and G.K. Miley 693 - 698

POSTER PRESENTATIONS

Spectrophotometry of Brackett Lines
in Very Luminous IRAS Galaxies

D.L. DePoy 701 - 705

Evidence for Extended IR Emission
in NGC 2798 and NGC 6240

G.S. Wright, R.D. Joseph,
P.A. James and N.A. Robertson 707 - 710

Models Relating the Radio Emission
and Ionized Gas in Seyfert Nuclei

A. Pedlar, S.W. Unger,
D.J. Axon and J.E. Dyson 711 - 715

Structure in the Nucleus of NGC 1068 at 10 μm

R. Tresch-Fienberg, G.G. Fazio, D.Y. Gezari
W.F. Hoffmann, G.M. Lamb, P.K. Shu and
C.R. McCreight 717 - 721

Far-Infrared Properties of Optically-Selected
Quasars and Seyfert Galaxies

R.A. Edelson and M.A. Malkan 723 - 725

Infrared-Ultraviolet Spectra of
Active Galactic Nuclei

M.A. Malkan and R.A. Edelson 727 - 729

IRAS Observations of BL Lac Objects

C. Impey, G. Neugebauer and G.K. Miley 731 - 735

Spectral Classification of
Emission-Line Galaxies

S. Veilleux and D.E. Osterbrock 737 - 740

F. CONFERENCE SUMMARIES

Low Luminosity Sources

F.H. Shu 743 - 752

Morphology of Luminous IRAS Galaxies

E.E. Becklin 753 - 756

INDICES

Author Index 759 - 761

Subject Index 765 - 779

Object Index 783 - 788

A. THE GALAXY

ORAL PRESENTATIONS

HIGH MASS STAR FORMATION IN THE GALAXY[1]

N.Z. Scoville
Astronomy Department 105-24
California Institute of Technology
Pasadena, CA 91125

J.C. Good
Infrared Processing and Analysis
Center 100-22
Pasadena, CA 91125

ABSTRACT. The Galactic distributions of HI, H_2 and HII regions are reviewed in order to elucidate the high mass star formation occurring in galactic spiral arms and in active galactic nuclei. Comparison of the large scale distributions of H_2 gas and radio HII regions reveals that the rate of formation of OB stars depends on $\langle n_{H_2} \rangle^{1.9}$ where $\langle n_{H_2} \rangle$ is the local mean density of H_2 averaged over 300 pc scale lengths. In addition the efficiency of high mass star formation (per unit mass of H_2) is a decreasing function of cloud mass in the range 2×10^5 - 3×10^6 M_o. These results suggest that high mass star formation in the galactic disk is initiated by cloud-cloud collisions which are more frequent in the spiral arms due to orbit crowding. Cloud-cloud collisions may also be responsible for high rates of OB star formation in interacting galaxies and galactic nuclei.

Based on analysis of the IRAS and CO data for selected GMCs in the Galaxy, the ratio L_{IR}/M_{H_2} can be as high as 30 L_o/M_o for GMCs associated with HII regions. This is a factor of ten higher than the mean value of 2.75 L_o/M_o for the H_2 in the galactic disk. The total far infrared luminosity at λ=1-500 μm associated with the molecular disk in the Milky Way is 6×10^9 L_o. The L_{IR}/M_{H_2} ratios and dust temperature obtained in many of the high luminosity IRAS galaxies are similar to those encountered in galactic GMCs with OB star formation. High mass star formation is therefore a viable (but certainly not unique) explanation for the high infrared luminosity of these galaxies.

---

1. Throughout this article, we have scaled all derived parameters to the new Sun-Galactic center distance R_o=8.5 kpc.

1. INTRODUCTION

Star formation is central to our understanding of both the structural evolution of galaxies and their energetics. The formation of high mass stars is a key element in both the spiral structure of galaxies and the highly luminous galactic nuclei since in both instances, rapid, OB star formation has been proposed as an efficient mechanism for generating a high luminosity with a small expenditure of interstellar gas. Although massive star formation is often invoked to account for the enormous energy output of extragalactic nuclei, the underlying cause for the bias toward high mass stars is not at all understood.

In this contribution, we review the results of several recent investigations specifically designed to elucidate the formation of OB stars in the Galaxy. These studies also provide us with the diagnostics needed to distinguish high and low mass star formation in external galaxies.

Carol J. Lonsdale Persson (Editor)
Star Formation in Galaxies

2. GENERAL CONSIDERATIONS

Numerous millimeter and infrared studies of nearby star formation regions have demonstrated that virtually all star formation activity in the Milky Way occurs within molecular (not atomic) hydrogen clouds. The bulk of the molecular gas is contained in giant molecular clouds (GMCs) of mass 10^5-10^6 $M_\odot$. For a GMC of diameter 40 pc, the mean internal density is $\sim$200 H_2 cm^{-3} (see Scoville and Sanders 1986 for a review).

The total mass of molecular gas in the Milky Way is estimated to be approximately 2.3×10^9 $M_\odot$ based on CO line surveys of the inner galaxy. The maximum global star formation rate for the Milky Way would be 10^3 $M_\odot$ yr^{-1} if these clouds were undergoing free-fall collapse ($\tau_{ff}=3 \times 10^6$ years for a density of 200 cm^{-3}). Since the actual star formation rate is estimated to be approximately 5 $M_\odot$ yr^{-1}, it is immediately apparent that the GMCs are generally stable against collapse. That is, the overall efficiency for star formation on the free fall collapse time is <1%. We should therefore view the gas parcels within the molecular clouds as being in an "inactive" state 99% of the time; only occasionally (presumably by unusual circumstances) are they activated to collapse and form stars.

Two alternative viewpoints can be taken with regard to star formation mechanisms. On the one hand, we may picture star formation as a percolation process, ie. once the clouds form, star formation proceeds inevitably, albeit at a slow rate. In this picture, the overall star formation rate within any region of the galaxy should vary linearly with the total mass of molecular gas. A second possibility is that external, environmental factors occasionally initiate the star formation at a high efficiency for a short time. For example, the shocks associated with galactic spiral arms, expanding HII regions (Elmegreen and Lada 1977) or supernovae remnants (Herbst and Assousa 1977) have been proposed as the initiation mechanism of high mass star formation on cloud surfaces. A fourth mechanism (not discussed much in recent years but for which we believe there is considerable observational support) is the compression of molecular gas in the interface between colliding GMCs. This latter process is consistent with observed concentration of high mass stars in the spiral arms where the cloud-cloud collision frequency is highest (due to orbit crowding in the spiral arms) and with observations of the star formation efficiency as a function of cloud mass (see below).

3. THE LARGE SCALE DISTRIBUTION OF MOLECULES

The most striking characteristic of the molecular gas distribution in the galaxy is the existence of a ring-like maximum midway between the Sun and the galactic center. This feature (at R=3-7 kpc), containing 75% of the total molecular gas, was first identified in the early survey of Scoville and Solomon (1975) and it has been confirmed by all subsequent CO emission surveys (eg. Burton et al 1975, Cohen et al 1980, Robinson et al 1984, and Sanders, Solomon and Scoville 1984).

In Figure 1, we show the galactic radial distribution of molecular gas derived from the 40,000 point Massachusetts-Stony Brook CO survey in the first galactic quadrant (Clemens, Sanders, and Scoville 1986). For comparison the distributions of radio HII regions and atomic hydrogen are also shown. The ring-like distribution seen in both the molecular hydrogen and the HII regions, is totally absent in HI (which has a relatively flat distribution outside R=3

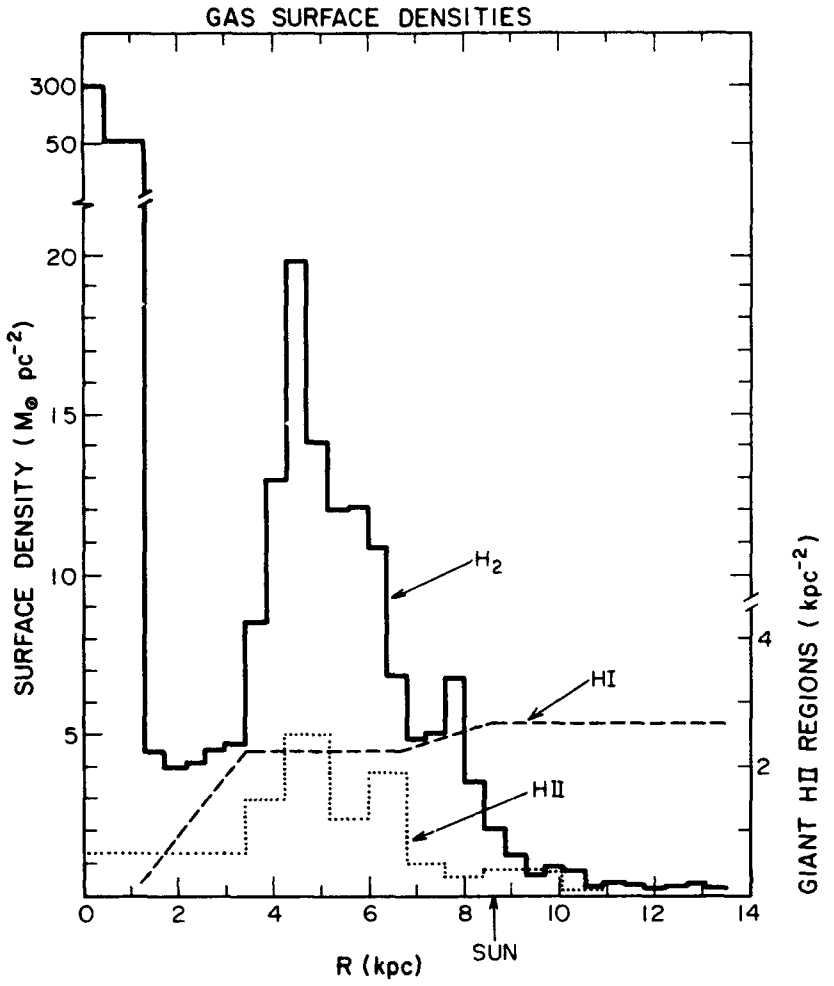

Figure 1. Comparison of the H_2, HI, and giant HII regions surface densities in the Galaxy. Values for H_2 and HI include a 1.36 correction for He. The HI distribution is from Burton and Gordon (1978) and the H_2 from Clemens, Sanders, and Scoville (1986) and corrected to R_o=8.5 kpc.

kpc and a hole in the central region). A second major feature of the molecular gas distribution is the sharp peak within 400 pc of the galactic center. The total mass of molecular gas within the galactic center peak and the molecular cloud ring at 3-7 kpc are 2×10^8 M_o and 1.8×10^9 M_o, respectively. The total H_2 and HI masses at R<14 kpc are each $\sim2.3\times10^9$ M_o (assuming R_o=8.5 kpc, cf. Scoville and Sanders 1986). The Z distributions of molecular gas and HII regions are also very similar with the thickness (FWHM) of approximately 90 pc in the area of the molecular ring, whereas the diffuse atomic hydrogen has approximately twice this scale height.

Although all investigators using CO to survey the large scale distribution of molecular clouds agree that there are large concentrations of CO emission corresponding to the tangential directions (l=32 and 50°) of the inner spiral arms, there is still controversy concerning the density contrast between the arm and inter-arm regions. For example, Sanders (1981) estimates an arm-interarm

contrast of approximately 3:1 averaged over length scales of 500 pc, yet Cohen et al (1980) assert that virtually all giant molecular clouds are confined to the arms. The principle reasons for this disagreement are the loose definition of the spiral arm locations and widths and uncertainities in the distances assigned to emission features due to the two-fold ambiguity in the kinematic distance and the finite velocity dispersion of the clouds.

Perhaps the best approach to the spiral arm question is to appeal to high resolution observations in nearby external galaxies similar to the Milky Way. In this spirit, it is significant that Rydbeck et al (1985) find only a 20% enhancement in the molecular emission along the spiral arms in M51 as compared with the mean emission at each radius when averaged over a length of approximately 1 kpc. In M83, Allen, Atherton and Tilanus (1986) found the HI emission peaks downstream from the dust lanes and they point out that the absence of HI emission from either the dust lanes themselves or the upstream side of the spiral arms implies that the interarm gas must be largely molecular. The latter investigation didn't provide a quantitative estimate of the density contrast, but it does at least clearly settle the issue of whether molecular clouds can occur outside of the spiral arms.

Within the Milky Way (at R=3-7 kpc), all the observations are consistent with at least 50% of the molecular gas being in interarm regions and a density contrast of >3:1. The interarm gas fraction could be even higher if a tight definition is adopted for the spiral arms. The much greater arm-interarm contrast seen in the galactic HII regions then implies that the spiral arm clouds are either intrinsically different in a way which favors high mass star formation or that OB star formation is induced by environmental factors such as galactic spiral shocks or cloud-cloud collisions (which are more frequent in the arms).

4. GMCS ASSOCIATED WITH HIGH MASS STAR FORMATION

We have recently undertaken a comparative study of discrete CO emission regions from the Massachusetts/Stony Brook galactic CO survey (Sanders et al 1986) and radio HII regions. From the CO survey, we have compiled three samples of giant molecular clouds (Scoville et al 1986). The first sample, which we take to be the general cloud population, contains 1,427 emission regions with CO temperatures exceeding 5 K. A second sample, which is a subset of the first, contains 255 hot CO emission cores (delineated at the 9 K level). The cloud cores are regions of molecular gas subject to strong heating--presumably active, star forming gas. The third sample of GMCs consists of 95 clouds associated with 171 radio HII regions (Downes et al 1980 and Lockman 1986).

4.1 Correlation of Hot Cloud Cores with Spiral Arms

Not surprisingly, the clouds associated with HII regions appear significantly hotter than the general cloud population. The mean peak CO temperature within the HII region clouds is 11.4 K while that in the general cloud population is 7.4 K. This correlation between hot molecular clouds and the spiral arm HII regions has been pointed out by Sanders, Scoville, and Solomon (1985), Solomon, Sanders and Rivolo (1985), and Scoville et al (1985).

The longitude-velocity distributions of the three cloud samples are shown

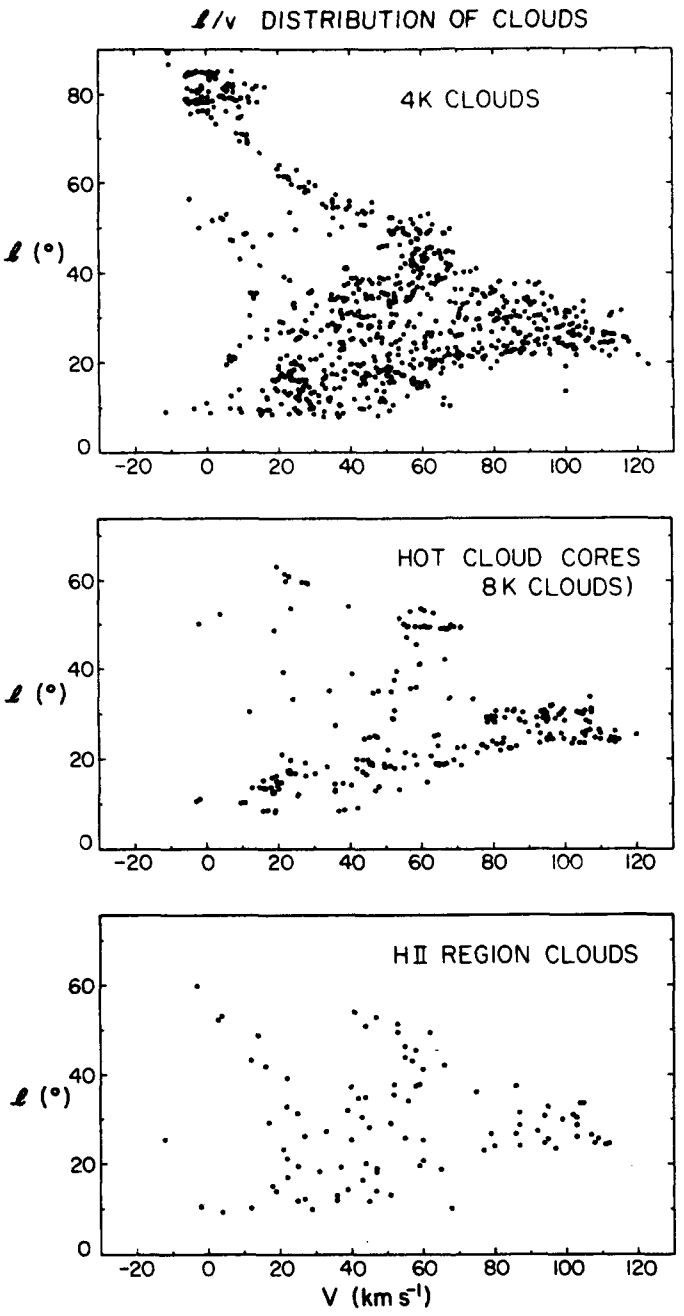

Figure 2. The longitude-velocity distribution of the general cloud population in the first galactic quadrant is contrasted with that of hot cloud cores and clouds associated with HII regions (Scoville et al 1986).

in Figure 2. There it can be seen that the hot cloud cores and HII region clouds exhibit a much tighter confinement within the longitude-velocity plane than the general cloud population. Indeed, the hot cloud cores appear to fall along two arcs stretching from $l=0°$, $V=0$ km s^{-1} to the terminal velocities at $l=32$ and $50°$ -- the Scutum and Sagittarius arms.

The tight confinement of hot cloud cores to the spiral arms does not address the fundamental question of why the OB star formation favors the GMCs in the spiral arms since clouds undergoing massive star formation will have higher temperatures due to the presence of the luminous embedded stars.

4.2 The Decreasing Efficiency of OB Star Formation in Massive GMCs

The more interesting question is whether the spiral arm clouds are intrinsically different (eg. have a different mass spectrum or internal density) than the more widely distributed disk population clouds. It is therefore of interest to note that the mean diameter of the HII region clouds (at the 4 K CO boundary) is 52 pc, effectively a factor of two larger than that of the general GMC population measured at the same threshold temperature (Scoville et al 1986). Although it is clear that massive star formation tends to prefer the larger GMCs, this may simply reflect the greater mass and therefore, the larger number of sites for star formation in the larger clouds.

In order to analyze the efficiency (per unit mass of H_2) for massive star formation in clouds of varying mass, we show in Figure 3 the HII region free-free luminosity normalized by the cloud mass for clouds in five mass bins between 2×10^5 and 3×10^6 $M_\odot$. Also shown is the normalized number of giant HII regions as a function of cloud mass. The figure demonstrates that the efficiency (per unit mass of H_2) for both uv emission and formation of separate OB star clusters decreases for high mass clouds compared to lower mass clouds over this mass range. Thus, the formation rate for massive stars is not simply proportional to the total mass of H_2, but must depend on other factors such as the galactic location or the internal properties of the clouds.

The decreasing efficiency for OB star formation in higher mass clouds argues rather strongly against mechanisms involving internal stimulation of the clouds to initiate star formation. This is because an internal stimulation process should generally have a higher efficiency in more massive clouds where there is more material (surrounding the trigger) ready to be stimulated. For this reason, sequential star formation models such as the compression of shells at the edges of HII regions (Elmegreen and Lada 1977) do not appear to dominate in the formation of massive stars.

4.3 Cloud-Cloud Collisions to Form OB Stars

An alternative mechanism for forming massive stars is the compression of gas in the interface between colliding clouds and cloud clumps (cf. Scoville, Sanders, and Clemens 1986). This mechanism is strongly supported by comparison of the galactic distributions of molecular clouds and HII regions. Recently, Clemens et al (1986) have analyzed the Massachusetts-Stony Brook CO survey to yield an approximate face-on distribution for the molecular gas in the inner galaxy using scale height information to resolve the distance ambiguities.

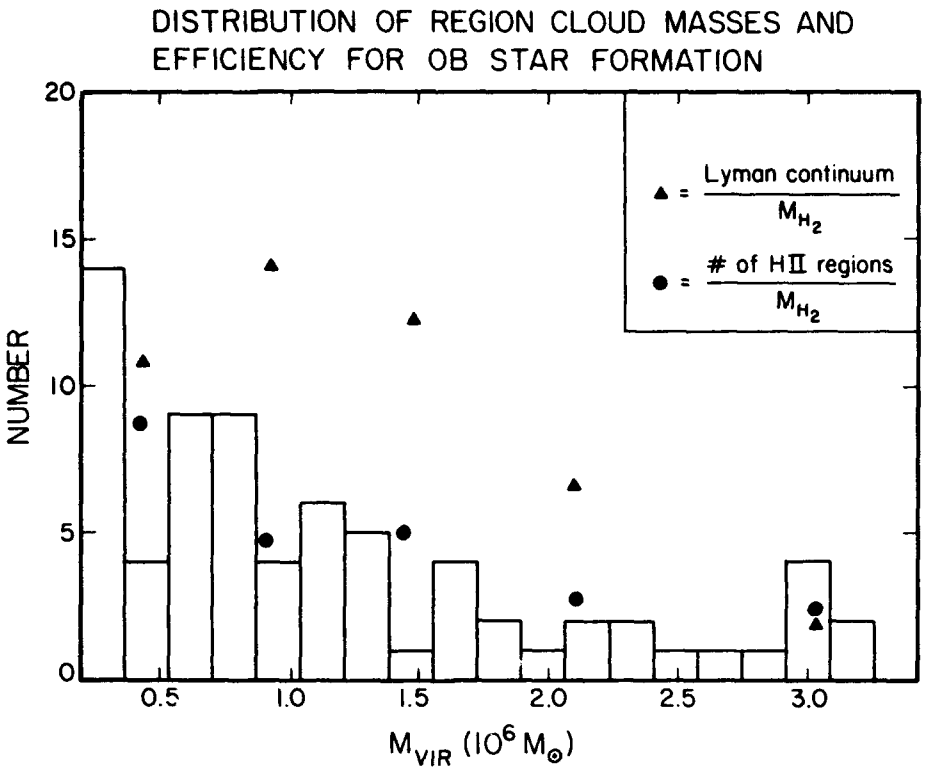

Figure 3. The distribution of virial masses and OB star formation efficiencies (per unit mass of H_2) are shown for 71 GMCs with associated HII regions at known distances (Scoville et al 1986).

Figure 4 shows the dependence of the number of HII regions on the molecular hydrogen density averaged over length scales of ∿300 pc. The best fit power law is

$$N_{HII} \propto \langle n_{H_2} \rangle^{1.9\pm0.2} \quad .$$

The quadratic dependence of the HII region density (presumably the OB star formation rate) on the molecular hydrogen density is strongly suggestive that OB stars form as a result of a collision process, such as cloud-cloud collisions.

Since the 4 km s^{-1} rms velocity dispersion of giant molecular clouds (Clemens 1985) is comparable to or less than the typical internal velocities in the clouds, it is clear that most collisions between GMCs will result in a bound complex rather than disruption of the clouds. During a cloud-cloud collision, the interface gas will remain molecular but be heated to peak temperatures of 10^3-2×10^3 K. Since the Jeans length at the highest temperatures is much greater than the thickness of the hottest zone in the interface, stars would not be expected to form until the post-shock gas has cooled to approximately 100 K. At that point, the highest mass stars will form first in the cooling gas, thus favoring massive stars in the initial mass function.

The mechanism of cloud-cloud collisions to form OB stars is consistent with a number of previous observations of OB star formation. Most important

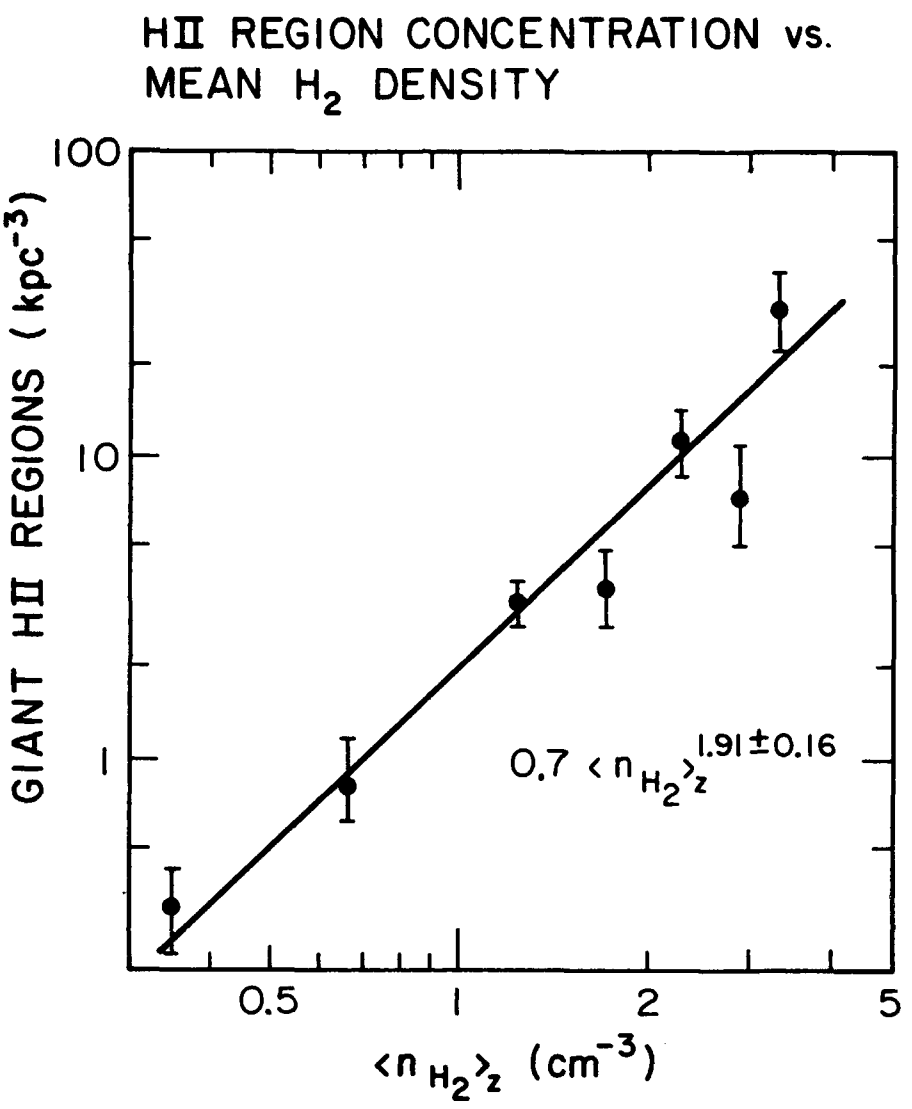

Figure 4. The number density of HII regions depends quadratically on the local H_2 density (averaged over ∿300 pc in the galactic plane). The face-on density of H_2 is taken from Clemens, Sanders, and Scoville (1986).

is the fact that one may now understand the concentration of HII regions along the spiral arms as resulting from the convergence of cloud orbits in the spiral potential minimum associated with the density wave. With a modest 5% spiral perturbation, Kwan and Valdes (1983) found that the number density of clouds increased by a factor of approximately three in the spiral arms which would result in an increase of the collision rate by a factor of nine. This corresponds well to the observed contrast between arm and interarm HII regions -- Mezger and Smith (1977) find 15% of the giant HII regions in classic interarm areas of the l-V plane. In addition, it has often been noted that OB star formation occurs with a low duty cycle in molecular clouds, that is, the time during which massive star formation occurs is relatively short compared to the spread of ages for lower mass young stars within the clouds. In the collision model,

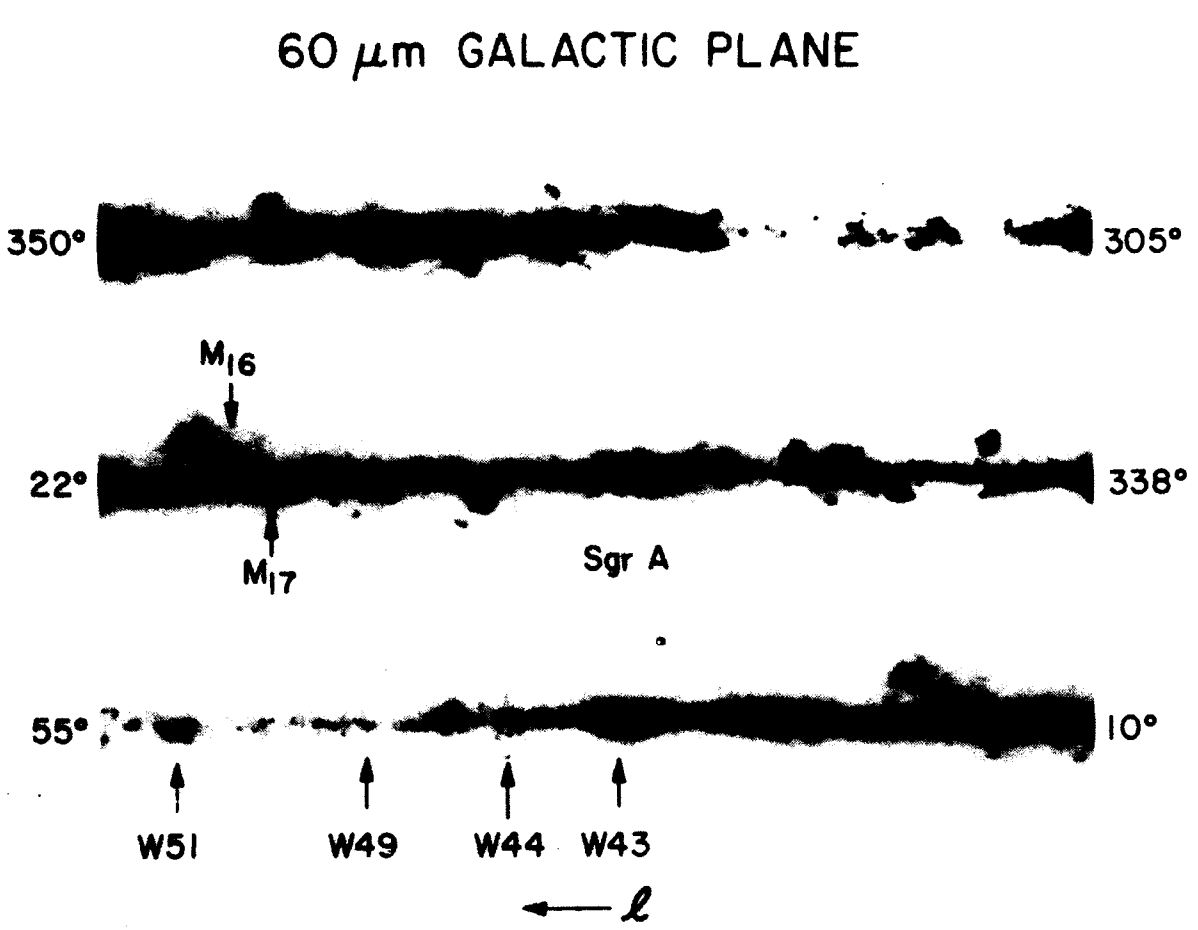

Figure 5. The 60 μm IRAS data were used to produce a constant, logarithmic stretch image of the first galactic quadrant. The image was prepared at IPAC by G. Laughlin.

it is natural to expect a low duty cycle as a result of the fact that the cloud crossing time (that is, the interaction time) is a factor of 5-10 less than the mean time between cloud collisions.

The HII regions formed during cloud collisions could be found deep in the cloud interior or near the edge of the merged cloud, depending on the relative masses of the initial two clouds. Since the largest fraction of the gas will be activated in collisions of equal mass clouds, one would also naturally predict a peak OB star formation efficiency (per mass of H_2 gas) at intermediate cloud masses. Finally, we note that the resulting HII regions will line up along the collision interface; thus, the model will be consistent with all the observational evidence which has been summoned to support sequential star formation models (cf. Elmegreen and Lada 1977).

5. THE INFRARED EMISSION ASSOCIATED WITH MOLECULAR CLOUDS

As a result of the IRAS survey, there now exists reasonably complete spectral

and spatial information for the infrared emission associated with the GMCs detected in the Massachusetts-Stony Brook CO survey. Identification of discrete CO emission complexes with concentrations of far infrared emission in the IRAS survey also enables us to determine the kinematic distances for numerous far infrared sources and thus to estimate luminosities from the IRAS flux measurements. Figure 5 is a far infrared image of the first galactic quadrant constructed from the 60 μm data with a constant logarithmic stretch. Each of the three strips contains 10° of latitude and 45° of longitude.

5.1 The Total Far Infrared Luminosity From Molecular Clouds

In Figure 6, we compare the longitude distributions of the far infrared luminosity, molecular hydrogen mass, and dust temperature (derived from the 60 and 100 μm fluxes with a dust emissivity $\propto \lambda^{-1}$, see Appendix B of Lonsdale et al 1985). For both the CO and IRAS data, the fluxes were averaged over a window of $\Delta b=2°$ and $\Delta l=2.5°$, and in the infrared, a background was subtracted corresponding to the fluxes at $b=\pm 1°$. The far infrared luminosity includes the bolometric correction for λ=1-500 μm (Lonsdale et al 1985). For both the H_2 mass and the infrared luminosity, the units are displayed in solar units for a reference distance of 1 kpc. Since the bulk of the emission in the range l=10-50° arises from regions at a distance of 5-15 kpc, the vertical scale should generally be multiplied by factors of 25-225.

The dominant feature in both the CO and far infrared luminosity distributions is the molecular ring at l=20-50°. For the range l=8-50° the mean ratio of l_{IR}/m_{H_2} is 2.75 L_o/M_o and the mean far infrared dust temperature is 29.3 K. There are, however, very notable departures from a constant IR:CO ratio in the vicinity of high luminosity HII region complexes, for example, at l=24, 34, 50 and 75°.

Assuming that, on average, the far infrared emission arises with the same distribution of source distances as the CO, we may use existing CO mass estimates to derive the total far infrared luminosity of molecular clouds in the galactic plane. That is, global models for the CO emission distribution in the galactic disk (for which the source distances were derived from the CO velocities and scale heights) may be applied directly to yield the d^2 factors needed to convert the far infrared fluxes in Figure 6 into luminosities. For a solar distance of 8.5 kpc, Clemens, Sanders, and Scoville (1986) deduce a molecular mass of 2.1×10^9 M_o for the region R>1.5 kpc. Using the mean ratio of far infrared luminosity to CO mass (2.75 L_o/M_o), we obtain a total far infrared luminosity from the same region of 5.8×10^9 L_o.

The luminosity in the galactic center region may be estimated directly from the observed flux assuming that all of the radiation observed at l=-2.5 to +2.5° originates at a distance of 8.5 kpc. The luminosity from this region, corresponding to $R\leq 375$ pc, is 7×10^8 L_o.

It should be noted that this luminosity estimate does not include emission components with large latitude thickness since we removed the "background" flux at $b=\pm 1°$. Although part of the emission which varies slowly in latitude is undoubtedly local and therefore does not represent a significant addition to the overall Galactic luminosity, some of the high latitude emission must originate in the 3-7 kpc ring on the basis of the longitude variation which shows a maximum

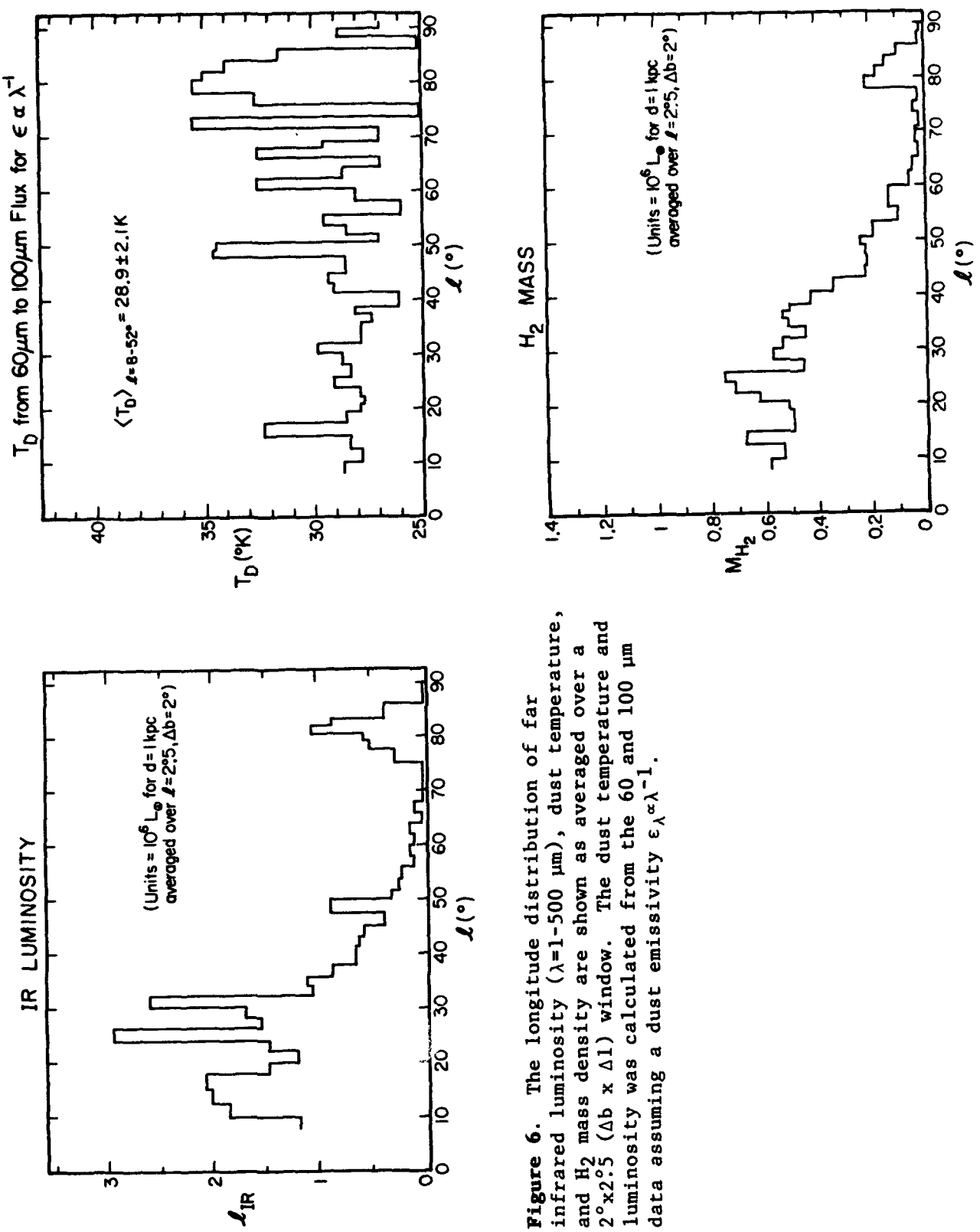

Figure 6. The longitude distribution of far infrared luminosity (λ=1-500 μm), dust temperature, and H_2 mass density are shown as averaged over a 2°x2°.5 (Δb x Δl) window. The dust temperature and luminosity was calculated from the 60 and 100 μm data assuming a dust emissivity $\varepsilon_\lambda \propto \lambda^{-1}$.

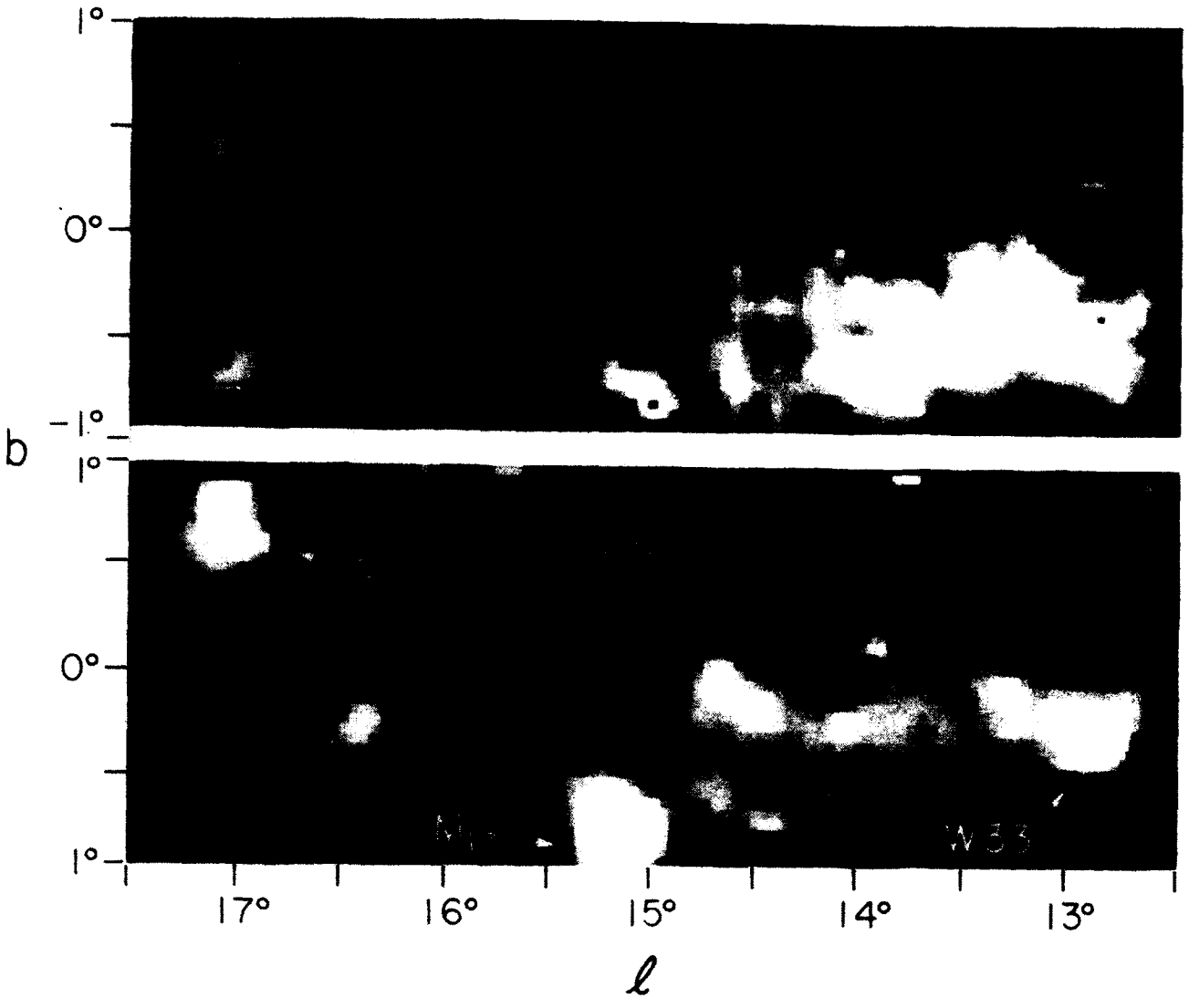

Figure 7a. The far infrared luminosity (λ=1-500 μm) and CO (V=10->40 km s^{-1}) distributions are shown for a 2x5° area of the galactic plane including M16 and M17. Pixels are 3x3'.

in the range l=20-50° (Puget et al 1986). This diffuse component could constitute as much as 50% of the total far infrared luminosity. Although the emission, seen at $|b|>1°$, is probably emitted by dust associated with non-molecular ISM, the energy sources of this luminosity are presumably situated closer to the galactic plane in the molecular cloud ring.

5.2 The Infrared Luminosity of Individual Clouds

In Table 1, the far infrared and CO properties are summarized for GMCs associated with the high luminosity HII regions M17, M16 and W51. Measurements are given for regions of varying diameter in each cloud -- including both the primary infrared sources associated with the HII regions and the more extended

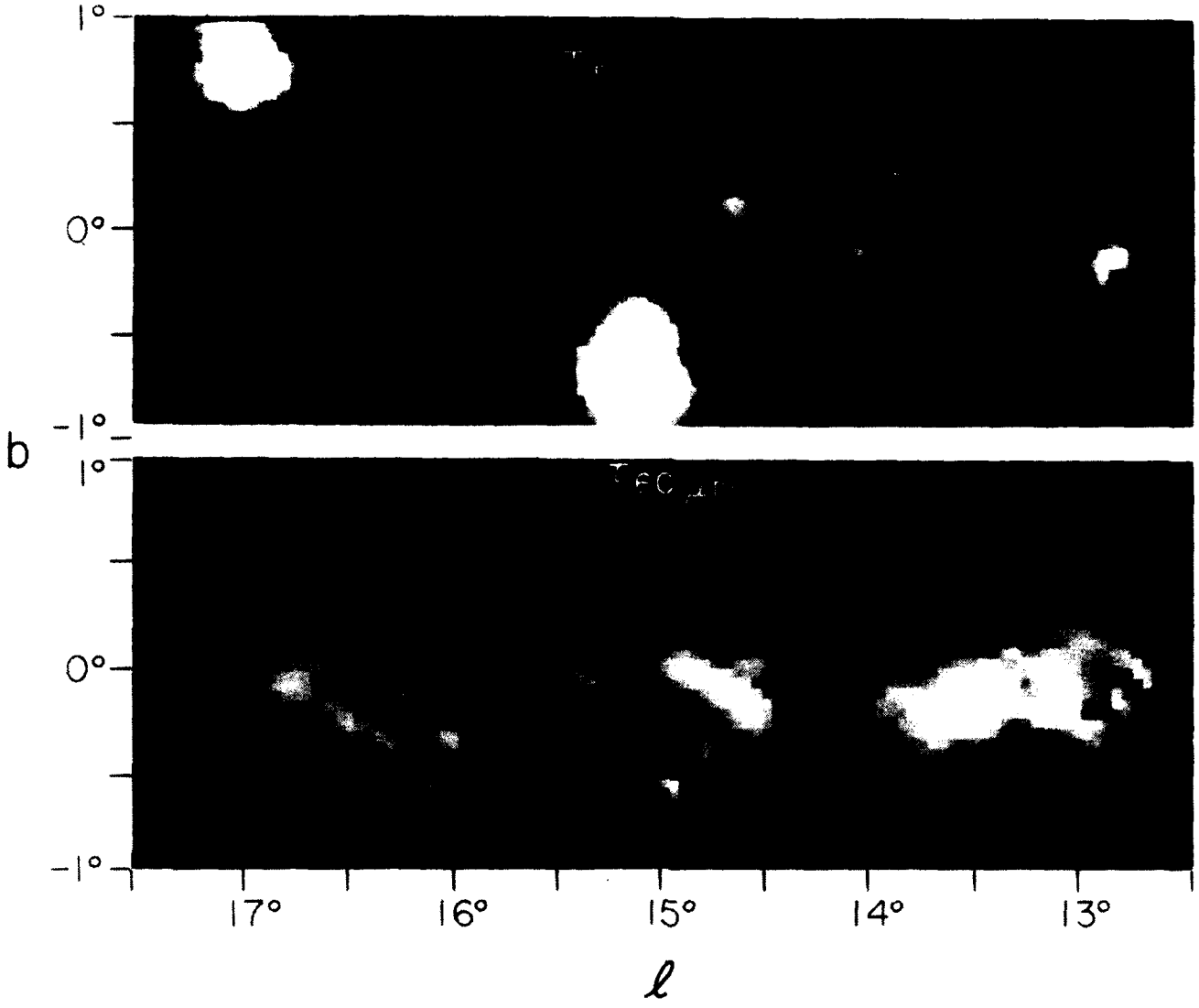

Figure 7b. The far infrared optical depth and dust temperature maps are shown for the same area as Figure 7a including M16 and M17. The opacity and temperatures were derived from the 60 and 100 μm IRAS data following the prescription given by Lonsdale et al (1985) for $\varepsilon_\lambda \propto \lambda^{-1}$. The image stretch is $\tau_{60\ \mu m}$=0-0.5 and T_D=25-45 K.

emission associated with the much larger molecular clouds.

The ratio of far infrared luminosity to molecular mass is a factor of ten higher than the galactic plane average of l_{IR}/m_{H_2}=2.75 L_o/M_o in the immediate vicinity of the luminous HII regions. The maximum value for L_{IR}/M_{H_2} (25.7 L_o/M_o) is obtained on M16. It is noteworthy that even though the ratio of far infrared luminosity to H_2 mass decreases as one includes larger areas of the cloud, inclusion of the entire GMC (100 pc in diameter) still yields a high L_{IR}/M_{H_2} ($\sim$10 L_o/M_o) which is much greater than the mean value obtained for the galactic plane.

Images of the CO and far infrared emission in a 2x5° (bxl) area of the

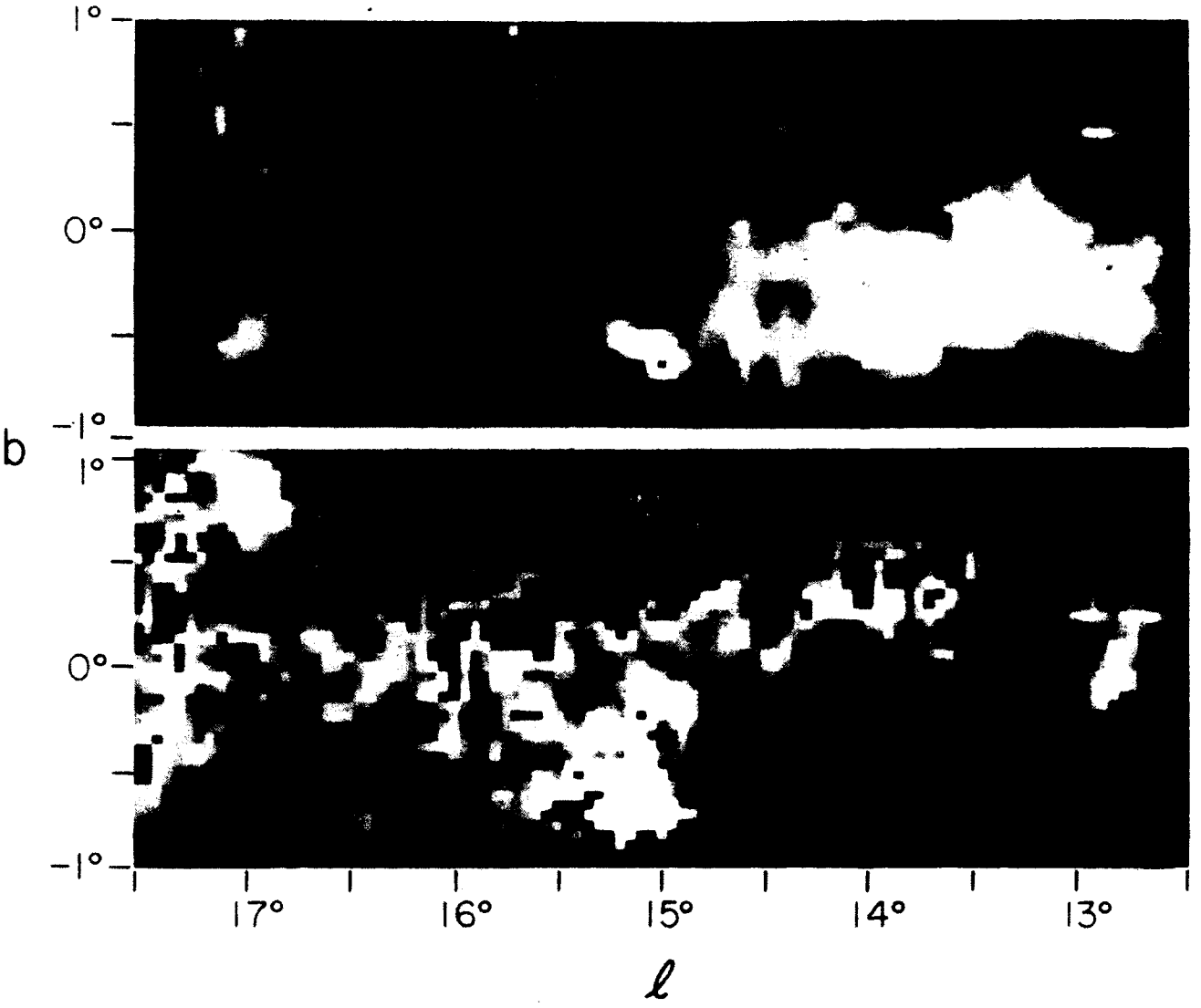

Figure 7c. The CO and L_{IR}/M_{H_2} maps for M16 and M17. The stretch for L_{IR}/M_{H_2} is from 3 to 30 L_o/M_o and the image is blanked where the CO measurement is less than 7σ.

galactic plane including M16 and M17 are shown in Figure 7. The CO emission was integrated from V_{LSR}=-10 to 40 km s^{-1} and the infrared optical depth, dust temperature and luminosity were computed assuming an emissivity $\varepsilon_\lambda \propto \lambda^{-1}$ (see Lonsdale et al 1985). The infrared emission in the vicinity of the HII regions is characterized by low opacity, high temperature and high luminosity density. In areas of the GMCs away from the HII regions, the dust appears significantly colder than even the galactic background and hence, the GMCs show up on the dust temperature map as dark areas (which also have high opacity). The L_{IR}/M_{H_2} map clearly shows the tendency for high values in the vicinity of the HII regions and in general along the cloud boundaries where the interstellar uv probably heats the peripheral dust.

Table 1

IR Properties of High Mass Star Formation Regions[a]

Region	Diameter (pc)	M_{H_2}[b] ($M_\odot$)	L_{IR}[b] ($L_\odot$)	L_{IR}/M_{H_2} ($L_\odot/M_\odot$)	IRE[b]	T_D (K)
M16	20	9×10^4	1.3×10^6	15	14	36
M17	18	9×10^4	3.4×10^6	37	2.4	43
	75	1×10^6	1.3×10^7	13	6.9	31
W51	50	8.7×10^5	1.3×10^7	15	4	39
	135	2.8×10^6	2.7×10^7	9.6	6.9	35
Galactic Center[c]	740	2×10^8	6.8×10^8	3.5		31
Galactic Disk[d]		2.2×10^9	6×10^9	2.8		29

Notes

a) Assumes R_o=8.5 kpc throughout.

b) M_{H_2} evaluated from $N_{H_2}=3.6\times10^{20}$ H_2 cm^{-2} (K km $s^{-1})^{-1}$ (Scoville *et al* 1986). L_{IR} obtained from 60 and 100 μm IRAS fluxes with an assumed λ^{-1} emissivity law (see Appendix B of Lonsdale *et al* 1985). The infrared excess (IRE) was evaluated from L_{IR} and the radio free-free flux (cf. Myers *et al* 1986).

c) l=-2°.5 to +2°.5, b=-1° to +1°. The IR background at |b|=1° was removed.

d) R<1.5 kpc. The IR galactic background at |b|=1° was removed.

6. APPLICATION TO HIGH LUMINOSITY IRAS GALAXIES

Recently, Sanders et al (1986) have obtained single dish CO measurements for some of the distant IRAS galaxies. Their results indicate typical L_{IR}/M_{H_2} ratios in the range 10-50. These values are generally consistent with those obtained for Galactic GMCs associated with HII regions (Table 1), suggesting that high mass star formation is a viable energy source in the luminous IRAS galaxies. However, it is then required that virtually all the clouds in these galaxies have conditions similar to the most active areas in W51 and M17 and this may be somewhat implausible.

With regard to the suggestion by Scoville, Sanders and Clemens (1986) that most massive star formation in our own galaxy results from cloud-cloud collisions, it is noteworthy that Sanders et al (1986) have found that the majority of the distant high luminosity IRAS galaxies are in fact interacting galaxy pairs in which one would expect a high frequency of collisions between the interstellar clouds of the two galaxies.

We acknowledge support for this work under the IRAS General Investigator Program (NS) and NSF Grant AST 84-12473.

7. REFERENCES

Allen, R.J., Atherton, P.D., and Tilanus, R.P.J. 1986, Nature, **319**, 296.
Burton, W.B. and Gordon, M.A. 1978, Astron. Astrophys., **63**, 7.
Burton, W.B., Gordon, M.A., Bania, T.M., and Lockman, F.J. 1975, Ap.J., **202**, 30.
Clemens, D.P. 1985, Ap.J., 295, 422.
Clemens, D.P., Sanders, D.B., and Scoville, N.Z. 1986, Ap.J. (submitted).
Cohen, R.S., Cong, H., Dame, T.M., and Thaddeus, P. 1980, Ap.J. (Letters), **239**, L53.
Cohen, R.S., Tomasevich, G.R., Thaddeus, P. 1979, in IAU Symposium 84, The Large Scale Characteristics of the Galaxy, ed. W.B. Burton (Dordrecht: Reidel), p.53.
Downes, D., Wilson, T.L., Bieging, J., and Wink, J. 1980, Astr. Ap. Suppl., **40**, 379.
Elmegreen, B.G. and Lada, C.J. 1977, Ap.J., **214**, 725.
Herbst, W. and Assousa, G.E. 1977, Ap.J., **217**, 473.
Kwan, J. and Valdes, F. 1983, Ap.J., **271**, 604.
Lockman, F.J. 1986 (in preparation).
Lonsdale, C.J., Helou, G., Good, J.C., and Rice, W.L. 1985, Catalogued Galaxies and Quasars Observed in the IRAS Survey (Washington : U.S. Government Printing Office).
Myers, P.C., Dame, T.M., Thaddeus, P., Cohen, R.S., Silverberg, R.F., Dwek, E., and Hauser, M.G. 1986, Ap.J., **301**, 398.
Mezger, P.G. and Smith, L.F. 1977, Star Formation, IAU Symposium No. 75, ed. de Jong, T. and Maeder, A., (Dordrecht: Reidel), p. 133.
Puget, J.L., Falgarone, E., Perault, M., and Ryter, C. 1986, in Star Formation in Galaxies, ed. C. Persson.
Robinson, B.J., Manchester, R.N., Whiteoak, J.B., Sanders, D.B., Scoville, N.Z., Clemens, D.P., McCutcheon, W.H., and Solomon, P.M. 1984, Ap.J. (Letters), **283**, L31.

Rydbeck, G., Hjalmarson, A., and Rydbeck, O.E.H. 1985, Astron. Astrophys., **144**, 282.
Sanders, D.B. 1981, Ph.D. thesis, State University of New York at Stony Brook.
Sanders, D.B., Clemens, D.B., Scoville, N.Z., and Solomon, P.M. 1986, Ap.J. Suppl., **60**, 1.
Sanders, D.B., Scoville, N.Z., and Solomon, P.M. 1985, Ap.J., 289, 373.
Sanders, D.B., Scoville, N.Z., Young, J.S., Soifer, B.T., Schloerb, F.P., Rice, W.L., and Danielson, G.E. 1986, Ap.J. (Letters), **305**, L45.
Sanders, D.B., Solomon, P.M., and Scoville, N.Z. 1984, Ap.J., **276**, 182.
Scoville, N.Z. and Sanders, D.B. 1986, in Interstellar Processes, ed. Thronson, H. and Hollenbach, D. (Dordrecht: Reidel) (in press)
Scoville, N.Z., Sanders, D.B., and Clemens, D.P. 1986, Ap.J. (Letters), (November 15).
Scoville, N.Z. and Solomon, P.M. 1975, Ap.J. (Letters), **199**, L105.
Scoville, N.Z., Yun, M.S., Clemens, D.P., Sanders, D.B., and Waller, W.H. 1986, Ap.J. Suppl. (submitted).
Solomon, P.M., Sanders, D.B., and Rivolo, A. 1985, Ap.J. (Letters), **292**, L19.

DISCUSSION

ELMEGREEN:

Molecular clouds are clumpy and stars form in the dense clumps. The average density in cloud complexes decreases with increasing cloud mass, so the star-forming cores represent a smaller and smaller fraction of the overall cloud mass as this overall mass increases. This may explain why the efficiency decreases with increasing mass; this decrease may be independent of sequential star formation processes. The observed clumpiness also explains the low star formation efficiency without the need for physical assumptions about cloud stability. The clumps dissipate their kinetic energy in only several crossing times and eventually form cores dense enough for star formation. The efficiency in these cores can be large (10%-50%), but the overall efficiency in the whole cloud, low. Cloud complexes need not be 'stable' for any longer time than this clump dissipation time. Star formation is not necessarily the same as clump formation because the clumps could be primordial, that is, the big clouds may form by a coalescence of smaller clouds, which are still visible as clumps.

SCOVILLE:

If the decreased efficiency for massive star formation in higher mass clouds is the result of the decreased fraction of the cloud mass in dense clumps, then this also implies that 'sequential star formation' has little to do with the OB star formation i.e., the formation of massive stars is simply due to the pre-existing clump structure in the clouds. In any case, there are as yet no observational studies suggesting that the fraction of mass in dense clumps is any different in high-mass clouds than in low-mass clouds. The mean density is probably higher in the latter case, but it does not follow that this is the result of a higher clump fraction.

HUNTER:

You have said that galaxies with low 'CO contents' would preferentially form low-mass stars. What about irregular galaxies which have low CO luminosities and yet plenty of high-mass star formation?

SCOVILLE:

The critical factor is not the absolute 'CO content' but rather the concentration of the molecular gas. You could certainly have situations in which the overall molecular gas content of a galaxy was low but the clouds were restricted to a small region (or had a high velocity dispersion) so that the frequency of cloud-cloud

collisions was high, resulting in a high rate of OB star formation. One should also note that massive star formation in the irregular galaxies with low H_2/HI ratios could result from collision of HI clouds.

HUNTER:

But in NGC 4449, for example, the high mass star formation is scattered throughout the galaxy, so clouds would have to be colliding over the entire disk. This implies a lot of molecular mass.

BEGELMAN:

Is there actually time for gravitational collapse to occur at the cloud-cloud interface during the collision? Even if cooling is very rapid, collapse can occur no faster than the free-fall time. In the limit of rapid cooling, the interface would cool isochorically rather than isobarically.

SCOVILLE:

Depending on the size of the GMCs undergoing a collision, the collision time could be up to 10^7 years which is much greater than the 10^6 year free-fall time at density $\geq 10^3$ cm^{-3}.

ELIAS:

With regard to the point about HII regions being at the center of molecular clouds, I noticed, first, that the specific examples you showed had the HII region toward the edges, and, second, that the clouds were very non-spherical. How does this affect your statistical discussion?

SCOVILLE:

I agree that the interpretation of the HII region offsets is very dependent on the assumed geometry of the clouds, i.e., whether they are spherical or elongated.

DIFFUSE INFRARED EMISSION OF THE GALAXY:

LARGE SCALE PROPERTIES

J.L. Puget, M. Perault, F. Boulanger, and E. Falgarone
Radioastronomie
ENS, 24 rue Lhomond, 75231 Paris Cedex 05

ABSTRACT

A quantitative analysis of IRAS data in the galactic plane shows that:

- about 2/3 of the power radiated in the 100μm band comes from diffuse medium (atomic, molecular and ionized components), the other 1/3 coming from well identified luminous sources (GMC/HII complexes).

- the diffuse emission has almost constant colours throughout the Galaxy, similar to the local "cirrus" colours.

- the sources have a much lower 12μm/25μm and a much higher 60μm/100μm emission ratio than the diffuse component, giving a very striking anticorrelation in the colour-colour diagrams.

- the separation between one narrow (molecular) and a second broader (atomic) component shows that the molecular component does not provide much more than 1/2 of the diffuse emission in the "molecular ring": this implies a $4\pi\ \nu I(\nu)$ emissivity at 100μm for the atomic component of about 2.4 10^{-30} watts per H atom, 10 times higher than the emissivity of the molecular component at the same galactocentric radius (4-6 kpc). The atomic component emissivity measures the interstellar radiation field density.

The temperature distribution of the 2 components is discussed comparing IRAS data with new measures of the 900μm emission of the galactic plane, which appears to be dominated by cold dust in the narrow (molecular) component.

Carol J. Lonsdale Persson (Editor)
Star Formation in Galaxies

The Origin of the Diffuse Galactic IR/Submm Emission: Revisited after IRAS

P. Cox and P.G. Mezger
Max-Planck-Institut für Radioastronomie,
Auf dem Hügel 69, D-5300 Bonn 1, F.R.G.

Abstract

In three previous papers we have investigated the origin of the diffuse galactic IR/Submm emission by fitting model computations to balloon-borne surveys. In this paper we compare the balloon observations with IRAS observations. For the longitude profiles we find good agreement. However, the dust emission observed by IRAS - contrary to balloon observations which show dust emission only within $|b| \leq 3°$ - extends all the way to the galactic pole. We repeat the model fits, using more recent parameters for the distribution of interstellar matter in galactic disk and central region. IR luminosities are derived for the revised galactic distance scale of $R_\odot$ = 8.5 Kpc. A total IR luminosity of 1.2 $E10L_\odot$ is obtained, which is about one third of the estimated stellar luminosity of the Galaxy.

The dust emission spectrum λI_λ attains its maximum at ~ $\lambda 100\mu m$. A secondary maximum in the dust emission spectrum occurs at ~$\lambda 10\mu m$, which contains ~ 15% of the total IR luminosity of the Galaxy. To this hot dust emission contribute both OH/IR stars (~ 1/3) and very small grains down to few Å size (~ 2/3). OH/IR stars are M giants with (for optical/NIR radiation) opaque dust shells. The very small grains could be polycyclic aromatic hydrocarbon (PAH) molecules.

We compare the galactic dust emission spectrum with the dust emission spectra of external IRAS galaxies. The emission spectra observed between $\lambda 30\mu m$ and $1300\mu m$ can be fitted by a minimum of two dust components: Cold dust with temperatures of ~14-25 K, which is associated with diffuse atomic hydrogen and with molecular hydrogen, respectively, and which is heated by the general interstellar radiation field; and warm dust with temperatures of ~30-50 K, located in HII regions and dense molecular cloud cores, which is heated by O and early B stars. The warm dust luminosity relates to the present OB star formation rate, while flux densities observed at longer submm wavelengths are dominated by cold dust emission and thus can be used to estimate gas masses.

I. The Galactic Disk between Galactic Radii $2 \leq R/kpc \leq 10$

The diffuse galactic IR/Submm emission is due to stellar radiation, which is absorbed and reradiated by interstellar dust particles. About one third of the total stellar luminosity of the galactic disk is reemitted as IR emission. For an investigation of the origin of this dust emission three basic parameters must be known: i) The dust characteristics; ii) the spatial distribution of both

interstellar dust and stars of different luminosity and evolutionary stage; iii) the geometrical association between stars and interstellar dust, which determines dust temperatures and luminosity.

We have investigated the origin of the galactic submm/IR emission in three successive papers (Mezger, Mathis and Panagia, 1982. Mathis, Mezger and Panagia, 1983. Cox, Krügel and Mezger, 1986. This last paper is referred to in the following as Paper I). As input parameters to our model computations we use the distribution of the interstellar gas as derived from HIλ21cm and CO(J=1-0) line emission. The distribution of different stellar populations adopted for our model computations are discussed in Mathis et al., who also derive the intensity and spectral distribution of the interstellar radiation field (ISRF) as function of galactic radius R.

We use the Mathis, Rumpl and Nordsieck (MRN, 1977) dust model (which consists of graphite and silicate grains), as extended beyond λ10μm by Mezger et al. (1982), but with optical constants as revised by Draine and Lee, (1984; see also Paper I). We scale the gas-to-dust mass ratio as a function of R with the observed galactic O/H abundance gradient. The MRN grain size distribution has the form $f(a) \alpha\ a^{-3.5}$, with a lower and higher cut-off at radii a_{min} ~100 Å (=0.01 μm) and a_{max} ~0.25μm. In dense molecular clouds one expects grains with radii $>a_{max}$ due to formation of ice mantles. In the diffuse atomic hydrogen (HI) recent observations suggest an extension of the grain size distribution to radii as small as a few Å (Boulanger et al., 1985). The existence of these very small grains (VSG) in interstellar space, probably polycyclic aromatic hydrocarbon molecules (PAH), was first suggested by Léger and Puget (1984).

We first compute the temperature of dust located in the diffuse HI and in quiescent giant molecular clouds (GMC) heated by the general ISRF. The dust emission predicted as a function of galactic longitude l and wavelength λ is then compared to observations. The spectrum of the dust emission within the solar circle (but without contributions from the region around the galactic center) is shown in Figs. 1a and 1b. Fig. 1a shows the spectrum taken from Paper I, which is based on a compilation of balloon observations by Pajot et al. (1986). Open circles relate to a preliminary evaluation of IRAS observations. The revised spectrum in Fig. 1b contains the final IRAS results (filled circles), which are obtained by integrating the IRAS maps after subtraction of the contributions by zodiacal dust. Very recently new and improved balloon observations at λ145μm and λ380μm became available (Caux and Serra, 1986). We cannot incorporate their surface brightness directly in the spectrum Fig. 1b, since their integration extends over $|b| < 1^\circ.25$ rather than over $|b| < 1^\circ$ used by us. However, we adopt their spectral shape for $\lambda \geq 100\mu$m.

It is found that the contributions from very cold dust (vcd) associated with quiescent molecular clouds and from cold dust (cd) associated with atomic hydrogen, as derived from our model computations (see Table 1), can account for only part of the spectrum between λ30μm and 1000μm. Remember that both these dust components are heated by the ISRF, whose radiation density is primarily determined by contributions from stars with $T_{eff} <$ 10,000 K. Subtraction of the contributions by (vcd) and (cd) leaves the dotted curves in Figs. 1a and b, which represent the contribution by warm dust (wd, T ~ 30-50K) to the diffuse galactic emission $\lambda \geq 30\mu$m. Detailed model computations

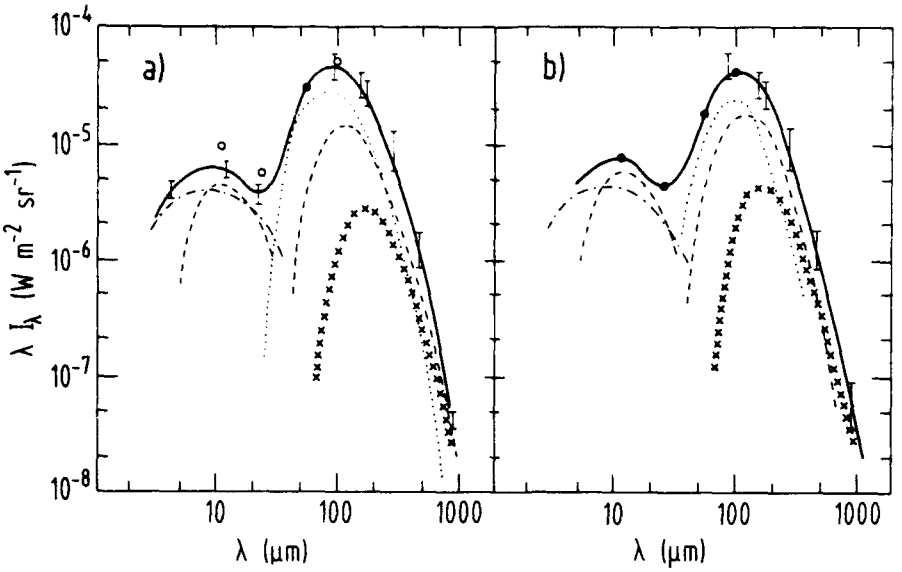

Figure 1. Spectrum of the dust emission between 4 and 900 μm from the inner part (R ≤ 8 kpc) of our galaxy, averaged over galactic longitudes 3 - 35° and latitudes |b| < 1°. a) This is *the spectrum reproduced from Paper I; open circles refer to preliminary IRAS results. b)* This is *the revised spectrum based on final IRAS data (filled circles). The three components which are used to fit both spectra for λ ≥ 30μm are: cold dust (dashed curve), very cold dust (crosses) and warm dust (dotted curve). Two components contribute to the* (hd) *spectrum in the middle IR λ ≤ 30μm, viz. very small grains (dashed curve) and OH/IR stars (dashed-dotted curve). The solid line shows the superposition of the five dust components.*

(Paper I) show that only O and early B stars located in HII regions and dense molecular cores can heat dust to these (wd) temperatures and provide the luminosity required to explain the observed galactic (wd) emission. These model computations further suggest that ~2/3 of the (wd) luminosity is due to heating by O stars and ~1/3 is due to heating by B stars. Comparison of the hydrogen masses associated with (wd) and (cd, vcd), respectively (see Table 1) shows, that only ~1% of the interstellar hydrogen is associated with warm dust, while the (wd) and (cd) luminosities are about equal. Of further interest is the fact that the submm part of the spectra shown in Figs. 1, for λ>500μm, is dominated by (cd) and (vcd) emission. Taking these facts together we arrive at the important conclusion that the (wd) luminosity of the diffuse galactic emission is related to the formation rate of O and early B stars during the past few million years; and that flux densities at submm wavelengths λ ≥ 500μm are dominated by contributions from (cd) and (vcd), which represent the bulk of the interstellar dust.

The emission between λ4μm and 20μm is due to hot dust (hd) of several hundred K. Our model computations, adjusted to the most recent IRAS results, suggest that ~ 1/3 of the total (hd) luminosity comes from normal MRN grains located in circumstellar shells of M giants, which are in their asymptotic giant branch (AGB) evolutionary stage, where heavy mass outflow occurs(the so-called OH/IR stars). The other 2/3 of the (hd) luminosity is contributed by very small grains (VSG) which are heated temporarily by absorption of single

energetic photons to temperatures of several hundred K. If these grains are made of PAH molecules, they would emit the absorbed energy via a "forest of lines" at MIR wavelengths rather independent on the exact grain temperature, and thus could account for the MIR shoulder in the spectra Fig. 1.

While the basic heating sources of the galactic dust are the same as described in Paper I, some of the model parameters have been changed for the fit of the revised spectrum presented here in Fig. 1b. Original and modified model parameters are given in Table 1 for $R_\odot$ = 10 kpc.

Table 1 Parameters for the Model Fit to IR/submm Emission from our Galaxy within the Solar Circle (2 ≤ R/kpc ≤ 10)

Dust component	used in Paper I and Fig.Ia	used here and in Fig.Ib	Reference
Very cold dust (vcd)			
$\langle T^{vcd} \rangle$ in K	14	14	(Puget, 1983)
L_{IR}^{vcd} in $L_\odot$	5 E 8	8 E 8	
M_{H_2} in $m_\odot$	9 E 8	1.5 E 9	(Puget, 1983)
Cold dust (cd)			
T^{cd} in K	15 - 25	15 - 25	
L_{IR}^{cd} in $L_\odot$	4.4 E 9	6.6 E 9	
M_{HI} in $m_\odot$	6 E 8	9 E 8	(Bloemen et al., 1986)
Warm dust (wd)			
T^{wd} in K	30 - 40	30 - 40	
L_{IR}^{wd} in $L_\odot$	7.3 E 9	6 E 9	
M_{gas}^{wd} in $m_\odot$	4 E 7	3 E 7	
Hot dust (hd)			
T^{hd} in K	200 - 500	200 - 500	
L_{IR}^{hd}(VSG) in $L_\odot$	1.3 E 9	2 E 9	
L^{hd}(OH/IR) in $L_\odot$	1.2 E 9	1.4 E 9	(Habing, 1986 priv. comm.)
A_V (10 - 2Kpc)			
A_V^{tot} in mag	20	25	(Puget, 1983)
A_V^{HI} in mag	9	13.5	
$A_V^{H_2}$ in mag	11	11.5	

The main difference of the parameters used in the revised model is an increase of the mass of interstellar matter associated with (vcd) and (cd) by factors of ~1.7 and ~1.5, respectively, accompanied by a corresponding increase in the IR luminosities. VSG appear to exist only in the diffuse interstellar matter (HI).Hence their contribution to the (hd) luminosity also increases by a factor 1.5. In paper I we adopted a luminosity ratio $L^{hd}(VSG)/L^{cd}$ ~ 0.25, which we here increase to ~ 0.30 based on the latest evaluation of IRAS results (Cox and Leene, 1986).

Ridge line intensities of the dust emission in the galactic plane as derived from IRAS observations are shown together with our model fits in Figs. 2a,b,c and d. Fits for surveys at other wavelengths can be found in Paper I. Ridge line intensities, derived from balloon and IRAS surveys, generally agree very well. Latitude profiles derived from IRAS surveys – contrary to balloon surveys – show dust emission at all latitudes. The extended IRAS latitude profiles are well reproduced by our model computations (see Paper I, Fig. 4). This high-latitude dust emission increases the radiation density contained in the FIR part of the ISRF by nearly an order of magnitude, as compared to the estimates by Mathis et al.(1983).

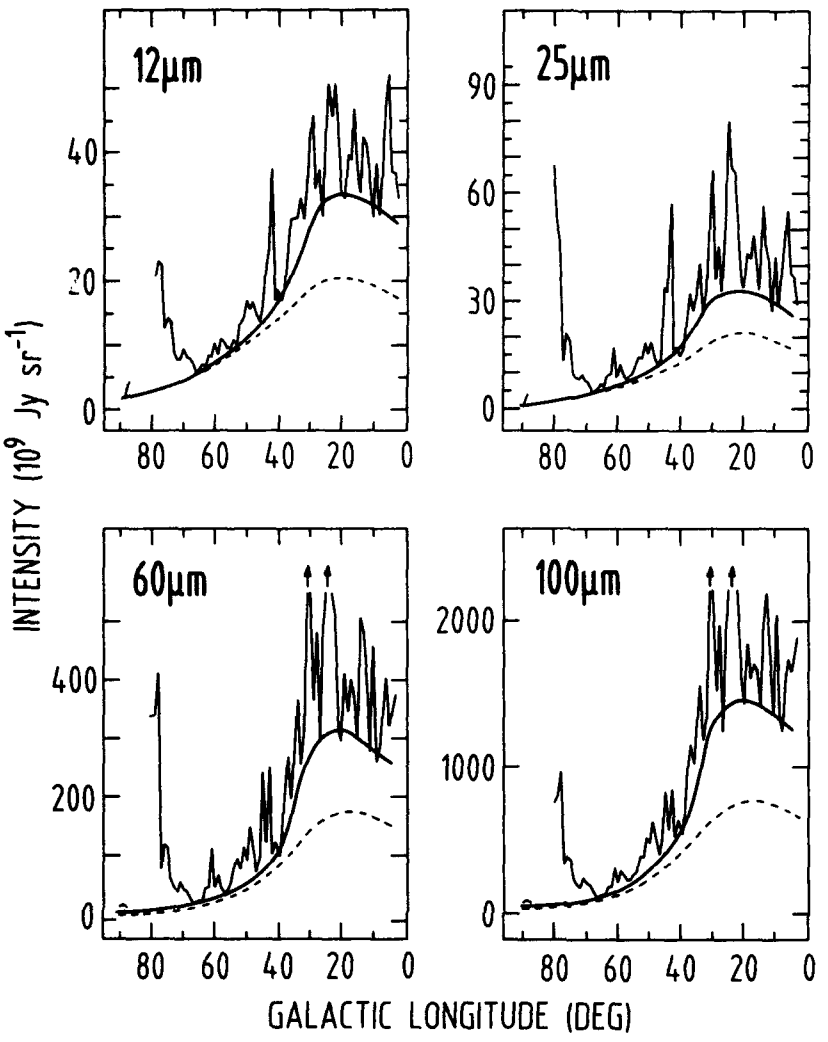

Figure 2. Ridge line intensities of the infrared emission for 3° ≤ l ≤ 90° in the four IRAS bands. The data are averaged over |b| ≤ 0°.5. The dashed curves represent at λ = 12μm and λ = 25μm the contributions of very small grains and show at λ = 60μm and λ = 100μm the contribution of cold dust. Solid curves are the sum of the contribution of cold, very cold and warm dust at 60μm and 100 μm, and of very small grains and hot dust in the shells of OH/IR stars at 12μm and 25μm.

II. The Galactic Center Region

The central regions of many external spiral galaxies are prominent IR sources. In analyzing their integrated dust emission one would like to know if and how the emission spectra of nuclear regions (R ≤ 1 kpc) deviate from those of the spiral arm regions, where most of the OB stars form. For most external galaxies the angular resolution of IRAS is not sufficient to resolve disk and nucleus. However, for the center region of our galaxy the IRAS data can be used to estimate the characteristics of its dust emission.

The surface density of both atomic and molecular hydrogen falls to a minimum between galactic radii R ~1-2kpc, then starts to increase again at R ≤ 0.7 kpc. The total mass of interstellar matter within this radius amounts to several 10E8 $m_\odot$. Free-free and warm dust emission, however, which indicate OB star formation, are only found within an area $\Delta l \times \Delta b \sim 2^\circ \times 0^\circ.5$, corresponding to ~ 350 x 90 pc surrounding the galactic center. The dust emission from this region will be investigated in this section.

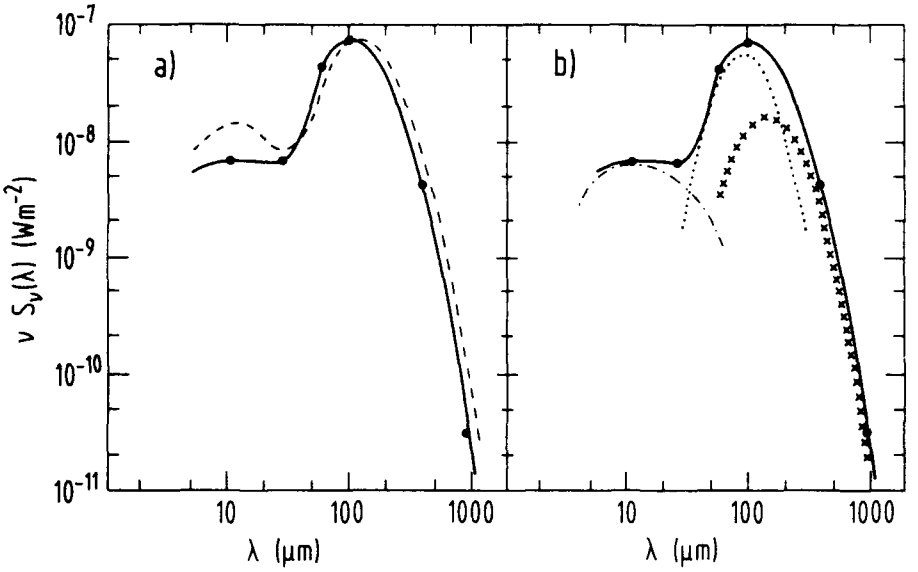

Figure 3. Average spectrum of the dust emission associated with the galactic center, integrated within an area $\Delta l \times \Delta b \sim 2^\circ \times 0^\circ.5$ (dots and full line). a) is a comparison with the spectrum of the galactic disk taken from Fig. 1b (dotted line); b) is a decomposition of the galactic center spectrum into the contributions of very cold dust (crosses), warm dust (dotted line) and hot dust (dash-dotted line), as described in the text.

In Fig. 3a we have plotted flux densities integrated within this area. The flux densities relate to the galactic center, i.e. an underlying extended component due to dust emission from the galactic disk has been subtracted. Flux densities at 900μm and 300μm are those estimated by Mezger et al. (1986 and references therein), flux densities at shorter wavelengths have been derived from IRAS data. The dashed curve in Fig. 3a represents the spectrum of the surface brightness of dust emission from the galactic disk as shown in Fig. 1b, but normalized to coincide with the galactic center flux density at λ100μm. The full curve connects the observed flux densities and represents the true IR/submm spectrum of the center region to the best of our present knowledge. Again, the spectral shape for λ ≥ 100 μm has been adopted from Caux and Serra (1986).

An investigation of the cold dust emission at λ300μm and λ900μm yielded a total mass of hydrogen of ~1.5E7 $m_\odot$ within 2° x 0°.5, comparable to the total mass of molecular hydrogen as estimated from CO observations. This led to the conclusion that most of the hydrogen in the central region is in form of molecules located in GMCs, whose average dust temperature of $\langle T^{vcd} \rangle$ ~ 20K,

however, appears to be higher than in disk GMCs. Also, kinetic gas temperatures derived for the center GMCs are much higher than gas temperatures derived for disk GMCs (Mezger et al., 1986, and references therein).

The (vcd) spectrum, for M_H = 1.5E7 $m_\odot$ and $\langle T^{vcd} \rangle$= 20K, is shown by crosses in Fig. 3b. Subtraction of this (vcd) contribution from the observed spectrum leaves the dotted line, which corresponds to the emission from (wd) with T^{wd} ~ 35–45K. Due to the absence of atomic HI we consider the contribution from (cd) emission negligible. This also agrees with the considerably lower (hd) emission as compared to the galactic disk (Fig. 3a). Since VSG dust is to be correlated with diffuse atomic hydrogen, which appears to be absent in the central 2°x0°.5, only OH/IR stars will contribute to the (hd) emission.

Table 2

Parameters for the Model Fit to the IR/submm Emission from a Region Δl x Δb ~ 2°x 0°.5 surrounding the Galactic Center. Adopted Distance to the Galactic Center is $R_\odot$ = 10 kpc.

Dust component	Parameters	References
Very cold dust (vdc)		
$\langle T^{vcd} \rangle$ in K	20	
L^{vcd} in $L_\odot$	7E7	Mezger et al.: 1986
M_{H_2} in $m_\odot$	1.5E7	
Cold dust (cd) not considered		
Warm dust (wd)		
T^{wd} in K	35 - 45	Dent et al.: 1983
L^{wd} in $L_\odot$	2.3E8	
M^{wd}_{gas} in $m_\odot$	1E6	
Hot dust (hd)		
T^{hd} in K	200 - 500	
L^{hd}_{IR} (VSG) in $L_\odot$	—	
L^{hd}_{IR} (OH/IR) in $L_\odot$	3E7	

The parameters used for the model fit of the dust emission from the central 2°x0°.5 are given in Table 2. The corresponding dust luminosity amounts to ~ 2% of the total luminosity. Estimates of the formation rate of OB stars in the central 350 x 90 pc – based on free-free flux densities and warm dust luminosity – range from ~ 10–4% of the total OB star formation rate in the Galaxy. The nucleus of our Galaxy thus exhibits only mild star formation activity.

III. Comparison with external galaxies

The average spectrum of 18 Sb,c type galaxies, taken from Chini et al. (1986), is shown in Fig. 4. This spectrum can be decomposed into a minimum of three components, which we identify – in analogy to the dust emission from our Galaxy – with contributions from i) (vcd) + (cd) emission (which cannot be separated), ii) (wd) emission and iii) (hd) emission, respectively.

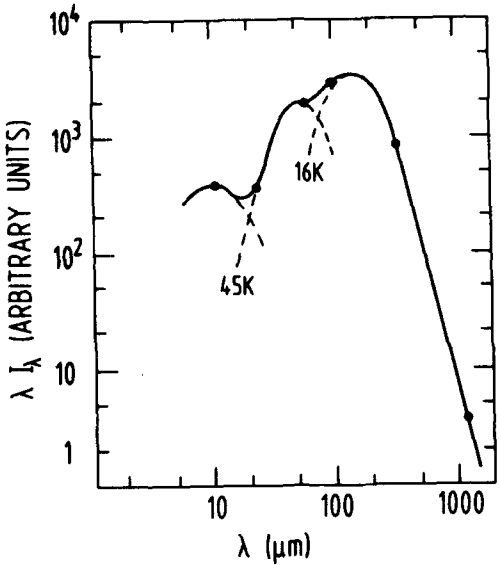

Figure 4. The average spectrum of 18 Sb,c type galaxies normalized at λ100μm (from Chini et al., 1986). The solid curve is the sum of the contributions from very cold dust and cold dust (16 K), warm dust (45 K) and hot dust (of a few hundred K).

Compared with the decomposition of the galactic dust emission spectrum in Fig. 1, which is based on model computations, the decomposition of the observed spectra of external galaxies in contributions from (cd) and (wd) is somewhat arbitrary and appears to represent a rather extreme solution, since the (wd) spectrum has been forced to fit the IRAS observations at λ25μm and 100μm, respectively. This is also born out by the fact that the ratio T^{wd}/T^{cd} ~ 2.9, derived for the external galaxies, is considerably higher than the ratio $T^{wd}/(\langle T^{cd}\rangle + T^{vcd})0.5$ ~ 2.1, obtained for our Galaxy (with temperatures taken from Table 1). It has been shown, however, by Chini et al. that this uncertainty in the decomposition barely affects the determination of L^{wd}. The uncertainty in the (cd) + (vcd) luminosity, on the other hand, does not affect estimates of the gas content of these galaxies, which are based on their λ1200 μm flux densities. The gas content of external galaxies estimated in this way (see e.g. Chini et al.) promises to be considerably more reliable than estimates based on the luminosity of the opaque ^{12}CO emission line. For the Sb,c galaxies a ratio L^{wd}/L^{cd} ~ 0.7 is found as compared to a ratio ~ 0.8 for our Galaxy (with luminosities taken from Table 3). The dust emission characteristics of our Galaxy appear to fit in with Sc galaxies (see Chini et al., 1986, Fig. 2).

IV. Dust luminosities of the Galaxy

Dust emission characteristics of the galactic disk as given in Table 1 extend to 10 kpc. In Paper I we have extended model computations beyond 10 kpc. Adding both the contributions for R >10 kpc (Paper I) and R <2 kpc (Table 2, this paper) to the luminosities given in Table 1 yields the total dust luminosities of the Galaxy, as given in the second column of Table 3. Note that

the (hd) luminosities from Tables 1 and 2 have been decreased by a factor of 1.4 to account for opacities at MIR wavelengths (see Paper I). The absorbed MIR luminosity is reradiated at longer wavelengths.

Table 3

Total Dust and Stellar of the Galaxy

$R_\odot$ =	10 kpc	8.5 kpc
L_{IR}^{vcd} in $L_\odot$	1.0 E9	7.2 E8
L_{IR}^{cd} in $L_\odot$	7.3 E9	5.2 E9
L_{IR}^{wd} in $L_\odot$	6.5 E9	4.7 E9
L_{IR}^{hd} in $L_\odot$	2.5 E9	1.8 E9
L_{IR}^{tot} in $L_\odot$	1.7 E10	1.2 E10
L_*^{tot} in $L_\odot$	5 E10	3.6 E10

The total stellar luminosity in Table 3 comes from Mathis et al.(1983). All luminosities have been obtained for a distance $R_\odot$ = 10 kpc between solar system and galactic center. Recently, the Working Group on Galactic Constants of the IAU Commission 33 (see, e.g. Kerr and Lynden-Bell, 1986) has recommended to use the distance $R_\odot$ = 8.5 Kpc. In this case all luminosities are reduced by a factor 0.85^2 = 0.72. These reduced luminosities are given in the third column of Table 3. The ratio L_{IR}^{tot}/L_*^{tot} ~0.34 means that one third of the stellar emission in the Galaxy is absorbed and reemitted by dust.

V. Dust Luminosities and Star Formation Rates

At present the most reliable way to estimate the global star formation rate (SFR) of O and early B stars, ψ_{OB}, is via the Lyman continuum (Lyc) photon production rate, which can be derived from the integrated free-free flux density of a galaxy. In a second step the OB SFR is connected to the total SFR, ψ, by adopting an initial mass function (IMF). It has first been suggested by Mezger and Smith (1977) that in our Galaxy (and in external galaxies probably as well) we deal with two different star formation processes, viz. "spontaneous SF", where stars form in the total mass range $0.1 \leq m/m_\odot \leq 100$ according to a rather general IMF, and "induced SF", where only stars form above a critical mass m_c. In our Galaxy induced SF appears to occur primarily in main spiral arms and (probably) in the center region, with $m_c \sim 3\ m_\odot$. The ratio of induced to spontaneous SF is $\alpha = \psi^{ind}/\psi^{spon} \sim 2$-2.5. This hybrid process of SF, also referred to as "bimodal SF", was put into a quantitative form by Güsten and Mezger (1983) in order to explain galactic abundance gradients. As a by-product it was found that bimodal SF also solves the problem of an apparently too high SFR, which is estimated on the basis of the Lyc-photon production rate.

From the Lyc-photon production rate in our Galaxy, using the IMF obtained by Miller and Scalo (1978), one derives a present-day SFR of $\psi(t_0)$ = 10.4 $m_\odot\ yr^{-1}$. The change of the galactic distance scale mentioned above reduces this value to ~ 7.5 $m_\odot\ yr^{-1}$. The contribution to the total SFR from the central region appears to be less than 10%, that from outside the solar

circle accounts for ~ 10%. This leads to an estimated total present galactic SFR of $\psi(t_0) \sim 9 m_\odot$, which is the value given in Table 4 for $\alpha = 0$. The corresponding lock-up rate in low mass stars $m < 1\ m_\odot$ and dead stellar remnants is $dM_*/dt = (1-r)\psi = 5.2 m_\odot yr^{-1}$, with r = 0.42 the fractional rate of "instantaneous return" to the interstellar space of matter transformed into a newly formed generation of stars. These values are close to the SFR and lock-up rate averaged over the lifetime of the Galaxy. In other words this would mean a time-independent SFR and lock-up rate, which - for various reasons - appears to be an unlikely situation. In the upper line of Table 4 is shown, for $m_c = 3 m_\odot$ and two values of α, how bimodal SF reduces both ψ and $\dot{M}_*$ in our Galaxy. Analytical formulae to compute SFRs and lock-up rates in the case of bimodal SF are given by Mezger (1985).

Table 4

Present Star Formation Rates $\psi(t_0)$ and Lock-up Rates $(dM_*/dt)_t = M_*$ in our Galaxy and in an IR Galaxy with $L^{wd} = 1E12\ L_\odot$, computed for mc 3 $m_\odot$ and three values of $\langle\alpha\rangle = \langle\psi^{ind}/\psi^{spon}\rangle$.

$\langle\alpha\rangle$=	0		2.5		∞	
Rates in $m_\odot yr^{-1}$	ψ	$\dot{M}_*$	ψ	$\dot{M}_*$	ψ	$\dot{M}_*$
Our galaxy $L^{wd} = 4.7E9 L_\odot$	9.0	5.2	4.5	1.8	2.6	0.34
IR Galaxy $L^{wd} = 1E12_\odot$	1.9E3	1.1E3	9.5E2	3.8E2	5.5E2	7.2E1

For external galaxies a determination of the Lyc photon production rate is difficult, since in most cases for $\lambda > 2$mm synchroton emission, and for $\lambda < 2$mm dust emission dominate over the free-free emission. It therefore would be desirable, if the easily observed total IR luminosity of a galaxy could be used to estimate its SFR. Most authors who have tried to do this, however, have oversimplified a rather complex problem. As pointed out above, it is only the warm dust luminosity which is directly linked to the number of recently formed O and early B stars. But a quantitative relation between L^{wd} and ψ_{OB} is difficult to establish. Factors f(m) enter into such a relation, which measure the fraction of the MS lifetime of a star of mass m, during which it is associated closely enough with dust in surrounding HII regions and shells to heat it to the (wd) temperatures (see the discussion in Paper I, Appendix A). Rather than using such a quantitative relation we combine values ψ and L^{wd} from Tables 3 and 4 to derive the empirical relation $\psi\ (\langle\alpha\rangle = 0) = 1.9\ 10^{-9}\ L^{wd}$, valid for our Galaxy and $\langle\alpha\rangle = 0$ (i.e. no induced SF). Here $L^{(wd)}$ is given in solar luminosities and ψ in $m_\odot yr^{-1}$. This empirical relation can be generalized for bimodal SF. Then, assuming that this relation also holds for external galaxies, we estimate the SFR and lock-up rate for a hypothetical IR galaxy with $L^{wd} = 1E12 L_\odot$. Without bimodal SF a SFR of nearly 2000 $m_\odot\ yr^{-1}$ would be required to sustain the (wd) luminosity of $1E12 L_\odot$. In one million years this galaxy would transform 2E9 $m_\odot$ into stars and lock up one half of this mass in stellar remnants. Remember that the total gas content of our Galaxy is ~ 4E9 $m_\odot$.

Considerations like these have probably helped to popularize explanations of high IR luminosities of galaxies in terms of "bursts of star formation". If,

however, in such actively star forming galaxies induced SF dominates (i.e. $\langle\alpha\rangle \rightarrow \infty$) both ψ and $\dot{M}_*$ are drastically reduced. E.g. in the case of the galaxy with $L^{wd} = 1E12L_\odot$, as shown in the second line of Table 4, a SFR of 550 $m_\odot yr^{-1}$ is required to sustain this luminosity, of which only 64 $m_\odot yr^{-1}$ would be permanently locked up. This example shows that galaxies can derive their high IR luminosities for a long time without consuming extensive amounts of gas or piling up too much mass in dead stars. Moreover, as shown by Chini et al. (1986) high IR luminosities in Galaxies are not necessarily a sign of star burst, but rather of very massive galaxies, whose SFR is proportional to their gas content, i.e. $\psi \propto M_H$.

VI. Estimated Uncertainties

This paper and related previous papers were aimed to derive a model , which both explains the diffuse galactic IR/Submm emission correctly, and is consistent with observations pertaining to dust characteristics and the distributions of stars and interstellar matter. How accurate are these parameters known today?

Derived dust luminosities depend primarily on the quality of the IR surveys and on the galactic distance scale, but only marginally on a particular model. Provided $R_\odot$ = 8.5 Kpc is the correct distance to the galactic center, $L^{tot} = 1.2E10L_\odot$ should be correct within ~ 20–30%. There are indications that $R_\odot$ is still overestimated.

Model computations related to the emission from dust associated with HI and H_2, which is heated by the general ISRF, depend on i) the dust absorption cross section per H-atom; ii) the distribution of interstellar gas in the galactic disk; iii) the density and spectral distribution of the ISRF. At present, we believe that dust cross sections between $\lambda 0.1\mu m$ and ~ $40\mu m$ are known with uncertainties of a few 10%. At longer wavelengths absorption cross sections could be up to twice as high as those adopted here and in Paper I.
The intensity and spectral distribution of the ISRF in the solar vicinity and for wavelengths $\lambda \leq 2\mu m$ appear to be rather well established. The FIR part of the ISRF, as given by Mathis et al. (1983), may be underestimated, however, by an order of magnitude and more, since contributions from dust at high galactic latitudes were neglected. This would affect primarily the temperature of dust deep inside GMCs. This is the reason why we adopted a rather uniform temperature $\langle T^{vcd}\rangle$ ~ 14 K of dust inside GMCs, rather than the lower values suggested by the model computations by Mathis et al. (1983). Extrapolation of the ISRF becomes more uncertain with increasing distance from the sun. We are nearly completely ignorant regarding the contribution of newly formed medium and low mass stars to the heating of dust in quiescent molecular clouds.
Estimates of the surface density of atomic and molecular hydrogen as a function of galactic radius appear slowly to converge. In the case of HI self-absorption of the λ21cm line appears to be the main source of uncertainty. The determination of H_2 surface densities based on ^{12}CO surveys is highly uncertain on a number of accounts. We refer to recent critical reviews by Puget (1983) and Bloemen et al.(1986).

Acknowledgements
We thank H. Habing (University of Leiden Observatory) for providing us with his most recent estimate of the total luminosity of OH/IR stars, which is based on IRAS observations. We acknowledge stimulating discussions with R. Chini, E. Krügel and T.L. Wilson.

REFERENCES

Bloemen, J.B.G.M., Strong, A.W., Blitz, L., Cohen, R.S., Dame, T.M., Grabelsky, D.A., Hermsen, W., Lebrun, F., Mayer-Hasselwander, H.A., Thaddeus, P.: 1986, Astron. Astrophys. 154, 25
Boulanger, F., Baud, B., van Albada. G.D.: 1985, Astron. Astrophys. 144, L9
Caux, E., Serra, G.: 1986, Proc. ESA Workshop on "A space-borne submm astronomy mission" Segovia, Spain, June 4-7, (in press)
Chini, R., Kreysa, E., Krügel, E, Mezger, P.G.: 1986, Astron. Astrophys. 157, L1
Cox, P., Leene, A.: 1986, Astron. Astrophys. (subm.)
Cox, P., Krügel, E., Mezger, P.G.: 1986, Astron. Astrophys. 155, 380

Dent, W.A., Werner, M.W., Gutley, I., Becklin, E.E., Hildebrand, R.H., Keene, J., Whitcomb, S.E.: 1982 in "The Galactic Center," AIP conf. proc. (R. Riegler, R.D. Blandford, eds.) p. 33
Draine, B., Lee, H.: 1984, Astrophys. J. 285, 89
Güsten, R., Mezger, P.G.: 1983, Vistas in Astronomy 26, 159
Kerr, F.J., Lynden-Bell, D.: 1986, Review of Galactic Constants (preprint)
Léger, A., Puget, J.L.: 1984, Astron. Astrophys. 137, L 5
Mathis, J.S., Rumpel, W., Nordsieck,K.: 1977, Astrophys. J. 217, 425
Mathis, J.S., Mezger, P.G., Panagia, N.: 1983, Astron. Astrophys. 128, 212
Mezger, P.G.: 1985, in proc. IAU symp. No. 116 (in press)
Mezger, P.G., Chini, R., Kreysa, E., Gemünd, H.-P., 1986 Astron. Astrophys. 160, 324
Mezger, P.G. Smith, L.F.: 1977, Proc. IAU Symp. Nr. 75 (T.de Jong, A.Maeder, eds.) p.133
Mezger, P.G., Mathis, J.S., Panagia, N.: 1982, Astron. Astrophys. 105, 372
Miller, G.E., Scalo, J.M.: 1978, Astrophys. J. Suppl. 41, 513
Pajot, F., Gispert, R., Lamarre, J., Peyturaux,R., Puget,J., Serra, G., Coron, N., Dambier, G, Leblanc, J., Moalic, J.P., Renault, J.C., Vitry, R.: 1986, Astron. Astrophys. 154, 55
Puget, J.L.: 1983, Proc. of XVI Les Houches meeting "Birth and infancy of stars" Lucas, Omont and Stora, eds., North-Holland, p. 77

DISCUSSION

TELESCO:
For your Sbc galaxy energy distribution, what do you claim is the origin of the 10μm emission?

MEZGER:
Presumably OH/IR stars and small grains.

TELESCO:

Shouldn't one be able to separate out these contributions to some extent, since small grains and others associated with 'starbursts' should be spatially distributed differently from the OH/IR stars? The OH/IR stars should be more uniformly distributed since they are not necessarily starburst products.

MEZGER:

Yes.

GALLAGHER:

Which initial mass function did you use?

MEZGER:

We used the Miller/Scalo IMF.

GALLAGHER:

More recent results, from both the Milky Way and Large Magellanic Cloud, suggest a flatter slope for the upper IMF than adopted by Miller and Scalo. This will help remove some of the energetics problems that you discussed. Going from an upper IMF slope of $\sim$3 to the Salpeter value of $\sim$2.35 might gain a factor of 3-10 in predicted L_{IR} per $M_{\odot}$ of stars formed.

MEZGER:

I agree.

PUGET:

In your discussion of the Galactic Center region, you don't mention the fact that the heating is due mostly to an old disk population-type spectrum peaking at 1μm, which is quite different from what happens in the disk and could explain the low 12μm/100μm ratio.

MEZGER:

In the Galactic Center region, $\Delta l \times \Delta b \sim 2^{\circ} \times 0^{\circ}.5$, we identify OH/IR stars as the principal contributors to the MIR emission, while the warm dust ($\sim$ 35 – 45 K) is heated by O stars and early B stars. The contribution from cold dust associated with atomic hydrogen is absent, and the very cold dust associated with molecular hydrogen is warmer ($\sim$20K) than in the Galactic disk. Although I agree that the density of the interstellar radiation field in the central region is higher than in the disk and is dominated by M giants, I doubt if these stars contribute anything to the 12μm flux density. Apart, of course, from those M giants which happen to be in their AGB evolutionary stage. In fact, we believe that all MIR emission in the central region comes from such OH/IR stars.

MASSES, LUMINOSITIES, AND DYNAMICS OF GALACTIC MOLECULAR CLOUDS

P. M. Solomon
A. R. Rivolo
T. J. Mooney
J. W. Barrett
L. J. Sage

Astronomy Program, State University of New York—Stony Brook

Star formation in galaxies takes place in molecular clouds and the Milky Way is the only galaxy in which it is possible to resolve and study the physical properties and star formation activity of individual clouds. In this paper we describe and analyze the masses, luminosities, dynamics and distribution of molecular clouds, primarily giant molecular clouds in the Milky Way. The observational data sets are the Massachusetts–Stony Brook CO Galactic Plane Survey and the *IRAS* far IR images. The molecular mass and infrared luminosities of galactic clouds are then compared with the molecular mass and infrared luminosities of external galaxies.

Section 1 describes how molecular clouds are observationally defined from the CO survey. We then show in section 2 that molecular clouds have well defined empirical laws governing their size–linewidth and virial mass–CO luminosity relationships (Solomon *et al.* 1986a). The virial mass–CO luminosity law establishes a physical basis for the use of CO as a tracer of molecular cloud mass, primarily H_2. The size–linewidth law combined with the dynamical mass from the virial theorem leads to mass–linewidth and CO luminosity–linewidth laws. Section 3 presents the molecular cloud mass spectrum.

In order to determine the current star formation activity in GMC's we have measured their far IR luminosity from a comparison of the *IRAS* and CO data. Section 4 shows that the IR luminosity is proportional to the CO luminosity and that the (IR luminosity / cloud mass) is independent of mass. There is a maximum to the $L_{IR}/M(H_2)$ ratio in galactic molecular clouds indicating that star formation activity is well regulated within the clouds. Section 5 briefly discusses the comparison between far IR and CO emission on a galactic scale and section 6 shows a face on picture of molecular clouds in the galaxy. In section 7 we briefly summarize our results on far IR and CO luminosities in external galaxies. We compare the star formation activity in isolated and interacting galaxies with that of galactic molecular clouds. The interacting galaxies have (IR luminosity / molecular mass) ratios substantially higher than any galactic molecular cloud.

1. CO Observations and Cloud Definition

The CO survey observations were carried out during 1981 and 1982 on the FCRAO

Carol J. Lonsdale Persson (Editor)
Star Formation in Galaxies

14 meter antenna operating at a frequency of 115.271 GHz (HPBW = 47 arc seconds). Approximately 40,000 CO spectra were obtained between the limits of 8° to 90° in longitude, −1° to +1° in latitude and −100 to +200 km·s^{-1} in velocity with a typical rms noise level of 0.35 K. The survey spacing of 3 arc minutes (over the range ℓ = 18° to 54°) was chosen to enable measurement of essentially all molecular clouds inside the solar circle with size greater than 20 pc. For example on the far side of the galaxy at distances of 14 kpc the spacing is 13 pc; on the near (wrt the tangent point) side in the molecular ring at a distance of 4 kpc the spacing is 3.5 pc. A more complete discussion of the observations and calibration procedures along with maps of the complete data in latitude-velocity space is in Sanders *et al.* (1986); longitude-velocity maps and spatial (longitude-latitude) maps at fixed velocities are given in Clemens *et al.* (1986) and Solomon *et al.* (1986b). Inspection of the actual survey contours in the above references shows that many clouds easily stand out from the background and can be defined with little difficulty. However there are also regions of strong emission with blending of features in which the definition of cloud boundaries in the three dimensional (ℓ, b, v) space is complicated and may be subject to different interpretations by different observers. In our first analysis of the Massachusetts–Stony Brook CO Galactic Plane Survey (Solomon, Sanders and Rivolo 1985) we overcame the boundary problem by defining CO sources, representing the cores of molecular clouds, as local maxima in ℓ, b, v space. We showed that the galaxy had two populations characterized by (1) warm molecular cloud cores with one-quarter of the population and about one-half of thte emission; they exhibit nonaxisymmetric galactic distribution, are clearly associated with H II regions, appear to be clustered, and are a spiral arm population; and (2) cold molecular cloud cores containing three-quarters of the total number; they are a widespread disk population located both in and out of spiral arms.

In this work we adopt a procedure which unambiguously defines cloud boundaries in three dimensions in order to obtain an objective cloud data set and to study cloud structure and dynamics. Clouds are defined as closed surfaces in the three dimensional space at fixed intensity levels T_R^* = 3, 4, 5, 6, 7 K. The galactic plane emission is thus broken up into a set of discrete clouds for each intensity. For the purpose of this analysis a cloud was required to have a minimum total integrated intensity summed over all locations inside the surface of 40 K·km·s^{-1} for T_R^* = 6 and 7 K and 60 K·km·s^{-1} for T_R^* = 4 and 5 K. Each set corresponds to a cloud catalog containing about 400 clouds. There are about 1,000 clouds smaller than the minimum. Large sections of the galactic plane are blended at the 3 K level with features extending over as much as 5° and 60 K·km·s^{-1}. By contrast there is very little blending of the surfaces at the 6 K level. The 4 K catalog was adopted except for the most confused regions between longitudes of 8° and 32° and velocities $v > 60$ km·s^{-1}. Here a selection was made of the lowest intensity surface cloud which was not severely blended. A quantitative measure of the cloud asymmetry was utilized to eliminate spatially blended clouds. The final catalog is thus composed of a mixture of clouds defined at the 4, 5 and 6 K levels. Above longitudes of 54°, where the emission is weaker, the 3 K

clouds were substituted for the 4 K clouds.

Each cloud in the final catalog is described by a set of parameters including the location of the emission peak in ℓ, b, v space, the minimum and maximum extent (in ℓ, b, v) of the emission surface, a total CO flux inside the surface, a galactocentric radius R determined from circular rotation, and the rms dispersions from the means in all three coordinates. There is a two fold (near-far) distance ambiguity for all kinematic distances in the inner galaxy. We have resolved the ambiguity by utilizing a boot strap process based on the cloud physical properties measured for a subset of clouds with known distances which serve as calibrators. The calibrator clouds include those with small near-far distance ratios (tangent point clouds), and clouds which can be assigned either near or far on the basis of an association with an H II region (Downes 1980) with a radio frequency absorption line for which an assignment has been made.

2. The Size–Linewidth and Virial Mass–CO Luminosity Relations

For the calibrators a direct relationship between cloud size, defined as the geometric mean of the ℓ–b dispersions [$S = D\tan(\sqrt{\sigma_\ell \sigma_b})$] and the velocity linewidth, is established. Although the cloud boundaries have been defined at the particular level ($T_R^* = 3, 4, 5, 6, 7$ K) we have included all emission down to the 1 K level within a cube circumscribing the cloud boundaries for the purpose of determining the cloud size, linewidth and luminosity. Measuring S in parsecs we find (see Figure 1)

$$\sigma_v = \left(\frac{S}{1.01}\right)^{0.5} \quad (\mathrm{km \cdot s^{-1}}) \tag{1}$$

with a logarithmic dispersion in σ_v of ± 0.13 or 40%.

Near or far distances to all remaining clouds in the final list were assigned using three criteria: 1) choosing the distance with the better fit to the size-linewidth relation, 2) choosing the near side if the far distance places the cloud more than 150 pc out of the plane, and 3) choosing near or far based on the best fit for the scale height of the emission in the longitude and velocity range of the cloud. The third method utilizes the well determined value for the half width at half maximum of the molecular layer of 60 parsecs (see *e.g.* Sanders, Solomon and Scoville, 1984). The details of these methods are explained elsewhere (Solomon *et al.* 1986a). For the purposes of this paper the accuracy of distance assignments is not critical since the result using only calibrator clouds is virtually identical to that using all clouds.

For each of the clouds a virial theorem mass can now be determined from the measured velocity and size dispersion

$$M_{VT} = \frac{3\, f_p\, S\, {\sigma_v}^2}{G} \quad (\mathrm{M_\odot})$$

where f_p is a projection factor (taken herein as π, this being consistent with a cylindrical truncation of spherically symmetric clouds), and $G = 1/232$ in units of $\mathrm{km \cdot s^{-1}}$ and

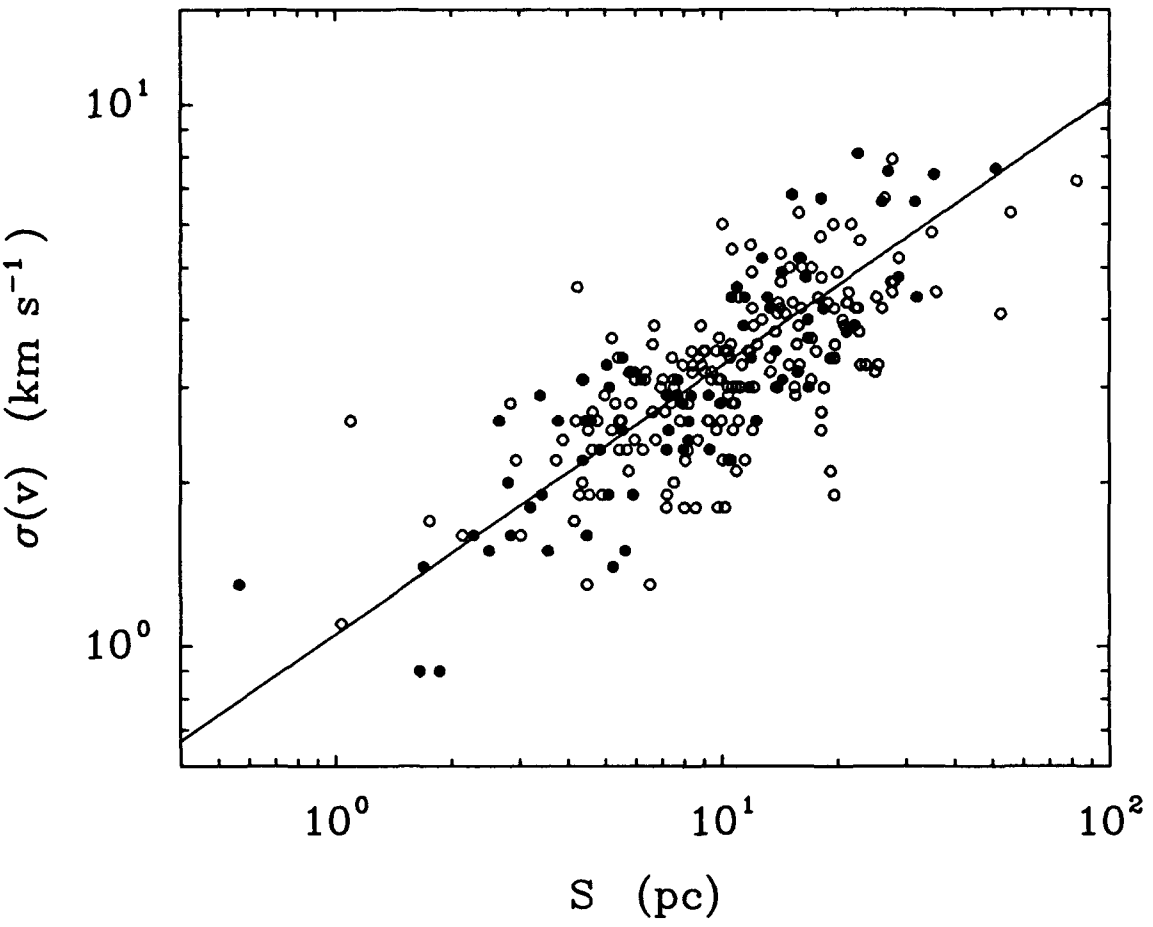

Figure 1. Molecular cloud velocity dispersion $\sigma(v)$ as a function of size dispersion S for 250 clouds in the inner galaxy. The solid circles are calibrator clouds with known distances and the open circles are for clouds with the near-far distance ambiguity resolved by the three techniques discussed in the text. The fit line is $\sigma_v = (S/1.0)^{0.5}$ km $\cdot$ s^{-1}. For virial equilibrium the 0.5 power law requires clouds of constant surface density.

parsecs. In addition, a cloud's CO luminosity is obtained directly from the survey data within the cloud boundaries as

$$L_{CO} = D^2 \int\int\int T_R^*(\ell, b, v)\, d\ell\, db\, dv \quad (\mathrm{K \cdot km \cdot s^{-1} \cdot pc^2}) \tag{2}$$

where $T_R^*(\ell, b, v)$ is the antenna temperature at location (ℓ, b, v). Figure 2 shows the virial mass as a function of CO luminosity for all clouds with calibrators shown as filled symbols. A least squares fit to all of the data shows an extremely tight power-law fit over a range of four decades given by

$$M_{VT} = 42\ (L_{CO})^{0.81} \quad (\mathrm{M_\odot}) \tag{3}$$

with a dispersion of 0.14 in $\log(M_{VT})$ or 38% in M_{VT}.

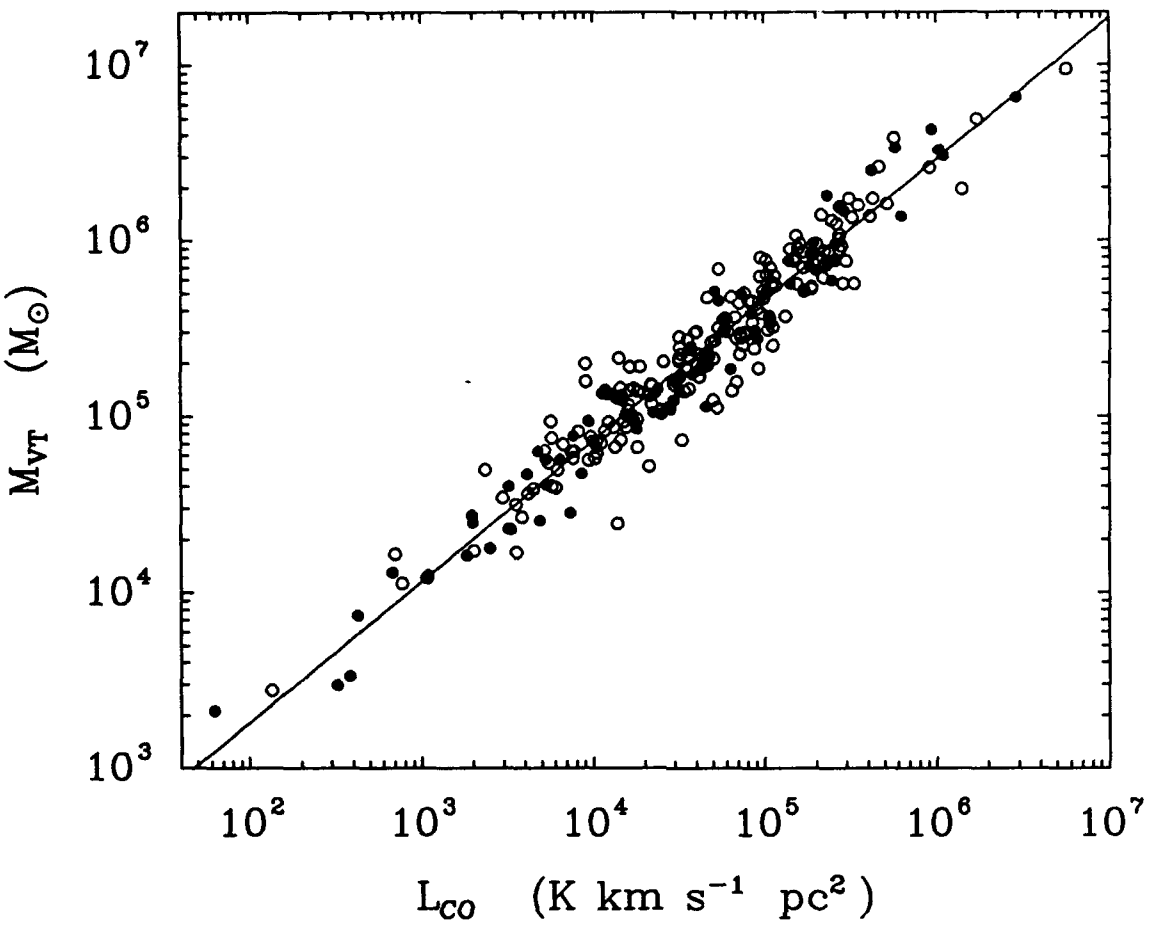

Figure 2. The Virial Mass–CO Luminosity relation for molecular clouds. The clouds range in distance from 1 to 15 kpc and in flux over more than two orders of magnitude. The solid circles and open circles are the same as in Figure 1. The fit is $M_{VT} = 42\,(L_{CO})^{0.81}$ $M_\odot$. For a given L_{CO} the dispersion in M_{VT} is 0.13 in the log.

The observed cloud mass–CO luminosity relation can be translated into a molecular hydrogen column density $N(H_2)$ as a function of the average CO integrated intensity over the cloud velocity range Δv, $\bar{I} = \int_{\Delta v} T\, dv$. The mass is the product of the mean column density and the surface area; the luminosity is the product of $\bar{I}$ and the surface area. Letting $N(H_2) = a\,\bar{I}$, we find $a = 4.7$, 3.1 and $2.0(10)^{20}$ for CO luminosities of 10^4, 10^5 and 10^6 $K \cdot km \cdot s^{-1} \cdot pc^2$. Thus, although the mass is not strictly a linear function of CO luminosity, the conversion factor varies by only a factor of two between clouds of mass 5×10^4 and 2×10^6 $M_\odot$. We adopt $a = 3.1$ as the effective conversion factor for clouds of mass 3×10^5 $M_\odot$ which are close to the median of the mass distribution.

The only other technique which has determined the CO luminosity to mass conversion factor for giant molecular clouds with $m > 10^5$ $M_\odot$ uses the observed γ-ray flux resulting

from cosmic ray interactions with hydrogen molecules. As summarized in Table 1 for the Orion Molecular Cloud $a = 2.6 \pm 0.8$ and for the galactic plane emission between $R = 5$ kpc and $R = 10$ kpc, $a = 2.8 \pm 1$ (Bloemen *et al.* 1984, 1986). The conversion factor based on the variation of optical extinction measured along the lines of sight with measured CO or ^{13}CO integrated intensity also gives good agreement although the clouds are typically of lower mass.

The close agreement of these conversion factors with our dynamical measurement demonstrates that the assumption of virial equilibrium in the clouds is correct. Molecular clouds are therefore bound by self gravity and not by pressure equilibrium with a hot phase of the ISM.

The agreement between these techniques and between the local and molecular ring calibrations provides an empirical basis for the measurement of the total mass of molecular hydrogen in the galactic disk (see *e.g.* Sanders, Solomon and Scoville, 1984 and Table 2). The agreement between the dynamical conversion factor which is heavily weighted to clouds in the molecular ring at $R = 5$ kpc, the γ-ray conversion factor determined for a mixture of the molecular ring and relatively local clouds and the γ-ray conversion factor determined for the nearby Orion molecular clouds shows that a constant conversion factor for the galactic disk between $R = 4$ kpc and $R = 10$ kpc may be used to determine the total H_2 mass. There is no evidence of a radial gradient in the conversion factor between $R = 5$ and 10 kpc as suggested by Bhat *et al.* (1985) and Blitz and Shu (1980).

One of the more interesting empirical results which follows directly from the size-linewidth relation (equation 1) and the assumption of virial equilibrium, is the constant surface density of the clouds $\Sigma = 230 \ \ M_\odot/pc^2$. Equivalently the mass-velocity law is

$$M = 2230 \, \sigma_v{}^4 \quad (M_\odot) \tag{4}$$

Expressed in terms of CO luminosity using equation 3 (Figure 2) yields a relation between velocity-width and size analogous to the Fisher-Tully or Faber-Jackson relation for galaxies

$$L_{CO} = 143 \, \sigma_v{}^5 \quad (K \cdot km \cdot s^{-1} \cdot pc^2) \tag{5}$$

The empirical mass-luminosity law (equation 3 and Figure 2) provides a basis for understanding the use of optically thick CO emission as a tracer of mass, primarily molecular hydrogen, in interstellar clouds. Both the existence and the form of the mass-luminosity law are a consequence of the structure and gravitational equilibrium of giant molecular clouds. If we assume that a cloud consists of a large number of small, optically thick regions (clumps), then emission intensity, T_R^*, along a line of sight at a velocity v will be proportional to the filling factor of the clumps at v and the temperature of the clumps T. For a Gaussian line profile the average surface brightness of the cloud is $\overline{I} = (2\pi)^{1/2} T_0 \, \sigma_v$ where σ_v is the velocity dispersion and T_0 is the peak intensity at the line center averaged over the cloud. The average filling factor of the cloud at line center is T_0/T. The CO luminosity is then the product of the surface area $3\pi S^2$ and the surface brightness

$$L_{CO} = 3\sqrt{2} \, \pi^{3/2} \, T_0 \, \sigma_v \, S^2 \tag{6}$$

TABLE 1

CALIBRATION OF CO INTEGRATED INTENSITY WITH H_2 COLUMN DENSITY

Method	Location	$a = \overline{N}(H_2)/\overline{I}_{CO}$ $(cm^{-2}/K \cdot km \cdot s^{-1})$	References
$A_v \leq 4$ (in dark clouds)	Local	$2.2(10)^{20}$	Dickman 1975
$A_v \geq 5$	Local	$5.0(10)^{20}$	Liszt 1982
$A_v > 5$	Local	$3.6(10)^{20}$	Sanders, Solomon & Scoville 1984
γ rays	Orion	$2.6(10)^{20}$	Bloemen *et al.* 1984
γ rays	$5 \leq R \leq 10$ kpc	$1.0(10)^{20}$	Bhat *et al.* 1985
γ rays	$5 \leq R \leq 10$ kpc	$2.8(10)^{20}$	Bloemen *et al.* 1986
Virial Theorem	$4 \leq R \leq 8$ kpc	$3.1(10)^{20}$	Solomon *et al.* 1986a

TABLE 2

TOTAL GALACTIC H_2 MASS FOR $2 < R < 10$ kpc

Reference	M $(10^9\ M_\odot)$	a $(cm^{-2}/K \cdot km \cdot s^{-1})$
Scoville & Solomon (1975)	1–3	—
Gordon & Burton (1976)	2.1	—
Solomon, Sanders & Scoville (1979)	3.9	5×10^{20}
Thaddeus & Dame (1984)	0.7	$(1\text{–}2) \times 10^{20}$
Sanders, Solomon & Scoville (1984)	2.6	3.6×10^{20}
Bronfman *et al.* (1986)	1.3†	2.8×10^{20}
This Work	2.0‡	3.0×10^{20}

† The difference between this and 2.0 is primarily due to a different weighting used to obtain the radial emissivity and to a 20% lower CO intensi ty calibration.

‡ The emissivity has been calculated using equal weight p er unit of projected face on area for each radial bin.

Combining equation (6) with the virial theorem, and utilizing the empirical size-linewidth relation (equation 1) yields a mass-luminosity relation

$$M_{VT} = 174 \left(\frac{L_{CO}}{T_0}\right)^{4/5} \quad (7)$$

For the clouds in our catalog T_0 ranges from 5 K to about 15 K with a mean of about 7 K which gives $M_{VT} = 37 \left(L_{CO}\right)^{4/5}$ in close agreement with the empirical results in equation 3. Thus the effective conversion factor from luminosity to mass is lower for hotter clouds than for cooler ones, and is lower for more luminous or massive clouds. For a fixed luminosity the mass-to-luminosity ratio can be expressed as a function of the average density $\bar{\rho} = 100/S$ ($M_\odot$ pc^{-3}).

$$\left(\frac{M_{VT}}{L_{CO}}\right) = 12 \frac{(\bar{\rho})^{1/2}}{T_0} \quad (8)$$

Thus the small scatter in Figure 2 is evidence of a fairly small scatter in the mean density of the clouds at a fixed luminosity.

3. The Molecular Cloud Mass Spectrum

Figure 3 shows the mass spectrum of clouds $dN/dm \propto m^{-3/2}$. This is consistent with previous determinations by Solomon and Sanders (1980), Liszt and Burton (1981), and Sanders *et al.* (1985) although it is based on a much larger sample of clouds. The turnover below $m = 5 \times 10^4$ $M_\odot$ is due to the undercounting of clouds, (even warm clouds) on the far side of the galaxy with diameter < 16 pc. The mass fraction of clouds per logarithmic mass interval $m \cdot dN(m)/d\log m \propto m^{1/2}$ demonstrating that most of the mass in molecular clouds is in the high end of the spectrum (Solomon and Sanders, 1980).

As can be seen from Figure 4 the most massive clouds are a few million solar masses and the single most massive object just below 10^7 $M_\odot$.

4. Far Infrared Luminosity of Galactic Molecular Clouds

The *IRAS* survey at 60 μm and 100 μm has an angular resolution similar to that of the Massachusetts–Stony Brook CO Survey of the Galactic Plane. Although the far infrared emission is severely blended it is possible to utilize the velocity information of the CO survey to identify individual molecular cloud/H II region complexes in the far IR. The far IR luminosity originatin from newly formed stars in, or associated with, the molecular cloud can then be determined from the *IRAS* maps utilizing the distance to the molecular cloud. The most luminous and hottest molecular clouds (with high peak CO intensity) are readily apparent on the *IRAS* 100 and 60 micron images. Most of the warm molecular clouds have IR counterparts which correspond to H II regions in or on the border of the clouds. An overlay of the locations of the predefined molecular clouds on the

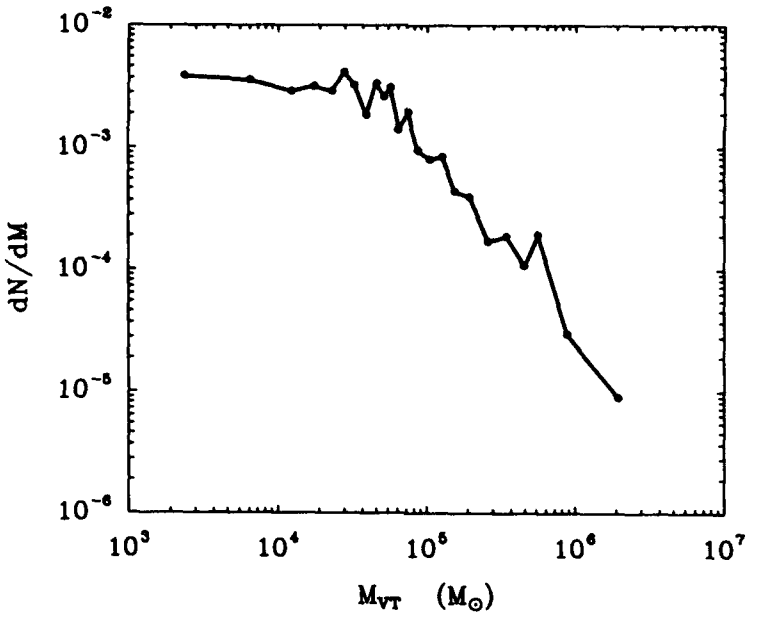

Figure 3. The molecular cloud mass spectrum dN/dm. A fit above 7×10^4 $M_\odot$ gives $dN/dm \propto m^{-3/2}$ (see text). There are 15 clouds in each bin and thus the standard deviation of each point is $\pm 24\%$. The turnover at low mass is due to undercounting of smaller clouds in the more distant parts of the galactic disk.

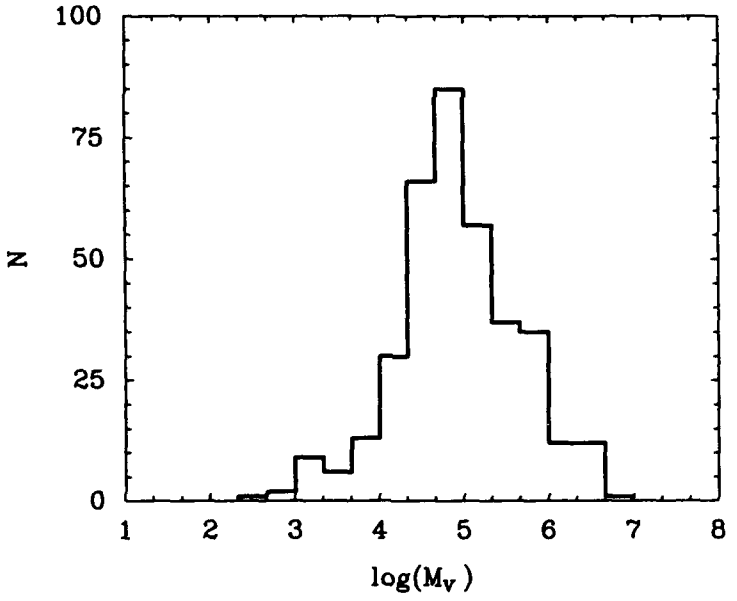

Figure 4. The number of clouds as a function of virial mass in the sample.

IRAS 60 and 100 micron galactic plane images shows a very good, although not complete, correspondence. In particular, almost all of the CO clouds with high CO luminosity and peak intensity above 10 K have obvious IR counterparts. However in regions of the galactic plane where there is a substantial overlap of several strong CO clouds at different velocities,

the infrared emission associated with each cloud may be difficult to separate. We have therefore picked a subset of molecular clouds which are the dominant feature in velocity space over their latitude and longitude extent. For each CO defined cloud a detailed comparison was carried out with the *IRAS* maps smoothed to 3 arc minute resolution. The boundaries of the molecular cloud were slightly adjusted to include *IRAS* sources which were sometimes at the edge of the cloud. In order to be certain that the infrared emission was associated with the velocities of the candidate CO cloud, an interactive program was developed which displayed the average CO spectral line profile over any specified region of (ℓ, b) space. The program would then calculate the total CO flux within the velocity and spatial limits of the cloud and the IR flux above the background but within the cloud boundaries. The IR background which consists principally of galactic background not associated with the candidate cloud and some contribution from the zodical light at 60 microns, was measured by three techniques. The first consists of a point by point comparison of the IR flux as a function of the CO flux.

As can be seen in the example in Figure 5, there is substantial far IR emission uncorrelated with the CO integrated intensity below about 40 $K \cdot km \cdot s^{-1}$. This uncorrelated emission provides a measure of the background level with respect to the molecular clouds. Similar correlations can be carried out for the restricted velocity range of a single cloud. The second technique finds the background by measuring the radially averaged IR profile around a source associated with a CO cloud. The radially averaged IR flux generally decreases approximately exponentially approaching a background level about two or three scale lengths from the peak. This technique works only for strong or well defined sources. The third method is a standard clipping (κ-σ) technique which iteratively finds the background by eliminating signals more than two standard deviations above the mean.

Figure 6 shows the far infrared luminosity as a function of the CO luminosity for 46 clouds. The clouds range in flux over two orders of magnitude and in luminosity over three orders of magnitude. They include such well known objects as M17, W51, and W43, as well as many previously uncatalogued molecular clouds. A formal fit shows that the infrared luminosity is proportional to the first power of the CO luminosity.

$$L_{IR} = 14\ (L_{CO})^{0.97 \pm 0.08} \quad [L_\odot] \tag{11}$$

The molecular cloud mass M can be obtained from equation 3. Figure 7 shows the ratio of infrared luminosity to cloud mass as a function of the mass. There is a substantial degree of scatter with L_{IR}/M varying from about 1 to 12 with the only significant exception being the M17 cloud with a $L_{IR}/M = 23$. Our cloud defining algorithms have broken the M17 complex into two regions. The well known and strong H II region is associated with a molecular cloud of 2×10^5 $M_\odot$ and the remainder of the complex is in a cloud which we refer to as M17B with mass of 7×10^5 $M_\odot$ and a very low luminosity to mass ratio. If we combine these two clouds into one, the ratio becomes 5, near the mean of all other clouds.

The most interesting feature of Figure 7 is the lack of dependence of L_{IR}/M on the cloud mass itself. The star formation rate per unit of available molecular mass is thus

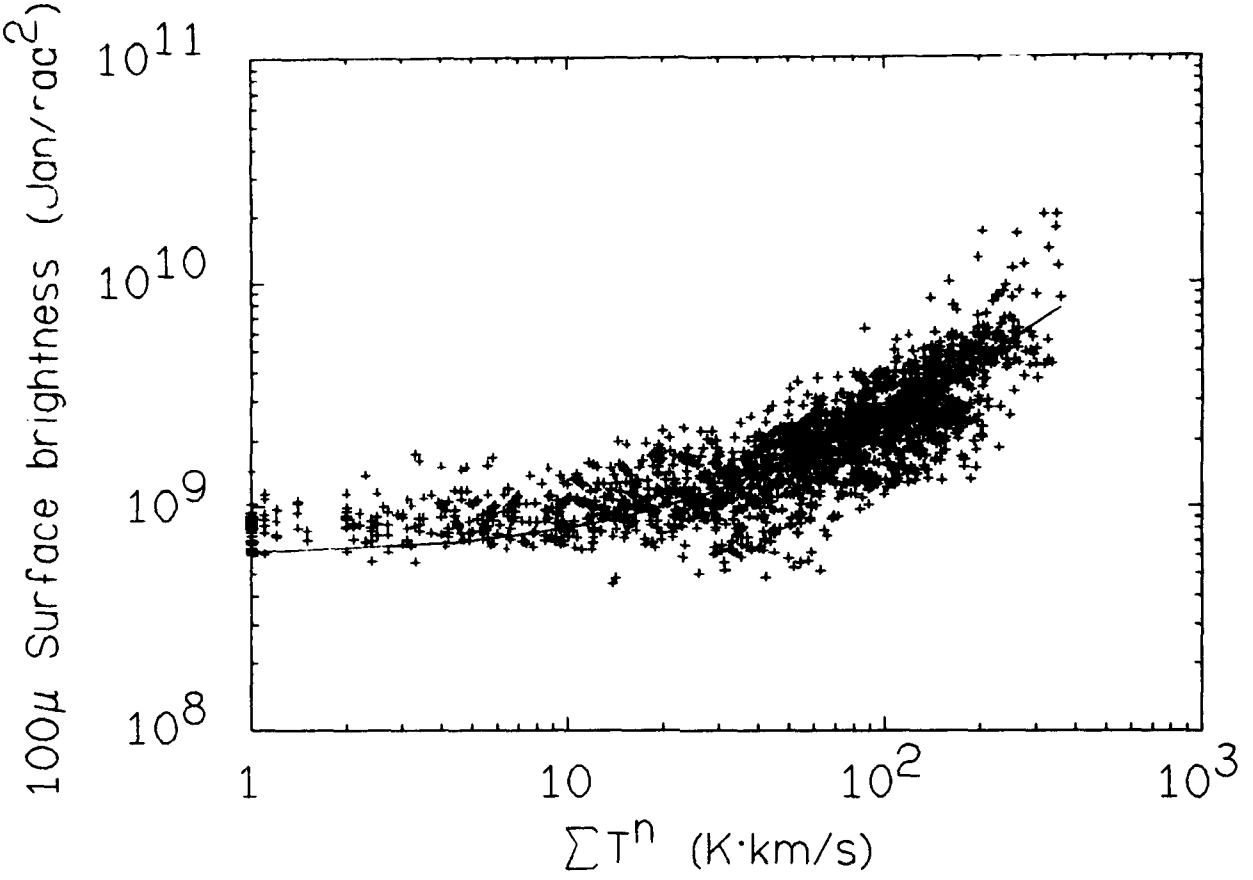

Figure 5. A point by point correlation of IR brightness as a function of CO integrated intensity ($T_R^* > 1$ K; $-40 < v < +140$ km $\cdot$ s^{-1}) for a 2° by 2° region of the galactic plane between $\ell = 29°$ to 31°, $b = -1°$ to $+1°$. There is substantial far IR emission uncorrelated with CO integrated intensity below about 40 K $\cdot$ km $\cdot$ s^{-1}, which provides an estimate of the IR background wrt the molecular clouds. The 100 micron background here is about 8×10^8 Janskys/steradian.

independent of the mass of the cloud. There appear to be no cases of uninhibited star formation. The star formation process appears to be equally efficient (or inefficient) in clouds of mass as low as 5×10^4 or as high as 5×10^6 $M_\odot$. This is evidence against nonlinear processes within a cloud, such as star-formation-induced star formation or supernova-induced star formation. Both of these processes would lead to a higher rate of star formation in the most massive clouds since the probability of forming a star per unit of available mass would be proportional to the number of recently-formed stars in the cloud. In fact, Figure 7 shows that there are many massive giant molecular clouds with no more than one O star. Twelve of the clouds in Figures 6, 7, and 8 (indicated by open circles) have no obvious IR sources; for these clouds the infrared luminosity should be regarded as an upper limit and there are probably no O stars. There are thus some giant molecular clouds with very little or no massive star formation.

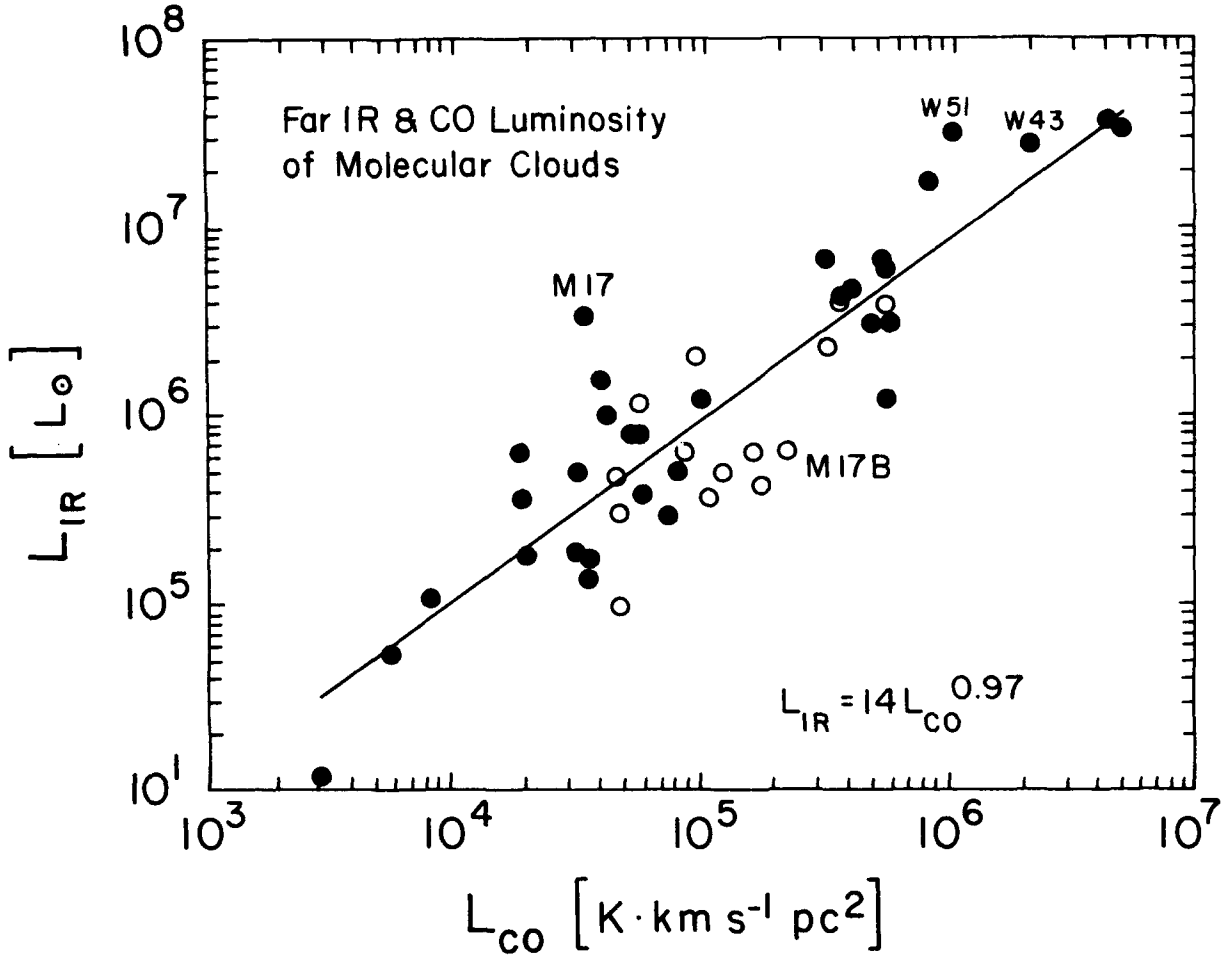

Figure 6. Far infrared luminosity as a function of CO luminosity for 46 molecular clouds in the galactic plane. The solid circles are molecular clouds with well defined IR sources which are H II regions associated with the cloud. The open circles are molecular clouds with no obvious IR.

Figure 8 shows the luminosity-to-mass ratio as a function of the far infrared color, F_{100}/F_{60}. The systematic decrease in the luminosity-to-mass ratio with decreasing far infrared color temperature is expected for thermal radiation. Expressed in terms of dust color temperature T_d we find, assuming an infrared emissivity proportional to the 1.5 power,

$$\left(\frac{L_{IR}}{M_{cloud}}\right) \propto (T_d)^{5.5}.$$

Thus the primary effect resulting in strong far infrared luminosity is simply hotter dust rather than more dust. Not surprisingly the far infrared emission at these wavelengths is not a good tracer of the mass of interstellar dust since there are some very massive cold clouds (see Figures 7 and 8) with relatively little far IR, such as M17B.

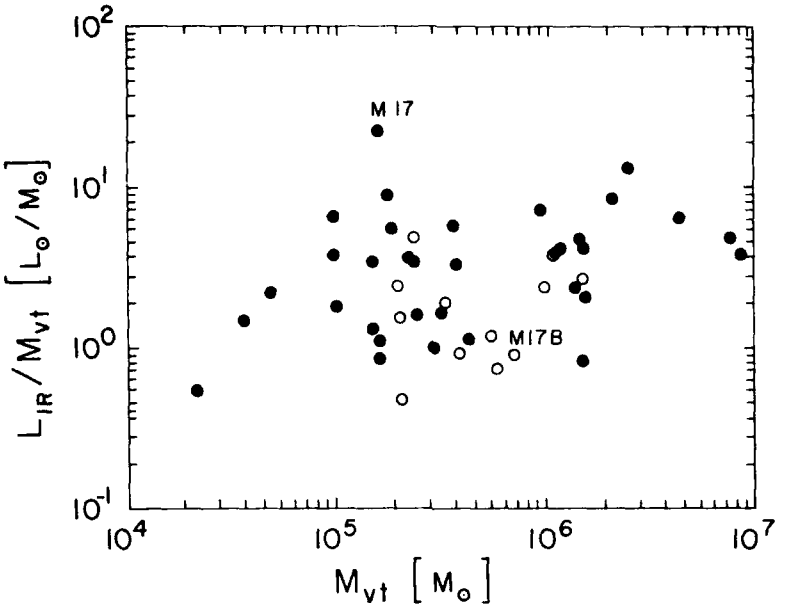

Figure 7. The ratio of infrared luminosity to cloud mass as a function of cloud mass. The solid and open circles are same as Figure 6. The star formation rate per unit of available molecular mass as measured by L_{IR}/M_{VT} is independent of the mass of the cloud.

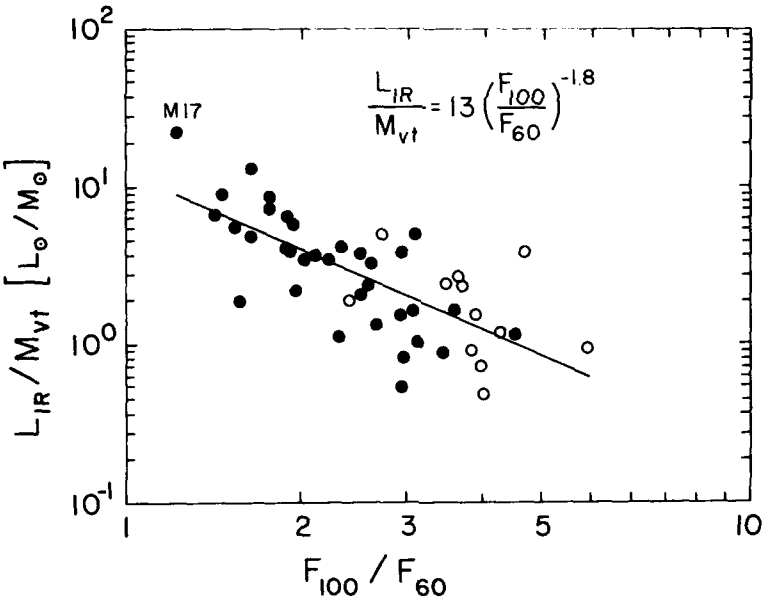

Figure 8 The ratio of infrared luminosity to cloud mass as a function of infrared color. The solid and open circles are the same as Figures 6 and 7. An emissivity $\epsilon \propto \lambda^{-1.5}$ is assumed.

5. Galactic Plane IR–CO Emission

Figure 9 shows the 100 micron and CO flux from a region 1° in ℓ by 2° in b as a

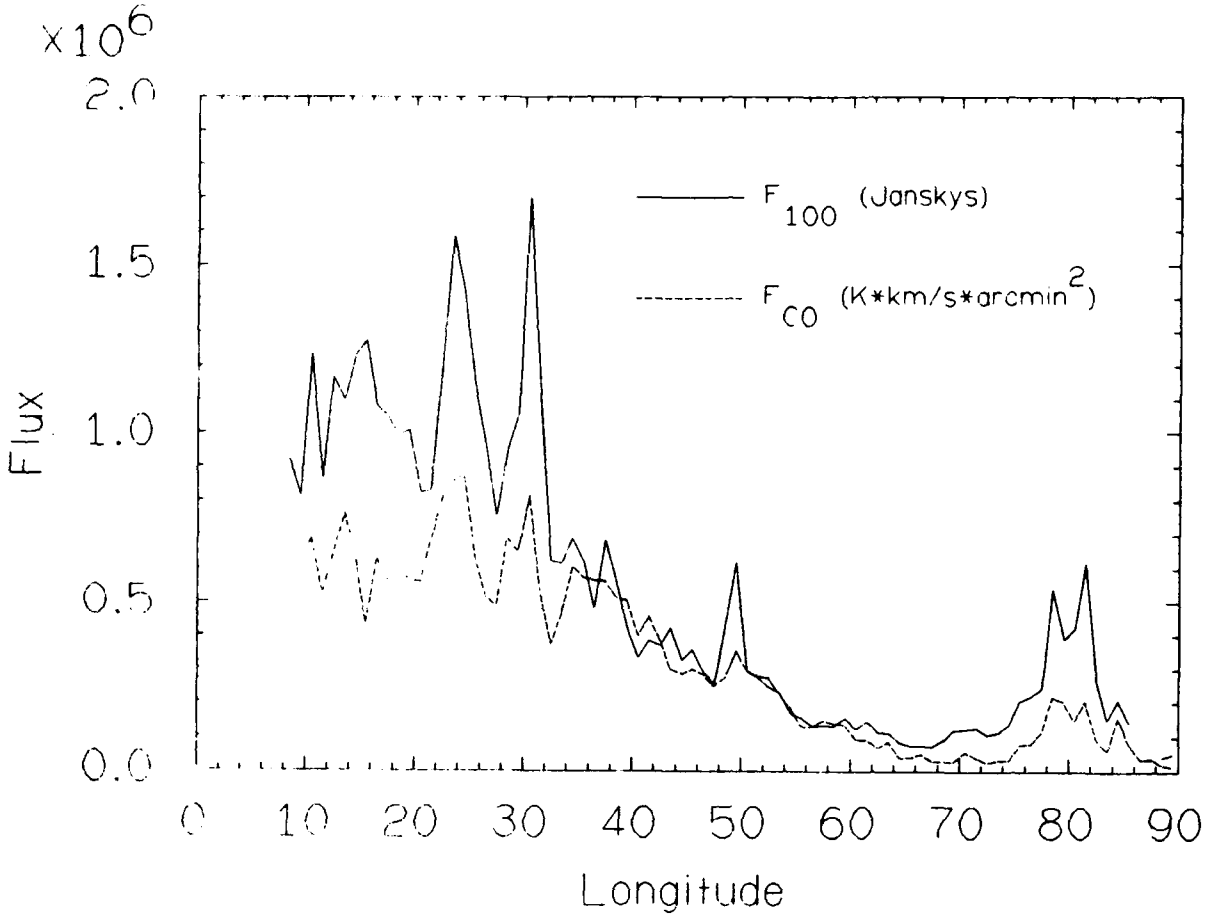

Figure 9. The 100 μm and CO flux binned every 1° in ℓ between $b = -1^\circ$ to $+1^\circ$, as a function of galactic longitude. The strong peaks near 23°, 31°, 50°, and 80° correspond to prominant molecular clouds in the galaxy (see text). The general trend with ℓ of the 100 μm and CO flux indicate that the molecular ring is a major feature of the *IRAS* data.

function of galactic longitude between the latitude range of $+1^\circ$ and -1°. The peaks in longitude and the general trend in longitude are the same for the 100 micron and CO flux. The strong peaks correspond to the most luminous molecular clouds in the galaxy located at (ℓ, b, v) : $(23.0, -0.4, 74)$ at a distance of $D = 12$ kpc, W43 $(30.8, -0.05, 92)$ at $D = 7$ kpc, and W51 $(49.5, -0.4, 57)$ at $D = 7$ kpc. Their IR luminosities are all about 4×10^7 $L_\odot$. The peak at $\ell \sim 80^\circ$ is from the relatively nearby Cygnus clouds. The fall off beyond longitudes of 35° is a characteristic not shared by the 21 cm emission from atomic hydrogen. Thus the molecular ring is clearly a major feature of the *IRAS* data as well as the CO data. On the basis of our assignments of infrared luminosity to molecular clouds, we estimate that about half of the far infrared flux is associated with the molecular component.

6. Face-on Picture of Warm Molecular Clouds in the Milky Way

Figure 10a is a face-on picture between $\ell = 8°$ and 90°, of the distribution of molecular clouds that we have found from the Massachusetts-Stony Brook CO Galactic Plane Survey and the Cloud Catalog discussed previously. Small and low luminosity clouds have been left out of this picture. The most prominent feature is the ring-like structure at about $R = 5$ kpc (we assume $R_0 = 10$ kpc) which is seen here to wind around to the far side of the galaxy at a distance of 14 kpc from the sun. Almost one-half of the CO luminosity in the warm component is in this feature, which corresponds to the traditional Scutum spiral arm tangent to the line of sight at a longitude near 30°. There are two other ring-like structures at approximately 7 kpc and 9 kpc from the galactic center which appear merged together on the far side of the galaxy. The 7 kpc feature is the well known Sagitarius spiral arm which is seen here to continue on to the far side of the galactic plane. While the accuracy of kinematic distances does not allow a conclusive statement regarding the pitch angle of these arms, their reality will remain regardless of distance errors due to noncircular motions such as streaming. In particular, the gap between $R = 6$ and 7 kpc is very prominent and appears even in the radial distribution of these objects (see Solomon, Sanders and Rivolo, 1985). Figure 10b is similar to Figure 10a but with the size of the molecular cloud image in proportion to the size of the molecular cloud. This gives a much more realistic appreciation of the space between the GMC's. Although the GMC's are the largest and most massive objects in the galaxy, the space between them or between the clusters of GMC's is much larger than their size.

It is important to note that these clouds represented in the picture are primarily those with peak intensities $T_R^* > 5$ K. As we have previously shown from an analysis of CO sources, these are the spiral arm population. The cold clouds which are more difficult to define by their outer boundaries, would fill in the spaces between the spiral arms just as the cold CO sources fill in the longitude velocity space (see Solomon, Sanders and Rivolo, 1985). Approximately one half of the galactic CO emission is in the warm clouds.

7. The Ratio of Far IR Luminosities to Molecular Mass in Interacting and Isolated Galaxies

As part of a program to investigate the content and distribution of molecular gas in external galaxies, we have observed λ 2.6 mm CO emission along the major axis of approximately 100 galaxies. In this section we briefly describe the results of a comparison of the CO and far infrared luminosities of these galaxies. We compare the results found for these external galaxies with those of molecular clouds in our own galaxy discussed in previous sections. The candidate galaxies were drawn from three separate samples. The first was a study of nearby large angular size spiral galaxies generally of type Sb or later with optical diameters greater than 7 arc minutes and distances greater than 4 Mpc. The second sample was drawn from early *IRAS* Circulars, particularly Circular 15. The third

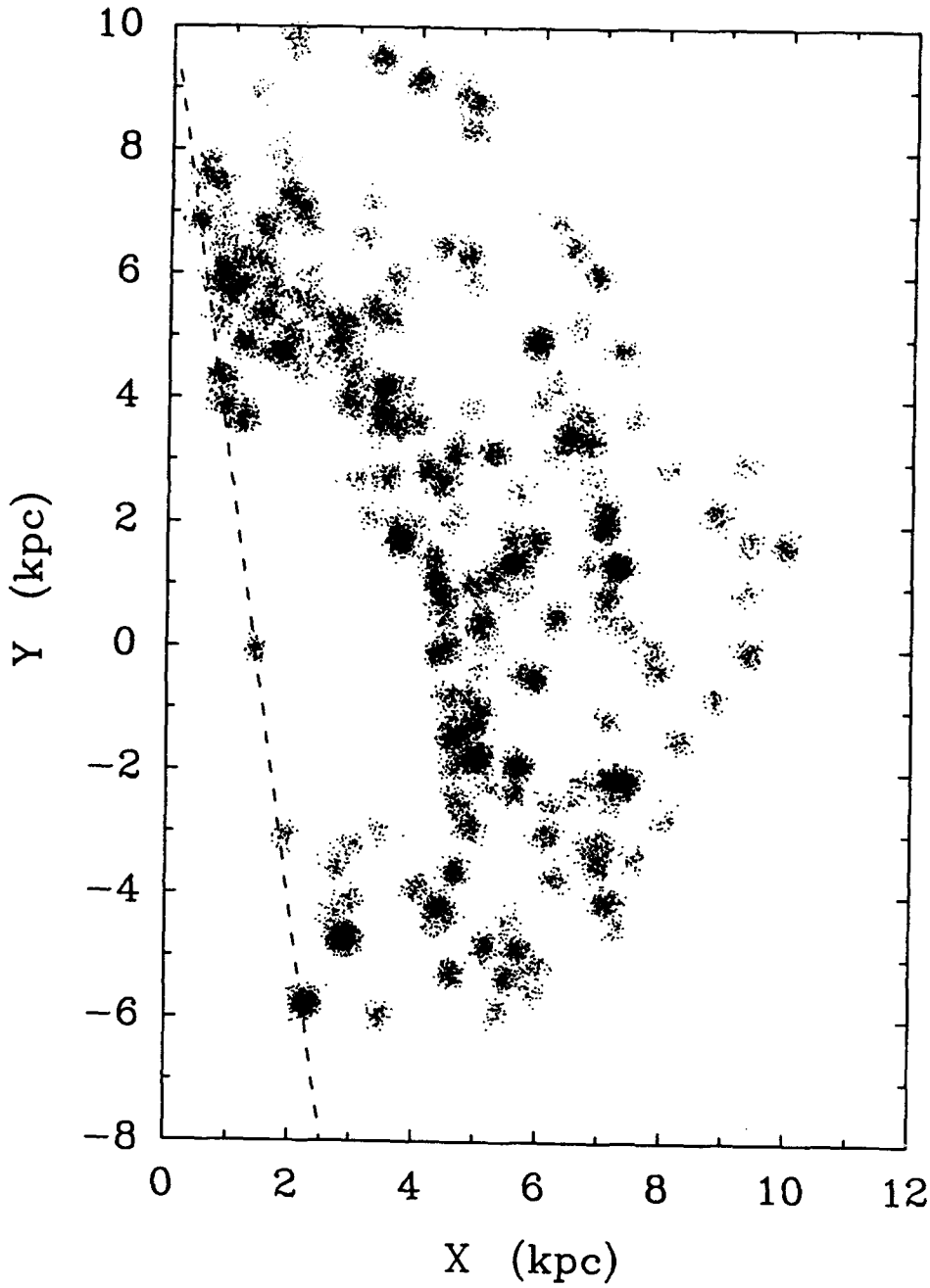

Figure 10a. Unresolved face-on picture of molecular clouds in the galaxy between $\ell = 8^\circ$ to 90°. The grey scale was generated with a Gaussian distribution of N points with $\sigma = 100$ pc about each cloud peak location. The contrast is achieved by setting $N = 150\,(L/10^5)^{0.75}$. The dashed line is the low longitude cutoff. Clouds with $L_{CO} < 1{\times}10^4$ $L_\odot$ were excluded.

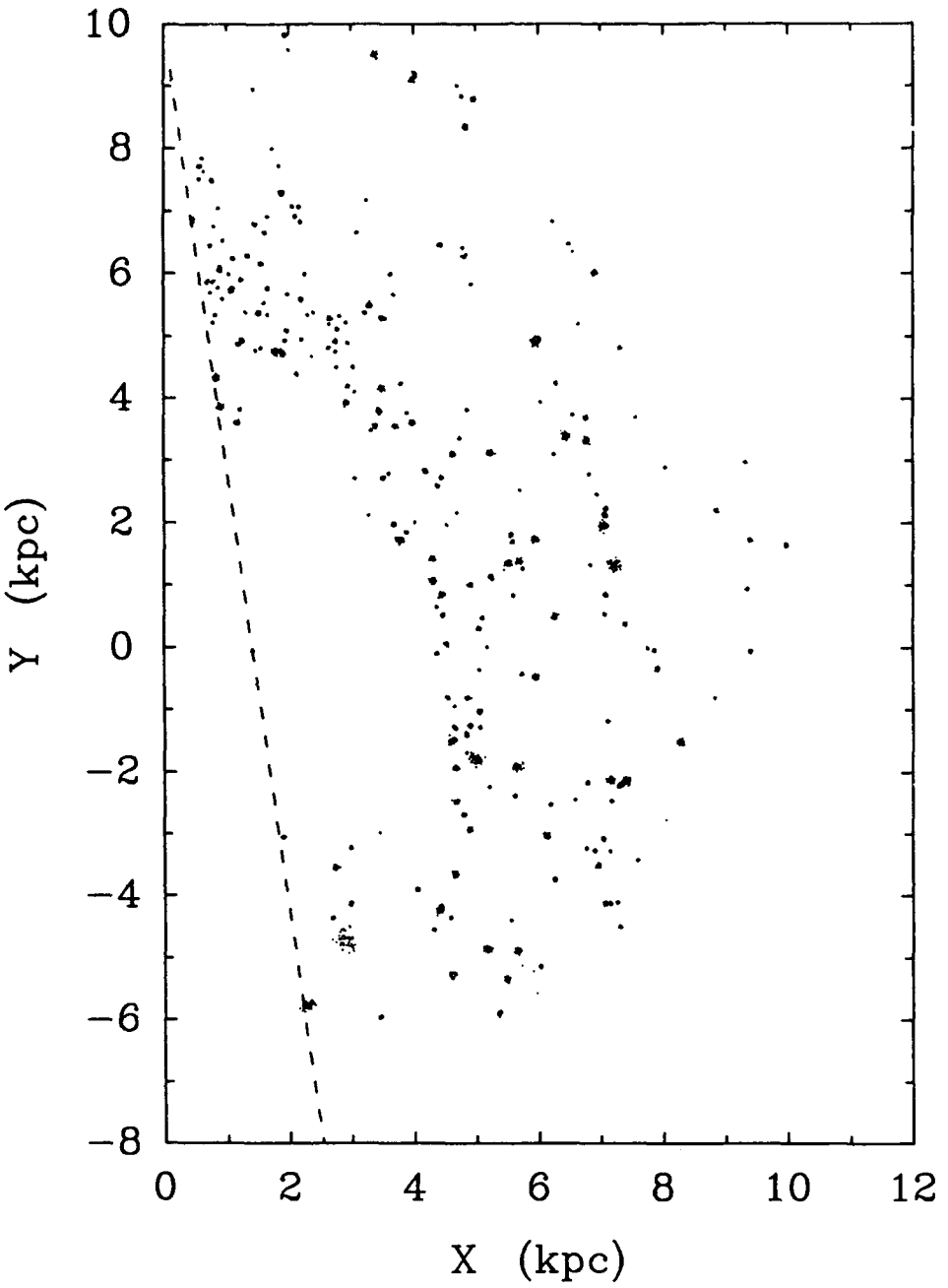

Figure 10b. Resolved face-on picture of the galaxy with same clouds as in figure 10a. The grey scale was fixed at 20 points per cloud with the size dispersion σ equal to the size dispersion of the clouds S.

sample consists of all *IRAS* galaxies at declination $\delta > 0^{\circ}$, 100 μm flux > 30 Janskys and velocity $v > 700$ km$\cdot$s^{-1}. The observations were carried out using primarily the FCRAO 14 meter antenna between 1982 and 1986 and more recently the NRAO 12 meter antenna. These observations are reported in detail elsewhere (Solomon, Sage and Barrett, 1986 and Sage, 1987). Previous studies but with smaller samples have been carried out by Sanders and Mirabel (1985) and Young *et al.* (1986).

Galaxies were classified as either isolated, interacting or merging based on their optical appearance. Interacting galaxies are those with disturbed appearances and/or neighbors closer than about 7 optical diameters. Merging galaxies are those with 2 nuclei as well as some of the extremely luminous peculiar galaxies such as MKN231, ARP220 and N6240. The combined sample has almost a 3 order of magnitude range in infrared flux.

Figure 11 shows the far infrared luminosity as a function of the CO luminosity for approximately 80 of these galaxies, both interacting and isolated. The CO luminosity was calculated from the major axis observations spaced every beamwidth taking account of the inclination of the galaxy and integrating out to at least half of the Holmberg radius. The far infrared luminosity was determined from the 60 and 100 μm fluxes in either the *IRAS* point source or extended source catalog. For large angular size nearby galaxies the far infrared luminosity was determined from the *IRAS* images.

As can be seen from Figure 11, there is generally a good correlation of the IR and CO luminosities but with a wide dispersion. The interacting galaxies are systematically higher in their infrared to CO ratio than the isolated galaxies although there is significant overlap between the two groups. In Figure 11 two lines have been drawn which indicate the range of the IR to CO ratio for galactic clouds. While many of the isolated galaxies could be understood as a collection of molecular cloud–H II regions similar to those in the galaxy, it is clear that the interacting, and particularly the merging galaxies, have IR to CO ratios substantially greater than any individual clouds in the Milky Way. Even some of the isolated galaxies appear a factor of two higher in this ratio than any clouds in our galaxy. This however could be explained if our galaxy has only about half of its far infrared emission associated with GMC's.

Figure 12 shows the infrared and CO luminosities separately for interacting and isolated galaxies along with a fit to the data. The interacting galaxies are systematically higher in the IR to CO ratio than the isolated galaxies by a factor of 3–5 with extreme cases such as MKN231 and ARP220 higher than the isolated galaxies by a factor of 10 to 20. If we utilize a constant conversion factor to obtain the molecular mass from the CO luminosity and regard the far infrared luminosity as an indicator of recent star formation, then we find that the star formation rate per unit mass of molecular hydrogen (as indicated by $L_{IR}/M(\mathrm{H_2})$) is 3–5 times greater in interacting than isolated galaxies.

The interacting, and particularly the merging, galaxies are also systematically hotter than the isolated galaxies. The merging galaxies in our sample have an average dust temperature (assuming a λ^{-1} emissivity) of $\sim$ 45 K while the isolated galaxies have an

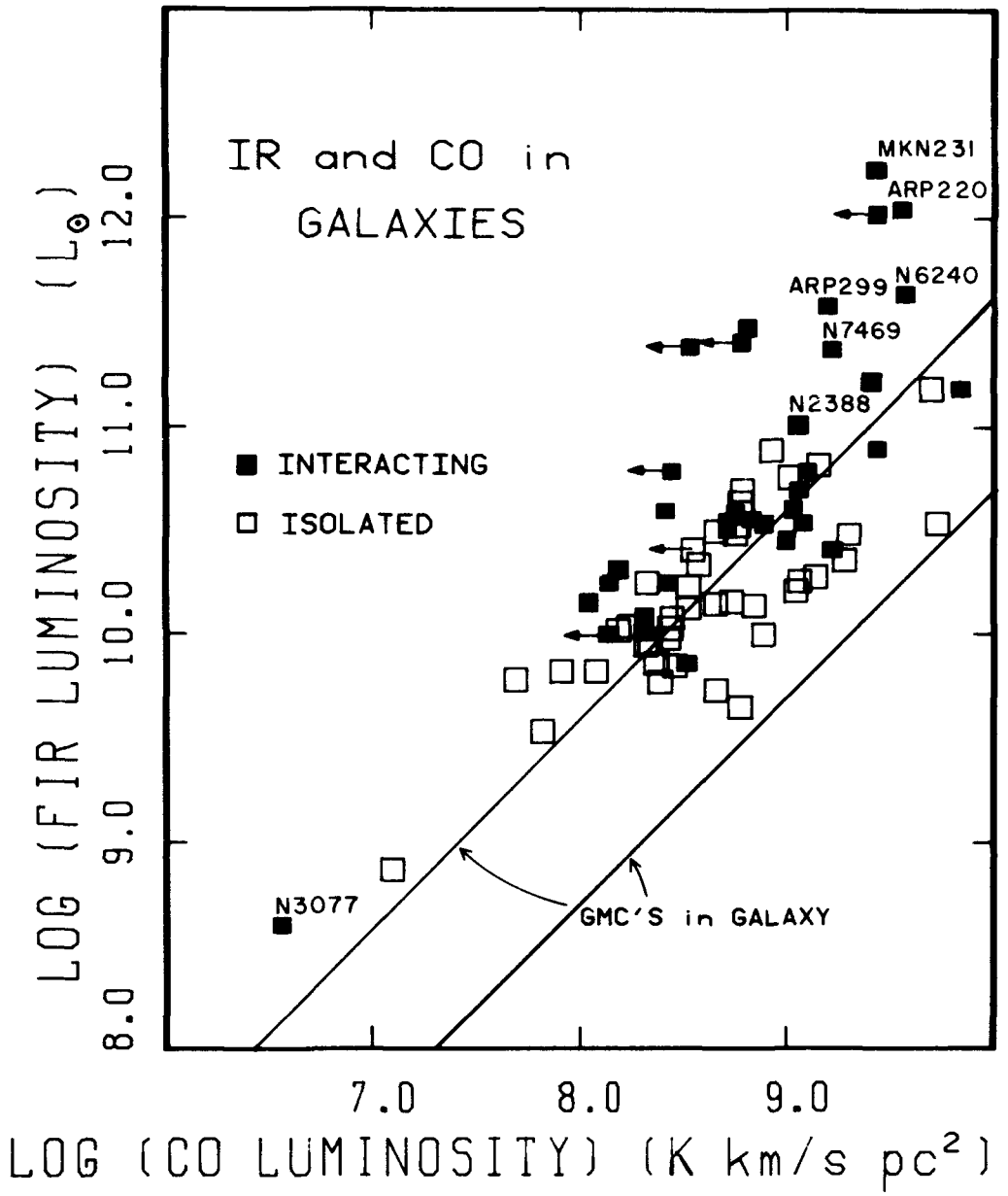

Figure 11. The Infrared and CO Luminosity of isolated and interacting galaxies. The two lines represent the range of L_{IR}/L_{CO} for the galactic molecular clouds. The interacting galaxies are systematically above the galactic GMC's.

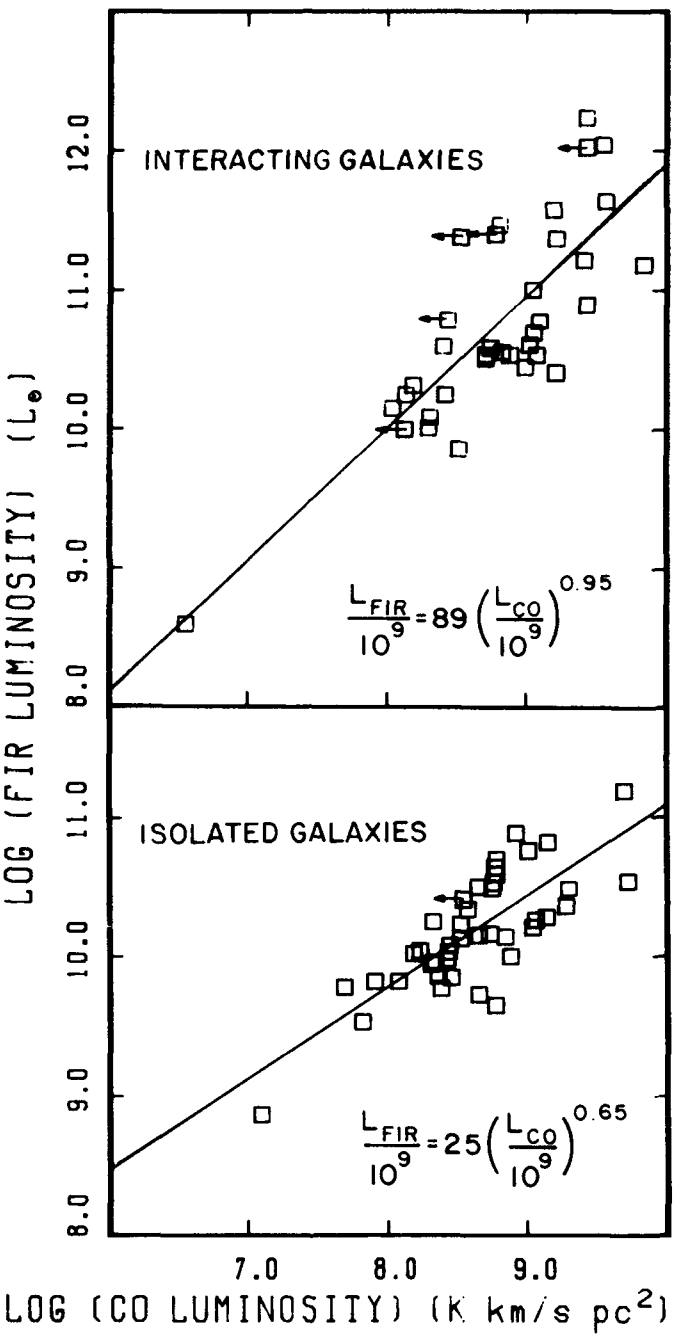

Figures 12a,b The Infrared and CO Luminosities separately with fits for a) interacting galaxies and b) isolated galaxies. The interacting galaxies are 3 to 5 times more luminous per unit of molecular mass (see text). The difference in the exponents of the fits needs to be tested with larger samples.

average dust temperature of $\sim$ 33 K. Much of the dispersion in $L_{IR}/M(H_2)$ is thus due to dust temperature variations since $L_{IR} \propto (T_d)^5$. Young *et al.* (1986) have treated the dust temperature as an independent parameter and fit the $L_{IR}/M(H_2)$ relation separately for galaxies of different temperature. However, the temperature dependence of L_{IR} on dust temperature is a necessary consequence of thermal radiation and selecting on dust temperature is almost equivalent to selecting on luminosity.

The dust temperature is therefore a result of the high luminosity and not a cause. We note that if the gas in the molecular clouds is also systematically hotter in interacting galaxies the CO–H_2 conversion factor will be smaller and $L_{IR}/M(H_2)$ will be even higher.

We thus find that the effect of an interaction appears to be to increase the star formation rate within preexisting molecular clouds rather than primarily creating new molecular clouds. Our finding that none of the molecular clouds in our galaxy has as high a ratio of IR to CO as the interacting or merging galaxies suggests a fundamental change in the star formation initiating mechanism in galaxy interactions.

8. Summary

From an analysis of several hundred galactic molecular clouds we have shown:

1) the velocity linewidth is propotional to the 0.5 power of the size $\sigma_v \propto (S)^{0.5}$. Combined with virial equilibrium this shows the clouds are characterized by a constant mean surface density and have a mass $M \propto {\sigma_v}^4$.

2) The virial mass–CO luminosity law is $M \propto (L_{CO})^{0.81}$. This establishes a calibration for measuring the total cloud mass from CO observations.

3) Molecular clouds are in or near virial equilibrium since their mass per unit CO luminosity determined dynamically, agrees with other measurements. The cloud CO luminosity $L_{CO} \propto {\sigma_v}^5$. This is the molecular cloud version of the Fisher-Tully or Faber-Jackson law for galaxies.

4) The far IR luminosity per unit cloud mass L_{IR}/M is independent of the cloud mass. Since the source of the far IR luminosity is primarily young massive stars, this argues against star formation induced star formation which is a nonlinear process that should spread throughout a cloud. There are some giant molecular clouds of mass 10^5–10^6 $M_\odot$ with little or no embedded far IR sources (O or early B stars).

5) Star formation activity is well regulated in galactic molecular clouds with a maximum (IR luminosity / cloud mass) ratio observed.

From an analysis of CO and far IR obsevations of external galaxies we conclude:

6) The fir IR luminosity and CO luminosity are well correlated but with a wide dispersion.

7) Interacting galaxies have systematically higher IR luminosities per unit molecular mass than isolated galaxies and more importantly have higher $L_{IR}/M(H_2)$ ratios than any galactic molecular clouds. This indicates that the star formation mechanism in interacting

and particularly merging galaxies is substantially more efficient than even the most active molecular cloud–H II region complexes in the galaxy. Star formation still appears as a viable mechanism for the luminous IR galaxies since the efficiency need only be enhanced by about one order of magnitude. The increase in efficiency may possibly be due to a compression of existing molecular clouds by cloud-cloud collisions during the interaction. The lack of efficient or even runaway star formation in giant molecular clouds in the galactic disk may be just as hard to explain as a "starburst" in luminous IR galaxies. Both systems have more than sufficient material in molecular clouds to account for their observed star formation.

References

Bhat, C. L., Issa, M. R., Houston, B. P., Mayer, C. J., and Wolfendale, A. W. 1985 *Nature* **314**, 511.

Blitz, L., and Shu, F. H. 1980 *Ap. J.* **238**, 148.

Bloemen, J. B. G. M., Caraveo, P. A., Hermsen, W., Lebrun, F., Maddalena, R. J., Strong, A. W., and Thaddeus, P. 1984 *Astron. Astrophys.* **139**, 37.

Bloemen, J. B. G. M., Strong, A. W., Blitz, L., Cohen, R. S., Dame, T. M., Grabelsky, D. A., Hermsen, W., Lebrun, F., Mayer-Hasselwander, H. A., and Thaddeus, P. 1986 *Astron. Astrophys.* **154**, 25.

Bronfman, L., Cohen, R. S., Alvarez, H., May, J., and Thaddeus, P. 1986 *preprint.*

Clemens, D. P., Sanders, D. B., Scoville, N. Z., and Solomon, P. M. 1986 *Ap. J. Suppl.* **60**, 297.

Dickman, R. L. 1975 *Ap. J.* **202**, 50.

Downes, D., Wilson, T. L., Bieging, J., and Wink, J. 1980 *Astron. Astrophys Suppl. Ser.* **40**, 379.

Gordon, M. A., and Burton, W. B. 1976 *Ap. J.* **208**, 346

Liszt, H. S., and Burton, W. B. 1981 *Ap. J.* **243**, 778.

Liszt, H. S. 1982 *Ap. J.* **262**, 198.

Sage, L. J. 1987 *thesis, in preparation*

Sanders, D. B., Clemens, D. P., Scoville, N. Z., and Solomon, P. M. 1986 *Ap. J. Suppl.* **60**, 1.

Sanders, D. B., Mirabel, I. F. 1985 *Ap. J.* **298**, L31.

Sanders, D. B., Scoville, N. Z., and Solomon, P. M. 1985 *Ap. J.* **289**, 373.

Sanders, D. B., Solomon, P. M., and Scoville, N. Z. 1984 *Ap. J.* **276**, 182.

Scoville, N. Z., and Solomon, P. M. 1975 *Ap. J.* (*letters*) **199**, L105.

Solomon, P. M., Rivolo, A. R., Barrett, J. W., and Yahil, A. 1986a *submitted to Ap. J.*

Solomon, P. M., Sage, L. J., Barrett, J. W. 1986 *submitted to Ap. J.*

Solomon, P. M., Sanders, D. B., and Scoville, N. Z. 1979 In *IAU Symposium 84, The Large Scale Characteristics of the Galaxy*, ed. W. B. Burton (Dordrecht: Reidel), p. 35.

Solomon, P. M., and Sanders, D. B. 1980 In *Giant Molecular Clouds in the Galaxy*, eds. P. M. Solomon and M. G. Edmunds, (New York:Pergamon), pp. 41.

Solomon, P. M., Sanders, D. P., and Rivolo, A. 1985 *Ap. J. (letters)* **292**, L19.

Solomon, P. M., Sanders, D. B., Scoville, N. Z., and Clemens, D. P. 1986b *Ap. J. Suppl. (in press)*.

Thaddeus, P., and Dame, T. M. 1984 Proceedings of Workshop on Star Formation, in *Occasional Reports of Royal Observatory, Edinburgh*, ed. R. Wolstencroft.

Young, J. S., Kenney, J., Lord, S. D. and Schloerb, F. P. 1984 *Ap. J.* **287**, L65.

Young, J. S., Schloerb, F. P., Kenney, J. D. and Lord, S. D. 1986 *Ap. J.* **304**, 443.

POSTER PRESENTATIONS

REGIONS OF STAR FORMATION

IRAS Colors of VLA Identified Objects in the Galaxy

Michel Fich
Astronomy Department
University of Washington, Seattle, WA 98195

Susan Terebey
High Altitude Observatory
NCAR, Boulder, CO 80307

ABSTRACT

IRAS sources found within 4 degrees of $l = 125^{\circ}$, $b = 2^{\circ}$ on the 3rd HCON 60μ Sky Brightness Images have been observed at the VLA. The intent of this project was to identify regions where massive stars are forming by looking for small areas of radio continuum emission. The IRAS sources could be divided into three groups by their IRAS $12\mu/25\mu$ and $60\mu/100\mu$ colors. The group identified with star forming regions contained essentially all of the objects with extended radio emission. In all of these cases the extended radio emission showed a morphology consistent with the identification of these objects as HII regions. The conclusion that may be drawn from this project is that star formation regions can be distinguished from other objects by their infrared colors.

INTRODUCTION

Our long term goal is to study star formation on a large scale in the Galaxy. To use IRAS observations for studying star formation in our Galaxy it is important to first learn how to distinguish star formation regions from other possible sources of infrared emission. This paper presents a first step in that direction. It might be expected that many of the pre-main sequence O stars will be shielded from view optically because of the high extinction of their progenitor cloud. However these objects should produce both infrared and radio continuum emission. The infrared emission for these objects will come from two separate regimes, hot dust near the star (possibly in a small HII region) and much cooler dust at large distances from the star. The radio continuum emission will come from the very young HII regions formed by such stars.

The method used here is to locate all of the infrared emitting objects within some field in the galactic plane and identify them. The field chosen was centered on $l = 125^{\circ}$, $b = 2^{\circ}$ and the IRAS 3rd HCON 60μ Sky Brightness Image for this area (plate number 13) was used to locate emission sources. One of these objects (Sharpless 187) was almost 30 arcminutes in diameter but the rest were smaller than 14 arcminutes, including 9 that were not resolved (ie. smaller than 4 arcminutes). A total of 35 were found with peak flux densities above our threshold of 2.3×10^7 Jy/sr within 4 degrees of the central position.

This particular field was not chosen strictly randomly. It is in the outer Galaxy where confusion is less and kinematic distances are not ambiguous. This field is not contaminated with any extremely large (several degrees or larger) objects and is in the area where kinematic distances are most accurately determined, although we are not con-

cerned with the distances in this paper. It is slightly above $b = 0^{\circ}$ because HI images show that the galactic plane warps up by a few degrees here. For these reasons we have been studying this field at a variety of wavelengths, this project being the most recent in our study.

OBSERVATIONS

All 35 of the objects were observed at the VLA in the C array configuration at a wavelength of 6 cm in a snapshot mode of 3 minute observations. This provides a resolution of 4 arcsec and a field of view of approximately 10 arcmin, however it is not sensitive to structures larger than 1 arcmin and there is some loss of sensitivity (a factor of 2 for point sources) at the edge of the field. The snapshots were converted to images that covered the entire field of view at slightly lower resolution in order to search for radio emission anywhere in the field. Then the data were re-imaged at the maximum resolution, but with smaller areas, around each possible source of emission. These images were then CLEAN'd to a flux density of 0.5 mJy/beam using the standard AIPS (NRAO data reduction package) routine MX. The final images had an rms noise level of 0.4 mJy/beam.

In addition to the above observations, the single-dish radio continuum surveys by Kallas and Reich (1980), Taylor and Gregory (1983), and Condon and Broderick (1986) were examined at the position of each of the 60μ sources.

RESULTS

Radio continuum emission characteristic of HII regions was found in 19 out of the 35 objects from the IRAS 60μ image. Although the identification of these all of these objects as HII regions is not firm, this is highly suggestive. An even more suggestive result comes from comparing the radio emission to the infrared colors of the objects.

Most (25 out of 35) of the 60μ sources were found in all four bands of the IRAS images. Their peak brightnesses at 12μ, 25μ, 60μ and 100μ were measured. Figure 1 shows a color-color plot of these objects using all four bands. These objects can be split into three groups: (I) those with low $60\mu/100\mu$ flux density ratios (0.1 to 1.0, T = 20°K to 50°K) but high $12\mu/25\mu$ flux density ratios (0.3 to 1.2, T = 160°K to 300°K), (II) those with moderate $60\mu/100\mu$ flux density ratios (0.8 to 2.0, T = 50°K to 80°K) and low $12\mu/25\mu$ flux density ratios (0.1 to 0.3, T = 120°K to 160°K), and (III) those with high $60\mu/100\mu$ flux density ratios (greater than 4, T > 180°K). The group I objects all lie in the bottom right of Figure 1, group II objects all lie to the left of the center, and the group III objects are in the top right side of the figure.

All but one (ie. 15 out of 16) objects with radio emission in this plot (as indicated by open squares) lie in group I. (There are three objects with radio emission that are not shown in this plot since they were not detected at 12μ.) There are only 3 (of 18) objects in group I that show no radio emission. In contrast, only 1 of the 5 objects in group II shows any radio emission, and neither of the two objects in group III show radio emission.

Of those 10 objects with no emission at 12μ and therefore not shown in Figure 1 only 3 had detectable radio continuum emission. This is no surprise since these 10 objects are also the weakest infrared sources in this sample.

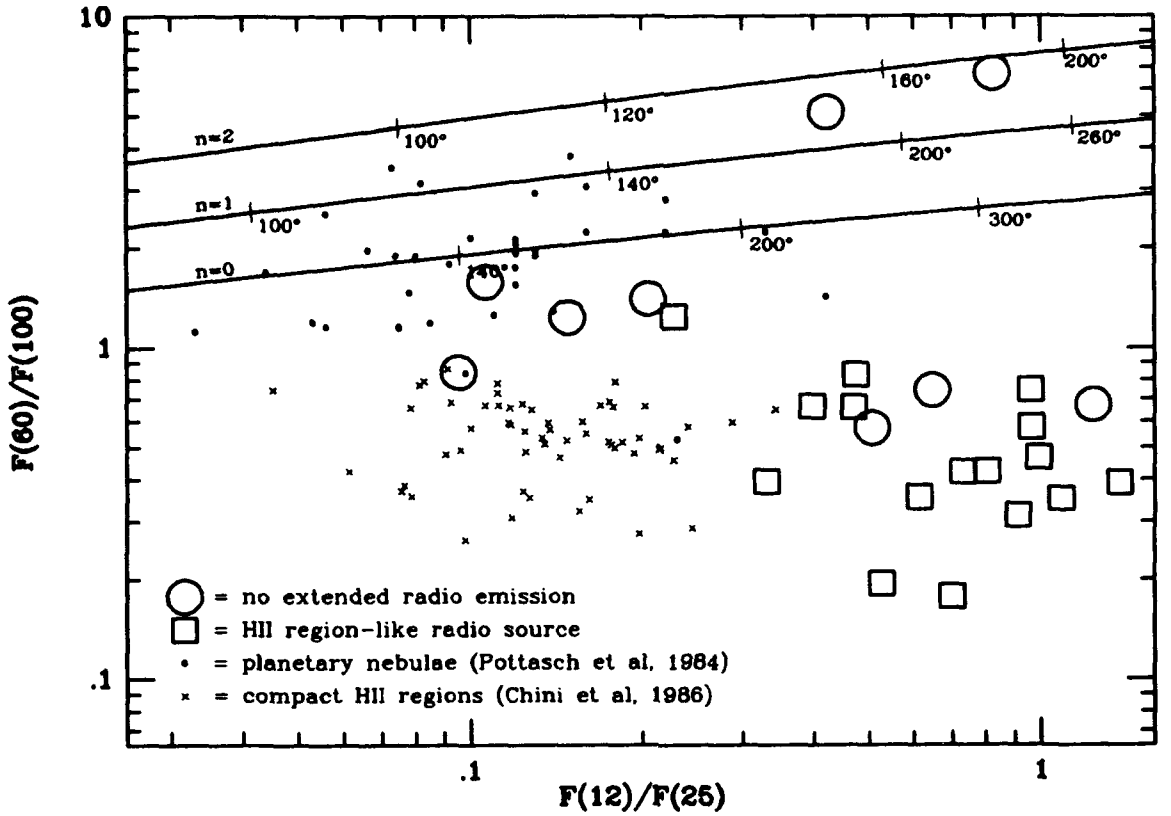

Figure 1: A color-color plot of all objects in VLA survey that were detected in all four IRAS bands. The solid lines show the Planck curves for emissivities of λ^{-n} for n = 0, 1, 2. The objects in the lower right hand corner all appear to be star forming regions. Also plotted here, for color comparison, are the planetary nebulae measured by Pottasch et al (1984) and the compact HII regions detected by Chini et al (1986).

DISCUSSION

It is possible to tentatively identify the objects in group I as star formation regions. Essentially all of the objects with radio continuum emission are in this group and most of the members of this group have radio continuum emission. This also indicates that most of these new stars must be earlier than B2 in order to produce the ionizing photons seen in these HII regions. The physical explanation for these colors is probably the following: at the longer wavelengths emission from cool dust around the HII region is seen while at the shorter wavelengths the heated dust within the HII region dominates the emission.

The colors of objects in group II correspond with the colors of planetary nebulae (plotted in Figure 1 using data from Pottasch et al). Most of them do not have any detected radio continuum emission and planetary nebulae are normally quite weak in the radio. For these reasons group II is tentatively identified as planetary nebulae. The group III objects are probably cool giant stars.

There is a problem reconciling these results with those of Chini et al (1986) shown

plotted in Figure 1. The compact HII regions in their sample are hotter in the 12 and 25 micron bands but are not as hot as those in our sample. This may be due to some physical difference between their objects and ours. Their sample contains very young HII regions excited predominantly by very early types of stars (earlier than O8) and ours may be excited by somewhat later stars or the HII regions may be older. Another possibility is that there may be a difference due to selection effects inherent in their use of the IRAS Point Source catalog and our use of the Sky Brightness Images. Despite this difference in the $12\mu/25\mu$ colors, the $60\mu/100\mu$ colors of the compact HII regions still match the colors of the objects in our survey and are different from those of the planetary nebulae.

In summary: this project indicates that it is possible to distinguish star forming regions from other objects on the basis of their infrared colors. Star forming clouds have Sky Brightness Image peak flux density ratios of $F(60\mu)/F(100\mu) < 1$ and (possibly depending on type of star forming object) $F(12\mu)/F(25\mu) > 0.3$.

REFERENCES

Chini, R., Kreysa, E., Mezger, P. G., and Gemund, H.-P. 1986, *Astr. Ap.*, **154**, L8.

Condon, J. J., and Broderick, J. J. 1986, *A. J.*, **91**, 1051.

Kallas, E., and Reich, W, 1980, *Astr. Ap., Suppl.*, **42**, 227.

Pottasch, S. R., Baud, B., Beintema, D., Emerson, J., Habing, H. J., Harris, S., Houck, J., Jennings, R., and Marsden, P. 1984, *Astr. Ap.*, **138**, 10.

Taylor, A. R., and Gregory, P. C. 1983, *A. J.*, **88**, 1784.

Star Formation in Carina OB1: Observations of a Giant Molecular Cloud Associated with the η Carinae Nebula

D.A. Grabelsky,[1,2] R.S. Cohen,[1] and P. Thaddeus[1,3]
[1]Columbia University, Department of Astronomy, New York, NY
[2]Northwestern University, Dept. of Physics and Astronomy, Evanston, IL
[3]Goddard Institute for Space Studies, 2880 Broadway, New York, NY

ABSTRACT. A giant molecular cloud associated with the η Carinae nebula has been fully mapped in CO with the Columbia Millimeter-Wave Telescope at Cerro Tololo. The cloud complex has a mass of roughly 7 x 10^5 $M_\odot$ and extends about 140 pc along the Galactic plane, with the giant Carina HII region situated at one end of the complex. Clear evidence of interaction between the HII region and the molecular cloud is found in the relative motions of the ionized gas, the molecular gas, and the dust; simple energy and momentum considerations suggest that the HII region is responsible for the observed motion of a cloud fragment. The molecular cloud complex appears to be the parent material of the entire Car OB1 Association which, in addition to the young clusters in the Carina nebula, includes the generally older clusters NGC 3324, NGC 3293, and IC 2581. We estimate the overall star formation efficiency in the cloud complex to be ~0.02.

1. INTRODUCTION

The η Carinae nebula (NGC 3372) is among the brightest giant HII regions in the Galaxy, and the young clusters that supply the ionizing radiation -- Tr 14, Tr 16, and Cr 228 -- comprise one of the largest known Galactic concentrations of massive stars: 16 main sequence O stars, including 5 classified O3V (Walborn 1971, 1973). Interstellar absorption lines observed toward many of the member stars display velocities ranging over 550 km s^{-1} (Walborn 1982), and it is generally agreed that the Carina nebula is pumping a lot of energy into the surrounding medium. Within about 2° along the Galactic plane lie the three somewhat older and less spectacular clusters NGC 3324, NGC 3293, and IC 2581, which, together with the clusters in the Carina nebula, make up the Carina OB1 Association.

Because it lies in the Southern skies, CO observations of the region in and around the Carina nebula were, until recently, limited either to single detections (Gillespie *et al.* 1977; White and Phillips 1983) or to small region mapping (de Graauw *et al.* 1981). In 1983 we installed the Columbia Southern Millimeter-Wave Telescope at Cerro Tololo and carried out the first well-sampled CO survey of the entire Southern Milky Way. As part of that survey, we mapped a large molecular cloud complex that is the parent material of the Car OB1 Association. In this paper we present the observations of the η Carinae molecular cloud complex, point out the interesting dynamical relationship between the molecular cloud and the HII region, and give an estimate of the overall star formation efficiency in the molecular cloud.

2. OBSERVATIONS

The CO observations were made between 1983 January and November at Cerro

Tololo with the Columbia Southern Millimeter-Wave Telescope (Grabelsky 1985; Bronfman 1986). The telescope has a beamwidth of 8.8′ at 2.6 mm, and its pointing accuracy is better than 1′. The detection system consists of a liquid nitrogen cooled superheterodyne receiver with a single-sideband noise temperature of ~380 K, and a filterbank spectrometer with 256 channels, each 1.3 km s^{-1} wide at 2.6 mm for a total bandwidth of 333 km s^{-1}. Spectra were calibrated against a blackbody reference following the standard chopper wheel technique (Kutner 1978), and only linear baselines were subtracted. Integrations times were typically 5 minutes, yielding an rms noise per channel of ~0.14 K.

The region in and around the Carina nebula was covered in a survey of molecular clouds in the Carina spiral arm (Grabelsky 1985). Observations were space every 1/8° in l and b in the range $270^\circ \leq l \leq 300^\circ$, $|b| \leq 1^\circ$, with latitude extensions as needed to cover all nonlocal emission. The spectrometer bandwidth, centered at v = 0, was more than adequate to cover all Galactic plane emission within the longitude range of the survey.

3. IDENTIFICATION OF THE CLOUD COMPLEX

A mosaic of ESO J plates showing the η Carinae nebula and its surroundings is displayed in Figure 1; the bright gas between $l = 287^\circ$ and 288° is the Carina HII region. Although the young clusters in the Carina nebula are washed out in this photograph, the other Car OB1 clusters can be identified: IC 2581 (l,b = 284.7°,0.1°), NGC 3293 (285.9°,0.1°), and NGC 3324 (286.2°,-0.2°). Various published distances place these clusters, as well as the Carina nebula, at 2.7 kpc. The overlaid concours in Figure 1 show CO emission integrated over velocity from -50 to -9 km s^{-1}. Along the Galactic plane a sequence of molecular clouds from l,b = 285°,0° to 288°,-1° is evident. Each molecular cloud in the apparent grouping is physically related to one or more of the Car OB1 clusters, thus placing each cloud at the same distance and establishing the identity of the molecular cloud complex. In each case the evidence for the association of a cluster with a molecular cloud in the complex is the spatial proximity and similar velocities; cluster velocities were determined either from member stars or from associated HII regions. In the case of the Carina nebula, discussed in the next section, there is, additionally, clear evidence for direct contact between the HII region and the molecular cloud.

With the now widely-used assumption that integrated CO line temperature, denoted W(CO), is proportional to $N(H_2)$, the H_2 column density, and adopting the γ ray calibration of Bloemen *et al.* (1986) of the W(CO)-$N(H_2)$ relation, we obtained a mass of 6.7 x 10^5 $M_\odot$ for the entire molecular cloud complex. We call this the CO mass to indicate that it is based on W(CO). This value is within about a factor of two of the virial mass derived by assuming that the observed bulk motions in the complex support the cloud against gravity.

4. INTERACTION BETWEEN THE CLOUD AND THE HII REGION

One of the prominent features of the Carina nebula is the dark dust lane that crosses the face of the bright gas. The generally good spatial correlation between the CO and the dust suggests that a portion of the molecular cloud must lie in front of the HII region, while the coincidence of the strong CO peak at l,b = 287.5°,-0.5° with the bright gas indicates that

FIGURE 1. Mosaic of ESO J plates showing the η Carinae nebula and its surroundings. The overlaid contours show CO emission integrated over velocity from -50 to -9 km s^{-1}. The contour interval is 5 K km s^{-1}. Note the good correlation between the CO and the dust lanes in the vicinity of the bright gas. This dust represents a fragment of the molecular cloud that is being driven out by the HII region.

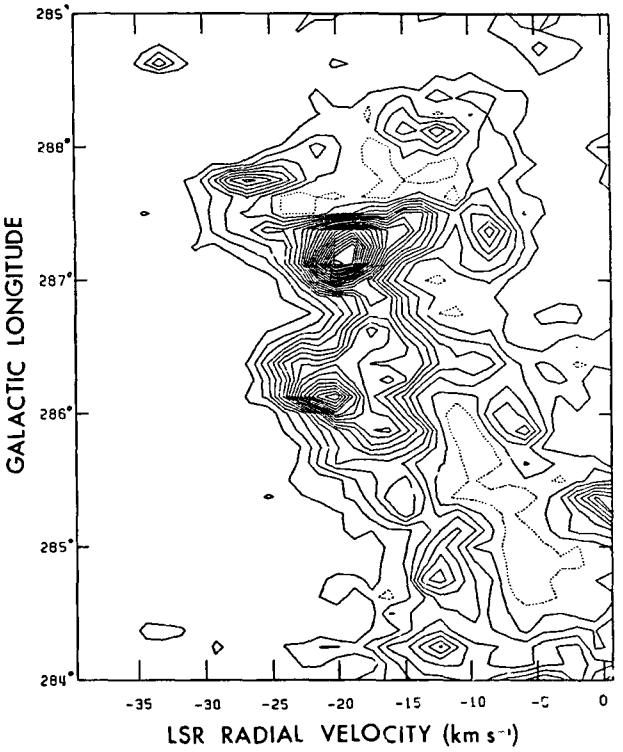

FIGURE 2. Longitude-velocity map of the η Carinae molecular cloud complex. The CO emission is integrated in latitude from b = -1^0 to 0^0; the contour interval is 0.125 K-deg. The mean velocity of the emission is -19 km s^{-1} but near the longitude of the HII region ($l \approx 287.5^0$) a cloud fragment with a velocity of about -26 km s^{-1} is seen. This fragment or filament corresponds to the dust lane in front of the Carina nebula, and its appearance as a blue-shifted feature (relative to the mean cloud velocity) indicates that it is moving out from the main body of the cloud. The CO mass of the filament is ~2 x 10^4 $M_\odot$ and its velocity relative to the mean cloud velocity is 7 km s^{-1}. The HII region is evidently driving the filament outward.

much of the molecular cloud is located behind the HII region. A longitude-velocity map integrated from b = -1^0 to 0^0 is shown in Figure 2. The mean velocity of the cloud complex is -19 km s^{-1}, quite close to the mean HII region

velocity of -20 km s^{-1}; but at the longitude of the Carina HII region there a CO "filament" with a velocity of about -26 km s^{-1}. This blue-shifted filament corresponds to the dust lane and the HII region may be driving the filament outward with a relative velocity of ~7 km s^{-1}. The spatial correlation of the blue-shifted CO filament and the dust lane is confirmed in spatial maps which sample narrow velocity "slices" through the cloud (not shown here).

To check whether the HII region could be the source of the filament's motion, we considered two possible mechanisms for driving the filament out from the main body of the cloud: a stellar wind-driven bubble, and the rocket effect. Following Castor *et al.* (1975), the velocity of the swept-up shell around a wind-driven bubble can be expressed $v_s = 2.7 \times 10^3 (\dot{M} v_w^2 n_o^{-1})^{1/5} t^{-2/5}$ km s^{-1}. With the assumption that the CO filament is a piece of swept-up shell and reasonable values in the Carina nebula for the stellar mass loss rate ($\dot{M}$), wind velocity, (v_w), ambient cloud density (n_o), and age (t), a stellar wind-driven bubble can easily account for the observed motion of the filament. Similarly, in the Carina nebula there is enough ionizing radiation to make the rocket effect of ionized gas streaming off the filament a plausible mechanism for accelerating the filament. Evidently, the HII region is severely disrupting the cloud.

5. STAR FORMATION EFFICIENCY

The star formation efficiency, SFE, is the ratio of stellar mass to total stellar plus molecular cloud masses. For the cloud mass we used the CO mass found above (§ 3.). To estimate the stellar mass we simply tallied up the mass in all the observed stars with spectral types earlier than B0.5, and used the IMF of Miller and Scalo (1979) to determine the total mass in spectral types B0.5 and later. The IMF was calibrated to the number of observed B0.5V stars. Our assumption that a reasonable total mass in early type stars can be attained by simply counting them is based on the unusually large number of early type stars observed in the Carina nebula. Using this method we obtained SFE = 0.02. This result is in good agreement with SFE determined by Myers *et al.* (1986) for about 50 inner-Galaxy giant molecular clouds.

REFERENCES

Bloemen, J.B.G.M. *et al.* 1986, *Astr. Ap.*, **154**, 25.
Bronfman, L. 1986, Ph.D. thesis, Columbia University.
Castor J., McCray, R., and Weaver, R. 1975, *Ap. J. (Letters)*, **200**, L107.
de Graauw, T., Lidholm, S., Fitton, B., Beckman, J. Israel, F.P., Nieuwenhuijzen, H., and Vermue, J. 1981, *Astr. Ap.*, **102**, 257.
Gillespie, A.R., Huggins, P.J., Sollner, T.C.L.G., Phillips, T.G., Gardner, F.F., and Knowles, S.H. 1977, *Astr. Ap.*, **60**, 221.
Grabelsky, D.A. 1985, Ph.D. thesis, Columbia University.
Kutner, M.L. 1978, *Ap. Letters*, **19**, 81.
Miller, G.E., and Scalo, J.M. 1979, *Ap. J. Suppl.*, **41**, 513.
Myers, P.C., Dame, T.M., Thaddeus, P., Cohen, R.S., Silverberg, R.F., Dwek, E., and Hauser, M.G. 1986, *Ap. J.*, **301**, 398.
Walborn, N.R. 1971, *Ap. J. (Letters)*, **167**, L31.
Walborn, N.R. 1973, *Ap. J.*, **179**, 517.
Walborn, N.R. 1982, *Ap. J. Suppl.*, **148**, 145.
White. G.J., and Phillips, J.P. 1983, *M.N.R.A.S.*, **202**, 255.

STAR FORMING REGIONS OF THE SOUTHERN GALAXY

T. B. H. Kuiper
Jet Propulsion Laboratory, 169-506
California Institute of Technology
Pasadena, California 91109
U.S.A.

J. B. Whiteoak
Division of Radiophysics
Commonwealth Scientific and Industrial Research Organization
P.O. Box 76, Epping, New South Wales 2121
Australia

J. W. Fowler
Infrared Processing and Analysis Center
California Institute of Technology, 100-22
Pasadena, California 91125
U.S.A.

ABSTRACT: A catalogue of southern dust cloud properties is being compiled to aid in the planning and analysis of radio spectral line surveys in the southern hemisphere. Ultimately, images of dust temperature and column density will be produced. For the interim, a list of the 60 and 100 μm fluxes has been prepared for the cores and adjacent backgrounds of 65 prominent dust clouds. Dust temperatures and column densities have been derived.

1. INTRODUCTION

Radio line surveys of southern molecular clouds have generally been based on catalogues of visible nebulae and radio continuum sources (e.g. Whiteoak 1983). Thus sites of star formation without such indicators may have been missed by such surveys. The IRAS far-infrared sky survey enables a more complete identification of molecular clouds by pinpointing the associated dense dust clouds.

Additionally, estimates of the temperature and column density within the clouds can be made by combining the data of the four IRAS spectral bands. The data for band 3 (60 μm) and band 4 (100 μm) are particularly useful for this purpose.

We have begun a project to identify and study southern molecular clouds present in the IRAS survey. Ultimately, we plan to produce images of estimated dust temperature and column density for these objects. In this paper we briefly discuss the method to be applied in the creation of the images, and present some preliminary results. The latter consist of the identification of 65 bright southern dust concentrations and estimates of temperature and column density towards their centers.

2. MATERIALS AND METHODS

2.1. Determination of Temperature and Column Density

Given a gas column density and dust temperature we can compute the flux measured by IRAS as discussed below. We have assumed that the optical depth of

the dust can be computed from

$$\tau = \left(\frac{\text{column density}}{10^{21}\ \text{cm}^{-2}}\right) * \left(\frac{0.5\ \mu\text{m}}{\lambda}\right).$$

This corresponds to a standard gas to dust ratio, and an inverse wavelength dependence for dust opacity. The brightness was then calculated from brightness

$$= B_\lambda(T_{dust}) * (1-\exp(-\tau)) ,$$

where B_λ is the blackbody wavelength spectrum. This brightness was integrated over the bandpasses of the IRAS detectors (Beichman et al., 1985). Using a Newton Raphson iteration, we can invert the above equations to determine estimated dust temperature and gas column density from the 60 and 100 μm fluxes. We intend to produce images of estimated dust temperature and gas column density for southern molecular clouds by applying the NewtonRaphson method on a pixel by pixel basis to coadded grids of 60 and 100 μm survey data. We prefer to reconstruct the images from the Calibrated Reconstructed Detector Data to using the Sky Brightness Images for a number of reasons. The data from the entire survey can be combined in the images, providing higher sensitivity and the potential for enhanced spatial resolution. Software is available which can remove scan-to scan variations, due to detector baseline effects, and field gradients due to extended background emission. The principal challenge will be to find a satisfactory algorithm for removal of background emission. We are presently using interactive image processing to evaluate the merits of various approaches, such as no background removal, removal of a background equivalent to the lowest pixel value, and subjective determination of cloud boundaries.

2.2. Selection of southern dust clouds

The 100-μm Sky Brightness Images were used initially for the identification of the southern dust concentrations. Bright discrete regions that could be effectively separated from the superimposed background emission of the galactic plane were selected for further processing with the facilities of the Infrared Processing and Analysis Center (IPAC). The positions of peak brightness were estimated using maps of the HCON1 series. For a comparison of 60-μm and 100-μm brightnesses, the different angular resolution for the two sets of data had to be taken into account. Accordingly, in our preliminary investigation, for each wavelength band we derived the average brightness for a 3 x 3 pixel grid centred on the pixel with the highest brightness. (The pixel spacing in the maps is 2 arcmin). The associated mean background levels around each object were also estimated. By means of the method discussed earlier, these results were then converted into temperatures and column densities.

3. RESULTS

Sixty-five of the brightest dust concentrations at 100 μm for declinations south of -10 degrees have been examined. However, because of its complexity the extended dense region near the galactic centre has been excluded. Virtually all the objects are centered near the bright HII regions listed in Gardner and Whiteoak (1974). In some cases the galactic background

level is high and somewhat uncertain, and this uncertainty carries over to the brightness estimates. To examine the consequences for the derived parameters, temperatures and column densities have been computed both with and without background removal. In addition, the temperature and column density of the background has been computed. The results are represented in the three histograms of Figure 1. The similarity of the top two histograms shows that the determination of temperature is not significantly dependent on the background subtraction. In both cases, the source temperature (averaged over a 6x6 arcmin square) is about 40K. The other thing to be observed is that the background temperature appears to be very uniform, varying only between 20 and 30 K over the 113 deg of longitude covered by the sample.

Although individual objects without groups of dust regions often have similar temperatures, some exceptions exist. A prominent example is seen in the complex near l = 298°. 298.2-0.3 has a dust temperature of 52 K; 298.9-0.4 has a temperature of 44 K. 298.2-0.8 has a temperature of about 30 K. The associated background dust temperature is about 20 K. Figure 2 shows the image of the ratio of the 60 to 100 micron flux for the complex. In this instance, we adjusted the background to be zero for the lowest pixel value. A temperature image will be similar to the colour image, since the flux ratio is nearly a function of temperature alone. We have therefore selected the contour levels in the figure to correspond to colour temperatures from 20 to 60 K degrees in steps of 5 K.

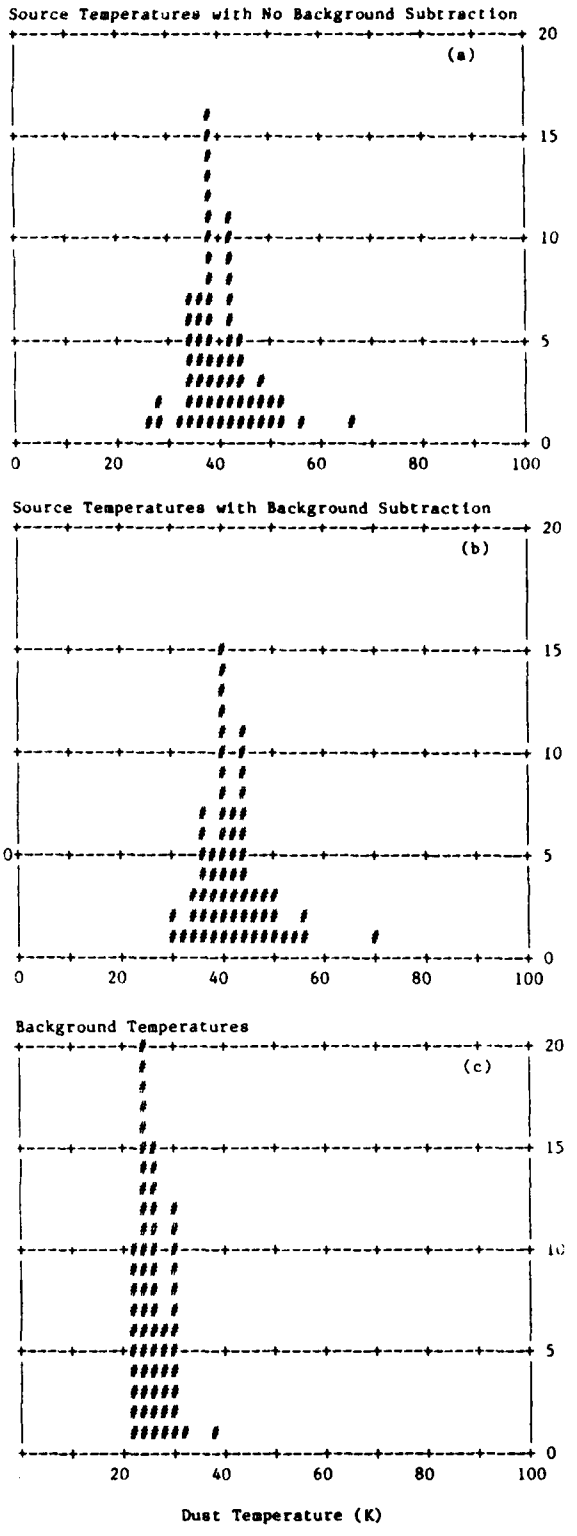

4. DISCUSSION

Comparison of the histograms in Figures 1a and 1b suggests that the temperatures derived for the cores of prominent isolated dust clouds are not strongly affected by what is assumed for the

Figure 1 - Histograms of derived dust temperatures towards cores of isolated dust clouds (a) without and (b) with background emission subtract. Dust temperatures of the background emission are shown in (c).

background emission. Comparing either of those histograms with the one in Figure 1c shows that there is very little overlap; the core regions are typically 15 K warmer than the background, averaged over 9 square arcmin. Also, the background temperature is quite uniform over a large part of the Galaxy.

5. ACKNOWLEDGEMENTS

We wish to thank Gwen Manefield of CSIRO for help in compiling the cloud core data, and Walter Rice of IPAC for help in developing the image processing tasks.

The research described in this paper was carried out in part at the Jet Propulsion Laboratory, California Institute of Technology, under contract to the National Aeronautics and Space Administration.

6. REFERENCES

Beichman, C. A., Neugebauer, G., Habing, H. J., Clegg, P. E., and Chester, T. J., eds. 1985, IRAS Explanatory Supplement, (Jet Propulsion Laboratory, Pasadena), Table II.C.5.

Whiteoak, J. B. 1983, in Surveys of the Southern Galaxy, ed. Burton and Israel (Reidel), p.31.

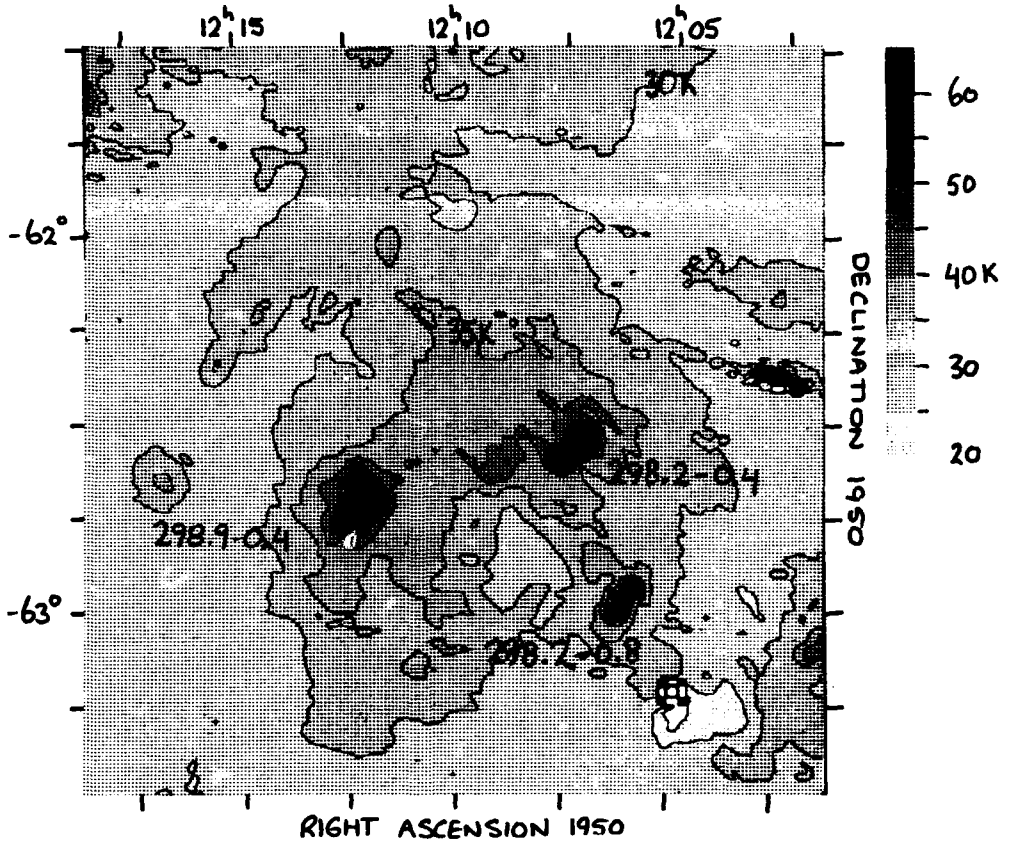

Figure 2 - Map of derived dust temperature of a 2 x 2 degree field which contains three dust condensations. The feature near the middle of the right border is an artifact.

ON THE REDISTRIBUTION OF OB STAR LUMINOSITY AND THE WARMING OF NEARBY MOLECULAR CLOUDS

D. Leisawitz
National Research Council-GSFC Research Associate
NASA Goddard Space Flight Center Code 697
Greenbelt, MD 20771

ABSTRACT

IRAS observations of the neighborhoods of six outer-Galaxy HII regions were combined with CO observations to show that most of the far infrared (FIR) luminosity from within ~25-75 pc of the ionizing stars is contributed by dust in molecular clouds, not by dust in the low-density ionized gas. Dust associated with the clouds is warmed by absorption of UV and visible light from the cluster of stars responsible for the ionization. Most ($\gtrsim$70%) of the OB cluster starlight is not absorbed locally.

A fraction of the order of 10% of the OB cluster luminosity is absorbed by nearby molecular clouds and reradiated as FIR light. The luminosity per unit mass for the heated clouds is ~3-13 $L_\odot/M_\odot$, approximately one order of magnitude greater than the corresponding ratio for clouds found near clusters without O stars, and two orders of magnitude greater than the ratio for dark clouds heated primarily by the interstellar radiation field. If the observations of clouds near outer-Galaxy HII regions are used to characterize the molecular clouds heated by HII regions in the inner-Galaxy, then at most 30% of the Galaxy's molecular cloud mass is actively engaged in the formation of massive stars at the present time.

INTRODUCTION

One can infer from a number of articles that appear in this volume that the "warm dust" (Cox, Krügel, and Mezger 1986) in many spiral galaxies has been heated by massive stars. As a rule, massive stars are concentrated in the arms of spiral galaxies and are accompanied by molecular clouds and diffuse atomic gas, as well as ionized gas. In order to successfully interpret correlations between indicators of massive star formation (e.g., radio continuum, recombination line, and blue luminosity observations) and the FIR emission of galaxies, it is necessary to understand how the luminosity of massive stars is distributed among dust grains associated with the various components of the interstellar medium (ISM). To put it succinctly: as we appreciate the beauty of the forest, let's not forget what the trees are!

Analysis of the infrared emission from the neighborhoods of HII regions in the Galaxy can be used to answer two important questions. First, how much of the ionizing cluster starlight is absorbed locally? Second, what are the relative proportions of the locally-absorbed starlight involved in heating dust associated with diffuse ionized gas, diffuse atomic gas, and molecular clouds?

Carol J. Lonsdale Persson (Editor)
Star Formation in Galaxies

OBSERVATIONAL PARAMETERS

We analyzed six regions, all of which lie outside the solar circle where a molecular cloud can be associated with an HII region almost unambiguously, and where the galactic infrared background is relatively uncomplicated. Table I shows the star cluster coordinates (Alter, Ruprecht, and Vanysek 1970) and distances, and the angular and linear radii of the regions.

Table I. Analyzed Regions

Star Cluster	HII Region	Galactic Coordinates (l,b) (deg)	d[a] (kpc)	Region Radius (deg)	(pc)
NGC 7380	S142	107.08-0.90	3.60	1.0625	66.8
NGC 281	S184	123.13-6.24	1.66	0.8125	23.5
IC 1848	W5/S199	137.19+0.92	2.31	1.0625	42.8
NGC 1624	S212	155.35+2.58	6.00	0.5625	58.9
NGC 1893	IC410/S236	173.59-1.70	4.00	1.0625	74.2
NGC 2175	S252	190.20+0.42	1.95	1.5625	53.2

[a] References for distance: NGC 7380, IC 1848, NGC 1893, and NGC 2175 from Lynga 1981, NGC 281 from Walker and Hodge 1968, and NGC 1624 from Moffat, FitzGerald, and Jackson 1979.

Observations of ^{12}CO J=1→0 emission were obtained with the Columbia University 1.2m millimeter wave telescope (Leisawitz 1985; Leisawitz, Thaddeus, and Bash 1986, hereafter LTB). A circular region, centered on the star cluster coordinates of the size indicated in Table I was mapped with a uniform sampling interval of 7.5'. The antenna beamwidth is 8.7', the velocity resolution of the spectrometer is 0.65 km s^{-1}, and the RMS baseline noise in all spectra is $T_A^* \sim 0.28$ K. A catalog and maps of the molecular clouds in the six regions of interest are given by LTB.

Maps of 12, 25, 60, and 100μm emission corresponding to the regions mapped in CO were extracted from the IRAS sky flux images (IRAS Explanatory Supplement). The spatial resolution of the IRAS images is modestly better than that of our CO observations. For comparison with the infrared data, the CO data were interpolated and mapped into 2'X2' pixels.

RESULTS

After subtraction of an appropriate background (Leisawitz and Hauser 1986), in-band and bolometric FIR luminosities were calculated for the regions of Table I and for each of the molecular clouds in these regions. Bolometric luminosities were derived from the 60 and 100μm observations (cf. Appendix B of Catalogued Galaxies and Quasars in the IRAS Survey). Two methods were applied

to estimate the background levels in the directions of molecular clouds and consistent results were obtained. Most of the uncertainty in the luminosity measurements is due to uncertainty of the background intensity.

The region luminosities (bolometric) range from ~5×10^4 to ~5×10^5 $L_\odot$ with uncertainties $\gtrsim$10%. A fraction between 5 and 30% of the total OB cluster luminosity is reradiated in the FIR by dust within the regions studied. Dust associated with molecular clouds accounts for ~50-80% of the FIR luminosity from the regions considered; the rest of the emission from these regions comes, in roughly equal proportions, from dust in the low-density ionized gas and dust in diffuse atomic gas surrounding the nebulae.

Individual molecular clouds have luminosity-to-mass ratios $\langle L/M\rangle \sim 3 - 13$ $L_\odot/M_\odot$ (cloud masses were derived from the CO observations assuming $N_{H2} \simeq 2\times10^{20}$ $cm^{-2}K^{-1}km^{-1}s\int T_R^* dv$). For comparison, the molecular clouds found in regions near star clusters with members of spectral type B0 or later (LTB) have $\langle L/M\rangle \sim 0.1 - 1$ $L_\odot/M_\odot$ and the molecular clouds in the LTB survey that appear to be isolated, local clouds have $\langle L/M\rangle \lesssim 0.1$ $L_\odot/M_\odot$ and generally were not detected by the IRAS.

DISCUSSION

If the luminosity of massive stars generally is distributed among the various components of the ISM as it appears to be in the regions that we have analyzed, then it is possible to deduce the fraction, f_{wmc}, of a galaxy's molecular cloud mass that consists of warm molecular clouds heated by nearby massive stars:

$$f_{wmc} \simeq f_{loc} L_{OB}(gal)/[M_{mc}(gal)\langle L/M\rangle_{wmc}],$$

where f_{loc} is the fraction of an OB cluster's luminosity absorbed by nearby molecular clouds and $\langle L/M\rangle_{wmc}$ is the luminosity-to-mass ratio for these clouds. Radio continuum observations can be used to derive $L_{OB}(gal)$, the luminosity from a galaxy's OB star clusters and CO observations can be used to estimate a galaxy's molecular mass, $M_{mc}(gal)$. Our analysis suggests that $f_{loc} \sim 2 - 13\%$ and $\langle L/M\rangle_{wmc} \sim 3 - 13$ $L_\odot/M_\odot$. For the inner Galaxy, Dame, Elmegreen, Cohen, and Thaddeus (1986) estimate $M_{mc}(gal) \simeq 9.1\times10^8$ $M_\odot$ and, from the Lyman continuum photon production rate obtained by Güsten and Mezger (1983), we derive $L_{OB}(gal) \simeq 6\times10^9$ $L_\odot$. Accordingly, f_{wmc} should be between ~1.3 and 29% for the inner Galaxy. Observations of 13 well-studied spiral galaxies summarized by Israel and Rowan-Robinson (1984) suggest that a ratio $L_{OB}(gal)/M_{mc}(gal)$ similar to the ratio derived for the Milky Way is applicable to these galaxies as well. Apparently, it is often the case that only a small fraction of a galaxy's molecular cloud mass is actively forming massive stars at a given time.

CONCLUSIONS

From analysis of the infrared emission from regions surrounding six OB clusters in the outer Galaxy, we conclude that:

(a) at most 30% of the cluster luminosity is absorbed by dust grains within ~25-75 pc of the stars,

(b) ~50-80% of the locally-absorbed starlight is absorbed by dust associated with molecular clouds while the remainder is absorbed, approximately in equal proportions, by dust embedded in low-density ionized gas and dust associated with diffuse atomic gas, and

(c) the fraction of cluster starlight absorbed by nearby molecular clouds is of the order of 10% and the FIR bolometric luminosity-to-mass ratios that characterize such clouds are approximately a few to 13 solar units. This information can be used to estimate the fraction of a galaxy's molecular mass that is in the form of molecular clouds heated by nearby clusters of massive stars: in the Milky Way, and in 13 well-studied spiral galaxies, probably less than 30% of the molecular gas is involved in the production of the current generation of massive stars.

REFERENCES

Alter, G., Ruprecht, J., and Vanysek, V. 1970, The Catalog of Star Clusters and Associations (Budapest: Akademiai Kiado).

Catalogued Galaxies and Quasars in the IRAS Survey, eds. C. J. Lonsdale, G. Helou, J. C. Good, and W. Rice 1985, NASA Jet Propulsion Laboratory.

Cox, P., Krügel, E., and Mezger, P. G. 1986, Astr. Ap., **155**, 380.

Dame, T. M., Elmegreen, B. G., Cohen, R. S., and Thaddeus, P. 1986, Ap. J., **305**, 892.

Güsten, R., and Mezger, P. G. 1982, Vistas in Astr., 26, 159.

IRAS Explanatory Supplement 1985, eds. C. A. Beichman, G. Neugebauer, H. J. Habing, P. E. Clegg, and T. J. Chester.

Israel, F. P., and Rowan-Robinson, M. 1984, Ap. J., **283**, 81.

Leisawitz, D. 1985, Ph. D. thesis, The University of Texas at Austin.

Leisawitz, D., and Hauser, M. G. 1986, in preparation.

Leisawitz, D., Thaddeus, P, and Bash, F. N. 1986, in preparation (LTB).

Lynga, G. 1981, Catalog of Open Cluster Data, NASA Data Center, Greenbelt, MD.

Moffat, A. F. J., FitzGerald, M. P., and Jackson, P. D. 1979, Astr. Ap. Supp. Ser., **38**, 197.

Walker, G. A. H., and Hodge, S. M. 1968, Publ. Ast. Soc. Pac., **80**, 290.

MAPS OF MILLIMETER WAVE EMISSION FROM THREE GALACTIC STAR-FORMING REGIONS

Mary Barsony
Division of Physics, Mathematics, and Astronomy
California Institute of Technology
Mail Code 103-33
Pasadena, CA 91125

ABSTRACT

In order to investigate the gas dynamics around young stellar objects, we have mapped three sources which exhibit supersonic velocities in the 115 GHz, J=1-0 transition of CO (Bally and Lada 1983). The maps, made with the Owens Valley Radio Observatory Millimeter Interferometer, are the highest spatial resolution (5" x 5") images currently available of millimeter-wave continuum and line emission from the sources S106, S87, and LkHα101. Observations were made in the CS (J = 2-1) and ^{13}CO (J = 1-0) transitions. In all the sources, our observations indicate that the ionized stellar wind is sweeping up ambient molecular gas. The molecular gas is found adjacent to the outer edges of the ionized winds, which originate in embedded infrared sources. From the observations presented here, we may infer that the outflowing ionized winds are channeled by the surrounding dense, neutral gas.

I. Observations

The inteferometer observations of S87 in the CS (J = 2-1) line were made with 32 channels at 3 km s^{-1} velocity resolution, while for S106 and LkHα101, the ^{13}CO maps were made at 0.14 km s^{-1} resolution. Because the interferometer resolves out 50-90% of the emission due to missing spatial sampling of large-scale (>30") features, these sources have also been mapped with the FCRAO 14-m antenna. The single-dish map of S87 in this contribution is in ^{13}CO, observed with 256 channels at 0.3 km s^{-1} per channel, sampled every 15" on a 9 x 9 element grid.

II. Results

S87 is an HII region buried in the center of a hot molecular cloud, associated with an extremely reddened IR source (Bally and Predmore 1983). It is the clearest example of a bipolar flow among the three sources discussed in this work. Figure 1 shows the single-dish map of S87 in the wings of the ^{13}CO line, while Figure 2 shows the same source as seen by the interferometer in CS. The position angles and morphologies of the emission agree over a factor of ten in length scale between the interferometer and single-dish maps, indicating that the bipolar flow is collimated within 10^{17} cm of the central star.

Carol J. Lonsdale Persson (Editor)
Star Formation in Galaxies

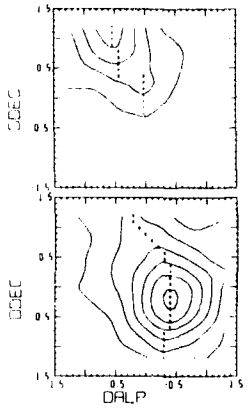

Figure 1
FCRAO 14-m map of S87 as seen in the J = 1-0 transition of ^{13}CO. Map center (1950) coordinates are α=19h 44m 13.7s, δ=24°28′05.1″. V_{LSR} = 22 km s^{-1}, so the top part of the figure is red-shifted emission (V_{LSR} = 24.5→28 km s^{-1}), while the bottom half is blue-shifted (17→21.5 km s^{-1}).

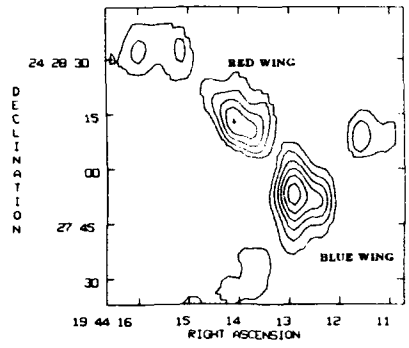

Figure 2
Same source, center coordinates, and V_{LSR} as in Figure 1, but as seen in the CS J = 2-1 transition with the OVRO interferometer. The red wing is emission integrated over V_{LSR}=19→22 km s^{-1}, while the blue wing is integrated over 22→25 km s^{-1}.

LkHα101 is a highly obscured emission line star which illuminates a roughly fan-shaped reflection nebula. In this source, there is a clear anti-correlation between the optical morphology and the molecular line emission. An unresolved 110 GHz continuum source is centered on the embedded young stellar object. Our line observations suggest that the stellar wind of LkHα101 has already cleared out most of the surrounding molecular cloud environment (Figure 3).

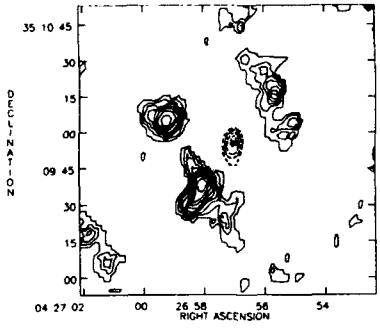

Figure 3
The ^{13}CO J = 1-0 interferometer map of the environs of LkHα101 α(1950)=04h 26m 57.23s, δ(1950)=35°09′55″, V_{LSR}=1.5 km s^{-1}. The dotted contours outline the unresolved 0.35 Jy continuum source coincident with the Hα emission line star.

S106 is a bipolar optical nebula with a dark lane across its center, making it a prime candidate for the detection of an edge-on interstellar molecular disk. The optical emission exhibits a complicated velocity structure; however, the northern lobe is generally red-shifted, while the southern lobe is blue-shifted (Solf and Carsenty 1982). Figure 4 shows the ^{13}CO emission from S106. Figure 5 shows the CS emission from S106 superimposed on the 1.3 cm VLA map (Bally 1985). We find no evidence of the molecular disk claimed by observers at the Hat Creek Interferometer

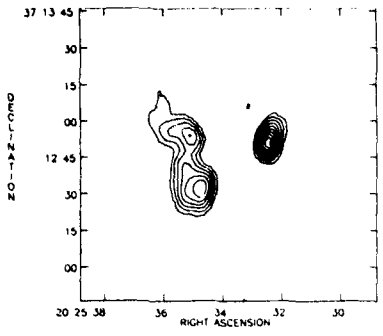

Figure 4
The interferometer map in ^{13}CO of S106. The map is centered on IRS4 (Gehrz et al. 1982) $\alpha(1950)$=20h 25m 33.8s, $\delta(1950)$=37°12′48″ V_{LSR}=-1.0 km s^{-1}. Note the similar morphologies of CS and ^{13}CO.

Figure 5

The interferometer map of CS emission from S106 overlaid on its 1.3 cm radio continuum emission. Note the anti-correlation of the spatial distribution of the molecular and ionized gas. There is no evidence for a disk-like structure. The white speck at map center is IRS4.

(Bieging 1984). Instead, the putative disk breaks up into two dense condensations on opposite sides of the HII region, as seen in our higher resolution observations.

III. Conclusions

High velocity CO emission associated with active star-forming cloud cores has been interpreted as outflows from embedded young stellar objects. In some cases, these flows appear to be bipolar on arc-minute angular scales (Lada 1985). Some authors have postulated massive (100 $M_\odot$), large-scale, rotating molecular disks as the energy source and/or focussing agent for the outflows. The observations presented here show no direct evidence of the hypothesized disks. In particular, the high-resolution data for S106 (one of the sources with best prior evidence for a disk) show that the presumed disk is, in reality, two dense knots of neutral gas on opposite sides of the conical HII region. These dense concentrations of neutral gas are probably responsible for constricting the HII region's expansion along its minor axis.

A preliminary interpretation of the data presented here lends support to the idea that a hot, ionized wind sweeps out the surrounding cloud material soon after stellar formation. However, it must be noted that the three regions studied here were already known from optical and radio studies to contain ionized gas.

Acknowledgements

I am happy to thank my advisor, N.Z. Scoville, for his encouragement and support, without which this contribution would not have been written. I would also like to thank Mark Claussen for his help and dedication in obtaining the single-dish data at FCRAO. Partial funding for this research was provided by the NSF through grants AST-8412473 and AST-8403054, and is gratefully acknowledged.

References

Bally, J. 1985, private communication.

Bally, J. and Lada, C. 1983, *Ap. J.*, **265**, 824.

Bally, J. and Predmore, R. 1983, *Ap. J.*, **265**, 778.

Bieging, J. H. 1984, *Ap. J.*, **286**, 591.

Gehrz, R. D., Grasdalen, G. L., Castelaz, M., Gullixon, C., Mozurkewich, D., Hackwell, J. A. 1982, *Ap. J.*, **254**, 550.

Lada, C. 1985, *Ann. Rev. Astr. Ap.*, **23**, 267.

Solf, J. and Carsenty, U. 1982, *Astron. Ap.*, **113**, 142.

Shock Heated Dust in L1551: L(IR) > 20 Solar Luminosities

F.O. Clark(1,2), R.J. Laureijs(1), G. Chlewicki(1), C.Y. Zhang(1),
W. van Oosterom(1), and D. Kester(1)

(1)Laboratory for Space Research Groningen and Kapteyn Laboratory
Postbus 800, 9700 AV Groningen, The Netherlands
(2)Department of Physics and Astronomy, University of Kentucky
Lexington, KY 40506, USA

ABSTRACT. The infrared bolometric luminosity of the extended emission from the L1551 flow exceeds 20 solar luminosities. Ultraviolet radiation from the shock associated with the flow appears to heat the dust requiring shock temperatures from 10,000 to 90,000 K in L1551, velocities of ~50 km/s near the end of the flow, and a minimum mechanical luminosity of ~40 solar luminosities. The total energy requirement of the infrared emission over a 10,000 year lifetime is 10^(46-47) ergs, two orders of magnitude higher than previous estimates for L1551. Infrared radiation offers a new method of probing interstellar shocks, by sampling the ultraviolet halo surrounding the shock. At least one current model for bipolar flows is capable of meeting the energetic requirements.

I. Introduction

The extended infrared emission from dust around the L1551 flow reported by Clark and Laureijs (1986), is analyzed. Bipolar flows from young stars have heretofore been detected by means of broad wings on spectral lines (usually CO, or Hα). The detection of infrared emission from dust surrounding bipolar flows offers a new method of observing such flows. From the extended infrared emission from the L1551 flow, the total infrared luminosity is calculated, the heating mechanisms is analyzed, the mechanical luminosity of the shock is estimated, and the energy requirements calculated over the lifetime of the flow.

II. Data

IRAS HCON3 survey data, CPC images, AO edge detector data, and HCON1, 2, and 3 raw detector data have been analyzed. We have examined the spatial extent and morphology of the infrared emission by analyzing GEISHA IRAS HCON1, 2, and 3 raw detector data, and small scale structure from CPC images.

III. Observed Flux, Dust Temperature, and Ambient Density

Table 1 illustrates the derived spatially resolved data from IRAS HCON3 survey data, shown as strip averages from northeast to southwest: spatial offset in arc minutes, IRAS flux, infrared luminosity, dust temperature (dust emissivity varying inversely with wavelength), and ambient density from Snell (1981).

The extended flux contains a small model correction for the contribution near IRS5 estimated with a cylindrical model which matched the observed cloud properties (Snell 1981, Snell and Schloerb 1985, and Mundt et al. 1985). L(IRAS) is the luminosity observed by the IRAS filters. The bolometric IRAS luminosity, corrected for that portion of a Planck curve with appropriate dust emissivity not detected by the IRAS detectors, is 20-29 solar luminosities (Lo), with the range representing uncertainty in dust emissivity, and dust temperature.

Table 1

Offset '	F(60) Jv	F(100) Jy	L(IRAS) Lo	T(dust) K	n_o cm^-3
-31.8	1.4	20.1	0.15	21	36
-26.5	1.0	22.8	0.17	20	52
-21.2	2.0	24.9	0.19	21	81
-15.9	6.1	30.0	0.23	29	143
-10.6	9.6	52.0	0.40	27	315
-5.3	19.8	192.3	1.47	25	1114
0	25.9	414.6	3.16	22	7295
5.3	15.2	238.6	1.82	22	1114
10.6	10.4	128.1	0.98	22	315
15.9	7.4	87.6	0.67	23	143
21.2	2.5	60.8	0.46	23	81
26.5	0.6	32.6	0.25	20	52
31.8	0.2	15.1	0.11	21	36

The extended infrared flux increases strongly towards IRS5, in good agreement with the model of Snell (1981), while the dust temperature is quite uniform across the flow. The comparison of the data near IRS 5 with the cylindrical model described above indicates a significant reduction in dust emission from near IRS5, perhaps from lower dust temperature, or less warm dust.

IV. Dust Heating Mechanism

The dust exhibits a near constant temperature of 22-26 K, with a radiative lifetime of days, requiring the dust heating source to be active at the present time. Three likely possibilities for heating the dust are: 1) radiative heating from IRS5, 2) mechanical heating from the neutral shock heated gas, and 3) radiative heating by shock-produced ultraviolet.

The uniform dust temperature over .5 to 2 pc speaks against the star as the heating source for the dust. Collisional heating of dust by hot post shock gas requires coexistence of the dust and hot gas which, under the range of conditions of interest to the L1551 flow, is less efficient at heating the dust than ultraviolet heating. The post shock region should have a thickness (.007 -.02 pc) which is small compared to the total width (0.4 pc), and the infrared emission should be strongly limb brightened for collisional heating.

The dust in the L1551 cloud surrounding the flow can be quite effective at trapping radiation which escapes from the flow. The conditions necessary to heat the dust by ultraviolet radiation from the shock in L1551 are estimated as an average shock temperature of 40,000 to 80,000 K, and an average shock velocity of 24 to 36 km/s (Hollenbach and McKee 1979). Ultraviolet heated dust will occupy the volume defined by the ultraviolet opacity reaching approximately 1. The surface of ultraviolet opacity = 1 (at 1500 Angstroms) has been modeled, and unveils the ultraviolet halo around the shock, producing a very distinctive morphology which blooms out at greater radii where the ambient density falls.

Figure 1 illustrates the observed infrared emission (solid), the CO flow (dotted) which coincides with the collisional heating morphology, and the UV heating morphology (dashed). UV heating offers a natural explanation of the excess infrared length and excess width at the ends of the infrared emission, although not of the excess infrared width near IRS5.

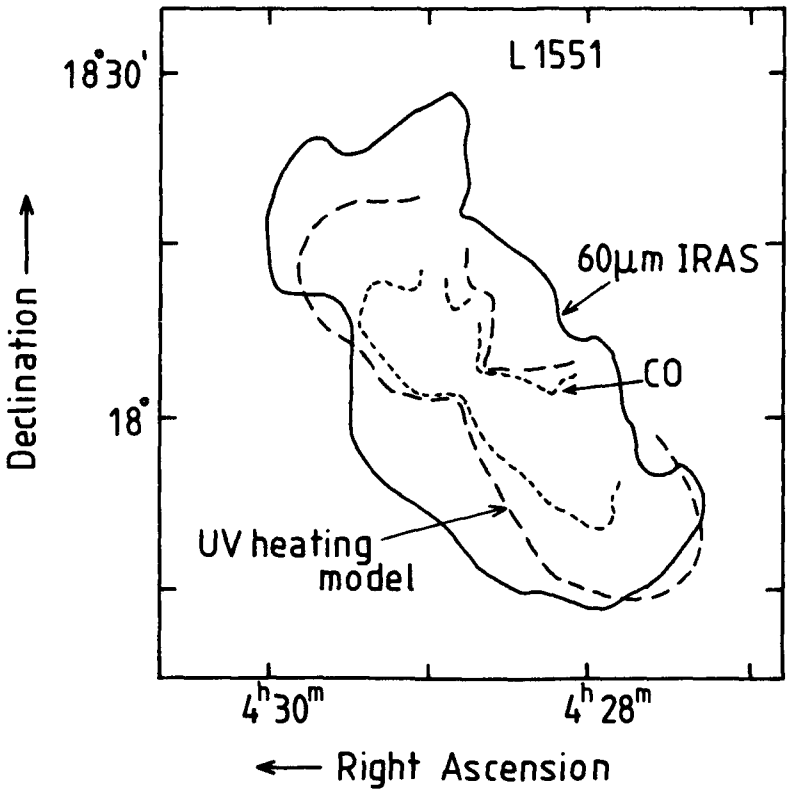

Figure 1. CO map - also the collisionally heated morphology (dotted), the ultraviolet morphology (dashed), and the observed infrared emission (solid).

Raw Detector Data - The raw survey detectors from HCON1, HCON2, and HCON3, which offer 1.5' resolution for the in scan direction, have been analyzed to determine the morphology with preliminary data from the GEISHA project. These confirm that the infrared morphology is as long and as wide as indicated by the IRAS survey data, and that the morphology of the infrared emission is that of a filled image with no suggestion of limb brightening, as predicted for ultraviolet heating of the dust.

V. The Mechanical Luminosity of the Shock

The dust heating has been modeled to determine the minimum heating requirements. The ultraviolet radiation field (Hollenbach and McKee) necessary to heat the dust requires shock temperature ~60-90,000 K at the low density end of the flow (2 pc out), falling to ~10-18,000 K within .3 pc of IRS5, with corresponding shock velocities of ~50 km/s and ~20 km/s, the variation presumably due to projection effects of the shock upon the ambient material. The mechanical luminosity is estimated as 40-140 Lo.

VI. The Mechanism Responsible for the L1551 Flow

The infrared luminosity of the L1551 flow is 20-29 Lo and the mechanical luminosity is estimated as 40-140 Lo. Emerson et al. estimate the bolometric luminosity of IRS5 as 38 Lo, and Mundt et al. classify IRS5 as a G-K star. These data indicate that IRS5 may not be energetically capable of providing sufficient energy to radiatively drive the L1551 flow (Draine 1983). A luminosity range of 20-140 Lo over a flow lifetime of 10^4 years implies an energy of >10^(46-47) ergs, two orders of magnitude larger than previous estimates (Snell and Schloerb). Several times 10^48 ergs is released in the collapse of a solar type star to the main sequence, and the model of Draine (1983) easily converts energies of this order via a magnetic bubble which can drive flows. The L1551 infrared parameters place L1551 well within Draine's two asymptotic limits on his figure 7.

VII. Summary

The detection of extended infrared emission from the L1551 flow offers a new technique for probing bipolar flows, and a new method of estimating the energetic requirements of the flows. The infrared luminosity is 20-29 Lo. The dust appears to be heated by ultraviolet radiation from the shock requiring velocities ~50 km/s. The infrared dust emission appears to unveil the ultraviolet halo around the L1551 shock. The shock mechanical luminosity is estimated as 40-140 Lo. Over a 10^4 year lifetime, this presents an energy requirement of 10^(46-47) ergs, two orders of magnitude larger than previous estimates. The magnetic bubble model for the bipolar flow is capable of supplying energies of this magnitude.

Acknowledgements: We acknowledge stimulating discussions with E.E. Becklin.

References

Clark, F.O. and Laureijs, R.J. 1986 A.&A. 154, L26.
Draine, B.T. 1983 Ap.J. 270, 519.
Draine, B.T., Roberge, W.G., and Dalgarno, A. 1983 Ap.J. 264, 485.
Emerson, J.P., Harris, S., Jennings, R.E., Beichman, C.A., Baud, B., Beintema, D.A., Marsden, P.L., and Wesselius, P.R. 1984 Ap.J. Letters 278, L49.
Hollenbach, D. and McKee, C.F. 1979 Ap.J. Suppl. 41, 555.
Mundt, R., Stocke, J., Strom, S.E., and Strom, K.M., and Anderson, E.R. 1985 Ap.J. Letters 297, L41.
Phillips, J.P., White, G.J, Ade, P.A.R., Cunningham, C.T., Richardson, K.J., Robson, E.I., and Watt, G.D. 1982 A.&A. 116, 130.
Richardson, K.J., White, G.J., Avery, L.W., Lesurf, J.C.G., and Harten, R.H. 1985 Ap.J. 290, 637.
Snell, R. 1981 Ap.J. Suppl. 45, 121.
Snell, R. and Schloerb, F.P. 1985 Ap.J. 295, 490.

MECHANISMS FOR THE CIRCULAR POLARIZATION OF ASTROPHYSICAL OH MASERS IN STAR-FORMING REGIONS AND THE INFERRED MAGNETIC FIELDS

Shuji Deguchi[1] and William D. Watson[1,2]
Departments of Physics[1] and Astronomy[2]
University of Illinois at Urbana-Champaign
Urbana, IL 61801

Abstract

Results of further calculations to explore the cause for the circular polarization of astrophysical OH masers in regions of star-formation are presented. New calculations are given for both the non-linear, Zeeman overlap mechanism and the Cook mechanism. The authors previous result that magnetic field strengths of a few milligauss or greater are required still survives.

Introduction

A striking feature of astrophysical masers is the strong, net circular polarization of the OH masers associated with regions of star formation. Linear polarization is also common though not so prominent as the circular which exceeds fifty percent in perhaps half of the masers (see, e.g., Reid and Moran 1981 for a review). One might reasonably suspect that, in addition to gaining an understanding of a widely observed astrophysical phenomenon, a quantitative knowledge of the mechanism might yield valuable information about the structure and physical conditions in the gas in regions of star formation. Although the striking polarization characteristics of these OH masers have been recognized for some twenty years, no cause for the polarization has been established by detailed calculations. The Cook mechanism (Cook 1966), which depends upon the accidental matching of the gradients of the velocity and the magnetic field, has been a possibility. The widespread occurence of the necessary correlations in the magnetic and velocity fields would seem to be surprising, however. We (Deguchi and Watson 1986) have recently recognized an entirely new physical mechanism -- the non-linear effects of the overlap of Zeeman components caused by a velocity gradient -- and have obtained a quantitative formulation utilizing the Sobolev approximation. In the presentation at this meeting, we extend our exploration of the polarization properties of OH masers by presenting additional results for the Zeeman overlap mechanism and results from an initial formulation of the Cook mechanism, also utilizing the Sobolev approximation. Calculations are performed for an angular momentum J=1-0 transition which is expected to be representative.

Non-Linear Effects in the Overlap of Zeeman Components

In this section, we augment our previous study (Deguchi and Watson 1986) by presenting results in Figure 1 for the two linear Stokes components Q and U as a function of the strength of the magnetic field. A description of the calculations is contained in our previous paper. The calculations of Figure 1 suggest a tendency at $\Delta v_Z \gtrsim 1$ for the circular polarization V to exceed the

Carol J. Lonsdale Persson (Editor)
Star Formation in Galaxies

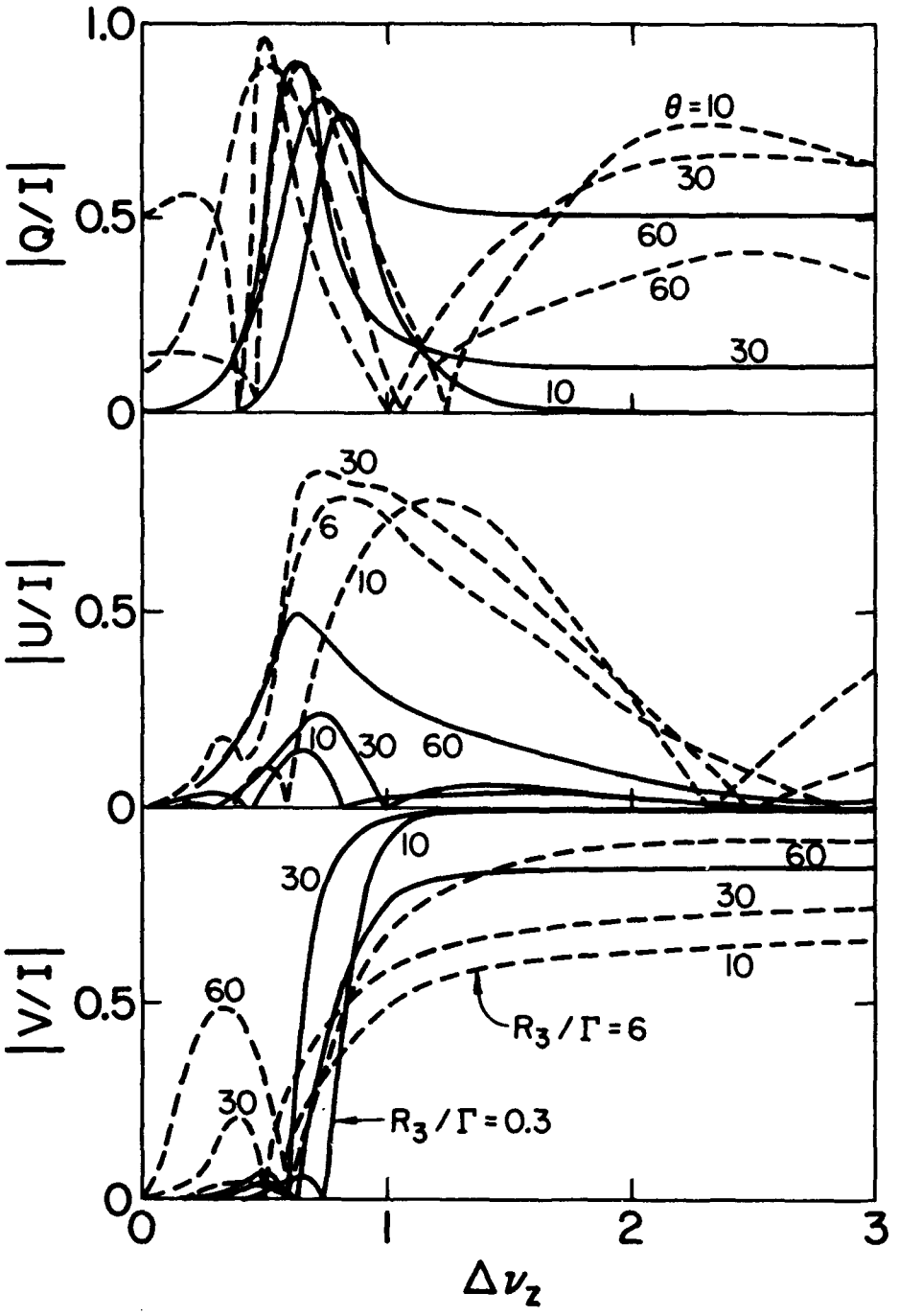

Figure 1. Ratios of the Stokes parameters Q, U and V to the intensity I as a function of the ratio $\Delta\nu_z$ of the Zeeman splitting to the local breadth of the spectral line. The angle between the magnetic field and the axis for the velocities is designated by θ. Solid and dashed lines give the degree of saturation R_3/Γ for the most saturated transition of the Zeeman triplet.

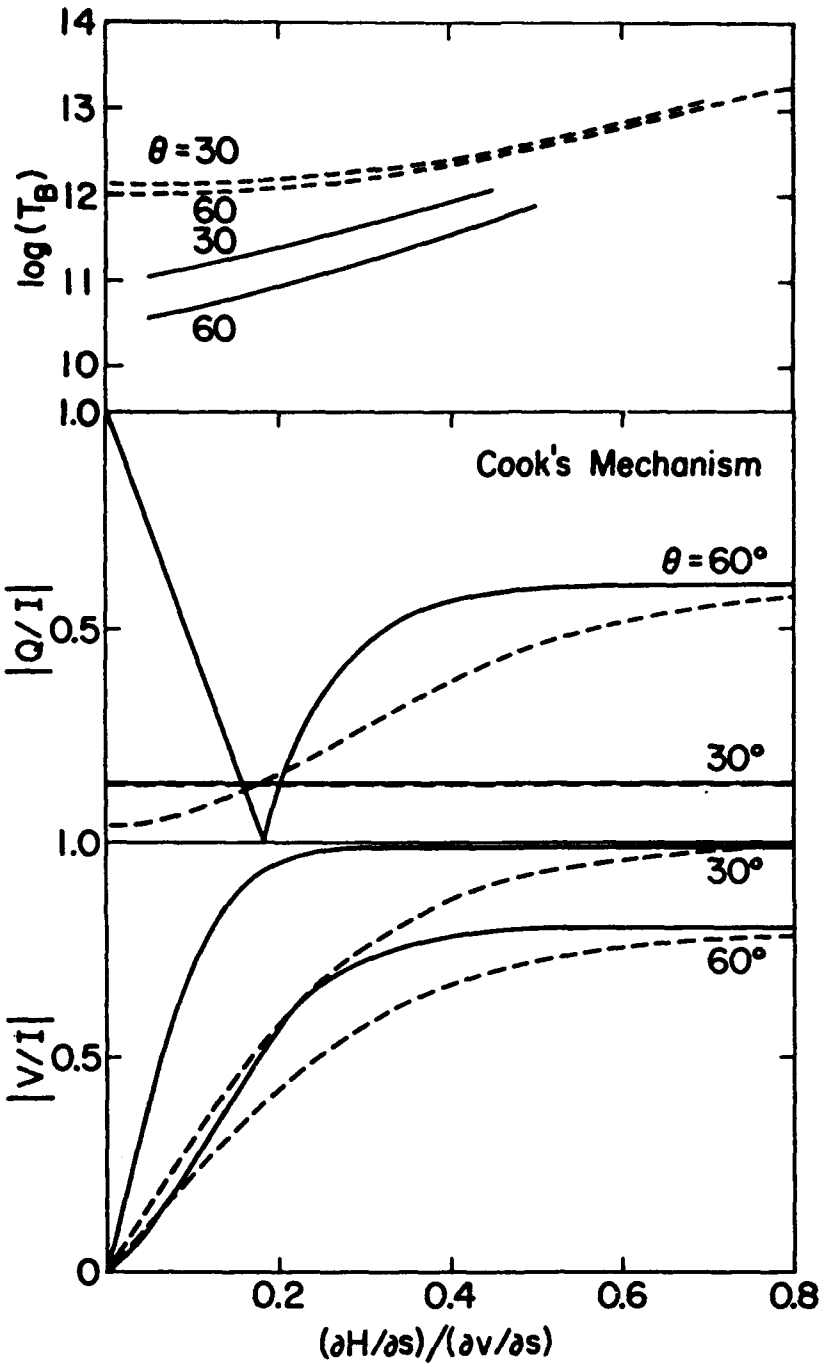

Figure 2. Calculations for the Stokes parameters and for the brightness temperature T_B (in Kelvins) viewed along the velocity axis. Quantities are given as a function of the ratio of the spatial derivatives, along the velocity axis, of the magnetic field and of the velocity in units of $(cg\mu_m/h\nu_o)$. Here, g is the Landé g-factor, μ_m the Bohr magneton and ν_o is the rest frequency for the transition. The dashed and solid lines represent different pump rates; they give the same (R_3/Γ) as in Figure 1 for $(\partial H/\partial s)/(\partial v/\partial s) = 0$. All three lines are summed to produce this Figure.

strength of the linear components Q and U -- a result that is in harmony with the observations of OH masers. This seems to be especially the case for the lower degree of saturation (R_3/Γ). Of course, the chief new information derived from the association of this mechanism with the observations is a measure of the strength of the magnetic field which is based on the requirement from Figure 1 that $\Delta v_Z \gtrsim 1$ to obtain large fractional polarizations. For the parameters of the OH masers, this implies magnetic fields of a few milligauss or stronger in these condensations in the gas in star-forming regions.

Evaluation of the Cook Mechanism

To our knowledge, the Cook mechanism for the circular polarization has not been evaluated quantitatively -- that is, transfer equations for the maser radiation have not previously been solved to exhibit the effect. In Figure 2, we present the results of such calculations, again utilizing the Sobolev approximation as described in Deguchi and Watson (1986). A qualification is necessary. The ideal matching of the gradients of the magnetic field and of the velocity corresponds to $(\partial H/\partial s)/(\partial v/\partial s) = 1$ in our units. The Sobolev approximation can not be used at exactly this value because the spectral line is not shifted out of the local, resonance profile by the gradients. In our calculation, the three components of the J=1-0 Zeeman triplet are considered to be so widely separated that they never overlap.

The calculations thus tend to support the idea that the Cook mechanism can be operative at the necessary maser power, given the proper correlations between the gradients of the velocity and magnetic field. What is perhaps surprising is its effectiveness over a wide range (not completely delineated here) of values for the ratio of the relevant gradients. This tends to improve the statistical likelihood for its occurence. However, the Cook mechanism (just as the Zeeman overlap mechanism) requires that the Zeeman splitting be comparable with or greater than the local breadth of the spectral lines; that is, $\Delta v_Z \gtrsim 1$ from Figure 1 and the limits of at least a few milligauss for the magnetic fields still hold (cf. Cook 1975).

The authors' research has been supported by the National Science Foundation.

References

Cook, A. H., 1966, Nature, 211, 503.

Cook, A. H., 1975, MNRAS, 171, 605.

Deguchi, S., and Watson, W. D., 1986, Ap. J. (Letters), 300, L15.

Reid, M. J. and Moran, J. M., 1981, Ann. Rev. Astr. Ap., 19, 231

DIFFUSE EMISSION

SURVEY OF THE GALACTIC DISC FROM l = -150° TO l = 82° IN THE SUBMILLIMETER RANGE

Emmanuel CAUX and Guy SERRA
C.E.S.R. - CNRS/UPS BP 4346
31029 TOULOUSE CEDEX FRANCE

Abstract

We present new results about the emission of the galactic disc from l=-150° to l=82°in the submm range (λ_{eff}=380μm). Observations have been made with the AGLAE83 balloon-borne instrument launched from Brazil in November 1983. In-flight calibration of the instrument was made on Jupiter. The longitude profile obtained exhibits diffuse emission all along the disc with bright peaks associated with resolved sources. The averaged galactic spectrum is in agreement with a temperature distribution of the interstellar cold dust.

1 Introduction

The FIR emission of the Galaxy is produced by thermal radiation of dust grains mixed with the interstellar gas and heated by the stellar radiation field. Actually, most of the power radiated by stars in the inner Galaxy is converted into FIR radiation. The galactic emission in the FIR range is mostly dominated by temperature effects. Thus, observations in the submillimeter (submm) range are necessary to assess more accurately the average spectrum of the diffuse galactic emission. We report in this paper the first almost complete survey of the galactic disc (from l=-150° to l=82°) in the submm range (λ_{eff} = 380μm) performed with the AGLAE balloon-borne intrument, modified to include a new submm channel. The FIR channel (λ_{eff} = 145μm) of the previous AGLAE flights was kept.

2 Instrumentation and observational procedure

The AGLAE83 experiment is a new configuration of the balloon-borne AGLAE intrument which has been launched four times and has mapped the galactic emission in the FIR range (Serra et al., 1978, 1979; Boissé et al., 1981; Gispert et al., 1982, Caux et al., 1984, 1985). The detectors (composite bolometers) and filters are located on the cold plate of a ^{4}He cryostat operating at a temperature lower than 1.5K (natural pumping at balloon altitude, p < 4mb). The detectors' output signals are amplified by low noise preamplifiers located on the wall of the cryostat. The sampling and 12 bit digitization was performed on board. The whole gondola was continuously rotating at a constant angular velocity of about 2RPM. In order to cover large wings on both sides of the galactic plane, and to provide good zero level for the absolute reference of the emission, a 360° azimuthal rotation on the sky of the experiment beams was adopted. The knowledge of the direction viewed by the telescopes was obtained 32 times per turn with a monitoring magnetometer locked onto the earth's magnetic field. The digitized scientific and housekeeping data were then transmitted to the ground in real time by PCM telemetry.

Carol J. Lonsdale Persson (Editor)
Star Formation in Galaxies

The observations presented in this paper were obtained during a twelve hour flight of the instrument launched from Sao Manuel (Brazil) on November 1st, 1983 at 0630 UT. The observational procedure allowed the coverage of the galactic plane from -150° to 82°, measurements of the sources close to the disc, and the observation of the fluxes from Venus and Jupiter in both wavelength channels. The photometric calibration was based on Jupiter (assuming a blackbody spectrum of T=125K, Wright, 1976). For the submm channel, the results obtained are in agreement to within 20% with the laboratory calibration using extended sources (blackbodies) filling the beam. For the submm channel, the rms fluctuation remaining after signal processing can be estimated, in most parts of the profile, at $\lambda I_\lambda = 3\ 10^{-7}\ W.m^{-2}.sr^{-1}$.

Table 1: Instrument Characteristics

Primary mirror diameter:	140mm	Beam diameter: 0.4°
Scanning velocity:	$12°s^{-1}$	
Bolometer N.E.P.:	$2\ 10^{-14}\ W.Hz^{-1/2}$	
Submm channel:	$\lambda_{eff} = 380\mu m$	$\Delta\lambda_{eff} = 150\mu m$
FIR channel :	$\lambda_{eff} = 145\mu m$	$\Delta\lambda_{eff} = 40\mu m$

3 Results and discussion

The results are presented as a profile of the submm brightness of the galactic disc (averaged over $|b| < 1.25°$), displayed as a function of the galactic longitude between l=-150° and l=82° in Figure 1. They are averaged in 1° longitude bins from -105° to 82° and in 5° bins from -150° to -105°.

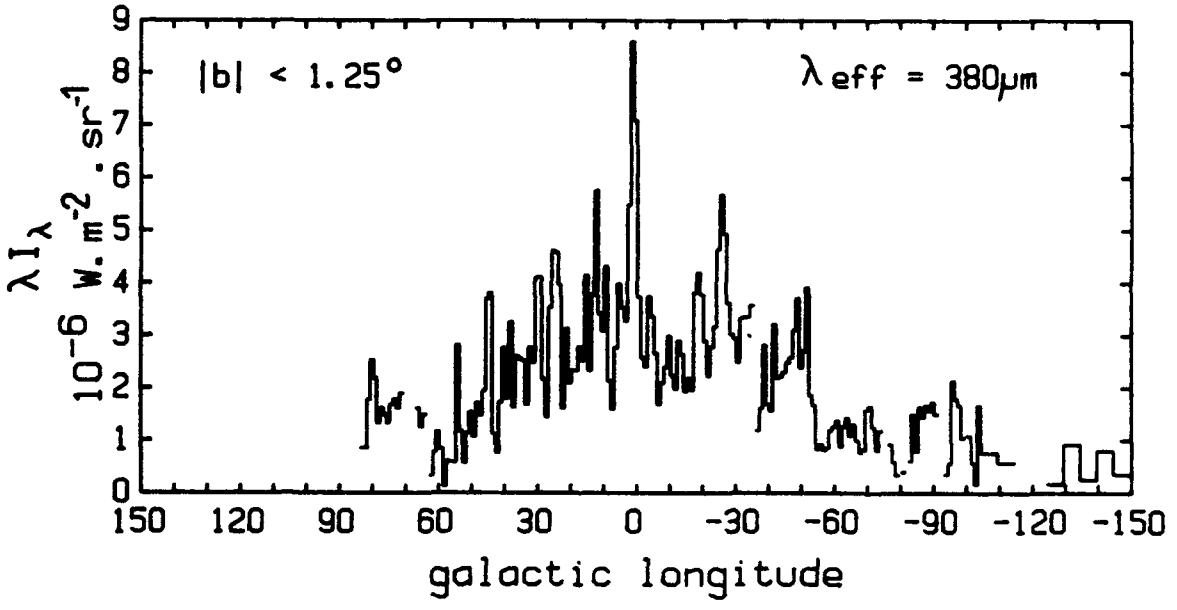

Figure 1. Longitude profile of the averaged submm brightness of the galactic disc.

This submm profile reveals, as in the FIR, a diffuse emission all along the

galactic disc and the presence of resolved bright sources. Most of them are related to FIR sources associated with HII region and molecular cloud complexes. Emission peaks in the tangential direction of spiral arms are very apparent in the submm, as they were in the FIR profile (Caux et al., 1984). The FIR profile displays more contrast than the submm one, as would be expected because of the steeper dependence on temperature of the FIR intensity. The longitude profile (averaged over 1°x2.5° bins) of a color index defined as the ratio of the fluxes measured in the two channels (145μm/380μm) and expressed in terms of λI_λ is displayed in Figure 2. No obvious large scale galactic effects are apparent in the longitude interval $-80° < l < 60°$, and the mean value of this ratio is the same for positive longitudes as for negative longitudes.

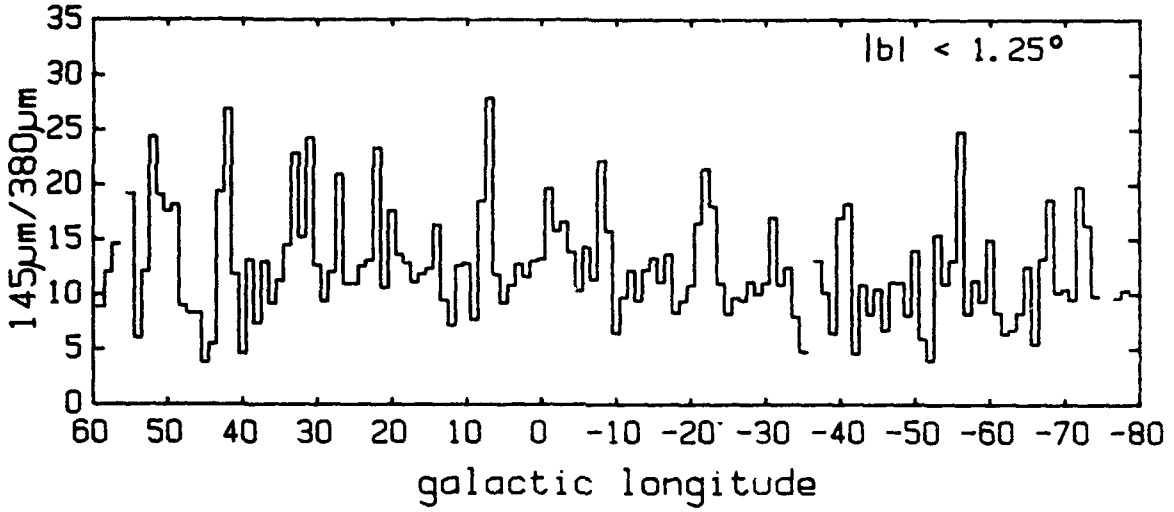

Figure 2. Longitude profile of the averaged ratio 145μm/380μm. The right scale shows the equivalent temperature (computed assuming a blackbody spectrum modified by a λ^{-2} emissivity law) corresponding to the 145μm/380μm ratio values.

The local apparent variations of this ratio are associated with bright sources and reflect temperature effects. Our submm channel records the emission by dust at about 10-30K while the emission in the FIR channel is dominated by dust with temperatures ranging from 15K to 45K (see Figure 5 in Pajot et al., 1986b). Thus the peaks of the 145μm/380μm ratio are related to sources of warm dust. The average value of the color index in the longitude interval $-80° < l < 70°$ is about 12 and leads to a typical dust temperature of 20K, assuming a blackbody spectrum modified by a λ^{-2} emissivity law. This temperature is only indicative. In fact, it can be seen on Figures 3a and 3b that the spectra of the inner Galaxy and galactic center respectively, are characteristic of a temperature distribution in the 100μm-1mm range.

For all points plotted on these spectra, the emission is averaged in the same way and reflects all the emission of the given region. Assuming a blackbody spectrum modified by a λ^{-2} emissivity law, we have computed the variation with temperature of the ratios (in λI_λ) for each pair of effective wavelengths used in the FIR and submm ranges to plot the spectra of Figure 3a and 3b. The ratios obtained with the measured fluxes in the average galactic spectrum correspond to typical dust temperatures given in Table 2. Note that the different typical temperatures displayed in Table 2 reflect a true distribution of the interstellar

dust temperature, and not only uncertainties in the determination of galactic fluxes at a given wavelength: an error of ± 20% in the 145μm/380μm ratio or the 60μm/100μm ratio leads to a temperature variation of only ± 1K.

Table 2: typical temperatures deduced from the spectrum of the inner Galaxy

wavelengths	60/100	60/145	100/145	60/380	100/380	145/380
ratios	0.42	0.51	1.22	6.1	14.6	12
T (K)	24	24	23	22	21	20

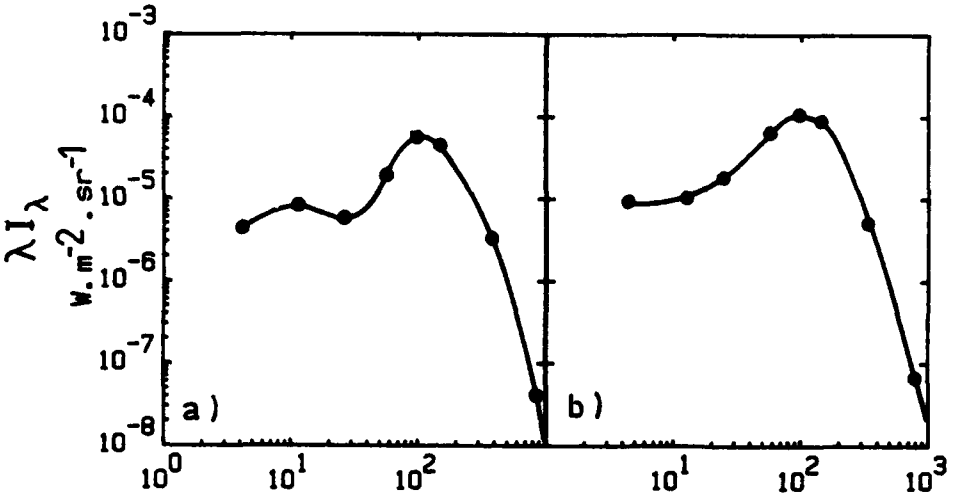

Figure 3a and 3b. Spectra of the averaged inner galactic emission, 3°<l<33°, |b|< 1.25° (3a) and galactic center region, |l|< 1.5°, |b|< 1.25° (3b). Data points on the two spectra are from: Pajot et al., 1986: 900μm, this work: 380μm and 145μm, IRAS data corrected for the zodiacal light emission (Caux et al., in preparation): 100μm, 60μm, 25μm and 12μm, Price, 1981: 4.4μm.

4 References

Boissé, P., Gispert, R., Coron, N., Wijnbergen, J.J., Serra, G., Ryter, C., Puget, J.L.: 1981, Astr. Ap. 94, 265

Caux, E., Serra, G., Gispert, R., Puget, J.L., Ryter, C., Coron, N.: 1984, Astr. Ap. 137, 1

Caux, E., Puget, J.L., Serra, G., Gispert, R., Ryter, C.: 1985, Astr. Ap. 144, 37

Caux, E., Chambon G.: 1986, in preparation

Gispert, R., Puget, J.L., Serra, G.: 1982, Astr. Ap. 106, 293

Pajot, F., Gispert, R., Lamarre, J.M., Peyturaux, R., Puget, J.L., Serra, G., Coron, N., Dambier, G., Leblanc, J., Moalic, J.P., Renault, J.C., Vitry, R.: 1986a, Astr. Ap. 154, 55

Pajot, F., Boissé, P., Gispert, R., Lamarre, J.M., Puget, J.L., Serra, G.: 1986b, Astr. Ap. 157, 393

Price, S.D.: 1981, A. J. 86, 193

Serra, G., Puget, J.L., Ryter, C., Wijnbergen, J.J.: 1978, Ap. J. 222, L21

Serra, G., Boissé, P., Gispert, R., Wijnbergen, J. , Ryter, C., Puget, J.L.: 1979, Astr. Ap. 76, 259

Wright, E.L.: 1976, Ap. J., 210, 250

DIFFUSE INFRARED EMISSION OF THE GALAXY: LARGE SCALE PROPERTIES

M. Pérault, F. Boulanger, E. Falgarone and J.L. Puget.
Radioastronomie, ENS, 24 rue Lhomond, 75231 Paris Cedex 05.
IPAC, Caltech 100-22, Pasadena CA 91125.

The IRAS survey is used to study large scale properties and the origin of the diffuse emission of the Galaxy. A careful subtraction of the zodiacal light enables us to present longitude profiles of the galactic emission at 12, 25, 60 and 100 μm.

1. About 2/3 of the power radiated in the 100 μm band comes from the diffuse medium (atomic, molecular and ionized components), the other 1/3 coming from well identified luminous sources (complexes of giant molecular clouds (GMC) and HII regions). The sources have a much lower 12μm/25μm and a much higher 60μm/100μm emission ratio than the diffuse component, giving a very striking anticorrelation in the colour-colour diagrams. The emission from the sources will not be further discussed here.

2. The diffuse radiation observed at 12 and 25 μm represents a large fraction of the far-infrared emission. The absence of any strong colour gradient across the Galaxy implies that most of the emission up to 60 μm is produced by small particles through temperature fluctuations.

3. The large scale galactic structure is clearly seen at b=1°, and even much higher. The dust producing the strong emission excess for longitudes smaller than 30° at b=1° is located about 150pc above or below the galactic plane, a height where the gas is mostly atomic hydrogen. The clear difference in gas scale height between the narrower molecular component and the broader atomic (and partially ionized) component is used to determine the contribution of each of these two components to the diffuse emission. Using an axisymmetric assumption for the infrared production rate, and taking optical depth effects into account, we simultaneously invert the diffuse infrared longitude profiles (successively for each of the 4 bands) at b=0° and b=1°.

4. At all radii in the Galaxy the diffuse emission is dominated by the broad atomic component. In the "molecular ring" half of the 100μm emission is produced by this broad component, half by the sum of the cool molecular component and the bright sources.
In the solar neighbourhood the dust infrared emission per H atom is 4 times larger in the atomic gas than in the quiet molecular clouds. For atomic gas this emissivity is 6 to 8 times larger in the "molecular ring" than in the solar neighbourhood. These numbers imply that dust in molecular clouds is efficiently shielded from the external radiation, and that a significant part of the luminosity of O and B stars is absorbed in the atomic component. The emissivity in this widespread component measures the interstellar radiation field energy density (with strong weight in the ultra-violet), which increases almost by a factor of 10 between the solar neighbourhood and the "molecular ring".

A paper is in preparation, and will be submitted to Astronomy and Astrophysics.

THE LARGE SCALE GAS AND DUST DISTRIBUTION IN THE GALAXY: IMPLICATIONS FOR STAR FORMATION

T.J. Sodroski[1,2], E. Dwek[1], M.G. Hauser[1], F.J. Kerr[2]
[1]NASA/Goddard Space Flight Center
[2]University of Maryland

ABSTRACT

We present IRAS observations of the diffuse infrared (IR) emission from the galactic plane at wavelengths of 60 and 100 μm and derive the total far infrared intensity and its longitudinal variation in the disk. Using available CO, 5 GHz radio-continuum, and HI data, we derive the IR luminosity per hydrogen mass, and the infrared excess (IRE) ratio in the Galaxy.

We linearly decompose the longitudinal profiles of the 60 and 100 μm emission into three components that are associated with the molecular (H_2), neutral (HI), and ionized (HII) phases in the interstellar medium (ISM), and derive the relevant dust properties (ie. temperature, IR luminosity per hydrogen mass, total IR luminosity) in each phase. Implications of our findings for various models of the diffuse IR emission and for star formation in the galactic disk are discussed.

I MORPHOLOGY OF THE FIR EMISSION FROM THE GALACTIC PLANE

Figures 1(a) and 1(b) show the longitudinal profiles of the observed 60 and 100 μm galactic plane emission, from which the contribution of the zodiacal emission was subtracted using the empirical model of Boulanger (1986). The profiles represent average intensities over the latitude interval $|b| < 0.^{\circ}25$ in longitude increments of $0.^{\circ}5$. As seen in Figure 1, the far infrared (FIR) emission originates primarily from within the solar circle. Most of the discrete sources are in the direction of, and likely associated with, known HII region/molecular cloud complexes. Figure 1(c) is a profile of the total IR intensity, integrated over all wavelengths, assuming the dust at a given longitude emits at the corresponding line-of-sight temperature, with an emissivity index of n = 2. The mean value of the total IR intensity in W m^{-2} sr^{-1} is 4 x 10^{-5} over the longitude range $l = 270^{\circ}$ to 90° and 2 x 10^{-5} over the entire Galaxy (Note: The $0.^{\circ}5$ position error in the original Zodiacal History File data has been corrected).

II COMPARISON WITH CO, HI, AND 5 GHZ SURVEYS

1) Correlation of Mean Intensity Profiles

We have compared Figure 1(c) with longitudinal profiles of the velocity-integrated ^{12}CO and HI emission, and 5 GHz radio-continuum emission from the galactic plane, all profiles representing the mean intensity over $-0.^{\circ}25$ to $0.^{\circ}25$ in latitude. The data used to derive the profiles comprise the galactic plane surveys of ^{12}CO from the Goddard Institute of Space Studies (GISS), the

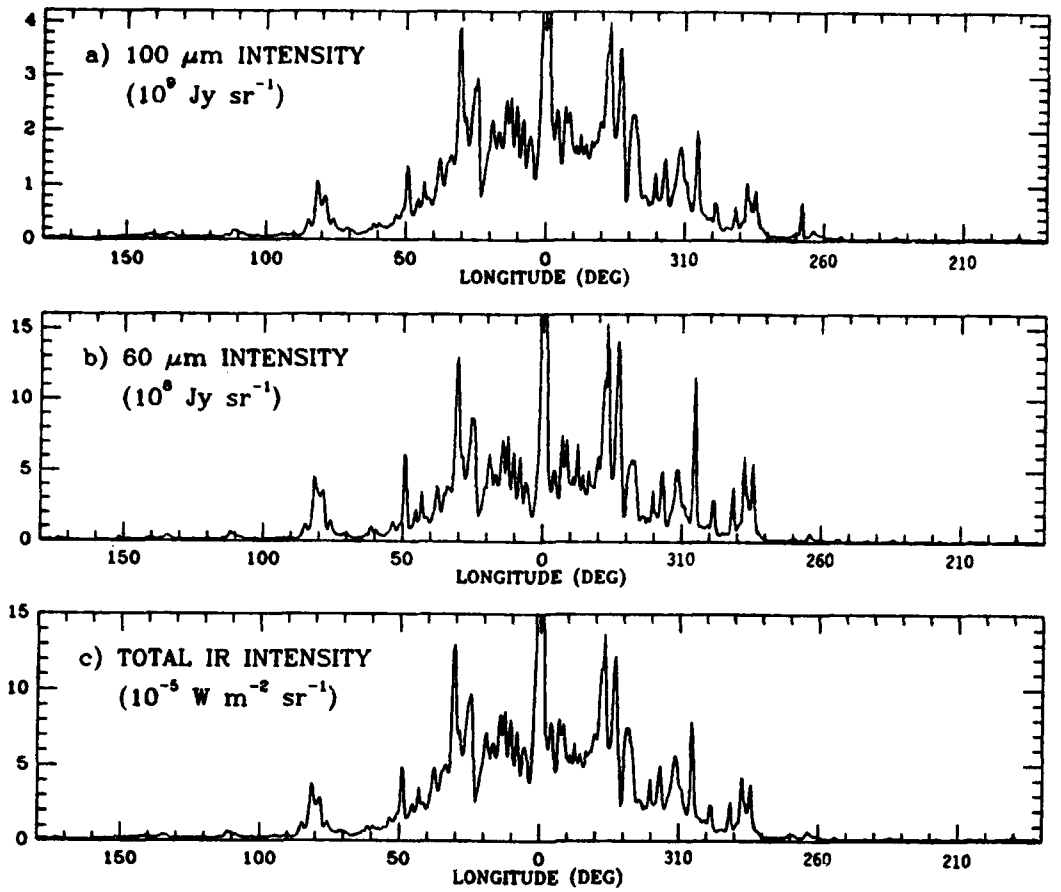

Figure 1. (a) and (b) Longitudinal profiles of the galactic plane emission as observed by IRAS and corrected for the zodiacal emission. (c) Profile of the total IR intensity.

Berkeley (Weaver and Williams 1974) and Parkes (Kerr et al 1986) galactic plane surveys of neutral atomic hydrogen, and the Haynes-Caswell (1979) galactic plane survey of the 5 GHz radio-continuum. The longitudinal variation of the total IR intensity closely correlates with both the CO and 5 GHz continuum emission, which originate from regions associated with the younger galactic populations (i.e. molecular cloud complexes, extended low density (ELD) HII regions), primarily located in the vicinity of spiral arms.

ii) The Infrared Luminosity Per Hydrogen Mass, and Infrared Excess (IRE) Ratio

The total hydrogen column density along a given line-of-sight can be derived from the velocity-integrated ^{12}CO and HI intensities. It can be used together with the total IR intensity to calculate the infrared luminosity per hydrogen mass, L_{IR}^{H} . The longitudinal profile of L_{IR}^{H} is plotted in Figure 2(a) in units of $L_{\odot}/M_{\odot}$. Many of the peak values shown in the figure lie in the directions of spiral arms. The mean value of L_{IR}^{H} over the entire range of longitudes is ~ 3 $L_{\odot}/M_{\odot}$, a value similar to that in clouds heated only by the interstellar radiation field (Weiland et al 1986).

The infrared excess ratio, defined as the IR-to-Lyα luminosity ratio, is plotted in Figure 2(b). The IRE ratio is relatively constant with longitude,

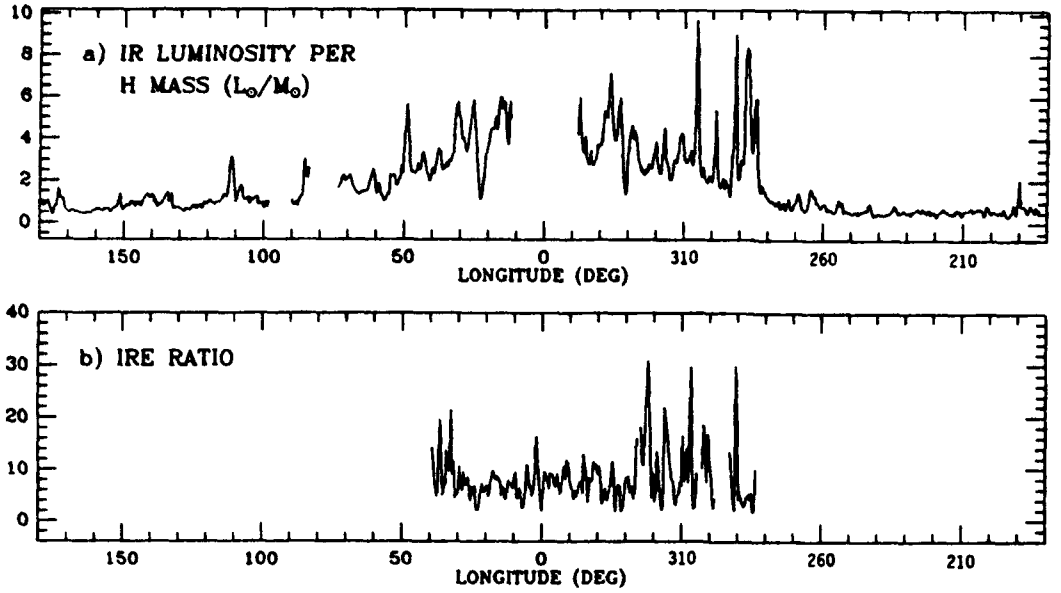

Figure 2. (a) Galactic longitude profile of the infrared luminosity per hydrogen mass. The mean value is ~ 3 $L_\odot/M_\odot$. (b) The IRE ratio.

suggesting that the stellar initial mass function (IMF) is largely unchanged throughout the inner Galaxy. This observed behavior contradicts the claim of Gispert et al (1982) that there exists a marked increase of the IMF with decreasing galactocentric radius, and, as must follow, that the inner galaxy is deficient in producing OB stars relative to the solar vicinity. The mean value of IRE is ~ 6 , and implies that known (instead of embedded) OB stars can provide a large fraction of the radiation needed to heat the dust that is responsible for the diffuse IR emission.

III A NEW APPROACH: A LINEAR DECOMPOSITION OF THE IR INTENSITY INTO ITS GAS PHASE CONTRIBUTIONS

We have linearly decomposed the IRAS data into three emission components associated with the most massive gas phases (H_2 , HI, and HII) in the ISM as follows. We assumed a constant gas-to-dust mass ratio and grain temperature in each of the three phases. Then, at every longitude l, the observed intensity in an IRAS band i(=1,2) is given by the linear combination of the dust emissivity per unit gas mass, e_{ij} , in each gas component j(=1,2,3), multiplied by the column density of that component. In order to obtain the column density of the ionized gas we assumed a gas density of 10 cm^{-3} in the ELD HII regions. The best fit to the flux in each band was found by adjusting the e_{ij}'s. A statistical analysis of our decomposition algorithm has confirmed that the parameters of the three components are linearly independent. The resulting e_{ij}'s were used together with an adopted emissivity index of n = 2 to obtain the dust temperature, the total IR intensity, the IR luminosity per hydrogen mass, and the gas-to-dust mass ratio in each gas phase component. Our results are summarized in Table 1.

TABLE 1: DERIVED DUST QUANTITIES IN THE VARIOUS ISM PHASES

Gas Phase	Dust Temp (K)	Gas-to-Dust Mass Ratio	FIR Luminosity per H Mass ($L_\odot/M_\odot$)	%Contribution 60 μm	100 μm	Total FIR	Total Mass ($M_\odot$)	Total Luminosity ($L_\odot$)
H_2	20	190	2.3	20	40	40	2.0×10^9 [a]	4.6×10^9
HI	24	270	2.8	30	33	30	2.6×10^9 [b]	7.3×10^9
HII	31	190	28.0	50	27	30	3.7×10^7 [c]	1.0×10^9
Mass-averaged Values		200	3.8					

References: (a)Cohen (1978); (b)Baker and Burton (1975); (c)Mezger (1978)

SUMMARY

We have calculated the contribution of the H_2 , HI, and HII regions to the galactic 60 and 100 μm emission. The major results of our calculations are listed in Table 1 and can be summarized as follows.

1) The molecular, neutral atomic, and ionized gas components contribute about equally to the total IR intensity. The total IR luminosity of the Galaxy is about 1.3×10^{10} $L_\odot$, with 35, 55, and 10 percent from H_2 , HI, and HII regions respectively.

2) The IR luminosity per hydrogen mass is ~ 2 - 3 for the H_2 and HI components, comparable to that of interstellar clouds heated by the interstellar radiation field alone. Therefore, molecular and HI clouds typically do not seem to have highly luminous, embedded heating sources.

3) The IRE ratio is ~ 6, implying that known OB stars can provide a large fraction of the energy needed to heat the dust. Its constancy with longitude implies that the stellar IMF does not vary significantly in the disk.

References:
Baker, P.L., and Burton, W.B., 1975, Ap. J., 198, 281
Boulanger, F., 1986, private communication
Cohen, R.S., 1978, Ph.D. thesis, Columbia University, (NASA TM 78071)
Gispert, R., Puget, J., and Serra, G., 1982, Astr. Ap., 106, 293
Haynes, R.F., Caswell, J.L., Simons, L.V.J., 1979, Austr. J. Phys., Astrophys. Suppl., 48, 1
Kerr, F.J., Bowers, P.F., Kerr, M., Jackson, P.D., 1986, Astr. Ap., Suppl. Ser., (in press)
Mezger, P.G., 1978, Astr. Ap., 70, 565
Weaver, H., Williams, D.R.W., 1974, Astr. Ap., Suppl. Ser., 8
Weiland, J.L., Blitz, L., Dwek, E., Hauser, M.G., Magnani, L., and Rickard, L.J., 1986, Ap. J., 306, L101

A Correlation Between the IRAS Infrared Cirrus at 60 or 100 μm and Neutral Atomic Hydrogen in the Outer Galaxy

Susan Terebey
High Altitude Observatory
NCAR, PO Box 3000, Boulder CO 80307

Michel Fich
Astronomy Department
University of Washington, Seattle WA 98195

ABSTRACT

We find a linear correlation between the infrared cirrus at 100 or 60 μm and neutral atomic hydrogen near the galactic plane. IRAS Sky Brightness images were compared to the 0.5° resolution Weaver-Williams HI survey in two regions of the outer Galaxy near l= 125° and l=215°. The dust temperature inferred is nearly uniform and in reasonable agreement with theoretical predictions of thermal dust emission.

INTRODUCTION

The IRAS Satellite Survey has given us a wealth of information on the diffuse galactic infrared emission, strongest in the 100 μm band, which has become known as the infrared cirrus (Low et al. 1984). Boulanger, Baud, and van Albada (1985) have found a correlation between the 100 μm cirrus and several high latitude HI clouds. Weiland et al. (1986) have found an association between the cirrus and several high latitude molecular clouds.

We discuss the properties of the infrared cirrus, and the physical conditions necessary for the observed emission. A more extensive discussion of the data can be found in Terebey and Fich (1986).

DATA

The two IRAS image fields are from the original release of the third HCON Sky Brightness Survey with central positions at (1.6h,60°) and (7.0h,0°) and linear extents of 16.5°. We smoothed the IRAS data to 0.5° resolution and subtracted a smooth zodiacal background from both the 60 and 100 μm data.

The HI data (Weaver and Williams 1973) have an angular resolution of 0.5° and galactic latitude range (-10°,10°). We constructed integrated brightness temperature maps from the HI data, then converted to neutral hydrogen column density assuming optical depth much less than one.

RESULTS

The 60 μm data show a linear correlation with the 100 μm data. Least squares derived values for the slope give 0.207 $\pm$ 0.022 and 0.205 $\pm$ 0.026 for the l = 125° and l = 215° fields, respectively. The small scatter in the correlation implies that the physical conditions leading to the infrared emission are very uniform in the outer Galaxy.

Carol J. Lonsdale Persson (Editor)
Star Formation in Galaxies

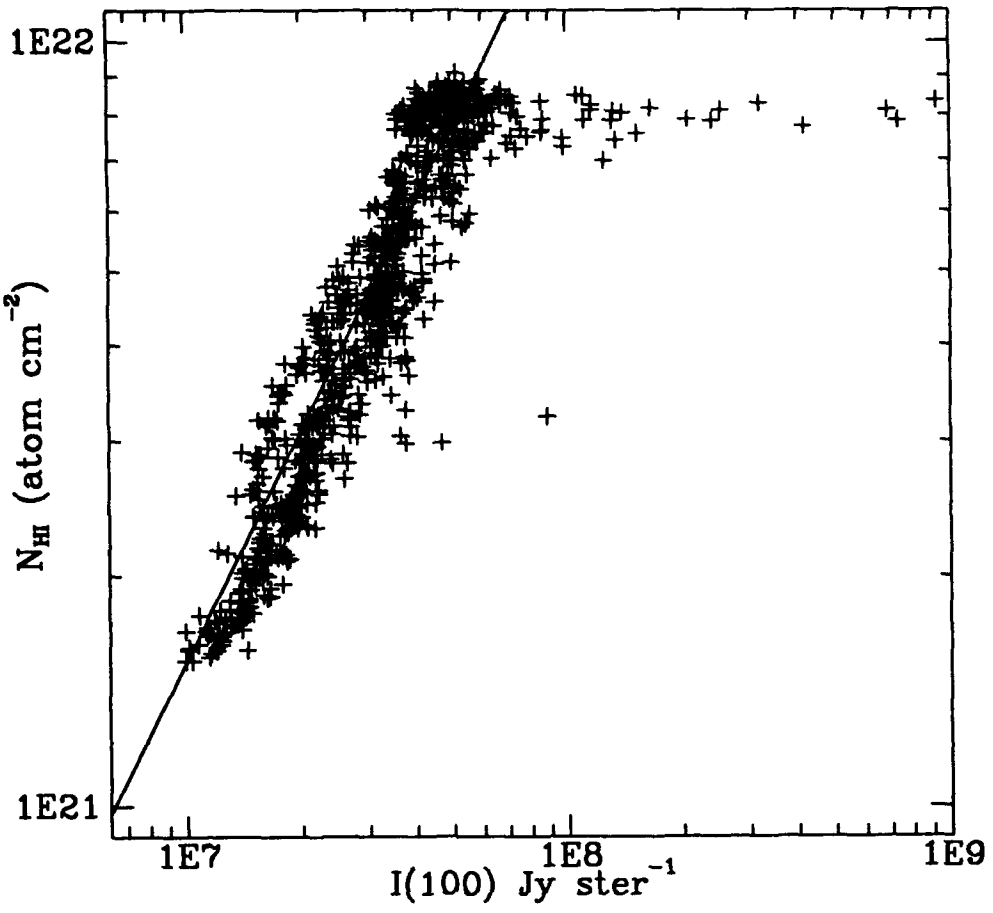

Figure 1. The HI column density is plotted against the IRAS 100 μm intensity in the $l = 125^\circ$ field. Contamination by non-cirrus infrared sources produces the high intensity 100 μm points that don't follow the correlation. Solid line shows a least squares fit to the data (excluding non-cirrus sources).

If the infrared emission is due to thermal emission from dust grains, then galactic properties such as the dust to gas ratio and the interstellar radiation field are relatively uniform in these regions. The infrared emissivity is a strong function of dust temperature. If the dust temperature is uniform then we might expect a linear relationship between the infrared intensity, which would be proportional to dust column density, and the gas column density. In the outer Galaxy the interstellar medium is predominantly neutral atomic hydrogen suggesting there should be a correlation between HI and the infrared cirrus.

Figure 1 shows there is a strong linear correlation between the 100 μm intensity and HI column density. A least squares fit gives slopes of $6.4 \pm 1.1\ 10^{-15}$ and $4.2 \pm 0.8\ 10^{-15}$ Jy ster^{-1}/ HI atom cm^{-2} in the $l = 125^\circ$ and $l = 215^\circ$ fields, respectively. This can be compared with the value of $1.4 \pm 0.3\ 10^{-14}$ found by Boulanger, Baud, and van Albada (1985) for several high latitude HI clouds.

Assuming the emission is thermal emission from dust grains then the ratio of the 100 μm intensity to HI column density can be used to calculate the characteristic dust temperature. Following Hildebrand (1983) and using for illustrative purposes a dust opacity proportional to $\lambda^{-1.5}$ gives a dust temperature of 16.7 and 15.9 K for the $l = 125^\circ$ and $l = 215^\circ$ fields, respectively. These results are in reasonable agreement with average dust temperatures predicted by models of thermal dust emission from dust grains (de Muizon and Rouan 1985, Draine and Anderson 1985).

REFERENCES

Boulanger, F., Baud, B. and van Albada, G. D. 1985, *Astr. Ap.*, **144**, L9.
de Muizon, M. and Rouan, D. 1985, *Astr. Ap.*, **143**, 160.
Draine, B. T. and Anderson, N. 1985, *Ap. J.*, **292**, 494.
Hildebrand, R. H. 1983, *Q.J.R.A.S.*, **24**, 267.
Low, F. J. et al. 1984, *Ap. J. Letters*, **278**, L19.
Terebey, S., and Fich, M. 1986, submitted to *Ap. J. Letters*.
Weiland, J. L., Blitz, L., Dwek, E., Hauser, M. G., Magnani, L. and Rickard, L. J. 1986, Ap. J., 306, L101.
Weaver, H. and Williams, D. R. 1973, *Astr. Ap. Suppl.*, **8**, 1.

THE ARP RING : GALACTIC OR EXTRAGALACTIC ?

J.A. ABOLINS
RUTHERFORD APPLETON LABORATORY
CHILTON, DIDCOT, OXFORDSHIRE, U.K.

W.L. RICE
IPAC, CALTECH
PASADENA, CA., U.S.A

ABSTRACT

The Arp Ring is a faint, loop-like structure around the northern end of M81 which becomes apparent only on deep optical photographs of the galaxy. The nature of the Ring and its proximity to M81 are uncertain. Is it simply foreground structure - part of our own galaxy, or is it within the M81 system ? IRAS maps of the region show a far-infrared counterpart of the Ring. The new infrared data are compared with previous optical and radio observations to try to ascertain its physical nature. The poor correlation found between the common infrared/optical structure and the distribution of extragalactic neutral hydrogen, and the fact that its infrared properties are indistinguishable from those of nearby galactic cirrus, imply that the Arp Ring is simply a ring structure in the galactic cirrus.

INTRODUCTION

Deep optical pictures of M81 taken by Arp (1965) showed a faint and fascinating loop-like structure around the northern end of the galaxy. Arp originally considered the feature to be associated with M81, i.e. extragalactic, and interpreted it as a manifestation of an electromagnetic interaction between electrons from M82 (then assumed to be exploding) and the magnetic field of M81. Gottesman and Weliachew (1975) considered the Ring to be the optical counterpart of the satellite neutral hydrogen they found around M81. However, more recent deep plates by Sandage (1976) revealed widespread, low-level diffuse optical emission throughout much of the region of sky about M81. IRAS extended emission maps (IRAS Explanatory Supplement) of the area show a good correlation between much of the diffuse optical emission and the infrared "cirrus" (Low et al, 1984) thought to be local to our galaxy. The Arp Ring could now be seen as simply a fortuitous alignment of a cirrus loop in the foreground of M81. Very recently Karachentsev et al (1985) have added a further twist in the tale with their reported detection, within the Ring, of young star clusters at recession velocities corresponding to the distance of the M81 group. So, is the Ring galactic or extragalactic ? Data obtained by IRAS show an infrared counterpart of the optical Ring; we compare the infrared and optical structure with the distribution of extragalactic neutral hydrogen to try to resolve the uncertainty.

OBSERVATION and RESULTS

Figures 1 and 2 show, respectively, the 100 and 60 micron maps of M81 made by coadding the data from IRAS pointed-mode observations (Young et al, 1985) of the area. The beam is 5 x 3 arcminutes at 100 microns and 4.7 x 1.5 arcminutes at 60 microns, with the long axis oriented perpendicular to the mean scan direction - indicated by the jagged line marking the edge of

Carol J. Lonsdale Persson (Editor)
Star Formation in Galaxies

the area observed. The maps have been flatfielded using techniques described in Rice et al (1986). The infrared counterpart of the Arp Ring is the extensive low surface brightness structure outside the northern half of the disc of M81.

Figure 1

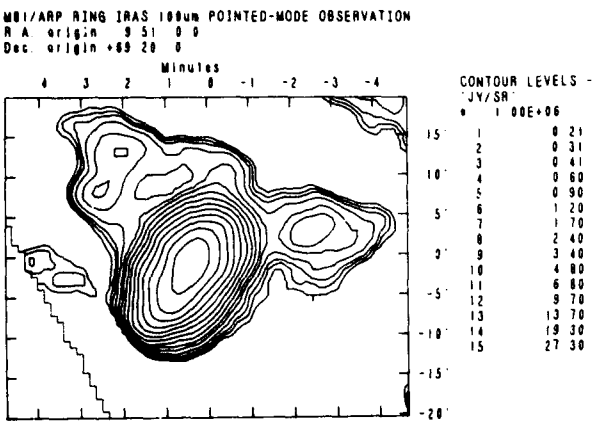

Figure 2

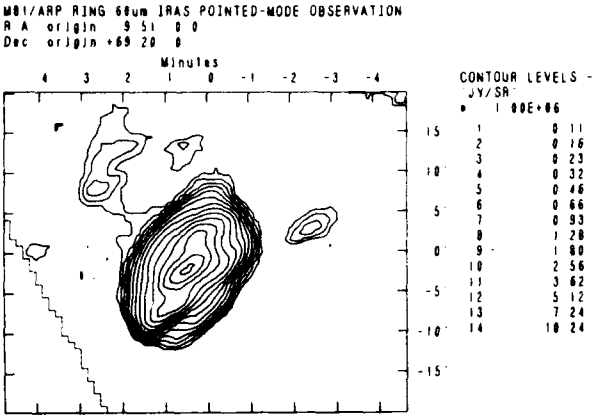

DISCUSSION

COMPARISON WITH SANDAGE'S DEEP OPTICAL PHOTOGRAPH

Inspection of Sandage's(1976) deep optical image reveals little to distinguish the Arp Ring from other cirrus/reflection nebulosity in the vicinity. Until recently only the relative sharpness of the Ring in the optical, and its curious orientation about M81, were compelling enough to suggest the Ring as a possible component of the M81 system; originating perhaps in the interaction between M81 and M82. However, Karachentsev et al now claim to have resolved "blue diffuse and star-like objects" on plates obtained with the Soviet 6 metre telescope (1986 and priv. comm.) Unfortunately details of where in the Ring this recent star-formation has taken place have yet to be disclosed.

The IRAS maps of M81 can be used to compare the infrared and deep optical appearance of the region immediately surrounding the galaxy. Despite the lower spatial resolution of the infrared maps, superimposing them on the deep optical image shows a one-to-one correspondence between the infrared and optical bright spots of the Ring. This is particularly clear at 60 microns where the spatial resolution is better and there is less confusion from nearby cirrus.The glaring difference between the infrared and optical views is the absence of the dwarf Magellanic irregular companion of M81, DDO 66, from both the 60 and 100 micron images. DDO 66 is of considerably higher optical surface-brightness than any part of the Ring, and, unlike the Ring, can even be seen on the blue sky-survey print. If the Ring was to be considered extragalactic, it would be unique as the only extended infrared feature, in any nearby galaxy observed by IRAS, to have no optical counterpart on sky-survey prints. (See "Atlas of IRAS Extended Galaxies" Rice et al, this conference.)

FAR-INFRARED COLOURS

Can the Arp Ring be distinguished from nearby cirrus on the basis of far-infrared colour ? The answer appears to be no ! The 100-over-60 micron flux ratio has been determined for many cirrus features within two degrees of M81 (Abolins and Rice, 1986). The values obtained are all greater than 5.5, ranging mainly between 6 and 8, corresponding to dust grains with colour temperature $T \lesssim 25$ K assuming emissivity proportional to ν^{+1}, or $T \lesssim 22$ K assuming emissivity proportional to ν^{+2}. The value for the Ring as a whole is 6 ± 1. This value does not change appreciably if smaller regions about the peaks are sampled, i.e. when possible contamination from cirrus not associated with the Ring is minimised.

21cm LINE DATA

Having established a close correspondence between the optical and infrared structure, we now compare both with the distribution of extragalactic neutral hydrogen from the published 21cm line data. The entire M81 group has been extensively observed : Gottesman and Weliachew (1975) showed the existence of clumps of satellite neutral hydrogen around M81, Cottrell (1977) and Gottesman and Weliachew(1977) showed the neutral hydrogen bridge connecting M81 with M82, van der Hulst (1979) described the bridge connecting M81 with NGC 3077 and Roberts(1972) and Davies(1974) showed that M81,M82 and NGC 3077 are enveloped in a giant cloud of neutral hydrogen. Is there then any close similarity between the optical/infrared structure and neutral hydrogen distribution, from which an extragalactic distance to the Ring could be inferred ? There is no detected counterpart of either the giant enveloping cloud or the connecting bridges (Abolins and Rice,1986). Gottesman and Weliachew(1975) interpreted the Ring as the optical counterpart of the satellite neutral hydrogen close to M81, but remarked that the radio emission was "very patchy" by comparison. In fact only the eastern parts of the Ring show any coincidence with the radio emission. Cottrell (1977) noticed this and pointed out that the bright portion of the Ring due north of M81 is coincident with a minimum in the HI distribution. The brightest of the satellite HI features is that associated with DDO 66, also the brightest optical feature outside M81, but undetected in the infrared. A cloud due north of DDO 66 is the only HI feature to overlap with the infrared structure. Its total mass and surface density are similar to, but rather lower than, those of DDO 66 (Gottesman and Weliachew, 1975), and therefore, if the Ring is extragalactic and its infrared emission is from heated dust grains, the gas-to-dust ratio must be quite unlike that of DDO 66.

INFRARED COUNTERPARTS OF EXTRAGALACTIC HI CLOUDS ?

Searches for infrared [dust] counterparts of extragalactic clouds of neutral hydrogen, using IRAS data, are underway in the USA and Europe (eg this work and priv. comms.). It is now clear that the task is likely to be severely hampered by confusion from galactic cirrus if dust grains present attain temperatures $T \sim 20$K (Pierce and Tully, 1985). Extragalactic HI clouds in cirrus-free areas are clearly the most promising candidates in this respect.

CONCLUSIONS

The far infrared maps and colour temperature of the Arp Ring are entirely consistent with the Ring being composed of galactic cirrus. The app-

arent conflict between this conclusion and the report of recent [extragalactic] star-formation within the Ring is resolved if there is a faint dwarf Im galaxy behind the [cirrus] Ring. This is not an unlikely event in a group known to be rich in dwarf systems.

REFERENCES

Abolins,J.A. and Rice,W.L. 1986, In preparation.
Arp,H.C. 1965, Science,148, 363.
Cottrell, G. 1977, M.N.R.A.S.,178, 577.
Davies,R.D. 1974, IAU Symp. 58, The Formation and Dynamics of Galaxies, 119, D.Reidel, Holland.
Gottesman,S.T. and Weliachew,L. 1975, Ap.J.,195, 23.
Gottesman,S.T. and Weliachew,L. 1977, Ap.J.,211, 47.
Hulst,J.M. van der 1979, Astr.Ap.,75, 97.
Karachentsev,I.D.,Karachentseva,V.E. and Borngen.F. 1985, M.N.R.A.S.,217, 731.
Low,F.J. et al. 1984, Ap. J. Lett., 278, L19.
Pierce,M.J. and Tully,R.B. 1985, A.J.,90, 450.
Rice et al, 1986, in preparation
Roberts,M.S. 1972, IAU Symp. 44, External Galaxies and Quasi-Stellar Object, 12, D.Reidel, Holland.
Sandage,A.R. 1976, A.J.,81, 954.
Young,E.T.,Neugebauer,G.,Kopan,E.L.,Benson,R.D.,Conrow,T.P., Rice,W.L. and Gregorich,D.T. 1985, A Users Guide to IRAS Pointed Observation Products,IPAC preprint no. pre-008n.

DUST GRAINS

Infrared Properties of Dust Grains Derived from IRAS Observations

G. Chlewicki[1,2], R.J. Laureijs[1,2], T.O. Clark[1,3], P.R.Wesselius[1]

[1] Laboratory for Space Research, Groningen, The Netherlands.
[2] Kapteyn Astronomical Institute, Groningen, The Netherlands.
[3] Department of Physics and Astronomy, University of Kentucky, Lexington, Kentucky, U.S.A.

ABSTRACT The paper presents the analysis of several diffuse interstellar clouds observed by IRAS. The 60/100 μm flux ratios appear to be nearly constant in clouds with up to 1^m of visual extinction at the centre. Observations of a highly regular cloud in Chamaeleon show that the 12/100μm ratio peaks at an intermediate radial distance and declines towards the centre of the cloud. These observations indicate that non-equilibrium emission accounts only for the 12 and 25 μm bands; strong emission observed at 60 μm band is probably due to equilibrium thermal radiation. The correlation of 12 μm emission with a red excess observed for a high latitude cloud, L1780, is shown to be consistent with the assumption that both features are due to fluorescence by the same molecular species.

1. Introduction

The early analysis of IRAS observations of dust in the diffuse interstellar medium concentrated on the discovery of the infrared cirrus (Low et al., 1984) and the universal occurrence of strong emission at 12 and 25 μm. These observations provided a clear indication that existing grain models must be modified by including a contribution of particles emitting as a result of transient rather than equilibrium radiative heating. In order to provide more restrictive constraints on grain models, we have analyzed data for individual well-defined clouds and studied the dependence of IR emission on the visual optical depth. This paper summarizes the most important preliminary results of the study.

2. Data reduction

The data base used in this study consisted of IRAS HCON3 scans (IRAS Explanatory Supplement, 1985). The maps were corrected for detector sensitivity effects (striping) by two-dimensional Fourier filtering. The zodiacal light contribution was estimated by masking bright sources and fitting a cosecant law to the remaining extended emission. After these reductions, the background level was determined as the average of weak galactic emission surrounding each cloud.

3. A 'typical' diffuse cloud

The object, for which the data have been summarized in Fig. 1, does not appear in the catalogues of galactic clouds. Its IR emission, however, is seen clearly in the IRAS maps of the Chamaeleon area; the cloud can also be identified in the ESO/SERC J-plate. The cloud appears highly regular with nearly circular IR isophotes, particularly at 100 μm. The brightness distribution

within the cloud derived by averaging intensities in concentric rings, has been shown in Fig. 1, which also presents pixel-to-pixel correlations between intensities in individual bands.

The results of our study of the Chamaeleon object can be summarized as follows:
(1) The 60/100 μm ratio remains constant over the entire radial extent of the cloud. The colour temperature implied by this ratio is 27K (assuming a λ^{-1} emissivity law). This number is somewhat higher than the temperatures obtained for several other clouds (Low et al., 1984; Laureijs et al., 1986); however, it may be due to the inaccurate calibration of HCON3, since the analysis of the cloud in HCON1 data yields a lower temperature of 24-25K (H. Walker, private communication). (3) The ratio of 12 and 25 μm intensities does not vary strongly but after improved background correction, the data imply a slight decrease towards the centre of the cloud. The value of the ratio is ~ 0.3. (3) The 12/100

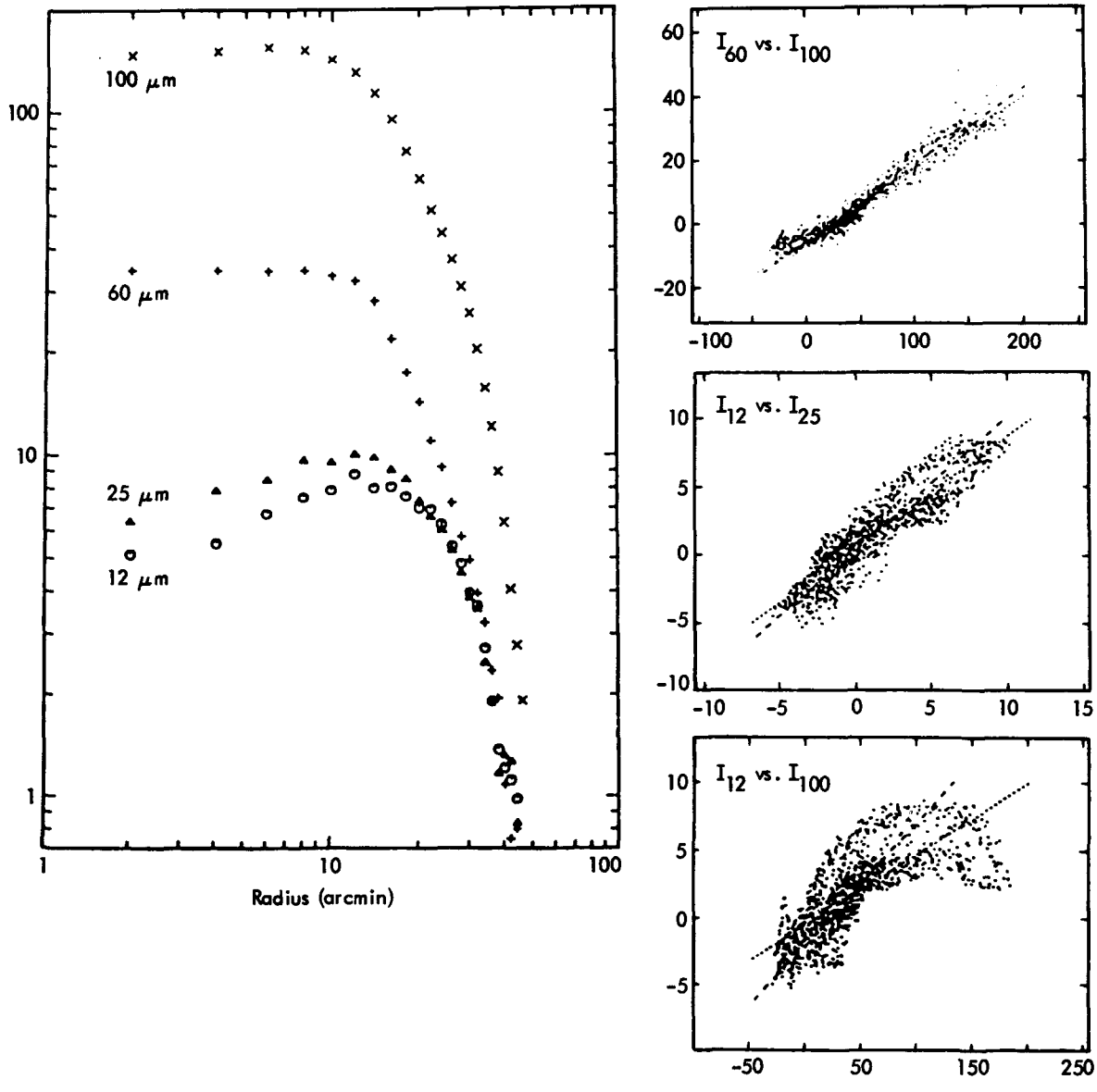

Fig. 1. Left: radial brightness distribution. Right: pixel-to-pixel correlations between individual IRAS bands. Intensities are in units of 105 Jy/sr.

μm ratio peaks at an intermediate radial position in the cloud and declines towards the centre.

The visual extinction at the centre of the cloud has not been measured (the work on star count analysis is in progress), but a comparison with L1642 (Laureijs et al., 1986) implies $A_V \approx 1^m$.

The high 60/100 μm temperature observed for the Chamaeleon object and almost all of the clouds so far extracted from the IRAS data base, cannot be explained by the current grain models, which predict equilibrium temperatures of less than 20K. The constant 60/100 μm ratio for the Chamaeleon object appears to contradict the suggestion that the additional emission at 60 μm is due to non-equilibrium emission from graphite particles with sizes of less than 0.005 μm (Draine and Anderson, 1985; the 60/100 μm ratio can be made to vary more slowly in this model if the power-law size distribution for the small particles is assumed to be steeper than λ^{-4}). The same argument appears to exclude the hypothesis which associates the 60 and 100 μm emission with fine structure lines of OI and OIII (Harwit et al., 1986), since the fall-off in the degree of fractional ionization with optical depth should lead to a rapid variation in the ratio of the two intensities.

As an alternative possibility, we have considered equilibrium emission from a population of particles whose temperatures are higher than those obtained in current grain models. The calculations related to this hypothesis have been carried out for thin graphite discs modelled as oblate spheroids with an axial ratio of ~10, for which the equilibrium temperature in the diffuse interstellar radiation field can be demonstrated to be ~25K (the increased temperature of spheroids with respect to spherical particles considered in current grain models is due to a combination of the properties of a conductor with a strong anisotropy, which is peculiar to graphite; Chlewicki, 1985). The required abundance of the additional particles is relatively low: with the distance to the cloud estimated at ~100 pc on the basis of its location with respect to the more extended cirrus emission, the volume concentration of the particles is only $\sim 10^{-6}$ cm^{-3}. The abundance of particles responsible for visual extinction is most easily derived from the three-population model (Hong and Greenberg, 1980), with the 'large' particles represented by 0.15 μm dielectric spheres. The extinction of 1^m at the centre of the cloud leads to a concentration of 'visual' particles of $\sim 5 \times 10^{-10}$ cm^{-3}. The volume ratio for the entire populations of 60 μm particles and large 'visual' grains is then ~0.1. The ratio is almost unchanged if the MRN (Mathis et al., 1977) model is used as a representation of the interstellar extinction curve, since both models impose similar requirements on the volume of material locked up in grains responsible for visual extinction. One of the most important implications of this hypothesis is that algorithms for estimating masses and volumes of interstellar clouds -such as the method described by Hildebrand (1983) - which are based on parameters derived from submillimetre data sensitive only to the IR properties of large particles, cannot always be used in the analysis of IRAS observations at significantly shorter wavelengths.

3. L1780: correlated visual and IR fluorescence?

L1780 appears to be the only interstellar cloud for which a red visual spectrum has been obtained (Mattila, 1979). The spectrum shows a pronounced peak at ~6500A, which cannot be explained by scattered light, unless substantial modifications in the optical properties of the grains are assumed (the intensities of the scattered diffuse galactic light predicted at these wavelengths by both the MRN and the three-population model are nearly constant). The position and shape of the feature (as far as they can be determined in the inevitably

noisy spectrum) are almost identical with the broad-band emission observed in the Red Rectangle (Schmidt et al., 1980). Recent interest in the polycyclic aromatic hydrocarbons as a possible explanation for the unidentified IR features and the IRAS 12 μm emission (PAH's, Leger and Puget, 1984; Allamandola et al., 1985), has led to suggestions that the Red Rectangle feature is due to fluorescence by such molecules. We have analyzed the IR data for L1780 in order to test the hypothesis that both the short wavelength IRAS emission and the red feature observed by Mattila can be due to fluorescence from the same molecular species. Since the basic parameters of the cloud have been determined by Mattila (A_B = 3^m, r = 100pc, $n_H = 10^3$ cm^{-3}; l = 359^o, b= 36^o), the energies contained in both visual and IR features can be estimated. By subtracting a scattering component predicted by grain models from Mattila's spectrum, we have obtained a total energy in the red feature of $8*10^{32}$ erg s^{-1} = 0.2 $L_\odot$. Table 1 contains the fluorescence yields required to reproduce this number for molecules in the gas phase and species locked up in grain mantles. The core-mantle grains containing the molecules were assumed to be 0.15μm spheres with a normal gas-to-dust ratio, $n_{gr} = 10^{-12} n_H$. Gas phase molecules were assumed to consist of 20 carbon atoms and to have a UV absorption cross-section of 10^{-16} cm^{-2}; the total content of carbon in the species was taken to be 1% of the cosmic abundance.

For aromatic molecules, the energy of a typical exciting photon (~4 eV) should be distributed almost equally between visual and IR fluorescence (the IRAS 12 μm band). If both the visual excess and the 12 μm emission are associated with the PAH's, the ratio of the energy contained in each wavelength range should have a value close to the fluorescence yield. The 12 μm intensity in the part of the cloud observed by Mattila is $I_{12} = 9*10^{15}$ ergcm $^{-2}s^{-1}sr^{-1}$. With the intensity of the red excess of $4*10^{-5}$, the intensity ratio is 0.45 in perfect agreement with fluorescence fields expected for aromatic species. A stronger confirmation of the PAH hypothesis for L1780 could only be obtained if more visual spectra of galactic clouds become available.

Table I
Fluorescence yields derived from the L1780 emission

Excitation threshold	Grain mantles	Free molecules
3.5 eV (UV)	0.03	~1
2 eV (UV+Vis)	0.01	0.4

REFERENCES

Allamandola, L. J., Tielens, A.G.G.M., Barker, J.R., 1985, Ap.J., 290, L25.
Chlewicki, G., 1985, Ph.D. Thesis, University of Leiden.
Draine. B.T., Anderson, N., 1985, Ap.J., 292, 494.
Harwit, M., Houck, J.R., Stacey, G.J., 1986, Nature, 319, 646.
Hildebrand, R.H., 1983, QJRAS, 24, 267.
Hong, S.S., and Greenberg, J.M., 1980, Astr. Ap., 88, 194.
Laureijs, R.J. et al., 1986, in preparation.
Leger, A., and Puget, J.L., 1984, Astr. Ap., 137, L5.
Low, F.J., et al., 1984, Ap.J., 278, L19.
Mathis, J.S., Rumpl, W., Nordsieck, K.H., 1977, Ap.J., 217, 425.
Mattila, K., 1979, Astr. Ap., 78, 253.
Schmidt, G.D., Cohen, M., Margon, B., 1980, Ap.J., 239, L133.

IRAS Observations of the Pleiades

P. Cox[1] and A. Leene[2]

1. Max Planck Institut für Radioastronomie
   Auf dem Hügel 69, D-5300 Bonn 1, F.R.G
2. Kapteijn Astronomical Institute
   Groningen, The Netherlands

Abstract

IRAS observations of the Pleiades region are reported. The data show large flux densities at 12 μm and 25 μm, extended over the optical nebulosity. This strong excess emission, implying temperatures of a few hundred degrees Kelvin, indicates a population of very small grains in the Pleiades. It is suggested that these grains are similar to the small grains needed to explain the surface brightness measurements made in the ultraviolet.

I. Introduction

At a distance of 126 pc, the Pleiades offer a beautiful opportunity to observe the fine structure occuring in interstellar clouds. The well known geometry of the cloud is of great help in characterizing the scattering properties (albedo and phase function) of interstellar dust. The chemistry is unusual in the sense that the column density of CH^+ is exceptionally high towards the Pleiades cluster. Previous models, based on optical and ultraviolet observations, required that the dust in the Pleiades will be an extended and complex radiation source in the infrared.

We present the IRAS observations of the Pleiades region and give preliminary results of the dust characteristics derived fron the infrared data. A paper on this subject is in preparation and will be submitted to Astronomy and Astrophysics. Here we give a summary of the salient results.

II. Observational Material and Data Reduction.

The data base consists of IRAS HCON3 scans (IRAS Explanatory Supplement, Ref. 1). The maps were corrected for detector sensitivity effects by two dimensional Fourier filtering. The zodiacal light contribution was estimated by fitting a linear baseline on the entire map and using averaged values derived from a geometrical model of the zodiacal emission (Ref. 2).

The resulting corrected and destriped maps are presented for 12 μm and 100 μm in figures 1 and 2, respectively.

III. Results

The brightness distribution of the infrared emission for the Pleiades is very similar in all four IRAS bands. A ridge of high brightness extends over the western half of the cluster. Three main emission peaks

Carol J. Lonsdale Persson (Editor)
Star Formation in Galaxies

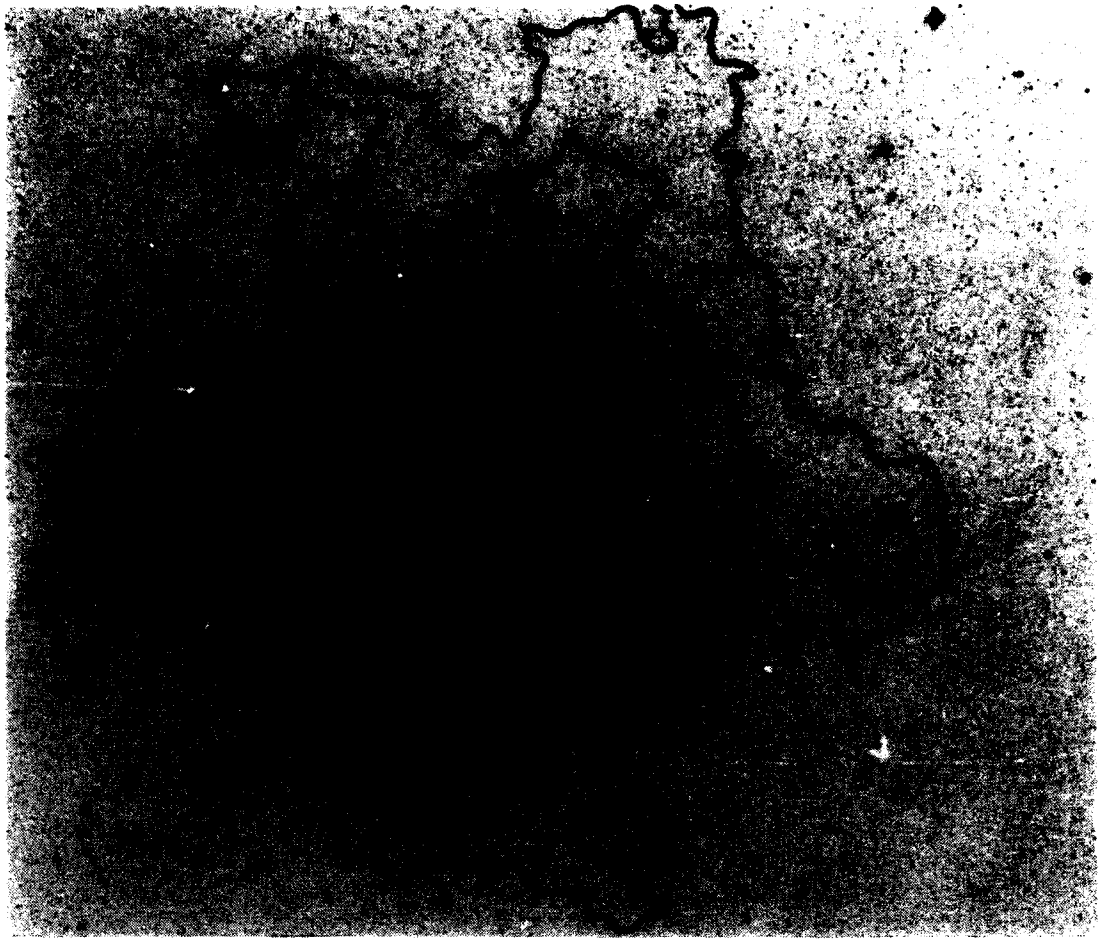

Figure 1: The 12 μm emission map of the Pleiades overlayed on the Red Print of the Palomar Sky Survey.

are apparent, of which the southern is the more intense. A weakening in the infrared distribution is noticeable east of this ridge. A diffuse emission extends from this ridge several degrees across the region.

In figure 1, the 12 μm image is presented superimposed on a copy of the Red Palomar Sky Survey. The brightest infrared component lies south of 23 Tau (Merope) and the two northen peaks correspond to the nebulosities associated with 20 and 17 Tauri.

Figure 2 shows the CO measurements (10 $km.s^{-1}$) and the HI emission at 7 $km.s^{-1}$ (Ref. 3-4). The CO cloud is slightly shifted with respect to the main infrared peak: note however that the sharp edge of the molecular cloud corresponds with the brightest region of the nebulosity, south of Merope. This feature coincides with a region of obscuration recognizable on visible photographs of the cluster. The HI ridge northen peak corresponds with a decrease in the infrared distribution. No infrared counterpart however is found for the southern HI peak.

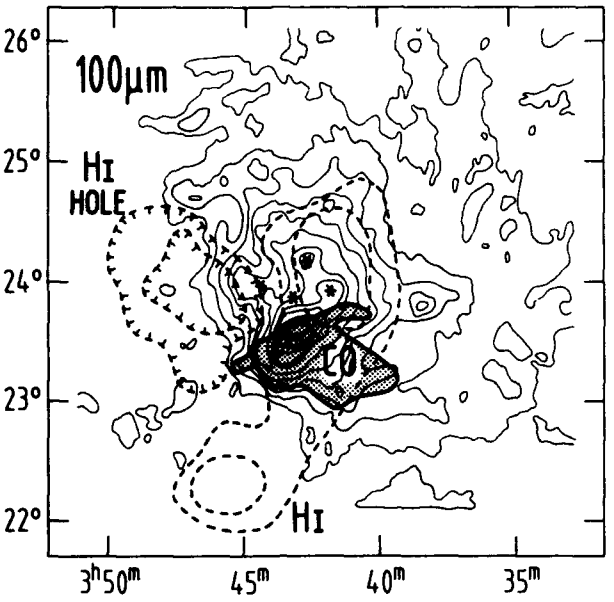

Figure 2: The HI contours (7 km.s^{-1}) and the CO emission (10 km.s^{-1}) superimposed on the 100 μm emission map.

In figure 3, the 12/100 μm ratio is presented superimposed on the blue Palomar Sky Survey. The large values of this ratio are striking. The first contour lies at 0.05 and is as extended as the diffuse blue reflection nebulosity.

The 60/100 μm ratio is also very extended and uniform over the nebulosity, indicating temperatures of the order of ~25K.

IV. Discussion

The strong excess emission at 12 μm which is extended over all the region definitely indicates the presence of very small grains (~10 Å sized) in the Pleiades (Ref. 5). The high values attained by the 12/100 μm ratio suggest that a conspicuous amount of carbon is locked into these grains i. e. up to 10% of the total carbon mass.

The presence of a large population of grains in the 10 Å size has been independently suggested by Witt et al. (Ref. 6) on the basis of ultraviolet measurements. According to these authors the ultraviolet data can only be understood if the scattering phase function becomes more isotropic in the far-ultraviolet, which is a behaviour expected for particles small compared to the wavelength of ultraviolet light. These particles are reminiscent of the free radicals (or 'Platt particles') as described by Andriesse and de Vries (Ref. 7), which have a high albedo in the far-ultraviolet and isotropic scattering i.e. g~0.2.

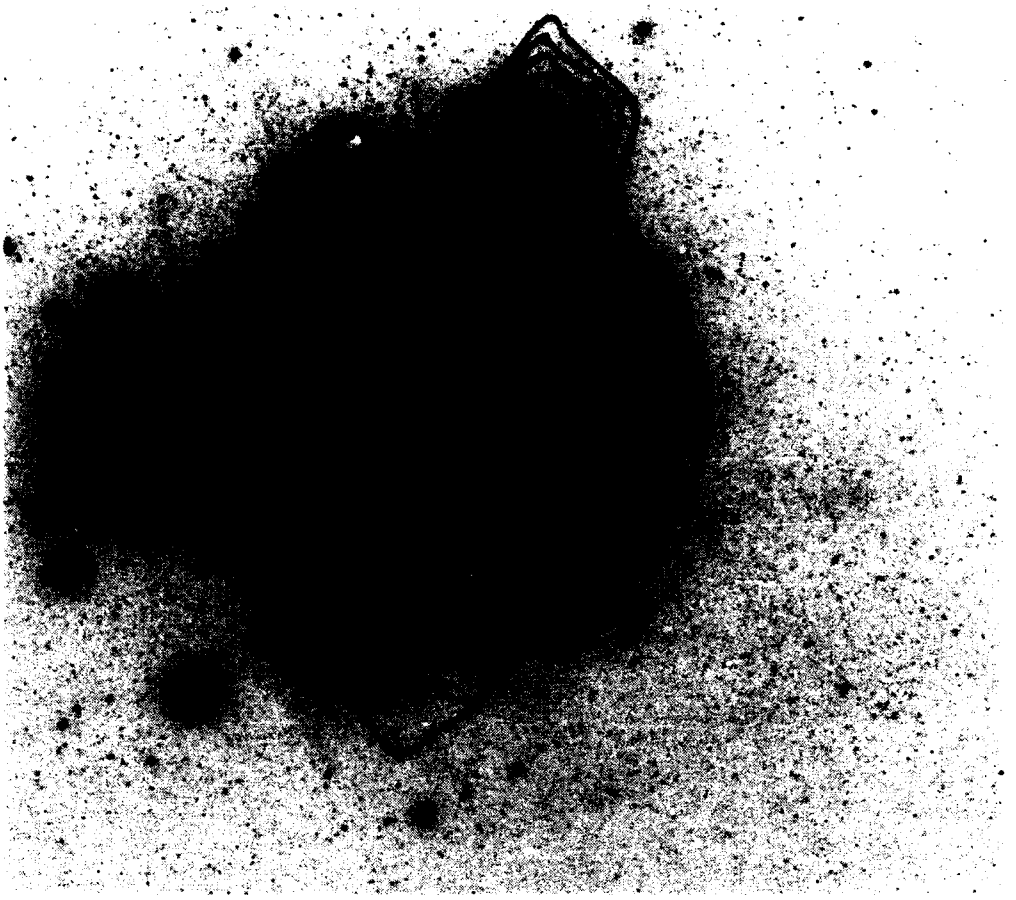

Figure 3: The 12/100 μm ratio overlayed on the blue print of the PSS. Contours are at 0.05 to 0.09 with steps of 0.01.

V. Conclusions

IRAS observations of the Pleiades are presented. The observations reveal a large flux density at 12 μm and 25 μm, extended over the optical nebulosity, implying temperatures of a few hundred degrees Kelvin. The 60 μm and the 100 μm fluxes give temperatures of the order of 25 K.

The strong excess emission at 12 μm can only be understood in terms of a large population of very small grains (in the 10 Å size range). We suggest that these grains are similar to the small grains needed to account for the ultraviolet measurements made on the Pleiades, i. e. isotropic ($g \sim 0.2$) scatterers in the far-ultraviolet. Finally, we note that the unusually high column density of CH^+ towards the Pleiades (Ref. 8) may perhaps be the key to the origin of these small graphitic particles.

References

1. IRAS Explanatory Supplement, 1985, eds Beichman et al.
2. Cox, P. and Leene, A. 1986, Astron. Astrophys. to be published.
3. Cohen, R. S. 1975, unpublished data.
4. Gordon, K. J. and Arny, T. T. 1984, Astron. J. 89, 672
5. Puget, J-L, Lêger, A. and Boulanger, F. 1985, Astron. Astrophys.142, L19
6. Witt, A.N., Bohlin, R.C. and Stecher, T.P. 1986, Astrophys. J. 302, 421
7. Andriesse, C.D. and de Vries, J. 1974, Astron. Astrophys. 30, 51
8. Hobbs, L.M. 1972, Astrophys. J. Letters 175, L145

B. NORMAL GALAXIES

ORAL PRESENTATIONS

STAR FORMATION IN NORMAL GALAXIES

C. G. Wynn-Williams
University of Hawaii, Institute for Astronomy
2680 Woodlawn Drive, Honolulu, Hawaii 96822

1. INTRODUCTION

In this review I shall be mainly concerned with the ways in which recent infrared observations, particularly by IRAS, have influenced our ideas about star formation in "normal" galaxies.

2. IRAS SURVEYS AS A POINTER TO STAR FORMATION

That strong infrared emission is common in spiral galaxies became clear at the time of publication of the first group of IRAS papers. De Jong et al. (1984) examined a sample of 165 galaxies in the Shapley-Ames catalog and found that over 80% of spirals (Sa and later) were detected by IRAS, though none of the ellipticals were seen. Since the publication of the IRAS point source catalog it has been possible to examine the incidence of infrared emission from galaxies on a proper statistical basis. The infrared luminosity function has been calculated by several groups (Lawrence et al. 1986; Soifer et al. 1986; Rieke and Lebofsky 1986). In general it resembles that of galaxies at visible wavelengths except that there appears to be an excess of sources with luminosities above about 10^{10} $L_{\odot}$. These high luminosity objects include active galaxies and "starburst" galaxies that will be receiving much attention elsewhere in this volume. I will generally be discussing lower-luminosity spiral galaxies in this paper, although I will present evidence that a number of early-type barred spiral galaxies may be exhibiting signs of low-level nuclear activity.

A crucial problem in trying to use infrared luminosities as a guide to star formation activity in galaxies is the difficulty of distinguishing emission from the diffuse interstellar medium and emission from dust heated by newly formed or still-forming stars. Attempts have been made to use various flux ratios for this purpose. de Jong et al. (1984) found that the ratio L_{IR}/L_B increases with the 60-100 μm color temperature. From this result has come the idea that spiral galaxy disks contain a cool dust component that corresponds to the diffuse or "cirrus" emission, plus a warmer component that dominates in cases of galaxies that are undergoing large amounts of star formation.

The separation of the infrared emission into a "cirrus" and a star formation component may be tested by comparing the IRAS data with some independent parameter, such as the Hα or the CO fluxes. The results are not conclusive. Two groups have compared the IRAS fluxes from a number of spiral galaxies with the star formation rates calculated by Kennicutt from measurements of Hα spectrophotometry; Moorwood, Veron-Cetty, and Glass (1986) conclude that the infrared emission from Kennicutt's galaxies matches that expected on the basis of Hα emission from star formation regions, but Persson and Helou (1986) conclude that the bulk of the infrared emission from these galaxies comes from the

Carol J. Lonsdale Persson (Editor)
Star Formation in Galaxies

interstellar "cirrus" component. Young (1986) finds a correlation between infrared luminosity and the luminosity in the 2.6 mm CO line, supporting the idea that much of the infrared emission is associated with star formation. Since some of the galaxies in her study are of very high luminosity, however, the result does not necessarily apply to "normal" galaxies.

A challenge to the idea that the 60-100 μm color temperature is an indicator of the role of star formation in galaxies has been raised by Burstein and Lebofsky (1986). They present evidence that the apparent far-infrared luminosity of Sc galaxies varies with inclination. This result would imply that the disks of these galaxies are optically thick at 100 μm, which in turn would require that the emission be concentrated within the central 1 kpc diameter region. Burstein and Lebofsky's conclusions are disputed by Rice, Elias, and Persson (1986), who point out that problems arise due to the difficulties of correctly classifying galaxies that have high inclinations. Another difficulty with Burstein and Lebofsky's hypothesis is that Devereux, Becklin and Scoville (1986) found that the emission from most Sc galaxies is not concentrated within the central 1 kpc, at least at 10 μm.

The strongest correlation that has appeared so far from the IRAS data is the very close proportionality between the 60 μm flux density from warm dust and the centimeter-wavelength nonthermal emission (de Jong et al. 1985; Helou, Soifer, and Rowan-Robinson 1985). This correlation has not yet been satisfactorily explained. One popular model has it that the radio emission is dominated by synchrotron emission from individual supernova remnants and that both the infrared luminosity and the supernova rate are proportional to the star formation rate. A problem with this model is that in the two cases where adequate data are available, namely M82 (Kronberg et al. 1985) and the Galaxy, individual supernova remnants are responsible for only a small fraction of the total synchrotron emission from the galaxy disk. In an alternative model the radio emission originates from relativistic electrons in the general interstellar medium. The difficulty with this model is that synchrotron emission depends strongly on the magnetic field strength as well as the number density of relativistic particles. To explain the proportionality of infrared and radio emission it is necessary to identify a mechanism that controls the interstellar magnetic field strength in various different star-forming regions. As yet no such mechanism has been identified.

3. DEPENDENCE OF STAR FORMATION RATE ON HUBBLE TYPE

The principle of the Hubble classification of spiral galaxies is that the bulge-to-disk ratio is higher in early-type galaxies (Sa-Sb) than in late-type galaxies (Sc-Sd). The ratio of the current to the historical star formation rate is higher in late-type galaxies than early-type galaxies (Kennicutt 1983).

Devereux, Becklin, and Scoville (1986) present evidence that the IRAS emission from spiral galaxies is mainly a disk phenomenon. They find that their measurements of the 1.65 μm nuclear (5.5 arcsec or 500 pc diameter) flux densities of Virgo cluster spirals is much better correlated with the 60 μm flux densities in disk-dominated late-type spirals than in bulge-dominated early-type spirals. On the whole, however, the dependence of infrared luminosity on Hubble type is weak for spiral galaxies. Devereux (1986) finds no statistically significant differences between the fractional luminosity functions of galaxies

of Hubble types in the range Sa to Sc, though there appear to be deficiencies of high-luminosity galaxies in the very late and very early classes. There are strong resemblances between the infrared fractional luminosity function and the radio continuum fractional luminosity function of spiral galaxy disks, as derived by Hummel (1981).

The 60-100 μm color temperature shows more dependence on Hubble type than does the bolometric luminosity. Table I summarizes an analysis by Devereux (1986) of a sample consisting of all 227 known galaxies in the distance range 15-40 Mpc, the galactic latitude range $|bII| > 20°$, and with a 60 μm luminosity (νS_ν) > 2 x 10^9 $L_\odot$. There is a statistically significant excess of "hot" galaxies among early types. He has also measured the "compactness" of many of the sample galaxies at 10 μm by comparing the flux in a 5.5 arcsec IRTF beam with the color-corrected 12 μm flux measured through the much larger IRAS beam. He finds that galaxies in which the 10 μm emission is compact are significantly more common among early-type than among late-type galaxies. A similar result was found by Hummel (1981) for the central radio sources of disk galaxies, but observations in the 2.6 mm CO emission line show a different trend with a number of early-type galaxies displaying a central hole rather than an enhancement (Young 1986).

Table I
Classification of 227 Nearby Galaxies
by Hubble Type and by 60-100 μm color temperature

	"Hot" >44 K	"Cold" <44 K
Early (S0/a-Sb)	35	49
Late (Sbc-Sm)	25	118

4. ROLE OF BARS

The first evidence that the infrared properties of galaxies were affected by the presence of bars was presented by Hawarden et al. (1986), who showed that a number of barred galaxies exhibit an energy distribution that is characterized by high 25μm/12μm and low 100μm/25μm flux density ratios. They estimated that over 30% of barred luminous galaxies show a flux excess at 25 μm and attributed this excess flux to a circumnuclear region of intense star formation.

The sample analyzed by Hawarden et al. includes only galaxies that have 12 μm and 25 μm flux densities above the IRAS point source catalog limit. Devereux (1986) has examined the effect of bars in the somewhat larger volume-selected sample of galaxies that was defined in section 3. He finds that the effect of bars is much more important in early-type galaxies than in late-type galaxies. He finds that most of the early-type galaxies exhibiting high compactness are barred, as are 29 of the 35 galaxies in the "hot" and "early" class in Table I. This work is described in more detail elsewhere in this volume.

On a smaller scale, aperture synthesis observations in the 2.6 mm CO line have provided evidence for bar-like structures of molecular material in the inner regions of IC 342 (Lo et al. 1984) and NGC 6946 (Ball et al. 1985).

5. COMPACT AND DWARF GALAXIES

Many galaxies for which there was preexisting evidence for nuclear (or, at least, localized) rapid star-forming activity are strong IRAS sources. These include many of the non-Seyfert Markarian galaxies and the compact blue "H II region" galaxies like II Zw 40. A large number of papers incorporating IRAS observations have recently appeared (Gondhalekar et al. 1986; Hunter et al. 1986; Klein et al. 1986; Kunth and Sevre 1986; Sramek and Weedman 1986; Thronson and Telesco 1986; Wynn-Williams and Becklin 1986). The IRAS observations generally confirm that these galaxies have high star formation rates. Specifically, Kunth and Sevre (1986) find that blue, compact emission-line galaxies generally have higher IR/blue flux density ratios and higher 60μm/100μm color temperatures than spiral galaxies in the Shapley-Ames catalog.

6. ELLIPTICAL AND S0 GALAXIES

Very few ellipticals were detected in the IRAS survey. A higher success rate was achieved by Impey, Wynn-Williams, and Becklin (1986), who looked for 10 μm emission from a sample of 65 bright elliptical galaxies using a 5.5 arcsec beam on the IRTF. One third of the sample showed emission above that expected from pure photospheric emission, but this emission is more likely to arise from circumstellar shells around late-type giant stars than from regions of current star formation.

S0 galaxies are much more common in the IRAS catalog than are ellipticals. Devereux, Becklin, and Scoville (1986) found that 7 out of 34 S0 galaxies in the Virgo cluster were detected by IRAS. The 60μm/100μm color temperatures of these galaxies are similar to those of normal spirals, which led Becklin (1986) to suggest that star formation may be the source of luminosity in these galaxies. However, their radio continuum emission (Hummel and Kotanyi 1982) appears to be lower than would be expected from an application of Helou, Soifer, and Rowan-Robinson's (1985) radio/infrared relation to the measured IRAS fluxes.

7. STUDIES OF INDIVIDUAL REGIONS

Future progress in understanding star formation in galaxies will require detailed studies of individual regions as well as a statistical examination of suitably chosen samples. Very few galaxies have angular sizes large enough that they can be mapped by IRAS. M31 has been described by Habing et al. (1984); a few others, including M33, are being presented by Walter Rice (this volume). Wainscot, de Jong, and Wesselius (1986) have used the chopped photometric channel on IRAS to produce scans along the disks of several edge-on galaxies. In the case of NGC 891 they find good agreement among the 50 μm, 21 cm continuum, and CO profiles, all of which are considerably narrower than the 21-cm H I emission.

The best far-infrared resolution achieved to date on an extragalactic

source is the study of the central regions of M51 by Lester, Harvey, and Joy (1986) using a 24 arcsec slit in the Kuiper Airborne Observatory. They find that much of the far-infrared luminosity of this galaxy comes from a small, sharply bounded region within a 700 pc radius of the nucleus. Finer detail than this can only be achieved by moving to shorter wavelengths and using large ground-based telescopes such as the IRTF. Maps at 10 μm of the central regions of galaxies such as NGC 2903 (Wynn-Williams and Becklin 1985), and NGC 3310 (Telesco and Gatley 1984) tend to show agreement in general, but not in detail, between the regions of strongest radio, infrared, and optical emission. Much more mapping at infrared wavelengths will be needed to disentangle the effects of dust extinction and of variations in the stellar formation histories in these regions.

Infrared spectroscopy is another area where important contributions can be expected from ground-based observations in the next few years. Roche and Aitken (1985) have shown that the 8-13 μm spectra of spiral galaxy nuclei show much stronger 11.6 μm features than are seen in H II regions in our Galaxy. It remains to be seen whether this effect is also seen in extragalactic spiral-arm star formation regions.

8. UNANSWERED QUESTIONS

I conclude with a list of questions I think we need to address before claiming to understand the nature of infrared emission from normal galaxies.

- Is there a fundamental difference between normal and "starburst" galaxies?
- What is the best way to separate "cirrus" emission from emission from star-forming regions?
- Do measurements of visible H II regions provide a reliable guide to the current star formation rate?
- Is the far-infrared optical depth in spiral galaxy disks large enough to produce self-absorption at high inclination?
- Does the radio emission come from supernova remnants or from cosmic rays in the interstellar medium?
- What is going on in early-type barred galaxy nuclei?
- Is there star formation in S0 galaxies?
- Do star formation conditions in the central regions of spiral galaxies resemble those in the disks?

9. ACKNOWLEDGMENTS

I thank Nicholas Devereux for allowing me to quote at length from work he is undertaking towards his Ph.D. thesis at University of Hawaii, and many colleagues for useful discussions and the receipt of preprints. This work was supported under NSF grant AST 84-18197.

10. REFERENCES

Ball, R., Sargent, A. I., Scoville, N. Z., Lo, K. Y., and Scott, S. L. 1985, Ap. J. (Letters), 298, L21

Becklin, E. E. 1986, in Light on Dark Matter, ed. F. P. Israel (Dordrecht: Reidel), 415.

Burstein, D., and Lebofsky, M. J. 1986, Ap. J., 301, 683.

de Jong, T., Clegg, P. E., Soifer, B. T., Rowan-Robinson, M., Habing, H. J., Houck, J. R., Aumann, H. H., Raimond, E. 1984, Ap. J. (Letters), 278, L67.

de Jong, T., Klein, U., Wielebinski, R., and Wunderlich, E. 1985, Astr. Ap., 147, L6.

Devereux, N. A. 1986, in preparation

Devereux, N. A., Becklin, E. E., and Scoville, N. 1986, Ap. J., submitted.

Gondhalekar, P. M., Morgan, D. H., Dopita, M., and Ellis, R. S. 1986, M.N.R.A.S., 219, 505.

Habing, H. J., et al. 1984, Ap. J. (Letters), 278, L59.

Hawarden, T. G., Fairclough, J. H., Joseph, R. D., Leggett, S. K., Mountain, C. M. 1986, in Light on Dark Matter, ed. F. P. Israel (Dordrecht: Reidel), 455.

Helou, G., Soifer, B. T., and Rowan-Robinson, M. 1985, Ap. J. (Letters), 298, L7.

Hummel, E. 1981, Astr. Ap., 93, 93.

Hummel, E., and Kotanyi, C. G. 1982, Astr. Ap., 106, 183.

Hunter, D. A., Gillett, F. C., Gallagher, J. S., Rice, W. L., and Low, F. J. 1986, Ap. J., 303, 171.

Impey, C. D., Wynn-Williams, C. G., and Becklin, E. E. 1986, Ap. J., in press.

Kennicutt, R. C. 1983, Ap. J., 272, 54.

Klein, U., Heidmann, J., Wielebinski, R., and Wunderlich, E., 1986, Astr. Ap., 154, 373.

Kronberg, P. P., Biermann, P., and Schwab, F. R. 1985, Ap. J., 291, 693.

Kunth D., and Sevre, F. 1986, in Star-Forming Dwarf Galaxies and Related Objects, ed. D. Kunth, T. X. Thuan, and J. T. T. Van (Gif Sur Yvette, France: Editions Frontieres). 331.

Lawrence, A., Walker, D., Rowan-Robinson, M., Leech, K. J., and Penston, M. V. 1986, M.N.R.A.S., 219, 687.

Lester, D. F., Harvey, P. M., and Joy, M. 1986, preprint

Lo, K. Y., et al. 1984, Ap. J. (Letters), 282, L59.

Moorwood, A. F. M., Véron-Cetty, M.-P., and Glass I. 1986, Astr. Ap., 160, 39.

Persson, C. J., and Helou, G., 1986, preprint.

Rice, W. L., Elias, J. A., and Persson, C. J., 1986, private communication.

Rieke, G. H., and Lebofsky, M. J. 1986, Ap. J., 304, 326.

Roche, P. F., and Aitken, D. K. 1985, M.N.R.A.S., 213, 789.

Soifer, B. T., Sanders, D. B., Neugebauer, G., Danielson, G. E., Lonsdale C. J., Madore, B. F., and Persson, S. E. 1986, Ap. J. (Letters), 303, L41.

Sramek, R. A., and Weedman, D. W. 1986, Ap. J., 302, 640.

Telesco, C. M., and Gatley, I. 1984, Ap. J., 284, 557.

Thronson, H. A., and Telesco, C. M. 1986, Ap. J., in press.

Wainscot, R. J., de Jong, T., and Wesselius, P. R., 1986, preprint.

Wynn-Williams, C. G., and Becklin, E. E. 1985, Ap. J., 290, 108.

Wynn-Williams, C. G., and Becklin, E. E. 1986., Ap. J., in press.

Young, J. S. 1986, in IAU Symposium 115, Star Formation, ed. J. Jugaku and M. Peimbert (Dordrecht: Reidel), in press.

DISCUSSION

ELMEGREEN:

Early-type bars are different from late-type bars with respect to brightness profile, relative size and kinematics (Elmegreen and Elmegreen 1985, *Ap.J.*, **288**, 438). The early-type bars apparently contain inner Lindblad resonances and inner spirals, whereas the late-type bars may end at the ILR and contain no additional resonances. The inner spirals in early-type barred galaxies are modeled by Sanders and Tubbs (1980, *Ap.J.*, **235**, 803) and others as pure-gas spiral shocks, responding to the inner resonances. Apparently these spiral shocks promote unusually high star formation rates. This would explain the effect described by Hawarden *et al.*, but in addition, why early early-type galaxies show it more than late types.

YOUNG:

I think it is important to clarify the use of the term 'starburst.' A galaxy which is luminous in the IR and has a high H_2 mass may simply be a scaled-up version of the Milky Way, while a lower luminosity galaxy which has very little H_2 may be very efficiently forming stars. What is your definition of starburst?

WYNN-WILLIAMS:

I am not particularly fond of the term. I expect Dan Weedman will provide us with a definition of it tomorrow.

FROGEL:

You showed a viewgraph which indicated that a larger fraction of early-type galaxies have a warm dust component than late-type galaxies. According to Mezger's bimodal model, early types would have more star formation than late types. This appears to contradict widespread belief that late-type galaxies are more active. Would you please comment on this.

WYNN-WILLIAMS:

The galaxies with a warm dust component tend to be early-type barred galaxies and there is evidence that this extra component is associated with the central regions rather than the disk.

MODELS FOR INFRARED EMISSION FROM IRAS GALAXIES

M. Rowan-Robinson

Theoretical Astronomy Unit,
Queen Mary College,
Mile End Road, London, E1 4NS

ABSTRACT. Models for the infrared emission from IRAS galaxies by Rowan-Robinson and Crawford, by de Jong and Brink, and by Helou, are reviewed. Rowan-Robinson and Crawford model the 12-100 μ radiation from IRAS galaxies in terms of 3 components: a normal disc component, due to interstellar 'cirrus'; a starburst component, modelled as hot stars in an optically thick dust cloud; and a Seyfert component, modelled as a power-law continuum immersed in an $n(r) \propto r^{-1}$ dust cloud associated with the narrow-line region of the Seyfert nucleus. The correlations between the luminosities in the different components, the blue luminosity and the X-ray luminosity of the galaxies are consistent with the model. Spectra from 0.1 to 1000 μm are predicted and compared with available observations.

de Jong and Brink, and Helou, model IRAS non-Seyfert galaxies in terms of a cool (cirrus) component and a warm (starburst) component. de Jong and Brink estimate the face-on internal extinction in the galaxies and find that it is higher in galaxies with more luminous starbursts. In Helou's model the spectrum of the warm component varies strongly with the luminosity in that component. The 3 models are briefly compared.

1. INTRODUCTION

In this paper I review 3 attempts to interpret the far infrared spectra of IRAS galaxies, by Crawford and Rowan-Robinson (1986), by de Jong and Brink (1986) and by Helou (1986).

The main properties we have to explain are:
(i) the great range of far infrared luminosities in IRAS galaxies, from 4×10^{7}-4×10^{12} $L_{\odot}$ at 60 μ (Fig 1).
(ii) the great range of ratio of far infrared to optical luminosity, in IRAS galaxies, from 0.05 to several hundred (Soifer et al 1984, Rowan-Robinson et al 1986),
(iii) the correlation of L_{FIR}/L_{opt} with $S(100\mu)/S(60\mu)$ (de Jong et al 1984, Rowan-Robinson et al 1986),
(iv) the distribution of IRAS galaxies in the IRAS colour-colour diagrams,
(v) the fact that many Seyferts show a peak at 25 μ (Miley et al 1984, de Grijp et al 1985).

Carol J. Lonsdale Persson (Editor)
Star Formation in Galaxies

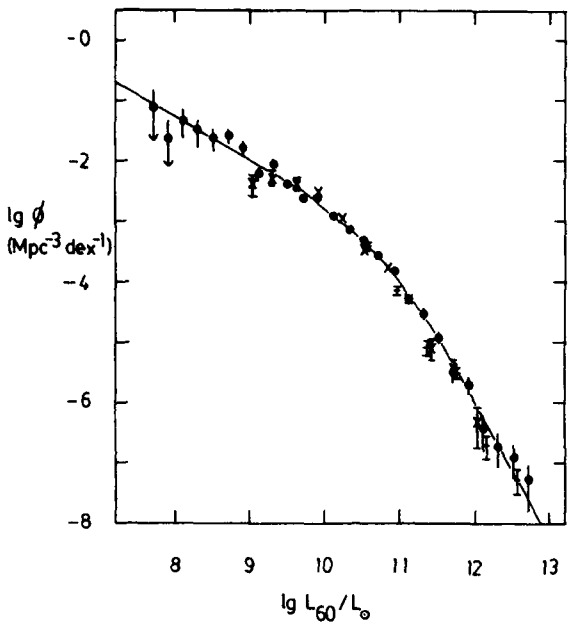

Fig 1 60 μm luminosity function for IRAS galaxies: filled circles (Lawrence et al 1986), crosses (Soifer et al 1986), x's (Rieke and Lebofsky 1986, assuming their $L_{IR} = 2.7\ L_{60}$), calculated for $\Omega = 1$, $H_0 = 50$. The solid curve is the two power-law fit of Lawrence et al.

Far infrared (10-1000μ) radiation can be expected from a normal spiral galaxy due to a variety of mechanisms. Dust in interstellar neutral hydrogen clouds, illuminated by the general interstellar radiation field, radiates prominently at 100 μ and in our Galaxy has been called the infrared 'cirrus' (Low et al 1984). The cirrus is also seen at 60 μ and more recently has been found to be radiating surprisingly stongly at 25 and 12 μ (Gautier and Beichman 1985, Boulanger et al 1985). To radiate significantly at 12 μ, interstellar grains must include a grain population much hotter than the thermal equilibrium temperature and it has been postulated that this population consists of very small grains (radius 0.001-0.003 μ, ~ 50 atoms) or, alternatively, of large molecules (Sellgren 1984, Leger and Puget 1984). Dust in the surface layers of molecular clouds will also be heated by the interstellar radiation field and in addition may be heated by young OB associations recently formed from the cloud complex. However uv photons will not be able to penetrate further than $A_V \sim 1$ into the clouds, so the bulk of the dust within molecular clouds should be at a temperature significantly lower than that in the HI clouds. Dust in the vicinity of protostars and newly formed stars embedded in molecular clouds will also radiate strongly in the far infrared. Crawford and Rowan-Robinson (1986) have shown that compact, high surface-brightness IRAS sources in the Galactic plane, many of which are associated with compact HII regions, can be modelled as hot stars embedded in a high optical depth dust cloud.

Finally high optical-depth circumstellar dust shells around late type stars, OH-IR sources and young planetary nebulae, form a related population of far infrared emitters which dominate the 12 and 25 μ emission from the bulge of our Galaxy (Habing et al 1985, Rowan-Robinson and Chester 1986) and could make a significant contribution to the 10-25 μ emission from the discs of some quiescent spirals like M31.

Turning to active galaxies, some categories like 'starburst' galaxies (Balzano 1983) may differ from normal spirals in the far infrared only in the relative proportions of the different ingredients discussed above. On the other hand galaxies with a quasar-like nucleus, eg Seyfert 1 galaxies, might be expected to produce additional far infrared radiation. Both quasars and Seyferts are known to have power-law spectra in the wavelength range 1-10 μ, with spectral index α ($S(\nu) \propto \nu^{-\alpha}$) in the range 0.5 -2 (Neugebauer et al 1979, Ward et al 1986). At visible and ultraviolet wavelengths quasars also have roughly power-law continua with a mean spectral index around 0.5 (Richstone and Schmidt 1980, Cheney and Rowan-Robinson 1981). Where such a nuclear source is located in a galaxy containing dust, for example a spiral galaxy, some of this visible and ultraviolet light will be absorbed by dust and reemitted in the far infrared.

The papers by de Jong and Brink and by Helou specifically exclude Seyferts from consideration. All three papers attempt to account for starburst and 'cirrus' components.

2. THE ROWAN-ROBINSON AND CRAWFORD STUDY

2.1 The Sample Studied

We have selected from the IRAS Point Source Catalog all those sources which have high-quality fluxes in all 4 IRAS bands (12, 25, 60, 100 μ), which are not flagged as associated with months-confirmed small extended sources (SES) in any band, and which are associated with catalogued galaxies. Associations were only accepted if they were within 2′ of the IRAS position. Where accurate optical positions are available for the galaxy the positional agreement with the IRAS source is generally better than 10″ for this sample. After deletion of 2 sources whose far infrared spectra were clearly those of stars (and for which there were also stellar associations) and of the planetary nebula NGC 6543, which picked up a spurious association with a nearby galaxy, the sample consisted of 208 galaxies.

The SES-flag condition was necessary both to eliminate contamination by cirrus emission and to ensure that the fluxes measured by IRAS represent the total flux from the galaxy. Where the emission from a galaxy is extended with respect to the IRAS beam the fluxes reported in the Point Source Catalog may be seriously underestimated and corresponding IRAS colours will be distorted.

167 have measured velocities. For the 41 which do not, we clearly have no information on their activity type either (see below). 24 are elliptical or lenticular, 127 are spiral or irregular, 57 are of unknown Hubble type, 18 are starburst or HII galaxies, 15 are Seyfert 1, 23 are Seyfert 2. Arp, Vorontsov-Velyaminov and Zwicky compact galaxies appear to be represented on a basis proportional to their frequency in the general galaxy population.

2.2 IRAS Colour-Colour Diagrams

Figures 2 a,b show the 12-25-60 and 25-60-100 μ colour-colour diagrams for the sample, with different symbols for starburst (+HII), Seyfert and other galaxies. Some striking features of this distribution are immediately apparent. (a) The starburst galaxies occupy well-defined areas of the 2 diagrams and in fact have colours very similar to those of compact HII regions in our Galaxy (Crawford and Rowan-Robinson 1986); (b) the bulk of the 'normal' galaxies (non-Seyfert, non-starburst) lie in a band stretching from the zone occupied by the starburst galaxies towards warmer S(25)/S(12) colours in Fig 2a and towards cooler S(100)/S(60) colours in Fig 2b; (c) the Seyferts spread out from this band towards lower values of S(60)/S(25), indicating the presence of a component peaking at 25 μ. Such a component was first noticed by Miley et al (1984) in 3C390.3. Low values of S(60)/S(25) have been successfully used as a criterion for selecting Seyfert galaxies by de Grijp et al (1985).

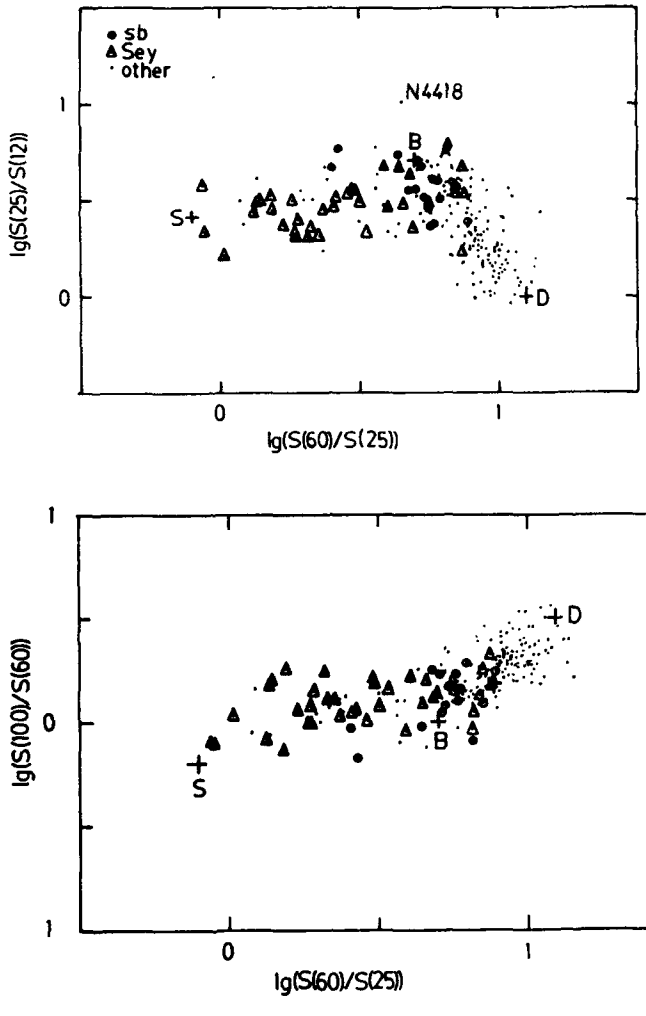

Fig 2 IRAS colour-colour diagrams for unresolved IRAS galaxies with high-quality fluxes in all 4 bands. Circled dots are star-burst (or HII) galaxies, triangles are Seyferts, dots are neither of these or unclassified to date. The crosses labelled D, B, S, are the adopted colours of the 'disc', 'starburst' and 'Seyfert' components used to synthesize the observed far infrared spectra.

2.3 A 3-Component Model for Far Infrared Spectra of Galaxies

As a first step towards understanding the range of galaxy far infrared spectra implied by Fig 2, we postulate that these spectra can be considered as a mixture of 3 components: (1) a normal 'disc' component, (2) a 'starburst' component, (3) a 'Seyfert' component. The colours adopted for these 3 components are indicated in Fig 2 by the letters D, B and S, and Fig 3 shows the corresponding spectra of the 3 components normalised to 12 μ, after colour-correction for the effect of the IRAS pass-bands. We now discuss models for each of these 3 components.

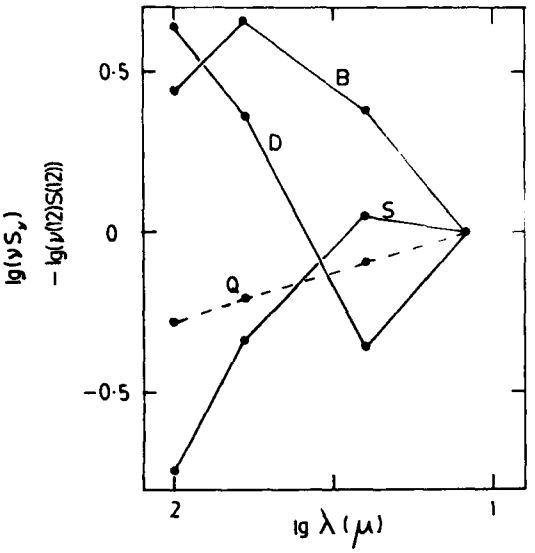

Fig 3 12-100 μ spectra, normalized to 12 μ, of adopted model components: D('disc'), B('starburst') and S('Seyfert'). The broken curve Q is the α = 0.7 power-law ('quasar') component considered for 3C273 (Fig 8c).

In Fig 4a the spectrum of the 'disc' component is compared with the spectrum of an isolated piece of cirrus in our Galaxy, a small cloud of interstellar neutral gas and dust with $A_V \sim 0.15$ presumably illuminated by the interstellar radiation field (Boulanger et al 1985). The agreement is remarkably good, showing that it is plausible to regard the 'disc' component as radiation from interstellar dust in the galaxy illuminated by the general galaxy starlight. Rowan-Robinson and Chester (1986) have estimated that emission from the bulge component identified by Habing et al (1985) would not make a significant contribution to the integrated flux from most galaxies at 12-100 μ. We have also shown an empirical fit to the 'disc' component spectrum of the form $\alpha\nu B_\nu$ (30K) + $\beta\nu B_\nu$ (210K).

Fig 4b shows the spectrum of the 'starburst' component compared with the spectrum of the 3 kpc disc observed in NGC1068 by Telesco et al (1984), with the average spectrum of star-forming clouds in our Galaxy calculated by Rowan-Robinson (1979) and with a simple model for a cloud containing a newly-formed massive star (stellar temperature T_s = 40000K, grain condensation temperature T_1 = 1000 K, uniform density, ratio of inner radius of dust cloud, r_1, to outer radius, r_2, r_1/r_2 = 0.0015, composite interstellar grain properties adopted by Rowan-Robinson (1982), ultraviolet optical depth, τ_{UV} = 100). The latter model is one from a sequence used by Crawford and Rowan-Robinson (1986) for high surface brightness sources in the

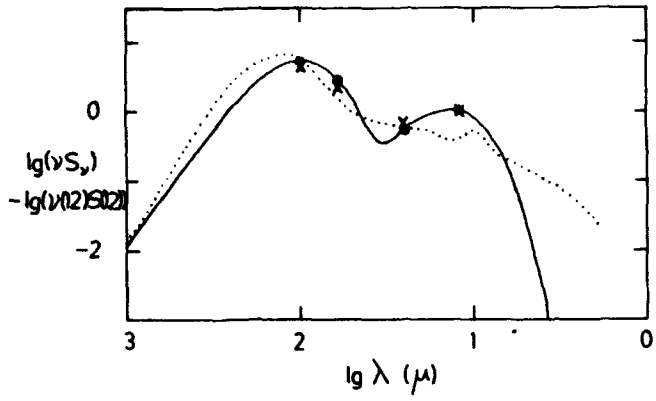

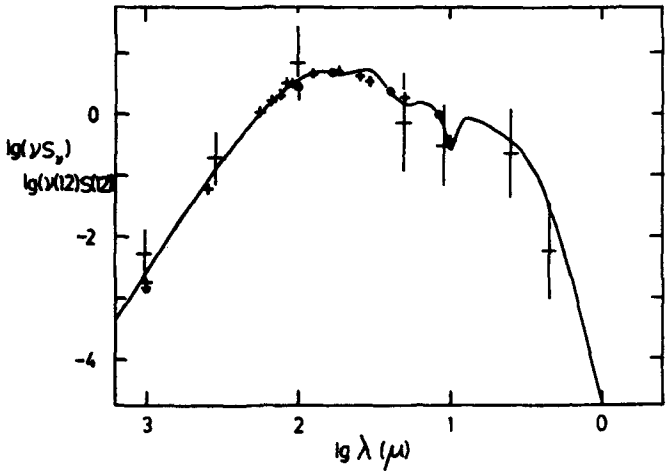

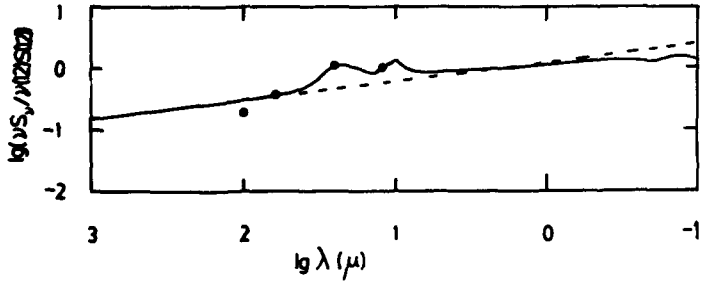

Fig 4 Model fits to the spectra of the adopted components (filled cirlces). (a) 'disc' component. The x's denote the spectrum of an isolated cirrus cloud in our Galaxy studied by Boulanger et al (1985). The dotted curve is the interstellar grain model of Draine and Anderson (1985). The solid curve is an empirical fit of the form $S_\nu = \alpha\nu B_\nu(30K) + \beta\nu B_\nu(210K)$.

(b) 'starburst' component. The small crosses are the data of Telesco et al (1984) for the 3-kpc ring in NGC 1068, which they attribute to a starburst. The large crosses are the average spectrum for regions of massive star formation in our Galaxy derived by Rowan-Robinson (1979). The solid curve is a simple model for a star-forming region of the type discussed by Crawford and Rowan-Robinson (1986), a uniform spherically symmetric dust cloud illuminated by a hot star (T_s=40000K), with optical depth τ_{uv} = 100, ratio of inner to outer cloud radius r_1/r_2 = 0.0015.

(c) 'Seyfert' component. The solid curve is a model consisting of an α = 0.7 power-law continuum source (indicated by the broken line) embedded in a spherically symmetric dust cloud with density distribution $n(r) \propto r^{-1}$, $r_1 < r < r_2$, optical depth τ_{uv} = 1 (A_v=0.23), temperature of the hottest grains T_1 = 1000K, and r_1/r_2 = 0.0055.

Galactic plane associated with star-forming regions and compact HII regions.

The agreement of the 'starburst' component spectrum with the model, with the average spectrum for star-forming clouds in our Galaxy, and with the 3 kpc disc in NGC1068 which Telesco et al (1984) argue to be a burst of star formation, is excellent.

Fig 4c compares the spectrum of the 'Seyfert' component with a simple model consisting of a central source with a power-law continuum extending from $\lambda = 0.1\ \mu$ to 1 mm embedded in a dust cloud with density distribution $n(r) \propto r^{-1}$, $T_1 = 1000$ k, $r_1/r_2 = 0.0055$, $\tau_{uv} = 1$ ($A_v = 0.23$). The agreement is satisfactory. The spectral index $\alpha = 0.7$ was selected because quasars detected by IRAS appear to have 12 - 100μ spectral indices centred on this value (Neugebauer, Soifer and Rowan-Robinson 1986). Models with $\alpha = 0.5$, 0.9 also give a reasonable fit. The dust is presumably located in the narrow-line region of the quasar-like object (see section 7). We were not able to obtain a satisfactory fit with $n(r) \propto r^{-2}$ or $n(r) =$ constant.

We conclude that there is a reasonable observational and theoretical basis for the separation into the 3 components of Fig 3 and that this separation may give valuable insight into the nature and energetics of infrared-emitting galaxies.

2.4 Deconvolution into Components

Let $\Delta\nu_i$, i = 1-4, be the effective bandwidths for the IRAS 12, 25, 60 and 100 μ bands (i.e. 13.48, 5.16, 2.58 and 1.00 x 10^{12} Hz respectively, IRAS Explanatory Supplement 1984) and suppose S_i are the fluxes in Jy in each band for a particular galaxy.

$$\text{Let } S_{tot} = \sum_{i=1}^{4} S_i \ \Delta\nu_i \qquad (1)$$

$$\text{and } y_i = S_i / S_{tot}\ ,\ i = 1\text{-}4. \qquad (2)$$

For the 'disc' component (j = 1), 'starburst' component (j = 2) and 'Seyfert' component (j = 3), let the flux in band i be $T_{j,i}$ (Jy) and let

$$T_{j,tot} = \sum_{i=1}^{4} T_{j,i}\ \Delta\nu_i \qquad (3)$$

$$t_{j,i} = T_{j,i} / T_{j,tot}. \qquad (4)$$

We then look for the least-squares solution of the over-determined set of equations

$$y_i = \sum_{j=1}^{3} \alpha_j\ t_{j,i}\ ,\ i = 1\text{-}4, \qquad (5)$$

to determine the relative proportions, α_j, j = 1-3, of the spectrum attributable to component j. If any of the α_j are found to be negative, the most negative is set to zero and the equations re-solved with one fewer variable. If one of the α_j is still negative, the remaining one is set to be 1.

Table 1 summarizes the number of each mixture combination for each galaxy type. All Seyferts but one have a 'starburst' component and all but 3 have a 'Seyfert' component. The 3 exceptions are all Type 2 Seyferts.

Table 1: Numbers of galaxies with different combinations of 'disc' (D), 'starburst' (B) and 'Seyfert' (S) components

type	number	
D	5	(NGC 2076, 4750, 5078, 5530; 23260-413)
B	5	(NGC 1614, 4418; UGC 8335; 20551-425, 23128-591)
S	1	(IC 4329A)
DB	124	
DBS	51	
DS	7	(NGC 4047, 5656, 7624, 7817; 01091-382, 02069-233, 20243-022)
BS	15	(NGC 1275, 1377, 4253, 5253, 6552; UGC 3426, 4203, 8058, 8850, 9412; 00344-334, 08171-250, 08341-261, 13197-162, 20481-571)

2.5 Correlations Between Luminosities in Components

To calculate the far infrared luminosities in each component we need to apply a correction for the incomplete wavelength coverage of the IRAS bands. Lonsdale et al (1985) have shown that the quantity $1.26(S_3\ \Delta\nu_3 + S_4\ \Delta\nu_4)$ is an excellent approximation to the 42.5–122.5 μ integrated spectrum of sources with blackbody or powerlaw spectra. The great range of spectral behaviours over the wider range 10–100 μ make it impossible to achieve as good a result over this whole wavelength range. However the quantity

$$1.26\ S_{tot} = 1.26 \sum_{i=i}^{4} S_i \Delta\nu_i \qquad (6)$$

is a good approximation to the integrated spectrum from 10–120 μ of the 'Seyfert' component model adopted here and is within 15% for the 'starburst' model, so we adopt this as a measure of the 10–120 μ far infrared flux from galaxies.

We have then calculated luminosities in each component, using

$$L_j = 1.26\ \alpha_j\ S_{tot}\ .4\ \pi d^2 \qquad (7)$$

where d is the luminosity distance calculated in an $\Omega = 1$ universe for $H = 50$. We have also calculated optical luminosities based on $\nu\ S_\nu$ in the B-band applying the de Vaucouleurs et al (1976) internal extinction correction. Corrections for interstellar extinction have been derived from the maps of Burstein and Heiles (1978), assuming $A_B = 4\ E(B-V)$. Optical luminosities have not been quoted for galaxies with $/b/ < 10^o$ unless direct estimates of interstellar extinction are available.

Fig 5 shows the correlation of L_D, the luminosity in the 'disc' component, with L_{opt}, the B-band optical luminosity, with different galaxy types indicated by different symbols. If the 'disc' component is interpreted as emission from interstellar dust as a result of absorption of starlight, then the ratio of these two luminosities can be interpreted in terms of a characteristic optical depth in dust

$$L_D/L_{opt,tot} \simeq (1 - e^{-\tau}) \quad , \qquad (8)$$

where $L_{opt,tot} \simeq \int_{opt-u\nu} L_\nu d\nu = 3.3\ L_{opt}$ by integration over the interstellar radiation field model of Mathis et al (1983). Lines of constant τ as given by (8) are indicated in Fig 5. As might be expected, early-type galaxies (E and L) have lower values of L_D/L_{opt}, consistent with a low dust content. Any contribution from dust near newly-formed stars or from circumstellar dust shells would also be lower for early-type galaxies. The values of τ are consistent with internal extinction formula of de Vaucouleurs et al (1976). We see that there is no evidence for exceptionally high internal extinction in IRAS galaxies, even where L_{IR}/L_{opt} is exceptionally high. This appears to be in contradiction to the conclusions of Moorwood et al (1986) (and also of de Jong and Brink, see section 3 below). However the corrections for interstellar extinction are very significant for several galaxies in this sample. It is possible that the minisurvey galaxies studied by Moorwood et al lie behind molecular gas associated with the Ophiuchus complex and hence that their interstellar extinction estimates based on neutral hydrogen column density are underestimates.

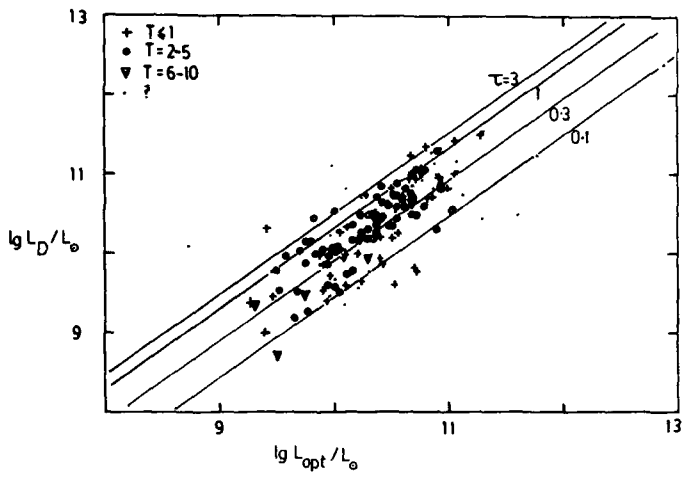

Fig 5 The correlation of the luminosity in the 'disc' component, L_D, in solar units, versus the blue luminosity of the galaxy. H_0 = 50 km s^{-1} Mpc^{-1}, and Ω_0 = 1, throughout this paper. Different symbols are used for different ranges of galaxy types, based on the parameter T of de Vaucouleurs et al (1976): + E-S0a, ⊙ Sa-Sbc, ▽ Sd-Irr, · type unknown.

The solid lines give values of the characteristic optical depth τ derived from eqn (8).

Fig 6 shows the correlation of L_B, the luminosity in the 'starburst' component with L_{opt}. Here there is a great deal of scatter, consistent with the idea of a transient, high luminosity event. There is clear evidence that barred spiral galaxies have significantly more

luminous starburst components than non-barred spirals and this is the explanation of the correlation of far infrared colour with the presence of a bar, found by Hawarden (1985).

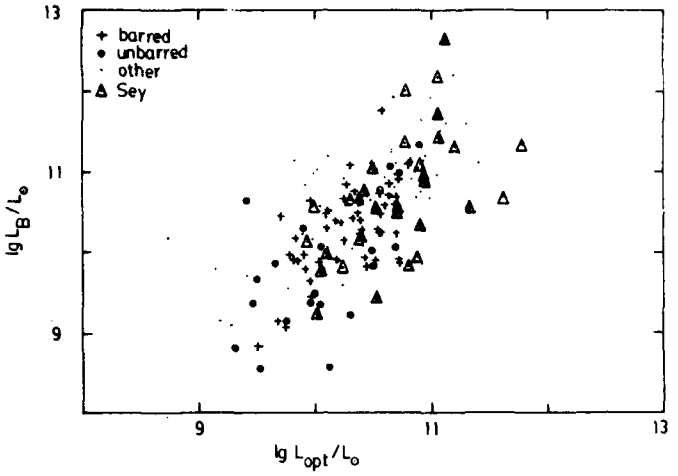

Fig 6 The correlation of the luminosity in the 'starburst' component, L_B, in solar units, versus the blue luminosity of the galaxy. The symbols denote: + barred galaxies (SB or SAB), ⊙ un-barred galaxies (SA), · bar-type unknown or not relevant, Δ Seyfert.

A broad correlation is found between L_S, the luminosity in the 'Seyfert' component, and L_B suggesting that there may be a common cause (for example, the sudden feeding of a galactic nucleus with gas) for the starburst and power-law continuum source. Fig 7 shows L_S versus L_X, the X-ray luminosity showing a good correlation, consistent with the idea that the 'Seyfert' component is dust illuminated by the central quasar-like source.

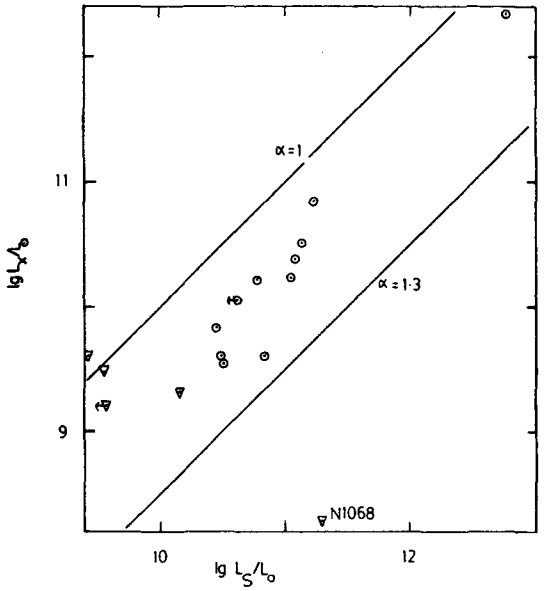

Fig 7 The correlation of the 2-10 keV ('hard') X-ray luminosity, in solar units, with the luminosity in the 'Seyfert' component. Seyferts of type 1 and 2 are denoted by circles and triangles, respectively. The straight lines are labelled with the infrared to X-ray spectral index.

Of the 14 galaxies in our sample which have $L_{IR} > 3.10^{11} L_o$ the far infrared spectra of 11 are dominated by starburst components (including the galaxy NGC6240 studied by Joseph et al 1984, Becklin et al 1985). The exceptions are the quasar 3C273, the Seyfert 1 galaxy I Zw 1, and the Seyfert 2 galaxy Mk 463.

2.6 Model Fits to the Infrared Spectrum of Selected Galaxies

For several galaxies in our sample the spectra are known at wavelengths outside the 12-100 μ range studied by IRAS, in some cases covering the range from ultraviolet wavelengths to 1 mm. These spectra provide a strong test of our models. The main conclusion of this comparison is that while our models give an excellent fit to the infrared spectra of more than 60% of the galaxies with good spectral data, the remainder require modification to give a good fit in the range 1-10 μ. These cases are almost all Seyfert galaxies and the modification required is that the optical depth across the dust cloud in the narrow-line region should be $\gg$ 1.

There are 2 other galaxies which require an additional ingredient to bring their predicted spectra into line with observations. Arp 220 (not actually in our sample) and NGC 4418 both have anomalously high {S(25)/S(12)} ratios, most easily understood as due to heavy extinction by interstellar dust in the parent galaxy.

We now discuss these 3 classes of galaxy in turn:

2.6.1.Galaxies for which the models of section 4 are a good fit. Fig 8a,b shows the visible to far infrared spectra of several galaxies for which the basic model of section 4 gives a good fit. These include the galaxy NGC 6240, for which we attribute most of the far infrared emission to a starburst component (α_2 = 0.95). The contribution of starlight can be seen at wavelengths shorter than 3 μ (except for NGC 7469, for which it has been subtracted). Fig 8c shows the data for 3C273 compared with our 3-component model and for a model with an additional pure power-law component. Although the latter improves the fit to the IRAS data, the fit to the overall spectrum is not improved. Although we can not resolve the issue of whether dust is present in the emission line region of 3C273, the IRAS data do point to the existence of a starburst in this galaxy.

2.6.2.Galaxies for which a higher optical depth Seyfert component is required. The best observed galaxy in this category is NGC 1068. Fig 8d shows the spectrum of the core ($\lesssim$100 pc) of this galaxy compared with our standard 'Seyfert' component and with a high optical depth model (β=1, T_1=500K, τ_{UV}=75, r_1/r_2=0.00215). The latter model, which involves a dust mass of 3×10^5 $M_\odot$ distributed between 4 and 180 pc from the central power-law source, is a much better fit to the observations.

On rerunning our deconvolution programme with this higher optical depth Seyfert model, there are several other galaxies for which this gives a much better fit to the overall spectra: NGC 1275, 1386, 3783, 5253 and 6764 and Mrk 3 and 231, illustrated in Fig 8c and e.

2.6.3.Arp 220. Fig 8f shows two possible models for the unusual galaxy Arp 220. This galaxy does not actually qualify for the sample studied in the present paper, since the 12 μ flux is not of sufficient quality, but the interest generated by it (Soifer et al 1984) warrants trying to understand its far infrared spectrum within the framework of the present paper.

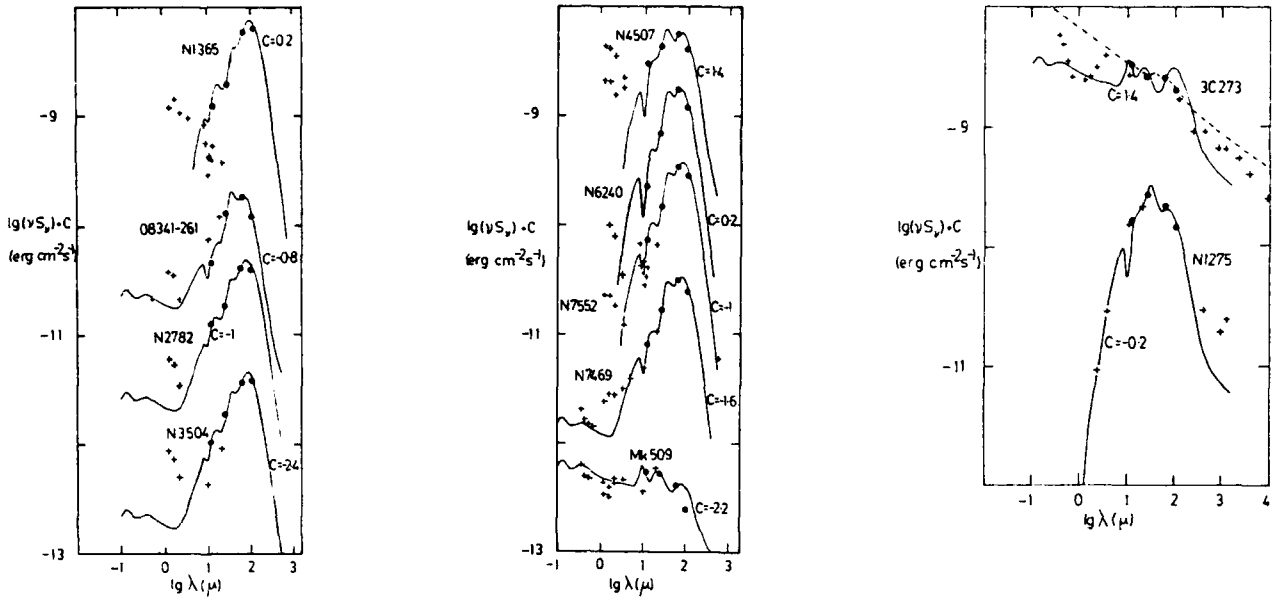

Fig 8 Ultraviolet to millimetre wavelength spectra predicted by the models of the present paper, compared with observations, for selected galaxies. The filled circles are the colour-corrected IRAS data to which the models were fitted.
(a) NGC 1365, 08341-261, NGC 2782, NGC 3504.
(b) NGC 4507, 6240, 7552, 7469 and Mk 509.
(c) Contemporaneous observations of 3C273 (solid curve: 3-component model, broken curve: 'starburst' plus α = 0.7 power-law model) and NGC 1275 (τ_{uv}=75, T_1=500K model, see Fig 8d), the latter with the contribution of starlight subtracted.
(d) The core of NGC 1068 (data from Telesco et al 1984) compared with τ_{uv}=75 Seyfert model, with T_1 = 1000K (dotted curve) and 500K (solid curve).
(e) Galaxies for which the τ_{uv} = 75, T_1 = 500K model of Fig 8d gives a better fit to the overall spectrum than our standard model: NGC 1386. Mk 3, NGC 3783, Mk 231, NGC 5253.

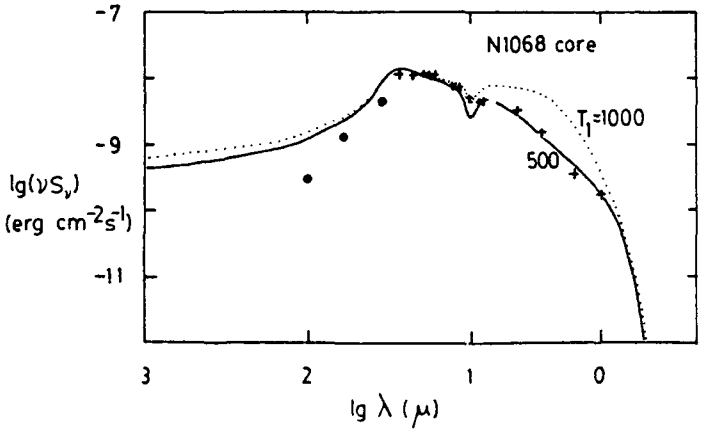

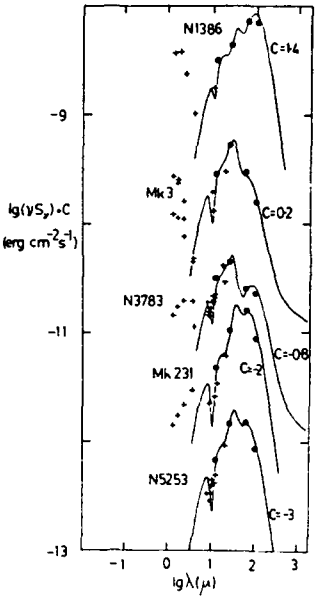

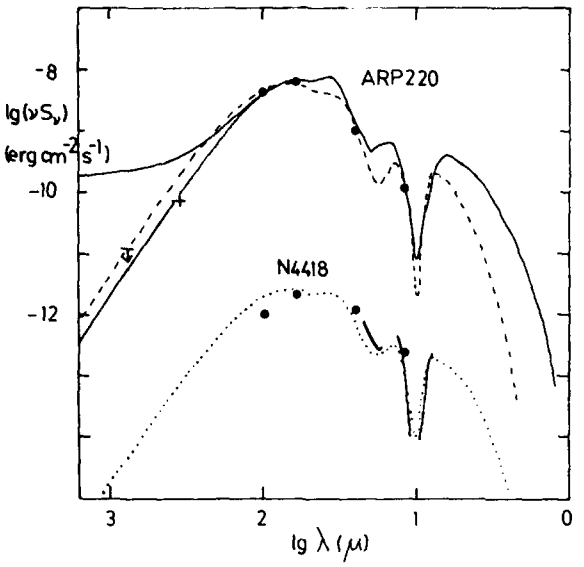

(f) Models for Arp 220 (broken curve: 'starburst' model with an additional A_V = 78 mag. of extinction by interstellar dust. Solid curve: power-law (α=0.7) continuum source embedded in uniform spherically symmetric dust cloud with τ_{uv} = 186 (A_V=40). The upper and lower solid curves at larger wavelengths correspond to whether the power-law source continues beyond 100 μ or not.) and NGC 4418 (dotted curve: 'starburst' model with an additional A_V = 39 mag. of extinction by interstellar dust).

The IRAS colours of this galaxy are unique (for example, Log{S(25)/S(12)}=1.25) and it cannot be understood as a mixture of the 3 components used in section 4. It can however be modelled either as a starburst behind very strong (A_V = 78 mag.) interstellar extinction (arising perhaps because the galaxy is seen virtually edge-on) or as a quasar embedded in a high optical depth (τ_{uv} = 186, A_V = 40) dust cloud. The predicted outer angular radii of the dust clouds are 1".7 for the starburst model with extinction and 0".37 for the embedded quasar model, and since the 20 μ emission tends to come from the inner edge of the dust cloud these are both consistent with the $\lesssim$ 1" size at 20 μ reported by Becklin et al 1986.

2.6.4.NGC 4418. This galaxy has an unusually high S(25)/S(12) ratio and a very deep 10 μ absorption feature (Roche et al 1986), both of which suggest exceptionally high extinction. It is located at l=290, b=61, where the interstellar extinction is low. Our model for this (Fig 8f) consists of a pure starburst model with an additional A_V=37 magnitudes of extinction, most of this presumably due to internal extinction in NGC 4418, which would again have to be almost edge-on.

2.7 Discussion

The model fits to the far infrared spectra of the assumed components illustrated in Figure 3 can be used to estimate the dimensions and masses of the dust clouds responsible for the infrared emission. For the 'starburst' and 'Seyfert' component models, which involve a specific optical depth in dust, the angular and linear radius of the dust cloud can be derived from the integrated flux, S_{tot} (eqn (1)) and the luminosity L_j (eqn (7)) respectively.

For the 'starburst' model we find, for a spherically symmetric cloud illuminated by a central cluster of stars,

$$\lg \theta_2(") = -7.83 + 0.5 \lg (1.26 \alpha_2 S_{tot})$$

and (9)

$$\lg r_2(cm) = 14.59 + 0.5 \lg (L_B/L_\odot)$$

The inner edge of the dust cloud is defined by

$$r_1/r_2 = 0.0015.$$

The corresponding dust mass is

$$\lg(M_d/M_\odot) = -6.32 + \lg(L_B/L_\odot). \quad (10)$$

For the galaxies in the present sample, r_2 lies in the range 3 pc to 250 pc, so the starburst activity is confined to a small region of the galaxy, presumably in most cases the nucleus. However our assumption of spherical symmetry clearly underestimates the extent if the stars are distributed through the cloud or if the starburst is actually located in a ring. For example for the NGC 1068 'starburst' component we find $\theta_2 = 3"$ and $r_2 = 30$ pc, considerably smaller than the observed 3 kpc diameter ring.

For the 'Seyfert' model we find

$$\lg \theta_2(") = -7.32 + 0.5 \lg (1.26 \alpha_3 S_{tot})$$

and (11)

$$\lg r_2(cm) = 15.11 + 0.5 \lg(L_S/L_\odot)$$

with a corresponding dust mass

$$\lg (M_D/M_\odot) = -7.81 + \lg(L_S/L_\odot). \quad (12)$$

The inner edge of the dust cloud is defined by

$$r_1/r_2 = 0.0055.$$

For the galaxies in the present sample r_2 lies in the range 30 pc to 400 pc, consistent with the dust being located in the narrow line region of the Seyfert nucleus.

For the 'disc' model we assumed $\tau_\nu \propto \nu$, but the model does not involve any specific value of τ_{UV} so we can only calculate $\tau_{100}^{1/2}\,\theta_2$, where $\tau_\nu = \tau_{100}(100\mu m/\lambda)$ is the optical depth in 30K grains. We find

$$\lg \{\tau_{100}^{1/2} r_2(cm)\} = 16.02 + 0.5 \lg(L_D/L_\odot)$$

or (13)

$$\lg\{\tau_{100}^{1/2}\ e_2(")\} = -6.90 + 0.5\ \lg\ \{1.26\ \alpha_1\ S_{tot}\}.$$

The optical depth at 12 μ in 210 K grains, τ_{12}, is related to that in 30 K grains by $\tau_{12} = 0.98 \times 10^{-4}\ \tau_{100}$. For a source to be a point source at 60 and 100 μ, the full width at half-power cannot be greater than 1'. Galaxies with $\alpha_D > 0.5$ yield $\tau_{100}^{1/2}\ e_2(")$ in the range 0.6 to 1.2 and this implies $\tau_{100} > 0.0004$. Using the interstellar grain model of Rowan-Robinson (1986), we can translate this lower limit on τ_{100} to one on A_V and find $A_V > 0.8$. This is broadly consistent with the optical depth estimates derived from Fig 5. As many of the galaxies in the present sample have Holmberg diameters considerably greater than 1', we must presume that the bulk of the far infrared emission comes from the inner part of the galaxy. This is still consistent with being reemission of starlight obscured by interstellar dust, since the halfpower width of the optical light is much smaller than the Holmberg diameter.

3. THE DE JONG AND BRINK STUDY

de Jong and Brink decompose the far infrared energy distribution into two $Q_\nu B_\nu(T)$ components with $Q_\nu \propto \nu$ and the dust temperatures T = 15, 60 K.

The warm component is heated by recently formed stars (T_S=30000 K) inside molecular clouds. 50% of the luminosity of these stars is assumed to be absorbed inside the clouds and 50% is assumed to escape and contribute to the cool component.

The cool component is heated partly by older disk stars (T_S=7000 K) in the general interstellar medium and partly by light from recently formed stars which escapes from the molecular clouds where the stars have formed.

They solve for A_B^o, the face-on extinction, L_1, the luminosity of the disk stars, and L_2, the luminosity of recently born stars, such that the IRAS 60 and 100 μ fluxes and the observed blue magnitude are reproduced. The calculation takes account of the inclination of the galaxy and the λ^{-1} dependence of extinction (so there are different optical depths for 30000 and 7000 K radiation). The analysis has been applied to two samples: a representative sample of 120 galaxies from the Revised Shapley Ames Catalog, and a subset of 20 minisurvey galaxies studied in detail by Moorwood et al (1986).

de Jong and Brink conclude that:
(i) A large fraction of the disk infrared luminosity is emitted at wavelengths >100 μm.

(ii) For the RSA galaxies the values of A_B^o and their dependence on galaxy type agree well (within a factor of two) with those derived from optical data by Sandage and Tammann (1981) and by de Vaucouleurs et al (1976). Their Fig 1 gives the average value of A_B^o for each Hubble type.

(iii) The minisurvey galaxies show enhanced star formation (higher values of L_2/L_1), higher values of A_B^o (50% of the sample have $A_B^o>1$, compared with 9% for the RSA sample), and a tendency to be more highly inclined (40% of the sample have a/b > 2.5 compared with 15% for the RSA sample). The minisurvey sample can be subdivided into 40% which are highly inclined normal galaxies and 60% which have ~3 times larger star formation rates. Galaxies in the latter group are about twice as dusty as normal galaxies.
(iv) The model gives a natural explanation of the distribution of galaxies in the L_{IR}/L_{BT} versus S(100)/S(60) diagram.

4. THE HELOU STUDY

The sample studied by Helou consists of all galaxies in 'Catalogued Galaxies and Quasars Oberserved in the IRAS Survey' (Lonsdale et al 1985) having high quality fluxes in all four IRAS bands and not flagged as extended. Most galaxies with S(60)/S(25) < 5.5 are Seyferts (de Grijp et al 1985) and are not considered further by Helou. Fig 9a shows S(60)/S(100) versus S(12)/S(25) for 'normal' galaxies (those with S(60)/S(25) > 5.5). They spread out along a band such that the warmer they are in S(12)/S(25), the cooler they are in S(60)/S(100).

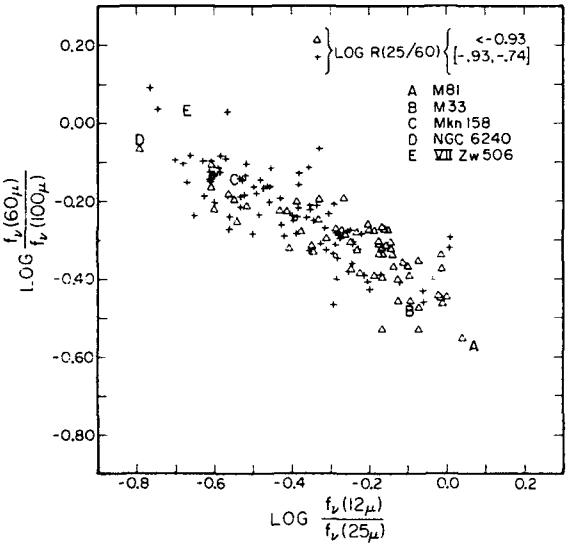

Fig 9 (a) The IRAS colour–colour diagram for 'normal' galaxies, with a few galaxies identified by letters.

The band corresponds to progressively greater star formation activity as it proceeds from the lower right hand corner to the upper left hand corner of the diagram. Galactic cirrus (Low et al 1984, Gautier 1986, Leene 1986) is found at the lower end of the band, together with very quiescent spirals such as M31 and M81. In contrast the upper end of the band is occupied by starburst galaxies like NGC 6240 (Wright, Joseph & Meikle 1984) and blue compact galaxies or 'extragalactic HII regions' such as Mrk 158, and compact Zwicky galaxies (Kunth and Sevre 1986, Wynn-Williams and Becklin 1986). This interpretation is supported by a model in which a realistic

mixture of grains including polycylic aromatic hydrocarbons (PAH) is subjected to increasingly intense radiation fields (Desert 1986: see the curve labelled D in Fig 9b).

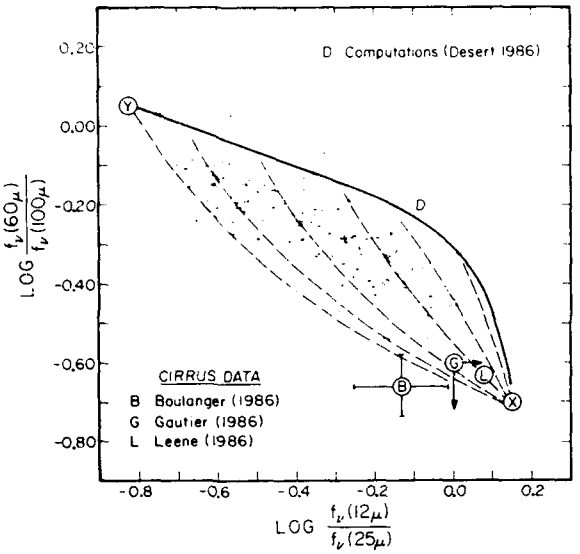

(b) As above, compared to the model by Helou. Various cirrus measurements are shown.

Two other samples of IRAS galaxies confirm the reality of the band in Fig 9: a sample of Virgo cluster spirals complete to B = 12.8 (Helou 1986), and a sample of near-by galaxies, roughly complete to an apparent diameter of 10' (Rice et al 1986). However the restriction to unresolved galaxies in the Helou and Rowan-Robinson and Crawford studies does lead to underpopulation of the low surface brightness, cooler (in S(60)/S(100)) end of the band.

Helou argues that the spread across the band implies that a simple mixing of two fixed components, C ('cirrus') and A (active component related to HII regions) is inadequate. He argues that two physical parameters are required to characterize the distribution: the intensity in its active regions, A, and the ratio A/C, where C is the (fixed) cirrus component. As the ambient radiation field goes from solar neighbourhood intensity to several hundred times this value, A traces out the curve D in Fig 9b from X to Y. As this is an upper envelope to the observed band the model is capable of explaining all galaxy colours.

The C component is due in large part to older disk stars and cannot be identified with recent star formation. The close relation between non-thermal radio and far infrared emission becomes even more intriguing, as it seems to apply independent of IRAS colour (Helou, Soifer and Rowan-Robinson 1985).

5. DISCUSSION

These 3 models for the observed normal galaxy - starburst sequence are strikingly different in their predictions of the optical properties of IRAS galaxies. In the Rowan-Robinson and Crawford model, the

starburst component is immersed in over 50 magnitudes of visual extinction, so there would be virtually no additional radiation observed in the visible. de Jong and Brink allow 50% of the radiation from the starburst to escape, so that IRAS galaxies with strong starbursts should differ in colour and intensity profile from normal galaxies. Helou's calculation (curve D in Fig 9b) is essentially an optically thin one, so would imply drastic changes to the visible appearance of a strong IRAS starburst galaxy. However Helou (1986a) argues that the dust optical depth must in fact increase for strong starburst galaxies because of the high value of L_{IR}/L_{opt}. Further study is needed to establish whether the presence of a strong, warm component at 60 and 100 μ is accompanied by changes in the visible appearance of the galaxy. My impression of the work published to date is that there is in general no drastic change. A preliminary look at the distribution of L_D/L_{opt} versus L_B/L_{opt} in the model of Rowan-Robinson and Crawford shows no evidence of the strong correlation that would be expected in the de Jong and Brink model.

The question raised by de Jong and Brink as to whether galaxies with high values of infrared-to-optical luminosity ratio also have abnormally high internal extinction deserves further study, as also does the question of whether edge-on-galaxies are over-represented (de Jong and Brink) or under-represented (Burstein 1986) in the IRAS survey. My own recommendation is that these studies should not be carried out on the minisurvey sample, much of which lies near the Ophiucus and Taurus molecular clouds, where the magnitude of interstellar extinction in our own Galaxy cannot be reliably estimated. Finally it is clear that the current star formation rate in a galaxy can not be calculated simply by multiplying the far infrared luminosity by an appropriate constant.

Acknowledgement: I am very grateful to G. Helou for presenting this paper at very short notice and for helpful comments on the manuscript.

REFERENCES

Balzano V.A., 1983, Astrophys.J. 268, 602
Becklin E.E., De Poy D.L. and Wynn-Williams C.G., 1985, Proceedings of the Infrared Detector Workshop, Laramie, Wyoming
Boulanger F. Baud B. and van Albada G.D., 1985, Astron.Astrophys 144, L9
Burstein D., 1986, preprint
Burstein D. and Heiles C., 1978, Astrophys.J. 225, 40
Cheney J. and Rowan-Robinson M., 1981, Mon.Not.R.astr.Soc. 195, 831
Crawford J. and Rowan-Robinson M., 1986, Mon.Not.R.astr.Soc., 221, 53.
de Jong, T., et al 1984, Astrophys. J., 278, L67.
de Jong, T., and Brink, K. 1986, these proceedings.
Desert, F.X. 1986, in 'Light on Dark Matter', First IRAS Symposium, ed. F. Israel (Reidel) p.213.
Draine, B.T., and Anderson, N. 1985, Astrophys. J., 292, 494.
Gautier, T.N.III 1986, in 'Light on Dark Matter', First IRAS Symposium, ed. F. Israel (Reidel) p.49.

Gautier T.N. and Beichman C.A., 1985, BAAS 16, 968
de Grijp M.H.K., Miley G.K., Lub J. and de Jong T., 1985, Nature 314, 240
Habing H.J., Olnon F.M., Chester T., Gillett F., Rowan-Robinson M. and Neugebauer G., 1985, Astron.Astrophys. 152, L1
Hawarden T., 1985, in 'Light on Dark Matter' ed. F.P. Israel (Reidel), 455.
Helou, G. 1986a, these proceedings.
Helou, G. 1986b, in 'Star Forming Dwarf Galaxies and Related Objects, eds. Kunth, D., Thuan, T.X., and Tran Thanh Van, J. (Gif-sur-Yvette; Editions Frontieres) p.319.
Helou, G., Soifer, B.T., and Rowan-Robinson, M. 1985, Astrophys. J., 298, L7.
IRAS Explanatory Supplement, 1984, C.A. Beichman, G. Neugebauer, H.J. Habing, P.E. Clegg and T.J. Chester, eds., JPLD-1855.
Joseph, R.D., Wright, G.S. and Wade, R. 1984, Nature, 311, 132.
Kunth, D., and Sevre, F. 1986, in 'Star Forming Dwarf Galaxies and Related Objects, eds. Kunth, D., Thuan, T.X., and Tran Thanh Van, J. (Gif-sur-Yvette; Editions Frontieres) p.331.
Lawrence A., Walker D., Rowan-Robinson M., Leech K.J., and Penston M.V., 1986, Mon.Not.R.astr.Soc. 219, 687
Leene A., 1986, Astron.Astrophys. 154, 295
Leger A. and Puget J.L., 1984, Astron.Astrophys. 137, L5
Lonsdale C.J., Helou G., Good J.C., and Rice W., 'Catalogued Galaxies and Quasars Observed in the IRAS Survey', 1985, (Jet Propulsion Laboratory)
Low F.J. et al, 1984, Astrophys.J. 278, L19
Miley G.K., Neugebauer G., Clegg P.E., Harris S., Rowan-Robinson M., Soifer B.T. and Young E., 1984, Astrophys.J. 278, L79
Moorwood A.F.M., Veron-Cetty M.-P. and Glass I.S., 1986, preprint
Neugebauer G., Becklin E.E., Oke J.B. and Searle L., 1976, Astrophys.J., 205, 29
Neugebauer G., Soifer B.T. and Rowan-Robinson M., 1986, in 'Structure and Evolution of Active Galaxy Nuclei', ed. G. Giuricin et al (Reidel). p.11
Neugebauer G., Oke J.B., Becklin E.E. and Matthews K., 1979, Astrophys.J. 230, 79
Rice W.L., et al 1986, preprint
Rieke G.H., and Lebofsky M.J., 1986, Astrophys.J. 304, 326
Richstone D.O. and Schmidt M., 1980, Astrophys.J. 235, 361
Roche P.F., Aitken D.K., Smith C.H., and James S.D., 1986, preprint
Rowan-Robinson M., 1979, Astrophys.J. 234, 111
Rowan-Robinson M., 1982, Mon.Not.R.astr.Soc. 201, 289
Rowan-Robinson M., 1986, Mon.Not.R.astr.Soc. 219, 737
Rowan-Robinson M., Helou G. and Walker D., 1986, Mon.Not.R.astr.Soc. (in press)
Rowan-Robinson M. and Chester T., 1986, Astrophys.J. in press
Sandage A. and Tammann G.A., 1981, 'Revised Shapley Ames Catalog of Bright Galaxies' (Carnegie Inst. Washington)
Sellgren K., 1984, Astrophys.J. 277, 623
Soifer B.T. et al, 1984, Astrophys.J. 283, L1
Soifer B.T. et al, 1986, Astrophys.J. 303, L41
Soifer B.T. et al, 1985, Astrophys.J. 278, L71

Telesco, C.M., Becklin, E.E., Wynn-Williams, C.G., and Harper, D.A. 1984, Astrophys. J., 282, 427.
de Vaucouleurs, G., de Vaucouleurs, A., and Corwin, H.Jr., 1976, 'Reference Catalogue of Bright Galaxies' (Univ. of Texas, Austin)
Ward M., Elvis M., Fabbiano G., Carleton N., Willner S.P., Lawrence A., 1986, preprint
Wright G.S., Joseph R.D., and Meikle W.P.S., 1984, Nature 309, 430
Wynn-Williams C.G., and Becklin E.E., 1986, Astrophys.J. (in press)

DISCUSSION *

PUGET:

If you consider the cirrus component in our Galaxy, about half of the heating is due to UV coming from B stars, so that component is related to star formation.

HELOU:

Yes, but it is difficult to deduce the amount of star formation from the infrared emission, because of the uncertain fraction of B star luminosity that is being re-radiated by the cirrus. The point of all this is that the relation between total infrared emission and massive star formation rate in a galaxy is not linear, but must depend on the IRAS colors.

de JONG:

I would like to react to a question that has been raised by several people this morning concerning the correlation between the far-infrared and the radio continuum emission of galaxies. The fact that not only the 60μm but also the 100μm fluxes correlate extremely well with the radio continuum flux indicates that a substantial fraction of the recently formed stars have moved out of the molecular cloud in which they were born, within their lifetime. These stars contribute significantly to the general interstellar radiation field that is supposed to heat the cool dust responsible for the 100μm emission. In our simple two-component galaxy model, presented at this meeting, this has been taken into account.

YOUNG:

On the one hand, the tight correlation between L_{IR} and radio continuum is not surprising, since within individual galaxies the continuum resembles the Hα, CO and blue light. On the other hand, I find it puzzling that the L_{IR} is so tightly correlated given that it depends on the 5th power of T_{dust}.

HELOU:

The scaling with T_{dust} is in this case an irrelevant truth, because what determines L_{IR} in the end is the amount of heating luminosity available. The reason I find the correlation puzzling is the long chain of intervening steps between L_{IR} and $L_{1.4GHz}$. On one hand, you heat dust grains with the starlight, on the other, you wait for the stars to go supernova and produce cosmic ray electrons, then take those and put them in the magnetic field to radiate. There must be a dozen free parameters, and yet the ratio $L_{IR}/L_{1.4GHz}$ is constant!

* Note: The paper was read by G. Helou.

ON THE ORIGIN OF THE 40-120 MICRON EMISSION OF GALAXY DISKS: A COMPARISON WITH H-ALPHA FLUXES

Carol J. Lonsdale Persson and George Helou
Infrared Processing and Analysis Center
California Institute of Technology, 100-22
Pasadena, CA 91125

Abstract

A comparison of 40-120 micron IRAS fluxes with published H-alpha and UBV photometry shows that the far infrared emission of galaxy disks consists of at least two components: a warm one associated with OB stars in HII-regions and young star-forming complexes, and a cooler one from dust in the diffuse, neutral interstellar medium, heated by the more general interstellar radiation field of the old disk population (a 'cirrus'-like component). Most spiral galaxies are dominated by emission from the cooler component in this model. A significant fraction of the power for the cool component must originate with non-ionizing stars. For a normal spiral disk there is a substantial uncertainty in a star formation rate derived using either the H-alpha or the far infrared luminosity.

1. INTRODUCTION

There is now a general consensus that the far infrared flux of the Galactic disk originates in part in the diffuse neutral and ionized media, heated by the general interstellar radiation field in these regions (eg. Cox and Mezger 1987). In this paper, which summarises the results of Lonsdale Persson and Helou (1987), we explore the extent to which the IRAS-measured 40-120 micron fluxes of a sample of normal disk galaxies can be attributed to the different regimes (young HII-region/GMC complexes, the diffuse neutral medium and low density HII-regions) and stellar populations (OB stars, A and later stars) which contribute to the Galactic far infrared (1-1000 micron) emission, by comparison of the 40-120 micron flux with the H-alpha flux. If the emission of galaxy disks in the IRAS bands is dominated by emission from young OB stars (either optically visible or GMC-embedded), then the IRAS fluxes might be expected to be highly correlated with H-alpha fluxes. Conversely, a poor correlation of far infrared with H-alpha flux might imply large dispersion in H-alpha extinction, far infrared emission from a mixture of HII-regions of varying density and dustiness, or a substantial contribution to the far infrared emission from older and less massive stars.

The H-alpha fluxes are taken from Kennicutt and Kent (1983), who made large aperture H-alpha+[NII] observations of over 100 disk galaxies. Our restricted sample of 54 galaxies represents all those in Kennicutt and Kent's list with high quality H-alpha, 60 micron and 100 micron fluxes, and with 60 micron flux density

Carol J. Lonsdale Persson (Editor)
Star Formation in Galaxies

greater than 2 Jy. Also, galaxies for which a significant part (>20%, as defined by Kennicutt and Kent) of the H-alpha emission originates in the nucleus, or which are known to possess Seyfert or starburst nuclei, were excluded since the primary interest here is disk emission. The measured H-alpha+[NII] fluxes were corrected for extinction and [NII] emission as recommended by Kennicutt (1983).

2. RESULTS

In Figure 1 we plot the 40-120 micron flux of the sample against the H-alpha flux and the blue flux. This far infrared flux is derived from the sum of the fluxes in the 60 and 100 micron bands (Cataloged Galaxies in the IRAS Survey, 1985, Appendix B). We have chosen not to extrapolate to 'total' (1-1000 micron) far infrared/submillimeter fluxes for the general analysis because of the uncertainties in the dust grain emissivity law and temperature distribution.

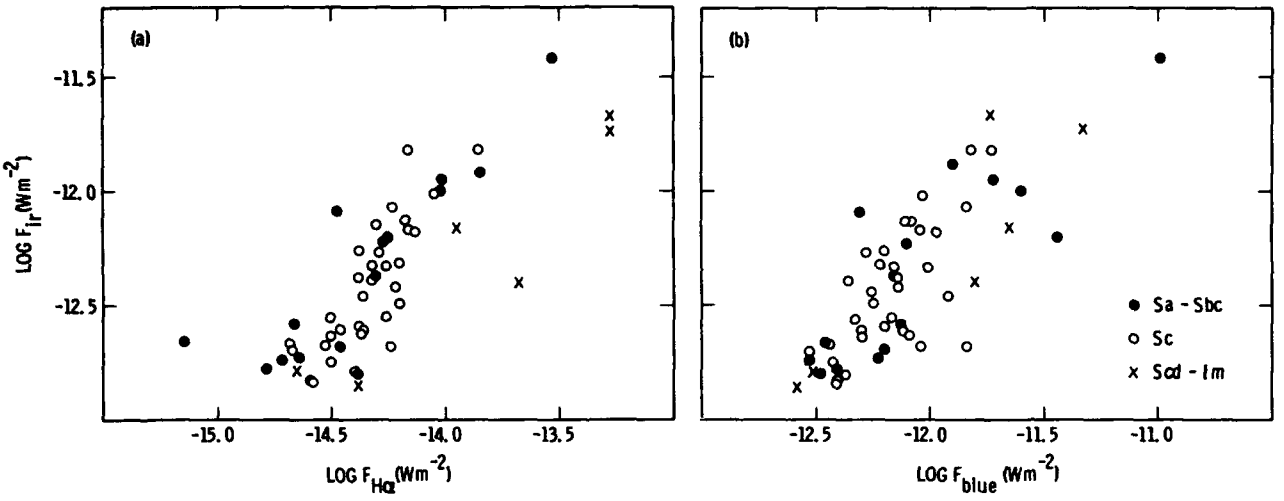

Figure 1. Correlation between far infrared and (a) H-alpha and (b) blue fluxes (derived from the extinction and inclination corrected blue magnitudes in de Vaucouleurs, de Vaucouleurs and Corwin 1976) The 54 galaxies are binned by revised Hubble type (Sandage and Tammann 1981).

The correlation between the far infrared and H-alpha flux seen in Fig 1a is quite good, with a slope consistent with unity and a Spearman's rank-order correlation coefficient r=0.81. Fig. 1b, however, shows just as good a correlation (r=0.79) between the far infrared flux and the flux within the blue filter. Good correlations still exist when both axes in these figures are normalised by the square of the angular diameter or when luminosities are plotted instead of fluxes (not shown), thus the correlations are not due to underlying correlations with distance or mass.

To investigate further the contribution to the far infrared flux by the stellar population responsible for the blue light, we derive the infrared excess, IRE, defined as the ratio of the infrared luminosity (here taken as the 40-120 micron luminosity) to the Lyman alpha luminosity (derived from the H-alpha luminosity). In Figures 2 and 3 we show the relationships of IRE and of the 60/100 micron color temperature to the equivalent width of H-alpha and the (B-V) color, respectively. IRE is proportional to the ratio of the axes of Fig. 1a, so since the slope of the relationship in that figure is consistent with unity, IRE is a measure of the residuals from the mean relation.

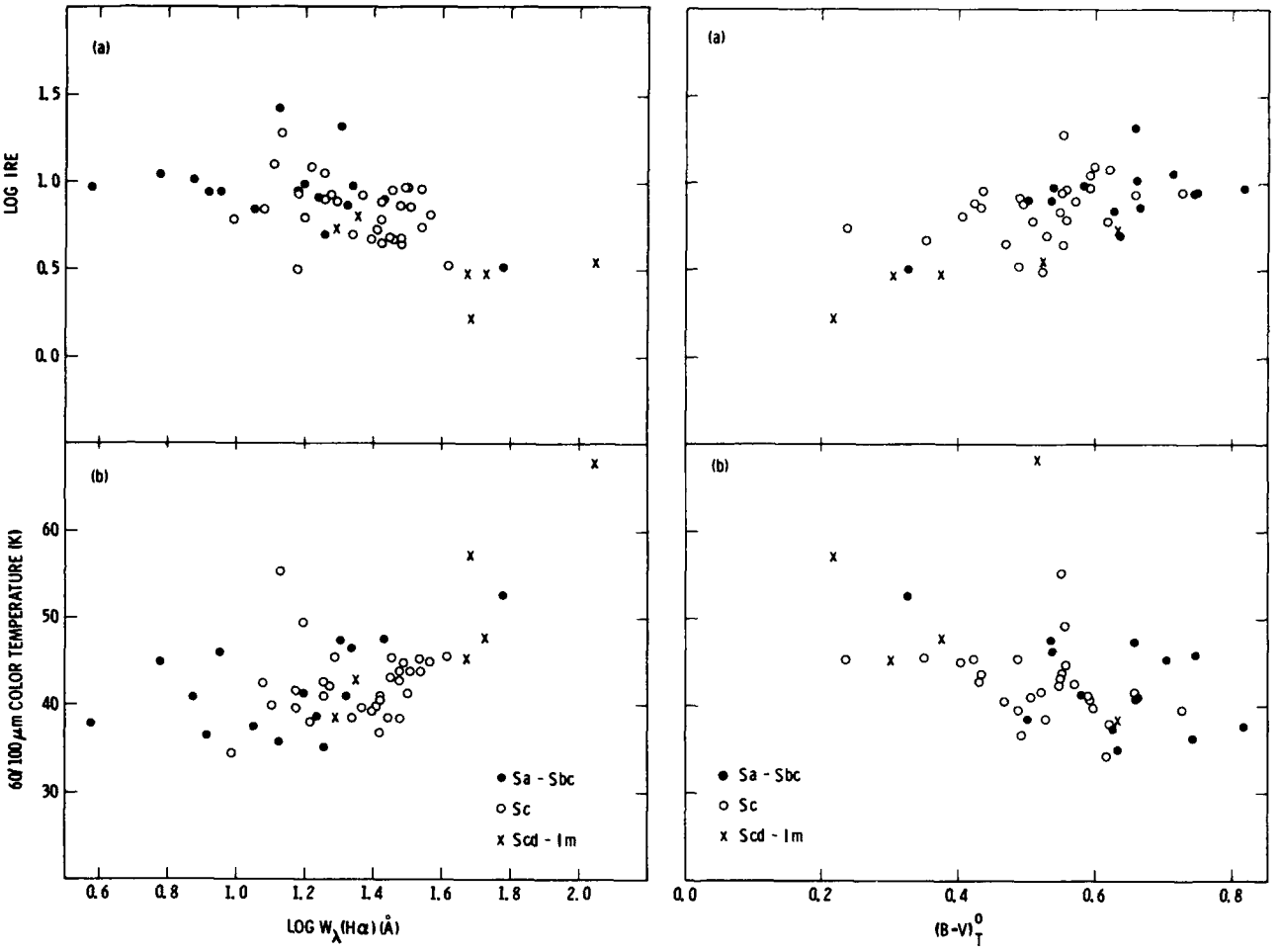

Figure 2. Relationships between the equivalent width of H-alpha and (a) the infrared excess (the 40-120 micron flux in units of the Lyman alpha flux) and (b) the 60/100 micron color temperature.

Figure 3. Relationships between (B-V) color (from de Vaucouleurs, de Vaucouleurs and Corwin 1976) and (a) the infrared excess and (b) 60/100 micron color temperature.

There is a tendency for IRE to decrease, and the color temperature to increase with the H-alpha equivalent width, which is a measure of the current relative star formation rate (Kennicutt 1983). Also, galaxies which are red in (B-V) tend to be cooler in the far infrared, and to have larger IRE. Similar relationships are seen with (U-B). It is also apparent that IRE decreases towards later morphological type, but no general gradient in color temperature can be distinguished with type, apart from the fact that very late types tend to be relatively warm, as also found by others.

3. INTERPRETATION AND MODELLING

On the basis of Fig. 1 we conclude that the 40-120 micron flux of galaxies may be powered in part by the stellar populations responsible for the blue flux, in addition to the HII-regions. The blue flux is dominated by old disk stars of 1-2 solar mass characteristic mass (Searle, Sargent and Bagnuolo 1973; Lequeux 1986; Renzini and Buzzoni 1986), which implies significant input to the far infrared flux from non-ionizing stars.

Figures 2 and 3 indicate that the coolest galaxies, which have 60/100 micron ratios similar to that of Galactic cirrus emission (Gautier 1986), tend to have high IRE, low H-alpha equivalent width and red UBV colors, while warm galaxies have 60/100 micron values which are more typical of compact HII-regions (Chini et al. 1986a,b). For these objects, IRE tends to be low, the equivalent width high and the UBV colors blue. Thus high IRE is apparently anti-correlated with optical indicators of a high star formation rate, and with dust temperature.

The simplest ways to explain this result are (i) that the far infrared flux is powered predominantly by OB stars and the trends seen in Figures 2 and 3 are due to a large dispersion in dust optical depth; (ii) that there are at least two far infrared flux components contributing to the IRAS-observed emission: a warm, low-IRE one originating with the OB star population and a cooler high-IRE one powered by the general interstellar radiation field and not strongly related to the HII-regions; and (iii) that the variations in observed IRE are driven by a changing IMF, such that the HII-regions in the high equivalent width galaxies are powered by hotter stars, resulting in higher dust temperatures and lower IREs (Panagia 1974).

We favor the second possibility described above as the most likely scenario for spiral disks with steady state star formation, which make up the bulk of our sample. A strong objection to the first model is that if the decrease in B-V in Fig. 3a were to be attributed to reddening, a visual extinction of more than two magnitudes would be required. This is much larger than typical galaxian internal extinctions. Also, there is a rough separation by Hubble-type in Fig. 3 in a sense consistent with dominance of the

B-V color by stellar populations rather by reddening. An objection to effect (iii) is that though it is likely to be operating to some extent in the high star formation rate late type galaxies such as NGC 4449 and NGC 1569, it is somewhat artificial for large disks undergoing steady state star formation.

Besides these objections raised to the other models, we favor the second interpretation because (a) there exist normal HI-rich spirals with little or no detectable H-alpha flux, which are not particularly dusty yet have normal IRAS-measured far infrared fluxes (Bothun 1986); (b) it is similar in concept to the current understanding of the situation in our own Galaxy (eg. Cox and Mezger, 1987); and (c) galaxies are known to possess substantial flux at wavelengths greater than the IRAS limit (Telesco and Harper 1980; Smith 1982; Rickard and Harvey 1984; Chini *et al.* 1984a,b) which would be identified with the cooler of the two components we propose.

To estimate the approximate contribution of the two components to the total far infrared flux we have constructed a simple two component model: a 'warm' component to be associated with the young OB star population, and a 'cool' one associated with interstellar radiation field heating of diffuse neutral material. All the H-alpha flux is associated with the warm component. Each model is defined by the 60/100 micron flux density ratio of the warm and cool component, selected to lie at or beyond the extrema of the observed distribution of this ratio and to be consistent with colors of HII complexes (Chini *et al.* 1986a,b) and of cirrus (Gautier 1986), respectively. Three values of each temperature were considered. For each galaxy and each model the combination of the two components was found that matches the observed far infrared flux and 60/100 micron ratio.

Models with warm and cool model component color temperatures of approximately 50 to 80 and 20 to 26 K, respectively, are able to fit all the sample galaxies. For these models, the contribution to the 'total' far infrared luminosity (an extrapolation of the 40-120 micron luminosity over a Planck function assuming that dust emissivity falls as the square of the wavelength) of the galaxy disks from the two components is roughly equal, with somewhat more arising in the cooler component. The 'total' IRE (derived from the 'total' far infrared luminosity) of the warm component lies in the range 2-10 for the bulk of the sample.

4. DISCUSSION

We have concluded from our simple model that in most disk galaxies a cool component, interpreted as 'cirrus' emission (dust in the diffuse neutral interstellar medium heated by the interstellar radiation field) is responsible for >50% of the 'total' far infrared flux, and that the intrinsic 'total' IRE of the remaining warm OB star-powered emission lies in the range 2-10.

We have checked that there is sufficient power in the interstellar radiation field to account for the observed infrared luminosity of the cool model component, and a large enough optical depth in the diffuse medium to absorb this energy for re-radiation in the far infrared, by comparison with the solar neighborhood cirrus models of Draine and Anderson (1985). We find that the ratio of the 100 micron flux to the HI line flux (Huchtmeier et al. 1983) is quite comparable to that predicted by the models of Draine and Anderson (1985) for most of our sample.

A good test of the existence of the cool component cirrus emission is long wavelength photometry. Only two of our sample galaxies have been measured at wavelengths longer than the IRAS limit. For these, NGC 4449 (Thronson et al. 1986) and NGC 4736 (Chini et al. 1984b), the long wavelength photometry is in better agreement with our two component model than with a single component interpretation of the far infrared data.

The infrared excess of our model warm component may be compared with predictions for model HII-regions, which vary from values as low as about 3 for low density HII-regions (Caux et al. 1984; Mezger, Mathis and Panagia 1982) to >9 (Hauser et al. 1984) depending on assumptions about the IMF, the optical depth of the gas and dust to the ionizing and non-ionizing continuum and the lines, and the gas density. Larger values can occur if very young dust-embedded stars dominate the emission, or if non-ionizing (late B and early A) stars belonging to the OB associations contribute a significant heating flux.

About 10% of the galaxies have an IRE of 2-3 for the warm model component, including half of the Sd-Im galaxies. Hence for these galaxies there is little evidence that the integrated H-alpha emission is seriously affected by extinction, or that GMC-embedded stars or very compact HII-regions are a significant fraction of the total OB star population (see also Hunter et al. 1986 and Kunth and Sevre 1986). Thus the far infrared flux of these galaxies comes primarily from the vicinity of the low density HII-regions, and the H-alpha-derived star formation rates are probably reasonably accurate.

For the remainder of the sample, which have relatively large IREs, it is not possible to rule out (a) a significant H-alpha extinction, (b) a significant trapping of the ionizing continuum by dust, or (c) a contribution to the warm component far infrared flux from either non-ionizing stars or from very young dust-embedded OB stars. Thus it is possible for these galaxies that star formation rates derived from H-alpha fluxes are severely underestimated. In view of the ambiguities associated with the interpretation of the warm component far infrared luminosity of these galaxies, it is not possible to derive reliable star formation rates from the IRAS far infrared data either.

Acknowledgements: We thank W. Rice for communication of data prior to publication, and G. Bothun for making available his UBV and H-alpha observations. We also thank G. Bothun, S.E. Persson, C. Beichman, B.T. Soifer, G. Neugebauer for critical comments. The IRAS project was managed by the Jet Propulsion Laboratory for NASA. IPAC is supported by NASA.

REFERENCES

Bothun, G. D. 1986, private communication
Cataloged Galaxies and Quasars Observed in the IRAS Survey 1985, Prepared by Lonsdale, C. J., Helou, G., Good, J. C., and Rice, W., (Washington: Government Printing Office).
Caux, E., Serra, G., Gispert, R., Puget, J. L., Ryter, C., and Coron, N. 1984, Astr. Ap., **137**, 1.
Chini, R., Mezger, P. G., Kreysa, E.,and Gemund, H.-P.1984a, Astr. Ap., **135**, L14.
Chini, R., Kreysa, E., Mezger, P. G.,and Gemund, H.-P. 1984b, Astr. Ap, **137**, 117.
Chini, R., Kreysa, E., Mezger, P. G., and Gemund, H.-P. 1986a, Astr. Ap, **154**, L8.
Chini, R., Kreysa, E., Mezger, P. G., and Gemund, H.-P. 1986b, Astr. Ap., **157**, L1.
Cox, P.,and Mezger, P. G. 1987, this volume
de Vaucouleurs, G., de Vaucouleurs, A., and Corwin, H. 1976, Second Reference Catalog of Bright Galaxies (Austin: University of Texas Press)
Draine, B. T., and Anderson, N. 1985, Ap. J., **292**, 494.
Gautier, T.N.III. 1986, in Light on Dark Matter, ed. F. P. Israel (Dordrecht: Reidel).
Hauser, M. G., Silverberg, R. F., Stier, M. T., Kelsall, T., Gezari, D. Y., Dwek, E., Walser, D., Mather, J. C., and Cheung, L. H. 1984, Ap. J., **285**, 74.
Huchtmeier, W. K., Richter, O.-G., Bohnenstengel, H.-D., and Hauschildt, M. 1983, ESO Preprint No. 250.
Hunter, D. A., Gillett, F. C., Gallagher, J. S., Rice, W. L., and Low, F. J. 1986, Ap. J., in press.
Kennicutt, R. C. 1983, Ap. J., **272**, 54
Kennicutt, R. C., and Kent, S. M. 1983, A. J., **88**, 1094
Kunth, D., and Sevre, F. 1986,in Star Forming Dwarf Galaxies and Related Objects, ed. D.Kunth and T. X. Thuan (Paris: Frontieres)
Lequeux, J. 1986, in Spectral Evolution of Galaxies, eds C. Chiosi and A. Renzini (Dordrecht: Reidel).
Lonsdale Persson, C. J., and Helou, G. 1987, Ap.J., in press
Mezger, P. G., Mathis, J. S., and Panagia, N. 1982, Astr. Ap., **105**, 372.
Panagia, N. 1974, Ap. J., **192**, 221.
Renzini, A. and Buzzoni, A, 1986,in Spectral Evolution of Galaxies, eds C. Chiosi and A. Renzini (Dordrecht: Reidel).
Rickard, L. J., and Harvey, P. M. 1984, A. J., **89**, 1520.

Sandage, A., and Tammann, G. 1981, A Revised Shapley-Ames Catalog of Bright Galaxies (Washington, D.C.:Carnegie Institute of Washington)
Searle, L., Sargent, W. L. W., and Bagnuolo, W. G. 1973 Ap. J., 179, 427.
Smith, J. 1982, Ap. J., 261, 463.
Telesco, C. M., and Harper, D. A. 1980, Ap. J., 235, 392
Thronson, H. A., Hunter, D. A., Telesco, C. M., Harper, D. A., and Decher, R. 1986, Ap. J., submitted.

DISCUSSION

MEZGER: This is more a comment than a question. In all cases in which we have extended the spectra of IRAS galaxies by observations at 350 and 1300 microns we find that (i) the 100-1000 micron luminosity is comparable to the 25-100 micron luminosity, and (ii) cold dust emission contributes a non-negligible fraction to the 100 micron flux density. This certainly complicates a spectral analysis based on IRAS data alone, and makes the interpretation of the 60/100 micron ratio in terms of a color temperature somewhat questionable.

REPLY: I agree. In fact the cold dust contribution to the 100 micron flux is just the point that we are making. Our approach is based on the fact that it is IRAS data that we now have available for thousands of galaxies, and we must understand clearly the limits to which we can use it. After making the model decomposition based on 60/100 micron color temperature, we made a correction to both the warm and cool component fluxes for flux beyond the IRAS limits. These corrections are about a factor of 1.5 - 2, similar to what you find. Also, we find a similar fraction of the total (1-1000 micron) far infrared flux to be coming from the cool component as you do.

MEZGER: Yes, we are in general agreement.

STAR FORMATION IN THE MAGELLANIC CLOUDS

Jay A. Frogel
Kitt Peak National Observatory
National Optical Astronomy Observatories
P. O. Box 26732
950 North Cherry Avenue
Tucson, AZ 85726

ABSTRACT. Because of their proximity, the Magellanic Clouds provide us with the opportunity to conduct a detailed study of the history and current state of star formation in dwarf irregular galaxies. There is considerable evidence that star formation in the Clouds has been and is proceeding in a manner different from that found in a typical well-ordered spiral galaxy. Star formation in both Clouds appears to have undergone a number of relatively intense bursts. There exist a number of similarities and differences in the current state of star formation in the Magellanic Clouds and the Milky Way. Examination of IRAS sources with ground based telescopes allows identification of highly evolved massive stars with circumstellar shells as well as several types of compact emission line objects.

1. A BRIEF OVERVIEW OF STAR FORMATION IN THE CLOUDS

We are all familiar with the well-worn cliche concerning the inability to see forests because of the trees. In astronomy the converse is often true: while global properties of galaxies can easily be studied, the extent to which the individual constituents can be observed is severely limited. But it is these individual constituents - stars and clouds of gas - that determine the appearance and evolution of a galaxy. The Magellanic Clouds present us with a unique opportunity to study the stellar content of two galaxies in considerable detail and to provide some insight to the problems of star formation and evolution in a galaxy-wide context. In this first section I will briefly review some ideas of the history of star formation in the Magellanic Clouds.

1.1 Old Stars

There is a population of stars in both Clouds which is the equivalent of the halo population of the Milky Way. These stars are old, $\geq 10^{10}$ yr, and metal poor. The two most obvious examples of this stellar population are RR Lyrae variables, found throughout both Clouds, and star clusters similar to metal poor globular clusters in the Milky Way. These stars have a metallicity between 30 and 100 times less than solar. The SMC's old population is more metal poor than the LMC's. These old stars constitute about 6% by mass of both Clouds, the same as that for the Galaxy's halo population interior to the solar circle (Frogel 1984).

Carol J. Lonsdale Persson (Editor)
Star Formation in Galaxies

1.2 Intermediate Age Stars

About 5 Gyr ago there appears to have been a major burst of star forming activity in the Clouds. Strong evidence for this comes from optical color-magnitude diagrams and luminosity functions constructed for a number of fields in both Clouds (*e.g.* Butcher 1977; Stryker 1984); from the discovery of large numbers of luminous asymptotic giant branch (AGB) M and C stars located throughout both Clouds (Blanco, McCarthy, and Blanco 1980); and, finally, from the relative number of clusters of intermediate age (*e.g.* Bica, Dottori, and Pastoriza 1986), although this line of argument has been questioned by Elson and Fall (1985).

As is the case for the oldest stars, the intermediate age population in the LMC has a higher mean metallicity than that of the SMC. On the whole, metal enrichment of the interstellar medium in the LMC appears to have occurred at a higher rate over time than that in the SMC. But even in the LMC, enrichment has proceeded much more slowly than in the Milky Way (*e.g.* Twarog 1980). References to discussions of these topics may be found in a more lengthy review article (Frogel 1984).

1.3 Young Stars

There is a significant population of objects in the Magellanic Clouds with an age of order 10^8 yrs. It is best typified by the so-called blue globular clusters and the Cepheid variables. Morphologically, the blue globulars resemble Galactic globular clusters. However, their turn-off mass is about 5-7 $M_\odot$ and their metallicity is only a factor of two down from solar. They have no obvious Galactic counterparts and appear to have formed in regions of very low gas density (Freeman 1980). The conditions which brought about their formation seem to be quite different from those which occur in the Galactic disk.

The blue globulars and AGB stars of similar age in the field of the Magellanic Clouds appear to be the result of an enhanced epoch of star formation with a production about 10% of that in the intermediate age stellar component (Frogel and Blanco 1983).

2. CURRENT STAR FORMATION

Scoville pointed out in his review talk this morning that essentially all star formation in our galaxy takes place in giant molecular clouds (GMC) which are delineated by their CO line emission. In the Magellanic Clouds there is clearly a great deal of current star forming activity. For example there are large numbers of OB stars and late type supergiants in the field of both Clouds as well as many young stellar associations and HII regions. However, the preliminary evidence from the Columbia CO survey of both the LMC and SMC pointed to a low molecular abundance.

Results of a CO survey of the LMC reported by Cohen, *et al.* (1984) indicated that H_2/HII is 5-10 times lower than in the Milky Way. A similar survey of the SMC by Rubio, *et al.* indicated an even lower ratio there. These results of course depend critically on the assumption that the CO to H_2 ratio is the same as in the Galaxy. With the possible exception

of the N159 region in the LMC, Israel (1984) found no unambiguous evidence on the basis of CO line strengths for GMC complexes in the Clouds as exist in the Milky Way.

More recently, Israel, *et al.* (1986) have argued that the CO abundance of both clouds is low not just, or even primarily, because of the low overall abundance of heavy elements, but because of the high destruction rate of molecules due to the strong interstellar UV radiation field and lower gas-to-dust ratios; the latter results in less shielding of the CO molecules. Hence, use of a Galactic H_2/CO ratio will result in gross underestimation of the H_2 abundance since this molecule is much less affected by the interstellar UV field than CO. Their model also qualitatively accounts for the relative CO strengths between the Large and Small Cloud. A search for H_2 from HII regions in the Clouds has in fact revealed its presence in quite a few objects (Israel 1986). Its discovery supports Israel, *et al.*'s contention that its true abundance cannot be inferred from observations of CO.

As reported in the poster paper at this conference by Jones, Hyland, and Harvey (hereafter PI) there appears to be a lack of high surface brightness, compact infrared cores to HII regions in the Clouds as are found in many Galactic HII regions where star formation is taking place. Elias and Frogel, in another poster paper (hereafter PII), note that they have been able to identify only a few IRAS sources associated with HII regions that are compact. "Compact" here means that the IRAS 12 and 25μm fluxes are only slightly greater than equivalent fluxes measured from the ground in apertures of a few arcseconds in diameter. In any case, the point is that such objects are rare in the Clouds. Most IRAS sources associated with HII regions are quite extended (PII). There also is an absence of highly obscured but IR/radio luminous HII regions in the Clouds (PI).

Catley, *et al.* (1981, 1982) have found obscured compact objects in the SMC and LMC which they identify as protostars but Jones, *et al.* (1986 and PI) note a general absence of low luminosity protostellar objects. Also, they find an apparent under luminosity of the HII regions for the number of ionizing photons that are inferred when compared with Galactic HII regions and the IMF of stars therein. Their interpretation of this result is that the cause is a lack of intermediate mass stars in regions of star formation. This conclusion is quite dependent on the assumption that all of the light from OB stars in the HII region is absorbed by dust and subsequently reradiated in the infrared. On the other hand, Hunter, *et al.* (1986) find that L(IR/Hα) is about the same for all dwarf galaxies with IRAS data and that this ratio is "roughly consistent with both luminosities measuring the integrated OB stellar luminosity output."

There is, of course, a danger in trying to derive an IMF from a sample of stars that represents an extremely limited slice of space and time. While there may well be some differences within HII regions, globally the IMFs for the LMC and the solar neighborhood appear to be quite similar, even for the massive stars (Humphreys and McElroy 1984).

Elias and Frogel (PII) have been attempting to identify and obtain near infrared and optical spectroscopy of IRAS sources in the Magellanic Clouds. They have observed about 65 sources, two-thirds of which have IRAS colors typical of stars. Two general results of their survey are: 1) The

relative scarcity of compact infrared sources in association with HII regions (discussed above); and, 2) a generally lower level of star forming activity in the SMC relative to the LMC.

The IRAS data by themselves cannot distinguish between luminous stars in the Magellanic Clouds and nearby field stars. Near infrared data, though, divides the IRAS sources up into three reasonably well separated categories. The first of these, about half of the star-like sources found, have *JHK* colors, CO, and H_2O indices quite similar to those of late-type giants in the solar neighborhood. Most of these can be identified with visually bright stars. Their *K* magnitudes are brighter than seventh; with very few exceptions no LMC or SMC supergiants are this bright (Elias, Frogel, and Humphreys 1985).

A second category of stellar sources consists of objects with colors and indices typical of late-type giants with circumstellar shells. CCD spectroscopy of the ones with optical counterparts usually reveals exceptionally strong TiO bands. At least one of these, in the SMC, is a carbon star. A few of the sources in this second category have no optical counterparts and probably are extreme examples of dust-enshrouded evolved objects. None, however, are as red or as luminous as the two LMC supergiants found by Elias, Frogel, and Schwering (1986) in their first look at Magellanic Cloud IRAS sources. One of these two has recently been identified as the first OH/IR star in the Magellanic Clouds by Wood, Bessell, and Whiteoak (1986). It should be remembered that although these cool, luminous stars are highly evolved, they are quite young and as such can yield important information on current star formation in the Magellanic Clouds. In particular they must play an important role in the enrichment and recycling of interstellar material.

The third category into which Magellanic Cloud IRAS sources can be divided on the basis of ground based data is compact or stellar emission line objects. Some of these are in HII regions. Others appear to be emission line stars. Some have optical spectra - permitted emission lines from neutral atomic species and from the calcium triplet - characteristic of pre-main sequence objects surrounded by a relatively dense cloud of gas and dust, presumably the remnant out of which they formed (*cf.* McGregor, Persson, and Cohen 1984). An advantage of studying such objects in the Clouds is the fact that they are all at the same distance so that the accuracy of a derived luminosity function will be limited only by the ability to find them.

In summary, we see that the history of star formation in the Magellanic Clouds and its current status, various aspects of which are considered in some of the poster papers presented at this conference, differ in a number of significant features from the situation in the Milky Way. Globally, star formation in the Clouds would be expected to be different from that in the Galaxy because of their smaller mass and lack of ordered spiral structure. The increasingly well-documented low metallicity of the Clouds, particularly of the SMC, appears to have resulted from a significantly lower rate of enrichment of the interstellar medium in these irregular systems than in the Milky Way. A lower enrichment rate could come about, for example, because of the inability of a low mass galaxy to retain the metal-enriched material present in supernova-driven winds. As pointed out by Vader (1986), such winds, even with a moderate total mass

loss rate, can carry away a substantial fraction of the heavy metal production resulting in a substantially reduced yield. A low present day abundance of heavy metals can be expected to have important effects on current star formation.

The Magellanic Clouds present us with the opportunity to study in great detail star formation in an environment different from that which obtains in the Galactic disk. Let us proceed to examine the trees and the leaves that grow on them so we may be better able to comprehend and appreciate the beauty and complexity of the forest as a whole.

I thank Terry Jones for material based on work in progress by him and his collaborators, Frank Israel for drawing my attention to his recent work on molecules in the Magellanic Clouds, and Jay Elias for considerable discussions about our own work.

REFERENCES

Bica, E., Dottori, H., and Pastoriza, M. 1986, *Astr. Ap.*, **156**, 261.
Blanco, V. M., McCarthy, M. F., and Blanco, B. 1980, *Ap. J.*, **242**, 938.
Butcher, H. 1977, *Ap. J.*, **216**, 372.
Cohen, R., Montani, J., and Rubio, M. 1984, in *I. A. U. Symp. No. 108, Structure and Evolution of the Magellanic Clouds*, ed. S. v. d. Bergh, and K. S. de Boer (Dordrecht: Reidel), p. 401.
Rubio, M., Cohen, R., and Montani, J. 1984, in *I. A. U. Symp. No. 108, Structure and Evolution of the Magellanic Clouds*, ed. S. v. d. Bergh, and K. S. de Boer (Dordrecht: Reidel), p. 399.
Elias, J. H., Frogel, J. A., and Humphreys, R. M. 1985, *Ap. J. Supp.*, **57**, 91.
Elias, J. H., Frogel, J. A., and Schwering, P. B. W. 1986, *Ap. J.*, **302**, 675.
Elson, R. A. W., and Fall, S. M. 1985, *Ap. J.*, **299**, 211.
Freeman, K. C. 1980, in *I. A. U. Symp. No. 85, Star Clusters*, ed. J. E. Hesser (Dordrecht: Reidel), p. 317.
Frogel, J. A. 1984, *Pub. A. S. P.*, **96**, 856.
Frogel, J. A., and Blanco, V. M. 1983, *Ap. J. (Letters)*, **274**, L57.
Gallagher, J. S., and Hunter, D. A. 1984, *Ann. Rev. Astr. Ap.*, **22**, 37.
Gatley, I., Becklin, E. E., Hyland, A. R., and Jones, T. J. 1981, *M.N.R.A.S.*, 197, 17P.
Gatley, I., Hyland, A. R., and Jones, T. J. 1982, *M.N.R.A.S.*, **200**, 521.
Humphreys, R. M., and McElroy, D. B. 1984, *Ap. J.*, **284**, 565.
Hunter, D. A., Gillett, F. C., Gallagher, J. S., Rice, W. L., and Low, F. J. 1986, *Ap. J.*, **303**, 171.
Israel, F. P. 1984, in *I. A. U. Symp. No. 108, Structure and Evolution of the Magellanic Clouds*, ed. S. v. d. Bergh, and K. S. de Boer (Dordrecht: Reidel), p. 319.
Israel, F. P. 1986, Proceedings of the Haystack Workshop, *Masers, Molecules, and Mass Outflows in Regions of Star Formation*, in press.
Israel, F. P., de Graauw, Th., van de Stadt, H., and de Vries, C. P. 1986, *Ap. J.*, **303**, 186.
Jones, T. J., Hyland, A. R., Straw, S., Harvey, P. M., Wilking, B. A., Gatley, I., Joy, M., and Thomas, J. A. 1986, *M.N.R.A.S.*, 219, 603.
McGregor, P. J., Persson, S. E., and Cohen, J. G. 1984, *Ap. J.*, **286**, 609.

Stryker, L. L. 1984, in *I. A. U. Symp. No. 108, Structure and Evolution of the Magellanic Clouds*, ed. S. v. d. Bergh, and K. S. de Boer (Dordrecht: Reidel), p. 79.
Twarog, B. A. 1980, *Ap. J.*, **242**, 242.
Vader, J. P. 1986, *Ap. J.*, **305**, 669.
Wood, P. R., Bessell, M. S., and Whiteoak, J. B. 1986, *Ap. J.*, 306, L81.

DISCUSSION

GALLAGHER:

Can you say anything about the number of OH/IR stars with regard to the death of AGB stars via 'superwinds'?

FROGEL:

Not at this time because our sample is restricted to the outer region of the Clouds where source confusion would not be a problem.

ISRAEL:

Under the extreme conditions exemplified by the Magellanic Clouds (e.g., low heavy-element abundances, relatively strong UV radiation field) one cannot expect CO to be a reliable tracer of H_2. In fact, despite the weakness of CO, there are several indications that the clouds may contain significant amounts of H_2. The most indirect indication is that several dark cloud silhouettes can be seen in both clouds with dimensions similar to those of Galactic GMCs.

The second indication is found in the IRAS maps, where several warm, high dust column density sources can be seen that do not have clear HI counterparts. Unless one is willing to accept wildly fluctuating and at times very high dust-to-gas ratios (in a low-z environment!) the obvious explanation is that these sources contain mostly molecular gas.

Third, Koorneef and I have detected several sources of 2μm H_2 emission, in fact in a large fraction of all sources looked at. Although it is very difficult to derive physical parameters such as mass, etc., from these detections, the frequent occurrence of H_2 emission (often at positions where CO is weak or absent) indicates that H_2 may be widespread in both Magellanic Clouds.

FROGEL:

Great! Finding large amounts of H_2 will help with one of the major problems I noted with regard to star formation in the Clouds.

ROCHE:

Did you not find any carbon stars in the Clouds?

FROGEL:

One SMC object is a C star. Without optical spectra, we cannot tell from the IR data we have whether the blank field SMC and LMC sources are C stars or M stars.

MEASURING STAR FORMATION RATES IN BLUE GALAXIES *

John S. Gallagher, III
National Optical Astronomy Observatories, Kitt Peak National Observatory,
Box 26732, Tucson, Arizona 85726

Deidre A. Hunter
Department of Terrestrial Magnetism, Carnegie Institute of Washington,
5241 Broad Branch Rd., N. W., Washington, DC 20550

ABSTRACT. The problems associated with measurements of star formation rates in galaxies are briefly reviewed, and specific models are presented for determinations of current star formation rates from Hα and FIR luminosities. The models are applied to a sample of optically blue irregular galaxies, and the results are discussed in terms of star forming histories. It appears likely that typical irregular galaxies are forming stars at nearly constant rates, although a few examples of systems with enhanced star forming activity are found among HII regions and luminous irregular galaxies.

1. INTRODUCTION

In this paper we briefly review methods for deriving star formation rates (SFRs) in galaxies with an emphasis on techniques based on the Hα and IRAS infrared luminosities (see also Güsten and Mezger 1982). Conversion of measured quantities into SFRs involves model-dependent assumptions, and it is interesting to intercompare SFRs derived by different methods as a means to test the reliability of the models. The blue irregular galaxies which we discuss include objects that are espcially well suited for this test for a variety of intrinsic and practical reasons outlined in Hunter and Gallagher (1986).

The strong emission lines and blue colors of galaxies in our sample sometimes are taken as evidence for "star burst" events. This view conflicts with results from the analysis of Gallagher, Hunter and Tutukov (1984; hereafter GHT), where a near constant SFR was found to fit most blue Irrs in agreement with earlier studies by Searle, Sargent and Bagnuolo (1973). The IRAS data base provides a new way to explore the star burst issue (as emphasized in many talks and poster papers during this conference), and we have developed a working definition for star bursts that is applicable to most types of galaxies.

2. MEASURING CURRENT STAR FORMATION RATES IN GALAXIES

To illustrate the factors involved in calculating SFRs, consider some quantity Q which is a measurable property of a stellar population in a galaxy (i.e. Q could be a luminosity, color, or mass estimate). Formally we then have

$$Q = \int_t \int_V \int_m q(m)\ \phi(m)\ w(\underset{\sim}{r})\ g(t)\ dm\ dV\ dt \cdot H(D). \qquad (1)$$

* See erratum, page 257.

This equation illustrates the many parameters that affect any apparently simple measurement of Q: q(m) is the weighting factor in stellar mass, $\phi(m)$ is the stellar initial mass function, g(t) is a description of the time evolution of the system, $w(\underset{\sim}{r})$ takes internal structural properties such as extinction into account, and $\underset{\sim}{H}(D)$ is the distance factor which is $(4\pi D)^{-2}$ for fluxes. Thus we require either good models or simple galaxies if we are to obtain reliable measurements of Qs that can be converted into SFRs, and in our work we have chosen the latter route in concentrating on studies of irregular galaxies (see Gallagher and Hunter 1984; Hunter and Gallagher 1986).

To get a current SFR for a galaxy, we must observe a Q that is sensitive to short-lived stars. If τ_g is the time scale for significant variations in SFRs over galactic scales, then we require that $q(m^*) \to 0$, where the stellar evolution lifetime τ for stars of mass m^* is $\tau(m^*) \sim \tau_g$. Unfortunately, we do not currently have good theoretical predictions for τ_g, and furthermore τ_g may vary between galaxies. A reasonable choice is $\tau_g \lesssim 10^8$ yr, which corresponds to typical dynamical time scales within galaxies. For $\tau_g = 10^8$ yr, the critical stellar mass is $m^* \sim 5\ M_\odot$. On the other hand, one should not choose too narrow a time interval to probe SFRs, since statistical noise associated with small samples of objects or small numbers of star forming sites will become a problem. For example, counting the luminosities of HII regions in the short-lived compact phase (Habing and Israel 1979) would not necessarily give a statistically reliable indicator of the current SFR in a galaxy.

To measure current galactic star formation rates, we therefore must estimate the numbers of OB stars, which is a well known result. A variety of measurable quantities Q can be used to trace OB stellar populations in galaxies: (1) Rocket ultraviolet luminosities reflect the numbers of hot stars in galaxies, but the interpretation is complicated by major extinction effects which are not easily disentangled (e.g. Huchra *et al.* 1983; Donas and Deharveng 1984; Lamb, Hunter and Gallagher 1986). (2) In a few nearby galaxies, OB stars can be directly counted and the resulting luminosity functions converted to star formation rates (Dennefeld and Tammann 1980; Hoessel and Danielson 1983). A difficulty in this approach lies in obtaining complete samples of OB stars, which is proving to be a major challenge even in the Magellanic Clouds. (3) Thermal radio emission and hydrogen recombination line luminosities measure the fluxes of Lyman continuum photons and thus the populations of hot, young stars. This approach has been successfully adopted by several groups including Smith, Biermann and Mezger (1978), GHT, Hunter and Gallagher (1986), Israel (1980), and Kennicutt (1983). These results also are sensitive to effects of dust and to the choice of model to convert observables into Lyman continuum luminosities (see the excellent summary by Güsten and Mezger 1982). (4) The far infrared luminosity *may* arise from dust heated primarily by OB stars. Our lack of understanding of the details of radiation processes responsible for L(FIR), as discussed by several papers during this meeting, introduce uncertainties into the choices of $w(\underset{\sim}{r})$ and q(m) that are needed to drive SFRs. In the pre-*IRAS* era, L(FIR) primarily was used to probe SFRs in 'star burst' galaxy candidates (e.g. Telesco and Harper 1980; Rieke *et al.* 1980; Gehrz, Sramek and Weedman 1983) and only recently has this Q been applied to galaxy populations in the general sense. (5) Radio continuum luminosities of galaxies are well-correlated with all other indicators of

current SFRs (see Klein 1982; Kennicutt 1983; de Jong et al. 1985; Helou et al. 1985; Sanders and Mirabell 1985), but suffer from a lack of understanding of the basic physical process which produces the correlation (i.e. both $w(\underset{\sim}{r})$ and $q(m)$ are not properly known). Thus at present radio continuum data must be taken as a secondary method for deriving SFRs, which relies on other techniques for absolute calibration.

3. A COMPARISON OF SFRS BASED ON FIR AND Hα LUMINOSITIES

In the spirit of eq. (1), we compress the problem of measuring a corrected Hα luminosity $L^{\circ}(H\alpha)$ from an Hα flux corrected for Galactic extinction $F^{\circ}(H\alpha)$,

$$L^{\circ}(H\alpha) = F^{\circ}(H\alpha) \cdot \exp \tau(H\alpha) \cdot (1+\gamma^{*}) \cdot (4\pi D^{2}). \qquad (2)$$

Here D is the distance, γ^{*} is a correction factor for underlying Hα stellar absorption, and $\tau(H\alpha)$ is some mean optical depth in the Hα line due to internal dust in the galaxy. From simple recombination theory, the Lyman continuum photon luminosity N_c is proportional to $L^{\circ}(H\alpha)$, $N_c = 7.3\times10^{11}\ L^{\circ}(H\alpha)\ s^{-1}$.

N_c is linked to the stellar population through the initial mass function (IMF), and following the notation of GHT with a Salpeter IMF,

$$N_c = \alpha_c \int_{m^{*}}^{m_u} (m^{-2.35})\ [\overline{n_c(m)t(m)}]\eta\ dm. \qquad (3)$$

We have adopted the Renzini-Tinsley approach in assuming a constant SFR over the time interval of interest here, in which case the time evolution of the luminosity for stars of mass m, $n_c(m)$, is replaced by an average over the appropriate stellar lifetime at mass m for the production of H-ionizing photons (see Renzini 1981). The other parameter η is an efficiency factor, and we wish to solve for the normalized SFR, α_c ($\dot{M}(H\alpha) = 5.8\alpha_c M_o\ yr^{-1}$ with a minimum stellar mass of 0.1 M_o; see GHT for details.)

The integral in eg. (3) is also sensitive to the choice of the maximum stellar mass m_u, as $\overline{n_c(m)t(m)}$ rises nearly as steeply as the Salpeter IMF falls to masses of $\gtrsim 100M_o$ (Güsten and Mezger 1982). For an $m_u = 100m_o$, we estimate

$$\dot{M}(H\alpha) = (2.5\times10^{-8})\ \eta^{-1}\ L^{0}(H\alpha)\ M_o\ yr^{-1} \qquad (4)$$

where $L^{\circ}(H\alpha)$ is measured in units of the sun's bolometric luminosity. The coefficient in eq. (4) depends on several factors, including the choice of IMF parameters, stellar evolution models, and the derivation of $n_c(m)$ as a function of time, effective temperature, surface gravity, abundance, etc. Hidden in the efficiency factor η are the escape of ionizing photons and the loss of ionizing photons due to the effects of dust. Since most of the contribution to $\dot{M}(H\alpha)$ must come from stars with lifetimes $\tau(m^{*}) \lesssim 10^{7}$ yr; Hα observations in principle provide particularly clean snapshots of star forming processes in galaxies.

An SFR can be derived from measurements of L(IR) under the assumption that massive stars play a major role in heating dust. The analog to eq. (3) is then (cf. Hunter *et al.* 1986a)

$$L^{*}(FIR) = \alpha_{I} \int_{m^{*}}^{m_{u}} (m^{-2.35}) \sum_{j} (\overline{L(m)\ \tau(m)})_{j} \beta\ dm. \qquad (5)$$

This is a more extreme simplification than in the Hα case, as the efficiency factor β should be a function of stellar temperature and the geometry of the galaxy should be taken into account in calculating the absorption of radiation. We will assume that $\beta \sim 0.5$ for all stars with an effective temperature above some threshold. The sum is over stellar evolutionary phases, and following the Renzini-Tinsley approach, we need only bolometric energies which stellar evolution models predict reasonably well (cf. Renzini 1981). Finally, we must account for infrared luminosity that is not associated with young stars, e.g. we probably should exclude the cold dust luminosity component (see Hunter *et al.* 1986a). Thus for an observed $L^{\circ}(IR)$, we have $L^{*}(FIR) = \delta L^{\circ}(IR)$ where $\delta < 1$.

For $m^{*} = 10\ M_{\odot}$ and modern stellar evolution models which include mass loss (e.g. from Maeder 1981; Brunish and Truran 1982), we find

$$\dot{M}_{1}(FIR) = 2.5\times10^{-10}\beta^{-1}\delta\ L^{\circ}(IR)\ M_{\odot}yr^{-1} \qquad (6)$$

where $L^{\circ}(IR)$ is again in bolometric solar units. The relevant time scale for eg. (5) is $\tau(m^{*}) \sim 2\times10^{7}$ yr, and we are including only stars and evolutionary phases with $\log T_{e} > 4.3$. If cooler stars are effectively heating dust, then the coefficient in eq. (6) is reduced. For example, reduction of the stellar temperature limit to $\log T_{e} > 4.0$ corresponds to $m^{*} \sim 2\ M_{\odot}$ and $\tau(m^{*}) \sim 10^{9}$ yr, while the coefficient changes only slightly to $2.1\times10^{-10}\ M_{\odot}\ yr^{-1}\ L_{\odot}^{-1}$.

Taken on their own, the FIR data thus involve a time average of the SFR over a somewhat indeterminate period, which could vary depending on physical conditions within galaxies. Dusty galaxies can have high optical depths for the absorption of radiation at visible wavelengths, and even comparatively cool stars can contribute to $L^{\circ}(IR)$. Most blue irregular galaxies lie at the opposite extreme, and have low dust optical depths in the visible (Hunter and Gallagher 1986). In these types of galaxies, UV heatings by younger stars is likely to be favored, and thus $L^{\circ}(IR)$ may be a good indicator of the current SFR.

4. APPLICATIONS TO REAL GALAXIES

4.1 Current SFRs

Blue irregular galaxies provide a way to test our ideas about SFRs and evolutionary processes in galaxies for the following reasons: (1) We have collected a large body of optical data, which includes Hα fluxes (cf. Hunter and Gallagher 1986). (2) Due to the low internal optical depths found in most Irrs, star forming sites usually are optically visible (Hunter 1982). (3) Irrs have the bluest optical colors for 'normal' (i.e. non-active) galaxies, and thus are logical candidates for star formation bursts on galactic

scales. (4) The majority of the less luminous Irrs are structurally simple and close to single zone systems, which allows primitive models to be used in interpreting observations.

We have recently collected IRAS observations of Irr galaxies included in our various optical samples (see Hunter and Gallagher 1986; Hunter et al. 1986a,b). These data are shown in Figure 1, where the Irrs basically form a continuation of the normal spirals to higher far infrared color temperatures, and perhaps somewhat more surprisingly, to higher values of L(IR)/L(B). A complete discussion of these data is currently in preparation by Hunter, Rice, Gallagher and Gillett.

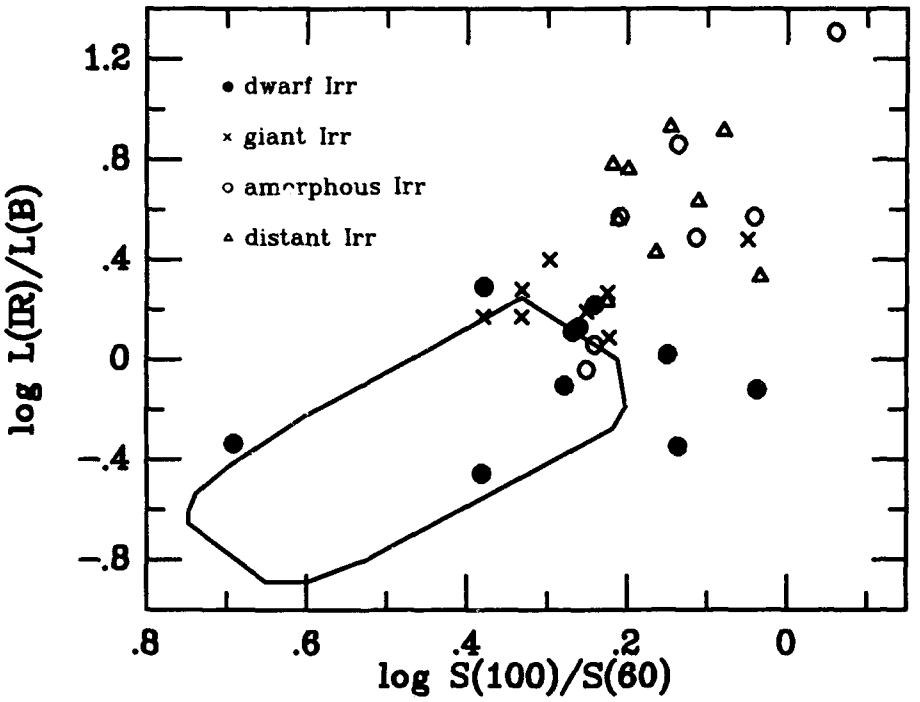

Figure 1. Irr galaxies are plotted on a luminosity-color diagram after de Jong et. al. (1984). L(B) is the blue luminosity, and S(60) and S(100) are IRAS flux measurements at 60 and 100 microns. L(IR) is derived from $\nu f(\nu)$ at 80 microns. The various structural class samples of Irr galaxies defined by Hunter and Gallagher (1986) are shown, and the approximate area occupied by spirals is outlined.

The two indicators for current SFRs, $\dot{M}(H\alpha)$ and $\dot{M}_1(IR)$, can be directly intercompared using the data for Irrs. Making the approximation that $(1+\gamma^*) = 1.0$ in eq. (2), we have

$$\frac{\dot{M}(H\alpha)}{\dot{M}_1(IR)} = 100 \frac{\exp \overline{\tau(H\alpha)} \beta L(H\alpha)}{\eta \delta L(IR)}. \qquad (7)$$

For the assumptions of high efficiencies, ($\beta = \eta \approx 1$) and low $\overline{\tau(H\alpha)}$, we obtain the limit that L(IR) = 100 L(Hα) if both luminosities measure the current SFR, and star formation has continued at a constant rate over $\gtrsim 2\times10^7$ yr (cf. eqns. 5 and 6). A minimum ratio of L(IR) = 16 L(Hα) can also be derived by assuming that, as in HII regions, equal amounts of power from O stars goes into dust heating and the eventual production of Hα emission (see Hunter et al. 1986a). The minimum model thus is appropriate where L(IR) is dominated by contributions from HII regions. The results of these models are shown in Figure 2.

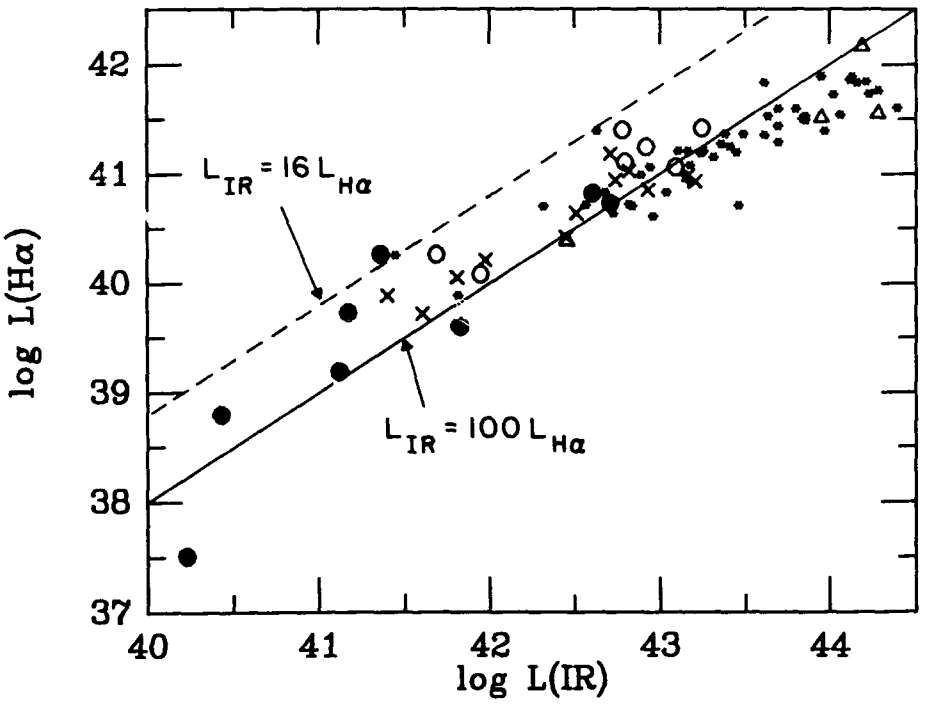

Figure 2. Hα and FIR luminosities are plotted for Irr galaxies (same symbols as in Figure 1) and spiral galaxies for which Hα fluxes have been measured by Kennicutt and Kent (1983) (plotted as stars). Model relationships are also shown.

Figure 2 is encouraging in th L(IR) α L(Hα) over a factor of ~10^4 in luminosity and the proportionality constant lies near the expected value of 100. Thus we see tht L(IR) empirically is a useful tracer of the current SFR. This diagram also shows that many details remain to be sorted out. Luminous spirals and Irrs have high L(IR)/L(Hα) ratios, which could be due to high optical depths or heating by older stellar populations. Just as puzzling are the normal Irrs where L(IR)/L(Hα) falls near our minimum estimate. It is possible that only very massive stars are contributing to the observed L(IR) in these systems, and further work is needed.

4.2 Star Formation Histories and the Existence of Star Formation Bursts

Following the approach of GHT, we can chart the evolutionary histories of galaxies by comparing SFR indicators that are sensitive to long term integrals over the SFR with estimates of current SFRs. GHT and Kennicutt (1983) have argued that most disk galaxies with active star formation have produced new stars at roughly time-constant rates during the past several Gyr. We can test the constant SFR, fixed IMF model by using the blue luminosity L(B) to estimate the average SFR over ~3Gyr (GHT).

In this case, a simple model which includes evolved stars as in eq. (5) and adopts a Salpeter IMF predicts L(B)/L(IR) ~1, where we have taken a mean optical depth at B of $\tau_B = 1.0$. Note that L(B) is the luminosity in terms of solar luminosities on the Johnson B system (one must be careful to properly define luminosities in the various color bands!). The results of this model are shown in Figure 3. Most galactic SFRs are within a factor of 3 (which is still quite large, but our model is primitive) of the constant SFR line. We will define a 'star burst' to be an epoch in which the SFR has increased by a substantial ($\gtrsim$ 3) factor over its historical mean value. Thus short-lived bursts (this diagram is most sensitive to bursts over time intervals of $\lesssim 10^9$ yr) are not common in field blue galaxies, and the only obvious burst candidate in our sample is the extragalactic HII region IIZw40. A similar result has been found by Thronson and Telesco (1986), although we have used a slightly different approach in analyzing our data.

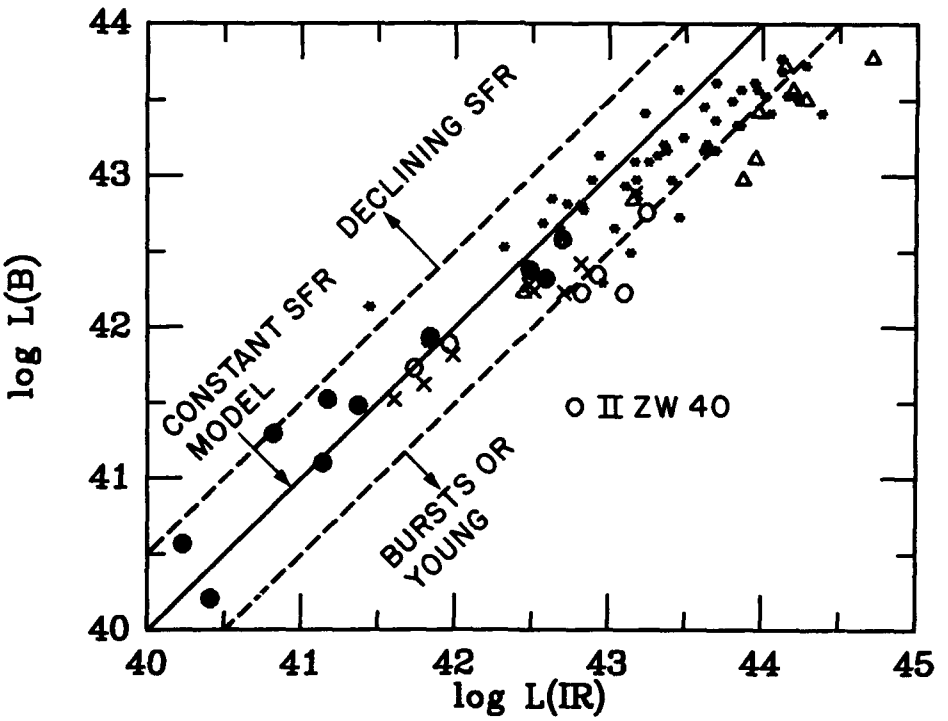

Figure 3. Predicted correlations for L(B) vs. L(IR) are shown with observed properties of spiral and irregular galaxies.

The L(B) vs. L(IR) diagram is not a useful diagnostic for systems such as M82, where τ_B is high. In these cases one can use mass-to-light ratios to detect anomalously luminous stellar populations. This approach was pioneered by Telesco and Harper (1980) and by Rieke et al. (1980), who pointed out that very low values of stellar mass-to-light ratios are indicative of overpopulations of massive stars. Using our models, we would predict $M_*/L(IR) = 2.5$ in solar units for a constant SFR, and $M_*/L(IR) \lesssim 0.5$ for high amplitude SFR bursts. Observed $M_*/L(IR)$ values in the centers of galaxies suspected of harboring star bursts are often < 0.1, which argues very strongly for the existence of bursts or some other anomaly, such as an IMF that is skewed in favor of massive stars (see Telesco 1985).

Another way to look at star formation histories is shown in Figure 4. Galaxies in region 1 have near constant SFRs in combination with either moderate $\overline{\tau(H\alpha)}$ or dust heating by older stars to give high values of L(IR) relative to optical luminosities. Area 2 contains galaxies where both L(B) and L(Hα) are very low, and these systems are likely to be very dusty and effectively opaque at visible wavelengths. The physical nature of the power sources in these hidden galaxies cannot be determined from optical observations. Area 3 contains optically thin, constant SFR galaxies, and area

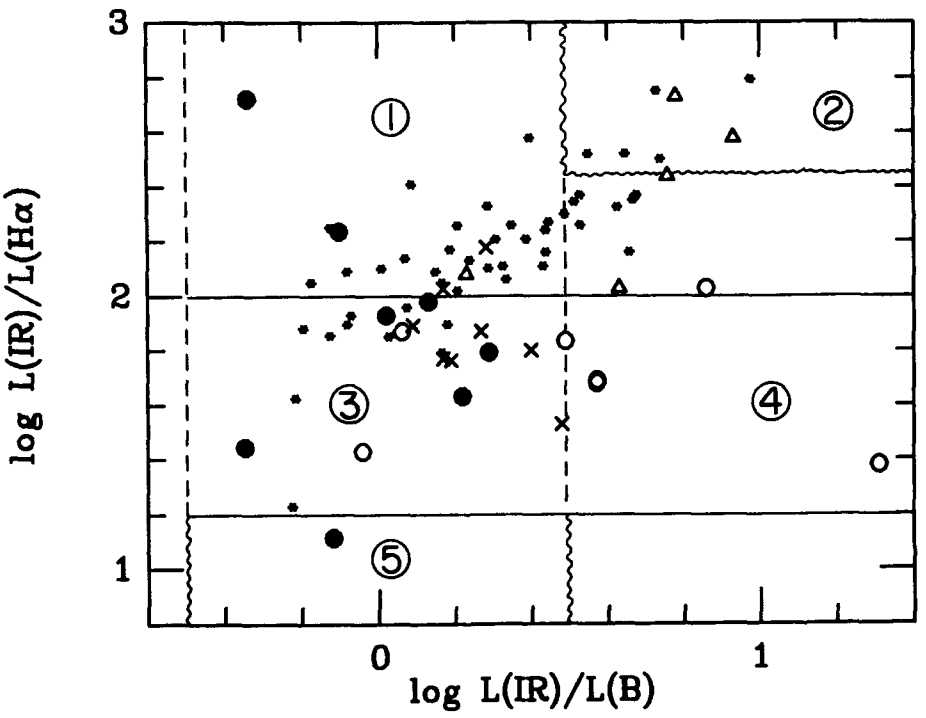

Figure 4. Irregular and spiral galaxies are plotted on a color-color diagram which can be used to study star forming histories. Different numbered regions are discussed in the text. Galaxies with high optical depths, which are effectively hidden at optical wavelengths, are found in the upper right corner, HII-region-like objects fall to the center right, and constant SFR galaxies cluster near the left-center.

4 shows the presence of a few low optical depth burst galaxy candidates. Finally Zone 5 includes galaxies which have extreme excesses of L(Hα). Very metal-poor galaxies with low dust-to-gas ratios could populate this region of the diagram, but we have no outstanding candidates for such galaxies.

5. CONCLUSIONS AND CAUTIONS

i) Both L(IR) and L(Hα) provide useful measures of current SFRs in galaxies, at least to the levels of factors of 2 or 3. It is not clear, however, what stellar lifetime should be associated with L(IR), and there are indications that the average age of the stellar populations responsible for L(IR) varies between galaxies.

ii) The majority of normal blue Irrs in our sample (which is not a complete sample; see Hunter and Gallagher 1986) have properties consistent with constant SFRs over the past 2-4 Gyr. Thus the IR observations give results that agree with the GHT optical studies (see also Thronson and Telesco 1986), and one cannot assume that galaxies with blue colors or strong emission lines are in a star burst phase. Furthermore, if the SFR is roughly constant over time, luminosities arising from different age stellar population components are correlated, and thus it is not easy to isolate the stellar population component responsible for L(IR).

iii) Optical depths may play a substantial role in determining properties of FIR-luminous galaxies. In general we expect that as the internal optical depth increases, L(IR) rises while L(Hα) and L(B) decline. We see some evidence for this trend to occur among the luminous Irrs (see Figure 4) which suggests that optical SFR measurements do not give a complete picture in these systems.

iv) SFR bursts are not common among the dwarf and normal Irr galaxies in our sample. IIZw40 has all the properties that would be expected for a high amplitude SFR burst in a small system. The very high values of L(IR)/L(B) and L(IR)/L(Hα) in combination with the substantial optical luminosities of the luminous Irrs suggest that many of these galaxies could also be in SFR burst evolutionary phases. We suspect, on the basis of optical observations, that the majority of the luminous Irrs are results of enhanced star forming activity associated with galaxy-galaxy interactions. High levels of star formation are also seen in the strongly interacting galaxy sample being investigated by H. Bushouse (1986a,b) and interactions thus may be the main source of star bursts among more luminous galaxies in nearby samples.

ACKNOWLEDGEMENTS. We thank Fred Gillett and Walter Rice for their numerous contributions to this project. We also thank the staffs at IPAC and at the National Optical Astronomy Observatories for their support of this research. Partial funding for the IRAS investigation of blue galaxies has been provided through a contract from JPL.

References

Brunish, W. and Truran, J. W. 1982, Ap. J. Suppl., **49**, 447.

Bushouse, H. A. 1986a, Ph.D. Thesis, Univ. Illinois-Urbana.

Bushouse, H. A. 1986b, this conference.

de Jong, T., Clegg, P. E., Soifer, B. T., Rowan-Robinson, M., Habing, H. J., Houck, J. R., Aumann, H. H. and Raimond, E. 1984, Ap. J. (Letters), **278**, L67.

de Jong, T., Klein, U., Wielebinski, R. and Wunderlich, E. 1985, Astron. Ap., **147**, L6.

Dennefeld, M. and Tammann, G. A. 1980, Astron. Ap., **83**, 275.

Donas, J. and Deharveng, J. M. 1984, Astron. Ap., **140**, 325.

Gallagher, J. S. and Hunter, D. A. 1984, Ann. Rev. Astron. Ap., **22**, 37.

Gallagher, J. S., Hunter, D. A. and Tutukov, A. V. 1984, Ap. J., **284**, 544.

Gehrz, R. D., Sramek, R. A. and Weedman, D. W. 1983, Ap. J., **267**, 551.

Güsten, R. and Mezger, P. G. 1982, Vistas in Astron., **26**, 159.

Habing, H. and Israel, F. 1979, Ann. Rev. Astron. Ap., **17**, 345.

Helou, G., Soifer, B. T. and Rowan-Robinson, M. 1985, Ap. J. (Letters), **298**, L7.

Hoessel, J. and Danielson, G. 1983, Ap. J., **271**, 65.

Huchra, J., Geller, M., Gallagher, J., Hunter, D., Hartmann, L., Fabbiano, G. and Aaronson, M. 1983, Ap. J., **274**, 125.

Hunter, D. A. 1982, Ap. J., **260**, 81.

Hunter, D. A., Gillett, F. G., Gallagher, J. S., Rice, W. L. and Low, F. L. 1986a, Ap. J., **303**, 171.

Hunter, D. A., Rice, W. L., Gallagher, J. S. and Gillett, F. 1986b, this conference.

Hunter, D. A. and Gallagher, J. S. 1986, P.A.S.P., **98**, 5.

Israel, F. P. 1980, Astron. Ap., **90**, 246.

Kennicutt, R. C. 1983, Ap. J., **272**, 54.

Kennicutt, R. C. and Kent, S. M. 1983, A. J., **88**, 1094.

Klein, U. 1982, Astron. Ap., **116**, 175.

Lamb, S., Hunter, D. A. and Gallagher, J. S. 1986, this conference.

Maeder, A. 1981, Astron. Ap., **102**, 401.

Renzini, A. 1981, Ann. Phys., **6**, 87.

Rieke, G., Lebofsky, M., Thompson, R., Low, F. and Tokunaga, A. 1980, Ap. J., **238**, 24.

Sanders, D. and Mirabell, I. F. 1985, Ap. J. (Letters), **298**, L31.

Searle, L. E., Sargent, W. L. W. and Bagnuolo, W. 1973, Ap. J., **179**, 427.

Smith, L. F., Biermann, P. and Mezger, P. G. 1978, Astron. Ap., **66**, 65.

Telesco, C. M. 1985, in Extragalactic Infrared Astronomy, ed. P. M. Gondhalekar (Chilton: Rutherford Appleton Lab.), p.87.

Telesco, C. and Harper, D. 1980, Ap. J., **235**, 392.

Thronson, H. and Telesco, C. 1986, Ap. J., in press.

DISCUSSION

YOUNG:

In your plot of $L_{H\alpha}$ vs. L_B was NGC 1569 included?

GALLAGHER:

Yes, it looks normal. This is probably an indication that the epoch of enhanced star formation has been going on for $\sim 10^9$ yr. For time scales of $\gtrsim 10^9$ yr, the $L_B/L_{H\alpha}$ ratios rapidly approach their equilibrium values for constant SFR systems.

CO OBSERVATIONS OF GALAXIES WITH THE NOBEYAMA 45-M TELESCOPE

Y. SOFUE[1,2], T. HANDA[1,2], M. HAYASHI[2], and N. NAKAI[2]
1. Department of Astronomy, University of Tokyo, Bunkyo-ku, 113 Tokyo,
2. Nobeyama Radio Observatory, Minamisaku, 384-13 Nagano, Japan

ABSTRACT

High-resolution (15"), filled aperture maps of the CO (J=1-0) line emission have been obtained of several nearby, CO-bright galaxies like M82, M83, IC342, NGC891, etc. in order to study star forming activity in these galaxies.

1. INTRODUCTION

Star formation in galaxies is intimately related to their molecular hydrogen content from which stars form. In order to obtain high-resolution, high-sensitivity and filled aperture maps of H_2 gas in spiral galaxies, we have conducted a survey of the CO (J=1-0) line emission at 115 GHz using the 45-m telescope at the Nobeyama Radio Observatory. The survey already includes nearby, CO-bright galaxies like M82, M83, M51, NGC253, NGC891, IC342, and NGC6946. We have obtained an almost complete map of M82, a map of the bar and central region of M83, a map of the central region of IC342, high-sensitivity scans along the major and minor axes of the edge-on galaxy NGC891, and several incomplete maps of the other galaxies. The survey is being extended to more galaxies. In this paper we report the results for NGC891, M83, IC342, and M82.

2. NGC891

The large-scale distribution of the CO line emission in disk galaxies has an important implication for understanding the structure and dynamics of gaseous content and the evolution of star-forming activity on a galactic scale. In the case of edge-on galaxies, one dimensional scan maps can give fairly complete information about the large-scale CO distribution in a realistic observing time.

NGC891, a typical edge-on Sb, shows a very similar property to our Galaxy. It has been observed in CO using the FCRAO 14-m telescope with a resolution of 45" (Solomon 1981;1983). The CO intensity distribution is characterised by a ring-like concentration at radius 5 kpc and a central hole. It is well known that the Milky Way, a typical Sb galaxy, has a strong central concentration of molecular gas forming a dense nuclear disk (e.g. Liszt and Burton 1978). It is therefore interesting to clarify by high-resolution observations whether Sb galaxies like NGC891 have a nuclear molecular disk. Another important implication of the CO observations of edge-on galaxies is to derive a rotation curve of molecular gas without the ambiguity of inclination angle. A CO rotation curve is especially important to see the dynamics of the central region, for the HI emission has a depression, giving poor information about the central region (Sancisi and Allen 1979).

Observed CO line spectra along the major axis are shown in figure 1. The intensities are corrected antenna temperature calibrated with respect to Ori A

Carol J. Lonsdale Persson (Editor)
Star Formation in Galaxies

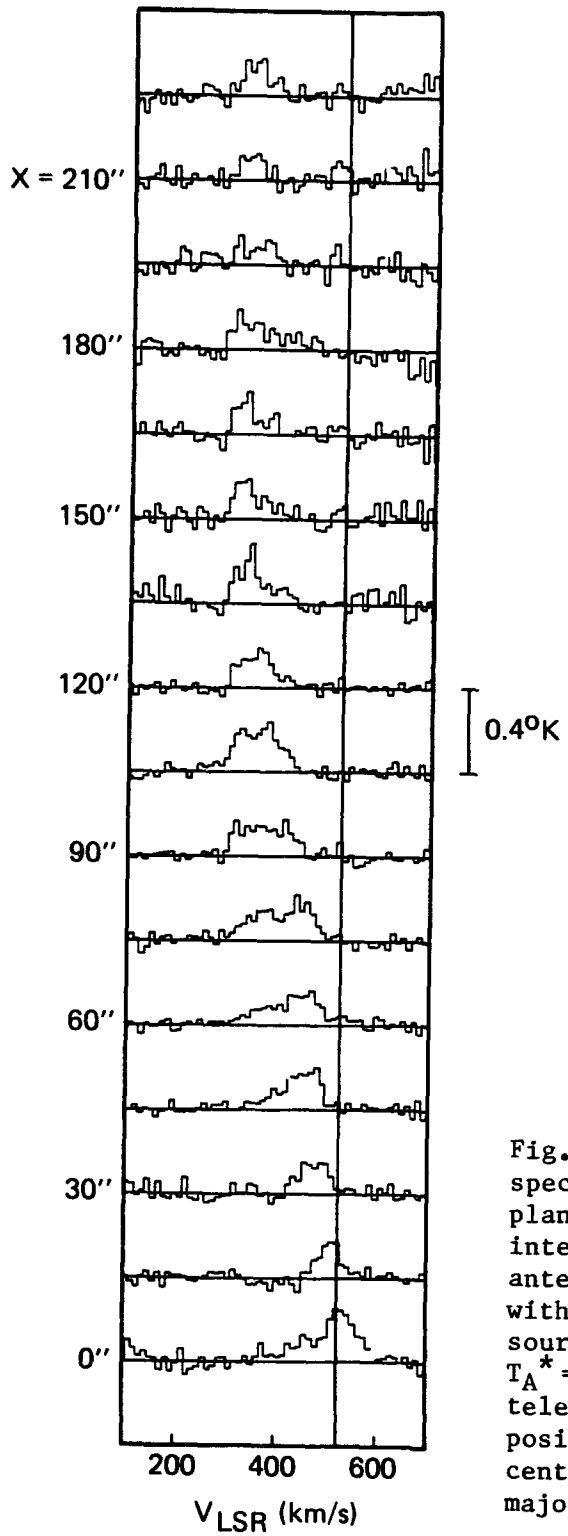

Fig. 1. ^{12}CO (J=1-0) line spectra along the galactic plane of NGC891. The intensity is the corrected antenna temperature T_A^* with respect to a standard source Ori KL which had $T_A^* = 35$ K with the 45-m telescope. Here X is the position off-set from the centre toward NE along the major axis.

with $T_A^* = 35$ K. Figure 2 shows a position-velocity diagram along the major axis. The rotation curve as derived from the terminal velocities (as drawn with the dashed line) coincides with the HI rotation curve of Sancisi and Allen (1979). From the rotation curve the dynamical mass contained within 15 kpc (225") is estimated to be 2×10^{11} $M_\odot$. The diagram shows that there exist many clumpy structures, which we identify with tangential directions of spiral arms, except for the central strong peak.

The distribution of integrated CO intensity is shown in figure 3. We find that the radial CO distribution is composed of two components: a broadly spread main-disk with the maximum at 60" (5 kpc) radius, tailing as far as to 15 kpc from the center, and a strong concentration toward the center, having a sharp peak of $I_{CO} = 26$ K km s^{-1}, which we refer to as the nuclear disk.

The main disk is distributed on a broad ring of radius 5-15 kpc with its peak at about 5 kpc. This well resembles that of our Galaxy which has the 5-kpc molecular ring. The main disk is well visible at least up to 15 kpc and appears to extend further beyond this radius. The total mass of molecular hydrogen gas, as derived using the same conversion factor as that used in Solomon (1983) but taking care of the difference between the antenna temperature of Ori A for the 45-m telescope and the 14-m telescope, is about 7×10^9 $M_\odot$. This shares 4 percent of the dynamical mass and this fraction is comparable to that in our Galaxy.

The nuclear disk has a radius of about 0.5 kpc, but the thickness is not resolved. This component has been detected for the first time for an external Sb galaxy, which confirms that NGC891 has a similar characteristics to our Galaxy, as the size and mass, 3×10^8 $M_\odot$, of molecular gas, are comparable to the nuclear disk in our Galaxy. The velocity dispersion near the center of this component is more than 100 km s^{-1}. The high dispersion may be partly due to internal motion of gas and partly to the steep gradient of the rotation curve. From the velocity dispersion a dynamical mass of 10^9 $M_\odot$ is derived. This leads to a fractional mass of molecular gas in the nuclear disk as high as 30 percent, much higher than that observed in the main disk. This suggests either that the molecular gas is really rich or that the conversion factor from I_{CO} to H_2 mass adopted here (Solomon 1983; Young and Scoville 1982) was too large. If the latter is the case, we have a higher rate of production of heavy elements in the central region than in the main disk: if the molecular mass shares $\sim$10% of the dynamical mass as in the main disk, the CO abundance in the nuclear region is about three times as large as that in the main disk.

Figure 3 compares the CO distribution with those of HI (Sancisi and Allen 1979) and radio continuum (Allen et al. 1979). The CO main disk has a similar distribution to that of the broad disk of the continuum emission. The HI gas is more widely distributed than CO and continuum. The CO nuclear disk coincides well in position with the central peak of continuum. This shows a significant correlation between the nuclear activity and the existence of a dense molecular disk in the center. A detailed description is given in Sofue et al. (1986).

2. M83

The SABc galaxy M83 is the nearest barred spiral (3.7 Mpc distance). The bar structure in a galaxy gives a deep nonlinear potential wave in the rotating material. The interstellar gas suffers a strong shock wave in such a deep

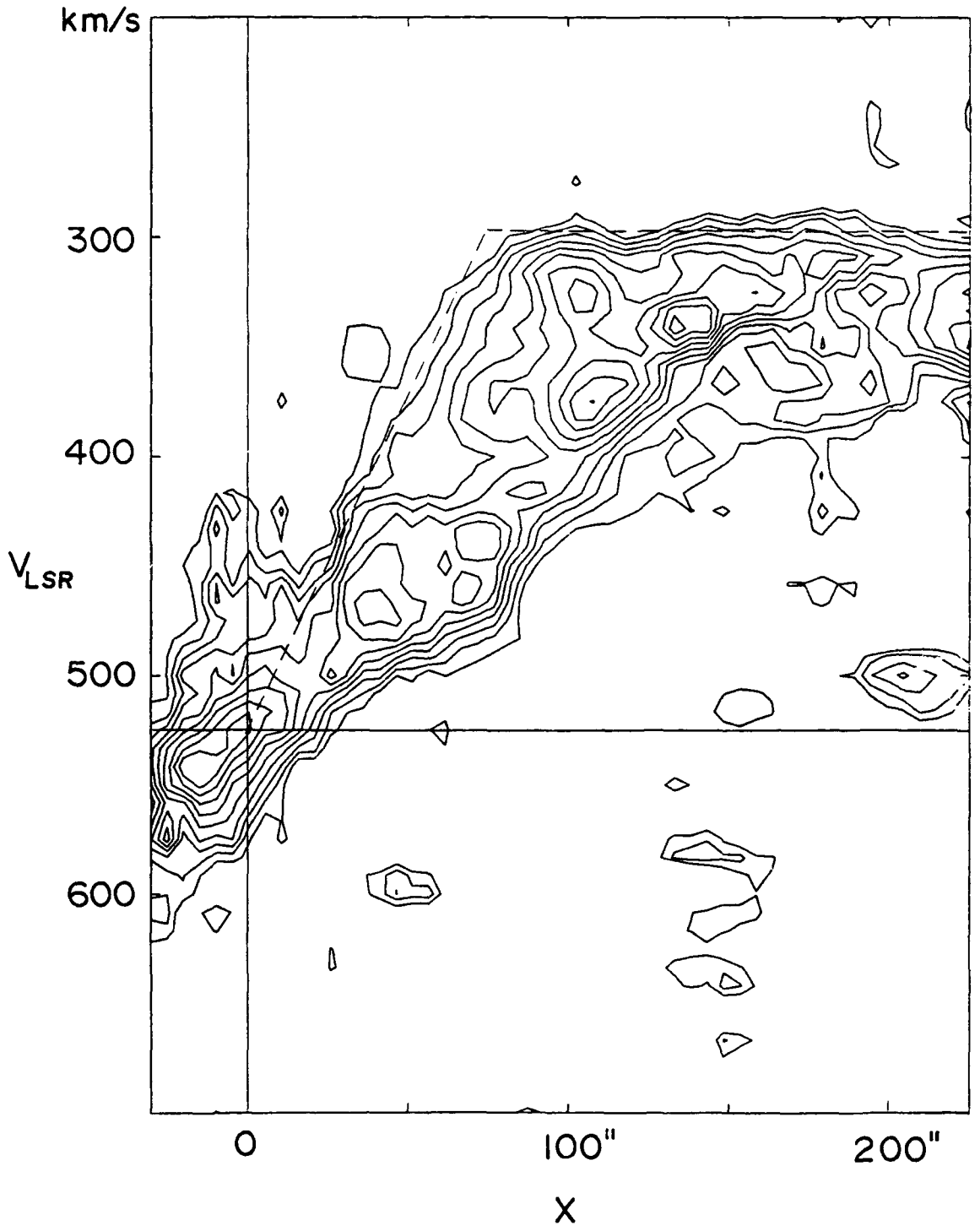

Fig. 2. Position-velocity diagram along the galactic plane of NGC891. The contours are in steps of 20 m K T_A^* and the lowest contour is at 40 m K.

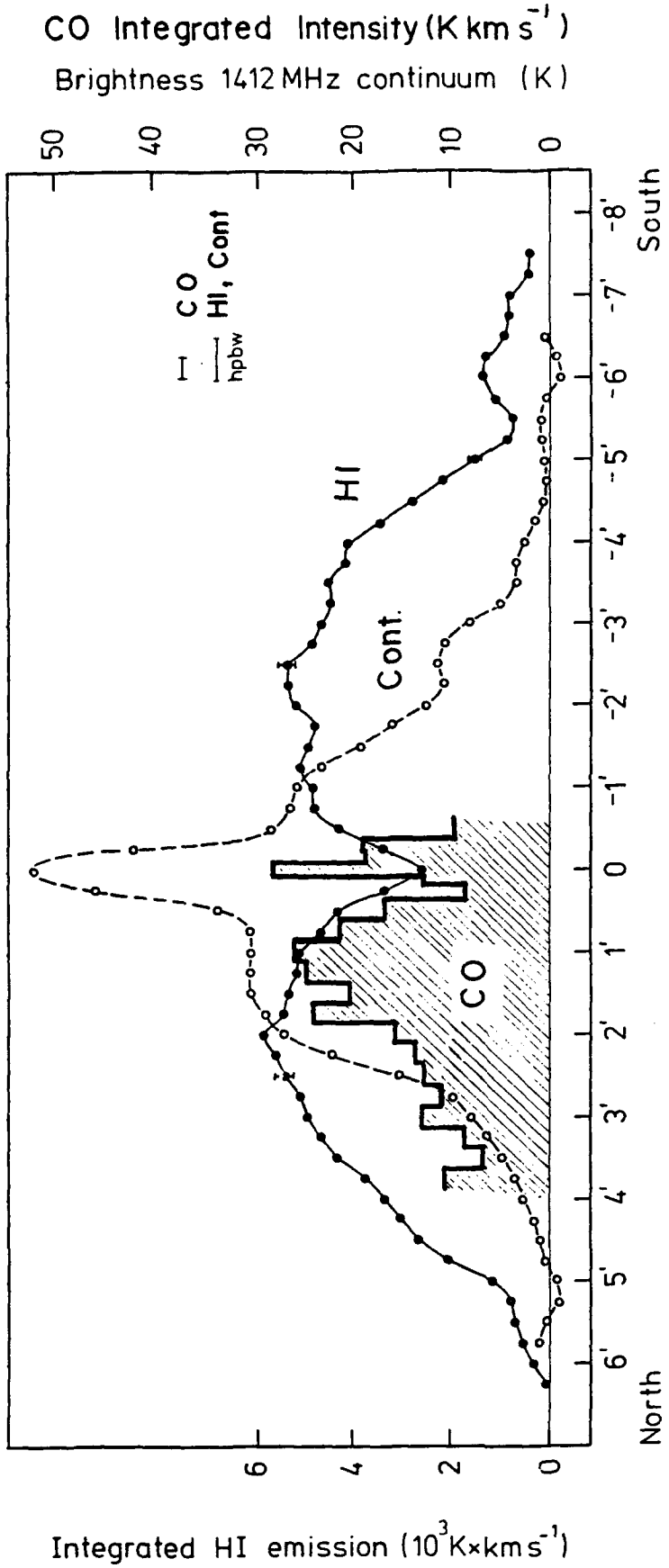

Fig. 3. Intensity distribution of the integrated CO line emission along X (hatched diagram). The HI (Sancisi and Allen 1979) and radio continuum (Allen et al. 1978) intensity distributions are superposed for a comparison. Note the coincidence of the CO main disk with the continuum disk and of the CO nuclear emission with the continuum nuclear emission.

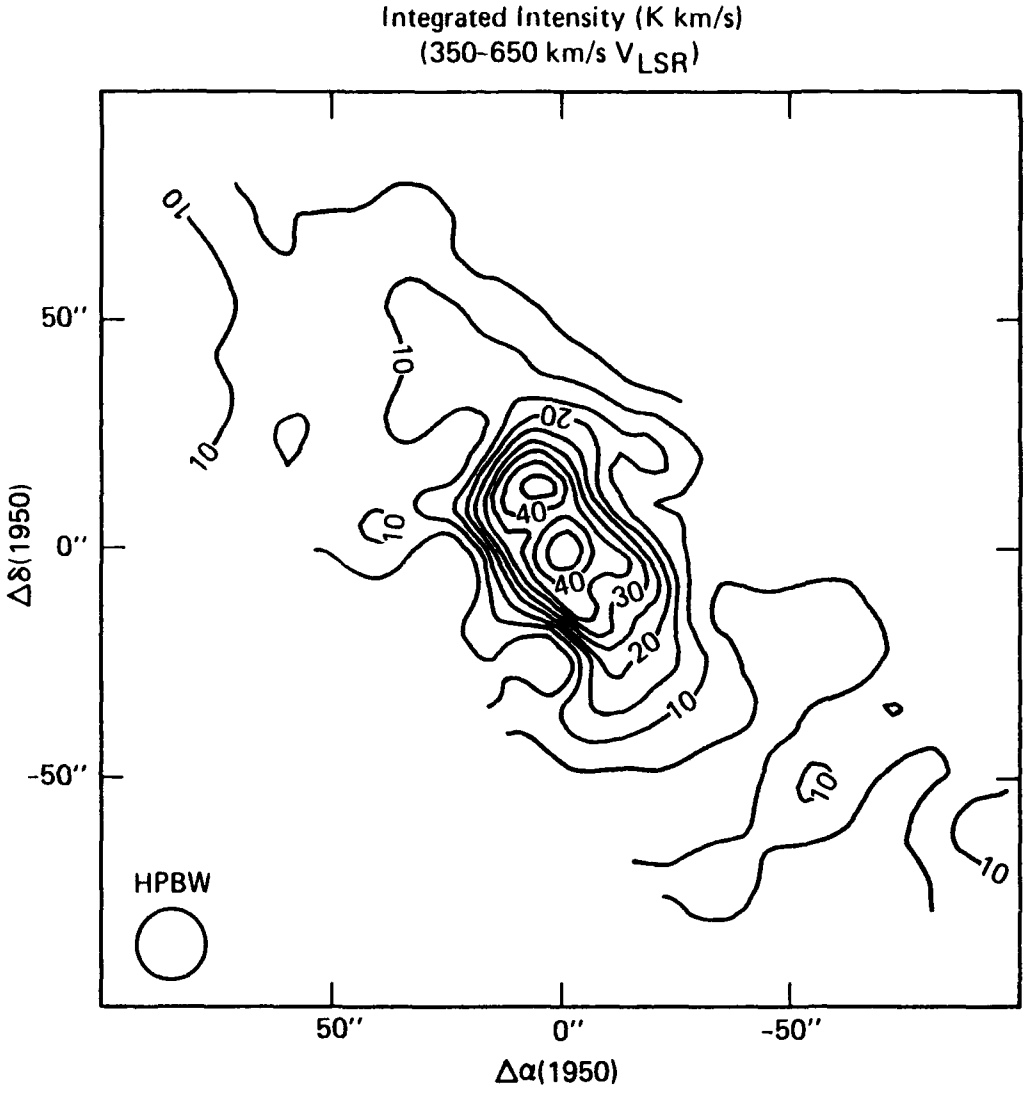

Fig. 4. CO intensity map of the barred region of M83. Note the strong concentration in the central 20".

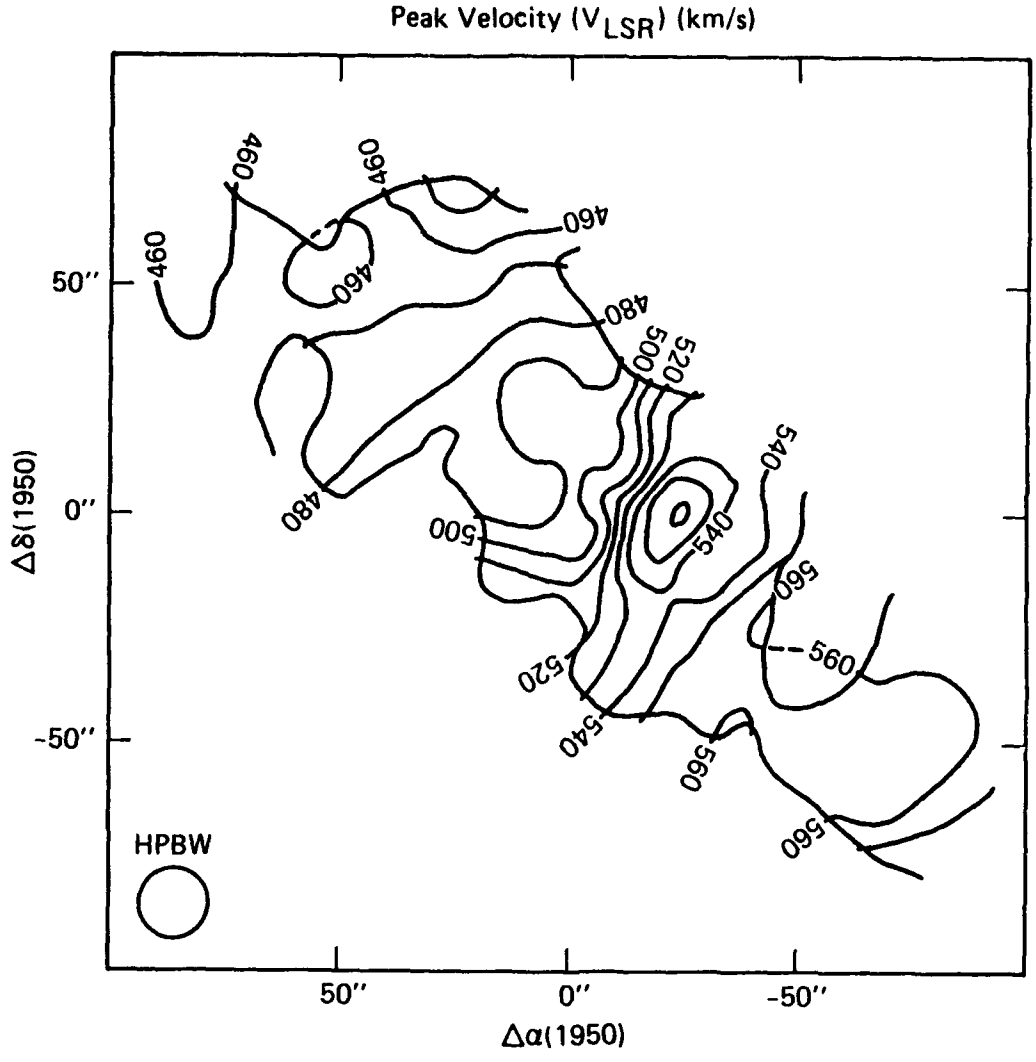

Fig. 5. Peak velocity distribution of CO gas in the bar of M83. A non-circular motion of 20 - 30 km s^{-1} is seen near the center.

potential (Sørensen et al. 1976; Roberts et al. 1979). In fact well developed dark lanes are found along the leading sides of the bar of M83 indicative of a shocked concentration of molecular gas. The strong shock will cause loss of angular momentum, leading to an accumulation onto the galactic center. Infall of gas toward the center may result in a high rate of star bursting, which is observed as the strong radio continuum emission near the center (Ondrechen 1985). The radio continuum observations show evidence of nonthermal emission along the barred shocked region. It is therefore important to investigate the motion of gas in and around the central barred region.

The high resolution map of HI line emission by Allen et al. (1986) shows, however, a depression in the central region including the bar, giving no information about the motion of gas there. In order to see the motion in the bar and gaseous concentration toward the center we have performed a survey of the CO line emission as the tracer of the molecular hydrogen gas. Our CO map covers a region of 3.5' x 1' along the bar, where most of the bar is included. Figures 4 and 5 show the distributions of total intensity, namely the H_2 column density, and the velocity field, respectively (Handa et al.1986).

The gas is concentrated in the central 1' x 0.5' (1 x 0.5 kpc) region, where about 40% of the gas in the observed region is found. The central gas distribution is elongated roughly along the bar, but shows an S-shaped ridge with two strong peaks, one is associated with the center, and the other is more shifted from the center by 10" (200 pc).

In the barred region a rather broad CO distribution is found, and the peak positions of the CO intensity runs approximately along the leading sides of the bar.

A clear noncircular motion is found in the central 1' (1 kpc). The amount of the noncircular motion subtracted for the circular rotation is about 20-30 km s^{-1}. This may be a superposition of deceleration by the shock and the infall motion. Beyond 1' from the center the velocity field resembles the circular rotation, although the sensitivity of the present observations might not be enough to detect weak noncircular motion.

The strong concentration of molecular hydrogen toward the center and its noncircular motion is suggestive of the infall of matter due to the barred shock wave, and must be intimately related to the activity of star formation observed in optical, infrared, UV, X-ray, and radio observations (Rieke 1976; Bohlin et al. 1983; Trinchieri et al. 1986; Ondrechen 1985).

4. IC 342

Extensive CO line observations of this bright S_{cd} galaxy have been made by Rickard and Palmer (1981) and Young and Scoville (1982). IC342 has a bright optical nucleus with a dark lane elongated in the north-south direction. A prominent molecular bar has been found lying on the dark lane using the Owens Valley interferometer (Lo et al. 1984). Their field of view was spatially limited by the primary beam as well as by the velocity coverage of the spectrometer. It is therefore not known whether the molecular bar is connected to the outer spiral arms, whether the bar is surrounded by more broad gas distribution, etc. We have made a highest resolution CO map accessible by a single-dish with

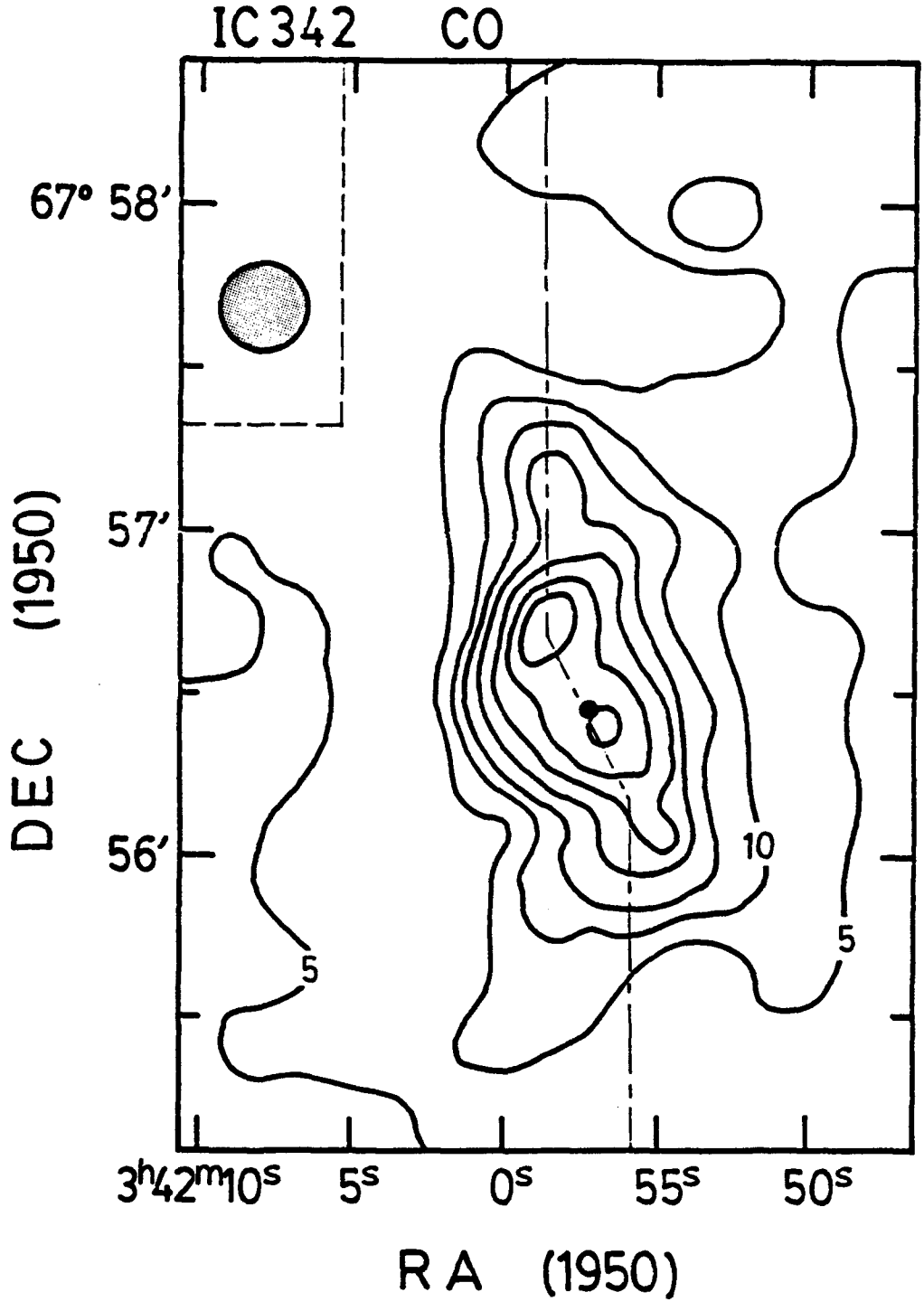

Fig. 6. Distribution of the integrated CO intensity of the bar of IC342. The 2.2 μm peak position is marked with the dark circle. Contour unit is in K km s^{-1}.

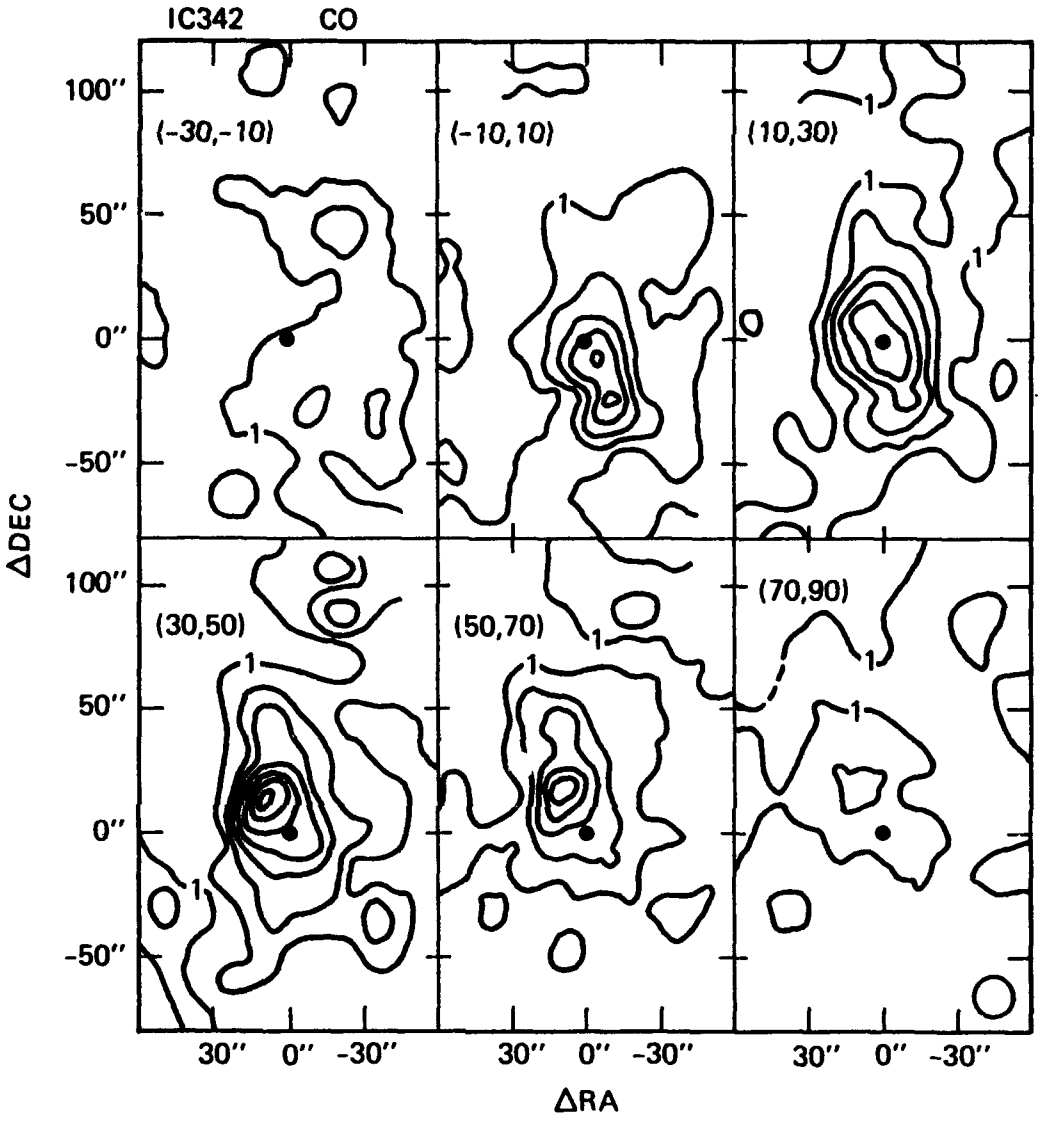

Fig. 7. Equal-velocity integrated CO intensities of IC342.

a sufficient velocity coverage (Hayashi et al. 1986).

Figure 6 shows a distribution of the integrated intensity of CO line emission. The dark circle is the center of the galaxy as determined by 2.2 μm infrared emission (Becklin et al. 1980). The CO emission is concentrated in the central bar whose size is 1.3x0.6 kpc after being deconvolved from the beam. Little CO emission is seen outside the bar: the molecular bar is localized within the optical bulge and is not connected to the outer spiral arms. The result is consistent with that of Lo et al. (1984), but our result suggests that the bar is more spread in the minor axis direction than the interferometer result. The beam-deconvolved width of the bar is 0.6 kpc and is considerably wider than that measured by Lo et al. (1984). The narrower width of their CO map might be caused by the limited velocity coverage of their spectrometer.

The CO bar has a double-peaked structure with a shallow dip toward the nucleus, being symmetric with respect to it. The two maxima lie about 200 pc away from the nucleus. The molecular hydrogen mass of the nuclear bar is estimated to be 2×10^8 $M_\odot$. Five percent of the total H_2 mass is accumulated in the central small area. This may explain the vigorous star forming activity in the nuclear region of this galaxy (Becklin et al. 1980; Turner and Ho 1983).

Figure 7 shows equal-velocity intensity maps, where intensities at every 20 km s^{-1} are shown in the form of contour maps. At the systemic velocity, the intensity distribution has a symmetric bar structure, whereas at 30 - 50 km s^{-1} there exists a dense complex at 15" to the NE of the center, and no counterpart to this complex is seen at the opposite side at $-10 \sim 10$ km s^{-1}. The velocity distribution shows a significant displacement from a circular rotation consistent with Lo et al. (1984). The noncircular motion may be related to the formation of the bar concentration of gas in the central region.

5. M82

The peculiar edge on galaxy M82 is well known with its filamentary structure running perpendicularly to the galactic plane, which suggests an intensive outflow of gas from the disk (Lynds and Sandage 1963). The dynamic state of the galaxy may be caused by star formation activity near the center (Rieke et al. 1980; Kronberg et al. 1985). The active star formation must be deeply related to the dense molecular hydrogen gas concentrated near the central region (Olofson and Rydbeck 1984; Nakai et al. 1986; Lo et al. 1986).

Figure 8 shows the intensity distribution of the CO line emission in the central 40" of M82 as observed with the 45-m telescope. Figure 9 shows a distribution of volume density of H_2 gas obtained by deconvolving the observed CO intensity on the assumption of a cylindrical symmetry around the rotating axis. It is remarkable that there exists a hole at the center, surrounding which we find a "200-pc ring", or a doughnut-shaped structure. This ring has a steep density gradient toward the center, whereas it is widely spread towards the outer side. The ring is further associated with spur-like protrusions extending toward the halo. The protrusions make a large-scale cylindrical structure with the height 500 pc from the galactic plane.

Velocity variation along the major axis shows a normal rotation of the disk at velocity of 100 km s^{-1}. Along the minor axis and along the cylindrical struc-

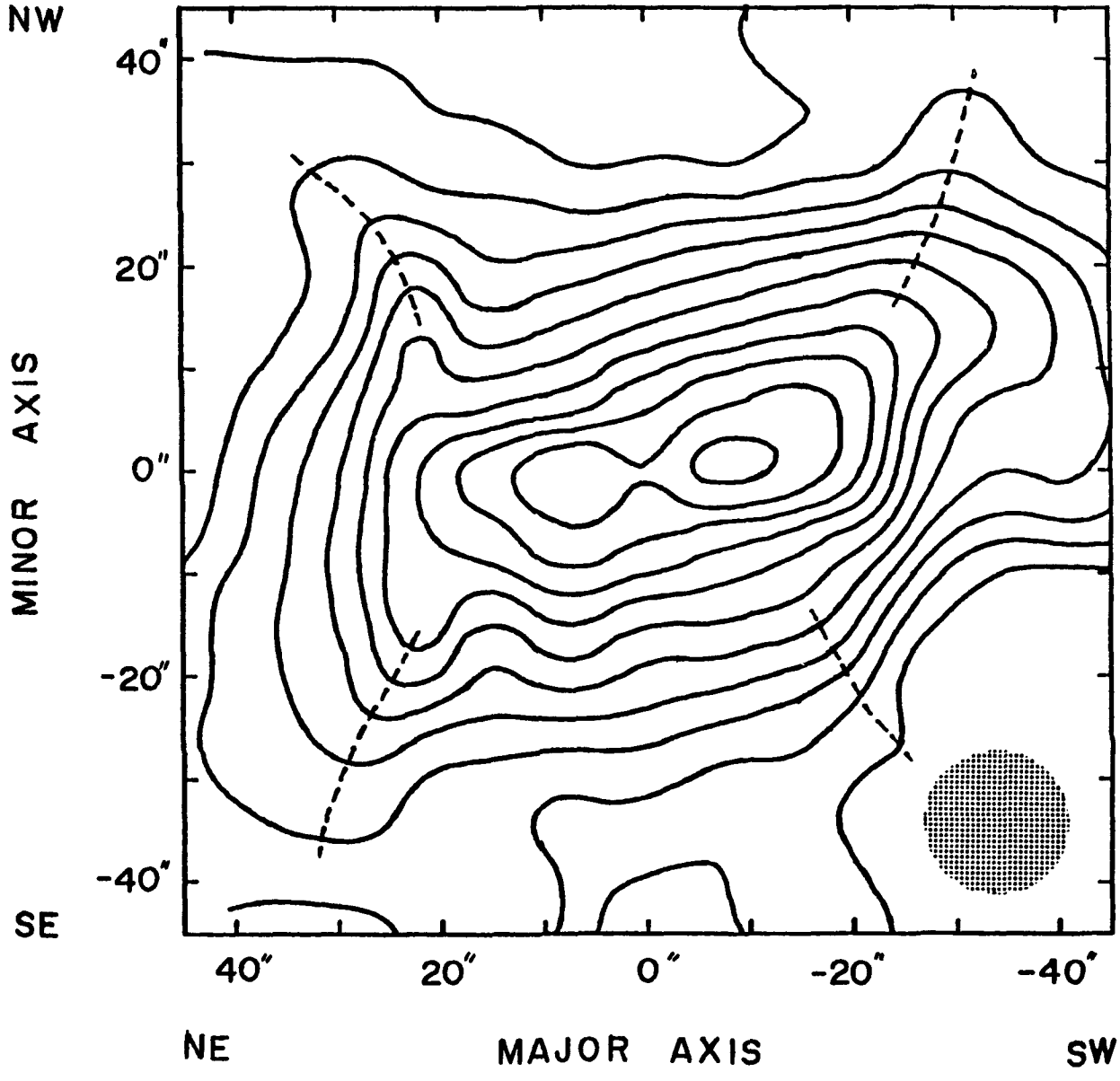

Fig. 8. Integrated intensity of CO line emission of M82. Note the double peaks which indicates the ring-like structure. Dashed lines show CO ridges extending toward the halo, which we interpret as due to cylindrical distribution of molecular gas perpendicular to the galactic plane. The lowest contour level and the contour intervals are 20 K km/s. The maximum intensity is 230 K km s^{-1}.

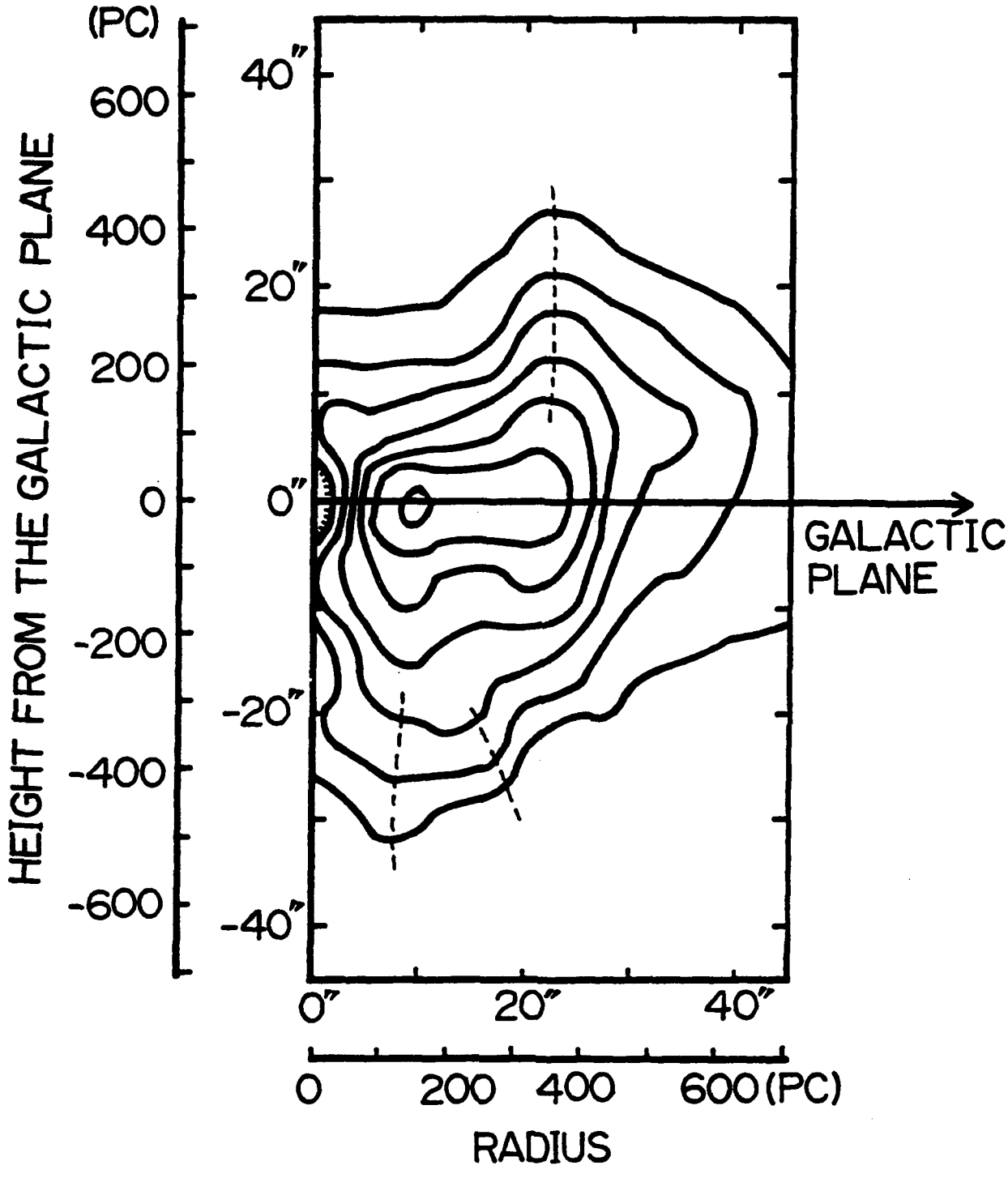

Fig. 9. Distribution of the volume density of molecular hydrogen calculated based on an axisymmetric model from figure 8. The first contour and contour intervals are 1 H_2 cm^{-3}.

ture in the halo we find also a velocity gradient. If we take into account the inclination of the galaxy disk, this gradient is well attributed to an outflow motion of molecular gas. The outflow velocity is from 100 to 500 km s^{-1} perpendicular to the disk plane, depending on the inclination angle, 70°-85°.

As the total mass involved in the cylinder is estimated to be 5×10^7 Mo, the kinetic energy of the outflow motion is of the order of $0.1\text{-}1.4 \times 10^{56}$ ergs. According to the star bursting model of Rieke et al. (1980) the rate of supernova explosions in the central few hundred pc is about 0.3 SN y^{-1} and the duration of the bursting activity is 5×10^7 y. Then the total energy released by SN explosions is 2×10^{58} ergs for a single SN energy of 10^{51} ergs. If the fraction of energy converted to kinetic energy of the gas is 0.03 (Chevalier 1974), enough energy is given to the gas to drive the outflow motion of the molecular cylinder.

Another fraction of the released SN energy may be used to heat up the ISM to high temperature, and the heated-up gas will expand into the halo, forming an X-ray halo. This is actually observed as an elongated halo of X-ray emission perpendicular to the disk plane (Watson et al. 1984). It must be noticed that the X-ray halo is confined by the wall of the molecular cylinder. It is likely that the interface of the X-ray halo and the molecular cylinder has an intermediate temperature, radiating H alpha emission. The H alpha filamentary structure may be a view of the interface region as seen through the dusty (molecular) cylinder with outflow motion. Figure 10 illustrates this picture.

From the observed facts we may propose the following scenario of evolution of M82: More than 10^7 years ago there appeared a dwarf galaxy ('proto-M82') with very rich content of molecular gas, possibly induced by an inflow of gas from M81 through a tidal interaction. The gas accumulated toward the center and produced a dense molecular disk. In the central region there occurred intensive star formation which propagated outward through the disk. Subsequent SN explosions and mass outflows from stars caused compression of the disk gas into a ring of high density molecular gas. In such a dense ring, especially near the inward shock-compressed side, further star formation occurred. The ring and star bursting sites are now observed as the 200-pc ring and associated nonthermal radio emisson. Plowed HI gas has been accumulated in an HI ring outside the molecular ring (Weliachew et al. 1984).

Released energy through the subsequent SN events escapes into the halo, a part of which goes to heating up the surrounding gas and a part goes to the kinetic energy of the high-velocity outflow of gas perpendicular to the disk, and is readily observed as the X-ray halo and the molecular cylinder as described above.

The shock-compressed 200 pc ring is probably expanding. In fact, the velocity dispersion toward the center of M82 is as high as 200 km s^{-1} in full width. This cannot be attributed to the rotation alone, and suggests an expansion of the ring gas at velocity 100 km s^{-1}. Then the expansion should have begun before 2×10^6 years ago, consistent with the duration of star bursting activity. The kinetic energy of the expanding motion is 3×10^{54} ergs as the total mass of the ring is 3×10^7 Mo, again enough driven by the SN energies.

6. Discussion

The galaxies reported here all show dense molecular disks in their central

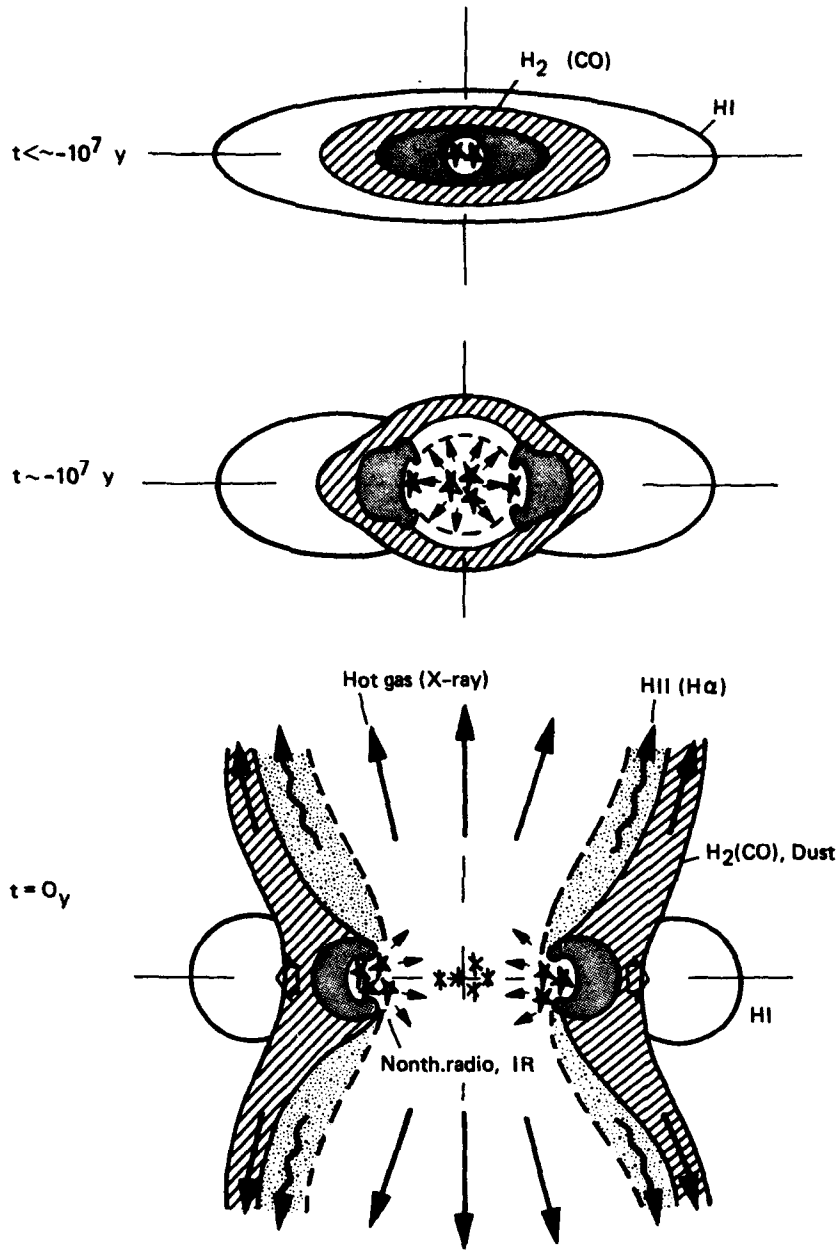

Fig. 10. Schematic illustration of possible evolution of M82.

regions. They show more or less central activity, and some show bursting star formation. Such activity may therefore depend on the molecular gas content in the central regions.

Table 1 lists the molecular to dynamical masses in the central few hundred pc of the galaxies reported here, and compares their ratios of molecular to dynamical masses. Here the molecular mass was estimated using the formula given in Sofue et al. (1986) except for M82 for which we used the value of Nakai et al. (1986). All the galaxies show that the ratio is 0.2-0.3, which is significantly higher than that known for the main disk of NGC891 or than in our Galaxy disk.

Table 1. Molecular and dynamical masses in the central few hundred pc.

Galaxy	Type	Distance	Region	M_{dyn}	M_{H_2}	M_{H_2}/M_{dyn}
NGC891	Sb	14 Mpc	$R \leq 500$ pc	$\sim 10^9$ Mo	$\sim 3\times10^8$ Mo	~ 0.3
M83	SABc	3.7	350	5×10^8	1×10^8	0.2
IC342	Scd	4.5	500	5×10^8	1×10^8	0.2
M82	Pec.	3.3	200	4×10^8	10^8	0.2

It is interesting to note that the ratio is almost constant for these galaxies, which include a normal galaxy such as NGC891, though all of them show some central activity. This implies that the anomalous star bursting activity in M82 is affected not only by the gas density alone, but also by some other mechanism. A hint may come from its ring structure: the 200-pc ring of M82, which likely arises from a shock compression by a more central activity, may play an essential role in the burst. Namely the degree of star forming activity depends on dynamics and morphology of the molecular disk as well. A comparative study in a more quantitative way is in progress. Finally we mention that the difference in the activity might be due to different I_{CO} to H_2 conversion rate in those galaxies: the high molecular content in NGC891, IC342 and M83 might be an apparent phenomenon caused by a higher content of heavy elements in their central regions than in M82 or in normal disks of NGC891 and our Galaxy, because we have used the usual conversion factor as noted above.

References

Allen,R.J., Baldwin, J.E. and Sancisi, R., 1978, Astron. Astropys. 62, 397
Allen,R.J., Atherton, P.D. and Tilanus, R.P.J. 1986, Nature 319, 296
Becklin,E.E., Gatley,I., Matthews, K., Neugebauer,G., Sellgren,K., Werner,M.W. and Wynn-Williams,C.G. 1980, Ap.J., 236, 441

Bohlin,R.C., Cornett,R.H., Hill, J.K., Smith, A.M. and Stecher,T.P. 1983, Ap.J. (Letters) 274, L53
Chevalier, R.A. 1974, Ap.J., 188, 501
Handa, T., Sofue, Y., Nakai,N., Fujimoto, M., and Hayashi, M., 1986, in "Star forming regions", IAU Symp. 115, Eds.M.Peimbert and J.Jugaku, D.Reidel Publ. Co., in press.
Hayashi,M., Handa, T., Sofue,Y., Nakai, N. and Hasegawa, T., 1986, ibid, in press.
Kronberg, P.P., Biermann, P., and Schwab, F.R., 1985, Ap.J. 291, 693
Lo, K.Y., Berge, G.L., Claussen, M.J., Heiligman, G.M., Leighton, R.B., Masson,C.R. Moffet, A.T., Phillips, T., Sargent,A.I., Scott,S.L., Wannier, P.G., and Woody, D,P,, 1984, Ap.J. (Letters), 282, L59
Lo, K.Y., Cheung,K.W., Masson,C.R., Phillips,T.G., Scott,S.L., Woody,D.P., 1986 Ap.J., submitted.
Liszt, H.S. and Burton, W.B. 1978, Ap.J., 226, 790
Lynds, C.R. and Sandage, A.R. 1963, Ap.J., 137, 1005.
Nakai, N., Hayashi, M., Hasegawa, T., Sofue, Y., Handa, T., and Sasaki, M. 1986, in "Star forming regions", IAU Symp. 115, Eds. M.Peimbert and J.Jugaku, D. Reidel Publ. Co., in press.
Olofsson,H., Rydbeck, G. 1984, Astron. Astrophys. 136, 17
Ondrechen, M.P. 1985, A.J., 90, 1474
Rickard, L.J., and Palmer, P. 1981, Astron. Astrophys., 102, L13
Rieke, G.H. 1976, Ap.J. (Letters), 206, L15
Rieke, G.H., Lebofsky, M.J., Thompson, R.I., Low, F.J. and Tokunaga, A.T. 1980, Ap.J., 238, 24
Roberts, W.W.Jr., Huntley, J.M. and van Albada, G.D. 1979, Ap.J. 233, 67
Sancisi,R. and Allen, R.J. 1979, Astron. Astrophys. 74, 73
Solomon, P.M. 1981, in "Extragalactic molecules", Proc. Workshop at NRAO, Eds. L.Blitz and M.Kutner, p.41.
Solomon, P.M., 1983, in "Internal kinematics and dynamics of galaxies", IAU Symp. No. 100, Ed. E.Athanassoula, D.Reidel Publ. Co., p.35.
Sofue, Y., Nakai, N., Handa, T., 1986, Publ. Astron. Soc. Japan, submitted.
Sørensen, S.-A., Matsuda, T., and Fujimoto, M. 1976, Astrophys. Sp. Sci., 43, 491
Trinchieri , G., Fabbiano, G. and Palumbo, G.G.C. 1986, Center for Astrophys. Preprint No. 2065.
Turner, J.L. and Ho,P.T. 1983, Ap.J. (Letters), 268, L79
Watson, M.G., Stanger, V., and Griffiths, R.E., 1984, Ap.J., 286, 144
Weliachew, L., Fomalont, E.B., and Greisen, E.W., 1984, Astron. Astrophys. 137, 335
Young,J. and Scoville, N. 1982, Ap.J., 258, 467.

DISCUSSION

UNGER:

A VLA map of OH absorption in M82 shows a rotating molecular ring on a scale of a few hundred pc (Weliachew *et al.* 1984, *A and A* 137 335). How does this relate to your expanding CO ring?

SOFUE:

Positionally it coincides with the CO ring, though I haven't done detailed comparisons. Neither have I checked whether the OH ring is expanding. But it is quite likely that they are both in the same site on a ring, being illuminated and compressed by the star formation burst and the central activity.

HECKMAN:

Pat McCarthy, Wil van Breugel, and I have recently obtained long-slit optical spectrophotometry of the emission-line filaments in M82. These new data strongly support the type of bi-polar wind model you have described. First, we find that the gas pressure in the filaments drops roughly like $1/r^2$, as a simple wind model would predict. Second, the relative emission-line strengths can be well fit by standard shock models. I will be discussing these and other related data during my talk Thursday afternoon.

SOFUE:

That's important information. Thank you for the comments.

CO Observations of Nearby Galaxies and the Efficiency of Star Formation

Judith S. Young
Department of Physics and Astronomy
University of Massachusetts
Amherst, MA

ABSTRACT. We have observed the CO distributions and total molecular content of 160 galaxies using the 14 meter millimeter telescope of the FCRAO (HPBW = 45"). For the luminous, relatively face-on Sc galaxies, the azimuthally averaged CO distributions are centrally peaked, while for the Sb and Sa galaxies the CO distributions often exhibit central CO holes up to 5 kpc across. None of the Sc galaxies have CO distributions which resemble that in the Milky Way.

The shapes of the azimuthally averaged CO distributions in the face-on Sc galaxies are similar to those observed in Hα, blue light, and radio continuum, and markedly different from the flat extended distributions of atomic gas. The relative constancy of the Hα/CO ratio as a function of radius in NGC 6946 suggests that the massive star formation rate is proportional to the mass of molecular clouds present, or that the star formation efficiency is constant as a function of radius. In contrast, the spiral arm structures in M51 appear to be regions of enhanced star formation efficiency; we find that the Hα/CO ratio (at 45" resolution) is a factor of 2 higher on the arms than between the arms in M51.

We find a general correlation between total CO and IR luminosities in galaxies, as noted previously (Rickard and Harvey 1984; Young et al. 1984; Sanders and Mirabel 1985; Young et al. 1986a). The scatter in this relation is highly correlated with dust temperature, in that there is a tight correlation between IR and CO luminosities within 3 distinct ranges of dust temperature. We find no strong correlation of IR luminosities with HI masses, and thereby conclude that the infrared emission is more directly tied to the molecular content of galaxies.

The ratio of IR/CO luminosities increases roughly as T^4, consistent with the IR emission of thermal origin at the characteristic temperature given by the dust temperature. If the IR/CO luminosity ratio is a measure of the emergent stellar luminosity per unit molecular mass, or the star formation efficiency (SFE), we find that this efficiency varies over two orders of magnitude from galaxy to galaxy. We suggest that galaxies which have high SFEs produce more stars per unit molecular mass, thereby increasing the average temperature of the dust in star forming regions. Irregular galaxies and galaxies previously identified as mergers have the highest observed star formation efficiencies. For the mergers, we find evidence that the IR/CO luminosity ratio increases with the merger age estimated by Joseph and Wright (1985).

Lastly, we find that isolated galaxies have a mean value of $L_{IR}/M(H_2)$ of 11 $L_\odot/M_\odot$, while the ratio for the interacting galaxies in our sample is 44 $L_\odot/M_\odot$. Clearly, the environment has a strong influence on the efficiency of star formation in galaxies.

Carol J. Lonsdale Persson (Editor)
Star Formation in Galaxies

1. INTRODUCTION

The evolution of a galaxy must depend in part on the distribution and abundance of molecular clouds within it, since stars form in molecular clouds. Furthermore, the evolution of a galaxy can be described in terms of the star formation history of the disk: the distribution of blue light from the disk indicates the past sites of star formation, the distribution of far-infrared emission indicates the currently forming stellar population, and the distribution of molecular clouds indicates the underlying potential for star formation. A synthesis of the details of the distributions of past, present, and future sites of star formation is one key to expanding our picture of the evolution of galaxies.

Since the earliest detection of molecular clouds in external galaxies (Rickard et al. 1975), there have been a large number of investigations of CO in galaxies, including both detailed studies of nearby galaxies, and comparisons of the global properties of selected samples of galaxies. These observations have been used to determine (1) the shapes of the CO distributions in galaxies and the dependence of this shape on galaxy type, (2) the relationship between the molecular content and the star formation rate within galaxies and from galaxy to galaxy, and (3) the relationship between the molecular and atomic gas distributions and masses in galaxies. In this paper, I shall use both studies of individual galaxies as well as large samples of objects to address the question of the star formation efficiency in galaxies.

The data upon which this discussion is based consist of CO observations at 2.6 mm (115 GHz) of 160 galaxies made primarily by myself, J. Kenney, L. Tacconi, and S. Lord using the 14 meter millimeter telescope of the Five College Radio Astronomy Observatory (HPBW = 45", for references see Young 1986). Of these 160 galaxies, CO was detected in 2/3, and mapped along the major axis in more than half. While the galaxies we have surveyed do not constitute a complete sample, since they were chosen to span a wide range of luminosity, morphological type, and environment, most of the objects are brighter than 10 Jy at 100 μm.

Also, I shall not use the common terms "normal" galaxy or "starburst" galaxy. Rather, in order to characterize the present state of star formation in a galaxy, I shall refer to the star formation rate per unit molecular gas mass, or the star formation efficiency (SFE). In this context, "starburst" galaxies are ones with high SFEs, and "normal" galaxies are galaxies with low SFEs; whether, in fact, a low SFE turns out to be the norm for galaxies remains to be determined.

2. CO RADIAL DISTRIBUTIONS IN NEARBY SPIRAL GALAXIES

In this section, I shall describe the CO radial distributions in the galaxies more nearby than the Virgo cluster (45" corresponds to 4.4 kpc for D = 20 Mpc) and for which we have made more than 5 CO measurements along the major axis. Throughout this paper, I will assume that H_2 surface densities are directly proportional to integrated intensities of CO emission (cf. Young and Scoville 1982a; Dickman, Snell and Schloerb 1986), with a constant of proportionality given by $N(H_2)/I_{CO} = 4 \times 10^{20}$ cm^{-2}/(K km s^{-1}).

2.1. Sc Galaxies

The CO radial distributions have been measured in 7 relatively face-on nearby Sc galaxies — NGC 598 (M33) and NGC 2403 (Young 1986), NGC 5194 (M51) (Scoville and Young 1983), NGC 5236 (M83) (Combes et al. 1978; Lord, Strom and Young 1986, this conference), NGC 5457 (M101) (Solomon et al. 1983), NGC 6946 and IC 342 (Young and Scoville 1982a). Figure 1 shows the CO radial distributions corrected to the plane of the galaxy (i.e. corrected for inclination) for 6 of the galaxies listed above. In each galaxy, the azimuthally averaged distribution of CO integrated intensities peaks in the center and decreases with radius in the disk. Also shown in Figure 1 is the Milky Way CO distribution at 1 kpc resolution, indicating the central peak, absence of gas between 1 and 4 kpc, and molecular annulus between 4 and 8 kpc (cf. Scoville and Solomon 1975; Burton et al. 1975; Sanders, Solomon, and Scoville 1984). None of the Sc galaxies have distributions which resemble that in the Milky Way.

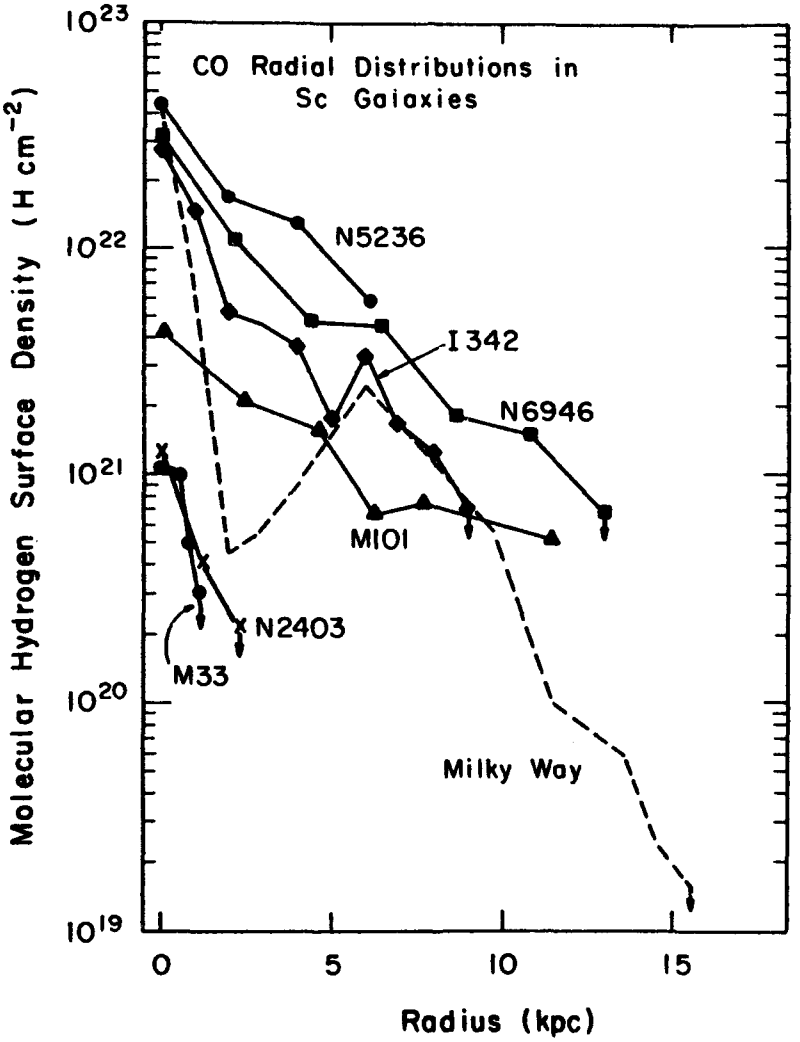

Figure 1. CO radial distributions corrected to the plane of the galaxy in 6 Sc/Scd galaxies (Young and Scoville 1982a; Solomon et al. 1983; Young 1986; Lord, Strom, and Young 1986) at 45" resolution. Also shown (dashed line) is the distribution found for the Milky Way (Sanders, Solomon, and Scoville 1984).

It is clear from Figure 1 that there is a wide range of molecular hydrogen surface densities found in Sc galaxies: the high luminosity galaxies M83 and NGC 6946 have the highest H_2 surface densities at all radii, while the low luminosity galaxies M33 and NGC 2403 have the lowest H_2 surface densities. In contrast, the atomic gas distributions in these same galaxies show little variation from one object to the next. This is illustrated in Figure 2, which compares the H_2 and HI radial distributions in high and low luminosity Scd galaxies (HI from Rogstad and Shostak 1972; CO from Young and Scoville 1982a and Young 1986). Although the low luminosity galaxies are small, so their HI disks have a small radial entent, the azimuthally averaged HI surface densities reach the same peak value of $\sim 10^{21}$ cm^{-2} as the high luminosity galaxies, in addition to exhibiting central HI holes. Thus, the ratio of H_2/HI surface densities is highest in the centers of the Sc galaxies, and is lower in the disks. Furthermore, the inner disks of the high luminosity galaxies have higher molecular-to-atomic gas ratios than the low luminosity galaxies.

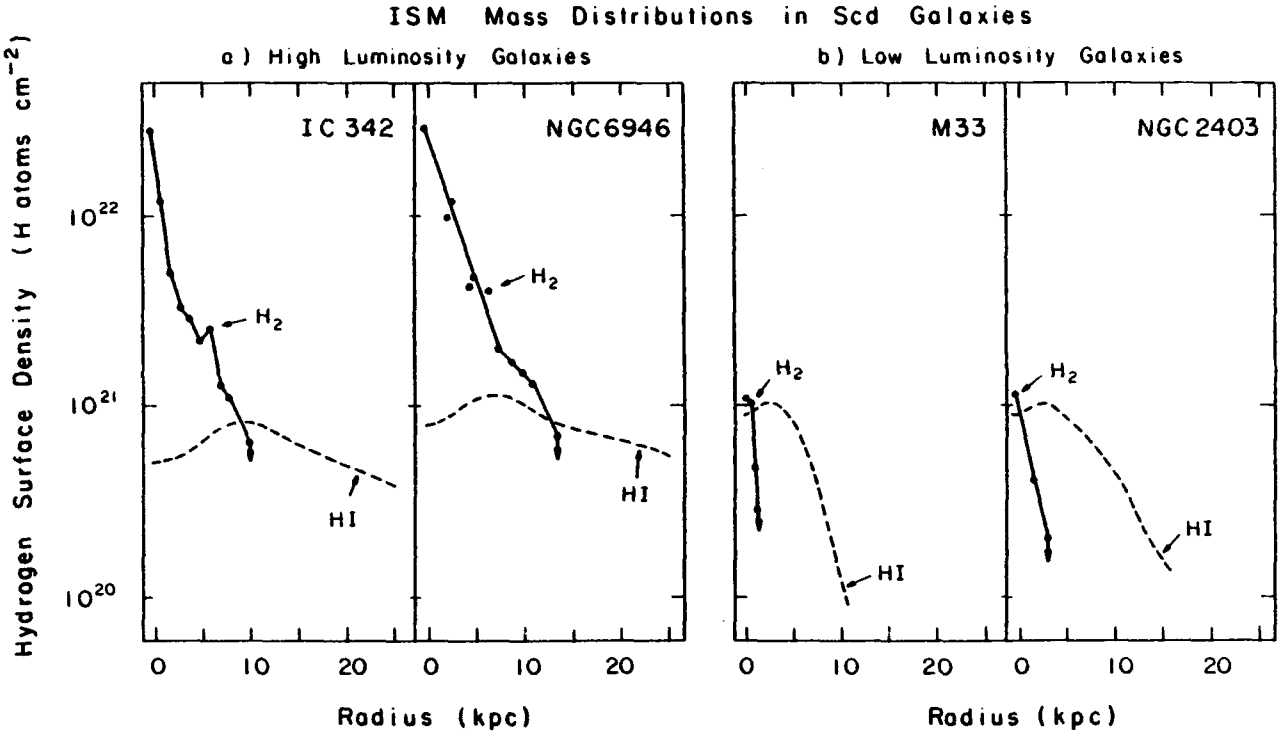

Figure 2. Comparison of the H_2 and HI radial distributions in high and low luminosity Scd galaxies (HI from Rogstad and Shostak 1972; CO from Young and Scoville 1982a and Young 1986).

2.2. Sa and Sb Galaxies

The CO morphologies of some of the early type spiral galaxies are distinctly different from those of the Sc galaxies. Of the 14 nearby Sa and Sb galaxies whose CO distributions have been measured, 5 have been observed to exhibit central CO depressions. These are NGC 224 (M31; Stark 1979), NGC 891 (^{12}CO by Solomon et al. 1983, ^{13}CO and ^{12}CO by Sanders and Young 1986), NGC 2841 and NGC 7331 (Young and Scoville 1982b), and NGC 4736 (Garman and Young 1986).

Additionally, it has been suggested that NGC 1068 also has a central CO minimum (Scoville, Young, and Lucy 1983), based on a deconvolution of the CO intensity distribution with the assumption that the CO velocity field mimics that of Hα. Thus, 6 out of 14 galaxies surveyed, or 40% of the early type spiral galaxies have central CO depressions. For NGC 2841 and NGC 7331, Young and Scoville (1982b) have pointed out that the central CO hole is coincident with the extent of the nuclear bulge, as determined from the separation of the blue light distribution into bulge and disk components (Boroson 1981). Obviously, higher resolution CO observations may reveal central CO depressions in more of the Sa and Sb galaxies.

Figure 3 shows a comparison of the H_2 and HI distributions in the Sb galaxies NGC 7331 and NGC 2841. As for the Sc galaxies in Figure 2, the HI distributions exhibit central holes (Bosma 1978), and the H_2 surface densities are greater than those of HI in the inner disk. The difference here is that for the Sb galaxies there are holes in both the atomic and molecular gas distributions, although the extents of the H_2 and HI holes differ.

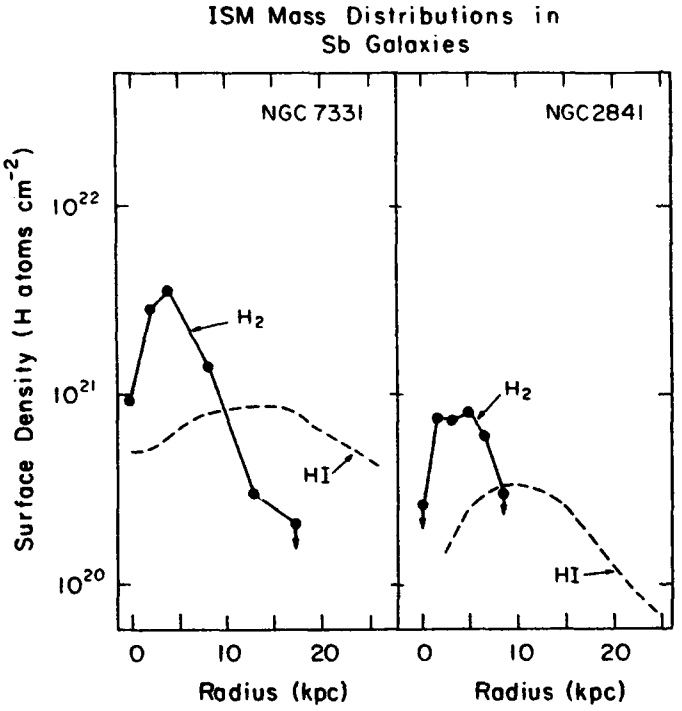

Figure 3. Comparison of the H_2 and HI radial distributions in two Sb galaxies, showing central holes in both CO and HI (HI from Bosma 1978; CO from Young and Scoville 1982b).

3. THE STAR FORMATION HISTORIES OF INDIVIDUAL GALAXIES

3.1. NGC 6946

The measurement of the CO distribution in a galaxy enables us to determine the star formation history of the galaxy through a comparison of tracers of star formation in the disk which are sensitive on different time scales. In the case of NGC 6946, observations have been made of Hα (DeGioia-Eastwood et al. 1984), HI (Rogstad, Shostak and Rots 1973; Tacconi and Young 1986a), CO (Rickard and Palmer 1981; Young and Scoville 1982a; Tacconi and Young 1986a), radio continuum (van der Kruit, Allen and Rots 1977; Klein et al. 1982), and blue light (Ables

1971; Elmegreen and Elmegreen 1984), as discussed in detail in Tacconi and Young (1986a). Figure 4 shows the azimuthally averaged radial distributions of H_2, HI, Hα, blue light and radio continuum emission for NGC 6946 (see also Tacconi and Young 1986b, this conference). It is remarkable that all of the radial distributions show similar behavior except that of the atomic gas. Furthermore, the same features in the various radial distributions are seen in most luminous Sc galaxies (see also Kenney and Young 1986b, this conference), and therefore the conclusions stated in this section apply more generally than simply to NGC 6946.

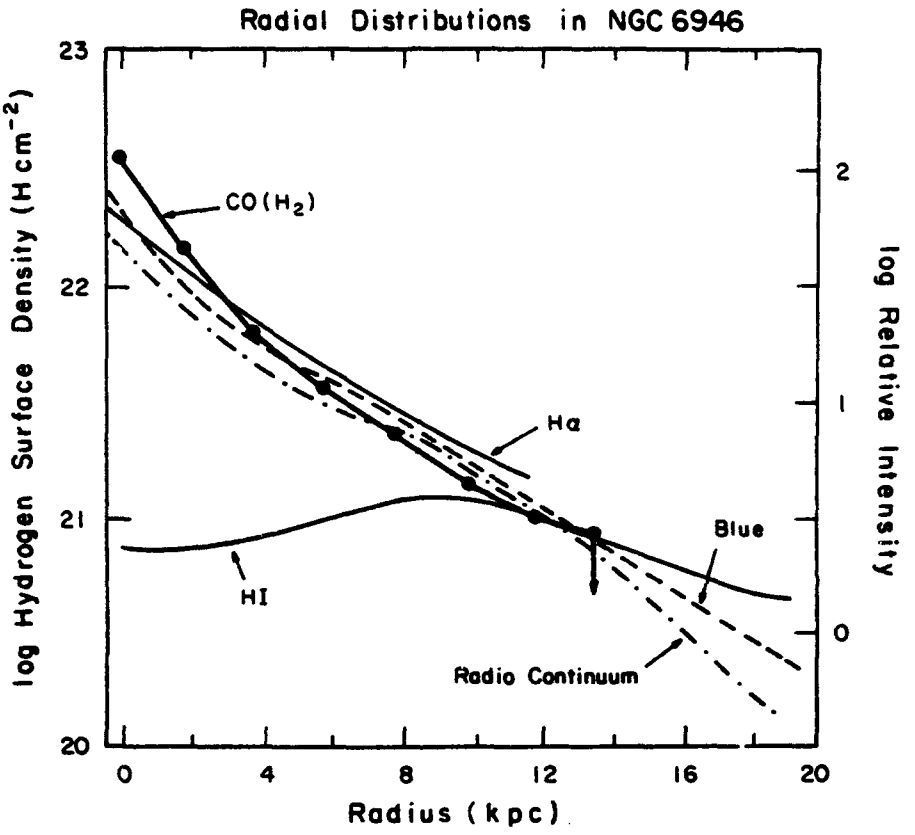

Figure 4. Comparison of the CO (H_2), HI, Hα, blue light, and radio continuum radial distributions in NGC 6946 (for references see text). All intensity scales are relative except that for the HI, which is plotted relative to H_2.

The fact that the CO, blue light, and Hα distributions in NGC 6946 all show similar radial behavior is significant in terms of the evolution of this galaxy. If the blue light from a late-type spiral galaxy is a measure of the star formation which has occurred over the last 2×10^9 years (cf. Searle, Sargent and Bagnuolo 1973), and the Hα flux indicates the massive star formation rate (SFR), the fact that the ratio of blue/CO surface densities is constant (Young and Scoville 1982a), and the ratio of Hα/CO surface densities is constant (DeGioia-Eastwood et al. 1984), indicates that the amount of star formation which occurs is proportional to the available supply of molecular gas. That is, the star formation efficiency is constant as a function of radius in NGC 6946.

From a comparison of the ISM surface density distributions in NGC 6946, it is apparent that the shapes of the atomic and molecular gas distributions are very different (see also §2.1). The ratio of H_2 to HI surface densities decreases from a central value of 30, to approximately 1 at a radius of 10 kpc (Tacconi and Young 1986a). If the ratio of H_2 to HI surface densities is a measure of the efficiency with which molecular clouds form, the radial behavior of the H_2 to HI ratio indicates that the molecular cloud formation efficiency decreases with radius in NGC 6946.

3.2. M51

While the star formation efficiency is constant as a function of radius in the disk of NGC 6946 and other luminous Sc galaxies, there are azimuthal structures in the disks of galaxies which are known as spiral arms. If the star formation efficiency were constant at all locations in a disk, then the spiral patterns which are so apparent optically should also be apparent in the molecular gas. However, searches over the years in a wide range of Sc galaxies and with a variety of resolutions have indicated that molecular spiral patterns are not the dominant feature of the molecular gas distributions. Indeed, studies of M51 with the OVRO interferometer resolve out more than half of the emission (Lo et al. 1984), indicating that the arm/interarm contrast in CO is not as high as that in Hα.

To determine the star formation efficiency on and off the arms in M51, we have compared the Hα image of Kennicutt (1985) with our fully sampled CO map, both at 45" resolution (Lord and Young 1986). In Figure 5 (top), we plot the Hα and CO surface brightnesses as a function of spiral phase, where the dust lanes are specified to be at phases 90° and 270°. While the spiral pattern in

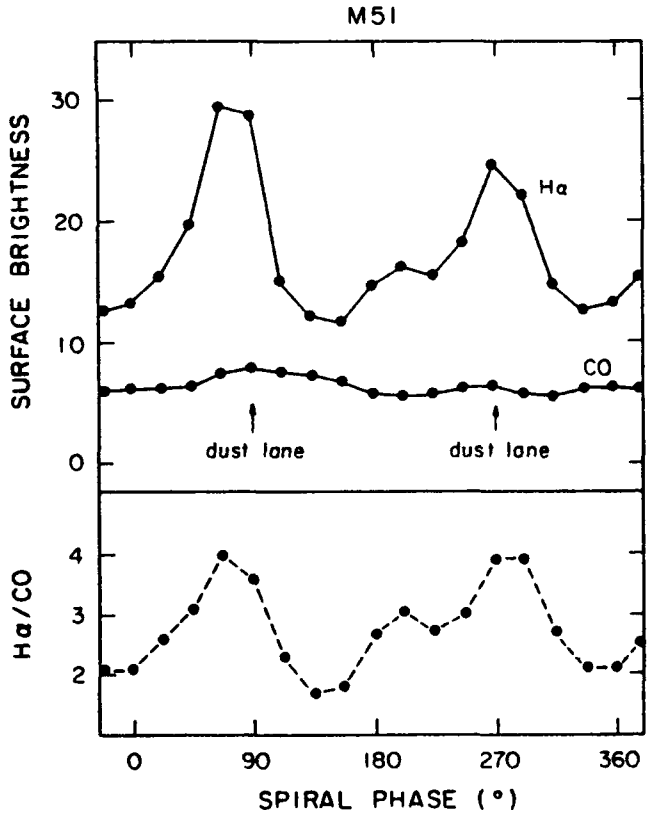

Figure 5. Hα and CO azimuthal distributions in M51 at 45" resolution (top) plotted as a function of spiral phase, with 90° and 270° chosen to be the locations of the arms (Hα from Kennicutt 1983; CO from Lord and Young 1986). Also shown (bottom) is the Hα/CO ratio as a function of spiral phase; the highest values of this quantity are found on the spiral arms in M51.

Hα is apparent, even at 45" resolution, that in CO is not. At the bottom of Figure 5, the ratio of Hα/CO surface brightnesses is shown to vary in azimuth, with the highest values on the arms. Thus, the star formation efficiency is higher on the arms than between the arms in M51. This result requires that star formation is not simply a local process, depending only on the mass of available gas, but that some mechanism has operated to produce more stars per unit molecular mass in the arms of M51.

4. THE STAR FORMATION EFFICIENCY FROM GALAXY TO GALAXY

4.1. Correlation of Total CO and IR Luminosities

With the success of the IRAS, the IR flux densities and color temperatures have now been measured for galaxies over the entire sky. These observations provide a measure of the star formation occurring within a galaxy, since the far infrared (far-IR) emission is believed to arise from dust heated by young stars forming in molecular clouds (cf. Rieke et al. 1980; Telesco and Harper 1980). The comparison of the IR luminosity, which provides a measure of the currently forming stellar population, with the CO luminosity, which traces the molecular content, enables us to deduce the star formation efficiency in galaxies.

Only a small number of CO-IR comparisons have been made in galaxies because of the limited amount of IR data previously available. From observations between 40 and 160 μm using the KAO, Rickard and Harvey (1984) found a rough correlation between CO and IR fluxes in the central 1' for 30 galaxies. Young et al. (1984) searched for CO emission in 20 galaxies reported during 1983-4 in the IRAS Circulars and for which radial velocities were available in the literature; CO emission was detected in 10 of these galaxies, including Arp 220 and NGC 6240, and a general correlation between CO and 100 μm luminosities was found. Sanders and Mirabel (1985) compared the central 1' CO luminosities and 40 to 120 μm IR luminosities for a sample of 21 galaxies chosen on the basis of their strong radio continuum emission, and found a similar correlation. All of the above CO-IR comparisons exhibit more scatter than would be expected based on a constant efficiency of star formation from galaxy to galaxy. However, the above galaxy samples are too inhomogeneous to determine which parameters are primarily responsible for this scatter.

From a comparison of total CO and IR luminosities in 27 IR bright galaxies, Young et al. (1986a) found that the scatter in the L_{CO} - L_{IR} plot is highly correlated with dust temperature, in that there is a tight correlation between the IR and CO luminosities for galaxies in each of three distinct ranges of dust temperature.

Figure 6 shows the total IR and CO luminosities for 122 galaxies — 27 from Young et al. (1984 and 1986a), 15 from Sanders et al. (1986), 23 in Virgo from Kenney and Young (1986), 13 galaxies of large angular size (Young and Scoville 1982a and 1982b; Scoville and Young 1983; Young, Tacconi and Scoville 1983; Scoville, Young and Lucy 1983; Solomon et al. 1983; Young and Scoville 1984; Scoville et al. 1985; Sanders and Young 1986), and 44 major axis CO maps observed during the past six months (Young et al. 1986b). The data shown in Figure 6 are coded by dust temperature, from which it is clear that there is a good correlation between IR luminosity and CO luminosity (or H_2 mass) within each dust temperature bin.

We have fitted the data in Figure 6, with a power law, and find that

$$L_{IR} \propto M(H_2)^{0.8 \pm 0.1} . \quad (1)$$

with an overall correlation coefficient of 0.90. For each dust temperature bin, the IR luminosity is roughly proportional to the first power of the H_2 mass. Also shown in Figure 6 is the position of the Milky Way (from Scoville, this conference), indicating a similarity to the galaxies with the coldest dust temperatures.

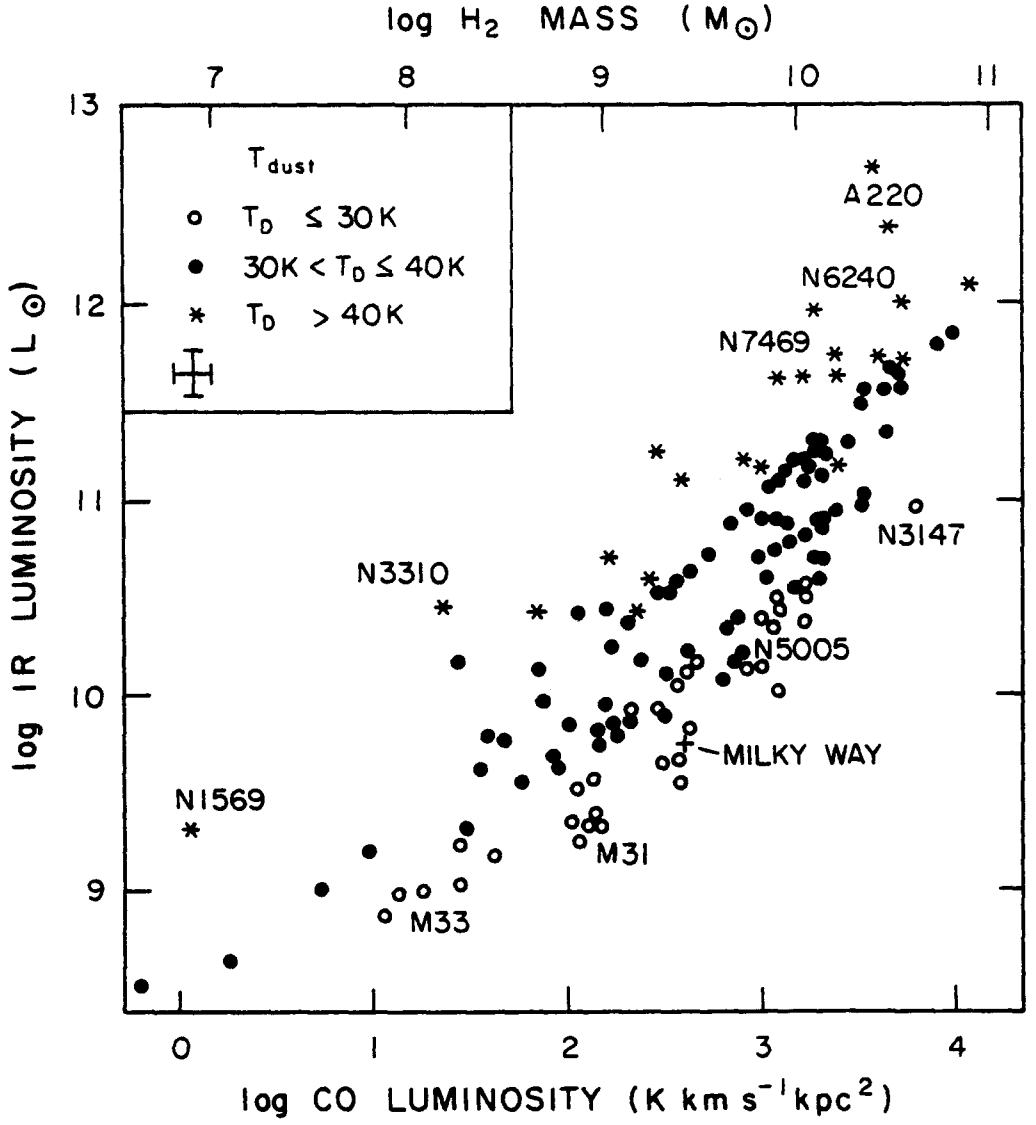

Figure 6. Comparison of the total IR and CO luminosities for 122 galaxies (27 from Young et al. 1984 and 1986a; 23 in Virgo from Kenney and Young 1986a; 15 from Sanders et al. 1986; 13 galaxies of large angular diameter -- for references see Young 1986; and 44 IR bright galaxies from Young et al. 1986b). The data plotted include total CO luminosities from both major axis maps and single CO observations. The IR luminosities are from the IRAS Point Source Catalogue (JISWG 1985) and from coadded survey data (Young 1986), following the method outlined by Lonsdale et al. (1985). Data points are coded by dust temperature as indicated in the upper left hand corner of the plot.

The data in Figure 6 can alternatively be illustrated as in Figure 7, where the ratio of L_{IR}/L_{CO} for each galaxy is plotted against the ratio of 60/100 μm flux densities, or the dust temperature. The ratio of the IR/CO luminosities is observed to depend on roughly the fourth power of the dust temperature, which is what one expects if the infrared emission is thermal emission related to dust in molecular clouds, as noted by Young et al. (1986a). This result is further emphasized by the fact that we find no correlation of the IR luminosities with HI masses. For the galaxies with the coldest dust temperatures, the mean value of $L_{IR}/M(H_2)$ is 5 L_o/M_o, while for the galaxies with the highest dust temperatures the mean value is 56 L_o/M_o.

Young et al. (1986a) interpret the ratio L_{IR}/L_{CO} as the reradiated stellar luminosity per unit molecular mass, or the galaxy-wide star formation efficiency (SFE). Thus, the SFE varies by almost 2 orders of magnitude from one galaxy to another, with higher SFEs in galaxies with higher dust temperatures.

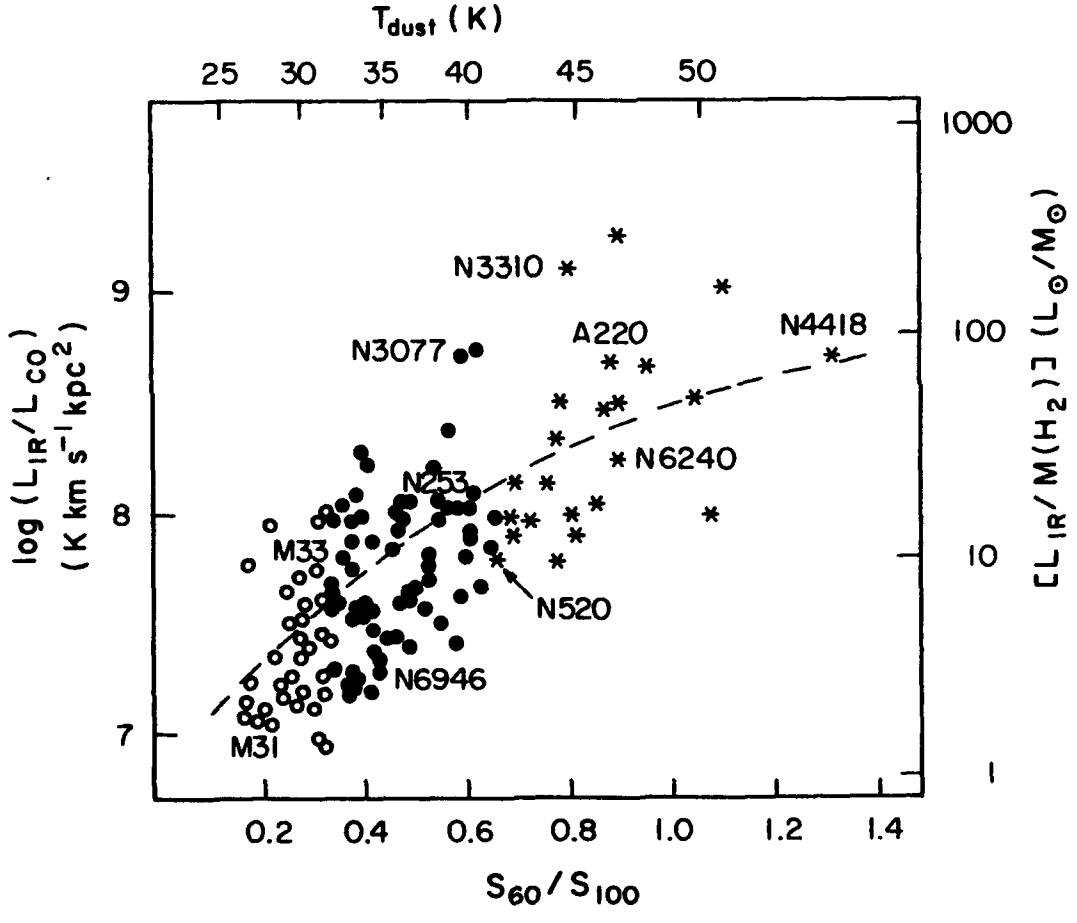

Figure 7. Ratio of IR/CO luminosities versus the ratio of 60/100 μm flux densities for the galaxies plotted in Figure 6. The dust temperatures indicated at the top of the figure were derived from the ratio of 60/100 μm flux densities, assuming a λ^{-1} emissivity law. The dashed line superposed on the data is not a fit, but represents a T^4 dependence of the L_{IR}/L_{CO} ratio, which is what one expects if the IR luminosity has a T^5 dependence, and the CO luminosity has a T^1 dependence (cf. Young et al. 1986a). The different symbols represent the same three different dust temperature bins as in Figure 6.

Furthermore, the galaxies previously identified as mergers (cf. Joseph and Wright 1985) are among the galaxies with the highest SFEs. We suggest that efficient star formation is responsible for the high dust temperatures observed, through the formation of more stars per unit molecular mass. Thus, the interacting galaxies which are luminous in the IR and therefore have high rates of star formation (cf. Lonsdale, Persson, and Matthews 1984) also have high efficiencies of star formation. However, even if the rate of star formation is low, as for the merger NGC 3310 and the irregular galaxy NGC 1569, the efficiency of using the molecular gas in these systems is high as well.

Finally, Young et al. (1986a and 1986b) find that the dust mass is well correlated with the molecular gas mass from galaxy to galaxy even though IRAS is only sensitive to that fraction of the dust which is warmer than ~ 25 K and emitting at 100 μm. Figure 8 is a plot of the mass of warm dust versus the H_2 mass in 122 galaxies, indicating a good correlation over 4 orders of magnitude, such that

$$M(H_2) \propto M_D^{1.2 \pm 0.1} . \qquad (2)$$

However, the mean value of the molecular gas-to-warm dust ratio is 500, not ~ 100 as it is for the Milky Way (cf. Hildebrand 1983). The most likely explanation for this discrepancy is that IRAS is sensitive only to the warm dust in a galaxy. If the gas to dust ratios in the external galaxies are the same as that in the Milky Way, we are observing as little as 20% of the dust mass with IRAS. However, due to the strong temperature dependence of the IR luminosity, IRAS is sensitive to the majority of the dust luminosity in a galaxy.

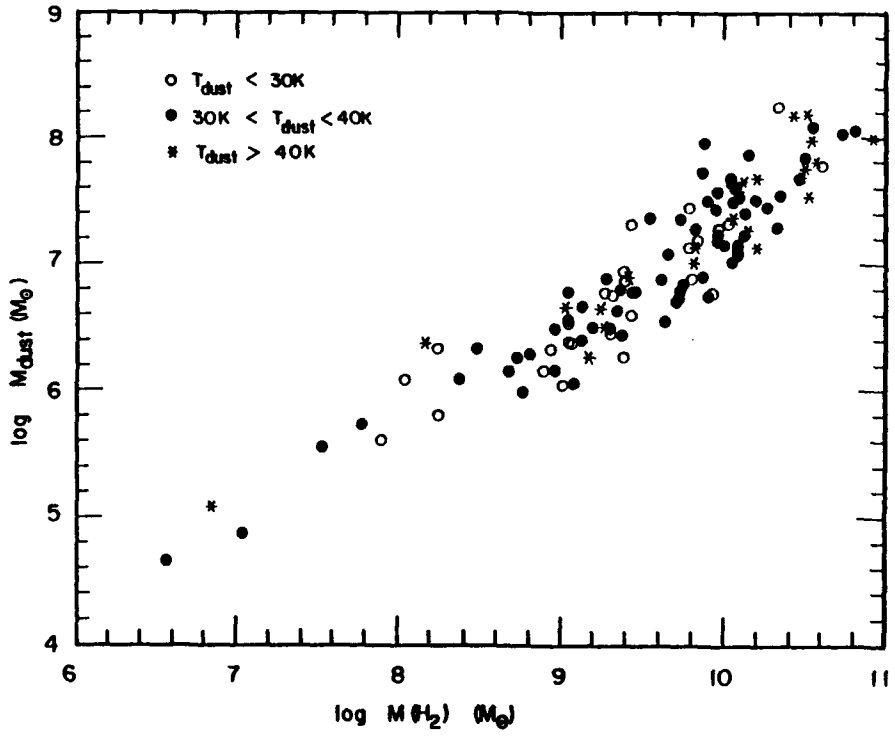

Figure 8. Comparison of the mass of dust, derived from the IRAS observations (cf. Hildebrand 1983), with the H_2 mass inferred from CO. The fit to all galaxies is given by $M(H_2) \propto M_D^{1.2 \pm 0.1}$ with a correlation coefficient of 0.91.

4.2. The Effect of Environment on the Efficiency of Star Formation

It is apparent from the above studies that galaxy mergers are among the galaxies with the highest values of $L_{IR}/M(H_2)$ (i.e. NGC 3310, NGC 6240, and Arp 220). Therefore, we have searched for CO in 30 objects specifically chosen to represent the extremes of environments: isolated galaxies, and merging or strongly interacting galaxies (Young et al. 1986b).

Isolated galaxies were taken from the Karachentseva Catalog of Isolated Galaxies (1973), with the additional requirement that they not be included in any groups (Sandage and Tammann 1975; Turner and Gott 1976; Geller and Huchra 1983). This selection procedure yielded 26 isolated galaxies brighter that 13th magnitude, of which 13 were observed in CO. Examples of galaxy mergers were selected from the paper of Joseph and Wright (1985); interacting galaxies were selected from the Arp Atlas of Pecuiar Galaxies (1966) to be pairs of galaxies in contact. This sample of galaxies includes 15 mergers and interacting galaxies. One striking difference between the galaxies in these samples is that the ratio of 60/100 μm flux densities for the isolated galaxies is 0.35 ± 0.11, while that for the interacting galaxies is 0.83 ± 0.21.

The principal difference between these two galaxy samples is in the value of the IR luminosity per unit H_2 mass, or the star formation efficiency. Figure 9 shows a plot of the ratio $L_{IR}/M(H_2)$ as a function of the 60/100 μm flux density ratio, with the data points coded by environment: stars indicate mergers and interacting galaxies, while circles indicate the isolated galaxies.

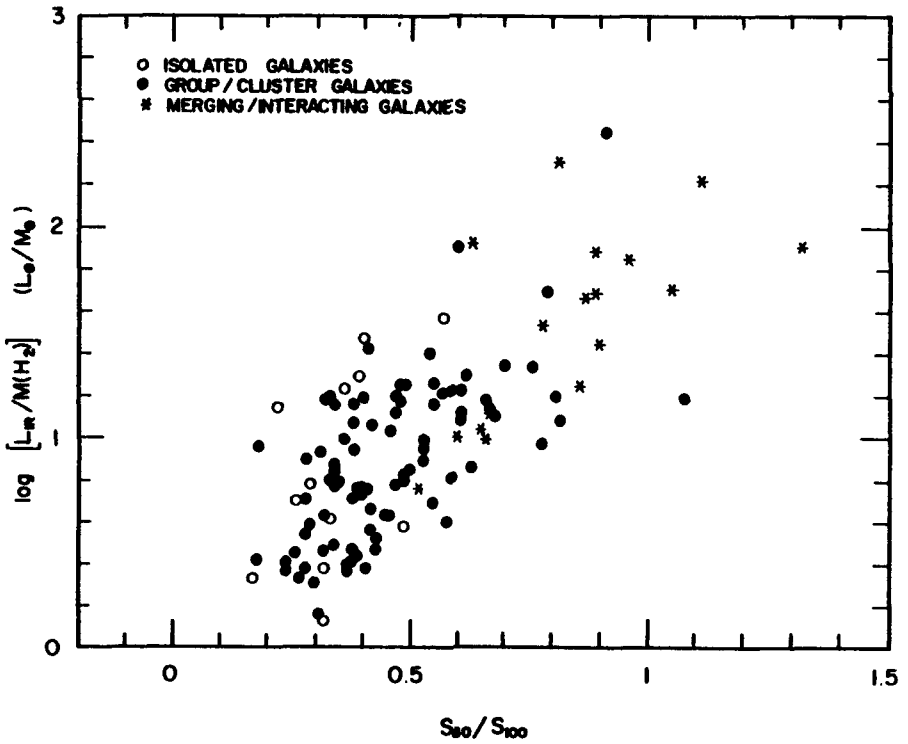

Figure 9. Comparison of the ratio of IR luminosities to H_2 masses with the ratio of 60/100 μm flux densities for the galaxies plotted in Figure 7. Here, the data for each galaxy are coded by the environment, with circles for isolated galaxies, and stars for interacting galaxies. Both the $L_{IR}/M(H_2)$ ratio and dust temperature are high in interacting galaxies and low in isolated galaxies.

We find clear separation between the two samples, in that the isolated galaxies have low values of $L_{IR}/M(H_2)$ and dust temperature, while the interacting galaxies have high values of both quantities; the mean value of $L_{IR}/M(H_2)$ is 11 L_o/M_o in the isolated galaxies and 44 L_o/M_o in the interacting galaxies.

However, within each sample we find a range of more than two orders of magnitude in both the IR luminosities and H_2 masses. The isolated galaxies were found to contain between 3×10^7 and 10^{10} M_o of H_2, while the range for the interacting galaxies is between 10^8 and 3×10^{10} M_o of H_2. Similarly, the IR luminosities are between 4×10^8 and 10^{11} L_o for the isolated galaxies and between 2×10^{10} and 2×10^{12} L_o for the interacting galaxies. The physical mechanism which causes star formation to be more efficient in interacting galaxies must operate over a wide range of masses and luminosities since even low luminosity galaxies with low star formation rates may have high star formation efficiencies.

4.3. Gas Depletion Timescales

Assuming that the observed IR and blue luminosities are produced primarily by O, B, and A stars, it is possible to estimate the inferred global rates of star formation in these galaxies. If the early type stars produce energy using the CNO cycle, and process 13% of their mass while on the main sequence, Scoville and Young (1983) have shown that the star formation rates are given by $M_{O,B,A} = 7.7\times10^{-11}\ L_{tot}/L_o$, where L_{tot} is the sum of the IR and blue luminosities, and $M_{O,B,A}$ is in $M_o\ yr^{-1}$. Figure 10 is a plot of the total luminosities ($L_{IR} + L_B$) and total ISM gas masses (H_2 + HI) for the galaxies in our sample.

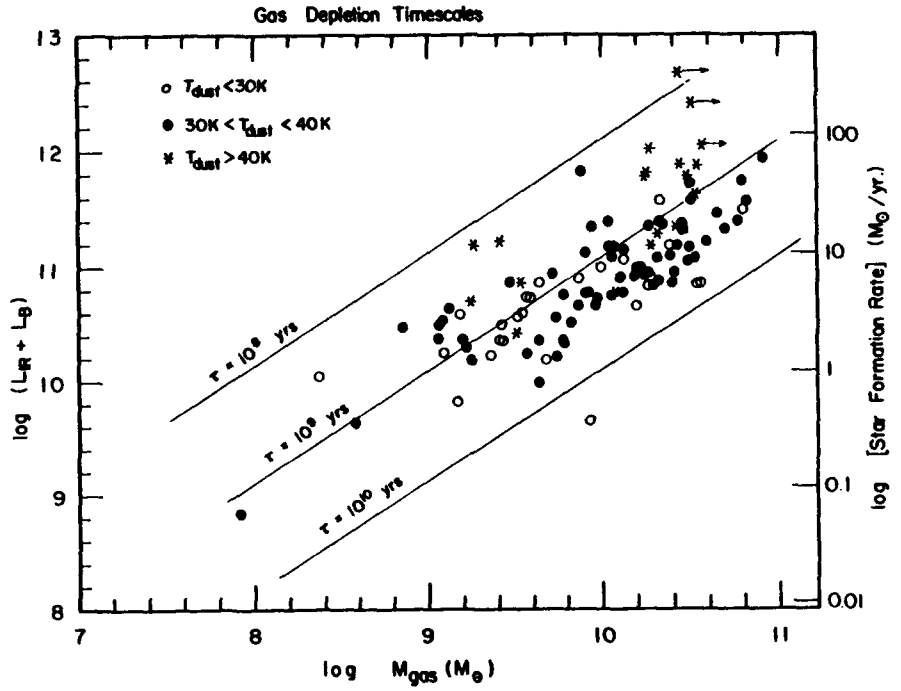

Figure 10. Comparison of the total luminosity ($L_{IR} + L_B$) with the interstellar gas mass (H_2 + HI) for the 114 galaxies in Figure 6 for which HI masses and blue luminosities were available. For galaxies with HI absorption profiles, only lower limits to the gas masses are plotted. The star formation rates were computed following Scoville and Young (1983), and the solid lines indicate the depletion times for the ISM gas masses.

The lines drawn in Figure 10 indicate the times in which the present gas masses will be depleted at the current rates of star formation implied by the total luminosities.

For the galaxies illustrated in Figure 10, the timescales for gas depletion range from 10^8 years to 6×10^9 years. In the sample of 27 galaxies studied by Young et al. (1986a), the galaxies with the highest star formation efficiencies and highest dust temperatures have an average gas depletion timescale of 1×10^9 years, while those with lower efficiencies and dust temperatures have an average gas depletion timescale of 4×10^9 years. Obviously, if the episodes of intense star formation in merging and interacting galaxies are relatively short-lived compared to 10^8 years, then the gas depletion timescales for these objects could in fact be considerably longer.

5. THE VIRGO CLUSTER

In order to understand the effect of environment on star formation for nearby galaxies, we have observed the molecular content of a complete optically selected sample of spiral galaxies in the Virgo cluster (Kenney and Young 1985 and 1986a). The Virgo cluster environment appears to be altering the atomic gas content of some of the member galaxies (cf. Giovanelli and Haynes 1983), and the star formation rates of Sc galaxies in the cluster core seem to have been reduced (Kennicutt 1983). Thus, the Virgo cluster serves as an environment for investigating the histories of star formation and molecular cloud formation in galaxies.

From HI observations of large samples of galaxies, it has been demonstrated that the atomic gas content of spiral galaxies in the Virgo cluster is lower by a factor of 2 in the mean, with some galaxies deficient by more than a factor of 10, from comparisons with isolated galaxies of the same type and optical diameter (cf. Haynes, Giovanelli, and Chincarini 1984). The presently favored explanation for the HI deficiency is stripping of the atomic gas as the galaxies move through the intracluster medium. Recent maps of the HI disks of Virgo spirals indicate that the HI radial extents have been reduced in the HI deficient galaxies (Giovanelli and Haynes 1983; van Gorkom and Kotanyi 1985; Warmels 1985), and that the stripping occurs primarily in the outer parts of the disk.

Kenney and Young (1986a and this conference) have shown that the ratio of H_2/HI masses is lower in the HI-normal galaxies and higher in the HI-deficient galaxies, consistent with stripping of the atomic and not the molecular gas. Additionally, they find that the ratio of CO diameters to HI diameters decreases with distance from M87, providing further evidence for the conclusion that only HI is stripped from the galactic disks. Furthermore, Kenney and Young (1986b) have shown that the atomic gas is stripped even from the inner disks of the HI-deficient galaxies, where the CO appears normal. Since the CO has not responded to the atomic gas removal, then this implies a long lifetime for the molecular phase of the ISM, of order 10^9 years which is the cluster crossing time.

A question which remains unanswered relates to the Hα emission from the Virgo galaxies. If the CO is not stripped, then why are the Hα properties of Virgo Sc galaxies different from those in the field (cf. Kennicutt 1983) ? This could be for any of several reasons. First, it is possible that some of

the Hα emission from field galaxies arises in the outer disk where it is difficult to detect CO. In the outer disks of the Virgo galaxies where the HI has been stripped, subsequent molecular cloud formation (and the resulting star formation) has been truncated. This could explain the lower Hα fluxes for the Virgo galaxies. On the other hand, the molecular cloud size distribution in the Virgo spiral galaxies may have been altered as a result of the HI stripping. If the IMF depends on the molecular cloud size distribution, then the consequent Hα flux may have been reduced. More detailed Hα and far-IR observations of galaxies in the Virgo cluster are needed to address this question.

6. CONCLUSIONS

From observations of the CO content and distributions in galaxies, we have investigated questions related to star formation and its efficiency in galaxies and found the following.

1) The CO radial distributions show central peaks in the Sc galaxies and central CO holes in 40% of the Sb galaxies.

2) The azimuthally averaged distributions of CO, Hα and blue light are similar in the disks of luminous, relatively face-on, late-type spiral galaxies. In NGC 6946, we conclude that the star formation efficiency is constant as a function of radius.

3) The distribution of Hα emission in M51 at 45" resolution shows an enhancement of a factor of 2 on the spiral arms relative to the interarm regions, while that of CO shows at most a 25% enhancement on the arms. Thus, the efficiency of star formation on the arms of M51 appears to be higher by a factor of two relative to the interarm regions.

4) From CO maps of the disks of IR bright galaxies, we find that the CO emission is distributed throughout the disks, and not concentrated solely in the nucleus of the galaxy.

5) We find a general correlation between the total IR luminosity and total CO luminosity of a galaxy, in that galaxies with high CO luminosities (H_2 masses) have high IR luminosities. The scatter observed in the IR luminosity-H_2 mass comparison is highly correlated with dust temperature; for a given H_2 mass the IR emission observed is higher for galaxies with higher dust temperatures.

6) The ratio of $L_{IR}/M(H_2)$ is observed to depend on roughly the fourth power of the dust temperature, which is what one expects if the infrared emission is thermal emission related to dust in molecular clouds. This is further emphasized by the result that there is little correlation between the IR luminosities and HI masses in galaxies.

7) The dust masses are well correlated with the H_2 masses from galaxy to galaxy, even though we are only observing that fraction of the dust which is emitting at 100 μm. If the gas to dust ratios in the external galaxies are the same as that in the Milky Way, we are observing as little as 10% - 20% of the dust mass in some galaxies with IRAS. However, IRAS is sensitive to the majority of the dust luminosity in these galaxies.

8) The implied rates of massive star formation required to produce the observed total luminosities range from 0.4 to 190 M_o yr^{-1}. If the galaxies are in a steady state, the available supplies of ISM (H_2 + HI) will therefore be depleted in 10^8 to 6 x 10^9 years.

9) The star formation efficiency, as measured by the ratio of IR luminosities to H_2 masses, is found to vary by two orders of magnitude from galaxy to galaxy. The galaxies with high values of $L_{IR}/M(H_2)$ are galaxies with high dust temperatures, independent of whether or not they have high values of the total luminosity. Thus, Arp 220 and NGC 1569 both have high dust temperatures and ratios of $L_{IR}/M(H_2)$, even though they have IR luminosities which differ by 4 orders of magnitude. We suggest that the high efficiency of star formation in these galaxies is probably responsible for the high dust temperature.

10) Those galaxies previously identified as mergers are among the galaxies with the highest star formation efficiencies and dust temperatures. Conversely, a sample of isolated galaxies we have studied is characterized by low star formation efficiencies and low dust temperatures. This indicates that the star formation efficiency from galaxy to galaxy does depend on global factors, and not only on the amount of molecular gas present.

ACKNOWLEDGEMENTS

I would like to thank J. Kenney and L. Tacconi for help with the CO observations, and K. Olson for help preparing the figures for this paper. The Five Collge Radio Astronomy Observatory is operated with support from the National Science Foundation under grant AST-82-12252 and with the permission of the Metropolitan District Commission, Commonwealth of Massachusetts. That portion of the research described above which involved access to IRAS data was supported under NASA's IRAS Data Analysis Program and funded through the Jet Propulsion Laboratory.

REFERENCES

Ables, H.D. 1971, Publ.U.S.Naval Obs., Series II, Vol. 20, Part 4.
Arp, H. 1966, Ap.J.Suppl., 14, 1.
Boroson, T. 1981, Ap.J.Suppl., 46, 177.
Bosma, A. 1978, Ph.D. thesis, University of Groningen.
Burton, W.B., and Gordon, M.A., Bania, T.M., and Lockman, F.J. 1975, Ap.J., 202, 30.
Combes, F. Encrenaz, P.J., Lucas, R., and Weliachew, L. 1978, Astron.Ap., 67, L13.
De Gioia-Eastwood, K., Grasdalen, G.L., Strom, S.E., and Strom, K.M. 1984, Ap.J., 278, 564.
Dickman, R.L., Snell, R., and Schloerb, F.P. 1986, Ap.J., in press (October).
Elmegreen, D.M., and Elmegreen, B.G. 1984, Ap.J.Suppl., 54, 127.
Garman, L., and Young J.S. 1986, Astron.Ap., 154, 8.
Geller, M.J. and Huchra, J.P. 1983, Ap.J.Suppl., 52, 61.
Giovanelli, R., and Haynes, M.P. 1983, A.J., 88, 881.
Haynes, M.P., Giovanelli, R., and Chincarini, G.L. 1984, Ann.Rev.Astr.Ap., 22, 445.
Hildebrand, R.H. 1983, Quart.J.R.A.S., 24, 267.

Joint IRAS Science Working Group. 1985, IRAS Point Source Catalogue (Washington, D.C.: US Government Printing Office).
Joseph, R.D., and Wright, G.S. 1985, M.N.R.A.S., 214, 87.
Karachentseva, V.E. 1973, Comm.Spec.Astrophys.Obs., 8.
Kenney, J. and Young, J.S. 1985, in ESO Workshop on the Virgo Cluster of Galaxies, ed. O.-G. Richter and B. Binggeli (Garching: ESO), p. 165.
----- 1986a, Ap.J.(Letters), 301, L13.
----- 1986b, this conference.
Kennicutt, R.C. Jr. 1983, A.J., 88, 483.
Klein, U., Beck, R., Buczilowski, U.R., and Wielibinski, R. 1982, Astron.Ap., 108, 176.
Lo, K.Y., et al. 1984, B.A.A.S, 16, 977.
Lonsdale, C.J., Helou, G., Good, J.C., and Rice, W.L. 1985, "Catalogued Galaxies and Quasars Observed in the IRAS Survey," JPL preprint.
Lonsdale, C.J., Persson, S.E., and Matthews, K. 1984, Ap.J., 287, 95.
Lord, S.D., Strom, S.E., and Young, J.S. 1986, this conference.
Lord, S.D., and Young, J.S. 1986, Ap.J., submitted.
Rickard, L.J., and Harvey, P.M. 1984, A.J., 89, 1520.
Rickard, L.J., and Palmer, P. 1981, Astron.Ap., 102, L13.
Rickard, L.J., Palmer, P., Morris, M., Zuckerman, B., and Turner, B. 1975, Ap.J.(Letters), 199, L75.
Rieke, G.H., Lebofsky, M.J., Thompson, R.I., Low, F.J., and Tokunaga, A.T. 1980, Ap.J., 238, 24.
Rogstad, D.H. and Shostak, G.S. 1972, Ap.J., 176, 315.
Rogstad, D.H., Shostak, G.S., and Rots, A.H. 1973, Astron.Ap., 22, 111.
Rydbeck, G., Hjalmarson, A., and Rydbeck, O.E.H. 1985, Astron.Ap., 144, 282.
Sandage, A. and Tammann, G.A. 1975, 1975, Ap.J., 196, 313.
Sanders, D.B., and Mirabel, I.F. 1985, Ap.J., 298, L31.
Sanders, D.B., Scoville, N.Z., Young J.S., Soifer, B.T., Schloerb, F.P., Rice, W.L., and Danielson, G.E. 1986, Ap.J.(Letters), 305, L45.
Sanders, D.B., Solomon, P.M., and Scoville, N.Z. 1984, Ap.J., 276, 182.
Sanders, D.B., and Young, J.S. 1986, Ap.J., submitted.
Scoville, N.Z., Soifer, B.T., Neugebauer, G., Young, J.S., Matthews, K., Yerka, J. 1985, Ap.J., 289, 129.
Scoville, N.Z., and Solomon, P.M. 1975, Ap.J.(Letters), 199, L105.
Scoville, N.Z. and Young, J.S. 1983, Ap.J., 265, 148.
Scoville, N.Z., Young, J.S., and Lucy, L.B. 1983, Ap.J., 270, 443.
Searle, L., Sargent, W.L.W. and Bagnuolo, W. 1973, Ap.J., 179, 427.
Solomon, P.M. 1982, in "Greenbank Workshop on Extragalactic Molecules," p. 41.
Solomon, P.M., Barrett, J. Sanders, D.B. and de Zafra, R. 1983, Ap.J.(Letters), 265, L103.
Stark, A.A. 1979, Ph.D. Thesis, Princeton University.
Tacconi, L.J., and Young, J.S. 1985, Ap.J., 290, 602.
----- 1986a, Ap.J., in press (September).
----- 1986b, this conference.
Telesco, C.M. and Harper, D.A. 1980, Ap.J., 235, 392.
Turner, E.L. and Gott, J.R. 1976, Ap.J Suppl., 32, 409.
van der Kruit, P.C., Allen, R.J., and Rots, A.H. 1977, Astron.Ap., 55, 421.
van Gorkom, J., and Kotanyi, C. 1985, in ESO Workshop on the Virgo Cluster of Galaxies, ed. O.-G. Richter and B. Binggeli (Garching: ESO), p. 61.
Warmels, R.H. 1985, in ESO Workshop on the Virgo Cluster of Galaxies, ed. O.-G. Righter and B. Binggeli (Garching: ESO), p. 51.
Young, J.S. 1986, in preparation.
Young, J.S., Gallagher, J.S., and Hunter, D.A. 1984, Ap.J., 276, 476.

Young, J.S., Kenney, J., Lord, S. and Schloerb, F.P. 1984, Ap.J.(Letters), 287, L65.
Young, J.S. et al. 1986b, Ap.J., submitted.
Young, J.S., Schloerb, F.P., Kenney, J., and Lord, S.D. 1986, Ap.J., 304, 443.
Young, J.S. and Scoville, N.Z. 1982a, Ap.J., 258, 467.
----- 1982b, Ap.J. (Letters), 260, L41.
----- 1984, Ap.J., 287, 153.
Young, J.S., Tacconi, L., and Scoville, N.Z. 1983, Ap.J., 269, 136.

DISCUSSION

SOLOMON: The Hα emission in M51 only gives a measure of the ionized gas or star formation rate from photons which escape out of the HII region. Much of the star formation may be inside molecular clouds and the Hα may be trapped and heat the dust. Thus, only the far-infrared could give a true measure of the star forming activity.

YOUNG:

There are sources of far-infrared emission which are not directly linked to star formation, such as dust in planetary nebulae, or dust in HI clouds heated by the ambient stellar radation field and more closely linked to older, stellar populations. Thus, the far-infrared is not a better measure of star forming activity, but an alternative measure to the use of Hα. Unfortunately, the Hα emission has extinction uncertainties; there are problems with Hα if more HII regions are on the far side of clouds (which is, of course, unlikely), or if there are radial gradients in the extinction. At the present time, however, the Hα distributions in galaxies have much higher resolution than the infrared, and continue to be essential for comparisons with CO.

SOLOMON:

The separation of galaxy properties such as L_{IR}/L_{CO} according to the 100μm – 60μm color or dust temperature does not really tell us anything about the galaxy. As I mentioned in my talk, for molecular clouds within the galaxy, $L_{IR}/L_{CO} \alpha\ T^{5.5}$. This is exactly what is expected for thermal radiation. The fact that hotter galaxies (hotter dust) have higher L_{IR}/L_{CO} is just a consequence of the Planck law and the dust emissivity. The $T^{5.5}$ dependence overwhelms any possible difference in the infrared luminosity due to differences in the percentage of dust which is heated.

YOUNG:

Phil, I agree completely. In my recent *Ap J.* paper, I pointed out that the dependence of L_{IR}/L_{CO} on T^4 in galaxies is precisely what is expected for thermal emission. However, if the IR emission is of thermal origin, then why do some galaxies have hotter dust? I have suggested that a higher efficiency of star formation, thus producing more stars per unit molecular mass, will heat the dust to a higher temperature in some galaxies.

BECKLIN:

In M51 what is the spiral arm enhancement in the far-infrared?

YOUNG:

The IRAS data do not have sufficient resolution to see arm structures in M51, since they are ~30" across. The 49" resolution 170μm map of Smith (1982) does not show spiral arms to the extent that the Hα (at 45" resolution) does. However, at 170μm, the cold dust should agree more with the CO, since IRAS measures only warm dust.

FORREST:

The Brackett α emission could be a good tracer of the star formation rate, being less affected by extinction.

YOUNG:

It would be interesting if the emission could be mapped over the optical disk.

Submm Observations of IRAS Galaxies

R. Chini, E. Kreysa, E. Krügel and P.G. Mezger
Max-Planck-Institut für Radioastronomie,
Auf dem Hügel 69, D-5300 Bonn 1, F.R.G.

As most of the talk is contained in a paper which will appear in a Letter of Astronomy and Astrophysics, we present in the following only the summary:

26 galaxies from the IRAS point source catalogue have been observed at 350 and 1300 μm. The FIR spectra from 25 to 1300 μm are interpreted in terms of two dust components of about 16 and 53 K. Flux densities at 1300μm are used to estimate the total gas mass M_g. The warm dust luminosity L^W is considered to be proportional to the star formation rate of massive stars. L^W is found to be proportional to $M_g^{0.9}$ in the mass range $3\ 10^8 \leq M_g/M_\odot \leq 10^{12}$. The efficiency of star formation seems to be four times higher in barred and peculiar galaxies than in Sc types.

Carol J. Lonsdale Persson (Editor)
Star Formation in Galaxies

STELLAR BARS AND THE SPATIAL DISTRIBUTION OF INFRARED LUMINOSITY

NICHOLAS DEVEREUX[1]
University of Hawaii, Institute for Astronomy
Honolulu, Hawaii 96822 USA

ABSTRACT. New ground-based 10-μm observations of the central region of over 100 infrared luminous galaxies are presented. A first order estimate of the spatial distribution of infrared emission in galaxies is obtained through a combination of ground-based and IRAS data. The galaxies are nearby and primarily noninteracting, permitting an unbiased investigation of correlations with Hubble type. Approximately 40% of the early-type barred galaxies in this sample are associated with enhanced luminosity in the central (~1 kpc diameter) region. The underlying luminosity source is attributed to both Seyfert and star formation activity. Late-type spirals are different in that the spatial distribution of infrared emission and the infrared luminosity are not strongly dependent on barred morphology.

INTRODUCTION

I am using the IRAS data to investigate the infrared emission from normal galaxies and in particular correlations with optical morphology. Here, I would like to present some preliminary results on stellar bars and the spatial distribution of infrared luminosity.

The primary motivation for this particular study was the discovery made by Hawarden et al. (1986) that the IRAS $S_{25\mu m}/S_{12\mu m}$ flux ratio could actually segregate barred from unbarred galaxies.

THE METHOD

I have investigated the role of bars separately in early- and late-type spiral galaxies. The sample was divided into two broad categories segregating early (Sb and earlier) and late (Sbc and later) spiral types. Each category was further subdivided on the basis of barred morphology. I then compared the distributions of some property, such as luminosity or color, by using a statistical Kolmogorov-Smirnoff (K-S) test. This enabled me to quantitatively estimate whether the "bars" differ from the "unbars" in that property. I will argue the new result that the most significant differences between the bars and the unbars are seen in the early-type spirals.

---

[1]Visiting Astronomer, Infrared Telescope Facility, which is operated by the University of Hawaii, under contract with the National Aeronautics and Space Administration.

Carol J. Lonsdale Persson (Editor)
Star Formation in Galaxies

THE SAMPLE

The galaxies are selected from a volume-limited (distance $\leq$ 40 Mpc) catalog compiled by Dr. Brent Tully of the University of Hawaii. I believe that I have identified all galaxies with 60-μm luminosity $>2.2 \times 10^9$ $L_\odot$, corresponding to a far-infrared luminosity, L (40-120 μm) $> 3 \times 10^9$ $L_\odot$, for $S_{100\mu m}/S_{60\mu m} \sim 3$. The lower luminosity limit was chosen to ensure completeness in the sense that IRAS would have detected all galaxies with $L_{60\mu m} > 2.2 \times 10^9$ $L_\odot$ in a volume of radius 40 Mpc, which is the outer distance limit of the catalog. Nearby galaxies, D $<$15 Mpc, were excluded, thereby reducing the number of galaxies whose large angular size would require more extensive observations. Galaxies with close neighbors were also excluded, since it was uncertain what fraction of the total IRAS flux was emitted by each galaxy. The selection criteria yielded a sample of ~230 galaxies.

RESULTS

The first property I investigated was the effect of bars on the luminosity of the central region. IRAS did not resolve the emission from most of the galaxies, and so I have used the IRTF to obtain new ground-based 10-μm observations with a small 6" aperture. These observations have enabled me to estimate the luminosity of the central (0.5-1 kpc diameter) region for a subsample of 127 galaxies in the RA range $5 \leq \alpha \leq 16$ hr.

The distribution of central 10-μm luminosity ($4\pi D^2 \nu S_\nu$) observed for early-type spirals is shown in Figure 1. The shaded area indicates barred galaxies,

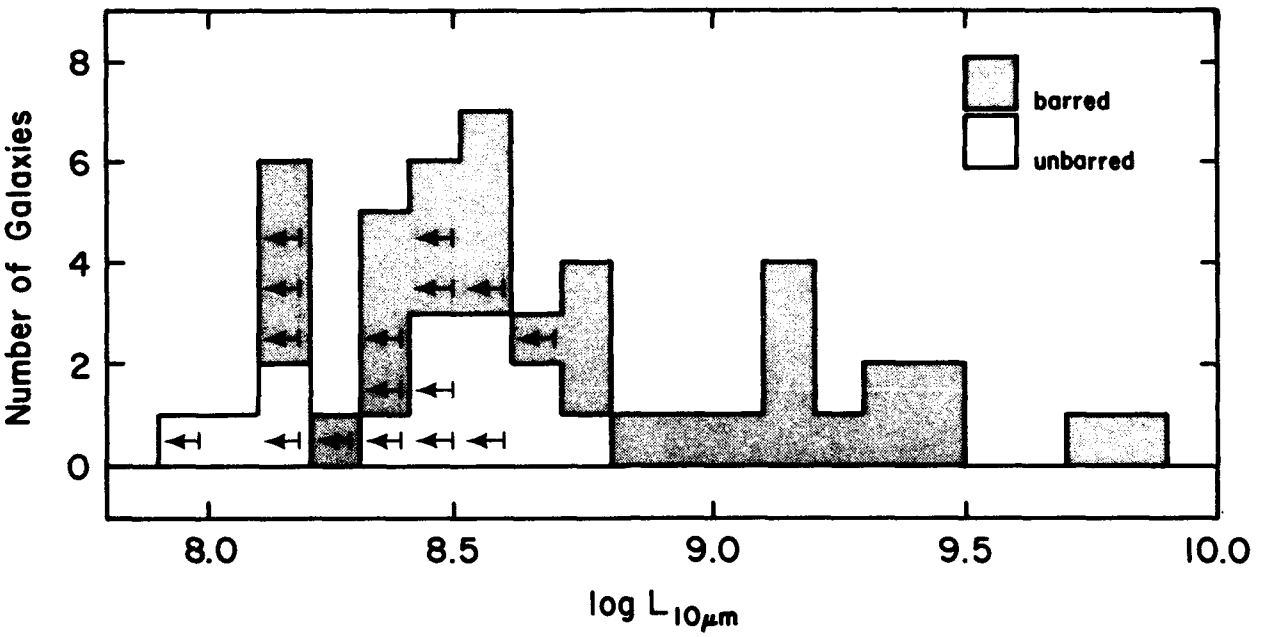

Figure 1. The distribution of central 10-μm luminosity for early-type barred and unbarred spirals. Arrows indicate 2σ upper limits. The central 10-μm luminosity in ~40% of the barred spirals exceeds the maximum central 10-μm luminosity in the unbarred spirals.

and the arrows indicate 2σ limits. The distributions for barred and unbarred galaxies are significantly different at the 95% level. The distributions are different because there is an excess component of 10-μm luminosity in ~40% of the bars that is not present in the unbars. Figure 2 illustrates the distribution for late type spirals; the K-S test indicates that the bars are not significantly different from the unbars (<90%).

The second property I investigated was the IRAS 25-μm/12-μm flux ratio to see if the effect, described by Hawarden et al. (1986), is related to the central 10-μm luminosity distributions described above.

The point source measurements for many of the sample galaxies were limits or unreliable because of extended emission. The IRAS point source measurements of 134 galaxies (~60% of the sample) were improved by line coadding raw IRAS scans. This was achieved using the facilities available at *IPAC*.

In Figure 3, I present the distributions of 25-μm/12-μm flux ratio for early- and late-type spirals. The distributions are significantly different at the 95% level. The difference arises because a larger fraction of the early types have $S_{25\mu m}/S_{12\mu m} > 2$.

When considering just the early-type spirals (Figure 3, top), the distribution of the bars (shaded area) is significantly (95%) different than that of the unbars. The difference arises in that a larger fraction of the bars (50%) than the unbars (17%) has $S_{25\mu m}/S_{12\mu m} > 2.5$. Considering the distribution for late-type galaxies illustrated in Figure 3 (bottom), the K-S test indicates a less significant (<90%) difference between the bars and the unbars.

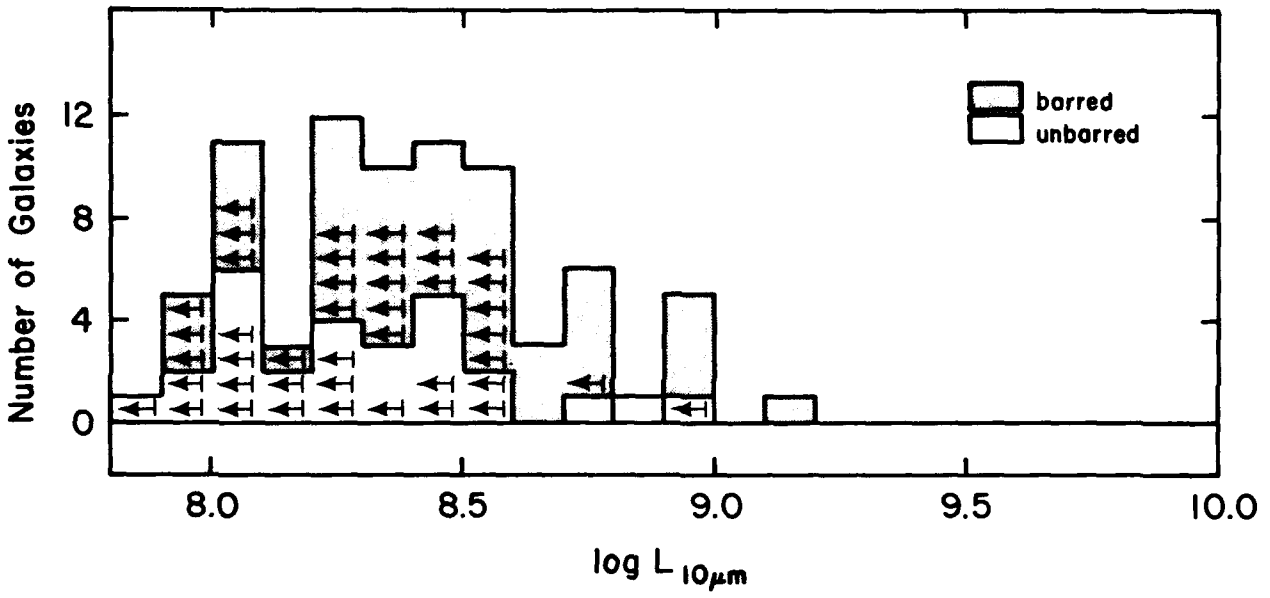

Figure 2. The distribution of central 10-μm luminosity for late-type barred and unbarred spirals. Arrows indicate 2σ upper limits. The distributions for barred and unbarred spirals are similar.

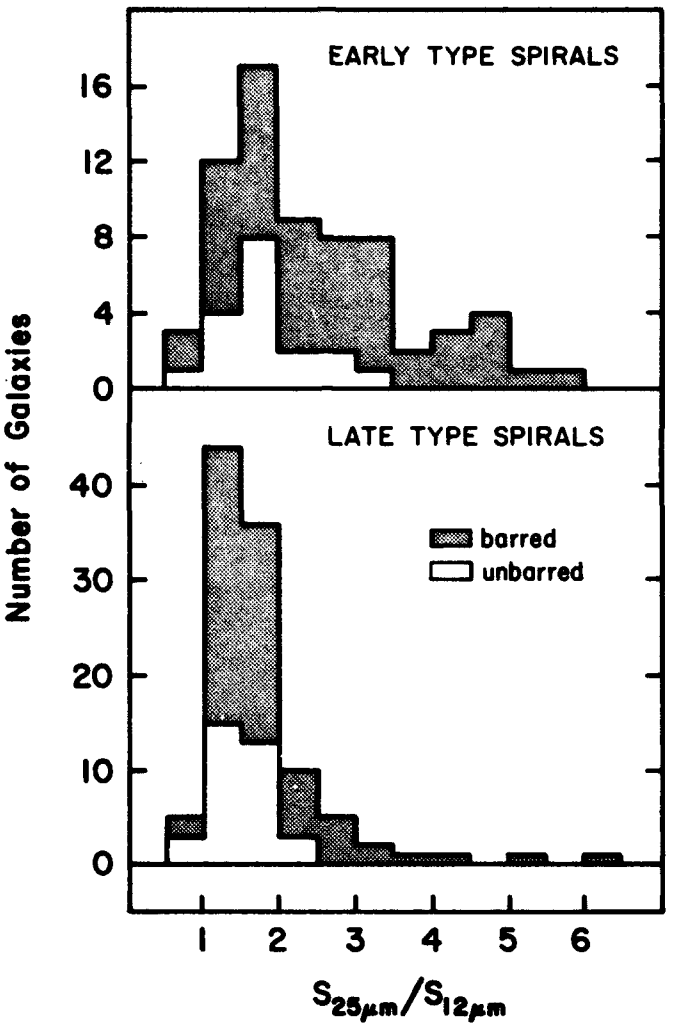

Figure 3. The distribution of the IRAS $S_{25\mu m}/S_{12\mu m}$ flux ratio for (top) early-type and (bottom) late-type spiral galaxies. The distributions for early- and late-type spirals are different largely because of an excess of early-type barred spirals with $S_{25\mu m}/S_{12\mu m} > 2.5$.

To summarise these results, I have shown that for the late-type spirals there was no significant difference between the bars and the unbars in both the ground-based and the IRAS data. In contrast, the early-type spirals did exhibit differences between the bars and the unbars, in both the ground-based and the IRAS data.

DISCUSSION

A reasonable hypothesis to explain the observations in the early-type bars would be that the luminosity of the central region is sufficient to dominate the IRAS 12-μm and 25-μm fluxes. To test this hypothesis, I define a parameter that I call the "compactness," which is the ratio of the ground-based small

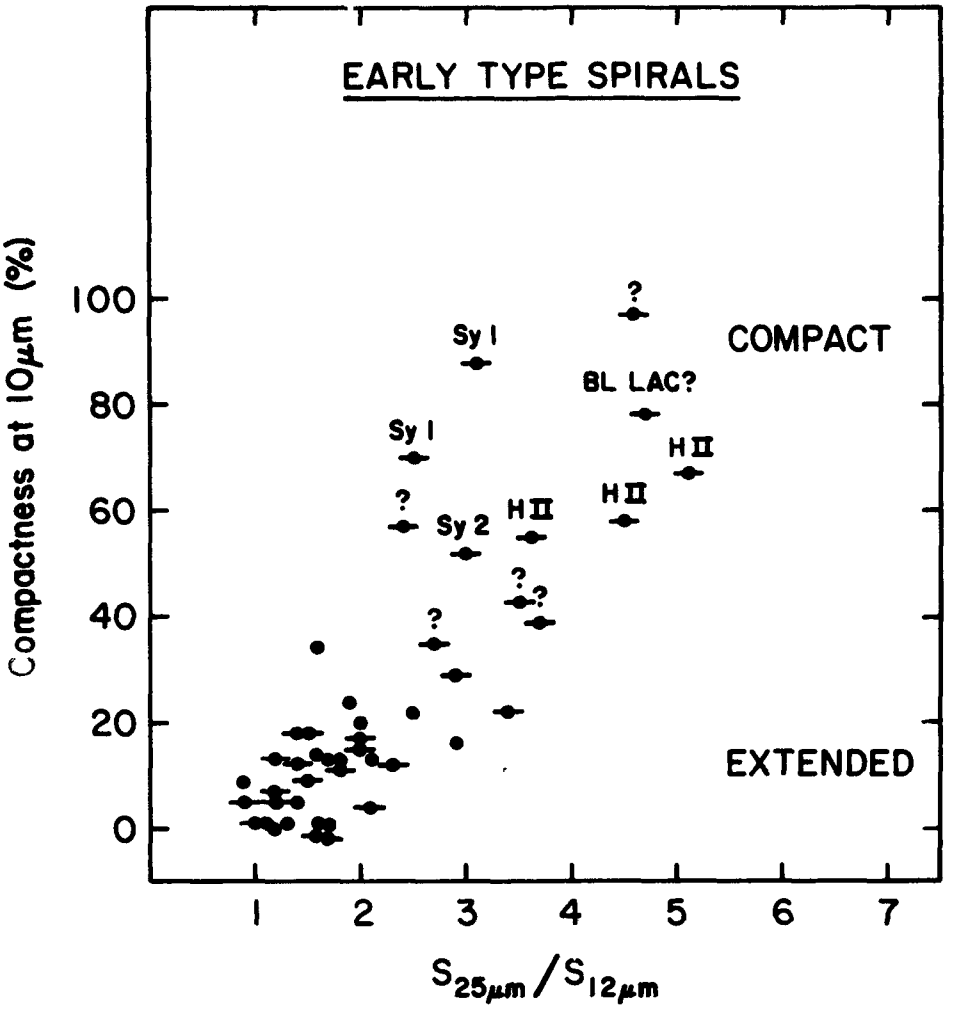

Figure 4. Compactness at 10 μm versus IRAS $S_{25\mu m}/S_{12\mu m}$. Galaxies for which the central region dominates the flux at 12 μm are compact. The IRAS $S_{25\mu m}/S_{12\mu m}$ colors for the compact galaxies indicate that the central region dominates the 25-μm flux also. Barred galaxies are indicated by horizontal bars.

beam 10-μm measurement to the larger beam IRAS 12-μm measurement, color corrected to 10 μm by extrapolating the IRAS 12-μm to 25-μm energy distribution. The compactness enables me to identify galaxies for which the central region dominates the IRAS 12-μm and quite likely the 25-μm emission.

The result of plotting compactness against the IRAS 25μm/12μm ratio is shown in Figure 4. The figure demonstrates that compact galaxies (i.e., >~30% compactness) all have 25-μm/12-μm flux ratios consistent with those observed previously in Seyfert and starburst nuclei (Lawrence et al. 1985). I have indicated the classification of the nuclei based on optical spectra when available. The figure shows that the optical classifications are consistent with the anticipated 25-μm/12-μm flux ratio in the sense that the H II region nuclei have larger ratios that the Seyfert nuclei (Lawrence et al. 1985). This supports the idea that where a galaxy's central region dominates at 12 μm it also dominates at 25 μm.

There is actually only a small number of galaxies in which the central region dominates the IRAS 12-μm and 25-μm fluxes. I estimate that there are only about 30 early-type barred galaxies with a central 10-μm excess, in the distance range 15-40 Mpc. Approximately 10% of all early-type barred galaxies are associated with enhanced central activity. The far-infrared luminosities L(40-120 μm) of the active early-type bars is $>1 \times 10^{10}$ $L_{\odot}$.

It is of interest to consider these results in the context of previous studies concerning the association of central activity with stellar bars. Seyfert nuclei are found predominantly in early-type spirals, although the association with stellar bars is of less statistical significance (Heckman 1978; Simkin 1980). On the other hand, H II region nuclei are found to be significantly biased to barred galaxies of all spiral types (Heckman 1980).

There is a difference between this study and those referenced above, in that the latter investigated only the frequency with which characteristic optical emission lines were observed in the central region of barred and unbarred galaxies. I have investigated the frequency with which high central 10-μm luminosity occurs in barred and unbarred galaxies. I found that in early-type galaxies, bars are essential for high central 10-μm luminosity. Perhaps the important parameter, distinguishing the bars from the unbars, is not the frequency with which a particular form of activity is observed, but rather the intensity of the activity.

QUESTIONS TO BE ADDRESSED

These results raise some interesting questions regarding the role of the bar in the early-type spirals. Is the bar somehow stimulating star formation? Is it supplying additional fuel for star formation and/or active nuclei? Perhaps a more fundamental question may be, Why is the bar more important in the early-type spirals? The latter may indicate that the stellar mass distribution is as important as a gas reservoir in fueling activity in the central region.

ACKNOWLEDGEMENTS

I would like to thank Gareth Wynn-Williams, Steve Eales, and Eric Becklin for their enthusiastic support of this work. Thanks also to the IPAC staff, in particular Walter Rice, Carol Persson, and George Helou, for ensuring that my stay was both enjoyable and scientifically rewarding. I would also like to thank the IRTF staff, in particular Charles Kaminski.

QUESTIONS

Solomon: With regard to the question of fuel in the bar, I have mapped the CO emission in the barred spiral NGC 1530. Along the bar the CO flux is an order of magnitude greater than off the bar, thus there is more fuel.

Helou: Did you not find the early-type galaxies to be more compact than the later types? Does that not contradict the result by Judy Young and coworkers that the CO distributions are centrally peaked in the late types and have holes in the early types?

Reply: Yes, the early types are more compact than the late types. The compactness of the late-type spirals, however, is not inconsistent with the exponential distributions observed by Judy for both the CO and blue luminosity in the late-type Virgo spirals. Regarding the CO holes, I think it is important to establish the distribution of CO in the early-type galaxies in question.

Kenney: Regarding the question about CO holes in the early types, I have mapped the CO emission in about a dozen early-type Virgo spirals; most of these are centrally peaked with a resolution of 45" (~4 kpc). Only one has a definite CO hole at this resolution.

Simkin: Models of gas flows in spirals induced by bars show that the rate of flow depends on the mass distribution in the galaxy. It may be that your association of central activity with early-type barred galaxies reflects the different mass distribution in these objects.

Reply: I am aware of these results and hope to obtain observations to investigate them further. In particular I plan to obtain multiaperture photometry at near-infrared wavelengths to establish the spatial distribution of starlight in the central regions of the spiral galaxies under discussion here.

Rieke: The result shown earlier (Wynn-Williams) from Rieke and Lebofsky that showed a strong tendency for Sa's not to have high-infrared luminosities was derived only for unbarred galaxies. It would imply that a bar was nearly essential for high luminosity in an early spiral. Is that consistent with your results?

Reply: Yes.

Kennicutt: Several years ago Sersic noted that nuclear hot-spots occur almost exclusively in barred spirals. Maybe you are seeing the same thing. Could the predominance of centrally concentrated sources in early-type spirals be a contrast effect due to the lower disk star formation in the early-type galaxies?

Reply: The Sersic result is now in question in the light of a recent study by Heckman (1978). Regarding the second part of your question, I do not believe that this is a contrast effect for two reasons. Firstly, Wynn-Williams showed that the far-infrared luminosity distributions of early- and late-type spiral galaxies are similar, thus there is no evidence that the disk star formation is lower in the early types. Secondly, the effect in the early-type bars is evident not only in the colors, but also the luminosity, of the central region. The luminosity of the central region of ~40% of the early barred galaxies is greater than that observed in the late-type galaxies and the early unbarred galaxies.

Joseph: There is an important additional parameter that could undercut your comparison of early- and late-type galaxy infrared luminosities. In our J,H,K,L' study of the spirals in the Virgo cluster we found that late-type galaxies are significantly fainter than early-type spiral galaxies in this cluster. Would this systematic bias in luminosity, and therefore also in the mass of gas present, not account for the differences between early- and late-type galaxies which you find in this sample?

Reply: In the study of those same Virgo galaxies carried out by myself,

Becklin, and Scoville, we found two results: the 10-μm luminosity of the central region of all spirals is comparable, whereas the near-infrared luminosity tended to be higher, on average, in the early types. Regarding my presentation, I am investigating the differences between bars and unbars separately in early and late types. I am not considering the differences between early- and late-type spirals here.

REFERENCES

Hawarden, T. G., Fairclough, J. H., Joseph, R. D., Leggett, S. K., and Mountain, C. M. 1986, in Light on Dark Matter, ed. F. P. Israel (Dordrecht: Reidel), pp.455-462.

Heckman, T. M. 1978, Pub. A.S.P., 90, 241.

_____. 1980, Astr. Ap., 88, 365.

Lawrence, A., Ward, M., Elvis, M., Fabbiano, G., Willner, S. P., Carleton, N. P., Longmore, A. 1985, Ap. J., 291, 117.

Simkin, S. M., Su, H. J., Schwarz, M. P. 1980, Ap. J., 237, 404.

STAR FORMATION AND SPIRAL STRUCTURE IN M81

Michele Kaufman[1] and Frank N. Bash[2]

[1]Department of Physics
The Ohio State University
Columbus, OH 43210

[2]Department of Astronomy
The University of Texas at Austin
Austin, TX 78712

ABSTRACT. High resolution digitized images of M81 in the radio continuum, Hα, H I, and I band are used to see how well various density wave models agree in detail with observations. We find that the observed width of the nonthermal radio arms favors a cloudy version of a density wave model (e.g., the model of Roberts and Hausman). The radial distribution of the set of giant radio H II regions disagrees with the simple expression of Shu and Visser for star formation by a density wave. The observed displacements of the giant radio H II regions from the spiral velocity shock indicate that some revisions in the details of the ballistic particle model of Leisawitz and Bash are necessary.

1. INTRODUCTION

In classical density wave theory, the compression of the gas by a spiral shock is responsible for triggering the formation of new stars. Some recent versions of density wave theories take into account the clumpy nature of the interstellar medium. For example, in the cloudy density wave model of Roberts and Hausman (1984), star formation is enhanced in the spiral arms because collisions between giant clouds occur more frequently there. Digitized high resolution radio and optical images of galaxies can now be made for checking the predictions of these various theories. We selected M81 for such a study because (i) the observed H I velocity contours show a spiral velocity shock (Visser 1980 a,b, Hine and Rots 1986) and thus provide strong evidence for a density wave in this grand design spiral, and (ii) theoretical density-wave models of this galaxy are available from Visser (1980 a,b) and Leisawitz and Bash (1982) for comparison with observations.

We present three tests of density wave models for M81. These tests involve using VLA radio continuum data from Bash and Kaufman (1986), VLA H I data from Hine and Rots (1986), Hα observations by Hodge and Kennicutt (1983), and I band data from Elmegreen (1981). We compare these observations of M81 with some predictions of the following density-wave models:

(a) the hydrodynamic density-wave model for M81 by Visser (1980 a,b), who treats the interstellar gas as a continuous, single component medium;

(b) the ballistic particle model for M81 by Leisawitz and Bash (1982), who use Visser's model for the H I gas but assume that stars form in giant clouds that orbit as ballistic particles;

(c) the cloudy density wave model for our Galaxy by Roberts and Hausman (1984), who impose a spiral gravitational perturbation but use an N-body calculation to simulate a cloudy interstellar medium.

Carol J. Lonsdale Persson (Editor)
Star Formation in Galaxies

The models of Roberts and Hausman and Leisawitz and Bash both involve clouds and a spiral gravitational perturbation but differ in the assumptions made about the clouds and the processes that lead to star formation.

Our goal is to see how well the above models agree in detail with the available data.

2. FIRST TEST: OBSERVED WIDTH OF THE NONTHERMAL RADIO ARMS

Classical density wave theory predicts a narrow nonthermal emission ridge on the inside edge of the spiral arms, where a spiral shock compresses the interstellar gas and magnetic fields. Since M81 is not seen face-on, the width of the ridge in the plane of the sky would depend on the scale height of the shocked layer. If the appropriate shocked layer is the H I disk, then Visser's model predicts a nonthermal ridge that is, at most, 260 pc wide in the plane of the sky. Roberts and Hausman did not do a model for M81. For our Galaxy their model produces a spiral "shock front" 300 - 600 pc wide and a spiral density enhancement 1 kpc wide; we expect that their calculations would yield similar results for M81.

To determine the width of the nonthermal radio arms for comparison with these values, Bash and Kaufman (1986) have made VLA observations of M81 at wavelengths of 6 and 20 cm. We detect radio continuum emission from the spiral arms and the mini-Seyfert nucleus, but not from the disk. On a series of radio continuum and spectral index maps that range in resolution from 10" to 15" (160 - 240 pc if the distance of M81 is 3.3 Mpc), we are able to separate giant H II regions from the more extended nonthermal arm emission (see Figure 1). The good correspondence between H II regions and many of the bright knots on the radio continuum arms is shown in Kaufman et al. (1986), where an Hα image is superimposed on a 20 cm radio image, both at a resolution of 10". A spectral index map with a resolution of 18" shows that much of the more extended emission from the arms is mildly nonthermal. Either the extended emission is a combination of nonthermal and diffuse free-free emission or the electron energy spectrum is not very steep. In the latter case, our spectral index values would agree with Duric's (1986) proposed mechanism for diffusive shock acceleration of relativistic electrons by spiral density-wave shocks.

Bash and Kaufman (1986) show examples of intensity profiles obtained by slicing across the radio continuum arms at various positions that avoid the giant H II regions. The intensity profiles were made on a 20 cm map with a resolution of 9.5" (150 pc) and on one with a resolution of 17" (270 pc). On both maps the nonthermal arms are patchy and well resolved, with a typical width of 1 - 2 kpc. Therefore the nonthermal arms are too broad to fit Visser's hydrodynamic model and seem to agree better with the width of the density enhancement in the cloudy density wave model of Roberts and Hausman.

From their VLA H I maps of M81, Hine and Rots (1986) conclude that the observed width of the velocity shock is too broad to agree with Visser's model but appears consistent with the width of the shocked layer in the model of Roberts and Hausman for our Galaxy. Therefore both the synchrotron radiation and the H I data point to the same conclusion.

3. SECOND TEST: THE RADIAL DISTRIBUTION OF GIANT RADIO H II REGIONS IN THE PLANE OF M81

Kaufman et al. (1986) study 42 giant H II regions with high surface brightness that are detected in the radio continuum maps of M81. Figure 1 shows the distribution of these giant radio H II regions deprojected into the plane of M81 and superimposed on a gray-scale display of the deprojected 20 cm map. The set of giant radio H II regions is more sharply confined to the spiral arms than the total optical samples plotted by Connolly et al. (1972) and Hodge and Kennicutt (1983). The total optical sets include faint H II regions as well as bright ones. We conclude that the giant radio H II regions are more likely to be related to a density wave. Rumstay and Kaufman (1983) find a similar phenomenon in M83 and M33 and suggest that the low luminosity H II regions are more likely to occur in smaller clouds and to involve sporadic star formation.

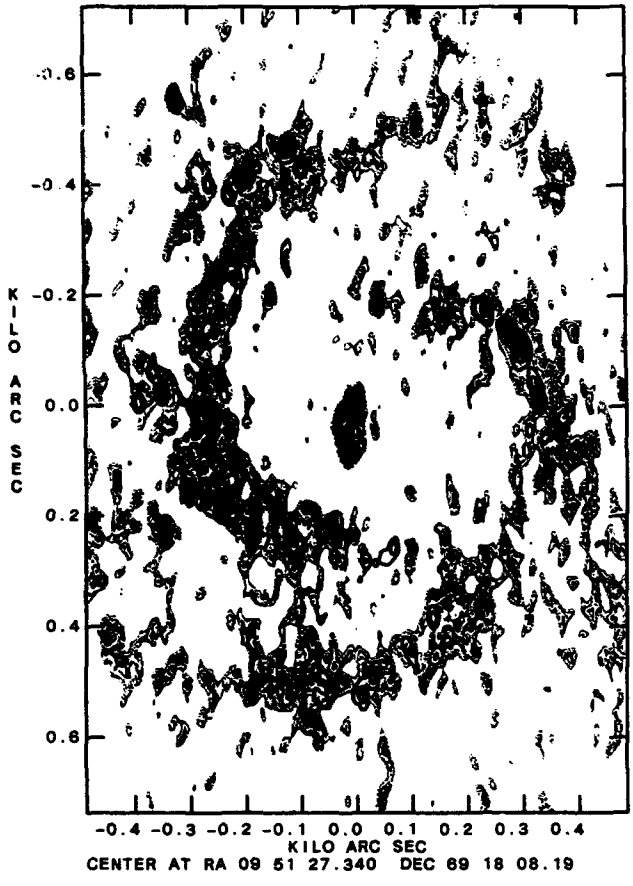

Figure 1. A gray-scale display of the 20 cm emission after deprojection into the plane of M81. The superimposed contours show the positions of the giant H II regions that are detected in the radio. The bright compact source in the nucleus was subtracted before making this map. The major axis is horizontal.

We use the radial distribution of giant radio H II regions in the plane of M81 to test the following simple relation proposed by Shu (1974) for star formation by a density wave:

$$N(\text{H II}) \sim \sigma_{HI}[\Omega(R) - \Omega_p] \, (\sigma_{shock}/\sigma_g)^n , \quad n = 1, 2, \qquad (1)$$

where N(H II) is the number of H II regions per kpc^2, σ_{HI} is the mean surface

density of H I at galactocentric distance R, $\Omega(R)$ is the angular rotation speed of the matter, Ω_p is the pattern speed, and σ_{shock}/σ_g is the spiral shock compression of the gas. The lower bar graph in Figure 2 is the observed radial distribution of the set of giant radio H II regions, while the dashed curve is obtained from Shu's expression with parameter values from the Visser model that gives the best fit to the observed distribution. Although the peak occurs at about the same location in both distributions, the observed distribution is more sharply peaked than the predicted one.

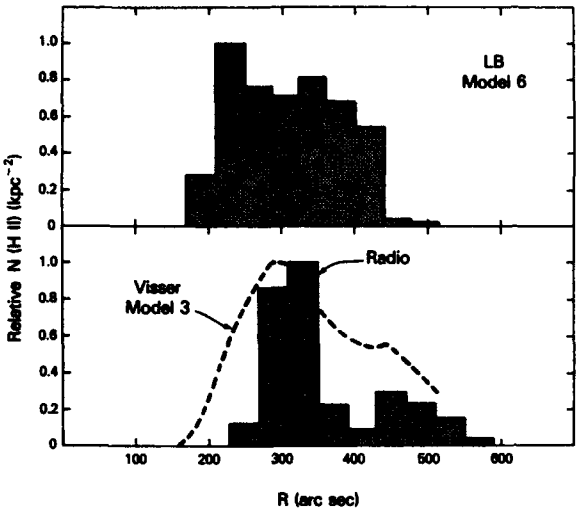

Figure 2. Comparison of the observed radial distribution of the set of giant radio H II regions (the bar graph labeled "radio") with the predictions of models for M81 by Visser (1980b) and Leisawitz and Bash (1982).

CO measurements and upper limits suggest that the surface density of H_2 in M81 is very low; therefore replacing σ_{HI} in Equation (1) by the surface density of atomic plus molecular hydrogen would not change the clear disagreement between theory and observation. We know of only one convincing detection of CO in M81: using a 102" FWHP beam (1.6 kpc at the distance of M81) centered near the two most luminous H II regions in the peak of the radial distribution, Stark (1986) obtains an integrated $T\Delta v$ of only 0.3 ± 0.1 K km s^{-1} for the J = 1 → 0 transition of ^{12}CO. This suggests that H_2 is a very minor constituent compared to H I.

The upper bar graph in Figure 2 is the prediction of a ballistic particle model adopted by Leisawitz and Bash for M81; it disagrees with our observations. To get their model to produce the narrow peak in the observed radial distribution requires a different choice for the assumed radial distributions of either the small clouds or of the birth sites of the giant clouds.

4. THIRD TEST: THE LOCATIONS OF THE SPIRAL ARMS DEFINED BY VARIOUS TRACERS

Figure 3 shows the H I intensity data from Hine and Rots (1986) after deprojection into the plane of M81, with the major axis horizontal. Rots (1975) suggests that the faint inner H I ring is produced by the inner Lindblad resonance. Our 20 cm observations support this interpretation (see Bash and Kaufman 1986). The position of the velocity shock measured by Hine and Rots is along the inside edge of the H I arms. Notice that the inner edge

of the arms is more sharply defined than the outer (downstream) edge. Near the northern major axis (the left-hand side in Fig. 3), the H I arm spreads out. This may be the result of a tidal distortion by M82.

Elmegreen's (1981) I band plate shows the spiral arms defined by the old stars; the I band ridge indicates the location of the spiral potential minimum. When we superimpose a sharp-masked I band image on the H I image, we see that the potential minimum defined by the old stars lies just downstream from the spiral shock. This agrees qualitatively with Visser's hydrodynamic model and with the cloudy density wave model of Roberts and Hausman. Figure 3 shows the positions of the giant H II regions that are detected in the radio. All but one of the giant radio H II regions are located on either the H I arms or the inner H I ring. Essentially all of these regions lie downstream from

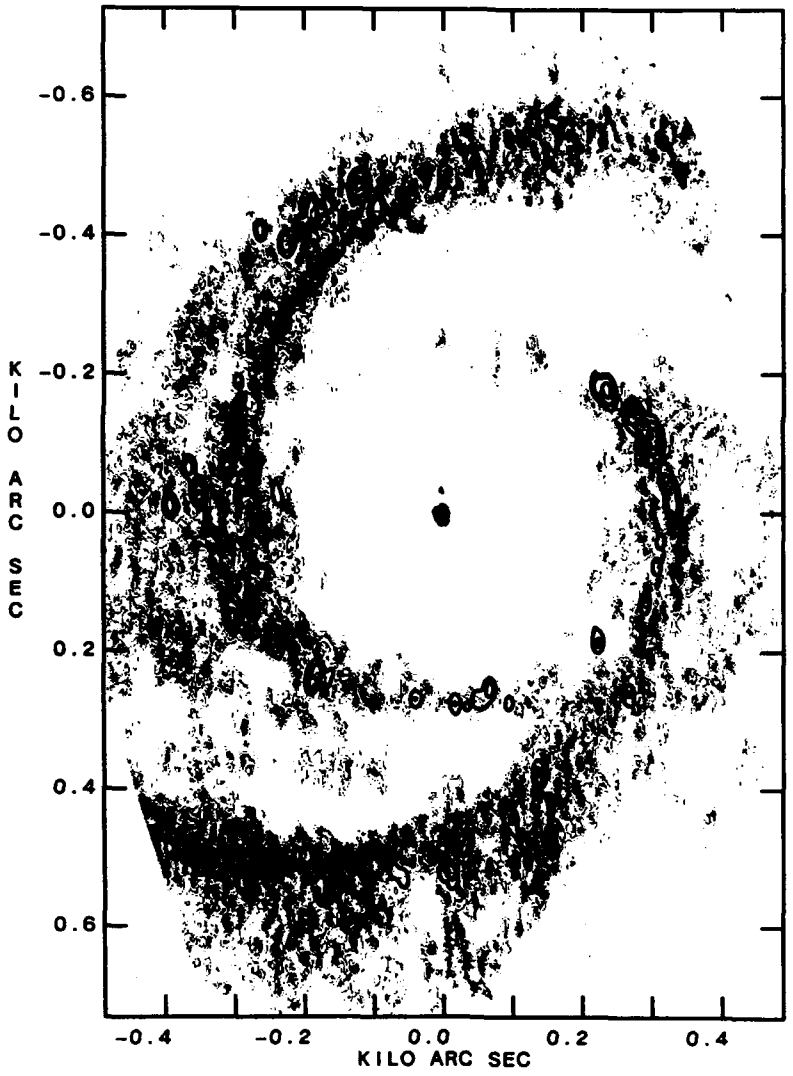

Figure 3. A gray-scale display of the rectified H I intensity map from Hine and Rots (1986). The superimposed contours show the locations of the giant radio H II regions. The compact nucleus is not an OB association but is retained here as a fiducial point. The major axis is horizontal.

the spiral shock. If the H I image, the distribution of giant radio H II regions, and the sharp-masked I band image are all superimposed (as was shown in a colored slide in the lecture), then one sees that some of the giant radio H II regions lie along the potential minimum defined by the old stars; the others, particularly at large R, are farther downstream.

To illustrate how this data can be used to test density wave models, we consider the angular distribution of H II regions that Leisawitz and Bash obtain with their adopted ballistic particle model for M81. Near the major axis, the model predicts two clumps of H II regions: one just upstream from the shock and the other stretching appreciably downstream. Near the southern major axis all the observed giant H II regions lie along the spiral potential minimum (i.e., just downstream from the shock); near the northern major axis some are located still farther downstream. At large galactocentric R, the model predicts that all H II regions should lie just upstream from the shock, but here the observed regions are significantly downstream from the shock. It appears that some change is required in the values used in their model for the launch speed and the time delay before the onset of star formation.

5. CONCLUSIONS

The observations of M81 are consistent with the presence of a density wave; this paper is concerned with how well the details fit. The width of the nonthermal radio arms favors a cloudy version of a density wave model. A comparison between the predictions of the ballistic particle model of Leisawitz and Bash (1982) and the observed radial and azimuthal distributions of giant radio H II regions indicates that some revision in the details of their model is necessary.

ACKNOWLEDGMENTS. We thank Butler Hine, Arnold Rots, Debra Elmegreen, Robert Kennicutt, and Paul Hodge for supplying us with copies of their digitized data. We thank Burton Jones for measuring the α, δ coordinates of the bootstrap standard stars that we used in doing the plate solutions. We thank Tony Stark for providing his unpublished results. This paper was written while M.K. held a National Research Council - NASA Research Associateship at Goddard Space Flight Center, Greenbelt, MD.

The National Radio Astronomy Observatory is operated by Associated Universities, Inc., under contract with the National Science Foundation. We thank the NRAO staff for this assistance.

REFERENCES

Bash, F.N., and Kaufman, M. 1986, Ap.J., in press.
Connolly, L.P., Mantarakis, P.Z., and Thompson, L.A. 1972, Pub. A. S. P., 84, 61.
Duric, N. 1986, Ap.J., 304, 96.
Elmegreen, D.M. 1981, Ap. J. Suppl., 47, 229.
Hine, B., and Rots, A.H. 1986, in preparation.
Hodge, P.W., and Kennicutt, R.C. 1983, Ap. J., 267, 563.

Kaufman, M., Bash, F.N., Kennicutt, R.C., and Hodge, P.W. 1986, preprint.
Leisawitz, D., and Bash, F.N. 1982, Ap. J., 259, 133.
Roberts, W.W., and Hausman, M.A. 1984, Ap. J., 277, 744.
Rots, A.H. 1975, Astr. Ap., 45, 43.
Rumstay, K.S., and Kaufman, M. 1983, Ap. J., 274, 611.
Shu, F.H. 1974, in The Interstellar Medium, ed. K. Pinkau (Dordrecht: Reidel), p. 219.
Stark, A.A. 1986, private communication.
Visser, H.C.D. 1980a, Astr. Ap., 88, 149.
_____. 1980b, Astr. Ap., 88, 159.

DISCUSSION

DICKEY:

I was not surprised to see a mixture of thermal and non-thermal emission shown by the spectral index map for the south-eastern spiral arm, but I was surprised that there is not a gradient in the spectral index representing a variation in the mixture of thermal and non-thermal emission. Are you confident that you have resolved the spiral arm?

KAUFMAN:

First of all, this is VLA data, not data taken with a filled aperture, so one should exercise some caution in interpreting the spectral index values. We checked on a spectral index map made with 160 pc resolution that the bright Hα sources have spectral indices consistent with optically-thin free-free emission. The slide showed a spectral index map with a resolution of 290 pc, and at this lower resolution the emission from an HII region is convolved with surrounding non-thermal arm emission. We use this map to distinguish between free-free, mildly non-thermal, and strongly non-thermal emission, but I would be wary of making finer distinctions. We find that most of the extended arm emission is mildly non-thermal.

Secondly, the intensity profiles across the arms show that the arm emission is resolved.

THE HII REGIONS IN M51: RADIO AND OPTICAL OBSERVATIONS

J.M. van der Hulst
Netherlands Foundation for Radio Astronomy
Postbus 2
NL - 7990 AA Dwingeloo
The Netherlands

R.C. Kennicutt Jr.[1]
Department of Astronomy
116 Church St. SE
Minneapolis, MN 55455
U.S.A.

ABSTRACT. High resolution, dual frequency radio observations and calibrated H_α surface photometry of the spiral galaxy M51 are used to determine the physical properties of the 40 brightest HII region complexes. M51 appears to have a normal HII region population when compared with other nearby Sc galaxies for which good data exist. We used the radio and H_α data to measure the extinction toward the HII regions. The extinction is very patchy but appears to have a weak trend to become on average smaller toward large galactocentric radii. This trend is consistent with a possible metallicity gradient in M51. We compared the radio determined extinctions with Balmer decrement extinctions and found good agreement between the two, contrary to previous studies of M51 and other galaxies.

1. INTRODUCTION

Several observable properties of galaxies provide information about recent, massive star formation. Each of these, however, has its drawbacks. The far infrared emission, for example, measures not only the energy absorbed by warm dust around HII regions, but also represents emission from cool dust illuminated by the interstellar radiation field. (Cox and Mezger, this volume, Persson and Helou, this volume). These components are difficult to separate so that an assessment of the massive star formation rate is difficult. A similar problem exists when one tries to measure the thermal radio emission from HII regions. The thermal free-free emission in principle measures all ionizing photons. The usual observational handicap, however, is that the thermal radio emission one measures is contaminated with non-thermal emission from the underlying disk and spiral arms, so that here also one cannot simply use the total radio emission from the HII regions as an indicator of the ionizing photon flux. First the thermal and non-thermal emission must be separated. A third way of measuring star formation is to observe the H_α emission. The prime difficulty with this method is that one needs to correct the H_α emission for the extinction, which is often not well known.

We have used dual-frequency radio maps and calibrated H_α surface photometry to investigate the distribution of extinction and to study the HII region population in the spiral galaxy M51. The radio maps allowed us to measure the free-free emission from the HII regions so that it is possible to estimate the extinction by comparing the free-free radio emission with the H_α emission of the same region. The exact procedures and results will be discussed briefly in the next two sections.

Carol J. Lonsdale Persson (Editor)
Star Formation in Galaxies

2. OBSERVATIONS

The radio observations were obtained with the Very Large Array (VLA) of the NRAO[2] in 1981-1982. (for details see Van der Hulst et al. 1987). The maps used for this study are maps at 6 and 20 cm wavelength obtained from the multi-array data which have a resolution of 8" (372 pc at the 9.6 Mpc distance of M51). This resolution appeared best for detecting the most HII regions. The reason is that some of the lower surface brightness regions begin to resolve out at higher resolution.

The H_α data were obtained with the two stage Carnegie Image tube on the KPNO 2.1 m telescope. Two plates, one at H_α and one in the red continuum were scanned on the KPNO PDS microdensitometer, calibrated, and then subtracted. The resulting H_α emission image was then smoothed to 8" resolution to match the radio resolution. The H_α data were calibrated using spectrophotometric data taken with the IDS scanner on the UCSD-UM 60" telescope at Mt. Lemmon. Spectrophotometry was obtained through 9" apertures for 15 HII regions (for a detailed description see Van der Hulst and Kennicutt 1987).

The radio maps and H_α map were interpolated onto a common grid and then blinked to identify the HII regions which have been detected in both data sets. The radio data are essentially noise limited and restrict the number of regions that can be identified and used. We detected 32 regions at H_α and in the radio and found another 8 with probable detections in the radio. These are the 40 brightest HII regions in M51. We then measured fluxes at 6 and 20 cm in the radio and in Hα through circular apertures varying in diameter from 12" to 21" depending on the extent of the region. A correction for background emission was made as described in Van der Hulst and Kennicutt (1987). The 6 cm radio fluxes were decomposed into a thermal and a non-thermal contribution assuming a non-thermal spectrum with a slope of α=-0.9 ($S \propto \nu^\alpha$), as indicated by the total, largely non-thermal emission of M51 (Klein and Emerson 1980). About half of the HII regions have 6 cm fluxes which are entirely thermal. For the other regions the fraction of thermal emission at 6 cm varies from 50 to 80 %. The extra non-thermal emission is probably due to small scale structure in the underlying disk or objects like supernova remnants. It should be pointed out that supernova remnants, and in particular young supernovae, may have a flat radio spectrum (Reynolds and Chevalier, 1984) and are therefore inseperable from the thermal emission of the HII regions. We then used standard recombination theory to calculate HII region properties (following Schraml and Mezger 1969) and the extinction in the visual (A_V). For these calculations we assumed an electron temperature of 7000 K, based on the average excitation of the HII region spectra. (see also McCall et al., 1985)

3. RESULTS

The HII region properties as determined from the radio fluxes are quite normal and not drastically different from earlier results in M51 (Israel, 1980) or recent results on the HII region population in M33 (Viallefond and Goss, 1986). Electron densities typically range from 2 - 5 cm^{-3}, HII masses are 3 - 8 x 10^6 $M_\odot$ and the emission measures are 10^3-10^4 cm^{-6}pc. The excitation parameter ranges from 350 to 700 which indicates the equivalent of 20 to 150 O 5 stars required to ionize the HII regions. The large number of radio detections enables us to construct the HII region luminosity function more reliably than in the past. Figure 1 shows both the radio and the H_α luminosity function for the HII

regions we detected. The two luminosity functions are fairly similar and agree quite well with the radio luminosity function Kaufman et al. (1987) find for the HII regions in M81. Israel (1980) found a much steeper luminosity function for M51. This is almost certainly a result of the large errors in his fluxes for the HII regions due to the low resolution and low sensitivity of the data he used.

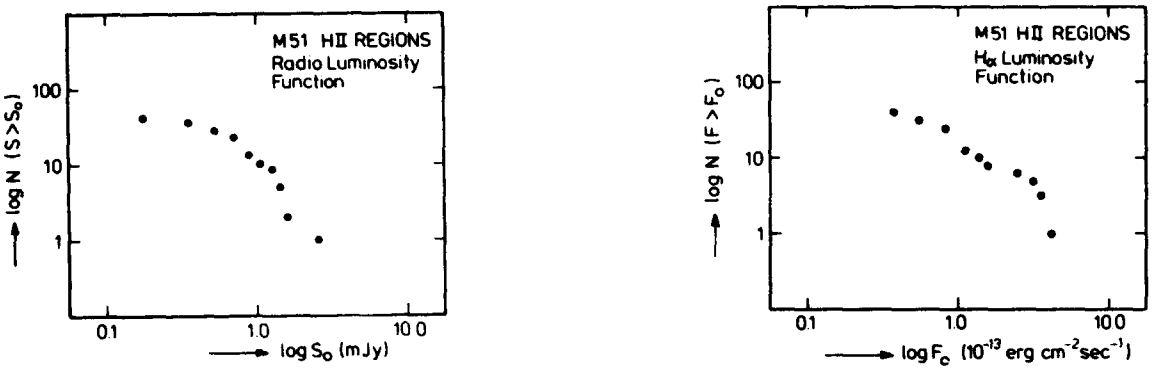

Figure 1. Radio luminosity function (left panel) and H_α luminosity function (right panel) of the HII regions in M51.

We can use the radio and H_α data to probe the extinction in the direction of the HII regions to give us some idea of the variation of extinction within the galaxy. The extinctions found vary from A_v=0.4 to 4 magnitudes with a median value of A_v=1.8. The extinction appears to be very patchy. An extreme example is 3 neighbouring HII regions in the eastern spiral arm where we find A_v=2.8, 0.7 and 2.5 respectively. Although the spread in extinction is quite large there appears to be a slight trend toward lower extinction at larger galactocentric radii. Figure 2 illustrates this trend. The inner two points and the outermost point are based on single measurements and therefore placed between parentheses.

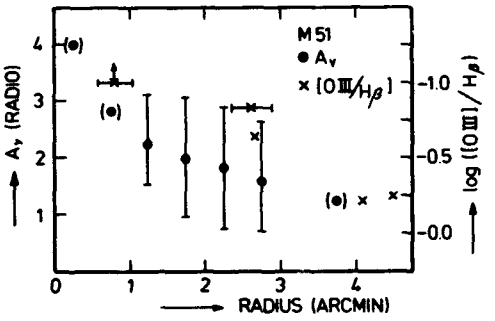

Figure 2. Radial dependence of A_v in M51. The excitation gradient in M51 is indicated by the crosses.

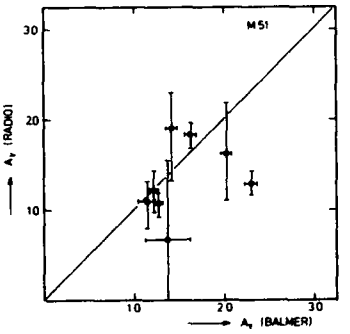

Figure 3. Comparison of A_v as determined from the Balmer decrement and A_v as derived from the radio - H_α flux ratios.

There nevertheless appears to be a slow decrease in average A_v when going from a radius of 1 to 3 arcminutes. This trend is in the same sense as the [OIII]/H_β excitation gradient found by Smith (1975) (plotted as crosses in Figure 2), and indicates that the extinction gradient is probably related to a metallicity gradient in M51.

It has been shown in the past that extinctions determined using the radio - H_α comparison method as described above are systematically larger by on average 1.2 magnitudes than extinctions derived form the Balmer decrement (Israel and Kennicutt 1980). Two ways to account for this are absorption internal to the HII regions or heavy clumping of the absorbing material inside or in front of the HII regions. Since we have Balmer decrements from the Mt. Lemmon spectrophotometry for 15 HII regions of which 8 overlap with the radio sample we can investigate this further in M51. Figure 3 shows the 8 regions with A_V determined from both the Balmer decrement and the radio - H_α comparison. For these regions one would conclude that both methods agree well and that no systematic difference exists. Recent work by Caplan and Deharveng (1986) in the Large Magellanic Cloud indicate that there a systematic difference exists of only 0.3 magnitudes, also much less than found in the past for galaxies in general. Requirements for internal and/or clumped extinction are therefore much milder. Caplan and Deharveng (1986) discuss various geometries for the dust distribution and suggest that the extinction is a combination of mostly general interstellar dust, partly clumped, and some scattering dust in and around the HII regions.

4. ACKNOWLEDGEMENTS AND NOTES

We gratefully acknowledge NATO travel grant 82-0592 and a NRAO/NSF travel grant. RCK anknowledges NSF grant AST 81-11711A01. Mt. Lemmon is supported by NSF grant AST 84-20374.

1. Visiting Astronomer, Kitt Peak National Observatory, National Optical Astronomical Observatories, which are operated by AURA, Inc., under contract with the National Science Foundation.

2. The National Radio Astronomy Observatory is operated by Associated Universities Inc., under contract with the National Science Foundation.

5. REFERENCES.

Caplan, J. and Deharveng, L.: 1986, Astron. Astrophys. **155**, 297.
Cox, P. and Mezger, P.G.: this volume.
Israel, F.P.:1980, Astron. Astrophys., **90**, 246.
Israel, F.P. and Kennicutt, R.C.Jr.: 1980, Astrophys. Lett. **21**, 9.
Kaufman, M., Bash, F.N., Kennicutt, R.C.Jr. and Hodge, P.W.; 1987, in preparation.
Klein, U. and Emerson, D.T.: 1981, Astron. Astrophys. **94**, 29.
McCall, M.L., Rybski, P.M. and Shields, G.A.: 1985, Astrophys. J. Suppl. **57**,1.
Persson, C.J., and Helou, G.: this volume.
Reynolds, S.P. and Chevalier, R.A.: 1984, Astrophys. J. **278**, 630
Schraml, J. and Mezger, P.G.: 1969, Astrophys. J. **136**, 26
Smith, H.E.: 1975, Astrophys. J. **199**, 591
Van der Hulst, J.M. and Kennicutt, R.C.Jr.: 1987, in preparation.
Van der Hulst, J.M., Crane, P.C. and Kennicutt, R.C.Jr.: 1987, in preparation.

POSTER PRESENTATIONS

THE MAGELLANIC CLOUDS AND IRREGULAR GALAXIES

IRAS AND GROUND-BASED OBSERVATIONS OF STAR FORMATION REGIONS IN THE MAGELLANIC CLOUDS

Jonathan H. Elias
Physics Dept., California Institute of Technology
320-47, Pasadena, CA 91125, and
Jay A. Frogel
Kitt Peak National Observatory
National Optical Astronomy Observatories
P. O. Box 26732, Tucson, AZ 85726

ABSTRACT

The Infrared Astronomical Satellite (IRAS) detected several hundred individual regions of star formation in the Large and Small Magellanic Clouds. Nearly two dozen of the brightest such sources have been searched for from the ground at 10 microns; most of these have been located and measured at wavelengths from 0.6 to 20 microns. Three principal results emerge from this study: First, the IRAS data show that star formation is considerably less active in the SMC than in the LMC, relative either to mass, luminosity, or H I content. The reduced activity in the SMC is consistent with the smaller amount of molecular material inferred from CO observations. Second, the sizes of the objects range from less than a few arcsec - objects which look like extremely compact HII regions, with little or no extended radio, optical, or infrared emission - to some tens of arcsec across - giant H II regions, of which the largest and brightest is 30 Doradus. Third, there are no obvious differences in the characteristics of the central portions of the LMC and SMC sources; all look like compact Galactic H II regions of similar luminosity.

IRAS DATA BASE

IRAS detected over 400 12 micron sources in the general direction of the LMC, and roughly 100 such sources in the direction of the SMC. Most of these have the characteristics of star formation regions: flux rising steeply from 12 to 100 microns. Specifically, star formation regions can be distinguished from evolved Magellanic Cloud or foreground objects on the basis of their 25 to 12 micron flux density ratios, which are typically greater than 4, and always greater than 3. Furthermore, only star formation regions have 60 to 25 micron flux density ratios significantly greater than 1. Many of the star formation regions are resolved by IRAS, which implies angular sizes of the order of an arcminute. Many, but not all, can be identified with catalogued visible or radio H II regions. In an effort to better understand these sources, we embarked on a ground-based observational program of LMC and SMC IRAS star formation regions detected by IRAS. The program had three aims: to identify and

Carol J. Lonsdale Persson (Editor)
Star Formation in Galaxies

locate precisely the stronger IRAS sources; to extend wavelength coverage to shorter wavelengths - into the visible in some cases - and to obtain information on sizes, by comparison of the small-beam ground-based data with the IRAS data (principally at 10 microns) and by mapping. The ultimate goal of the program is to make a comparison between the SMC, the LMC, and the Galaxy. A separate but related program is a study of evolved objects in the Magellanic Clouds detected by IRAS (Elias, Frogel and Schwering, 1986; Elias and Frogel, in preparation).

The principal result from the IRAS data themselves is that the SMC contains far fewer bright star formation regions that the LMC; the brightest 12 micron point sources in the SMC have flux densities of roughly 1 Jy, while the brightest LMC sources (excluding 30 Dor) are roughly 10 Jy, and there are more than 100 1 Jy sources. (In fact, confusion limits over much of the LMC are greater than 1 Jy.) Similar comparisons can be made at 25, 60, and 100 microns. This parallels the relative weakness of CO emission from the SMC, as compared with the LMC (e.g. Cohen, Montani, and Rubio 1984; Rubio, Montani, and Cohen 1984; Israel *et al.* 1986). Since the IRAS data measure most of the star formation luminosity in these galaxies, it appears that the simplest explanation of these observations is that star formation is currently much less active in the SMC than it is in the LMC. The much higher flux limits in the LMC, compared with the SMC, account for the fact that the total numbers of IRAS sources in the two Clouds do not show so great a disproportion.

Another interesting result is that in the SMC, the brightest sources are located in the eastern portions of the galaxy, with the brightest object (IRAS 01228-7324) located outside the main body. Since the distribution of H I in the SMC also shows more concentration to the east than do the stars, it may be that ongoing star formation is occurring in a different pattern than in the past.

IDENTIFICATION OF IRAS SOURCES

Two main considerations led us to search primarily at 10 microns rather than at some shorter wavelength. The first was a desire to be certain that the IRAS sources were being correctly identified, and the position of maximum flux located; this could in practice be done only at 10 microns. A second concern was confusion at shorter wavelengths; since some of the star formation sources proved to be extremely red, they could not be reliably located at wavelengths less than 10 microns.

Most of the searches were done on the CTIO 1.5m telescope, using the "D2" bolometer system and a beam size of 12.7 arcsec; follow-up observations were made on the CTIO 4m telescope with beams sizes of 4 to 7 arcsec. A total of 12 LMC sources and 6 SMC sources were searched. With the exception of 4 of the fainter SMC sources, 10 micron flux was measured from all objects and an approximate position of peak flux located. In many cases, the sources were extended, with peak fluxes several times less than the total IRAS flux, extrapolated to 10 microns. In two cases, however, the flux in a 5 arcsec beam was not significantly less than the IRAS flux, suggesting a very compact source. Both of the these objects (IRAS 01228-7324 [=N88a; cf. Testor and Pakull 1985] and 05216-6753) have visible counterparts with H II region spectra, but no strong radio emission. Energy distributions of these objects

are shown in Figure 1. One should note, though, that because of the distance of the Magellanic Clouds, these "compact" objects may easily be up to a parsec in extent. Nevertheless, it appears that there exist regions in both the SMC and LMC similar to compact H II regions in the Galaxy.

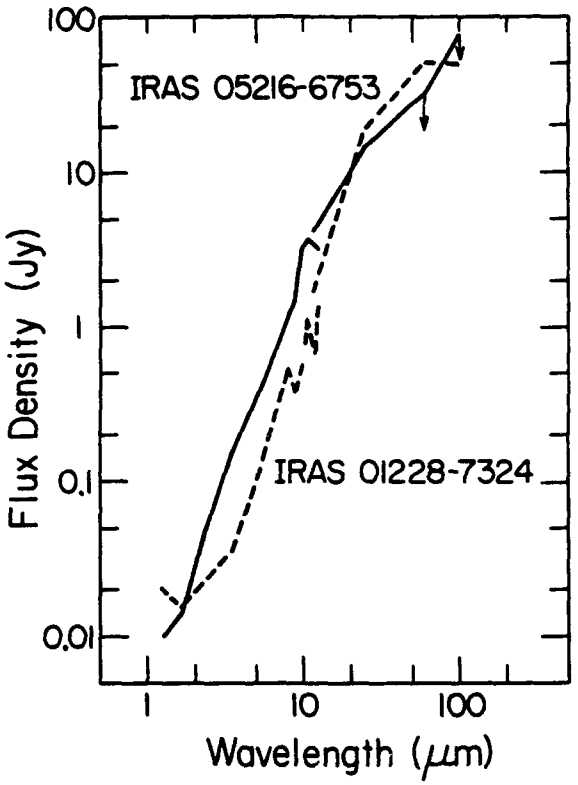

Figure 1. Flux Density Distributions of Two Compact Magellanic Cloud H II Regions. The data from 1 to 12 microns are ground-based measurements with a 4.5 arcsec beam, and the 12 to 100 micron data are IRAS Point Source Catalog data. The data for IRAS 05216-6753 are shown with a solid line, and the data for IRAS 01228-7324 are shown with a dashed line. The 60 and 100 micron upper limits for IRAS 05216-6753 are set by confusion.

Another noteworthy aspect of the IRAS "star formation" sources searched for is that all those that were identified proved to have one or more characteristics identifying them as including H II regions: that is, regions with stars producing substantial amounts of ionizing radiation. Most of the objects have obvious,compact, visible counterparts, whose spectra are characteristic of H II regions; the remainder are most likely H II regions obscured by intervening molecular cloud material, and show generally redder near-infrared energy distributions. Most sources, also, could be identified with thermal radio sources. What is not clear is that these H II regions are in fact the dominant source of far-infrared flux, since there are indications that the 10 micron sources are not precisely coincident with the visible compact H II regions. This apparent association of IRAS sources with H II regions suggests that luminous star formation regions containing only pre-main-sequence objects are relatively rare - possibly because pre-main-sequence lifetimes are so short compared with main-sequence lifetimes. A survey at high spatial resolution might not be so dominated by H II regions, since (as noted above) much of the flux from the IRAS sources come from regions several arcseconds or tens of arcseconds across.

ACKNOWLEDGMENTS

Portions of this work were supported under the IRAS extended mission program, and by the National Science Foundation. Cerro Tololo Interamerican Observatory is operated by AURA, Inc., under contract with the National Science Foundation.

REFERENCES

Cohen, R. S., Montani, J., and Rubio, M. 1984, in *IAU Symposium 108, Structure and Evolution of the Magellanic Clouds*, ed. S. van den Bergh and K. S. de Boer (Dordrecht: Reidel), 401.

Elias, J. H., Frogel, J. A., and Schwering, P. B. W. 1986, *Ap.J.*, **302**, 675.

Israel, F. P., deGraauw, Th, van de Stadt, H., and deVries, C. P. 1986, *Ap.J.*, **303**, 186.

Rubio, M., Cohen, R., and Montani, J., 1984, in *IAU Symposium 108, Structure and Evolution of the Magellanic Clouds*, ed. S. van den Bergh and K. S. de Boer (Dordrecht: Reidel), 399.

Testor G., and Pakull, M. 1985, *Astr.Ap.*, **145**, 170.

STAR FORMATION IN THE LARGE MAGELLANIC CLOUD

Terry Jay Jones, University of Minnesota
A.R. Hyland, Mt. Stromlo and Siding Springs Obs.
Paul M. Harvey, University of Texas

This conference has concerned itself largely with the properties of galaxies that are very much more luminous than the Milky Way and shine predominately in the far and mid-infrared. One might ask what role the Large Magellanic Cloud, a dwarf irregular, can play in this endeavor. There are two main reasons the LMC may prove helpful in our attempt to understand the infrared luminous galaxies. One, the LMC is only 55 kpc away, very nearby compared to the much rarer high luminosity systems. Second, the environment in the LMC is distinctly different than in the Milky Way, at least those parts of the Milky Way interior to the sun, where most of the studies of massive star formation have been concentrated. The environment in the LMC is not, of course, likely to be similar to that in the infrared luminous galaxies, but the fact that it is different than in the Milky Way does provide a test for the universality of our theories of star formation.

Despite the title of this conference, the star formation process in galaxies was *not* the central topic. Rather, the observed properties of infrared luminous galaxies have dominated the discussion. There is plenty of observational evidence for and theoretical understanding of how to push a large amount of gas around (say in an encounter) and we also know that massive star formation results in a large amount of mid and far-infrared luminosity. The connection between the two, however, has yet to be established. That is, the star formation process itself in these galaxies (if star formation is the correct explanation) is simply not well understood. The study of the infrared luminous galaxies as a class is still in its infancy, so this state of affairs is to be expected. As pointed out by Becklin (these proceedings) only by detailed groundbased studies will we be able to improve our understanding of these galaxies.

We sometimes forget that the LMC is an interacting system with a large amount of neutral hydrogen that has been pushed around by the galaxy's encounter with the Milky Way. Perhaps a good understanding of the star formation process in the LMC will provide guidance in our study of the infrared luminous galaxies. The two questions I wish to address are: 1) How is star formation in the LMC similar to our galaxy, and 2) How is it different?

SIMILARITIES

1) The field IMF in the LMC is similar to the Milky Way (Humphreys and McElroy 1984), although the very top of the IMF is probably hidden from optical view by plasma and dust.

2) At least two LMC HII regions contain point IR sources with no Lyman continuum or photospheric absorption features (i.e., protostars, Gatley et al. 1981, 1982).

3) There is some dust in the LMC star forming regions as evident in the FIR emission (IRAS, Werner et al. 1978, Jones et al. 1986), near IR reddening (Gatley et al. 1982, Jones et al.) and silicate absorption at 10μm (Epchtein et al. 1984).

4) A few H_2O and OH masers have been found in LMC HII regions.

DIFFERENCES

1) There is proportionately more HI mass in the LMC than in the Galaxy. There is plenty of raw material for making stars, the problem is how to go from HI to massive stars.

2) The CO luminosity of the LMC is very low compared to the FIR luminosity and Hα luminosity of the LMC, both of which are in the expected proportion to one another based on observations of a wide range of galaxy luminosities. This MAY indicate a significant lack of molecular hydrogen in the LMC, despite the vigorous star formation going on. Israel (private communication) has argued that there could still be large amounts of molecular hydrogen in the LMC without the corresponding amount of CO and dust expected for a galactic molecular cloud in the Milky Way.

3) There are no deeply imbedded, high surface brightness, very luminous FIR cores in any of the LMC HII regions. This is further indication that the giant molecular cloud phase may not be necessary (or considerably reduced in importance) in the LMC.

4) The six protostars found to date (Jones et al., Hyland et al. 1986), tend to lie behind what appear to be the intersections of giant mass loss bubbles. This suggests that direct compression of the HI gas results in the formation of stars in the LMC.

5) There appears to be an excess of very early O stars in at least two of the LMC giant HII regions (Jones et al.). This is best explained by a truncation of the IMF below about 30 $M_\odot$. The lack of any protostars below a few$\times 10^4$ $L_\odot$ supports this contention. Thus, the LMC may be producing more total luminosity and Lyman continuum flux per unit mass of available gas than is the case in galactic giant molecular clouds.

Without further study we can't be certain, but the LMC may be showing us that massive star formation does not require exorbitant amounts of mass in gas, molecular or otherwise, and that once the process gets going in the presence of a large amount of neutral hydrogen, mass loss bubbles and supernovae keep the process continuing at a high rate.

Epchtein, N., Braz, M.A., and Sevre, F., 1984, A. & A., 140, 67.
Gatley, I., Becklin, E.E., Hyland, A.R., and Jones, T.J., 1981, MNRAS, 197, 17P.
Gatley, I., Hyland, A.R., and Jones, T.J., 1982, MNRAS, 200, 521.
Humphreys, R.M., and McElroy, D.B., 1984, Ap.J., 284, 565.
Hyland, A.R., Straw, S., and Jones, T.J., 1986, in preparation.
Jones, T.J., Hyland, A.R., Straw, S., Harvey, P.M., Wilking, B., Joy, M., Gatley, I., and Thomas, J., 1986, MNRAS, 219, 603.
Werner, M.W., Becklin, E.E., Gatley, I., Ellis, M.J., Hyland, A.R., Robinson, G., and Thomas, J.A., 1978, MNRAS, 184, 365.

INFRARED EMISSION AND EXCITATION IN LMC HII REGIONS

V. Ungerer
Ruimteonderzoek Groningen, Postbus 800
9700 AV Groningen, The Netherlands

F. Viallefond
DEMIRM, Observatory of Meudon
F-92190 Meudon, France

ABSTRACT. The infrared excess (IRE) of LMC HII nebulae is found to correlate positively with the temperature of the ambient radiation field or with the He^+/H^+ abundance ratio. This result is discussed in terms of a selective absorption of the photons in the range 504-912Å relative to the He ionizing photons. This interpretation may explain the paradox of finding highly excited nebulae with only relatively moderate equivalent width of their Balmer lines.

1. INTRODUCTION

The excitation in HII nebulae is sensitive to the metallicity and to the energy distribution of the radiation field in the far UV ($\lambda < 912$Å). The metallicity as traced by the abundance of oxygen is known to be fairly uniform across irregular galaxies in contrast to the case of spiral galaxies. Thus restricting to a sample of HII nebulae in the Large Magellanic Cloud allows the study of the relative variations of the temperature of the radiation field from nebula to nebula, minimizing any possible influence of abundance variations.

2. OBSERVATIONAL DATA

The IRAS AO maps of the LMC (P. Schwering, in preparation) have been analyzed in order to separate the emission originating from sources and the underlying diffuse large scale component. About 200 sources have been identified with HII regions outside the 30 Doradus region (Ungerer et al., in preparation). In this catalogue we have selected the HII regions detected in the 5 GHz radio continuum survey (McGee et al. 1972) and having optical spectroscopic measurements (Pagel et al. 1978 and references herein). We rejected the source N44 whose radio continuum flux is contaminated by the SNR emission. For the HII nebula N91 an extended north-south plateau shows up at 5 GHz in contrast with the infrared and 408 MHz emission. We thus used the 408 MHz flux density. We have redetermined the electron temperature, the abundance of He^+ relative to H^+ and O/H in a homogeneous way using the atomic data compiled by Mendoza (1983). The ambient radiation field in an HII nebula can be conveniently characterized by an effective temperature T_{eff} which measures the relative number of the photons shortward of 504Å to those from 504 to 912Å. Stasinska (private communication) has demonstrated that this quantity is relevant for the excitation of nebulae, no matter if there is one or several exciting stars and which stellar atmosphere model is used. Thus we have defined T_{eff} for the ambient field inside a nebula as the T_{eff} of a stellar atmosphere model having the same ratio of He to H ionizing photons. Based on the NLTE stellar atmosphere models from Mihalas (1972) and the grid of photoionization models (Stasinska,

Carol J. Lonsdale Persson (Editor)
Star Formation in Galaxies

1982), we assign to each nebula of our sample a Teff, this temperature reflecting directly the temperature of the ionizing star cluster if there was no dust mixed with the ionized gas. This T_{eff} has been determined from the relative intensities of [OII]3727, [OIII]4363, [OIII]4959+5007 and Hβ4860, and we checked that it was also consistent with the He^+/H^+ ratios (Fig. 1).

The total infrared emission has been determined by multiplying the sum of the four in-band fluxes with a bolometric correction factor of 1.8: this factor is actually insensitive to the dust temperature over a large range of values from 30 to 200K (Boulanger, private communication) allowing us to get reliable bolometric infrared emission for HII regions. The IRE is deduced: by definition it has a value of 1 corresponding to all the bolometric infrared luminosity originating from Lyman α absorption (we further assumed that all Lyman continuum photons which ionize the gas degrade into Lyman α photons).

3. RESULTS AND DISCUSSION

In Fig. 2 the comparison between the IRE and T_{eff} is presented. The IRE tends to increase with the radiation field temperature. More striking is the very similar correlations in Fig. 1 and Fig. 2 which indeed implies that the IRE correlates positively with the He^+/H^+ ratio.

If the absorption of Lyc photons by dust were negligible, the IRE would measure directly the contribution of the nonionizing stars relative to the exciting stars (>15$M_\odot$), and we would predict a decrease of the IRE with increasing T_{eff} caused either by different Initial Mass Functions (IMF) or by age effects for the different nebulae. Thus we are forced to conclude that dust in HII nebulae plays a major role for the excitation, and the IRE may not directly reflect the properties of the young star cluster. One explanation for the increase of the IRE with T_{eff} is the existence of selective absorption of the 504-912Å photons relative to the He-ionizing photons. If the 504-912Å photons are preferentially absorbed, the effective temperature of the ambient radiation field will be increased relative to the effective temperature T^*_{eff} of the star cluster. This effect is illustrated in Fig. 3 where we have computed the IRE based on the NLTE Mihalas atmosphere models and ignoring absorption of all photons longward of 912Å. The solid lines are related to the fraction of 504-912Å photons absorbed by the dust, and the dashed lines show the evolution of T_{eff} as the amount of selective absorption of Lyc photons increases.

In Tab. 1 we show the effects on derived star cluster properties for two HII regions with extreme physical conditions when this selective absorption is considered. The IMF parameters (i.e., the slope x and the upper mass cut-off m_U), duration of star formation τ, star formation rate SFR, and the total luminosity are based on an evolutionary model for a star cluster which gives $T^*_{eff}(x,m_U,\tau)$ and $W^*_\beta(x,m_U,\tau)$.

TABLE 1

	N214C		N105	
$T_{eff}(10^4K)$	3.58	3.52	4.3	3.6
IRE (from phot.>912Å)	1.7	0.0	3.7	1.0
Equivalent width W_β(Å)	115	137	85	170
H phot. absorbed by dust	0%	16%	0%	50%
Ionization rate ($10^{50}s^{-1}$)	1.0	1.0	2.5	2.5
Stellar Lyc rate ($10^{50}s^{-1}$)	1.0	1.2	2.5	5.0
IMF upper cut-off $m_U(M_o)$	40	25	140	35
CSF duration (Myr)	4.5	0	>>10	0
SFR ($10^3M_oMyr^{-1}$)	3.9		- -	
Stellar mass formed (10^3M_o)	18	3.0	- -	70
Present day $L_{Tot}(10^6L_o)$	8.1	8.0	- -	25
L_{FIR}/L_{Tot}	0.09	0.10	- -	0.1

Table 1: Correction effects on star cluster properties for the far UV selective absorption: two columns are given for each nebula corresponding respectively to the extreme cases of no selective absorption and Zero Age Main Sequence star clusters. The last six lines of this table are based on a star cluster model very briefly presented in the paper of Viallefond and Thuan (1983) and revised by using the NLTE Mihalas stellar atmosphere model (Viallefond, unpublished). An IMF slope of 1.3 was assumed corresponding to the Salpeter IMF slope for the solar neighborhood: continuous star formation was also assumed. If these two assumptions are relaxed, the star cluster parameters will be different: however it will not affect the conclusions of this paper. An unreasonable solution is indicated by "- -".

Let A_β(radio)-A_β(Balmer) be the apparent "excess" of extinction derived by comparing the extinction A_β (radio), obtained from the relative strength of the Hβ Balmer line to the radio free-free emission, with A_β (Balmer), obtained from the relative strengths of the Hα and Hβ Balmer lines (Caplan and Deharveng, 1985). This "excess" extinction is believed to be at least partly caused by the presence of dust mixed with the ionized gas: it might then be related to the amount of selective extinction. The "excess" extinction for N214 is only 0.16 mag. compared to 0.54 mag. for N105, consistent with our analysis, which suggests very little selective absorption for N214 compared to N105. This trend is supported by the analysis of the full sample. The case of N105 illustrates how partial correction for selective absorption can solve the problem of finding many extragalactic HII regions with high effective temperatures (40,000 to 50,000K) and very low values of W_β (Stasinska and Viallefond, in preparation). On the contrary, less excited HII regions such as N214C can be interpreted without any selective absorption. Another important implication which emerges from this discussion is that a substantial fraction of the nonionizing radiation may escape the ionized regions contributing to the large scale interstellar radiation field in the LMC: only 10 to 20% of the total luminosity from the young star clusters would be degraded into far infrared emission locally inside the plasma, i.e., in the sites of star formation. Finally it is interesting to notice that the absorption efficiency of small graphite and silicate grains (with typical sizes of 30 to 100Å) does peak near 700 to 800Å (Draine and Lee, 1984). In this respect, the study of the excitation in HII regions may give

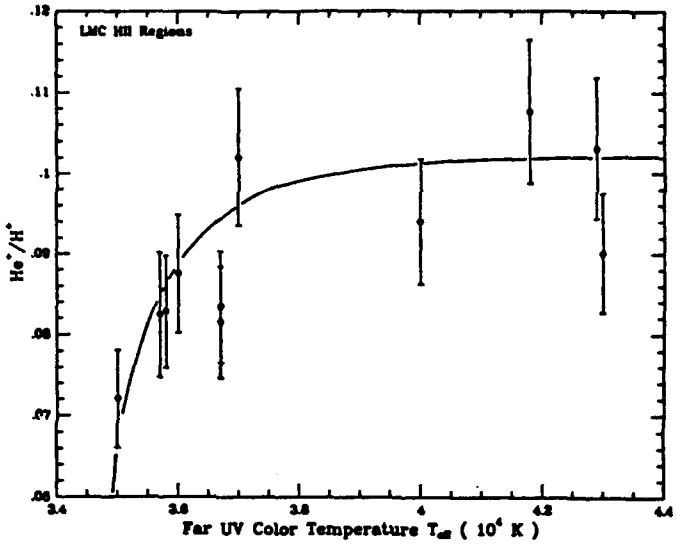

Fig. 1: Abundance of He^+ relative to H^+ as a function of the far UV color termperature of the radiation field in LMC HII regions. This temperature is expressed in terms of an effective temperature as defined in the text. The curve is based on photoionization models (Stasinska, 1982).

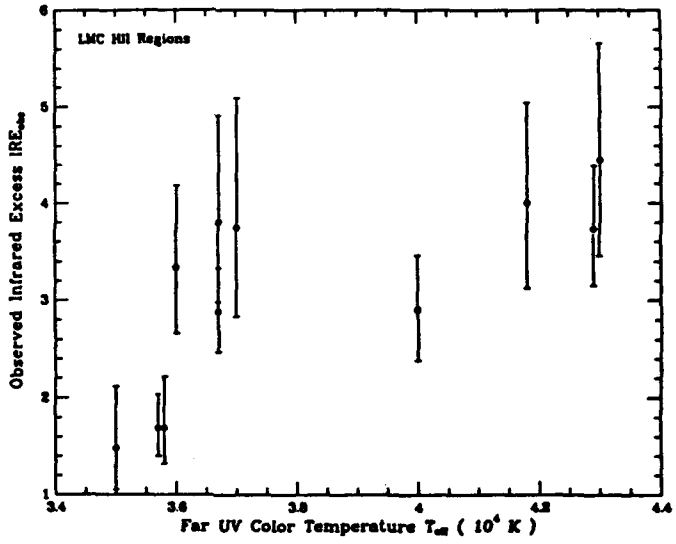

Fig. 2: Observed infrared excess as a function of the temperature of the radiation field in LMC HII regions: the sample of nebulae is common with Fig. 1. All Lyman continuum photons which are absorbed by the gas are supposed to be degraded into Lyman α photons. By definition the IRE is unity if all the bolometric infrared emission is entirely caused by dust absorption of these Lyman α photons.

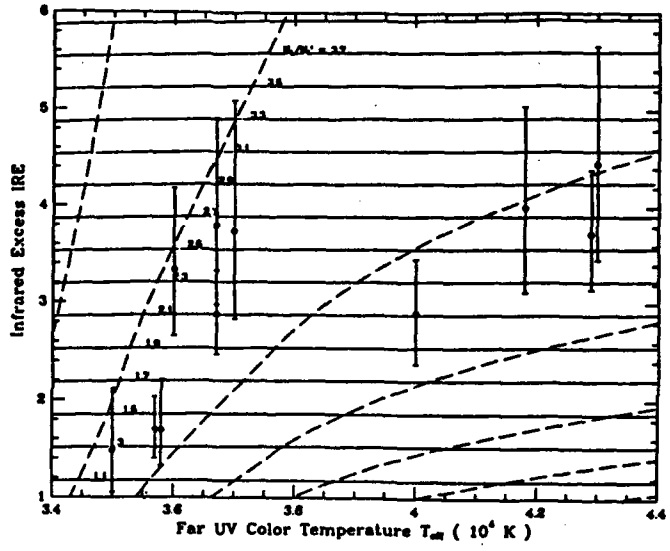

Fig. 3: Grid of a simple model for the IRE if it is caused exclusively by dust absorption of the 504-912Å photons. The dashed lines correspond to the evolution of the IRE and of the radiation field temperature relative to the amount of selective absorption. The continuous lines correspond to different values of the ratio N_L/N'_L of the 504-912Å photons, N_L being the number of these photons emitted by the star cluster and N'_L the number of these photons which effectively ionized the gas. For an IRE of unity the radiation field temperature is equivalent to the star cluster temperature T^*_{eff}.

valuable new constraints on the lower part of the size distribution of the grain population. The 2200Å bump of the extinction curve of the LMC is apparently weak (Prevot et al. 1984) compared to the bump for the standard galactic curve (Savage and Mathis, 1979): the properties of the grain population must be different in the LMC and in the solar neighborhood: selective absorption in the far UV would be primarily caused by the small silicate grains in the LMC if the small graphite grains are responsible of the 2200Å bump of the standard extinction curve.

4. CONCLUSIONS

From a sample of LMC HII regions for which all relevant information is available, a positive correlation is found between the IRE and the effective temperature of the ambient radiation field or the He^+/H^+ abundance ratio. We suggest the presence of selective absorption in the far UV to explain this observed phenomenon. While this result introduces a lot of complications for the interpretation of the IRAS measurements of the young star-forming regions in galaxies, it may solve the apparent paradox of finding many highly excited HII nebulae with only very moderate values for their equivalent width of Hβ.

REFERENCES:

Caplan, J., Deharveng, L. 1985, Ast. Ap. Suppl. 62, 63
Dottori, H.A., Bica, E.L.D. 1981, Astr.Ap.,102, 245
Draine, B.T., Lee, H.M. 1984, Ap.J.,285,89
McGee, R.X., Brooks, J.W., Batchelor, R.A. 1972, Australian J. Phys.25, 581
Mendoza, C. 1983, in Planetary Nebulae IAU Symp. 103, p143
Mihalas, D. 1972, Non LTE model atmospheres for B and O stars, NCAR-TN/str-76
Pagel, B.E.J., Edmunds, M.G., Fosbury, R.A.E., Webster, B.L. 1978, M.N.R.A.S., 184, 569
Prevot, M.L., Lequeux, J., Maurice, E., Prevot, L., Rocca-Volmerange, B. 1984, Astr.Ap., 134, 389
Savage, B.D., Mathis, J.S. 1979, Ann.Rev.Astr.Ap., 17, 73
Stasinska, G., 1982, Ast.Ap.Suppl., 48, 299
Viallefond, F., Thuan, T.X. 1983, Ap.J. 269, 444

IRAS Observations of Irregular Galaxies *

D. Hunter
Dept. of Terrestrial Magnetism, CIW
Washington, D.C.
W. Rice
Infrared Processing and Analysis Center, CIT
Pasadena, CA
J. Gallagher and F. Gillett
Kitt Peak National Observatory, NOAO
Tucson, AZ

Abstract

Normal irregular galaxies seem to be unusual in having vigorous star formation yet lacking the many dark nebulae typical of spirals. IRAS observations of a large sample of irregulars are used to explore the dust contents of these galaxies. Compared to normal spirals, the irregulars generally have higher L_{IR}/L_B ratios, warmer f(100)/f(60) dust color temperatures, and lower globally-averaged dust/gas ratios. The relationship between the infrared data and various global optical properties of the galaxies is discussed.

In spiral galaxies dust seems to be intimately connected with star-forming regions. In normal irregular galaxies, however, there appears to be a dearth of dark nebulae and reddenings are low relative to spirals. This is in spite of the vigorous, apparently normal, star formation often found in irregular galaxies. We present preliminary results from an investigation of the dust content of a large sample of irregulars based on IRAS (co-added survey) infrared observations at 12, 25, 60, and 100 μm (see also Hunter et al. 1986).

The irregular galaxies are divided into four groups: 1) "Dwarf"-- low surface brightness Magellanic-type irregulars, 2) "Giant"-- high surface brightness Magellanic-types, 3) "Amorphous"-- noted for their smoothness and lack of resolution into stars and clusters, and 4) "Distant"-- distant, clumpy irregulars. Systems in the first three grouups are primarily nearby, non-interacting galaxies. The distant irregulars, however, are at such large distances that morphological distinctions are more difficult and many of the systems have been found to be interacting. The galaxies in these four groups have many similar optical properties which are summarized and compared by Hunter and Gallagher (1986). For comparison with spiral galaxies we have chosen systems from Kennicutt's (1983) list of Hα observations and taken infrared data from the Cataloged Galaxies and Quasars Observed in the IRAS Survey.

In comparing the different groups of irregular galaxies, we find that the distant irregulars tend to have higher ratios of $L_{IR}/L_{H\alpha}$ and L_{IR}/L_B and somewhat warmer f(100)/f(60) dust color temperatures. However, differences in the infrared properties could be due to the fact that many of these systems are

* See erratum, page 257.

Carol J. Lonsdale Persson (Editor)
Star Formation in Galaxies

interacting. The dwarf irregulars tend to have somewhat lower L_{IR}/L_B ratios, but otherwise the groups have fairly similar infrared properties.

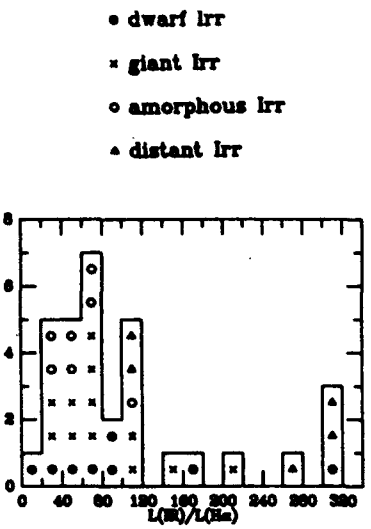

Fig. 1-Ratio of infrared to Hα luminosity of the irregulars.

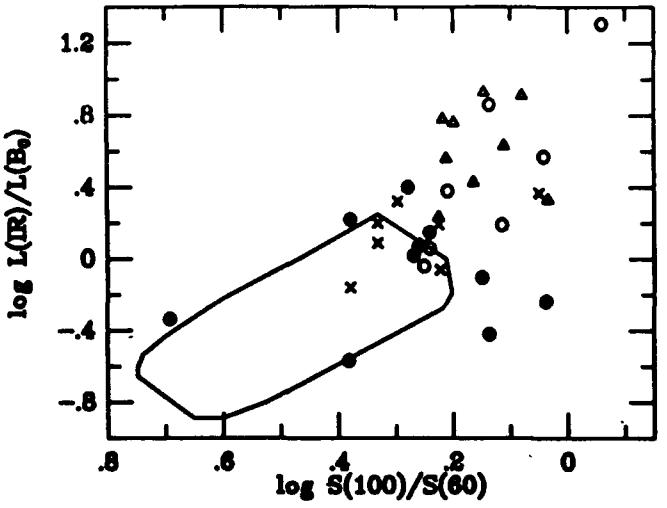

Fig. 2-The outlined region shows the area occupied by normal spiral galaxies (de Jong et al. 1984).

In a comparison of irregulars with spiral galaxies, on the other hand, there are some general differences. When irregulars are put on the plot of log L_{IR}/L_B vs. log f(100)/f(60) of de Jong et al. (1984), one finds that on average the irregulars have warmer f(100)/f(60) dust color temperatures and somewhat higher L_{IR}/L_B ratios than the spirals. However, in terms of the f(25)/f(12) dust color temperature, the spirals are on average somewhat warmer. Also, spirals generally have higher $L_{IR}/L_{H\alpha}$ ratios.

Because dust at a range of temperatures contributes to the global IRAS fluxes, the ratio f(100)/f(60) does not refer to a single temperature of the dust. However, the ratio does give an idea of the average temperature of the dust contributing to those passbands. One can then ask why this temperature-sensitive ratio varies and why irregulars are warmer in general than many spirals. One factor affecting the dust color temperature is the composition of the dust grains. One might expect that, if composition of the grains is the dominant factor affecting the overall temperature variation in the dust between galaxies, that the temperature ratio f(100)/f(60) would be correlated with the metallicity of the galaxies. Irregulars are in general more metal poor than spirals. However, a plot of f(100)/f(60) against the oxygen abundance shows that the average temperature of the dust does not depend on the metal abundance of the irregular in any simple fashion.

Dust masses have also been estimated using f(60) and a silicate model. It is important to note that the dust and gas masses are global measurements rather than measurements of individual star-forming regions; and the gas beyond the optical galaxy is not expected to contain dust that contributes to the IRAS infrared flux. Keeping this in mind, one finds that irregulars generally have lower global dust/gas ratios than spirals. Studies (Werner et al. 1978; Viallefond, Goss, and Allen 1982; Viallefond, Donas, and Goss 1983; references

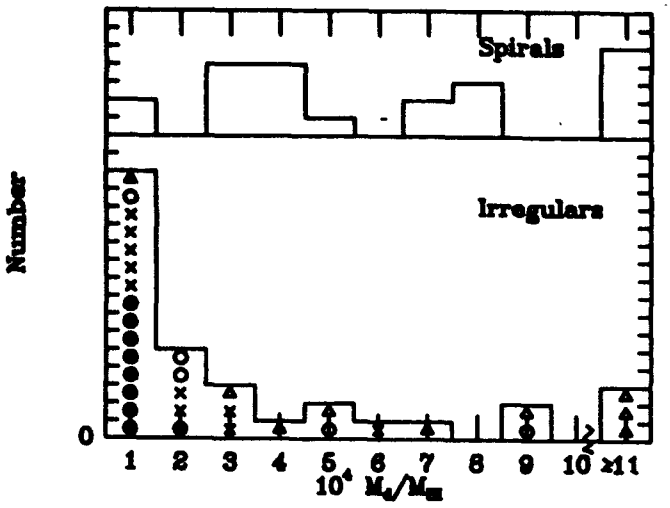

Fig. 3-The dust/hydrogen gas ratio. Dust masses have been estimated using f(60) and a silicate model. These are globally-averaged values.

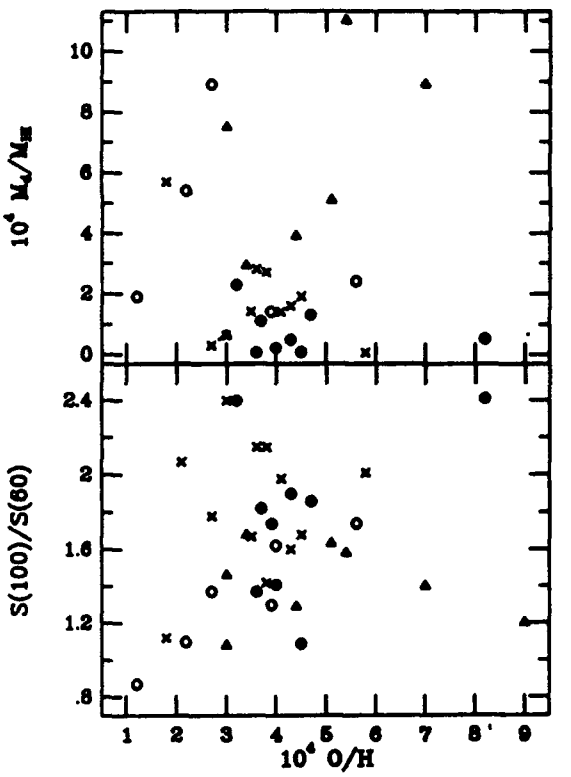

Fig. 4-Dust color temperatures and global dust/hydrogen gas ratios vs. oxygen abundance of the irregular.

in Koornneef 1984) of a few individual star-forming regions in the LMC suggest that local dust/gas ratios are also lower than regions in spirals although large optical depths due to dust can occur (Gatley et al. 1981). There is no correlation of the dust/gas ratio with the metallicity of the irregular.

Traditionally people have thought that radiation from stars in star-forming regions is responsible for heating the dust (cf. Wynn-Williams and Becklin 1974). But, with IRAS people have found that "cirrus" (Low et al. 1984) can also contribute to a galaxy's total far-IR flux. It is possible then that part of the far-IR flux of a galaxy comes from stars not connected with the current star-forming activity (see also Helou 1986; Persson and Helou, 1986). The problem in dealing with integrated fluxes of galaxies is in determining the relative contributions of these two sources.

The SFR (star formation rate)/area is a measure of the star-formation related radiation field in the galaxy, and the optical surface brightness is more a measure of the general stellar radiation field. There is no correlation between the temperature-indicators, f(25)/f(12) and f(100)/f(60), and the SFR/area although there may be a trend between f(100)/f(60) and surface brightness. There are also hints of trends of both SFR/area and surface brightness vs. L_{IR}/L_B, but they are far from clean. When spirals are added to these plots, they increase the scatter. Part of the difficulty in using these

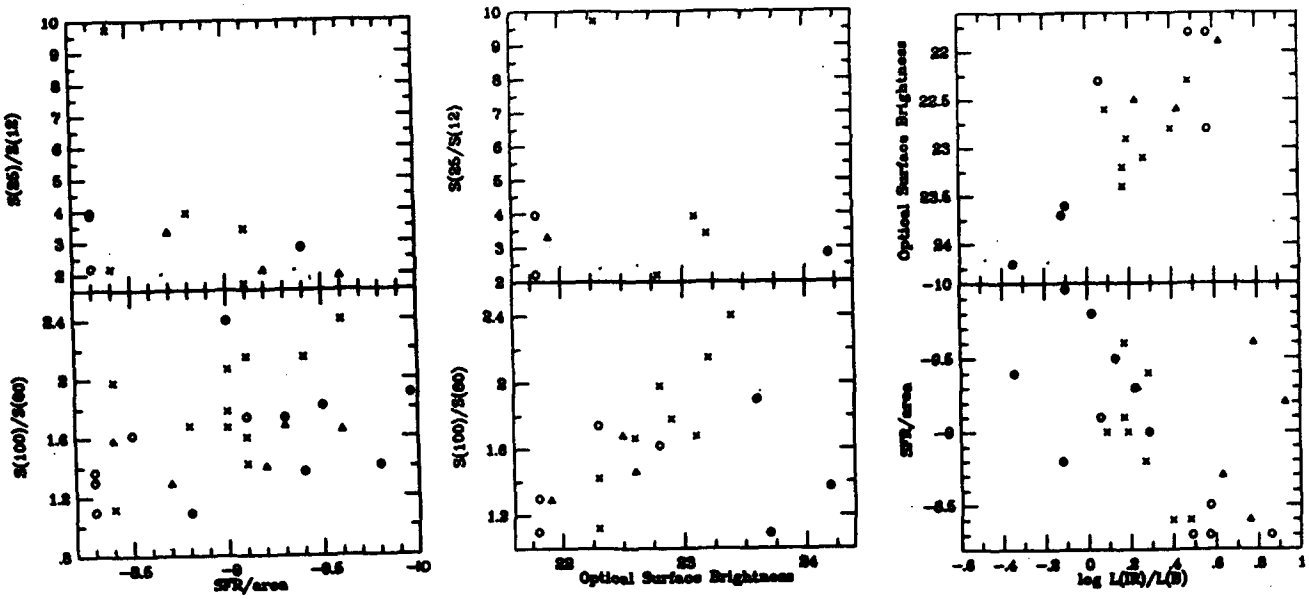

Figs. 5,6,7-The star formation rate per unit area and the blue optical surface brightness vs. infrared properties of the galaxies.

parameters is that we are looking at local processes through global averages. In addition the irregular galaxies have formed stars at approximately constant rates, so the stellar radiation field is not independent of the current SFR and it is difficult to separate the two. (See Gallagher and Hunter, these proceedings, for a discussion of star-formation rates and histories).

We are grateful to all of the people involved in the IRAS project for an excellent infrared data base and to the people at IPAC for their assistance in extracting the data. This work is supported in part by a grant from NASA as part of the IRAS General Investigator program.

References

de Jong, et al. 1984, Ap. J. (Lett), 278, L67.
Gatley, I., Becklin, E. E., Hyland, A. R., and Jones, T. J. 1981, M. N. R. A. S., 197, 17p.
Helou, G. 1986, Ap. J. (Lett), submitted.
Hunter, D. A. and Gallagher, J. S. 1986, Pub. A. S. P., 98, 5.
Hunter, D. A., Gillett, F. C., Gallagher, J. S., Rice, W. L., and Low, F. J. 1986, Ap. J., 303, 171.
Kennicutt, R. C. 1983, Ap. J., 272, 54.
Koornneef, J. 1984, in Structure and Evolution of the Magellanic Clouds, eds. S. van den Bergh and K. de Boer (Dordrecht: Reidel), p. 333.
Low, F. J., et al. 1984, Ap. J. (Lett), 278, L19.
Persson, C. J. and Helou, G. 1986, Ap. J., in press.
Viallefond, F., Donas, J., and Goss, W. M. 1983, Astr. Ap., 119, 185.
Viallefond, F., Goss, W. M., and Allen, R. J. 1982, Astr. Ap., 115, 373.
Werner, M. W., Becklin, E. E., Gatley, I., Ellis, M. J., Hyland, A. R., Robinson, G., and Thomas, J. A. 1978, M. N. R. A. S., 184, 365.
Wynn-Williams, C. G., and Becklin, E. E. 1974, Pub. A. S. P., 86, 5.

ERRATUM: IRAS OBSERVATIONS OF IRREGULAR GALAXIES

D. A. Hunter and J. S. Gallagher
Lowell Observatory, Flagstaff, Arizona 86001

In "IRAS Observations of Irregular Galaxies" by D. Hunter **et al.** and "Measuring Star Formation Rates in Blue Galaxies" by J. Gallagher and D. Hunter in these proceedings, as well as in D. Hunter **et al.** (1986, **Ap. J.**, 303, 171), galactic blue luminosities are based on standard optical definitions. Thus we derive L_B from the blue absolute magnitude M_B using

$$L_B = 7.81\times10^{34}\ \mathrm{dex}(-0.4\ M_B)\ \mathrm{erg\ s^{-1}}, \qquad (1)$$

or from the in band flux derived via

$$f_B = \int B_\lambda S_\lambda(B) d\lambda = \mathrm{dex}\ (-0.4B_T - 5.19)\ \mathrm{erg\ s^{-1}\ cm^{-2}}, \qquad (2)$$

where $S_\lambda(B)$ is the Johnson B response function.

However, the L_B system adopted by de Jong **et al.** (1984, **Ap. J. (Letters)**, 278, L67) for spiral galaxies was based on quasi-bolometric (rather than in band) fluxes given by

$$f^*_B = \lambda_B\ f_\lambda(4400\ \mathrm{A})\ \mathrm{erg\ s^{-1}\ cm^{-2}}. \qquad (3)$$

The L^*_B on this system are a factor of 4.5 times larger than the L_B from eq. (1). Thus our statements that the L(IR)/L(B) ratios for irregular galaxies are systematically higher than those of spirals are an incorrect result of comparing data on two different L_B systems. In fact, the irregulars cover roughly the same range in L(IR)/L(B) as the spirals when a consistent L_B system is used. A corrected L(IR)/L(B) versus S(100)/S(60) plot is given below.

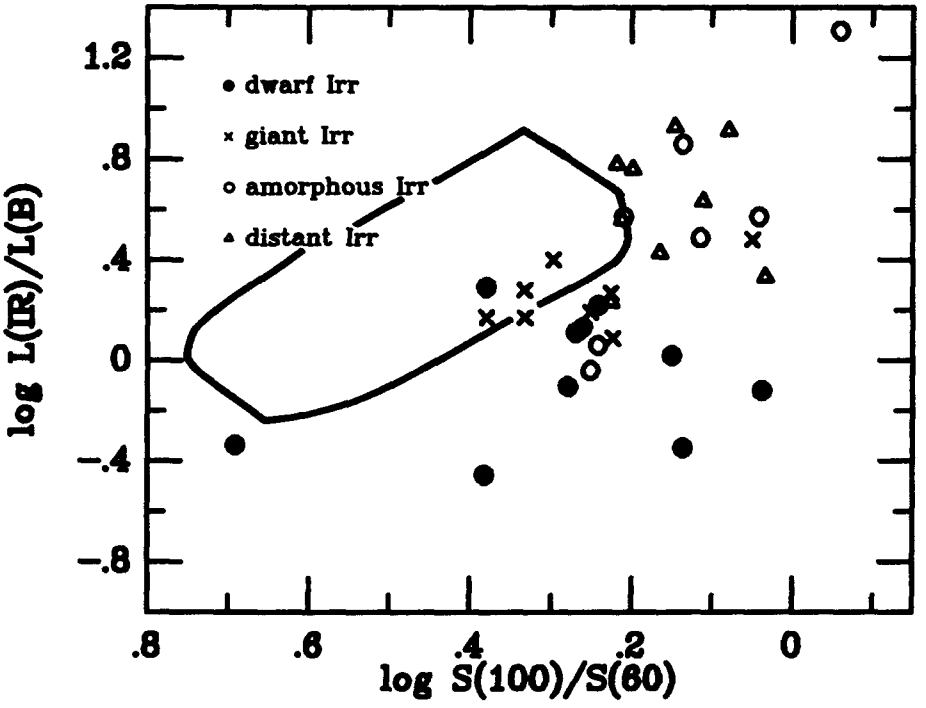

Carol J. Lonsdale Persson (Editor)
Star Formation in Galaxies

IUE OBSERVATIONS OF LUMINOUS BLUE STAR ASSOCIATIONS IN IRREGULAR GALAXIES

S.A. Lamb
NASA-Ames Research Center and
Departments of Physics and Astronomy
University of Illinois at Urbana-Champaign
Urbana, IL 61801

D.A. Hunter
Department of Terrestrial Magnetism
Carnegie Institution of Washington
5241 Broad Branch Road
Washington, D.C. 20015

J.S. Gallagher, III
National Optical Astronomy Observatories
Kitt Peak National Observatory
P.O. Box 26732
Tucson, AZ 85726-6732

ABSTRACT

Two regions of recent star formation in blue irregular galaxies have been observed with the IUE in the short wavelength, low dispersion mode. The spectra indicate that the massive star content is similar in these regions and is best fit by massive stars formed in a burst and now approximately 2.5-3.0 $x10^6$ years old.

I. INTRODUCTION

Irregular galaxies offer a special opportunity for the study of massive star formation. They are the bluest of galaxies, as a class, and this, together with the optical emission line spectra observed for some, indicates that massive stars are currently being formed. We are particularly interested in exploring the high mass end of the initial mass function (IMF) and the spatial patterns of star formation for the massive stars in these systems.

The irregular galaxies span a considerable range in morphology. The majority are blue, clumpy Im (Magellanic type) galaxies which have very obvious HII regions and associated OB associations. The remaining irregulars are classified IO or Irr II, some of which are red, like M82. An interesting subset of the latter class are the Amorphous galaxies, which were first classified by Sandage and Brucato (1979). These Amorphous systems can be as blue or bluer than Im galaxies, but OB associations are not resolved, despite the relative proximity of the galaxies to us. Extensive HII regions are observed in these systems, however.

Ultraviolet spectra provide a means of exploring the hot stellar content of these galaxies. In a previous paper (Lamb et al. 1985) we investigated the massive star content of two amorphous irregulars - NGC 1705 and NGC 1800, through IUE (International Ultraviolet Explorer Satellite) observations, together with optical spectra. In this paper we continue the exploration of irregular galaxies through IUE ultraviolet spectra of two systems which have very different star-forming patterns: 1) NGC 1140 is a typical Amorphous system. It contains a large blob of ionized gas at its center upon which the IUE aperture was placed. 2) NGC 4449 is a classical, well-resolved Magellanic Irr with many star-forming

Carol J. Lonsdale Persson (Editor)
Star Formation in Galaxies

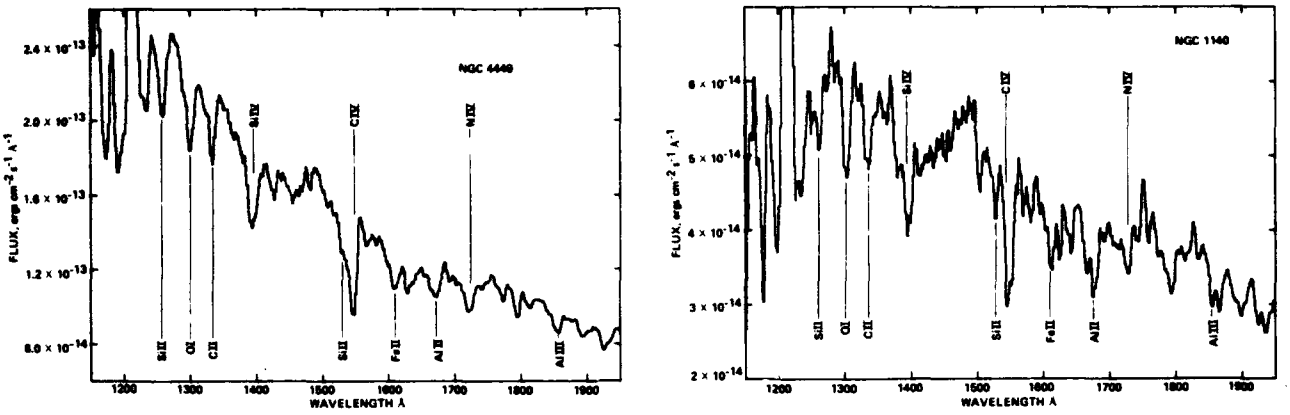

Fig. 1. IUE short wavelength spectra of NGC 4449 and NGC 1140. The two spectra of NGC 1140 were summed with a weighting proportional to their signal-to-noise. The spectrum for each galaxy was smoothed with a 5-point smoothing function. Lines of primarily stellar origin are identified above the spectra.

HII regions. One large HII region at the southwest end of the bar is in the form of an arc with a cluster of stars nestled in this arc (see Hunter and Gallagher 1985) and the IUE aperture was centered on this cluster.

Short-wavelength ultraviolet spectra were obtained at low-dispersion of these two galaxies in 1984 June and December. Setting with the 10"x20" aperture was by blind offset from bright stars. SWP 23262 of NGC 4449 is a 210 minute exposure, and SWP 24623 and SWP 24624 of NGC 1140 are respectively 180 and 185 minute exposures.

Data reductions and analysis were done using the Goddard Space Flight Center Regional Data Analaysis Facility. The results are shown in Figure 1, and we see that the primary stellar lines present are Si IV λ 1394, 1403Å, C IV λ 1548, 1551Å and N IV λ 1720Å. The other prominent absorption features arise from interstellar sources within the external galaxies, and there can be a substantial but unknown contribution from the interstellar medium of our own galaxy.

2. THE MASSIVE STAR CONTENT

2.1 Fitting the Ultraviolet Spectra

We have chosen to fit the overall shapes of the spectral lines, including P Cygni profiles when they are present, and to give considerable weight to the ratio of the equivalent widths of the SiIV and CIV features. This latter has been shown by Walborn and Panek (1984 a,b) to be a sensitive indicator of whether an individual massive star is on the main sequence or evolved into a supergiant. They have also demonstrated that the presence of SiIV P Cygni profiles is another indication of the luminosity class, as these develop only as the massive stars move off the main sequence.

We have constructed spectra of stellar clusters using the IUE stellar atlas (Wu et al. 1983) and relative contributions of stellar groups based on a standard

Salpeter (1955) initial mass function. The weighting factor is a product of the star's relative luminosity, number (the initial mass function), and lifetime (for evolved models). The relative luminosity at λ 1400-1500Å for a star was determined from the ratio of LF_λ (1400-1500Å) to T_e^4, where F_λ was determined from Kurucz (1979) model stellar atmospheres ($Z=Z_o$, log g=4). The relationship between T_e and stellar spectral class, mass and luminosity were obtained from Humphreys and McElroy (1984, see their Fig. 1), and the lifetimes of the stars were taken from models by Maeder (1981, 1983). Six stellar masses (9,15,30,60,85,120 M_o) were chosen as representative of six stellar groups, and average main sequence and evolved properties were determined for them. The atlas stellar spectra were extracted as point sources, corrected for reddening, and normalized to ~1500Å.

In constructing the synthesised models we attempted to span reasonable possibilities in the upper mass cut-off and the time dependence of the star formation rate. We did not vary the IMF, but our results are such that we can exclude a very flat IMF for the most massive stars. We constructed nine models. These included single burst models which varied from all main sequence stars to a burst now 3×10^6 years old, and extended production models in which the massive stars are either constantly formed or in which the production rate has fallen off by a factor of five from a maximum 3×10^6 years ago.

The best fit to our spectra of NGC 4449 and NGC 1140 were obtained from synthesised spectra of single bursts of star formation. The burst of age ~2.5 x 10^6 years with an upper mass cut off of ~120M_o gave an equally good fit to that of the single burst of age ~3.0 x 10^6 years with an upper mass cut off of ~70-80 M_o. The main features needed to provide a good fit are plenty of massive supergiants and a lack of the most massive ($M>50M_o$) main sequence O stars. The emission hump in the spectra of NGC 1140 at λ 1400-1500Å was not fit by our synthesised spectra. This feature is due to Wolf Rayet stars (see Nussbaumer et al. 1982). Their spectra are not available in the IUE spectral atlas and are not included in our models.

2.2 Comparison with Spectra of Giant HII Regions.

Rosa et al. (1984) have published IUE spectra for a variety of extragalactic HII regions and we compare these to our spectra. The majority of the systems have quite similar short-wavelength spectra. That is, most giant extragalactic HII regions have spectra which are similar to those of late C, early B stars. A few systems have weaker stellar absorption features without having the strong emission lines of very hot stars, and a few systems are of higher excitation, having NIV] λ 1483,1486 Å emission (These latter systems include NGC 1140.)

Thus we conclude, from the similarity between our results and those for extragalactic HII regions, that the OB star population is roughly comparable in these systems. Small variations observed in these spectra indicate varying mixes of evolved massive stars which can most easily be attributed to an age spread from ~2.5 x 10^6 years to 10^7 years amoung the various regions.

In addition to the stellar features the energy distributions, i.e. the slopes of the continua, are all roughly similar for the giant HII regions and for our Amorphous galaxies. The similarities in the ultraviolet continua are actually quite remarkable. One might expect that dust contents and distributions would vary greatly from region to region and with time within a given region. We

conclude that dust does not play a large role in those parts of the galaxies which we are observing in the ultraviolet.

3. THE SPATIAL PATTERNS OF STAR FORMATION.

Among the five Irr galaxies we have investigated (the two discussed here, plus NGC 1705, NGC 1800 and DDO 50, see Lamb et al. 1985 and Lamb et al. 1986), none are resolved into multiple clumps in the ultraviolet. Two of these galaxies, NGC 4449 and DDO 50, are Im type and do have a clumpy appearance in the optical. Although unresolved into clumps, the ultraviolet sources are broader than a point source. Our other three galaxies (NGC 1140, NGC 1705 and NGC 1800) are of the blue Amorphous type. These galaxies are more distant than our Im galaxies (ranging from 8.7 Mpc to 30 Mpc), and the large aperture of the IUE covers a considerable fraction of the galaxy. In each case the aperture was centered on the optical center of the object and in each case the ultraviolet source was point like.

It appears that the ultraviolet spectra are dominated by the youngest and brightest regions within the star forming complexes in all these galaxies. The Amorphous systems appear to experience massive star production in very condensed regions but the population of massive stars is not obviously different from that in normal Magellanic type irregulars.

We wish to acknowledge support from NASA grant NAG5-404 and to thank the staff at the IUE observatory and at the Data Reduction Facility at Goddard Space Flight Center for their help. S.A.L. was a NRC senior fellow during the completion of this work.

REFERENCES

Humphreys, R. M. and McElroy, D.B. (1984), *Ap.J.*, **284**, 565.
Hunter, D.A. and Gallagher, J.S. (1985) *Astron, J.*, **90**, 80.
Kurucz, R. (1979) *Ap.J. Suppl.*, **40**,1.
Lamb, S.A., Gallagher, J.S., Hjellming, M.S., and Hunter, D.A. (1985) *Ap.J.*, **291**, 63.
Lamb, S.A., Hunter, D.A. and Gallagher, J.S. (1986) in preparation.
Meader, A. (1981) *Astron. Astrophys.*, **102**, 401.
Maeder, A. (1983) *Astron. Astrophys.*, **120**, 113.
Nussbaumer, H., Schmutz, W., Smith, L.J., and Willis, A.J. (1982), *Astron. Astrophys. Suppl.*, **47**, 257.
Rosa, M., Joubert, M., and Benvenuti, P. (1984) *Astron. Astrophys. Suppl.* **57**, 361.
Salpeter, E.E. (1955), *Ap.J.*, **121**, 161.
Sandage, A. and Brucato, R. (1979) *Astron. J.*, **84**, 472.
Walborn, N.R. and Panek, R.J. (1984a), *Ap.J.*, **280**, L27.
Walborn, N.R. and Panek, R.J. (1984b) *Ap.J.*, **286**, 718.
Wu, C.-C. et al. (1983), 'IUE Ultraviolet Spectral Atlas', *IUE NASA Newsletter No. 22.*

Neutral Hydrogen and Star Formation in Irregular Galaxies

Evan D. Skillman
Netherlands Foundation for Radio Astronomy, Radiosterrenwacht Dwingeloo
Postbus 2, 7990 AA Dwingeloo, The Netherlands

Abstract

VLA and WSRT H I synthesis observations of seven irregular galaxies are presented. The total H I images of four Local Group dwarf irregular galaxies and three larger more distant irregular galaxies are constructed at the identical resolution of 500 pc (FWHM). When compared to H II region distributions derived from Hα images, all galaxies studied show an excellent correlation between the H I surface density and the presence of H II regions. This correlation is most easily interpreted in terms of a requisite threshold H I surface density for massive star formation. This threshold is 1 x 10^{21} H I atoms/cm^2 for a resolution of 500 pc. Giant extragalactic H II regions - star formation events of the magnitude of 30 Doradus or more luminous - are only found near H I surface densities of a factor of three to five times this threshold level. The observed threshold implies a Jeans length of 150 pc, which is the same as the size scale at which the structure in the H I complexes correlates well with the H II region distribution. This, combined with the fact that in none of the galaxies observed is there H I above the threshold level without concomitant H II regions, implies an exclusively gravitational origin for the star formation events. That is, there is no need to involve a "trigger" as in the SSPSF theory (Seiden 1983) or feedback as in Dopita (1985).

Introduction

Since neutral hydrogen represents the ultimate raw material for star formation, it is natural to study the relationship of the spatial distribution of the source to that of the product. It is possible to do this in external galaxies by measuring the H I 21cm emission and comparing it to a tracer of massive star formation - the Balmer emission. Irregular galaxies provide a logical starting point for this type of investigation, since the interpretation is not complicated by the presence of spiral density waves or abundance gradients.

Method

H I synthesis maps of seven irregular galaxies were produced at a resolution of 500 pc (FWHM). In order for valid inter-galaxy comparisons to be made, it is important that all galaxies be analyzed at the same resolution because surface density varies as a function of resolution. The inclinations of the galaxies were determined by studying the total H I distributions and velocity fields and modelling the H I distribution as a thin disk in dominantly circular motion. Images representing the H I

surface density were then produced by scaling the column density maps by cos(inclination). H II region catalogues derived from Hα photography were then taken from the literature, and the H II region distributions were compared with the neutral hydrogen surface density images.

Results

The observed galaxies divide into two groups. Four of the galaxies are Local Group dwarf irregular galaxies with $M_B > -16$ (NGC 6822, IC 1613, DDO 75 - Sextans A, DDO 216 - Pegasus). The other three irregulars are more luminous with $M_B < -18$ (NGC 4214, NGC 3239, NGC 4449). In addition to luminosity, the two groups are distinguished by one other feature, velocity field. The velocity fields of the dwarf galaxies were very regular, showing predominantly solid body rotation. The velocity fields of the more luminous irregulars range from very disturbed (NGC 4449) to moderately disturbed (NGC 3239) to warped (NGC 4214). (Images of the H I surface densities with superposed H II region distributions were presented in the poster, but, since there is insufficient space to display those images here, a written description follows.)

The H I distributions in the Local Group galaxies are highly clumped. Both holes (minima reching the zero level) and dense clouds (surface densities > 2 x 10^{21} atoms/cm^2) are observed. In NGC 6822 and IC 1613, there is an obvious correlation between the presence of H II regions and high H I surface density. This is especially striking in IC 1613 where there is one strong H I concentration with an H I surface density higher by a factor of two than anywhere else in the galaxy. Clustered around this H I concentration are 15 of the 18 catalogued H II regions. Most of the H II regions in NGC 6822 and IC 1613 are associated with regions of H I surface density in excess of 1 x 10^{21} atoms/cm^2. The H I distribution in Sextans A is dominated by two large H I concentrations exceeding the 10^{21} atoms/cm^2 level. Although there is no available deep Hα photography of Sextans A, Hodge (1974) has reported detections of 3 H II regions, and optical images of the galaxy show three obvious stellar associations. The reported H II regions and associations are coicident with the H I maxima. There are no immediately obvious H II regions in the Pegasus dwarf galaxy, although there exists no published Hα photography. The H I surface density in Pegasus is everywhere low (< 0.5 x 10^{21} atoms/cm^2 throughout the disk).

From the four Local Group irregulars two trends emerge. The first is a very good correlation between the presence of H II regions and peaks in the H I surface density distribution. The second is a threshold effect. No H II regions are found in regions with peak H I surface densities less than about 1 x 10^{21} atoms/cm^2.

The three high luminosity irregular galaxies all show strikingly large numbers of H II regions. Here the correlation between H I surface density and the presence of H II regions is again very good. These galaxies also support the idea of an H I surface density threshold. In NGC 4214, H I is detected across a disk of 10' extent, but the H II regions are confined to a narrow strip through the galaxy where the H I surface density exceeds 1 x 10^{21} atoms/cm^2. All three galaxies have regions of H I surface density in excess of 3 x 10^{21} atoms/cm^2. Coincident with these regions are giant H II

regions (NGC 4214 and NGC 3239) or a large complex of H II regions (NGC 4449).

Discussion

The proposed threshold surface density value of 1×10^{21} atoms/cm^2 can be converted to a characteristic central volume density by assuming an exponential distribution in z. An assumed scale height of 200 pc yields a central volume density of 0.8 atoms/cm^3. Next, this characteristic volume density can be used to estimate a Jeans length (assuming the effects of magnetic fields and the galactic gravitational potential are not important). From:

$$\lambda_J = 6 \times 10^7 \left(T/\mu\rho_o\right)^{.5} \text{ cm}$$

and values of T = 100 K and μ = 1, a Jeans length of ≈ 150 pc is derived. This is comparable to the resolution in the highest resolution maps available for NGC 6822. At this resolution the correspondence of the presence of H II regions to H I surface density peaks is even more striking than in the lower resolution images discussed earlier. This suggests that gravitational instability is the cause of the massive star formation in these irregular galaxies.

The observed threshold may have an additional significance. It is most likely that the formation of molecular cloud cores is an intermediate step between the formation of the large neutral hydrogen clouds and the onset of star formation. It may be that the observed threshold represents a requisite column density of dust for shielding the molecular cores from the ambient uv radiation field of the galaxy. If this is the case, one would predict a lower threshold value in regions of higher abundance where the dust to gas ratio is higher. Finding appropriate galaxies to test this hypothesis may prove difficult as dwarf irregular galaxies span a range of only about one decade in heavy element abundance. This picture also suggests an upper limit to the surface density of H I, as any atomic gas in excess of the requisite shielding thickness is quickly converted to molecular gas. Note that in the larger irregular galaxies the disturbed kinematics imply that large scale dynamical processes are most likely responsible for piling up large column densities of H I, and therefore fueling the observed prodigious star formation.

Having assembled a collection of H I distributions of irregular galaxies, it is of interest to assess them in light of current theories of star formation. The stochastic self propagating star formation (SSPSF) theory of Gerola and Seiden (1978) has been attributed with the ability to produce an accurate picture of the global properties of dwarf galaxies (Gerola, Seiden, and Schulman 1980). This theory has been laid on a more credible structure by the inclusion of a gaseous component in the models. However, this inclusion dramatically altered the interpretation of the modeling experiments. It was shown that it is more appropriate to think in terms of stochastic self propagating cloud formation (Seiden 1983). The key words then become self-propagating. Is it reasonable to link the cloud building stage causally to the star formation events in dwarf galaxies? Whereas the compression of small clouds by supernova blast waves and stellar winds must certainly be occuring, can the construction of the large (200 pc

to 1000 pc) H I clouds typically seen in irregulars be attributed to the older star formation events? Or alternatively, are the majority of the star formation events in the models of dwarf galaxies initiated stochatically in pre-existing neutral clouds, while the self-propagating mechanism merely insures that the "burst" has access to all of the available fuel. If the latter explanation holds true, then it may be that the self-propagating aspect of the theory is without a physical basis. It could be that the gravitationally bound aspect of the H I complexes insures that most of the constituent gas is available for star formation.

Finally a comment on the recent paper of Dopita (1985) regarding a law of star formation in disk galaxies. If the concept of an H I surface density threshold is valid for not only irregular galaxies, but all disk galaxies, then a tight relationship between the star formation rate and the product of the total mass and H I surface density (his figure 1) is difficult to understand. A requisite H I surface density for star formation implies that the star formation rate will be determined by the amount of gas above the threshold value, and not the total H I content of a galaxy (the H I surface density used by Dopita is really the total H I divided by the optical area of the galaxy). Dopita notes that the scatter in the diagram may be attributable to several factors. Perhaps the clumpiness of the gas distribution is an additional factor causing the scatter. A threshold effect would predict a good correlation between the star formation rate and the total neutral hydrogen above the cutoff.

Acknowledgements

All of the galaxies, except the Pegasus dwarf, have been observed with the Very Large Array of the National Radio Astronomy Observatory which is operated by the Associated Universities Inc., under contract with the National Science Foundation. Pegasus was observed with the Westerbork Synthesis Radio Telescope of the Netherlands Foundation for Radio Astronomy which is financially supported by the Netherlands Organization for the Advancement of Pure Research (ZWO). This paper discusses data taken from a number of research projects concentrating on the distribution of H I in irregular galaxies done in collaboration with J. Albinson, G. Bothun, P. Hodge, R. Sancisi, R. Terlevich, R. Warmels, and H. van Woerden. Discussions with F. Israel and B. Elmegreen are gratefully acknowledged.

References

Dopita, M. A. 1985, Ap. J., 295, L5
Gerola, H., and Seiden, P. E. 1978, Ap. J., 223, 129
Gerola, H., Seiden, P. E., and Schulman, L. S. 1980, Ap. J., 242, 517
Hodge, P. W. 1974, Ap. J. Suppl., 27, 113
Seiden, P. E. 1983, Ap. J., 266, 555

CARBON MONOXIDE EMISSION FROM SMALL GALAXIES

Harley A. Thronson, Jr.
Wyoming Infrared Observatory

John Bally
AT&T Bell Laboratories

ABSTRACT. We have searched for J = 1 → 0 CO emission from 22 galaxies, detecting half, as part of a survey to study star formation in small- to medium-size galaxies. Although we find substantial variation in the star formation efficiencies of the sample galaxies, there is no apparent systematic trend with galaxy size.

1. INTRODUCTION AND BACKGROUND

A correlation between far-infrared and CO emission from galaxies was discovered by Telesco and Harper (1980) and discussed recently and more fully by Rickard and Harvey (1984) and Young *et al.* (1986). Dust reprocesses starlight into far-infrared radiation. Massive young stars, which are signposts of ongoing star formation are usually surrounded by warm (30 to 60 K) dust which re-emits much of the radiation into the 60 and 100 μm bands surveyed by the IRAS satellite. Thus, the far-infrared flux should be a tracer of the global rate of star formation in a galaxy. To first order, the CO emission is a tracer of the principle reservoir of mass from which the stars are produced. Given that the far-infrared emission arises from dust heated by young stars, L_{IR}/L_{CO} is proportional to the star formation efficiency, defined as the rate of star formation per unit H_2 mass.

We are conducting a survey of the J = 1 → 0 $^{12}C^{16}O$ emission from a sample of galaxies of modest size in order to estimate the amount of material available to form stars. Dwarfs are the most abundant type of galaxy in the universe. They appear to be structurally simple and without the complex gas dynamics, such as spiral shocks, which can complicate the interpretation of processes in large star-forming galaxies. On the average, dwarf galaxies are closer than the giants and may therefore be studied in greater detail.

2. OBSERVATIONS

We have used the AT&T Bell Laboratories 7-m telescope and the National Radio Astronomy Observatory 12-m telescope to search for CO emission from 22 galaxies to date. Our sample is deliberately heterogeneous, reflecting the variety of small galaxies. Our selection criteria are: (1) modest angular size so that the observed CO line strength is a good measure of the total line flux; (2) detection in the IRAS Point Source Catalog, so that the total far-infrared luminosity is known; (3) far-infrared luminosities less than about $10^{10}L_{\odot}$. Our results are presented in Table 1 and Figures 1 and 2.

3. ANALYSIS

In Figure 1 we present a plot of far-infrared luminosity versus CO luminosity, along with three lines showing the L_{CO}/L_{IR} relations found by Young *et al.* to fit data for giant galaxies of different average dust temperature. These relations

Carol J. Lonsdale Persson (Editor)
Star Formation in Galaxies

TABLE 1

J = 1 → 0 CO Observations of Galaxies of Modest Size

Name		Type	Distance (Mpc)	$\int T_R^* dv \equiv S$ (K^R - km/s)	$4\pi D^2 S$ (K-km/s-Mpc^2)	V_{LSR} (km/s)	L_{FIR} ($L_\odot$)	M_{HI} ($M_\odot$)	M_{H_2} ($M_\odot$)	$2.58F_{60} + F_{100}$ (Jy)
CPG 330	[B]	SBcII	3.1	-0.01 ± 0.15	-0.1 ± 1.8 x 10^1	359	7.2 x 10^7	8.8 x 10^7	<3.0 x 10^6	12.5
Haro 2	[N]	Im(p)	20.5	0.94 ± 0.22	5.0 ± 1.2 x 10^3	1435:	4.4 x 10^9	4.6 x 10^8	1.7 x 10^8	17
Haro 3	[N]	Sm?	13.9	0.96 ± 0.28	2.3 ± 0.7 x 10^3	930:	2 x 10^9	5.4 x 10^8	7.8 x 10^7	17
DDO 154	[B]	-	10	0.19 ± 0.10	2.4 ± 1.2 x 10^2	375	<1.5 x 10^8	2.5 x 10^9	<4.1 x 10^7	< 2.5
IC 10	[B]	I	3.0	1.01 ± 0.10	1.1 ± 0.1 x 10^2	-330	1.9 x 10^8	--	9.4 x 10^6	35
Mk 86	[B]	ScIIIp	7.0	0.05 ± 0.27	0.3 ± 1.7 x 10^2	449	4.2 x 10^8	2.4 x 10^8	<3.2 x 10^7	14
Mk 527	[B]	-	47.4	0.40 ± 0.12	1.1 ± 0.3 x 10^4	3554	2.5 x 10^{10}	8.4 x 10^8	9.4 x 10^8	18.5
NGC 185	[B]	dE3p	0.7	0.35 ± 0.15	2.2 ± 0.9	195	9.5 x 10^5	4 x 10^5:	1.9 x 10^5	3.2
NGC 205	[B]	SO/E5p	0.7	-0.02 ± 0.25	-0.1 ± 1.5	230	1.4 x 10^6	4 x 10^5:	<2.5 x 10^5	4.8
NGC 1569	[B]	SmIV	3.1	-0.24 ± 0.19	-2.8 ± 2.3 x 10^1	-83	9.8 x 10^8	1.7 x 10^8	<1.5 x 10^6	170
NGC 2814	[B]	-	23.2	-0.03 ± 0.17	-0.2 ± 1.1 x 10^3	1740	1.9 x 10^9	--	<1.7 x 10^8	5.9
NGC 2976	[B]	SdIII	3.1	1.2 ± 0.2	1.5 ± 0.2 x 10^2	13	3.2 x 10^8	--	1.3 x 10^7	56
NGC 3274	[B]	SIV	6.4	0.1 ± 0.14	5.0 ± 7.2 x 10^1	540	1.3 x 10^8	7 x 10^8	<1.7 x 10^7	5.3
NGC 3738	[B]	SdIII	5.4	-0.02 ± 0.06	-0.6 ± 2.1 x 10^2	225:	1.3 x 10^8	3 x 10^8	<3.1 x 10^6	7.4
NGC 4449	[N]	SmIV	5.4	>2.5 ± 0.5	>9.2 ± 1.8 x 10^2	244	3.2 x 10^9	2 x 10^9	>3.2 x 10^7	180
NGC 4605	[B]	ScIII	4:	1.3 ± 0.3	2.6 ± 0.6 x 10^2	141	5.8 x 10^8	--	2.2 x 10^7	60
NGC 5506	[B]	-	24.2	0.31 ± 0.28	2.3 ± 2.1 x 10^3	1815	1.1 x 10^{10}	1.2 x 10^9	<5.5 x 10^8	31
NGC 7800	[N]	Im	25.8	-0.38 ± 0.37	-3.2 ± 3.0 x 10^3	1950	2.4 x 10^9	3.4 x 10^8	<9.5 x 10^7	6.0
I Zw 33	[B]	Smp?	34.6	1.55 ± 0.19	2.3 ± 0.3 x 10^4	2502	6.0 x 10^{10}	1.7 x 10^9	2.0 x 10^9	84
I Zw 89	[B]	Sb	31.1	1.96 ± 0.26	2.4 ± 0.3 x 10^4	2329	8.4 x 10^9	2.4 x 10^9	2.0 x 10^9	14
II Zw 40	[N]	-	10.1	0.62 ± 0.29	7.9 ± 3.7 x 10^2	800	1.4 x 10^9	4.5 x 10^8	2.7 x 10^7	23
III Zw 102	[B]	Sp	21.7	3.0 ± 0.24	1.8 ± 0.1 x 10^4	1626	1.2 x 10^{10}	2.3 x 10^9	1.5 x 10^9	42

Telescope: [B] Bell Telephone Laboratory 7m; [N] NRAO 12m

1. M_{H_2} was calculated from $M_{H_2}(M_\odot) = 1.07 \times 10^6 D^2(\text{Mpc}) \int T_R^* dv$ [Bell 7m] and $M_{H_2}(M_\odot) = 4.25 \times 10^5 D^2(\text{Mpc}) / \int T_R^* dv$ [NRAO 12m]. Observations with the signal-to-noise ratio greater than 2 were treated as detections. Upper limits for M_{H_2} are 2σ.
2. $[2.58F_{60} + F_{100}] \propto L_{IR}(L_\odot)/6 \times 10^5 D^2(\text{Mpc})$ and is proportional to the integrated far-infrared flux.

extend reasonably well to include the objects of low luminosity in our sample. The center line in the figure corresponds to $L_{IR}/L_{CO} = 25$, which is about the average value for our sample.

Luminosity-luminosity plots such as Figure 1 demonstrate that both CO and infrared emission scale with the size of the galaxy: larger galaxies, on average, have more CO and infrared emission than do smaller galaxies. Although the range of far-infrared luminosities (presumably roughly proportional to mass of young stars) reported in the literature vary over almost 7 orders of magnitude, the range of star formation efficiencies is less than 2 orders of magnitude. Moreover, some of the more efficient star-forming galaxies are dwarfs. We suggest that concentration upon infrared-luminous galaxies in a study of star formation may be misplaced effort.

Such plots alone, however, cannot be used to infer a good correlation between CO and infrared emission since, in converting the observed fluxes to luminosities, both species are multiplied by a common factor: the distance (D) squared. If the range in the quantity D^2 is comparable to or greater than the range of fluxes, then even an uncorrelated set of CO and infrared fluxes will produce a correlation in a plot of luminosity! The situation is made worse by the presence of errors

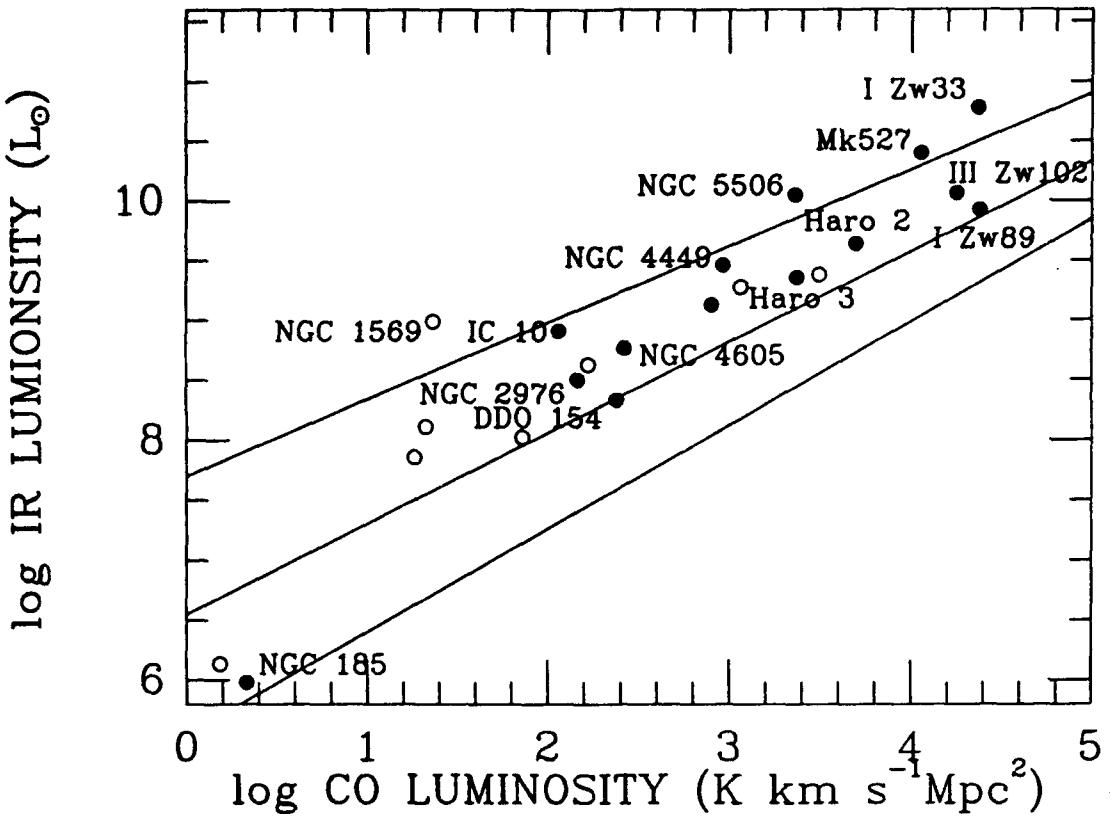

Figure 1 -- The far-infrared luminosity versus the J = 1 → 0 CO line luminosity for the sample of galaxies observed in this program. The three lines are those found by Young *et al.* for more luminous galaxies.

in the distance of the galaxies, which will tend to increase the dispersion in the common weighting factor. A distance-independent plot, such as Figure 2, is a better way to investigate the relationship between infrared and CO emission.

Figure 2 presents the CO surface brightness versus the total infrared flux, measured by $F_{IR} = 2.58S_{60}(Jy) + S_{100}(Jy)$. This plot clearly demonstrates the range of star formation efficiencies which are encountered in our sample of smaller galaxies. Objects located in the upper left of the figure are energetic star-forming galaxies: they have $L_{IR}/L_{CO} = 50$, and perhaps as high as 500! These objects include the energetic galaxies NGC 1569 and NGC 4449, as well as the mega-maser dwarf IC 10 (Henkel, Wouterloot, and Bally 1986). Although Young, Gallagher, and Hunter (1984) report a detection of NGC 1569 using the FCRAO telescope, we failed to detect it at a level 4 times fainter, indicating that the CO emission from this object comes from an area smaller than the beam of the 14-m FCRAO telescope. Objects located in the lower right of the diagram are lethargic star forming galaxies, with $L_{IR}/L_{CO} < 7$. These galaxies have a relatively large molecular content, but are not putting it to use in forming stars at a rapid rate. Objects in this category include I Zw 89 and III Zw 102.

It is interesting to note that these lethargic galaxies are relatively large spirals, whereas all of the very energetic galaxies in our sample are irregulars. Extensive spiral structure is obviously not necessary for a high efficiency of star formation.

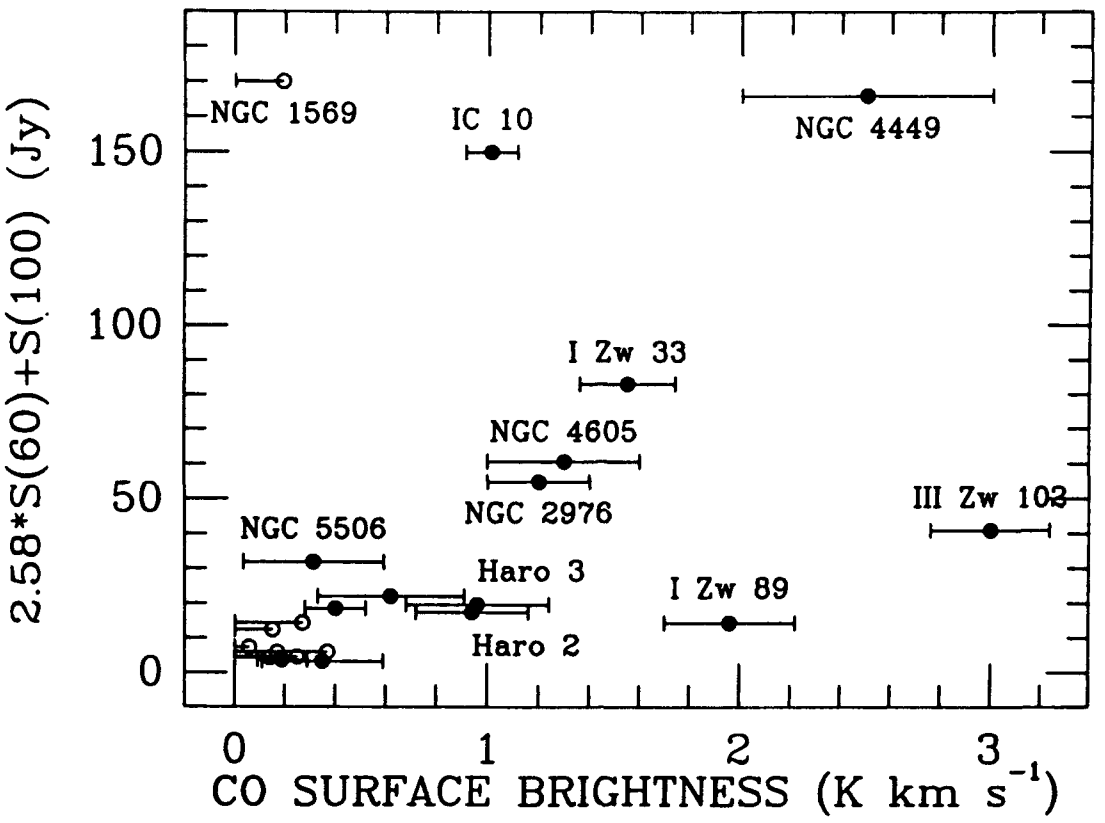

Figure 2 -- The far-infrared flux versus the J = 1 → 0 CO line flux. Upper limits are open circles. Note the wide variation in F_{IR}/F_{CO}.

A possible explanation for the high star-forming activity in irregular systems may be a higher efficiency of induced star formation (or, more significantly, molecular cloud formation) in a system having a thick gas layer. Within a thin disk, with a small scale-height gas layer, much of the pressure generated by massive star formation might be released above and below the plane of the gas layer. Only an annular region within the plane is compressed. Within an irregular galaxy or a thick disk, this pressure is confined and may therefore produce compression in all directions.

H. Thronson was partially supported by NASA grant NAG 2-134.

REFERENCES

Henkel, C., Wouterloot, J. G. A., and Bally, J. 1986, *Astr. Ap.*, 155, 193.

Rickard, L. J, and Harvey, P. M. 1984, *Astron. J.*, 89, 1520.

Telesco, C. M., and Harper, D. A. 1980, *Ap. J.*, 235, 392.

Young, J. S., Gallagher, J. S., and Hunter, D. A. 1984, *Ap. J.*, 276, 476.

Young, J. S. *et al.* 1986, *Ap. J.*, 304, 443.

SPIRALS

CHARACTERISTICS OF UGC GALAXIES DETECTED BY IRAS

Carol J. Lonsdale Persson and W. Rice
IPAC, California Institute of Technology

and G. D. Bothun
California Institute of Technology

Abstract

IRAS detection rates at 60 μm have been determined for the Uppsala General Catalogue of Galaxies (Nilson 1973; the UGC). Late-type spirals, characterised by a 'normal' IR/B ratio of $\sim$0.6, are detected to a velocity of $\sim$6000 km/s for $L_B = L^*$. Contrary to the situation for IRAS-selected galaxy samples, we find little evidence for a correlation bewteen IR/B and 60/100 μm in this large optically-selected sample. Thus a significant fraction of the IRAS-measured far-infrared flux from normal spirals must origionate in the diffuse interstellar medium, heated by the interstellar radiation field. We do not find support for Burstein and Lebofsky's (1986) conclusion that spiral disks are optically thick in the far-infrared.

1. INTRODUCTION

The UGC catalog is the most uniform catalog of optically selected galaxies available, being reasonably complete for high surface brightness galaxies to a blue size limit of 1'. As one approach to the question of the nature of the power source(s) of the far-infrared emission of galaxies, we have begun an analysis of the characteristics of the subset of the UGC galaxies detected by IRAS. In this contribution we present initial results of our study. A more substantial analysis, including a far-infrared luminosity function, will be submitted to the Ap. J. (Bothun, Lonsdale Persson and Rice 1987).

2. RESULTS AND DISCUSSION

The detection rate of UGC galaxies at 60 μm as a function of morphological type is illustrated in Figure 1a. As first noted by de Jong et al. (1984) the detection rate is low for E and S0 galaxies and increases towards later types. Figure 1b displays the detection rates of early- and late-type spirals in blue magnitude bins. At an equivalent blue magnitude the detection rate of the later spiral types is higher than that of the early types.

Figure 1b also shows that the IRAS detection rate drops steeply beyond about 13.5 mag. Another way to look at the situation is in terms of the IRAS detectability of an L^*_{opt} galaxy

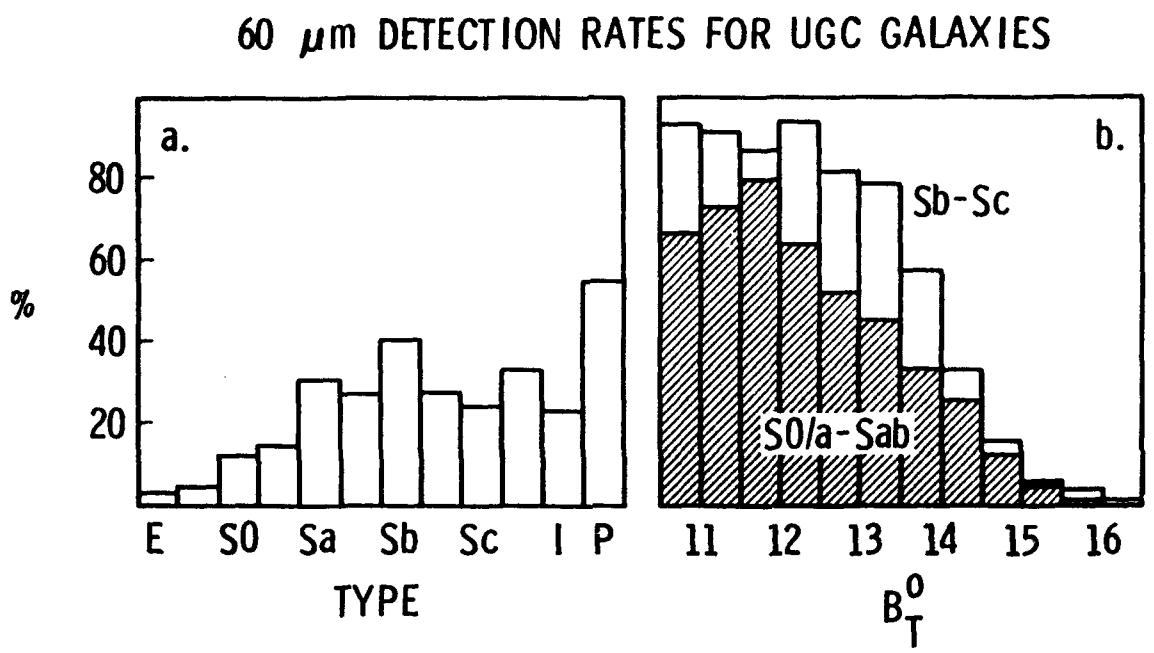

Figure 1 The 60 μm detection rate of UGC galaxies is shown as a function of Hubble type (a), and, for two type ranges, as a function of blue magnitude (b). The 'I' class refers to Irrs, and the 'P' class to Peculiars. The blue magnitude is corrected for Galactic and internal extinction as in de Vaucouleurs, de Vaucouleurs and Corwin (1976).

(ie. a galaxy at the 'knee' of the optical luminosity function; Schechter 1976). For an IR/B ratio of 0.6, which is typical of 'normal', optically-selected spirals (see Figure 2), an L^*_{opt} galaxy can be seen by IRAS to a velocity of 6000 km/s, and would have a blue magnitude of 14.2 at the limit of detectability (see Bothun, Lonsdale Persson and Rice 1987 for full details). Thus an galaxy sample extending to significantly fainter magnitudes or higher velocities will be biased towards starburst and active galaxies with high IR/B ratios. In particular, we would point out that the IRAS catalog is not an unbiased survey of structure on a 2-300 Mpc scale, as claimed by Lawrence et al. (1986), and that studies of the large-scale distribution of matter using the IRAS catalog as a data base (Yahil, Walker and Rowan-Robinson 1986; Meiksin and Davies 1986) must take into account the possibilty that infrared-luminous galaxies may not trace the matter very well (cf. Smith et al. 1987).

The apparently high detection rate for 'peculiar' galaxies (Figure 1a) is undoubtedtly largely due to a selection effect in the UGC such that an object with clearly evident morphological peculiarities is likely to be a high surface brightness (high specific star formation rate) interacting galaxy.

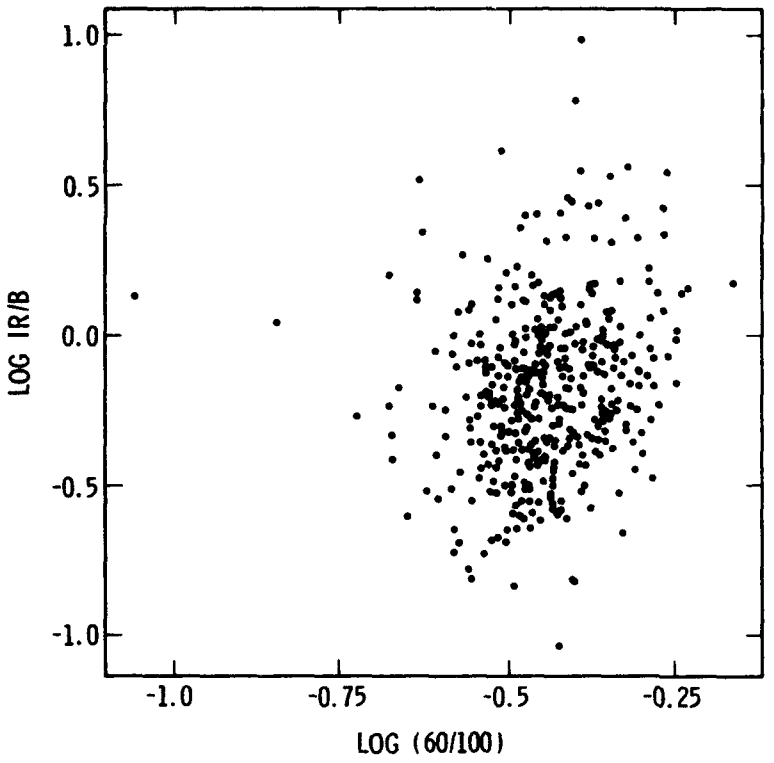

Figure 2 Dependence of the IR/B luminosity ratio on 60/100 μm color.

In Figure 2 we plot infrared-to-blue luminosity ratio versus 60/100 μm color. Here the infrared flux is the 40-120 μm flux derived as in Persson and Helou (1987), and the blue flux is defined as νf_ν(blue). Several authors have found a general trend for the 60/100 μm color to increase with IR/B in IRAS-selected galaxy samples. We find little evidence for such a correlation in our large optically-selected sample. We also find a very large scatter in plots of the blue surface brightness vs. IR/B ratio and 60/100 μm color (not shown here). Thus while it may be true that the most luminous IRAS galaxies are warm objects powered by starbursts or active nuclei, it does not follow that star formation is the primary source of the far-infrared luminosity of a typical late-type galaxy. It is, rather, likely that for many galaxies, much of the far-infrared emission is from the diffuse interstellar medium, heated by the interstellar radiation field (cf. Lonsdale Persson and Helou 1987).

Burstein and Lebofsky (1986) have found that the IRAS detection rate of UGC galaxies decreases with increasing inclination. We have verified this important result, but are unable to find support for Burstein and Lebofsky's interpretation that galaxies are optically thick in the far-infrared, and that the far-infrared emission must arise predominantly in the nuclear regions. As illustrated in Figure 3, there is no dependence of 60/100 μm color on inclination, which would be expected if the disks are optically thick. We do

not find any strong dependence of IR/B ratio on inclination either. Burstein and Lebofsky's conclusion is also inconsistent with the IRAS maps of nearby, spatially resolved galaxies (Rice et al. 1987), which show that the far-infrared flux is not strongly confined to the nuclear regions.

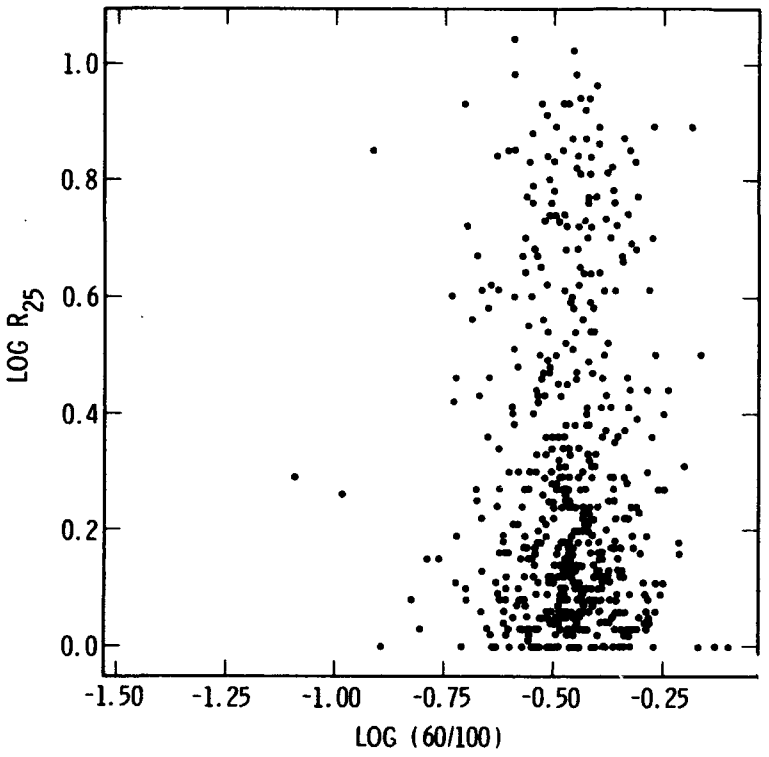

Figure 3 Inclination dependence of the 60/100 μm ratio of UGC galaxies. R_{25} is the major to minor axis ratio at the 25th mag. isophote, thus edge-on galaxies lie at the top of the figure.

3. REFERENCES

Bothun, G. D., Lonsdale Persson, C. J., and Rice, W. L., 1987, in preparation
Burstein, D. and Lebofsky, M. J. 1986, Ap.J. **301**, 683
de Jong, T. et al. 1984, Ap.J.Lett., **278**, L67
de Vaucouleurs, G., de Vaucouleurs, A., and Corwin, H. 1976, Second Reference Catalog of Bright Galaxies, (Austin: University of Texas Press)
Lonsdale Persson, C. J., and Helou, G. 1987, Ap.J., in press
Lawrence, A., Walker, D., Rowan-Robinson, M., Leech, K.J., and Penston, M.V. 1986, M.N.R.A.S., **219**, 687
Meiksin, A., and Davies, M. 1986, A.J., **91**, 191
Nilson, P. 1973, Uppsala General Catalogue of Galaxies
Rice, W., Lonsdale Persson, Carol. J., Soifer, B. T., Neugebauer, G., and Kopan, E. L. 1987, in preparation
Schechter, P. 1976, Ap.J., **203**, 297
Smith, B. J., Kleinmann, S. G., Huchra, J. P., and Low, F. J. 1987, this volume
Yahil, A., Walker, D., and Rowan-Robinson, M. 1986, Ap.J.Lett., **301**, L1

FAR-INFRARED PROPERTIES OF CLUSTER GALAXIES

M.D. Bicay[1,2] and R. Giovanelli[1]

(1) Arecibo Observatory, NAIC
P.O. Box 995
Arecibo, Puerto Rico USA 00613

(2) Center for Space Science and Astrophysics
Stanford University
Stanford, California USA 94305

ABSTRACT. Far-infrared properties are derived for a sample of over 200 galaxies in seven clusters: A262, Cancer, A1367, A1656 (Coma), A2147, A2151 (Hercules), and Pegasus. The IR-selected sample consists almost entirely of "IR normal" galaxies, with $< \text{Log } [L(FIR)] > = 9.79\ L_\odot$, $< [L(FIR)/L(B)] > = 0.79$, and $< \text{Log } [S(100\mu m)/S(60\mu m)] > = 0.42$. None of the sample galaxies has $\text{Log } [L(FIR)] > 11.0\ L_\odot$, and only one has a FIR-to-blue luminosity ratio greater than 10. No significant differences are found in the FIR properties of HI-deficient and HI-normal cluster galaxies.

I. INTRODUCTION

The synthesis of optical, radio, and X-ray measurements of galaxies and clusters has provided evidence of interaction of galaxies with an intracluster medium (ICM). IRAS observations allow us to expand the scope of studies to examine what effect environmentally driven mechanisms have on a galaxy's rate of star formation. Of particular interest is the question of whether the passage of a spiral disk through the ICM serves to stimulate star formation, especially in the central regions of the disk, or whether the stripping of the interstellar gas quenches star formation processes. We examine the far-infrared (FIR) properties of galaxies in seven clusters and attempt to find correlations with HI deficiency, a quantity that serves as a global probe of a galaxy's interstellar gas content and that is assumed to expose recently stripped galaxies.

II. THE SAMPLE

The noise-limited sample was obtained by coadding months-confirmed IRAS observations for fields six degrees square, centered roughly at the cluster cores. The resultant maps contained over 1700 points which satisfied the criterion $S(60\mu m) > 3\sigma$; this figure was typically 0.15-0.2 Jy. The flux-weighted IR positions were then matched to optical positions listed in the RCBG2, UGC, MCG, and CGCG catalogs, using a search radius of 90 arcsec (2 arcmin for galaxies of large angular extent). This procedure yielded a set of ~350 galaxies. By using redshift information to identify foreground and background objects, and by selecting the most probable IR source in confused fields (based on positional coincidence, morphology, and angular size), we were left with a sample of 206 galaxies with known redshift. The basic parameters for the seven clusters studied can be found in Giovanelli and Haynes (1985:GH).

TABLE I

MEAN OPTICAL / HI / INFRARED PROPERTIES OF CLUSTER GALAXIES

(1) Cluster	(2) N(IR)	(3) N(HI)	(4) a	(5) m	(6) r/r(A)	(7) Log L(B)	(8) Log D(L)	(9) Log M(H)	(10) HI def	(11) Log S(60)	(12) Log S(100)	(13) IR color	(14) Log (FIR)	(15) Log L(FIR)	(16) IR excess
A262	36	24	1.56	14.29	0.77	10.02	1.31	9.37	>0.17	−0.28	0.20	0.45	−13.21	9.62	−0.41
CANCER	32	27	1.58	14.83	0.90	9.78	1.33	9.45	>0.02	−0.25	0.23	0.44	−13.18	9.70	−0.09
A1367	34	28	1.10	15.05	1.01	9.87	1.33	9.38	0.09	−0.25	0.24	0.37	−13.16	9.99	0.07
A1656	56	36	1.01	15.01	1.29	9.93	1.33	9.30	>0.21	−0.36	0.09	0.41	−13.31	9.90	−0.05
A2147	20	15	0.88	15.39	1.34	10.21	1.46	9.71	>0.17	−0.37	0.10	0.40	−13.29	10.28	0.04
A2151	28	20	0.86	15.30	1.79	10.20	1.45	9.75	>0.16	−0.39	0.07	0.40	−13.33	10.25	0.02
PEGASUS	19	10	1.53	14.80	0.65	9.55	1.16	9.29	0.01	−0.23	0.28	0.42	−13.12	9.45	−0.09
ALL CLUSTERS	208	148	1.24	14.89	1.10	9.92	1.33	9.42	>0.12	−0.30	0.17	0.42	−13.23	9.79	−0.10
HI-DEFICIENT	43	43	1.38	14.70	0.78	10.00	1.37	8.99	>0.58	−0.31	0.20	0.46	−13.21	9.84	−0.18
NON HI-DEF	103	103	1.31	14.88	1.21	9.93	1.36	9.55	−0.07	−0.24	0.23	0.41	−13.18	9.89	−0.06

Note that the A2147 and A2151 fields overlap. All distant-dependent quantities assume a Hubble constant of 100 km/s/Mpc.

BRIEF EXPLANATION OF TABLE:
Col. 1 – "HI-deficient" galaxies are those with (HI def) > 0.3; see explanation for col. 10.
Col. 2 – Number of galaxies with IRAS measurements.
Col. 3 – Number of galaxies with high-quality HI measurements.
Col. 4 – Major blue diameter (arcmin).
Col. 5 – Apparent photographic magnitude.
Col. 6 – Projected distance of galaxy from cluster center, in units of Abell radius.
Col. 7 – Optical luminosity (solar units), with corrections applied for systematic effects in the CGCG, galactic extinction, redshift, and internal absorption.
Col. 8 – Linear (major) diameter of galaxy (kpc), obtained from angular diameter in Col. 4.
Col. 9 – Neutral-hydrogen mass (solar units).
Col. 10 – HI-deficiency (logarithmic units), as defined in Giovanelli and Haynes (1985). Positive values denote an HI-deficiency with respect to a suitably defined sample of isolated galaxies.
Col. 11 – IRAS 60um flux density (Jy).
Col. 12 – IRAS 100um flux density (Jy).
Col. 13 – IR color index, Log (S(100um)/S(60um)).
Col. 14 – Total far-infrared (FIR) flux, in units of W/(m*m). FIR is computed from eq. (1) of Soifer et al. (1986), under the assumption that the grain emissivity function is proportional to frequency.
Col. 15 – Total FIR luminosity (solar units).
Col. 16 – FIR to blue luminosity ratio, Log (L(FIR)/L(B)), a measure of infrared excess.

III. INFRARED PROPERTIES AND CORRELATIONS WITH HI PROPERTIES

The mean optical, HI, and infrared properties of the sample galaxies are given in Table I. Note that the A2147 field (~3 degrees square) is fully contained within the A2151 field. Furthermore, the central Hercules cluster (A2151) was examined to a flux density level of S(60μm)=50 mJy by Young et al. (1984). The quantities in columns 7 and 9 of Table I are derived following the precepts of Haynes and Giovanelli (1984:HG). The HI-deficient galaxies are those with HI content less than half (HI def > 0.3) of the value found for an isolated galaxy of the same morphology and linear diameter (see GH for details). The mean values in Table I were computed on a reduced sample (i.e. upper limits excluded), with the exception of "HI def" (for which lower limits were included). Since the sample is flux-limited, it clearly suffers from the Malmquist bias, as seen in the figures of col. 15. In the context of the current study, however, the most important derived FIR properties are Log [S(100μm)/S(60μm)], the IR color index, and the FIR-to-blue luminosity ratio Log [L(FIR)/L(B)]. For convenience, we will refer to these quantities as "IR color" and "IR excess", respectively.

The sample galaxies in our study are found in clusters of various morphologies, ranging from centrally concentrated clusters (A262, A1656) to loosely organized systems (Cancer, Pegasus). Yet, inspection of Table I reveals that there is little variation in the mean values of IR color and IR excess, with one exception: the IR excess of A262 is significantly lower than any of the other clusters. This is due, in part, to the high proportion of early-type galaxies in the A262 sample and the associated high values of optical luminosity. The fraction of E-S0 galaxies in A262 is 10/34, twice that of the other clusters. Table II shows that, on the whole, IR excess is lower in E-S0 cluster galaxies than in later types. This is certainly not surprising, in light of the fact that E and S0 galaxies have low amounts of the dust associated with FIR emission.

TABLE II

DISTANCE-INDEPENDENT FIR PROPERTIES AS FUNCTIONS OF MORPHOLOGICAL TYPE

	IR COLOR Log [S(100)/S(60)]			IR EXCESS Log [L(FIR)/L(B)]		
	All	HI-def	non HI-def	All	HI-def	non HI-def
All galaxies	0.42(0.14)	0.46(0.17)	0.41(0.13)	-0.10(0.35)	-0.18(0.34)	-0.06(0.31)
E - S0a	0.45(0.15)	——	——	-0.30(0.35)	——	——
Sa - Sab	0.40(0.18)	0.54(0.17)	0.37(0.13)	-0.14(0.42)	-0.36(0.34)	-0.09(0.41)
Sb - Sbc	0.43(0.15)	0.47(0.16)	0.40(0.13)	-0.12(0.32)	-0.13(0.31)	-0.11(0.32)
Sc - Scd	0.45(0.08)	0.39(0.03)	0.45(0.08)	-0.08(0.21)	0.06(0.02)	-0.09(0.22)
Pec., Dist.	0.34(0.10)	0.39(0.03)	0.33(0.10)	-0.02(0.39)	-0.32(0.21)	-0.03(0.28)

Figures in parentheses are standard errors of the mean.

In Figure 1, the IR color is plotted as a function of HI deficiency for all cluster galaxies within a projected Abell radius [r/r(A)] of 1.4. This latter constraint not only gives us uniform IRAS coverage for each of the clusters but is also the radius within which most of the HI-deficient galaxies reside. If one considers only the reduced sample (dashed line), no correlation is found. However, a very marginal correlation is apparently present when the limits are incorporated (solid line), using the algorithm for doubly-censored data given in Schmitt (1985). This "correlation" must be considered suspect, however, when one notes that typical logarithmic uncertainties are 0.15-0.2 in both HI deficiency and IR color. To quantitatively judge the significance of this result, we applied nonparametric statistical tests suitable for censored data. We find that the difference in the IR color distributions of HI-deficient and HI-normal galaxies to be less than a 2σ effect.

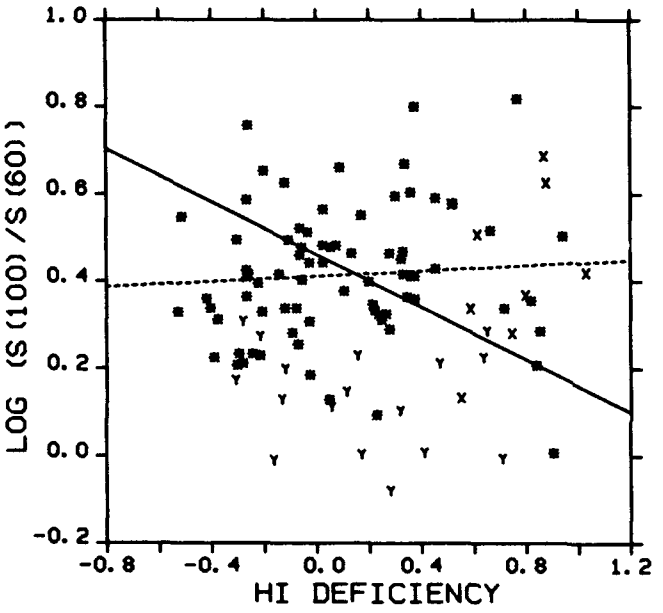

Figure 1

A plot of IR color as a function of HI deficiency for all cluster galaxies with known redshift and [r/r(A)] < 1.4. "X" denotes a lower limit in HI deficiency; "Y" denotes an upper limit in IR color. The results of two regressions are superimposed. The dashed line excludes IR limits, but includes HI limits. The solid line is a result of applying the Schmitt (1985) algorithm for doubly-censored data. The correlation coefficients are 0.07 and 0.49, respectively.

IV. SUMMARY AND CONCLUSIONS

The following points are made with respect to the > 200 sample galaxies:

(1) The sample consists almost entirely of "IR normal" galaxies. Included in the noise-limited sample are 31 E-S0a galaxies (18% of the sample galaxies with known morphology).

(2) The derived IR properties are (nearly) normally-distributed, with < Log [L(FIR)] > ~ 9.8 $L_\odot$, < [L(FIR)/L(B)] > ~ 0.8, and < Log [S(100μm)/S(60μm)] > ~ 0.4. None of the galaxies has Log [L(FIR)] > 11.0$_\odot$. Only one, the distorted double system NGC 3808 (VV 300) in A1367, has a FIR-to-blue luminosity ratio > 10.

(3) 12% of the galaxies with known morphology are classified as peculiar, disturbed, interacting, etc. Clearly, the tidally-induced disruption of a galaxy is not a necessary condition for FIR emission.

(4) Under the assumption that dust emissivity is proportional to frequency, the mean FIR color temperature is 30-35 K, with no variation seen among different spiral types. There is no way to tell if this is an integrated temperature due to the two components suggested by de Jong et al. (1984).

(5) There is NO significant correlation between derived IR properties and either projected Abell radius or, more importantly, HI deficiency.

(6) The absence of IR luminous galaxies leads us to conclude that if star formation is stimulated by the interaction of cluster galaxies with the ICM or the general cluster environment, it occurs at a negligible rate or over a time scale that is very small when compared with that of determinable HI gas deficiency.

This study was partially supported by NASA grant NAS7-918 and by the National Astronomy and Ionosphere Center, operated by Cornell University under contract with the National Science Foundation.

REFERENCES

de Jong, T., Clegg, P.E., Soifer, B.T., Rowan-Robinson, M., Habing, H.J., Houck, J.R., Aumann, H.H., and Raimond, E. (1984). Astrophys. J. Lett. 278, L67.

Giovanelli, R., and Haynes, M.P. (1985). Astrophys. J. 292, 404. (GH)

Haynes, M.P., and Giovanelli, R. (1984). Astron. J. 89, 758. (HG)

Schmitt, J.H.M.M. (1985). Astrophys J. 293, 178.

Soifer, B.T., Sanders, D.B., Neugebauer, G., Danielson, G.E., Lonsdale, C.J., Madore, B.F., and Persson, S.E. (1986). Astrophys. J. Lett. 303, L41.

Young, E., Soifer, B.T., Low, F.J., Neugebauer, G., Rowan-Robinson, M., Miley, G., Clegg, P.E., de Jong, T., and Gautier, T.N. (1984). Astrophys. J. Lett. 278, L75.

PRESENT STAR FORMATION IN SPIRALS OF THE VIRGO CLUSTER

B. GUIDERDONI
Institut d'Astrophysique
98 bis, Bd Araqo, F-75014 PARIS

ABSTRACT. From a study of spiral qalaxies in the Virqo Cluster (VC), it is shown that RDDO anemics with smooth arms and no siqn of present formation of (massive) stars have HI surface densities below a threshold value of 2 to 5×10^{20} atom cm^{-2}. This value is very consistent with predictions of theoretical models. It is likely that the HI disks of VC HI-deficient RDDO anemics have been deeply affected by ram pressure strippinq in the qaseous intracluster medium, while VC HI-deficient RDDO spirals have been only peripherally stripped.

1. RDDO ANEMICS IN THE VIRGO CLUSTER

The anemics of the RDDO classification introduced by Van den Berqh, 1976, are smooth-arms disk galaxies with no "knots" characterizinq HII regions and OB associations. Consequently they have a low present star formation rate of (at least) massive stars. Since most RDDO anemics are assigned RSA type Sa (Sandaqe and Tammann, 1981, Bothun and Sullivan, 1980) and since they do exist in the field, anemics might be simply the normal transition stage of the Hubble sequence between spirals which actively form stars and lenticulars (Sandaqe, 1983). On the other hand, since rich clusters actually have a large population of smooth-arms, faint disks (Wirth and Gallaqher, 1980), anemics might be a staqe of the evolution of spirals after interactions with an aqqressive cluster environment (Van den Berqh, 1976, Strom and Strom, 1978).

Guiderdoni and Rocca-Volmeranqe, 1985 (hereafter GRV), studied the observational properties of 107 spirals and irregulars (S0/a to Im, that is $0 \leq T \leq 10$ accordinq to de Vaucouleurs et al., 1976, RC2) in the VC, from a compilation of HI and photometric data. Amonq this sample, 38 qalaxies have a RDDO class from Van den Berqh, 1976, or Giovanardi et al., 1983: 24 are anemics (A or S0, S0/A, A ?, A/S) and 14 are normal, "healthy" spirals (S): Guiderdoni, 1986, studied the properties of these objects and some results are hereafter summarized.

2. EVIDENCE FOR A THRESHOLD IN STAR FORMATION PROCESSES

It is well known that spiral qalaxies in the VC are HI-deficient relative to reference counterparts with the same RC2 morphological type and optical surface (Davies and Lewis, 1973, Chamaraux et al., 1980, GRV). The deficiency parameter is here $Def(q_H) = (\langle \log q_H \rangle_T - \log q_H)/\sigma_T$. q_H is the ratio of HI mass to optical surface inside the B-isophote $\mu_B = 25.0$ mag arcsec^{-2} and the means $\langle \log q_H \rangle_T$ and dispersions σ_T are computed in GRV at fixed RC2 morphological type T from a reference, "field" sample.

It is hereafter shown that HI-deficient RDDO spirals and anemics have different HI surface densities in the central regions of their disks. Giovanardi et

Carol J. Lonsdale Persson (Editor)
Star Formation in Galaxies

al., 1983, gave HI diameters at 1/3 x central peak and the derived HI surface densities $\Sigma_H = M_H / \frac{\pi}{4} D_H^2$ closely approximate the HI surface densities in the central regions of the disks. For 13 anemics, $\langle \log \Sigma_H \rangle = -0.43 \pm 0.11$ ($\Sigma_H \simeq 2.2 \times 10^{20}$ atom cm^{-2}) while for 10 RDDO spirals, $\langle \log \Sigma_H \rangle = 0.26 \pm 0.06$ ($\Sigma_H \simeq 1.1 \times 10^{21}$ atom cm^{-2}). Figure 1 readily shows that the HI surface densities of RDDO spirals are always higher than those of anemics, whatever the deficiency may be. The separation value between the two RDDO classes corresponds to $\Sigma_H = 6.0 \times 10^{20}$ atom cm^{-3}.

Bosma, 1981, gave HI diameter $D_{H,5}$ at the isophote 5×10^{20} atom cm^{-2}. For 17 spirals, $\langle D_{H,5}/D^{o}_{25} \rangle = 1.64$. Similarly, lenticulars mapped at λ 21 cm have disk column densities lower than 5×10^{20} atom cm^{-2} (Sancisi, 1983). So no formation of (at least) massive stars is expected for this value of HI surface density. Thus the global star formation is a threshold process, with a regulating parameter strongly related to Σ_H.

Two theoretical models of star formation predict the existence of such a threshold related to the HI surface density (Elmegreen, 1979 and Seiden, 1983; Dopita, 1985). Guiderdoni, 1986, showed that both models lead to numerical values of the threshold $\simeq$ 2 to 5 x 10^{20} atom cm^{-2}, in remarkable agreement with the observational results.

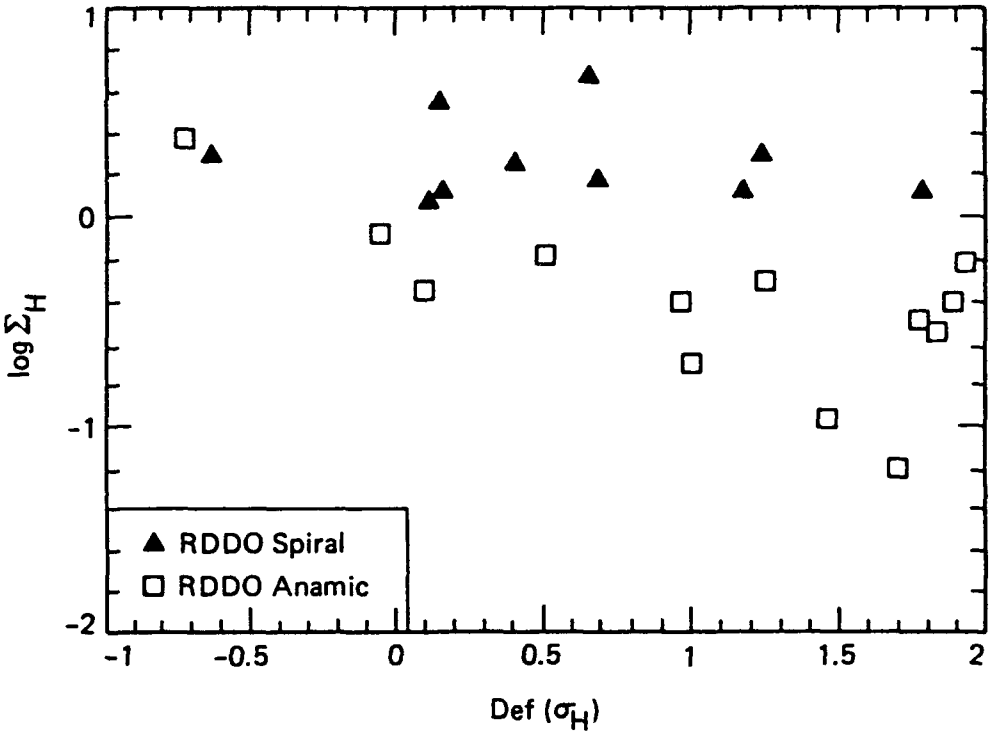

Figure 1 - HI surface density log Σ_H (in 10^{-3}g cm^{-2}) versus deficiency parameter Def(σ_H). See text for definitions. Triangles = RDDO spirals. Squares = RDDO anemics.

3. THE FATE OF SPIRAL GALAXIES IN THE VIRGO CLUSTER

There is a now good evidence that in the VC as well as in some other clusters, the HI disks are altered by ram pressure stripping (and evaporation) in the gaseous intracluster medium (see references in Guiderdoni, 1986). It appears in figure 2 that RDDO spirals and anemics have been affected by the stripping in a different way. The inner disk value log Σ_H for RDDO spirals does not depend on Def(q_H), supporting an effective stripping only in the peripheral regions. As a matter of fact, figure 2 shows that D_H/D^o_{25} well correlates with Def(q_H). On the contrary, the inner disk value log Σ_H for anemics roughly depends on Def(σ_H) while D_H/D^o_{25} does not depend on Def(q_H). That seems to support a stripping occurring in the whole disk. So the present HI disks of VC anemics might originate from stellar ejecta or conversion of molecular gas into atomic gas.

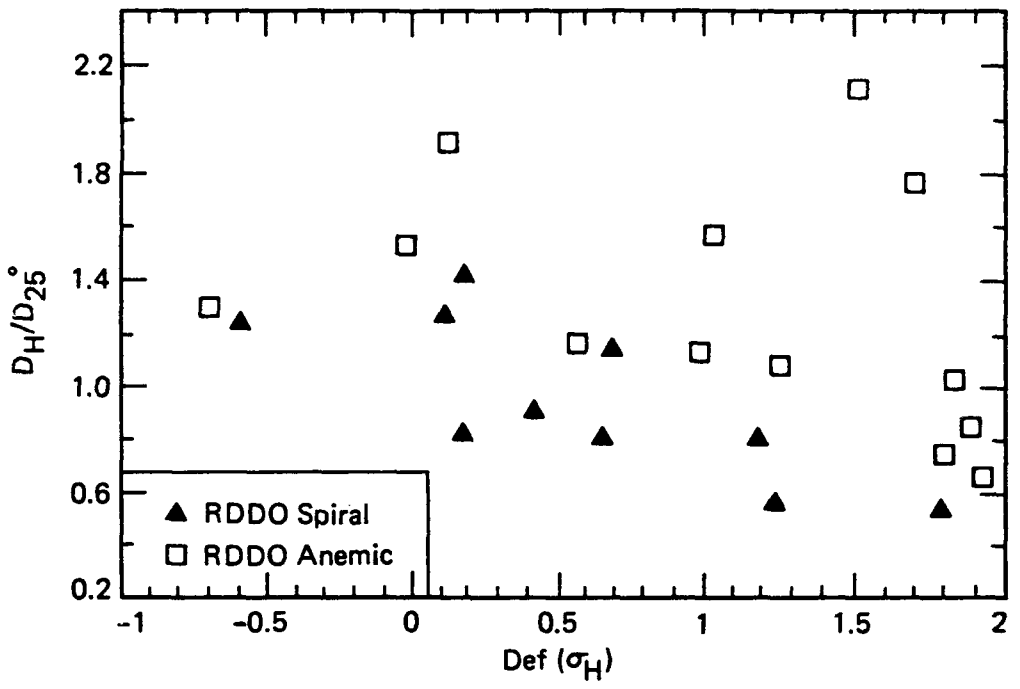

Figure 2 - HI/optical diameter ratio D_H/D^o_{25} versus deficiency parameter Def(q_H). See text for definitions. Triangles = RDDO spirals. Squares = RDDO anemics.

REFERENCES

Bosma, A., 1981, A.J., **86**, 1825
Bothun, G.D., Sullivan, W.T., 1980, Ap.J., **242**, 903
Chamaraux, P., Balkowski, C., Gerard, E., 1980, Astr.Ap., **83**, 38
Davies,.R.D., Lewis, B.M., 1973, M.N.R.A.S., **165**, 231
de Vaucouleurs, G., de Vaucouleurs, A., Corwin, H.G., 1976, The Second Reference Catalogue of Bright Galaxies, Austin, University of Texas Press.
Dopita, M.A., 1985, Ap.J., **295**, L5
Elmegreen, B.G., 1979, Ap.J., **231**, 372

Giovanardi, C., Helou, G., Salpeter, E.E., Krumm, N., 1983, Ap.J., **267**, 35
Guiderdoni, B., Rocca-Volmerange, B., 1985, Astr.Ap., **151**, 108
Guiderdoni, B., 1986, submitted
Sancisi, R., 1983, in Internal Kinematics and Dynamics of Galaxies, IAU Symp. n°100, p.55
Sandage, A., Tammann, G.W., 1981, A Revised Shapley-Ames Catalog of Bright Galaxies, Carneqie Institution of Washington.
Sandage, A., 1983, in Internal Kinematics and Dynamics of Galaxies, IAU Symp. n°100, p.367
Seiden, P.E., 1983, Ap.J., **266**, 555
Strom, S.E., Strom, K.M., 1978, in Structure and Properties of Nearby Galaxies, p.69
Van den Bergh, S., 1976, Ap.J., **206**, 883
Wirth, A., Gallagher, J.S., 1980, Ap.J., **242**, 469

Molecular Gas and Star Formation in HI-Deficient Virgo Cluster Galaxies

Jeffrey D. Kenney and Judith S. Young
Department of Physics and Astronomy
University of Massachusetts
Amherst, Massachusetts 01003

ABSTRACT Mapping of the CO emission line in 42 Virgo cluster galaxies reveals that the molecular gas contents and distributions are roughly normal in severely HI-deficient Virgo spirals. The survival of the molecular component mitigates the impact of the HI-stripping on star formation and subsequent galactic evolution. For spirals which are deficient in HI by a factor of 10, far-infrared, Hα line, and non-thermal radio continuum luminosities are lower by no more than a factor of 2. The fact that the inner galactic disks are stripped of HI, while CO is normal, suggests that the lifetime of the molecular phase is $\sim 10^9$ years in the inner regions of luminous spirals.

1. INTRODUCTION & OBSERVATIONS

Many spiral galaxies in the Virgo cluster have far less atomic gas (HI) than typical isolated spirals, probably because the galactic atomic gas is stripped away as the galaxies rush through the intracluster gas surrounding M87 (for a review, see Haynes, Giovanelli, and Chincarini 1984). Since many of these galaxies appear to have lost over 90% of their original HI supply, the evolution of Virgo galaxies has unquestionably been altered to some degree by the harsh cluster environment (e.g. Kennicutt 1983). However, the fate of star formation in HI-deficient galaxies depends critically on the response of the molecular gas to the HI-stripping event: in luminous spirals, molecular gas is a significant fraction of the total interstellar gas mass, and is the component of the interstellar medium out of which stars form.

To determine the fate of molecular gas in HI-deficient galaxies, we have mapped CO(J=1→0) emission in 42 Virgo spirals with the 14-meter telescope of the Five College Radio Astronomy Observatory (HPBW=45"). All Sa-Sm galaxies brighter than $B_T^0=12.0$ in a 16°x16° field centered on M87 were surveyed in 3-9 positions along the major axis. Of the 42 galaxies surveyed, 33 were detected in at least one position. Both the radial distribution of CO emission and the total CO flux have been determined from the observations by modeling the sources to correct for inclination and source-beam coupling. Results for a subset of the present sample, focussing on the normal CO emission in the HI-deficient galaxies, have been published elsewhere (Kenney and Young 1985, 1986). In this paper, we concentrate on the relationship of the gas content to the present star formation in the HI-deficient Virgo spirals.

2. RESULTS

2.1. CO and Tracers of Star Formation vs. HI Deficiency

As a measure of the HI content of Virgo galaxies, we employ the HI deficiency

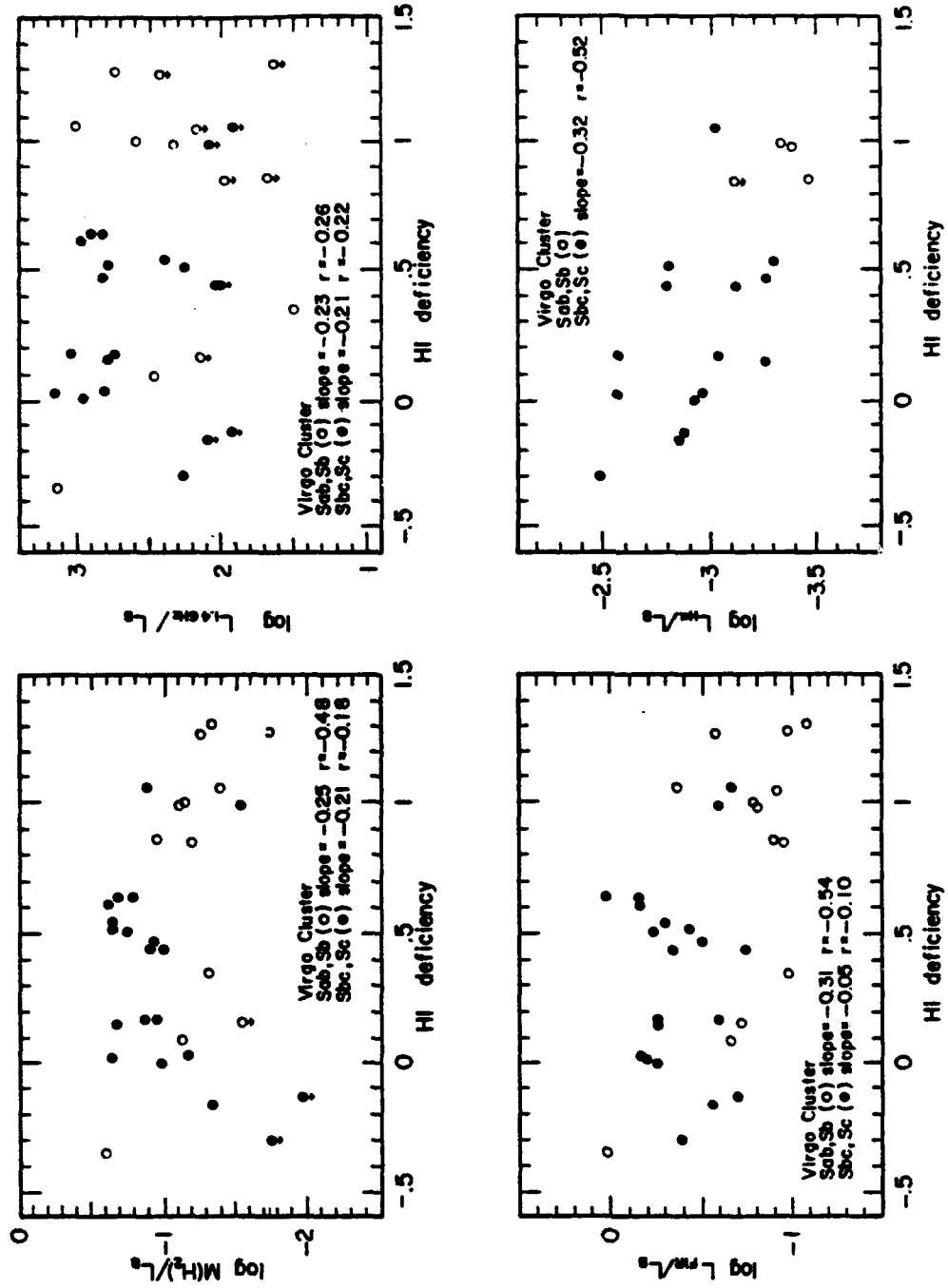

Figure 1. HI deficiency vs. H_2 masses; FIR, radio continuum, and Hα luminosities, all normalized to blue luminosities. The least squares slopes and correlation coefficients (r) have been computed using the 2σ upper limit values for non-detections. Omitting the upper limits does not significantly change the slope or correlation coefficient of any of the fits. (a) H_2 mass is assumed to be proportional to the CO luminosity. Units are $M_\odot/L_\odot$. (b) FIR luminosity derived from single thermal component fit to coadded 60μm and 100μm IRAS fluxes. (c) 1.4 GHz radio continuum. (d) Hα+[NII] luminosities. References--HI: Helou et al. (1981, 1984); Giovanelli and Haynes (1983, 1985). Blue light: RC2 (1976). Far-infrared: IRAS coadds (1986). 1.4 GHz radio continuum: Kotanyi (1980). Hα+[NII]: Kennicutt and Kent (1983).

parameter, as formulated by Giovanelli and Haynes (1983). Its definition is: HI def = log[M(HI expected)/M(HI actual)], where M(HI expected) is the HI mass of a typical isolated galaxy of the same morphological type and optical diameter. The HI deficiency is a logarithmic ratio, so that HI def = 0 (±0.3) denotes a normal HI content, and HI def = 1.0 denotes a galaxy with 10 times less HI than normal. In Figure 1, the HI deficiency is compared with global measures of CO emission and three tracers of current star formation. In order to compensate for the range in galaxy masses, we normalize these quantities by the blue optical luminosity.

Figure 1a shows that the CO luminosities of the HI-deficient galaxies are roughly normal, since the L_{CO}/L_B ratios are similar for the HI-normal and severely HI-deficient galaxies. Further discussions of the CO luminosities and distributions in Virgo spirals, including comparisons with non-Virgo spirals, are presented in Kenney and Young (1985, 1986). Stark et al. (1986) also find normal CO emission in Virgo spirals. Throughout this paper, the H_2 mass is assumed to be proportional to the CO luminosity ($\sigma(H_2) \sim 3.9\ \int T_R(CO)dv\ M_\odot pc^{-2}$; Dickman, Snell, and Schloerb 1986). Although the $^{12}CO(J=1\rightarrow0)$ line is generally optically thick, the fact that more massive molecular clouds have larger linewidths (at least in our galaxy, e.g. Sanders, Scoville, and Solomon 1985) allows the use of CO emission as a valid tracer of molecular mass. The $CO\rightarrow H_2$ conversion does depend linearly on the mean gas temperature (and weakly on the mean gas density and the cloud mass spectrum). However, we find that the $S_{60\mu m}/S_{100\mu m}$ ratios (a measure of dust temperature) are uncorrelated with HI deficiency. Thus, it is unlikely that the $CO\rightarrow H_2$ conversion is significantly different in the HI-deficient galaxies.

Figures 1b and 1c show that the far-infrared and 1.4 GHz radio continuum luminosities are not strongly correlated with HI deficiency. Figure 1d indicates some degree of correlation between HI deficiency and Hα luminosity for Virgo Sc's, as discovered previously by Kennicutt (1983). However, the maximum slope in any of these relations, of -0.32 in the log, means that galaxies which are HI-deficient by a factor of 10 are deficient in current star formation by a maximum of a factor of 2. We argue below that this is due to the survival of the molecular component.

2.2 Radial Distributions of Gas, New Stars and Old Stars

That the survival of H_2 is responsible for maintaining high global rates of star formation despite the severe HI deficiencies is elucidated by the radial distributions in Figure 2. There are 2 features of the radial distributions which are worth emphasizing: 1) In all galaxies, the distributions of CO, HII regions, and radio continuum emission are similar. This demonstrates that star formation occurs where the molecular gas exists. 2) In galaxies with normal amounts of HI, the surface densities of HI and H_2 are typically equal at some radius. In the severely HI-deficient spirals, the surface density of HI is significantly below that of H_2 over the entire region where CO is detected.

One reason that the molecular gas has resisted removal, while the atomic gas has not, is that the HI and H_2 generally have such different distributions. The gravitational force per unit area binding a gas cloud to a galactic disk is approximately $2\pi G\sigma_{TOT}(R)\sigma_{gas}$, where σ_{gas} is the gas mass surface density, and $\sigma_{TOT}(R)$ is the total mass surface density, which is a function of galactocentric radius R. Typically, a large fraction of a galaxy's molecular gas resides in the inner galaxy, where $\sigma_{TOT}(R)$ is large. Most of the HI exists in the outer galaxy, and thus is more easily removed, since $\sigma_{TOT}(R)$ is smaller.

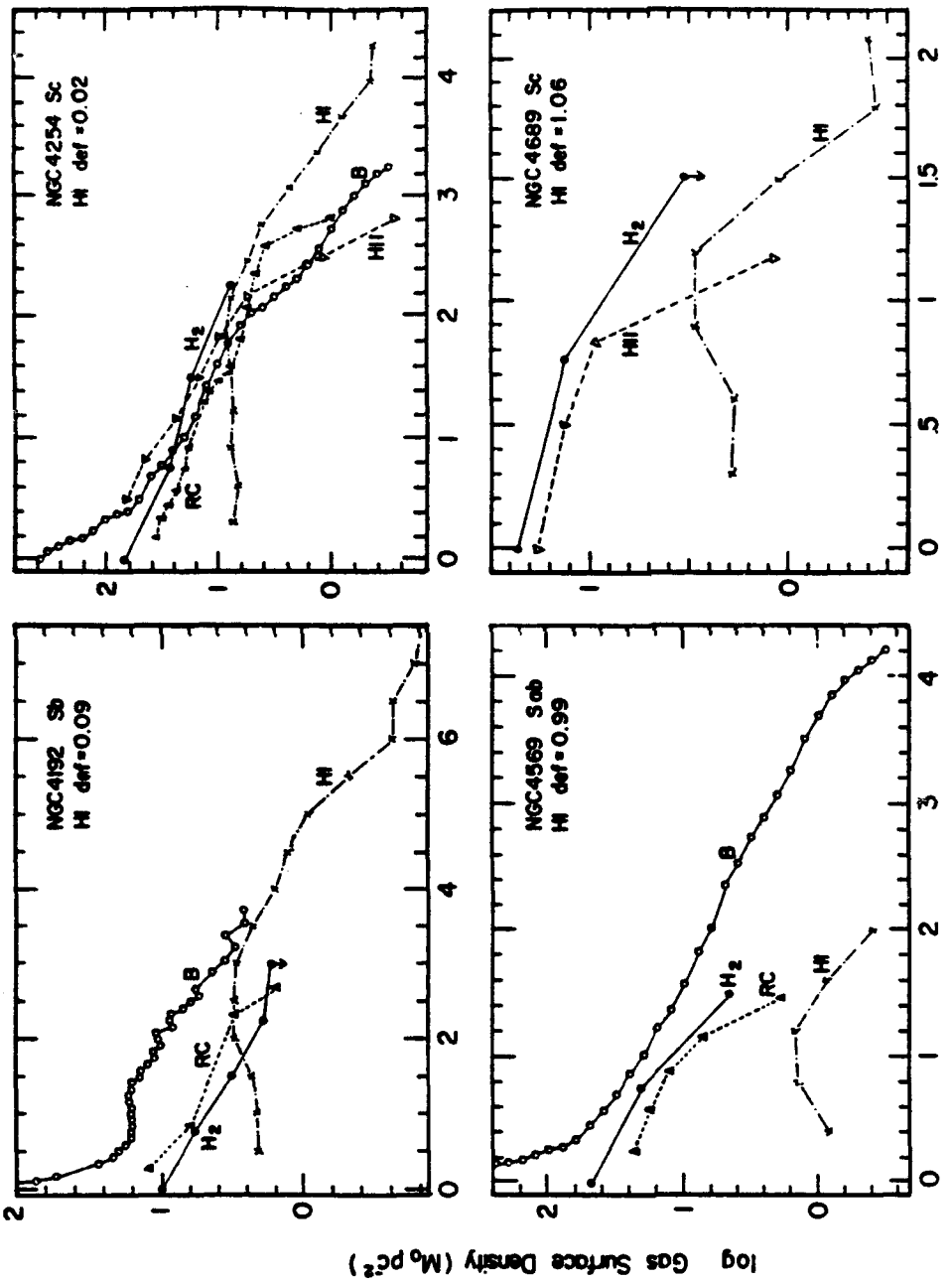

Figure 2. Radial distributions of CO (H_2), HI, 1.4 GHz radio continuum (RC), HII regions (HII), and blue light (B) in 4 Virgo spirals, selected to show a range in HI deficiency and morphological type. The vertical scaling for HI and H_2 is M_o pc-2. All other quantites have been scaled by an arbitrary factor which gives a good fit to the H_2 distribution in 3 luminous Sc galaxies. Although the scaling factor for B, RC, and HII is arbitrary, it is the same for every galaxy. References--HI: Warmels (1986). Blue light: Whitmore and Kirshner (1982); Fraser (1977). 1.4 GHz continuum: Condon (1983); Warmels (1986). HII region counts from Hodge and Kennicutt (1983), normalized by global Hα+[NII] fluxes (Kennicutt and Kent 1983). The HII region counts may be underestimated in the galaxy centers due to plate burnout.

The greater column density of molecular clouds (and corresponding greater σ_{gas}) is the second property of molecular gas which makes it more difficult to strip than atomic gas. This property is relevant, since even the inner regions of the Virgo galaxies have less HI, as shown in Figure 3a. This figure displays the (global) HI deficiency vs. the mean HI surface density over the inner half of the optical disk, normalized to the typical value for a more isolated galaxy of the same type (Warmels 1986). The slope of this relation, -0.38 in the log, means that galaxies which are globally HI-deficient by a factor of 10, are HI-deficient in the inner galaxy by a factor of ~2-3. Thus even the inner galaxy, where the bulk of the molecular gas exists, has been stripped of atomic gas. Figure 3b shows explicitly that the $M(HI)/M(H_2)$ ratio is significantly lower over the region where CO is detected (which is typically $D_0/4$) in the HI-deficient spirals. The slope of this relation, -0.50 in the log, indicates that the inner galaxy HI deficiency is the same (within the uncertainties) whether measured with respect to the HI in isolated galaxies, or with respect to the molecular gas.

2.3 The Long Lifetime of the Molecular Gas Phase

While perhaps unsurprising that the dense H_2 has survived the stripping, it is significant that the molecular gas has not yet responded to the atomic gas removal. The large number of Virgo galaxies with small HI/H_2 ratios suggests that the molecular gas has not responded during a cluster crossing time (~10^9 years), which is approximately how long the stripping events have been going on.

Inasmuch as the HI-deficient Virgo galaxies can be considered once-normal spirals subjected to modification in a cluster 'laboratory', we may conclude that the molecular phase is long-lived in the inner disks of all luminous (non-starburst) spiral galaxies. Energetic events associated with star formation

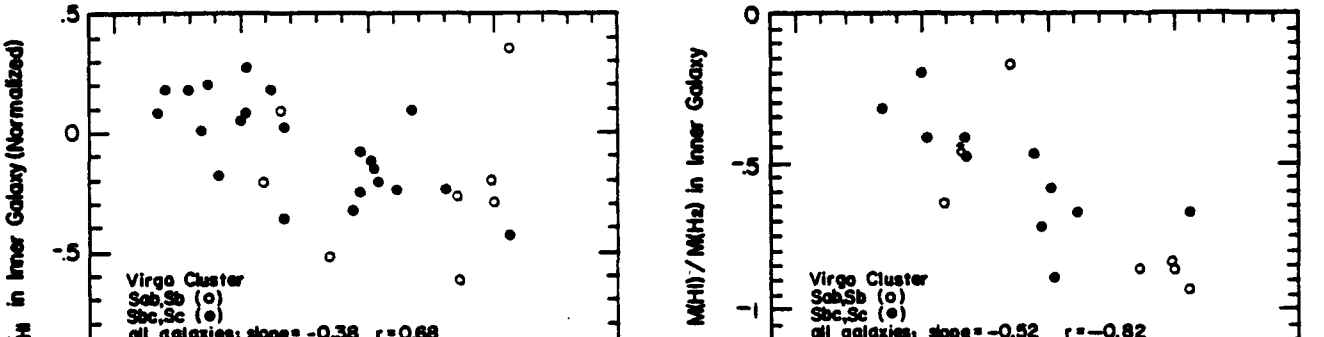

Figure 3. (a) Mean HI surface density for Virgo spirals over the inner half of the optical disk (out to a radius of $D_0/4$, where D_0 is the optical diameter from the RC2), normalized to the typical value for a more isolated galaxy of the same type (Warmels 1986), vs. HI deficiency. (b) HI/H_2 mass ratio, over the region where CO is detected, vs. HI deficiency.

undoubtedly act to partly ionize and disrupt molecular clouds, but the conversion of H_2 back into HI appears to be an inefficient process in these galaxies. Apparently, once gas enters the molecular phase in the inner regions of luminous spiral galaxies, it tends to remain molecular for $\sim 10^9$ years. The predominant disruptive influence of star formation on molecular clouds may be to break apart the cloud into smaller fragments.

3. CONCLUSIONS

1) CO fluxes and distributions are roughly normal in HI-deficient Virgo cluster spirals. This is easily understood, since molecular clouds are difficult to strip. Two charactersistics of molecular gas are responsible for its survival: its high surface density (with respect to most of the HI), and its location deep in the gravitational well of the galaxy.

2) The survival of the molecular component mitigates the impact of HI removal on star formation and subsequent galactic evolution. In galaxies which are globally HI-deficient by a factor of 10, global tracers of star formation (FIR, radio continuum, Hα) are lower by no more than a factor of 2.

3) Atomic gas has been stripped even in the inner galaxy, where the molecular gas resides. Molecular gas has not significantly responded to the HI removal in over a cluster crossing time, or $\sim 10^9$ years. This implies that gas in the inner regions of luminous spirals does not cycle rapidly between the atomic and molecular phases. Instead, once a typical nucleon enters the molecular phase, it remains molecular for $\sim 10^9$ years.

REFERENCES

Condon, J.J. 1983, Ap.J.Supp., 53, 459.
deVaucouleurs, G., deVaucouleurs, A.,and Corwin, H.G. 1976, Second Reference Catalogue of Bright Galaxies (Austin: University of Texas Press) (RC2).
Dickman, R.L., Snell, R.L., and Schloerb, F.P. 1986, Ap.J., in press.
Fraser, C.W. 1977, Astr.Ap.Supp., 29, 161.
Giovanelli, R., and Haynes, M.P. 1983, A.J., 88, 881.
Giovanelli, R., and Haynes, M.P. 1985, Ap.J., 292, 404.
Haynes, M.P., Giovanelli, R., and Chincarini, G.L. 1984, Ann.Rev.Astr.Astr., 22, 445.
Helou, G., et al. 1981, Ap.J.Supp., 46, 267.
Helou, G., Hoffman, G.L., and Salpeter, E.E. 1984, Ap.J.Supp., 55, 433.
Hodge, P.W., and Kennicutt, R.C. 1983, A.J., 88, 296.
Kenney, J.D., and Young, J.S. 1985, in ESO Workshop on the Virgo Cluster of Galaxies, ed. O.-G. Richter and B. Binggeli (Garching: ESO), p. 165.
Kenney, J.D., and Young, J.S. 1986, Ap.J.(Letters), 301, L13.
Kennicutt, R.C. 1983, A.J., 88, 483.
Kennicutt, R.C., and Kent, S.M. 1983, A.J., 88, 1094.
Kotanyi, C.G. 1980, Astr.Ap.Supp., 41, 421.
Sanders, D.B., Scoville, N.Z., and Solomon, P. 1985, Ap.J., 289, 373.
Stark, A.A., et al. 1986, Ap.J., 306, L17.
Warmels, R.H. 1986, Ph.D. thesis, Groningen.
Whitmore, B.C., and Kirshner, R.P. 1982, A.J., 87, 500.

STAR FORMATION RATES AS A FUNCTION OF GALAXY MASS

W. ROMANISHIN
Physics Department
Arizona State University
Tempe AZ 85287

ABSTRACT

Several groups have found correlations between the colors and absolute magnitudes of spiral galaxies. Using optical and/or near IR (1.6 micron) colors, they find that lower luminosity spirals are systematically bluer than higher luminosity spirals. I have used IRAS far IR luminosities to investigate the suggestion that one prime cause of these color- absolute magnitude correlations is a systematic variation with galaxy mass of the current star formation rate (SFR) per unit mass. To the extent that the IRAS fluxes actually measure disk SFR, I find NO correlation of SFR/ unit mass and galaxy mass. Other possible explanations of the color- absolute mag. correlations are discussed, as well as caveats on the use of IRAS fluxes as a means of comparing SFRs in galaxies of differing mass.

INTRODUCTION

Several groups (Tully, Mould, and Aaronson 1982; hereafter TMA; Wyse 1982, and Visvanathan 1981) have reported finding color- absolute magnitude correlations for spiral galaxies. All find that lower luminosity galaxies are bluer than higher luminosity galaxies. The most striking relation is shown by TMA, who plot the optical minus infrared color BT(b,i)- H(-0.5) versus the HI line width. Their B magnitude is a total magnitude corrected for Galactic absorption and internal galaxy absorption (galaxy tilt). Their H (1.6 micron) magnitude encompasses a diameter corresponding to about 1/3 the B=25 mag/sq. arcsec isophotal diameter. This B-H color changes by almost 2 magnitudes as W, the HI line width corrected for galaxy inclination, ranges from 200 to 600 km/sec. TMA postulate that much of this effect is caused by a higher star formation rate (SFR) per unit mass in lower mass galaxies.

I am studying the role of SFR in explaining the B-H relation for spirals using IRAS far infrared fluxes. The rationale, of course, is that the far IR flux might be a good measure of the current SFR for massive stars, as the massive stars are presumably the heating source for the dust radiating at 60-100 microns.

SAMPLE AND ANALYSIS

My sample is similar to that in TMA. The TMA sample was drawn from "A Catalog of Infrared Magnitudes and HI Velocity Widths for Nearby Galaxies" (Aaronson et al 1982, hereafter the "HI CATALOG").

The primary sample consists of all galaxies in the HI CATALOG meeting the following criteria:

1) Only galaxies smaller than 3.5 arcmin diameter were included , as the fluxes in the Cataloged Galaxies in the IRAS Survey (Lonsdale et al 1985) for larger galaxies may be seriously underestimated.

2) Galaxies with inclinations larger than 80° were ignored, to avoid the worst of the possible inclination dependent detection problems (Burstein and Lebofsky 1986).

Approximately 120 galaxies from the HI CATALOG meet these 2 criteria. Of these, about 80% had positive detections at 60 and 100 microns listed in Cataloged Galaxies in the IRAS Survey (Lonsdale et al,1985).

A more restricted sample was also chosen, for which good B magnitudes could be determined. These were chosen from the galaxies meeting 1) and 2) which also:

3) Had BT magnitudes listed in the Second Reference Catalog (RC2) or had Zwicky magnitudes which were converted to BT estimates using the procedure in Auman, Hickson, and Fahlman (1982).

4) Had Galactic latitude greater than 30°, following TMA.

Of this restricted sample of 88 galaxies, 76% had positive IRAS 60 and 100 micron detctions.

Far IR luminosities (LFIR) were found using LOG(FIR) listed in Cataloged Galaxies in the IRAS Survey (Lonsdale et al 1985) and galaxy distances from the HI CATALOG. These distances are based on a Virgocentric infall model. I assumed a value of 15.7 MPC for the distance to Virgo.

Galaxy masses (Mgal) were derived from the simple relation (Faber and Gallagher 1979)

$$Mgal = R\,(\Delta V)^2 \;/\; G$$

where R is the galaxy radius (derived from the diameters in the HI CATALOG) and ΔV is an estimate of the rotational velocity (derived from the HI line width).

RESULTS AND DISCUSSION

In Figure 1 I have plotted Log(LFIR/Mgal) , which should be a measure of the SFR per unit mass, against the galaxy mass. This figure shows NO OBVIOUS CORRELATION OF SFR/UNIT MASS WITH MASS. Notice that the scatter is large. If there is any trend, it is actually for lower mass galaxies to have a lower Log(LFIR/Mgal) than higher mass galaxies. However, this is not statistically significant with the present sample.

The LFIR/ blue luminosity ratios for this sample are similar to the lower to middle range found for Shapley- Ames spirals (de Jong et al 1984, ApJ 278, L67). This implies that galaxies in the present sample are not unusually active.

Several points must be kept in mind:

1) If lower mass, lower metallicity galaxies have a lower dust mass/ total mass ratio, LFIR might not be a good measure of current SFR. Arguing against the importance of this effect is the fact that LFIR does seem to measure SFR in small

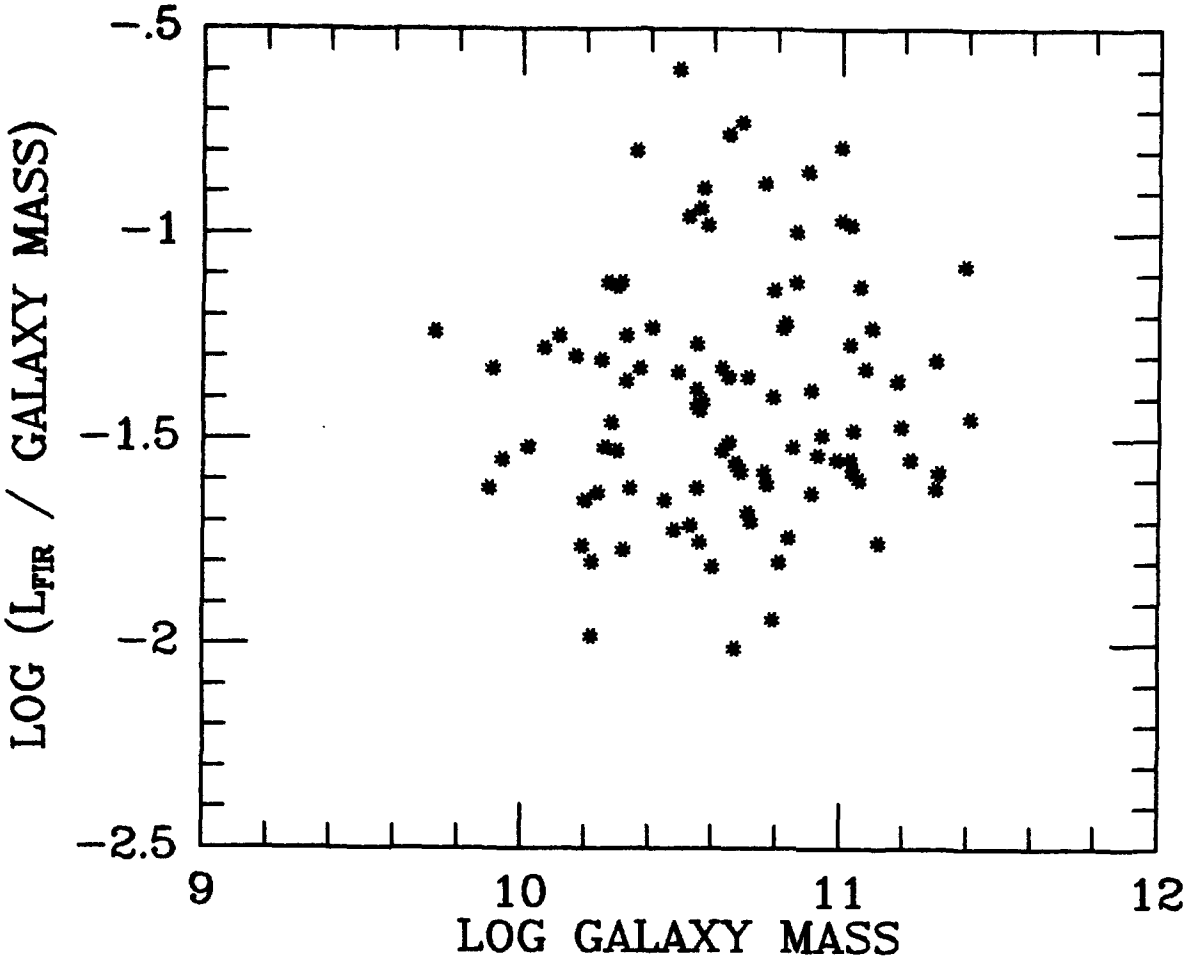

FIGURE 1. Plot of Log(Far IR Luminosity / Galaxy Mass) vs. Log (Galaxy Mass). Luminosity and mass are measured in Solar units.

blue irregular galaxies (Hunter, Gillett, Gallagher, Rice and Low 1986).

2) There may be strong contamination of the disk emission by nuclear sources (Burstein and Lebofsky 1986). I hope that analysis of IRAS pointed observations of nearby galaxies will settle this question.

3) Possible problems with overestimation of the flux for sources near the survey limits have not been dealt with yet.

4) Galaxies with upper limits to LOG(FIR) have not been included. There is a slight trend for the lower mass galaxies to have a lower detection rate. Thus, proper inclusion of upper limit data might actually accentuate any tendency for lower mass galaxies to have lower SFR/ unit mass.

What are some other possible explanations for the (B-H)- absolute magnitude relation? Some possibilities include:

1) GALAXY AGE- Lower luminosity galaxies might well be younger (in some sense) than higher mass galaxies. If this is true, they might have far less of the old "Population II" component which is red in (B-H). (see discussion in Bothun, Romanishin, Strom and Strom 1984).

2) IMPORTANCE OF BULGE POPULATION TO H(-0.5) - The manner in which the H magnitude is measured (to a fraction of the standard isophotal diameter) emphasizes the contribution from the center of a galaxy. This accentuates the importance of any old (red) bulge population. If bulge/ total galaxy population increases with galaxy mass (on average) this could help explain the correlation. (Note however that TMA find little type dependence of the correlation, arguing against the importance of this poiunt.)

3) SYSTEMATIC METAL ABUNDANCE VARIATIONS- TMA do point out the possibility of a contribution of a change in stellar metal abundance with galaxy luminosity to the (B-H)-W correlation. Perhaps this is more important than previously thought (see Bothun et al 1984 for a discussion of systematic metal abundances in spirals).

4) EXTINCTION VARIATIONS - If lower luminosity spirals have less dust, they will tend to be bluer optically simply because they have lower internal extinction.

Possibly all these factors play some role in the color- absolute magnitude relation.

ACKNOWLEDGEMENT

This research has been supported in part under the IRAS extended mission program by JPL contract 957317, for which I am grateful.

REFERENCES

Aaronson, M. et. al. 1982, Ap.J.Suppl.,50,241.
Auman, J.R., Hickson, P., and Fahlman, G.G. 1982, Pub. A.S.P. 94,19.
Bothun, G.D., Romanishin, W., Strom, S.E., and Strom, K.M. 1984, A.J., 89, 1300.
Burstein, D., and Lebofsky, M.J. 1986, Ap.J.,301,683.
de Jong, T., Clegg, P.E., Soifer, B.T., Rowan-Robinson, M., Habing, H.J., Houck, J.R., Aumann, H.H., and Raimond, E. 1984,Ap.J.(Letters),278,L67.
Faber, S.M., and Gallagher, J.S. 1979, Ann. Rev. Astr. Ap. 17, 135.
Hunter, D.A., Gillett, F.C., Gallagher, J.S., Rice, W.L., and Low, F.J. 1986, Ap.J., 303,171.
Lonsdale, C.J., Helou, G., Good, J.C., and Rice, W. 1985, Cataloged Galaxies and Quasars Observed in the IRAS Survey (Jet Propulsion Laboratory)
Tully, R.B., Mould, J.R., and Aaronson, M. 1982, Ap.J.,257,527 (TMA).
Visvanathan,N. 1981, Astr. Ap., 100, L20.
Wyse,R. 1982, M.N.R.A.S. 199, 1P.

Global Properties of the Nearby Spiral M101

C. Beichman, F. Boulanger, W. Rice, C. Persson

Infrared Processing and Analysis Center,
California Institute of Technology and
Jet Propulsion Laboratory
Pasadena, CA 91125

and

F. Viallefond
Institute d'Astrophysique, Paris

M101 (NGC 5457) is a classic Sc I spiral galaxy located sufficiently nearby, 6.8 Mpc, (Aaronson, Mould and Huchra 1980) that its structure can be studied even with the coarse angular resolution of IRAS. This work addresses the global infrared properties of M101 including the radial dependence of its infrared emission.

IRAS pointed observations were combined to construct maps of M101 at 12, 25, 60 and 100 micron. The processing included subtraction of a linear baseline from each detector stream to remove residual electronic offsets and zodiacal emission (Rice *et al.* 1986). The emission from the galaxy was integrated using a circular area of 28' diameter to obtain the integrated fluxes of M101 presented in Table 1. The flux densities include small color correction factors derived by fitting an intrinsic source spectrum consisting of the sum of Planck functions at two temperatures times an emissivity proportional to frequency. The best fit temperatures are 200 K and 31 K.

Table 1. Global Properties of M101

A. Observations[1]		B. Derived Properties	
$f_\nu(12)$	9 ± 2 Jy	F(IR)[2]	5.74E-12 W m^{-2}
$f_\nu(25)$	12 ± 2 Jy	L(12-100 um)	1.3E10 L_o
$f_\nu(60)$	95 ± 15 Jy	IR/B[3]	0.40
$f_\nu(100)$	260 ± 40 Jy	L(0.15-100 um)	1.0E11 L_o

Notes: 1)Color-corrected values measured in a 28' diameter aperture; 2)flux between 40 and 120 micron as defined by Helou *et al.* 1985; 3) see text.

A spectrum of the galaxy from the UV to the far-infrared is presented in Fig. 1. The UV data are from Code and Welch (1982), the visible results from Okamura *et al.* (1976) and the near IR from Elmegreen (1980) and all have been corrected for reddening (A_V=0.17 mag) within our galaxy. In making Figure 1 a geometric correction factor was applied to the data to account for the

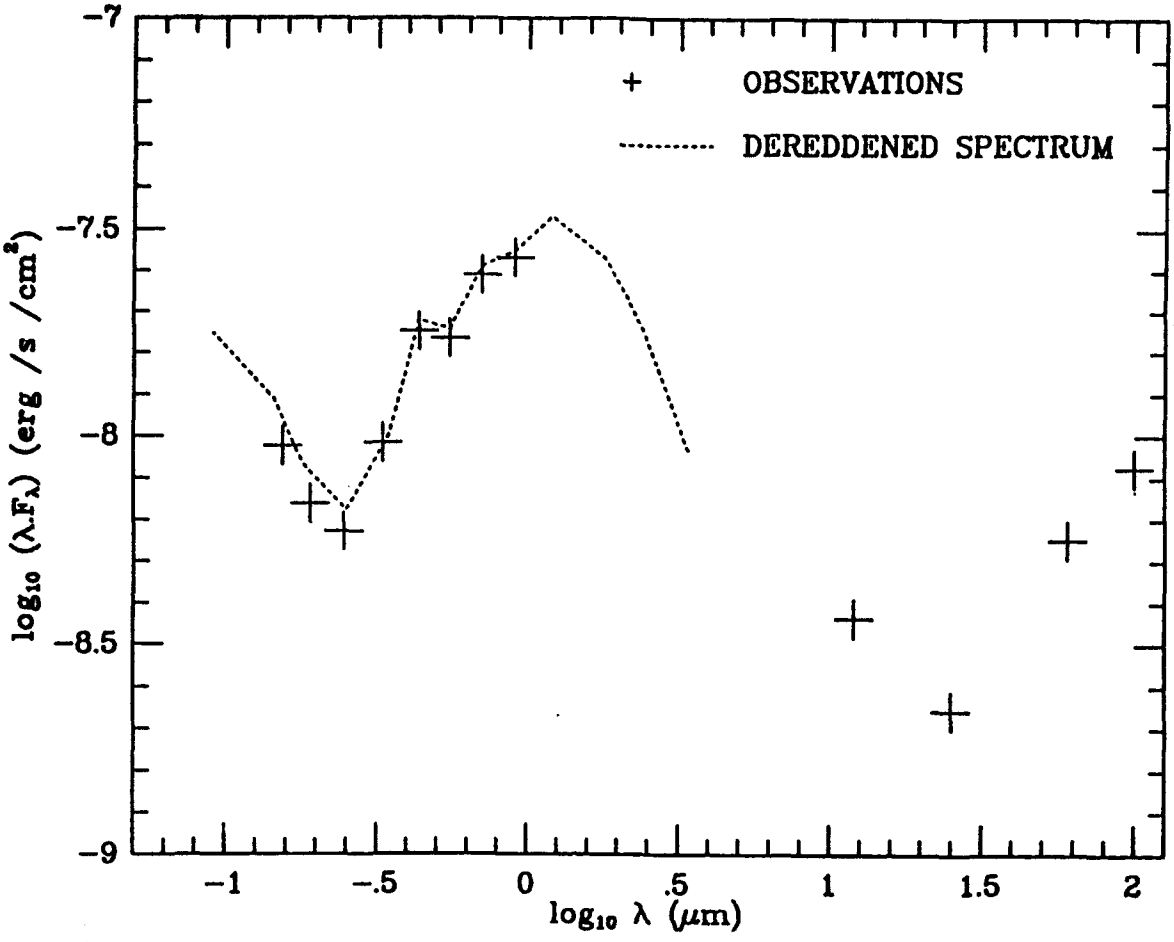

Figure 1. Spectral energy distribution of M101 from UV to far infrared wavelengths.

fact that observations at the various wavelengths were obtained with different sized apertures. This factor was based on extending an exponential disk at each wavelength to infinite radius.

The determination of the radial dependence of the infrared emission is complicated by the fact that the size of the galaxy (~10') is comparable to the resolution of the IRAS detectors (about 0.75'x4.5' at 12 and 25 micron, 1.5'x4.5' at 60 micron and 3'x5' at 100 micron) and because a number of giant HII regions are bright at these wavelengths. The following procedure was invoked to separate these two components. Data from scans which crossed the galaxy in the same direction were fitted to a model consisting of an axisymmetric exponential disk of amplitude I and scale length h convolved with the detector response; data from the vicinity of the HII regions were excluded. Fits were made in the scan direction at a number of different position angles and the results averaged. Table 2 lists the properties of the M101 disk.

Table 2. The M101 Disk

Wavelength (μm)	Amplitude (MJy/sr)	Scale Length (')	Scale Length (kpc)	Integrated Model Disk (D>>28')(Jy)
12	3.1	3.0±0.2	5.9±0.4	14
25	3.4	3.2±0.2	6.3±0.4	18
60	18	3.4±0.4	6.7±0.8	110
100	45	3.4±0.5	6.7±1.0	280
CO		3.6[1]		
Visual Light		2.2-2.6		

Notes: 1) Solomon *et al.* 1982.

Figure 2 shows a 25 micron map of M101 before and after subtraction of exponential disks. While the fitting procedure is not yet perfect, as evidenced by the negative parts of the maps, the procedure enables one to detect five of the major HII regions in the galaxy, N5447, N5455, N5461, N5462 and N5471. Even preliminary estimates of the brightnesses of the HII regions allow one to state that the emission from M101 is dominated its disk. The influence of the major optical HII regions is negligible at 12 and 25 micron and less than 20% of the total at 60 and 100 micron.

Overall Properties

M101 is similar to other spirals detected by IRAS with an infrared luminosity and 12/25 and 60/100 micron colors consistent with those of a galaxy with modest amounts of star formation (Helou, this conference). A number of authors have used the IR to blue luminosity ratio, defined as $\nu f_\nu(80)/\nu f_\nu(B)$ where $f_\nu(80)$ is the average of the 60 and 100 micron flux densities, as a measure of infrared activity. M101 has an IR/blue ratio of 0.4, similar to that inferred for our own galaxy and close to the median for spirals detected by IRAS (Soifer *et al.* 1984).

Origin of the Infrared Emission

M101 is an average spiral galaxy and it is therefore important to understand the nature of its infrared emission mechanism and to distinguish it from the more luminous infrared galaxies. We argue that much of the infrared emission from M101 originates in the neutral medium, and not in the ionized component.

First, the ratio of 12 to 25 micron flux densities (Table 3) implies a temperature of 200 K and, as shown by the scale lengths in Table 2, is roughly constant across the face of the galaxy. This emission accounts for approximately 25% of the 12-100 micron luminosity of the galaxy. The existence of large amounts of hot, 200 K, material outside of HII regions cannot be accounted for within the context of equilibrium heating of

grains in the interstellar radiation field of the galaxy. Further, the lack of a radial temperature gradient runs counter to the expectation that, for equilibrium heating of dust, the temperature in the disk should decrease as the radiation field falls off with increasing radius.

Table 3. M101 Colors

	M101 Disk	Galactic Cirrus
$\log(f_\nu(12)/f_\nu(25))$	-0.12	-0.2 to 0.1[1]
$\log(f_\nu(25)/f_\nu(60))$	-0.92	-0.65 ± 0.05[2]
$\log(f_\nu(60)/f_\nu(100))$	-0.34	-0.81 ± 0.02[2]

Notes: 1) Boulanger *et al.* 1985; 2) Weiland *et al.* 1986.

A solution to this problem may be found in the similarity of the 12/25 micron color of the M101 disk to that of the hot cirrus found within our own galaxy (Boulanger, Baud and van Albada 1985; Weiland *et al.* 1986). The warm Galactic cirrus has been attributed to small (<10 Angstrom) grains, possibly polyaromatic hydrocarbons (Puget, Leger and Boulanger 1985) transiently heated by the absorption of single UV photons. In this process the maximum temperature reached by a grain is independent of the intensity of the radiation field; the intensity of emergent spectrum, but not its shape, depends on the input intensity. We suggest that the existence of large amounts of 12 and 25 micron emission in the disk of M101 is due to the existence of such small, stochastically heated grains.

The poorer spatial resolution of the 60 and 100 micron maps makes it harder to separate the disk component from the HII regions. The 60/100 micron color of the disk is considerably hotter than that seen toward typical Galactic cirrus and may partially be due to unresolved HII regions. However, not all of the infrared emission can originate in HII regions. On the basis of a catalog of 21 cm continuum observations of HII regions in M101 and the integrated intensity of the galaxy at 2.8 cm (Klein and Emerson 1981), Viallefond (1986) has estimated that about 100 mJy of the 21 cm emission from M101 is thermal. From this one calculate that the infrared excess (IRE) of this disk exceeds 16, far higher than for typical HII regions with values of 5 (Myers *et al.* 1986). Such a high IRE suggests that predominantly non-ionizing photons, from A or later type stars and not from OB stars, dominate the heating of the disk.

References

Aaronson, M. Mould, J. and Huchra, J. 1980, *Ap. J.*, 237, 655.
Boulanger, F., Baud, B. and van Albada, T. 1985, *Astr. Ap.*, 144, L9.
Code, A.D. and Welch, G. A. 1982, *Ap. J.*, 256, 1.
Elmegreen, D. M. 1980, *Ap. J. (Suppl)*, 43, 37.
Helou, G., Soifer, B.T. and Rowan-Robinson, M. 1985, *Ap. J.*, 298, L7.
Klein, U. and Emerson, D.T. 1981, *Astron. and Astrop.*, 29, 94.

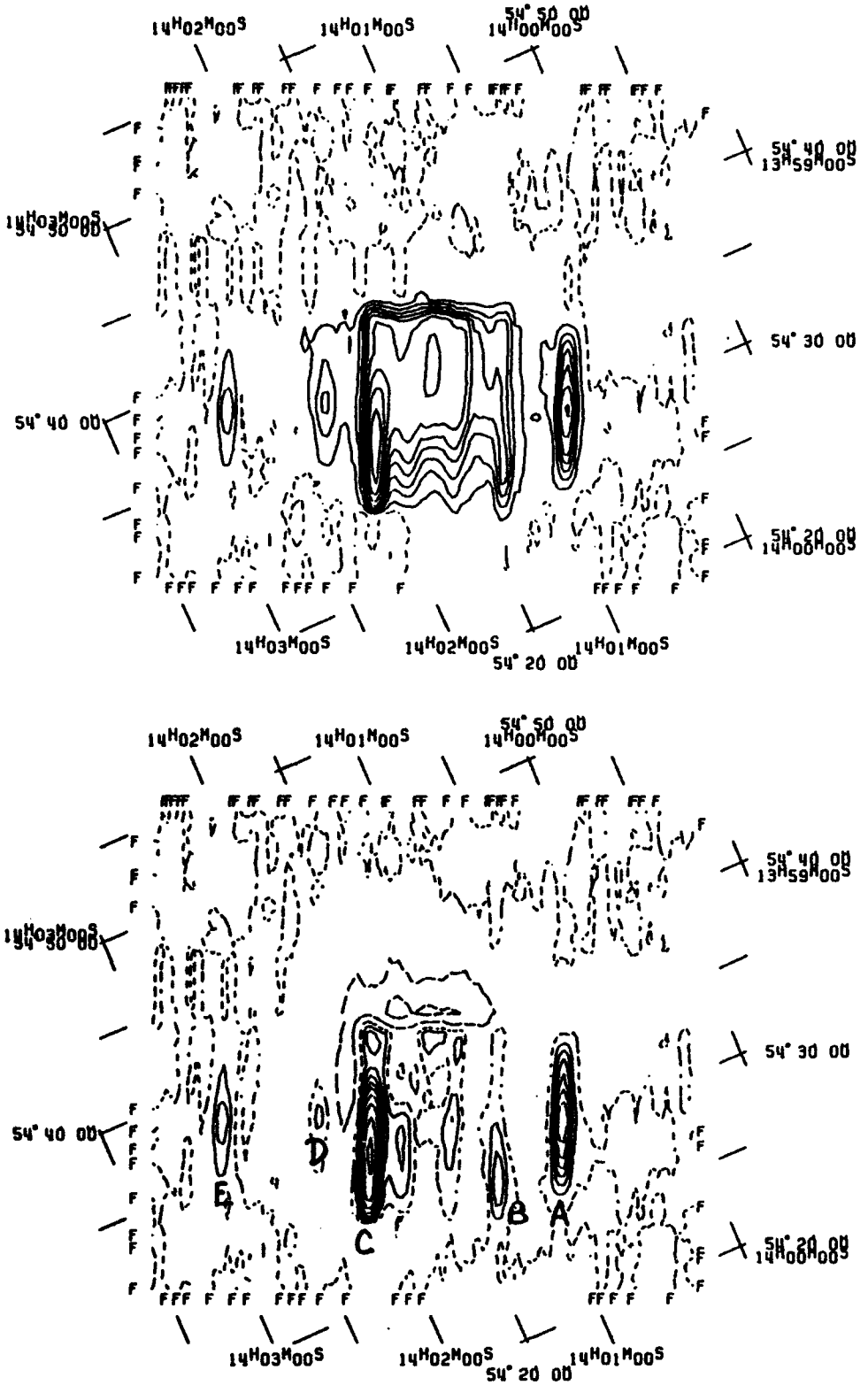

Figure 2: a) 25 micron map of M101; b) 25 micron map after subtraction of an exponential disk (dashed contours are negative). The HII regions N5447, N5455, N5461, N5462 and N5471 are marked with letters a-e.

Myers, P. C. Dame, T.M., Thaddeus, P., Cohen, R.S.
Silverberg, R.F., Dwek, E., and
Hauser, M.G. 1986, Ap.J., in press.
Okamura, S., Kanazawa,T., Kodaira, K. 1976, P.A.S.J.,28,329.
Puget, J.L., Leger, A. and Boulanger, F. 1985,
Astr. Ap., in press.
Rice et al. 1986, in preparation.
Soifer, B.T. et al. 1984, Ap. J., 278, L71.
Solomon, P. Barrett, J., Sanders, D.B. and
de Zafra, R. 1983, Ap.J. (Letters), 255, L99.
Viallefond, F. 1986, private communication.
Viallefond, F., Goss, W. M. and
Allen, R. J., 1981, Astr. Ap., 104,127.
Weiland, J.L., Blitz, L., Dwek, E., Hauser, M.G.,
Magnani, L. and Rickard, L.J. 1986 preprint.

EFFICIENT STAR FORMATION IN THE BRIGHT BAR OF M83

S.D. Lord, S.E. Strom, and J.S. Young

Department of Physics and Astronomy
University of Massachusetts
Amherst, MA 01003

ABSTRACT. We have detected the bright molecular bar in M83 standing out as a 100% enhancement of molecular emission with respect to the off-bar emission at the same radii. We compare the spatial variations in the star formation efficiency, as traced by Hα emission and the surface density of the interstellar gas, in M83 and M51. Both the central bar of M83 and the spiral arms of M51 are regions characterized by high massive star formation rates. For M83, we ascribe the fact that both the gas surface density and the star formation efficiency are high to the hydrodynamics of the central region.

1. INTRODUCTION

In recent years, detailed molecular studies of nearby disk galaxies have helped to identify the role played by the molecular cloud population in the presence of spiral density waves and central bars. The detection of molecular bars in optically barred and unbarred galaxies, such as IC342 (Lo et al. 1984), NGC 6946 (Ball et al. 1985), NGC 1530 (Solomon 1985), and possibly NGC 4548 (Kenney 1986), demonstrates the propensity of this phenomena to occur. Here we report the detection of a luminous molecular bar, extending 8 Kpc (assuming a distance of 8.9 Mpc) in the nearby spiral M83 (SAB) and examine the galaxy's star formation efficiency as traced by the Hα emission and gas surface density. We compare our results to a similar study in the galaxy M51, and contrast the efficiency of massive star formation in a bar and in spiral arms.

2. OBSERVATIONS

We have observed the grand design spiral galaxies M83 and M51 in the (J=1→0) transition of CO using the 13.7 m telescope of the Five College Radio Astronomy Observatory during 1984 to 1985. Emission was detected in 21 positions (HPBW = 45") for M83 and 57 positions for M51, with the observations extending out to a radius of 2.6' in each galaxy. The observed positions (spaced radially by 1 HPBW) and contours of integrated intensity are shown for M83 in Figure 1. We have compared the intensity of molecular emission in each aperture with Hα intensities obtained from the photometric database of Talbot, Jensen, and Dufour (1979). These data had been corrected for extinction by the authors using their detailed UBVR color results and the Whitford reddening law. Contours of Hα intensity are displayed in Figure 2, with the same spatial scale as Figure 1. We have used the initial mass function (IMF) of Jensen, Talbot, and Dufour (1981) to relate the Hα flux in each aperture to the star formation rate, and have converted the CO emission to an H_2 mass surface density (as per Dickman et al. 1986). Likewise, for M51, we have used the calibrated Hα data of Kennicutt (see van der Hulst and Kennicutt, this volume), corrected with their radial extinction estimate, to obtain the star formation rate in each aperture. A Saltpeter IMF was choosen in this case, because it has been found to consistently model the integrated colors of this galaxy (Kennicutt 1983). The

Carol J. Lonsdale Persson (Editor)
Star Formation in Galaxies

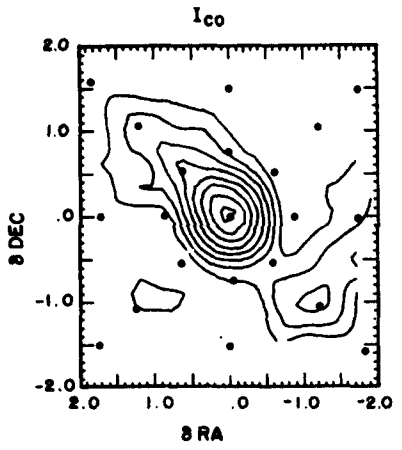

Figure 1. The CO integrated intensity in M83. Points marks the aperture positions separated 45" (1 HPBW) apart. The contours start at 15 K km s^{-1} and are separated by 5 K km s^{-1}.

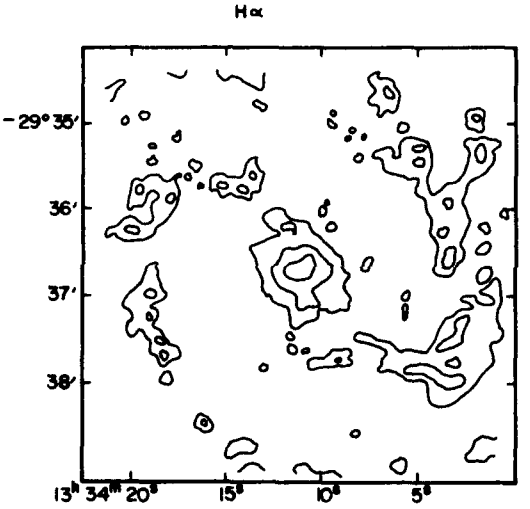

Figure 2. The H α flux in M83. The contour levels are 23.5, 22.0, and 20.5 mag arcsec^{-2}. (Adapted from de Vaucouleurs, et al. 1983).

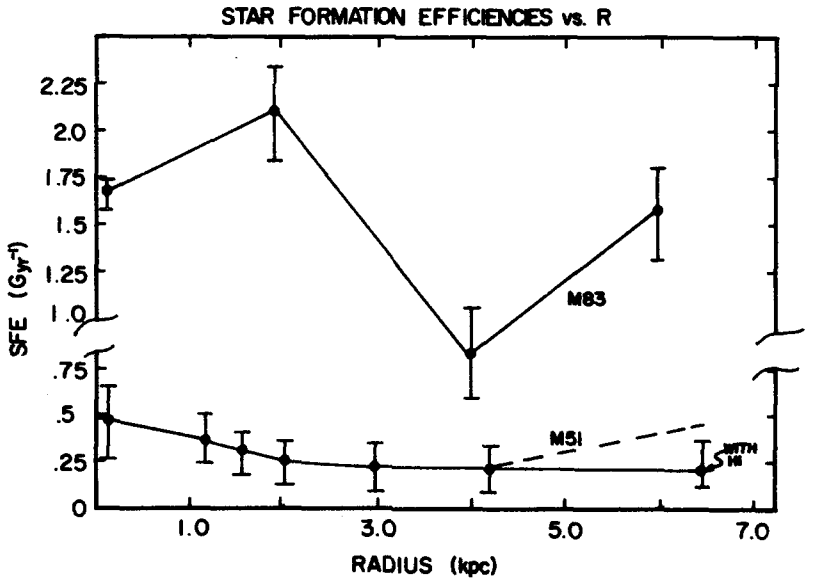

Figure 3. The star formation efficiency for M83 and M51 plotted as a function of galactic radius after azimuthal averages have been made. The vertical scale shows the SFE for all stellar types. Considering the relative freedom involved in choosing an IMF for each galaxy, we advise caution, and have placed a break in the axis. We do however conclude that the massive star formation efficiency in M83 is a factor of 4 higher than in M51.

star formation rates (SFRs) and star formation efficiencies (SFEs) have been calculated for each aperture. Here the SFE is defined as the ratio of the star formation rate in $M_\odot$ pc^{-2} Gyr^{-1} to the total surface density of the ISM, $\sigma(HI) + \sigma(H_2)$, in $M_\odot$ pc^{-2}. In this sense, the SFE may be thought of as measuring the reciprocal gas depletion time, measured in Gyr^{-1}, given the current rate of star formation and no gas recycling. The results are discussed in detail in Lord and Young (1986) for M51, and Lord (1986) for M83, with the major results given below.

3. RESULTS

In Figure 2 it can be seen that the HII regions in M83 delineate its central bar, the spiral arms, and the "cusp" regions where the inner arms connect to the bar (see also Rumstey and Kaufman 1983). The Hα brightness in this galaxy is very strong in comparison to other spiral galaxies, and about a factor of 10 higher than that of M51 at comparable radii. Likewise, the CO brightness in the barred inner region of M83 is strong (in molecular emission this galaxy is among the brightest spiral galaxies known) and the emission is seen to be clearly organized into a central bar (c.f. Sofue, this volume) as well as a region at the end of the bar in the southwest, displaced about 30" closer to the nucleus than the corresponding Hα feature (Figure 1). Dynamical information is provided by our observations. The molecular isovelocity contours show a weak S-shaped distortion in crossing the central bar, characteristic of oval orbits in the presence of a bar potential, and the velocity dispersions of the line profiles along the bar are found to be greater in general than those measured off-bar. The bar of M83 lies nearly colinear with the major axis, so our dispersion results are just the opposite of the situation usually encountered in unbarred disk galaxies, where the major axis profiles are the narrowest due to the minimal projection of non-circular motions into the line of sight. Our results for the M83 SFE calculations are presented as an azimuthal average in Figure 3, with the star formation along the bar dominating the results.

In M51 we find an extremely high point-to-point spatial correlation between the spiral pattern and regions exhibiting a high SFE. This high efficiency is manifested in the production of massive stars and HII regions in the absence of any correspondingly large excess in the gas surface density. At any given radius in this galaxy, the molecular surface density remains a constant in azimuth to within about 40% while the Hα intensity makes 200% departures from a mean value, if regions 45" (2.2 Kpc) in diameter are considered. However, if the Hα and CO emission are averaged azimuthally, the star formation efficiency is found to be a constant, SFE = 0.25 Gyr^{-1}, as function of radius, as shown in Figure 3.

Only in the region from R=1.5' to R=2.6' in M51 do we clearly see an enhancement in molecular emission (of 80%) when crossing the spiral pattern, as displayed in Figure 4. This is also the radius at which the HI surface density begins to become an appreciable fraction of the molecular density, with $\sigma(HI)/\sigma(H_2) = 0.2$, and increasing outward. The inclusion of the HI component in the SFE calculation serves to maintain a constant SFE, as shown in Figure 3. In M83 the HI contribution is negligible throughout the the area under consideration (Allen et al. 1986).

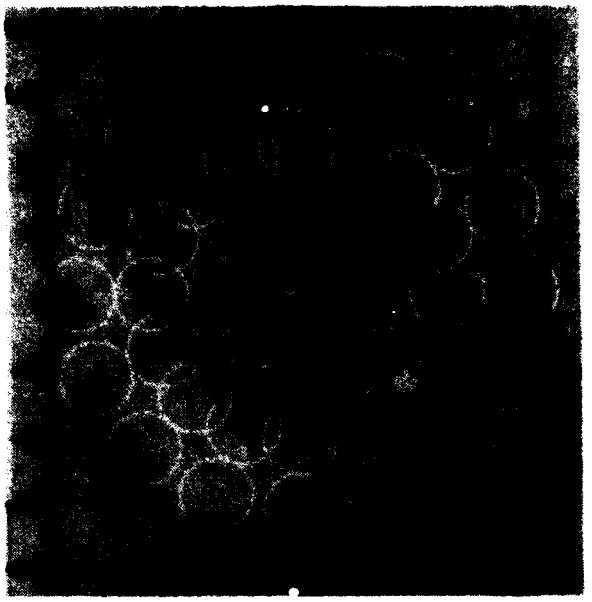

Figure 4a. Hα image of M51 showing the aperture positions (white) and the spiral pattern. The Hα emission was smoothed to the resolution of the CO observations and sampled at the same points for the analysis below.

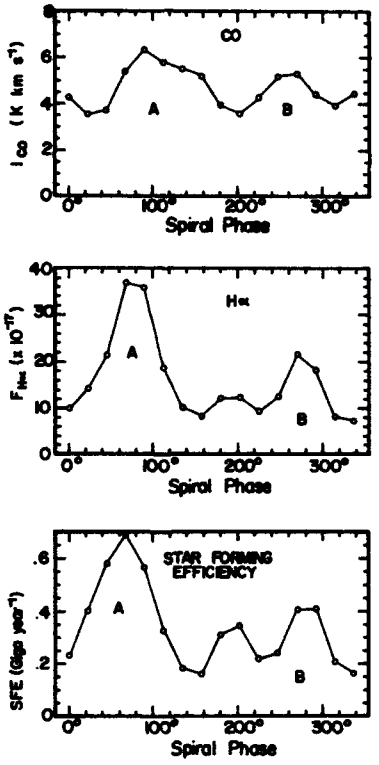

Figure 4b. CO emission, Hα emission, and SFE for the annulus 1.5' < R_{gal} < 2.6'. The data were interpolated to give intensity as a function of position angle relative to the spiral pattern in the plane of the galaxy, with arm crossings at 90° and 270°. The regions around the HII complexes A and B stand out in emission in both in Hα and CO.

4. DISCUSSION AND CONCLUSIONS

What causes the molecular cloud population to form a bar in M83? It is, most likely, the convergence of the oval streamlines in the gas motions thought characteristic of barred spirals and evidenced dynamically in spectroscopic studies. Of the hydrodynamic models for barred spirals we have considered, the model of Roberts et al. (1979), seems favored by these results. This model, incorporating a disk and spheroidal potential, manifests "shock focusing", where disk material from both inner and outer regions tends to converge at the ends of the central bar in hook shapes that connect with the spiral pattern. The convergence of gas streamlines can set up a shock front along the leading edge of the arm and bar. We think that the molecular material at the southwest end of the bar may have arrived there as a result of such focusing action.

In comparison to M83, M51 shows a constant SFE with radius in the disk, a high efficiency on the arms, and an overall lack of molecular spiral structure. The last result is in part an effect of the spatial resolution employed, since Rydbeck, et al. (this volume), with finer resolution, find 20% on-arm enhancements typical. Even so, the result still holds that the molecular cloud population is largely ubiquitous. The dominant portion of the molecular distribution is uniformly distributed in azimuth and monotonically falling-off in radius. It scarcely resembles the Hα distribution, even when the latter is smoothed to comparable resolution. We must therefore conclude that the principle action of the spiral density wave in this galaxy is not in gathering clouds, but triggering the star formation within them.

5. ACKNOWLEDGEMENTS

The FCRAO is operated with the support from the National Science Foundation under grant AST 82 12252 and with the permission of the Metropolitan District Commission, Commonwealth of Massachusetts. We wish to thank R. Dufour, M. Kaufman, R. Kennicutt, and L.J. Rickard for the generous loan of data sets, and R. Kennicutt for valuable advice.

REFERENCES

Allen, R.J. Atherton, P.D., and Tilanus, R.P.J. 1986, Nature, 319, 296.
Ball, R., Sargent, A.I., Scoville, N.Z., Lo, K.Y., and Scott, S.L. 1985, Ap.J. Lett., 298, L21.
de Vaucouleurs, G., Pence, W.D., and Davoust, E. 1983, Ap.J.Supp., 53, 17.
Dickman, R.L., Snell, R.L., and Schloerb, F.P. 1986, Ap.J., in press.
Jensen, E.B., Talbot, R.J., Jr. and Dufour, R.J., 1981, Ap.J., 243, 716.
Kenney, J. 1986, Personal Communication.
Kennicutt, R.C.,Jr. 1983, Ap.J., 272, 54.
Lo, K.Y., Berge, G.L., Claussen, M.J., Heiligman, G.M., Leighton, R.B., Masson, C.R., Moffet, A.T., Phillips, T.G., Sargent, A.I., Scott, S.L., Wannier, P.G., Woody, D.P. 1984, Ap.J., 282, L59.
Lord, S.D. and Young, J.S. 1986, in preparation.
Lord, S.D. 1986, in preparation.
Roberts, W.W., Huntley, J.M., and van Albada, G.D. 1979, Ap.J., 233, 67.
Rumstay, K.S. and Kaufman, M. 1983, Ap.J., 274, 611.
Solomon, P. 1985, Personal communication.
Talbot, R.J.,Jr., Jensen, E.B., and Dufour, R.J. 1979, Ap.J., 229, 91.

LARGE SCALE DISSOCIATION OF MOLECULAR GAS IN THE SPIRAL ARMS OF M51

R.P.J. Tilanus[*#] and R.J. Allen[#]

[#]Department of Astronomy
University of Illinois
1011 W. Springfield Ave.
Urbana, Il 61801
U.S.A.

[*](on leave from)
Kapteyn Astronomical Institute
University of Groningen
Postbus 800, 9700 AV Groningen
The Netherlands

Abstract. In this paper we compare the distribution of the atomic and ionized hydrogen along the inner spiral arms of M51. As is the case in M83, the location of both these phases of the interstellar medium with respect to the major dust lanes suggests that molecular hydrogen is dissociated on kpc scales in active star-forming regions, and that this dissociation process may strongly affect the observed morphology of atomic hydrogen in spiral arms.

1. INTRODUCTION

Since the introduction of the notion of spiral density-waves by C.C. Lin and F.H. Shu in the mid-1960's the gaseous spiral arms observed in galaxies have been explained as shocked gas arising from the non-linear response of the gaseous disk to a relatively weak density-wave disturbance in the gravitational field of the old stellar disk (summarized e.g. in Shu 1982). In this picture the shock is thought either to stimulate the formation of giant cloud complexes or to cause the collapse of pre-existing clouds, eventually resulting in the formation of new stars downstream from the the shock. Young, bright stars and giant HII complexes are distributed like 'beads on a string' along the outer edges of spiral arms. The position of the shock front is outlined by the dust lanes, which thus represent the locus of highest (total) gas density. However, in several cases, e.g. M81 (Visser 1980) and M83 (Allen et al. 1986), the highest density of the atomic gas is observed to be shifted downstream with respect to dust lanes. In the case of M83 the shift puts the atomic gas along the same locus as the HII complexes. Visser has shown that such a shift could arise from beam-smoothing, but we have ruled out this possibility in the case of M83 (Allen et al. 1986). We suggest that, since no atomic and ionized gas is observed at the position of the dust lane, the interstellar gas is apparently mostly molecular there and remains molecular for some time downstream of the shock. After the formation of sufficiently hot stars the molecular gas is dissociated giving rise to the observed arm of atomic gas, or ionized yielding giant HII complexes. In this scenario the correspondence between the ridge of highest HI density and the 'string' of HII regions is thus explained quite naturally.

Carol J. Lonsdale Persson (Editor)
Star Formation in Galaxies

We have emphasized however that the region studied in M83 is exceptional in that the displacements described are very clear. Our interpretation of this fact is that, for this region, the density-wave streaming is well-ordered enough to allow the time sequence of star formation to be stretched out in space. Since such large-scale ordered motions have been identified previously in M51 (Segalovitz 1976), we have obtained high resolution HI and Hα observations of this galaxy.

2. OBSERVATIONS

High resolution HI observations of M51 were carried out using the Westerbork Synthesis Radio Telescope in a 2 x 12 hrs. observation. The data have been Hanning smoothed resulting in a resolution of 16.5 km s^{-1}, the 63 channels spanning a total range in velocity of 520 km s^{-1} centered on the systemic velocity of 440 km s^{-1}. The spatial resolution is 12" x 18" (α x δ). The data showed some moderate phase errors resulting in extra grating rings at 10', and we are still in the process of removing these errors. The inner parts presented appear to be unaffected by these problems, except possibly for a region close to the nucleus. The continuum has been formed by averaging the channels free from line emission. Subsequently the continuum-subtracted line channels have been added using a cutoff of 3σ. The resulting total HI map is shown in Figure 1, with the contours representing -4, 4, 8, 14, and 20 mJy/beam (4 mJy/beam $\simeq$ 3σ; for this resolution, 1 mJy/beam $\simeq$ 4.6 x 10^{19} atoms/cm^2 along the line of sight through M51).

Hα observations were obtained using the TAURUS imaging Fabry-Pérot spectrometer (Atherton et al. 1982) attached to the Isaac Newton telescope on La Palma. The total velocity range observed is 400 km s^{-1} over 72 channels, the resulting resolution in velocity is 15 km s^{-1}, sampling slightly less than 3 channels per resolution element. Again the continuum was formed by averaging line-free channels and a total Hα map was obtained adding the continuum-subtracted line channels using a cutoff of 3σ. The distribution of the Hα emission in the inner region of M51 is shown in Figure 2, where the contours are -250, 250, 500, 1000, 2000, 4000, and 6250 in units which scale linearly with the number of photons observed. This map and a velocity integrated map of the original cube showing also the continuum sources are in excellent agreement with broad-band Hα observations of M51 by Kennicutt (1986, private communication). We have used his observations and positions of reference sources from Mathewson et al. (1972) to obtain a position calibration of the TAURUS observation accurate to approximately 1". Figure 3 shows the Hα distribution of Figure 2 smoothed to the resolution of the HI observation (Figure 1).
The thick lines in Figures 1,2 and 3 represent the major dust lanes along the inner spiral arms of M51, obtained from overlaying a large scale optical photograph with the Hα observations.
We emphasize that a more thorough analysis of both the Hα and HI data is in progress, using more advanced methods of treating the data.

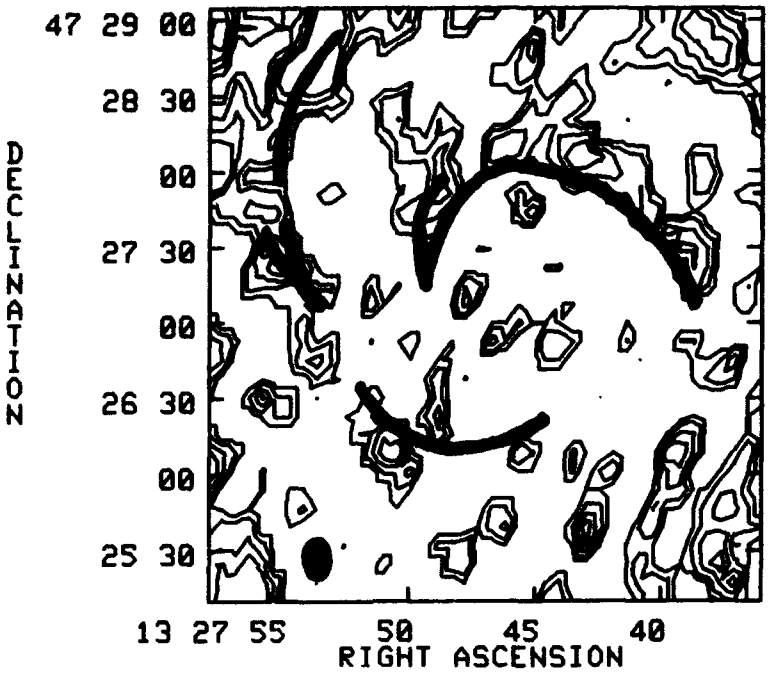

Fig. 1 HI density distribution in the central region of M51. contours: -4, 4 (=3σ), 8, 14, and 20 mJy/beam. The beam (12"x18") is shown in the bottom left corner. The thick contours indicate the main dust lanes.

3. DISCUSSION

Although the separation is not as pronounced as in M83, comparing Figure 1 with Figures 2 and 3 shows that the ridge of highest HI density is more closely coincident with the Hα distribution than with the dust lanes, in particular along the inner northern arm. This suggests that in the inner parts of M51, as in M83, the interstellar gas is molecular at the position of the shock and remains molecular downstream of the shock until the newly formed stars dissociate or ionize the molecular gas on a kpc scale. Furthermore, our observations indicate that this dissociation process may significantly affect the HI morphology in the inner regions of galaxies and that the HI clouds need not always have key role as precursors of molecular clouds.

More so than in M83, the observed distribution of the ionized gas is likely to be affected by obscuration effects. High resolution radio continuum observations at several frequencies have been obtained which should be free of obscuration, allowing a precise indication of the location of both the thermal (HII regions) and the non-thermal (shock region) radio continuum (van der Hulst 1986, private communication).

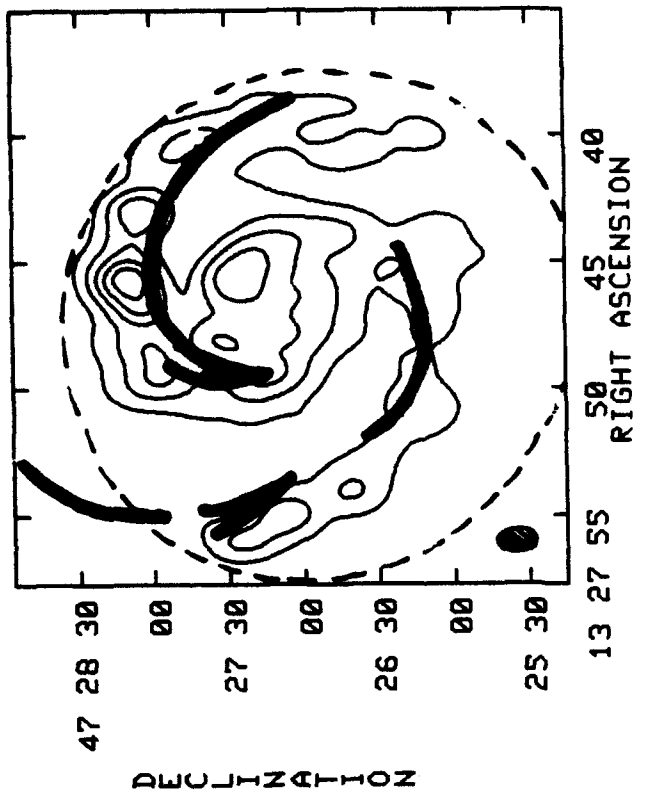

Fig. 3 The Hα emission of fig. 2 smoothed to a resolution of the HI distribution shown in fig. 1. contours: 45, 135, 270, 450, 675 units. The beam (12"x18") is shown in the bottom left corner. The thick contours indicate the main dust lanes, the broken contour shows the field of view.

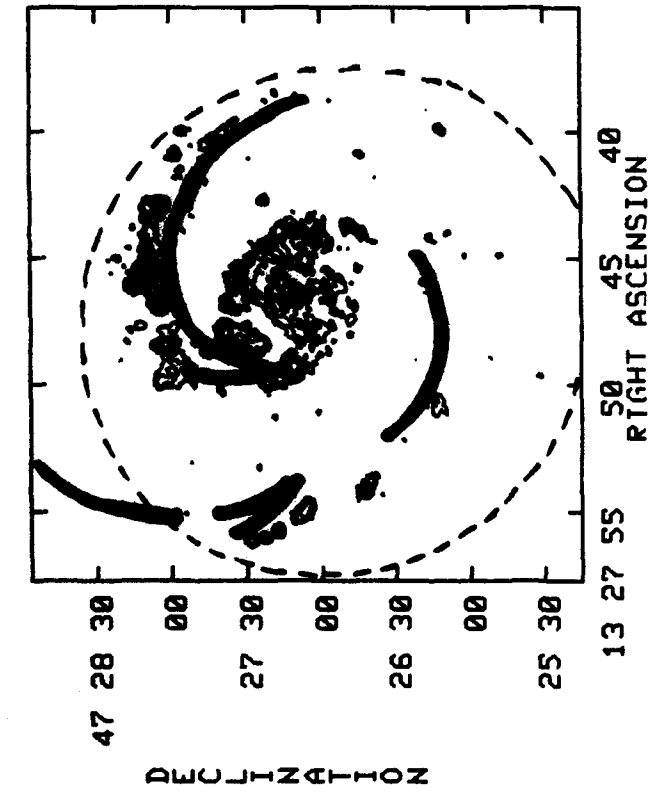

Fig. 2 Hα emission in the central region of M51 (continuum subtr.). contours: -250, 250, 500, 1000, 2000 4000, 6250 (units scale linearly with the number of photons detected). The thick contours indicate the main dust lanes, the broken contour shows the field of view.

Acknovledgements. We would like to thank F. (K-Y) Lo, J.M. van der Hulst and R. Sancisi for usefull discussions, R. Kennicutt for the use of his Hα plates of M51 and F. Lo for providing us with an excellent optical photograph of the central region of M51. P.D. Atherton and K. Taylor generously provided expertise in obtaining the TAURUS data. The Westerbork Radio Observatory is operated by the Netherlands Foundation for Radio Astronomy with the financial support of the Netherlands Organization for the Advancement of Pure Research (Z.W.O.). R.P.J. Tilanus is financially supported by Z.W.O.

REFERENCES

Allen, R.J., Atherton, P.D., Tilanus, R.P.J. 1986, Nature 319, 296

Atherton, P.D., Taylor, K., Pike, C.D., Harmer, C.F.W., Parker, N.M., Hook, R.N. 1982, MNRAS 201, 661-696

Mathewson, D.S., van der Kruit, P.C., Brouw, W.N. 1972, Astr. Ap. 17, 468-486

Segalovitz, A. 1976, Astr. Ap. 52, 167-174

Shu, F.H. 1982, The Physical Universe (University Science Books, Mill Valley, California), p. 281-284

Visser, H.C.D. 1980, Astr. Ap. 88, 159-174

STRUCTURE AND KINEMATICS OF THE MOLECULAR SPIRAL ARMS IN M51

G. Rydbeck, Å. Hjalmarson, L.E.B. Johansson,
O.E.H. Rydbeck and T. Wiklind
Onsala Space Observatory
S-439 00 Onsala, Sweden

Mapping of the CO(1-0) emission from the spiral galaxy M51 has been made with the Onsala 20 m antenna (HPBW≈33"). The observations show that the emission is considerably enhanced - above the background disk distribution - in spiral arms which appear to originate as intense ridges of emission about 1 kpc from the nucleus (assuming a distance of 9.6 kpc). Inside this region there is virtually no emission (Rydbeck et al., 1985b; cf. also the FIR results by Lester et al., 1986). Arm-interarm ratios (defined as in Rydbeck et al., 1985b) along the observed arm (arm r,p in Tully, 1974, Fig. 10), vary between 1.1 and 2.5, with an average of about 1.4. The beam deconvolved arm-interarm contrasts are likely to be higher, however. The excess emission along the arm is broken up into large scale patches of up to a few kpc in size. This suggests that the "on-arm" molecular clouds are assembled into giant complexes with hydrogen masses estimated to be up to 10^8 $M_\odot$, using the Young and Scoville (1982) "empirical" conversion factor of integrated CO to H_2 mass. Cloud parameters could be very different in this case, however, making the determination rather uncertain.

One of the main objectives for the 1986 observations was to study the variations of the tangential velocity component of molecular gas across a spiral arm. The radial velocity component was studied in Rydbeck et al. (1985a,b) where it was found to have a velocity shift similar to that predicted by density wave theory. Note that tangential and radial velocities are observed along the major and minor axis, respectively.

The present (1986) observations of the inner southern spiral arm of M51 (containing the southern part of the major axis, its position angle being -10°) show that also the tangential velocity component behaves in a way which conforms with density wave theory. As one crosses the spiral arm radially outwards (see Figure) the tangential velocity first displays a gradual decrease followed by a sudden increase the velocity slowly decreases again. As was found for the radial velocity component the sudden change in tangential velocity is rather large (50-70 km s^{-1}, depending on the inclination) compared to what is usually expected from density wave models (≈30 km s^{-1}, Roberts and Hausman, 1984, cf. also numerical simulations of tidal interactions by Sundelius et al., 1986). It thus appears that the density wave in M51 is comparatively strong.

Looking more closely at the rapid velocity change in the position-velocity maps, we find that going radially outwards this velocity shift, in most cases appears as a new component spatially overlapping the old one, while in general there appear to be less clouds with "intermediate" velocities. In some cases, however, e.g. in crossing the largest cloud complex (around position 8,8 in Rydbeck et al., 1985a, or near position p in Tully, 1974, Fig. 10), the clouds appear to evenly fill the whole velocity gap (c.f. Figure 12a in Rydbeck et al., 1985b), but still overlap spatially.

Carol J. Lonsdale Persson (Editor)
Star Formation in Galaxies

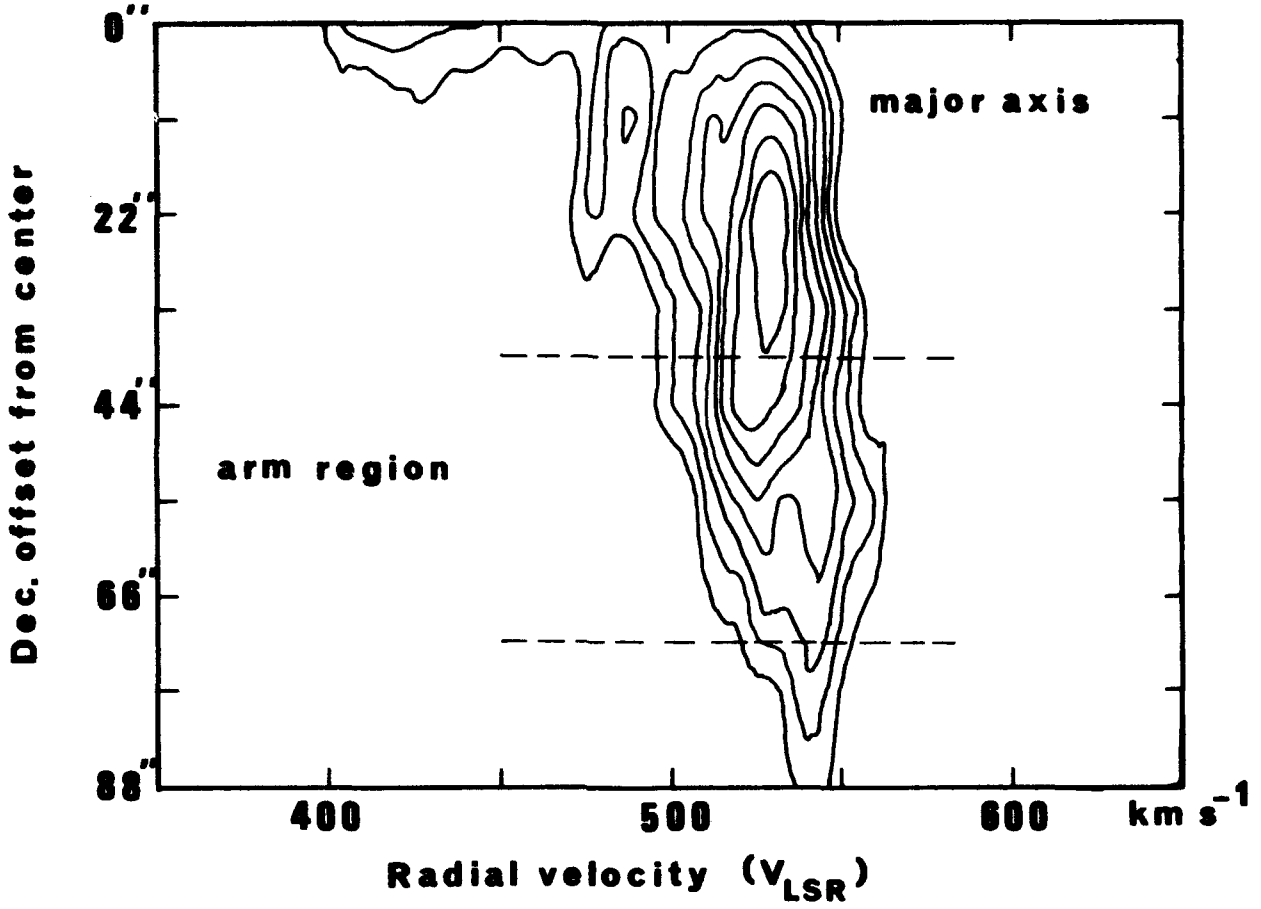

From the structure of our position-velocity maps it seems that these results cannot be explained by beam or sidelobe effects. Higher resolution maps of some of these arm-regions would be highly desirable. Assuming that our interpretation above is correct it seems that fairly violent cloud-cloud collisions may occur in the arm regions. The occurance of high velocity cloud-cloud collisions may be important to the formation of massive stars in the spiral arms.

We have compared the molecular arms with the Hα ionized gas arms of Tully (1974) and find that the ionized gas appears to have its maximum intensity slightly outside the molecular arm. This apparent phase shift may be due to extinction by dust. However, the molecular gas seems to have a systematically lower velocity than the ionized gas (Rydbeck et al., 1985b, Fig. 9), so a correlation between the arm maxima for the molecular and the ionized gas is not obvious, though the most intense non-central Hα emission does occur on the north-eastern molecular cloud complex.

Onsala Space Observatory is operated by Chalmers University of Technology with financial support from the Swedish Natural Science Research Council (NFR).

REFERENCES

Lester, D.F., Harvey, P.M. and Joy, M.: 1986, Astrophys. J., 302, 280
Roberts, W.W. and Hausman, M.A.: 1984, Astrophys. J., 277, 744
Rydbeck, G., Hjalmarson, Å., Johansson, L.E.B. and Rydbeck, O.E.H.: 1985a, in *U.R.S.I. International Symposium on Millimeter and Submillimeter Wave Radio Astronomy*, Granada, Spain, p. 219.
Rydbeck, G., Hjalmarson, Å. and Rydbeck, O.E.H.: 1985b, Astron. Astrophys., 144, 282.
Sundelius, B., Thomasson, M., Valtonen, M.J. and Byrd, G.G.: 1986, Astron. Astrophys., submitted.
Tully, R.B.: 1974, Astrophys. J. Suppl., 27, 449.
Young, J.S. and Scoville, N.Z.: 1982, Astrophys. J., 258, 467.

MODELLING THE *IRAS* COLORS OF GALAXIES

George Helou
I P A C, California Institute of Technology

ABSTRACT: A physical interpretation is proposed for the color-color diagram of galaxies which are powered only by star formation. The colors of each galaxy result from the combination of two components: cirrus-like emission from the neutral disk, and warmer emission from regions directly involved in on-going star formation. This approach to modelling the emission is based on dust properties, but independent evidence for it is found in the relation between the color sequence and the luminosity sequence. Implications of data and interpretation are discussed and possible tests mentioned for the model.

1. INTRODUCTION

While still unfolding, the contribution of *IRAS* to extragalactic astronomy has already attained remarkable proportions. Perhaps the most dramatic quantitative expression of this contribution has been the staggering increase in the number of objects accessible to study: from fewer than a hundred in the pre-*IRAS* era to about 20,000 detections in the Point Source Catalog (Helou 1986a), and the promise of at least another 10,000 sources at the completion of the Faint Source Survey (which will average the individual detector output from all survey scans before searching for detections). Even though the spectral coverage of *IRAS* is limited to four bands (12, 25, 60 and 100 μm), and most galaxies are detected in only two of these bands (60 and 100 μm), it is the large number of objects that both demands and makes possible a detailed interpretation of the origin of the infrared flux. The starting hypothesis, predating *IRAS* (Wynn-Williams 1982), that needs improvement is that far-infrared emission is proportional to the rate of formation of massive young stars in the system. Rowan-Robinson (in this volume, hereafter RR) reviews several attempts at an improved interpretation, all of which try to decompose a galaxy's *IRAS* emission into physically distinct components.

The present contribution summarizes (§2) the model presented in Helou 1986b (hereafter H86), and addresses in some detail (§3) two specific aspects of that model, namely the assumption of small optical depths in the infrared, and luminosity constraints on the model. Implications and tests are reviewed briefly in §4. In what follows objects whose emission is dominated or affected by a Seyfert or quasar-like nucleus are excluded from the discussion, so the mid- and far-infrared emission from all systems considered is mostly due to thermal radiation from interstellar dust grains heated by starlight.

2. MODEL SUMMARY

A scatter diagram of $R(60/100)=f_\nu(60\mu m)/f_\nu(100\mu m)$ *vs* $R(12/25)=f_\nu(12\mu m)/f_\nu(25\mu m)$ shows "normal galaxies" spreading out along a band such that R(12/25) and R(60/100) are *anti-correlated* (Figure 1 of H86 or Figure 9 of RR). While R(12/25) increases along the band, apparently signalling hotter dust, R(60/100) decreases, signalling cooler dust! The resolution to this paradox is found in the properties of the dust rather than in those of the galaxies.

Carol J. Lonsdale Persson (Editor)
Star Formation in Galaxies

In part as a result of the *IRAS* data, it is now recognized that realistic models of interstellar dust must include a population of very small grains (Beichman 1987), extending the size distribution into the range of polycyclic aromatic hydrocarbons, *i.e.* a few Å. As such a mixture of dust is heated by increasingly intense radiation fields (Désert 1986), the *IRAS* colors of its emission trace out a curve like the one labelled D in Figure 2 of H86, or Figure 9 of RR. The shape of that curve is dictated by the presence of very small grains and by the emission features of polycyclic aromatic hydrocarbons at 7.7, 8.6 and 11.3 μm (Puget, Léger and Boulanger 1985), and reflects in particular the transition from the dominance of temperature fluctuations at low intensity of heating flux (Draine and Anderson 1985) to dominance by single temperature emission from grains in equilibrium at high intensity. As can be seen in Désert (1986), the smallest grains transiently heated to very high temperatures emit with a spectrum extending down to a few μm, and with an intensity scaling roughly linearly with the intensity of heating radiation. This emission dominates at low heating intensities, i.e. for cirrus, at the lower end of curve D. As the heating increases, larger grains reach higher equilibrium temperatures, and their blackbody spectrum starts moving into the *IRAS* bands, until it dominates and determines the colors at the uppper end of curve D.

Since the emission from any galaxy is a mixture of components all of which lie on curve D, galaxies are expected to fill out a region of the color–color plane whose upper envelope is the "heating curve" D. Rather than assume arbitrary mixing between any number of points on the heating curve to generate galaxy colors, H86 proposes a simple model with two components: (1) $C(\nu)$, cirrus–like emission whose colors are constant from one galaxy to the next, typified by emission from the neutral interstellar medium in the solar neighbourhood, and (2) $A(\nu)$, emission directly associated with active star formation, especially from dust within HII regions and their immediate surroundings, such as outer layers of molecular clouds. This second component $A(\nu)$ is assumed to have variable colors: if the galaxy is forming stars mostly in high density regions, the dust exposed to high heating intensities will place $A(\nu)$ at the upper left hand side of curve D. If on the other hand the majority of HII regions in a galaxy are mature, extended low density objects, then the colors of the active component will place it lower on that curve. Thus the model relates the infrared colors of a galaxy to two physical parameters, the ratio between active region and cirrus emission, and the effective gas density in regions of active star formation.

3. MODEL DISCUSSION

The heating curve D is of course a function of properties and size distribution of the dust grains, which is a serious limitation to the accuracy to which it can be specified. Its over–all character however is quite unlikely to change. A basic assumption in using Désert's (1986) calculations is that optical depths *in the infrared* are never large enough over so large a fraction of the emitting medium that infrared colors are affected. Burstein and Lebofsky (1986) have found evidence suggesting that the disks of galaxies are optically thick in the infrared, but Persson, Rice and Bothun (1987) show data suggesting otherwise. The assumption that most galaxies are optically thin in the infrared is supported in the Milky Way, where the 12 μm extinction in the direction of the Galactic center is only about one magnitude, low enough to allow detection of 12 μm sources in the Galactic nucleus and beyond, without any patchiness in their projected distribution (Habing *et al.* 1985). That assumption should therefore hold in a galaxy whose interstellar medium mass is less than a few times the corresponding mass in the Milky Way. It may break

down in a few cases, namely those with very massive *and* dense concentrations of gas and dust, e.g. systems containing mega-masers (Baan and Haschick 1984).

In defining the components in this model, the approach is phenomenological in essence. There are clearly many possible choices for emission components (see RR), and no obvious way to decide where to place them in the color-color diagram in the absence of "perfect" dust models. One additional constraint however results from the luminosity sequence associated with the galaxy distribution in the color-color diagram. Total infrared luminosity and especially infrared to blue ratio increase substantially from the lower right hand end to the upper left hand end of the galaxy band. For instance, in the sample used in H86 the median value of $f_\nu(25\mu m)/D^2$ (where D in the optical diameter of the galaxy) increases by almost an order of magnitude when R(60/100) goes from 0.37 to 0.65. This trend can become a constraint on the emission models: Suppose a galaxy's spectrum is being synthesized by adding to the cirrus spectrum (component *C*) a gradually increasing contribution from a component *A* whose colors place it above and to the left of the observed galaxy band. Then the associated increase in the amplitude of the synthesized spectrum can be interpreted as the luminosity trend and constrained to be of the appropriate amount to agree with the observations. It turns out that the large increase in infrared luminosity (scaled to the size of the system) from one end of the band to the other forces a choice of components whose colors fall basically at the boundary of the galaxy distribution. This argument for the general placement of curve D is completely independent of the curve's physical justification above.

4. IMPLICATIONS

The most significant implication of the observed color-color diagram is in demonstrating that emission from some galaxies is dominated by cirrus, and from others by recent star formation. The model proposed in H86 quantifies the relation between far infrared emission and the recent star formation rate in a galaxy, with the unavoidable conclusion that the number of young stars in a galaxy is not simply proportional to the infrared luminosity. This proportionality holds for many galaxies (*e.g.* star-burst objects), but fails by uncertain and varying amounts for the others. Other implications of the model can be used as potential tests:

(i) In the *IRAS* color-color diagram, the model expects the colors of HII regions to place them near curve D. Unfortunately, the relevant data are not yet available, mostly because of difficulties in extracting HII regions in the *IRAS* data from the surrounding background (Pérault 1986).

(ii) Another prediction is that the active component should correlate with tracers of recent star formation such as thermal radio or Hα emission, and should do so better than the total infrared emission. A first investigation (Persson and Helou 1987) has shown encouraging results, even though using a more rudimentary model which keeps the colors of both active and cirrus components fixed.

(iii) An indirect test related to selection effects is suggested by the fact that for any reasonable choice of curve D, the model expects more galaxies to appear just below the band which is now filled out. Since the galaxies shown on the color-color diagram were chosen to be detected in four bands *and* unresolved by *IRAS*, they are biassed towards high infrared luminosity and high surface brightness. Optically selected galaxy samples may provide indirect confirmation for the model if they tend to fill the area just below the band in the color-color plane.

I would like to thank Chas Beichman for a critical reading of this manuscript. This work was supported as part of the *IRAS* Extended Mission Program by the Jet Propulsion Laboratory (JPL), California Institute of Technology, under contract with the National Aeronautics and Space Administration.

REFERENCES

Baan, W. A., and Haschick, A. D. 1984, Ap. J., 279, 541.

Beichman, C. A. 1987, *The IRAS View of the Galaxy and the Solar System*, Ann. Rev. Astron. Ap., in press.

Burstein, D., and Lebofsky, M. J. 1986, Ap. J., 301, 683.

Désert, F. X. 1986, in Light on Dark Matter, proceedings of the First IRAS Conference held in Noordwijk, 10–14 June 1985, ed. F. P. Israel. (Dordrecht: Reidel), p. 213.

Draine, B. T., and Anderson, N. 1985, Ap. J., 292, 494.

Habing, H. J., Olnon, F. M., Chester, T., Gillett, F., Rowan-Robinson, M., and Neugebauer, G. 1985, Astr. Ap., 152, L1.

Helou, G. 1986a, in Star-Forming Dwarf Galaxies and Related Objects, proceedings of the Workshop held in Paris, 1–3 July 1985, ed. Kunth, D., Thuan, T. X., and Tran Thanh Van, J. (Gif-sur-Yvette: Editions Frontières), p. 319.

Helou, G. 1986b, Ap. J. (Letters), 311, in press.

Pérault, M. 1986, private communication.

Persson, C. J., and Helou, G. 1987, Ap. J., in press.

Persson, C. J., Rice, W. L., and Bothun, G. D. 1987, *Characteristics of UGC Galaxies Detected by IRAS*, these proceedings.

Puget, J. L., Léger, A., and Boulanger, F. 1985, Astron. Ap., 142, L19.

Rowan-Robinson, M. 1987, *Models for Infrared Emission from IRAS Galaxies*, these proceedings.

Wynn-Williams, C. G. 1982, Ann. Rev. Astr. Ap., 20, 587.

A SIMPLE TWO-COMPONENT MODEL FOR THE FAR-INFRARED EMISSION FROM GALAXIES

T. de Jong and K. Brink
Astronomical Institute "Anton Pannekoek", University of Amsterdam
Roetersstraat 15, 1018 WB Amsterdam, The Netherlands

ABSTRACT. We have constructed a simple model to calculate the far-infrared emission of galaxies made up of a disk component containing cool dust heated by the general interstellar radiation field and of a molecular cloud component containing warm dust heated by recently formed massive stars. This model is fitted to the optical and far-infrared data of 120 Shapley-Ames galaxies and of 20 optically studied mini-survey galaxies, resulting in the determination of blue face-on extinctions and of the total luminosities of recently born massive stars and of disk stars. The ratio of these two luminosities is a more reliable star formation activity index than the previously often used ratio L_{IR}/L_B. The results show that infrared selected galaxies are on the average almost three times more dusty than optically selected ones. Only about 10% of the mini-survey galaxies exhibits strongly enhanced star formation.

1. INTRODUCTION

A large fraction of the energy emitted by recently formed massive stars is reradiated in the far-infrared by dust grains in molecular clouds - the dominant site of massive star formation in a galaxy. This makes the infrared by far the most suitable wavelength range to study the energetics of star formation and to derive global star formation rates in galaxies.

However there are additional sources of infrared radiation in a galaxy that complicate the picture. Dust particles in the general interstellar medium, predominantly heated by much older field stars, also contribute to the total infrared emission. This dust is probably cooler than the dust in molecular clouds (cf. Mezger et al. 1982, de Jong et al. 1984). Furthermore, hot dust has been shown to be present in the nuclei of active galaxies (de Grijp et al. 1985).

If infrared observations of galaxies with high spatial resolution would be available the different infrared components could be separated directly. However, because of the large detector sizes (typically several arcminutes, cf. Neugebauer et al. 1984) the IRAS data, on which our study will be based, provide only total energy information.

Thus to study star formation in galaxies the observed infrared emission has to be decomposed into several components. In this paper we present some preliminary results of fitting simple two-component models to the IRAS 60 and 100 μm fluxes of about 140 galaxies.

Carol J. Lonsdale Persson (Editor)
Star Formation in Galaxies

2. THE MODEL

The purpose of our model calculation is to fit the observed 60 and 100 μm fluxes and the B_T magnitude of a galaxy. In addition to these three observables the model also makes use of the observed galaxy inclination (or equivalently the axial ratio b/a).

First we fit two infrared components to the observed infrared spectral energy distribution. To do so we assign a dust temperature T_w to the warm dust in molecular clouds and T_c to the cool dust in the general interstellar medium (the disk component). We further assume that the dust emissivity is proportional to λ^{-1}. This fit results in 60 and 100 μm fluxes for each component, that add up to the observed fluxes. We then calculate the total luminosity of each component, L_w and L_c, by integrating over all wavelengths.

Next we calculate the total luminosity of recently formed massive stars, L_2, by assuming that half of the luminosity of these stars is completely converted to infrared radiation inside molecular clouds, so that $L_2 = 2L_w$. The other half is emitted by stars that have moved away from the molecular clouds in which they were born within their lifetime. The 50% estimate above has been derived for stars born with a Salpeter initial mass function (IMF) and a cloud residence time of $3\ 10^6$ yrs (cf. Garmany et al. 1982), i.e. for stars moving with velocities of 10 km s^{-1} in clouds with sizes of order 60 pc. The fact that we do observe OB stars is convincing evidence that an appreciable fraction of them indeed escapes from clouds within their lifetimes.

To calculate the luminosity L_1 of disk stars, that are largely responsible for the blue luminosity of a galaxy and for the heating of the cool interstellar dust, we assume a surface black-body temperature for these stars of T_1 = 7000 K. Anticipating the result that in a typical spiral galaxy $L_2/L_1 \approx 0.5$ (see section 3) and taking T_2 = 30,000 K (see below) the mean colour temperature of the interstellar radiation field is found to be 12,000 K, close to the canonical value of 10,000 K.

However, OB stars outside molecular clouds also contribute to the heating of the interstellar dust and to the observed blue light. The effective temperature of these stars is about 30,000 K, another result of the calculation of the fraction of the luminosity emitted outside clouds by stars born with a Salpeter IMF inside molecular clouds. Taking account of the fact that the interstellar absorption roughly scales with $1/\lambda$ so that the effective optical thickness of the disk for 7000 K and 30,000 K radiation is different, we iteratively solve for the dust optical thickness at λ4400, τ_B, of the galactic disk (equivalent to the face-on extinction) and L_1. To fit the observed blue magnitude we take into account that the blue light is attenuated by optical thickness $(a/b)\tau_B$. The face-on extinction is then found from the relation $A_B^0 = 1.086\ \tau_B$.

Our model thus results in the determination of the face-on blue extinction A_B^0 of a galaxy and of the luminosities L_1 and L_2. The quantity L_2/L_1 is a much better measure of the ratio of present-to-past star formation rates than the often used quantity L_{IR}/L_B (de Jong et al. 1984, Soifer et al. 1984).

3. RESULTS AND DISCUSSION

We have fitted our simple two-component model to infrared and optical data of 120 galaxies in the Revised Shapley-Ames Catalog of Bright Galaxies (Sandage and Tammann 1981) and to the data of 20 mini-survey galaxies (Soifer et al. 1984) for which morphological classifications, detailed optical and infrared photometry and optical spectra have recently been presented by Moorwood et al. (1986). Infrared flux densities of these galaxies were taken from the IRAS Point Source Catalog (JISWG 1985), supplemented by flux densities from the IRAS Small Scale Structure Catalog (JISWG 1986), if listed. Optical blue magnitudes of both the RSA galaxies and of the mini-survey galaxies were corrected for extinction in our own galaxy according to the prescriptions given by Sandage and Tammann (1981).

For our model calculations we took T_w = 60 K and T_c = 16 K. These are not arbitrary choices but were selected as follows. T_w was chosen to be somewhat larger than the largest dust temperature as derived from the observed S_{100}/S_{60} flux density ratios. T_c was chosen such that the average face-on extinction derived for the RSA galaxies agreed with optically determined values (see fig.1 and discussion below). The low temperature of the cool component implies that a substantial fraction of the total infrared luminosity of galaxies (more than 50% in most cases) is emitted at wavelengths longward of 100 μm.

We note that our adopted values of T_w and T_c are remarkably close to the ones recently derived by Chini et al. (1986) by combining sub-millimeter observations with IRAS data for about 20 bright galaxies. This agreement may be somewhat fortuitous because Chini et al. assumed a λ^{-2} dust emissivity law.

We have verified that the results are rather insensitive to changes in the adopted parameters. The largest effect is observed for T_c, understandably because L_c changes significantly if T_c changes by only a few degrees. We emphasize that the value adopted for T_c is found by fitting optical extinction measurements of galaxies and is thus rather well-determined.

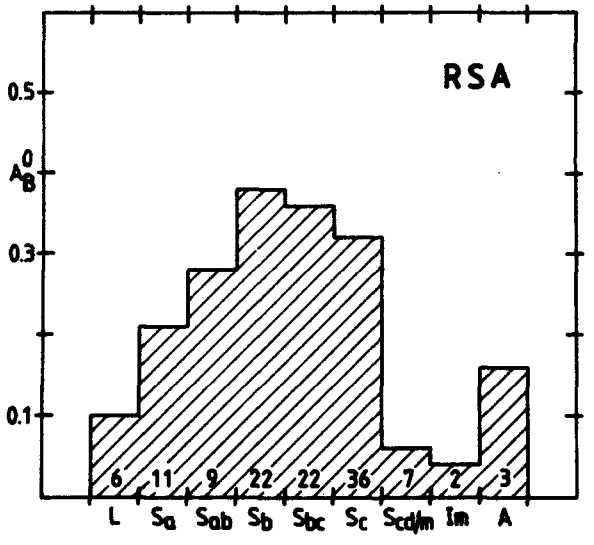

Figure 1. Mean values of the face-on blue extinction A_B^0 as a function of morphological type. The numbers of galaxies on which this mean value is based, are listed.

The distribution of average face-on blue extinctions as a function of morphological type for the RSA galaxies is shown in fig.1. Formal uncertainties in the averages are typically of order 10% - 20%. As noted above the temperature of the cool dust has been fixed by requiring that the weighted mean of A_B^0 over all spirals equals that calculated using the prescriptions of Sandage and Tammann (1981). The somewhat higher values for S_a and S_{ab} galaxies quoted by Sandage and Tammann may be due to the exclusion of dust-poor galaxies in their determination of A_B^0 for the earliest morphological types.

The variation of A_B^0 with morphological type is quite interesting and seems intuitively rather plausible. A_B^0 is small for early-type galaxies because they contain relatively small amounts of interstellar matter and thus also of dust. Proceeding to later morphological types the mass fraction of interstellar matter increases and so does the face-on extinction. For the latest morphological types we deal with galaxies in which evolution has been so slow or in which star formation has started so late that their metallicity is still relatively low, showing up here as a low face-on extinction.

In fig.2 we compare values of A_B^0 and of the recent star formation activity index $\log(L_2/L_1)$ for an optically complete sub-set of about 50 bright RSA spirals ($B_T < 12.5$, $V_R > 500$ km s^{-1}) and for the sub-set of the infrared-complete mini-survey galaxies studied by Moorwood et al. (1986). The most important conclusion to be drawn from this comparison is that the mini-survey galaxies are on the average almost three times more dusty while the present star formation activity is only about twice as large as in the RSA spirals. The

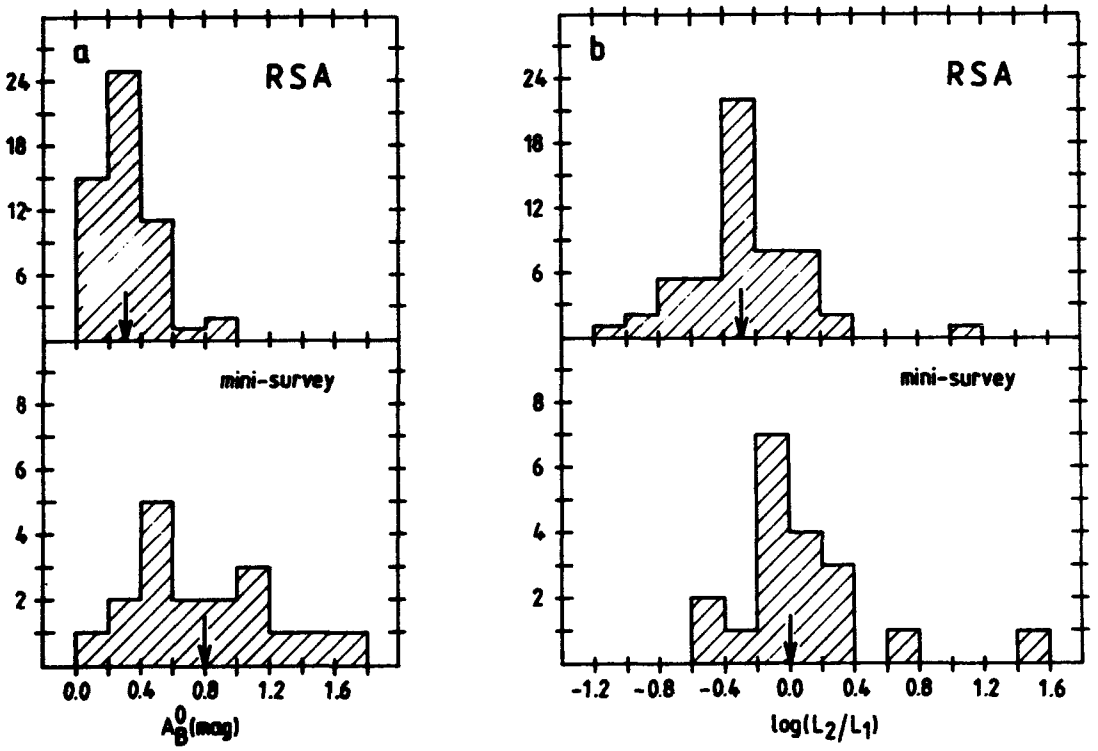

Figure 2. The distribution of: (a) blue face-on extinction A_B^0, and (b) star formation activity index $\log(L_2/L_1)$ for bright optically selected RSA spirals and infrared selected mini-survey galaxies.

latter may be fully explained by realizing that galaxies with higher present star formation rates are expected to be overrepresented in an infrared complete sample of galaxies. Thus we conclude that infrared selected samples of galaxies are apparently dominated by dusty galaxies.

This possibility was already briefly discussed in the discovery paper by Soifer et al. (1984). Later excitement about the alternative possibility of enhanced star formation may have resulted in the somewhat premature conclusion that an appreciable fraction of infrared detected galaxies are "starburst" galaxies (e.g. de Jong 1986). In fact fig.2b suggests that only 10% of the galaxies in an infrared complete sample shows anomalously enhanced star formation ($L_2/L_1 > 10$). It is interesting to note that the two deviating galaxies (IRAS 0413+081 and IRAS 0414+001) are the most morphologically peculiar in the sample studied by Moorwood et al.. The one galaxy with $L_2/L_1 > 10$ among the RSA galaxies is NGC 2146, a well-known peculiar galaxy.

The fact that most of the mini-survey galaxies are probably anomalously

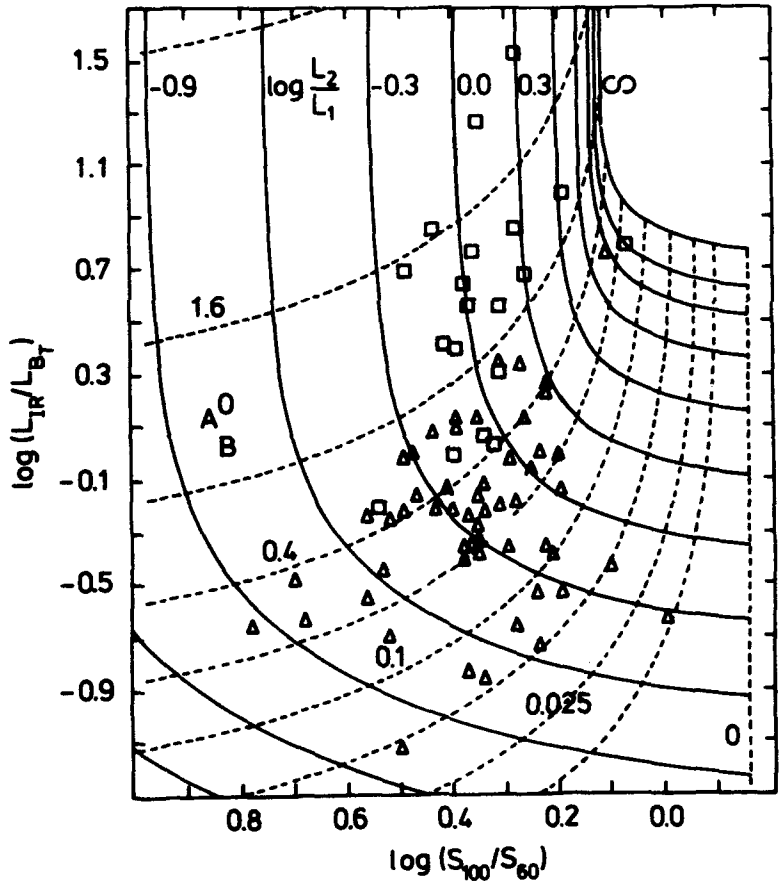

Figure 3. A theoretical L_{IR}/L_{B_T} versus S_{100}/S_{60} diagram. Lines of equal A_B^0 (dotted) and L_2/L_1 (full-drawn) are shown, calculated for a representative value of b/a = 0.6. As indicated by the labelling of these lines the values of the parameters increase by a factor two from one line to the next. Data points for bright optical RSA spirals (triangles) and mini-survey galaxies (squares) are plotted.

dusty was derived from near-infrared photometry by Moorwood et al. (1986). Our model analysis nicely confirms their findings.

Another way to illustrate our results is shown in the (L_{IR}/L_B) versus (S_{100}/S_{60}) diagram in fig.3 where data points for the optically complete RSA sub-set (triangles) and for the mini-survey sub-set (squares) have been plotted. Using our simple two-component model we have drawn lines of equal A_B^0 and L_2/L_1 in this diagram. These lines are calculated for a representative value of $b/a = 0.6$. For $A_B^0 > 1$ almost all optical radiation is reemitted in the infrared so that the ratio L_2/L_1 fixes the infrared color ratio S_{100}/S_{60} independent of the value of A_B^0, whereas L_{IR}/L_B is determined almost exclusively by the extinction. For small values of A_B^0 the quantity L_{IR}/L_B is most strongly dependent on L_2/L_1. The upper right hand corner in the diagram is forbidden because L_2/L_1 cannot exceed infinity.

Fig.3 clearly shows that the mini-survey galaxies are much more dusty than the optically selected bright RSA spiral galaxies while the star formation activity is only about twice as large in the mini-survey galaxies. It is quite rewarding that in spite of the simplicity of our model it is so remarkably succesful in explaining the differences between optically and infrared selected samples of galaxies. A more extensive discussion of our results will appear elsewhere.

The research of K.B. is supported by a grant from the Netherlands Foundation for Astronomical Research (ASTRON) with financial aid from the Netherlands Foundation for the Advancement of Pure Research (ZWO)

REFERENCES

Chini, R., Kreysa, E., Krugel, E., and Mezger, P.G. 1986, Astr. Ap. 157, L1
Garmany, C.D., Conti, P.S., and Chiosi, C. 1982, Ap. J. 263, 777
Joint IRAS Science Working Group 1985, IRAS Point Source Catalog, US Government Printing Office, Washington
Joint IRAS Science Working Group 1986, IRAS Small Scale Structure Catalog, US Government Printing Office, Washington
de Grijp, M.H.K., Miley, G.K., Lub, J., and de Jong, T. 1985, Nature 314, 240
de Jong, T. 1986, in "Spectral Evolution of Galaxies", C.Chiosi and A.Renzini, Reidel Publ. Co., Dordrecht, p.111
de Jong, T., et al. 1984, Ap. J.(Letters) 278, L67
Mezger, P.G., Mathis, J.S., and Panagia, N. 1982, Astr. Ap. 105, 372
Moorwood, A.F.M., Veron-Cetty, M.-P., and Glass, I.S. 1986, Astr. Ap. 160, 39
Neugebauer, G., et al. 1984, Ap. J.(Letters) 278, L1
Sandage, A., and Tammann, G.A. 1981, A Revised Shapley-Ames Catalog of Bright Galaxies, Carnegie Institution of Washington, Publ. 635
Soifer, B.T., et al. 1984, Ap. J.(Letters) 278, L71

EARLY-TYPE GALAXIES

DETECTION OF CO (J=1-0) IN THE DWARF ELLIPTICAL GALAXY NGC 185

Tommy Wiklind and Gustaf Rydbeck
Onsala Space Observatory
S-439 00 Onsala, Sweden

We report the first detection of CO(J=1-0) emission in the dwarf elliptical galaxy NGC 185. The observations were performed with the Onsala 20 m telescope equipped with a SSB tuned Schottky mixer and, for the most recent observations, a SIS mixer. The previously reported tentative detection of CO in NGC 185 by Johnson and Gottesman (1979) does not agree with our results, see also Knapp (1983).

NGC 185 is a companion to M31 and classified as dE3p (Sandage and Tammann, 1981). It is classified as peculiar owing to the presence of dust patches and a population of blue stars situated in the centre region (Hodge, 1963). It contains $1.5 \cdot 10^5$ $M_\odot$ of atomic hydrogen, which is asymmetrically distributed with respect to the centre (Johnson and Gottesman, 1983).

The presence of both dust and atomic hydrogen made NGC 185 a prime object for a deep search for molecular gas. We detected CO emission at a level of 37 mK; intensities are given as main beam brightness temperature, $T_{mb} = T_A^* / \eta_{mb}$ ($\eta_{mb} \approx 0.3$). So far we have observed two positions; the center and a prominent dust cloud. Emission was detected from both places. The emission profile consists of two distinct peaks, centered at $V_{LSR} = -203$ km s^{-1} and $V_{LSR} = -292$ km s^{-1}, respectively.

The HI seen by Johnson and Gottesman was centered at $V_{LSR} \simeq -190$ km s^{-1}, their observations did not cover a possible HI component around -290 km s^{-1}. With only two observed positions it is impossible to determine whether the two peaks correspond to an ordered motion or not.

Conservative estimates of the mass of molecular gas can be made by assuming Galactic factors for the conversion of CO intensity to H_2 mass. In the case of optically thick emission we get approximately $1.5 \cdot 10^5$ $M_\odot$ of H_2 within the observed region. Should the emission be optically thin we get $5 \cdot 10^3$ $M_\odot$. We emphasize that these mass estimates are very uncertain, but most probably represents lower limits for both cases.

REFERENCES

Hodge, P.W.: 1963, *Astron. J.*, 68, 691.
Johnson, D.W. and Gottesman, S.T.: 1979, in *Photometry, Kinematics and Dynamics of Galaxies*, ed. D.S. Evans (Austin, Univ. of Texas Press).
Johnson, D.W. and Gottesman, S.T.: 1983, *Astrophys. J.*, 275, 549.
Knapp, G.R.: 1983, in *Internal Kinematics and Dynamics of Galaxies*, IAU Symp. No. 100, ed. E. Athanassoula.
Sandage, A.R. and Tammann, G.A.: 1981, *A Revised Shapley-Ames Catalogue of Galaxies*, Carnegie Institution of Washington, Washington, D.C.

Carol J. Lonsdale Persson (Editor)
Star Formation in Galaxies

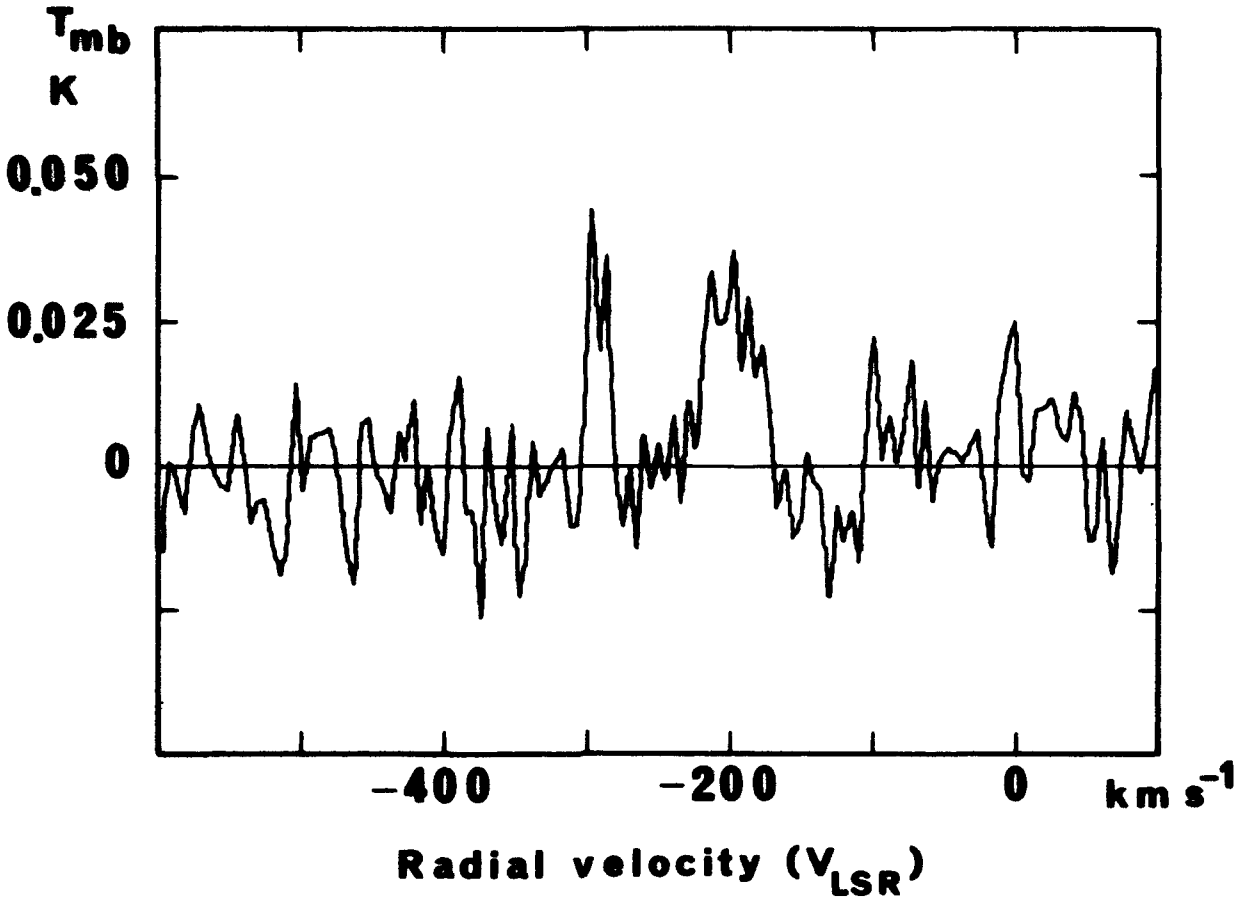

Figure CO(J=1-0) spectra of NGC 185. The velocity resolution is 5.2 km s^{-1} and the intensity is given as main beam brightness temperature, $T_{mb} = T_A^* / \eta_{mb}$. No baseline correction has been applied.

Star Forming Regions in Gas–Rich S0 Galaxies

Richard W. Pogge
Lick Observatory, University of California, Santa Cruz, CA 95064
and
Paul B. Eskridge
Dept. of Astronomy FM–20, University of Washington, Seattle, WA 98195

ABSTRACT

We present the first results of an Hα imaging survey of HI rich S0 galaxies, in which we are searching for HII regions and other sources of emission (*e.g.*, nuclear emission). CCD Hα interference filter images have been made of 16 galaxies. Eight of these galaxies show evidence for on–going star formation (HII regions), one has nuclear emission but no HII regions, and the remaining seven have no emission detected within well defined upper limits. With the exception of one notably peculiar galaxy in which the emission from HII regions appears pervasive, the HII regions are either organized into inner–disk rings or randomly distributed throughout the disk. A few of the galaxies are found to be clearly not S0's, or peculiar objects atypical of the S0 class. Using simple models we have estimated star formation rates (SFRs) and gas depletion times from the observed Hα fluxes. In general, the derived SFRs are much lower than those found in isolated field spiral galaxies (Kennicutt 1983) and the corresponding gas depletion time scales are also longer.

I. Introduction

The gas content of early–type galaxies is a subject of great interest, especially because of its application to understanding the evolution of these systems. Early-type galaxies as a class are deficient in gas and dust relative to later types. For a long time, only a few S0 galaxies and no E galaxies had been detected in 21-cm emission surveys. Recently, however, more sensitive techniques and instruments have increased the number of detected galaxies, and a few E galaxies have now been detected (see the extensive compilations in Wardle and Knapp 1986 for S0 galaxies; and Knapp, Turner, and Cuniffe 1985 for E galaxies). Among S0's with similar properties, there seems to be a broad range in gas content from relatively strong ("HI Rich S0's") to undetected ("HI Poor S0's").

It is of interest to ask to what extent this gas is attended by current star formation. We have used CCD imaging through redshifted Hα interference filters to search for HII regions in a sample of HI rich S0 galaxies selected out of the literature. By subtracting the underlying stellar continuum using images taken through filters sampling emission–free regions of the spectrum, it is possible to isolate not only the brightest HII regions (if any), but also to detect faint HII regions whose surface brightness may be below that of the surrounding starlight.

Carol J. Lonsdale Persson (Editor)
Star Formation in Galaxies

II. Sample and Observations

From the literature published up to June 1985, a total of 103 S0 galaxies have detectable HI emission, contrasted with about 220 HI poor S0's for which there is either no HI detection or only an upper limit. For the present imaging survey at Lick Observatory, the galaxies must be accessible to our redshifted interference filter set, which excludes all galaxies with $V \gtrsim 3800$ km sec^{-1}. In addition, the galaxies must be within the declination limits of the 1-meter Anna Nickel telescope at Lick Observatory, which limits the sample to the range $+62° \gtrsim \delta \gtrsim -25°$. The final redshift and pointing limited sample contains 62 HI rich S0's.

Observations were made using the 1-meter Anna Nickel telescope at Lick Observatory using the $f/17$ GEC CCD direct camera during Spring 1985, and using the TI CCD Cassegrain spectrograph in direct imaging mode during Fall 1985. For each program galaxy, two images were taken, the first through an interference filter isolating Hα+[N II]λ6548,6583 emission at the galaxy redshift, and a second through a filter centered on emission–free stellar continuum 40Å redward or blueward of the emission line filter. The filters have a typical width of 22Å and peak transmission of 80%. Reduction and analysis of the images was done using the VISTA image processing program developed at Lick Observatory. Atmospheric extinction corrections were made following Hayes (1970). An approximate flux calibration was accomplished by observing white dwarf standard stars from the lists of Oke (1971) and McCook and Sion (1984). The fluxed continuum image was subtracted from the fluxed emission image to produce an *essentially starlight–free Hα+[N II] emission line image of the galaxy.* In cases where emission regions were not evident after continuum subtraction, a "detection limit" was evaluated.

III. Results and Discussion

Of 16 S0 galaxies observed so far, eight galaxies have detectable HII regions, and one (NGC 7743) has nuclear emission but no HII regions. The remaining seven galaxies have no emission detected with well defined upper limits. Total Hα fluxes, or appropriate upper limits, are given in Table 1 The Hα fluxes have been corrected to account for a contribution due to [N II]λ6548,6583 emission following Kennicutt (1983).

In the S0's with detectable HII regions, we find the star forming regions are either distributed into inner rings near the central regions, or randomly distributed throughout the disk of the galaxy. With the exception of NGC 694, in which the star formation appears to be global, the observed HII regions sparsely populate the disk compared with the covering seen in later type spirals (Hodge and Kennicutt 1983). A few of the galaxies (*e.g.,* NGC 7013) also show signs of nuclear emission. HI maps of NGC 7013 (Knapp *et al.* 1984) and NGC 4138 (Shane and Krumm 1983) suggest that the HI gas rings are associated with the HII region rings. Two galaxies (NGC 4670 and UGC 12713) turn out to be irregular galaxies misidentified as S0's.

Following roughly the procedures used by Gallagher, Hunter and Tutukov (1984) and Kennicutt (1983), we have used these fluxes to estimate the total star for-

mation rates (SFRs) in these galaxies. Details of the derivation may be found in Pogge and Eskridge (1986). The total star formation rates in $M_\odot$/year are given in Table I. By comparison, Kennicutt (1983) found that for field Sa and Sb spiral galaxies the mean SFR is $\sim$ 1.6 $M_\odot$/yr, and for field Sbc and Sc spirals it is $\sim$ 3.5 $M_\odot$/yr. (Kennicutt's method of estimating the SFR differs slightly from ours, so it was necessary to multiply his estimates by 0.64 to bring the two methods into agreement.) For the detected S0 galaxies the SFRs are typically $\sim$ 0.4 $M_\odot$/yr, smaller than for field spirals.

In Table I, we give estimates of the total gas depletion time in years for the S0 galaxies with detected HII regions assuming that all of the HI gas is available for star

TABLE I. HII Regions in HI Rich S0 Galaxies.

Galaxy	Type[1]	D (Mpc)[2]	M_{HI} (10^9 $M_\odot$)[3]	H II Dist[4]	log F(Hα)[5]	SFR ($M_\odot$/yr)	τ (yr)
NGC 473	S0	45.4	...[6]	R	−12.33	0.66	...[6]
NGC 680	S0	58.6	2.96		< −15.4	<0.0006	
NGC 694	S0p	60.0	4.20	G	−12.42	0.94	1.1×10^{10}
NGC 936	SB0	31.6	1.80		< −15.7	<0.0001	
NGC 1023	SB0	15.2	3.72		< −15.1	<0.0001	
NGC 4138	S0	8.6	0.3	R	−12.39:	0.02:	9.5×10^{10}:
NGC 4385	SB0	50.4	11.7	P	−11.36:	7.6:	3.9×10^{9}:
NGC 4670	SB0p	24.6	1.84	G	−11.51	1.28	3.6×10^{9}
NGC 5631	S0	40.2	2.40		< −14.9	<0.0015	
NGC 6501	S0	60.0	5.96		< −15.4	<0.0006	
NGC 7013	S0/a	20.0	2.04	R	−11.88	0.36	1.4×10^{10}
NGC 7180	S0/a	30.4	0.18		< −16.2	<0.00003	
NGC 7280	S0	41.2	1.08		< −15.4	<0.0003	
NGC 7742	S0p	35.2	4.16	P	−14.75	0.016	6.5×10^{11}
NGC 7743	SB0	38.2	1.00	n	< −15.5	<0.0001	
UGC 12713	S0/a	9.2	0.26	G	−13.11	0.0044	1.5×10^{11}

Notes:

A colon (:) means fluxes are uncertain to greater than 20%, hence greater uncertainty in SFR and τ.

1.) From de Vaucouleurs *et al.* (RC2) or Sandage and Tammann (RSA).

2.) Based on H_0 = 50 km/sec/Mpc and V_{Virgo} = 1350 km/sec.

3.) From literature, see references in Pogge and Eskridge (1986).

4.) Emission Region Distribution Codes: R=Ring, G=Global, P=Patchy, n=nuclear.

5.) Log of integrated Hα flux in erg/cm^2/sec.

6.) Promised updated value of M_{HI} not available at press time.

formation. The total gas mass is found by correcting the observed HI mass to account for helium, molecular gas, and gas recycling by evolved stars (see Kennicutt 1983; Larson *et al.* 1980). The gas depletion time (τ) is the amount of time required to use up the available gas at the current SFR. For field spirals, the median value of τ is $\sim 4 \times 10^9$ yr (Kennicutt 1983). For our detected S0's τ varies from 1.1×10^{10} yr for NGC 694 to as high as 6.5×10^{11} yr for NGC 7742. A bright nuclear starburst in NGC 4385 makes its estimate of τ uncertain as our simple SFR models may not be valid. If all of the HI gas is not be available for star formation, then our estimates of τ would be reduced. For example, if only the gas in the inner regions of NGC 7013 ($M_{\rm HI} = 1.92 \times 10^9$ $M_\odot$– Knapp *et al.* 1984) is available for star formation, this implies that $\tau \sim 5 \times 10^9$ yr, compared with $\sim 1.4 \times 10^{10}$ yr using the total HI mass.

Both the SFRs and gas depletion times suggest that on–going star formation in most of these systems is likely to have little impact on their subsequent evolution unless the SFRs increase dramatically. This is consistant with the evolutionary theory of Larson *et al.* (1980), suggesting that S0's may be fossil spiral galaxies with only vestigial star formation continuing to the present.

IV. Conclusions

We have demonstrated that in at least a few HI rich S0 galaxies, the gas is accompanied by current star formation. Much work remains. In particular, it is essential to have detailed HI maps made of more of these systems to be able to determine to what extent the gas is directly associated with the star forming regions.

References

Gallagher, J.S., Hunter, D.A. and Tutukov, A.V., 1984, *Ap. J*, **284**, 544.

Hayes, D.S., 1970, *Ap.J.*, **159**, 165.

Hodge, P.W. and Kennicutt, R.C., 1983, *An Atlas of H II Regions in 125 Galaxies.* AIP Physics Auxiliary Publication Service Document ANJOA–88–0296–300.

Kennicutt, R.C., 1978, Ph.D. Thesis, University of Washington.

Kennicutt, R.C., 1983, *Ap.J.* **272**, 54.

Knapp, G.R., Turner, E.L. and Cunniffe, P.E., 1985, *A.J.*, **90**, 454.

Knapp, G.R., van Driel, W., Schwarz, U.J., van Woerden, H. and Gallagher, J.S., 1984, *Astr.Ap.*, **133**, 127.

Larson, R.B., Tinsley, B.M. and Caldwell, C.N. (1980). Astrophys. J. **237**, 692.

McCook, G.P. and Sion, E.M., 1984, *Villanova Obs. Cont.*, No. 3.

Oke, J.B., 1974, *Ap.J.Suppl.*, **27**, 21.

Pogge, R.W. and Eskridge, P.B., 1986, *in preparation.*

Shane, W.W., and Krumm, N., 1983, *IAU Symposium No. 100, Internal Kinematics and Dynamics of Galaxies*, E. Athanassoula ed., (Dordrecht:Reidel), p.105.

Wardle, M. and Knapp, G.R., 1986, *A.J.*, **91**, 23.

MODELS

A SIMPLE THEORY OF BIMODAL STAR FORMATION◇

Rosemary F.G. Wyse[1,2] and J. Silk[2]
1. Space Telescope Science Institute, Baltimore, MD 21218
2. Astronomy Dept., University of California, Berkeley, CA 94720

ABSTRACT. We present a model of bimodal star formation, wherein massive stars form in giant molecular clouds (GMC), at a rate regulated by supernova energy feedback through the interstellar medium, the heat input also ensuring that the initial mass function (IMF) remains skewed towards massive stars. The low mass stars form at a constant rate. The formation of the GMC is governed by the dynamics of the host galaxy through the rotation curve and potential perturbations such as a spiral density wave. The characteristic masses, relative normalisations and rates of formation of the massive and low mass modes of star formation may be tightly constrained by the requirements of the chemical evolution in the Solar Neighborhood. We obtain good fits to the age metallicity relation and the metallicity structure of thin disk and spheroid stars only for a narrow range of these parameters.

1. THE MASSIVE STAR FORMATION RATE

The effects of massive stars on the surrounding interstellar medium and subsequent star formation may be envisaged to be either to *suppress* further star formation for some time by destroying the cold (molecular) gas from which stars are presumed to form, or to *induce* further star formation through the increase in pressure compressing and destabilising clouds. These two effects in fact operate simultaneously, leading to self regulated (massive) star formation (cf. Cox 1983; Franco and Cox 1983; Dopita 1985). The lower mass stars are effective over much longer timescales and may be neglected for the regulation of the formation of short-lived stars. Assuming that the most important energy injection process is due to supernova explosions, which maintain a velocity dispersion in the system of GMC that governs the cloud-cloud collision time and hence energy dissipation and star formation time, leads to the following dependence of global massive star formation rate (SFR) per unit (molecular) gas mass on the surface densities (Σ) of total material, and gas :

$$\frac{\dot{M}_*}{M_{gas,CO}} \sim (\Sigma_{tot}\Sigma_{gas,CO})^{1/2}$$

The self regulation allows one to understand why only a small fraction of GMC cores have associated HII regions (Solomon, Sanders and Rivolo 1985; Scoville, Sanders and Clemens 1986) *ie.* why massive star formation is in this sense inefficient.

The massive SFR in external galaxies may be estimated from the UV flux, or the far IR assuming it is mainly due to dust reradiation of the UV from massive stars. Unfortunately, large discrepancies in these two estimates exist for the galaxies that have measurements of the quantities in the above equation, which may indicate either that a significant fraction of the IRAS flux is due to a cirrus component of dust heated by the general stellar radiation field, or that extinction problems remain with the quantitative interpretation of the UV, or both. Thus a direct quantitative testing of this relation is not yet possible.

◇Supported in part by Calspace.

2. THE RADIAL DEPENDENCE OF GMC AND MASSIVE STARS.

The dependence of the global massive SFR on total surface density found above suggests that the rotation curve may be of importance. Many models for the formation of GMC complexes analyse the effect of a spiral density wave and postulate that the potential causes an increase in the lengthscale which is gravitationally unstable, or simply aids the coagulation of small diffuse clouds of either atomic or molecular gas (eg. Cowie 1980; Balbus and Cowie 1985). We here present a phenomenological model for GMC, whereby the rate of their formation, and CO emission, depends on the rate at which a parcel of gas encounters a spiral perturbation, and on the square of the HI density. We are most interested in understanding the *radial profiles* of CO in disk galaxies – why they are so different from the atomic gas profiles, but similar to the blue light. In this respect it is only important that the progenitors of GMC have the same radial profile as the HI, as may be the case for the analogs of the small high latitude CO clouds found by Blitz, Magnani and Mundy (1984). Thus

$$CO(r) \propto n_{HI}^2(r)(\Omega(r) - \Omega_P)m$$

where Ω is the local angular frequency, Ω_P and m being the pattern speed and number of arms in the spiral pattern. For situations where no underlying density wave occurs but the arms are due to a simple shear instability and swing amplifier, we set $\Omega_P = 0$, since then $\Omega(r)$ mimics the Oort constant of differential rotation, which controls the instability (Toomre 1981). A dependence on the rate of encounters of spiral arms was also postulated by Shu *et al.* (1972) in their modelling of the SFR in density wave theory, and by Güsten and Metzger (1982) for massive stars in the spiral arms of our Galaxy. The dependence on the square of the HI density assumes that two-body processes such as binary cloud-cloud collisions dominate. We are also equating a rate with a luminosity and hence mass.

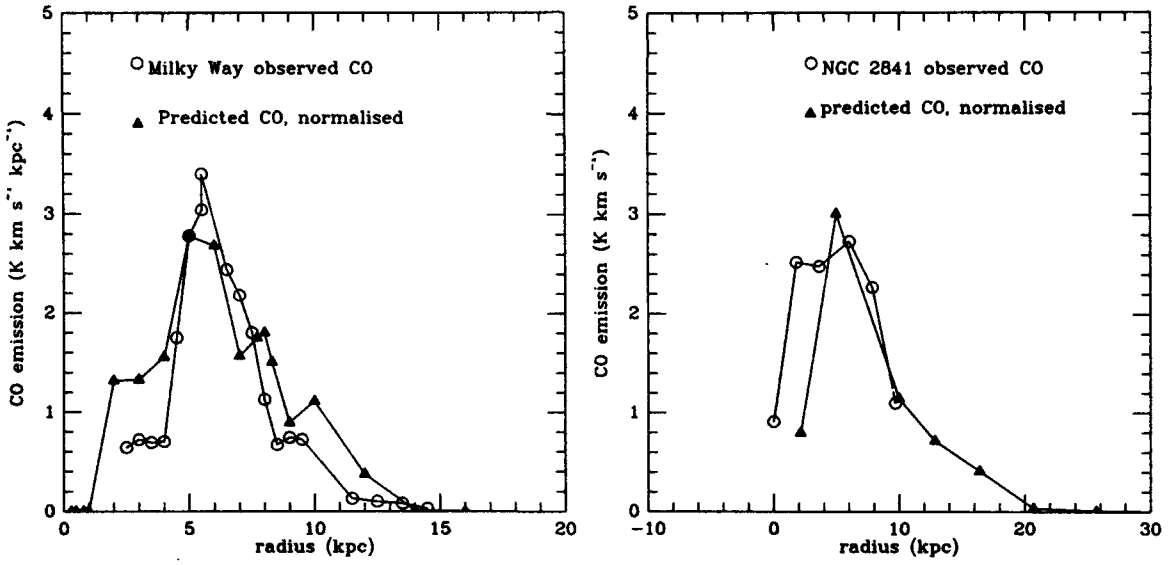

Figure 1. Predicted CO emission (filled triangles), arbitrarily normalised, compared to the observations (open circles) for the Milky Way (Sanders, Solomon and Scoville 1984) and NGC 2841 (Young and Scoville 1982).

We have made predictions for of order ten galaxies with the necessary observations, obtaining encouraging results. Interesting features are that galaxies which are believed to have a density wave are best fit by corotation in the outer regions, as predicted by theory (Shu *et al.* 1972) and have a significantly poorer fit if we set $\Omega_P = 0$, while the galaxies with more filamentary arms (eg NGC 2841) are well fit by the theory for arbitrary values of the

pattern speed, as may be expected. Results for the Milky Way and NGC 2841 are shown in Figure 1. We obtain equally good agreement with the CO observations for galaxies with a CO 'ring' and those with monotonic CO. The radial fall-off of the CO emission to large radii while the HI remains flat reflects the near exponential behavior of $\Omega(r) - \Omega_P$, which in turn reflects the profile of the stellar disk since disk galaxies are essentially self-gravitating within a few scale-lengths. Thus fitting an exponential to the CO results in a scale-length close to that of the stars, or equivalently, the blue light.

3. CHEMICAL EVOLUTION IN A BIMODAL MODEL.

Any reasonable model for the time dependence of the gas mass, together with the regulation equation above, yields a massive SFR that decreases sharply with time. This contrasts strongly with the derived constant Solar Neighborhood low mass SFR (Twarog 1980) – hence the star formation process is bimodal in time as well as space (cf Larson 1986). Matteucci and Greggio (1986) showed that a constant SFR for stars of all masses would overproduce oxygen and other elements due to massive stars. The effect of the new $^{12}C(\alpha,\gamma)^{16}O$ reaction rate on the chemical yields of massive stars was investigated subsequently (Matteucci 1986) and silicon and iron are still overproduced. A decreasing massive SFR appears to offer a solution.

We have investigated the chemical evolution in a particular parameterisation, where the two modes are taken to be 1). 'low mass' mode : Miller-Scalo IMF, all masses, constant SFR $A_1 M_\odot Gyr^{-1}$ and 2) 'massive' mode : only stars above M_{L2}, SFR $A_2 e^{-t/\tau_2} M_\odot Gyr^{-1}$. The lower mass cutoff of the 'massive' mode is made as low as possible, to avoid introducing a time dependence into isotopic ratios which would arise were the nucleosynthetic properties of the two modes different and which is not observed. The models are required to fit the Solar Neighborhood age-metallicity relationship for low mass F stars and also to reproduce the present day gas content and total disk surface density, 70 $M_\odot pc^{-2}$ (any dark matter being stellar remnants). A gas consumption time of at least several Gyr is also required. These quantities are shown in Figure 2 for a model we deem satisfactory.

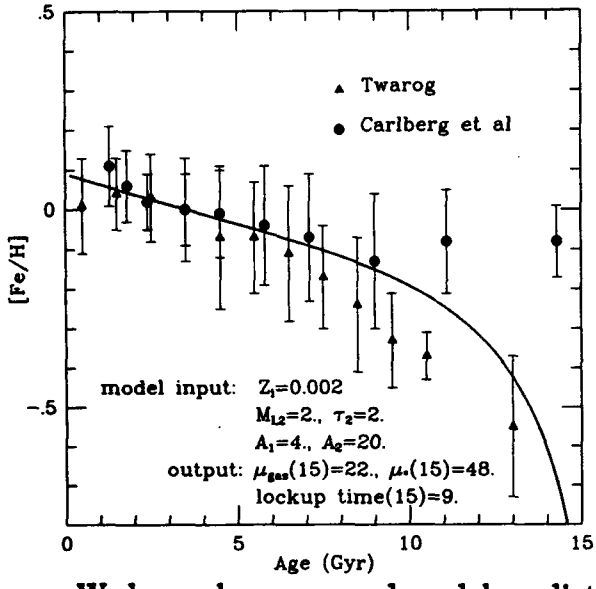

Figure 2. The predicted age metallicity relation for long-lived F stars in the Solar Neighborhood (solid line), for a model for the thin disk with initial metallicity a tenth solar, consistent with the spheroid model in Figure 3(b), and with low mass mode SFR 4 $M_\odot Gyr^{-1}$, high mass mode, with lower mass of 2 $M_\odot$, normalisation 20 $M_\odot Gyr^{-1}$ and e-folding time of 2 Gyr. The observational data of Twarog (1980) and Carlberg *et al.* (1985) are also shown. The model and observations are in good agreement, and the model output values, at 15Gyr, for the gas and stellar surface density μ $M_\odot pc^{-2}$ and the gas lockup (consumption) time are entirely satisfactory, although the gas content is somewhat high.

We have also compared model predictions with the cumulative metallicity distributions of thin disk stars and extreme spheroid stars, allowing for ejecta from the spheroid (leaving at a rate λ times the star formation rate) to pre-enrich the thin disk material (see Figure 3). There is a narrow range of parameter values which provides a good fit to *all* these observational constraints.

We are currently working on fully self consistent models, using the equations above for the time and radial dependences of the massive SFRs. Extension of the model to different environments such as IRAS galaxies is underway to help understand the starburst phenomenon.

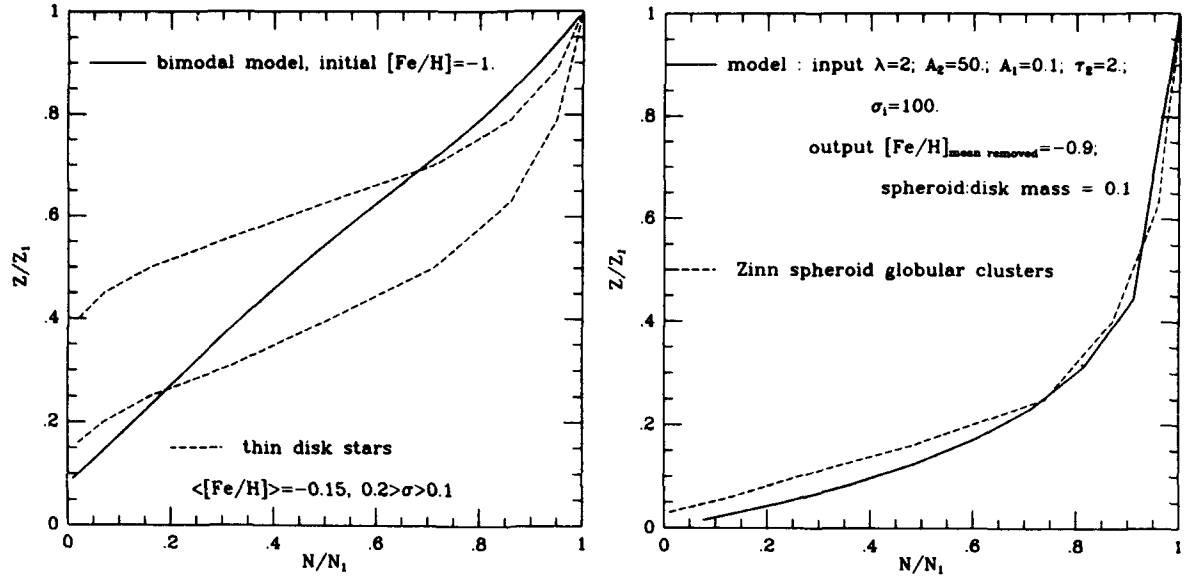

Figure 9 (a). Cumulative metallicity distribution for the low mass stars of our favored model (solid line) compared to estimates of the true distribution, which are $\pm 2\sigma$ truncated gaussians, of mean −0.15 dex (dashed lines delimiting range of dispersion $0.1 < \sigma < 0.2$ dex).

(b). Cumulative metallicity distribution for spheroid stars. The model (solid line) has star formation parameters as indicated, with outflow at twice the total SFR, and a total initial surface density (σ_i) of $100 M_\odot pc^{-2}$. The observations are the metal poor spheroid globular clusters (Zinn 1985). The model predicts reasonable values for the initial enrichment of the thin disk and for the spheroid to thin disk mass ratio.

REFERENCES

Balbus, S.A. and Cowie, L.L., 1985, *Ap. J.*, **297**, 61.
Blitz, L., Magnani, L. and Mundy, L. 1984, *Ap. J. (Lett.)*, **282**, L12.
Carlberg, R. *et al.*, 1985, *Ap. J.*, **294**, 674.
Cowie, L.L., 1980, *Ap. J.*, **236**, 868.
Cox, D.P., 1983, *Ap. J. (Lett.)*, **265**, L61.
Dopita, M.A., 1985, *Ap. J. (Lett.)*, **295**, L5.
Franco, J. and Cox, D.P., 1983, *Ap. J.*, **273**, 243.
Güsten, R. and Metzer, P.G., 1982, *Vista in Astr.*, **26**, 159.
Larson, R.B., 1986, *M.N.R.A.S.*, **218**, 409.
Matteucci, F., 1986, *Ap. J. (Lett.)*, **305**, L81.
Matteucci, F. and Greggio, L., 1986, *Astr. Ap.*, **154**, 279.
Sanders, D.B., Solomon, P.M. and Scoville, N.Z., 1984, *Ap. J.*, **276**, 182.
Scoville, N.Z., Sanders, D.B. and Clemens, D.P., 1986, preprint.
Solomon, P.M., Sanders, D.B. and Rivolo, A.R., 1985, *Ap. J. (Lett.)*, **292**, L19.
Toomre, A., 1981. *Normal Galaxies*, eds. S.M. Fall and D. Lynden-Bell (CUP) p111.
Twarog, B., 1980, *Ap. J.*, **242**, 242.
Shu *et al.*, 1972, *Ap. J.*, **173**, 557.
Young, J.S. and Scoville, N., 1982, *Ap. J. (Lett.)*, **260**, L41.
Zinn, R., 1985, *Ap. J.*, **293**, 424.

THE HISTORY OF GAS IN SPIRAL GALAXIES

Philip Maloney
Department of Planetary Sciences
University of Arizona
Tucson, AZ 85721

The general association of luminous young stars with spiral arms in galaxies has led to widespread acceptance of the idea that the formation of massive stars, at least, is somehow triggered by the interaction of interstellar gas clouds with a spiral density wave . The observed increase in C/H and N/H with decreasing galactic radius receives a natural explanation in this scenario, as gas closer to the galactic nucleus has more encounters with the spiral density wave. This picture may only be applicable to grand design spirals, since non-grand design spiral galaxies may not have long-lived density waves (Kormendy and Norman 1979).

Consider a very simple model for the gas in such a spiral galaxy, with a specified initial surface density $\sigma(r)$ and angular velocity $\Omega(r)$. A spiral density wave (pattern speed Ω_p) is present. In each encounter with the density wave some fraction f of the gas is permanently lost in the form of low mass stars and stellar remnants. The actual nature of the density-wave trigger is unimportant (e.g., whether the density wave causes HI clouds to coalesce into molecular clouds which then form stars, or causes star formation in pre-existing molecular clouds). The fraction of gas remaining after n encounters with the density wave is just $(1-f)^n$, where f has been assumed constant with time. An assumed initial gas distribution can be evolved back to T years before the present or followed forward in time. If the conversion factors used to infer H_2 column densities from CO J=1-0 emission are correct, then H_2 dominates the mass of the ISM for radii less than $\approx$ 10 Kpc, and the present-day radial gas distributions in spirals are roughly exponential.

Typical results from this simple model, with parameters appropriate to NGC 6946, are shown in Figures 1a and b. The H_2 distribution is from Young and Scoville (1982); Ω_p is from Roberts, Roberts and Shu (1975). Gas profiles have been calculated only for the region of nearly solid-body rotation. Figure 1a shows an initial exponential distribution that has been evolved for 10^{10} years; Figure 1b gives the initial (T=0) distribution implied by a present-day exponential distribution. It is evident that a gas distribution that was exponential 10^{10} years ago would now be very flat. A general result is that the gas distibutions inferred from CO observations require too much gas in the past, exceeding the dynamical mass derived from the rotation curve.

Carol J. Lonsdale Persson (Editor)
Star Formation in Galaxies

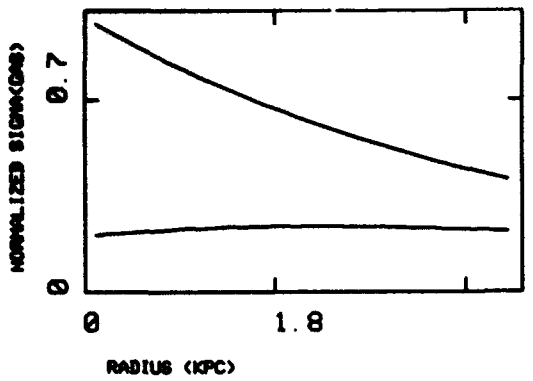

Figure 1a. Upper curve is initial exponential gas distribution; lower curve is gas profile after 10^{10} years. Gas density is normalized to initial R=0 density.

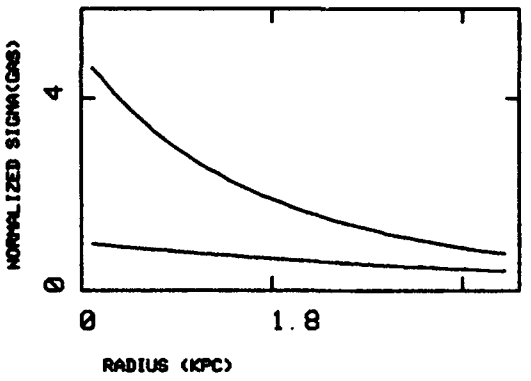

Figure 1b. Upper curve is initial distribution 10^{10} years ago implied by present-day exponential distribution. Normalization as in 1a.

The idea that encounters between spiral density waves and interstellar clouds would lead to depletion of gas at small radii was first suggested by Oort (1974) to explain the distribution of HI in spirals. Possible explanations for this discrepancy are:

1) The conversion from integrated CO intensity (I_{CO}) to H_2 column density ($N(H_2)$) is in error. Since linear conversions of this form implicitly assume that all clouds are identical, they almost certainly overestimate the amount of H_2 in the inner region of the galaxy relative to the disk, regardless of the absolute error.

2) The star-forming efficiency f is much less than 1%. Note that f as defined above is the amount of gas that is permanently locked up in stars and stellar remnants. This fraction is related to the amount of gas that is turned into stars as a result of the density wave, F, by a factor that depends on the amount of mass returned to the ISM by evolved stars. If only high-mass stars are formed as a result of the density wave (e.g., the lower mass cut-off is $\geq 3\ M_\odot$) then f would be expected to be $\approx 0.1F$, unless remnants with very large masses are formed. The idea that the initial mass function may be bimodal has been extensively discussed by Larson (1986).

3) Grand design spiral structure doesn't persist over galactic lifetimes.

4) Our understanding of the effects of density waves on the ISM is very inadequate.

5) Infall of gas into the inner disk is extremely important in the evolution of spiral galaxies.

Unfortunately, it is very difficult to make any quantitative statements regarding 2) - 5). Therefore, for the rest of this paper I shall discuss the issue raised by 1), namely: how accurately can we really presume to know the molecular gas distributions in galaxies, based upon observations of CO J=1-0 emission?

It has been suggested that there should be a linear conversion between I_{CO} and $N(H_2)$ if the antenna temperature T_R^* effectively measures the fraction of the beam that is filled with clouds. Then, if all the clouds have the same excitation temperature, and are virialized so that the linewidth of each cloud depends on its mass and thus column density, it is claimed that there will be a constant conversion factor between I_{CO} and $N(H_2)$ (Young and Scoville 1982). Dickman, Snell and Schloerb (1986) (DSS) have made a study of this relation, using a number of simplifying assumptions. However, no rigorous analysis of this suggestion has yet been made, and no study has been made of the errors in H_2 column densities which might result if the assumptions involved are violated.

In order to perform this analysis, a model has been constructed which simulates the observation of molecular clouds in galaxies in a completely general way. A model galaxy is assigned a rotation curve, z-velocity dispersion and inclination. The overall parameters of the cloud distribution (total number, form of radial distribution,etc.) are specified, and a random number algorithm assigns coordinates and z-velocities to the clouds. Cloud velocity dispersions, excitation temperatures, and radii are all assigned individually and may be arbitrarily complicated functions of position. The positions and velocities of all the clouds are projected onto the plane of the sky. Convolution of the cloud brightness distribution with a gaussian antenna (with FWHM $\Theta_{1/2}$)is performed numerically, without any simplifying assumptions. Cloud-cloud shielding is explicitly taken into account.

Under what conditions is I_{CO} proportional to $N(H_2)$? For simplicity, let us consider a face-on galaxy and assign all clouds the same radius and velocity dispersion, σ_c. The surface density of molecular clouds falls off exponentially with radius, in accordance with the distributions inferred using a constant conversion factor. If the clouds all have T_{EX} = 10 K and virialized linewidths, then I_{CO}/H_2 is a constant. However, since $I_{CO} \propto \sigma_c$ and $\langle N(H_2) \rangle$, the cloud-averaged column density, is $\propto \sigma_c^2$, the value of the constant depends on σ_c and hence on the mean density. For $\langle n \rangle$ = 200 cm^{-3}, the value used by DSS, the conversion factor is $N(H_2) = 2 \times 10^{20} I_{CO}$. Here $N(H_2)$ is the column density of H_2 averaged over the beam FWHM. This is 2X smaller than the value advocated by Young and Scoville (1982). It is also smaller than the value of DSS for the same $\langle n \rangle$. This is a result of their neglect of contribution to I_{CO} from clouds outside the FWHM.

Under restricted conditions, then, I_{CO}/N_{H2} is constant, with a value within a factor of two of that suggested for it. The key question then becomes how strongly this ratio is affected by deviations from these restrictive conditions. As mentioned above, clouds must not only be in virial equilibrium, but have the same mean density for I_{CO}/N_{H2} to be strictly constant. This last

condition is very unrealistic. It is not even clear that clouds are in virial equilibrium. In studies of dark clouds, Leung, Kutner and Mead (1982) and Myers (1983) have suggested that these objects are in virial equilibrium, but there is reason to suspect that this is not true (Maloney 1986). If clouds have linewidths that do not reflect their masses, the correlation between CO emission and H_2 column density will cease to be linear.

Of perhaps more importance is the effect of variations in the excitation temperature of the CO J=1-0 line. The models show that, as expected, I_{CO} depends linearly on T_{EX}. Figure 2 shows I_{CO} versus radius for two model galaxies which are identical except that one has T_{EX} = 10 K everywhere, while the other has an exponential $T_{EX}(r)$, with $T_{EX}(0)$ = 40 K and T_{EX} (15 Kpc) = 5 K. Figure 3 shows $N(H_2)$ versus R obtained using a constant conversion factor, as well as the actual $N(H_2)$ distribution. A T_{EX} gradient of this size will lead to an error of an order of magnitude in the inferred H_2 mass between the center and edge of the disk.

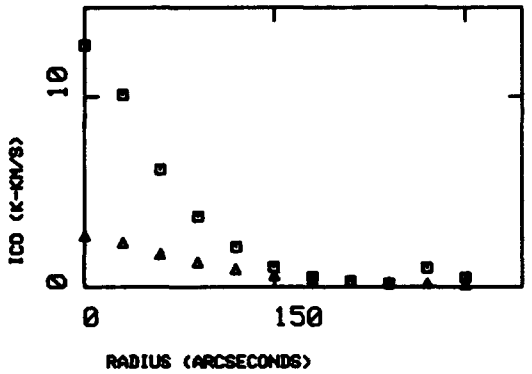

Figure 2. Integrated CO intensity vs. R (20"=1 kpc) for model with exponential T_{EX} (boxes) and constant T_{EX} (triangles).

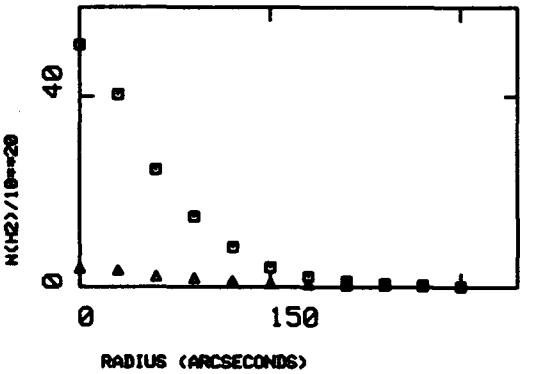

Figure 3. Actual $N(H_2)$ distribution (triangles) and distribution inferred from $I_{CO}/N(H_2) = 4 \times 10^{20}$. $N(H_2)$ in units of 10^{20} cm^{-2}.

It is apparent that large errors in H_2 mass within a galaxy are possible when using a constant $I_{CO}/N(H_2)$ conversion, with the result that the actual gas distribution may be considerably different from what is inferred from CO observations. In the absence of information on the actual variation of excitation temperature across a galaxy, caution must be exercised in the use of such conversions.

I would like to thank John Black for numerous helpful discussions.

REFERENCES

Dickman, R.L., Snell, R.L., and Schloerb, F,P. 1986, in press.
Kormendy, J., and Norman, C.A. 1979, Ap.J. 233, 539.
Larson, R.B. 1986, M.N.R.A.S. 218, 409.

Leung, C.M., Kutner, M.L., and Mead, K.N. 1982, Ap.J. 262, 583.
Maloney, P.R. 1986, in preparation.
Myers, P.C. 1983, Ap.J. 270, 105.
Oort, J. 1974, IAU Symp. 58, 375.
Roberts, W.W.,Jr., Roberts, M.S., and Shu, F.H. 1975, Ap.J. 196, 381.
Young, J.S., and Scoville, N.Z. 1982, Ap.J. 258, 467.

C. STARBURST AND INTERACTING GALAXIES

ORAL PRESENTATIONS

STARBURST GALAXIES

Daniel W. Weedman
Department of Astronomy
525 Davey Laboratory
Pennsylvania State University
University Park, PA 16802
U.S.A.

ABSTRACT. The infrared properties of star-forming galaxies, primarily as determined by IRAS, are compared to X-ray, optical, and radio properties. New luminosity functions are reviewed and combined with those derived from optically discovered samples using 487 Markarian galaxies with redshifts and published IRAS 60μ fluxes, and 1074 such galaxies in the Center for Astrophysics redshift survey. It is found that the majority of infrared galaxies which could be detected are low luminosity sources already known from the optical samples, but non-infrared surveys have found only a very small fraction of the highest luminosity sources. Distributions of infrared to optical fluxes and available spectra indicate that the majority of IRAS-selected galaxies are starburst galaxies. Having a census of starburst galaxies and associated dust allows several important global calculations. The source counts are predicted as a function of flux limits for both infrared and radio fluxes. These galaxies are found to be important radio sources at faint flux limits. Taking the integrated flux to $z = 3$ indicates that such galaxies are a significant component of the diffuse X-ray background, and could be the dominant component depending on the nature of X-ray spectra and source evolution. The dust which must be associated with the known infrared galaxies obscures a significant portion of the universe beyond $z = 3$. Depending on the scale size of dusty galaxies, this effect may prevent the observation of distant quasars and primordial galaxies.

1. INTRODUCTION

Infrared astronomers can be defined as those individuals whose primary source of reward is hot dust. Studying hot dust might be considered as just another one of those things people do in California, but the census of this dust revealed by the IRAS has dramatic implications, at least for astronomy. In this paper, I summarize some implications of IRAS discoveries for understanding various astronomical problems, including consequences for X-ray, optical, and radio astronomy as well as fundamental cosmological interpretations of galaxies and quasars. In all cases, the results discussed arise because the extra-galactic sources seen by IRAS are predominantly star forming regions visible in the infrared by re-radiation from dust heated by the hot, massive, young stars. It is now obvious that this is the most efficient locator of star forming regions, so that these new data give us the most complete accounting yet available of star formation in the universe.

This paper emphasizes the starburst galaxies because it is clear that the great majority of the most luminous infrared galaxies are made luminous by star-bursts. This was already suspected from ground based observations, but was quantified by studies of IRAS sources (e.g. Lawrence et al. 1986, Rieke and Lebofsky 1986). Galaxies whose fundamental power sources are non-thermal, such as Seyfert galaxies, can be notable infrared sources, but do not exceed 10% of the infrared-luminous galaxies in any surveys. Even some bright Seyferts, such

Carol J. Lonsdale Persson (Editor)
Star Formation in Galaxies

as NGC 1068, are found when observed carefully to have their infrared luminosity arising primarily from starbursts rather than non-thermal processes (Telesco et al. 1984). Consequently, I am not going to distinguish any further in this review between thermal and non-thermal infrared sources, and will simply group all galaxies into a single infrared luminosity function.

The term "starburst" connotes an object in which star formation is proceeding at a rate that cannot be maintained in equilibrium over the life of a galaxy. A corollary is that the observed properties of a galaxy undergoing a starburst are dominated in many wavebands by radiation originating in the starburst: X-rays from supernova remnants and compact accretors associated with massive stars, ultraviolet and optical continua from the hot stars themselves, emission lines from ionization by these stars, infrared continua from dust re-radiation, and radio continua from the hot gas and the supernova remnants.

It is no surprise that starburst galaxies show up on lists of interesting objects derived in many different ways. While the most luminous infrared galaxies fulfill this definition of starburst galaxy, there are many fainter infrared galaxies which are luminous because of star formation processes proceeding at more or less their equilibrium rate. There is no defined luminosity at which such "normal" galaxies separate from starburst galaxies. To facilitate my analysis, I will group all galaxies into a single 60μ luminosity function, whether starburst or not.

I feel there is no real purpose in defining precisely when the star formation rate is abnormally high, but if one wishes a rigorous definition of a starburst system, it could probably best be derived using the ratio of infrared to optical flux. In the discussion below, I consider the infrared properties of some optically derived samples--the bright, generally normal galaxies in the Center for Astrophysics redshift survey (Huchra et al. 1983) and the Markarian galaxies, most all of which are detected because excessive star formation makes their optical continua unusually blue. Utilizing the ratio "r" of infrared to optical flux as defined by Soifer et al. (1984), the distribution of r in these samples is as in Table I for those CfA and Markarian galaxies detected by IRAS. It is seen that Markarian galaxies are systematically about four times as luminous in the infrared relative to the optical. This is comparable to the distribution of r for galaxies discovered as infrared sources by Wolstencroft et al. (1985). My primary objective in the remainder of this paper is to consider some overall consequences of star formation in the universe as revealed by infrared results, so I worry no further about precise definitions for the various galaxies in which such star formation is revealed via the infrared luminosity.

2. LUMINOSITY FUNCTION FOR GALAXIES AT 60μ

The correct way to determine the luminosity function for any sample of celestial objects is to define the sample on the basis of a flux limit and then determine the actual fluxes and redshifts of every object in the sample. This procedure has begun for samples of infrared galaxies found by IRAS, utilizing primarily the 60μ fluxes at which detections are optimized. Two such studies based primarily on new redshift data have already appeared (Lawrence et al. 1986, Soifer et al. 1986). The importance of continuing these efforts is so obvious that I should not bother to mention it. It would be useful if authors

Table I
Distribution of Infrared to Optical Flux Ratio r

bin of log r	# of Markarian galaxies	# of CfA galaxies
-1.6 to -1.2	1 (0.2%)	3 (0.28%)
-1.2 to -0.8	1 (0.2%)	21 (1.20%)
-0.8 to -0.4	5 (1.0%)	125 (11.6%)
-0.4 to 0	62 (12.7%)	531 (49.4%)
0 to +0.4	188 (38.6%)	307 (28.9%)
0.4 to 0.8	177 (36.3%)	71 (6.6%)
0.8 to 1.2	43 (8.8%)	15 (1.4%)
1.2 to 1.6	9 (1.8%)	0 (0%)
1.6 to 2.0	1 (0.2%)	1 (0.1%)
2.0 to 2.4	0 (0%)	0 (0%)

always include their redshift and flux values in papers, because it is impossible otherwise to reproduce calculations of luminosity functions, and comparison between different samples then involves interpolation to other luminosity bins, normalizing of different cosmologies, and a lot of wondering as to whether I or one of the other parties did it wrong in the first place.

In Table II are shown the results for the two studies mentioned, normalized to the best of my ability to the same luminosity intervals and H_o = 75 km s^{-1} Mpc^{-1}. Both studies derive from faint IRAS sources in small areas of the sky and refer to relatively luminous galaxies. The results do not agree particularly well, but the average of them should give a real luminosity function that does not err by more than a factor of two in any bin.

Table II
Space Densities of Galaxies for 60μ Luminosities

d log L_ν (erg/s/Hz)	d log νL_ν (erg/s)	Lawrence $\#Mpc^{-3}$ (294 galaxies)	Soifer $\#Mpc^{-3}$ (141 galaxies)	CfA $\#Mpc^{-3}$ (1051 galaxies)	Markarian $\#Mpc^{-3}$ (487 galaxies)
28.6-29	41.3-41.7	-	-	-	-
29 -29.4	41.7-42.1	-	-	3.2×10^{-2}	1.2×10^{-2}
29.4-29.8	42.1-42.5	9.7×10^{-3}	-	9.6×10^{-3}	9.7×10^{-4}
29.8-30.2	42.5-42.9	5.5×10^{-3}	-	3.2×10^{-4}	3.5×10^{-4}
30.2-30.6	42.9-43.3	4.7×10^{-3}	-	10.6×10^{-4}	2.0×10^{-4}
30.6-31	43.3-43.7	1.8×10^{-3}	-	3.0×10^{-4}	1.2×10^{-4}
31 -31.4	43.7-44.1	6.2×10^{-4}	3.5×10^{-4}	5.7×10^{-5}	3.8×10^{-5}
31.4-31.8	44.1-44.5	2.1×10^{-4}	5.6×10^{-5}	5.7×10^{-6}	6.8×10^{-6}
31.8-32.2	44.5-44.9	4.1×10^{-5}	8.5×10^{-6}	1.2×10^{-7}	6.6×10^{-7}
32.2-32.6	44.9-45.3	6.5×10^{-6}	2.0×10^{-6}	1.7×10^{-8}	3.6×10^{-8}
32.6-33	45.3-45.7	9.4×10^{-7}	1.9×10^{-7}	1.0×10^{-9}	8.7×10^{-10}
33 -33.4	45.7-46.1	1.8×10^{-7}	5.1×10^{-8}	-	-

To supplement these results at low luminosities, it is necessary to have nearby galaxies, which are found spread over the entire sky. Limiting values to the space densities at low luminosities can be derived from the CfA sample, using IRAS fluxes for those galaxies. This sample contains redshifts for the approximately 2500 brightest galaxies, defined by their optical magnitude, in the most accessible 9000 deg^2 of the sky. I found 60μ fluxes for 1074 of them excluding Markarian galaxies (to be discussed separately) in the catalog of Lonsdale et al. (1985). Calculating distances and luminosities is problematical for some because of the very low redshifts. To keep the procedure simple, I ignored those with $cz < 500$ km s^{-1} and determined distances to the rest using $H_o = 75$ km s^{-1} Mpc^{-1}. The CfA sample is a large and important data base for use with IRAS results; there are many more sophisticated things which could be done.

Most of the CfA galaxies are found in low luminosity 60μ bins. The space densities of such galaxies in the infrared luminosity function only represent a lower limit to the true space densities, because they are defined by an additional optical selection effect that may or may not affect the infrared selection. That is, there may be more low luminosity infrared galaxies Mpc^{-3} than have already been found as optically bright galaxies. On the other hand, the fact that these low luminosity infrared galaxies exist in the CfA sample as known objects means that they must be included in the complete infrared luminosity function; that function cannot be truncated at only those luminosities seen in the samples derived from IRAS discoveries alone.

The largest other sample of optically discovered galaxies having redshifts is the Markarian sample, which gives another set of minimum limits to the infrared-luminous galaxies which must exist. Of the 1500 known Markarian galaxies, I found 487 with both redshifts and 60μ fluxes. Existing data on Markarian galaxies including 60μ fluxes are summarized by Mazzarella and Balzano (1986); their catalog was completed after my calculations so may include a few more redshifts than I utilized. Space densities from the CfA and Markarian samples are also listed in Table II, calculated assuming an IRAS 60μ flux limit for source detection of 0.5 Jy.

In Table III, the space densities of Table II are summarized into a single luminosity function that is adopted for the remainder of this paper. This Table also shows the proportion of galaxies in any luminosity bin that would already have been known from the optically derived samples compared to the number found from IRAS-derived samples. There are two interesting conclusions from this comparison; a few examples of the most infrared luminous galaxies were already known among optically discovered galaxies (such as Markarian 231, 171, NGC 7469, IC 4553), but infrared discovery observations find an increasingly higher percentage of the most luminous galaxies. This is a simple demonstration of the importance of IRAS for finding many examples of the most dramatic starburst systems. (It is fair to note that these percentages greatly underestimate the potential of optical techniques for finding such galaxies. No completeness corrections have been applied to the Markarian sample, and no allowance has been made for improved objective prism observations such as in Wasilewski (1983) that can significantly increase compared to Markarian's search the number of starburst galaxies found optically.)

Table III
Space Densities and Luminosity Function Adopted at 60μ

d Log L_ν	Space Density # Mpc^{-3}	minimum known optically	log L_ν	log Ψ Ψ has units # $Mpc^{-3}>L_\nu$
29 -29.4	$>4.4\times10^{-2}$	100%	29	>-1.18
29.4-29.8	$>1.0\times10^{-2}$	100%	29.4	>-1.64
29.8-30.2	5.5×10^{-3}	65%	29.8	-1.90
30.2-30.6	4.7×10^{-3}	28%	30.2	-2.15
30.6-31	1.8×10^{-4}	23%	30.6	-2.61
31 -31.4	4.8×10^{-4}	20%	31	-3.19
31.4-31.8	1.3×10^{-5}	9%	31.4	-3.80
31.8-32.2	2.5×10^{-6}	3%	31.8	-4.52
32.2-32.6	4.3×10^{-7}	1%	32.2	-5.30
32.6-33	5.7×10^{-7}	0.3%	32.6	-6.16
33 -33.4	1.2×10^{-7}	0%	33	-6.92

3. SOURCE COUNTS IN INFRARED AND RADIO, AND THE X-RAY BACKGROUND

3.1. Results at 60μ

The luminosity function in Table III, derived from various uses of IRAS fluxes, provides a starting point for predictions for how many star-forming galaxies should be seen in the universe with various observing techniques. Such predictions are commonly presented in terms of source counts as a function of flux limit, or "log N - log S" plots. The easiest way to make such calculations is as a sum of the number of galaxies seen in successive volume shells of the universe. Let dN(z) be the number of galaxies within a redshift interval dz having volume interval dV seen to a given flux limit. Then $dN(z) = \Psi[L(z)]dV$, for L(z) the minimum luminosity which can be reached for observations at z with the flux limit used. All of the results presented use a cosmology with q_o = 0.1, although the precise form is not important for most results, and H_o = 75. The methodology and necessary cosmological equations are summarized in Weedman (1986). All calculations for the infrared use a continuous spectrum of form $f_\nu \propto \nu^{-2}$, an index corresponding to that between 25μ and 60μ for typical galaxies in the samples used to construct the luminosity function.

Expectations for observations at 60μ are in Table IV, carried to a final flux limit of 0.5 mJy. Not surprisingly, the number of sources to be found increases rapidly with flux limit. The characteristic redshift of sources also increases but does not reach very large values even for faint flux limits because source counts are contaminated by the many low luminosity, nearby objects. If the most luminous objects could be traced, they would be visible to great distances. This is shown by the values of maximum redshift at which a galaxy with log L_ν = 33 could be seen.

Table IV
Predicted Source Counts and Redshifts for 60μ Flux Limits

Flux limit (Jy)	# deg^{-2}>f(60μ)	most probable z	highest z
11	0.01	0.0030	0.07
4.4	0.038	0.0045	0.10
1.8	0.15	0.0070	0.15
0.7	0.53	0.011	0.23
0.28	1.9	0.017	0.33
0.11	6.5	0.026	0.48
0.045	21	0.040	0.66
0.018	67	0.065	0.90
0.0072	200	0.095	1.22
0.0029	580	0.14	1.61
0.0012	1540	0.21	2.10
0.0005	3800	0.28	2.70

3.2. Relation to Radio Source Counts

Contrary to some expectations, deep radio surveys with the VLA did not reveal progressively increasing fractions of radio sources to be faint and distant quasars. Instead, a new population of intrinsically faint but relatively nearby galaxies begins to appear at flux levels of a few times 10^{-4} Jy (Condon 1984, Windhorst et al. 1985). From their blue colors, these seem to be starburst galaxies. The radio properties of starburst galaxies and IRAS sources in general deserve increased attention, and are getting it (see papers by Dressel, Wielebinski, Fich, and Eales and Wynn-Williams, this meeting). Data so far available indicate very similar ratios of infrared to radio flux, as would be expected if both are the consequence of the same starburst (e.g. Helou, Soifer and Rowan-Robinson 1985). For my calculations, I adopt the mean ratio f(60μ)/f(20cm) = 350 from the 8 starburst systems measured with both the VLA and IRAS from Sramek and Weedman (1986). Applying this to the luminosity function of Table III predicts the radio counts at 20 cm given in Table V. Fluxes associated with the counts in Table V can be rescaled proportionally if another value is adopted for the f(60μ)/f(20cm) ratio.

These expectations are consistent with the observed radio counts to the extent that the infrared galaxies predict a significant portion of but do not exceed the observed source counts. For example, Windhorst, Kron and Koo (1984) find 50 sources deg^{-2} to 6×10^{-4} Jy at 20 cm. There is much room and great potential for new and exciting results in correlating the infrared and radio properties of faint starburst systems. These may prove to be the dominant component for the faintest radio counts. Conversely, the radio counts can provide useful constraints to deductions from infrared data, which encourages further efforts at improved correlations between data from the two wavebands.

3.3. The Extragalactic Diffuse X-ray Background

The most outstanding puzzle in observational X-ray astronomy is that of the source of the diffuse X-ray background at energies above one KeV (Boldt 1981). This background seems to fill the extragalactic sky evenly and so must

Table V
Radio Source Counts of Starburst Galaxies at 20 cm

Flux limit (Jy)	# deg^{-2}>f(20cm)
0.29	0.0003
0.12	0.0014
0.047	0.006
0.0019	0.023
0.0075	0.088
0.0030	0.34
0.0012	1.2
0.0005	4.5
0.0002	16

arise from very distant sources. (The lower energy background has structure that correlates with the Milky Way Galaxy, so is attributed to various Galactic sources.) Much effort has gone into asking what sources could explain this background. Quasars, for example, could with sufficient evolution arise in adequate numbers to explain the background, except that the observed steep X-ray spectra of quasars are in gross disagreement with the flatter, seemingly thermal, spectrum of the background. Perhaps the background is associated with diffuse processes in the early universe, or perhaps it hints at an as yet unobserved population of objects. The exciting result from the infrared data is that starburst galaxies can play a significant, perhaps dominant, role in explaining this X-ray background.

Once again, I start with the starburst galaxy luminosity function in Table III. The answer for the predicted background will simply be a lower limit. The reasons are several. Low luminosity galaxies in large numbers could be significant for any background, which is by definition the integrated flux from many sources too faint to be resolved. Yet, the infrared luminosity function in Table III is truncated at log L(60μ) = 29, with no allowance for fainter galaxies that could conceivably exist in large numbers, given the steepness of the luminosity function. Furthermore, star formation should have been more common in the early universe, but no evolution is included in my calculation. Finally, the sum of sources is carried only to z = 3, because that is where the high redshift observables (quasars) cease, even though the presence of heavy elements in those same quasars shows that star formation must have predated their epochs.

It is possible empirically to ratio infrared and X-ray fluxes using a few star-forming systems with both Einstein and IRAS fluxes. The result I adopt arises from 12 galaxies in Fabbiano, Feigelson and Zamorani (1982) whose mean ratio $f(60\mu)/f(2keV) = 2.7 \times 10^{8}$. Extremes of this value range from 4.7 to 0.4. An improved determination of this ratio could be folded into the calculation simply by scaling the predicted X-ray background in proportion, as long as the ratio is not taken as a function of luminosity. Another uncertainty lies in the X-ray spectrum of starburst systems, of which nothing is known. (This ignorance may be considered an advantage for the modeler since that lessens demands on one's model.) Because existing galaxy observations are at 2 keV, that is the energy of the background calculation made. It is necessary to

adopt a spectrum to account for K-corrections at high redshifts; because matching the background is the target, I adopt a spectral index of -0.4 to resemble that observed for the background near this energy.

The results are quite exciting, predicting without source evolution a 2 keV background from faint, unresolved X-ray sources of 1.3×10^{-7} Jy deg^{-2}, or 13% of the observed background. The sources are so common (over 10^6 deg^{-2}--see next section) that this background would appear unstructured. Applying source luminosity evolution proportional to $(1+z)^2$, not unreasonable since quasars evolve as about $(1+z)^4$, approximately doubles the background. The most critical need at the moment to pursue this idea further is improved X-ray data on starburst galaxies; it is obvious, however, that with relatively minor modifications to the parameters used the starburst galaxies could prove to be the primary source of the extragalactic X-ray background.

4. THE SHROUD OF THE UNIVERSE

Among the more pressing cosmological mysteries are the issues of why no primordial galaxies can be seen (e.g. Sunyaev et al. 1978) and why quasar numbers rapidly diminish beyond redshift of about 2.5 (Osmer 1982, Schmidt, Schneider and Gunn 1986). Various speculators have wondered if one or both of these effects might be caused by dust obscuring the background universe. Here, as well, the infrared galaxy luminosity function is a necessary step toward learning the answer. For this use, we no longer care what is heating the dust, but simply use the infrared-luminous galaxies as tracers of dust. Obviously, the results will be lower limits, because we omit objects containing dust that is not heated enough to radiate and omit objects with luminosities too low to be included in Table III.

To consider dusty galaxies as obscurers rather than emitters requires some modifications in cosmological considerations. Fluxes and luminosities no longer are relevant; all that counts is the total area of the sky covered up by all galaxies to a given redshift, regardless of the luminosities of these galaxies. A very important cosmological effect enters, which is that the angular diameter of galaxies decreases very little with redshift beyond z about unity. Unlike its contribution to flux, the obscuring ability of a galaxy changes little with redshift in those redshift regimes where the total number of galaxies is increasing dramatically. For example, with $q_o = 0.1$ and $H_o = 75$, the angular diameter subtended by 10 kpc remains almost constant at 1.3" for all $z>1$.

As was done for the source count calculations, the numbers of galaxies per shell of volume are summed to the cutoff redshift, also taken here as $z = 3$. Truncating the luminosity function at the luminosity in Table III, there are at least 6.6×10^{-2} dusty galaxies Mpc^{-3}. Carrying these to $z = 3$ with the cosmology assumed yields 1.1×10^6 galaxies deg^{-2}. It is easy enough to weight each of these by actual size, because the great majority of them are at $z>1$ where their angular size no longer changes with z. From this result, it is found that the fraction of the universe beyond $z = 3$ which is obscured by these galaxies closer than $z = 3$ is $4.5 \times 10^{-3} R^2$, for R the effective radius of the absorbing material in kpc.

This result illustrates the critical importance of obtaining infrared imaging data on galaxies to determine reasonable values for R. Note presentations at this meeting by Telesco, Low, and Rice. Recalling that most of the galaxies in the luminosity function are normal spirals, R may approach 10 kpc. In that case, the obscured fraction approaches unity, and could easily exceed unity if allowance were made for the faint or cold but dusty galaxies not included in the luminosity function used. Regardless of the conclusions finally reached, the IRAS data give us unambiguous proof that dust plays a significant role in governing the observable properties of the distant universe.

5. PUZZLES AND PROGRESS

There are many other aspects of investigating starburst galaxies whose importance is not diminished by the fact that I did not review them thoroughly. For example, I trust that A. Toomre will give what is due to those theorists who are struggling commendably with understanding why starbursts happen at all. Work by Struck-Marcell and Scalo discussed at this meeting is particularly relevant and diligent. Another area exciting in its own right is the molecular radio astronomy which attempts to understand how the presence of giant molecular clouds couples to the starburst phenomenon. There is no question that extensive CO emission correlates with infrared flux, as discussed in the literature and at this meeting by Young et al., Lo et al., and Solomon. Which ingredient was needed first; did the dust have to be there to make the molecules, or are the stars which made the dust there because of the raw material in the molecular clouds?

Another intriguing molecular observation is that of the megamasers such as originally emphasized by Baan and Haschick (1984) and discussed here by Bottinelli et al. and by Norris. These require not only dense molecular clouds between the observer and galactic nucleus, but also strong continuum radio sources in those nuclei. Such sources, as the ones in IC 4553, NGC 3079 and NGC 3690, are usually unresolved and accompanied by strong infrared sources (see the paper by Becklin and Wynn-Williams). To me, these sources are great puzzles. It is hard to understand how a starburst of the luminosity required, especially to explain the radio fluxes, can be compressed in such a small volume. These objects may prove to be important hybrids of starbursts plus something more mysterious. The entire question of why there are starbursts in and near galactic nuclei and how these relate to other forms of active nuclei is a basic one. Observationally, note papers here as well as earlier work by Turner, Keel, and Wilson which illustrate the various techniques being used to probe these nuclei; Norman has been worrying about the theory to explain these events and their consequences.

Various programs underway for intensive spectroscopic follow ups of IRAS sources are reported here by Houck, Savage et al., Dennefeld, and Smith et al. Beyond making major progress toward understanding the luminosity function and distributions of galaxy types, such observations are also the opportunity for finding really weird things. For example, are there more galaxies out there like Markarian 231? We knew 15 years ago that this object has a very strange optical spectrum, having a Seyfert 1 broad line region, absorption lines from young stars, and blueshifted absorption lines from dense interstellar material. I thought initially it was a more or less normal Seyfert galaxy with an absorbing cloud which happened to be in front of the nucleus, but the

exceptional infrared luminosity now known implies that the absorption is much more widespread. Optical observers have found no other similar objects. Are there many hidden in the IRAS lists?

Seeking to answer such questions illustrates a basic value of surveys such as that of IRAS: these produce a treasure trove that keeps astronomers in many specialties busy and excited for years. Closing on that note, the IRAS teams deserve much commendation for their efficiency in making this marvelous data base so quickly and easily available to the rest of us.

REFERENCES

Baan, W. A. and Haschick, A. D. 1984, Ap.J., 279, 541.
Boldt, E. 1981, Comments Ap. 9, 97.
Condon, J. J. 1984, Ap.J., 284, 44.
Fabbiano, G., Feigelson, E., and Zamorani, G. 1982, Ap.J., 256, 397.
Helou, G., Soifer, B. T., and Rowan-Robinson, M. 1985, Ap.J. (Letters), 298, L7.
Huchra, J., Davis, M., Latham, D., and Tonry, J. 1983, Ap.J. Suppl., 52, 89.
Lawrence, A., Walker, D., Rowan-Robinson, M., Leech, K. J., and Penston, M. V. 1986, M.N.R.A.S., 219, 687.
Lonsdale, C. J., Helou, G., Good, J. C., and Rice, W. 1985, Cataloged Galaxies and Quasars Observed in the IRAS Survey (Pasadena: Jet Propulsion Laboratory).
Mazzarella, J. M. and Balzano, V. A. 1986, Ap.J. Suppl., in press.
Osmer, P. S. 1982, Ap.J., 253, 28.
Rieke, G. H. and Lebofsky, M. J. 1986, Ap.J., 304, 326.
Schmidt, M., Schneider, D. P., and Gunn, J. E. 1986, Ap.J., 306, 411.
Soifer, B. T. et al. 1984, Ap.J. (Letters), 278, L71.
Soifer, B. T., Sanders, D. B., Neugebauer, G., Danielson, G. E., Lonsdale, C.J., Madore, B. F., and Persson, S. E. 1986, Ap.J. (Letters), 303, L41.
Sramek, R. A. and Weedman, D. W. 1986, Ap.J., 302, 640.
Sunyaev, R. A., Tinsley, B. M., and Meier, D. L. 1978, Comments Ap., 7, 183.
Telesco, C. M., Becklin, E. E., Wynn-Williams, C. G., and Harper, D.A. 1984, Ap.J., 282, 427.
Wasilewski, A. J. 1983, Ap.J., 272, 68.
Weedman, D. W. 1986, Quasar Astronomy (Cambridge: Cambridge University Press).
Windhorst, R. A., Kron, R. G., and Koo, D. C. 1984, Astr. Ap. Suppl., 58, 39.
Windhorst, R. A., Miley, G. K., Owen, F. N., Kron, R. G., and Koo, D. C. 1985, Ap.J., 289, 494.
Wolstencroft, R. D., Clowes, R. G., Kalafi, M., Leggett, S. K., MacGillivray, H. T., and Savage, A. 1985, preprint.

DISCUSSION

MONTMERLE:

You made the suggestions that starburst galaxies could explain the diffuse x-ray background. However, this background extends out to several 10 kev, whereas, to my knowledge, such high energies in our Galaxy, relate only to x-ray sources like compact binaries, etc. The Galactic star forming regions themselves may be associated with temperatures of 10-12 kev at most (see the recent 'Tenma' results). Therefore, what kind of observational evidence in our Galaxy may support your suggestion? Or are you thinking in terms of special processes not observed in Galactic star-forming regions?

WEEDMAN:

I don't know the answer for our Galaxy. Because there are no extragalactic starburst systems with 10 kev data, I didn't consider that energy in my analysis.

LOW:

Have you used the new infrared luminosity function to re-calculate the diffuse infrared background? It is possible to extract a diffuse extragalactic component from the IRAS data at 100μm.

WEEDMAN:

I have determined a number, but did not present it because I wasn't aware of any meaningful measurements that could extract the extragalactic background from Galactic and zodiacal backgrounds.

BURBIDGE:

Since you have a 60μm luminosity function, can you look at the production of helium in galaxies? In effect, the amount of helium produced by hydrogen burning in galaxies is now greater than we originally expected it to be because the bolometric luminosity of galaxies integrated over the age of the universe is greater.

WEEDMAN:

What you suggest is an important consistency check that I have not done.

SCOVILLE:

Could you comment on the relative shapes and number densities of the IRAS galaxy and quasar luminosity functions.

WEEDMAN:

I have not compared them to determine the luminosity at which the space densities are comparable. At most luminosities, the galaxies greatly dominate, but at the very highest luminosities, there are only quasars. My definition of quasars includes Seyfert 1 galaxies, so the real issue should be to try to produce thermally vs. non-thermally derived luminosity functions.

GALLAGHER:

In considering the issue of 'extra' bolometric luminosity that has been found by IRAS (e.g., with regard to Geoff's questions about He production), don't you have to distinguish between blue, near constant SFR systems that surprise us by radiating much of their power in the infrared, and true bursts which surprise us by having a much larger bolometric luminosity than we would have expected from optical data? Do you have any estimates for the relative infrared luminosity contributions of these two classes of Markarian systems?

WEEDMAN:

I have not tried to distinguish starbursts at various levels from more equilibrium star formation in the luminosity function given. The hope is that we are observing a representative statistical sample of the total 60μm luminosity at a given epoch of the universe, and that the average would remain the same even as individual galaxies come and go.

INFRARED SPECTROSCOPY OF STAR FORMATION IN GALAXIES

Sara C. Beck
Northeastern University, Huntington Avenue, Boston, MA 02115

Paul T.P. Ho and Jean L. Turner
Harvard-Smithsonian Center for Astrophysics, Cambridge MA 02138

ABSTRACT

We have observed the Brackett α (4.05 μm) and Brackett γ (2.17 μm) lines with 7.2″ angular and 350 km s^{-1} velocity resolution in 11 infrared-bright galaxies. From these measurements we derive extinctions, Lyman continuum fluxes, and luminosities due to OB stars. The galaxies observed to date are NGC 3690, M83, NGC 5195, Arp 220, NGC 520, NGC 660, NGC 1614, NGC 3079, NGC 6946, NGC 7714, and Maffei 2, all of which have been suggested at some time to be "starburst" objects. The contributions of OB stars to the luminosities of these galaxies can be quantified from our measurements and range from insignificant (Arp 220, NGC 3079, NGC 5195) to sufficient to account for the total energy output (M83, NGC 1614). The OB stellar luminosities observed are as high as 10^{12} $L_{\odot}$ in the galaxy NGC 1614. It is noteworthy that star formation can play very different roles in the infrared energy output of galaxies of similiar luminosity, as for example Arp 220 and NGC 1614. In addition to probing the star formation process in these galaxies, the Brackett line measurements, when compared to radio and infrared continuum results, have revealed some unexpected and at present imperfectly understood phenomena: 1) in some very luminous sources the radio continuum appears to be suppressed relative to the infrared recombination lines; 2) in many galaxies there is a substantial excess of 10μm flux over that predicted from simple models of Lyman α heating of dust if young stars are the only significant energy source.

OBSERVATIONS AND METHODOLOGY

Young O and B stars are likely energy sources for the intense infrared emission observed in many galaxies (Telesco and Harper 1980; Rieke *et al.* 1980; Scoville *et al.* 1983), but non-stellar sources may also be involved (Rieke 1976; Wynn-Williams and Becklin 1985). The first priority in studying star formation in galaxies is to quantify the contribution of young stars to the total luminosity. For this purpose, we have observed the Brackett α (4.05 μm) and γ (2.17 μm) lines of hydrogen. From the Brackett line strengths one can derive the extinction, the flux of ultraviolet photons, and, with the assumption of an initial mass function, the total number of OB stars present. The properties of this deduced stellar population, including total luminosity, 10 μm luminosity, and thermal radio flux, are then compared to the observed values. Details of the method are found in Beck *et al.* (1986), and Turner *et al.* (1986). Uncertainties in the derived quantities depend on their sensitivity to the assumed values of electron temperature, which can affect both the total ionizing flux and extinction derived by 10 to 15 percent; dust temperature, which can change the predicted 10 μm flux by up to 50 percent; and the initial mass function, the largest uncertainty, which can change the total luminosity due to young stars by up to a factor of two.

Carol J. Lonsdale Persson (Editor)
Star Formation in Galaxies

The observations were made using the Cornell Cooled Grating Spectrometer (Beckwith *et al.* 1983) on the NASA Infrared Telescope Facility on Mauna Kea in March and October 1985. All of the galaxies observed are bright, have companions, and have been suggested to contain regions of rapid star formation, but the sample spans a range in morphology, luminosity, distance, and strength of tidal interactions with the companion.

RESULTS

The OB luminosities derived from the Brackett lines indicate that star formation contributes varying amounts to the total infrared luminosities in the galaxy sample. In the three galaxies NGC 5195, Arp 220, and NGC 3079, the OB stellar population was found to contribute only insignificantly (less than 20 percent of the total) to the far-infrared luminosity. Corrections between the small-beam Brackett observations and the large beams of far-infrared measurements used to find the total luminosity cannot explain these discrepancies. By contrast, in NGC 1614 and M83 the luminosity due to OB stars derived from a Miller and Scalo (1979) initial mass function with upper mass limit 30 $M_\odot$ is actually somewhat greater than the total observed luminosity, indicating that star formation is the primary energy source and that the initial mass function may be truncated. In NGC 6946, NGC 7714, Maffei 2, NGC 660, NGC 520, and NGC 3690 the luminosity of young OB stars is a significant portion of the total observed. When beam size corrections are considered, the observations of these galaxies suggest that star formation is their major luminosity source, although proof will require continuum measurements with higher angular resolution.

From the Brackett line flux, the UV flux and hence the thermal radio continuum flux can be derived. In almost all cases, the predicted thermal radio flux $S^{pr}_{radio} < 0.1 - 0.2\ S^{tot}_{radio}$, with the excess radio emission due to synchrotron emission. There are two possible exceptions in the galaxy sample. The predicted thermal flux from NGC 1614 is about half the total observed. In the most unusual source, M83, S^{pr}_{radio} ~70–100 mJy whereas S^{tot}_{radio} ~30 mJy. The deficiency in radio emission in M83 could result from a very low electron temperature in the ionized gas ($< 5 \times 10^3$ K) or from optically thick radio continuum emission. The latter possibility is intrinsically more interesting in that it suggests the presence of $> 10^3$ compact HII regions with possibly 10^7 $M_\odot$ tied up in young stars. We suggest that the burst of star formation in M83 has been short, $< 10^4$ yrs, and that the prodigious rate of star formation cannot be sustained (Turner *et al.* 1986).

The 10μm flux can also be derived from the Brackett line fluxes, assuming that dust heating is due solely to Lyman α radiation within HII regions. Small beam ($< 8''$) 10μm ground observations when compared to IRAS 10μm observations with a larger beam ($0.8' \times 5.0'$), indicate an excellent correlation with on average more than 50% of the 10μm emission coming from the nuclear regions. Yet the 10μm fluxes predicted from Brackett lines consistently underestimate the observed 10μm flux (measured with similar telescope beams) by an average factor of 5. This excess in 10μm emission suggests that the nominal ratio of 10μm flux to the ionizing flux as derived from Galactic HII regions may not be applicable to external galaxies, especially in the nuclear regions. The 10μm excess could be due to unusual distributions of stars and gas, small dust grains, or possibly to higher temperatures in regions with a high spatial density of hot young stars.

THE NATURE OF STAR FORMATION IN GALAXIES

The galaxies in this sample for which OB stars are the primary energy source cover a wide range of luminosities, morphologies, and interaction histories. The Brackett line observations suggest that the infrared luminosity, radio continuum flux, and 10 μm emission may not be practical quantitative predictors of star formation activity under these circumstances. In some of the galaxies observed the thermal radio flux is lower than that predicted from the Brackett lines; in all of the galaxies the 10μm flux is significantly higher than the OB stars can account for if the emitting region behaves as do "normal" Galactic HII regions. These results imply that it is very difficult to unambiguously predict the spectral signature of star formation. Complicating factors as optically thick HII regions or non-equilibrium heating of small grains may have to be considered in models of such objects. This sample of bright infrared galaxies appears to be a disparate group and difficult to model. This may be only what should be expected from galaxies known to be undergoing a shortlived, unusual, and highly energetic stage of development.

This research has been supported in part by the Alfred P. Sloan Foundation, and NSF Grant AST85-09907. The Infrared Telescope Facility is operated by the University of Hawaii under contract from the National Aeronautics and Space Administration.

REFERENCES

Beck, S.C., Turner, J.L., and Ho, P.T.P. 1986, *Ap. J.*, in press.
Beckwith, S., Evans, N.J. II, Gatley, I., Gull, G., and Russell, R.W. 1983, *Ap. J.*, **264**, 152.
Miller, G.E., and Scalo, J.M. 1979, *Ap. J., Suppl.*, **41**, 513.
Rieke, G.H. 1976, *Ap. J. (Letters)*, **206**, L15.
Rieke, G.H., Lebofsky, M.J., Thompson, R.I., Low, F.J., and Tokunaga, A.T. 1980, *Ap. J.*, **238**, 24.
Scoville, N.Z., Becklin, E.E., Young, J.S., and Capps, R.W. 1983, *Ap. J.*, **271**, 512.
Telesco, C.M., and Harper, D.A. 1980, *Ap. J.*, **235**, 392.
Turner, J.L., Ho, P.T.P., and Beck, S.C. 1986, *Ap. J.*, in press.
Wynn-Williams, C.G., and Becklin, E.E. 1985, *Ap. J.*, **290**, 108.

DISCUSSION

PUGET:

If your 10μm excess is due to small grains, the observations in our Galaxy show that the excess is much larger in the neutral medium than in HII regions, so the 10μm excess may be a handle on the relative distribution of O stars and B stars.

HO:

That is certainly a good suggestion. When more detailed mapping is available, we can compare the 10μm excess and the ionizing flux in terms of spatial distribution.

GALLAGHER:

What is the evidence for an outflow from the nucleus of NGC 3079?

HO:

Hummel and collaborators have published a radio continuum map which shows an extension perpendicular to the plane of the galaxy.

YOUNG:

In your comparison of 10μm fluxes in a 7" aperture, what was the source of IR data? The Point Source Catalog will underestimate the total flux in many of the galaxies which are extended, and the coadded survey fluxes are higher than those in the Extragalactic Catalog.

HO:

For examining the 10μm excess, we used the Brackett lines to predict a 10μm flux in a 7" beam. We compared this flux to 10μm flux actually observed in ground-based observations with angular resolution $\leq$8". To determine the dominance of nuclear 10μm emission, we compare the ground-based photometry with IRAS 12μm flux from the Extragalactic Catalog. We don't think extended emission (with respect to the IRAS beam) is likely for our sample, because these sources have high correlation coefficients, $\sim$99%, consistent with 'point-like' (with respect to IRAS beam) distributions.

TELESCO:

All the 12μm IRAS flux in M83 can be accounted for in a recent map at 10.8μm (Telesco *et al*; this conference). Nearly all falls within the central 20" diameter region. However, most of this is not in the central 7". The infrared source is compact, but not extremely compact.

HO:

In our comparison of 10μm and Brackett flux for M83, we have actually summed over the positions mapped in the Brackett line. We have been careful to compare data that are at the same positions and with similar beams. M83 was the strongest source in our sample so that a little mapping was possible.

MOLECULAR GAS IN THE STARBURST NUCLEUS OF M82

K. Y. Lo
California Institute of Technology
Pasadena, California

ABSTRACT. 7″-resolution CO(1-0) observations of the central 1 kpc of M82 have resolved 2 components of molecular gas: (1) A high concentration in the central 700 pc × 200 pc, and (2) extended features that may be gas expelled from the central concentration. The central concentration of molecular gas falls in the same confines as the other tracers of recent star formation, and may be identified directly with the star-burst region.

The molecular gas in the star-burst nucleus of M82 appears to be highly disturbed and has high kinetic temperature (> 40 K), likely consequences of the high density of young star clusters. Stellar winds and subsequent supernovae from the star clusters can effectively sweep up the interstellar medium. The flux of the stellar radiation throughout the M82 star-burst region ($\sim 10^5$ $L_\odot/pc^2$) is comparable to that in Orion, at $\sim$ 0.25 pc from the Trapezium stars, and can heat the gas to high temperature. The $N(H_2)/I_{CO}$ ratio is $\sim$ 10 times smaller than that for the galactic GMC, but indicates a substantial column density still—$N(H_2) \geq 3 \times 10^{22}$ cm^{-2} or ≥ 500 $M_\odot/pc^2$. L_{IR}/M_{H_2} for the M82 star-burst region is 170 $L_\odot/M_\odot$, much higher than the ratio for the extended molecular disks of nearby galaxies ($\sim$ 5 $L_\odot/M_\odot$).

The spatial distribution and kinematics of the nuclear concentration of the molecular gas, as well as the 2 μm light distribution, suggest the presence of a stellar bar in M82. While accretion from outside the galaxy could have contributed to the gas supply in the nuclear region of M82, the immediate mechanisms for both supplying and confining the gas in the central 1 kpc, and for triggering the star formation may have been provided by the stellar bar.

Comparisons of the M82 star-burst nucleus to a sample of IR luminous galaxies suggest that star-burst regions in general may have a higher gas temperature (therefore higher integrated CO intensity) and much higher L_{IR}/M_{H_2} than the galactic disk, and that *L_{IR} of the star-burst regions may be essentially proportional to their area.*

1. INTRODUCTION

M82, at a distance of 3.25 Mpc, serves a prototypical system for studying the star-burst phenomenon. The most persuasive explanation for the 3×10^{10} $L_\odot$infra-red luminosity (Telesco and Harper 1980) is that it is due to a recent burst of star formation that started $\sim 5 \times 10^7$ years ago with an exponential decay time of $\sim 2 \times 10^7$ years and produced primarily massive stars at high efficiency (Rieke et al 1980). Detailed optical studies show that very young star clusters exist in the nucleus of M82 (O'Connell and Mangano 1978, hereafter OM), and high resolution radio maps of M82 show the presence of >40 compact radio sources which are most likely young supernova remnants (Kronberg et al 1985). Thus, star-bursts in the nucleus of M82 seem well founded.

Carol J. Lonsdale Persson (Editor)
Star Formation in Galaxies

Extremely large infra-red luminosity is observed towards the central few hundred pc to kpc scale in many galaxies (cf. Telesco and Harper 1980). Recent IRAS observations have shown that galaxies with extremely large far-IR luminosity are fairly common (Soifer et al 1986). While star-bursts could be the natural explanation for the luminosity, the underlying mechanisms for star-bursts are not well understood. Questions concerning (i) the source of the molecular gas, the raw material for star formation, (ii) the mechanisms for collecting the gas in the star-burst regions, typically the central kpc, and (iii) the triggering of star-bursts need to be answered. In addition, some mechanism to regulate the runaway star formation may be required.

One of the most useful approaches to this problem is through an investigation of the molecular gas, the raw material for forming new stars, using observations of the relatively abundant trace molecule, CO. M82 is the brightest emitter of the CO radiation which has been studied extensively via single telescopes (Rickard et al 1977; Knapp et al 1980; Olofsson and Rydbeck 1984; Young and Scoville 1984; Nakai 1984). Even at the modest distance of M82, single telescope CO observations have rather poor linear resolution: a few hundred pc at best (e.g. Nakai 1984). With the Owens Valley millimeter-wave interferometer, we have observed the molecular gas distribution within the central $\sim$ 1 kpc region with a linear resolution of 110 pc, adequate to resolve spatially some of the prominent irregular dusty filaments visible in optical pictures.

In this paper, we present high resolution interferometric observations of the CO(1-0) emission from the central $\sim 1'$ region of M82. (For details, see Lo et al 1986.) They show that the molecular gas can be divided into 2 components: (1) a high concentration in the central 700 pc $\times$ 200 pc, and (2) extended regions that may be shell-like and filamentary in structure. We also discuss the properties of the interstellar medium in the nuclear region of M82 implied by our and related observations and the implications of our observations for star formation in M82 and in other galaxies.

2. NUCLEAR CONCENTRATION OF MOLECULAR GAS

2.1 Relationship to Star-burst Region

Figure 1 shows the integrated CO intensity map of the central $\sim 1'$ of M82 superposed on a print of an 103aO plate of the galaxy. The CO source, 1.5 kpc by 0.3 kpc in extent, is roughly aligned with the disk of the galaxy and shows two prominent peaks $\sim 25''$ ($\sim$ 450 pc) apart, with a weaker one in between. To illustrate the relative distribution of the molecular gas and other components in the nucleus of M82, we have superposed the integrated CO intensity maps on (i) a λ6 cm map, (ii) a 10 μm map and (iii) a 2.2 μm map of the nuclear region of M82 (figure 2;cf. Rieke et al 1980). Both the 6 cm and 10 μm emissions trace the locations of recent formation of massive stars within a region of $\sim$ 700 pc $\times$ 200 pc. Figure 2 shows that the region of recent star formation falls in the same confines as the central concentration of the CO distribution. However, the correspondence is not exact in detail.

The correlation of strong CO emission and recent star formation is further illustrated by figure 3 in which a $0''.15$-resolution λ 6 cm map (Kronberg et al 1985) is superposed on the integrated CO intensity map. The general 6 cm distribution is very well correlated spatially with the central concentration of CO emission. There are many compact radio sources in the 6 cm map, lying preferentially on the periphery of the overall 6 cm distribution (with the majority to the south). These compact sources are most likely supernova remnants, some of which have been observed to be decreasing in flux and must be quite young (Kronberg and Sramek 1985). However, the supernova remnants appear to be offset from peaks of the CO emission.

Figure 1: The integrated CO intensity map of the central 1' of M82 at 7" resolution is superposed on a copy of a 103aO plate taken with the Hale 5m telescope. This map made from the broadband channel emphasizes the large velocity dispersion emission and some of the more extended small velocity dispersion emission may be below the sensitivity of this map. The contours are multiples of 187.5 K-km s^{-1}.

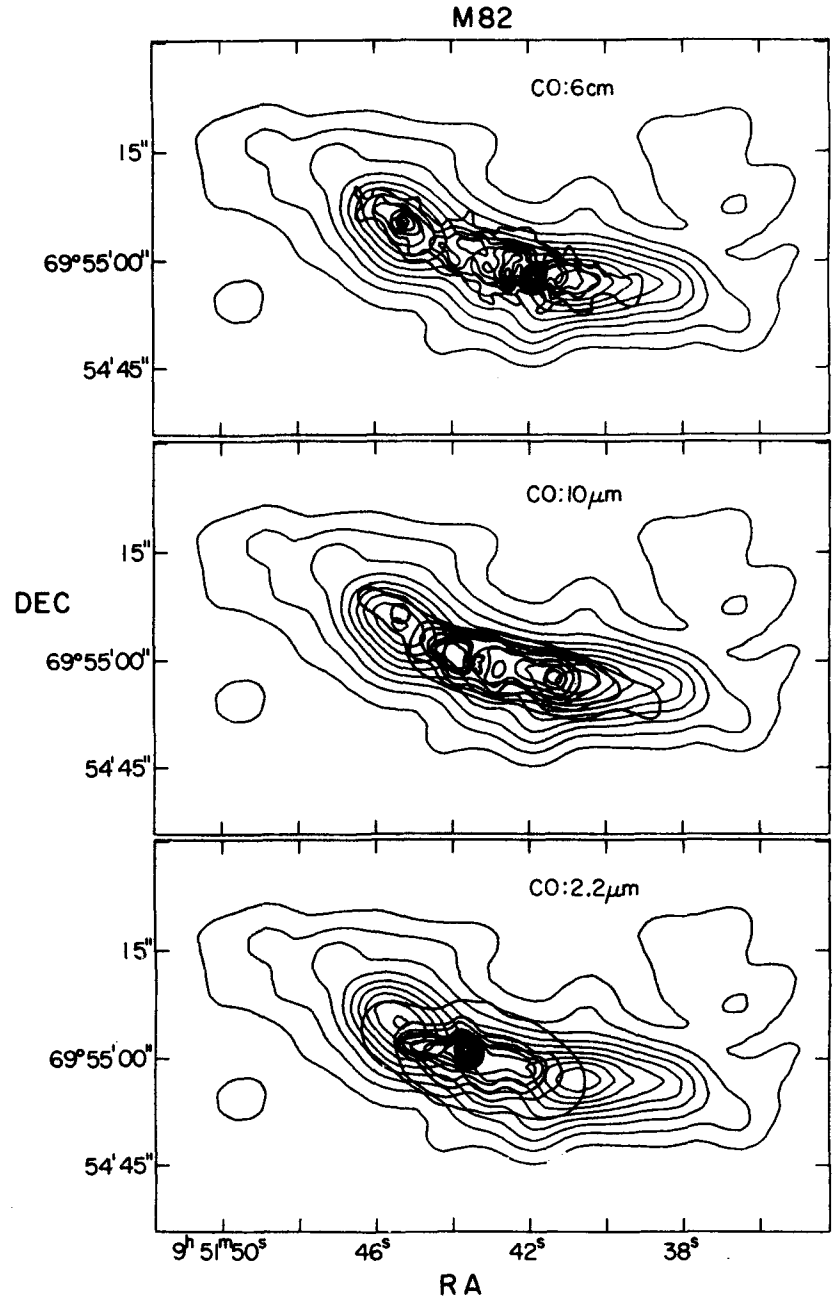

Figure 2: Comparisons of the integrated CO intensity map to λ 6 cm radio continuum (top), 10μm emission (middle), both tracers of recently formed stars, and 2.2 μm emission (bottom), presumably the underlying stellar nucleus and disk (Rieke et al 1980). Note that the CO peaks are not symmetrically placed about the 2.2 μm nucleus. The accuracy of the positional registration for all the maps is $\leq 1''$.

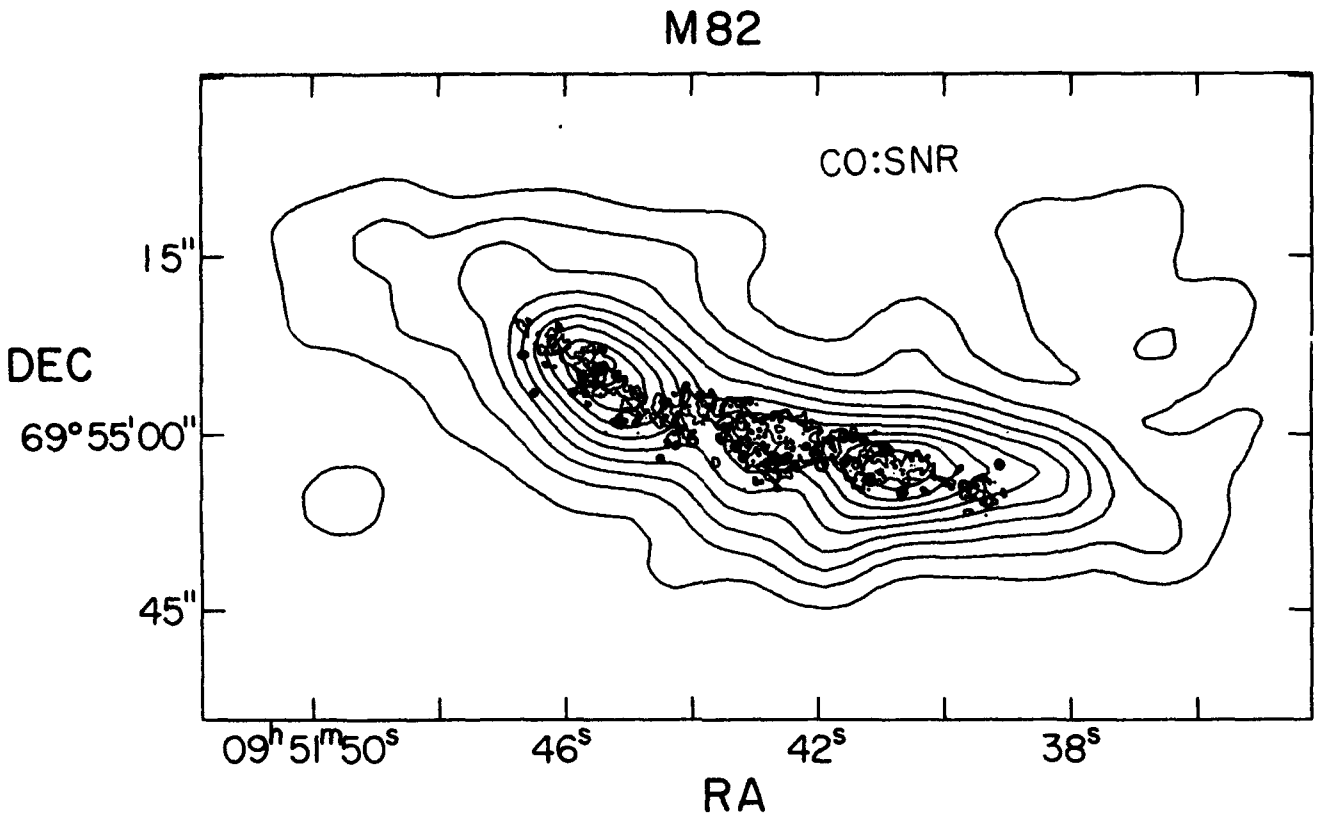

Figure 3: A 0.″15 resolution λ 6 cm radio continuum VLA map of M82 (Kronberg et al 1985), showing the discrete radio supernova remnants, is superimposed on the integrated CO intensity map. Note that the remnants are not situated on the CO intensity peaks.

2.2 Kinematics

From the available channel maps, an intensity-weighted velocity field of the CO emission measured with the spectrometer can be constructed, as shown in figure 4. The overall velocity gradient suggests a general rotation of the gas. The rotation axis would be at a PA of $\sim 130°$, about 20° offset from the stellar minor axis of M82. It appears that the kinematic and structural major axes of the CO emission are not aligned. Similar misalignment is observed in the velocity field derived from optical emission lines (Heckathorn 1972; OM; Williams et al 1985). Thus, the observed gas motion cannot simply be that of an inclined circularly rotating ring or disk. Within the central 300 pc region, the high brightness CO emission in the nucleus has a constant velocity gradient of 0.7 km s^{-1}/pc, compared to the Hα velocity gradient of ~ 0.9 km s^{-1}/pc within the central 180 pc (OM). The velocity gradient of the HI gas within the central 500 pc is ~ 0.5 km s^{-1}/pc (Weliachew et al 1984). The orbital time scale of the neutral and ionized gas within the central 500 pc of M82 is $\leq 10^7$ yr.

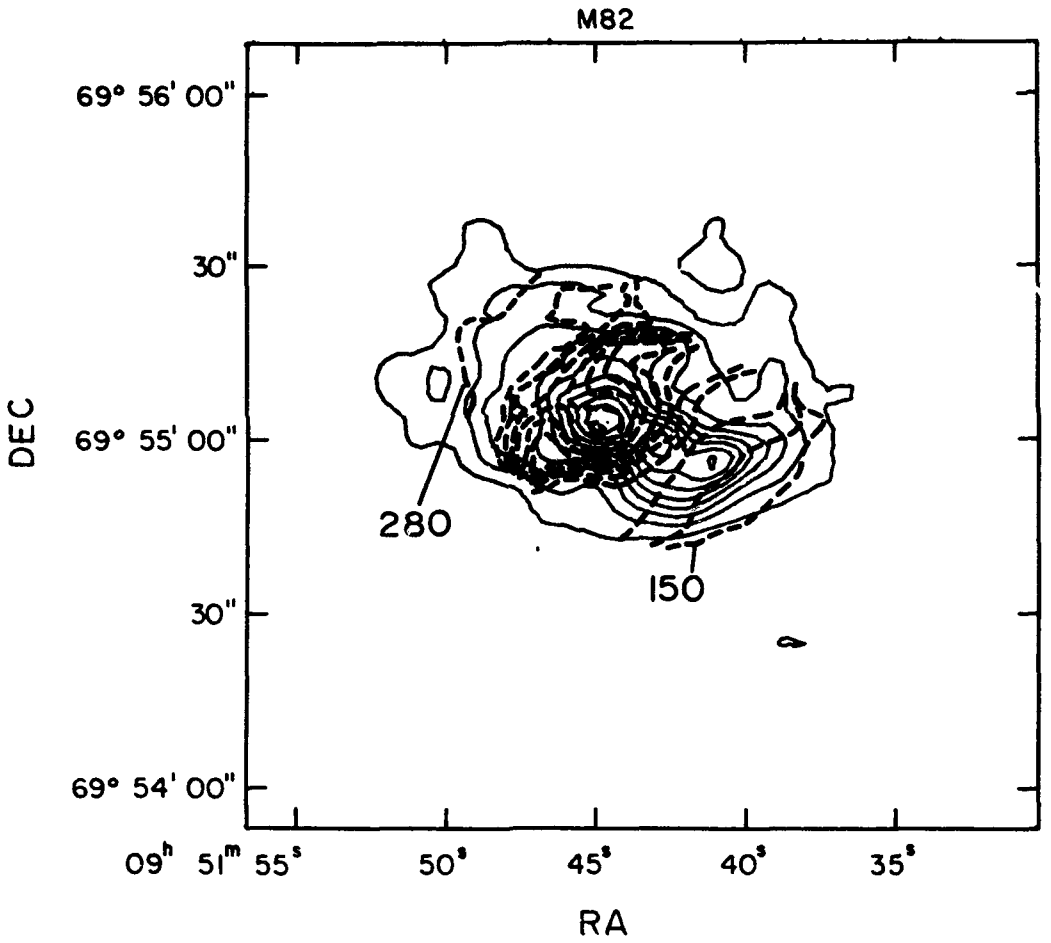

Figure 4: The dashed lines are the isovelocity contours at 10 km s^{-1} intervals, showing the velocity field of the CO emission falling within the spectrometer. The numbers are the LSR velocities in km s^{-1}. The solid contours show the CO intensity map obtained from summing all the emission in the observed channel maps and therefore does not represent all the emission in the central 1′. The contours of the solid lines are multiples of 54 Jy-km s^{-1}/beam.

3. EXTENDED EMISSION: MOLECULAR SUPERSHELLS ?

The channel maps (figure 5) show a bright, slightly resolved component as well as fainter extended emission. The bright component is CO emission from the central concentration, distinguishable from the extended emission by its higher brightness temperature and confinement. In many of the maps, the extended CO emission appears to show arc-like structures. As the linear resolution of the beam is ~ 110 pc, any distinctly resolved feature would have a scale > 200 pc. The arc-like structures at $V_{LSR} = 234.6$ km s^{-1} have scale size up to 400 pc. At other velocities, the extended emission may show overlapping arc-like structures, and sometimes, the structure retains some similarities over 2 to 3 channel maps (see, for example, $V_{LSR} = 286.2$, 297.0 and 307.4 km s^{-1} in figure 5.)

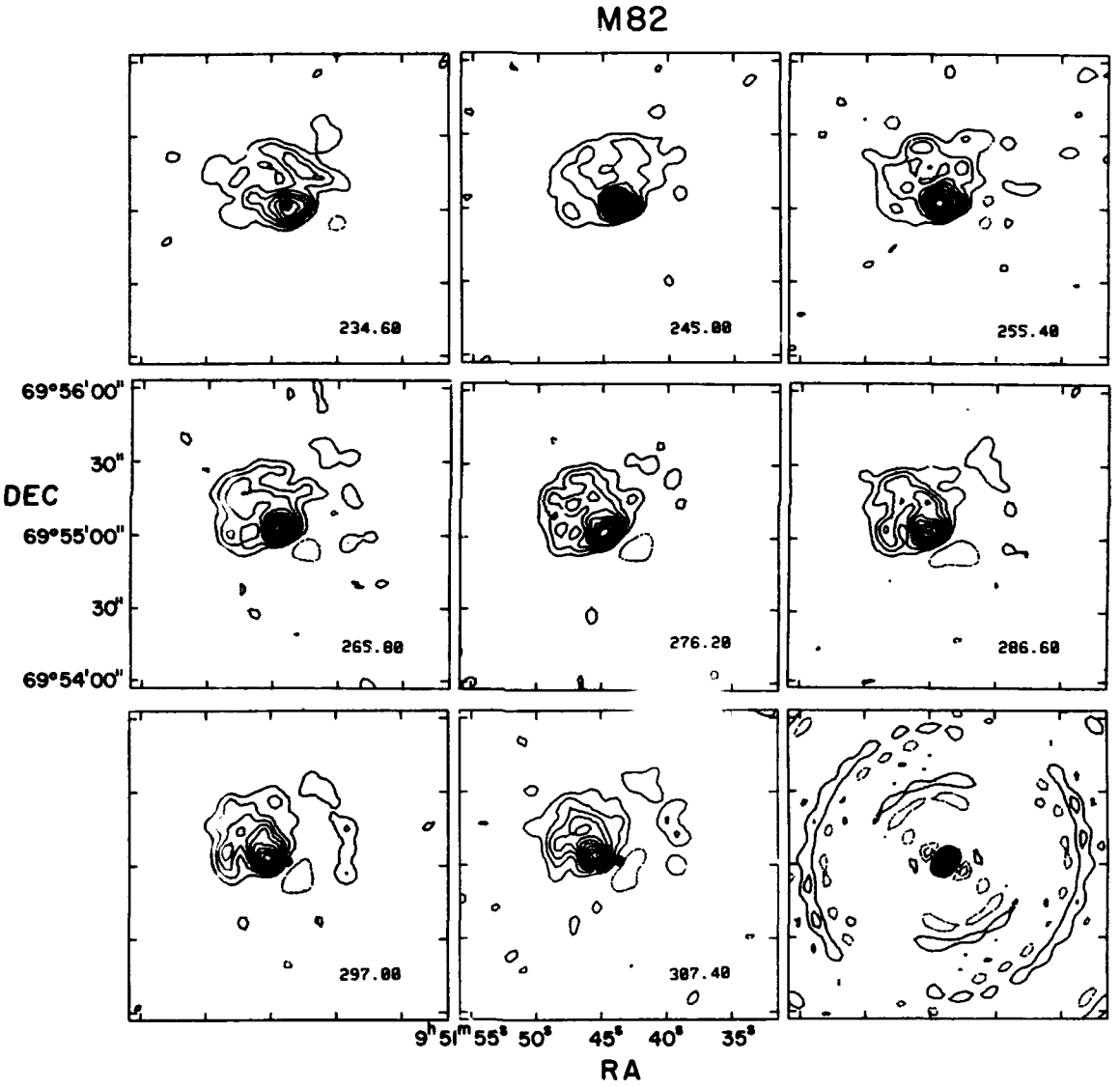

Figure 5: The "cleaned" 10.4 km s^{-1} channel maps all show the presence of a bright component and an extended fainter component (< 0.5 of peak brightness) which shows arc-like structures. The black dot denotes the 2.2 μm peak (cf. figure 2). The numbers refer to the V_{LSR} in km s^{-1} at the center of the 10.4 km s^{-1} channels. The shift in position of the emission relative to the 2 μm peak indicates a general velocity gradient. The contours are multiples of 0.7 Jy/beam or Rayleigh-Jeans brightness temperature of 1.1 K.

The total flux density from the extended emission is roughly twice that of the central concentration in each of the channels. This implies that the molecular gas mass involved in the extended emission is roughly twice that in the central concentration, if the same conversion factor from I_{CO} to H_2 column density applies to both. If the CO emission is optically thin (see below), then the H_2 mass in the extended emission is $\sim 10^8$ $M_\odot$.

If we identify the extended emission as largely due to gas expelled from the central concentration, perhaps in the form of incomplete shells, we may estimate the following parameters. The continuity of structure over only 2 to 3 channels may indicate that the present expansion velocity is low, $\leq$ 10 to 15 km s^{-1}. With scale size ranging up to $\sim$ 400 pc, the implied dynamical time scale is on the order of 10^7 yr. The expansion kinetic energy of the extended emission can be estimated as $\sim 1/2 \times 10^8 M_\odot \times$ (10 km s^{-1})^2 or $\sim 10^{53}$ ergs.

These shell-like structures may be similar to the HI supershells first identified by Heiles (1976, 1979) in our galaxy. Similar large and energetic HI shells have been identified in M101 (Allen et al 1978) and in M31 (Brinks 1984), as well as in other galaxies (cf. McCray and Kafatos 1985). A single supernova or the stellar wind from an individual O star cannot account for the large kinetic energy and scale size of one of these supershells (cf. Heiles 1979). A supershell can be formed from sweeping up the HI medium by the combined action of the stellar winds and subsequent supernovae from an OB association (Bruhweiler et al 1980; Tomisaka et al 1980; McCray and Kafatos 1985).

Given the enhanced level of recent star formation in the M82 nucleus, it may be natural to identify the extended CO emission with supershells. As the interstellar medium in the nucleus of M82 is quite different from those in the galactic disks (e.g. much higher mean density), the formation of such supershells requires more extreme energy input. The substantial mass ($\geq 10^8$ $M_\odot$) contained in the extended emission suggests that the interstellar medium is highly disturbed.

4. THE INTERSTELLAR MEDIUM IN THE NUCLEUS OF M82

4.1 Highly Disturbed Molecular Gas

While the gas in the nuclear concentration is only slightly resolved by the 7″ beam, its disturbed structure is suggested by a short exposure plate of M82 (cf figure 1 of OM) that shows a very patchy distribution of the obscuring dust on scales as small as $\sim$ 2″. Furthermore, the close correlation of a large number of young radio supernova remnants with the CO emission also implies that the medium would be highly disturbed by the explosions (cf. figure 4). The extended CO emission is most likely due to gas expelled from the central concentration. Thus, there exist both direct and indirect indications of a highly disturbed molecular gas medium in the central 1 kpc of M82.

4.2 High Gas Temperature

The peak T_b of CO emission from the central concentration of M82 ranges between 9 to 15 K. this is much higher than the brightness temperature of the clouds in our Galactic disk when averaged over $\sim$ 100 pc. The galactic values can be no larger than the 3 to 6 K (Sanders et al 1985; Blitz 1980). Taking into account the less than unity filling factor and probable small optical depth of the CO emission, one would infer that *the kinetic temperature of the gas in the central concentration (extent $\sim$ 700 pc) is greater than 40 K.*

Maintaining such high kinetic temperature for a substantial amount of gas over a large extent requires special circumstances. However, the nuclear region of M82 has a high space density of young massive stars (OM) and a very intense radiation field ($\sim 10^5$ $L_\odot/pc^2$ or ~ 45 ergs s^{-1} cm^{-2}, about 10^4 times that of the average galactic interstellar medium; Tielens and Hollenbach (1985)). *The molecular gas throughout the nuclear region of M82 is exposed to a radiation field not very different from that in Orion within 0.2 pc of the Trapezium stars.*

If the H_2 gas is highly disturbed by the stellar winds and supernova explosions from the young star clusters, with resultant sheet-like structures, large surface area of the molecular gas would be exposed to the intense radiation field external to the gas. Surface layers of hot molecular gas ($T_k \sim$ 100 K, thickness corresponding to $A_V \sim 2$) are obtained under such circumstances, heated primarily by photoelectric emission from dust grains (Tielens and Hollenbach 1985).

4.3 Column Density and Mass of H_2

Given the gas in the star-burst nucleus of M82 is found in very different conditions as the galactic disk GMC, the conversion from the observed integrated CO intensity to H_2 column density may be different. Since the observed properties of CO emission from the nucleus of M82 can be explained by a hot, optically thin source with a large area filling factor, the H_2 column density implied by the CO(1-0) intensity in this limit is 2.6×10^{19} I_{CO} cm^{-2} (cf. Knapp et al 1980), ~ 14 times smaller than that given by the conversion for galactic GMC (Sanders et al 1984). Also, the visual extinction implied by the CO intensity would then be consistent with that derived from other methods (Rieke et al 1980; Jaffe et al 1984). Within the central concentration (700 pc $\times$ 200 pc), the mean H_2 column density is 2.6×10^{22} cm^{-2}, or 430 $M_\odot/pc^2$ and the total H_2 mass is 6.0×10^7 $M_\odot$.

5. STAR FORMATION IN M82

5.1 Gas Supply

Detailed optical studies of M82 show that outside the central 2 kpc, the current star formation rate is abnormally low compared to normal late-type spirals (OM). In contrast, the central region has had very active star formation in the last 10^8 years, with the central star clusters being the youngest. The observations here show that a high concentration of neutral gas is found in the region of most recent star formation (central 700 pc), suggesting that a fresh supply of gas has entered the central 1 kpc to fuel the star formation during the last 10^8 years. To support the observed luminosity, massive stars must have been formed at a rate of $(L/10^{10}\ L_\odot)$ $M_\odot$/year or ~ 3 $M_\odot$/year (e.g. Scoville et al 1985) over the last 10^8 years, requiring a mean gas supply rate of > 3 $M_\odot$/year over the same period.

It has often been suggested that tidal interaction with M81 could be responsible for the observed properties of M82. The fuel for the last burst of star formation may have been accreted during the interaction with M81. There exists $\sim 10^9$ $M_\odot$of HI surrounding M82 (Cottrell 1977; Killian 1978).

5.2 Confinement Mechanisms

However, it is not clear how the tidal interaction confines the gas within the central kpc of M82. Furthermore, NGC253, another star-burst galaxy with properties very similar to M82 (Rieke et al 1980), is not in an interacting system, so that additional mechanisms besides tidal interaction may

be necessary. Both the spatial and kinematic distributions of the nuclear concentration of molecular gas may be consistent with the gas responding to a non-axisymmetric mass distribution in M82. 2.2 μm observations of Rieke et al (1980) and Scoville (private communications) show that the central 1′ of the M82 has a different PA from the galaxy as a whole. Furthermore, the 2.2 μm intensity profile of M82 shows a plateau with a scale size of 1′ in addition to an exponential profile typical of spiral galaxies. This profile is similar to those of barred spiral galaxies observed in the near-IR by Baumgart and Peterson (1986). Thus, there may be indirect indications of a stellar bar in M82, although the large inclination of the galaxy makes a definite identification difficult.

The effects of oval distortions in the nuclear bulges of spiral galaxies on the gas dynamics in the inner galaxy are significant (Huntley 1977; Zaritsky and Lo 1986), as perhaps illustrated in the high resolution observations of CO emission from nuclear regions in IC 342 (Lo et al 1984) and NGC 6946 (Ball et al 1985). An important consequence is the resulting radial transport of gas towards the center. In IC342, a few $\times$ 10^8 $M_\odot$ of gas are confined to a bar structure 1500 pc long, and the velocity field suggests the gas flow can be approximated by highly elliptical orbits. Thus, the orbital time scale of $\sim 10^7$ yr implies that on the average ≥ 10 $M_\odot$/yr of gas is brought towards the center. A similar process due to a stellar bar may have supplied the gas to the central kpc of M82.

5.3 Triggering Mechanisms ?

Do the star-bursts in M82 occur simply because a large amount of H_2 has been collected in the nuclear region, independent of external factors ? Kronberg et al (1985) identified > 40 radio supernova remnants of which the brighter (younger) ones are aligned along a quasi-linear feature $\sim$ 650 pc $\times$ 60 pc in extent and are offset from the peaks of the CO intensity distribution (figure 3). Unless the H_2 distribution follows that of the supernova remnants when viewed at sufficiently high resolution ($\leq 3''$), it seems unlikely that the precursors of the supernova remnants - massive stars - were formed along a "line" as a result of spontaneous collapse of the molecular clouds. A large-scale external mechanism was probably involved in initiating the formation of massive stars along the quasi-linear feature in the nucleus of M82 (cf. Kronberg et al 1985).

The same underlying mechanism responsible for supplying gas to the nuclear region and for aligning the gas may also be triggering star formation in the collected gas. A stellar bar can induce shock fronts in the gas (e.g. Roberts, Huntley and van Albada, 1979) which would lead to increased cloud collisions and growth of GMC's along the shock fronts, both of which may help to accelerate cloud-collapse to form stars (Lo et al 1984). A stellar bar in M82 may have played an important role in the star-bursts.

5.4 Regulation of Star Formation ?

The current state of the H_2 medium in the nucleus of M82 appears highly disturbed as a result of the recently formed stars. Such a medium may be unsuitable for further star formation until the gas has been collected into giant molecular clouds again by some large-scale gravitational mechanisms such as the ones discussed above. Thus the star-burst could be its own limiting factor in continuing star formation, due to its disruptive effects on the interstellar medium. Sustained continuous enhanced star formation may not be possible, which could explain why the gas supply is not exhausted in all the galaxies and star-bursts are still possible at the current epoch.

6. IMPLICATIONS FOR STAR-BURST GALAXIES

6.1 High CO Intensity from Star-burst Regions

The high gas temperature in the M82 star-burst nucleus is likely the result of the very high density of young star clusters there. It is therefore interesting to estimate the the star density within such regions of other IR luminous galaxies. We have listed in Table I a sample of IR luminous galaxies with measured IR luminosity, L_{IR}, (1 to 300 μm; Telesco and Harper 1980; Becklin et al 1980) and 10 μm size. Except for the nonthermal contribution to a fraction of the luminosity of Arp 220, NGC 6240 and NGC 1068 (Becklin et al, this conference; Wynn-Williams 1985; Telesco et al 1984), L_{IR} is predominantly due to the luminosity of young stars formed in the central regions (Telesco and Harper 1980) and the 10 μm size is a measure of the extent of the recently formed stars. Thus, if we assume that the stars are uniformly distributed in a flattened circular distribution, with extent d, given by the 10 μm size, $\Sigma = L_{IR}/\pi(d/2)^2$, the mean IR luminosity per unit area, is a measure of the stellar luminosity per unit area in the star-burst region and indirectly a measure of the surface mass density of young massive stars. Σ is within a factor of 2 of 10^5 $L_\odot/pc^2$ for all these galaxies, coresponding to a few B0 stars per square parsec (> 100 $M_\odot/$ pc^2).

The large Σ also indicates that the molecular gas throughout such star-burst regions is exposed to a high FUV radiation flux. In contrast, in an average region of the galactic disk, molecular clouds

TABLE I

LUMINOSITY AND SURFACE BRIGHTNESS OF SOME IR-LUMINOUS GALAXIES

GALAXY	L_{IR} (L)	$d_{10\mu m}$ (pc)	Σ ($10^5 L/pc^2$)
Milky Way	2×10^9	230[a]	0.5
NGC 253.....	3×10^{10}	$\leq$ 500[b]	$\geq$ 1.5
NGC 1068	2×10^{11}	3000[c]	0.3
NGC 2903	7×10^9	300 x 150[d]	1.6
NGC 3034 (M 82) ...	3×10^{10}	470[b]	1.5
NGC 5236 (M 83) ...	2×10^{10}	460[d]	1.2
NGC 6949	2×10^{10}	640 x 800[d]	0.4
IC 342	3×10^9	300[e]	0.4
Arp 220.....	1×10^{12}	2000 x 4500[f]	1.1
NGC 6240	5×10^{11}	2500[f]	1.0

[a] Low *et al.* 1977.
[b] Telesco and Harper 1980; Jaffe *et al.* 1984.
[c] Telesco *et al.* 1984.
[d] Rieke 1976.
[e] Becklin *et al.* 1980; Telesco, private commumication.
[f] Rieke *et al.* 1985.

are located in quite different conditions (cf Draine 1978; Goldsmith and Langer 1978). Furthermore, the cosmic ray ionization rate of H_2, ζ, if proportional to the much increased supernova rate per unit area in the star-burst regions, would lead to much more significant cosmic ray heating of the molecular gas (cf. Goldsmith and Langer 1978). *Thus in star-burst regions generally, the molecular gas is likely to be heated to higher temperature, resulting in higher CO intensity, compared to a GMC in our galactic plane.* The standard $N(H_2)/I_{CO}$ ratio of the galactic GMC may not apply to star-burst regions in general. However, the amount of H_2 mass could still be high, given the generally higher I_{CO} expected from the star-burst regions.

6.2 High Star Formation Efficiency

From our observations, we can estimate a mean star formation efficiency (ϵ, the fraction of gas that has been converted to stars in the star-burst) directly for the star-burst nucleus of M82. The total amount of gas (H_2 + HI + ionized gas) within the central 1 kpc is 1.8×10^8 $M_\odot$, including the extended gas which we assume to have been expelled from the central concentration. The amount of stellar mass involved in the star-bursts is 2×10^8 $M_\odot$, indicating that ϵ is 0.5 (see also Rieke et al 1980). This efficiency is much higher than inferred for our galaxy generally (Wilking and Lada 1985), but *the physical mechanisms for such high ϵ in star-burst regions are not clearly understood.*

6.3 L_{IR} depends on Area of Star-bursts

The nearly constant Σ (Table I), if upheld in larger samples of IR luminous galaxies, may mean that a nearly constant stellar surface density is formed in star-bursts. This suggests some saturation effects in the underlying mechanisms in the star-burst process. One factor could be that there is a limit to the maximum possible surface density of H_2 in a galaxy. Tightly packing galactic GMC's in a thickness of 100 pc would yield a surface H_2 density of ~ 500 $M_\odot/pc^2$. Another self-regulating process could be the disruption of the interstellar medium by the recently formed massive stars, as is perhaps seen in M82.

If there are physical limits to the surface densities of young stars that can be formed in the star-burst process, then the luminosity of the star-burst region would depend strongly on its extent. For galaxies with an extreme luminosity of $\sim 10^{12}$ $L_\odot$, the requisite star-burst, if limited to $\Sigma \sim 10^5$ $L_\odot/pc^2$, would take place over ~ 3.5 kpc. *This extent is much smaller than the typical galactic dimension* and subtends a very small angle for the more distant galaxies (3.5 kpc = 7″ at 100 Mpc). Under this hypothesis, galaxies with luminosities of 10^{11} and 10^{10} $L_\odot$ would have star-burst regions with characteristic dimensions of ~ 1 and ~ 0.3 kpc, respectively. High resolution far-IR observations are required to verify this hypothesis.

6.4 Why are the More IR Luminous Galaxies Mergers ?

The more luminous IR galaxies ($L > 10^{11}$ $L_\odot$), if due to star-bursts, cannot be easily supported in isolated or loosely interacting galaxies (Lo et al 1986). In strongly interacting or merging galaxies, the twin requirements of sufficient gas supply and of triggering simultaneous star formation over a large extent are more likely to be satisfied. In such cases, strong tidal disruption of the underlying galaxies and the gas distribution could initiate star-bursts over a few kpc extent, perhaps via direct cloud collisions or as a result of concentration of large amount of gas in the same place. Thus, while the amount of gas in the merger may be only the sum of the gas in the two galaxies, *the resulting L_{IR}, if proportional to the area of interaction, can be many times higher than would be implied if the luminosity is simply*

proportional to the mass of gas present. Also, the star-burst regions in such mergers need not coincide with the nuclear regions.

7. CONCLUSIONS

The aperture synthesis CO observations of the central 1 kpc of M82 presented here provide the highest resolution probe yet achieved of the molecular gas within a star-burst nucleus. They have enabled a closer examination of the underlying processes involved.

1. The 7″ resolution observations have identified a 700 pc × 200 pc concentration of H_2 gas in the same confines as tracers of recent star formation in the nucleus of M82, amounting to 6×10^7 $M_\odot$. The gas temperature is very high ($T_k > 40$ K) throughout this region and is most likely due to the high stellar radiation flux there ($\sim 10^5$ $L_\odot/pc^2$, comparable to that in Orion). L_{IR}/M_{H_2} for the M82 star-burst nucleus is ≥ 170 $L_\odot/M_\odot$, reflecting very high star formation efficiency.

2. The observations have also identified extended CO emission that may be due to gas expelled from the central concentration. It suggests that the molecular gas in the nucleus of M82 is highly disturbed, most likely resulting from the stellar winds and subseqent supernovae from the OB associations formed in the star-burst. The kinetic energy involved in the extended gas is $\geq 10^{53}$ ergs. The extended emission may have structures similar to the HI supershells seen in the Galaxy and other galaxies.

3. The concentration of H_2 within the central $\sim$ 700 pc of M82 requires an explanation. The distribution and kinematics of the central gas concentration, as well as the 2.2 μm light distribution, all suggest the presence of a stellar bar in the central region of M82. Such a bar may provide the underlying mechanisms both to transport the molecular gas towards the center and to trigger the star-burst. While tidal interaction with M81 may provide some of the gas needed for star-formation, the more direct cause of star-burst in M82 is probably provided by the stellar bar.

4. Comparisons of the nucleus of M82 to a sample of other IR luminous galaxies suggest that the flux of stellar radiation in all the star-burst regions is high and comparable in magnitude. This implies that the gas temperature (and therefore the CO intensity) in the star-burst regions may generally be higher than that found in the galactic disk. The $N(H_2)/I_{CO}$ is likely to be smaller than the galactic ratio, but the higher I_{CO} expected from such regions could indicate substantial H_2 column density still.

5. Existing evidence for a sample of 10 IR luminous galaxies suggests that the star-burst regions may have a nearly constant mean IR luminosity per unit area, possibly a result of physical limits of the surface density of young stars that can be formed in the star-burst process. This would imply that L_{IR} of luminous star-burst galaxies is primarily proportional to the area of the star-burst. Such a dependence can explain why the more luminous galaxies are mergers.

8. REFERENCES

Allen, R.J., van der Hulst, J.M., Goss, W.M. and Huchtmeier, W., 1978, *Astr. and Ap.*, **64**, 359.

Ball, R., Sargent, A.I., Scoville, N.Z., Lo, K.Y. and Scott, S.L., 1985, *Ap.J.*, **298**, L21.
Becklin, E.E., et al 1980, *Ap. J.*, **236**, 441.
Blitz, L., 1980, *Third Gregynog Astrophysics Workshop, Giant Molecular Clouds in the Galaxy*, eds. P. M. Solomon, M. G. Edmonds (Pergamon, Elmsford, N.Y.), pp. 1 - 24.
Brinks, E., 1984, Ph.D. thesis, University of Leiden, Holland.
Bruhweiler, F.C., Gull, T.R., Kafatos, M. and Sofia, S., 1980, *Ap.J. (Letters)*, **238**, L27.
Cottrell, G.A., 1977, *M.N.R.A.S.*, **178**, 577.
Draine, B. T., 1978, *Ap. J. Suppl.*, **36**, 595.
Goldsmith, P., Young, J.S., and Langer, W.D., 1983, *Ap.J. Suppl.*, **51**, 203.
Heckathorn, H.M., 1972, *Ap.J.*, **173**, 501.
Heiles, C., 1976, *Ap.J. (Letters)*, **208**, L137.
Heiles, C., 1979, *Ap.J.*, **229**, 533.
Jaffe, D.T., Becklin, E.E., and Hildebrand, R.H., 1984, *Ap.J. (Letters)*, **285**, L31.
Killian, D. J., 1978, Ph. D. thesis, University of Florida, U.S.A..
Knapp, G.R., Phillips, T.G., Huggins, P.J., Leighton, R.B. and Wannier, P.G., 1980, *Ap.J.*, **240**, 60.
Kronberg, P.P., Biermann, P. and Schwab, F.R., 1985, *Ap.J.*, **291**, 693.
Kronberg, P.P., Sramek, R. A., 1985, *Science*, **227**, 28.
Lo, K.Y., et al., 1984, *Ap.J. (Letters)*, **282**, L59.
Lo, K.Y., et al. 1985 in *U.R.S.I. Symposium on Millimeter and Submillimeter Wave Astronomy* (Granada: URSI), p. 223.
Lo, K.Y., et al. 1986, accepted by Ap. J.
Low, F., Kurtz, R., Poteet, W., Nishimura, T., 1977, *Ap.J.(Letters)*, **214**, L115.
McCray, R. and Kafatos, M.C., 1985, preprint.
Nakai, N., 1984, Ph.D. thesis, University of Tokyo, Japan.
O'Connell, R.W. and Mangano, J.J., 1978, *Ap.J.*, **221**, 62.
Olofsson, H. and Rydbeck, G., 1984, *Astr. and Ap.*, **136**, 17.
Rickard, L.J., Palmer, P., Morris, M., Turner, B.E. and Zuckerman, B., 1977, *Ap.J.*, **213**, 673.
Rieke, G.H. 1976, *Ap. J. (Letters)*, **206**, L15.
Rieke, G.H., Lebofsky, M.J., Thompson, R.I., Low, F.J. and Tokunaga, A.T. 1980, *Ap.J.*, **238**, 24.
Rieke, G. H. *et al* 1985, *Ap. J.*, **290**. 116.
Roberts, W. W., Huntley, J., van Albada, G., 1979, *Ap. J.*, **233**, 67.
Sanders, D.B., Solomon, P.M. and Scoville, N.Z., 1984, *Ap.J.*, **276**, 182.
Sanders, D.B., Scoville, N.Z. and Solomon, P.M., 1985, *Ap.J.*, **289**, 373.
Sanders, D.B. et al, 1986, Ap. J. (Letters), June 15 issue.
Scoville, N.Z., Soifer, B.T., Neugebauer, G., Young, J.S., Matthews, K. and Yerka, J., 1985, *Ap.J.*, **289**, 129.
Soifer, B.T. et al, 1986, *Ap. J. (Letters)*, **303**, L41.
Telesco, C.M. and Harper, D.A., 1980, *Ap.J.*, **235**, 392.
Telesco, C.M., Becklin, E.E., Wynn-Williams, C.G. and Harper, D.A., 1984, *Ap.J.*, **282**, 427.
Tielens, A.G.G.M., Hollenbach, D. 1985, *Ap.J.*, **291**, 722.
Tomisaka, K., Habe, H. and Ikeuchi, S., 1980, *Prog. Theor. Phys. (Japan)*, **64**, 1587.
Weliachew, L., Fomalont, E., Greisen, E., 1984, *Astron. and Ap.*, **137**, 335.
Wilking, B., Lada, C. 1985, *Protostars and Planets II.*, eds. D. Black, M. Matthews (U. of Arizona, Tucson), 297..
Williams, T.B., Caldwell, N. and Schommer, R.A., 1984, *Ap.J.*, **281**, 579.
Wynn-Williams, C.G. 1985, in *IAU Symposium 115 on "Star Formation Regions"*, (Tokyo, Japan).
Young, J.S. and Scoville, N.Z., 1984, *Ap.J.*, **287**, 153.

Young, J.S. et al, 1986, *Ap. J.*, **304**, 443.
Zaritsky, D. and Lo, K.Y., 1986, *Ap.J.*, **303**, 66.

DISCUSSION

WATSON:

Given the structure of the molecular ring in M82 and the possibility of its being a resonant orbit in a bar potential, what do you 'predict' for the parameters of the bar, i.e., size, pattern speed, etc.? Is it consistent with the wings seen on the 2μm distribution?

LO:

As M82 is so highly inclined, none of the parameters of the 'molecular ring', or of a stellar bar is well determined. So, I have not made quantitative comparisons of the parameters involved. It is suggestive, however, that the wings seen of 2μm distribution have a comparable scale to the starburst region.

MEZGER:

You quote an $N(H_2)/I_{CO}$ ratio for M82 which is about a factor of 10 smaller than the value used for our Galaxy. This would lead to an underestimate of the total mass of gas in M82. I would have expected the opposite. How did you derive this value?

LO:

The $N(H_2)/I_{CO}$ ratio I quoted was derived from the CO emission in the optically thin limit. The resulting gas column density is consistent with the 400μm observations of the dust continuum of Jaffe *et al.* (1984, *Ap.J.* **285**, L31).

THRONSON:

How do your observations compare with single-dish data in (a) total intensity and (b) line shape and structure?

LO:

At the velocities at which the interferometric observations were made, the total flux is comparable to the single dish measurements.

SHULL:

If supernova remnants are common in M82, their evolution will be speeded up and the x-rays from their hot interior will be effective at ionizing, heating and exciting large volumes of molecular gas.

Have you looked for evidence of this excitation or of enhanced star formation due to supershells?

LO:

In the starburst nucleus of M82, the observed high gas temperature is very likely due to heating by a very high far-UV radiation field, as well as by the enhanced cosmic ray flux and the x-rays, as you have mentioned. The extended CO emission within the central 1' of M82 may be naturally identified with supershells. To look for enhanced star formation within the supershells requires higher resolution ($< 2'$) observations of both the molecular gas and the far-infrared emission.

YOUNG:

If the interstellar radiation field is heating the clouds in M82, the 2-1/1-0 ^{12}CO ratio may not be probing the same regions and cannot be used to argue that the gas is optically thin. And, if the CO is optically thin, the CO is not a good tracer of the H_2 mass.

LO:

The important point is that the observed gas properties within the star-burst nucleus of M82 are very different from those in our Galactic disk, presumably the result of very different physical conditions within the M82 nucleus. The optically thin CO limit leads to a gas column density consistent with the dust opacity derived from the 400μm observations of the central $\sim$40" of M82, if the gas to dust ratio is assumed to be the same as the Galactic value (Jaffe *et al.* 1984).

NUCLEAR STAR FORMATION ON 100 PARSEC SCALES: 10″ RESOLUTION RADIO CONTINUUM, HI, AND CO OBSERVATIONS

Jean L. Turner and Paul T. P. Ho
Harvard-Smithsonian Center for Astrophysics, Cambridge, MA 02138

Robert N. Martin
Steward Observatory, University of Arizona, Tucson, AZ 85721

ABSTRACT

We report on a program of radio line and continuum studies of star formation in nearby (< 10 Mpc) spiral galaxies. The objective is a search for hot gas and peculiar dynamics in spiral nuclei with 10″ to 30″ angular resolution. Vigorous star formation is found to be a common phenomenon in the inner kpc of spirals. Arcsecond-resolution observations of radio continuum emission at 6 and 2 cm have been used to separate the thermal and nonthermal radio components. We find that thermal and nonthermal emission are well-mixed even on sizescales of 10 pc. To understand the reason for the increased level of star formation activity in spiral nuclei, we are studying HI and CO emission in these galaxies. The CO ($J = 3 \rightarrow 2$) transition has been detected in M51, M82, NGC 253, NGC 6946 and IC 342 with T_a^* ~0.5–2.0 K, at 20″ angular resolution. The dynamics and spatial distribution of nuclear gas are being studied using VLA HI maps with 30″ synthesized beams. Evidence for noncircular motions in HI has been found in the nucleus of IC 342.

INTRODUCTION

It is clear that nuclear activity is common in spiral galaxies, as evidenced by strong radio continuum (*e.g.* Hummel 1981), infrared (*e.g.* Telesco and Harper 1980), and optical (*e.g.* Keel 1980) emission. In many cases, the emission regions resemble regions of intense star formation activity (Rieke *et al.* 1980). A useful approach toward understanding the "starburst" phenomenon is to study nearby galaxies, where the nuclear emission can be studied with great sensitivity and spatial resolution. We describe a program of radio observations of the ionized and neutral gas in spiral galaxies closer than 10 Mpc, where we can resolve regions of 100-200 pc extent. We use radio continuum emission to trace the ionized regions in these nuclei; dual-frequency observations allow estimates of the thermal emission, and hence the number of young stars and their spatial distribution. The hot molecular component associated with these OB stars can be studied using higher transitions of CO. The enormous numbers of young stars posited for these sources imply high rates of mass consumption. A central issue becomes: is this activity in the nucleus fed from gas in the disk? This question can be addressed with high resolution aperture synthesis maps of HI.

RADIO CONTINUUM STUDIES OF NEARBY SPIRAL NUCLEI

In order to accurately measure thermal radio continuum fluxes in spiral galaxies, it is desirable to spatially resolve out the extended synchrotron emission that dominates single-dish radio continuum observations (Klein and Emerson 1981). Observations of seventeen nearby

Carol J. Lonsdale Persson (Editor)
Star Formation in Galaxies

spiral galaxies were made with the NRAO Very Large Array, at 1″ resolution, corresponding to roughly 10 – 20 pc linear extent. Matched beam observations were obtained at 6 and 2 cm to allow spectral separation of the thermal and nonthermal emission (Turner and Ho 1983).

We detected nuclear radio continuum emission in sixteen of the seventeen galaxies. The nuclei show a range of activity, from 1 mJy in M101 at 7.2 Mpc, to 2 Jy in NGC 253 at 2.5 Mpc, a factor of more than 200 in luminosity. Spectral index maps show that the radio emission is usually dominated by nonthermal emission, even on 10 parsec sizescales. Spectral indices of -1.2 to -0.8 are common. However, flat and positive spectral indices have also been observed (M83; IC 342), possibly indicating the presence of large complexes of compact HII regions in the nuclei. In a number of cases, including Maffei 2, NGC 253, and NGC 4736, the radio continuum knots are organized in one-dimensional structures. In NGC 253, at 0.1″ resolution, there is a string of compact knots aligned to within a degree on the sky, and 5 degrees in the plane of the galaxy; this 100 pc jet-like structure may be related to ejection from the central compact (< 0.6 pc) nonthermal ($> 10^5$ K) nucleus (Turner and Ho 1985).

Even for our small sample of nearby spirals, the range in activity and the variety of morphologies are impressive. The overall impression is that nuclei in general are very active.

CO (J = 2 → 1) AND CO (J = 3 → 2) OBSERVATIONS

The goal of the CO observations is to detect molecular gas that has been heated by star formation in spiral nuclei, and to study the dynamics of this gas. High excitation CO lines have two advantages over the CO (J = 1 → 0) transition for studying warm gas in the nucleus: if the gas is optically thin, the warm gas will have significantly higher line intensities in CO (J = 2 → 1) and (3 → 2); if the gas is optically thick, the smaller beamsizes afforded by the higher observing frequencies will decrease beam dilution effects. The CO (J = 2 → 1) and (3 → 2) observations were made with the NRAO 12m telescope, with system temperatures of 2000 K and 12000 K and beamsizes of 35″ and 22″ at 230 and 345 GHz, respectively.

We have mapped CO (J = 2 → 1) in the nuclei of the nearby spiral galaxies IC 342, M51, NGC 253, and NGC 6946. The beam-diluted brightness temperature, which ranges from $T_a^*(2 \rightarrow 1)$ ~0.2 K in M51 to 1.4 K in NGC 253, is in each case similar to the CO (J = 1 → 0) temperature (*e.g.* Young and Scoville 1982). Since the (2 → 1) beam is four times smaller than the (1 → 0) beam, the CO most likely is optically thick, clumpy with respect to 30″, but with a total angular extent greater than the telescope beams. Mapping shows that the CO (J = 2 → 1) extent is confined to roughly the inner two kpc. The extent of the (2 → 1) emission in the nucleus of IC 342 is $\sim 2' \times 1'$, somewhat larger than that mapped interferometrically by Lo *et al.* (1984), but in agreement with the (1 → 0) Nobeyama map of Sofue (1986). The (2 → 1) maps also show that the rotation curve in these galaxies rises very steeply out of the nucleus: in NGC 253 the velocity centroid shifts by 150 km s^{-1} over 30″ (~360 pc), implying an enclosed mass of 2×10^8 $M_\odot$.

CO (J = 3 → 2) was detected in M82, NGC 253, IC 342, M51, and NGC 6946. These observations represent the first detection of extragalactic CO (J = 3 → 2). The peak antenna temperatures $T_a^*(3 \rightarrow 2)$ range from 0.7 K in NGC 6946, ~1 K in NGC 253, IC 342, and M51, to ~2 K in M82. In all cases, $T_a^*(3 \rightarrow 2)$ is very similar to $T_a^*(2 \rightarrow 1)$. This

supports the implications from the $(2 \rightarrow 1)/ (1 \rightarrow 0)$ ratio that we are observing well-distributed but clumpy molecular gas. Even for modest clumping factors, the detected CO temperatures are higher than the values commonly found in Galactic giant molecular clouds. For example, if the molecular scale length is 100 pc in M82, we deduce a gas temperature of ~30 K.

With the increasing angular resolution achieved by studying the higher frequency CO lines, we can begin to define the morphology and kinematics in the nuclear regions. However, it appears that arcsecond angular resolution will be needed to define the hotter gas component that is heated by star formation activity.

VLA HI MAPPING OF NEARBY SPIRAL NUCLEI: IC 342

The objective of HI mapping of nearby spiral nuclei is to study the relation of the disk gas (HI) and the molecular gas found in the nucleus, as described above. From the large numbers of stars derived for many spiral nuclei (*e.g.* Beck, Turner, and Ho 1986) it is clear that not many generations of such star formation activity can proceed before the nucleus is exhausted of gas. Is the nuclear gas replenished from the disk? Can we see evidence for nuclear feeding in the HI velocity distribution? To study this problem, we have observed IC 342 in HI with the C and D configurations of the VLA. The preliminary maps have 30″ angular resolution and 10 km s^{-1} velocity resolution.

The integrated intensity distribution in IC 342 shows a flat HI disk distribution and a ~2′ central HI hole, as shown in Westerbork (Rogstad, Shostak, and Rots 1973) and Cambridge (Newton 1980) maps. The higher resolution of the VLA map, however, reveals that the central hole is not completely devoid of HI. There are faint HI features in the nucleus. One HI filament lines up with the inner portion of a spiral arm, as traced by radio continuum emission. Another HI filament appears at the center of the nuclear region, slightly offset from the nuclear radio continuum source and the CO bar of Lo *et al.* (1984). This nuclear HI filament has an extent of roughly $2' \times 1'$, oriented north-south. This feature is very similar in extent to the CO $(J = 2 \rightarrow 1)$ feature mentioned in the previous section and the Nobeyama maps of Sofue (1986). The mass of this HI bar is ~1–2×10^6 $M_\odot$, or approximately 1% of the CO mass (Lo *et al.* 1984). The north-south orientation of the HI bar is ~20° different from the more northwesterly orientation of the disk HI gas at the same velocity.

The HI velocities also indicate that the central HI bar feature is not simply a continuation of the HI disk. Deviations from circular rotation appear in the central 2′. The HI bar rotates nearly north-south, with velocities similar in both direction and magnitude with those of CO (Lo *et al.* 1984). In contrast, the disk HI at these velocities (near the systemic velocity of IC 342) define a rotating structure with a position angle ~45° east of north. Other deviations from circular rotation appear at the edges of the HI hole near the ends of the bar. The deviations from circular motion are ~10 to 30 km s^{-1}.

The high angular resolution HI synthesis maps show that the molecular gas in the nucleus can be connected to the disk atomic gas. The correspondence between the HI filament and the CO bar, and the presence of noncircular velocities suggest flows into the nucleus and concurrent conversion of atomic gas to molecular form.

SUMMARY

We report here on a program of radio continuum, CO, and HI studies at high angular resolution in order to examine the kinematics and spatial distribution of key tracers of young star formation. These studies have been most fruitful and promising in demonstrating a link between the nuclear and the disk environments in the case of IC 342.

This research has been supported in part by the Alfred P. Sloan Foundation, NATO Grant 83/584, and NSF Grant AST85-09907. The National Radio Astronomy Observatory is operated by Associated Universities, Inc., under contract with the National Science Foundation.

REFERENCES

Beck, S.C., Turner, J.L., and Ho, P.T.P. 1986, this volume.
Hummel, E. 1981, *Astr. Ap.*, **93**, 93.
Keel, W. 1984, *Ap. J.*, **282**, 75.
Klein, U., and Emerson, D.T. 1981, *Astr. Ap.*, **94**, 29.
Lo, K.Y., *et al.* 1984, *Ap. J. (Letters)*, **282**, L59.
Newton, K. 1980, *M. N. R. A. S.*, **191**, 169.
Rieke, G.H., Lebofsky, M.J., Thompson, R.I., Low, F.J., and Tokunaga, A.T. 1980, *Ap. J.*, **238**, 24.
Rogstad, D.H., Shostak, G.S., and Rots, A.H. 1973, *Astr. Ap.*, **22**, 111.
Sofue, Y. 1986, this volume.
Telesco, C.M. and Harper, D.A. 1980, *Ap. J.*, **235**, 392.
Turner, J.L., and Ho, P.T.P. 1983, *Ap. J. (Letters)*, **268**, L79.
Turner, J.L., and Ho, P.T.P. 1985, *Ap. J. (Letters)*, **299**, L77.
Young, J. S., and Scoville, N. 1982, *Ap. J.*, **258**, 467.

DISCUSSION

APPLETON:

Can you be sure that the weak HI feature you see near the center of IC 342 is not a result of incomplete continuum subtraction from the line-containing maps? It seems suspicious to me that this weak HI feature corresponds so closely to the continuum emission.

TURNER:

The feature only shows up in four or five channel maps: it is clearly a spectral and not a continuum feature.

EXTREMELY LUMINOUS FAR-INFRARED SOURCES (ELFS)*

Martin Harwit and James R. Houck

Center for Radiophysics and Space Research, Department of Astronomy
Ithaca, New York 14853-6801

B. Thomas Soifer
Division of Physics, California Institute of Technology
Pasadena, California 91125

Giorgio G. C. Palumbo
NASA Goddard Space Flight Center
Greenbelt, Maryland 20771

ABSTRACT. The Infrared Astronomical Satellite (IRAS) survey uncovered a class of Extremely Luminous Far-Infrared Sources (ELFS), exhibiting luminosities up to and occasionally exceeding 10^{12} $L_\odot$. We present arguments to show that sources with luminosities $L \geq 3\times10^{10}$ $L_\odot$ may represent gas-rich galaxies in collision. The more conventional explanation of these sources as sites of extremely active star formation fails to explain the observed low optical luminosities of ELFS as well as their high infrared excess. In contrast, a collisional model heats gas to a temperature of $\sim10^6$K where cooling takes place in the extreme ultraviolet. The UV is absorbed by dust and converted into far-infrared radiation (FIR) without generation of appreciable optical luminosity. Gas recombining as it cools generates a Lyman-α photon only once for every two extreme ultraviolet ~50eV photons emitted by the 10^6K gas. That accounts for the high infrared excess. Finally, our model also is able to explain the observed luminosity distribution of ELFS as well as many other traits.

1. INTRODUCTION TO THE DATA

The most luminous sources identified through the IRAS survey exhibit these properties:

i) Their FIR luminosities approach and sometimes exceed 10^{12} $L_\odot$ (Soifer *et al.* 1986),

ii) The FIR flux appears uncorrelated with the optical and near infrared luminosity which typically remains around 10^{10} $L_\odot$ characteristic of fairly normal spirals (Houck *et al.* 1985, Allen *et al.* 1985),

iii) Many ELFS appear to be irregular, disturbed or interacting galaxies (Houck *et al.* 1985),

---

* The authors have submitted a more comprehensive article (Harwit *et al.* 1987) on the same topic to *The Astrophysical Journal*. Here we only summarize the findings presented in greater detail in that paper.

Carol J. Lonsdale Persson (Editor)
Star Formation in Galaxies

iv) The FIR luminosity is directly proportional to the 21-cm radio continuum luminosity (Sanders and Mirabel 1985),

v) CO observations at 2.6mm indicate a high molecular hydrogen content $\sim 10^{10}$ $M_\odot$ (Sanders and Mirabel 1985), and

vi) The CO lines are abnormally broad, indicating high-velocity motions.

vii) The infrared excess -- the ratio of FIR to Lyman-line radiation -- is higher by an order of magnitude than in HII complexes (Beck et al. 1986, DePoy et al. 1986).

viii) Low-ionization states of atoms are more prevalent than the more highly ionized species generally found in HII regions (Allen et al. 1985).

ix) The luminosity distribution function is roughly proportional to $L^{-5/2}$ for $L \geq 3\times10^{10}$ $L_\odot$ but declines less steeply below a break in the curve at $\sim 3\times10^{10}$ $L_\odot$ (Lawrence et al. 1986, Soifer et al. 1986).

x) Only one extragalactic source in $\sim 10^6$ has FIR luminosity above $\sim 10^{12}$ $L_\odot$ (Soifer et al. 1986).

xi) Intense vibrational H_2 emission characterizes many ELFS (Joseph et al. 1984).

2. MODEL FOR ELFS

We assume that ELFS are the byproduct of collisions among gas-rich galaxies. We picture most of the gas in each of the colliding partners to be concentrated in a central disk, roughly 1 kpc in radius, 0.1 kpc thick and containing $\sim 10^{10}$ $M_\odot$ of gas. The indicated pre-collision gas density then is $n_H \sim 10^3$ cm^{-3}. Galaxy-galaxy collisions are expected to occur at free infall velocities $\geq$ 500 km sec^{-1}. The observed CO line widths are consistent with such high velocities and the line strengths suggest the high gas content we have assumed.

If the disks collide face on, the dissipated kinetic energy gives rise to a luminosity $\sim 10^{12}$ $L_\odot$ for about 3×10^5y. More oblique collisions can account for lower luminosities, often with longer enduring interaction. A rough numerical calculation that takes into account a wide range of initial orientations and of center-to-center distances for the colliding pairs gives the luminosity (the dissipation) distribution function shown in Fig. 1. The line drawn through the data points has been arbitrarily anchored to the probability with which the most luminous galaxies are observed. There are no other assumptions aside from the above-listed disk dimensions and mass. The shaded extension of the curve around 10^{11} $L_\odot$ esimates the contribution of the many glancing (weak) collisions. Collisional activity should not make a pronounced contribution for luminosities well below 3×10^{10} $L_\odot$, and this appears to account for the break in the luminosity distribution below that luminosity.

Calculation of the luminosity of stars that could form from 10^{10} $M_\odot$ of gas suggest that a total luminosity of 10^{12} $L_\odot$ could only be reached with unusually efficient conversion of gas into stars and with an exceptionally high luminosi-

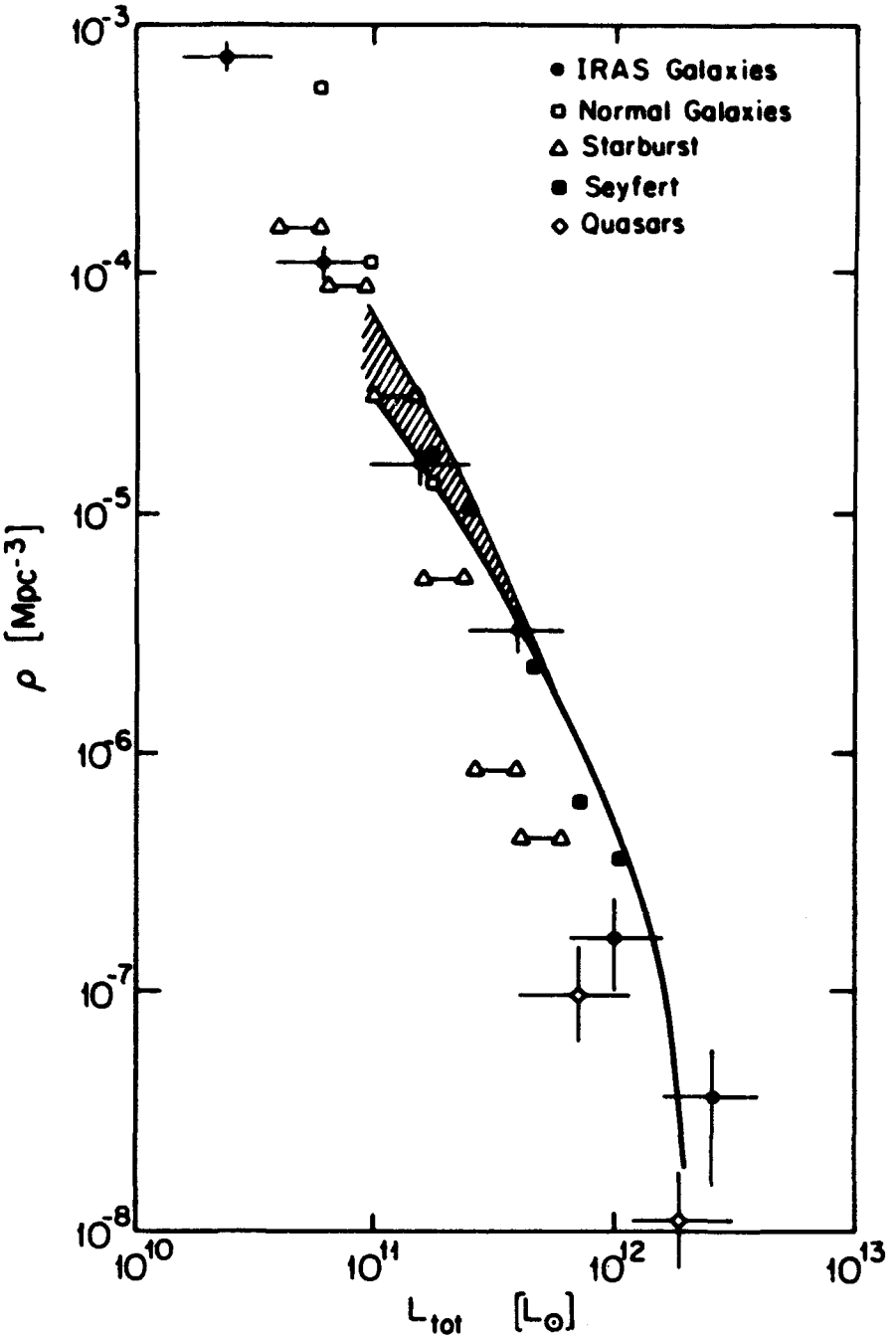

Figure 1 - Data on the luminosity distribution function among luminous FIR sources (Soifer et al. 1986) and a calculated fit (solid line and shaded area). A derivation of this fit is presented in a full-length paper by the authors (Harwit et al. 1987).

ty to mass ratio for the stars that are formed. Even then, however, we would have to account for the exceptionally low optical luminosity, since it is not clear how one could systematically block all but ~1 percent of the optical emission, converting all of that radiation instead into FIR. It would also be difficult to explain the low observed atomic hydrogen line-emission or the radiation from predominantly singly ionized, rather than multiply ionized species. All of these observations break with those traditionally characteristic of HII complexes around massive, luminous stars.

The collisional model does not face these difficulties. Observed gas masses and velocities can account for dissipation rates consistent with the observed luminosities. At collision (Fig. 2) gas temperatures rise to $\geq 10^6$K. At this temperature the bulk of the energy loss is via cooling through extreme ultraviolet (EUV) radiation. Photons with energies in the 50eV range are emitted. There is little optical flux. Much of the EUV emission is absorbed by grains and converted directly into FIR. Detailed considerations show that only every second EUV photon, on the average, leads to ionization followed by recombination -- to a a Lyman-α photon. This accounts for the high infrared excess. The optical line radiation emitted in this layered model (Fig. 3) comes largely from a dusty, partially ionized layer. The partial ionization of the hydrogen accounts for the absence of highly ionized species; those would quickly jump to a lower ionization state by charge exchange with a hydrogen atom. Molecular hydrogen is vibrationally excited in this same partly ionized regime, well upstream of the impact front.

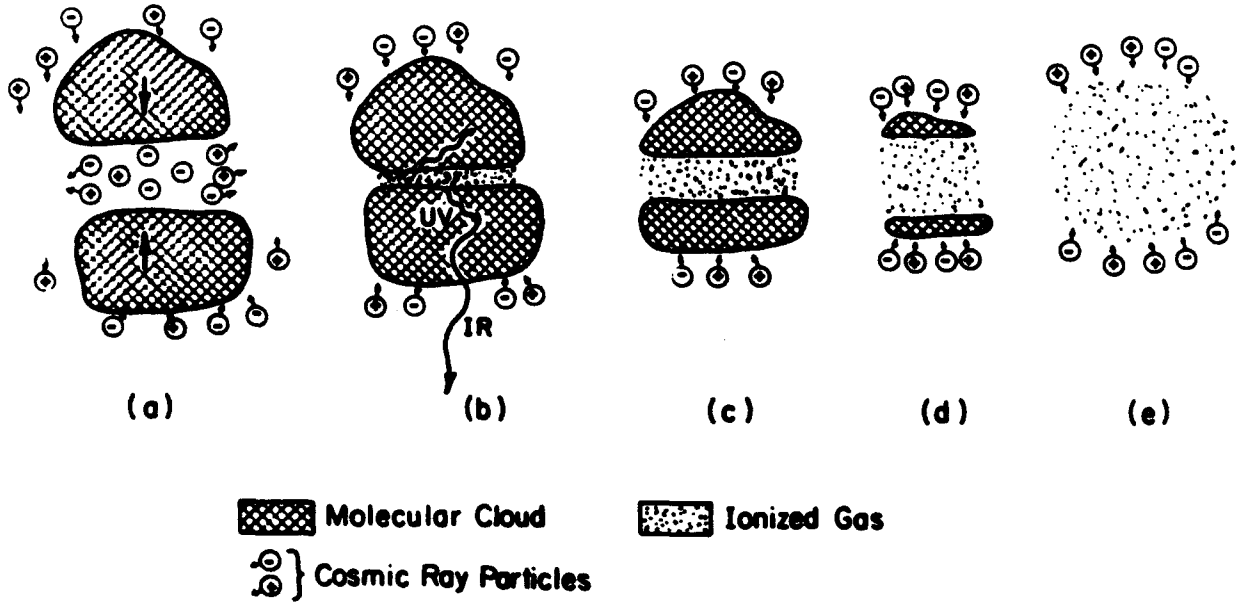

Figure 2 - Schematic Diagram of Colliding Gas Clouds. Two molecular clouds approach. (a) Upon contact, the gas between them is ionized and heated to temperatures above 10^6K. (b) Ionizing radiation escapes into the molecular gas and produces an ionized layer even before that gas has a chance to collide with the stationary layer of hot gas that has formed. As the collision proceeds, (c,d) the central layer thickens until no more molecular gas remains. Then the hot outer layers of the ionized cloud expand outward to meet trailing, more tenuous halo gas from each of the colliding galaxies (e).

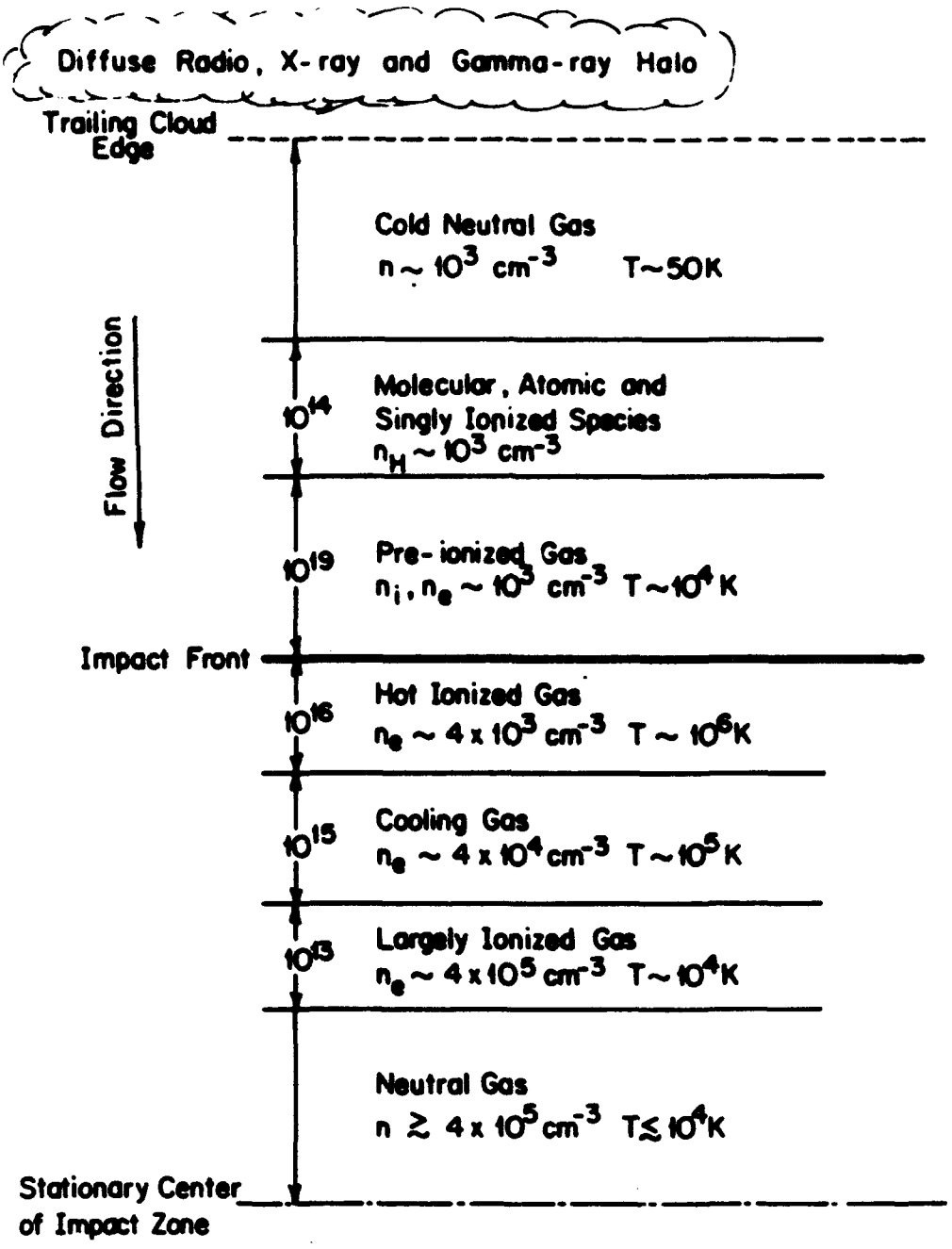

Figure 3 - Layered structure of colliding clouds. At the bottom is the central portion of the colliding disks. At the top the outer pre-collision gas.

More comprehensive arguments also suggest that the cosmic ray acceleration rate and hence the radio flux should be proportional to the gas content of colliding regions, leading to the observed proportionality of FIR to radio continuum emission.

3. PREDICTION

The 10^6K layer should give rise to highly ionized species such as OIV and

NeV, whose fine-structure emission, respectively at 25.87 and 24.28μm, should penetrate through obscuring dust layers, to be observable from Earth. That radiation would not be produced in HII regions and, if observed, would discriminate against starburst models.

ACKNOWLEDGEMENTS

At Cornell, this work was supported by NASA Grant NAGW-761 and JPL Contract 954603. B.T.S. is supported by NASA under the IRAS Extended Mission Program. G.G.C.P. appreciates the hospitality of Drs. E. A. Boldt and S. S. Holt during his stay at NASA/GSFC as a NRC/NAS Research Associate.

REFERENCES

Allen, D. A., Roche, P. F., Norris, R. P. 1985, M.N.R.A.S., 213, 67P.
Beck, S. C., Turner, J. L. and Ho, P. T. P. 1986, Ap. J., to be published.
DePoy, D. L., Becklin, E. E., and Wynn-Williams, C. G. 1986, Ap. J., 307, 116.
Harwit, M., Houck, J. R., Soifer, B. T., and Palumbo, G. G. C. 1987, Ap. J., submitted.
Houck, J. R., Schneider, D. P., Danielson, G. E., Beichman, C. A., Lonsdale, C. J., Neugebauer, G., and Soifer, B. T. 1985, Ap. J., 290, L5.
Joseph, R. D., Wright, G. S., and Wade, R. 1984, Nature, 311, 132.
Lawrence, A., Walker, D., Rowan-Robinson, M., Leech, K. J., and Penston, M. V. 1986, M.N.R.A.S., 219, 687.
Sanders, D. B., and Mirabel, I. F. 1985, Ap. J. (Letters), 298, L31.
Soifer, B. T., Sanders, D. B., Neugebauer, G. Danielson, G. E., Lonsdale, C. J., Madore, B. F., and Persson, S. E. 1986, preprint.

DISCUSSION

BURBIDGE:

First, I would like to remind everyone that more than thirty years ago collisions were thought to be the explanation of radio galaxies. The idea did not last! Second, I want to say that my own view is that the brightest IRAS galaxies are young galaxies forming their first generations of massive ($\sim 100\ M_\odot$) stars which give both line luminosity and the dust. A few times 10^5 stars are needed, and about 10 generations of them, to make enough dust.

HARWIT:

First, observations tell us that galaxy interaction appears involved. Many of the most extremely luminous sources clearly appear to be interacting partners.

Second, the most luminous phases may last $\sim 3 \times 10^5$ yr, perhaps an order of magnitude less than the lifetime of highly luminous stars. Lower luminosity, more oblique collisions will last an order of magnitude longer. But we are dealing with events of extremely low probability here. Only one galaxy in a million has a luminosity in excess of $10^{12}\ L_\odot$. Quantitatively, our model appears capable of explaining that number of extremely luminous sources.

SCOVILLE:

I don't think the high $L_{IR}/L_{Br\alpha}$ line ratio is an insurmountable problem for massive star formation models in interacting galaxies. The HII regions there will have higher dust abundances than standard Galactic HII regions because the cloud-cloud velocities are ≥ 100 km s^{-1} and fresh grains will be supplied continually to

the ionized gas surrounding the OB stars.

HARWIT:

I would really like to see quantitative estimates of such effects. It appears very difficult to provide a dust absorption shield which will have no holes, and will prevent all but 1% of the optical radiation from escaping. The luminosities involved are so high that dust and gas constituting a shrouding envelope could be blown away by radiation pressure if it did not already have the enormous approach velocities involved in our model.

SHULL:

Your large ratios of infrared to optical flux are predicated on the assumption that the emitting regions are buried deep inside large homogeneous slabs. If you take into account a cloudy interstellar medium, wouldn't much of the optical radiation escape through the 'holes'? Note that much of the cooling will take place in optically thin optical-IR forbidden lines.

HARWIT:

The emitting regions in our model primarily radiate in the far ultraviolet which is readily absorbed by the interstellar gas even if it escapes through holes between clouds. No direct optical radiation is involved. Recombination in tenuous ambient interstellar gas ionized in this way will be extremely slow and result in low luminosity emission from the galaxies' halos.

de JONG:

You have normalized the infrared luminosity function, predicted on the basis of your model, to the observed infrared luminosity function. This implies a certain collision frequency of galaxies at impact parameters of $\sim$1 kpc. Have you verified that this implied collision frequency is consistent with that directly derivable from observations?

HARWIT:

Schweizer, in a recent article in Science, estimates that one galaxy in every ten appears to have undergone an interaction in its past. Such figures are still not well established, but they appear sufficiently high, particularly if we recall that many initial encounters may be quite weak - just strong enough to bind two galaxies together in rather eccentric orbits. There may then be several relatively close passes before a substantial collision occurs. In summary, the number of passes two galaxies make past each other could be few times higher than the number of captures that take place.

STAR FORMATION AND DYNAMICS IN STARBURST NUCLEI

COLIN A. NORMAN
Department of Physics and Astronomy, Johns Hopkins University and
Space Telescope Science Institute,
Baltimore, Maryland 21218

ABSTRACT

A simple model is presented for gas inflow through a disk galaxy driven by interacting galaxies through the action of a non-axisymmetric disturbance acting on the disk whose gas is modelled as an ensemble of gas clouds. Cloud collisions, as well as being a vital process in forcing gas inflow to the centre of the disk, are also assumed to generate massive stars. This ever increasing rate of gas flow toward the centre of the galaxy and the associated rapid increase in cloud collisions leads to a centrally concentrated starburst.

Starbursts have important consequences for the immediate environment of galaxies. Mildly collimated outflows can be driven by a combination of multiple supernovae and OB star winds. Jets associated with activity in the galactic nucleus can interact strongly with a starburst environment.

Physical mechanisms proposed for generating starbursts and active nuclei via feeding the monster are rather similar and a strong inference is that starbursts and activity are intimately related. Among the obvious evolutionary implications are that powerful infrared sources could be forming a significant part of their central stellar mass--which is galaxy formation in action--a relatively delayed and hidden process. Furthermore, quasar-like nuclei embedded in such objects as Arp 220 will be powerful infrared sources until the gas and dust is depleted either by ejection and/or by transformation to stars.

I. INTRODUCTION

The remarkable observations of starburst systems discussed at this meeting require at least some theoretical modelling. The analysis I discuss here is quite simplified but may lead to some more physical insight. It will be assumed that it is necessary to explain why companions and mergers trigger starbursts, what skews the mass functions to predominantly OB stars in these systems, what drives the observed outflows, what is the relation between activity and starbursts? In addition we will discuss the implications of the infrared observations for theories of galaxy formation and quasar activity and for the metal enrichment of the intracluster medium.

II. INTERACTION DRIVEN INFLOW

Consider a normal disk galaxy with a significant gas content, say an Sc galaxy, and apply a significant perturbation to it in the form of a companion, bar, oval distortion or infalling or merging dwarf galaxy. Assume the pre-

Carol J. Lonsdale Persson (Editor)
Star Formation in Galaxies

existing stars provide a background potential and that the gas distribution is described as a mean cloud ensemble that can undergo various dissipative processes such as collisions, coagulation, disruption, fragmentation etc. To illustrate the relevant physics here we will simplify this system further by assuming the perturbation is a linear (~10%) non-axisymmetric distortion, cloud orbits can be described as test particles with drag and cloud collisions are the sources of the drag as well as providing the massive star formation mode.

The technique used to calculate the response is to follow the elegant stellar dynamical formulation of this problem by Lynden-Bell and Kalnajs (1971) and butcher it by adding a collisional drag component to some of the stars that are then called clouds. The general linear non-axisymmetric distortion is Fourier decomposed into spiral modes, a transformation is made to action angle variables, it is assumed the dominant collisional damping is on the radial action and the long wavelength limit is taken. The rate of change of angular momentum at any given radius in the disk is given by

$$\langle \dot{h} \rangle = \frac{2\gamma\, m^2\, k^2 S^2 (\Omega - \Omega_p)}{\left(m(\Omega + \Omega_p - \frac{K}{m})^2 + \gamma^2\right)\left(m\,(\Omega + \Omega_p + \frac{K}{m})^2 + \gamma^2\right)} \qquad (1)$$

where S is the potential wave amplitude, k is its radial wave number, γ is the drag collisional rate, Ω in the rotation frequency of the disk, Ω_p is the wave pattern speed, K is the epicyclic frequency and m is the number of arms associated with the perturbation (Norman 1984). The change of sign of the effect at corotation when $\Omega = \Omega_p$ is obvious, as is the crucial dependence of $\langle \dot{h} \rangle$ on the presence of **both** the cloud collisions and the presence of the perturbing wave. Physically, the clouds lead to the bar or general wave perturbation inside corotation by an angle that is of order γ. This is just the forced oscillator with drag response problem, where the drag gives a phase shift. These leading clouds form a system that is torqued down by the action of the corresponding stellar bar thus losing angular momentum and having the clouds move inwards. Outside corotation the clouds move outwards since the effect changes sign. This simple analysis fits the numerical simulations done by Schwarz (1981) and Combes and Gerin (1985). Away from resonances, which is the general case, the inflow velocities can be written, at radius R,

$$v_r \sim 2\gamma\, m^2 R\, [kR]^2 \left[\frac{S^2}{\Omega^2 R^2}\right] \left[\frac{\Omega - \Omega_p}{\Omega}\right] \qquad (2)$$

for $k \neq 0$, and for $k = 0$

$$v_r \sim 2\gamma\, m^2\, R \left[\frac{S^2}{\Omega^2 R_h^2}\right] \left[\frac{\Omega - \Omega_p}{\Omega}\right] \qquad (3)$$

Once again we see that the combination of enhanced cloud collisions and large amplitude perturbations will give greatly enhanced inflow. To estimate timescales we need to establish the nature of the drag. There are two cases here. If the drag is due to collisions with background clouds the inflow velocity will increase exponentially with time as $e^{t/\tau}$, and secondly if the drag is due to collision with other large clouds the temporal behaviour will be as $(1 - t/\tau)^{-1}$. The timescale $\tau = 1/\gamma$ is obtained from a $[n_{cl}\, \sigma_{cl}\, v_{cl}]^{-1}$

estimate and here taking quantities relevant to the central region of ARP 220 we find a timescale of 2 x 10^7 yr, and for a normal Sc ~ 10^9 yr, when in both cases a wave perturbation of order ~10% is assumed. Thus the mechanism is efficient and roughly fits even the rapid inflow rates required for starbursts. For Arp 220 there are also interesting implications for star formation and the details of the estimate for τ are found in the following section.

III. STAR FORMATION IN STARBURSTS

The question here is what is the physical process that skews the mass function to high mass only?? Theories are very ambiguous here. For example, in another high pressure environment such as a cooling flow it supposed that only low mass stars form. Low mass star formation may be inhibited by shear, turbulence or magnetic fields but may is the relevant word here. The approach I will take here is to base the model on powerful observationally based arguments presented by Scoville (this meeting) that cloud-cloud collisions generate massive OB stars, and by clouds it is generally meant molecular clouds. Taking relevant parameters for Arp 220 to be 10^{10} $M_\odot$ of gas in the inner 3 kpc and assuming 10^5 $M_\odot$ per cloud and a cloud radius of 5 pc and a velocity dispersion of 20 km s^{-1} and a wave amplitude of 10% and a star formation efficiency of ~10% we get $\tau \sim 2 \times 10^7$ years in the previous section and a rate of OB star formation of ~10^2 OB stars per year!

Cloud collisions rates can be significantly enhanced by the presence of bars and ovals that generate shocks and give substantial orbit crossings. In the central regions of triaxial systems there are many box orbits that have plunging radial trajectories with the possibility for much orbit crossing. In systems with strong central mass concentrations stochastic orbits can develop and these orbits wander stochastically around the central region greatly increasing the collision rate. This effect will be very significant for ratios of black holes (in other central mass concentrations) to core masses of order 10^{-3} to 10^{-1} (Norman and May 1984).

IV. OUTFLOWS FROM STARBURSTS

Outflows from starbursts systems seem ubiquitous (Heckman, these proceedings). The mechanical energy and momentum input is clearly very substantial. For a supernova rate of 1-10 yr^{-1} one finds a luminosity $L \sim \eta$ 10^{43} erg s^{-1} in an outflow where η is an efficiency factor. There are several ways to model these outflows. Chevalier and Clegg (1985) have given a spherical wind model with a wind velocity of order $V_w \sim 2000$ km s^{-1} at 200 pc and a terminal cloud velocity of $V_t \sim 400\ [(10^{21}\ cm^{-2}N)/(Ncl)]^{1/2}$ km s^{-1}. The x-ray emitting gas is produced by shocked clouds and filaments in the wind itself. Wind or explosion driven shell propagation and evolution has been studied by various authors (c.f. Sakashita and Hanami 1986, Norman 1986 plus references). A mild, wide-angled collimation of order 30-40° is found and various evolutionary sequences can be seen as the shell is embedded in and bursts out of the disk. These various stages can be compared with the data (Heckman, Sofue, this conference). In the final state we expect a steady state wind propagating in a core between two shock waves at the long edge of the core and a massive molecular ring in the disk at the boundaries of the outflow

region. The opening angle of the core is of order the inverse Mach number of the flow at one disk scale height. Shocked clouds, bullets and filaments will give the coronal x-rays and optical lines. Molecular lines may well be observed in these outflows. The Galactic Centre itself has many of these properties (Pudritz, Norman and Heyvaerts 1986) if associated with a relatively small starburst $\sim 10^7 - 10^8$ years ago.

The metallicity content of these outflows is rather interesting. A supernova rate of 1-10 supernovae per year producing approximately 1 $M_\odot$ of iron per supernova over a burst lifetime of $\sim 10^8$ years gives an injected iron mass of $10^8 - 10^9$ $M_\odot$ of Fe into the intracluster or intergalactic medium. We assume the gas does not cool and supernovae bubbles intersect before significant cooling at such high supernovae remnant densities found in starburst systems. This is a very significant metallicity input to the intra cluster or intergalactic medium. One needs of order greater than 10^{10-11} $M_\odot$ of processed material per luminous L_* galaxy injected into the intracluster medium (Henriksen 1985) to explain the metallicity of the intracluster medium. If the starburst outflow were ubiquitous in the early stages of cluster evolution this could solve the metallicity of clusters problem, essentially due to the distorted initial mass function of starbursts.

IV. ACTIVITY AND STARBURSTS

There are many ways in which starbursts and activity can be related and here I will briefly note a few of these. Jets can certainly trigger star formation as is discussed in the context of Minkowski's object by van Bruegel et al (1985) and Centaurus A (de Young 1981). Jet pressures are high compared to interstellar medium pressures

$$P_{jet} \sim 10^{-9} \left(\frac{L_{jet}}{10^{42}\ \mathrm{ergs}^{-1}}\right) \left(\frac{(100\ \mathrm{pc})^2}{A_{jet}}\right) \left(\frac{10^4\ \mathrm{km\ s}^{-1}}{v_{jet}}\right) \mathrm{dyne\ cm}^{-2} \qquad (4)$$

where L_{jet}, A_{jet} and v_{jet} are the jet luminosity, shear and velocity. The over pressure induced by a jet striking a cloud is very similar to the effect of a cloud-cloud collision and can therefore probably trigger massive OB star formation. In this picture clouds can either orbit into a jet or be struck by a jet propagating through the interstellar medium.

The structure of the molecular clouds and the interstellar medium can be significantly affected by the prescence of activity. For example the ionization balance in molecular clouds in the central region can be changed by more than an order of magnitude if a powerful central x-ray source is present. This can substantially lengthen the ambipolar diffusion time and possibly lead to more massive star formation (Silk and Norman 1983).

The presence of starbursts can feed the monster creating the active nucleus. Massive OB stars on radial box orbits or stochastic orbits can plunge toward the central black hole and accretion disk on timescales of order a core crossing time which is less than the time to evolve to a supernova. Thus high pressure and other direct mass injection processes can occur due to the action of starburst generated supernovae exploding near the central object. More generally, the processes discussed here for fuelling starbursts are the same as

those for fuelling quasars. Recall that for powerful quasars one needs 10-100 $M_\odot$ yr^{-1} and, conversely, it is difficult to see how such prodigious mass inflows could avoid forming stars!

V. SUMMARY

A model has been presented where the action of a companion on a gas-rich spiral galaxy can induce mass inflow rates typical of those required for Arp 220 and a starburst rate of massive OB star formation of ~10-10^2 per year where it is assumed cloud collisons trigger the massive star formation mode.

Supernovae and OB star wind driven outflows were discussed and various evolutionary stages were noted. The outflows would be significantly metal enhanced and could provide the major source of metals to the intracluster medium.

Starbursts and activity are intimately related--it is difficult to conceive of one without the other in massive gas rich system with central black holes. Massive starbursters appear to be forming a significant fraction of their central stellar mass. This is indeed galaxy formation by any other name. The process is apparently hidden by dust and occurs in bursts! Any quasar embedded in such a system would be quite successfully shrouded until the dust is removed. Arp 220 seems an excellent example. These points learned from the infrared work must be kept in mind when discussing both galaxy formation and quasar evolution.

It is a pleasure to acknowledge stimulating conversations with T. Heckman, J. Heyvaerts, R. Pudritz and N. Scoville.

REFERENCES

Chevalier, R. A. and Clegg, A. W. 1985, Nature, **317**, 44.
Combes, F. and Gerin, M. 1985, Astron. Astrophys., **150**, 327.
DeYoung, D. S. 1981, Nature, **293**, 43.
Heckman, T. 1986 (these proceedings).
Henriksen, M. 1985, Ph.D. thesis, Univ. of Maryland.
Lynden-Bell, D. and Kalnajs, A. 1972 M.N.R.A.S., **157**, 1.
Norman, C. and May, A. 1984, unpublished.
Norman, C. 1984, in Formation and Evolution of Galaxies, ed. J. Audouze and J. Tran Vanh 1984, D. Reidel, p. 327.
Norman, C. 1986, IAU, **116**, in press.
Pudritz, R., Norman, C. and Heyvaerts, J. 1986, in preparation.
Sakashita, S. and Hanami, H. 1986, PASJ, in press.
Schwarz, M. P. 1981, Ap. J., **247**, 77.
Scoville, N. 1986 (these proceedings).
Silk, J. and Norman, C. 1983, Ap. J. Letters, **272**, L49.
Sofue, I. 1986, these proceedings.
van Breugel, W., Filippenko, A. V., Heckman, T. and Miley, G. 1985, Ap. J., **293**, 83.

DISCUSSION

SCOVILLE:

The size of 3 kpc assumed for the gas distribution in Arp 220 is consistent with the new Owens Valley Interferometer maps of the CO as will be presented by Anneila Sargent tomorrow.

NORMAN:

Sounds good to me!

BURBIDGE:

You say that with a black hole and a starburst all of the phenomena can be explained. But how about a prediction? Which comes first, and how do these systems evolve?

NORMAN:

Good question. I have tried to answer this in the text.

INDUCED STAR FORMATION IN INTERACTING GALAXIES

R.C. Kennicutt and K.A. Roettiger, Dept. of Astronomy, University of Minnesota

W.C. Keel, Sterrewacht Leiden

J.M. van der Hulst, Netherlands Foundation for Radio Astronomy

E. Hummel, Max-Planck-Institut für Radioastronomie

ABSTRACT. We have used measurements of H-alpha emission-line fluxes and FIR fluxes in ~100 interacting spirals to investigate the effects of close tidal interactions on the disk and nuclear star formation rates in galaxies. Two samples of interacting spirals were studied, a complete sample of close pairs, and a set of strongly perturbed systems from the Arp atlas. Both the integrated H-alpha luminosities and FIR luminosities are enhanced in the interacting galaxies, indicating that the encounters indeed trigger massive star formation in many cases. The response of individual galaxies is highly variable, however. A majority of the interacting spirals exhibit normal star formation rates, while a small fraction are undergoing bursts with luminosities which are rarely, if ever, observed in noninteracting systems. Virtually all of the latter are in the Arp sample, indicating that the Arp atlas is heavily biased to the most active star forming systems.

INTRODUCTION

Although it is well known that many of the most spectacular examples of starburst galaxies are members of interacting systems, relatively little quantitative information is available on the effects of interactions overall on the star formation properties of galaxies. The few available prior studies have yielded contradictory results. For example, comparisons of optical colors and infrared fluxes of normal and interacting galaxies by Larson and Tinsley (1978) and Lonsdale et al. (1984), respectively, provided evidence for strong interaction-induced star formation bursts, while Hummel's (1981) study of radio emission in close pairs revealed no evidence of abnormal disk star formation.

Here we report preliminary results from a new optical and infrared study of the star formation properties of interacting spiral and irregular galaxies. We have obtained measurements of the Hα line emission and (IRAS) far-infrared fluxes for objectively-defined samples of interacting and isolated galaxies, in order to quantitatively assess the effects of interactions on the global star formation rate. The results summarized here are part of a more general survey of the effects of interactions on the disk and nuclear properties of galaxies. Results on the nuclear activity have been published previously (Kennicutt and Keel 1984, Keel et al. 1985). We also refer the reader to closely related papers by Bushouse and Cutri elsewhere in this volume.

MATERIALS AND METHODS

Following our earlier study of nuclear activity (Keel et al. 1985), we have studied two samples of interacting galaxies. We used an unpublished catalog of galaxy pairs by T. van Albada, along with published redshift catalogs, to

Carol J. Lonsdale Persson (Editor)
Star Formation in Galaxies

generate a magnitude-limited sample of 53 galaxies with close companions, selected independently of any abnormalities in structure, surface brightness, or star formation activity. While this sample (referred to hereafter as the complete pairs sample) may be contaminated by a few projected, noninteracting pairs, it is free of the potentially severe selection bias which may plague any sample which is selected according to purely morphological criteria. In order to assess the importance of this bias, and to explore the effects of unusually strong interactions, we also studied a subsample of pairs from the Arp (1966) Atlas of Peculiar Galaxies. This latter sample of 58 galaxies, including several members of the complete sample above, will be referred to hereafter as the "Arp" sample.

For comparison we used two control samples of noninteracting galaxies. For comparisons of Hα properties we used the survey of Kennicutt and Kent (1983), excluding elliptical and S0 galaxies, interacting systems, and Virgo cluster members. For the comparison of infrared properties we used in addition the magnitude-limited sample of Keel (1983), again excluding interacting galaxies. Both control samples exhibit very similar Hα and FIR properties.

We chose as our primary star formation indicator the integrated emission in the Hα emission line; this has proven to be a useful and sensitive tracer of the massive star formation rate (e.g., Kennicutt 1983, Gallagher et al. 1984). Digital images in Hα and in the red continuum were obtained during 1983-1985 on the 2.1m telescope at Kitt Peak National Observatory, using the ISIT Video Camera (53 galaxies), and a TI CCD direct camera (27 galaxies). The images were processed at KPNO to produce continuum-subtracted Hα + [NII] maps, as well as a normalized continuum frame of each galaxy. Final processing of the data, including sky background removal and simulated aperture photometry, was performed on the University of Minnesota image processing system. The main parameter of interest for this study is the integrated emission-line equivalent width of each galaxy, which is directly measurable from the relative fluxes in the net Hα and normalized continuum frames (and the bandwidth of the Hα filter). For data taken under photometric conditions we also derived the absolute emission line fluxes of the galaxies.

We also obtained photoelectric Hα and continuum aperture photometry for 27 galaxies, using the Schmidt Two-Holer photometer on the UM/UCSD 1.5m telescope on Mt. Lemmon. This provided a check on the equivalent widths derived from the imagery, as well as flux calibration data for images obtained on non-photometric nights. Comparison of the independent measurements indicates that the equivalent widths are accurate to ±5Å or better (or ±10% in galaxies with very high equivalent widths). Finally aperture photometry for a few nearby, large-diameter systems was taken from the surveys of Kennicutt and Kent (1983) and Kennicutt, Edgar, and Hodge (in preparation).

We have also used the IRAS 60μ and 100μ data to measure the integrated far-infrared (FIR) luminosities of the same galaxies. Roughly 30-40% of the galaxies in the control samples and in the complete pairs sample are larger than the IRAS detector resolution, so we determined integrated fluxes from the HCON1 sky flux maps, using a background-subtracting aperture photometry program on the University of Minnesota image processing system. Comparison of the derived fluxes with the IRAS Point Source Catalog (1985) fluxes for small faint galaxies in our program showed agreement to better than 15-25% on average, adequate for our purposes. For galaxies smaller than 4' diameter we used the PSC fluxes

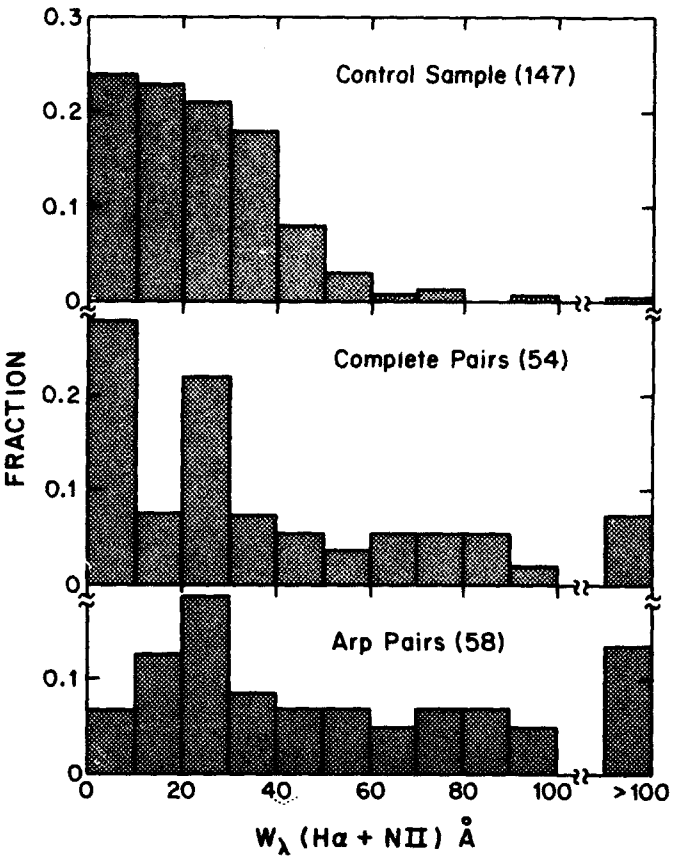

Figure 1: Distribution of H-alpha emission equivalent widths in the interacting galaxy and control samples. Numbers in parentheses refer to the number of galaxies in each sample.

directly. Detection rates, using either the PSC or the sky flux maps, were 90% for the control samples, 85% for the complete pairs, and 75% for the Arp pairs. Unfortunately the IRAS survey does not resolve the emission from many of the close pairs; this is especially a problem for the Arp pairs. We obtained flux co-added maps for the close pairs in our samples, but in most cases the emission from the individual members is hopelessly blended. For the statistical comparisons which follow (only!), we have used the relative Hα fluxes of the individual components in the IRAS-blended pairs to estimate the relative FIR contribution of each member. Alternatively one can throw out the blended pairs altogether, or compare pairs together instead of individual galaxies, and the qualitative conclusions are unchanged.

The 60μ and 100μ fluxes were combined using the algorithm in the IRAS Explanatory Supplement (1985) to obtain an estimate of the integrated FIR flux for each galaxy. Finally, we normalized this FIR flux to the blue flux (the latter taken from de Vaucouleurs et al. 1976), in order to obtain a luminosity-free index of relative FIR emission in each galaxy.

RESULTS

Both samples of interacting galaxies exhibit significant enhancements in total Hα emission and FIR emission on average. Figures 1-2 show the distributions of integrated Hα + [NII] equivalent width and L(FIR)/L(B) in the samples of interacting and isolated galaxies. Both quantities vary systematically with Hubble type, so it is best to compare the different samples on a type-by-type

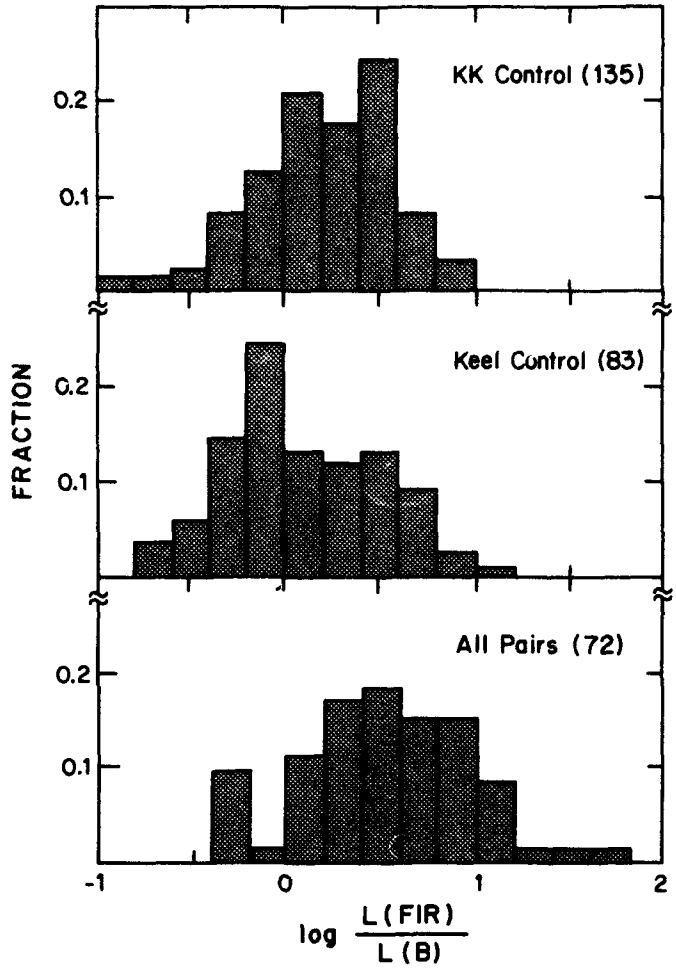

Figure 2: Distribution of the ratio of far-infrared to blue luminosity in the samples. The top two samples are the control samples as described in the text. The bottom is the combined interacting galaxy sample (complete and Arp).

basis, as is shown in Table 1 (also see Figs. 3-4). The distributions of morphological type in the three samples are very similar, however, so the type-averaged distributions shown in Figs. 1-2 can be directly compared.

Although the average levels of emission are significantly higher in interacting galaxies -- the average Hα equivalent widths and L(FIR)/L(B) ratios are both roughly a factor of two higher in the Arp sample than in the control samples -- the response of individual galaxies varies enormously. A large fraction of the interacting galaxies we studied, in fact, exhibit little or no enhancements in emission. In our complete sample, which should be the most representative of galaxies with close companions, the median emission levels are virtually identical to the control samples (though a few extreme starbursting systems are certainly evident). Virtually all of the starburst galaxies in the complete pairs sample are members of the Arp atlas. In contrast to the objectively-selected complete sample, the sample of galaxies selected solely on the basis of morphological peculiarity possesses, perhaps not surprisingly, a very high fraction of abnormally star forming systems, and a systematically high level of star formation overall. Clearly the star formation properties of a sample of interacting galaxies can be as dependent on the observational selection criteria as on the physical effects of the interactions themselves.

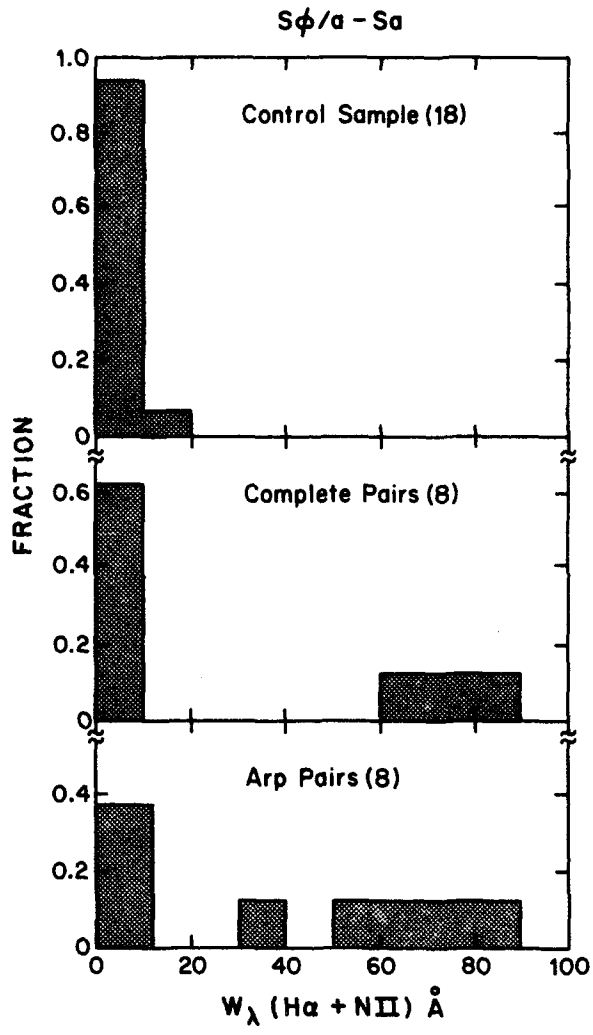

Figure 3: Same as Fig. 1, but showing only the early-type spirals. Note the broad dispersion in emission properties of the interacting galaxies.

Table 1
MEDIAN EMISSION PROPERTIES

	Control Sample	Complete Pairs	Arp Pairs
W_λ(Hα + [NII]) (Å)			
All Types	22	24	46
S0/a-Sa	2	4	45
Sab-Sb	10	10	28
Sbc-Scd	26	32	33
Sm-Im	37	125	110
log (FIR/B) (detection only)			
All Types	+0.23	+0.44	+0.66
S0/a-Sa	-0.24	+0.42	+0.78
Sab-Sbc	+0.16	+0.29	+0.90
Sbc-Scd	+0.32	+0.43	+0.52
Sm-Im	+0.42	+0.78	+0.67

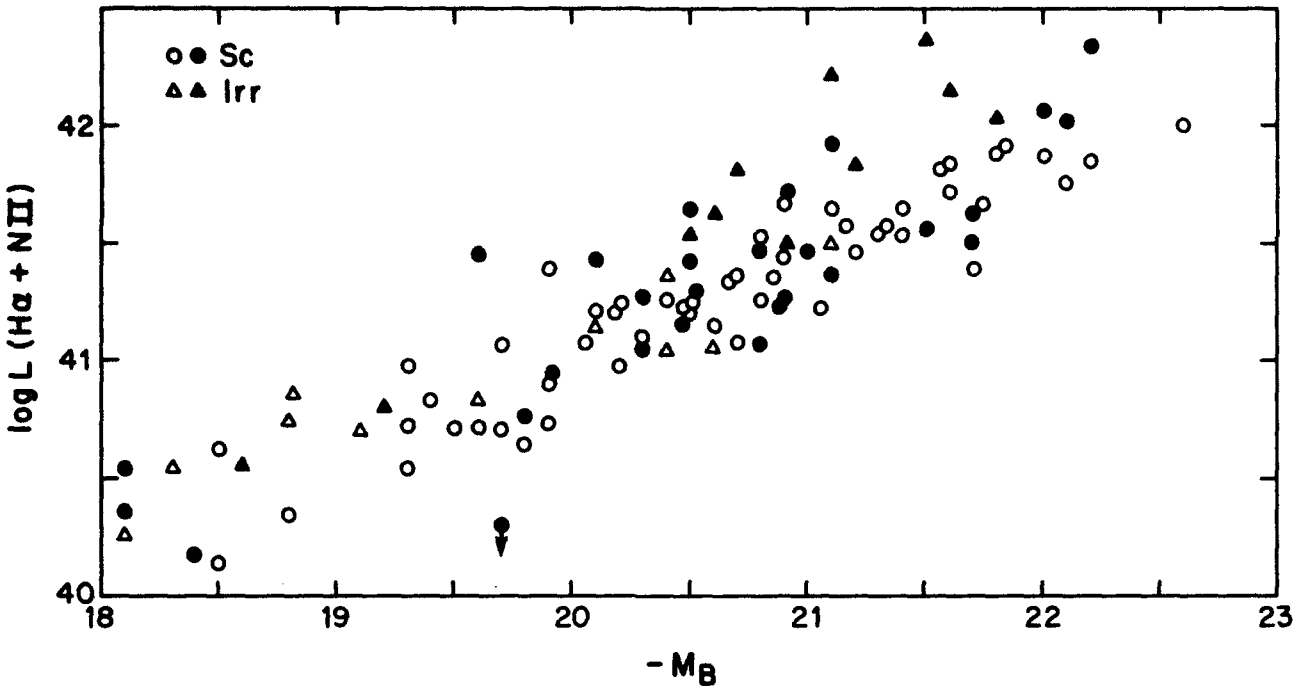

Figure 4: H-alpha luminosities for late-type galaxies. Closed symbols denote interacting galaxies, while open symbols denote galaxies in the control sample.

The emission properties of the galaxies illustrated in Figs. 1-2 appear to be continuous, but this is partly due to the mixing of different galaxy types. When we examine the distributions among galaxies of a fixed type, we observe a broader relative dispersion in properties, and in some cases a suggestion of bimodality in response. This is most clearly seen in the early-type spirals, as illustrated in Fig. 3. Isolated Sa galaxies normally exhibit only weak (if any) detectable Hα emission, indicative of a low massive star formation rate. Among the interacting Sa galaxies, however, we find both systems with normal (i.e., low) Hα equivalent widths, and several systems with emission levels which are abnormally high even for a late-type galaxy. In some cases this abnormally strong emission is primarily nuclear, in others it is primarily from disk emission, and in many both the disk and nuclear emission are enhanced.

For most of the galaxies we also have measured the total emission luminosities, and Fig. 4 illustrates the Hα properties of the late-type (Sc-Irr) galaxies in our study. On average the interacting galaxies exhibit stronger emission at all luminosities. The brightest systems, mostly members of the Arp sample, possess total Hα luminosities which are rarely if ever observed among isolated galaxies. Hence it is probably not surprising that such a large fraction of the luminous sources in the IRAS survey, Markarian catalogs, emission-line surveys, etc., are members of interacting systems.

DISCUSSION

The integrated Hα emission of a galaxy primarily measures the present star formation rate for massive (>10 $M_\odot$) stars, and hence our results confirm the hypothesis that close galaxy-galaxy interactions can induce bursts of star

formation in spiral and irregular galaxies. The degree of enhancement in the star formation rate varies over a large range, from galaxies which appear to be unaltered by the interaction (at least as observed at present) to galaxies with star formation bursts which are 10-100 times stronger than is typically observed in isolated systems.

Our results explain what had been an apparent inconsistency between the studies of Larson and Tinsley (1978) and Lonsdale et al. (1984), who had found evidence for strong star formation bursts in interacting galaxies, and the study of Hummel (1981), who found no evidence for increased disk star formation in his complete sample of galaxy pairs. We confirm the results of all 3 studies. For strongly interacting, peculiar galaxies selected from sources such as the Arp atlas, including those which made up the bulk of the Larson and Tinsley and Lonsdale et al. samples, we observe systematically high star formation rates. Bushouse (1986) has observed a sample of even more strongly perturbed systems and observes even higher average star formation rates. On the other hand, for our objectively-selected complete sample of galaxies with close companions, we observe a slight increase in the average star formation rate, confirming Hummel's conclusion.

What can we learn from this complicated set of results? Clearly galaxy-galaxy interactions are capable of inducing star formation in galactic disks, and under special conditions can trigger major star formation bursts of a magnitude which is rarely if ever observed in noninteracting galaxies. Such starbursts are rare, however. The enhancement in star formation activity must be very sensitive to the ambient conditions in the disks of the galaxies, as well as to the orbital properties of the interaction itself.

The high star formation rates in the Arp sample confirm the not-surprising result that the most strongly disturbed galaxies exhibit the strongest star formation bursts. It is also, likely, however, that catalogs such as the Arp atlas are strongly biased toward unusually luminous, high surface brightness systems, and will a priori exhibit abnormal star formation properties. The relatively normal emission in most of the members of our complete sample of close pairs suggests that while induced star formation in strongly interacting galaxies may be a very important physical process for understanding the IRAS source counts, statistics of active and starbursting galaxies, etc., it is probably not a major influence on the current evolution of most galaxies, even those with nearly companions.

Several important questions remain to be explored in more detail. We intend to use our imagery to study the spatial distribution of the star formation in the interacting galaxies, and in particular to study the relative enhancements in disk and near-nuclear star formation. Preliminary analysis of our data indicates that the bulk of the Hα emission in most of the galaxies originates from star formation in the disk, but that the fraction of emission from the nucleus (or from a near-nuclear disk) is significantly higher than in isolated galaxies (see also Keel et al. 1985 and especially Bushouse 1986). We are also measuring the properties of individual HII regions in the galaxies, in order to better understand the nature of the induced star formation. A better understanding of the physical origins of the star formation, however, and its wide diversity in different systems, will probably require detailed spatially-resolved kinematic observations and modelling of individual systems.

ACKNOWLEDGEMENTS

This work was supported by NASA grant JPL/957243 and NSF grant AST81-11711A01 to the University of Minnesota, and a NATO International Travel Grant 0592/82 to JMH and RCK. Mt. Lemmon Observatory is supported in part by NSF grant AST84-20347.

REFERENCES

Arp, H. 1966, Atlas of Peculiar Galaxies (Pasadena: California Institute of Technology).
Bushouse, H. A. 1986, Ph.D. Thesis, University of Illinois.
de Vaucouleurs, G., de Vaucouleurs, A., and Corwin, H. G. 1976, Second Reference Catalog of Bright Galaxies (Austin: University of Texas Press).
Gallagher, J. S., Hunter, D. A., and Tutukov, A. 1984, Ap. J., 284, 544.
Hummel, E. 1981, A. & A., 96, 111.
IRAS Catalogs and Atlases, Explanatory Supplement, 1985, ed. Beichman, C. A., Neugebauer, G., Habing, H. J., Clegg, P. E., and Chester, T. J. (Washington, D.C.: US Government Printing Office).
IRAS Point Source Catalog 1985, Joint IRAS Science Working Group (Washington, D.C.: US Government Printing Office).
Keel, W. C. 1983, Ap. J. Suppl., 52, 229.
Keel, W. C., Kennicutt, R. C., Hummel, E., and van der Hulst, J. M. 1985, A. J., 90, 708.
Kennicutt, R. C. 1983, Ap. J., 272, 54.
Kennicutt, R. C., and Keel, W. C. 1984, Ap. J. (Letters), 279, L5.
Kennicutt, R. C., and Kent, S. M. 1983, A. J., 88, 1094.
Larson, R. B., and Tinsley, B. M. 1978, Ap. J., 219, 46.
Lonsdale, C. J., Persson, S. E., and Matthews, K. 1984, Ap. J., 287, 95.

DISCUSSION

C. Magri: From your complete pairs sample, we see that proximity doesn't guarantee enhanced star formation in component galaxies. Have you found any discriminant (e.g., rotation velocity, HI content) of 'active' pairs vs. 'normal' pairs?

R. Kennicutt: It is very difficult to discern such second-order effects in our data, because the dispersion in emission properties among isolated galaxies is so large. Among the early-type spirals, we do notice that the 'active' galaxies often exhibit unusually strong nuclear emission.

M. Harwit: Since gas-gas interactions can be far more abrupt than stellar interactions in colliding galaxies, does one ever see galaxies in which the gas is clearly interacting, while the stellar components appear virtually unaffected?

R. Kennicutt: I do not think that enough data are available on gas distributions in galaxies to test your hypothesis. Most HI mapping studies of interacting galaxies, for example, are limited to pairs which show optical peculiarities. On the other hand, HI maps of a number of close groups (by M. Haynes, for example) do show prominent gaseous plumes among what are relatively undistorted galaxies in the stellar component.

THE FREQUENCY OF ENHANCED STAR FORMATION IN INTERACTING AND ISOLATED GALAXIES

Roc M. Cutri

Steward Observatory

ABSTRACT

It has become increasingly apparent that the physical state of galaxies can be influenced by their environment. To probe the sensitivity of the star formation rate and extent in galaxies to gravitational encounters, we have obtained ground based near and mid-infrared and IRAS far-infrared measurements of complete samples of isolated and interacting pairs of galaxies. The observed infrared properties of the isolated galaxies are used to gauge the magnitude of star formation in galaxies free from external influences, and to define the relationships between morphological type and infrared luminosity. We contrast these properties with those of the interacting sample to examine the extent to which interactions can enhance or alter the nature of star formation. The mechanisms by which interactions influence activity such as star formation are investigated through correlations of the infrared characteristics with radio and optical measurements, and with morphological and physical parameters such as galaxy types, separations, encounter velocities and interaction types. Limits to the physical extent of the star formation are obtained by comparing the large aperture measurements of IRAS with the small-aperture ground based photometry.

Carol J. Lonsdale Persson (Editor)
Star Formation in Galaxies

ULTRALUMINOUS INFRARED GALAXIES

D. B. Sanders[1], B. T. Soifer[1], G. Neugebauer[1], N. Z. Scoville[1],
B. F. Madore[1], G. E. Danielson[1,2], J. H. Elias[1], K. Matthews[1],
C. J. Persson[3], and S. E. Persson[4]

[1]Palomar Observatory, California Institute of Technology
[2]Division of Geological and Planetary Sciences, Caltech
[3]IPAC, California Institute of Technology
[4]Mount Wilson and Las Campanas Observatories

ABSTRACT. The IRAS survey of the local universe ($z \lesssim 0.1$) has revealed the existence of a class of ultraluminous infrared galaxies with $L(8\text{-}1000\mu m) > 10^{12} L_\odot$ that are slightly more numerous, and as luminous as optically selected quasars at similar redshift. Optical CCD images of these infrared galaxies show that nearly all are advanced mergers. Millimeter-wave CO ($1 \rightarrow 0$) observations indicate that these interacting systems are extremely rich in molecular gas with total H_2 masses $1 - 3 \times 10^{10} M_\odot$. Nearly all of the ultraluminous infrared galaxies show some evidence in their optical spectra for nonthermal nuclear activity. It is proposed that their infrared luminosity is powered by an embedded active nucleus and a nuclear starburst both of which are fueled by the tremendous reservoir of molecular gas. Once these merger nuclei shed their obscuring dust, allowing the AGN to visually dominate the decaying starburst, they become the optically selected quasars.

1. INTRODUCTION

Recent determinations of the luminosity function for IRAS galaxies (Lawrence *et al.* 1986, Rieke and Lebofsky 1986; Soifer *et al.* 1986) all show a significant population of luminous infrared galaxies with infrared luminosities exceeding $10^{12} L_\odot$ ($H_o = 75$ km s^{-1} Mpc^{-1}). Soifer *et al.* (1986) find that at luminosities above $10^{10} L_\odot$ the space density of infrared galaxies is comparable to, or greater than that for active and starburst galaxies, and at the highest luminosities the IRAS galaxies are slightly more numerous than optically selected quasars (Schmidt and Green 1983). The ultraluminous infrared objects with $L(8\text{-}1000\mu m) > 10^{12} L_\odot$ are the subject of this paper.

The data reported here are part of a larger study of the properties of the brightest galaxies in the IRAS survey. The bright galaxy sample includes all objects brighter than 5.4 Jy at $60\mu m$ with $|b| > 30°$ and $\delta > -30°$. Because these are the brightest galaxies in the sky at $60\mu m$, this sample represents the best opportunity for the study of the infrared emission processes in galaxies. A complete description of the survey and the luminosity function for these galaxies is given in Soifer *et al.* (1986, 1987). A preliminary description of the morphology and molecular gas content of 'high luminosity' members of the bright galaxy sample with $L_{FIR}(40\text{-}400\mu m) = 6 \times 10^{10} - 6 \times 10^{11} L_\odot$ is given in Sanders *et al.* (1986a).

2. THE ULTRALUMINOUS IRAS GALAXY SAMPLE

The ultraluminous objects in the IRAS Bright Galaxy Survey are listed in Table 1. Their tabulated luminosity was computed using the prescription outlined by Perault *et al.* (1986) which uses the data from all four IRAS bands to approximate $L(8\text{-}1000\mu m)$. Since several of the ultraluminous objects have substantial flux at $25\mu m$, this method provides a significantly better approximation to the bolometric luminosity than the more commonly used L_{FIR} fit to the 60 and $100\mu m$ data given in *Catalog of Galaxies*

and Quasars Detected in the IRAS Survey (1985). The dominance of the far infrared luminosity in the total energy budget for all of the ultraluminous galaxies can be seen from the tabulated ratio $\nu f_\nu(80)/\nu f_\nu(B)$ which has a median value of 25.

Table 1

Ultraluminous IRAS Galaxies

Object	RA (1950)	Dec (1950)	cZ [a] (km s^{-1})	L(8-1000μm) ($10^{12}L_\odot$)	$\frac{\nu f_\nu(80)}{\nu f_\nu(B)}$	Morph [b]	Optical [c] Spectra
IRAS	05 18 58.6	-25 24 40	12706	1.23	24	star	Sey 1.5
IRAS	08 57 13.0	+39 15 40	17480	1.25	10	M	HII
UGC5101	09 32 04.6	+61 34 37	12000	1.02	22	M	Sey 2
IRAS	12 11 12.2	+03 05 20	21703	1.94	68	M	LINER
Mrk231	12 54 04.8	+57 08 38	12623	3.45	22	M	Sey 1
Mrk273	13 42 51.6	+56 08 13	11400	1.47	.	T	Sey 2
IRAS	14 34 52.3	-14 47 24	24332	1.88	33	M	LINER/HII
IRAS	15 25 03.1	+36 09 00	16009	1.00	25	M	LINER
Arp220	15 32 46.3	+23 40 08	5450	1.58	59	M	Sey 2
IRAS	22 49 09.6	-18 08 20	22807	1.33	25	M	LINER

Note: Objects in the IRAS Bright Galaxy Survey (Soifer *et al.* 1986, 1987) with $L(8-1000\mu m) \geq 10^{12}L_\odot$

[a]Mean optical heliocentric redshift

[b]M - advanced merger; tidal tails observed.
T - single long tail of Mrk 273 due to recent strong interaction with disturbed companion 2' North.
star - appears star-like on Palomar print; obvious nebulosity on short CCD exposure.

[c]Based on linewidth of Hα+[NII] and/or [OIII]/Hβ line ratio from long-slit spectrum.

The majority of the objects in Table 1 have blue magnitudes greater than 15.5, hence are not found in the standard catalogs. The mean redshift of the sample is $\sim$ 16,000 km s^{-1}. The space density of these objects in the local universe ($z < 0.081$) is $\rho \sim 10^{-7}$ Mpc^{-3} M_{bol}^{-1}. The sample of objects listed in Table 1, although relatively small, is an impressive number when one realizes that the only other objects in the same volume of space of comparable luminosity are quasars of which there are only about half as many.

3. BASIC PROPERTIES OF ULTRALUMINOUS IRAS GALAXIES

We have undertaken a major program of optical, near-infrared and radio continuum observations of all of the galaxies in the bright galaxy sample in an attempt to understand both the nature of the host galaxy and the origin of the enhanced infrared radiation in the most luminous objects. Data for the ultraluminous sample are summarized here with a more complete accounting to appear in Sanders *et al.* (1987).

3.1 IMAGING

One of the most important results of the entire IRAS Bright Galaxy Survey is that nearly all of the ultraluminous objects appear to be merging spirals. Eight of the ten objects show obvious, long tidal tails which extend from almost completely merged disks. The symmetry and length of the tails are remarkably consistent of numerical simulations of mergers between two disks of nearly equal mass (e.g. Toomre and Toomre 1972). One of the remaining two objects, Mrk 273, has a single, long tail pointing directly away from an extremely blue, nearly point-like companion. The companion has apparently scored a direct hit on Mrk 273, leaving behind most of its disk gas to what is now seen as a heavily reddened, disturbed galaxy. The remaining ultraluminous object, IRAS 0518-25, appears stellar on the Palomar Sky Survey print, but shows distinct nebulosity on a short CCD exposure. A deeper image is required to detect evidence of a merged system.

Figure 1 shows deep CCD images of Arp 220 and Mrk 231 - the two galaxies from our list that have attracted considerable past interest because of their extreme infrared properties. Previous optical images have apparently not been deep enough to show the faint tidal tails that clearly implicate a recent merger as the trigger for the extreme luminosity of these objects.

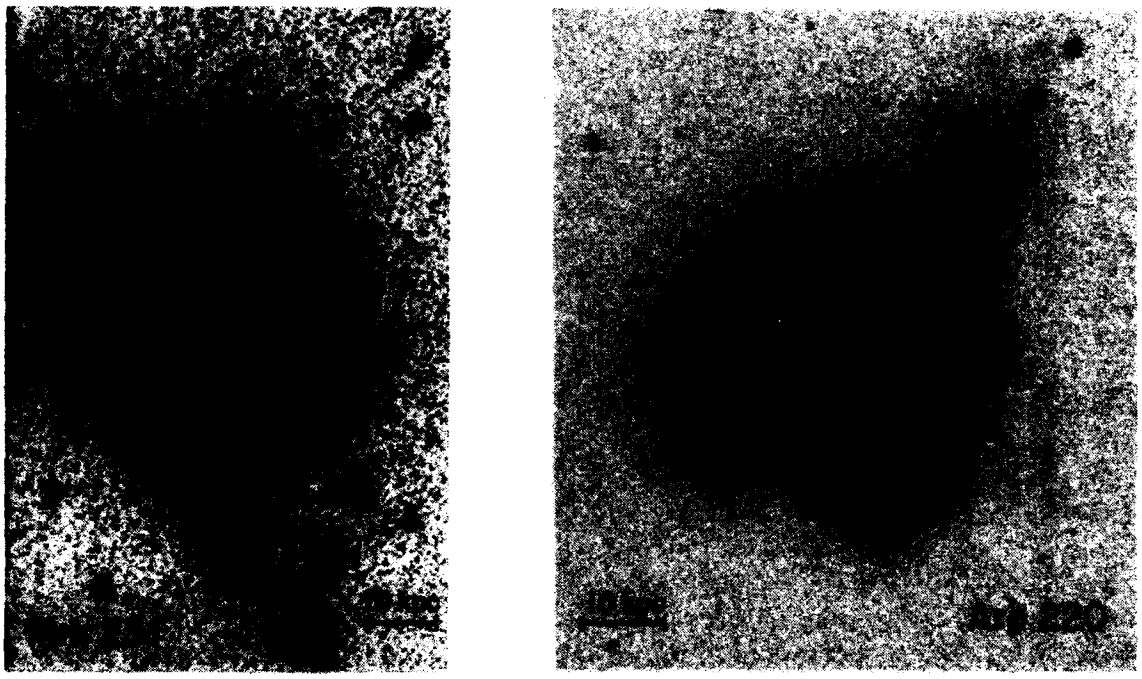

Figure 1: CCD images at 6500Å (Gunn r) of Arp 220 and Mrk 231. The scale is approximately 0".5/pixel and seeing was $\sim$ 1 arcsec.

3.2 OPTICAL SPECTRA

High-resolution, long-slit optical spectra (3800-8000Å) have been taken of the ultraluminous galaxies using the CCD double spectrograph on the Palomar 5m telescope. All are strong emission-line objects. Broad Hα emission was the primary diagnostic used to identify Seyfert activity. The remaining galaxies with narrow emission lines most often show [OIII]/Hβ line ratios characteristic of a LINER spectrum. Only one object bears strict resemblance to a thermal HII region spectrum. One galaxy has two clearly separable nuclei, one with a liner spectrum and the other of HII region type.

Our classification of the optical spectra is rather simplistic as several of these ultraluminous objects appear to have a mixture of nonthermal and thermal emission components. The most bizarre spectrum is that of Mrk 231 which shows broad Hα emission plus several strong absorption bands indicating a possible circumnuclear starburst (c.f. Boksenberg *et al.* 1976). Several other objects, most notably Arp 220 (Rieke *et al.* 1984), appear to have both strong thermal and nonthermal components, but in Table 1 we have emphasized nonthermal emission. As a class, the ultraluminous infrared galaxies differ dramatically from the majority of the galaxies with lower luminosity discovered by IRAS. The vast majority of the bright galaxies surveyed by us (Sanders *et al.* 1987) as well as the IRAS mini-survey galaxies studied by others (Elston, Cornell, and Lebofsky 1985; Lawrence *et al.* 1986) are narrow emission line objects with HII region type optical spectra.

3.3 ENERGY DISTRIBUTION

We have combined the IRAS data with ground-based optical and near-infrared photometry to determine the energy spectrum between 0.44 and 100μm for all of the ultraluminous galaxies as shown in Figure 2. The dominance of the far-infrared emission ($\lambda > 40\mu$m) in the total energy budget ranges from >95% for Arp 220 to ~50% in Mrk 231.

The distributions in Figure 2 are displayed approximately in order of increasing $f_\nu(60)\mu m/f_\nu(100\mu m)$ ratio of flux densities. The 60μm and 100μm IRAS data points have been fit with a single temperature dust emission ($\epsilon \propto \lambda^{-1}$) curve; dust temperatures range from 47 K for Arp 220 to 62 K in IRAS 0857+39. There is an obvious trend of increasing 12μm and 25μm emission with increasing $f_\nu(60\mu m)/f_\nu(100\mu m)$ color temperature, possibly due to a separate component of hotter dust associated with a Seyfert nucleus (c.f. Miley, Neugebauer, and Soifer 1985). There is also an obvious trend of increasing 1-5μm flux with increasing far-infrared color. This may still represent thermal emission from high temperature dust relatively close to a luminous nonthermal nuclear source, or it could be nonthermal emission directly associated with the region emitting the broad optical emission lines.

3.4 MOLECULAR GAS

Because of the relatively large distance of most of the ultraluminous objects and the limited sensitivity of current single dish millimeter-wave telescopes, direct measurement of the molecular gas content is limited to two objects – Arp 220 and Mrk 231. However, these data are extremely interesting in that both Arp 220 and Mrk 231 are among the most luminous CO sources known and their ratio of infrared luminosity to total H_2 mass is more extreme than observed in other high luminosity IRAS galaxies. Figure 3 shows that the total mass of H_2 in Mrk 231 is $1.4 \times 10^{10} M_\odot$ and the $L_{FIR}/M(H_2)$ ratio of 150 is ~35 times larger than that found for the ensemble of molecular clouds in the Milky Way (Sanders *et al.* 1986a; Scoville and Good 1986). For Arp 220 the values are $M(H_2) = 1.43 \times 10^{10} M_\odot$ and $L_{FIR}/M(H_2) = 95$ (Young *et al.* 1984; Sanders and Mirabel 1985. If the $L_{FIR}/M(H_2)$ ratio measures the efficiency of star formation (Sanders and Mirabel 1985; Young *et al.* 1986) then their molecular gas will be depleted in $\sim 10^8$ years.

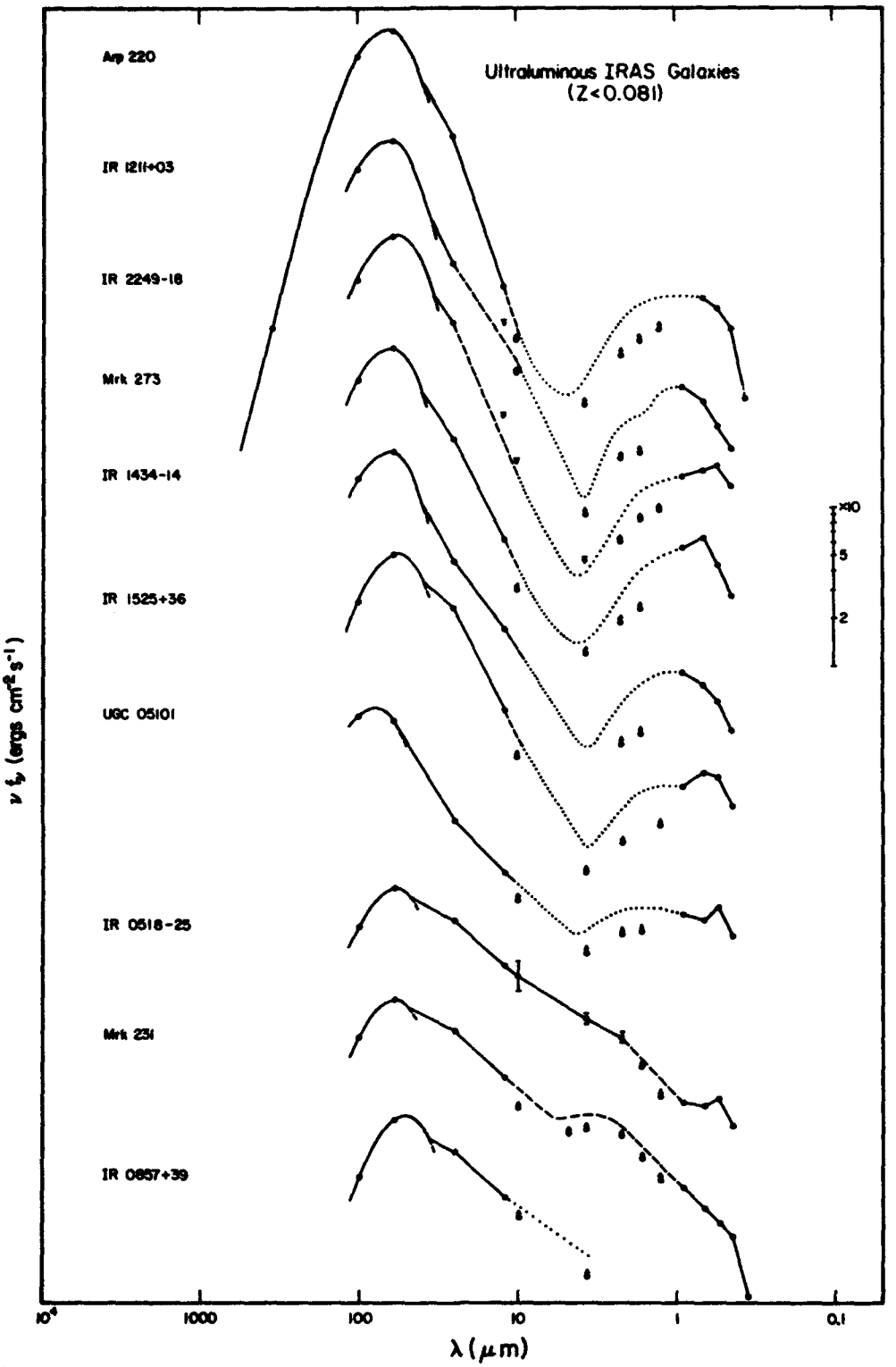

Figure 2: Spectral energy distributions from 0.33 to 100μm for ultraluminous infrared galaxies in the IRAS Bright Galaxy Survey. The data from 0.44 to 100μm is from this work. Additional data for Arp 220 at 350μm and 760μm are from Emerson *et al.* (1984). The 1-10μm data points are 5" or 10" aperture measurements. The shape of the energy distribution of the entire galaxy between 1 and 10μm (dotted line) was estimated from these small aperture measurements and the measured magnitude growth curve at I (0.88μm).

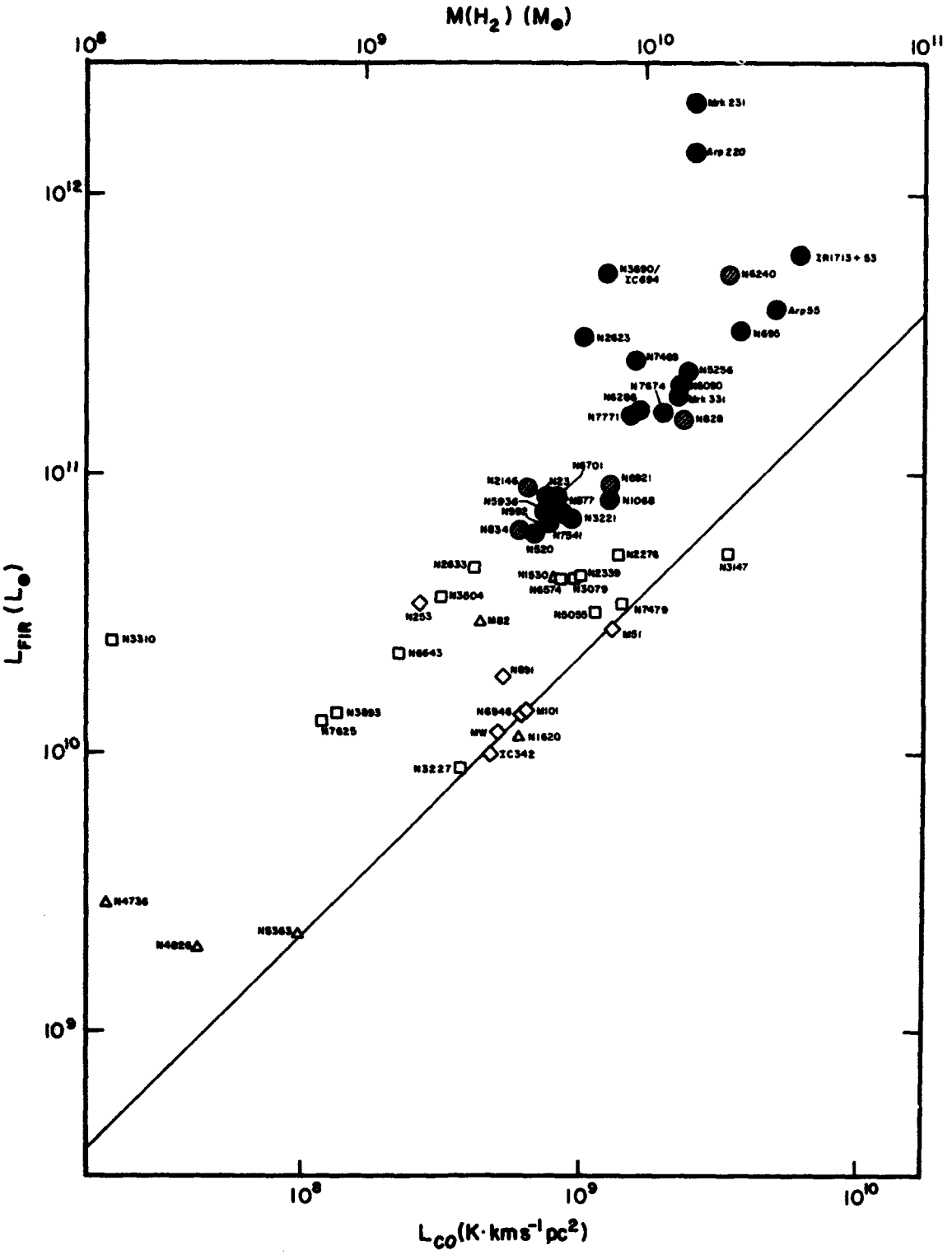

Figure 3: The total far-infrared luminosity determined from IRAS data vs CO luminosity and the total mass of H_2 in molecular clouds. Circles represent high luminosity IRAS galaxies which are an unbiased sample of all galaxies with L_{FIR} (40-400μm) $\geq 7 \times 10^{10}$ $L_\odot$. All other symbols represent CO observations of lower luminosity bright IRAS galaxies with known and unknown selection bias (see Sanders *et al.* 1986a).

4. DISCUSSION

The ultraluminous infrared galaxies represent the culmination of a trend toward an increasing percentage of interacting spirals with increasing infrared luminosity that has already been observed in previous studies of IRAS galaxies at lower luminosity (Sanders *et al.* 1986a). Table 2 compares the properties of the ultraluminous sample with galaxies at lower luminosity from the IRAS Bright Galaxy Survey. In addition to the increased frequency of merger candidates, there is evidence from the optical spectra that non-thermal AGN's play an increasing role in the energy budget at the highest luminosities.

Figure 3 strongly suggests that the fuel for the infrared luminosity in all of the bright IRAS galaxies is an abundant supply of molecular gas. Several possibilities exist for producing this luminosity, particularly if both collision partners were initially rich in molecular clouds. During the merger molecular clouds in the disks of the two spirals would be expected to undergo frequent collisions, potentially generating infrared luminosity directly (Harwit *et al.* 1986) and/or triggering massive star formation (Scoville, Sanders, and Clemens 1986). In addition, if the collision trajectory has the two galactic disks counter-rotating then the cancellation of angular momentum during cloud–cloud collisions should result in a pile-up of molecular material near the merger nucleus. This may further enhance the 'starburst' and supply fuel for a QSO nucleus. Recent CO observations of Arp 220 with the OVRO millimeter-wave interferometer (Scoville et al. 1986), show that most (> 70%) of the CO emission comes from a radius smaller than 750 pc centered on the bright radio and near-infrared nucleus.

Table 2
IRAS Galaxy Properties vs Increasing Infrared Luminosity[a]

Property		$(2-7\times10^{10}\ L_\odot)$	HL $(7\times10^{10}-7\times10^{11}\ L_\odot)$	UL $(>10^{12}\ L_\odot)$
No. Objects (BG Sample)		80	80	10
Morphology	merger	10%	40%	90%
	close pair	15	30	10
	isolated	75	30	0
Optical Spectra	Seyfert	< 10%	20%	50%
	LINER/?	> 90	80	40
	HII			10
$\nu f_\nu(80)/\nu f_\nu(B)$ (median)		1	5	25
$L_{FIR}/M(H_2)$ (median)		5	18	120

[a]Infrared luminosity = L(8-1000μm). Data for $2-7\times10^{10}\ L_\odot$ galaxies and High Luminosity sample is from Sanders *et al.* (1986a, 1987).

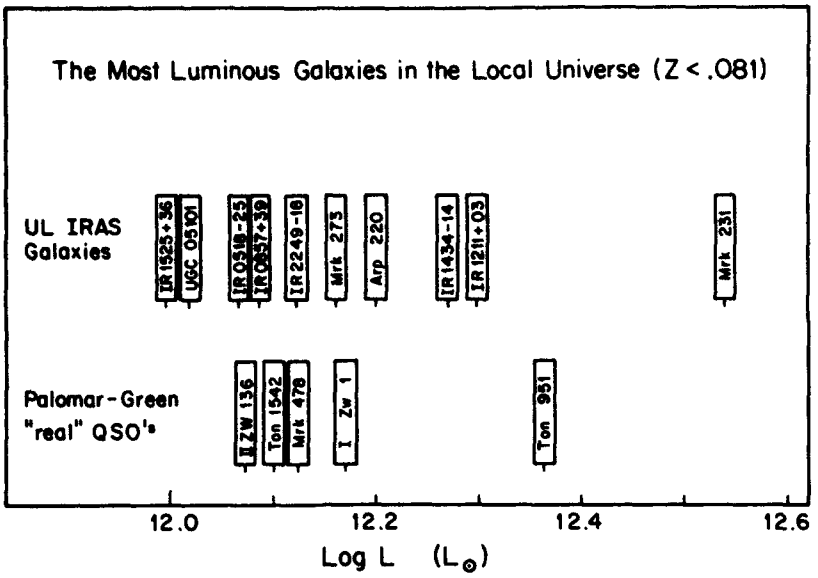

Figure 4: Objects with luminosities greater than 10^{12} $L_{\odot}$ at $z \leq 0.081$. For the infrared galaxies the plotted value is L(8-1000μm) which is $\gtrsim 0.9$ L_{Bol}. For the optically selected quasars (Schmidt and Green 1983) the luminosity is L_{Bol} as determined by Soifer *et al.* (1986).

As the most luminous infrared objects in the local universe the ultraluminous IRAS galaxies are all at, or near their peak luminosity. It appears likely that this coincides with a dense and massive concentration of molecular gas around a merger nucleus which is heated by both an embedded AGN and newly formed massive stars. Eventually this gas will be dispersed through the combined action of supernova explosions, stellar winds, and radiation pressure. Such housecleaning may have already begun in those objects listed in Table 1 whose broad-line Seyfert spectra suggest that we can see into the central nonthermal source. It seems reasonable to assume that these galaxies will shortly resemble optically selected QSO's characterized by a dominant central point source. The infrared-loud quasar IRAS 1334+24 (Beichman *et al.* 1986) might well represent just such a state. Figure 4 compares the total number of ultraluminous infrared objects and their luminosities with the bolometric luminosities of a complete optical sample of QSO's within approximately the same volume of space. If the lifetimes of the ultraluminous infrared and QSO phases are approximately equal, then Figure 4 suggests that nearly all ultraluminous infrared galaxies become QSO's and that the QSO phase may in fact be slightly less luminous than the infrared phase.

5. ACKNOWLEDGEMENTS

This research was funded partially by NASA under the IRAS extended mission program and partially by the NSF.

6. REFERENCES

Beichman, C. A., Soifer, B. T., Helou, G., Chester, T. J., Neugebauer, G., Gillett, F. C., and Low, F. J. 1986, *Ap. J. (Letters)*, **308**, L1.

Boksenberg, A. Carswell, R. F., Allen, D. A. Fosbury, R. A. E., Penston, M. V., and Sargent, W. L. W. 1977, *Mon. Not. R. A. S.*, **178**, 451.

Cataloged Galaxies and Quasars Observed in the IRAS Survey 1985, prepared by C. J. Lonsdale, G. Helou, J. C. Good, and W. L. Rice, Jet Propulsion Laboratory D-1932.

Elston, R., Cornell, M. E., and Lebofsky, M. J. 1985, *ApJ.*, **296**, 106.

Emerson, J. P., Clegg, P. E., Gee, G., Cunningham, C. T., Griffin, M. J., Brown, L. M. J., Robson, E. I., and Longmore, A. J. 1984, *Nature*, **311**, 237.

Harwit, M. O., Houck, J. R., Soifer, B. T., and Palumbo, G. G. C. 1986, *Ap. J.*, submitted.

Lawrence, A., Walker, D. Rowan-Robinson, M., Leech, K. J., and Penston, M. V. 1986, *Mon. Not. R. A. S.*, **219**, 687.

Miley, G. K., Neugebauer, G., and Soifer, B. T. 1985, *Ap. J. (Letters)*, **293**, L11.

Neugebauer, G., Green, R. J., Matthews, K., Schmidt, M. Soifer, B. T., and Bennett, J., 1986a, *Ap. J.*, in press.

Neugebauer, G. Miley, G. K., Soifer, B. T., and Clegg, P. E. 1986b, *Ap. J.*, **308**, in press.

Perault, M., Boulanger, F., Falgarone, E., and Puget, J. L. 1986, *Astron. Ap.*, submitted.

Rieke, G. H., Cutri, R. M., Black, J. H., Kailey, W. F., McAlary, C. W., Lebofsky, M. J., and Elston, R. 1985, *ApJ.*, **290**, 116.

Rieke, G. H., and Lebofsky, M. J. 1986, *ApJ.*, **304**, 326.

Sanders, D. B., and Mirabel, I. F. 1985, *ApJ. (Letters)*, **298**, L31.

Sanders, D. B., Scoville, N. Z., Young, J. S., Soifer, B. T., Schloerb, F. P., Rice, W. L., and Danielson, G. E. 1986a, *Ap. J. (Letters)*,, **305**, L45.

Sanders, D. B., Young, J. S., Scoville, N. Z., Soifer, B. T. and Danielson, G. E. 1986b, *Ap. J. (Letters)*, submitted.

Sanders, D. B., *et al.* 1987, in preparation.

Scoville, N. Z., and Good, J. C. 1986, this volume.

Scoville, N. Z., Sanders, D. B., and Clemens, D. P. 1986, *Ap. J. (Letters)*, in press.

Scoville, N. Z., Sanders, D. B., Sargent, A. I., Soifer, B. T., Scott, S. L., and Lo, K. Y. 1986, *ApJ. (Letters)*, in press.

Schmidt, M., and Green, R. F. 1983, *ApJ.*, **269**, 352.

Soifer, B. T., Sanders, D. B., Neugebauer, G., Danielson, G. E., Lonsdale, C. J., Madore, B. F., and Persson, S. E. 1986, *ApJ. (Letters)*, **303**, L41.

Soifer, B. T., Sanders, D. B., Madore, B. F., Neugebauer, G., Persson, C. J., Persson, S. E., and Rice, W. L. 1987, *ApJ.*, submitted.

Soifer, B. T., *et al.* 1984, *ApJ. (Letters)*, **283**, L1.

Toomre, A., and Toomre, J. 1972, *ApJ.*, **178**, 623.

Young, J. S., Kenney, J., Lord, S., and Scholerb, F. P. 1984, *ApJ. (Letters)*, **287**, L65.

Young, J. S., Schloerb, F. P. Kenney, J., and Lord, S. D. 1986, *ApJ.*, **304**, 443.

DISCUSSION

Thronson: How does the following selection effect affect your interpretation of your plot of L_{IR} vs L_{CO}, if at all: in a flux-limited sample, would you not tend to be strongly biased toward high-efficiency of star formation?

Sanders: Our flux limited sample is biased toward selecting objects with high L_{FIR}, whatever the cause of the FIR. Figure 2 should not be used to determine the true distribution of L_{FIR}/L_{CO} at a given L_{CO}, particularly at $L_{FIR} \leq 7 \times 10^{10} L_{\odot}$ where we have simply plotted all galaxies for which CO data was available from the literature plus a few of our own. However, above $L_{FIR} \sim 10^{11} L_{\odot}$ where most of the plotted data is from our Bright Galaxy survey, we attempted to uncover additional galaxies of comparable far-infrared luminosity which lie within the boundaries of the survey, by lowering the 60 μm limit to 0.5 Jy. But, essentially no new objects were found. Therefore, the Bright Galaxy sample does appear to give an accurate picture of the real distribution of L_{FIR}/L_{CO} at these high far-infrared luminosities.

Mundy: We have observed the nuclear region of NGC 253 in CO with the Owens Valley Interferometer. The CO emission is in a 40" $\times$ 10" bar with $L_{IR}/M_{gas} \sim 60$. Where does this fit in your sample and can't bars be very efficient at stirring up star formation?

Sanders: The data point for NGC 253 in Figure 2 represents the average L_{FIR}/L_{CO} over the inner 6 arcmin radius. Apparently, the small bar in your data has a ratio yet 3 times higher, which could presumably be due to either an increase in star formation efficiency, or heating from a non-thermal nucleus.

Mezger: You showed a diagram of M_{H2} vs L_{IR}, which deviates from a linear relation at the high luminosity end. This is in disagreement with a similar diagram shown by Krugel *et al.* (this symposium). The major difference is that you determined M_{H2} from the (optically thick) ^{12}CO line while Krugel *et al.* uses the (optically thin) $\lambda 1300 \mu$m dust emission. My question is: What makes you believe that you can extrapolate a relation between CO luminosity and H_2 column density, originally derived for our Galaxy, to galaxies which appear to have a gas content of two to three orders that of our Galaxy?

Sanders: I believe that the total I_{CO} from a galaxy is essentially influenced by the number of clouds. If the *mean* internal cloud properties (temperature, density, etc.) were to vary greatly from galaxy-to-galaxy then $M(H_2)$ as derived using the mean value of $M(H_2)/L_{CO} = 5.8$ found for the Milky Way would not be very accurate. For one of the most luminous galaxies in Figure 2, Arp 220, we have been somewhat surprised that our mass estimate agrees so closely with the mass determined by Emerson from 350 μm observations. The criticism raised most often concerning extragalactic H_2 masses is that ^{12}CO may be partially optically thin, a possibility that, presumably, is raised by the relatively large $^{12}CO/^{13}CO$ ratio observed in M82. Krugel's work to which you refer is the first I have seen which gives substantially larger H_2 masses then we derive from ^{12}CO.

EXTRAGALACTIC INFRARED SPECTROSCOPY

R D Joseph[1], G S Wright[2], R Wade[2], J R Graham[3], I Gatley[4], & A H Prestwich[1]
[1]Blackett Laboratory, Imperial College, London SW7, UK
[2]Royal Observatory, Blackford Hill, Edinburgh EH9 3HJ, Scotland
[3]Lawrence Berkeley Laboratory, 1 Cyclotron Road, Berkeley, CA 94720
[4]UK Infrared Telescope Unit, 665 Komohana Street, Hilo, HA 96720

ABSTRACT

We are engaged in a programme to explore the spectra of galaxies in the near-infrared (H & K) atmospheric transmission windows. We have detected emission lines due to molecular hydrogen, atomic hydrogen recombination lines, a line we attribute to [FeII], and a broad CO absorption feature. Lines due to H_2 and [FeII] are especially strong in interacting and merging galaxies, but we have also detected them in Seyferts and 'normal' spirals. These lines appear to be shock-excited. Multi-aperture measurements show that they emanate from regions as large as 15 kpc. We argue that starbursts provide the most plausible and consistent model for the excitation of these lines, but the changes of relative line intensity of various species with aperture suggests that other excitation mechanisms are also operating in the outer regions of these galaxies.

1. INTRODUCTION

Spectroscopy in the near-infrared atmospheric windows is an almost completely undeveloped tool for investigating physical processes in galaxies. Until recently there have been only two detections of H_2 in galaxies, in N1068 (Thompson, Lebofsky & Rieke 1978) and N3690-IC694 (Fischer, Simon, Benson & Solomon 1983). There have also been only two detections of the 1.644 μm lines which are attributed to [FeII] in the nuclei of galaxies, in M82 (Rieke, Lebofsky, Thompson, Low, & Tokunaga 1980) and in N4151 (Rieke & Lebofsky 1981). There have been a few more detections of H Brackett lines in galaxies, but in total probably less than ten (cf. Beck, Beckwith & Gatley 1984).

We have embarked on a programme to explore the spectra of several classes of galaxies in the H & K atmospheric windows. Our interest in attempting such spectroscopy arose from our studies of interacting and merging galaxies (Joseph, Meikle, Robertson & Wright 1984, Wright, Joseph & Meikle 1984, Graham, Wright, Meikle, Joseph & Bode 1984, Joseph & Wright 1985). The collision of two gas-rich galaxies must be one of the most likely places in the universe to look for shock-excited H_2, and we hoped to be able to use these lines as shock diagnostics and independent indication of a genuine physical interaction. This conjecture was supported by the discovery of strong H_2 emission in the interacting galaxies N3690-IC694 by Fischer et al. (1983), and subsequently by our discovery (Joseph, Wright & Wade 1984) and others' (Becklin, DePoy & Wynn-Williams 1984, Rieke et al. 1985) of extraordinarily luminous H_2 emission in two of the most intriguing 'IRAS galaxies,' N6240 and Arp220. We have extended this observing programme to include other classes of galaxies, partly for comparison purposes, but chiefly as a systematic exploration of the near-IR spectroscopic properties of spiral galaxies in general.

Carol J. Lonsdale Persson (Editor)
Star Formation in Galaxies

2. OBSERVATIONS

Our observations have been obtained at UKIRT, using a circular variable filter spectrometer. This instrument provides a spectral resolution $\lambda/d\lambda$ - 120, or about 2500 km/sec. Since the instrument employs re-imaging optics, this resolution is independent of aperture. Our approach has been to begin study of a given galaxy using the 19.6 arcsec aperture, and then to obtain spectra at successively smaller apertures. In one or two nearby galaxies we have also measured spectra in several different positions not centred on the nucleus. So far we have obtained complete spectra in the H & K windows for about 15 galaxies. Most of these are interacting and merging galaxies, but we have good spectra for four nearby bright spirals and two Seyfert galaxies.

The features which appear most frequently in these spectra are the quadrupole vibration-rotation lines of H_2, H recombination lines in the Brackett series, a line at 1.644 μm which we tentatively attribute to [FeII], and the stellar absorption feature due to CO. Examples of the spectra we measure are shown in Figs. 1 - 4. These spectra have been ratioed with the spectrum of a G-type star taken at similar airmass to remove effects of the atmosphere and instrumental response. The spectra illustrate how useful it is to work at the high altitude of UKIRT on Mauna Kea. For example, one can study the 1-0 Q-branch of H_2 in galaxies even at redshifts as large as that of N6240 (7500 km/sec).

3. RESULTS

We have done preliminary reduction of the spectra for a subsample of the galaxies so far observed to obtain fluxes for the H_2, Brackett γ, and [FeII] lines. In the following we summarise the physical parameters that characterise this data, and the apparent trends which seem to be emerging.

3.1 Excitation mechanisms

Both shocks and fluorescence following absorption of a UV photon in the Lyman or Werner bands have been suggested for the H_2 excitation. The evidence from relative line intensities in the data available so far is consistent with shock excitation. Table I shows relative line intensities expected for excitation by a 10 km/sec shock and for UV fluorescence. For comparison we give the relative intensities of several of the H_2 lines for N6240 and Arp220. The most critical indication is probably the intensity of the 2-1 S(1) line relative to that of the 1-0 S(1) line. The data for these two galaxies is clearly consistent with shock excitation and incompatible with the UV fluorescence model. We have also looked hard for the 2-1 S(1) line as evidence of UV fluorescence in the Seyfert galaxies we have observed. The line intensities favour collisional excitation in these galaxies as well. However, we intend to obtain spectra in still smaller apertures to distinguish the features of the active nucleus itself more clearly.

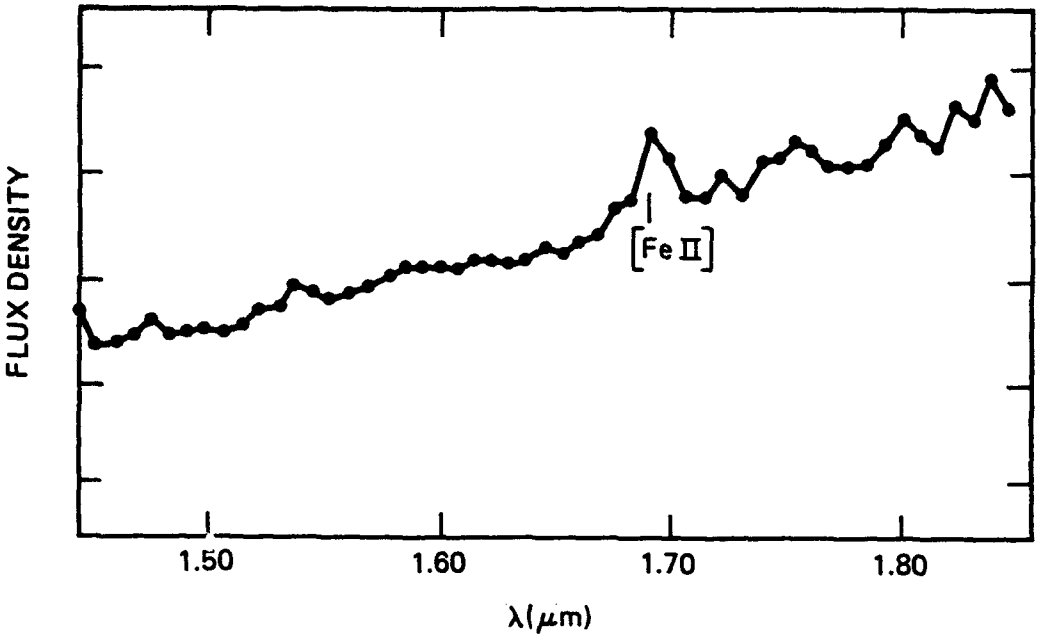

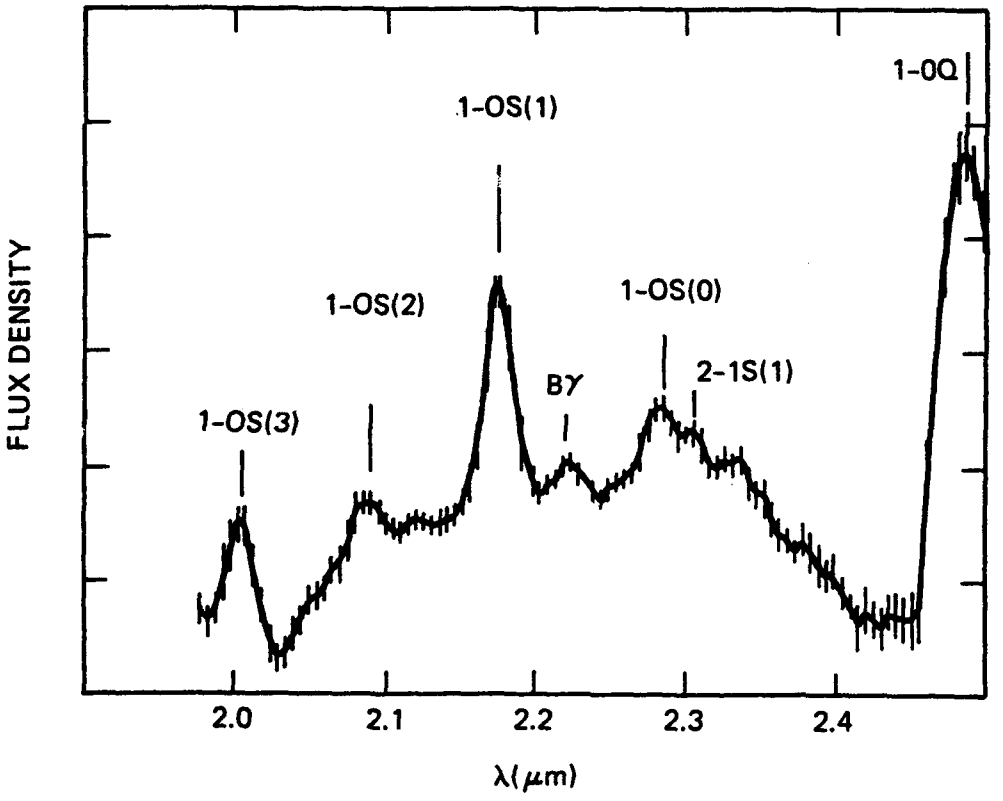

Figure 1. Spectra of the merging galaxy N6240 in a 19.6 arcsec aperture.

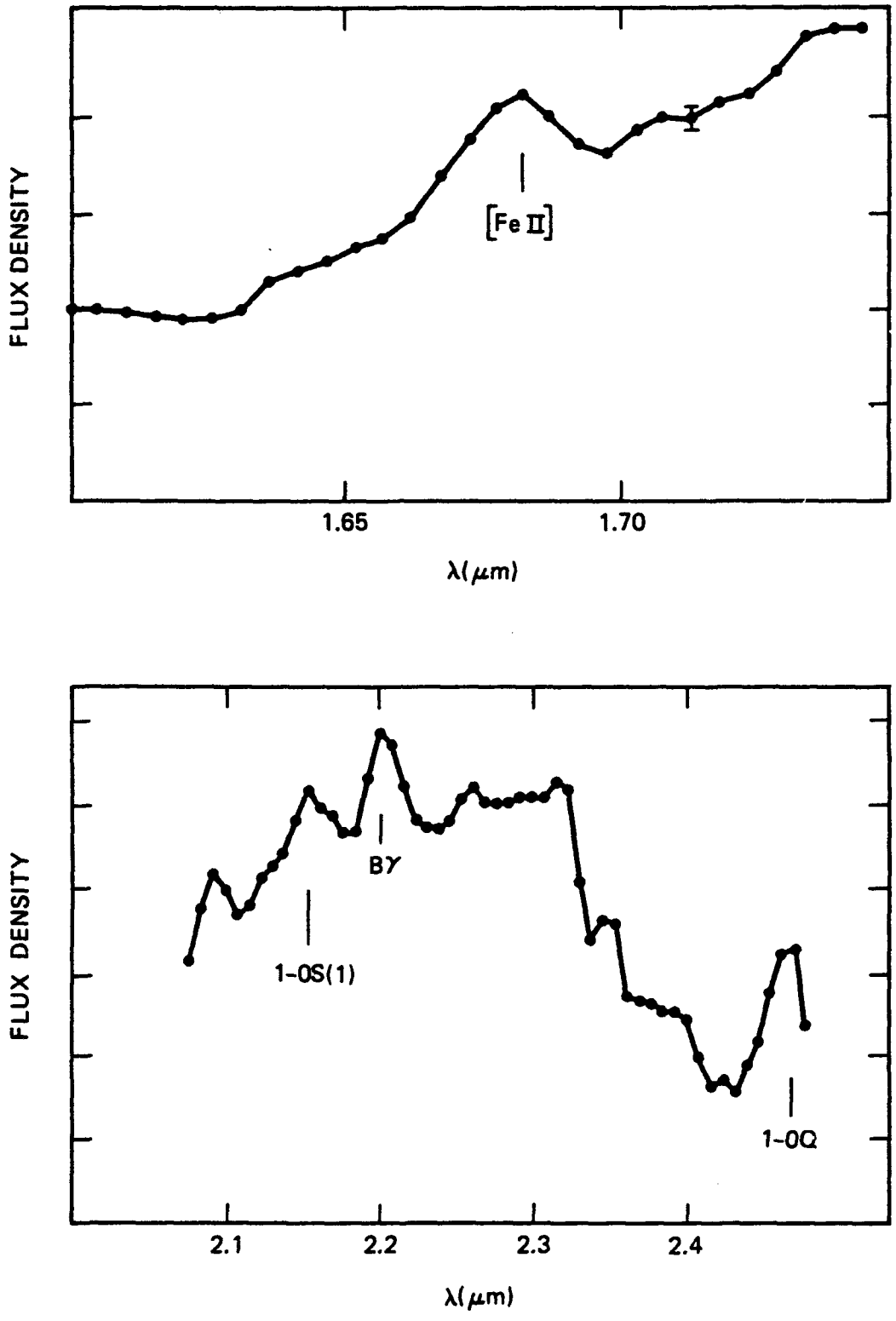

Figure 2. Spectra of the merging galaxy N1614 in a 19.6 arcsec aperture.

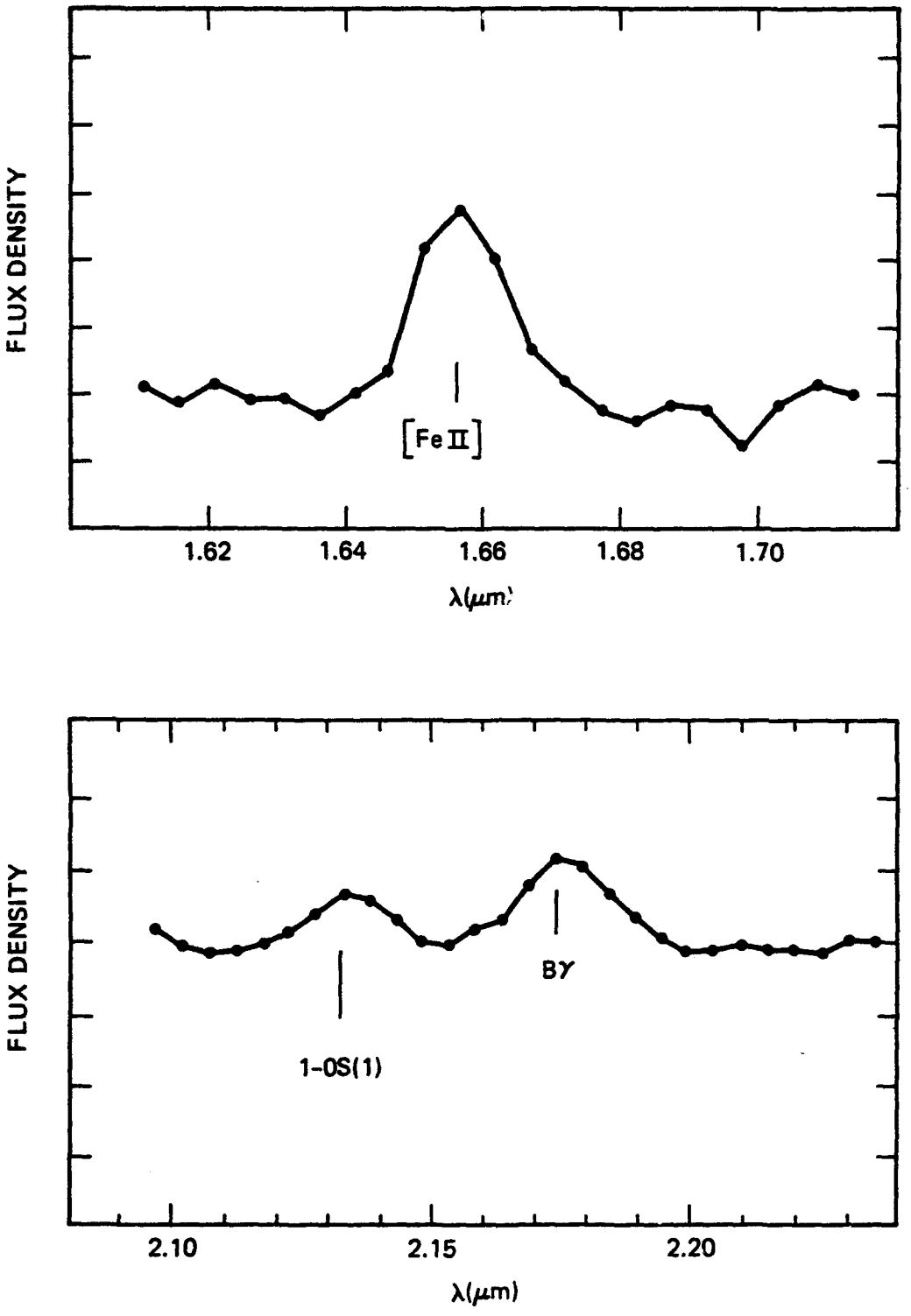

Figure 3. Spectra of the merging galaxy N3690A in a 19.6 arcsec aperture.

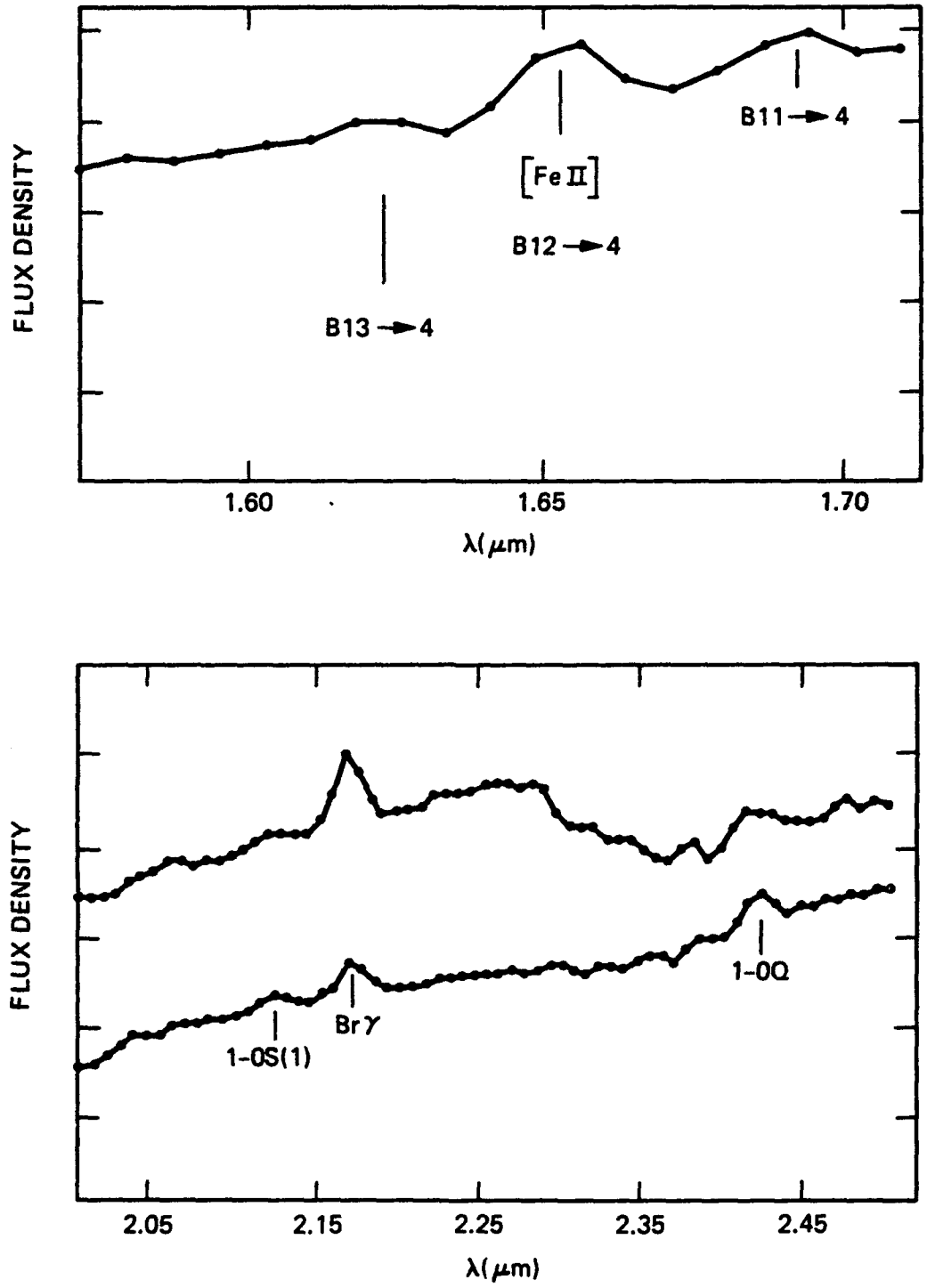

Figure 4. Spectra of N253 in a 19.6 arcsec aperture. The upper K window spectrum has been ratioed by the spectrum of an A-type star, which gives spuriously enhanced Brackett γ. The spectrum just below has been ratioed with the spectrum of a star with a very large CO index to remove the CO feature in the galaxy spectrum and show the Q-branch more clearly.

TABLE I. RELATIVE LINE INTENSITIES FOR H_2 EXCITATION

Line	N6240	Arp220	Shock*	UV†
1-0 S(0)	0.28	0.17	0.22	0.67
1-0 S(1)	1.0	1.0	1.0	1.0
1-0 S(2)	0.24		0.36	
1-0 S(3)	0.77		0.95	
1-0 Q(1-7)	2.2	4.5	2.4	2.7
2-1 S(1)	0.14	0.05	0.1	0.55

*Hollenbach & Shull (1977)
†Black & Dalgarno (1976)

The 1.644 μm [FeII] line is also collisionally-excited. If the [FeII] were emitted from an HII region, one would expect the ratio of the [FeII] λ1.644 μm line to Brackett γ λ2.166 μm to be ~ 0.06 (Graham, Wright & Longmore 1986). We find this ratio typically to be at least 10 times larger, suggesting that the line is not excited by photoionisation in an HII region. It is very difficult to excite this line by UV fluorescence, and we do not observe a line at 2.09 μm which we would expect to see if the relevant terms were populated by this mechanism. The line is therefore almost certainly shock-excited.

This is an important result. Shock speeds in excess of 30 km/sec are required to excite the [FeII] emission, whereas shock speeds as low as 5 km/sec can excite the H_2 1-0 S(1) line. Thus these lines provide powerful shock diagnostics. For example, their relative spatial extent can constrain the kinds of astrophysical source(s) driving the shocks. Comparison of these indicators with the extent of Brackett γ and infrared continuum maps should then provide rather detailed insight into the astrophysics associated with the nuclear infrared activity in these galaxies.

3.2 Luminosities in H_2 emission lines

The luminosities of the 1-0 S(1) emission lines discovered in 1984 in N6240 and Arp220 are astonishingly large, ~ 10^8 and 10^7 L⊙ respectively. How do these luminosities compare with those for a larger sample including other types of galaxies? The samples are still small, but some trends may be appearing. Table II presents the 1-0 S(1) luminosities (H_0 = 50 km sec^{-1} Mpc^{-1}) for the line fluxes obtained in a 19.6 arcsec aperture centred on the nucleus of each galaxy.

These luminosities are enormous! At the upper end they compare with the 10 μm continuum luminosities of starburst galaxies. Another way to appreciate the physical significance of these luminosities is to ask what masses of H_2 must be shock-excited to produce these luminosities. If the temperature is ~ 2000 K, these luminosities imply masses of excited H_2 of 10^2 to 10^5 M⊙, and excitation rates of 30 to 30,000 M⊙ of H_2 per year. The timescales of the processes producing this excitation must be large, since we have detected H_2 emission in virtually every interacting or merging galaxy we have observed, and in most other galaxies as well. If the excitation were a starburst, one expects a lifetime of $\gtrsim 3 \times 10^7$ years, whereas if it were due to spiral density waves or to gas flows

TABLE II. LUMINOSITIES IN THE H_2 1-0 S(1) LINE

Galaxy type	Luminosity range ($L_\odot$)
Mergers	$3 \times 10^6 - 3 \times 10^8$
Interacting (not merging)	$2 \times 10^5 - 1 \times 10^7$
Starburst (N253)	$\sim 7 \times 10^4$

induced by bar instabilities the lifetime would be $\sim 10^{10}$ years. Multiplying these timescales by the excitation rates we have inferred suggests that all the molecular gas must be excited over the lifetime of the starburst in N253. In the mergers, the result is even more striking: every H_2 molecule must be excited many times, in order to account for the high excitation rates we find in these systems.

3.3 Energy source driving these shocks

Because many of these galaxies are ultra-luminous IR sources, it might be expected that radiation pressure would be sufficient to drive the shocks we infer are present. However, the radiation pressure, L_{IR}/c, is $\ll \dot{m} v_s$ for the excitation rates given above, even for shock velocities v_s as low as 10 km/sec.

Alternatively, it may be that the relative kinetic energy of the collisions for the interacting and merging galaxies, or mass outflows from star formation regions or from the active nucleus in the case of the Seyferts, are the underlying energy sources driving the shocks. To investigate these possibilities we have compared the ratio of the luminosity in the 1-0 S(1) line to the total IR luminosity. This ratio should have a characteristic value for star formation regions, since the S(1) line luminosity is a measure of the mechanical energy in the outflow from a star formation region and the IR luminosity is a measure of the total energy of the starburst. The ratio is 1×10^{-5} for Orion (Shull & Beckwith 1982). For all the galaxies we have observed this ratio does not deviate above or below 1×10^{-5} by more than a factor of ~ 2, with one notable exception. For N6240 this ratio is at least 15 times larger. Our inference then is that mass outflows from star formation regions similar to Orion can account for the excitation of H_2 in all these galaxies, except for N6240, and in this case it is likely that the relative kinetic energy of the merger has produced the higher excitation rate we observe.

3.4 Spatial extent of the line emission

We have not yet completed our multi-aperture spectroscopy for this galaxy sample, but the data available for galaxies observed in more than one aperture suggests that the line emission has considerable spatial extent. In Table III we list the relative line intensities found in various apertures, with the corresponding linear dimensions associated with these apertures, for several galaxies. The most noteworthy feature is the large extent of the H_2 and [FeII]

emission, over much of the disc, in the two merging galaxies N6240 and N1614. There is spatial extent of at least 2 or 3 kpc for the H_2 emission in the Seyfert galaxy N3227 and in the interacting galaxy N2798. Although the Brackett γ is also spatially extended, it appears to be more centrally condensed in the latter two galaxies than is the H_2 emission. We emphasise that even these results on spatial extent are lower limits--19.6 arcsec is simply the largest aperture available in our spectrometer.

TABLE III. SPATIAL EXTENT OF LINE EMISSION

Galaxy	Line	Aperture				Linear scale for 20"
		5"	8"	12"	20"	
N6240	1-0 S(1)	1.0	1.5	2.1	2.6	14 kpc
	[FeII]	1.0	1.3	1.6	1.8	
N1614	[FeII]		1.0	2.0	3.0	9 kpc
N3227	1-0 S(1)		1.0		2.1	2 kpc
	S(1)/Bγ		1.0		1.3	
N2798	1-0 S(1)			1.0	2.3	3 kpc
	S(1)/Bγ			1.0	2.0	
N253	See text					

We have the most detailed information on the nearby starburst galaxy N253. Here we have achieved some spectral mapping. We find the H_2 emission extended to at least ± 20 arcsec, i.e. ± 300 pc, along the major axis. By contrast the [FeII] and Brackett γ emission are much more centrally condensed, and seem to follow the 10 μm emission mapped by Rieke & Low (1975).

4. STEPS TOWARD AN INTERPRETATION

There are several plausible mechanisms which might be responsible for the shock excitation we observe in these galaxies. (1) Mass outflows associated with starbursts have already been mentioned, and are one of the sources of H_2 excitation in our own galaxy. (2) Dynamical processes associated with the collision between two galaxies, as discussed by Martin Harwit elsewhere in this volume, are also a likely source of shock excitation. (3) Mass outflows associated with Seyfert nuclei may be responsible for shocks in the vicinity of the nucleus in this class of galaxies. (4) Shocks due to spiral density waves or due to flows associated with bar instabilities may also be a source of excitation. In the following we will use the results outlined above to work toward a consistent picture of the astrophysical processes which might account for the line emission seen in these galaxies.

Firstly, which of the above processes can be responsible for the greatly

extended H_2 emission? In N253, the [FeII] emission does not show similar spatial extent, and so the slower shock speeds characteristic of spiral density waves, or shocks associated with the bar in this galaxy are reasonable. The fact that Brackett γ is centrally condensed in this galaxy also suggests that outflow from star formation regions is not likely to be responsible for the extended H_2 emission in N253.

For the merging galaxies, the [FeII] emission seems to be as spatially extended as the H_2. Since the [FeII] requires rather fast shock velocities, gentler processes such as spiral density waves are not so likely to dominate the excitation. In this case either star formation or the energy of the interaction is likely to be responsible. If it were star formation, we would expect the outflows from massive young stars to be responsible for exciting the H_2, and outflows from supernova remnants to provide the fast shocks needed to excite the [FeII]. The strong emission from [FeII] in the 1.644 μm line in the supernova remnant IC443 (cf. Graham, Wright, & Longmore 1986) must be an archetypal example of this process.

Secondly, the approximate constancy of the ratio of S(1) line to total IR luminosity for nearly all galaxies helps to distinguish the relative importance of these processes. The constancy of this ratio from one merging galaxy to another might be understood in terms of the mechanical energy of the collision, but it is difficult to see why, in this case, it would be the same for non-merging interacting galaxies, a Seyfert, and a starburst galaxy. Moreover, that this ratio is quantitatively the same as that for a local star formation region (Orion) is strongly suggestive that, in general, the H_2 is excited by mass outflows from star formation regions in the central regions of these galaxies. N6240 is clearly the exception, and as we suggested some time ago (Joseph et al. 1984), it is likely that the relative kinetic energy of the interaction dominates the H_2 excitation in this merger.

If we adopt this interpretation, we can ask whether it is consistent with other information available for these galaxies. One of the most important questions is whether the H recombination line luminosity is consistent with a starburst model. In our original paper on H_2 emission in N6240 and Arp220 (Joseph et al. 1984) we called attention to an apparently low flux of Lyman continuum photons as evidenced by our failure to detect Paschen α at a similar sensitivity as that used when we first detected H_2. This point has been pursued by Becklin et al. (1986), who have detected the Paschen α line in a 5 arcsec aperture, and used the ratio of the luminosity in this line to the total IRAS luminosity as a major argument to support their suggestion that N6240 is not powered by a starburst at all, but by a quasar-like active nucleus. To investigate this point further we have calculated the ratio of the Brackett γ flux we have measured in a 19.6 arcsec aperture to the IRAS 25 μm flux for these galaxies, including N6240. We take the flux at 25 μm to indicate the starburst component of the far-IR emission, as the spectral synthesis models show is reasonable (cf. Helou et al. in this volume). Therefore, the Brackett γ/25 μm flux ratio should be roughly constant for galaxies powered by a starburst. The ratio, shown in Table IV, is remarkably constant, especially considering the rather heterogeneous collection of objects, and the fact that it will be somewhat sensitive to reddening. Clearly, on this criterion, N6240 is not weak in H recombination line strength among the galaxies measured. On the other hand, Arp220 may be a bit short of Brackett γ photons.

TABLE IV. RATIOS OF BRACKETT γ TO 25 μm FLUX

Galaxy	Bγ/25 μm (x10^5)
N6240	12
Arp220	1.7
N3256	3.9
N2623	4.6
N1614	6.6
N3227	6.2
N2798	7.4
N253	3.0

Finally we can use our spectroscopic data to infer what supernova rate is implied if the [FeII] emission is due to supernovae associated with the starbursts. Graham, Wright & Longmore (1986) have discovered the 1.644 μm [FeII] line in the galactic supernova remnant IC443. The lifetime and [FeII] luminosity of this supernova remnant, and the [FeII] luminosities of the galaxies in the present sample indicate a supernova rate of < 1 per year for the interacting and Seyfert galaxies, and 10 ~ 70 supernovae per year in the mergers. These are not unreasonable supernova rates.

However, the fact that the relative strength of the S(1) line flux to the Brackett γ flux seems to be changing with aperture, for some of the galaxies studied so far, as shown in Table III, suggests that starbursts alone may not be enough to account for all the excitation of H_2. It will be particularly germane to find out how the [FeII]/Bγ ratio varies with aperture to see how well the starburst picture holds up for the excitation well outside the central regions of activity in these galaxies.

5. SUMMARY AND CONCLUSIONS

We have measured near-IR emission lines due to H_2, Brackett γ, and [FeII] for a variety of classes of galaxies. The lines due to H_2 and [FeII] are especially strong in interacting and merging galaxies. Multi-aperture measurements show that the emission is generally extended over kiloparsec scales. The H_2 and [FeII] emission is apparently excited by shocks, in which case the latter requires shock velocities > 30 km/sec. Consideration of several processes which might produce emission lines from these three species shows that, in general, starbursts provide the most attractive and consistent model. In particular, the ratio of the H_2 flux to the total IR flux, the ratio of the Brackett γ flux to the 25 μm flux, and the luminosities of the [FeII] provide semi-quantitative support for this interpretation. However, starbursts cannot be the whole story for in some cases the ratio of H_2 to Brackett γ emission shows a marked increase with aperture, suggesting that shocks due to spiral density waves or to the interactions may become important outside the most active central regions in these galaxies.

More quantitative and detailed presentations of the IR spectroscopic data for these are other galaxies we have observed will soon be submitted for publication in Monthly Notices of the Royal Astronomical Society.

REFERENCES

Beck, S. C., Beckwith, S., and Gatley, I. 1984, Ap. J., 279, 563.
Becklin, E. E., DePoy, D., & Wynn-Williams, G. 1984, Infrared Detector Workshop, Laramie, Wyoming.
Becklin, E. E., DePoy, D., & Wynn-Williams, G. 1986, Submitted to Ap. J.
Black, J., & Dalgarno, A. 1976, Ap. J., 203, 132.
Fischer, J., Simon, M., Benson, J., and Solomon, P. M. 1983, Ap. J. (Letters), 273, L27.
Graham, J. R., Wright, G. S., Meikle, W. P. S., Joseph, R. D., and Bode, M. F. 1984, Nature, 310, 213.
Graham, J. R., Wright, G. S., & Longmore, A. J. 1986, Submitted to Ap. J.
Hollenbach, D. J., & Shull, J. M. 1977, Ap. J., 216, 419.
Joseph, R. D., Meikle, W. P. S., Robertson, N. A., and Wright, G. S. 1984, Mon. Not. R. Astr. Soc., 209, 111.
Joseph, R. D., Wright, G. S., & Wade, R. 1984, Nature, 311, 132.
Joseph, R. D., and Wright, G. S. 1985, Mon. Not. R. Astr. Soc., 214, 87.
Rieke, G. H., & Low, F. J. 1975, Ap. J. (Letters), 200, L67.
Rieke, G. H., Lebofsky, M. J., Thompson, R. I., Low, F. J., & Tokunaga, A. 1980, Ap. J., 238, 24.
Rieke, G. H., and Lebofsky, M. J. 1981, Ap. J., 250, 87.
Rieke, G. H., Cutri, R., Black, J. H., Kailey, W. F., McAlary, C. W., Lebofsky, M. J., and Elston, R. 1985, Ap. J., 290, 116.
Shull, J. M., and Beckwith, S. 1982, Ann. Rev. Astr. Ap., 20, 163.
Thompson, R. I., Lebofsky, M. J., and Rieke, G. H. 1978, Ap. J. (Letters), 222, L49.
Wright, G. S., Joseph, R. D., and Meikle, W. P. S. 1984, Nature, 309, 430.

DISCUSSION

SHULL:

The supernova shocks would be expected to destroy the H_2 at velocities above 25 km s^{-1}. Can you discuss this difficulty in your model of star formation excitation of the 2μm H_2 emission?

(Note, added afterwards: The Hollenbach-McKee idea of reforming H_2 behind the shock (by grains that survive shock destruction) may not work here, since the gas will have cooled well below 1000 K so that vibrational lines cannot be excited.)

JOSEPH:

There are shocks of three different origins in the model outlined: 1) those due to the galaxy-galaxy collision, 2) those due to outflow from star formation regions, and 3) those associated with supernovae. The Hollenbach-McKee idea of reforming H_2 on grains that survive the shock applies to the first case. We are probably seeing excitation mainly because of the second case for the H_2, and mainly because of the third case for the [FeII]. Of course, the localized regions emitting the H_2 are not the same as those emitting the [FeII],

but they both emanate from the same general volume. There are examples in the Galaxy in which one sees both [FeII] and H_2 emission, for example, in the supernova remnant IC443.

BURBIDGE:

Can you say anything about the Fe/H ratio in these objects. Is the ratio normal?

JOSEPH:

I don't think these measurements permit us to deduce much about the total Fe/H abundance ratio.

TELESCO:

1) How did you determine that the H_2 is extended in these sources?

2) Do you know the ratio of [FeII]/L_{IR} for the Seyfert NGC 4151 and how does it compare to the values for this sample?

JOSEPH:

1) Multi-aperture observations.

2) I don't recall the value for 4151, but for NGC 3227, the only clear-cut Seyfert in this sample, it is about 5, which is much higher than for the other galaxies shown here (except 6240).

RIEKE:

The ratio for 4151 is about unity.

CLOUD FLUID MODELS OF GAS DYNAMICS AND STAR FORMATION IN GALAXIES

Curtis Struck-Marcell
Astronomy Program
Physics Department
Iowa State University
Ames, IA 50011

John M. Scalo
Astronomy Department
University of Texas
Austin, TX 78712

P. N. Appleton
Astronomy Program
Physics Department
Iowa State University
Ames, IA 50011

ABSTRACT

The large dynamic range of star formation in galaxies, and the apparently complex environmental influences involved in triggering or suppressing star formation, challenge our understanding. The key to this understanding may be the detailed study of simple physical models for the dominant nonlinear interactions in interstellar cloud systems. We describe one such model, a generalized Oort model cloud fluid, and explore two simple applications of it. The first of these is the relaxation of an isolated volume of cloud fluid following a disturbance. Though very idealized, this closed box study suggests a physical mechanism for starbursts, which is based on the approximate commensurability of massive cloud lifetimes and cloud collisional growth times. The second application is to the modeling of colliding ring galaxies. In this case, the driving processes operating on a dynamical timescale interact with the local cloud processes operating on the above timescales. The result is a variety of interesting nonequilibrium behaviors, including spatial variations of star formation that do not depend monotonically on gas density.

Carol J. Lonsdale Persson (Editor)
Star Formation in Galaxies

I. INTRODUCTION

A. The Dynamic Range of Star Formation in Galaxies

The discovery of Sargent and Searle (1970) that several Zwicky irregular galaxies are essentially "extragalactic HII regions" provided one of the earliest indications that current star formation rates (SFRs) in other galaxies could be very high compared to the SFR in our galaxy. It was clear to these authors that the relatively high SFRs in these galaxies could not persist for any significant fraction of a Hubble time, if only because the implied gas consumption time was short. Later, Gerola and Seiden showed that relatively strong (i.e. enhancement factors ofan order of a few) bursts of star formation, separated by relatively long quiescent periods, could be a consequence of self-propagating star formation in relatively small and essentially three-dimensional systems like the dwarf irregulars (see e.g. the review of Seiden and Gerola 1982). At the same time, the discovery of Larson and Tinsley (1978) that bursts of star formation were apparently ubiquitous in Arp interacting galaxies showed that high SFRs were not unique to dwarf galaxies. More recently, the observation that merger remnants are undergoing very extended starbursts (e.g. Joseph and Wright 1985, and further references in the review of Schweizer 1986), provides very dramatic evidence that large galaxies are capable of very large net SFRs.

Moreover, these examples of high SFRs in galaxies do not show the full dynamic range of star formation in galaxies, since galactic SFRs extend to very low values as well. One example, is given by the class of anemic spirals of van den Bergh (e.g. 1977). However, these galaxies have low gas densities as well as small SFRs. A better example is provided by the gas-rich, low-surface-brightness (LSB) galaxies discovered by Thuan and Seitzer (1979), and further studied by Romanishin et al. (1982). As Schommer and Bothun (1983) point out, these galaxies may provide evidence for suppression of star formation in otherwise normal disk galaxies.

Many questions are raised by the existence of variations in star formation between galaxies as large as those between the LSB galaxies and the starburst galaxies. What are the mechanisms responsible? What are the circumstances required to induce bursts or the suppression of star formation in galaxies? What is the precise role of interactions? Is the star formation process in starburst galaxies an extreme extension of the normal mechanisms of star formation in disk galaxies or is it a different process entirely? How can we tell observationally?

With respect to the latter two questions, there is evidence that the star formation efficiencies per unit mass in starburst galaxies can range up to about two orders of magnitude higher than in normal spirals (Rieke et al. 1980, Sanders and Mirabel 1985, Young et al. 1986, Sanders et al. 1986). In itself this result does not answer the question of whether starbursts represent a nonlinear continuation of a normal (e.g. Schmidt-law) mode of star formation, or whether once some threshold is exceeded a qualitatively different mode appears. If there are two distinct modes of star formation, then the dispersion in optical and near-infrared colors in color-color diagrams gives an indication of the relative importance of burst versus continuous star formation

in galaxies (Larson and Tinsley 1978, Struck-Marcell and Tinsley 1978, and Telesco 1983). However, these models do not directly address the question of mechanisms.

At the present time, with radio continuum and optical line surveys, and with IRAS data and near-infrared mapping of individual galaxies, there is a wealth of new information available on star formation in galaxies. To decipher the systematics and mechanisms of star formation in galaxies, it has been and will continue to be especially important to have statistical studies of large sets of data, collected in a consistent way (e.g. the IRAS data (Lonsdale et al. 1985), or optical line work like that of Balzano 1983 and Keel et al. 1985). For the present, we leave the intriguing questions posed above, but will return in the concluding section to consider a possible explanation for the large dynamic range of star formation in galaxies, which is suggested by a simple physical model.

Following some discussion of the general role of simple models, a specific model is presented in section II. In sections III and IV two applications of the model are considered - relaxation in a closed box and the evolution of ring galaxies.

B. The Heuristic Role of Simple Physical Models

In order to model and understand the wide range of phenomena associated with star formation in galaxies, theorists have used a variety of tools and techniques, including continuum kinetic or fluid approaches, discrete N-body models with approximations to include interstellar gas cloud and cloud-star interactions, and modeling with a stochastic component of the star formation. This range parallels that in studies of fluid turbulence, and other nonlinear phenomena. The various approaches have different advantages and disadvantages, both from the point of view of faithfully representing the phenomena, and the practical point of view of being able to perform the calculations and interpret them, analytically or on existing computers. In the end, to derive a consistent interpretation of the many aspects of star formation in galaxies (and hopefully some predictions!), a variety of increasingly sophisticated approaches will be needed. Because of the extreme complexity of the numerical models, the various approaches must be carefully compared to each other and to observation.

On the other hand, to achieve a consistent physical understanding of a complex problem it is very helpful to begin with the study of a relatively simple phenomenological model which captures the essence of the phenomenon (e.g. the Ising model of ferromagnetism or the Kolmogorov model of turbulence). Of course, in using such a simple model one must remember that while it may succeed in mocking-up the dominant physical processes in some relevant range of parameter space, it may miss the full interplay of these processes in some other parameter range, or it may miss the emergence of new processes. For the problems of galaxy-scale star formation and gas dynamics the ideas behind the classic Oort cycle - i.e. that clouds are built up by collisional coalescence and massive clouds are broken up as a result of internal star formation activity - have provided the basis for such a simple model for some time. Examples of the usefulness of the Oort picture include the work of Field and Saslaw (1965), who showed that a kinetic (coalescence) equation for the evolution of the cloud spectrum with Oort cycle interactions yielded power-law

solutions like the observed solar neighborhood cloud spectrum, and implied a dependence of the star formation rate on gas density in accordance with the empirical Schmidt law. Another example of a cloud collisional model is provided by Larson's (1969, 1974, 1975, 1976) numerical models of collapsing protogalaxies, which included density-dependent star formation and energy dissipation in cloud collisions, and which yielded structures matching many observations of elliptical galaxies. More recently, a variety of numerical calculations (e.g. Casoli and Combes 1982, Combes and Gerin 1985, Kwan and Valdez 1983, Hausman and Roberts, 1984, Roberts and Hausman 1984 and Tomisaka 1984), which include Oort-type interactions, have shown that a spiral density wave can drive collisional processes, leading to the buildup of giant clouds or cloud complexes, and presumably, enhanced star formation.

These examples share in common the feature that the interstellar medium is assumed to consist of an ensemble of distinct clouds (with perhaps a large range of sizes and masses). The cumulative interactions among the clouds are used as a link between the large-scale disturbance and the gas dynamics and star formation on small-scales. This approach, like many turbulence theories (e.g. eddy viscosity or mixing length theories), is an essentially phenomenological treatment of intermediate-scale interactions (like the "inertial" range in incompressible turbulence). It attempts to model the cumulative effects of small-scale interactions, without incorporating the details of those interactions (e.g. the physics of the formation of an individual massive star). At the same time, the intermediate-scales (cloud ensembles) can be driven by large-scale disturbances or instabilities (e.g. density waves, gravitational or Parker-Jeans instabilities), and their nonlinear feedbacks can, in turn, effect the development of the large-scale instability. Thus, a model of the intermediate-scale interactions serves as an essential tool for applying knowledge of the physics of the interstellar medium in our Galaxy and other nearby galaxies, to a variety of galaxy-scale problems.

In the original Oort model, and many of the later versions (e.g. Field and Saslaw 1965), a number of physical processes of possible importance in the ISM were not considered. Several of these can be incorporated quite readily into a continuum formalism derived from a kinetic equation (see Scalo and Struck-Marcell 1984), such as the fact that cloud collisions at high relative velocity probably lead to cloud disruption, rather than coalescence (Hausman 1982, Gilden 1984), or that clouds can be formed from the more or less random local compression of the intercloud material by runaway O, B stars (Bania and Lyon 1980). The possible effects of an intercloud medium on the cloud ensemble (e.g. drag) could also be included; however, we have argued elsewhere (Scalo and Struck-Marcell 1984) that such effects are probably not dominant in most situations.

The interchange of material between cloud and intercloud media, or more generally, between multiple phases in the ISM, is an intricate subject in its own right. The view of the ISM as a gas in several co-existing thermal phases, with a dynamic, time-dependent balance (McKee and Ostriker 1977, Ikeuchi et al. 1984, Bodifee and de Loore 1985), is fundamentally orthogonal (though not contradictory) to the Oort picture. However, since most of the interstellar gas is located in relatively dense clouds, the multiple phase picture is probably more relevant to the study of the intercloud gas.

Another area of substantial ignorance is the role of magnetic fields on all scales. Most workers have concentrated on the effects of magnetic fields on small-scales (e.g. angular momentum transport, flux loss, etc.), but they may also contribute an effective viscosity and additional dissipation on intermediate and possibly large scales (e.g. Clifford and Elmegreen 1983, Clifford 1984, 1985, Elmegreen 1985). The effects of magnetic fields may be crudely included in a hydrodynamic model as additions to the cross sections or rates of viscous transport and dissipation.

Perhaps the most serious questions about the relevance of an Oort-type cloud model to gas in galaxies are raised by the conclusion of Scalo (1985, and references therein) that a hierarchical structure of clouds within clouds is implied by an analysis of observations in a variety of wave-bands of the ISM in our Galaxy on a wide range of scales. In Scalo (1985) it is suggested that about five levels of this hierarchy have been observed, with several clumps contained within each clump of the next higher level. The hierarchecal picture does not necessarily call into question the importance of cloud collisional interactions, and cloud-star interactions, which are the basics of the Oort model. However, at the least, it muddies the simple physical picture of the original Oort model, e.g. the definition of a "cloud" and the proper treatment of collisions in a hierarchecal structure, and in fact, makes the definition of statistical averages ambiguous.

Nonetheless, despite the difficulties and ambiguities a cloud ensemble or generalized Oort picture still provides a viable basis for building deterministic and physically understandable models of large scale gas dynamics and star formation in galaxies (see e.g. Chiang and Prendergast 1985). As a starting point for such a model, we have suggested (Scalo and Struck-Marcell 1984) a general kinetic equation for the joint coordinate position, velocity, and mass distribution of an interstellar cloud ensemble as a function of time. Unfortunately, this kinetic equation is too complex to serve as a very practical tool in itself (although N-cloud type calculations can simulate it). Thus, again following the tradition in the study of fluids and turbulence, we can take velocity and mass moments to derive hydrodynamic equations.[1]

To proceed from this point one must adopt specific models for the cloud interactions, which act like sources and sinks in the hydrodynamic equations. A variety of approximate forms were suggested in Scalo and Struck-Marcell 1984. In the next section we will discuss a relatively simple example of an Oort-type model. In later sections we will apply it to the ring galaxy problem in particular, and explore the insights it offers on the starburst problem in general.

---

[1]This procedure is of course quite idealized since we do not know the mass and velocity distributions or how they may vary with time. However, within the range of reasonable functional forms for these (where what is reasonable is based in part on what we know of the cloud distributions in the solar neighborhood), this amounts to uncertainty in coefficients or order unity.

II. AN OORT MODEL EXAMPLE

Given our great ignorance about the nature of the interactions in the interstellar medium in galaxies, the choice of what methods to use in a simple model, let alone the functional dependence of the interactions, will not be unique and must be partially based on considerations of practicality or feasibility. We have chosen to study, as a general-purpose model for a variety of applications, a hydrodynamic model, averaged over the mass and velocity distributions of clouds, with equations for the number density of clouds n, the mean mass of clouds m, and the cloud velocity dispersion c (or equivalently the internal energy). The equations are very similar to the normal hydrodynamic equations except for the presence of extra source terms. We include source terms for the usual Oort-cycle interactions, including: cloud collisional coalescence, collisional energy dissipation, the breakup of massive clouds and the acceleration of the fragments due to the stellar winds, expanding HII regions, and supernovae that result from massive star formation. We have also included the process of cloud disruption in high relative velocity collisions. Figure 1 gives a schematic overview of these processes.

Among the key 'philosophical' choices we have made in setting up this model are: 1) We assume that the characterization of the problem by the mean values of cloud number density, cloud mass, mean flow velocity, and velocity dispersion (i.e. the random motions of clouds), preserves much of the essential physics of the problem (more on this later), 2) we do not assume constant collisional cross sections and direct gas density-dependent star formation, and 3) we do not assume the cloud fluid is isothermal (motivated in part by the possible observational comparisons since velocity dispersions can be measured across the face of galaxies). In the remainder of this section we consider in a little more detail a couple of the key aspects of the adopted model (henceforth the Oort model), including the parametrizations of the collisional cross sections and the rate of cloud disruption by internal star formation activity. We also comment briefly on the role of time delays due to the finite lifetime of massive clouds, a role we have found to be crucial in controlling the qualitative and quantitative evolution of the models.

A. Collisional Rates

The form adopted for the rate of change of the number of clouds per unit volume due to coalescence or disruption in collisions is

$$\left(\frac{dn}{dt}\right)_{\text{collision}} = -\alpha_n f_c(m,c) m^{2/3} n^2 c, \tag{1}$$

where the n^2c factor gives the usual quadratic dependence on cloud number density and linear dependence on velocity dispersion for binary collisions. The factor $m^{2/3}$ represents the mass dependence of the geometric cross section, assuming that the internal density of clouds is roughly constant, and the factor α_n contains the generalized cross section amplitude (i.e. the ratio of effective to geometrical cross section). The additional collisional nonlinearities are contained in the function f_c, for which we have adopted the simple parametrized form

$$f_c = \left[\frac{1-(c/c_{cr}^r)}{1+(c/c_{cr}^r)}\right], \tag{2}$$

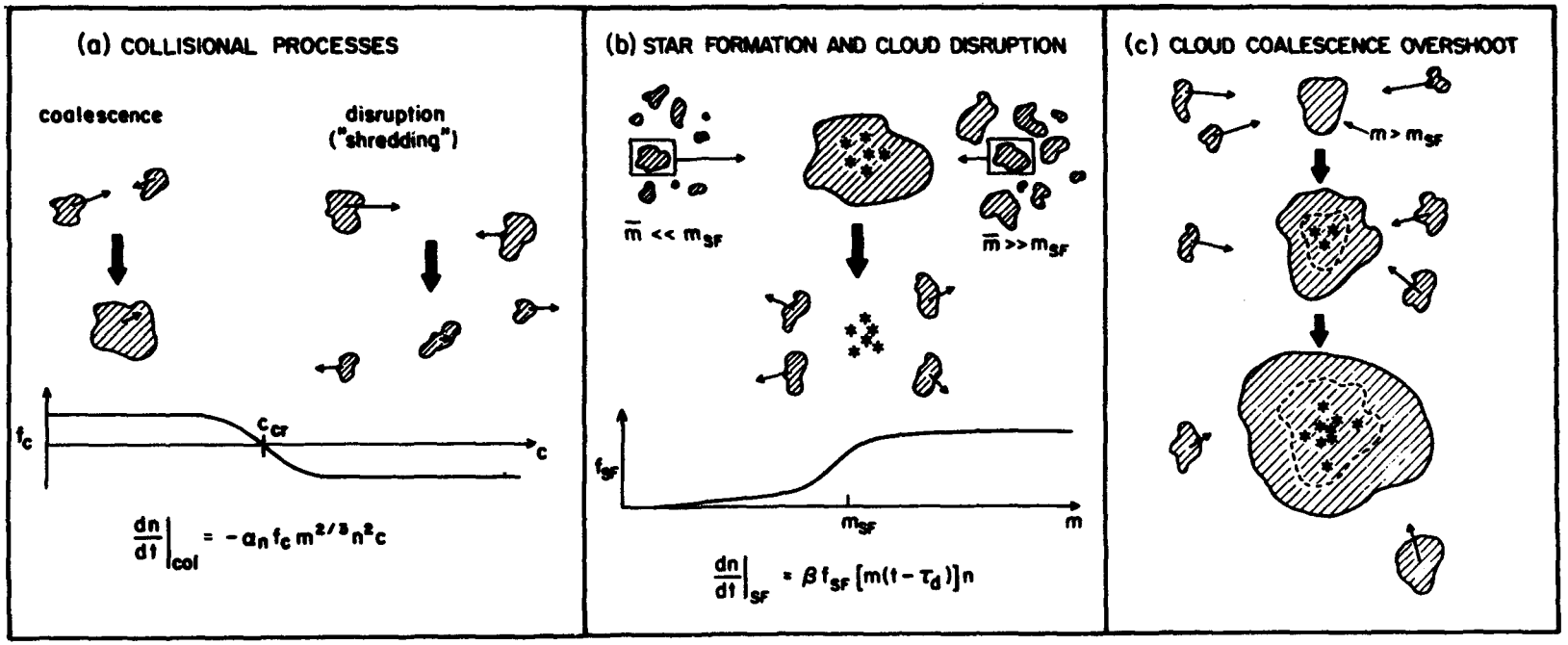

Figure 1. Schematic overview of the important processes in an Oort model of an interacting cloud system (from Struck-Marcell and Scalo 1986). The first panel shows cloud collisional coalescence (disruption) in low (high) relative velocity collsions and adopted parametrization for the rate this process. The second panel illustrates the process of massive cloud break-up as a result of internal star formation activity, and again the model parametrization is given. The third panel illustrates the 'coalescence overshoot', which occurs when the timescale for massive cloud collisional build-up is less than the cloud lifetime to internal star formation.

where c_{cr} is the characteristic velocity dispersion such that the average relative kinetic energy in collisions equals the mean gravitational binding of a cloud. Thus, for example, when c increases past the value $c = c_{cr}$, the sign of the collisional cross section changes, giving the assumed change from coalescence to disruption. The exponent r determines the abruptness or nonlinearity of this change, and is treated as a parameter of the model. The form of the function is such that it saturates at a maximum (minimum), where we have essentially 100% efficient coalescence (disruption) at $c<<c_{cr}$ ($c>>c_{cr}$). Examples of the function, with different values or r are shown in Fig. 2, taken from Scalo and Struck-Marcell 1986.

The simple binding energy approximation contained in eq. (2) does not by any means fully represent the complex physics involved in cloud collisions, see, for example, the recent numerical hydrodynamical calculations of Gilden (1984), Lattanzio et al. (1985) and Hunter et al. (1986). Moreover, even the numerical hydrodynamic calculations are highly idealized compared to real interactions between clouds containing internal hierarchecal clumping. Thus, it is presently hard to see how to substantially improve upon the physically plausible, if crude, approximation above.

B. Internal Star Formation

In this simple Oort model we also assume that at any time some fraction of the clouds are sufficiently massive to form stars efficiently and then suffer disruption as a result. (For a recent observational reference see Leisawitz 1985.) We have chosen the following parametrization for this fraction as a function of mean cloud mass compared to a critical cloud mass for star formation m_{SF},

$$f_{SF}(m) = \frac{(m/m_{SF})^s}{1+(m/m_{SF})^s} , \qquad (3)$$

where the exponent s, like the exponent r in eq. (2), is a parameter of the model, which characterizes the nonlinearity, or rapid turn-on of star formation, at $m \approx m_{SF}$ (see Fig. 2). The ratio $f_{SF}(m)/f_{SF}(m_o)$, for some characteristic (e.g. equilibrium) cloud mass m_o, gives the relative rate of cloud disruption by internal star formation, and also the relative fraction of clouds that are forming massive stars. If the mean gas density is constant this ratio can also be taken as an indicator of relative star formation rate. (Strictly speaking, this interpretation also requires particular assumptions about the evolution of the cloud spectrum, see Scalo and Struck-Marcell 1986.)

The particular form for f_{SF} in eq. (3) is somewhat arbitrary, but it embodies several physically relevant features quite naturally. First of all, the fraction of clouds massive enough to form stars (or at least the probability of massive cloud formation) is a monotonically increasing function

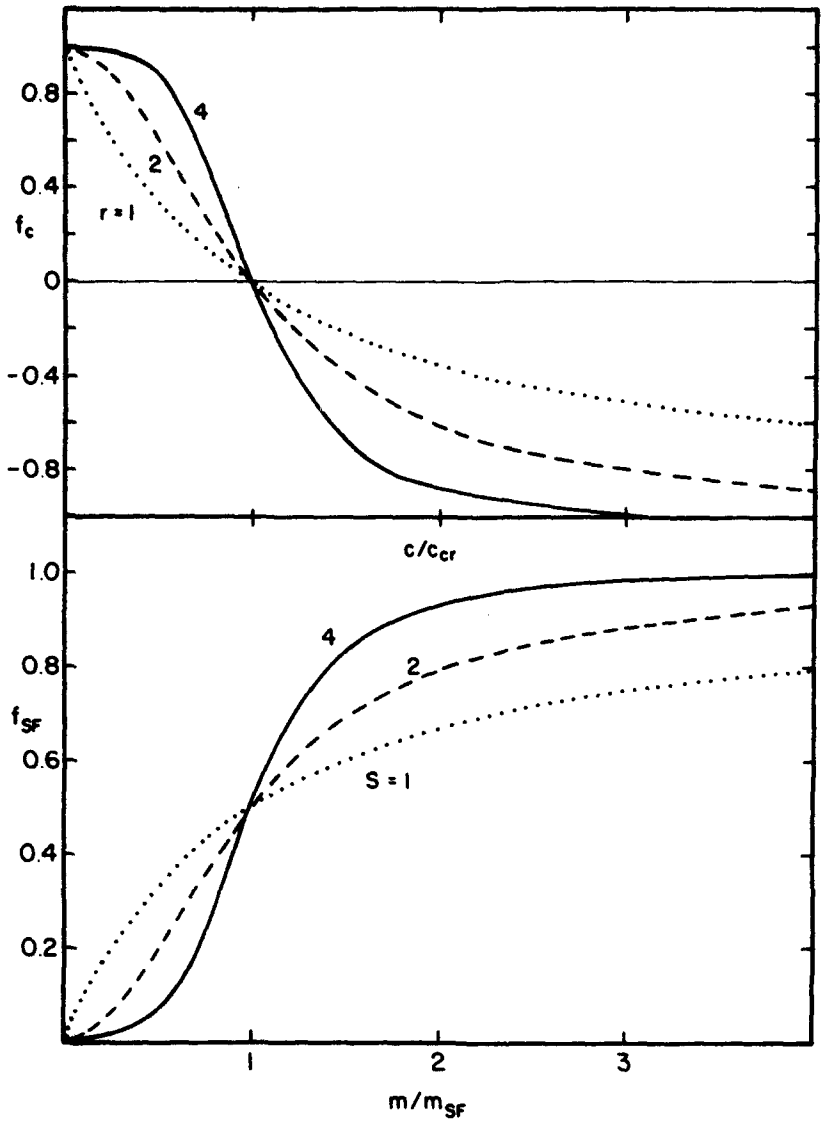

Figure 2. Several examples of the parametrized coalescence - disruption function f_c and star formation function f_{SF} are shown (from Struck-Marcell and Scalo 1986). Depending on the values of the parameters (especially the exponents r,s), the form of these functions can range from nearly linear to an almost step function form. The latter implies a strong threshold behavior.

of mean cloud mass. Secondly, since f_{SF} is defined as the fraction of clouds forming massive stars, it must have a maximum saturation value of $f_{SF,max}<1$. On the basis of the first point, we might simply choose to approximate f_{SF} by a power-law in m. The saturation effect, however, suggests the form of the denominator on the right hand side of eq. (3). The form of the denominator

also reflects an attempt to constrain $f_{SF}(m)$ based on the possible evolution of simple cloud mass spectra (see Appendix A in Struck-Marcell and Scalo 1986).

Note that a steep increase in f_{SF} occurs at $m = m_{SF}$ if $s \gg 1$. On the other hand, it is apparent from Fig. 2 that if $s < 2$, f_{SF} is sufficiently smooth that there is only a modest increase at 'threshold'.

As in the case of the collision function f_c, it is difficult to go beyond these qualitative considerations. Basically, the function f_{SF} is dependent on two highly uncertain quantities: 1) The efficiency of massive star formation as a function of cloud mass, and 2) the most probably time-dependent mass distribution of the cloud ensemble. Ongoing observations of star-forming regions in our Galaxy should provide helpful constraints on the first factor.

We might hope that N-body simulations of interacting cloud ensembles would provide useful constraints on the second quantity, in the same way that molecular dynamics experiments yield information on net chemical reaction cross sections. The analogy is imperfect of course, because we don't have a first-principles understanding of cloud interactions, and the detailed results of N-cloud calculations may depend sensitively on the assumptions made about these interactions. Nonetheless, we can illustrate the usefulness of these calculations with one example from the work of Kwan and Valdes (1983). The evolution of the mass spectrum (g(m)) of a cloud ensemble following passage through a spiral density wave, on a timescale which is assumed to be shorter than the massive cloud lifetime, is shown in Fig. 2 of their paper. The form of the mass spectrum does change significantly with time, but qualitatively, it is characterized by a single dominant peak at all times, supporting the basic consistency of a model based on the mean mass. Moreover, a narrowing of the mass distribution as the mean mass increases and a steepening at the high-mass end are apparent in their figure (for this essentially pure coalescence case). These features indicate a fairly rapid increase of the mass fraction greater than some (relatively large) critical mass as a function of the mean mass. If this is also convolved with a threshold behavior in the star formation efficiency, then it is quite plausible that the exponent $s > 2$ in eq. (3).

C. The Rate Equations with Time Delays

With the expressions above for the collision and star formation terms, the equations for the rate of change of the cloud number density and velocity dispersion squared due to these interactions in an isolated fluid element can be written

$$\frac{dn}{dt} = \alpha_n f_c m^{2/3} n^2 c + \beta_n f_{SF}(m(t-\tau_d)) n(t-\tau_d)$$

$$\frac{d(nc^2)}{dt} = \alpha_c m^{2/3} n^2 c^3 + \beta_c f_{SF}(m(t-\tau_d)) n(t-\tau_d) \qquad (4)$$

(see Scalo and Struck-Marcell 1984, Scalo and Struck-Marcell 1986 for more

details). With an additional assumption for the rate of conversion of gas into stellar remnants, dm/dt, the equation set is closed. The full hydrodynamical equations, with pressure terms and other spatial gradients, are derived and discussed in detail in Scalo and Struck-Marcell 1984.

As will be shown in the following section, it is essential to include the finite cloud lifetime in the cloud disruption terms in eqs. (4). (The importance of the cloud lifetime is readily apparent in several N-cloud studies of density waves, e.g. Hausman and Roberts (1984), Tomisaka (1984).) Specifically, massive clouds are assumed to have a fixed lifetime τ_d, and thus, the cloud disruption rate at time t is proportional to the number of massive star-forming clouds at time $t-\tau_d$, i.e. $n(t-\tau_d)f_{SF}(m(t-\tau_d))$. With the inclusion of the time delay effect our simple Oort model is complete.

To summarize, we have attempted to model, in a very general way, the principle nonlinear effects associated with cloud collisions and the feedbacks of massive stars on the cloud ensemble. To keep the model simple a number of processes noted in the introduction have not been included. Eventually, it would be interesting to extend the model to include some of these. In general, there is no reason that the hydrodynamic formalism must be restricted to Oort-type interactions. Many potentially interesting kinetic effects are excluded in a mean fluid model, but in this case some idea of what has been lost can be obtained by comparing to N-cloud calculations. (Multiple-fluid hydrodynamic models are also possible, and even two-scale models have proven of great use in atmospheric physics.)

Even with the many omissions this 'simple' model appears at first sight to be very complex, and dependent on many parameters. However, as far as the qualitative evolutionary behavior is concerned, this turns out not to be the case. First of all, the equation set (4) has a single equilibrium (with n_o, m_o, c_o real and > 0) at constant gas mass density, and if the equations are nondimensionalized in units of this equilibrium six dimensionless parameters remain. These include: the exponents r,s, the critical mass for star formation m_{SF}/m_o, (in units of m_o for convenience) the critical velocity dispersion for disruption in collisions c_{cr}/c_o, (in units of c_o) a dissipation efficiency factor, and T the ratio of the cloud lifetime to the equilibrium cloud collision time. The extensive parameter study in Struck-Marcell and Scalo 1986, shows that, as long a S>2, only the parameter T effects the qualitative behavior of the model, the quantitative effects of the other parameters decouple to the extent that their individual effects are fairly understandable physically (see the following section). Thus, we believe that this deterministic Oort model can serve as a useful tool for studying a variety of problems in galactic gas dynamics, and as an aid in the interpretation of other more complex calculations.

III. APPLICATIONS I: A MECHANISM FOR STARBURSTS

A. Evolution in a Closed Box

The simplest application of the model eqs. (4) is to the study of the

evolution of a cloud system in an isolated closed box with constant gas density $\rho = mn$, following a disturbance. Some of the essential results of such calculations were given in Scalo and Struck-Marcell 1986, and an extensive parameter study is reported in Struck-Marcell and Scalo 1986, so we limit the discussion in this section to a brief summary.

We have found, on the basis of an extensive grid of numerical integrations of eqs. (4) and linear stability analysis, that following an arbitrary disturbance, the closed box cloud system relaxes within a few cloud collision times to one of two generic behaviors. If T, the cloud lifetime to collision time parameter (henceforth simply the 'time delay' parameter T) is assumed to be less than some critical value T_{cr}, the system relaxes rapidly to the single stable equilibrium state (n_o, m_o, c_o). On the other hand, if $T>T_{cr}$ the system relaxes to a stable closed curve, rather than a point, in the (n,m,c) phase space. In this case the system undergoes nonlinear, self-excited oscillations. At $T=T_{cr}$ the system undergoes a so-called Hopf bifurcation, so that for T slightly greater than T_{cr} the attracting set is a single-period limit cycle. The bifurcation is characterized not only by the appearance of the limit cycle, but also by the fact that the original equilibrium state becomes unstable. Thus, even if the system is in a state near equilibrium, if $T>T_{cr}$, it will evolve out to the limit cycle.

The value of T_{cr} is found to be of order unity for virtually the whole range of astronomically interesting values of the other parameters. Thus, since cloud lifetimes are probably of the same order as cloud collision times, the bifurcation phenomenon is relevant to galactic cloud systems. Moreover, since T_{cr} is insensitive to the other parameters, it is not expected to be a singular or unusual phenomenon. Even more generally, the bifurcation is not restricted to the precise form of the Oort model terms of eq. (4), see Scalo and Struck-Marcell 1986.

If T is increased far enough beyond T_{cr}, a second bifurcation occurs, this time to a double-looped limit cycle with two bursts of different amplitude per cycle. Indeed, further increases of T lead to a series of bifurcations and eventually to deterministic chaos in the phase space. In this limit the SFR vs. time looks essentially stochastic, with frequent bursts (Scalo and Struck-Marcell 1986).

This result leads us to consider the physical meaning of high T. If the cloud lifetime consists essentially of the protostellar collapse time plus the main-sequence lifetime of massive stars, it should be more or less constant universally (at a given stellar metallicity). On the other hand, the equilibrium cloud collision time depends inversely on the cloud density and cross section, which turns out to be the product of the mean gas density of the cloud fluid and a slowly varying function. Thus, increased gas density implies increased T ($T \sim \rho$ roughly). Note, however, that m and f_{SF} are highly nonlinear functions of T. Thus, this is not a Schmidt law density dependence.

B. A Starburst Mechanism and Systematics

With the essentially mathematical questions of the generic existence and stability of the limit cycle bifurcation resolved, we can proceed to the

questions of the physical mechanism of the bifurcation and its consequences for galactic gas dynamics. First the mechanism: In Scalo and Struck-Marcell 1986 we attributed the bifurcation to a "coalescence overshoot", where, as a result of the relatively long cloud lifetime, a massive star-forming cloud can continue to grow for some time before suffering disruption. If the function f_{SF} is sufficiently nonlinear ($s>2$), and the cloud mean mass is near the threshold value m_{SF}, this extra growth translates into a great deal more (and presumably more efficient) star formation, i.e. build-up to a burst. Roughly one delay time later the system suffers the consequences of these excesses - severe cloud disruption. The energy input is quickly dissipated in (possibly disruptive) collisions, then the system finds itself in a shredded, quiescent state, and begins to regrow through coalescence.

The key step is the overshoot, or excess cloud growth past the equilibrium mean mass (see Fig. 2). This step is similar to the triple-alpha nuclear reaction in that a third-body (or more for the clouds) collision occurs before the outcome of the original collision is resolved.

If we consider a series of closed box models with successively larger values of $T>T_{cr}$, we find that both the amplitude and the period of the limit cycle increase in the system phase space. This implies an increased starburst amplitude, and a longer time between bursts (up to 10 times the burst duration, see Fig. 3). The burst duration is of order T at $T\approx T_{cr}$, i.e. of order a cloud collision time $\approx 3\times10^7$ yr. It varies quite slowly with T. It has been suggested (e.g. Loose et al. 1982) that starbursts are of short duration because the gas is blown out of the region (e.g. a galactic nucleus) by the resulting winds and supernovae. These one-zone models imply instead that the fundamental reason may be that the cloud system is simply broken down to a state where it is no longer capable of forming stars efficiently. The apparent low mass of the molecular clouds in the core of M82 (Knapp et al. 1980, Stark 1982, Olofsson and Rydbeck 1984), together with the possible polar outflow (Ungar et al. 1984), probably indicate that a combination of both processes is at work in that galaxy.

The density dependence of the bifurcation sequence, together with the notion of high gas consumption in bursts (see references in section I), implies another relaxation process, one which tends to drive the cloud system below the burst threshold. For example, consider the case of rapid gas infall into a galactic nucleus induced by a tidal encounter which boosts the gas density and time delay parameter above the value for the onset of chaos. With the system in the burst mode a large fraction of the time, gas consumption will be rapid, which in turn lowers the gas density. Figure 4 shows that a calculation in the limit cycle regime, and including gas consumption, yields rapid damping of burst amplitude. The gas consumption in these calculations is scaled to f_{SF}, and can range up to 30%. (Star formation is clearly very efficient.) Thus, galactic cloud systems are probably found in the chaotic regime only rarely (protogalaxies excepted?), and even successive limit cycle bursts are strongly damped. This calculation also indicates that the gas consumption timescale does not determine the duration of the bursts in the limit cycle or chaos regime (It is the breakdown of the clouds that turns off the burst even if there is still an ample gas supply.) This implies that apparent gas consumption timescales in galaxies are relatively meaningless if the galaxies burst.

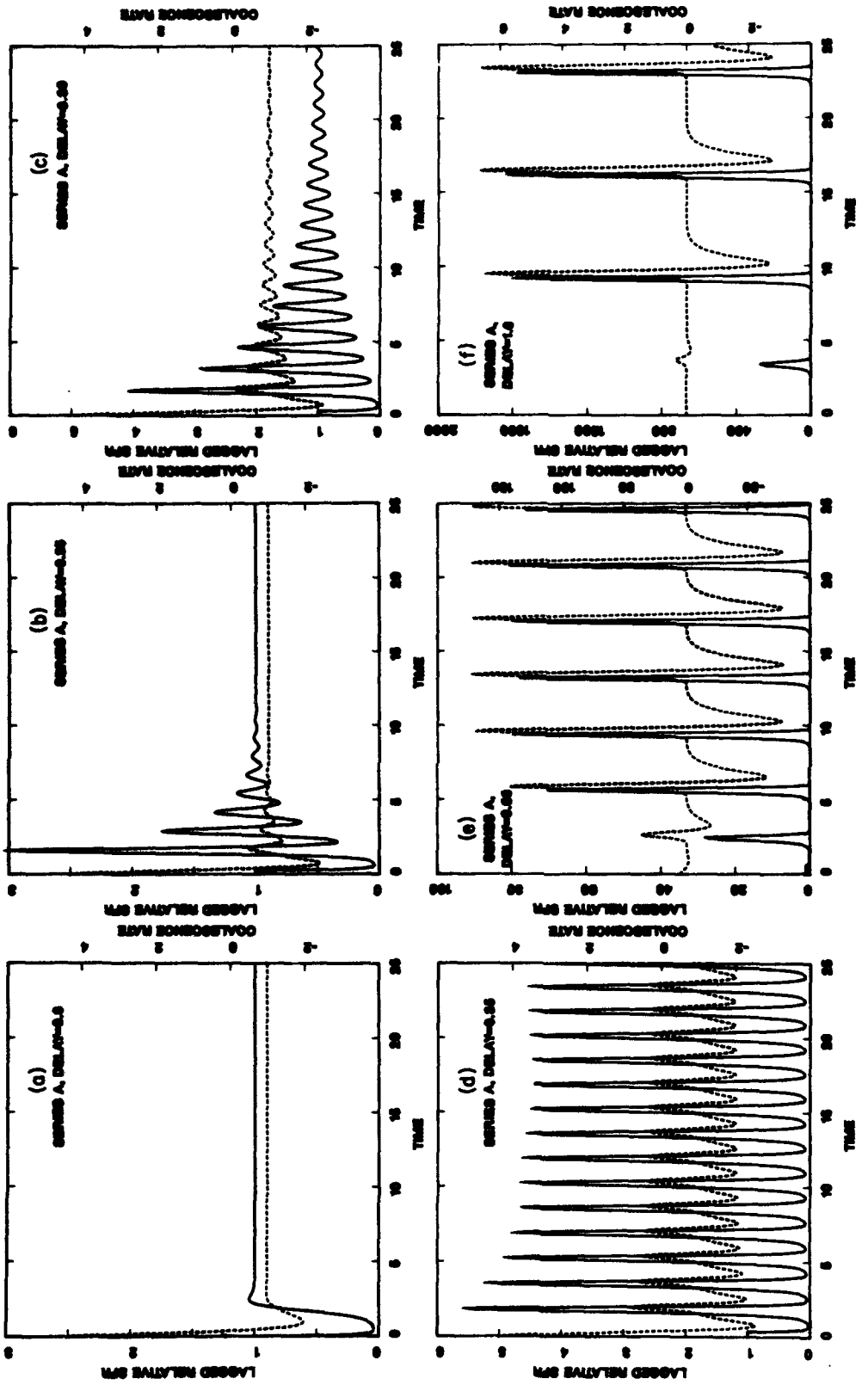

Figure 3. Time series of the function f_{SF}, an indicator of the relative star formation rate, is shown (solid line) for six closed box calculations with increasing values of the parameter T (from Struck-Marcell and Scalo 1986). Note the increasingly oscillatory response of the model, which leads eventually to the limit cycle bifurcation. Also shown (dashed lines) are the relative collisional coalescence-disruption rates.

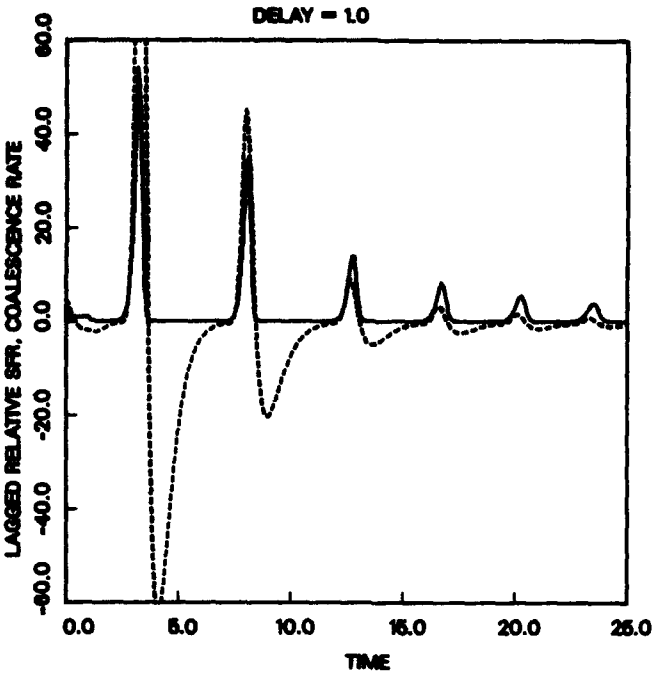

Figure 4. Time series of the function f_{SF}, as in Fig. 3, but for a calculation with gas depletion included (from Struck-Marcell and Scalo 1986).

C. Other Consequences and Parameter Dependences

The model also yields several other observationally relevant consequences. First of all, even within the limit cycle-starburst regime, the model has a strong tendency to remain nearly isothermal. There is some observational evidence for this result (see Lewis 1984, Gallagher and Hunter 1984). Even under conditons that show large variations in m, n, and f_{SF}, the velocity dispersion varies only by a factor of about a few.

Secondly, we note that, in the same way that the model predicts starbursts for $T>T_{cr}$, it also predicts bursts of energy dissipation in cloud collisions. These dissipation bursts might produce measurable shock emission, e.g. from H_2 and [OI]. Estimates are given in Struck-Marcell and Scalo 1986. An interesting complication is that in the models, the dissipation burst and star formation burst are out of phase.

Thirdly, there is commonly a delay of order several equilibrium cloud collision times between the occurrence of a disturbance in the cloud system and the starburst it triggers. Most disturbances act to break down the clouds initially and the delay is roughly equal to the regrowth timescale. This regrowth time depends on how severe the cloud breakdown is, and thus on the magnitude of the disturbance. Clearly, this effect can help account for the observation that many interacting galaxies do not have enhanced SFRs.

We conclude this discussion of the closed box model with a few comments on the role of parameters other than T. Apparently, the chief role of the parameter m_{SF}/m_o, is in determining the maximum value of the star formation function: $(f_{SF}/f_{SF}(m_o))_{max} \simeq (m_{SF}/m_o)^6$. Since m_{SF}/m_o (m_o mean equilibrium cloud mass) is an essentially unknown quantity, the model cannot predict absolute star formation rate amplitudes. On the other hand, the parameter c_o/c_{cr}^o plays the dominant role in determining variations in c. Small values of this parameter (i.e. when the equilibrium value c_o is much less than the cloud collisional disruption threshold), yield nearly perfect isothermality. Finally, decreasing the dissipation efficiency parameter increases the value of T_{cr} somewhat, and decreases $(f_{SF})_{max}$ for a given $T>T_{cr}$. This is not surprising since dissipation is an important part of the coalescence overshoot phenomenon.

IV. APPLICATIONS II: THE HYDRODYNAMICS OF RING GALAXIES

A. Why Study Rings?

The chief result of the preceding section was that above a critical value of the time delay parameter, i.e. above a threshold gas density, starbursts are a generic behavior of an Oort-type system. Taken together with the observational evidence that strong disturbances, e.g. strong density waves, induce starbursts, this result cries out for numerical modeling of the gas dynamics in interacting galaxies. In general, this modeling is a very formidable undertaking, although there have been several pioneering efforts (Theys and Spiegel 1977, Icke 1985, and Noguchi and Ishibashi 1986). Thus, in attempting numerical modeling with the Oort cloud fluid we have chosen to focus on what is probably the simplest case - ring galaxies.

Since ring galaxies are relatively rare objects, it is worthwhile to elaborate on the reasons why, among all types of interacting system, they are deserving of detailed study. These reasons include the following.

1. Relatively unambiguous observation comparisons.

Detailed studies of the optical morphology and kinematics of several ring systems have been carried out, including the Cartwheel galaxy (Fosbury and Hawarden 1977), the Lindsey-Shapley ring (Few, Madore and Arp 1982), and the Vela ring (Taylor and Atherton 1984). These studies revealed radially propagating rings of HII regions with companions at a distance of about one ring diameter. Thus, in these cases at least, the circumstantial evidence for a recent collision, and a resulting density wave (as in the Toomre 1978 models) is strong. The strength of the wave depends on the relative masses of the target and intruder galaxies, and, if the encounter is essentially impulsive, to a much lesser degree on orbital passage time.

The possibility of obtaining direct observational estimates of the density wave amplitude is clearly important, and is the first strong argument for studying rings. (Consider the long debate over the amplitude of density waves in spiral galaxies.)

2. Symmetry.

In a direct, head-on collision between a purely stellar intruder galaxy and a target system containing a cold disk, the formation of a cylindrically symmetric ring in the disk can be approximated as a one-dimensional problem. Indeed, even the examination of the evolution an isolated fluid element, driven by a time-dependent external perturbation can be useful in the ring galaxy problem (see Appleton et al. 1985). In general, some symmetry remains even in the more likely case of an off-center collision. In this case the response of the disk can be treated as approximately two dimensional, i.e. in the plane of the disk. Multidimensional numerical hydrodynamic calculations require a great deal of computer time, so having relevant low-dimensional approximations, within which it is practical to vary parameters and perform many computational runs, is extremely helpful.

3. Range of perturbation amplitude.

Collisions with small companions, as well as with larger intruders are of interest, as is the variation of response with companion mass. From a practical point of view, small disturbances are usually easier to model stably and accurately, so it is a useful check of the stability of the numerical approximation to verify that model behavior changes continuously as the disturbance is increased. Thus, both numerical and astronomical considerations converge here.

4. Extended starbursts.

It appears, on the basis of IRAS infrared luminosity and color temperature (S_{100}/S_{60}), that many of the rings are undergoing moderately strong, and of course, highly extended starbursts (see Appleton and Struck-Marcell 1986a). The large extent of the star formation in rings is not only intrinsically interesting, but also of practical importance for providing a class of galaxy where any nuclear activity is generally separated from starburst activity. The spatial extent also makes the more nearby rings good candidates for near-IR, radio continuum, 21 cm, and molecular observations of spatial variations in star formation and cloud characteristics. Some work is already underway (e.g. Ghigo et al. 1986).

In summary, the ring galaxies appear to possess a number of unique advantages for facilitating the comparison between observation and theory of star formation in galaxies, as well as being especially amenable to numerical modeling.

B. Approximations for Numerical Modeling

We have begun a two-pronged effort to model ring galaxies using the Oort model cloud fluid. The first part of this program consists of one-dimensional numerical hydrodynamic modeling of cylindrically symmetric rings, using a Lagrangian (moving) grid, and explicitly calculating the time-delay effects. The second part of the program consists of two-dimensional hydrodynamic calculations of the formation and evolution of both symmetric and off-center rings. Both computer programs use the well-known Flux-Corrected Transport algorithm (see Book 1981); details will be published elsewhere.

In the relatively (and only relatively!) inexpensive one-dimensional calculations, it is possible to include the full details of the cloud interaction model (e.g. density-dependent time delay parameters calculated accurately at each grid point), and to do a large enough number of calculations to fairly sample parameters and initial conditions. The two-dimensional calculations are better suited to study kinematic and dynamic questions (e.g. angular momentum transport), but they become impractical without some simplifications in the cloud fluid terms. For example, we typically assume isothermality and use a very coarse calculation of the memory effects in the two-dimensional calculations. Since here we are primarily interested in star formation in the ring(s), most of the discussion below will be limited to results from representative one-dimensional calculations.

We have not yet coupled a realistic treatment of the stellar dynamics to the hydrodynamic calculations (nor included self-gravity in the gas), but instead, assume that the potential of the target galaxy is dominated by a softened point mass, with a softening length of typically 40 equilibrium cloud mean free paths (e.g. $13(\lambda/0.3$ kpc.) kpc.). This large softening length yields a rather flat rotation curve, over a large range in radius. The companion galaxy is assumed to be a gas-free, softened point mass (softening length of 1/4 - 1/2 that of the target disk), on a free-fall trajectory. In the one-dimensional calculations, angular momentum is assumed to be conserved in each Lagrangian fluid element (i.e. each discrete radial ring).

Finally, in all of the calculations reported below, the gas density was assumed to be constant across the disk initially, with a value well below the threshold for bursts.

C. Numerical Results in One-Dimension

Several of the most interesting numerical results are well-illustrated by considering, either individually or in comparison, two representative one-dimensional calculations. These calculations have initial conditions as described above, with a companion mass equal to 20% of the softened point mass in the target galaxy. The companion orbit is such that it falls through the center very rapidly, yielding a somewhat unrealistically impulsive disturbance, but in this case the details of the orbit are unimportant. The values of the cloud fluid parameters are as follows: $c_o/c_{cr}^o = 0.924$, the equilibrium velocity dispersion is quite near the disruption threshold; $m_o/m_{SF} = 0.1$, the equilibrium mean mass is well below the threshold for efficient star formation; the dissipation efficiency is of order unity (i.e. almost completely inelastic collisions); and r=s=4, implying steep thresholds in f_c and f_{SF}. The only difference between the two calculations is that the initial, equilibrium value of the time delay parameter is 0.3 of the critical value in the first case, and 0.75 the critical value in the second. (For brevity we will refer to these as the 0.3 and 0.75 models.)

Figures 5 and 6 show the radial profiles of the mass density, star formation rate indicator $f_{SF}/f_{SF}(m_o)$, and radial velocity at one representative time in the 0.3 and 0.75 models, respectively. Although we will not discuss detailed dynamical questions here (see Appleton and Struck-Marcell 1986b), we note several very basic features in these figures. First, the radial velocity profile shows infall outside of the ring, positive velocity within the ring,

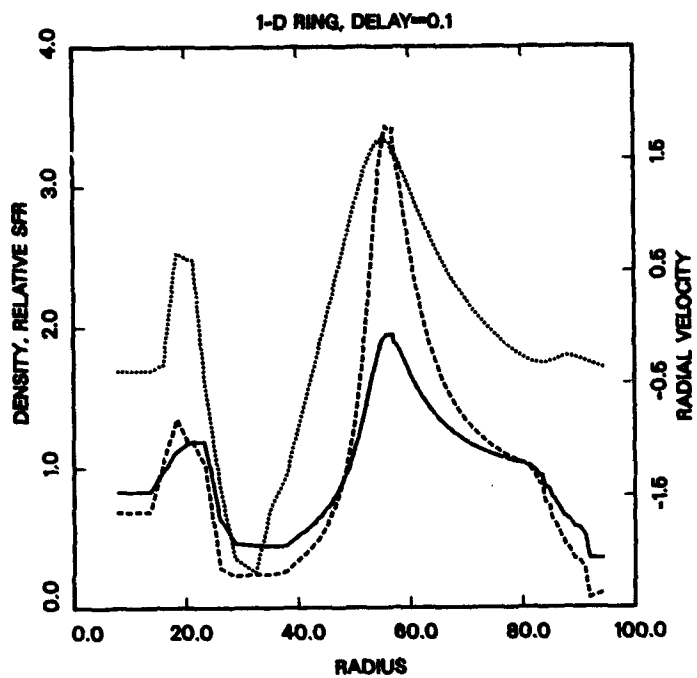

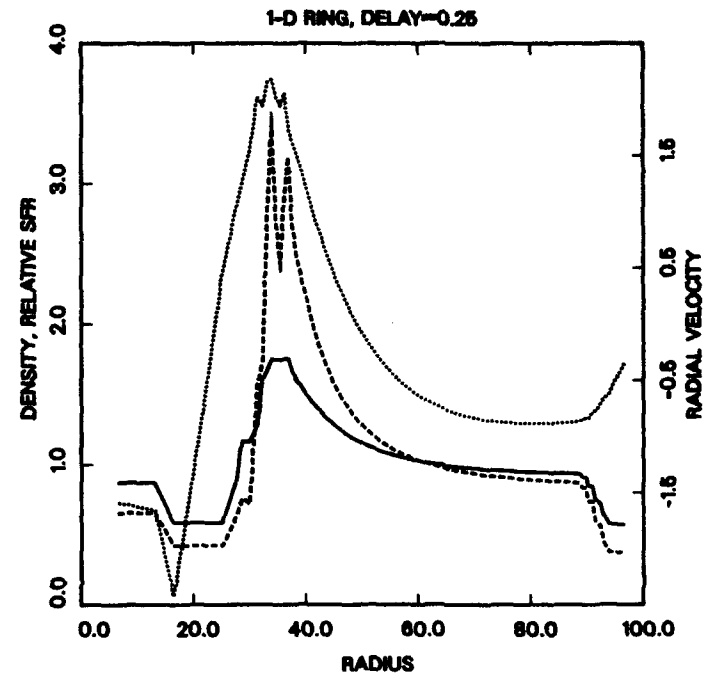

Figure 5. Radial profiles of gas mass density (solid curve), star formation function f_{SF} (dashed curve), and radial velocity (dotted curve) from a one-dimensional hydrodynamic ring galaxy calculation, with parameter T=0.3 T_{cr} initially, are shown at a representative time after the collision. All quantities are dimensionless, with ρ and f_{SF} normalized to their initial values, radius measured in units of equilibrium cloud mean free path, and radial velocity measured in free paths per mean collision time.

Figure 6. Radial profiles as in Fig. 5, but for a calculation with T=0.75 T_{cr} initially, i.e. with a gas density near to the critical value for the limit cycle-starburst bifurcation.

and, at late times, infall behind the ring into a second ring. Secondly, the density profiles show that most of the density variations are limited to within a factor of two of the initial value. This is one indication of the fact that the ring propagates through the gas; it is not a shell.

These comments on the density structure also provide a starting place for studying the star formation in the first or primary ring. It is clear from Figure 5 that the enhancement of the SFR in the primary ring is also typically no more than a factor of a few. A relatively small increase is expected on the basis of the closed box results: since the density increase is about a factor of two, the time delay parameter only increases through the density wave from 0.3 to about 0.6 of the critical value for the starburst bifurcation, so we expect rapid damping to equilibrium following a disturbance.

The situation in Figure 6 is quite different. Shortly after its appearance in this case, the primary ring exceeds the density enhancement factor of 4/3 needed to increase the time delay parameter beyond the critical value. Interestingly, the ring does not burst immediately. The disturbance is still modest, and we expect that, in the analogous closed box case, the system would execute several cycles of a growing oscillation to evolve from near the (now unstable) equilibrium out to the limit cycle. From the double-peaked structure of the star formation profile at the intermediate time shown in Figure 6 we see evidence of such an oscillation. At that time, it appears that a given fluid element passes out of the overdensity part of the wave, into the rarefaction zone where $T<T_{cr}$, before it can 'grow' a burst. The multiple peak structure is interesting in its own right, since several rings seem to show such small-scale filagree.

Later in the run the density profile steepens, making for a more unstable cloud system and a stronger disturbance (see Struck-Marcell and Appleton in preparation). The result is a starburst near the peak of the wave, with echo bursts behind, each with decreasing amplitude as the density decreases. The energy input from the bursts generates significant pressure, which begins to effect the density wave profile.

Up to this point, the simple closed box model has proved to be a useful tool for helping to understand the numerical hydrodynamic calculations, at least qualitatively. At the same time, the numerical hydrodynamics reaffirms, in a more general context, the existence of the starburst bifurcation, which was discovered in the closed box. However, the hydrodynamic flows are fairly modest at the times shown in Figures 5 and 6, at least in the primary ring.

Once the primary ring has propagated through a good fraction of the disk, a second ring forms and begins to move outward. It is apparent in Figures 5 and 6 that the infall velocities generated in the rarefaction behind the primary ring are larger than those in front of the primary. In this case the hydrodynamic flow times can become comparable to cloud interaction timescales, and the closed box analogue without external driving may no longer be very accurate (Appleton and Struck-Marcell 1986b). Thus, the compression is larger in the second ring, and the density enhancement soon exceeds that in the primary, leading to strongly enhanced star formation or bursts.

It is an interesting question whether third, fourth, etc. rings can form. We do not have a definitive answer at this time, but we know that the radial oscillation period of an individual fluid element is roughly equal to its free-fall time, which decreases with radius. Thus, the oscillations of adjacent fluid elements (or stars) grow progressively out of phase. This dispersion, coupled with dissipation damping, and the additional incoherence due to the pressure waves generated by starbursts will cancel out the coherent radial waves fairly rapidly.

The models above provide information on the spatial distribution of relative SFR, which may be usefully compared to optical observations and radio continuum maps. However, if there is substantial obscuration, the optical observations may not reveal all of the star formation. On the other hand, many of the nearby rings were detected at 60 and 100 μm by IRAS, although with its large beam size IRAS can provide no spatial resolution. The IRAS observations show that the integrated FIR luminosity of the rings is typically 2-6 times that of normal galaxies (see Appleton and Struck-Marcell 1986b). Are the models consistent with this result? To provide a partial answer to this question we integrate the SFR over the disk and compare to the initial unperturbed disk. Of course, the result of this integration depends on the choice of the outer radius (and on the value of the parameter m_{SF}/m_o), so it can only provide an estimate.

The first result of this integration exercise is that if the ring bursts, the net SFR can in fact reach a value of a few to 10 times the initial value. Most of this star formation does originate in the ring(s). Moreover, the models imply that to get a strongly enhanced net SFR requires a burst in a ring to offset the suppression in rarefaction regions. Such bursts can only occur in the model if there is a finite time delay, i.e. only if the local gas densities are sufficiently large.

D. Two-Dimensional Calculations

In order to treat more realistically the propagation of the density wave within a differentially rotating disk galaxy we have performed somewhat simplified cloud fluid calculations in two-dimensions. We consider both centered and off-center collisions of the companion with the disk (see Appleton and Struck-Marcell 1986b for details). The principal difference between the one- and two-dimensional calculations is the transport of angular momentum within the ring which leads to more compression of the outer edge of the ring and to stronger rarefaction behind the ring. Interesting behavior of the cloud fluid is found when the ring compression timescale becomes comparable with the cloud collision time. Even in the case when the massive cloud lifetime is zero (instantaneous cloud recycling), the models show that significant differences can exist between the spatial distribution of newly formed stars and the amplitude to the density wave. The situation is even more interesting when the amplitude of the density wave varies with position around the ring, as in the off-center collisions. As an example we show in Figure 7 the star formation rate distribution resulting from an off-center collision of a 1/5 mass companion galaxy. Observations of SFRs around off-center ring galaxies will be an important test of the cloud fluid models.

In the future, we plan to include the full set of Oort cycle interactions in the two-dimensional calculations. Eventually, we also intend to incorporate

a better treatment of the stellar gravity, and more realistic modeling of cloud interactions (e.g. of the processes wind-driven fragmentation and magnetic dissipation) in the cloud fluid equations.

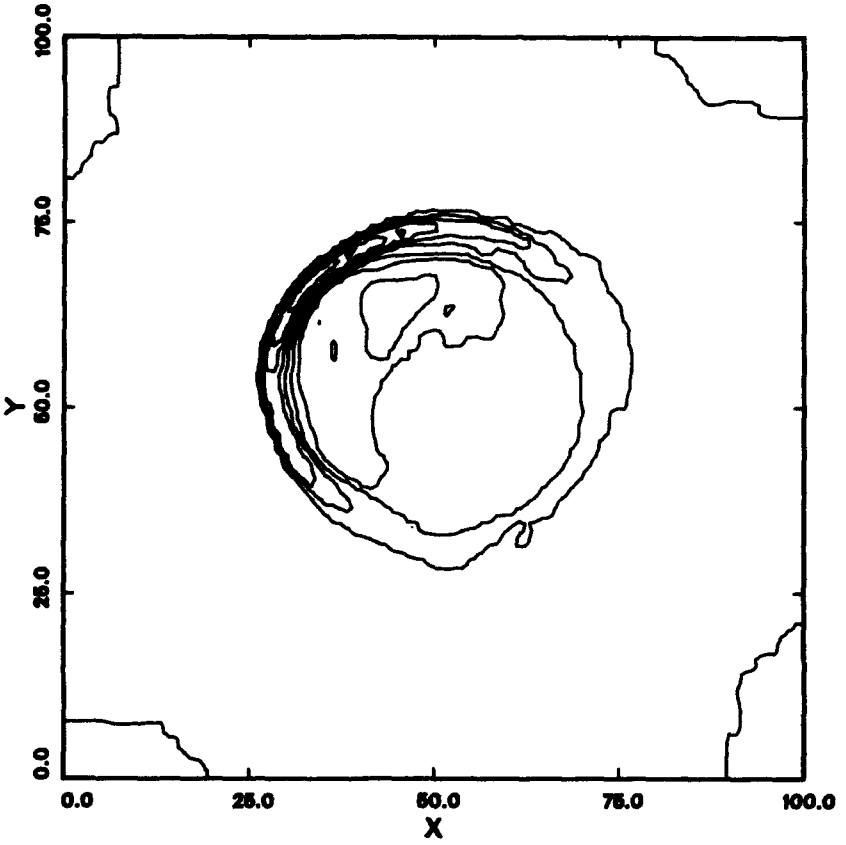

Figure 7. Contours of the star formation function f_{SF} from a two-dimensional hydrodynamic calculation of an off-center collision. As in collisions along the symmetry axis, star formation is clearly concentrated in a ring. However, in this case the ring is noncircular, and the star formation varies strongly with angle around the ring. The base level of the contours is $f_{SF}/f_{SF}^{o} = 0.5$, with increments of 1.0.

V. CONCLUSION: BEYOND RINGS

In conclusion, we recall that the arguments for studying ring galaxies were not only based on their intrinsic interest, but also in the hope that they might serve as a representative of many types of tidal interaction. This notion is a potentially rich vein that we have hardly begun to mine. There are some direct applications of course. Ring formation is probably the beginning of a small

impact parameter galaxy merger. The evolution from ring to completed merger could be explored by putting the companion in the ring calculations in a damping orbit, allowing multiple, nonimpulsive encounters. The elliptical rings produced in off-center collisions are first cousins to interaction-induced spiral waves. More specifically, we might hope that the results above on star formation in rings can be extended to arbitrary density waves.

The Oort model results suggest that, in general, the nature of the star formation and dynamics of a local cloud system will depend on which of several important timescales are commensurate. The first two of these timescales are the cloud collision time and the massive cloud lifetime. The former is basically the relaxation time of a dissipative cloud system, while the ratio of the latter to the former, T, provides a measure of the instability of the system. It was found in both the general applications, that above a critical value, T_{cr}, there is no longer a single stable equilibrium state, instead the system tends to 'relax' to an oscillatory attractor in phase space. A third timescale is the local dynamical or flow time, which is typically of the order as the local free-fall time. A fourth timescale, which is closely related to the third in many cases, is the global dynamical timescale, e.g. the time between perigalactic passages of a bound companion. If the local cloud environment is effected by strong disturbances, these timescales can be roughly commensurate with the cloud collision time, and the local cloud system can be forced far out of equilibrium. Even if the time delay parameter is small, so that the system is not unstable to oscillatory behavior, this nonequilibrium behavior can yield enhancements or suppressions of star formation, which do not necessarily correspond to the peaks and valleys in the gas density. If, however, all of the first three or all four of the timescales are comparable, then the system is driven relative to an 'equilibrium' that is inherently oscillatory. In this case, depending on the regularity of the driving forces relative to the natural system oscillation time, the dynamical evolution can appear quite stochastic.

Such behavior seems likely in strong interactions and mergers. In the burst regime of the model in general, and in the case of commensurate large-scale dynamical and cloud system timescales in particular, the dispersion in SFR, as a function of gas density for example, is large. Hopefully, these timescale considerations will be useful in interpreting observations, though the task will be complex.

Finally, these results suggest answers to some of the questions posed in the introduction, at least within the context of the Oort model. The mechanism of starbursts is the limit cycle bifurcation, or coalescence overshoot instability, which is a qualitatively different process than 'normal', equilibrium star formation. Unfortunately, the possibility of driven, nonequilibrium behavior superimposed on the limit cycle may confuse the application of this result to complex systems. However, a number of interesting comparisons between theory and observation should be possible in the simpler cases, like the ring galaxies.

The canonical description of the ring galaxies is that they are like dropping a pebble in a pond. For strongly interacting galaxies in general, the models suggest a better analogy might be to a storm at sea, with starbursts as the froth of a breaking wave.

REFERENCES

Appleton, P. N., and Struck-Marcell, C. 1986a, Ap. J. accepted for publication.
_____ 1986b, preprint.
Appleton, P. N., Struck-Marcell, C., and Foster, P. A. 1985, in Cosmical Gas Dynamics, ed. F. D. Kahn (Dordrecht: VNU Science Press).
Balzano, V. A. 1983, Ap. J. 268, 602.
Bania, T. M., and Lyon, J. G. 1980, Ap. J. 239, 173.
Bodifee, G., and de Loore, C. 1985, Astr. Ap. 142, 297.
Book, D. L. 1981, Finite Difference Techniques for Vectorized Fluid Mechanics, (New York: Springer-Verlag).
Casoli, F., and Combes, F. 1982, Astr. Ap. 110, 287.
Chiang, W.-H., and Prendergast, K. H. 1985, Ap. J. 297, 507.
Clifford, P. J. 1984, M.N.R.A.S. 211, 125.
_____ 1985, M.N.R.A.S. 216, 93.
Clifford, P. J., and Elmegreen, B. G. 1983, M.N.R.A.S. 202, 629.
Combes, F. and Gerin, M. 1985, Astr. Ap. 150, 327.
Elmegreen, B. G. 1985, Ap. J. 299, 196.
_____ 1986, in Star Forming Regions, I.A.U. Symp. 115, ed. M. Peimbert and J. Jugaku (Dordrecht: Reidel).
Few, J. M. A., Madore, B. F., and Arp. H. C. 1982, M.N.R.A.S. 199, 633.
Field, G. B., and Saslaw, W. C. 1965, Ap. J. 142, 568.
Fosbury, R. A. E., and Hawarden, T. G. 1977, M.N.R.A.S. 178, 473.
Gallagher, J. S., and Hunter, D. A. 1984, Ann. Rev. Astr. Ap. 22, 37.
Ghigo, F., Hine, B. P., III, and van der Hulst, J. M. 1986, preprint.
Gilden, D. L. 1984, Ap. J. 279, 335.
Hausman, M. A. 1982, Ap. J. 261, 532.
Hausman, M. A., and Roberts, W. W. 1984, Ap. J. 282, 106.
Hunter, J. H., Jr., Sandford, M. T., II, Whitaker, R. W., and Klein, R. I. 1986, Ap. J. 305, 309.
Icke, V. 1985, Astr. Ap. 144, 115.
Ikeuchi, S., Habe, A., and Tanaka, Y. D. 1984, M.N.R.A.S. 207, 909.
Joseph, R. D., and Wright, G. S. 1985, M.N.R.A.S. 214, 87.
Keel, W. C., Kennicutt, R. C., Hummel, E., and van der Hulst, J. M. 1985, Astron. J. 90, 708.
Knapp, G. R., Phillips, T. G., Huggins, P. J., Leighton, R. B., and Wannier, P. G. 1980. Ap. J. 240, 60.
Kwan, J., and Valdes, F. 1983, Ap. J. 271, 604.
Larson, R. B. 1969, M.N.R.A.S. 145, 405.
_____ 1974, M.N.R.A.S. 166, 585.
_____ 1975, M.N.R.A.S. 173, 671.
_____ 1976, M.N.R.A.S. 176, 31.
Larson, R. B., and Tinsley, B. M. 1978, Ap. J. 219, 46.
Lattanzio, J. C., Monaghan, J. J., Prongracic, H. and Schwarz, M. P. 1985, M.N.R.A.S. 215, 125.
Leisawitz, D. 1985, unpublished Ph.D. thesis, University of Texas.
Lewis, B. M. 1984, Ap. J. 285, 453.
Lonsdale, C. J., Helou, G., Good, J. C., and Rice, W. 1985, Catalogued Galaxies and Quasars in the IRAS Survey, Jet Propulsion Laboratory, Pasadena.
Loose, H., Krugel, E., and Tutukov, A. 1982, Astr. Ap. 105, 342.
McKee, C. F., and Ostriker, J. P. 1977, Ap. J. 218, 148.

Noguchi, M., and Ishibashi, S. 1986, M.N.R.A.S. 219, 305.
Olofsson, H., and Rydbeck, G. 1984, Astr. Ap. 136, 17.
Rieke, G. H., Lebofsky, M. J., Thompson, R. I., Low, F. J., and Tokunaga, A. T. 1980, Ap. J. 238, 24.
Roberts, W. W., and Hausman, M. A. 1984, Ap. J. 277, 744.
Romanishin, W., Krumm, N., Salpeter, E. E., Knapp, G. R., Strom, K. M., and Strom, S. E. 1982, Ap. J. 263, 94.
Sanders, D. B., and Mirabel, I. F. 1985, Ap. J. Letts. 298, L31.
Sanders, D. B., Scoville, N. Z., Young, J. S., Soifer, B. T., Schloerb, F. P., Rice, W. L., and Danielson, G. E. 1986, Ap. J. Letts. 305, L45.
Sargent, W. L. W., and Searle, L. 1970, Ap. J. Letts. 162, L155.
Scalo, J. M. 1985, in Protostars and Planets II, eds. D. C. Black and M. S. Mathews (Tucson: University of Arizona Press).
Scalo, J. M., and Struck-Marcell, C. 1984, Ap. J. 276, 60.
_____ 1986, Ap. J. 301, 77.
Schommer, R. A., and Bothun, G. D. 1983, Astron. J. 88, 577.
Schweizer, F. 1986, Science 231, 227.
Seiden, P. E., and Gerola, H. 1982, Funds. Cosmic. Phys. 7, 241.
Stark, A. A. 1982, in Extragalactic Molecules, N.R.A.O. Workshop, eds. L. Blitz and M. Kutner (Charlottesville: N.R.A.O.), pp.77-85.
Struck-Marcell, C., and Scalo, J. M. 1986, Ap. J., submitted.
Struck-Marcell, C., and Tinsley, B. M., 1978, Ap. J. 221, 562.
Taylor, K., and Atherton, P. D. 1984, M.N.R.A.S. 208, 601.
Telesco, C. M, 1983, in Edinburgh Star Formation Workshop, ed. R. D. Wolstencroft (Edinburgh: Royal Observatory) pg. 183.
Theys, J. C., and Spiegel, E. A. 1977, Ap. J. 212, 616.
Thuan, T. X., and Seitzer, P. O. 1979, Ap. J. 231, 680.
Tomisaka, K. 1984, P.A.S. Japan 36, 457.
Toomre, A. 1978, in The Large-scale Structure of the Universe, eds. M. S. Longair and J. Einasto (Dordrecht: Reidel) pg. 109.
Unger, S. W., Pedlar, A., Axon, D. J., Wilkinson, P. N., and Appleton, P. N. 1984, M.N.R.A.S. 211, 783.
van den Bergh, S. 1977, in The Evolution of Galaxies and Stellar Populations, eds. B. M. Tinsley and R. B. Larson (New Haven, Yale Observatory) p. 19-37.
Young, J. S., Schloerb, F. P., Kenney, J. D., and Lord, S. D. 1986, Ap. J. 304, 443.

Gallagher: Is there a regime where the model breaks down due to energy input by stars formed in a major burst?

Struck-Marcell: It is possible that in a violent burst most of the clouds are broken down completely, and all the material distributed more uniformly in an intercloud phase (e.g. Ikeuchi et al. 1984, and Bodifee and de Loore 1985). In the Oort model discussed here, there is a breakdown of the system into a large number of very low mass clouds following a strong burst. The clouds regrow by coalescence on a long timescale. It is tempting to think that this is at least part of the explanation for the tiny molecular clouds in the core of M82.

Begelman: What is your prescription for injecting kinetic energy into the clouds? Are your results sensitive to the details of this prescription?

Struck-Marcell: At the end of its lifetime a massive cloud is supposed to break up into N_c fragments, which fly off in random directions with a mean velocity dispersion c_{B_3}. The generic behavior of the model is not sensitive to the precise value of any parameter except the ratio of the cloud lifetime to the collision time, T. However, the quantities N_c, c_{B_3} are not allowed to vary freely, but are tied to the equilibrium values of the model and the dissipation efficiency, since dissipation balances energy input in equilibrium.

STARBURST-DRIVEN SUPERWINDS FROM INFRARED GALAXIES

Timothy M. Heckman and Lee Armus
Astronomy Program, University of Maryland
College Park, MD 20742

Patrick McCarthy and Wil van Breugel
Dept. of Astronomy, University of California
Berkeley, CA 94720

George K. Miley
Space Telescope Science Institute
Homewood Campus
Baltimore, MD 21218

ABSTRACT

We present new data that indicate that strong far-infrared galaxies commonly have largescale emission-line nebulae whose properties are suggestive of mass outflows ("superwinds"), presumably driven by the high supernova rate associated with the central starburst. These data include longslit spectra of M82 which show that the radial variation of the gas pressure in the emission-line nebula is in excellent agreement with the Chevalier and Clegg (1985) wind model. The M82 nebula also has a LINER spectrum, consistent with shock-heating. We find morphologically and spectroscopically similar emission-line nebulae in NGC253 (associated with the diffuse X-ray gas along the galaxy minor axis), and in Arp220 and NGC6240 (where the nebulae are tens of kpc in size). We have also conducted a longslit spectroscopic investigation of 20 additional very powerful (~ 10E12 L(sun)) far-infrared galaxies and find that they generally have spatially-extended emission-line nebulae whose spectra closely resemble that of the M82 nebula. If the "superwind" interpretation is correct, it could have many important consequences in extragalactic astronomy.

1. INTRODUCTION

The discovery of a class of galaxies with far-infrared luminosities of 10E11 to 10E12 L(sun) - 10 to 100 times larger than the corresponding optical luminosities - is probably the most significant extragalactic discovery made by IRAS. While these far-infrared galaxies ("FIRG's") are the subject of intense scientific scrutiny, the most fundamental questions are not yet answered: What powers the strong far-infrared emission? How are the observed optical emission-lines and nonthermal radio continuum emission related to the infrared power-source? What is the impact of the prodigious release of energy on the surrounding galaxy? The answers to these questions are likely to prove of considerable value to our quest to understand star formation, galaxy formation and evolution, and the nature of nuclear activity in galaxies.

In order to address these questions, we have embarked on two related investigations of FIRG's. The first is a detailed study of the physical state, kinematics, and morphology of the emission-line nebulae associated with the nearest FIRG's. The second is a systematic spectroscopic and direct imaging survey of a moderately large sample of optically faint IRAS galaxies with very powerful infrared emission. As we will discuss below, the data we have

Carol J. Lonsdale Persson (Editor)
Star Formation in Galaxies

collected so far strongly suggest that FIRG's are commonly associated with largescale mass outflows ("superwinds") of the kind hypothesized by Chevalier and Clegg (1985-hereafter CC). Further details concerning our data and their interpretation can be found in Heckman, Armus, and Miley (1986) and McCarthy, Heckman, and van Breugel (1986).

2. THE MODEL

We begin by briefly summarizing the model that will serve as the interpretational framework for the data we will present and review in section 3. This model was originally proposed by CC to account for the X-ray and emission-line nebula associated with the prototypical FIRG, M82.

The starburst underway in the circumnuclear (100 to 1000 pc-scale) molecular disk of M82 implies a high supernova rate. CC hypothesize that the kinetic energy of the supernova ejecta is efficiently thermalized as remnants intersect one another at high velocities, producing a central cavity of hot gas which then expands outward in the form of a fast (several*10E3 km/sec) wind. While the CC model is for a spherically-symmetric wind, both the data (see below) and physical intuition suggest that a bipolar wind will be produced as the hot gas preferentially escapes along the rotation axis of the circumnuclear disk. In the CC model the wind material itself is a negligible source of radiation. The nebula in M82 is instead produced by shock-heated clouds that have been entrained in the wind.

3. THE DATA

3.1. M82

As the nearest and best-studied FIRG, M82 is the "Rosetta Stone" for the wind model described above. We will therefore summarize all the relevant observational evidence, including the new results from our long-slit spectroscopic investigation.

First, as emphasized by CC, both the starburst models of Rieke et al. (1980) and the population of compact time-variable radio sources observed by Kronberg et al. (1985) imply that supernovae are occuring in M82 at the rate of one every several years.

Second, recent high-resolution CO maps of M82 (e.g. Nakai 1984) show clear evidence for a central cavity in the circumnuclear molecular disk (the "nozzle" for the wind). The molecular annulus is coincident with the region of intense infrared and radio emission, and is apparently coplanar with the largescale stellar disk of M82.

Third, both the well-known emission-line nebula and the cospatial X-ray nebula (Watson et al. 1984) are oriented perpendicular to the molecular annulus (they lie along the galaxy's minor axis).

Fourth, the kinematics of the emission-line gas in the M82 nebula are strongly suggestive of high-speed outflow (Axon and Taylor 1978; J. Bland and R.B. Tully, private communication).

Fifth, our new spectroscopy shows that the pressure in the emission-line

nebula falls smoothly and monotonically with radius (see Fig. 1). The form of P(r) is in excellent agreement with the predictions of the CC model. Moreover, the pressures in the emission-line gas agree with those estimated in the X-ray gas. We note that this directly observed radial variation in gas pressure rules out models in which most of the optical line-emission in M82 is dust-scattered nuclear light.

Finally, our new data also demonstrate that the M82 nebula has a LINER spectrum, very similar to the emission-line spectra of gas heated by shocks (e.g. old supernova remnants - see Table I).

Thus, the available data on M82 provide evidence for the supernovae to drive the wind, for the nozzle to channel the wind, and for the shock-heated material which traces the wind's passage and probes its physical properties.

Table I
Emission-Line Ratios in Far-Infrared Galaxies

(1) Name	(2) [OIII]/Hβ	(3) [OI]/Hα	(4) [NII]/Hα	(5) [SII]/Hα
SNR's	0.0 to 0.6	-1.1 to -0.3	-0.5 to 0.1	-0.4 to 0.2
Shock Model	0.2	-1.1	-0.2	-0.2
M82 Nebula	-0.1	-1.1	-0.4	-0.4
NGC253	-0.5	?	0.0	-0.3
Arp220	0.2	-0.7	0.0	-0.2
NGC6240	0.2	-0.6	0.0	-0.1
FIRG Sample	-0.2 to 0.6	-1.5 to -0.5	-0.5 to 0.1	-0.6 to 0.0

Notes to Table I.

Col. 1) Supernova remnants (SNR's) from Dopita et al. (1984) and references therein. The Shock Model line ratios are the average of models B and C in Raymond (1979) and models D and E in Shull and McKee (1979). The FIRG Sample is described in section 3.4 in the text.
Cols. 2-5) The logarithmic ratios of the fluxes of the [OIII]λ5007 and Hβ; [OI]λ6300 and Hα; [NII]λ6583 and Hα; [SII]λ6717+6731 and Hα lines.

3.2 NGC253

NGC253 is nearly a perfect match to M82 in both its distance and far-infrared luminosity. As such, it provides an important test of the generality of the phenomena discussed above. Like M82, NGC253 has i) a central circumnuclear molecular disk which is coincident with the region of intense infrared and radio emission (Scoville et al. 1985; Turner and Ho 1983), ii) an X-ray nebula extending along the galaxy minor axis (Fabbiano and Trinchieri 1984), and iii) a region of high-velocity outflow seen in the optical emission-line gas (e.g. Ulrich 1978).

Our new data considerably strengthen the resemblance between NGC253 and

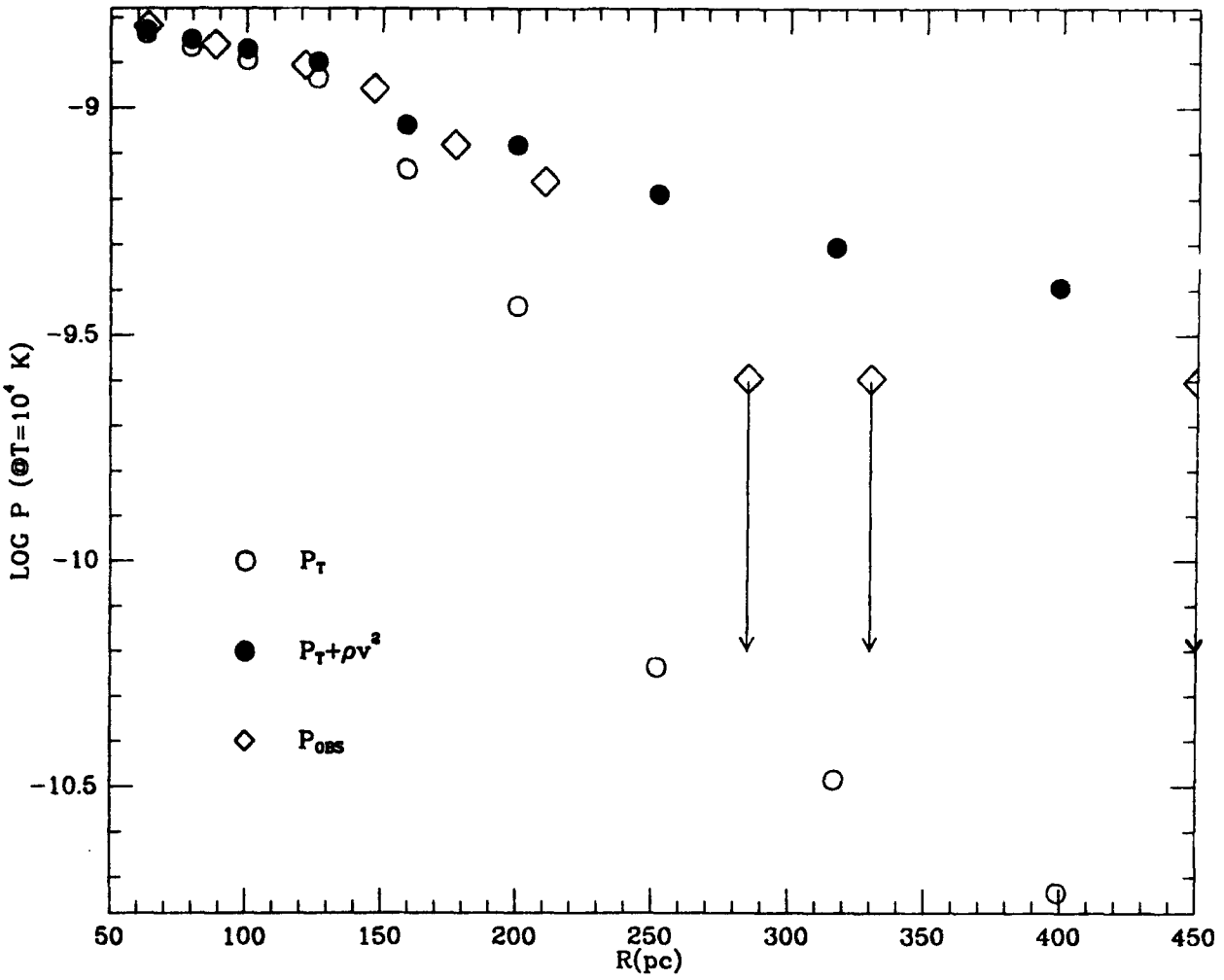

Figure 1. The observed radial dependence of the gas pressure in the M82 nebula (=2nkT, where n is the electron density as measured by the red [SII] lines and T is taken to be 10,000K) is plotted along with the predicted thermal and total (ram plus thermal) pressures in the wind model calculations of Chevalier and Clegg (1985). A best fit between the model and the data is achieved if the pressures are a factor of 5 below the maximum values allowed by the model (as shown).

M82. A narrowband (H-alpha) image shows that there is a striking morphological relationship between the optical and X-ray emitting gas along the minor axis, as in M82 (see McCarthy, Heckman, and van Breugel 1986). Moreover (again as in M82), this gas has a LINER spectrum, suggestive of shock-heating (Table I).

3.3 Arp220 and NGC6240

These galaxies are two of the closest examples of the class of very-powerful FIRG's, having luminosities one to two orders-of-magnitude larger than M82 or NGC253. Rieke et al. (1985) have recently shown that many of their properties can be explained by a scaled-up version of the starburst models they had successfully applied to M82 and NGC253.

Our new narrowband (H-alpha) images and longslit spectra suggest that superwinds are also occurring in these two FIRG's. Large (tens of kpc) and morphologically spectacular emission-line nebulae are present in both galaxies (see Figs. 2 and 3). The Arp220 nebula is strongly bipolar in appearance, consisting of a bright central "jet" and faint outer "bubbles". The inner feature is oriented roughly perpendicular to the central dust-lane in Arp220. The NGC6240 nebula is more complex, with a bright central "starfish" elongated along the galaxy's minor axis, and an outer region of filaments and arcs.

Both nebulae have classic LINER spectra, at least in the bright inner "jet" and "starfish" (Table I). They are thus similar to the M82 and NGC253 nebulae both spectroscopically and morphologically. Little is yet known concerning the kinematics of the gas in Arp220 and NGC6240, however high velocity (several hundreds of km/sec) noncircular gas motions are clearly present in both galaxies (see Table 2 in Heckman et al. 1986 and related discussion).

3.4 A Survey of Very Powerful FIRG's

We have recently undertaken a spectroscopic and multi-color direct imaging survey of a sample of optically-faint IRAS sources chosen to have the same far-infrared spectral-energy-distribution as Arp220 and NGC6240. Our principle results of special relevance to the present discussion are as follows:

First, most of the 20 galaxies observed spectroscopically resemble the M82 nebula (see Table I). About half can be comfortably classifed as LINER's, while most of the rest have spectra that are intermediate between a LINER and an HII region.

Second, the emission-line regions are often spatially resolved, and several nebulae are larger than 10 kpc in size. We have just begun a narrowband imaging program to determine the statistical properties of these nebulae.

Third, as is apparently the case for FIRG's in general, the galaxies are generally very disturbed in their optical morphology, suggesting that galaxy collisions/mergers are important in the FIRG phenomenon.

4. IMPLICATIONS

The evidence summarized above implies that the CC model for largescale

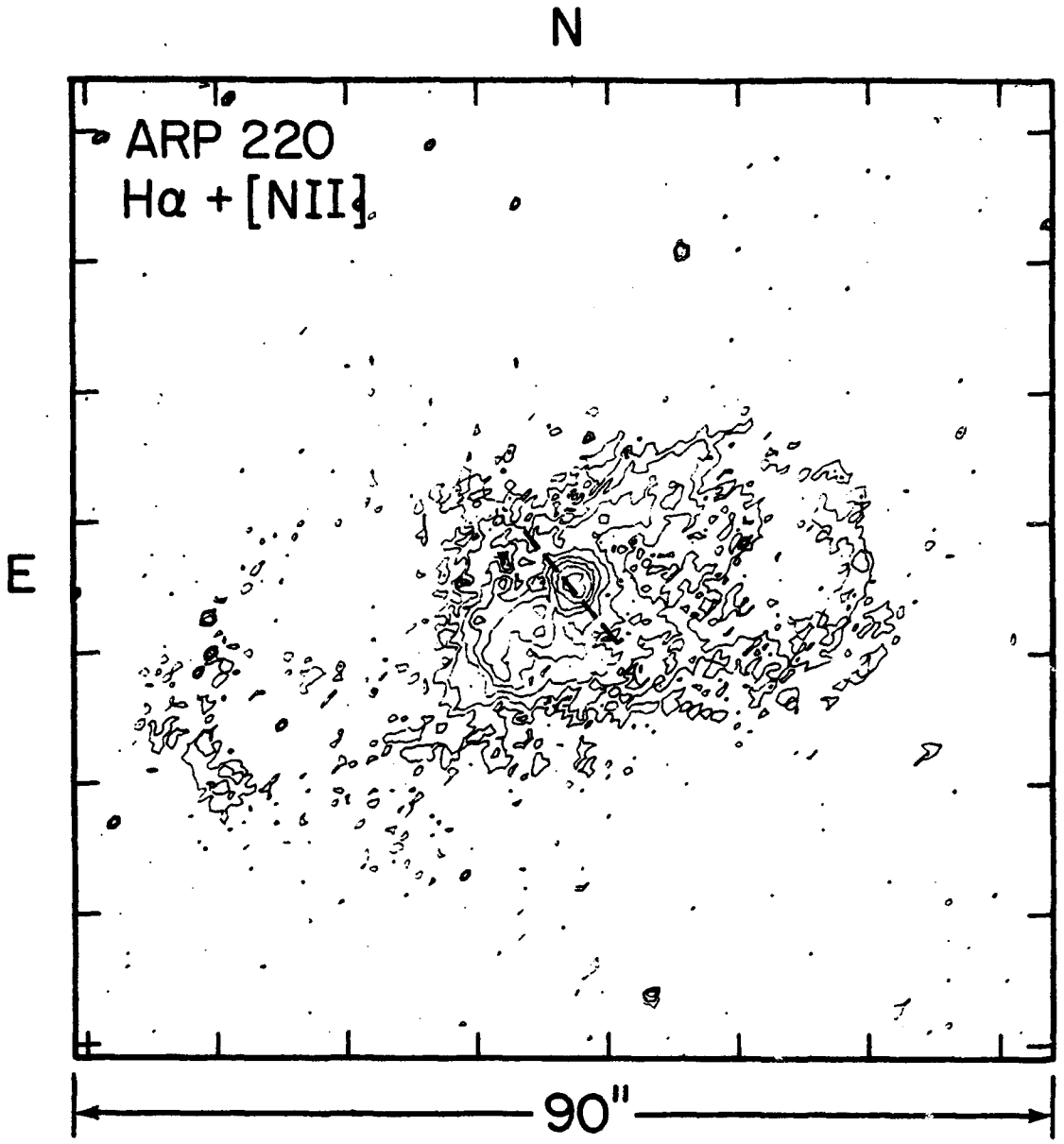

Figure 2. Contour plot of a continuum-subtracted H-Alpha image of Arp220. The first contour is at a surface brightness of 3.4E-17 ergs/(cm**2 sec arcsec**2) and each subsequent contour is at a factor 2 higher brightness. The dashed diagonal line represents the orientation of the central dust lane in Arp220.

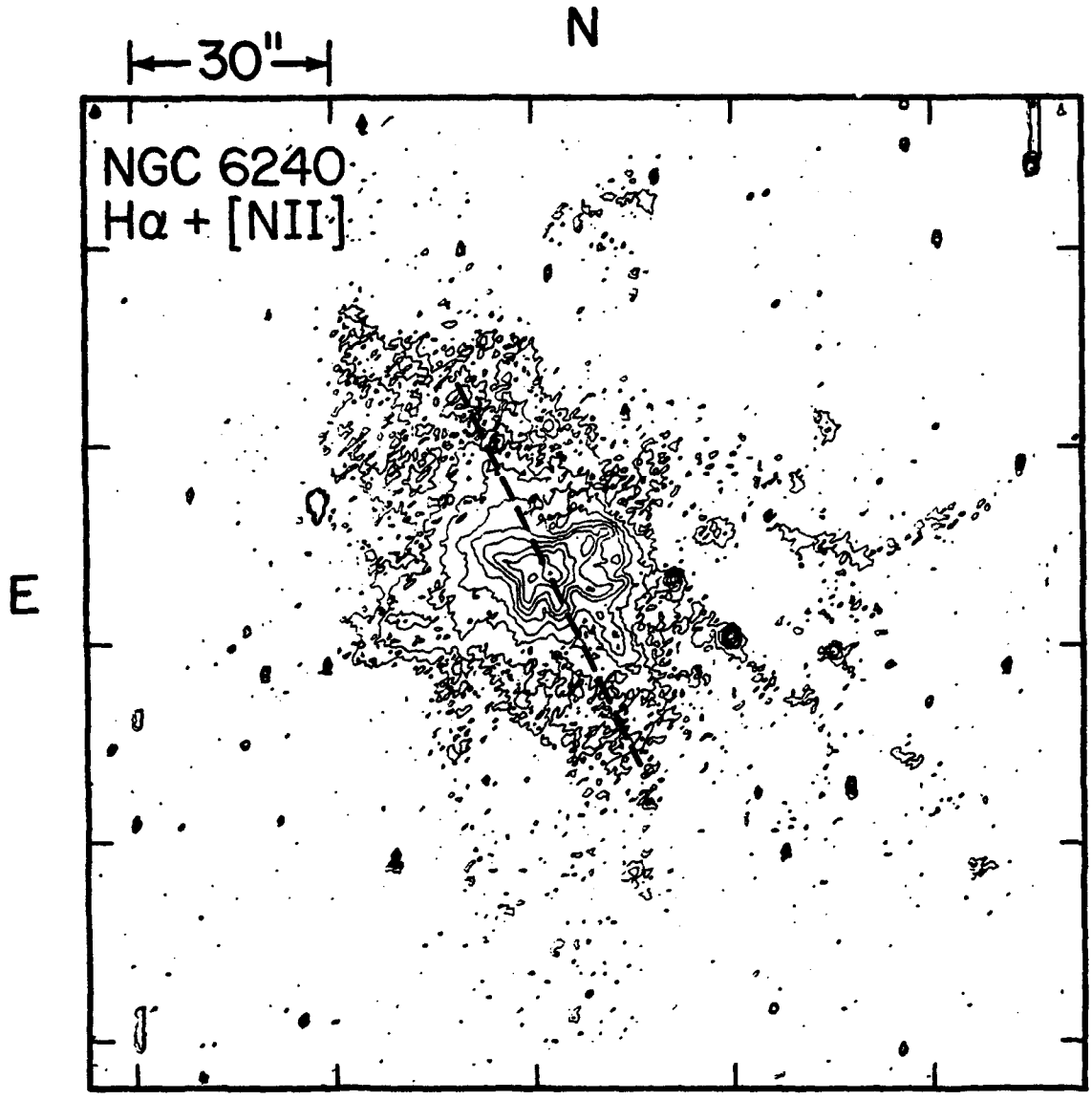

Figure 3. Contour plot of a continuum-subtracted H-Alpha image of NGC6240. The first contour is at a surface brightness of 6.6E-17 ergs/(cm**2 sec arcsec**2) and each subsequent contour is at a factor 2 higher brightness. The dashed diagonal line represents the orientation of the major axis of NGC6240.

mass outflows (superwinds) driven by circumnuclear starbursts may have general applicability to powerful far-infrared galaxies. If so, this will have many far-reaching implications.

Simply scaling the CC wind parameters for M82 by the far-infrared luminosity would mean that the superwinds in galaxies like NGC6240 and Arp220 have mass fluxes of 10 to 100 M(sun)/year of highly enriched material and kinetic energy fluxes of 10E44 to 10E45 ergs/sec. If, as suggested by the models of Rieke et al. (1980, 1985), starbursts last for about 10E8 years, then these galaxies will inject 10E9 to 10E10 M(sun) and 10E60 ergs into the intergalactic medium.

The consequences of the superwind model (if it is correct) may be profound for our understanding of galaxy formation, the chemical and thermal evolution of the intergalactic and interstellar media, the nature of QSO absorption-line clouds, and many related topics. The main need at present is to place the model on a more secure observational footing by combining detailed investigations of the nearest examples of possible superwinds with continued survey work on a large sample of FIRG's. Such work is underway.

REFERENCES

Axon, D.J., and Taylor, K. 1978, Nature, 274, 37.

Chevalier, R.A., and Clegg, A.W. 1985, Nature, 317, 44.

Dopita, M.A., Binette, L., D'Odorico, S., and Benvenuti, P. 1984, Ap. J., 276, 653.

Fabbiano, G., and Trinchieri, G. 1984, Ap. J., 286, 491.

Heckman, T.M., Armus, L., and Miley, G.K. 1986, submitted to A.J.

Heckman, T.M., Beckwith, S., Blitz, L., Skrutskie, M., and Wilson, A.S. 1986, Ap. J., 305, 157.

Kronberg, P.P., Biermann, P., and Schwab, F.R. 1985, Ap. J. 291, 693.

McCarthy, P., Heckman, T.M., and van Breugel, W.J.M. 1986, submitted to A.J.

Nakai, N. 1984, Ph.D. thesis, Univ. of Tokyo.

Raymond, J.C. 1979, Ap. J. Suppl., 39, 1.

Rieke, G.H., Lebofsky, M.J., Thompson, R.I., Low, F.J., and Tokanaga, A.T. 1980, Ap. J., 238, 24.

Rieke, G.H., Cutri, R.M., Black, J.H., Kailey, W.F., McAlary, C.W., Lebofsky, M.J., and Elston, R. 1985, Ap. J., 290, 116.

Scoville, N.Z., Soifer, B.T., Neugebauer, G., Young, J.S., Matthews, K., and Yerka, J. 1985, Ap. J., 289, 129.

Shull, J.M., and McKee, C.F. 1979, Ap. J., 227, 131.

Turner, J.L., and Ho, P.T.P. 1983, Ap. J. Lett., 268, L79.

Ulrich, M.H. 1978, Ap. J., 219, 424.

Watson, M.G., Stanger, V., and Griffiths, R.E. 1984, Ap. J., 286, 144.

DISCUSSION

WINDHORST:

I assume that the shock heated gas implied by your model would produce a fairly hard x-ray spectrum. Would not these star forming galaxies make up for the rest of the hard x-ray background, or even exceed it?

HECKMAN:

The x-ray spectrum need not be very hard, since the x-rays are produced by clouds that are shock-heated by the wind. These clouds will be heated to only modest temperatures ($T \lesssim 10^7$ K) if they are relatively dense.

INTERFEROMETRIC CO OBSERVATIONS OF THE ULTRALUMINOUS IRAS GALAXIES ARP 220, IC 694/NGC 3690, NGC 6240, and NGC 7469[1]

A. I. Sargent, D. B. Sanders, N. Z. Scoville, B. T. Soifer
Division of Physics, Mathematics and Astronomy
California Institute of Technology, Pasadena, CA 91125

ABSTRACT. High resolution CO observations of the IRAS galaxies Arp 220, IC 694/NGC 3690, NGC 6240 and NGC 7469 have been made with the Millimeter Wave Interferometer of the Owens Valley Radio Observatory. These yield spatial information on scales of 1 to 5 kpc and allow the separation of compact condensations from the more extended emission in the galaxies. In the case of the obviously interacting system IC 694/NGC 3690 the contributions of each component can be discerned. For that galaxy, and also for Arp 220, the unusually high luminosities may be produced by non-thermal processes rather than by intense bursts of star formation.

1. INTRODUCTION

IRAS observations have shown that the galaxies Arp 220, IC 694/NGC 3690, NGC 6240 and NGC 7469 are all extremely luminous with $L_{FIR} > 10^{11}$ $L_\odot$ (Sanders and Mirabel 1985). The molecular gas masses, $M(H_2)$, derived from single dish measurements (Sanders and Mirabel 1985) are considerably in excess of 10^9 $M_\odot$. In addition, the ratio $L_{FIR}/M(H_2)$, which can be interpreted as an indicator of star formation efficiency (Sanders *et al.* 1986a), is significantly enhanced. A comparison of the properties of these four galaxies with those of the starburst galaxy M82 is presented in Table I.

TABLE I

Galaxy	D[a] (Mpc)	$M(H_2)$[b] ($10^{10}M_\odot$)	L_{FIR}[b] ($10^{11}L_\odot$)	$L_{FIR}/M(H_2)$[b] ($L_\odot/M_\odot$)
Arp220	77	1.3	13.4	100
NGC6240	101	1.99	5.3	26
NGC7469	66	0.92	2.6	28
NGC3690 | IC694	48	0.73	5.3	72
M82	3	0.17	0.2	12

Notes:
a) Assumes $H_o = 75$ km s^{-1} Mpc^{-1}.
b) From Sanders and Mirabel (1985) and Sanders *et al.* (1986a).

Although the presence of a significant quantity of molecular gas in these galaxies was discernible from the single dish CO observations, their 45" resolution was not sufficiently high to determine the distribution. Here we report 5" resolution, aperture synthesis CO maps of the four galaxies. These

[1] These results are presented in full by Scoville *et al.* (1987) and Sargent *et al.* (1986).

Carol J. Lonsdale Persson (Editor)
Star Formation in Galaxies

observations permit a study of the detailed structure of the molecular gas and the origins of the unusually high luminosities.

2. OBSERVATIONS AND RESULTS

Observations were made in the 2.6 mm CO line, using the Owens Valley Millimeter Wave Interferometer in May, 1986. For each galaxy, two configurations of the three 10.4 meter telescopes were employed, with spacings out to 80 m north-south and 65 m east-west. The shortest projected baseline was 10m, so that the interferometer is insensitive to structures greater than 30" in size. A recently-completed, broad-band filterbank consisting of 32 channels, each 5 MHz wide, provided velocity coverage of 416 km s^{-1}, with 13 km s^{-1} resolution. System temperatures were typically 300 K (SSB).

The resulting contour maps of integrated CO intensity for Arp 220, IC694/NGC3690, and NGC 7469 are shown in Figures 1, 2, and 3, respectively, overlayed on optical images of the galaxies. No emission was detected from NGC 6240 up to a level of 15% of the single dish flux, suggesting that the molecular gas in this galaxy is distributed on scales > 30", rather than being confined to compact structures. In Arp 220 and NGC 7469, the CO emission is unresolved. This is also the case for each of the two compact regions detected in IC 694/NGC 3690. Upper limits to the diameters of the compact sources range from 1 to 2 kpc. Precise values, as well as the fraction of the single dish flux detected by the interferometer, F_i/F_s, are given in Table II. Average densities were calculated assuming a spherical distribution of gas and are also presented in Table II.

Figure 1: Contours of the integrated CO emission in Arp 220 superimposed on an optical photograph of the galaxy. Contour levels are spaced by 12 Jy/beam km s^{-1}, the lowest being 12 Jy/beam km s^{-1}.

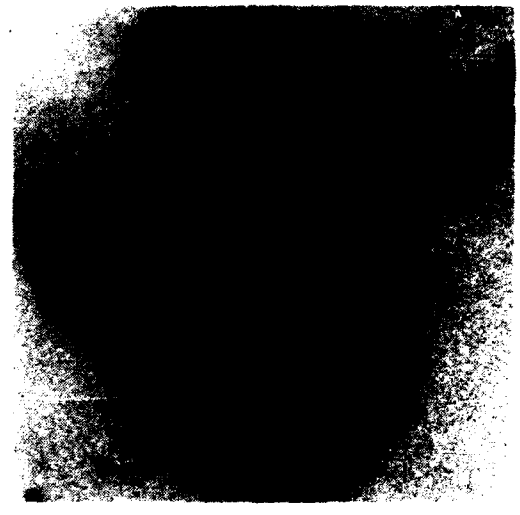

Figure 2: Contours of the integrated CO emission in Arp 299 (IC694–NGC3690) overlayed on an optical photograph of the galaxy. Contour levels begin at, and are spaced by, 10 Jy/beam km s^{-1}.

TABLE II

Galaxy	Phase Center		Beam	Scale	Fi/Fs	$M(H_2)$	N_{H2}
	∝(1950)	δ(1950)		(kpc)		($10^9 M_\odot$)	(cm^{-3})
Arp220	15 32 46.92	23 40 07.9	6".4 × 4".0	1.4	0.7	9.1	130
NGC6240	16 50 28.00	02 09 00.0	7".6 [illegible]	2.2	< 0.15	< 3	< 10
NGC7469	23 00 44.00	08 36 18.0	13".[illegible]	2.0	0.3	2.8	10
NGC3690 / IC694	11 25 42.60	58 50 14.0	8".3 × [illegible].8	1.0	0.5	3.2	70

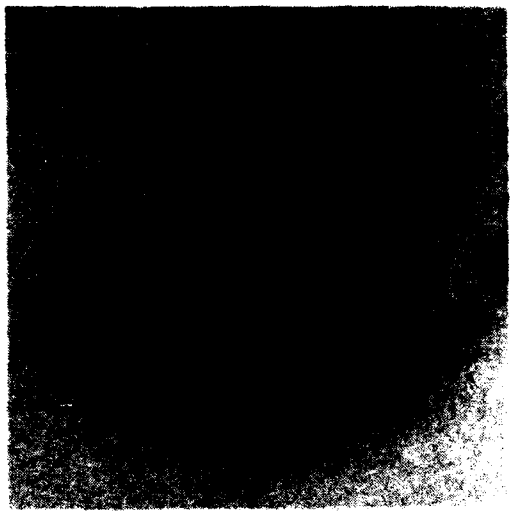

Figure 3: Contours of the integrated CO emission in NGC 7469 superimposed on an optical photograph of the galaxy. Contour levels are spaced by 8 Jy/beam km s^{-1}, the lowest being 8 Jy/beam km s^{-1}.

3. DISCUSSION

3.1. Arp 220

A substantial mass of molecular gas, $\sim 9 \times 10^9$ $M_\odot$, is concentrated in a region of radius < 700 pc at the nucleus of Arp 220 (Figure 1). The minimum mean density is 130 cm^{-3} and the ratio $L_{FIR}/M(H_2)$ is 100 $L_\odot/M_\odot$. The star formation rate could be considerably enhanced as a result of an increased frequency of cloud–cloud collisions (cf. Scoville, Sanders and Clemens 1986), and the unusually high luminosity could be attributable to an intense burst of star formation (cf. Reike *et al.* 1985). However, it has recently been discovered that the spatial extents of the 20 μm and radio continuum emission are comparable, and less than 1.5" (Becklin 1986). This extreme concentration of the infrared and radio emission, the fact that the Br α emission is both unusually broad (de Poy 1986) and much weaker than expected if the luminosity is the result of high mass star formation (Beck, Turner and Ho 1986), the compact, dense molecular core, and the uncommonly high value of $L_{FIR}/M(H_2)$, provide compelling evidence that the energy in Arp 220 derives from non–thermal processes.

3.2. IC 694/NGC 3690

The interacting system Arp 299 comprises the galaxies IC 694 and NGC 3690. In the interferometer maps, two compact CO components were detected (see Figure 2), each of mass $\sim 1.4 \times 10^9 M_\odot$. The eastern component coincides with the nucleus of IC 694 (Telesco, Decher and Gatley 1985) where there is an unresolved, flat spectrum radio source, termed A by Gehrz, Sramek, and Weedman (1983); the western component spans their compact radio components C and C', which span the region where IC 694 and NGC 3690 overlap. Although CO is known to be present at the nucleus of NGC 3690 (Sanders *et al.* 1986b), no emission was detected by the interferometer, indicating that there the molecular gas must be distributed on scales greater than 30".

Observations at 60 and 100 μm, at 20" and 30" resolution respectively (Harper 1984), show that about 75% of the total luminosity from Arp 299 arises from the nucleus of IC 694. If the luminosity source is as concentrated as the CO, $L_{FIR}/M(H_2)$ is ~ 280 $L_\odot/M_\odot$. The H_2 mass in a 16" region centered on this

nucleus is $\sim 2.4 \times 10^9$ $M_\odot$ (Sanders *et al.* 1986b), leading to $L_{FIR}/M(H_2) = 150$ $L_\odot/M_\odot$. These ratios are considerably greater than the values for the Milky Way, ~ 3, and for starburst galaxies, ~ 20 $L_\odot/M_\odot$ (Sanders *et al.* 1986a, Scoville and Good 1986, Young *et al.* 1986). Taken together with the presence of the flat-spectrum radio source at the nucleus, these results strongly suggest that the source of energy in IC 694 may well be nonthermal. By contrast the ratio $L_{FIR}/M(H_2)$ for the remainder of the Arp 299 complex is between 40 and 70 $L_\odot/M_\odot$, indicating that the energy source here is probably massive star formation.

The effect of the interaction between IC694 and NGC3690 appears to have been to channel a substantial mass into the nucleus of IC 694, thereby producing an unusual energy source, probably fuelled by non-thermal processes. It has also induced increased density and, by implication, enhanced star forming activity in the region of overlap between the two galaxies.

3.3. NGC 7469

NGC 7469 is a type 1 Seyfert galaxy. From Figure 3, it is evident that the one CO source detected is offset from the nucleus by about 8". Its mass, 2.8×10^9 $M_\odot$, is approximately 30% of the total molecular gas mass measured by Sanders and Mirabel (1985). On the basis of 3.3 μm emission measures, Cutri *et al.* (1984) have suggested that star formation complexes may reside in a 2–8" annulus around the nucleus of the galaxy. Since the interferometer observations were somewhat limited, the resolution here is not optimal and the precise location and extent of the CO emission region is not well-determined. However, it is tempting to speculate that it represents the densest part of such an annulus, perhaps similar to that found around another Seyfert nucleus, NGC 1068 (Myers and Scoville 1986).

Acknowledgements

This work was supported in part by NASA through the IRAS extended mission program and by NSF grant AST 84-12473.

REFERENCES

Beck, S. C., Turner, J. L, Ho, P. T. P. 1986, *Ap. J.*, in press.

Becklin, E. E. 1986, in *Star Formation in Galaxies*, ed. C. J. Persson (U. S. Government Printing Office).

Cutri, R. M., Rudy, R. J., Rieke, G. H., Tokunaga, A. T., and Willner, S. P. 1984, *Ap.J.*, **280**, 521.

dePoy, D. 1986 in *Star Formation in Galaxies*, ed. C. J. Persson (U. S. Government Printing Office).

Gehrz, R. D., Sramek, R. A., and Weedman, D. W. 1983, *Ap.J.*, **267**, 551.

Harper, D. A. 1984, in *Airborne Astronomy Symposium*, ed. H. A. Thronson, Jr., and E. F. Erickson, NASA Conference Publication No. 2353.

Myers, S., and Scoville, N. Z., 1986, *Ap. J. (Letters)*, submitted.

Rieke, G. H., Cutri, R. M., Black, J. H., Kailey, W. F., McAlary, C. W. and Elston, R. 1985, *Ap.J.*, **290**, 116.

Sanders, D. B., and Mirabel, I. F. 1985, *Ap. J. (Letters)*, **298**, L31.

Sanders, D. B., Scoville, N. Z., Young, J. S., Soifer, B. T., Schloerb, F. P., Rice, W. L., and Danielson, G. E. 1986a, *Ap. J. (Letters)*, **305**, L45.

Sanders, D. B., Young, J. S., Scoville, N. Z., Soifer, and Danielson, G. E. 1986b, *Ap. J. (Letters)*, submitted.

Sargent, A. I., Sanders, D. B., Scoville, N. Z., and Soifer, B. T. 1986, *Ap. J. (Letters)*, submitted.
Scoville, N. Z., and Good, J. C. 1986, in *Star Formation in Galaxies*, ed. C. J. Persson (U. S. Goverment Printing Office).
Scoville, N. Z., Sanders, D. B., and Clemens, D. P. 1986, *Ap. J. (Letters)*, Nov. 15.
Scoville, N. Z., Sanders, D. B., Sargent, A. I., and Soifer, B. T. 1987, *Ap. J. (Letters)*, submitted.
Soifer, B. T., et al. 1984, *Ap.J. (Letters)*, **278**, L71.
Telesco, C. M., Decher, R., and Gatley, Ian 1985, *Ap.J.*, **299**, 896.
Young, J. S., Schloerb, F. P., Kenney, J., and Lord, S. D. 1986, *Ap.J.*, **304**, 443.

DISCUSSION

A. S. Wilson. I'm a little puzzled by the offset of the CO emission from the nucleus of NGC 7469. The centimetric radio continuum and circumnuclear optical line emission center very well on the nucleus. Could atmospheric effects be responsible? It would be valuable if you could directly measure the relative positions of the CO and the radio continuum in your data.

Sargent. Our observations of NGC 7469 were somewhat limited so that the exact size and location of the compact CO region cannot be determined. It is possible that we have detected only the densest part of an annulus of gas centered on the nucleus. Higher sensitivity measures are needed to confirm this.

J. Carlstrom. Do you see any 3 mm continuum emission from these galaxies?

Sargent. We have not yet searched for continuum emission from the galaxies, although such a measurement might permit a more accurate determination of the CO offset from the nucleus.

POSTER PRESENTATIONS

STARBURST GALAXIES

THE INITIAL MASS FUNCTION IN HII GALAXIES

Alison W. Campbell
Center for Astrophysics
60 Garden Street
Cambridge, Mass

Abstract

Observation of a large sample of HII galaxies shows that the emission line ratios of the youngest objects change systematically with gaseous oxygen abundance, which we interpret as resulting from changes in the initial mass function (IMF) of the ionising cluster. Comparison with cluster/nebula models shows that both the slope and the upper mass limit of the cluster IMF vary with abundance. In HII galaxies with oxygen abundance about 1/10 that of Orion, the IMF for massive stars must have a slope which is about a factor of 2 smaller than in the Solar Neighbourhood.

Introduction

"HII galaxies", dwarf galaxies with the spectra of giant HII regions, are ionised by massive O stars formed during a recent intense burst of star formation. Although the very strong, narrow emission lines which characterise these objects have been used in several studies to determine physical conditions in the ionised region (eg Searle and Sargent 1972, French 1980, Kinman and Davidson 1981, Kunth and Sargent 1983, Campbell, Terlevich and Melnick 1986a; CTMa), little is known about their ionising clusters.

The nebular excitation of low-abundance HII galaxies is higher than can be explained by a solar neighbourhood IMF (Lequeux et al 1981, Bergvall 1985). Giant HII regions in spiral galaxies show trends in emission line ratios which indicate that the temperature of the ionising cluster, T_{ion}, increases smoothly as the abundance decreases (eg Shields and Tinsley 1976, Stasinska 1980). The observed change in T_{ion} can arise if the IMF of the ionising cluster in giant HII regions and HII galaxies is abundance-sensitive: Shields and Tinsley (1976) proposed a systematic change in the upper mass limit of the IMF, while Terlevich (1982) suggested that the slope of the IMF decreases with decreasing abundance.

Studies of the ionising cluster in HII galaxies have so far been based almost entirely on UV/optical/infrared colours, mass-to-light ratios, and recombination line equivalent widths; the easily-observed emission line ratios, which carry important information about the mass distribution and age of the ionising cluster, have been almost totally neglected. We report here the results of a comparison between the line ratios of a sample of ~ 50 HII galaxies and those of model nebulae ionised by clusters with a variable IMF.

Modelling strategy

The ionising clusters of HII galaxies evolve very rapidly, on timescales of order the lifetime of a massive star, a few Myr. As the cluster evolves, T_{ion} falls and the "hardness" of the ionising spectrum decreases, leading to a rapid change in the relative strength of lines from different ionisation stages of a

Carol J. Lonsdale Persson (Editor)
Star Formation in Galaxies

given element. A least-squares fit to the distribution of HII galaxies in a T_{ion} -sensitive emission line ratio will therefore always underestimate the T_{ion} of the cluster IMF (as distinct from the cluster's current T_{ion}) and consequently cause us to either overestimate the IMF slope or underestimate its upper mass limit. If we wish to study the abundance behaviour of the IMF, it is therefore crucial to remove the effect of cluster evolution.

In principle, there exists a set of HII galaxies, covering a range in abundance, in which the ionising cluster is at close to zero age: a "zero age sequence" (ZAS) which will appear as an upper envelope in T_{ion} -sensitive emission line diagrams. Identification and modelling of this ZAS using zero-age main sequence cluster models will allow us to determine the abundance behaviour of the HII galaxy IMF for stars more massive than $\sim 20\ M_\odot$.

Model HII galaxies

We have used the cluster code of Melnick, Terlevich and Eggleton (1985) to produce zero-age main sequence model clusters of mass $10^6\ M_\odot$. The cluster mass distribution is specified by a power-law IMF with slope α between $0.1\ M_\odot$ and a maximum of $200\ M_\odot$. We next pass the ionising part of the cluster's spectrum to a model nebula code (Ferland and Truran 1981) and construct low-density, clumpy, radiation-bounded HII regions with oxygen abundances spanning the range covered by the data. The models are discussed in greater detail in Campbell, Terlevich and Melnick (1986b; CTMb).

Comparison of models and data: the ([OIII]/[OII], O/H) diagram

The T_{ion} -sensitive line ratio [OIII]/[OII] is insensitive to O/H and thus allows us to examine directly the behaviour of T_{ion} with abundance. The ZAS, from which objects evolve downwards, is easily visible in figure 1. The curves in figure 1a are the loci of model HII galaxies ionised by clusters with a constant IMF specified by the M_u and α shown. All these models are poor fits to the data. Those with $\alpha = 3.0$ produce values of [OIII]/[OII] which fall nearly an order of magnitude below the ZAS for $O/H \simeq 4 \times 10^{-5}$, while those with $\alpha = 1.0$ grossly overestimate the position of the ZAS for 6×10^{-5}. It is immediately evident that for any M_u , a "flat" IMF ($\alpha \sim 1.0$) is required at low abundance. The steep turndown of the [OIII]/[OII] envelope with increasing abundance requires a systematic decrease in M_u or increase in α .

The strongest dependence of α and M_u on abundance which can be accommodated without conflicting with their observed values at the Solar Neighbourhood oxygen abundance are

$$M_u = 5.9\ (O/H)^{-0.3} \qquad (1)$$

$$\alpha = 1.2 \log (O/H) + 6.9 \qquad (2)$$

The loci of models in which M_u and α vary according to equations (1) and (2) are shown in figures 1b and 1c respectively. The fit of the variable-M_u models is little better than that of constant IMF models, owing to the small change in the cluster mass distribution caused by changes in M_u . Variable α models do much better, but still overestimate the position of the envelope for $O/H \gtrsim 1.5 \times 10^{-4}$.

It seems therefore that a systematic change with abundance of both α and M_u is required to fit the [OIII]/[OII] envelope. We have constructed two such models, one in which α increases with abundance in the variable-M_u model (equation (1)), and another in which M_u decreases with abundance in the variable-α model (equation (2)). Figure 1d demonstrates that these closely similar models both produce a very good fit to the ZAS.

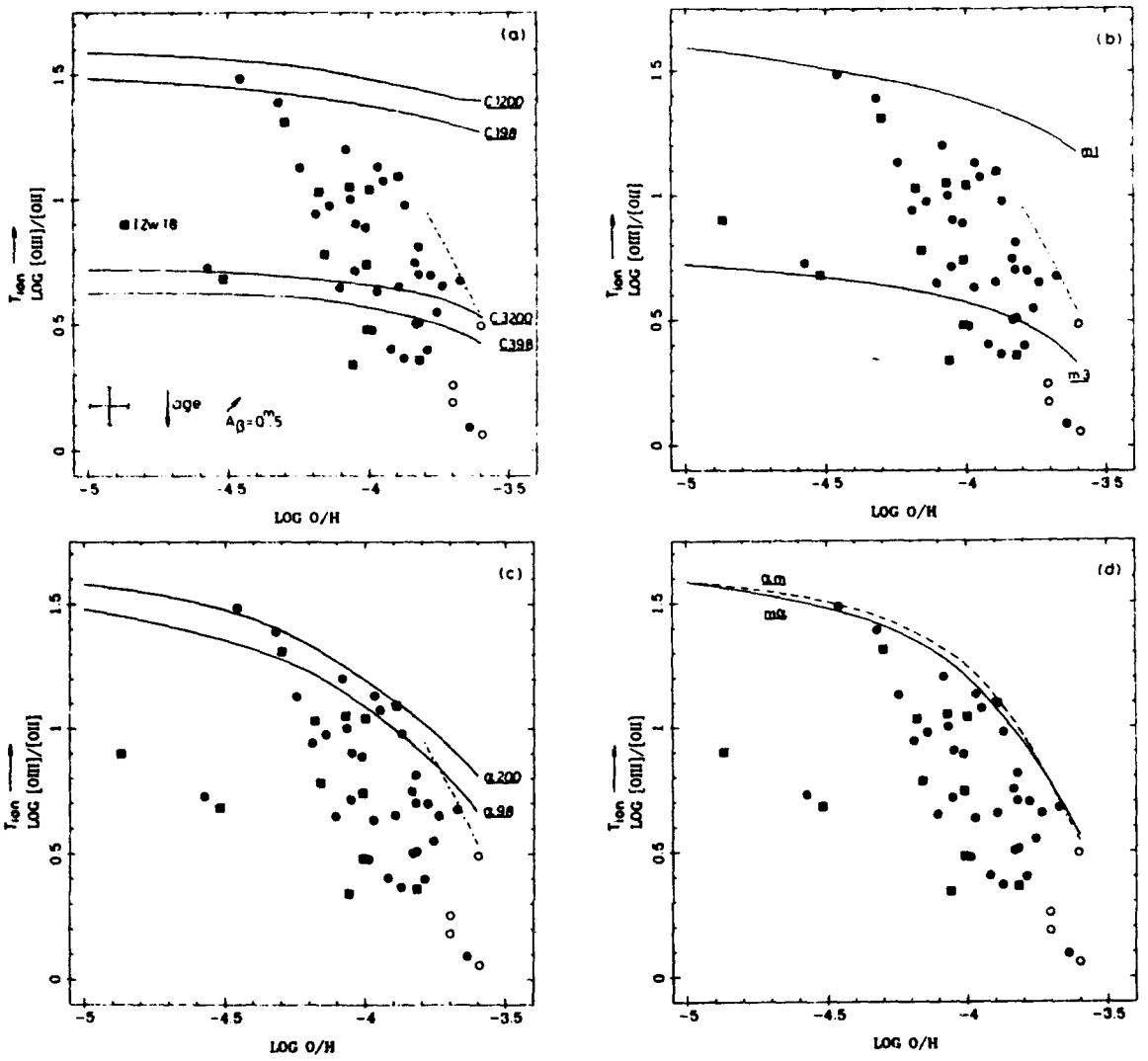

Figure 1

The distribution of the sample in the ([OIII]/[OII], O/H) plane. Circles: data from CTMa; squares: data from Kunth and Sargent (1983). IZw18 is from Kinman and Davidson (1981). The short dash-dot line represents the adopted zero-age envelope for O/H > 1.5 x 10^{-4}, as explained in CTMb. The model loci are labelled as follows: C398: constant IMF, α = 3.0, M_u = 98 $M_\odot$; C3200: constant IMF, α = 3.0, M_u = 200 $M_\odot$; C198: constant IMF, α = 1.0, M_u = 98 $M_\odot$; C1200: constant IMF, α = 1.0, M_u = 200 $M_\odot$; M3: IMF with α = 3.0 and variable M_u (eq.1); M1: IMF with α = 1.0 and variable M_u ; α 98: IMF with M_u = 98 $M_\odot$ and variable α (eq.2); α 200: IMF with M_u = 200 $M_\odot$ and variable α ; M α : the variable M_u model (eq.1) with 1.0 < α < 2.7; α M: the variable α model (eq.2) with 200 > M_u > 73 $M_\odot$.

Discussion

An excellent fit to our adopted zero-age sequence in the ([OIII]/[OII], O/H) diagram has been obtained by allowing the mass distribution of the ionising clusters of HII galaxies to vary systematically with abundance. Our models indicate a very pronounced change in the IMF in the oxygen abundance range 2.5 x

10^{-5} to 2.5×10^{-4}; α is required to vary from $\simeq 1.5$ to 2.7 and M_u from $\simeq 200$ to $\simeq 75\ M_\odot$. The dependence of the IMF slope on abundance is closely similar to that derived (using different methods) for giant HII regions and HII galaxies by Terlevich (1982).

Conclusions

Assuming trends in emission line ratios are due to changes in the stellar mass distribution of the ionising clusters of HII galaxies, the main results of the emission line modelling can be summarised as follows:
1) No constant IMF can reproduce the values of the T_{ion} -sensitive line ratio [OIII]/[OII] observed in the youngest ("zero age") objects over the oxygen abundance range $2.5 \times 10^{-5} < O/H < 2.5 \times 10^{-4}$.
2) A systematic change with abundance of M_u alone also fails to reproduce the zero age range in [OIII]/[OII], owing to the small effect which even large changes in M_u have on the mass distribution of the ionising cluster.
3) Models in which only α varies cover much more of the zero-age range in [OIII]/[OII] and if $M_u \simeq 200\ M_\odot$, are correct for oxygen abundances $\lesssim 1 \times 10^{-4}$. Above this they slightly overestimate the position of the [OIII]/[OII] envelope.
4) Models in which both α and M_u vary with abundance reproduce the data envelope very well over the full range in oxygen abundance of 2.5×10^{-5} to 2.5×10^{-4}. The detailed abundance behaviour of α and M_u is given in CTMb.
5) For the lowest-abundance HII galaxies, eg IZw18 ($O/H \simeq 1.5 \times 10^{-5}$), the predicted IMF slope is $\simeq 1.2$, irrespective of M_u. IZw18 is an evolved object in which T_{ion} is currently considerably lower than its zero-age value.

Acknowledgements

I thank Jorge Melnick, Roberto Terlevich and Gary Ferland for access to their model software, and Jack Baldwin and Belinda Wilkes for their helpful comments.

References

Bergvall N., 1985, A.& A. 146,269
Campbell A.W., Terlevich R.J. & Melnick J., 1986a, accepted by M.N.R.A.S. (CTMa)
Campbell A.W., Terlevich R.J. & Melnick J., 1986b, submitted to M.N.R.A.S. (CTMb)
Ferland G. & Truran J.W., 1981, Ap.J. 244,1022
French H.B., 1980, Ap.J., 240,41
Kinman T. & Davidson K., 1981, Ap.J. 243,127
Kunth D. & Sargent W.L.W., 1983, Ap.J. 273,81
Lequeux J., Joubert M.M., Deharveng J.M., Kunth D., 1981, A.& A. 103,305
Melnick J., Terlevich R.J. & Eggleton P.P., 1985, M.N.R.A.S. 216,255
Searle L. & Sargent W.L.W., 1972, Ap.J. 173,25
Shields G.A. & Tinsley B., 1976, Ap.J. 203,66
Stasinska G., 1980, A.& A. 84,320
Terlevich R.J., 1982, Ph.D. Thesis, University of Cambridge

VLA CONTINUUM OBSERVATIONS OF BARRED SPIRAL GALAXIES

J. Antonio García-Barreto
Instituto de Astronomía, Universidad Nacional Autónoma de México, Apartado Postal 877, Ensenada 22830, Baja California, Mexico.

P. Pişmiş
Instituto de Astronomía, Universidad Nacional Autónoma de México, Apartado Postal 70-264, México D.F. 04510, Mexico.

ABSTRACT

In this paper we report observations of NGC 613, NGC 1300, NGC 4314 and NGC 5383 using the VLA at frequencies of 1464.9 and 4885.1 MHz. These objects are a subset of galaxies from which we have searched for radio emission. Our selection criteria were: a) they are barred spiral galaxies preferentially with different Hubble type; b) they have a peculiar or hot-spot nucleus as reported by Sersic (1973, P.A.S.P. 85, 103) or Vorontsov-Vel'yaminov, Zaitseva and Lyutyi (1972, Soviet Astron. 16, No. 1, 71); c) they have been observed at far-infrared wavelengths by IRAS (1985, IRAS Catalogs and Atlases: the Point Source Catalog, Government Printing Office) and d) they are observable from the northern hemisphere. Their radio and far-infrared properties are summarized in Table I while their composite spectra are shown in Figure 1.

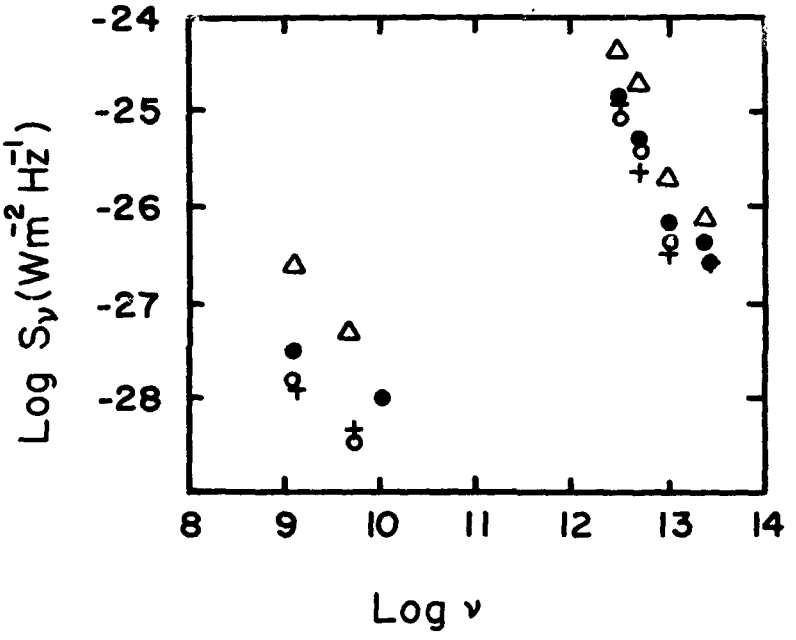

Figure 1. Composite spectra showing radio and far-infrared observations of NGC 613 (Δ), NGC 1300 (+), NGC 4314 (o) and NGC 5383 (●).

Carol J. Lonsdale Persson (Editor)
Star Formation in Galaxies

TABLE I. Radio and far-infrared properties.

Galaxy	Type	Frequency (GHz)	S_ν total (mJy)	S_ν central (mJy)	Ref.	Distance[a] (Mpc)	FIR Flux Density (Jy) 12μm	25μm	60μm	100μm	T_d (°K)	L_{FIR}[b] (erg sec^{-1})	M_g^{FIR}[c] ($M_\odot$)
NGC 613	SBb(rs)	1.4649	260 ± 10	82 ± 2	1,3	15.3	0.74	2.09	19.30	48.12	32	3.5×10^{43}	6.8×10^{7}
		4.8851	45 ± 5	15	1,3								
NGC1300	SBb(s)	1.4649	12	5	1,6	15.6	0.25	0.31	2.39	10.78	27	0.6×10^{43}	2.4×10^{7}
		4.8851		1	1								
NGC4314	SBa(rs) PEC	1.4649	15 ± 3	~11	1,2	8.8	0.25	0.39	3.71	7.30	35	0.2×10^{43}	3.0×10^{6}
		4.8851	5 ± 1	~ 3	1,2								
NGC5383	SBb(s)	1.4649	34 ± 1	~20	1,4	23.5	0.36	0.65	5.23	12.60	33	2.1×10^{43}	3.8×10^{7}
		10.7	8.8 ± 1		5								

References: (1) This paper; (2) García-Barreto, J.A. and Pismis, P., 1986, in preparation; (3) Hummel, E., van der Hulst, J.M. and Dickey, J.M., Astron. Astroph. 134, 207; (4) Sancisi, R. and Ekers, R.D., 1978, Astron. Astroph. 67, L21; (5) Gräve, R., Klein, U. and Wielebinski, R., 1981, Astron. Astroph. 95, 391; (6) Hummel, E., Pedlar, A., van der Hulst, J.M. and Davies, R.D., 1985, Astron. Astroph. Suppl. Series 60, 293.

[a] Assuming: $H_0 = 100$ km s^{-1} Mpc^{-1}.

[b] Assuming: $L_{FIR} = 4\pi D^2 FIR$, where $FIR = 1.26 \times 10^{-14} * [2.58\, f_\nu(60\mu m) + f_\nu(100\mu m)]$.

[c] Assuming: $M_g^{FIR} = 100\, M_d^{FIR}$, where $M_d^{FIR} = \rho L_{FIR}/3\sigma T^4 (Q_e/a)$.

A DUST SCATTERED HALO IN STARBURST GALAXY M82?

Michael Rohan, Philip Morrison, and Alberto Sadun

INTRODUCTION

The source of the halo about M82 has been under discussion for several years; one explanation for it is the dust model of Solinger, Morrison and Markert (1977) in which they propose a diffuse cloud of dust through the M81 group, with M82 travelling through the group holding a denser cloud of dust around it.

This paper looks at the feasibility of the "dust" theory in the X-ray range, using the halo in the X-ray image of M82 taken by the Einstein Observatory. To this end the X-ray cross section for dust is presented, along with the single scattered image of an X-ray source surrounded by a dust cloud; multiply-scattered images have been simulated with a Monte-Carlo program; profiles of the halo along the major and minor axes of M82 are presented. Also presented is an accounting for line spectrographs of M82 that show unusual splitting (e.g. Axon and Taylor, 1978), using the dust model.

The final model proposed for the X-ray image requires dust (typically SiO_2, although the result is not overly sensitive to the choice of dust material) of radius 50 Å-300 Å, with density on the order of 10^{-7} cm^{-3} to 10^{-9} cm^{-3}, out to a distance of about 9 kpc for some regions. The HRI image of M82 is shown in Fig. 1.

CROSS SECTION

The cross section for dust in the Rayleigh-Gans limit is

$$\frac{d\sigma}{d\Omega} = 4R^6k^4|m-1|^2\left(\frac{1+\cos^2\theta}{2}\right)\left[\frac{\sin x - x\cos x}{x^3}\right]^2$$

where $x = 2Rk\sin(\theta/2)$ has been used for brevity; R is the dust grain radius, and k is the wavenumber for the X-rays, m is the index of refraction, and θ is the scattering angle.

The total cross section is

$$\sigma = 2\pi R^4k^2|m-1|^2.$$

Note that $|m-1|^2 \propto k^{-4}$.

SINGLE SCATTERING

The image of a point source is strongly dependent on the location of the scattering cloud. For a cloud of radius r about the source, the image intensity is given by

$$\frac{dI_s}{d\Omega dt} = \frac{L_s n}{\pi d}R^6k^4|m-1|^2\left(\frac{0.21}{Rk\psi} - \frac{d}{8.5r}\right)$$

Carol J. Lonsdale Persson (Editor)
Star Formation in Galaxies

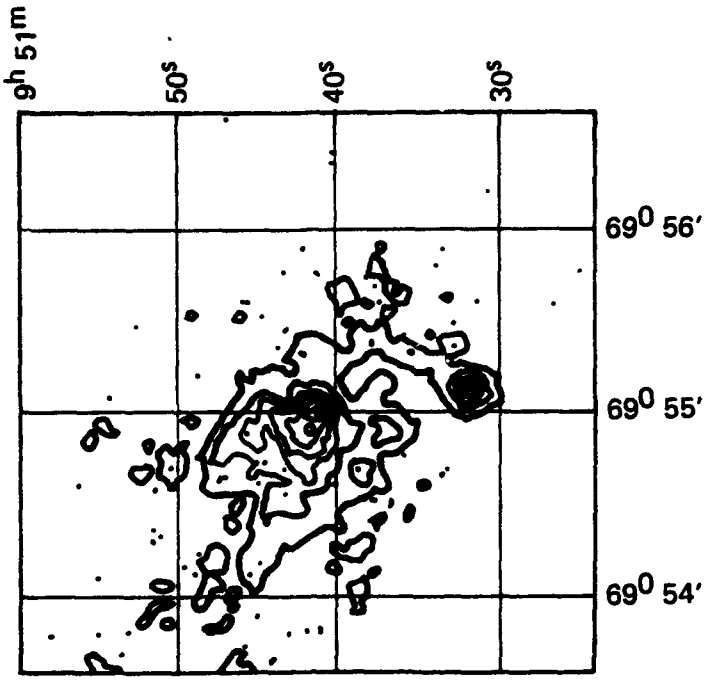

Fig. 1. The X-ray image of M82 taken by HRI-3 and smoothed with the point response function. Contours are at 0.1-0.7 counts/arcsec^2 for the observation.

where L_x is the luminosity in the range considered, n the dust density, d the source-observer distance, ψ is the separation in the sky from the source, and r is the extent of the cloud in front of the source.

In the case of M82, X-ray scattering by dust in our galaxy produces a halo with constant intensity beyond the field of the observing instrument; this is relegated to background.

It can be seen that the singly-scattered halo of the nucleus of M82 due to the diffuse dust proposed for the M81 group would be much smaller than the observed halo, and is 'washed out' by it.

MULTIPLE SCATTERING

Multiply-scattered images of a point source have been simulated by a Monte Carlo program. The program traces the photons to the surface of a spherical, homogeneous cloud of dust around the source, and notes the exit angle of each photon at the surface (from the normal). From this accounting, a distribution of exit angles can be obtained for any point on the surface; from this distribution an image can be calculated.

In the simulations done for M82 the dust used was SiO_2, we set a lower limit of 100 Å for the dust radius. The density had an upper limit of 10^{-7} cm^{-3}, and the cloud radius was kept at less than 10 kpc.

A further limit imposed was that the mass of the homogeneous sphere of scattering dust in the program was kept below 10^{11} solar masses. (This keeps the mass of dust required for M82 below 10^9 solar masses when we take into account filling factors and geometrical

considerations.)

The simulated images were convolved with a $\sigma = 6''$ gaussian cut at $10''$ to account for the extent of the core of M82.

The resulting multiply scattered images can be quantified using some results from Alcock and Hatchett (1978), who showed that the variance of the angle between the path of a multiply scattered photon and the source-to-photon position vector (ϕ), after being multiply scattered, is

$$< \phi^2 >= \frac{\tau}{3} < \theta^2 >$$

where $< \phi^2 >$ is the variance of the cross-section for the scatterers and τ the optical depth.

Thus, a rough estimate for the width is given by

$$\sqrt{<\psi^2>} \simeq r^{\frac{1}{3}} n^{\frac{1}{3}} R^2/k.$$

The simulations follow this prediction (although some are at the limit of the small angle approximation for ϕ).

DATA

The data below was taken in one observation (of 13,110.7 sec) with the High Resolution Imager (HRI) aboard the Einstein Observatory. The HRI has a 25' diameter field of 0.5"x0.5" pixels, resolution ~1 arcsec. The energy range is 0.1 keV-4 keV, with no energy resolution.

To study the scattering of the nucleus of M82, two 90° cuts of the image, one along the SE major axis and one along the SW minor axis, were radially binned to obtain profiles. The cuts are centered at $\alpha = 9^h\ 51^m\ 41.8^s$, $\delta = 69°, 55', 56.2''$; they are from 90° to 180°, and 180° to 270° on the image in Fig. 1, clockwise from the top (north). The numbers for the profiles are in units of counts/arcsec^2 for the whole (13110.7 sec) observation, a background of 0.017 counts/arcsec^2 (taken from an agreement between the edge of the field of the HRI and survey observations at similar galactic latitude) has been subtracted. The profiles are shown in Figures 2 and 3.

MODELS

A set of simulated profiles from the Monte-Carlo program, convolved with a gaussian nucleus of radius $10''$ and $\sigma = 6''$ are shown below in Figures 4 through 5, with the more extended profile from the two cuts superimposed. A successful model for M82 needs dust of radius <300 Å in a cloud between 2 kpc and 9 kpc deep, at optical depths $\geq$10. Lower limits can be set at 10^{-8} cm^{-3} density dust, 2 kpc cloud radius and with 5 optical depths of dust for workable models, though these can all be overcome by allowing more dust or much greater optical depths.

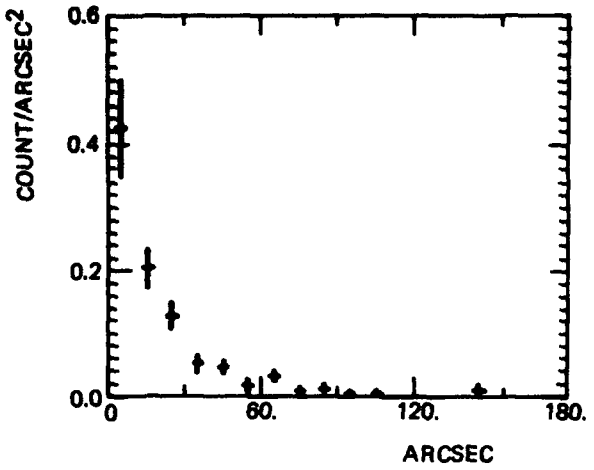

Fig. 2. Data from a 90° cut in the halo about the SW major axis

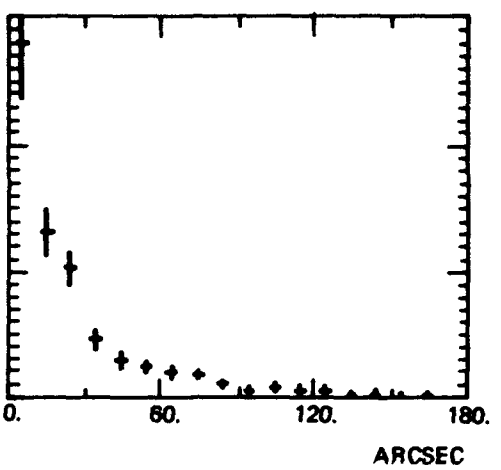

Fig. 3. Data from a 90° cut in the halo about the SE minor axis

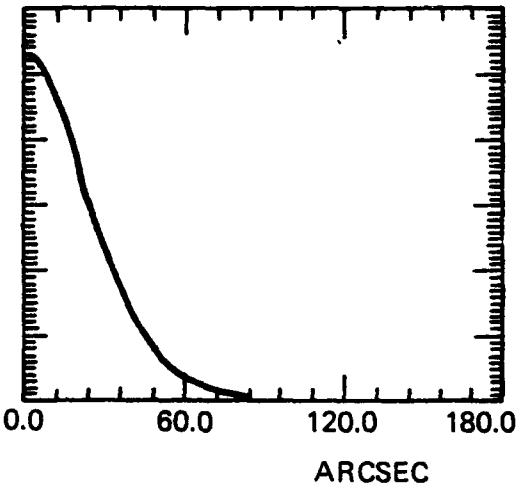

Fig. 4. Cloud radius 9 kpc
density $1.3 \times 10^{-7} cm^{-3}$
grain radius 100Å

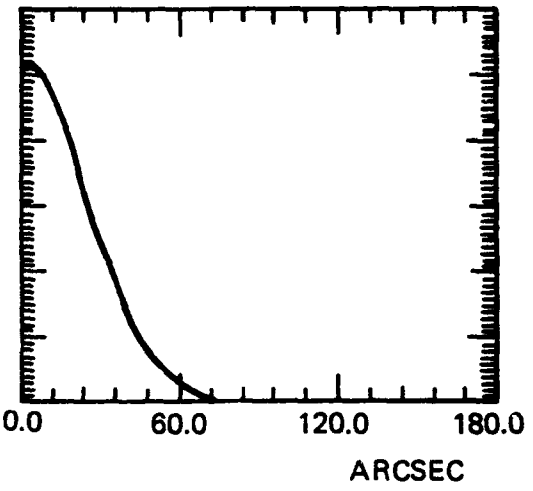

Fig. 5. Cloud radius 5 kpc
density $7.4 \times 10^{-7} cm^{-3}$
grain radius 100Å

SPECTROSCOPIC OBSERVATIONS

The line splitting that has been observed in spectroscopic observations of M82 (Axon and Taylor, 1978) can be produced by scattering by dust within the disk of the galaxy. Simple models using sources moving within the nucleus (the existence of such bright sources has been shown by O'Connell and Mangano, 1978) and the rotation curve for M82 (from Burbidge, Burbidge, and Rubin, 1964) can produce both published lines and more complex possibilities.

Two sample slit spectrographs have been constructed in Figure 6. The drawing shows the galaxy from the top with some velocities marked and four sources labelled in the nucleus. The sections of the disc observed by slits α and β are drawn and labelled, and

several sample scatterers have been placed on each slit. The shift for each scatterer-source pair has been plotted below the figure and the line splits interpolated, producing the observed line splitting.

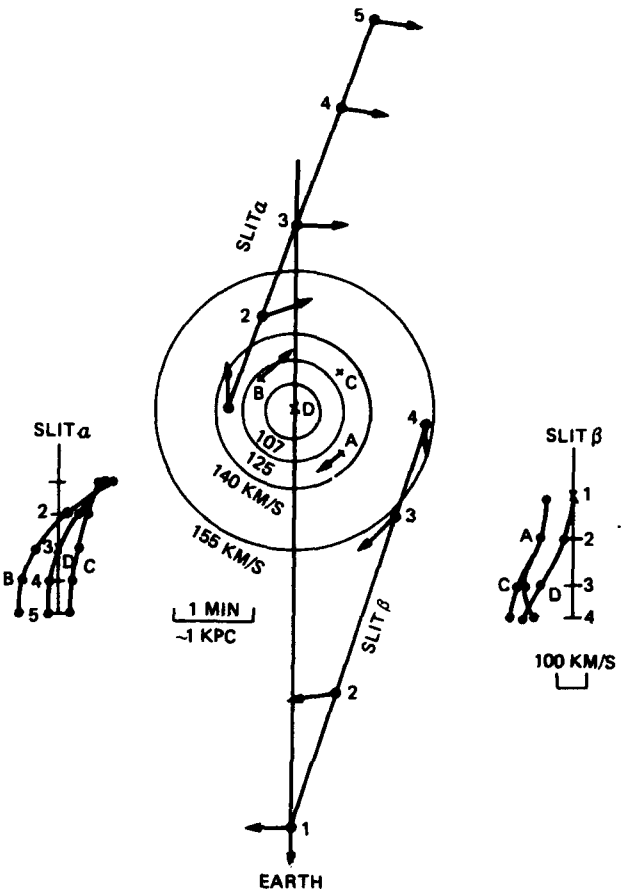

Fig. 6. M82 viewed from the top: "α" through "β" are the sections of the disk viewed by two slits. Several scatterers and their velocities have been placed on each slit. The line shift due to each scatterer-source pair is plotted on the graph for each slit, and the shifted line for each source, have been drawn in.

The line splitting constructed shows the possibility of line splitting at either end as well as splits and crossovers, using only one or two sources. Curling, horizontal lines and sharp turns can also be produced in a spectrograph with the consideration of one additional source.

1. Alcock, C., and Hatchett, S. Ap. J. *222* (1978), 456.
2. Axon, D.J., and Taylor, K. Nature *274* (1978), 37.
3. Burbidge, E.M., Burbidge, G. and Rubin, V.C. Ap. J. *140* (1964), 942.
4. Hulst, H.C. van de, *Light Scattering by Small Particles*, Dover Publications, New York, 1957, 1981.
5. Martin, P.G., Mon. Not. R. Astr. Soc. *149* (1970), 221
6. O'Connell, R.W., and Mangano, J.J. Ap. J. *221* (1978), 62
7. Solinger, A., Morrison, P., and Markert, T. Ap. J. *211* (1977), 707.

The Azimuthal and Radial Distributions of HI and H_2 in NGC 6946

Linda J. Tacconi-Garman and Judith S. Young
Five College Radio Astronomy Observatory
University of Massachusetts
Amherst, MA

Abstract. We have completed a study of the atomic and molecular components of the ISM in NGC 6946. The distribution of molecular clouds has been determined from a fully sampled CO map of the inner disk (R < 8 kpc) using the 14-meter telescope of the FCRAO (HPBW = 45"). The distribution of atomic gas was derived from VLA observations at 40" resolution in the D configuration. When comparing the global CO and HI properties with other components of the galaxy, we find that the azimuthally averaged radial distributions of CO, Hα, radio continuum and blue light all exhibit similar roughly exponential falloffs, while the azimuthally averaged HI surface densities vary by only a factor of 2 out to R = 16 kpc. This indicates that while the Hα/CO ratio is approximately constant with radius, the CO/HI ratio decreases by a factor of 30 from the center of the galaxy to R = 10 kpc.

INTRODUCTION

To better understand the cycling of the interstellar medium and the star formation efficiency in galaxies, we have undertaken a multi-wavelength study of the ISM of the face-on Scd galaxy, NGC 6946. This galaxy has been well-studied by a number of authors. Photometric data from Ables (1971) and Elmegreen and Elmegreen (1984) indicate the exponential nature of the blue and I band luminosity profiles. Hα studies by DeGioia-Eastwood et al. (1984) have been used to infer the massive star formation rate. The HI distribution has been determined at a resolution of 2' by Rogstad, Shostak and Rots (1973). Radio continuum emission has been observed at many wavelengths (cf. Klein et al. 1982; van der Kruit et al. 1977). Observations of the CO distribution have previously been determined (Morris and Lo 1978; Rickard and Palmer 1981; Young and Scoville 1982), and most recently, an interferometric study of CO in the central 1' of this galaxy (Ball et al. 1985) has uncovered a molecular bar ~45" long. In this paper we present the results of a complete ^{12}CO and HI study at moderate resolution.

DATA AND RESULTS

We have made ^{12}CO observations at more than 100 positions in NGC 6946 with the 14-meter antenna of the Five College Radio Astronomy Observatory, and have fully sampled the inner 6' of this galaxy. Figure 1 shows a sample of the CO spectra attained at radii < 2.'25, all plotted on the same scale. The CO intensities peak in the center of the galaxy, and then fall off fairly smoothly with radius, although azimuthal variations of factors of 3 are observed. We observe 2 smaller CO peaks to the northeast and northwest of the galaxy in the

Carol J. Lonsdale Persson (Editor)
Star Formation in Galaxies

direction of two major optical spiral arms. Using the standard conversion of CO intensities to H_2 surface densities (Young and Scoville 1982) we find the H_2 density in the central 45" to be 3.3×10^{22} atoms cm^{-2} with the lowest observed values of $<6\times10^{20}$ atoms cm^{-2} in the disk of this galaxy.

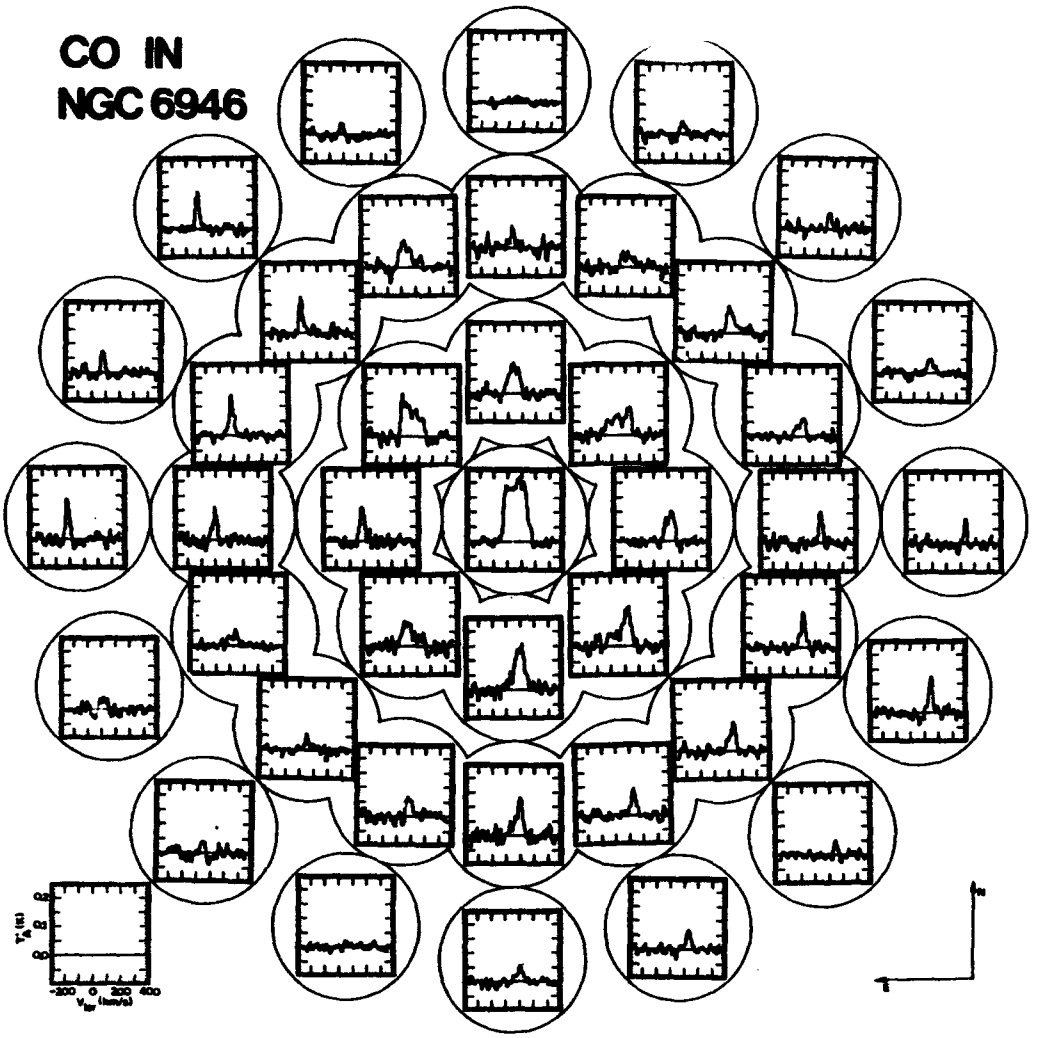

Figure 1. A sample of the CO spectra attained at radii <2'.25 all plotted on the same scale. The circles indicate the positions where the observations were made. These data represent ~1/2 of the complete CO map of NGC 6946. The box in the lower left hand corner indicates the scale of all the spectra.

The 21-cm line data were obtained with the VLA in the D configuration, where the resolution of the synthesized beam was 40"×37". We observe HI emission at greater than the 3σ level out to a radius of 30 kpc, with HI spiral structure apparent in the outer disk, well beyond where the optical arms are seen (see Figure 2). The central surface density of HI is 2.5×10^{20} H cm^{-2} with extreme values over the entire HI disk of 2.1×10^{20} to 2×10^{21} H cm^{-2}. There are two noticeable HI peaks located ~4' to the northwest and northeast of the center which are ~2'.5 × 2'.5. The peak to the northeast contains about 2.4×10^{8} M_0 of HI in an area of 19 kpc^2, and is roughly coincident with the largest, high surface brightness spiral arm in the optical disk. The stronger peak to the northwest of the center contains about 3.8×10^{8} M_0 of neutral gas in a region of 28 kpc^2, and is also coincident with an optical spiral arm. The HI surface densities in these regions are ~14 M_0 pc^{-2}. We also observe several resolvable

HI depressions larger than 45" (2.2 kpc) across in this galaxy to the north and southwest of the center, as well as in the central region itself.

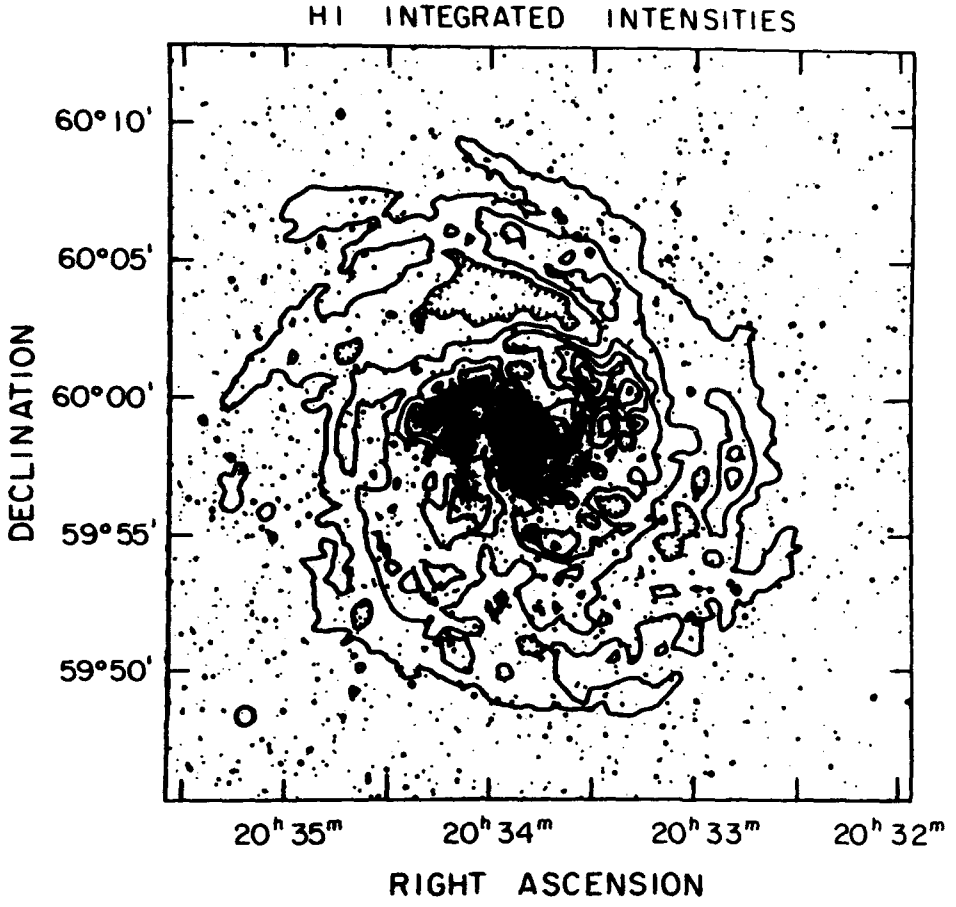

Figure 2. A contour representation of the total HI integrated flux distribution superposed on an enlargement of the Palomar Sky Survey print. The contour levels range from 0.2 to 3.0 Jy km s^{-1} and are separated by 0.4 Jy km s^{-1} intervals. Regions of HI depletion are represented by tic marks on the contours. The HI synthesized beam is shown in the bottom left hand corner of the figure.

COMPARISONS OF HI AND H_2

In Figure 3 we show the H_2/HI ratio as a function of the molecular and atomic surface densities for 89 positions at R < 3' in the galaxy. We have made linear fits to the data for each of the plots, and find that the H_2/HI ratio is correlated with H_2 surface density and anti-correlated with HI surface density. These plots indicate that an increase in the H_2/HI ratio is due to an increase in the H_2 density as well as a slight decrease in the HI density in the inner disk of NGC 6946. Thus, fluctuations in the ISM of this galaxy are dominated by the molecular component rather than the atomic gas.

We have computed the azimuthally averaged radial distributions of HI and H_2 in NGC 6946, and have compared them with the blue luminosity (Ables 1971), Hα (DeGioia-Eastwood et al. 1984), I band (Elmegreen and Elmegreen 1984) and radio continuum (van der Kruit et al. 1977) profiles in Figure 4. The radial distributions of CO, Hα, radio continuum, blue and I band all exhibit similar roughly exponential falloffs (scale lengths = 4-6 kpc), while the azimuthally averaged HI surface densities vary by only a factor of 2 out to R = 16 kpc.

Thus the atomic gas distribution is the only component of NGC 6946 whose shape differs from the rest. This indicates that while the Hα/CO ratio is approximately constant with radius, the CO/HI ratio decreases by a factor of 30 from the center of the galaxy to R = 10 kpc.

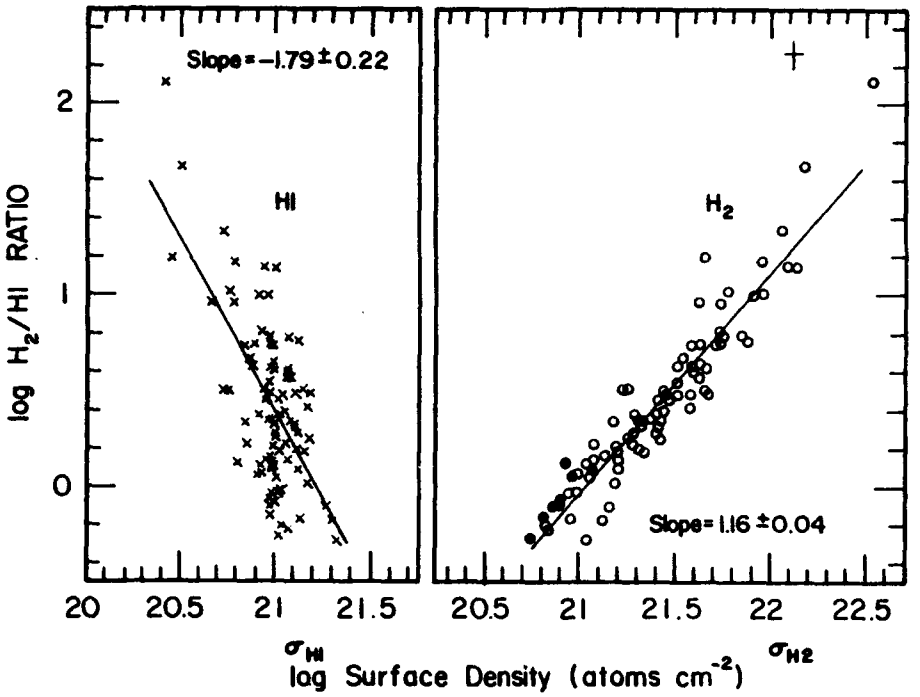

Figure 3. H_2/HI ratio as a function of the (a) atomic and (b) molecular surface densities for 89 positions in the galaxy. A typical error bar is shown in the upper right hand corner of the plot. Filled circles on the H_2 plot represent upper limits to the CO intensity, and thus the H_2 surface density.

We interpret the CO/HI ratio as the efficiency of molecular cloud formation from the atomic medium, and the Hα/CO ratio as the star formation efficiency (SFE) from the molecular medium. Therefore, while the SFE is constant with radius (DeGioia-Eastwood et al. 1984) the cloud formation efficiency decreases sharply with radius. That is, once molecular clouds are formed, stars are produced at a rate which is proportional to the mass of the molecular clouds. The formation of molecular clouds in the outer parts of NGC 6946 may be greatly reduced due to the decreasing volume density of atomic gas. The optical edges of galaxies, therefore, probably reflect the edges of the molecular disks where the formation of molecular clouds from atomic clouds is greatly reduced due to the increasing HI scale height.

Acknowledgements. The FCRAO is operated with support from the National Science Foundation under grant 82-12252 and with the permission of the Metropolitan District Commission, Commonwealth of Massachusetts. The National Radio Astonomy Observatory is operated by Associated Universities Inc., under contract with the National Science Foundation. L.T-G. acknowledges a Grant-in-Aid of Research from Sigma Xi, the scientific research society, for partial funding of this work.

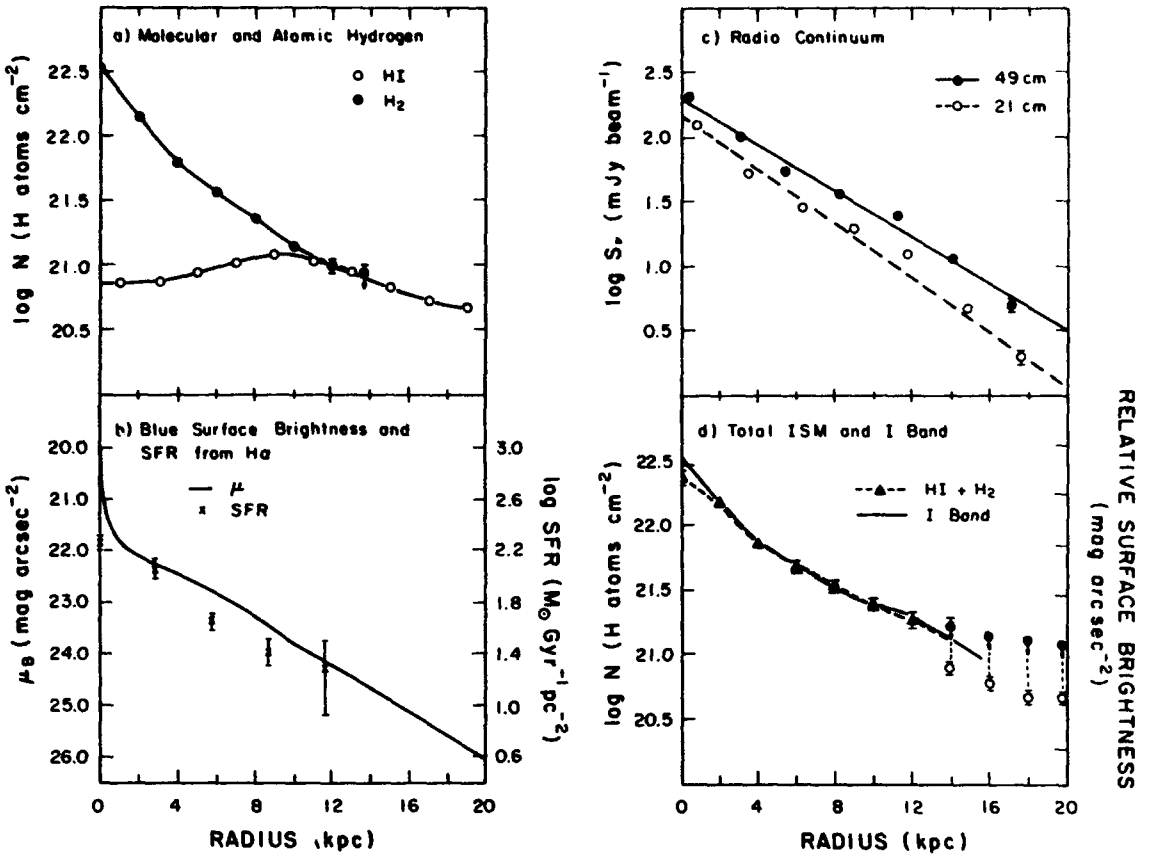

Figure 4. (a) The azimuthally averaged radial distributions of HI and H_2 surface densities. (b) The blue surface brightness radial profile from Ables (1971) and total SFR's calaculated from Hα observations of DeGioia-Eastwood et al. (1984). (c) Radial continuum radial distributions of van der Kruit et al. (1977). (d) I band (Elmegreen and Elmegreen 1984) and total ISM (HI + H_2) radial distributions. At radii greater than 12 kpc, the closed circles in panel d represent HI + H_2 upper limits and the open circles represent the HI lower limits to the total ISM density.

REFERENCES

Ables, H.D. 1971, Pub. US Naval Obs., Series II, Vol. 20, Part 4.
Ball, R., Sargent, A.I., Scoville, N.Z., Lo, K.Y., and Scott, S.L. 1985, Ap.J. Lett., 298, L21.
DeGioia-Eastwood, K., Grasdalen, G.L., Strom, S.E., and Strom, K.M. 1984, Ap.J., 278, 564.
Elmegreen, D.M. and Elmegreen, B.G. 1984, Ap.J. Suppl., 54, 127.
Klein, U., Beck, R., Buczilowski, U.R., and Wielebinski, R. 1982, Astr. Ap., 108, 176.
Morris, M. and Lo, K.Y. 1978 Ap.J., 223, 803.
Rickard, L.J. and Palmer, P. 1981, Astr. Ap.(Letters), 102, L13.
Rogstad, D.H., Shostak, G.S., and Rots, A.H. 1973, Astr. Ap., 22, 111.
van der Kruit, P.C., Allen, R.J., and Rots, A.H. 1977, Astr. Ap., 55, 421.
Young, J.S. and Scoville, N.Z. 1982, Ap.J., 258, 467.

THE INFRARED MORPHOLOGY OF GALACTIC CENTERS

C. M. Telesco, R. Decher, and B. D. Ramsey
Space Science Laboratory, NASA Marshall Space Flight Center

R. D. Wolstencroft and S. G. Leggett
Royal Observatory, Edinburgh

ABSTRACT. We present initial results of a program to map the centers of galaxies in the mid-infrared using the NASA-MSFC 20-pixel bolometer array. Maps at 10.8 μm of the galaxies NGC 5236 (M83), NGC 1808, NGC 4536, and NGC 4527 reveal complex emitting regions ranging in size from 500 pc to 2 kpc. The infrared spatial distributions generally resemble those in the visible and radio. In all cases a large fraction of the IRAS 12 μm flux originates in spatial structures prominent in the maps.

1. INTRODUCTION

The central regions of many galaxies emit intense radiation at $\lambda > 5$ μm usually attributed to warm dust. Complexes of young stars and, in some cases, non-thermal sources appear to play a key role in heating the dust, but our understanding of this phenomenon is severely limited by our not knowing how the emission is spatially distributed in the centers of a large sample of galaxies. We must be able to relate their infrared spatial structure to fundamental galactic properties determined throughout the spectrum.

Although numerous galaxies have been observed at $\lambda > 10$ μm by IRAS and from the ground, these survey data are either of low spatial resolution, as in the case of IRAS, or obtained with a single small focal-plane aperture (typically 6" in diameter) centered on a visually prominent position. Multi-aperture observations (e.g., Rieke 1976) have established scale sizes for central infrared-emitting regions in a few galaxies, while mapping (e.g., Telesco and Gatley 1984) has defined the details of the infrared spatial distributions in several others. However, single-beam infrared mapping is very time consuming, and the list of mapped galaxies is still short; only nine were mapped prior to the present study. To address this problem, we at NASA Marshall Space Flight Center have developed a 20-pixel bolometer spatial array for use at 10-30 μm. This array has substantially increased our mapping speed, as illustrated by the fact that the total time required to map the four galaxies discussed here was less than half an observing night.

2. OBSERVATIONS AND ANALYSIS

The maps were made at 10.8 μm ($\Delta\lambda$ = 5.3 μm) and were obtained at the NASA Infrared Telescope Facility in 1985 November (NGC 1808) and 1986 March (M83, NGC 4536, and NGC 4527). The 20 array pixels were arranged in a 5 x 4 (RA x Dec) configuration with each square pixel having dimensions (FWHM) 4".3 x 4".3. The pixel center-to-center separation was 4".5. All maps are presented here at the same scale, with the pixel size shown in Figure 2. Except for the lower 5" of

Carol J. Lonsdale Persson (Editor)
Star Formation in Galaxies

the map of NGC 1808, the separation between adjacent observed positions was one-half pixel. The lowest contours drawn in each map correspond to a signal-to-noise ratio $\gtrsim 2$, and the mapped regions are enclosed by dashed lines. In these maps, the cross designates the visually prominant position used for guiding at the telescope. We have also found that the 2 μm peaks, which correspond to the true nuclei as defined by the peaks in the mass distribution of old stars, are coincident with the visible nuclei in M83, NGC 4536, and NGC 4527.

The four galaxies are bright IRAS far-infrared sources also detected by IRAS at 12 and 25 μm. The quoted flux densities are for 10.8 μm, but before comparison of our and IRAS fluxes, our flux densities are converted to equivalent 12 μm values using the 12 and 25 μm spectral slope, which is also used to color-correct the 12 μm IRAS data. Presented flux uncertainties do not include the ± 10% inherent in the absolute flux calibration.

3. RESULTS

Our 10.8 μm maps are fully reduced, but our analysis of these data is in progress. These results are therefore presented without significant interpretation. Preliminary comparison of the central infrared sources with available radio and visual images shows that the shapes are similar. The study of detailed correspondance (or lack thereof) of structure at various wavelengths must await the accurate relative positioning of our maps with respect to radio and visual images, a procedure now underway. Note that quoted infrared luminosities correspond to the range 10-300 μm and have been estimated by assuming a reasonable extrapolation beyond 100 μm (see Telesco and Harper 1980). We have also assumed that the energy distribution at each position in a map resembles that observed from the whole region.

3.1 NGC 5236 (M83)

The total 10.8 μm flux density in our map of NGC 5236 (Figure 1) is 3.3 ± 0.2 Jy, which accounts for 80% of the IRAS 12 μm flux. The diameter of the lowest contour is 500 pc at 6 Mpc, and the total source luminosity is ~1 x $10^{10} L_\odot$. Each of the two 10.8 μm peaks emits ~1 x $10^9 L_\odot$ in a region 130 pc in size. It is noteworthy that no prominent infrared source occurs at the visual and 2 μm nucleus. The infrared map bears a striking resemblance to the 21 cm map presented by Condon et al. (1982). The visual properties of the region spanned by our map are dominated by normal

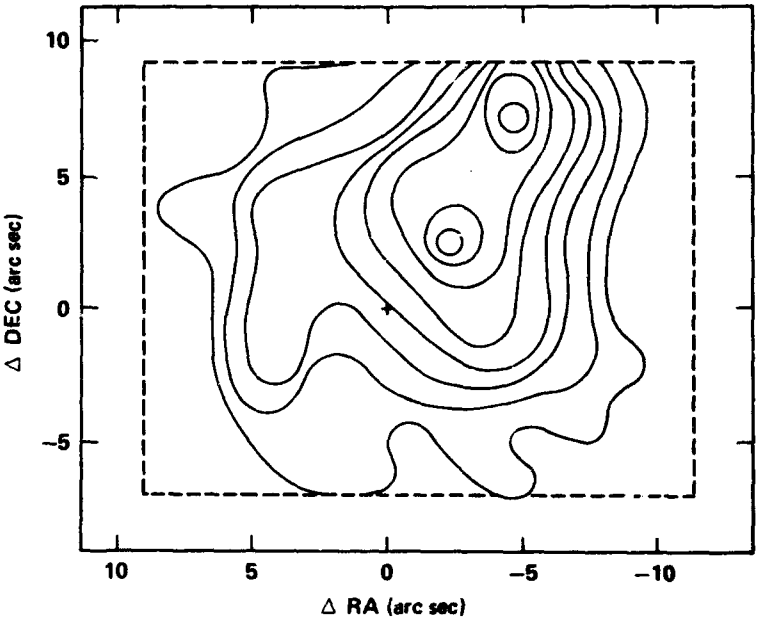

Figure 1. NGC 5236 (SBc) at 10.8 μm. The contour levels (mJy/pixel) are: 100, 150, 200, 250, 300, 350, 400, and 450.

HII regions (Pastoriza 1975), which, along with the infrared energy distribution, implies that the complicated and extended infrared emission is powered by young stars. A dust lane in the galactic bar enters the field near the bright infrared sources to the northwest. Another dust lane enters the field near the tongue-like feature in the southeast. We speculate that gas flow along the bar may be feeding the star formation which is occurring at rates (OBA stars) of 3 $M_\odot$ yr^{-1} throughout the mapped region and 0.4 $M_\odot$ yr^{-1} at the peaks.

3.2 NGC 1808

The 10.8 μm flux density within the lowest contour of our map of NGC 1808 (Figure 2) is 2.5 ± 0.1 Jy, which accounts for 69% of the flux in the IRAS 12 μm band. The remaining IRAS flux can be accounted for by lower level emission in the mapped region. The luminosity within the lowest contour, which has a maximum dimension of 1 kpc at 11 Mpc, is 2 x $10^{10} L_\odot$. The peak luminosity is 5 x $10^9 L_\odot$ from a region 230 pc in size. NGC 1808 appears to contain a weak Seyfert nucleus embedded in a bright emission-line region ionized by young stars (Véron-Cetty and Véron 1985). Our map implies that the Seyfert nucleus emits < 25% of the infrared luminosity. The most intense IR emission originates in a region 200 pc x 400 pc in size which, if the lower visual and infrared contours coincide, is centered on the Seyfert nucleus.

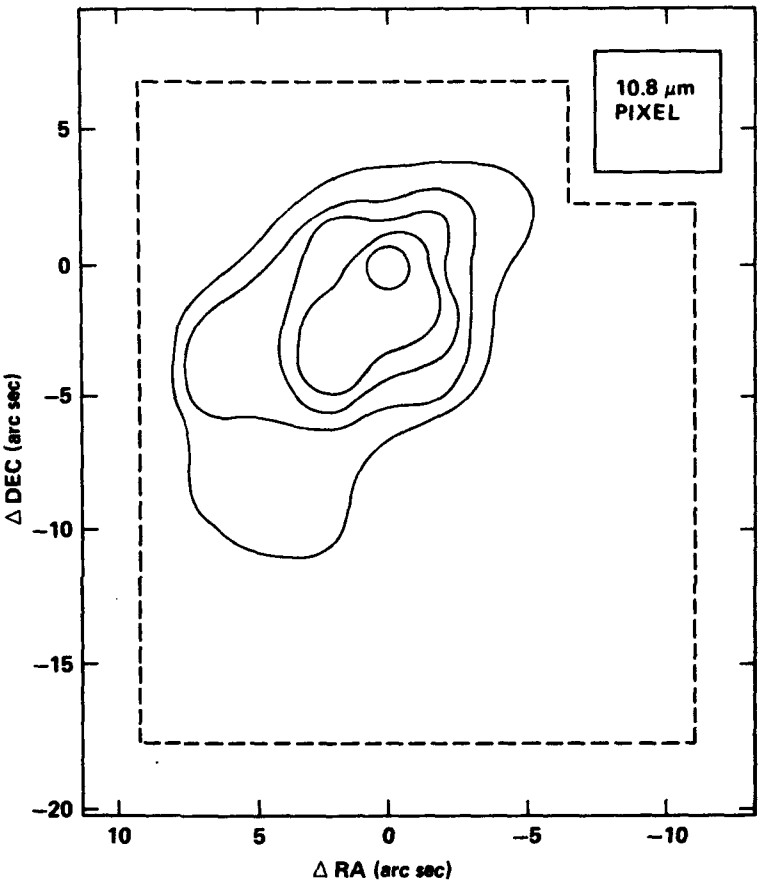

Figure 2. NGC 1808 (Sbc pec.) at 10.8 μm. The contour levels (mJy/pixel) are: 200 300, 400, 500, and 600.

3.3 NGC 4536 and NGC 4527

The 10.8 μm flux density within the lowest contour of our map of NGC 4536 (Figure 3) is 0.43 ± 0.03 Jy. From the entire mapped region, we detect 0.70 ± 0.09 Jy, which accounts for 57% of the IRAS 12 μm flux. The total infrared luminosity within the lowest contour, which has a long dimension of 1.4 kpc at 22 Mpc, is 1.4 x $10^{10} L_\odot$ The peak luminosity is 5 x $10^9 L_\odot$ from a region 460 pc in size and originates within 1" of the visual peak. The shape of the infrared source in NGC 4536 closely resembles that of the radio continuum emission (Condon et al. 1982).

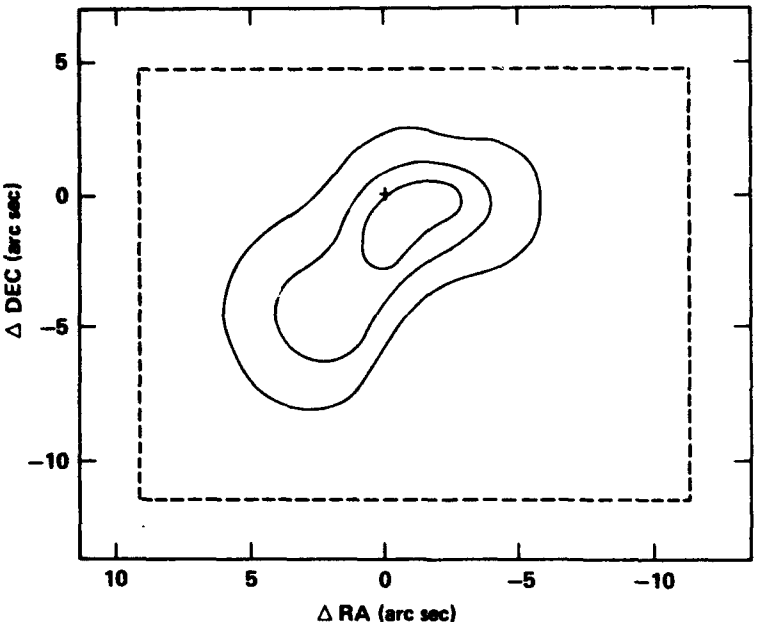

Figure 3. NGC 4536 (Sc) at 10.8 μm. The contour levels (mJy/pixel) are: 50, 100, and 150.

The 10.8 μm flux density from NGC 4527 (Figure 4) is 0.51 ± 0.04 Jy within the lowest contour, which accounts for 54% of the IRAS 12 μm flux. The lowest infrared contour has a long dimension of 2 kpc at 21 Mpc. The luminosity within the lowest contour is 3 x $10^{10} L_{\odot}$, with 7 x $10^{9} L_{\odot}$ originating in a 430 pc region centered on each of the two brightest peaks. Although the complicated emission region is roughly centered on the visual peak, no obvious infrared peak occurs there.

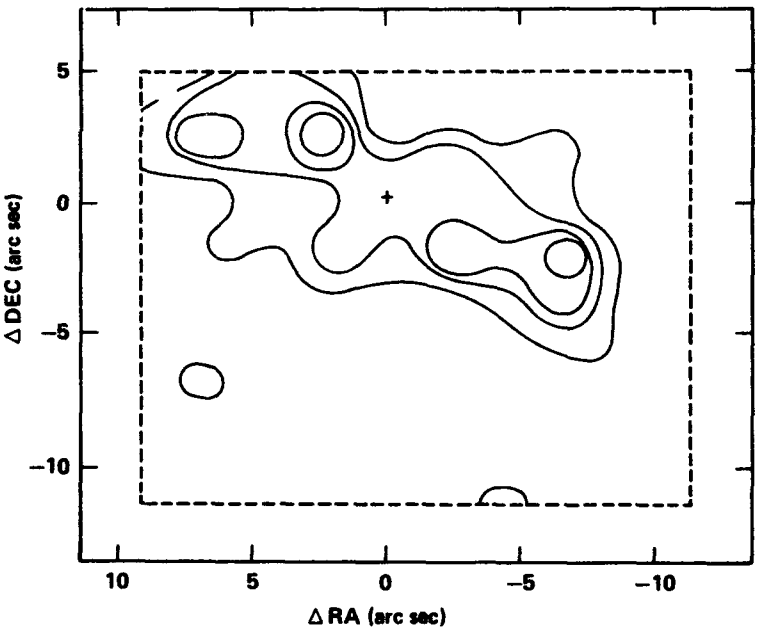

Figure 4. NGC 4527 (Sb) at 10.8 μm. Contour levels (mJy/pixel) are: 50, 75, 100, and 125.

REFERENCES

Condon, J. J., Condon, M. A., Gisler, G., and Puschell, J. J. 1982, Ap. J., 252, 102.
Pastoriza, M. G. 1975, Astrophys. Sp. Sci., 33, 173.
Rieke, G. H., 1976, Ap. J. (Letters), 206, L15.
Telesco, C. M., and Gatley, I. 1984, Ap. J., 284, 557.
Telesco, C. M., and Harper, D. A. 1980, Ap. J., 235, 392.
Véron-Cetty, M.-P., and Véron, P. 1985, Astron. Astrophys., 145, 425.

Far-infrared activity and starburst galaxies

P. Belfort, R. Mochkovitch, M. Dennefeld
Institut d'Astrophysique de Paris
98 bis, boulevard Arago
75014 Paris - France

Abstract

After the IRAS discovery of galaxies with large far-infrared to blue luminosity ratio, it has been proposed that an enhanced star formation could be the origin of the far-infrared emission through dust heating. We have investigated whether a simple photometric model is able to account for the FIR and optical properties of IRAS galaxies. The L_{IR}/L_B ratio, (B−V) color and H_α equivalent width of normal spirals are well reproduced with smooth star formation histories. In the case of starburst galaxies, several theoretical diagrams allow us to estimate the burst strength and extinction. L_{IR}/L_B ratio up to 100 can be rather easily reached, whereas extreme values (~500) probably require IMF truncated at the low end.

1.Introduction

One of the most striking IRAS discoveries is the discovery of galaxies with far-infrared activity (L_{IR}/L_B) of several tens, some extreme objects even exhibiting L_{IR}/L_B ratios of 100 or greater. According to the energy distribution and optical spectra of these galaxies, bursts of star formation have been proposed to explain their far-infrared (FIR) emission.

The purpose of this work was to check whether a simple photometric model could reproduce the FIR and optical properties of both normal and starburst galaxies.

A sample of "normal" spirals has been studied first. Then, the effects of bursts occuring in normal underlying galaxies have been investigated. Several theoretical diagrams were obtained which allow us to estimate the burst strength b (as defined by Larson and Tinsley, 1978) and internal extinction E_b(B−V) for two samples of starburst and interacting galaxies. Finally, the case of the most extreme IRAS galaxies (with $L_{IR}/L_B \sim 500$) is discussed.

2.Normal galaxies

The stellar population of a normal galaxy is computed for a given initial mass function (IMF) and a history of the star formation (ratio of the present SFR to the average past SFR). The dust content is described by the internal extinction E(B−V) and the fraction (1−f) of the Lyman continuum photons directly absorbed by dust.

The IMF proposed by Kennicutt (1983) for normal galaxies has been adopted. Both on observational (Vrba et al., 1984) and theoretical (Serra et al., 1980) grounds, we have assumed that massive stars, which spend most of their life inside or in the vicinity of molecular clouds, are on average more reddened than lower mass stars. So, a specific extinction e' for stars more massive than $\sim 20\ M_\odot$ has been introduced in addition to a uniform extinction e affecting all stars.

As shown in figures 1 and 2, the Hα equivalent width and FIR activity of our 44 sample galaxies are well reproduced with this model.

Carol J. Lonsdale Persson (Editor)
Star Formation in Galaxies

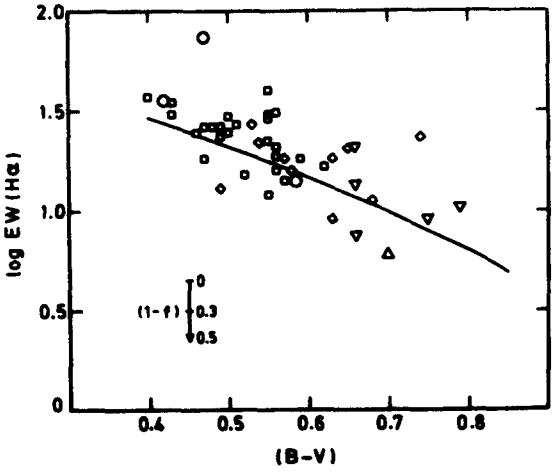

Figure 1

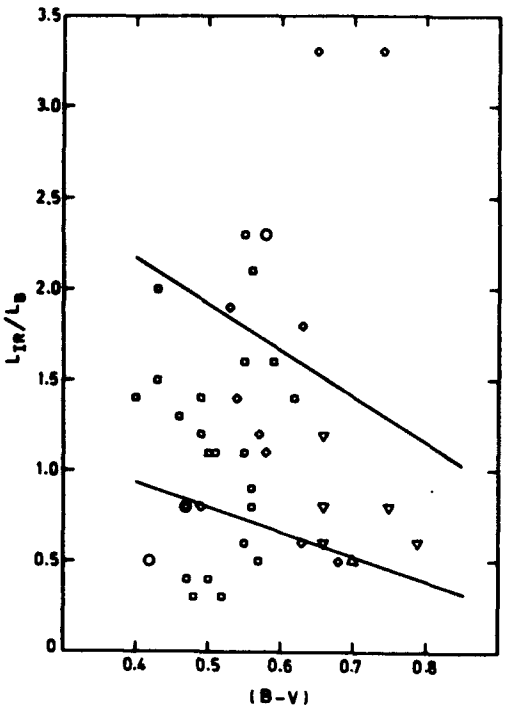

Figure 2

Figure 1. Log EW(H_α) vs (B−V) diagram : normal spirals.
The EW(H_α) are from Kennicutt et al. (1983) and (B−V) colors (corrected for galactic reddening) are from the RC2 catalog (1976). Morphological types : Δ Sab, ∇ Sb, ◇ Sbc, □ Sc, O Sm–S pec. The theoretical line has been obtained with e = 0.05, e' = 0.35, (1−f)=0.3 and a galactic extinction law (Savage et al., 1979).

Figure 2. L_{IR}/L_B vs (B−V) diagram : normal spirals.
The relation $F_{IR} = 1.75\,10^{-11}\,(12.66\,S_{12} + 5.00\,S_{25} + 2.55\,S_{60} + 1.01\,S_{100})$ erg.cm^{-2}.s^{-1} (Boulanger et al., 1985) has been used to estimate the FIR luminosities. The flux densities (in Jansky) are from the Point Source Catalog (1985). Most of the galaxies lie within the area between the two theoretical lines which may represent a realistic range of extinction for typical spirals (lower line : e = 0.02, e' = 0.35 and upper line : e = 0.10, e' = 0.35).

The few galaxies outside of the "normal" range in figure 2 can be accounted for by lower or larger internal extinction. However, NGC 4666 and NGC 6574 have a rather large L_{IR}/L_B (~ 3.3), more likely due to a slightly enhanced star formation.

3.Starburst galaxies

We have built starburst galaxies from normal ones by adding an enhanced star formation event, simply represented by a step function. Three new parameters are then required : the duration τ of the burst, its age Δt and its strength b (as defined in Larson and Tinsley, 1978). The IMF has been assumed identical in burst and host galaxy and we have adopted a uniform extinction E_b(B−V) in the burst where the stars have been formed recently and are then all located near their birth–place.

Figures 3, 4 and 5 show how the FIR activity, UBV colors and H_α equivalent width are affected by bursts of different strength and extinction.

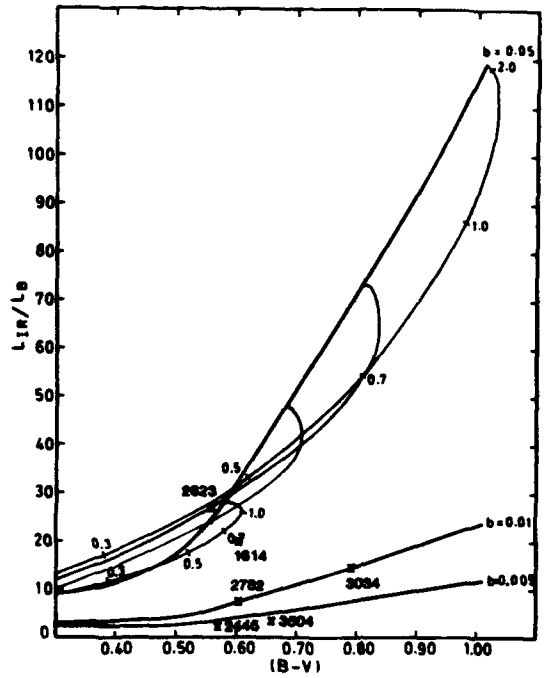

Figure 3. L_{IR}/L_B vs (B−V) : starburst galaxies.
The three heavy lines correspond to galaxies experiencing bursts of strength b = 0.005, 0.01, 0.05 and internal extinction $E_b(B-V) = 3$. Thin lines show the effect of a decreasing extinction on the FIR activity and (B−V) color (the $E_b(B-V)$ values are indicated).

This diagram can be used to estimate the strength b in starburst galaxies. The corresponding UBV and log EW(H_α) vs (B−V) diagrams (fig. 4 and 5) then give an estimation of the burst extinction $E_b(B-V)$. As an example, NGC 1614, 2445, 2623, 2782, 3034 and 3504 are reported. Estimation of b and $E_b(B-V)$ are summarized in the table.

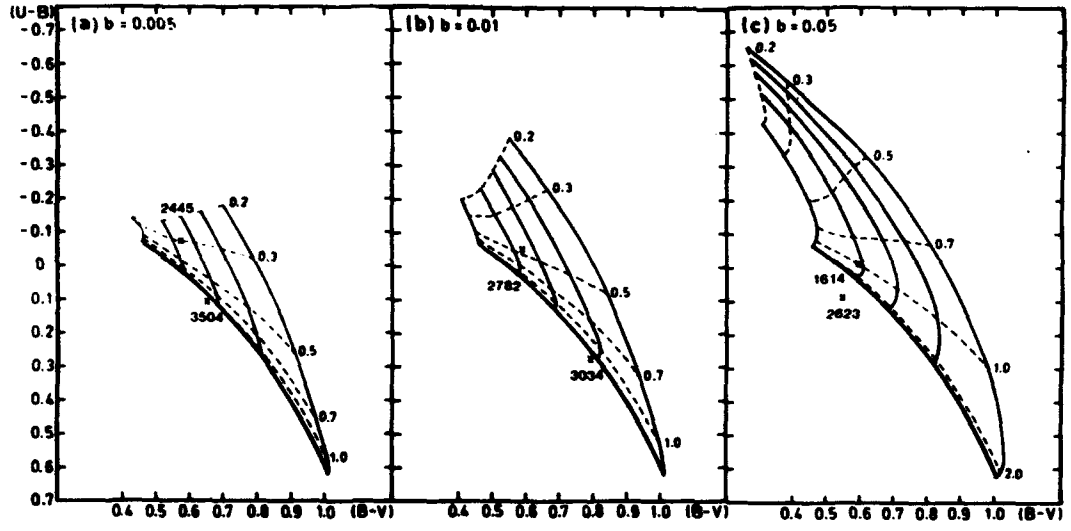

Figure 4. (U−B) vs (B−V) diagram : starburst galaxies.
Sequences of normal galaxies are represented by heavy lines. Thin lines show the effect of a

decreasing $E_b(B-V)$ on the UBV colors. Dashed lines are sequences of same $E_b(B-V)$.

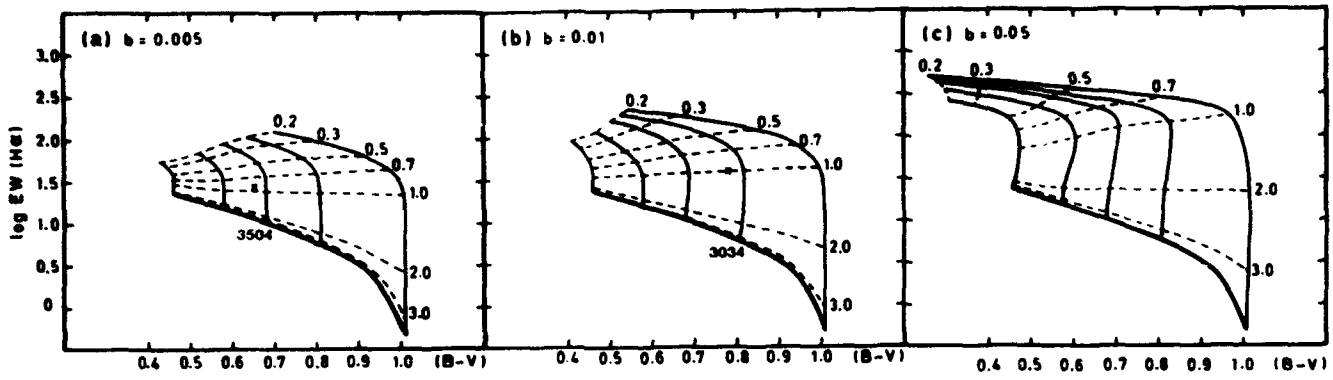

Figure 5. same as figure 4, but for logEW(H_α) vs (B−V) diagram

NGC	b	$E_b(B-V)$
1614	~0.04	>0.7
2445	<0.005	~0.3
2623	~0.05	>1
2782	~0.01	≥0.5
3034	~0.01	>1
3504	<0.005	0.5–1

Table : Estimation of the strength b and extinction $E_b(B-V)$ for the galaxies reported in fig. 3, 4, 5.

In the figures 3, 4 and 5, all the bursts have been assumed to be in progress since 2.10^7 years. Of course, when a burst gets old these figures cannot be used to estimate b and $E_b(B-V)$. However, as the L_{IR}/L_B ratio decreases quickly after the end of a burst, a galaxy with large FIR activity likely experiences a recent burst. Furthermore, if $E_b(B-V)$ is not too large, only a current or very young burst contributes significantly to the H_α equivalent width.

4.Extreme IRAS galaxies

Figure 3 shows that L_{IR}/L_B ratios up to 100 are rather easily reached (at least in red host galaxies) but extreme values ~ 500 are observed in IRAS 0404+101 and IRAS 0413+122 (Aaronson et al., 1984;Houck et al., 1985). Such FIR activities would imply bursts of strength b ~ 0.4– 0.5, clearly too large for a typical gas content. If these extreme L_{IR}/L_B ratios are actually due to starburst events (Allen et al., 1985), more reasonable b would be obtained with an IMF forming massive stars only. For instance, with a lower mass limit at ~ 9 $M_\odot$, a strength b of 8–10% could produce L_{IR}/L_B ~500.

5.Conclusion

Thus, a simple photometric model is able to account for the FIR and optical properties of both normal and starburst galaxies. Of course uncertainties in the duration and age of the burst complicate the interpretation of the observational data. However, bursts of star formation, put forward on observational evidences to explain many of the luminous IRAS galaxies, appear to be realistic from this theoretical study.

Effects of other choices for the burst parameters (age, duration, IMF) are discussed with more details in a paper submitted to Astronomy and Astrophysics, main journal.

References.

Aaronson, M., Olzewski, E.W. : 1984, Nature, **309**, 414.
Allen, D.A., Roche, P.F., Norris, R.P. : 1985, Monthly Notices Roy. Astron. Soc., **213**, 67p.
Boulanger, F., Baud, B., van Albada, G.D. : 1985, Astron. Astrophys. Letters, **144**, L9.
de Vaucouleurs, G., de Vaucouleurs, A., Corwin, N.C. : 1976, Second Reference Catalogue of Bright Galaxies, Austin : University of Texas Press.
Houck, J.R., Schneider,D.P. Danielson, G.E., Beichman, C.A., Lonsdale, C.J.,Neugebauer, G., Soifer, B.T. : 1985 , Astrophys. J. Letters, **290**, L5.
Joint IRAS Science Working Group : 1985, IRAS Point Source Catalog, Washington : US Government Printing Office.
Kennicutt, R.C. : 1983, Astrophys. J., **272**, 54.
Kennicutt, R.C., Kent, S.M. : 1983, Astron. J., **88**, 1094.
Larson, R.B., Tinsley, B.M. : 1978, Astrophys. J., **219**, 46.
Savage, B.D., Mathis, J.S. : 1979, Annu. Rev. Astron. Astrophys., **17**, 73.
Serra, G., Puget, J.L., Ryter, C.E. : 1980, Astron. Astrophys., **84**, 220.
Vrba, F.J., Rydgren, A.E. : 1984, Astrophys. J., **283**, 123.

IRAS Observations of Starburst Galaxies

Kazuhiro Sekiguchi
Department of Astronomy, New Mexico State University
Las Cruces, New Mexico 88003 U.S.A.

ABSTRACT

Far-infrared properties of Starburst galaxies were analyzed using IRAS observations at 25, 60, and 100 μm. Seventy-nine of 102 Starburst galaxies from the list of Balzano were detected. These galaxies have high IR luminosities of up to a few 10^{12} $L_\odot$ and concentrate in a small area of the IR color - color diagram. The IR power law spectral indices, α, lie within the ranges $-2.5 < \alpha(60,25) < -1.5$ and $-1.5 < \alpha(100,60) < 0$. These observed indices can be interpreted in terms of a cold (~30 K) disk component and a warm (~80-90K) component. More than 80% of the 60 μm emission comes from the warm component. The fraction of the 60 μm emission attributable to the warm component can be used as an activity indicator.

INTRODUCTION

Strong infrared excess is known to be a property of starburst galaxies. It has been suggested (Rieke and Low 1975; Rieke et al. 1980; Weedman et al. 1981; Gehrz, Sramek, and Weedman 1983) that this IR excess is from gas and dust heated by newly born massive stars. The maxima of these IR fluxes fall into the IRAS wavelengths ranges, 12, 25, 60, and 100 μm. There is an indication that a large fraction of the IRAS selected infrared luminous galaxies are starburst galaxies (Elston et al. 1985; Allen , Roche, and Norris 1985; Soifer et al. 1986). Some of them such as NGC 6240 (Wright, Joseph, and Meikle 1984) show high luminosities, up to 10^{12} $L_\odot$, comparable to those of quasars.

It is therefore of interest to examine the far-infrared properties of starburst galaxies. In this paper we present the infrared properties of starburst galaxies based on the IRAS survey data. Then we try to interpret these properties in terms of their star formation activity.

SAMPLE SELECTION

Galaxies studied by Balzano (1983) were used as the prime sample of starburst galaxies. These galaxies are known to have a nuclear starburst which dominates their observable properties in many wavelengths. In addition to the Balzano galaxies, two well known starburst galaxies NGC 3690 (Gehrz, Sramek, and Weedman 1983) and NGC 6240 (Rieke et al. 1985) were included in the sample. Eighty-one of 104 sample starburst galaxies are identified and listed in the Cataloged Galaxies and Quasars Observed in the IRAS Survey (Lonsdale et al. 1985). Quoted flux densities of 25, 60, and 100 μm in the catalogue were used. Since color correction for a black body source with T ~ 100 K is small at 60 and 100 μm (< 4%), and ~ 16% at 25 μm, no color corrections were applied.

Carol J. Lonsdale Persson (Editor)
Star Formation in Galaxies

RESULTS

Figure 1 is a plot of power law spectral index $\alpha(60,25)$ vs. $\alpha(100,60)$ for all the starburst galaxies observed by the IRAS survey. The spectral index is defined by $-\alpha(\lambda_2,\lambda_1) = \mathrm{Log}(f_2/f_1)/\mathrm{Log}(\lambda_2/\lambda_1)$, where f_i is the observed flux density at λ_i. This figure shows a large scatter of observed colors among the objects. Some are even located above the power law line. No apparent trend or tendency is seen from this plot. One reason for this large scatter is that not all of the observed flux values are of the same quality. (A detailed discussion of the uncertainties of IRAS measurements is given in IRAS Explanatory Supplement. Beichman et al. 1985)

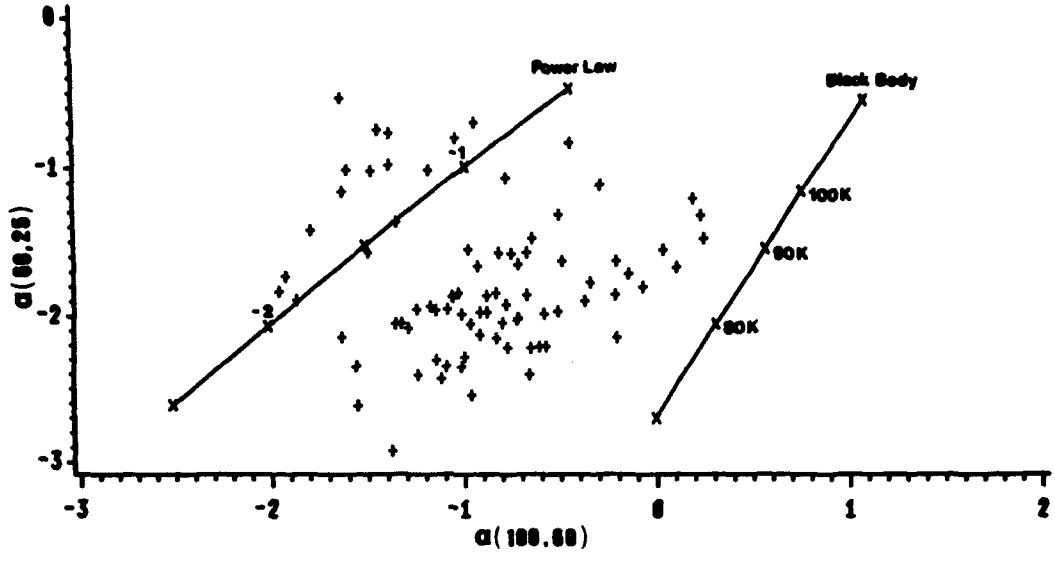

Figure 1. An infrared color-color plot for all starburst galaxies detected and identified by the IRAS survey. The spectral indexes are defined in the text. The loci for Black body and Power law sources have been plotted for comparison. The numbers along the Power law line are the spectral indices and along the Black body line are the temperatures.

To obtain more reliable far-infrared colors of the starburst galaxies, we imposed certain constraints on the sample. First, only flux densities of good quality were selected. Then, to reduce uncertainties, only quoted flux values with a 1σ flux uncertainty $\delta f_\nu/f_\nu < 0.12$ were used. Finally, to minimize possible effects of the different diaphragm sizes at 25 μm (~0'.76 x 4'.6), 60 μm (~1'.5 x 4'.75), and 100 μm (~3'.0 x 5'.0), a distance limit $z > .0067$ corresponding to distances exceeding 28 Mpc (A Hubble constant of 75 km s^{-1} Mpc^{-1} is used throughout this paper) was applied. If a typical galactic disk has a radius 20 kpc, then a distance of 23 Mpc implies 3'.0 in angular dimension. Therefore, at least for the flux densities at 60 and 100 μm used to obtain total infrared luminosity, the diaphragm size effect should be small.

After having applied these criteria, nineteen objects remained for further analysis. Table I gives the identifications of these galaxies along with other pertinent information. Figure 2 shows the infrared color of these 19 galaxies. From this figure it is apparent that starburst galaxies occupy a distinct and quite localized position in the diagram. The mean spectral indices for these galaxies are $\langle\alpha(60,25)\rangle = -2.02 \pm 0.16$ and $\langle\alpha(100,60)\rangle = -0.71 \pm 0.35$.

Table I

Object	IRAS Name	α(60,25)	α(100,60)	z[1]	Tw (°K)	P	Log(Lw) (ergs s-1)	Log(Lc) (ergs s-1)	Log(LIR) (ergs s-1)
Mk 133	09578+ 7222	- 1.97	- 1.15	0.0068	87	.92	43.43	42.93	43.55
Mk 158	10560+ 6147	- 2.22	- 0.66	0.0068	80	.89	43.85	43.14	43.93
Mk 161	10591+ 4529	- 2.13	- 0.92	0.0200	82	.85	44.25	43.68	44.36
Mk 201	12116+ 5448	- 1.87	- 0.22	0.0084	85	.93	44.52	43.54	44.56
Mk 213	12290+ 5814	- 1.99	- 1.02	0.0105	86	.84	43.92	43.36	44.02
Mk 286	14188+ 7148	- 2.02	- 0.73	0.0250	84	.87	44.72	44.06	44.81
Mk 326	23256+ 2315	- 1.85	- 0.84	0.0130	88	.86	44.12	43.48	44.21
Mk 496E	16104+ 5235	- 1.93	- 0.78	0.0290	86	.86	45.02	44.39	45.11
Mk 602	02572+ 0234	- 1.87	- 0.89	0.0099	88	.85	43.84	43.23	43.94
Mk 691	15447+ 1802	- 2.30	- 1.15	0.0110	80	.83	43.93	43.45	44.06
Mk 708	09395+ 0454	- 2.22	- 0.78	0.0070	80	.87	43.67	43.04	43.76
Mk 717	10078+ 2439	- 1.73	- 0.16	0.0212	88	.93	44.56	43.57	44.60
Mk 799	13591+ 5934	- 2.09	- 1.29	0.0110	85	.81	44.36	43.91	44.50
Mk 897	21052+ 0340	- 2.05	- 0.80	0.0260	83	.87	44.60	43.95	44.68
Mk 1089	04591 - 0419	- 1.99	- 0.59	0.0120	83	.89	44.04	43.31	44.12
Mk 1093	05053 - 0805	- 2.21	- 0.58	0.0140	80	.90	44.52	43.76	44.59
Mk 1379	14150 - 0711	- 2.03	- 0.73	0.0094	83	.87	43.90	43.24	43.98
NGC3690	11257+ 5850	- 1.81	- 0.08	0.0100	86	.94	45.35	44.29	45.38
NGC6240	16504+ 0228	- 2.15	- 0.21	0.0246	80	.94	45.43	44.43	45.47

1. Redshift Sources: Balzano (1983), for NGC 3690 Sandage and Tammann (1981) and for NGC 6240 Fosbury and Wall (1979).

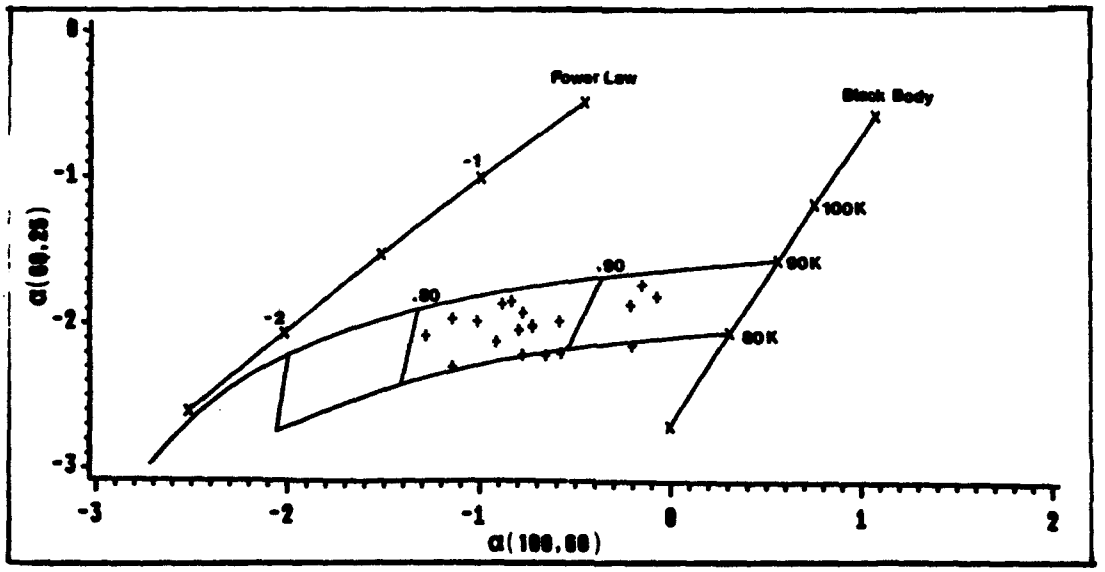

Figure 2. An infrared color-color plot for starburst galaxies with high quality measurement, 1σ flux uncertainty $\delta f_\nu / f_\nu < 0.12$, and redshift $z > .0067$. The loci for the two black-body model have been ploted in addition to the Black body and the Power law lines. Numbers along the two black-body model lines are the fraction of the warm component contribution to the total 60 μm flux.

To interpret the far-infrared colors of these galaxies, a two component black body model was used. A fixed cool temperature, Tc, of 30 K which represents the cold disk component was assigned. Then, a unique warm temperature, Tw, which represents all the IR sources except the 30 K component, can be obtained from the observed colors. In figure 2, we plotted loci of the two temperature model. Numbers along the two temperature model curves are the fractions, P, of the 60 μm warm component flux to the total 60 μm flux observed. The galaxies' Tw and P determined from observed colors are given in Table I.

Finally, using the procedure outlined by Lonsdale et al. (1985), the total IR luminosities from the two temperature model were computed. The total IR, L_{IR}, the warm, Lw, and the cool, Lc, component luminosities are given in Table I.

DISCUSSION

The far-infrared colors of the starburst galaxies are quite distinct. Their color indices α(60,25) are steeper than the range of Seyfert selection criterion, $-1.5<\alpha(60,25)<-0.25$ (de Grijp et al. 1985). Compared to the median color indices of Seyferts and H II region galaxies (Miley, Neugebauer, and Soifer 1985), separation from Seyfert 1's is clear. However, there is significant overlap with Seyfert 2's. As is expected, H II region galaxies show almost the same color as those of the starbursts. On the other hand, the indices α(100,60) of the starbursts are similar to those of the Seyfert's. They are much flatter than those of non-active spirals (de Jong et al. 1984) and infrared galaxies in the IRAS minisurvey (Soifer et al. 1984).

From Figure 2, it can be seen that the starburst galaxies occupy a relatively small range, ~80 to 90 K, of Tw and a wider range, ~.80 to .95 of P. Since the warm component mainly represents warm gas and dust associated with a star-formation region, Tw and P should indicate their physical state and degree of activity. The flat α(100,60) of starburst galaxies may be the result of a larger warm component contribution to the total IR flux than that of non-active spirals (ie. large P).

The total IR luminosity of the starburst galaxies ranges from 10^{10} to 10^{12} $L_{\odot}$. NGC 6240 is the most extreme. At the low luminosity end there is overlap with non-active spirals.

We thank K.S. Anderson for his valuable help and comments and S.W. Berrick for help with manuscript preparation.

REFERENCES

Allen, D.A., Roche,P.F.,and Norris, R.P., 1985, M.N.R.A.S., 213, 67P
Balzano, V.A., 1983, Ap. J., 268, 602
Beichman, C.A., Neugebauer, G., Habing, H.J., Clegg, P.E., and Chester, T.T., 1985, IRAS Explanatory Supplement.
de Grijp, M.H.K., Miley, G.K., Lub, J., and de Jong, T., 1985, Nature, 314, 240
de Jong, T., et al., 1984, Ap. J., 278, L67
Elston, R., Cornell, M.E., and Lebofsky, M.J., 1985, Ap. J., 296, 106
Fosbury, R.A.E. and Wall, J.V., 1979, M.N.R.A.S., 189, 79
Gehrz, R.D., Sramek, R.A., and Weedman, D.W., 1983, Ap. J., 267, 551
Lonsdale, C.J., Helou, G., Good, J.C., and Rice, W., 1985, Cataloged Galaxies and Quasars Observed in the IRAS Survey.
Miley, G.K., Neugebauer, G., and Soifer, B.T., 1985, Ap. J., 293, L11
Rieke, G.H., and Low, F.J., 1975, Ap. J., 197, 17
Rieke, G.H., Lebofsky, M.J., Thompson, R.I., Low, F.J., and Tokunaga, A., 1980, Ap. J., 238, 24

Rieke, G.H., Cutri, R.M., Black, J.H., Kailey, W.F., McAlary, C.W., Lebofsky, M.J., and Elston, R., 1985, Ap. J., 290, 116
Sandage, A. and Tammann, G.A., 1981, A Revised Shapley - Ames Catalog of Bright Galaxies.
Soifer, B.T., et al., 1984, Ap. J., 278, L71
Soifer, B.T., et al., 1986, Ap. J., 303, L41
Weedman D.W., Feldman, F.R., Balzano, V.A., Ramsey, L.W., Sramek, R.A., and Wu, C.C., 1981, Ap. J., 248, 105
Wright, G.S., Joseph, R.D., and Meikle, W.P.S., 1984, Nature, 309,430

INTERACTING AND MERGING GALAXIES

A NEAR-INFRARED STUDY OF THE LUMINOUS MERGING GALAXIES NGC 2623 AND ARP 148*

MARSHALL JOY† AND PAUL M. HARVEY†
Astronomy Department, University of Texas at Austin
Austin, Texas 78712

ABSTRACT

As part of an investigation of the physical mechanisms which produce large infrared luminosities in interacting systems, we have obtained multicolor near-infrared maps of the long-tailed galaxy NGC 2623 and the ring galaxy Arp 148. We decompose the near-infrared broadband spectrum to obtain the contributions of four processes: emission from evolved stars, nebular continuum emission, thermal reradiation, and extinction. This multicolor analysis, along with 2 μm maps and 10 μm measurements, is used to determine the structure of these interacting galaxies and to delineate regions of star formation.

Previous optical studies have suggested that both NGC 2623 and Arp 148 are in the process of merging. Although much of the optical structure in the nuclear regions is found to be an artifact of obscuration, our infrared analysis confirms that these galaxies are coalescing. Theoretical models indicate that the pair of narrow tails in NGC 2623 are the result of a tidal interaction between two spiral galaxies whose orbits are destined to decay within several revolutions; since a single nucleus is observed in the infrared, we conclude that the merger is complete. The ring galaxy Arp 148 is found to be the product of a close collision of two galaxies, and our multicolor analysis implies that this system is in a very early stage of coalescence. The nuclear regions of Arp 148 and NGC 2623 are extremely luminous in the infrared (~3.5 x 10^{11} $L_{\odot}$); evidence indicates that recently formed stars are the source of the infrared emission in NGC 2623.

---

* Manuscript submitted to the *Astrophysical Journal*, 4 June 1986.

†Visiting astronomers at the Infrared Telescope Facility, which is operated by the University of Hawaii under contract from the National Aeronautics and Space Administration.

Star Formation in the Merging Galaxy NGC3256

James R. Graham[1], G. S. Wright[2], R. D. Joseph[3], J. A. Frogel[4], M. M. Phillips[4], & W. P. S. Meikle[3]

[1]Lawrence Berkeley Lab., [2]Royal Observatory Edinburgh,
[3] Imperial College London, [4] CTIO.

Abstract

We have mapped the central 5kpc of the ultra-luminous merging galaxy NGC3256 (Graham et al. 1984) at J, H, K, L, & 10μm, and obtained 2μm spectra of the nuclear region. We use this data to identify and characterize the super-starburst which has apparently been triggered and fuelled by the merger of two gas-rich galaxies. We will also show that the old stellar population has relaxed into a single spheriodal system, and that a supernova driven wind might eventually drive any remaining gas from the system to leave a relic which will be indistinguishable from an elliptical galaxy.

1 Introduction

NGC3256 is a spectacularly disturbed galaxy which has been identified as a merger (Toomre 1977). At a distance of 50Mpc (H_0=50km/s/Mpc) this is one of the closest and most luminous such systems, and therefore it can be studied in some detail. The IR maps of NGC3256 were made at a resolution of 5", which corresponds to 1.3kpc. These maps show emission extending over 5kpc.

2 Mapping and Spectroscopy

The 10μm emission is quite remarkable both in its extent and luminosity (see figure 1). The 10μm luminosity (defined as νL_ν) in the central kpc corresponds to $1x10^{10} L_\odot$, this increases to $3x10^{10} L_\odot$ within 2kpc of the nucleus, and to $6x10^{10} L_\odot$ in IRAS band 1 (12μm, projected aperture of 12x70kpc). Thus not only does this galaxy rank among the most luminous galaxies known (e.g NGC6240 or Mrk231, Wright et al.; 1984, Rieke et al. 1978) but most of the IR luminosity arises from outside the central kpc!

Table 1

10μm Luminosity

Aperture (")	Corresponding Distance (kpc)	10μm Luminosity ($L_\odot$)
3.5	0.9	$8.4x10^9$
5	1.3	$1.4x10^{10}$
15	3.9	$3.4x10^{10}$

Carol J. Lonsdale Persson (Editor)
Star Formation in Galaxies

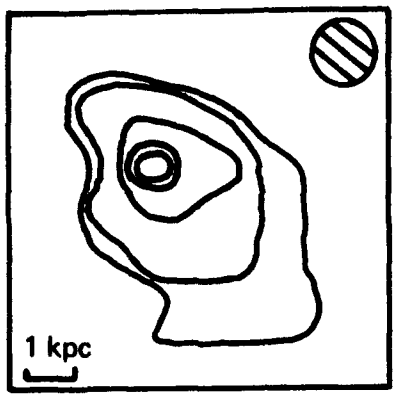

Figure 1

A map of NGC3256 at 10μm. The map was made at a resolution of 5" which corresponds to a distance of 1.3kpc. This map, and multi-aperture 10μm photometry shows that most of the emission at this wavelength arises from beyond the central kpc. The map contours are 44, 88, 175, 350, 700 mJy/beam.

Although this galaxy is thought to be the merger of two disc galaxies there is no evidence for two distinct systems from the near-IR colour maps (J, H, & K). These maps show that the distribution of old stars is relatively smooth. The structure which is present can be interpreted as due to extinction. The J-H map demonstrates that the structure to the south of the nucleus is caused by a dust lane with $A_v \sim 2$ mags. The near-IR colours can be explained in terms of emission from the old stellar population, reddened at J, and with some evidence for an additional hot dust component at K. The K-L colour on all pixels on and around the nucleus is > 1.0, indicating a strong non-stellar dust component at 3.5μm. The K-L colour map shows 2 off-nuclear 'hot-spots' indicating positions of high star formation efficiency. Multi-aperture photometry at K shows that the distribution of old red stars can be described accurately by a $r^{1/4}$ profile out to a radius of at least 5kpc. This indicates that as predicted violent relaxation has occurred following the collision producing a stellar distribution similar to that found in elliptical galaxies.

A spectrum of NGC3256 at 2μm shows two strong lines at $\lambda = 2.163$ and 2.134μm, which we identify as Bγ and H_2 1-0 S(1). The luminosity in these lines is approximately the same and equal to $7 \times 10^6 L_\odot$. The luminosity in these lines is high. In particular the H_2 flux exceeds that of NGC1068 (Thompson et al. 1978) and is comparable to Arp220, but an order of magnitude less than NGC6240 (Joseph et al. 1984)

Table 2

Spectroscopy

Wavelength (μm)	Line	Luminosity ($L_\odot$)
2.163	Bγ	7×10^6
2.134	H_2 1-0 S(1)	7×10^6

3 NGC3256 as a super-starburst.

The observational evidence overwhelmingly points to recent and extensive star formation triggered and fuelled by the merger of two gas-rich disc galaxies. The sheer extent of the luminosity at 10μm (5kpc), and its lack of confinement to nuclear regions is the single most persuasive piece of evidence in favour of star formation. Combining the above data the starburst within a radius of 1.5 kpc of the nucleus can be characterized by $4x10^6$ B0 stars producing a total of $3x10^{54}$ Lyman continuum photons per second, and a luminosity of $2x10^{11}L_\odot$ (see table 3).

Table 3

The Starburst within 1.5kpc of the nucleus

Total Luminosity ($L_\odot$)	$L_{B\gamma}/L_{IR}$	Spectral Type	# of Stars required
$2x10^{11}$	$4x10^{-5}$	B0	$4x10^6$

The ratio of H_2 emisssion in the 1-0 S(1) line to total luminosity is $4x10^{-5}$. A ratio of $1x10^{-5}$ would be expected for a star formation region such as Orion.

Finally we note that the energy that will be released when these young stars explode as supernovae exceeds the binding energy of the gas (as determined from the rotation curve) by a factor of 50. Thus, it is very likely that a supernova driven wind will blow away any gas remaining after the starburst has faded, and leave a relic which will be indistinguishable from an elliptical galaxy.

Acknowledgments

The observations described here were carried out at CTIO and ESO, and this work was partially supported by US Dept. of Energy Contract No. DE-AC03-76SF00098. J.R.G. is supported by research fellowships awarded by the Royal Commission for the Exhibition of 1851, and the UK SERC.

References

Glass I.S. & Moorwood A.F.M., 1985. *Mon. Not. Roy. astr. Soc.*, **214**, 429.
Graham J.R. Wright G.S. Meikle W.P.S. Joseph R.D. & Bode M.F., 1984. *Nature*, **310**, 213.
Joseph R.D. Wright G.S. & Wade R., 1984. *Nature*, **311**, 132.
Rieke G.H., 1978. *Ap. J.*, **226**, 550.
Thompson R.I. Lebofsky M.J. & Rieke G.H., 1978. *Ap.J.*, **222**, L49
Toomre A., 1977. In *Evolution of Galaxies and Stellar populations*, ed B.M. Tinsley & R.B. Larson, Yale University Observatory, 401.
Wright G.S. Joseph R.D. & Meikle W.P.S., 1984. *Nature*, **309**, 430.

D. SURVEYS

ORAL PRESENTATIONS

The Luminosity Function of the Brightest Galaxies in the IRAS Survey

B. T. Soifer[1], D. B. Sanders[1], B. F. Madore[1], G. Neugebauer[1],
C. J. Persson[2], S. E. Persson[3], W. L. Rice[2]

[1] Palomar Observatory, California Institute of Technology
[2] IPAC, California Institute of Technology
[3] Mt. Wilson and Las Campanas Observatory

ABSTRACT. Results from a study of the far infrared properties of the brightest galaxies in the IRAS survey are described. There is a correlation between the infrared luminosity and the infrared to optical luminosity ratio and between the infrared luminosity and the far infrared color temperature in these galaxies. The infrared bright galaxies represent a significant component of extragalactic objects in the local universe, being comparable in space density to the Seyferts, optically identified starburst galaxies, and more numerous than quasars at the same bolometric luminosity. The far infrared luminosity in the local universe is approximately 25% of the starlight output in the same volume.

1.0 INTRODUCTION

The IRAS survey was the first infrared all sky survey with sufficient sensitivity to detect a significant number of extragalactic sources. To understand the significance of the infrared emission from galaxies it is important to establish a census of the kinds of galaxies that are significant infrared emitters, to determine the space densities of these galaxies, and to compare infrared bright galaxies with other known classes of extragalactic objects.

We have begun a program to understand the properties of the brightest infrared galaxies discovered in the IRAS survey. This paper derives the far infrared luminosity function of this sample of galaxies. A preliminary description of the luminosity function for the most luminous members of this sample was reported by Soifer, *et al.* (1986a), while a detailed description of the entire sample is given by Soifer, *et al.* (1986b).

2.0 THE IRAS BRIGHT GALAXY SAMPLE

The objects selected for study in this survey were chosen to be a complete sample of far infrared emitting extragalactic objects. The final criteria defining the IRAS bright galaxy sample were all extragalactic objects having 60μm flux densities greater than 5.4 Jy and galactic latitude $| b | > 30°$. The area of sky where complete redshift information was obtained for candidate objects placed further areal constraints on the sample: Declination $\geq -30°$ for 0-12 hr, $\geq -15°$ for 12-14 hr, and $\geq -20°$ for 14-24 hrs.

The final sample was selected to be all extragalactic sources meeting the above constraints selected from the IRAS Point Source Catalog (1985), the Catalog of Small Scale Structures (1986), and the Catalog of IRAS Observations of Large Galaxies (Rice, *et al.* 1986). As would be expected, the data sampling the largest spatial scales always provided the largest 60μm flux density.

The total area covered in the Bright Galaxy survey is ~14,500 square degrees. There are 324 objects in the sample; 29 galaxies have 60μm flux densities taken from the Large Galaxy Catalog, 53 have 60μm flux densities taken from the Small Scale Structures Catalog, with the rest taken from the Point Source Catalog.

3.0 BASIC PROPERTIES OF THE BRIGHT GALAXY SAMPLE

The properties of the IRAS Bright Galaxy sample are important for describing the far infrared characteristics of the local Universe. A basic question is to determine the kind of objects contained in the sample. Although no morphological criterion was established for an object to be in the Bright Galaxy sample the vast majority of objects in the sample are cataloged galaxies. Furthermore only one object in the sample, IR0518-25 (Sanders, *et al.* 1986),

shows a predominantly stellar appearance on visible images. This object (described in detail by Sanders, *et al.*) has, in addition, broad emission lines and is clearly a Seyfert nucleus. Thus virtually all the infrared bright extragalactic objects in the local Universe are associated with galaxies.

All the galaxies in the Bright Galaxy sample have far infrared flux densities much greater than can be expected from a stellar population. None are known radio loud objects where the infrared emission could be expected to be an extension of a radio non-thermal source. Thus we assume that the far infrared peak in the energy distribution is due to thermal emission by dust.

The galaxies in the Bright Galaxy sample range in distances from 0.7 Mpc for M33 to >300 Mpc. The median distance is 32 Mpc, excluding Virgo galaxies. Thus the IRAS Bright Galaxy sample extends well beyond the local supercluster, but is not sampling objects at distances significant with respect to the size of the Universe, i.e. the sample is one of the far infrared properties of the local Universe. A total of 31 sample galaxies were identified as associated with the Virgo cluster. While the Virgo cluster presents a significant contribution to the Bright Galaxy sample, it by no means dominates the sample.

The range of observed far infrared luminosities extends from $\sim 10^8 L_\odot$ to $> 10^{12} L_\odot$, with the peak in the distribution occurring at $\sim 2 \times 10^{10} L_\odot$. For the IRAS Bright Galaxies the range in values of $\log(f_{ir}/f_b)$ is from -1 to 2.1, with a median value of $\log (f_{ir}/f_b)$ of 0.4, where f_{ir} is the far infrared flux from the galaxy, and f_b is the flux in the blue, defined as νf_ν (blue). This value is much greater that the corresponding value of $\log (f_{ir}/f_b)$ of $\sim$ -0.2 for an optically selected sample of galaxies. The infrared flux limited sample selects galaxies with much greater average infrared luminosity per unit blue luminosity than does a magnitude limited optical sample.

Figure 1 shows that f_{ir}/f_b correlates with L_{fir}, while there is no correlation between f_{ir}/f_b and L_b. The simplest explanation of this correlation is that the far infrared and blue luminosity components are uncorrelated, and the blue luminosities of the galaxies in the bright galaxy sample are roughly constant. Thus a larger f_{ir}/f_b ratio requires larger L_{fir} rather than extinction depressing the blue light. The absence of galaxies in the region of Figure 1 where $L_{fir} < 10^{10} L_\odot$ and $f_{ir}/f_b > 10$ shows that there are no dwarf galaxies in the Bright Galaxy sample with large f_{ir}/f_b ratios.

In Figure 2 the 60μm/100μm flux density ratio (effectively color temperature) is plotted vs far infrared luminosity. There is a correlation between the color temperature and the far infrared luminosity in the sense of higher luminosities generally implying higher 60μm/100μm color temperatures, while there is no correlation between the far infrared color temperature and the blue luminosity. The lack of correlation between far infrared color temperature and blue luminosity further supports the lack of coupling between the blue and far infrared luminosity components in these galaxies.

4.0 LUMINOSITY FUNCTION OF IRAS GALAXIES

The 60μm luminosity function derived from the Bright Galaxy sample is shown in Figure 3. Other 60μm luminosity functions have been derived based on other samples from the IRAS data (e.g. Lawrence, *et al.* 1986, Rieke and Lebofsky, 1986). We have compared these luminosity functions with that derived for the Bright Galaxy sample, and show this comparison in Figure 3. Here we have converted all the luminosity functions to the units used here, i.e. the bins represent the space density in galaxies per cubic megaparsec per magnitude interval in 60μm luminosity, where the 60μm luminosity is taken as νL_ν(60μm), and H_o is taken as 75 Km s^{-1} Mpc^{-1}. As can be seen from Figure 3 the agreement between the three luminosity functions, derived from completely different samples is excellent.

Two power laws, fit to the observed 60μm luminosity function, are shown in Figure 3. At low luminosity the best fit power law gives a slope $\rho \sim L^{-0.83}$, while at high luminosity the best fit slope is $\rho \sim L^{-2.05}$. The luminosity of the break between the two power laws is $\sim 2 \times 10^{10} L_\odot$. For comparison a Schechter function is also fit to the observed luminosity function.

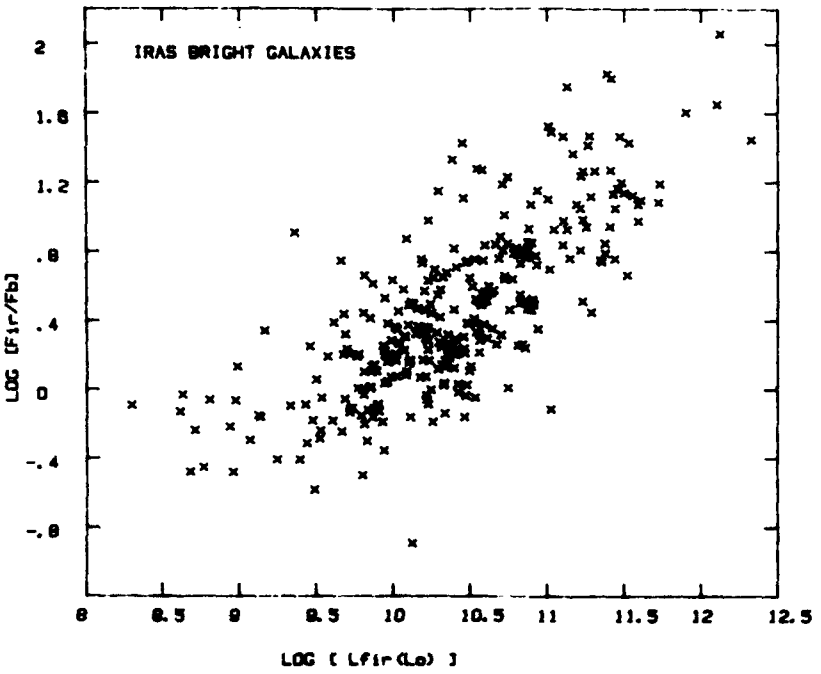

Figure 1: The ratio of the far infrared to blue flux plotted vs the far infrared luminosity for the galaxies in the Bright Galaxy Sample. The far infrared flux represents the integral of a single temperature Planck curve, convolved with an emissivity proportional to frequency, and fitted to the observed flux densities at 60μm and 100μm. The blue flux is taken to be νf_ν (blue). The luminosities were calculated using a Virgocentric velocity field where D_{Virgo} = 17.6 Mpc and H_o = 75 km $s^{-1}Mpc^{-1}$ at large distances.

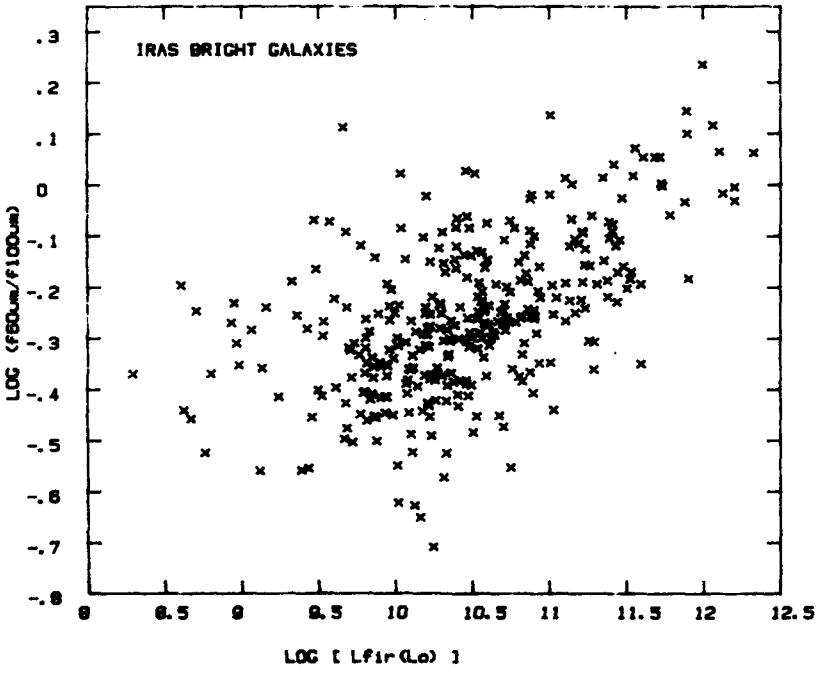

Figure 2: The ratio of the 60μm to 100μm flux densities plotted vs far infrared luminosity for the galaxies in the Bright Galaxy Sample.

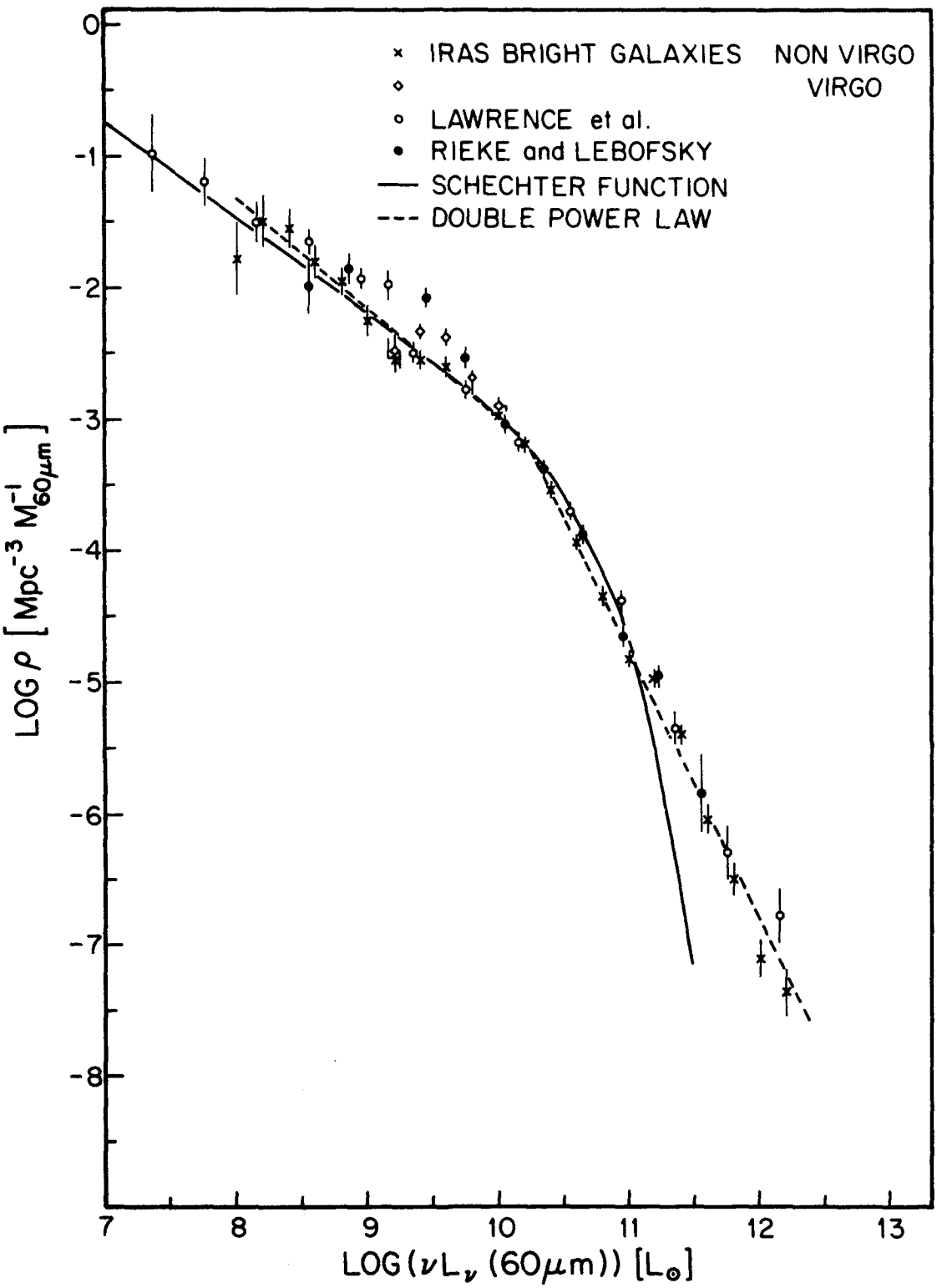

Figure 3: The 60μm luminosity function derived for the Bright Galaxy sample, plotted as space density in galaxies per cubic Megaparsec per magnitude range in 60μm luminosity vs 60μm luminosity. The 60μm luminosity is taken as νL_ν (60μm). For comparison the luminosity functions derived from different IRAS samples are shown as well. These are taken from Lawrence, *et al.* 1986 and Rieke and Lebofsky, 1986. Both a double power law and a Schechter type luminosity function are shown for comparison with the observed luminosity functions.

While the strict definition of the 60μm luminosity function is most appropriate for comparing the local luminosity function with the deeper surveys with IRAS (e.g. Hacking and Houck, 1986) and ultimately next generation space missions, one of the more immediate goals of the present study is to understand the significance of far infrared emission in the local Universe. This requires comparing the space densities of widely varying classes of objects. To do this in a meaningful way we have chosen to paramaterize the luminosities of objects by the bolometric luminosity. In Figure 4 the luminosity functions of a variety of different important classes of extragalactic objects are plotted. The far infrared luminosity has been adopted as the bolometric luminosity for the IRAS Bright Galaxy sample. The total far infrared luminosities calculated in this way are about 50 percent greater than the 60μm luminosities for the same galaxies.

For comparison with the luminosity function for the Bright Galaxy sample, luminosity functions taken from the literature for "normal galaxies," "starburst galaxies," Seyfert galaxies and quasars are included in Figure 4. The published luminosity functions are given in terms of M_b, i.e. absolute blue luminosity, and thus a different bolometric correction was estimated for each of the classes of objects. These corrections are described in detail in Soifer, 1986a,b.

Figure 4 shows that the infrared bright galaxies represent a significant component in the local Universe, being more numerous than all categories of extragalactic objects at very high luminosites, and more numerous than all except normal galaxies at those luminosities where normal galaxies contribute significantly to the global luminosity function.

The infrared galaxies are more numerous than (non-Seyfert Markarian) starburst galaxies at all luminosities. In the range $10^{10}L_\odot$ to $10^{11}L_\odot$, the two become quite comparable. As suggested by Soifer, *et al.* 1986a, this agreement suggests that these represent the same population, at least over this luminosity range. At higher luminosities the infrared selected galaxies become significantly more numerous than the starburst galaxies, suggestive of either dust affecting the UV selection of the more luminous Markarian galaxies, or possibly a new luminosity component becoming important at the highest luminosities.

Below $\sim 2 \times 10^{11}L_\odot$, normal galaxies dominate the space densities of objects in the local Universe. For luminosities above $\sim 2 \times 10^{11}L_\odot$ infrared luminous galaxies appear to be the dominant population in the local Universe, having virtually the same space densities as the Seyferts at the lower end of this range, and a significantly greater space density than quasars at the higher luminosities. How high the far-infrared luminosity function extends will await a survey of sufficient numbers of IRAS galaxies to be able to make a statistically significant statement on the content of the next luminosity bin.

From the luminosity functions the contribution to the luminosity density of the local Universe can be estimated. The galaxies with far infrared luminosites greater than $10^8L_\odot$ produce roughly $9 \times 10^7 L_\odot/\mathrm{Mpc}^3$ in far infrared emission, with $4 \times 10^7 L_\odot/\mathrm{Mpc}^3$ being generated in galaxies with luminosities greater than $10^{10}L_\odot$. By comparison the normal galaxies produce a bolometric luminosity density of $\sim 4 \times 10^8 L_\odot/\mathrm{Mpc}^3$, where the integrated blue luminosity density was taken from Felten (1977) and Yahil, Sandage, and Tammann (1980), corrected to bolometric luminosity and to H_o=75 Km s^{-1} Mpc^{-1}. Thus ~25 percent of the stellar luminosity luminosity of galaxies emerges in the far infrared. At luminosities greater than $\sim 10^{10}L_\odot$ it is likely than star formation is the dominant form of energy generation in infrared bright galaxies (this volume) at least until the very highest luminosities. Several authors (Persson and Helou, 1986, Helou, 1986, Rowan-Robinson, 1986, de Jong and Brink, 1986) have suggested that a significant fraction of the far infrared luminosity in less active galaxies is recycled stellar radiation not necessarily associated with star formation regions. Thus overall, star formation accounts for between 60 and 80 percent of the far infrared luminosity generated in the local Universe.

The total space density of galaxies with far infrared luminosities $> 10^{11}L_\odot$ is $\sim 2.2 \times 10^{-5}$ Mpc^{-3}. Figure 1 shows that 85 percent of these galaxies have blue luminosities $> 10^{10}L_\odot$. From Christensen (1975) the space density of normal galaxies with $L_b > 10^{10}L_\odot$ is 3.4×10^{-3}, or roughly 0.6 percent of the galaxies with $L_b > 10^{10}L_\odot$ have $L_{fir} > 10^{11}L_\odot$. If the infrared bright phase has a lifetime t_{ir} and the optical phase has a lifetime t_b then the fraction of galaxies that have undergone such an infrared active phase is $0.006 \times t_b/t_{ir}$. If $t_b \sim 10^{10}$ yrs, and the infrared bright phase is a starburst phase with $t_{ir} < 10^8$ yrs (Rieke, *et al.* 1980, Gerhz, Sramek, and Weedman, 1983) then

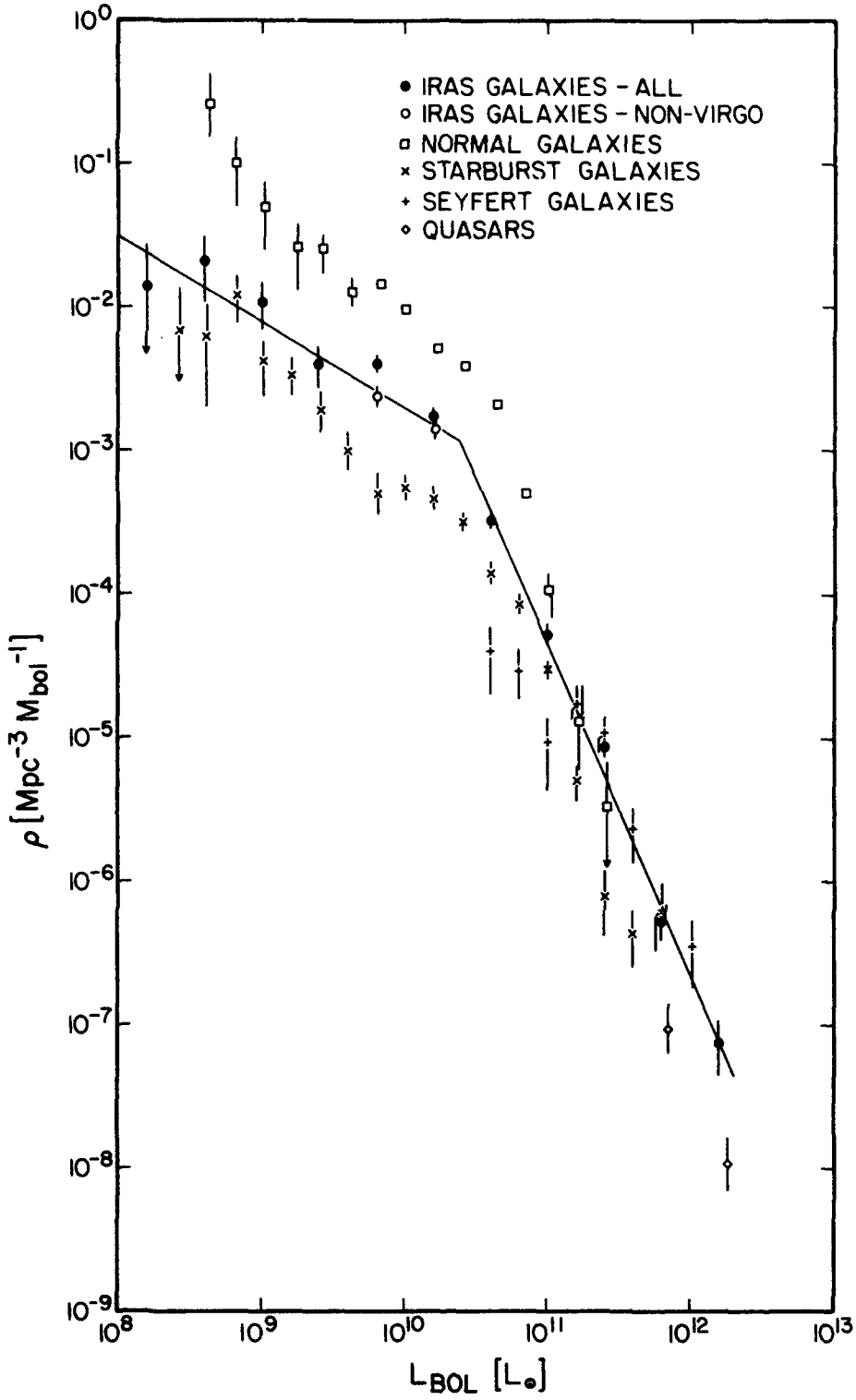

Figure 4: The far infrared luminosity function is shown for the Bright Galaxy sample, along with luminosity functions of a variety of classes of extragalactic objects, where the luminosity functions for the other classes of objects have been converted to bolometric luminosity.

a significant fraction, perhaps approaching 50 percent, of galaxies with $L_b > 10^{10} L_\odot$ must have undergone such an infrared active period over the course of their evoulution, if this is a non- recurring event stage in galaxy evolution.

5.0 Acknowledgements

This research was funded partially by NASA under the IRAS extended mission program and partially by the NSF.

6.0 References

Christensen, C. G. 1975, *A.J.*, **80**, 282.
de Jong, T. and Brink, K. 1986, this volume.
Felten, J.E. 1977, *A.J.*, **82**, 861.
Gehrz, R.D., Sramek, R.A. and Weedman, D.W. 1983, *Ap.J.*, **267**, 551.
Hacking, P. and Houck, J.R. 1986, this volume.
Helou, G. 1986, *Ap. J. Letters*, submitted.
IRAS Catalogs and Atlases: Point Source Catalog 1985, U. S. Government Printing Office.
IRAS Catalogs and Atlases: Small Scale Structures Catalog 1986, prepared by G. Helou and D. Walker, U.S. Government Printing Office.
Lawrence, A., Walker, D. Rowan-Robinson, M., Leech, K. J., and Penston, M.V. 1986, *Mon. Not. R.A.S.*, **219**, 687.
Persson, C.J. and Helou, G. 1986, this volume.
Rice, W.L. *et al.* 1986, in preparation.
Rieke, G. H., Lebofsky, M. J., Thompson, R. I., Low, F. J., and Tokunaga, A. T. 1980, *Ap.J.*, **238**, 24.
Rieke, G. H. and Lebofsky, M. 1986, *Ap.J.*, **304**, 326.
Rowan-Robinson, M. 1986 this volume.
Sanders, D. B., *et al.* 1986, in preparation.
Soifer, B. T., Sanders, D. B., Neugebauer, G., Danielson, G. E., Lonsdale, C. J., Madore, B. F., and Persson, S.E. 1986a, *Ap. J. (Letters)*, **303**, L41.
Soifer, B.T., *et al.* 1986b, in preparation.
Yahil, Sandage, and Tammann, 1980, *Ap.J.*, **242**, 448.

DISCUSSION

BECKLIN:

Is there any reason to suspect that the infrared luminosity function drops off at $L > 10^{12}\ L_\odot$ and thus drops below the QSO function?

SOIFER:

Not yet. This will require statistically complete redshift surveys of several thousand IRAS catalog galaxies to extend the 60μm luminosity function to greater luminosities than $\sim 2 \times 10^{12}\ L_\odot$.

LOW:

Why have we not found galaxies more luminous than Mkn231?

SOIFER:

Based on our Bright Galaxy luminosity function we would predict ~3 objects with far-infrared luminosity about 1 magnitude more luminous than Mkn231. We found no objects in that bin. Others have found individual objects having higher luminosity than Mkn231 in the IRAS survey (e.g., Mkn1014, 3C48, etc.) Until a large enough sample can be surveyed, where the number of sources at these luminosities is significant, we will not know whether there is a real cut off in the luminosities of IRAS galaxies.

ROCHE:

We have been taking optical spectra at the AAT of faint IRAS galaxies with no identified counterparts on the Sky Survey, and some of those have redshifts in the range 0.2-0.3. Even with fluxes of approximately 1 Jy at 60μm they have luminosities a few times greater than that of Mkn 231.

WINDHORST:

Given the apparently good correlation between 60μm flux and 21 cm continuum flux for spiral galaxies, did you translate your 60μm luminosity function to 21 cm and how does it compare with, for instance, Hummel's 21 cm radio luminosity function of spiral or interacting galaxies?

SOIFER:

Hacking has done this and finds excellent agreement between the 60μm source counts and the radio source counts for spirals done by Condon.

VLA OBSERVATIONS OF A SAMPLE OF GALAXIES WITH HIGH FAR-INFRARED LUMINOSITIES

S. A. Eales and C. G. Wynn-Williams
University of Hawaii, Institute for Astronomy
Honolulu, Hawaii 96822 USA

C. A. Beichman
California Institute of Technology
Pasadena, California 91125 USA

ABSTRACT. We present preliminary results from a radio survey of galaxies detected by the IRAS minisurvey. We find that the main difference between galaxies selected in the far-infrared and those selected in the optical is that the former have higher radio luminosities and that the radio emission is more centrally concentrated. There is some evidence that the strong central radio sources in the galaxies selected in the infrared are due to star formation rather than to active nuclei. If the radio emission is caused by star formation, the star formation rate divided by the volume in which the star formation is occurring is 100-1000 times greater in the galaxies selected in the infrared than in the disks of normal galaxies.

INTRODUCTION

We present preliminary results from a VLA survey of the galaxies detected by the IRAS minisurvey. The sample consists of the galaxies in the area of the IRAS minisurvey with $M_{pg} \lesssim 18$ and $S_{60\mu m} \gtrsim 0.5$ Jy (Soifer et al. 1984), together with the minisurvey sources that did not have optical counterparts on the Palomar Sky Survey (Houck et al. 1984) but that were later found to be galaxies (Aaronson and Olszewski 1984, Houck et al. 1985). Eighty-eight of the 92 galaxies in the sample have redshifts, measured either at Mauna Kea Observatory or at Palomar (Lonsdale, private communication). Because it was selected in the infrared, the sample is biased towards galaxies with high far-infrared luminosities; 76% of the galaxies have $L_{fir} > 10^{10} L_{\odot}$, compared with 5% of the spirals in an optical catalogue (Devereux, private communication).

We made 10-minute 'snapshot' observations of all the sources at 5 GHz with either the B- or C-array of the VLA, or with both. The data were reduced in a standard way, with extensive use being made of the CLEAN algorithm of Högbom (1974). To obtain structural information on the many sources that were just resolved by the VLA, we found the two-dimensional Gaussian brightness distributions that best represented the sources. This procedure gave us three structural parameters for each source: the distances between the half-intensity points along the major and minor axes and the position angle of the major axis. Flux densities were obtained either from the Gaussian fits or from integration over the maps in the vicinity of the significant components. Typical noise on the final maps was 0.2 mJy beam^{-1}.

Carol J. Lonsdale Persson (Editor)
Star Formation in Galaxies

RESULTS

Of the 92 objects in the sample, 57 were detected by the VLA. An additional 10 were detected at 5 GHz with the Effelsberg telescope by the Bonn group (Klein, private communication). Eighteen of the 57 VLA detections were unresolved. There is one double-lobed radio source (0421+040; Beichman et al. 1985), and three of the pairs of interacting galaxies in the sample have radio sources coincident with both galaxies.

Fig. 1 shows an unrepresentative collection of radio maps; most typical is 0402+212, an undistinguished blob of emission at the position of the IRAS source.

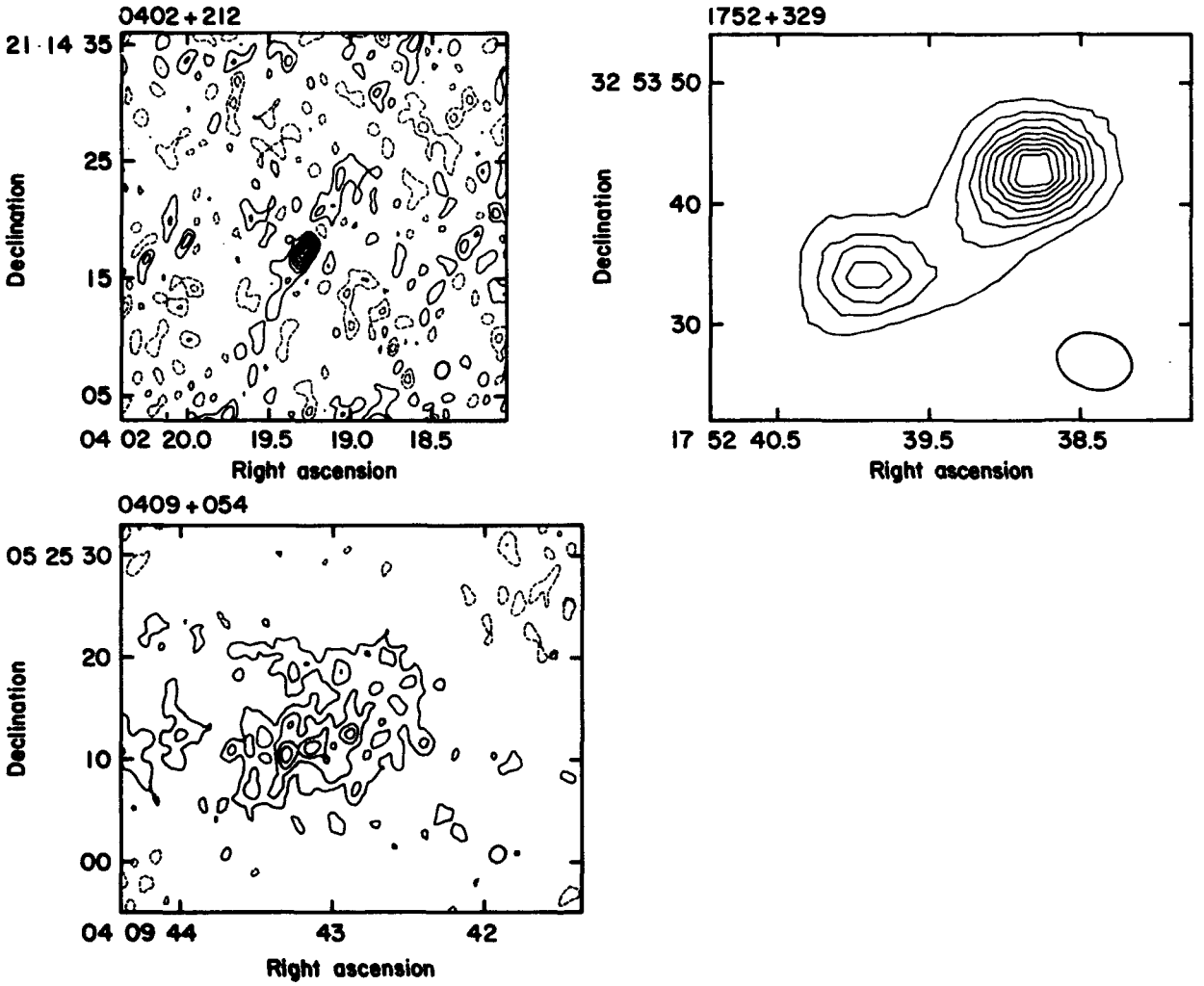

Figure 1. VLA maps of the IRAS sources 0402+212, 0409+054, and 1752+329. Negative contours are dashed, positive contours are solid lines, and the zero-level contour has been omitted. For the first two sources, the contour interval is 0.2 mJy beam^{-1}; for 1752+329, the contour interval is 7 mJy beam^{-1}. The ellipse in the bottom right-hand corner of each map shows the shape and size (FWHM) of the telescope beam. The 0409+054 source has a large physical size, ~7 kpc in diameter. 1752+329 is a pair of interacting galaxies. The radio peaks are coincident with the two galaxies.

DISCUSSION

Fig. 2 shows the P-D (radio luminosity-physical size) diagram for the minisurvey radio sources. The angular sizes used are mostly $(\theta_x\theta_y)^{1/2}$, where θ_x and θ_y are the distances between the half-intensity points along the major and minor axes of the best-fitting Gaussian brightness distribution. For sources with complex radio structures, angular sizes were measured off the maps between the lowest believable contours. The diagonal lines are lines of constant surface brightness. The undetected galaxies may have remained undetected because their radio luminosities are generally lower than those of the galaxies that were detected, or they may have similar radio luminosities but lower surface brightnesses and so fall on the P-D diagram to the right of the limiting surface brightness of the VLA--roughly the upper diagonal line in Fig. 2. The sizes of the sources range from 0.4 to 35 kpc, but most have sizes that bunch around the median, ~2 kpc.

How do the radio properties of these galaxies compare with those of galaxies selected from optical catalogues? Hummel (1980, 1981) used the Westerbork telescope to observe a large number of galaxies in the Reference Catalogue of Bright Galaxies. In Fig. 2 the horizontal lines show the luminosities above which 1% and 10% of Hummel's galaxies lie. The minisurvey radio sources are significantly more luminous (transforming between 5 GHz and 1.4 GHz, the frequency used by Hummel, by assuming $\alpha = 0.7$). The difference between the radio properties of infrared- and optically-selected galaxies becomes more marked when one considers that the radio emission from a typical minisurvey galaxy is coming from a much smaller physical region than the emission from a typical galaxy in an optical catalogue.

Another way to look at the difference between the radio properties of optically- and infrared-selected galaxies is to compare surface brightnesses; the minisurvey sources have surface brightnesses similar to those of the central sources in some well-known nearby galaxies (Fig. 2) (and much higher surface brightnesses than the disks of those galaxies) but higher luminosities and larger physical sizes. In the nine cases where we have accurate astrometry, to within the position errors (1-2 arcsec), the radio and optical centroids coincide, showing that the minisurvey radio sources occur in the centre of the galaxies.

What is causing the intense radio emission from the central regions of the minisurvey galaxies? Two possibilities, considering the high far-infrared luminosities, are star formation or active nuclei. The data are not good enough to reach a definite conclusion, but there are two arguments that suggest that the radio emission is caused by star formation.

The median physical size of a sample of Seyferts in which the radio emission is probably caused by collimated outflow from an active nucleus is only one-sixth that of the minisurvey galaxies (Ulvestad and Wilson 1984), which suggests that something different in the minisurvey galaxies is causing the radio emission. The second argument is that if the radio emission is caused by plasma beams from an active nucleus, the radio sources should be long and thin; which is not the case, as is shown in Fig. 3. There we plot for the minisurvey sources a histogram of eccentricity, defined as the distance between the half-intensity points along the major axis divided by the same distance along the

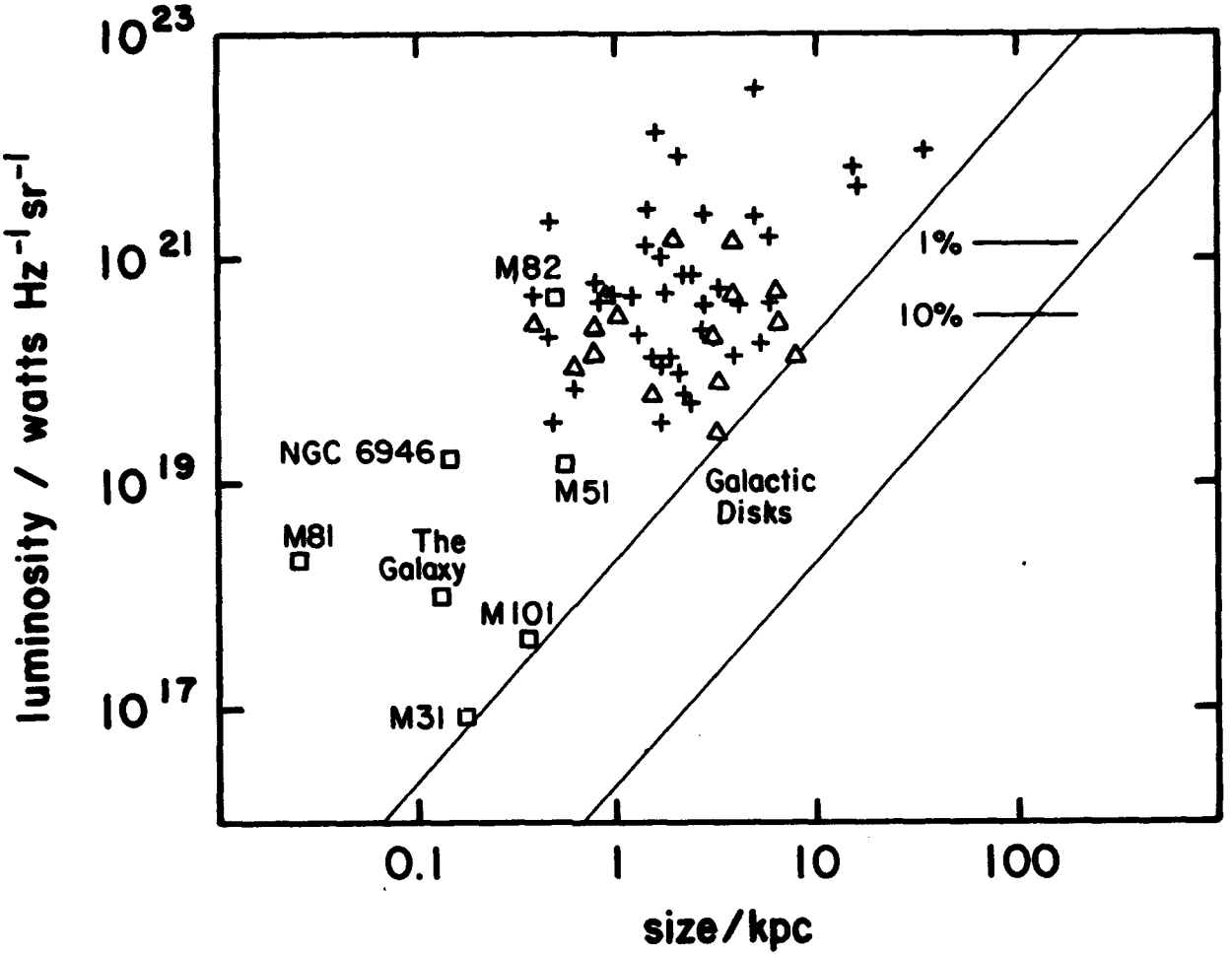

Figure 2. The luminosity-physical size diagram for the minisurvey sources. A Hubble constant of 75 km s^{-1} Mpc^{-1} has been assumed. Δ indicates an upper limit to the physical size. The squares show the positions of the central sources in some well-known nearby galaxies (Ekers 1975). The diagonal lines are lines of constant surface brightness. Galaxy disks have surface brightnesses that lie between these lines. The horizontal lines show the luminosities above which 1% and 10% of Hummel's galaxies lie.

minor axis. The median eccentricity is not much larger than the median expected from the effect of projection, if the sources consisted of thin circular disks.

A measure of the intensity of a starburst is the star formation rate divided by the volume in which the star formation is occurring, call this ε. If the radio emission is caused indirectly by star formation and directly by supernova remnants, $\varepsilon \propto$ radio surface brightness and is 100-1000 times greater than in the disks of normal galaxies.

Although star formation may be the cause of the radio emission in most of the minisurvey galaxies, there are a few galaxies in which the data point to an active nucleus. M82 is at once the prototype starburst and also the prototype

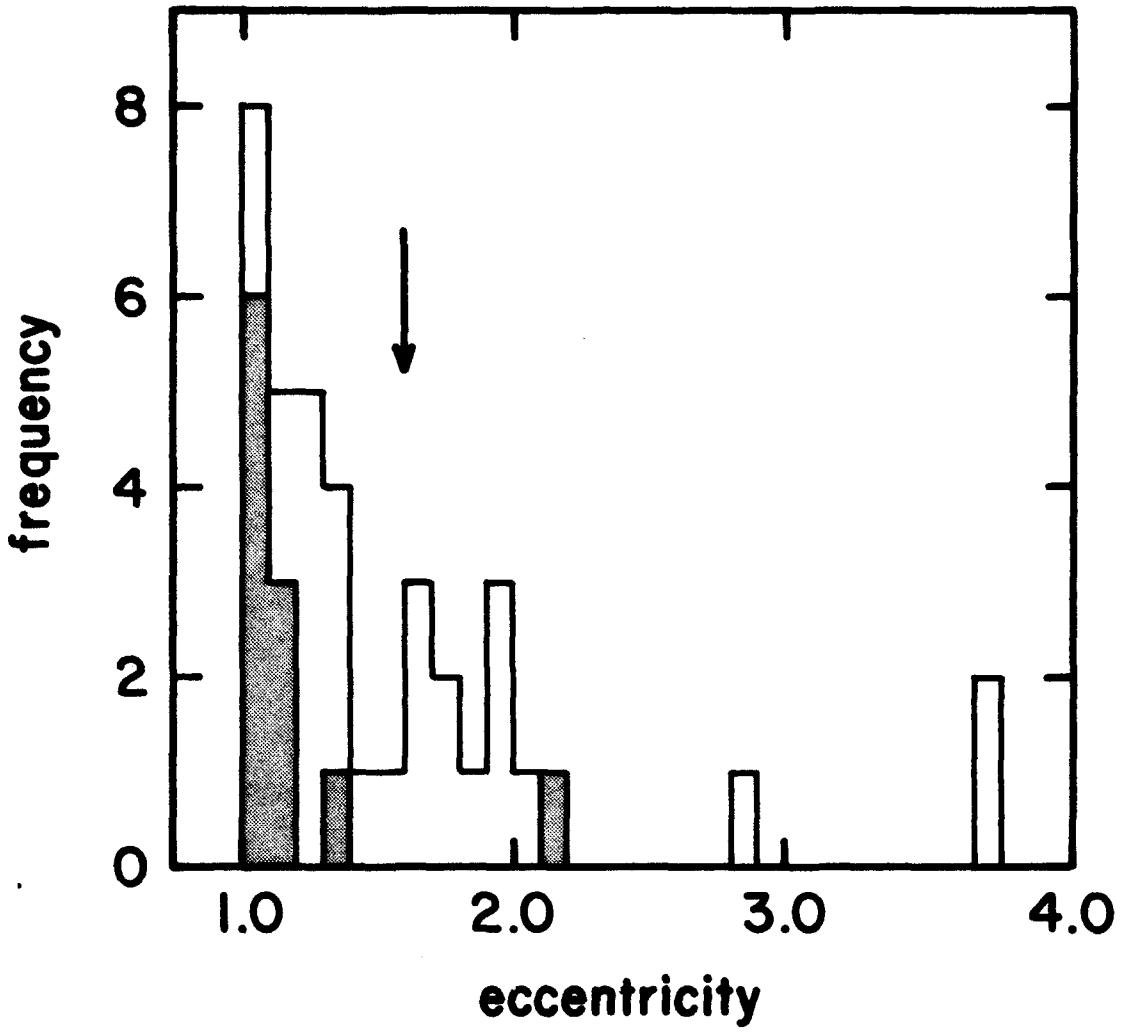

Figure 3. A histogram of eccentricity for the minisurvey galaxies. The hatching indicates lower limits. The median eccentricity is shown for those sources that have exact measurements. For comparison, the median expected from the effect of projection if the sources were just thin circular disks is 1.3.

exploding galaxy (Lynds and Sandage 1963; Bland and Tully, in preparation). Chevalier and Clegg (1985) have suggested that this is not a coincidence: that the explosion is caused by the large number of supernovae occurring in the starburst at the centre of the galaxy. We speculate that for a starburst, ε cannot exceed its value for M82, otherwise an explosion occurs. Three minisurvey sources have, however, higher values of ε, so these may be active nuclei rather than starbursts. One minisurvey source is certainly caused by outflow from an active nucleus--the double-lobed radio source 0421+040 (Beichman et al. 1985).

ACKNOWLEDGMENTS

We thank Dr. U. Klein and Dr. C. Lonsdale for communicating data prior to publication. We thank Drs. J. Heasley and E. Becklin and Mr. G. Hill for measuring redshifts for the minisurvey galaxies. This work was supported by NSF grant AST 84-18197. The National Radio Astronomy Observatory is operated by Associated Universities, Inc., under contract with the National Science Foundation.

REFERENCES

Aaronson, M., and Olszewski, E. W. 1984, Nature, 309, 414.
Beichman, C., et al. 1985, Ap. J., 293, 148.
Chevalier, R. A., and Clegg, A. W. 1985, Nature, 317, 44.
Ekers, R. D. 1975, in Structure and Evolution of Galaxies, ed. G. Setti (Dordrecht: Reidel), p. 217.
Högbom, J. A. 1974, Astr. Ap. Suppl., 15, 417.
Houck, J. R. et al., 1984. Ap. J. (Letters), 278, L63.
Houck, J. R., Schneider, D. P., Danielson, G. E., Beichman, C. A., Lonsdale, C. J., Neugebauer, G., and Soifer, B. T. 1985, Ap. J. (Letters), 290, L5.
Hummel, E. 1980, Astr. Ap. Suppl., 41, 151.
Hummel, E. 1981, Astr. Ap., 93, 93.
Lynds, C. R., and Sandage, A. 1963, Ap. J., 137, 1005.
Soifer, B. T., et al. 1984, Ap. J. (Letters), 278, L71.
Ulvestad, J. E., and Wilson, A. S. 1984, Ap. J., 278, 544.

SYSTEMATIC IDENTIFICATION OF IRAS POINT SOURCES

A. Savage, R.G. Clowes, H.T. MacGillivray, R.D. Wolstencroft
Royal Observatory, Edinburgh.

S.K. Leggett, P.J. Puxley
University of Edinburgh.

INTRODUCTION

A year ago we initiated a large scale programme to identify IRAS point sources. At ROE we have the ideal facilities to undertake such a large programme, viz. the rapid scanning capabilities of the COSMOS measuring machine to exploit the depth and resolution of the United Kingdom Schmidt Telescope (UKST) J survey plates. This automated procedure is more rapid than visual identification procedures and thus we have now covered about 1100 square degrees of sky containing about 1300 IRAS point sources. Figure 1 indicates the plates and areas that we have already processed together with those areas we hope to cover in the near future.

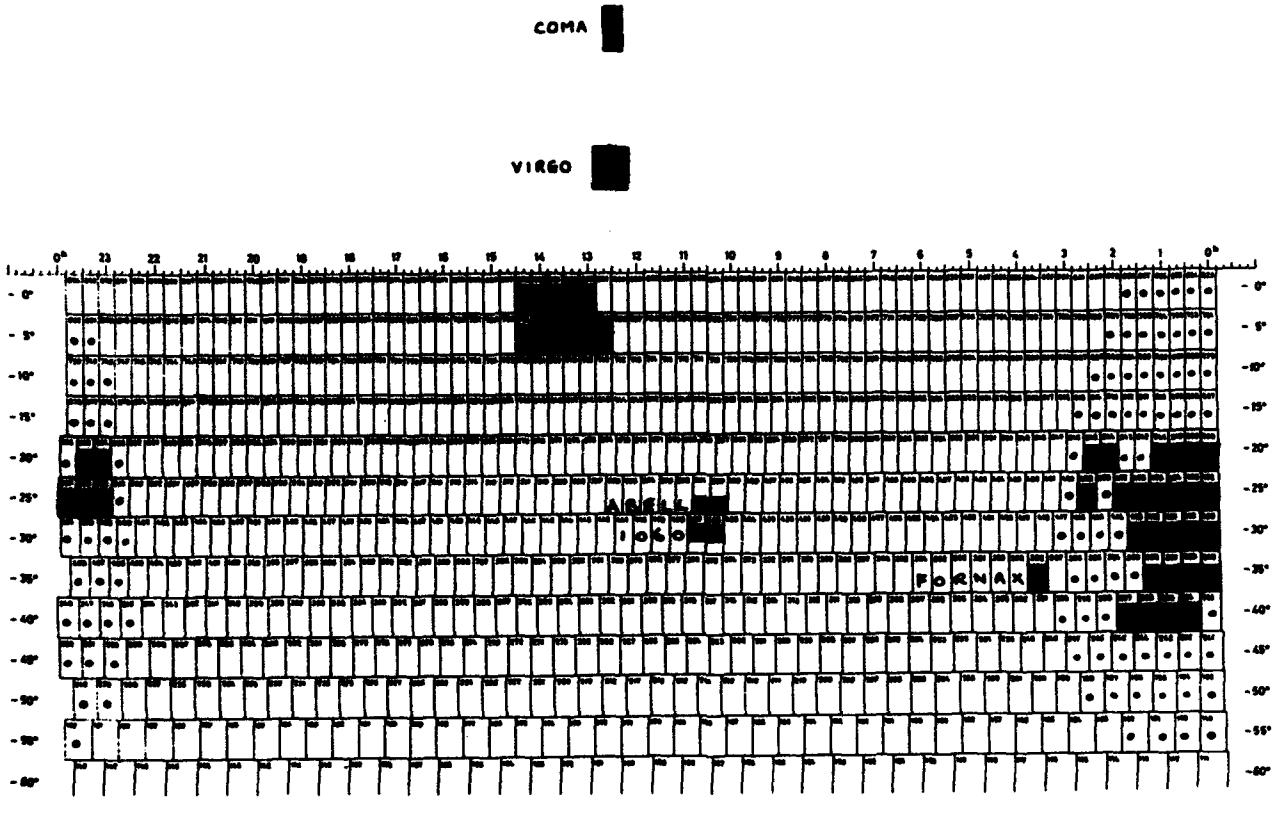

Figure 1. Distribution of UKST/SERC J survey fields showing those plates scanned by COSMOS (■) and to be scanned by COSMOS (•) as part of this project to systematically identify IRAS point sources.

Carol J. Lonsdale Persson (Editor)
Star Formation in Galaxies

The identification procedure has been thoroughly described in Wolstencroft et al. (1986) and will not be repeated here. These new results are preliminary, and mainly relate to the gross properties of the sample as a whole.

EMPTY FIELDS

Paper 1 (Wolstencroft et al. 1986) analyses the 10 empty field sources with no identification ($B_J < 21$) out of 312 IRAS sources in this SGP area. Likelihood criteria were used to estimate the reliability of individual identifications which should be a more conservative estimator than that from gaussian errors alone.

Table I compares the chance coincidence rates with the likelihood ratios LR for both low and high Galaxy densities.

TABLE 1

	All galaxies $B_J < 21^m$		All galaxies $B_J < 17^m$	
r	LR	N	LR	N
1.0	15.5	0.08	1197	0.001
2.0	3.5	0.33	267	0.004
3.0	0.28	0.74	22	0.009

N is the number of galaxies at the SGP expected by chance within a defined dimensionless angular distance, r, between the infrared and optical positions, it and all other parameters are defined in Paper 1. Our adopted limit of LR $\geq$ 3 corresponds in the limiting case, for an individual object, to a reliability of 75%: however the reliability of our identified sample as a whole is well over 90%. Also for some of the fainter galaxy identifications, if we are to have a fairly high reliability, the search radius has to be small to meet the LR constraint and thus some potential identifications may be excluded.

However for our 10 original empty fields 5 do have possible or probable identifications ($B_J < 21$) just outside the 2σ error ellipse derived from the known galaxy and stellar identifications, 1 is a confused source and 1 is a probable cirrus detection. The remaining 3 sources are either due to faint cirrus or may be true empty field sources. In reality the genuine empty field sources may be extremely rare. We have subsequently noticed whilst working through the new areas that all of the new 13 "empty field" sources have a cirrus 1 flag > 1 and tend to be associated with small localized clumps of cirrus. Examples are shown in Figure 2. In Figure 2(b) there is evidence of some very faint optical nebulosity on the original plate. Reappraisal of the original SGP and Virgo cluster areas confirms that some of the empty field sources in those samples also appear in such clouds. There probably remain very few, if any, distant galaxies to be identified which are not fairly easily visible in optical wavebands.

STELLAR IDENTIFICATIONS

Although it is possible in the great majority of cases to tell from the IRAS flux density ratios whether the source is a galaxy or a star we prefer to keep this information in reserve to be as objective as possible. Thus we are identifying all IRAS sources. This in retrospect has been a wise decision. Figure 3 shows a selection of unusual stellar objects which we have identified with IRAS sources. 3(c) IRAS 10299-2803 has a blue point-like image but a diffuse extended red image. It

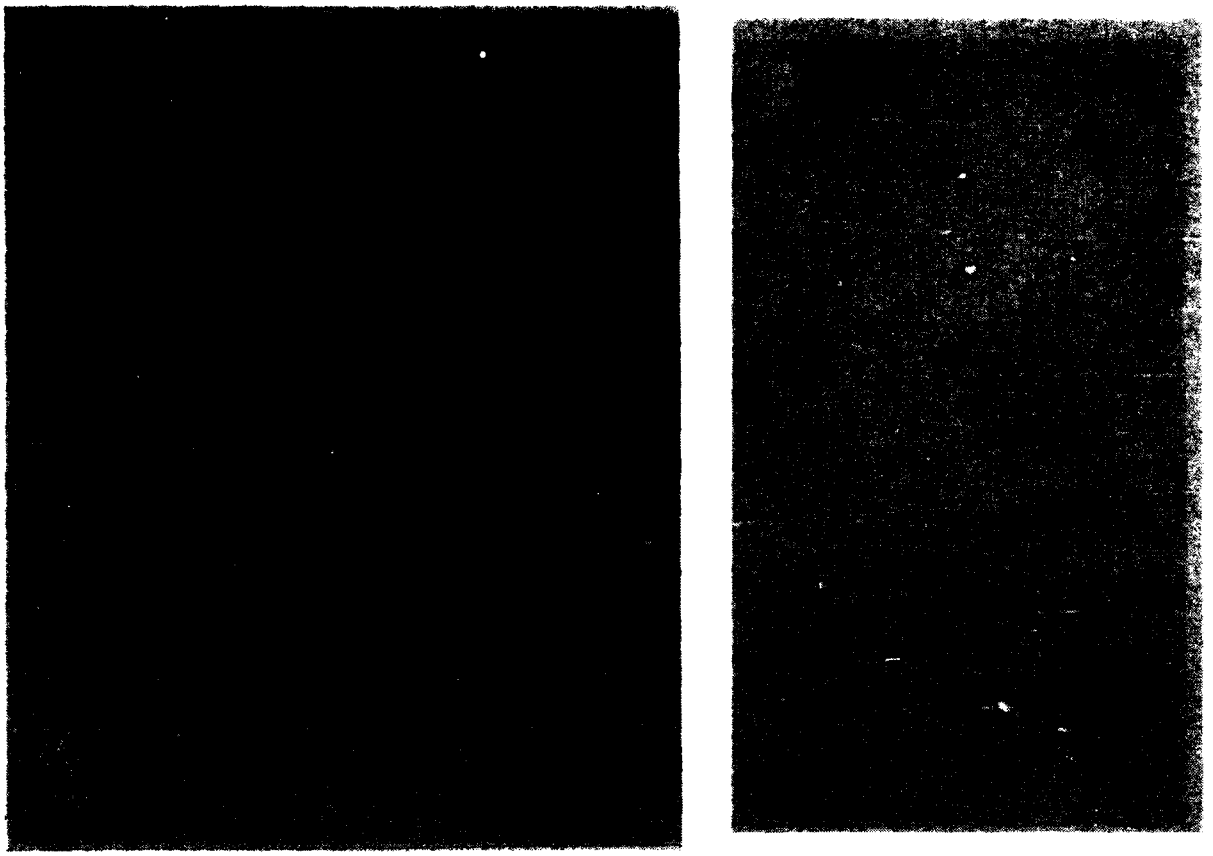

Figure 2. Reproductions from UKST/SERC J survey glass atlas showing the positions of definite IRAS cirrus sources, identifications and possible empty field identifications. All sources have a cirrus 1 flag > 1. Since these are closely associated in the sky and since optical nebulosity can be seen on the original plate at (B) these proposed empty field sources are probably low level cirrus detections.

has IRAS fluxes which do indicate a galaxy identification and its morphological appearance suggests an "N" galaxy or a low redshift quasar. An optical spectrum taken on the Anglo-Australian Telescope confirms the extragalactic nature of this object. Another advantage of this kind of objective systematic approach starting in areas of the lowest IRAS source densities is that we are able to distinguish new populations of stellar identifications. Figure 4 illustrates this.

Figure 4 shows the increasing numbers of fainter stellar identifications, Mira variables, extreme M and carbon stars which begin to appear at lower galactic latitudes. Optical spectra have been obtained on the Anglo-Australian Telescope of a representative sample of these stars having magnitude ~ 15. These spectra confirm that the stars are of late M spectral type. The availability of a wide variety of UKST/SERC/ESO plate material covering a range of epochs suggests that these stars may also be variable. Both the above are suggestive of Mira variables. A variety of Schmidt plate material is also required to identify such sources. Neither IRAS 00193-4033 nor IRAS 10299-2803 are visible on the J survey material but both are easily visible on R (5900-6900Å) or I (7150-9000Å) plate material (see Figure 3).

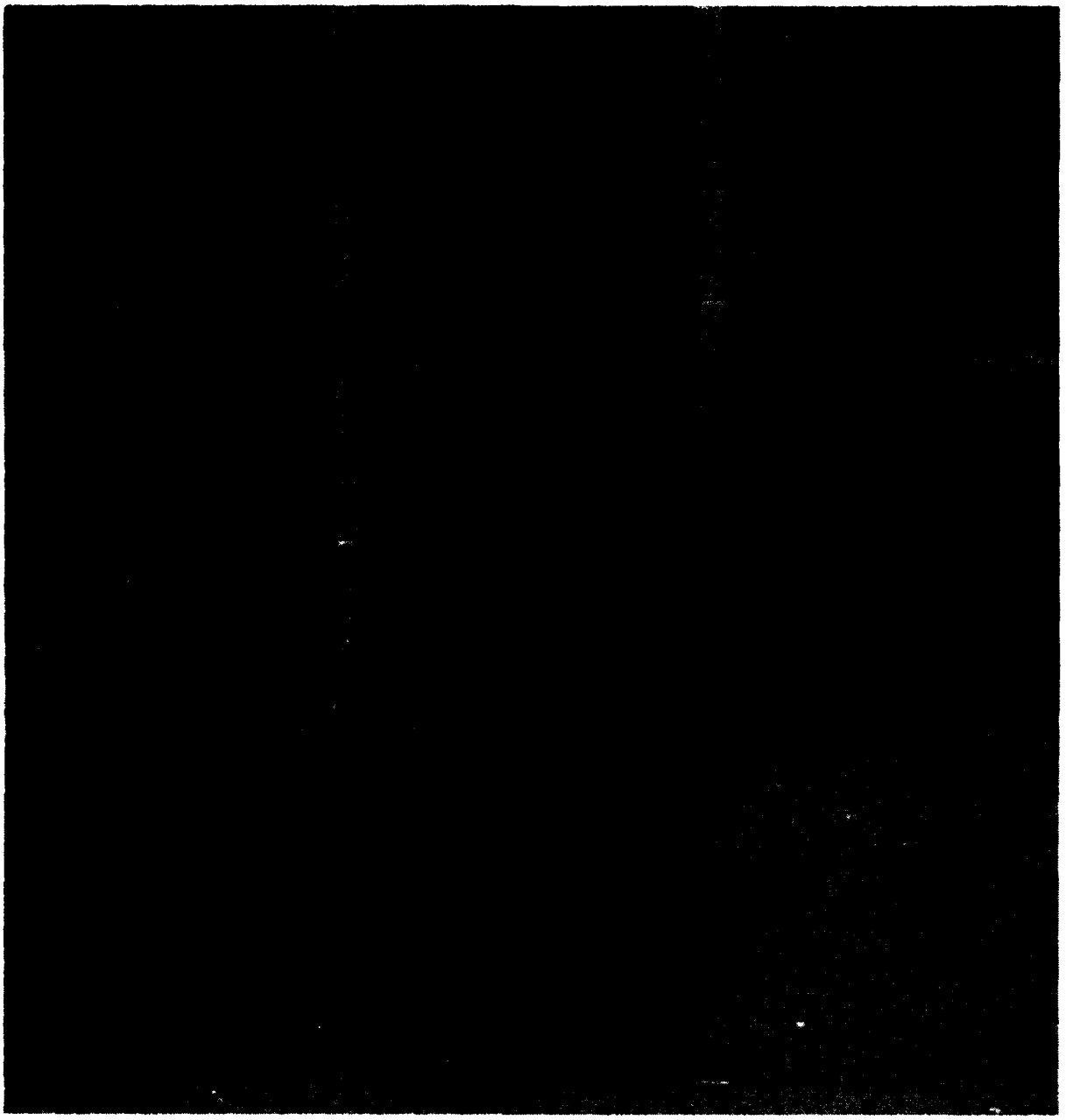

Figure 3. A selection of the more extreme types of stellar identifications.

(a) IRAS 00193-4033. Probably a dusty Mira star. The IRAS spectrum shows a strong 10μm silicate emission feature indicating an oxygen rich dust envelope. It is just visible with a very red spectrum on UKST objective prism plate material.

(b) IRAS 15194-5115. A similar type of stellar identification to (a) above.

(c) IRAS 10299-2803. A very blue star which appears slightly fuzzy on the red sensitive emulsion. It has IRAS fluxes which indicate a galaxy type identification. It is probably an "N"-galaxy or low redshift quasar with a redshift of about 0.3.

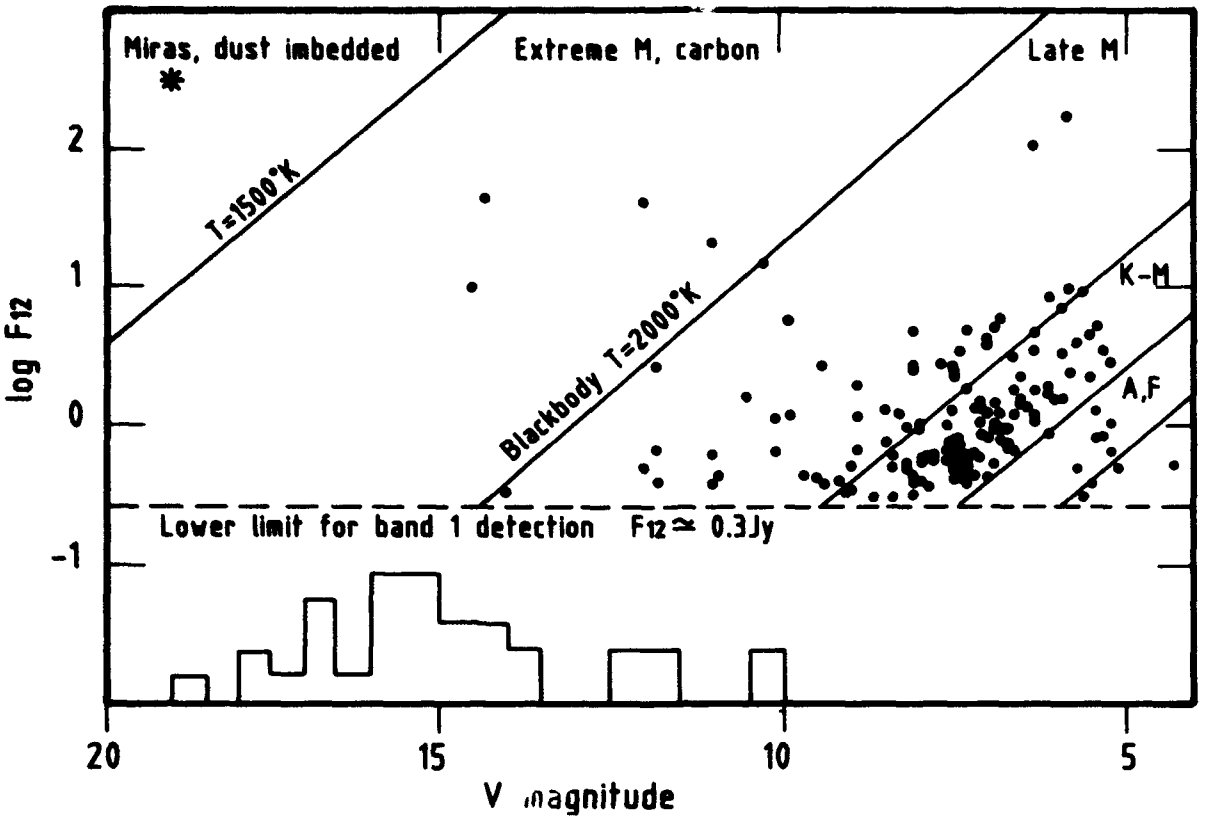

Figure 4. The relation between V magnitudes and $\log F_{12}$ for the 148 stars in Paper 1 (see text). Also indicated is an extremely red star, probably a Mira (*), found in the more recent identifications. The histogram indicates the increasing numbers of stars fainter than 10 magnitude being identified as we move to lower latitudes and found in the regions either side of the SGP area of Paper I.

GALAXY IDENTIFICATIONS

Our major aim with the galaxy identifications is to provide a database from which sound statistical analyses can be made. We are producing accurate blue magnitudes and morphological classifications for each identification. In addition other workers at ROE (MacGillivray et al.) are producing magnitude limited samples of field galaxies in each of the areas in which we are working. We should eventually be able to make firm statements about the proportions of all galaxies at a given magnitude which are IRAS sources and see if there are any strong correlations with morphological type. Clarification of the variation of L_{IR}/L_B with morphological type will also be possible with this large database; our present work indicates that many optically similar galaxies show a range in excess of 10^3 in L_{IR}/L_B, although our first paper (Wolstencroft et al. 1986) did find a trend with morphology.

So far the galaxy identifications still appear to be primarily a selection of field spirals. The combined galaxy error diagrams (Figure 5) for the total area that we have now covered are considerably worse than the similar diagram for the stellar identifications. In Figure 5 the error diagrams have been divided into two components (A) for galaxies brighter than $B_J \approx 15.5$ and (B) for galaxies fainter than $B_J \approx 15.5$.

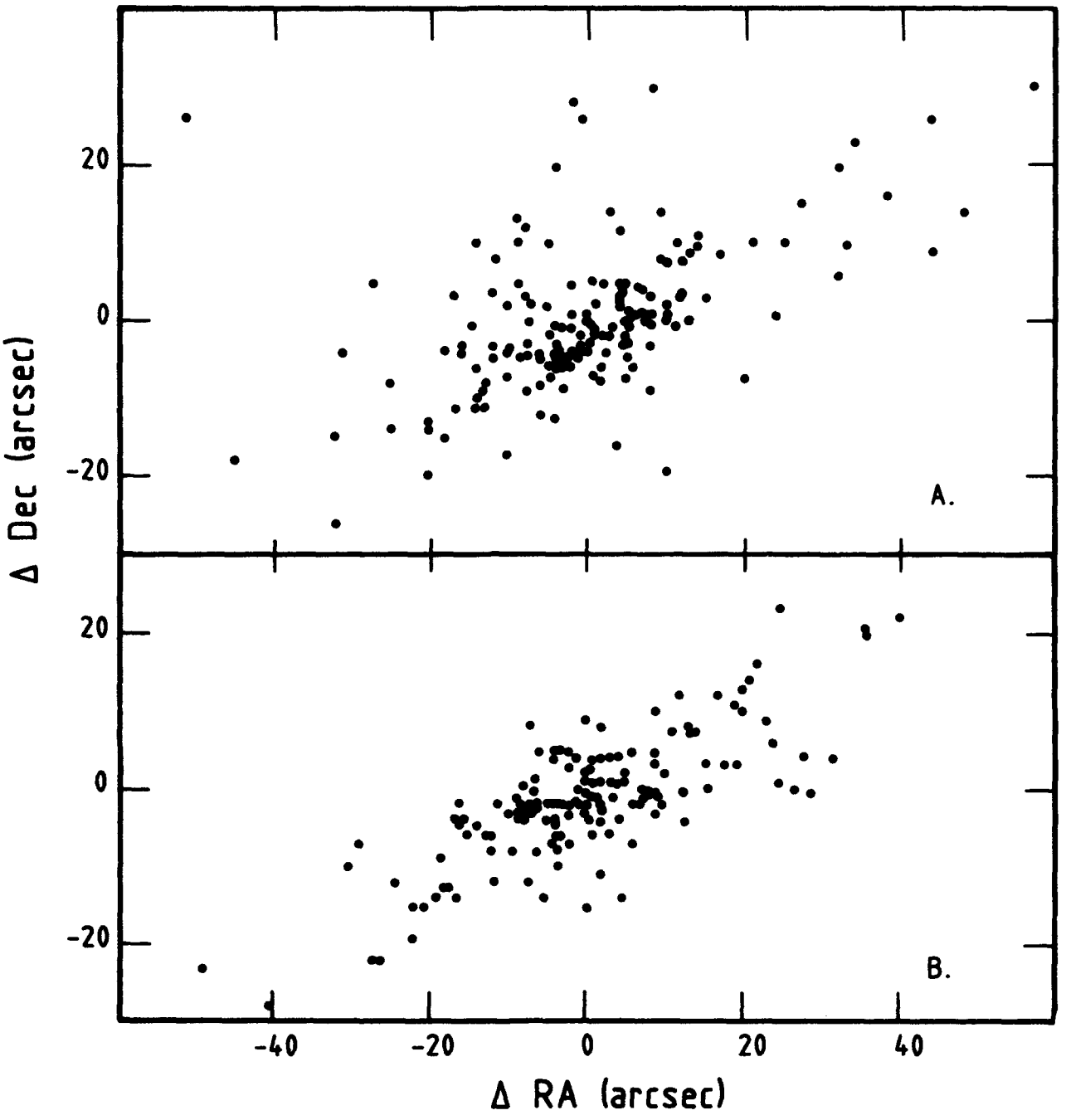

Figure 5. Position differences IRAS minus optical for (A) the IRAS galaxy identifications brighter than $B_J \approx 15.5$ and (B) $B_J > 15.5$ from the SGP area covered to date. It can be seen that the scatter is much larger for the brighter galaxies presumably because in some cases the IRAS source is not associated with the nucleus of the galaxy. The offsets for the fainter galaxies are similar to those for the stars and compatible with similar residuals quoted in the IRAS Explanatory Supplement, Beichman et al. 1985.

It appears to be the brighter galaxies that contribute most to this scatter. Figure 5 shows that for a significant number of the bright galaxies (which are unambiguous identifications) there is an offset between the optical and the IRAS point sources which is much larger than the IRAS position uncertainty. This indicates that regions of star formation are not confined solely to the nucleus but there may be a significant fraction of flux from the outer regions.

The UKST has a prism combination which acts as an intermediate dispersion objective prism with a reciprocal dispersion of 1200Å/mm at Hγ. On plates taken with this prism many bright galaxies show prominent HII regions by virtue of their emission-line spectra. It is hoped to use such prism plate material to investigate the distribution of star formation regions in individual galaxies. As an interim measure some low dispersion UKST prism plate material, which already exists for some of our fields has been inspected. This plate material has a dispersion of 2440Å/mm at Hγ and the wavelength range covered is 3200Å to 5400Å. At this low dispersion only those galaxies with very prominent emission show detectable features of the blend [0III] 5007/Hβ and of [0II] 3727 indicative of HII regions. Some galaxies with prominent features are shown in Figure 6. Unfortunately the dispersion is too low to investigate the distribution of HII regions in a reasonably large sample of galaxies nor is it possible to determine accurate redshifts. A programme to measure redshifts for the more luminous galaxies is under way and this is discussed in the poster paper by Wolstencroft et al. at this conference.

The average number of field galaxy identifications is 0.5 per square degree. Half of these are brighter than $B_J \approx 15.5$. The fainter galaxies appear to be uniformly distributed with no fields of 25 square degrees showing greater than a 2σ variation. However the brighter galaxies do seem to be clustered with some fields showing density variations in excess of three sigma. Similar variations are also seen in the field galaxy counts in two 25 square degree fields for galaxies brighter than $B_J \approx 15.5$ (Kalafi et al. 1986).

SUMMARY

We have now identified sources in 44 Schmidt plate areas including 1300 sources and covering 1100 square degrees. The identifications comprise 700 galaxy identifications (field and cluster members) and 600 stellar identifications. We hope to extend this area to cover some 3000 square degrees which should include some 1500 galaxy identifications. There are also about 40 sources with no obvious identification but which can be most easily explained by cirrus, confusion between two sources or sources just outside the 2 sigma error box. We feel confident that we can tackle the increased source densities, confusion and cirrus problems of lower galactic latitudes, and succeed in our aim of compiling a sound database for detailed statistical analyses.

ACKNOWLEDGEMENTS

We would like to thank Professor D.C. Morton for acquiring the AAT spectra for us. We would again like to thank the staff of the UKST Unit for continuing to produce such superb plate material. Special thanks are due to Brian Hadley and ROE Photolabs, together with Marjorie Fretwell and Dorothy Skedd for helping to prepare this paper at very short notice.

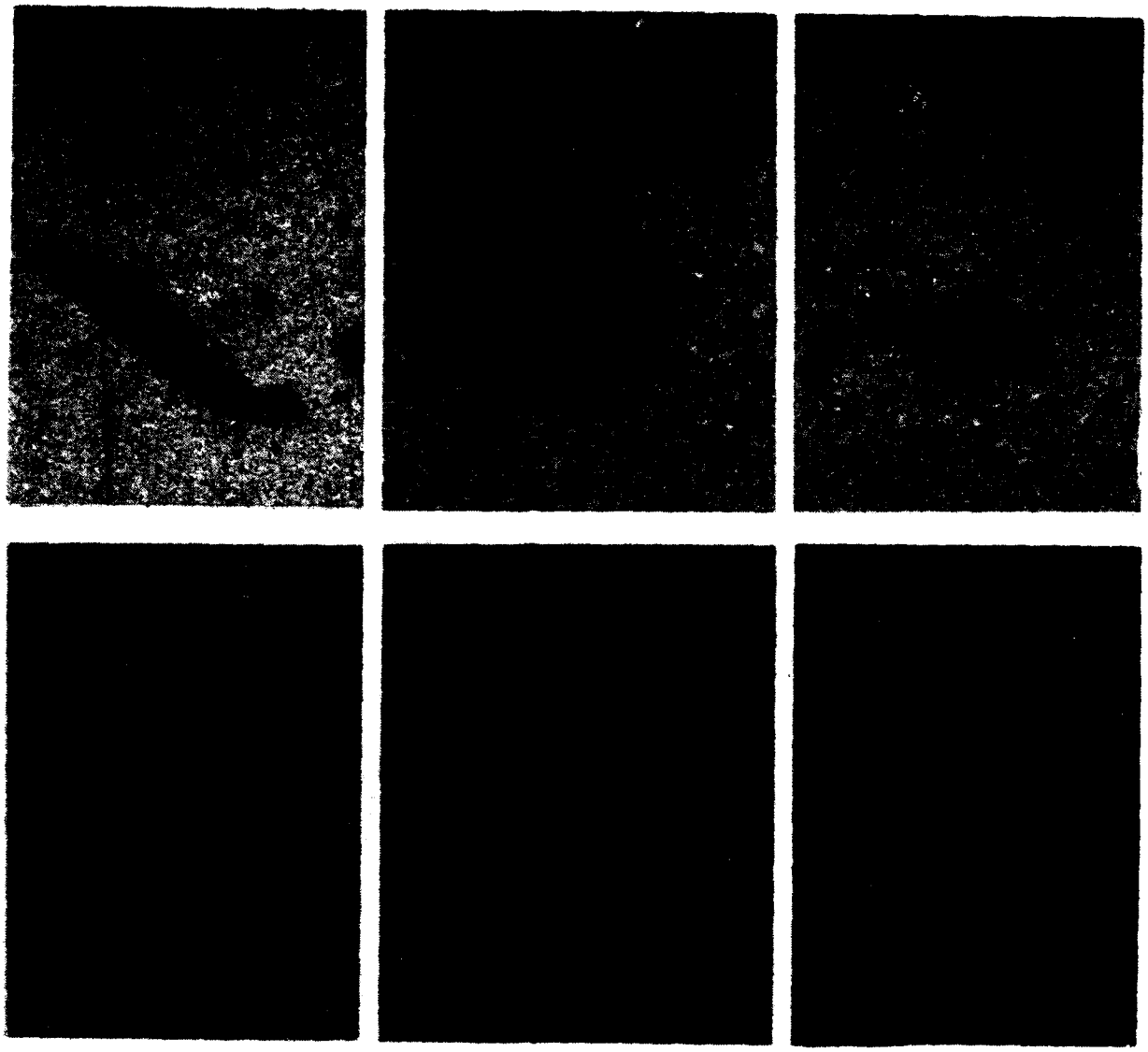

Figure 6. These are a selection of IRAS source counterparts for which UKST low dispersion objective prism plate material exists. This plate material has a dispersion of 2440Å/mm at Hγ and the wavelength range here is 3200Å to 5400Å. At this low dispersion only those galaxies with very prominent emission show detectable features of the blend [OIII] 5007/Hβ and [OII] 3727. For the galaxy at (a) the IRAS source may be related to the strong extragalactic HII region rather than the bright Sbc galaxy; (b) is the well studied galaxy complex "The Cartwheel" A0035-34 and (c) is clearly resolved into two compact nuclei or galaxies.

REFERENCES

Explanatory Supplement to the IRAS Catalogues and Atlases, ed. Beichman, C.A., Neugebauer, G., Habing, H.J., Clegg, P.E., and Chester, T.J., 1985. (US Government Printing Office, Washington DC).

Kalafi, M., Savage, A., Good, A.R., Yates, M.G., & Cannon, R.D., 1986. Proceedings of IAU Symposium 121, Byurakan, Armenia, USSR.

Wolstencroft, R.D., Savage, A., Clowes, R.G., MacGillivray, H.T., Leggett, S.K. and Kalafi, M., 1986. Mon.Not.R.astr.Soc., in press.

DISCUSSION

TELESCO:

Do you think there's a chance that the clustering of IRAS sources in the SGP is due to cirrus?

SAVAGE:

No.

A VERY DEEP IRAS SURVEY AT $\ell^{II} = 97°$, $b^{II} = +30°$

Perry Hacking and James R. Houck

Center for Radiophysics and Space Research
Ithaca, New York 14853-6801

ABSTRACT. A deep far-infrared (12-100μm) survey is presented using over one thousand scans made of a 4-6 deg^2 field at the north ecliptic pole by the Infrared Astronomical Satellite (IRAS). Point sources from this survey are up to one hundred times fainter than the IRAS point source catalog at 12 and 25μm, and up to ten times fainter at 60 and 100μm. The 12 and 25μm maps are instrumental noise-limited, and the 60 and 100μm maps are confusion noise-limited. The majority of the 12μm point sources are stars within the Milky Way. The 25μm sources are composed almost equally of stars and galaxies. About 80 percent of the 60μm sources correspond to galaxies on Palomar Observatory Sky Survey (POSS) enlargements. The remaining 20 percent are probably galaxies below the POSS detection limit. The differential source counts are presented and compared with theoretical models. The 12μm source counts are found to be consistent with what is predicted by the Bahcall and Soneira Standard Galaxy Model (1980) using the B-V-12μm colors of stars without circumstellar dust shells given by Waters, Cote and Aumann (1986). The 60μm source counts are inconsistent with those predicted for a uniformly distributed, nonevolving universe. The implications are briefly discussed. A detailed description of the survey appears in Hacking and Houck (1986). A discussion of the scientific implications of the source counts and colors are discussed in Hacking, Condon, and Houck (1986).

INTRODUCTION

There are two reasons for conducting an infrared survey to lower flux densities. The first is to detect trends in sources observed at higher flux densities. The changes might be detected in the shape of the luminosity function (i.e., changes in relative distribution of sources vs. luminosity) or the position of the luminosity function in the density -- luminosity plane (e.g., changes in the space density of sources or luminosity evolution at cosmological redshifts). The second is to search for new classes or types of objects. An obvious example would be the detection of a nearby, isolated brown dwarf. It is also possible that a new type of source, as yet unthought of, might be detected.

THE DATA

The survey is located at the north ecliptic pole, in the constellation of Draco, at 18^h, +66°; $\ell^{II} = 97°$, $b^{II} = 30°$, and covers 4.3 square degrees at 12 and 25μm and 6.3 square degrees at 60 and 100μm.

There are two types of data used in the survey: 488 scans from the IRAS all-sky survey and 141 pointed observations. The survey scans cover the entire

Carol J. Lonsdale Persson (Editor)
Star Formation in Galaxies

field approximately uniformly. Each survey scan map is 1/2° x up to 4° and consists of data from a single scan of the satellite across a portion of the field. The pointed observations are centered on NGC 6543, which is located very near the ecliptic pole and was used as a calibrator for the IRAS mission. Each pointed observation consists of three to six scans made at half the IRAS survey scan rate and results in a map of dimensions 1/2° x 1 to 1.75°. Since NGC 6543 was the target of the pointed observations, only the central three square degrees is covered by them, and the coverage is nonuniform, with the region around NGC 6543 (near the center of the field) observed the most. Over one thousand scans were combined to form the final maps, making this the deepest infrared survey to date. At 12 and 25μm it is likely to remain so until the next generation infrared satellite can be flown (e.g., SIRTF or ISO). At 60 and 100μm, it may prove possible to probe slightly deeper in the field (and a few other smaller select fields) using different filtering techniques. Point sources as faint as 5-10 mJy are in the 12 and 25μm maps with SNR > 3-5 (a factor of 50 to 100 times fainter than the IRAS point source catalog), 50 mJy at 60μm (ten times fainter than the IRAS PSC), and 100-200 mJy at 100μm (five to ten times fainter than the IRAS PSC).

Two images of each survey scan and each pointed observation were made: 1) A full-intensity image was made that approximates the true appearance of the infrared sky; 2) a point-source filtered image was made that improves the signal-to-noise ratio of point sources. Several preliminary maps were made from subsets of the data to check for moving or spurious sources. All of the images were then summed to form final intensity and point source filtered images.

The intensity maps indicate that there is a great deal of extended emission in the field at 60 and 100μm. The 60μm point source filtered map contains very little extended emission. The 100μm point source filtered map is contaminated with extended emission, however. This is due to the larger angular size of the 100μm point spread function that is similar in size to much of the structure present in the extended emission. For this reason, 100μm fluxes are quoted only for sources also detected at 60μm, where contamination from the extended emission is less likely.

RESULTS

The point source density in this field at 12 and 25μm is quite low compared to the effective beam size (10-15 sources per square degree brighter than 20 mJy), so that the 12 and 25μm surveys are limited by instrumental noise.

At 60μm, the effective beam size and the source density (20 sources per square degree brighter than 50 mJy) are larger, resulting in a confusion noise-limited survey (σ_{conf} = 20 mJy). Extended emission and confusion prevented an unbiased 100μm survey.

No moving or spurious (single event) sources were found in any of the preliminary maps.

The point source filtered maps were used to extract the point source sample. The point sources were compared with the Smithsonian Astrophysical

Observatory Star Catalog (1966) and the Palomar Observatory Sky Survey (POSS) plates. A summary of the comparison is presented in Table 1.

TABLE 1 - Summary of Point Sources from Deep Survey

λ	Total Number[a]	Stars %	Galaxies %	Unidentified %
12μm	46	89	11	0
25μm	36	50	47	3[b]
60μm	99	0	~80	~20[c]

[a] Excluding NGC 6543
[b] Probably a distant Seyfert galaxy
[c] Probably galaxies below POSS detection limit

The distribution of sources vs. flux density was modeled, assuming a power law of the form:

$$n_{>F_\nu} = A\, F_\nu^{-\alpha}$$

where $n_{>F_\nu}$ is the number of sources with flux density greater than F_ν per square degree; A and α are constants. Values of α of 0.76±0.11 and 1.79±0.17 were found for the 12μm (mostly stars) and 60μm (extragalactic sources) point source samples, using the method of maximum likelihood. The Kolmogorov test revealed that the power law distribution assumed for the source counts is consistent with the data at 12 and 60μm. Since the 25μm sample is composed of both stars and galaxies, the 25μm distribution is a linear combination of the 12 and 60μm distributions.

DISCUSSION

The 12μm source counts are consistent with star counts predicted by the Bahcall and Soneira Standard Galaxy Model*, using the B-V-12μm colors given by Waters, Cote, and Aumann (1986) for stars without circumstellar dust shells. In particular, the total number (33) and the value of $\alpha_{12\mu m}$ (0.78) is successfully predicted (see Hacking, Condon, and Houck 1986 for details). Figure 1 shows differential star counts extrapolated to very low flux densities at the north galactic pole (not covered in this survey) as predicted by the model. The 12μm counts above ~10Jy are dominated by stars with circumstellar dust shells (Hacking, et al. 1985), which are not included in Figure 1. The expected galaxy counts at 12μm are also plotted in Figure 1. As can be seen, galaxies should dominate the 12μm point source counts below ~10 mJy at the galactic poles.

The 60μm source counts were modeled in a similar fashion to the radio

*See Hacking, Condon, and Houck (1986) for a description of what was used, and Bahcall and Soneira (1980), for a detailed description of the model.

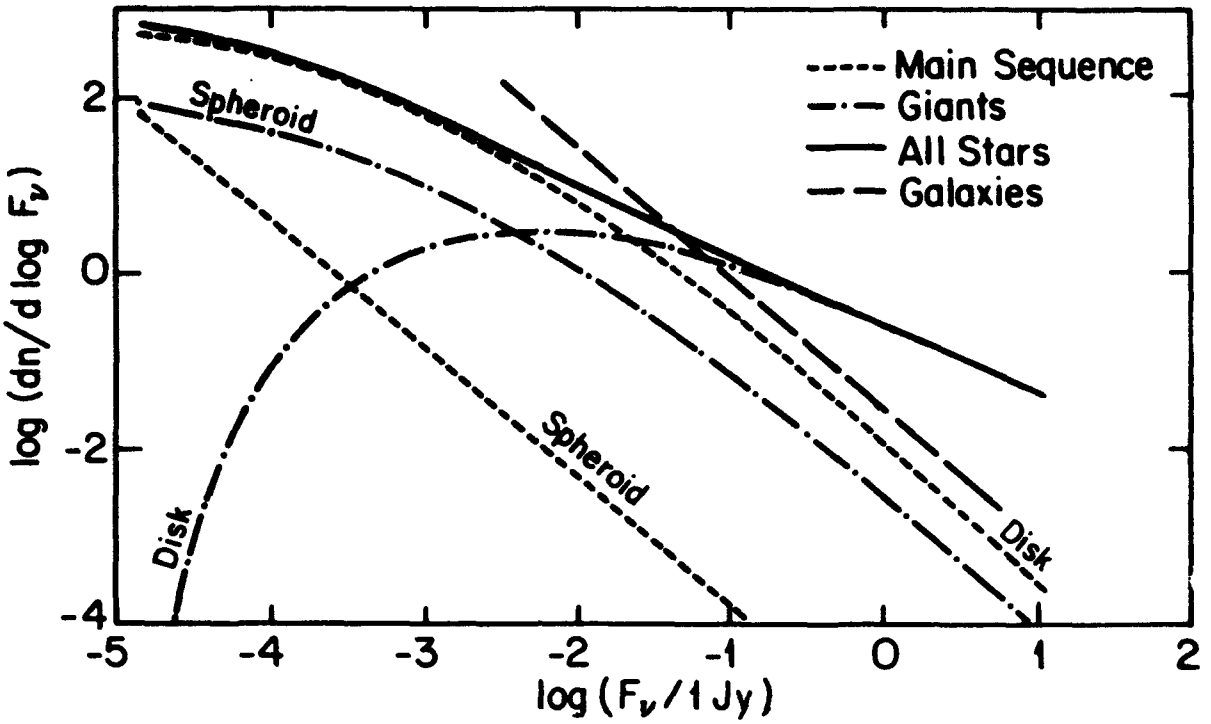

Figure 1 - Predicted 12μm differential star counts at the north galactic pole using the Bahcall and Soneira Standard Galaxy Model (1980) and B-V-12μm star colors from Waters, Cote, and Aumann (1986). The log of the number of sources per square degree, per decade of flux density is plotted versus log flux density (in Janskys). The differential counts for all stars are given by the solid line. In addition, the differential counts for main sequence and giant stars are each shown for the disk and spheroidal components. The expected galaxy counts at 12μm are also shown.

source counts using the model of Condon (1984) with and without evolution, using the 60μm luminosity function and color-luminosity data given by Soifer, et al. (1986). The predicted counts for an evolutionary model and a nonevolving model are compared with the observed counts in Figure 2. Although the source counts favor the evolving model, they do not constrain the type of evolution that may have been detected. In addition, evolution is not the only explanation for the discrepancy between the observed source counts and the source counts predicted for a nonevolving universe. In particular, a galaxy cluster in the direction of this survey with a redshift of ~0.2 could produce this effect. Clearly, redshift data are needed to resolve the nature of this discrepancy.

ACKNOWLEDGEMENTS

Space does not permit us to express our gratitude to all of the people that contributed to this work. Some of the more important contributors we would like to acknowledge are: the entire IPAC facility for their untiring help; Jim Condon at NRAO for many useful discussions; Jim Cordes, Martin Harwit, and Martha Haynes at Cornell for useful discussions; Barbara Boettcher for her help with the figures; and Sylvia Corbin for compiling the manuscript.

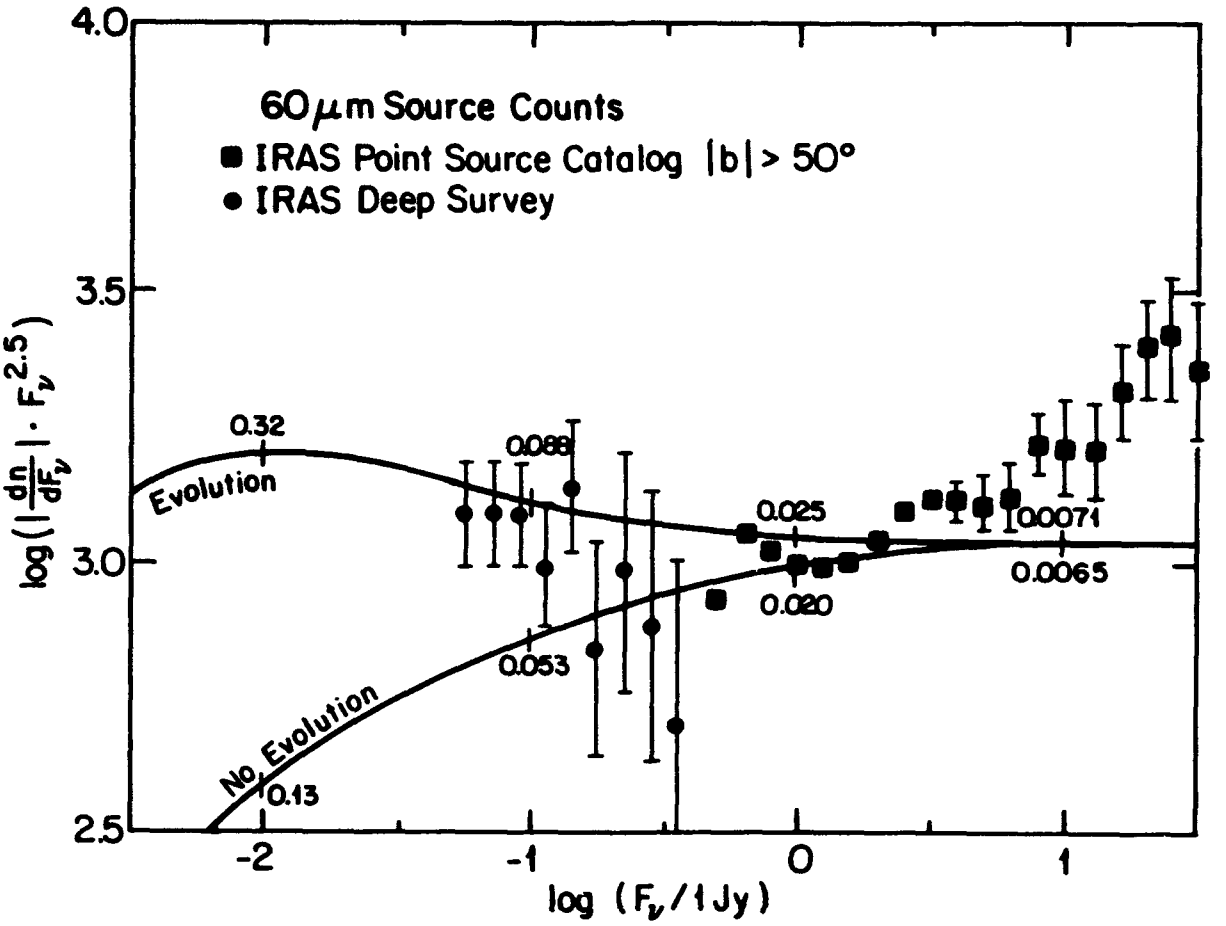

Figure 2 - Predicted 60μm differential galaxy counts with and without evolution, using the luminosity function and luninosity-color data from Soifer et al. (1986). Tick marks indicate median redshifts of the differential counts. The data from the deep survey are plotted as filled circles, and the data from the IRAS Point Source Catalog with $|b| > 50°$ are plotted as filled squares. Much of the increase in the source counts above 10 Jy is due to the Virgo cluster. The luminosity function has been shifted down by 15% so that the non-evolutionary model agrees with the differential counts at 1 Jy. See Hacking, Condon, and Houck (1986) for details.

REFERENCES

Bahcall, John J., and Soneira, Raymond M. 1980, Ap. J. (Supplements), 44, 73.
Condon, J. J. 1984, Ap. J., 287, 461.
Hacking, P. et al. 1985, P.A.S.P., 97 , 616.
Hacking, Perry, Condon, J. J., and Houck, J. R. 1986 (in preparation).
Hacking, Perry, and Houck, J. R. 1986, Ap. J. (Supplements), submitted.
Smithsonian Astrophysical Observatory 1966, Smithsonian Astrophysical Observatory Star Catalog.
Soifer, B. T., et al. 1986 (in preparation).
Waters, L. B. F. M., Cote, J., and Aumann, H. H. 1986, Astronomy and Astrophysics (submitted).

DISCUSSION

WYNN-WILLIAMS:

Are there other IRAS fields that can be analyzed to this depth, or have we hit the limit of what is possible with IRAS?

HACKING:

This is probably as deep as we can go at 12 and 25μm. There are smaller deep fields that are almost as deep as this field at 60 and 100μm. In addition, it may prove possible to reduce the confusion noise in this field using different filtering techniques, allowing a study up to a factor of 2 fainter in this field.

WEEDMAN:

Your counts at 60μm agree precisely with expectations from the average luminosity function now available. The very close agreement must be fortuitous, but it is pleasing that all of the data are coming together so consistently.

WHAT ARE 'CIRRUS' POINT SOURCES?[1]

CARL HEILES
PATRICK J. MCCARTHY
WILLIAM REACH
MICHAEL A. STRAUSS

Astronomy Department
University of California, Berkeley

ABSTRACT. Most 'cirrus' point sources are associated with interstellar gas. We have isolated a subset of these, together with other sources showing large band 4 to band 3 flux density ratios, that are *not* associated with interstellar gas. Most of the point sources are associated with diffuse cirrus emission. The sources appear to be distributed randomly on the sky, with the exception of six clusters, one of which is not associated with any known astronomical object.

Six sources out of seventeen that were observed for redshifted H I at Arecibo were found to be associated with relatively nondescript external galaxies. Most of the sources do not appear on the Palomar Sky Survey. Deep optical observations of eight fields revealed some fairly distant galaxies, one object with a very peculiar optical spectrum, and several blank fields.

I. INTRODUCTION

IRAS 'cirrus' point sources (*i.e.*, sources detected only in band 4, $\lambda \sim 100\ \mu$m) are suspected to arise from the same stuff as the diffuse cirrus background, namely interstellar dust. Since dust and gas are intermixed, we expect the presence of clumps of 21-cm emission at the positions of 'cirrus' point sources. However, our first cursory inspection of the distribution of these sources (Figure I.C.4 in the *IRAS* Explanatory Supplement, 1984) revealed that a small fraction are located in regions containing very little interstellar gas. By 'little' we mean HI column densities smaller than 10^{20} cm^{-2}, which is very low—typical of values toward the Galactic poles, and in other regions containing the very lowest column densities as measured with HI surveys using angular resolutions of 36 arcmin or more. This made us suspect that they are, in fact, *not* associated with interstellar gas.

We developed a source list for further study using a two-stage selection process. In the first stage, we included only those sources satisfying the following criteria: (1) reliable (quality 3) band 4 flux densities ($F4$); (2) $F4/F3 > 5$; (3) $F4 > 2$ Jy; (4) Galactic latitude $|b| > 10°$. This provided more than 20000 sources. In the second stage, this was reduced to 293 sources by requiring $F4$ to be larger than the limit determined from the H I column density described by equation (1) below.

From their locations in the sky, many of these sources are obviously associated with interstellar gas. Some are positionally coincident with known astronomical objects, many of which are galaxies. Some have no obvious association with known astronomical objects. Most sources have no corresponding image on the Palomar Sky Survey (PSS).

II. STATISTICS

Most of the 20000-odd sources chosen from the first stage selection are associated with interstellar gas. This is apparent from the scatter diagram of $F4$ *vs.* N(H I) presented in Figure 1: for N(H I) $\lesssim 150$, the upper envelope of the densely-populated portion of the $F4$-N(H I) plane has a

[1]This paper is based in part on observations performed at the Lick Observatory, operated by the University of California at Santa Cruz.

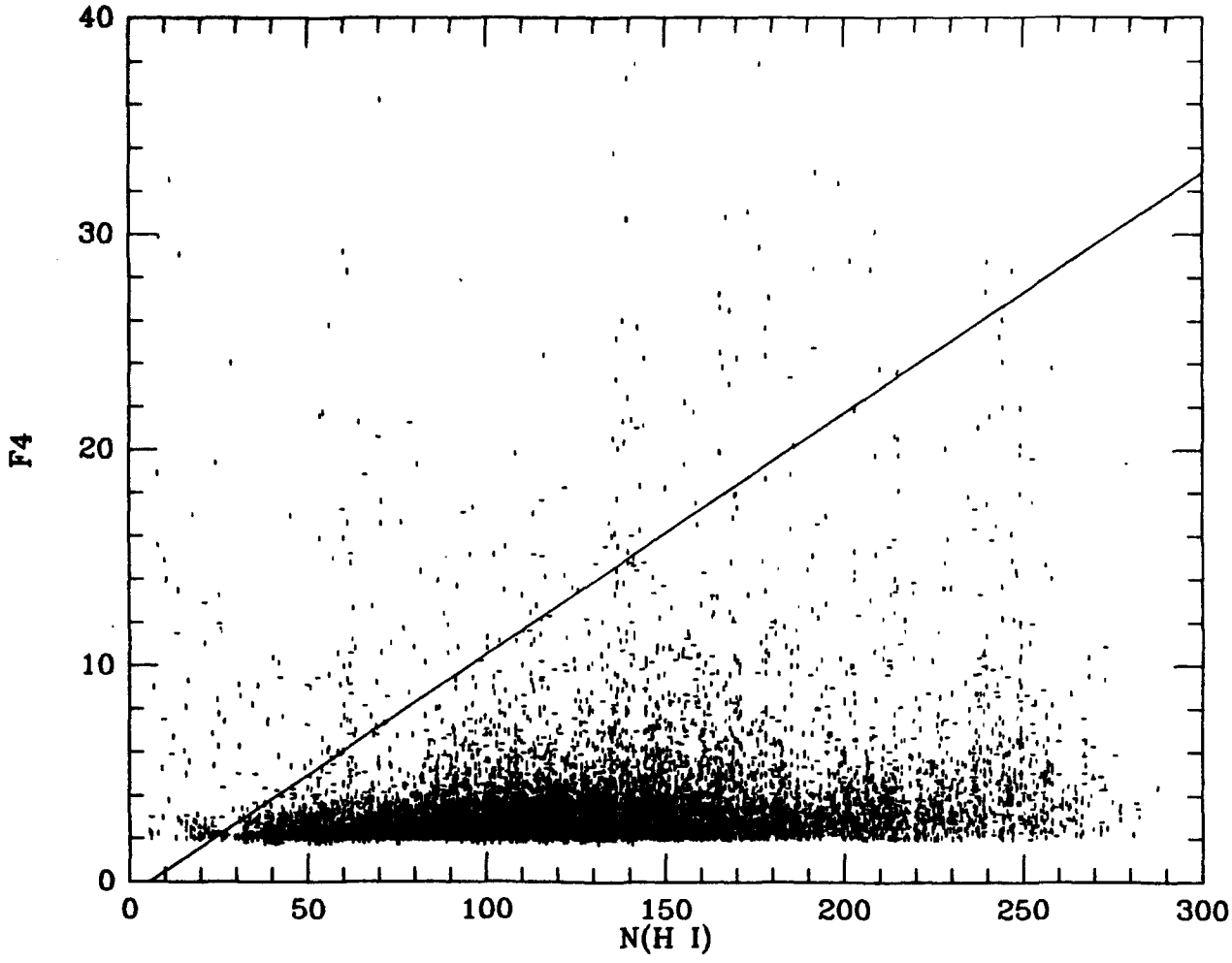

Figure 1. Scatter diagram of sources satisfying the first-stage selection process. $F4$ is the *IRAS* band 4 flux density in Jy; N(H I) is the H I column density in units of 9.96×10^{18} cm^{-2}, taken from Stark *et al.* (1986) for the Northern sky and from Cleary, Heiles, and Haslam (1974) for the Southern sky. This diagram does not include the full range of each variable, but does include the vast majority of the points. The solid line is the second-stage criterion of equation (1).

positive slope. For $F4$'s much larger than the majority, there is no obvious correlation with N(H I). We assumed that all sources with $F4$ exceeding a linear function of N(H I) should be considered as possible non-cirrus candidates, and determined the linear function by eye. The function, drawn in Figure 1, is

$$F4 = 0.1116\ \mathrm{N(H\ I)} - 0.625\ \ \mathrm{Jy}, \tag{1}$$

where the units of N(H I) are 9.96×10^{18} cm^{-2}, as on Figure 1.

The total number of sources satisfying the above criterion is 293. A bit fewer than half have positional coincidences with objects in astronomical catalogs other than the *IRAS* point source catalog. The distribution of the 293 sources on the sky is shown in Figure 2. The points tend to avoid low Galactic latitudes; this is a result of equation (1), because high H I column densities tend to lie at low latitudes.

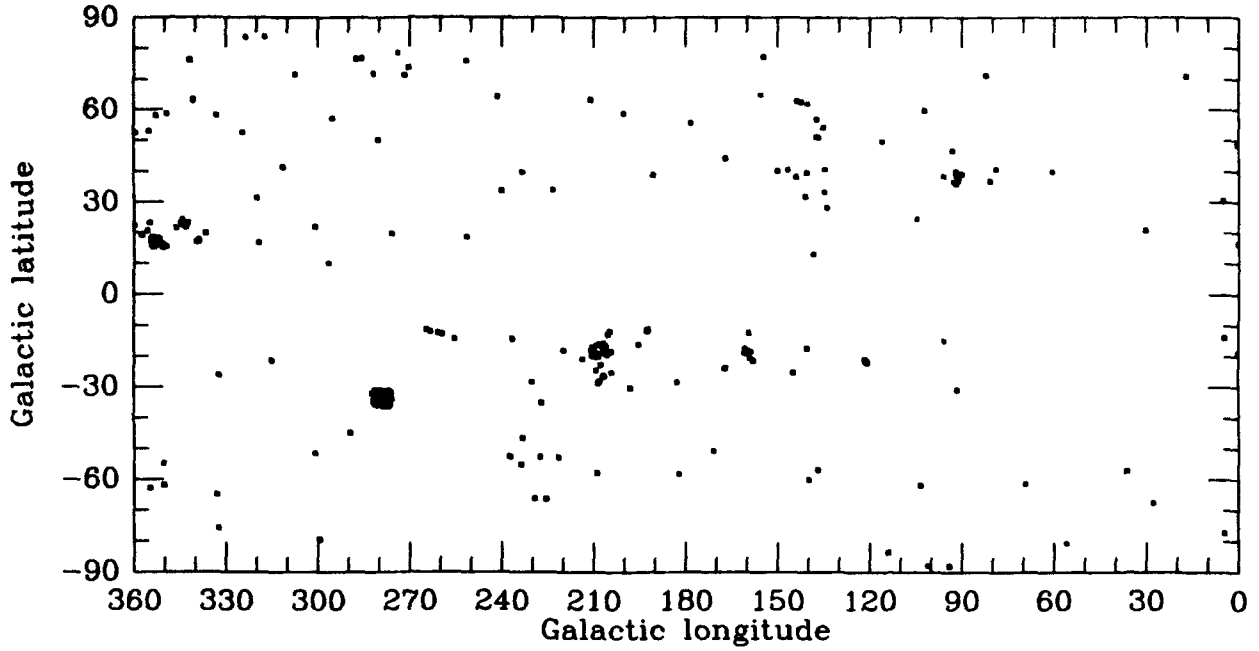

Figure 2. Distribution on the sky of sources above the solid line in Figure 1.

Some of the points are highly clustered. Five clusters can be identified with specific Galactic dust regions or extragalactic objects, as follows: $(l,b) \sim (122°,-22°)$, M31; $(161°,-19°)$, Perseus region; $(208°,-19°)$, Orion region; $(280°,-34°)$, Large Magellanic Cloud; $(353°,17°)$, Ophiuchus region. Two clusters have no obvious identifications: $(l,b) \sim (92°,38°)$, and the very sparse and possibly spurious cluster covering the large area centered near $(140°,50°)$. The former is located near the nondescript external galaxies NGC 6223, 6226, 6238, and 6244, and near the nondescript Abell cluster 2232. It is also located in a region containing high-velocity H I, but because other high-velocity H I regions do not exhibit clustered sources there is probably no real association. Sources with the largest $F4$'s (> 50 Jy) are associated either with dense clouds of Galactic interstellar matter, the Large Magellanic Cloud, or the external galaxy NGC 891.

Are these 293 sources unique or do they simply occupy the tails of the distributions of $F4$ and $F4/F3$? We are unable to tell. Our selected sources represent only a tiny fraction of all sources with interesting IR properties; the lion's share was discarded using equation (1). Answering the question would require generating a statistically unbiased list of *IRAS* point sources that are not associated with interstellar gas on arcminute scales. This might be done using high-resolution 21-cm line observations of a large unbiased sample, but this would be a tremendous undertaking.

III. GROUND-BASED OBSERVATIONS

A. 21-cm Observations

Equation (1) discriminates against regions of overall high H I column density, as measured with the large beamwidths ($\sim 1°$) used in the H I surveys. However, the possibility remains that small, arcminute-size clumps of H I exist within such regions. We used the NAIC Arecibo telescope[1] with

[1]The NAIC is a national facility operated by Cornell University under contract with the National Science Foundation.

its angular resolution of 3 arcminutes to check this possibility.

Out of 17 sources observed, 13 showed an H I column density excess relative to adjacent positions smaller than 10^{19} cm^{-2}, and the rest smaller than 3×10^{19} cm^{-2}. These are strict, absolute, and in many cases conservative upper limits. A point source with $F4 = 2$ Jy would produce an H I column density of 1.2×10^{21} cm^{-2} if the relation of Boulanger, Baud, and van Albada (1985) applies—100 times more H I than the observed upper limits. The most straightforward conclusion is the expected one, that these sources have nothing whatsoever to do with the interstellar gas.

We also used Arecibo to search for redshifted H I emission out to ~ 6000 km s^{-1}. Of the sample of 17 observed, 6 were detected. All 6 were positionally associated with ordinary nearby galaxies and were so designated in the *IRAS* point source catalog. For these 6 galaxies, the ratios of H I mass to IR luminosity were typically much higher than those of the IR-bright sample studied by Young *et al.* (1986), by factors ranging from ~ 10 to ~ 1000. These large factors result from the combined effects of our galaxies being overly abundant in H I and underluminous in the IR, with respect to the optical brightnesses of that sample. Our 6 galaxies are very easily visible on the PSS, and are therefore intrinsically different from the PSS blank-field objects discussed below.

B. Optical Observations

We used the CCD spectrograph in the direct imaging mode on Lick Observatory's Shane 3-m telescope (Miller *et al.*, 1983) to take optical images of fields centered on 8 PSS blank-field sources. One and possibly one other showed the streaks characteristic of interstellar cirrus. Two fields clearly contained external galaxies within the *IRAS* error ellipse: one a pair of galaxies, and one a compact galaxy. One field, 1645+37, contained three very faint galaxies within the error ellipse. The other three fields were blank with R $\gtrsim 22.5$ mag. The observations are summarized in Table 1, where the optical flux *densities* are compared to the IR flux *densities*.

TABLE 1

PROPERTIES OF OPTICALLY-OBSERVED SOURCES

SOURCE	IDENTIFICATION	R MAG	F4(Jy)	F4/(R-BAND FLUX)
0917+69	cirrus	-	3.5	
1148+58	compact galaxy	18	2.4	1.3E4
1149+61	pair of galaxies	16,19	2.0	1.8E3,2.8E4
1150-09	cirrus?	21	2.9	2.6E5
1231-05	?	>22.5	2.2	>7.8E5
1324+16	?	>22.5	2.8	>1.0E6
1325+16	?	>22.5	2.1	>7.4E5
1645+37	three galaxies	21.0-23.5	2.4	2.6E5-3.4E6

We also used the CCD spectrograph to obtain low-dispersion spectra of the three galaxies in the 1645+37 field. These data were taken very recently and are currently being analyzed. The easternmost galaxy exhibits a clear emission line. If this emission line is [OII] λ3727, then the redshift is 0.444 ± 0.002. With this redshift, the optical luminosity of the galaxy is roughly typical of L_* galaxies and the galaxy exhibits small internal reddening. The westernmost galaxy has a broadband

spectrum similar to that of the easternmost galaxy, but exhibits no emission line. The central object exhibits an unusual broadband spectrum, becoming spectacularly bright towards the blue.

There is a good *a priori* probability of finding the galaxies described in the above paragraph by observing eight *randomly-selected* fields to the depth that we observed. However, the central object in the 1645+37 field is very unusual, and the *a priori* probability of finding it in eight randomly-selected fields would appear to be small. Further observations and analysis are needed to determine just how unusual this object is.

C. 1.2 mm Continuum Observations

We used the NRAO 12-m telescope at Kitt Peak[1] to observe a selection of sources at 1.2 mm wavelength. Our goal was restricted to determining whether the sources are nonthermal emitters, *i.e.* similar to ordinary continuum radio sources with flux density rising toward lower frequencies. Sensitivity was low because of power outages, hardware failures, basic errors in system software, and (least of all) weather; the average 3σ flux density limit was 5.5 Jy. No source was detected. Thus *no* source was significantly stronger at 1.2 mm than at 100 μm. Any typical power-law synchrotron source would have been easily detectable. The most straightforward conclusion is that the sources are thermal emitters, perhaps modified by the wavelength-dependence of the emissivity of dust particles.

IV. DISCUSSION

Our 1.2 mm observations imply that the *IRAS* point-source emission is thermal. Nevertheless, it would be remiss not to mention the unlikely alternative that the IR emission is produced by an as-yet unspecified powerful process, making the situation analagous to the early days of radio astronomy when virtually nothing was known about the basic characteristics of nonthermal radio sources. If the radiation has a blackbody spectrum, $(F4/F3) > 5$ corresponds to T < 30.5 K; if the emission comes from dust, which radiates less efficiently at long wavelengths, then the physical temperature of the dust is smaller. For a blackbody emitter at T=30.5 K to produce $F4 = 2$ Jy, its angular diameter > 0.6 arcsec; if the radiation is from dust, this is a lower limit.

With such angular diameters, most of the objects can hardly be anything but diffuse matter. If Galactic, their lack of concentration toward the Galactic plane would imply that they are nearby, with typical distances smaller than their z-heights above the Galactic plane. If extragalactic, they would be truly spectacular because the ratios of IR to optical flux densities are enormous. For example, for objects fainter than 22.5 mag, the ratio of $F4$ to optical R-band flux *density* is $\gtrsim 10^6$. This is about 50 times larger than the corresponding ratio for the extremely far-IR bright starburst/Seyfert galaxy Arp 220 (Rieke *et al.*, 1985; Soifer *et al.*, 1984) and about 10 times larger than the ratio for the most extreme example in the lists of Aaronson and Olszewski (1984) and Houck *et al.* (1985).

Finally, we mention ripe areas for future observational work. Most intriguing is the unidentified cluster of sources, associated with diffuse cirrus, centered near $(l, b) \sim (92°, 38°)$ or $(\alpha, \delta) \sim (16^h47^m, 62°)$. IR observations longward of 100 μm should be successful because of the rapid rise of flux density with decreasing frequency, unless the radiation is line emission; very low-resolution spectroscopy is the best approach for this test. If these sources obey the same statistical relationships as external galaxies they should be detectable as radio continuum sources, typically with flux densities $\gtrsim 3$ mJy at 1.4 GHz (Helou, Soifer, and Rowan-Robinson, 1985) and as CO emitters, typically at the level $T\Delta v \gtrsim 0.5$ °K-km/s with the FCRAO 14-m telescope (Young *et al.*, 1986). Finally, we will continue our optical observations.

[1]The NRAO is operated by Associated Universities, Inc., under contract with the National Science Foundation.

We gratefully acknowledge the suppport of the Lick Observatory staff for their assistance in performing the optical observations. It is a pleasure to thank Prof. Frank Low for pointing out to us the preponderance of diffuse cirrus emission, and for providing the stimulus to write this paper in a timely fashion. This research was supported in part by a National Science Foundation grant to CH, and also under the *IRAS* extended mission program by a JPL contract to CH. MAS is supported by a Berkeley Graduate Fellowship.

REFERENCES

Aaronson, M., and Olszewski, E.W. 1984, *Nature*, **309**, 414.

Boulanger, F., Baud, B., and van Albada, G.D. 1985, *Astron. Ap.*, **144**, L9.

Cleary, M.N., Heiles, C. and Haslam, C.G.T. 1979, *Astron. Ap. Suppl.*, **36**, 95.

Helou, G., Soifer, B.T., and Rowan-Robinson, M. 1985, *Ap. J.*, **298**, L7.

Houck, J.R., Schneider, D.P., Danielson, G.E., Beichman, C.A., Lonsdale, C.J., Neugebauer, G., and Soifer, B.T. 1985, *Ap. J.*, **290**, L5.

IRAS Catalogs and Atlases, Explanatory Supplement 1985, edited by Beichman, C.A., Neugebauer, G., Habing, H.J., Clegg, P.E., and Chester, T.J. (Washingon D.C.: U..S. Government Printing Office).

IRAS Point Source Catalog 1985, Joint *IRAS* Science Working Group (Washington, D.C.: U.S. Government Printing Office).

Miller, J.S. 1983, The Lick 3-m Cassegrain Spectrograph, Lick Observatory, University of California, Santa Cruz, CA.

Rieke, G.H., Cutri, R.M., Black, J.H., Kailey, W.F., McAlary, C.W., Lebofsky, M.J., and Elston, R. 1985, *Ap. J.*, **290**, 116.

Soifer, B.T., Helou, G., Lonsdale, C.J., Neugebauer, G., Hacking, P., Houck, J.R., Low, F.J., Rice, W., and Rowan-Robinson, M. 1984, *Ap. J.*, **283**, L1.

Stark, A.A., Bally, J., Linke, R.A., and Heiles, C. 1986, in preparation.

Young, J.S., Schloerb, F.P., Kenney, J.D., and Lord, S.D. 1986, *Ap. J.*, **304**, 443.

Properties of the Unusual Galaxy PSC 09104+4109

S.G. Kleinmann[1] and W.C. Keel[2]

ABSTRACT

The IRAS source PSC 09104+4109 is tentatively identified with a faint ($m_R \sim +19$) emission line galaxy having $z = 0.442$. Assuming this identification is correct, the total infrared luminosity of this galaxy is estimated to be 5×10^{12} L_o, among the highest for galaxies detected by IRAS. This energy is concentrated at wavelengths less than 30 μm, and is ~50 times greater than the estimated optical luminosity. The serendipitous way in which this source was found in the PSC catalog suggests that many more similar objects may be found at the lowest levels of the IRAS survey.

1. Introduction

During the startup phase of a redshift survey of sources detected at $\lambda_{obs} \sim 60$ μm in the IRAS survey, we found an object, PSC 09104+4109 (IRAS Point Source Catalog), worthy of further study both for its high luminosity and its unusual infrared spectral energy distribution. Particular interest in this IRAS source was first evoked because it was one of ten 60 μm sources, out of a list of 500 located in a slice of the sky at high galactic latitudes, that was not located near a bright ($m_{pg} < 18$) star or galaxy. Houck *et al.* (1985) showed that many such sources could be identified with distant luminous galaxies.

2. Optical Identification

In search of its optical counterpart, a deep R-band image of the region surrounding PSC09104+4109 was taken at the 2.1-m telescope of the Kitt Peak National Observatory. A cluster of faint ($m_R > 21$) sources was detected on this plate, though none brighter than $m_R \sim 22$ fell within the IRAS error box. Two brighter objects, each having $m_R \sim 19$, were found just outside the error box. One of the these (Object 1) lies near the periphery of the cluster of faint objects, while the other (Object 2) lies near its center.

The PSC position for the infrared source is listed in Table 1; its error box, as given in the Point Source Catalog, has dimensions ±11" x ±24" at P.A. 108°. The positions of the two nearby 19^{th} mag. sources, which were measured on the two-axis Grant measuring engine at NOAO, are also given in the Table; the rms error in the measurements of the system of standard stars on the plates was 0.5". The distances of each of the objects in Table 1 from the center of the IRAS error box are listed in the table in units of the positional uncertainties of the infrared source.

[1]Department of Physics and Astronomy, University of Massachusetts.
[2]Leiden Observatory.

Carol J. Lonsdale Persson (Editor)
Star Formation in Galaxies

Table 1. Positions of Sources Near IRAS PSC 09104+4109

Designation	RA (1950)	DEC (1950)	Offset From Major Axis	Offset From Minor Axis	Total Offset
PSC 09104+4109	09 10 29.8	+41 09 04			
Object 1	09 10 29.13	+41 09 22.0	1.4σ	0.5σ	1.5σ
Object 2	09 10 32.92	+41 08 52.4	$.0\sigma$	1.5σ	1.5σ

Spectra of the two red objects listed in Table 1 were obtained with the Cryogenic Camera at the 4-m telescope at Kitt Peak. These showed that the cluster-center galaxy (Object 2) had an absorption line spectrum at $z \sim 0.3$, while the object near the cluster's edge (Object 1) had a strong emission line spectrum at $z = 0.442$. By analogy with many other 60 μm sources associated with faint optical objects, we have tentatively identified IRAS 09104+4109 with Object 1. In any case, if this infrared source is extragalactic, it probably lies at $z \geq 0.2$, since less distant galaxies should have been detected on the R-band image at a level brighter than $m_R = 22$.

If $H_o = 100$ km/s/Mpc, and $q_o = 1/2$, the the total Blue luminosity is estimated to be 2 x 10^{10} L_o. About half of this light is due to emission lines of O[III] 5007 and 4959, Hβ and Hγ. Weak emission from He II 4686 is also observed. These lines are all narrow; Hβ has a full width at half maximum of <1000 km/s. This line width and luminosity are typical for Seyfert II galaxies.

3. Infrared Photometry

The "Add-Scan" program at IPAC was used to obtain high signal-to-noise photometry of PSC 09104+4109 in the IRAS bands. Data from 11 scans of the object were co-added, yielding significant detections in IRAS Bands 1, 2, and 3, but a low upper limit in Band 4. Flux densities derived under the assumption that the observations were made in the rest frame of a source having a spectrum $F_\nu \sim \nu^{-1}$ (as in the PSC catalog) are given in Table 2. The upper limit quoted for Band 4 corresponds to 3σ. The low ratio of flux densities, $S(100)/S(60) < 0.7$, is one of the most peculiar features of this source. In contrast, the high-redshift galaxies studied by Houck *et al.* (1985) were all found to have $S(100) \geq 2\ S(60)$. Even higher ratios are typical of normal galaxies detected by IRAS at $\lambda = 60$ μm (deJong *et al.* 1984; Soifer *et al.* 1984).

Also given in Table 2 are the corrected flux densities for a thermal source at $z = 0.442$. In this case, the flux in each band was derived by assuming that the spectrum in adjacent bands is produced by a blackbody having color temperatures 330 °K, 180 °K, and 137 °K at wavelengths 12μm to 25μm, 25μm to 60μm, and 60μm to 100μm, respectively.

Table 2. Infrared Flux Densities for PSC 09104+4109

	S(12μm)	S(25μm)	S(60μm)	S(100μm)
z=0; F=ν^{-1}	0.17±0.03	0.39±0.03	0.55±0.05	<0.39
z=0.442; F=F(BB)	0.25	0.27	0.27	<0.17

The total infrared luminosity of PSC 09104+4109 is estimated to be 5 x 10^{12} $L_{\odot}$, most of it emerging at $\lambda < 30$ μm. This value is nearly 3 times greater than the infrared luminosity produced by Arp 220 or Markarian 231 (for the same cosmological constants).

If the energy per octave at optical wavelengths ($0.36 < \lambda(\mu m) < 1.0$) is constant and equal to that observed in the R band, then the total infrared luminosity of PSC 09104+4109 exceeds its optical luminosity by a factor of nearly 50. This ratio is much larger than values characteristic of quasars.

4. Conclusion

The IRAS source PSC 09104+4109 has an observed infrared energy distribution which is peculiar both for stars and for galaxies, in that it peaks near $\lambda_{obs} = 60$ μm. It also exhibits a large ratio of L_{IR}/L_{opt} (~50). It is tentatively identified with an emission line galaxy having $m_R \sim +19$, and $z = 0.442$. Confirmation of this identification would show that this source is one of the most luminous objects found in the survey. Further study is required to learn the extent to which the ratio of infrared to optical luminosity can be used to distinguish the most luminous galaxies found by IRAS, and what relationship exists between PSC 09104+4109 and other classes of luminous galaxies.

Only a dozen of the 500 galaxies in the flux-limited sample from which PSC09104+4109 was drawn have been observed spectroscopically. That fact suggests that many more galaxies having such high luminosity and peculiar flux distributions may be found among the faint sources detected in the IRAS survey.

We would like to thank Don Hamilton for providing us with the spectra he obtained at the KPNO 4-m, and Judy Young who obtained the Add-Scan photometry at IPAC. This work was supported by grant # AFOSR 85-0057.

REFERENCES

DeJong, T., Clegg, P. E., Soifer, B. T., Rowan-Robinson, M., Habing, H. J., Houck, J. R., Aumann, H. H., and Raimond, E. 1984, *Ap. J. Letters*, **278**, L67.

Houck, J. R., Schneider, D. P., Danielson, G. E., Beichman, C. A., Lonsdale, C. J., Neugebauer, G., and Soifer, B. T. 1985, *Ap. J. Letters*, **290**, L5.

IRAS Point Source Catalog, 1985, Joint IRAS Science Working Group, (Washington, D.C.: U.S. Government Printing Office).

Soifer, B. T., Rowan-Robinson, M., Houck, J. R., deJong, T., Neugebauer, G., Aumann, H. H., Beichman, C. A., Boggess, N., Clegg, P. A., Emerson, J. P., Gillett, F. C., Habing, H. J., Hauser, M. G., Low, F. J., Miley, G., and Young, E. T. 1984, *Ap. J. Letters*, **278**, L71.

POSTER PRESENTATIONS

FAR-INFRARED LUMINOSITY FUNCTIONS

A Redshift Survey of IRAS Galaxies

Beverly J. Smith[1], S.G. Kleinmann[1], J.P. Huchra[2], and F.J. Low[3]

ABSTRACT

We present results from a redshift survey of all 72 galaxies detected by IRAS in Band 3 at flux levels ≥ 2 Jy, and lying in the region $8^h < \alpha < 17^h$, $23.5° < \delta < 32.5°$. The 60 μm luminosities of these galaxies range from 1.4×10^8 $L_\odot$ to 5.0×10^{11} $L_\odot$. The luminosity function at the high luminosity end is proportional to L^{-2}, however, we observe a flattening at the low luminosity end indicating that a single power law is not a good description of the entire luminosity function. Only three galaxies in our sample have emission line spectra indicative of AGN's, suggesting that, at least in nearby galaxies, unobscured nuclear activity is not a strong contributor to the far-infrared flux. Comparisons between the selected IRAS galaxies and an optically complete sample taken from the CfA redshift survey show that they are drawn from different parent populations. The absolute blue luminosities of IRAS galaxies are more narrowly distributed than those optically selected, in the sense that the IRAS sample includes few galaxies of low absolute blue luminosity. We also find that the space distributions of the two samples differ: the density enhancement of IRAS galaxies is only ~1/3 that of the optically selected galaxies in the core of the Coma cluster.

1. Introduction

The study of IRAS galaxy source counts is important because IRAS offers the first all-sky survey sufficiently sensitive to detect galaxies, but relatively insensitive to surface brightness gradients. To interpret these source counts in terms of the space distribution of IR-bright galaxies, it is necessary to know their infrared luminosity distribution. Towards this end, we have exploited and extended the deep redshift survey carried out by de Lapparent, Geller, and Huchra (1986) over a selected "slice" of the sky (the CfA survey).

2. Materials and Methods

Our sample includes all sources listed in the IRAS Point Source Catalog or the Small Extended Source Catalog above a flux limit of 2 Jy at 60 microns, and lying within the 1072 square degree region between $8^h < \alpha < 17^h$, $23.5° < \delta < 32.5°$. Eighty-six sources met the selection criteria. Optical identifications were made on the basis of positional proximity. Thirteen are stars, one is a planetary nebula, and 72 are galaxies. Twenty-two of the galaxies in our sample were found to occur in groups of two or more. In cases where more than one galaxy falls in the quoted Point Source Catalog error box, the IRAS source was associated with the brightest galaxy.

Spectra with a resolution of 6-7 Å covering 4600-7200 Å were obtained at the F.L.Whipple 1.5m telescope and at the MMT. Several galaxies were observed in the confused cases; all of our pairs appear to be physically associated, i.e. at the same redshift. Redshifts

[1]Five College Astronomy Dept., University of Massachusetts, Amherst, MA 01003
[2]Center for Astrophysics, 60 Garden St., Cambridge, MA 02138
[3]Steward Observatory, University of Arizona, Tucson, AZ 85718

Carol J. Lonsdale Persson (Editor)
Star Formation in Galaxies

and equivalent widths of the Hα, Hβ, [OIII] λ5007, [OI] λ6300, and [NII] λ6585 lines were determined from these spectra. For galaxies brighter than $m_B \sim 15.7$, blue magnitudes were taken from the Zwicky Catalog. For fainter galaxies, eye estimates were made.

3. The 60 μm Luminosity Function

We define the 60 micron luminosity as the energy in the band:

$$L = 4\pi r^2 F_\nu \Delta\nu$$

where F_ν is the IRAS flux density and $\Delta\nu$ is the bandwidth ($= 3.75 \times 10^{12}$ Hz; Neugebauer *et al.* 1984). We calculate r by assuming $H_o = 100$ km/s/Mpc[3] and correcting for 300 km/s galactic rotation and deviation from the Hubble flow due to infall towards the Virgo cluster of 300 km/s as in Huchra and Geller (1982).

The distribution of luminosities and the luminosity function

$$\Phi(L) = \frac{4\pi}{\Omega}\frac{1}{\Delta L_i}\sum_j \frac{1}{V_j}$$

are shown in Figure 1. Here $\Omega/4\pi$ is the fraction of the sky covered by this survey, ΔL_i is the bin width, and V_j is the volume of the universe out to which a galaxy of luminosity L is observed at our flux limit. Uncertainties in the luminosity function were calculated assuming Poisson distribution errors, proportional to $\sqrt{N}$. Thus we have ignored errors in the luminosities due to uncertainties in the infrared fluxes and deviations from Hubble flow which are not completely eliminated by our corrections for Virgocentric motion. The data from Soifer *et al.* (1986), corrected to our units, are shown for comparison.

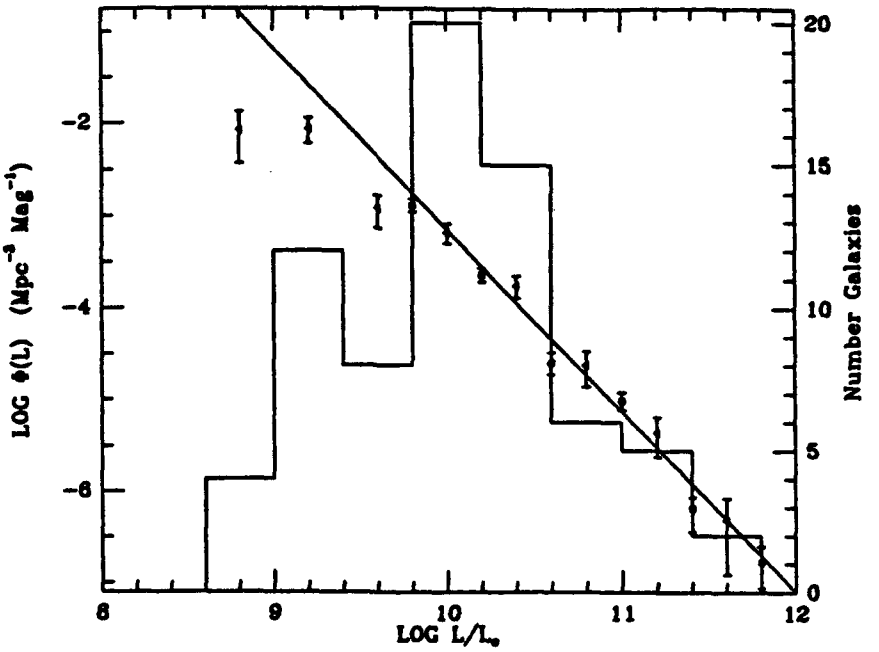

Figure 1. The 60 micron luminosity function. The triangles are the points derived from our sample; the squares are from Soifer *et al.* (1986). The units on Φ(L) are Mpc^{-3} mag^{-1}, and the error bars are proportional to $\sqrt{N}$. The histogram is the number count of galaxies in each luminosity bin (right axis).

To describe this data in a useful analytical form, we have tried both a Schechter (1976) function and a single power law. Neither yielded a good fit; at high luminosities the density lies below that expected for a Schechter function, and at low luminosities the density is less than expected for a single power law. However, the apparent flattening of the luminosity function at the low luminosity end may be due to incompleteness due to low surface brightness galaxies larger than 2 arcminutes. The line shown is a best fit power law to our data above $10^{10}L_{\odot}$ of $\phi(L) = 3.5 \times 10^{16}(L/L_{\odot})^{-2}$ $Mpc^{-3}mag^{-1}$. The slope is confined to a range of −1.7 to −2.1 with a 68% confidence. This fit is consistent with the fit derived by Soifer *et al.* (1986) from a brighter sample.

4. Comparison with Optical Sample

Figure 2 shows the absolute magnitude distribution of our infrared-selected sample, the Center for Astrophysics blue-selected sample from Huchra *et al.* (1983), and the CfA spirals. This figure clearly shows that the galaxies in our sample have a narrower range of absolute blue magnitude than those of an optically selected sample. The mean for this sample is −19.2 with a standard deviation of only 0.8. We find that IRAS undersamples galaxies of low absolute blue luminosity. There also appears to be a deficiency of galaxies of high blue luminosity. A Kolmogorov-Smirnov test gives an 95% probability that the two samples are not derived from the same parent population.

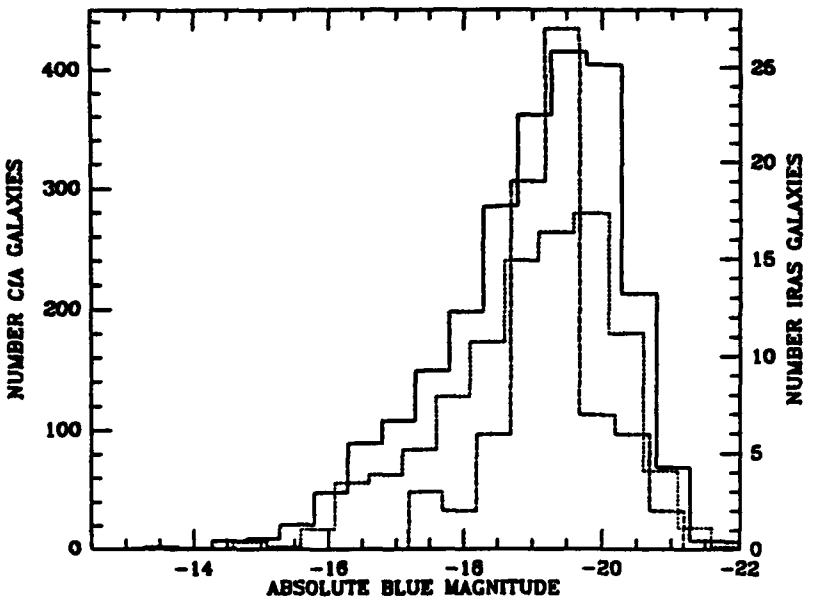

Figure 2. The absolute magnitude distribution of the IRAS sample (dashed histogram), the CfA blue-selected sample (solid histogram), and the CfA spirals (dotted histogram).

We also see a difference in the blue magnitude distributions of IRAS galaxies and CfA spirals. A Kolmogorov-Smirnov test gives a 99% probability that the IRAS galaxies are not drawn from the same parent population as the CfA spiral galaxies. However, a Mann-Whitney test shows that there is only a 1 sigma difference in the medians. We can thus conclude that the distributions are different in that the IRAS sample excludes galaxies of low blue luminosity, and therefore has a narrower range in blue luminosity.

A possible explanation is low metallicity in low mass galaxies. Metallicity has been shown to be correlated with blue luminosity, in ellipticals (Faber 1973) and in spirals (Bothun *et al.* 1984). If dust content is a function of metallicity, then we would expect the observed difference in the blue magnitude distributions of IRAS galaxies and CfA spirals. It is important to note that the blue luminosity is enhanced by recent star formation; M/L of the IRAS galaxies may differ from that of the CfA galaxies. It is thus not possible to conclude that only more massive galaxies are detected by IRAS. It is also important to emphasize that the infrared luminosity is both a function of the dust content and of the proximity of the dust to the heating sources. It may simply be the case that galaxies of low blue luminosity have a lower percentage of HII regions embedded in molecular clouds.

Two galaxies in this sample are Seyfert 2 galaxies; one is a Seyfert 1. The percentage of active galaxies in this infrared selected sample is thus not significantly different from that of the CfA sample. We find no correlation between [OIII]/Hβ and the infrared excess L_{60}/L_B, again indicating that unobscured nuclear activity is not a strong contributor to the 60 μm flux in this sample.

Comparing the space distribution of our sample with that of the CfA sample, we find that the IRAS galaxies follow the cellular pattern of galaxies observed by de Lapparent, Geller, and Huchra (1986), however, a density enhancement in the core of Coma the size of the CfA density enhancement is not observed. The IR density/B density ratio in Coma is ~1/3 that of the mean of the remainder of our box. This is most easily explained by the fact that IRAS preferentially detects spirals (Wolstencroft *et al.* 1985), while Coma is dominated by E's and S0's (Dressler 1980). We therefore expect that IRAS is systematically underestimating the mass in rich clusters; this introduces errors into the gravitational dipole moment derived by Yahil *et al.* (1985) and Meiksen and Davis (1986).

We would like to thank J.Peters, E.Horine, and S.Tokorz for help in obtaining and reducing the data. This work was partially supported by grant # AFOSR 85-0057 and by the Smithsonian Institution.

REFERENCES

Bothun, G.D., Romanishin, W., Strom, S.E., and Strom, K.M. 1984, *A.J.*, **89**, 1300.
de Lapparent, V., Geller, M.J., and Huchra, J.P. 1986, *Ap.J.(Letters)*, **302**, L1.
Dressler, A., 1980, *Ap.J.Supp.*, **42**, 565.
Faber, S.M. 1973, *Ap.J.*, **179**, 731.
Huchra, J.P., Davis, M., Latham, D., Tonry, J. 1983, *Ap.J.Supp.*, **52**, 89.
Huchra, J.P., and Geller, M.J. 1982, *Ap.J.*, **257**, 423.
Meiksin, A., and Davis, M., 1986, *A.J.*, **91**, 191.
Neugebauer, G., *et al.* 1984, *Ap.J.(Letters)*, **278**, L1.
Schechter, P. 1976, *Ap.J.*, **203**, 297.
Soifer, B.T., *et al.* 1986, *Ap.J. (Letters)*, **303**, L41.
Wolstencroft, R.D., *et al.*, 1986, in: Light on Dark Matter, F.P. Israel, ed., Reidel, p.425.
Yahil, A., Walker, D., Rowan-Robinson, M., 1986, *Ap. J. (Letters)*, **301**, L1.

OPTICAL AND IR LUMINOSITY FUNCTIONS OF IRAS GALAXIES

J. Patricia Vader
Department of Astronomy
Yale University
Box 6666
New Haven, CT 06511

M. Simon
Astronomy Program
State University of New York
Stony Brook, NY 11794

ABSTRACT

The optical and infrared luminosity functions are determined for a 60μm flux-limited sample of 68 IRAS galaxies covering a total area of 150 degrees squared. The IR function is in good agreement with that obtained by other authors. The shape of the optical luminosity function is similar to that of optically selected galaxy samples. The integrated light of most objects in our sample have [NII] to Hα line flux ratios characteristic of HII-region galaxies. In the absolute magnitude range M_J = -18, -22 about 14% of late-type galaxies are IRAS galaxies. The apparent companionship frequency is about twice as large as that for a comparable sample of non-IRAS late-type galaxies.

1. INTRODUCTION

The aim of this study is to construct the infrared luminosity function of IRAS galaxies and to compare various properties of an infrared selected sample of IRAS galaxies to those of optically selected non-IRAS galaxies.

We have selected all candidate galaxies listed in the IRAS Point Source Catalog (Beichman et al. 1984) with high or medium quality 60μm fluxes ≥ 0.5 Jy in six 5° x 5° fields at galactic latitude $|b| > 30°$. These fields are covered by the photographic plates of fields SP6, NP4, NP5, NP6, NP7, and NP8 used by Kirshner et al. (1978 (KOS), 1983 (KOSS)) to determine the optical luminosity function of field galaxies. This yields a sample of 81 IRAS candidate galaxies, 42 of which are previously catalogued galaxies, 38 are identified as galaxies on the KOS/KOSS plates, and 1 appears to be a blank field. The resulting density of these objects is ∿ 0.5 galaxy per degree squared. Published velocities are available for 24 objects. We have remeasured some of these (no discrepancies) and obtained new velocities for 45 galaxies, with an accuracy of 100 km/s, using the IIDS at the Kitt Peak 2.1-m telescope. Velocities are still missing for 12 galaxies in our sample, half of which are in field SP6, and most of which are optically faint.

Integrated optical magnitudes in the J band (KOS) have been measured with the Yale PDS microdensitometer from the KOS/KOSS plates. The zero-points of the photometry have been determined to an accuracy of 0.1 mag by comparing our results to those of KOS and KOSS. Our final magnitudes have an accuracy of better than 0.2 mag. They are corrected for galactic absorption as in KOS, but no k correction is applied. With the magnitude of 1 galaxy still missing, the sample of IRAS galaxies with available velocities and optical magnitudes considered here consists of 68 objects. No corrections for incompleteness will be made.

Carol J. Lonsdale Persson (Editor)
Star Formation in Galaxies

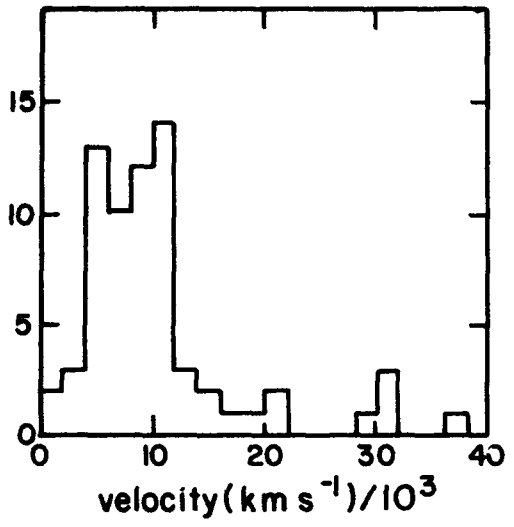

Fig. 1. Velocity distribution of our sample of 68 IRAS galaxies.

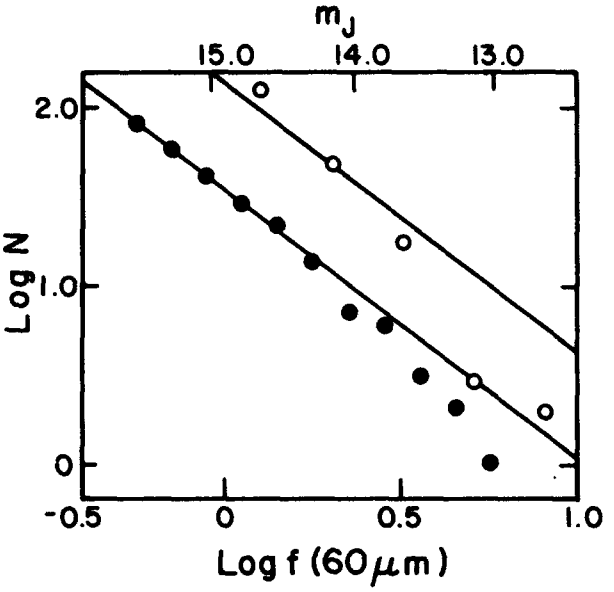

Fig. 2. Cumulative number of IRAS galaxies versus f(60μm) (•) and of KOS galaxies versus m_J (o). Solid lines indicate the expected slope for a complete sample.

2. THE INFRARED LUMINOSITY FUNCTION

The velocity distribution of our sample is shown in Fig. 1. A plot of the cumulative number of galaxies versus 60μm flux density shows that our sample is complete at the faint end but is deficient in bright objects (Fig. 2). A similar behaviour appears in the optical sample (m_J < 14.9) of KOS/KOSS in the same fields.

Absolute IR luminosities are calculated according to $L(60\mu m) = 4\pi D^2(\nu f_\nu(60\mu m))$, with D the distance of the galaxy assuming a uniform Hubble flow with H = 75 km/s/Mpc. Our differential IR luminosity function (Fig. 3a) and those obtained by Lawrence et al. (1986), Smith et al. (1986), Soifer et al. (1986), and Weedman (1986) all agree within a factor of 2 when the same units and scale factors are used.

3. THE OPTICAL LUMINOSITY FUNCTION

With only one exception all the objects in our IRAS sample can be identified optically on the KOS/KOSS plates. We therefore construct an optical luminosity function according to ϕ (opt,i) = sum(j) Nij/Vj, where Nij is the number of galaxies within absolute optical luminosity bin i and IR luminosity bin j and Vj is the corresponding volume sampled in the infrared.

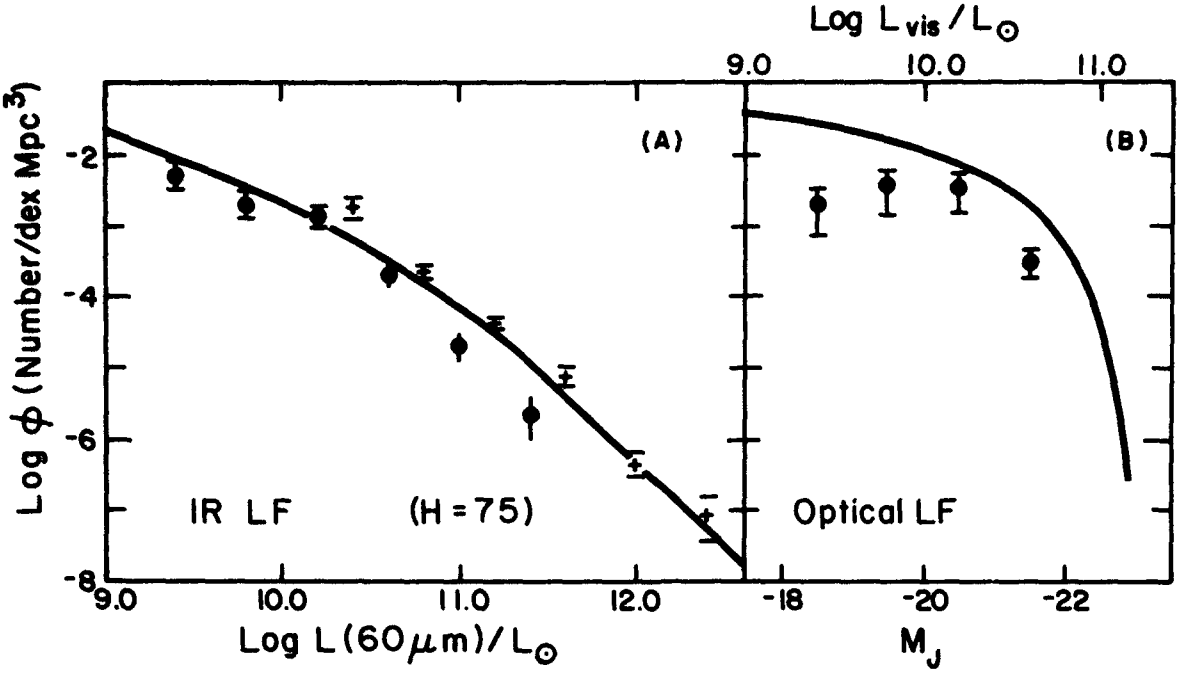

Fig. 3. (a) The differential IR luminosity function of our sample (•), of Lawrence et al. (1986, solid line), and of Soifer et al. (1986), +); (b) the optical luminosity function of our sample (•) and of Kirshner et al. (1979, solid line).

In other words, we assume that the volume sampling is determined by the IR flux limit. This hypothesis can be tested to some extent by varying the IR flux limit of our sample. We find that for 60μm flux limits ranging from 0.5 Jy (68 objects) to 0.9 Jy (31 objects) the optical luminosity functions thus derived are identical within the errors. The results for our 68 IRAS galaxies are displayed in Fig. 3b. The shape of this optical luminosity function is similar to that obtained by Kirshner et al. (1979) for their optically selected sample of field galaxies. For $-22 \leq Mj \leq -18$ the average ratio of IRAS to field galaxies is 1/7.

4. SPECTRAL CHARACTERISTICS AND COMPANIONSHIP FREQUENCY

Our spectrophotometry was principally in the red, so that the spectral diagnostics available are the Hα, [HII], and [SII] lines. The Hα line is invariably the strongest. The [NII] λ6584 to Hα line flux ratios lie in the range 0.1 to 1.0 characteristic of HII region-like galaxies (Baldwin et al. 1981). This suggests that the integrated optical spectrum of the majority of IRAS galaxies is dominated by starburst rather than nuclear activity. The absolute Hα luminosity (uncorrected for internal extinction) is proportional to the 60μm luminosity, but with a large scatter. Converting the Hα flux into Lyman continuum flux using standard recombination theory and assuming that the ionizing flux is solely due to OB stars (Salpeter IMF, mass range 6 to 40 M_0) whose optical luminosity is completely absorbed and reemitted at 60μm, we

predict a relation log L (Hα [erg/s]) = log ($L(60\mu m)/L_0$) + 30.8. While M82 approximately does obey this relation, the galaxies in our sample have Hα luminosities smaller than predicted by a factor of 20 on average. This is probably due to much larger optical extinction in our sample and a possible contribution to the 60μm luminosity of the general underlying stellar population besides that of the ionizing OB stars alone.

Enhanced star formation and nuclear activity are often found in interacting galaxies (e.g. R.M. Cutri, this volume). We have compared the frequency of apparent companions within a projected solid angle of 100 kpc for our sample of IRAS galaxies to that of 40 non-IRAS late-type galaxies in the same KOS/KOSS fields. We find that 43±8% of the IRAS galaxies have such a companion as compared to only 23±8% of the non-IRAS galaxies. In spite of the uncertainty due to projection effects, it is interesting that the apparent companionship frequency among IRAS galaxies appears to be higher, at a statistically significant level, than among the non-IRAS galaxies.

We have also compared the (J-F) colors of IRAS and non-IRAS galaxies in the KOS sample (excluding E and SO galaxies). The difference is not statistically significant: for the IRAS galaxies $(J-F)_{avg} = 0.84 \pm 0.04$, and for the non-IRAS galaxies $(J-F)_{avg} = 0.78 \pm 0.02$.

5. CONCLUSIONS

Within an absolute magnitude range $-22 \leq M_J \leq -18$ about 14% of late-type galaxies are IRAS galaxies. The integrated light of IRAS galaxies mainly reflects an enhanced star formation rate which, however, does not affect their J-F color. The probability of a galaxy being an IRAS source seems to be larger when a companion is present within a projected radius of 100 kpc.

A detailed account of this work will be submitted for publication to the Astronomical Journal.

We thank Dr. A. Oemler for kindly making available to us the KOS/KOSS plates and his PDS and photometry computer programs.

REFERENCES

Baldwin, J. A., Phillips, M. M., and Terlevich, R. J. 1981, Pub. A.S.P., 93, 5.

Beichman, C. A., Neugebauer G., Habing, H. J., Clegg, P. E. and Chester, T. J. 1984, IRAS Explanatory Supplement (National Space Science Center, Greenbelt, MD).

Kirshner, R. P., Oemler, A., and Schechter P. L. 1978, A.J. 83, 1549 (KOS).

Kirshner, R. P., Oemler, A., and Schechter P. L. 1979, A.J. 84, 951.

Kirshner, R. P., Oemler, A., Schechter P. L., and Shectman S. A. 1983, A.J. 88, 1285 (KOSS)

Lawrence, A., Walker D., Rowan-Robinson, M., Leech, K. J., and Penston M. V. 1986, M.N.R.A.S. 219, 687.

Smith, B., Kleinmann, S. and Huchra, J. 1986, this volume.

Soifer, B. T., Sanders, B. D., Neugebauer G., Danielson, G. E., Lonsdale C. J., Madore B. F., and Persson, S. E. 1986, Ap.J. (Letters) 303, L41.

Weedman, D. W., 1986, this volume.

THE RADIO-FAR INFRARED CORRELATION

The Correlation Between Far-IR and Radio Continuum Emission from Spiral Galaxies

John M. Dickey, Robert W. Garwood
University of Minnesota
Department of Astronomy
116 Church St. SE, Minneapolis, MN 55455
and
George Helou
California Institute of Technology
Image Processing and Analysis Center
Pasadena, CA 91125

ABSTRACT

We have observed a sample of 30 galaxies selected for their intense IRAS flux at 60 and 100 μm using the Arecibo telescope at 21 cm to measure the continuum and HI line luminosities. The centimeter-wave continuum correlates very well with the far-infrared flux, with a correlation coefficient as high as that found for other samples, and the same ratio between FIR and radio luminosities. Weaker correlations are seen between the FIR and optical luminosity and between the FIR and radio continuum. There is very little correlation between the FIR and the HI mass deduced from the integral of the 21 cm line. The strength of the radio continuum correlation suggests that there is little contribution to either the radio or FIR from physical processes not affecting both. If they each reflect time integrals of the star formation rate then the time constants must be similar, or the star formation rate must change slowly in these galaxies.

BACKGROUND

In spiral galaxies the 60μm and 100μm luminosity is closely tied to star formation processes, as indicated by its tight correlation with star formation tracers such as Hα emission, CO emission, and radio continuum emission. In this study we concentrate on the correlation with radio continuum among galaxies selected for their intense FIR (far-infrared) emission.

Correlations between FIR and centimeter-wave continuum have been found in many samples of galaxies chosen by many criteria and in diverse environments. Examples are spirals in clusters of galaxies (Helou et al. 1985, Dickey and Salpeter 1984), FIR flux limited samples such as the point source catalog (Gavazzi et al. 1986, Sanders and Mirabel 1985), and radio flux limited catalogs (Condon and Broderick 1986).

The question we address here is whether this correlation extends to the brightest FIR galaxies, and if so whether the radio continuum stays in the same proportion to FIR luminosity. We use the list of galaxies in IRAS circular #6 (1984) supplemented by galaxies from the point source catalog with extremely high FIR luminosity. This sample is essentially FIR flux-limited at 5 Jy, and relatively complete for the Arecibo declination range. We have used the Arecibo telescope to measure the 21cm line and continuum emission from these galaxies, as well as the 18cm OH line emission and absorption. Measured fluxes are tabulated and the spectra are shown and discussed in detail for each galaxy by Garwood et al. (1986); in this presentation we give a brief description of the major results. The most important result is that the same ratio of FIR to radio luminosity holds for these galaxies as for more normal spirals, and that the correlation is as good or better as for other samples.

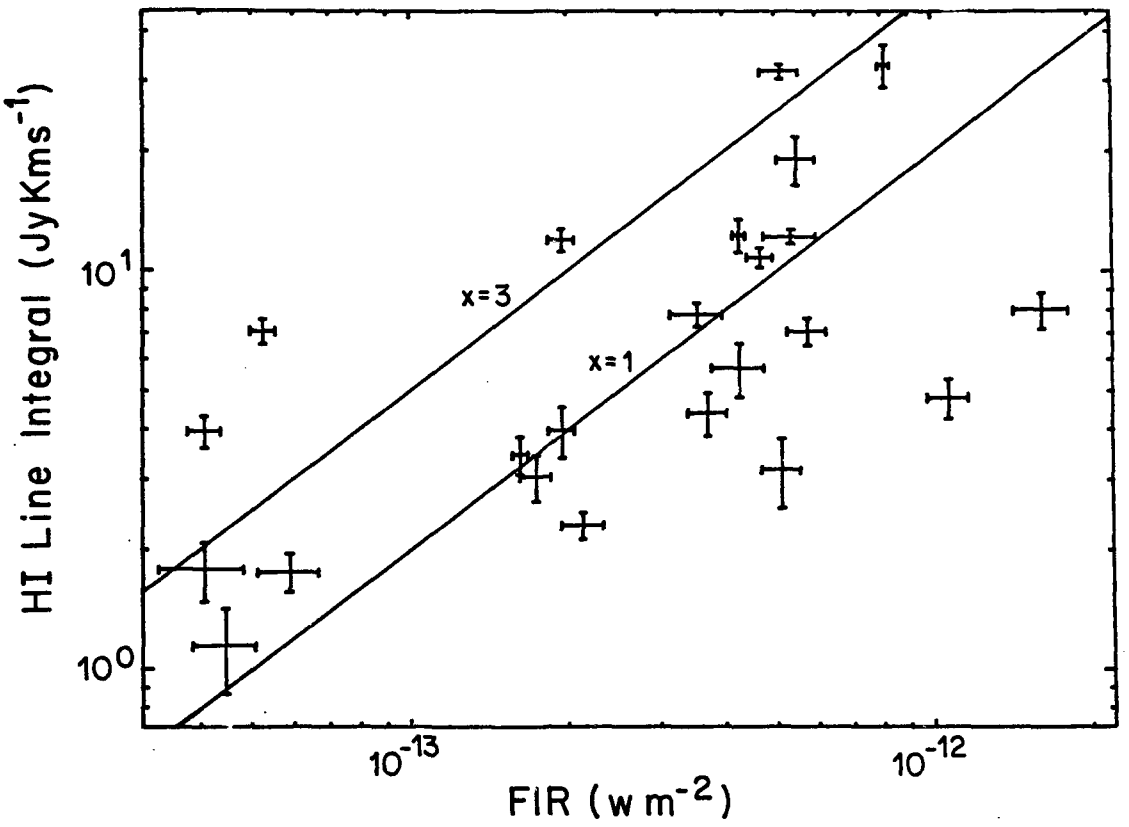

Fig. 2 - The relationship between the HI line integral and the FIR flux.

The main result of this project is to show that active spirals with FIR emission as high as 10^{38} watts may be described as having a higher level of activity of processes similar to those operating in more ordinary spirals with FIR of 10^{36} watts or less. The results imply that the same physical processes link the radio and FIR emission in these most luminous IRAS galaxies as in others. On the other hand, the intensity of the FIR is not simply a result of a larger and brighter system overall. The HI masses of these galaxies are not particularly large compared to ordinary spirals, indicating that these galaxies do not simply have scaled-up disks. As shown in figure 2, there is little correlation between HI mass and FIR luminosity, in contrast to CO emission (Young et al. 1986) which traces the molecular component. As figure 3 shows, the overall blue luminosity of these galaxies is somewhat correlated with their FIR and 21cm continuum emission, but not as well as the latter two are correlated with each other. This is partially due to high and variable extinction, but must also be in part the effect of the longer time scale (several times 10^8 years) associated with the population contributing to the blue luminosity (Bothun 1982).

The high correlation coefficient and the consistency of q in many samples has severe astrophysical implications. The total contribution to the FIR emission from sources unrelated to radio synchrotron emission must be small. Similarly, cosmic ray acceleration mechanisms which are unrelated to the massive star formation rate must be negligible in spiral galaxies. Since the characteristic energy loss lifetime for the cosmic ray particles emitting the radio continuum is 1.5 to 2×10^8 years, this may indicate that variations in the star formation rate do not occur much faster than this (Hummel 1986).

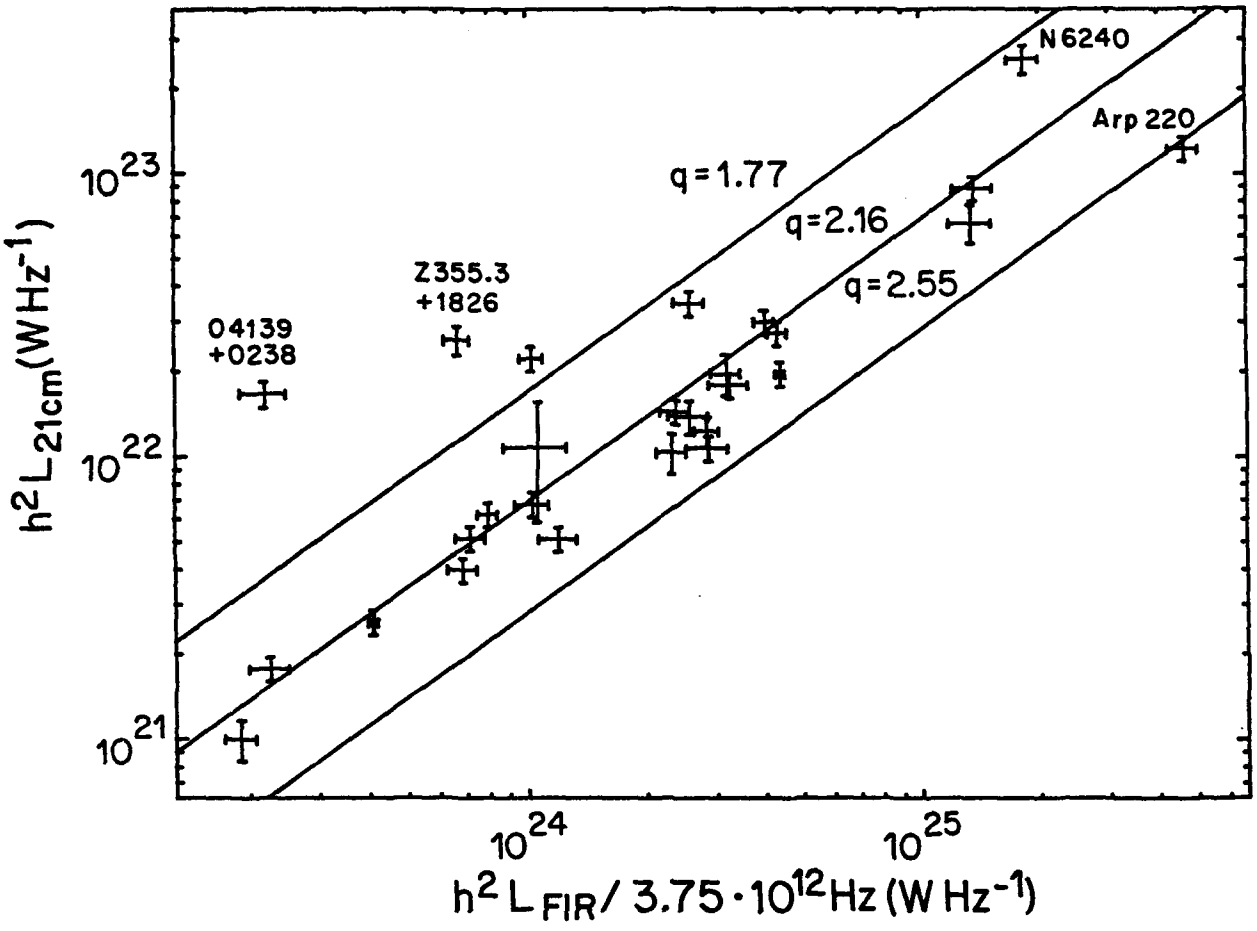

Fig. 1 - The relationship between radio continuum luminosity and FIR luminosity. Three values of q are indicated.

RESULTS

Figure 1 shows the relationship between luminosity at 21cm (watts/Hz) and FIR (watts) defined as an average of the 60μ and 100μ emission weighted by the two bandwidths. The best fit slope is indicated by the line, which corresponds to q = 2.16 where q is the average ratio of FIR to radio flux. The correlation coefficient is 85%, deleting the two galaxies with lowest q's (labelled 04139+0238 and Z355.3+1826) the correlation coefficient increases to 94%. This is as good a correlation as shown by most samples of normal spiral galaxies selected by other criteria.

The q value of 2.16 is similar to that found for many other samples, notably the Virgo cluster galaxies considered by Helou et al. (1985). As discussed by those authors this value is consistent with radio synchrotron emission by high energy electrons generated (indirectly) by the supernovae associated with a high rate of formation of massive stars. The FIR emission in this case is from dust in and around their HII regions. The supernova remnants are not the direct source of the radio continuum (assuming that they obey a normal Σ-d relation, Ulvestad 1982) but only a small fraction of the remnant energy is needed to power the radio emission through a secondary acceleration process such as interstellar shocks.

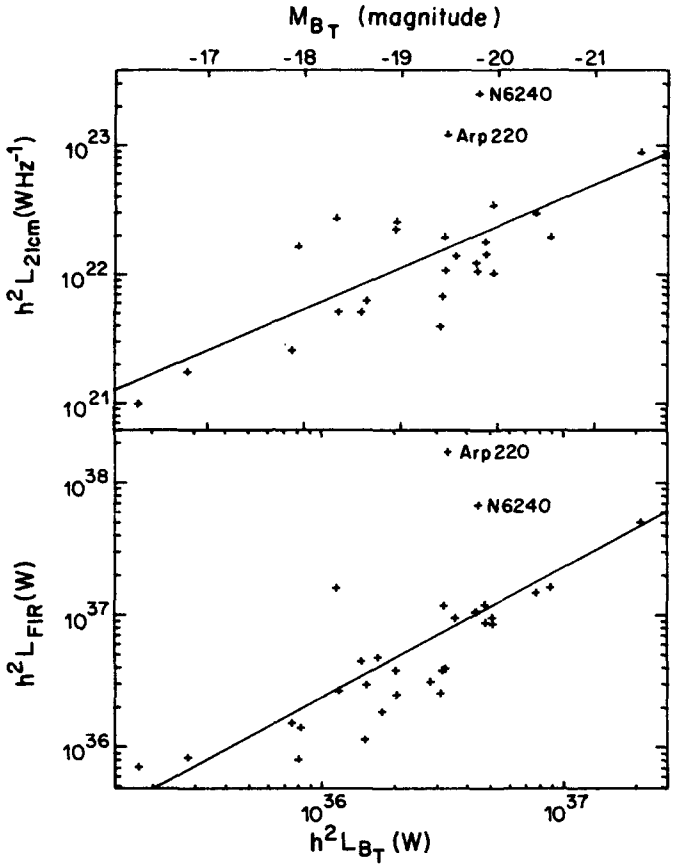

Fig. 3 - The relationships between blue luminosity (lower ordinate scale in watts, upper scale in B magnitudes) and radio continuum and FIR luminosities for galaxies in this sample.

REFERENCES

Bothun, G. D. 1982, Ap. J. Suppl., 50, 39.
Condon, J. J., and Broderick, J. J. 1986, Ap. J., in press.
Dickey, J. M., and Salpeter, E. E. 1984, Ap. J., 284, 461.
Garwood, R. W., Helou, G., and Dickey, J. M. 1986, preprint.
Gavazzi, G., Cocito, A., and Vettolani, G. 1986, Ap. J. (Letters), 305, L15.
Helou, G., Soifer, B. T., and Rowan-Robinson, M. 1985, Ap. J. (Letters), 298, L7.
Hummel, E. 1986, Astr. Ap., 160, L4.
IRAS Circular, No. 6, 1983.
Infrared Astronomical Satellite (IRAS) Catalogs and Atlases: The Point Source Catalog, 1985 (Washington: Government Printing Office).
Sanders, D. B., and Mirabel, I. F. 1985, Ap. J. (Letters), 298, L31.
Ulvestad, J. S. 1982, Ap. J., 259, 96.
Young, J. S., Schloerb, F. P., Kenney, J. D., and Lord, S. D. 1986, Ap. J., 304, 443.

RADIO AND INFRARED OBSERVATIONS OF (ALMOST) ONE HUNDRED NON-SEYFERT MARKARIAN GALAXIES

Linda L. Dressel
Department of Space Physics and Astronomy, Rice University
Houston, TX 77251

ABSTRACT. I have measured the 13 cm flux densities of 96 non-Seyfert Markarian galaxies at Arecibo Observatory. Far infrared flux densities have been published for 78 of these galaxies in the IRAS catalog. I have compared the radio, infrared, and optical fluxes of these galaxies and of a magnitude-limited sample of "normal" galaxies to clarify the nature of the radio emission in Markarian galaxies. I find that Markarian galaxies of a given apparent magnitude and Hubble type generally have radio fluxes several times higher than the fluxes typical of "normal" galaxies of the same magnitude and type. Remarkably, the ratio of radio flux to far infrared flux (i.e., the synchrotron power per stellar ultraviolet thermal power) is nearly the same for most of these "star-burst" galaxies and for normal spiral disks. However, the compact and peculiar Markarian galaxies consistently have about 60% more radio flux per unit infrared flux than the other Markarian galaxies and the normal spirals. It is not clear whether this difference reflects a difference in the evolution of the star-bursts in these galaxies or whether there is excess radio emission of non-stellar origin.

1. INTRODUCTION

Photometric and spectroscopic studies of Markarian galaxies (Markarian et al. 1979 and references therein) have shown that, while some of them harbor Seyfert nuclei or BL Lac objects, the vast majority are unusually blue because of recent massive "bursts" of star formation. Although these galaxies have been found in ultraviolet surveys, they are expected to emit more of their radiation in the infrared, since the star-forming regions show heavy extinction by dust. They should also be unusually bright radio sources for their Hubble type and optical luminosity, due to high supernova rates. The relationships between radio, infrared, and blue luminosity can be used to clarify how radio emission is produced in star-forming regions. Below, I describe radio and infrared data for a large sample of bright nearby non-Seyfert Markarian galaxies, and I use this data to interpret the nature of the radio emission.

2. OBSERVATIONS

I have measured the 13 cm flux densities of 96 non-Seyfert Markarian galaxies brighter than 14.5 pg mag at Arecibo Observatory. Thirty-eight of the galaxies have flux densities above the conservative detection limit of 15 mJy (3σ noise, 5σ confusion). The measured flux densities below 15 mJy are not very accurate individually, but they are still useful statistically. I have compared this Markarian galaxy sample with the complete sample of

Carol J. Lonsdale Persson (Editor)
Star Formation in Galaxies

galaxies brighter than 14.5 pg mag observed with the same system at Arecibo (Dressel and Condon 1978).

I have obtained far infrared fluxes for 78 of the 96 Markarian galaxies from the IRAS point source catalog (Lonsdale et al. 1985). (Five of the galaxies were not observed by IRAS, 11 were observed but not detected, and 2 were obviously confused). I have compared the far infrared flux from 43 to 123 microns ("FIR" in the catalog) to the 13 cm flux density for these galaxies.

3. RESULTS

3.1. Radio-to-Optical Luminosity Ratios

The radio detection rate of the Markarian galaxies brighter than 14.5 mag (40%) is much higher than that of the complete sample of galaxies brighter than 14.5 mag (22%). It is particularly high for Markarian SO galaxies (44%) relative to "normal" SO galaxies (12%). To make a more useful comparison of the physical properties of Markarian galaxies and normal galaxies, I have computed the ratio R of radio luminosity to optical luminosity for the galaxies in both samples. $R = S \text{ dex } [0.4 (m - 12.5)]$ where S is the 13 cm flux density in mJy and m is the corrected photographic magnitude (Dressel 1981).

Distributions of R are shown for Markarian galaxies of several Hubble types (Nilson 1973) in Table I. They are displayed beside R distributions derived for 370 SO galaxies, 820 spiral galaxies, and 225 peculiar galaxies in the normal galaxy survey. To facilitate comparison, each normal galaxy distribution has been normalized to have the same total number of galaxies as the corresponding Markarian galaxy distribution, with Sa, Sb, and Sc distributions being normalized separately within the spiral class. (Nilson's S... class has not been included.) Markarian galaxies show a definite shift away from the low R values found in many normal galaxies. The Markarian SO and peculiar galaxies peak at "intermediate" R values (R ~ 20), with medians several times greater than the normal galaxy medians. The Markarian spiral galaxies peak at R ~ 10, which is twice the median R of normal spirals.

Table I. Numbers of Galaxies in the Markarian Sample and Normalized Numbers of Galaxies in the Complete Sample as a Function of the Ratio R of Radio to Optical Luminosity.

R	SO Galaxies		Spiral Galaxies		Peculiar Galaxies	
	Markarian Sample	Complete Sample	Markarian Sample	Complete Sample	Markarian Sample	Complete Sample
<1.5	2	7.5	2	8.8	2	7.8
1.5- 4.5	0	2.8	9	6.2	2	3.7
4.5-13.5	5	2.9	8	8.0	5	7.7
13.5-40.5	9	1.6	7	3.7	16	8.8
40.5-122	0	0.7	1	0.5	6	3.0
>122	0	0.5	0	0.0	1	1.0

3.2 Radio-to-Infrared Luminosity Ratios

The 13 cm flux densities and far infrared fluxes are strongly correlated for the Markarian galaxies. Nearly all of the 28 galaxies with log FIR(W m^{-2}) $\geq$ -12.7 were above the 15 mJy detection limit of the radio survey. For these 28 galaxies, the mean difference Δ between log S (W m^{-2} Hz^{-1}) and log FIR (W m^{-2}) is -15.07 $\pm$ 0.03, and the dispersion in Δ is 0.18. The correlation persists at lower flux levels, where the radio flux densities have relatively large but random errors (σ = 3.6 mJy). For the 33 galaxies with -13.2 $\leq$ log FIR (W m^{-2}) < -12.7 and with S generally less than 15 mJy, the mean Δ is -15.15 $\pm$ .06 and the dispersion is 0.35. These values of Δ are not significantly different from the mean Δ of the Sc galaxies in the magnitude-limited complete sample, which is just the Δ of "normal" disk emission.

There are enough radio detections of Markarian galaxies in this sample to permit separate examinations of SO, spiral, and peculiar galaxies. Peculiar galaxies are defined here as those described by Nilson (1973) as "... peculiar," "... compact," or merely "...". They are usually only 0.5 to 1.0 arcmin in diameter, while other galaxies brighter than 14.5 mag are usually 1.0 to 2.5 arcmin in diameter. Values of Δ are shown in Table II for the SO, spiral, and peculiar galaxies detected at Arecibo and by IRAS. (Galaxies with obviously confused or low quality IRAS fluxes have been excluded. Only 2 galaxies were detected at Arecibo but not by IRAS.) The median Δ for the SO and spiral galaxies in Table II (excluding the anomalous value for Mar 321) is -15.10 $\pm$ 0.03, and the dispersion is 0.10. The median Δ for the peculiar galaxies is -14.88 $\pm$ 0.02, and the dispersion is 0.07. The peculiar galaxies thus emit roughly 60% more radio emission per unit infrared emission than the SO and spiral galaxies do.

Table II. Values of Δ = log S($Wm^{-2}Hz^{-1}$) - log FIR(Wm^{-2}) for SO, Spiral, and Peculiar Galaxies Detected at Arecibo and by IRAS.

SO Galaxies		Spiral Galaxies		Peculiar Galaxies	
Markarian Number	Δ	Markarian Number	Δ	Markarian Number	Δ
531	-15.21	319	-15.04	325	-14.93
534	-15.04	321	-14.43	363	-14.92
1002	-15.20	323	-15.03	418	-14.80
1088	-15.04	326	-15.12	432	-15.02
1194	-15.14	404	-15.02	479	-14.81
		545	-15.03	518	-14.92
		1183	-15.01	1027	-14.86
		1466	-15.34	1233	-14.88
				1304	-14.80

4. DISCUSSION

Markarian galaxies typically emit several times as much radio luminosity per unit optical luminosity as "normal" galaxies of the same Hubble type. This implies that most of the radio emission in Markarian galaxies is related to the "star-burst" population that produces their characteristically powerful ultraviolet emission. Since most of the ultraviolet emission is absorbed by dust and converted to infrared emission, the ratio of radio flux to infrared flux in these galaxies is a measure of the radio luminosity produced per unit of "star-burst" stellar luminosity. Remarkably, this ratio is similar to that produced by the disks of "normal" Sc galaxies. Star-forming regions thus appear to produce similar amounts of synchrotron power per unit stellar ultraviolet thermal power (roughly, synchrotron power per star recently formed) in a very wide range of physical conditions. This study confirms the conclusions of Helou et al. (1985), who compared a much smaller sample of "star-burst" galaxies to "normal" spiral galaxies.

The significant excess of radio emission per unit infrared emission of the peculiar galaxies, relative to the S0 and spiral galaxies, remains to be explained. It is not due to any power-dependent selection effect: the galaxies of each type span the same range in far infrared power. Nor is it due to resolution of the radio sources in the somewhat larger S0 and spiral galaxies: flux errors due to resolution should be less than 10% in most cases (Dressel and Condon 1978). The infrared fluxes are generally well above the level where systematic errors are known to exist in the IRAS point source catalog. The temperature-sensitive ratio of the fluxes at 60 and 100 microns covers the same range for the peculiar galaxies and the S0 and spiral galaxies. Since many of the peculiar galaxies are "disturbed" in appearance (Nilson 1973), it is possible that tidal interactions are involved in generating "extra" radio sources of non-stellar origin. Alternatively, these compact galaxies may have stronger magnetic fields, or may produce a higher proportion of supernova progenitors in their burst populations.

5. ACKNOWLEDGMENTS

This research was supported in part by a grant from NASA administered by the American Astronomical Society.

6. REFERENCES

Dressel, L. L. 1981, Ap J., 245, 25.
Dressel, L. L. and Condon, J. J. 1978, Ap. J. Suppl., 36, 53.
Helou, G., Soifer, B. T., and Rowan-Robinson, M. 1985, Ap. J., 298, L7.
Lonsdale, C. J., Helou, G., Good, J. C., and Rice, W. 1985, Cataloged Galaxies and Quasars Observed in the IRAS Survey (Pasadena: Jet Propulsion Laboratory).
Markarian, B. E., Lipovetsky, V. A., and Stepanyan, D. A. 1979, Astrofiz., 15, 549; also Astrophysics, 15, 363.
Nilson, P. 1973, Uppsala General Catalogue of Galaxies (Uppsala: Uppsala Astronomical Observatory).

THE RADIO-FAR INFRARED CORRELATION:

SPIRAL AND BLUE COMPACT DWARF GALAXIES OPPOSED

U. Klein
Radioastronomisches Institut der Universität Bonn
F.R.G.

E. Wunderlich
Max-Planck-Institut für Radioastronomie
F.R.G.

Abstract: The recently established correlation between radio continuum and far infrared emission in galaxies has been further investigated by comparing normal spiral and blue compact dwarf galaxies. The puzzling result is that the ratio of radio-to-far infrared luminosity and its dispersion is the same for both samples, although their ratios of blue-to-far infrared luminosity, their radio spectral indices and their dust temperatures exhibit markedly different mean values and dispersions. This suggests that the amount of energy radiated in the two regimes is enhanced in the same way although the mechanisms responsible for the two components are rather different and complex. The fact that the blue light does not increase at the same proportion shows that both the radio and the far infrared emission are connected with the recent star formation history.

1. INTRODUCTION

Soon after the successful IRAS mission, several groups of investigators reported a close correlation between the integrated radio continuum and far infrared (FIR) emission from galaxies, with the radio continuum radiation being predominantly of nonthermal origin (de Jong et al., 1985, Helou et al., 1985, Sanders and Mirabel, 1985). The most straight-forward interpretation was in terms of a close connection between dust heating and cosmic ray production via recent star-forming activity. Hummel (1986), investigating this correlation for a sample of Sbc galaxies, considered this relation as evidence for the validity of energy equipartition between cosmic rays and magnetic fields in Sbc spiral galaxies, with a uniform star formation rate during the past $\sim 10^9$ yrs.

A similar investigation was carried out by Kunth and Sevre (1986) for a sample of blue compact dwarf galaxies (BCDGs), and again drawing the attention to the amazingly tight correlation between radio and FIR emission, holding even for this outstanding class of galaxies.

In order to investigate this intriguing and puzzling correlation further, we have undertaken a comparison of the total radio and FIR emission from normal spiral galaxies (NSGs) and BCDGs.

2. THE SAMPLES AND THE DATA

Radio continuum measurements of BCDGs have been accumulating during the past decade, obtained primarily with single dishes (see the compilation of Klein, 1986). In some cases measurements at two or more frequencies exist so that (more or less accurate) spectral indices can be derived. Recently high-resolution VLA observations have been carried out by several groups of

Carol J. Lonsdale Persson (Editor)
Star Formation in Galaxies

investigators (e.g. Brinks and Klein, 1986, Wynn-Williams and Becklin, 1986, Sramek and Weedman, 1986) which, besides allowing more detailed studies, are indispensable as a check on the confusion problems naturally inherent to the single-dish measurements. Some 40 BCDGs have so far been detected in the radio continuum (mainly at 5 GHz), and for a few of them upper limits have been obtained. For nearly 30 of them spectral indices could be derived, but nearly half of these are still rather unreliable. All of the flux densities incorporated in the present work have been taken from the above-mentioned literature, supplemented by more recent measurements carried out with the Bonn 100-m telescope (Klein, in prep.). FIR flux densities of the BCDGs have been compiled by Kunth and Sevre (1986), in addition the work of Gondhalekar et al. (1986) and of Wynn-Williams and Becklin (1986) provided some more data. Blue optical magnitudes have been adopted from the list of Thuan and Martin (1981). All of the BCDGs for which radio continuum measurements exist have been used for the present analysis. This 'sample selection' may therefore bear the danger of being biased, but selection effects would probably have been more serious if the sample had been chosen using FIR detections.

As a comparison sample to represent what one would call normal spiral galaxies (in the sense that they have seen a uniform history of star formation over at least the past ~ 10^9 yrs) we have chosen that investigated by Gioia et al (1982) for which accurate flux densities over a wide frequency range and therefore reliable spectral indices, are available. The FIR data have been taken from the following sources: for all of the galaxies which are smaller than the detector sizes (i.e. galaxies with angular extents smaller than about 6') the data have been taken from the IRAS Point Source Catalogue (PSC). For those galaxies which have sizes between about 6' and 8' the data have been taken from the Small Scale Structure Catalogue, while galaxies larger than that have been analyzed in the IRAS maps of the HCON1 survey. The blue magnitudes of the NSG sample have been adopted from the list of Gioia and Gregorini (1980).

We have thus complete radio and optical data for the two samples investigated here. FIR data (and spectral indices in case of BCDGs) are available for only about 60% of the galaxies.

3. INTEGRATED RADIO AND FIR PROPERTIES

In Figure 1a-d we present all of the properties relevant to the current analysis for NSGs (upper row) and BCDGs (lower row). Some of the properties have already been derived and discussed previously: it is known that the radio index (ratio of radio-to-optical luminosity) of BCDGs is significantly higher than that of NSGs, and that the average radio spectrum of BCDGs is much flatter than that of NSGs (see Klein et al., 1984). Here we have supplemented the previously existing radio data with the more recent measurements mentioned in Section 2. High-resolution observations with the VLA (see e.g., Brinks and Klein, 1986) at λ20 cm and λ6 cm revealed that some of the single-dish fluxes were confused by nearby unrelated sources. The updated distributions of the radio index at λ6.3 cm, $R_{6.3B}$, and the spectral index, α *, are plotted in Figures 1a and d. Hyphens indicate spectral index uncertainties in excess of 0.2. Figures 1b and c display those histograms which incorporate the FIR data from the PSC. The ratio

* $R_{6.3B} = S_{6.3}\ 10^{x}\ ((m_B-12.5)/2.5) = 0.044\ S_{6.3}/S_B$, where $S_{6.3}$ and S_B are in mJy and $S_\nu \sim \nu^\alpha$

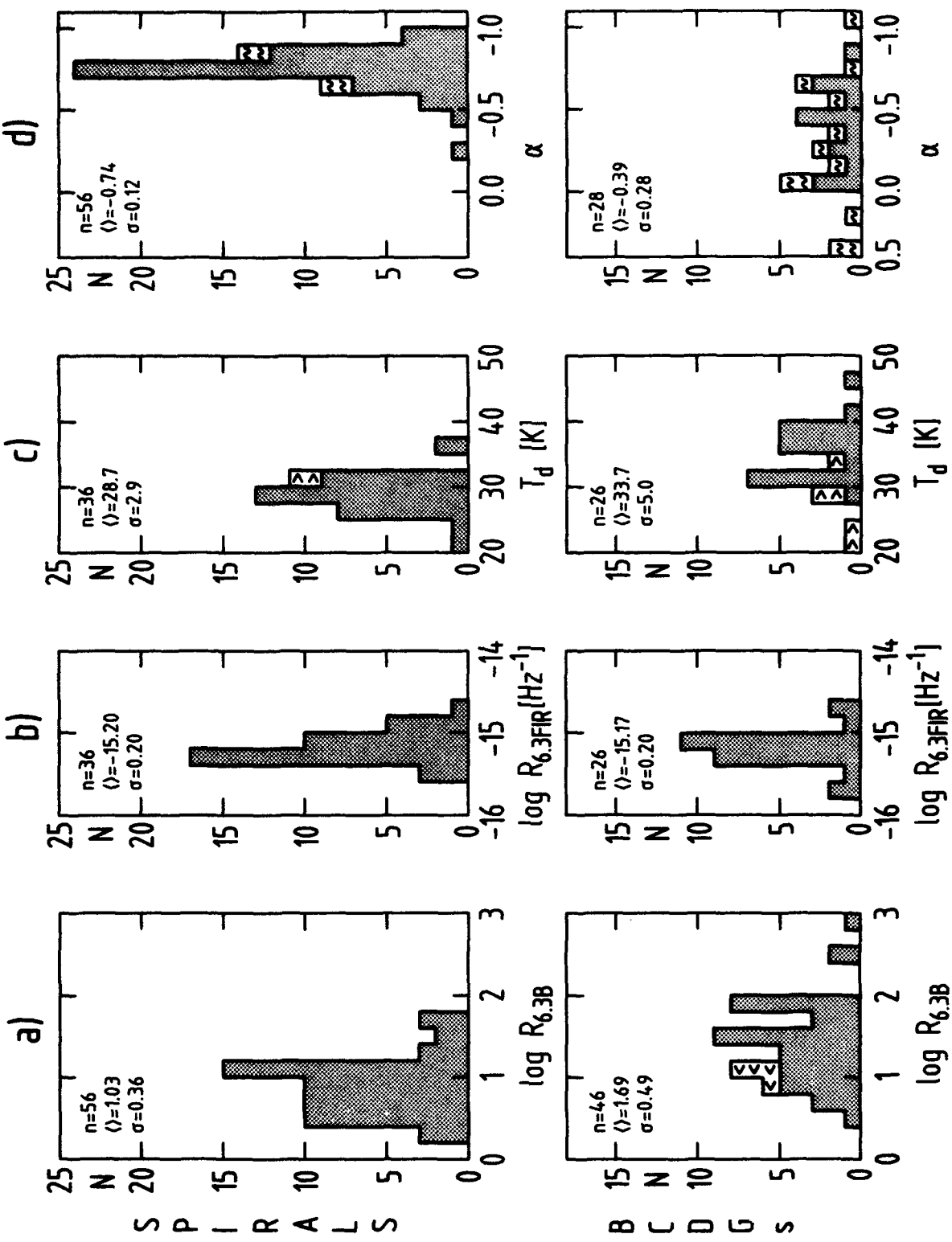
a)
b)
c)
d)
SPIRALS
BCDGs
N
n=56
⟨⟩=1.03
σ=0.36
n=36
⟨⟩=-15.20
σ=0.20
n=36
⟨⟩=28.7
σ=2.9
n=56
⟨⟩=-0.74
σ=0.12
n=46
⟨⟩=1.69
σ=0.49
n=26
⟨⟩=-15.17
σ=0.20
n=26
⟨⟩=33.7
σ=5.0
n=28
⟨⟩=-0.39
σ=0.28
log R6.3B
log R6.3FIR[Hz-1]
Td [K]
α

$R_{6.3FIR}$ of radio-to-FIR luminosity is shown in Figure 1b, the dust temperature in Figure 1c. The latter was derived from the ratio of the 100μ-to-60μ flux densities and by assuming an $F_\nu \sim \nu^{1.5} \cdot B_\nu(T_d)$ dust emission law. The ratio $R_{6.3FIR}$ was derived by computing the FIR luminosity using the 100μ and 60μ flux densities which reflect the bulk of the FIR luminosity and following the procedure of Helou et al. (1985). This ratio is then obtained as

$$\log R_{6.3FIR} = -15.10 + \log S_{6.3} - \log(2.58\, S_{60} + S_{100}),$$

where $S_{6.3}$ is in mJy and S_{60} and S_{100} are in Jy. All of the mean values and standard deviations given in each figure have been obtained by properly weighting the individual data.

Let us first turn to the spectral indices, obtained by applying least-squares fits to the data. As discussed by Gioia et al. (1982) the distribution of α for NSGs is extremely narrow indicating that both the nonthermal spectral indices (α_{nt}) as well as the thermal/nonthermal ratios ($f_{tnt}(\nu)$) do not vary among NSGs. This certainly does not hold for BCDGs for which (in spite of the large uncertainties still inherent to the data) the spectral indices show a large scatter around a mean value, which as stated already by Klein et al. (1984) suggests significantly flatter spectra for these than for NSGs. The strong 'thermal' wing in Figure 1d near $\alpha = 0$ indicates that thermal emission plays a major role in this galaxy type, but the spread of α down to about −0.8 implies that probably all combinations of α_{nt} and $f_{tnt}(\nu)$ may occur, in particular nonthermal spectra which may be <u>flatter</u> than those derived for NSGs.

There is also a pronounced difference between the distributions of dust temperature of NSGs and BCDGs: BCDGs appear to host much warmer dust on average than normal spirals do. The same conclusion had already been reached by Helou (1986) who compared samples of BCDGs and Virgo spirals. Another interpretation would be a lack of the cooler dust component in BCDGs which according to Cox et al. (1986) delivers about 40% of the total luminosity of the dust emission in the Milky Way. This cooler dust component, with a temperature range of $T_c \sim 15$–25 K (note that Cox et al. used an $F_\nu \sim \nu^2 \cdot B_\nu(T_d)$ law), is associated with atomic hydrogen and heated by the general interstellar radiation field (ISRF), while the warm dust component has $T_c \sim 30 - 40$ K and is associated with ionized gas in extended low-density (ELD) HII regions and heated by OB stars. According to Figure 1c this latter component contributes a much larger fraction to the total FIR emission in BCDGs than in NSGs, which once again emphasizes their similarity to HII regions, as was first pointed out by Sargent and Searle (1970). In addition the dust temperatures in BCDGs appear to occupy a wider range than those of NSGs.

What about the radio continuum – FIR relation? Looking at Figure 1b we immediately realize that there is <u>no difference at all</u> between BCDGs and NSGs, <u>neither</u> in the <u>mean values</u> <u>nor</u> in their <u>standard deviations</u>! This is a puzzling result: it means that regardless of what is the predominant mechanism of dust heating (OB stars in ELD HII regions or the ISRF for the diffuse component) and regardless of what is the thermal/nonthermal ratio and the energy spectrum of cosmic ray electrons, the ratio of radio-to-FIR luminosity is universal! Both (thermal and nonthermal) radio as well as thermal emission from dust must therefore be enhanced in the same way as the star formation activity increases. This obviously applies only to the recent star formation history, since otherwise we would expect the blue light to increase by about the same

proportion, which according to Figure 1a it does not.

It is remarkable that IZw18 and IIZw40, the BCDGs with the most extreme properties (they are particulary metal-poor and exhibit very high gas contents, IIZw40 has the highest radio index and the highest dust temperature) are well within the distribution of radio-to-FIR luminosity.

4. CONCLUSIONS:

It is puzzling that the two emission processes ((thermal and nonthermal) radio and FIR) which arise from very different mechanisms apparently follow the same relation and probably increase at the same rate as the star formation rate increases. The predominant dust heating process apparently has no influence on the total amount of FIR emission, and neither has the thermal/nonthermal ratio and the nonthermal radio spectrum on the total amount of radio radiation.

The lack of scatter in the radio-to-FIR ratios of BCDGs suggests that (at least in this galaxy type) the (thermal and nonthermal) radio emission must be connected with the most recent star formation as already stated by de Jong et al. (1985) because the - undoubtedly rapidly varying - star formation history in BCDGs would otherwise have resulted in a variation of this ratio. Hence this ratio is not very suitable for studying variations in recent star formation histories. The situation must be different for NSGs: under normal conditions (i.e., in the absence of tidal interactions, strong bars, etc.) their star formation rates did not vary over the last ~ 10^9 yrs. (Larson and Tinsley, 1978). Therefore the lack of scatter in the radio-to-FIR luminosity ratio of NSGs was to be expected. The larger scatter in the ratio of radio-to-optical luminosity for NSGs can be explained in terms of varying star formation rates before that epoch, since the blue light is about equally shared by stars younger and older than that. Consistent with this, the scatter in the radio-to-optical luminosity ratio of BCDGs is somewhat larger than that of NSGs because in these the relative contribution of young stars to the blue light is much higher than in NSGs so that the scatter of $R_{6.3B}$ partly reflects the violent recent star formation epoch.

We can finally rule out any obvious underabundance of dust in BCDGs as compared to NSGs because we would otherwise expect lower values of $R_{6.3FIR}$ for the former, or at least a wing of lower values. Normal amounts of dust in BCDGs would then contradict the view of them being 'young' galaxies (in the sense that most of them are undergoing their first burst of star formation).

References:

Brinks, E., Klein, U.: 1986, in "Star-forming Dwarf Galaxies and Related Objects". eds. D. Kunth, T.X. Thuan, and T.X. Thuan, and J. Tran Thanh Van. Edition Frontieres, Paris, p. 281

Cox, P., Krugel, E., Mezger, P.G.: 1986, A and A 155, 380

Gioia, I.M., Gregorini, L.: 1980, A and A Suppl. 41, 329

Gioia, I.M., Gregorini, L., Klein, U.: 1982, A and A 116, 164

Gondhalekar, P.M., Morgan, D.H., Dopita, M., Ellis, R.S.: 1986 MNRAS, 219, 505

Helou, G.: 1986, in "Star-forming Dwarf Galaxies and Related Objects", eds. D. Kunth, T.X. Thuan, and J. Tran Thanh Van, Edition Frontiers, Paris, p. 319

Helou, G., Soifer, B.T., Rowan-Robinson, M.: 1985, Ap.J.Lett. 298,L7

Hummel, E.: 1986, A and A 160, L4

de Jong, T., Klein, U., Wielebinski, R., Wunderlich, E.: 1985, A and A 147, L6

Klein, U.: 1986, in "Star-forming Dwarf Galaxies and Related Objects", eds. D. Kunth, T.X. Thuan, and J. Tran Thanh Van, Edition Frontieres, Paris, p. 371

Klein, U., Wielebinski, R., Thuan, T.X.: 1984, A and A 141, 241

Kunth, D., Sevre, F.: 1986, in "Star-forming Dwarf Galaxies and Related Objects".eds. D. Kunth,T.X. Thuan, and J. Tran Thanh Van, Edition Frontieres, Paris, p. 331

Larson, R.B., Tinsley, B.M.: 1978, Ap.J. 219, 46

Sanders, D.B., Mirabel, I.F.: 1985, Ap.J. 298, L31

Sargent, W.L., Searle. L.S.: 1970, Ap.J. 162, L155

Sramek, R., Weedman, D.W.: 1986, Ap.J. 302, 640

Thuan, T.X., Martin, G.E.: 1981, Ap.J. 247, 823

Wynn-Williams, C.G., Becklin, E.E.: 1986, Ap.J. in press

RADIO CONTINUUM, FAR INFRARED AND STAR FORMATION

R. Wielebinski and E. Wunderlich
Max-Planck-Institut für Radioastronomie, Bonn

U. Klein
Radioastronomisches Institut der Universität Bonn

E. Hummel
Max-Planck-Institut für Radioastronomie, Bonn

A very tight correlation has been found between the radio emission and the far infrared emission from galaxies. This has been found for various samples of galaxies (de Jong et al., 1985: Helou et al., 1985) and is explained in terms of recent star formation. The tight correlation would imply that the total radio emission (the sum of thermal and synchrotron emission) is a good tracer of star formation.

In Figure 1 we show the correlation between the radio power at 5 GHz and the far infrared luminosity. The galaxies are of various morphological types and were selected from the various IRAS circulars, hence the sample is an infrared selected sample. Noticeable is that we corrected the far infrared luminosities for the dust temperature. This turned out to be significant because it decreased the dispersion in the correlation.

As can be seen the correlation is very tight over 4 decades! There is strong evidence that the slope of the linear regression changes, in the sense that it is steeper at higher infrared luminosities ($L_{ir} > 5 \times 10^{36}$W). It could also be that the objects of the minisurvey, which preferentially occupy this region of the diagram, have a slight excess of radio emission.

The global correlation between radio power and far infrared emission is also seen in individual galaxies. Figures 2 and 3 show the distributions of the radio emission at 1.4 GHz (Haynes et al., 1986) and of the 100μm emission as observed with IRAS. This shows (as in a number of other galaxies studied in detail) an almost exact coincidence of the two kinds of emission. Note however that most of the radio background sources are not visible at 100μm.

It turned out that the brightest regions in the radio continuum and at 100μm are related to HII regions. There the radio emission is dominated by thermal emission as is indicated by the flat radio spectra. In the far infrared these regions show the highest temperature ($T_\alpha \sim 40^\circ$). The more extended component is dominated by radio emission due to the synchrotron mechanism and by far infrared emission from cooler dust ($T_\alpha \sim 20^\circ$). The heating mechanism for this hot dust and cooler dust is probably different. The hot dust is heated by the radiation from hot, young stars, while the cooler dust can be heated by the interstellar radiation field (Cox et al., 1986). These different heating mechanisms have to be considered when relating the radio continuum emission (in particular the nonthermal component) to star formation.

The separation between the nonthermal component and the thermal component, which is possible locally for individual galaxies, is in principle also possible for the integrated radio emission from galaxies. Assuming a nonthermal spectral

Carol J. Lonsdale Persson (Editor)
Star Formation in Galaxies

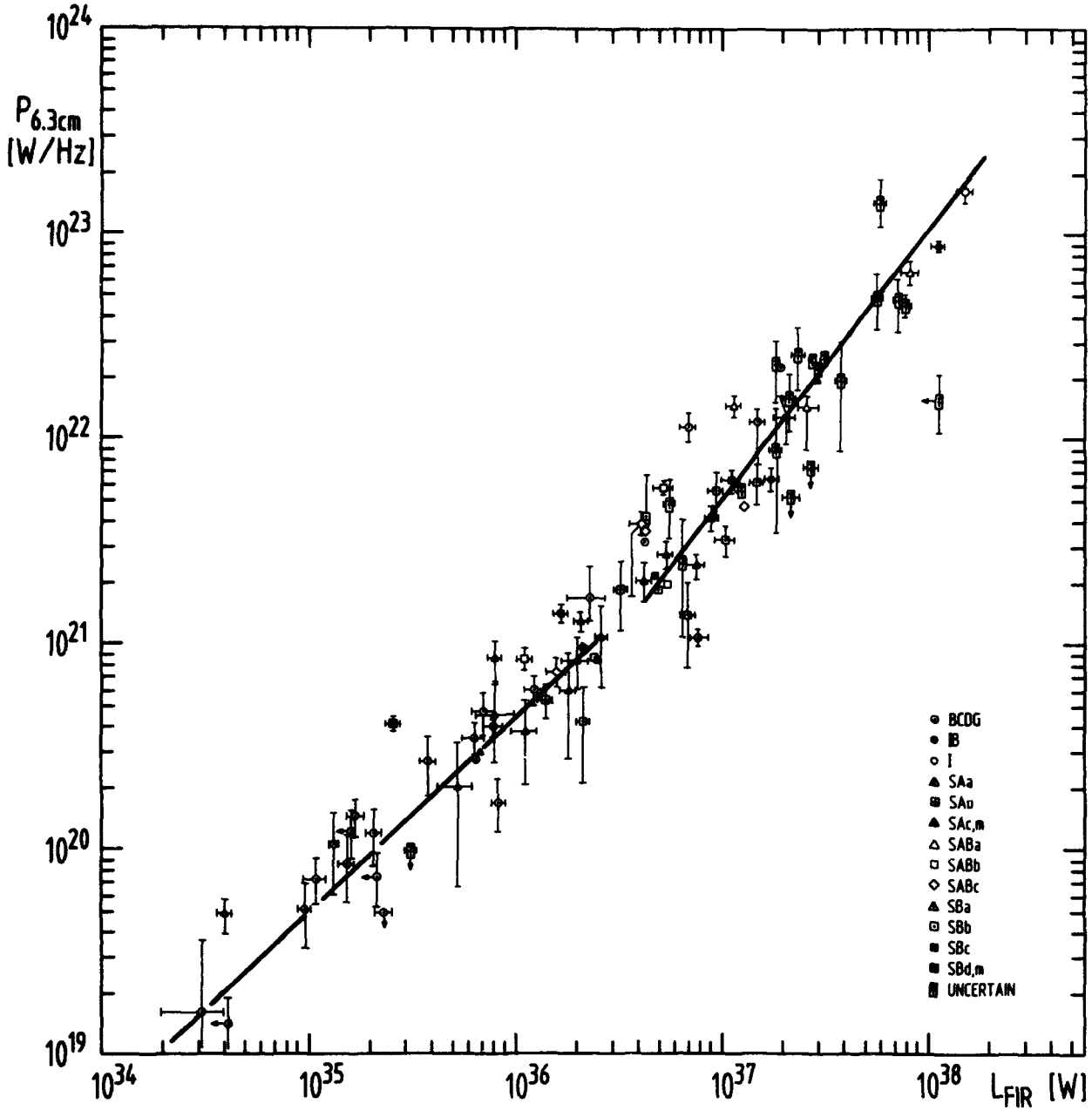
10^{24}
$P_{6.3cm}$ [W/Hz]
10^{23}
10^{22}
10^{21}
10^{20}
10^{19}
10^{34}
10^{35}
10^{36}
10^{37}
10^{38}
L_{FIR} [W]
BCDG
IB
I
SAa
SAb
SAc,m
SABa
SABb
SABc
SBa
SBb
SBc
SBd,m
UNCERTAIN

Figure 1

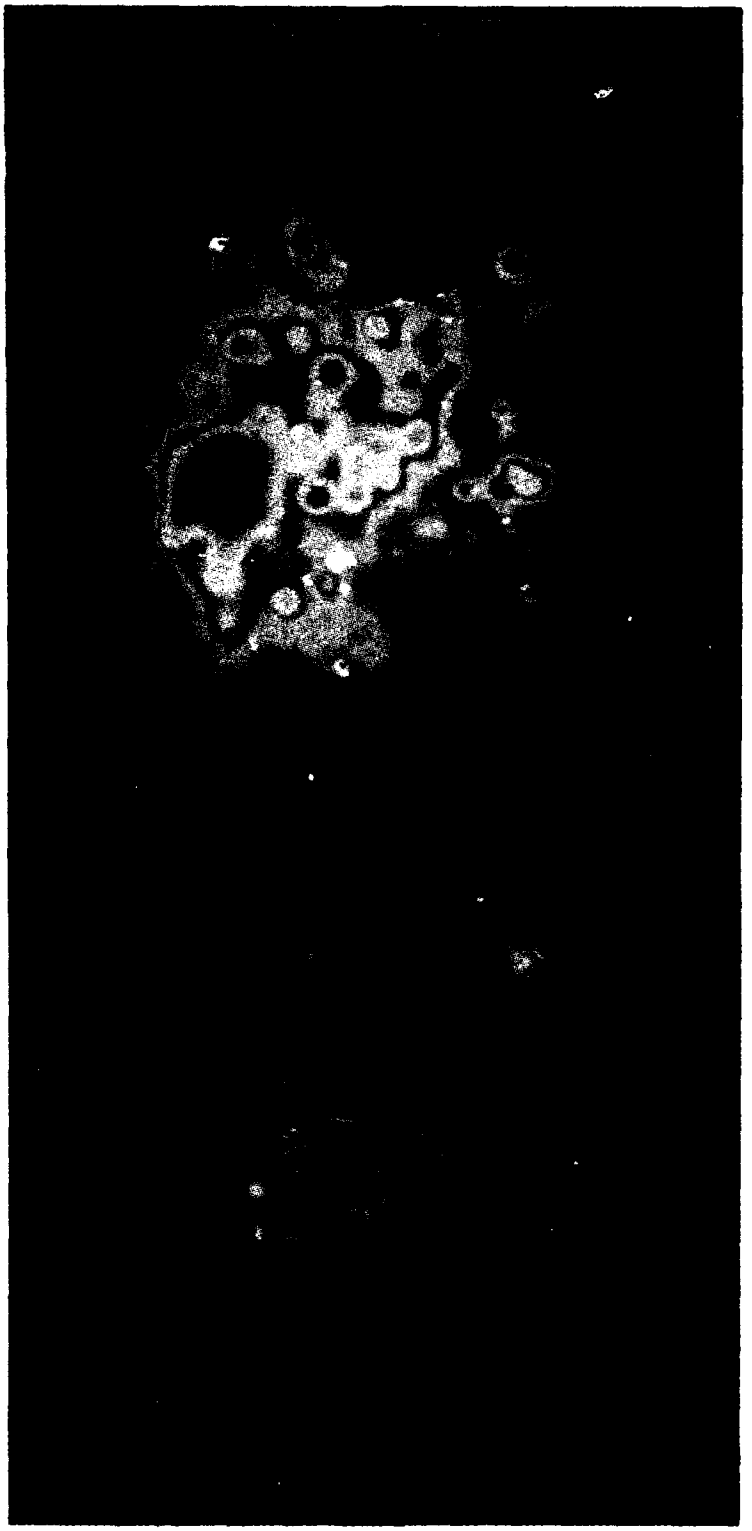

Figure 2

Figure 3

index, the observed spectral index could be a measure of the thermal fraction. As seen before, the thermal fraction is expected to correlate with hot dust. In this simplistic view one would expect a correlation between the observed radio spectral index (α) and the far infrared spectral index ($\log(S_{100\mu m}/S_{60\mu m})$), which is a measure of the dust temperature.

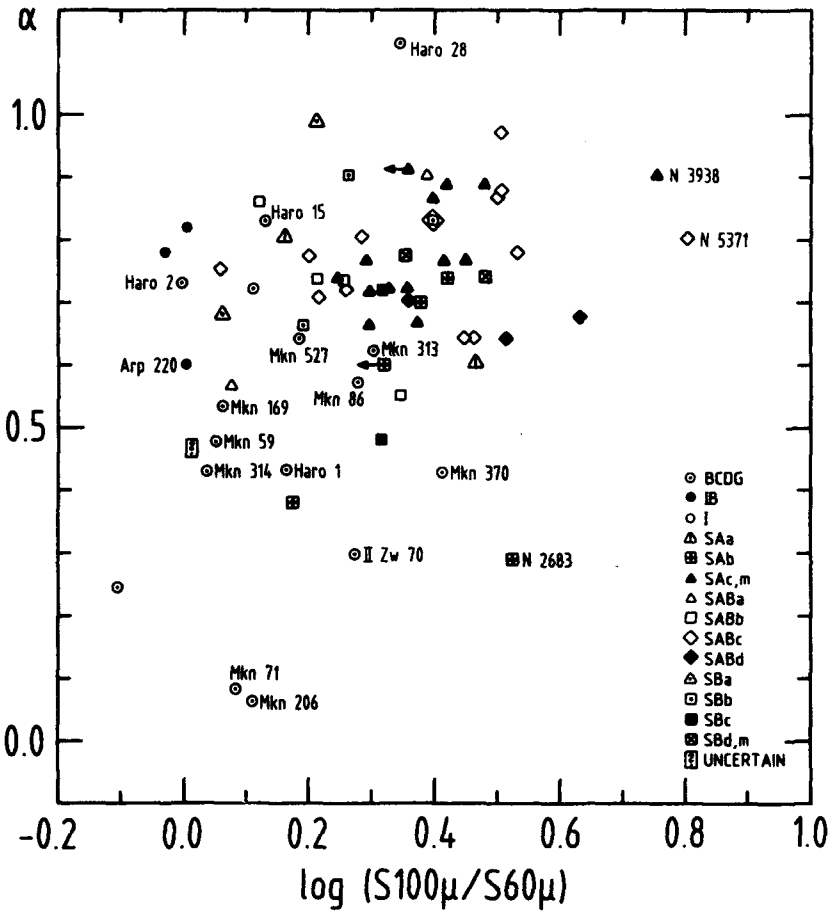

In Figure 4 we show this diagram for the far infrared selected sample. There is no obvious correlation. This can have several causes:

— Up to frequencies of 5 GHz the thermal fraction is in general still not dominating the total radio emission from spiral galaxies.

— The spectral index for the nonthermal component is not known exactly and can in fact, in particular for galaxies in an active star-forming phase, vary from galaxy to galaxy. Note that SNR usually have a relatively flat spectrum ($\alpha \cong 0.5$) compared to the spectra of galaxies. Low frequency ($\nu <$ 1.5 GHz) and high frequency ($\nu >$ 10 GHz) measurements are needed to accurately determine the thermal fraction.

We conclude:

i) The thermal radio component is a good tracer of star formation. It is related to the hot dust component.

ii) The coupling between star formation and the nonthermal component is less direct, perhaps mainly due to the relatively long confinement time of cosmic rays and to diffusion of cosmic rays.

iii) The nonthermal component probably contains information on the star forming history of galaxies over a time scale of ~10^8 yr (see Hummel, 1986: poster by Klein and Wunderlich).

iv) A correlation between the thermal fraction of the radio emission and the dust temperature is expected but not yet visible here because the spectral index is not an accurate enough measure of the thermal fraction.

References:

Cox, P., Krugel, E., Mezger, P.G.: 1986, Astron. Astrophys. 155, 380
de Jong, T., Klein, U., Wielebinski, R., Wunderlich, E.: 1985
Astron. Astrophys. 147, L6
Haynes, R.F., Klein, U., Wielebinski, R., Murray, J.D.: 1986,
Astron. Astrophys. 159, 22
Helou, G., Soifer, B.T., Rowan-Robinson, M.: 1985, Astrophys. J., 298, L7
Hummel, E.: 1986, Astron. Astrophys. 160, L4

THE NATURE OF IR-LUMINOUS GALAXIES

EXTRAGALACTIC OH MEGAMASERS IN STRONG IRAS SOURCES

L.Bottinelli[1,2], M.Dennefeld[3], L.Gouguenheim[1,2]
J.M.Martin[1], G.Paturel[4], A.M. Le Squeren[1]

(1) Observatoire de Meudon 92195 Meudon Cedex, France
(2) Université de Paris Sud 91405 Orsay Cedex, France
(3) Institut d'Astrophysique de Paris 75014 Paris,France
(4) Observatoire de Lyon 69230 Saint-Genis-Laval, France

From our OH and HI survey of the strongest far-infrared (λ= 60 or 100 μm) IRAS sources, we have discovered 3 new powerful OH megamasers in Arp 148, IRAS 1510+0724 and in the uncatalogued IRAS source,IRAS 17208-0014 (Bottinelli et al. 1985b, 1986).

The HI line, the OH 1667 and 1665 MHz main lines and the 21-cm continuum observations have been made with the Nançay radio telescope. The optical spectra and images have been obtained at the European Southern Observatory (Fig.1).

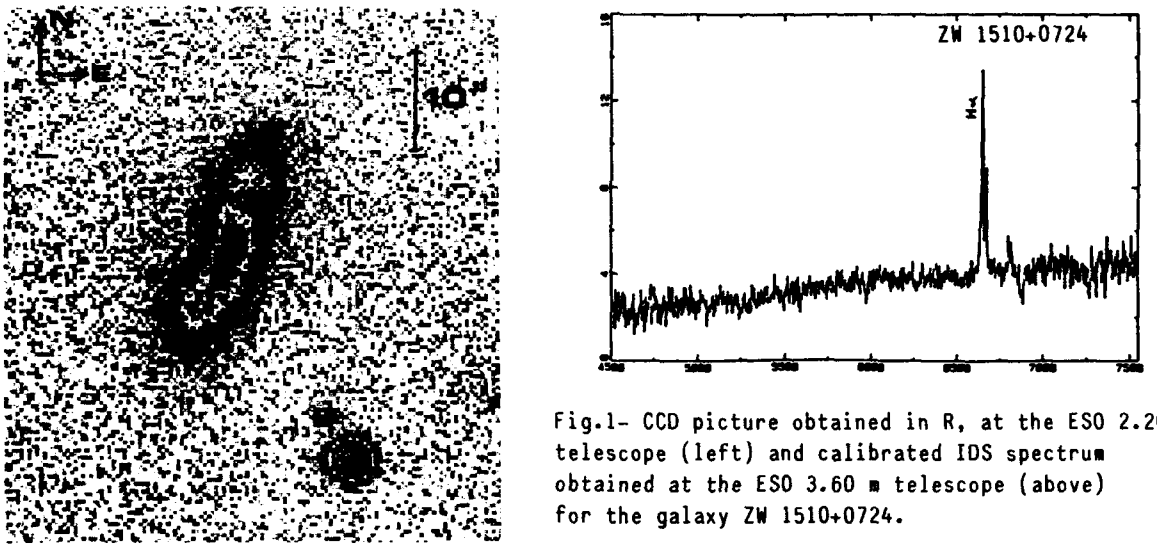

Fig.1- CCD picture obtained in R, at the ESO 2.20m telescope (left) and calibrated IDS spectrum obtained at the ESO 3.60 m telescope (above) for the galaxy ZW 1510+0724.

The spectra are displayed in the following figures (Fig. 2a-d) together with the main IR and OH properties of the 8 megamasers detected up to now, including IC 4553 (Baan et al., 1982), NGC 3690 and Mrk 231 (Baan, 1985), Mrk 273 (Bottinelli et al., 1985a) and III ZW35 (Chapman et al., 1986) (Figure 3).

Particularly striking features are :

1- strong IR luminosity.
2- nearly edge-on optical inclinations.
3- evidences of large optical thicknesses as judged from the 12, 25, 60 and 100 μm flux ratios and optical spectra.
4- correlated IR and OH (1667 MHz) luminosities (Fig.3).
5- evidence of non-circular motions from HI absorption lines. Among all OH mega-

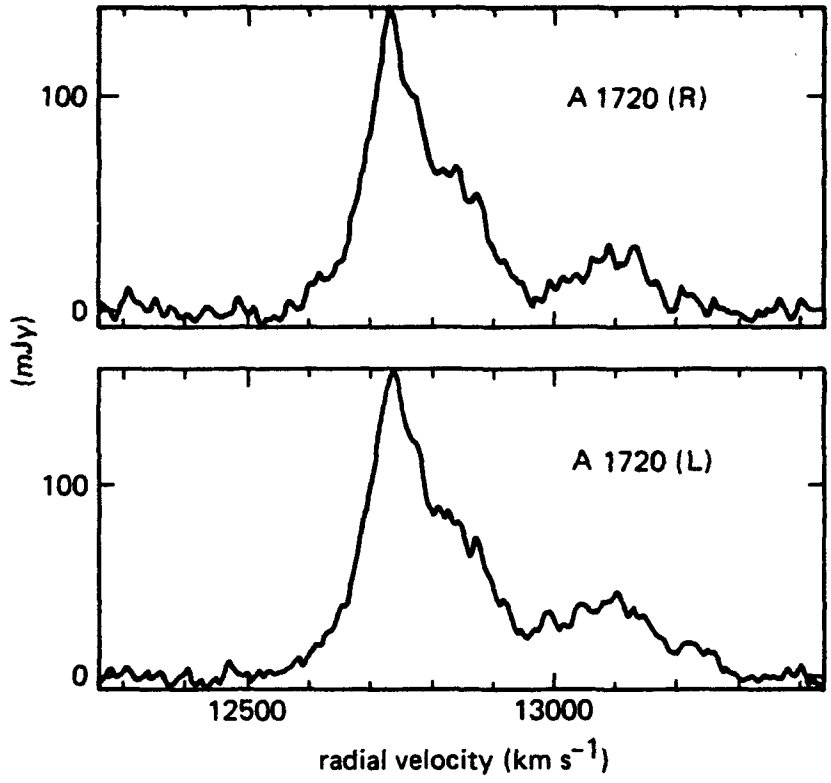

Figure 2a: OH spectrum of A 1720 centered for the rest frequency of the 1667 Mhz transition with a velocity resolution of 4.5 Km s^{-1}. Radial velocities are given in terms of heliocentric optical redshift $c\Delta\lambda / \lambda_o$. The central feature corresponds to the 1667 Mhz transition. The redshifted secondary feature corresponds to the 1665 Mhz transition. Upper part: right circular polarization. Lower part: left circular polarization. There is no evidence of circular polarization larger than about 15%.

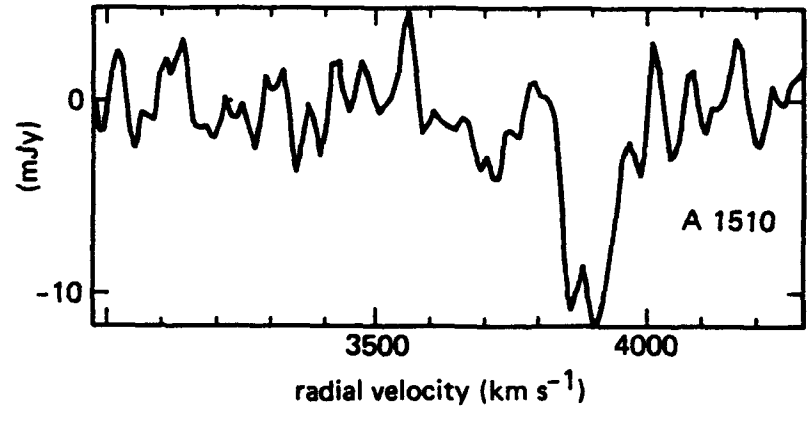

Figure 2b: HI profile of A 1510 with a velocity resolution of 10 Km s^{-1}. Radial velocities are given in terms of the heliocentric optical redshift $c\Delta\lambda / \lambda_o$.

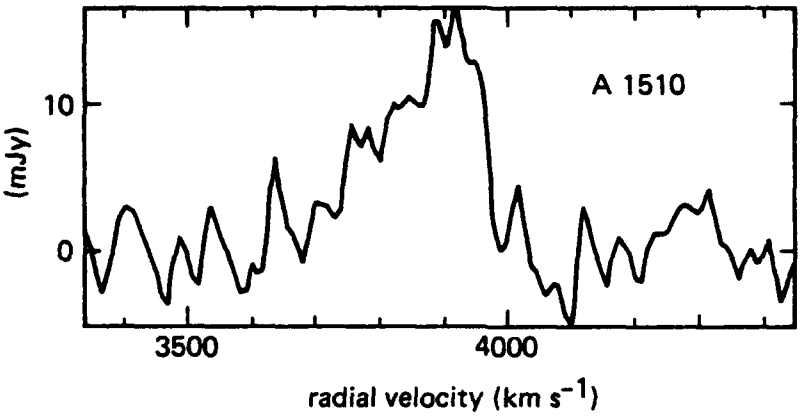

Figure 2c: OH spectrum of A1510 centered for the rest frequency of the 1667 Mhz transition with a velocity resolution of 9 Km s^{-1}. Radial velocities are given in terms of the heliocentric optical redshift $c\Delta\lambda / \lambda_o$. The secondary feature (at about 4300 Km s^{-1}) corresponds to the 1665 Mhz transition.

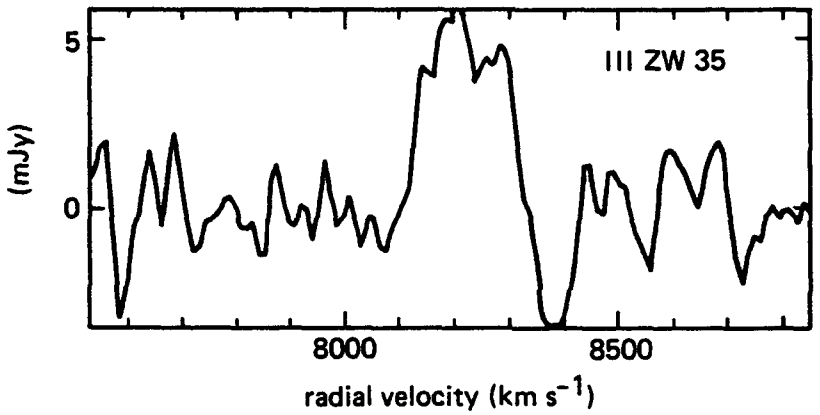

Figure 2d: HI profile of III Zw 35 with a velocity resolution of 10.5 Km s^{-1}. Radial velocities are given in terms of heliocentric optical redshift $c\Delta\lambda / \lambda_o$. (Note the absorption feature at about 8300 Km s^{-1}.)

masers presented in Figure 3, these motions seem to be the largest for the strongest IR emitters, thus suggesting a relation with the stronger star formation activity.

REFERENCES.

Baan, W.A. and Wood, P.A.D. 1982, Ap.J. 260, L49.
Baan, W.A. 1985, Nature 315, 26.
Bottinelli, L., Fraix-Burnet, D., Gouguenheim, L., Kazes, I., Le Squeren, A.M., Patey, I., Rickard, L.J., Turner, B.E. 1985a, Astron. & Astroph. 151, L7.
Bottinelli, L., Gouguenheim, L., Le Squeren, A.M., Dennefeld, M., Paturel, G. 1985b, IAU Circular No. 4106.
Bottinelli, L., Gouguenheim, L., Le Squeren, A.M., Martin, J.M., Dennefeld, M., Paturel, G. 1986, IAU Circular No. 4231.
Chapman, J.M., Cohen, R.J., Pointon, L., Staveley-Smith, L., Unger, S.W. 1986, IAU Circular No. 4180.

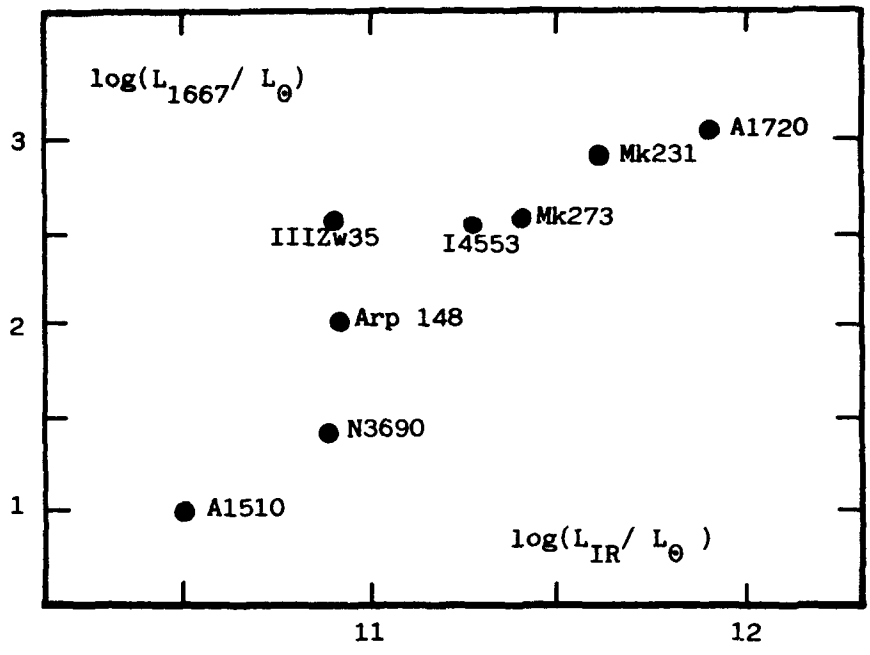

Fig 3 - Isotropic luminosity at 1667 MHz vs. far-infrared luminosity determined from IRAS data,for megamaser galaxies.

Near-Infrared Observations of IRAS Minisurvey Galaxies

David P. Carico, B. T. Soifer, J. H. Elias, K. Matthews, G. Neugebauer
Palomar Observatory, 320-47 Downs Laboratory
California Institute of Technology, Pasadena, CA 91125

C. Beichman, C. J. Persson
Infrared Processing and Analysis Center, 100-22
California Institute of Technology, Pasadena, CA 91125

S. E. Persson
Mount Wilson and Las Campanas Observatories
813 Santa Barbara St., Pasadena, CA 91101

ABSTRACT

Near-infrared photometry at J, H, and K has been obtained for 82 galaxies from the IRAS minisurvey. The near-infrared colors of these galaxies cover a larger range in J-H and H-K than do normal field spiral galaxies, and evidence is presented of a tighter correlation between the near- and far-infrared emission in far-infrared-bright galaxies than exists between the far-infrared and the visible emission. These results suggest the presence of dust in far-infrared-bright galaxies, with hot dust emission contributing to the 2.2 μm emission, and extinction by dust affecting both the near-infrared colors and the visible luminosities. In addition, there is some indication that the infrared emission in many of the minisurvey galaxies is coming from a strong nuclear component.

I. INTRODUCTION

The IRAS minisurvey contained a total of 86 galaxies that were detected at 60 μm with galactic latitude $|b| > 20°$, and that have visible counterparts on the Palomar Observatory Sky Survey (POSS) (see Soifer *et al.*, 1984, as well as Rowan-Robinson *et al.*, 1984 for an explanation of the IRAS minisurvey). As such, the galaxies in that survey represent a complete sample of infrared selected galaxies. Near-infrared observations of the IRAS minisurvey galaxies and the corresponding results are discussed in detail by Carico *et al.* (1986), and are summarized in what follows.

II. OBSERVATIONS AND DATA REDUCTION

The 86 galaxies analyzed by Soifer *et al.* (1984) which comprise the minisurvey sample are listed in *IRAS Circular No. 6* (1984). Of these, 82 were observed at 1.27 μm (J), 1.65 μm (H) and 2.2 μm (K) using the 5 m Hale telescope at Palomar Observatory. A solid nitrogen cooled InSb detector was used for the observations, and for most of the galaxies, a 10" diameter beam was used. Corrections were applied to the observed magnitudes and colors, ranging from 0 to 0.03 mag in J-H and H-K, to account for wavelength dependent distortions in the beam profiles. Statistical uncertainties in the observed colors are believed to be <0.04 mag.

K-corrections (from Neugebauer *et al.*, 1985) and galactic reddening corrections were also applied to the observed magnitudes of 80 galaxies for which redshifts were obtained or were available in the literature. For the galactic reddening corrections, the values of the color excess E_{B-V} were obtained for each galaxy individually by determining the reddening at that location on the reddening maps of Burstein and Heiles (1982), and the values of E_{B-V}/A_V, E_{J-H}/A_V, E_{H-K}/A_V, and A_K/A_V were taken from Cohen *et al.* (1981).

The near-infrared data, as well as the redshifts and the values of E_{B-V} for each galaxy, are tabulated in Carico *et al.* (1986).

III. RESULTS

a) *Near-Infrared Colors*

The near-infrared colors for the minisurvey galaxies, corrected for redshift and galactic reddening, are plotted in Figure 1. There is one galaxy, 04210+0400 (0421+040P06), which is distinct from the rest of the minisurvey sample with a value of 0.87 mag for H-K. This galaxy, which has near-infrared colors appropriate for a Seyfert nucleus, is discussed extensively by Beichman *et al.* (1985). The region in Figure 1 enclosed by a dashed line is the region occupied by the normal spiral galaxies of Aaronson (1977, converted to the CIT photometric system of Frogel *et al.*, 1978). Also included in Figure 1, indicated by the solid lines labeled A through D, are the changes in the near-infrared colors due to the effects of dust within the galaxies.

The near-infrared colors of the minisurvey galaxies differ from the normal galaxies of Aaronson primarily in that they represent a larger range in J-H and H-K than that spanned by the normal galaxy region, resulting in somewhat redder average colors. As is indicated in Figure 1, this can be understood by invoking

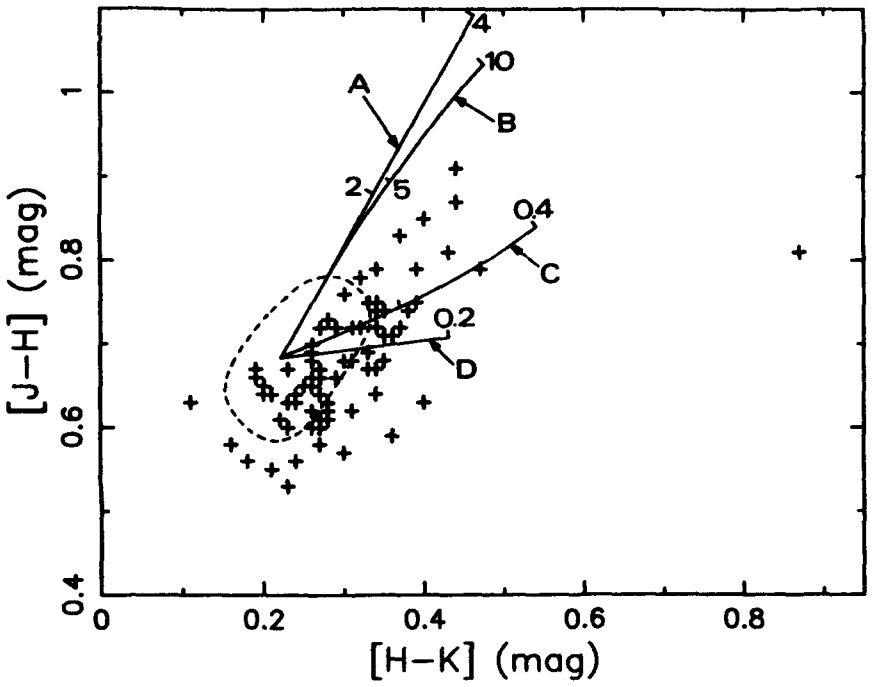

Figure 1 : Near-infrared colors for the IRAS minisurvey galaxies. The region enclosed by a dashed line is that occupied by the normal spiral galaxies of Aaronson (1977). The solid lines A through D are from Aaronson (1977) and represent the effect of dust on the near-infrared colors. Specifically, they are as follows: A corresponds to a reddening screen of purely absorbing dust, drawn as a function of the optical depth at V, τ_V; B to reddening from dust that is uniformly mixed with the emitting source, also drawn as a function of τ_V; C, D to 600 K and 1000 K dust, respectively, with emissivity, ϵ, given by $\epsilon \propto \nu^2$, where ν is the frequency. Lines C and D are labeled according to the fractional contribution to the 2.2 μm emission, assuming zero contribution from dust emission for a normal stellar population. All of the lines A through D are taken from Aaronson (1977).

the presence of dust in the minisurvey galaxies, affecting the near-infrared colors through absorption with visual optical depths up to about 5, for the case of dust uniformly mixed throughout the galaxy, coupled with hot dust emission. It can also be seen from Figure 1 that a large fraction of the minisurvey galaxies would be well fitted by the normal galaxy region were it not for a slight shift, amounting to barely 0.02 mag in both J-H and H-K. Considering the potential sources of systematic uncertainties inherent in the comparison between the two samples, we consider such a small systematic effect with some skepticism.

b) Near and Far-Infrared Luminosity Correlation

The near- and far-infrared luminosities (L_{NIR} and L_{FIR}, respectively) have been calculated using the flux densities given in the *IRAS Point Source Catalog* (1985). The corresponding distributions are plotted in Carico *et al.* (1986), where it is found that the distribution of near-infrared luminosities has a mean of $\log(L_{NIR}/L_{\odot}) = 9.6$ with a dispersion of $\log(L_{NIR}/L_{\odot})$ of $\sigma_{NIR} = 0.5$, and the far-infrared luminosity distribution has a mean of $\log(L_{FIR}/L_{\odot}) = 10.4$ with a dispersion of $\log(L_{FIR}/L_{\odot})$ of $\sigma_{FIR} = 0.5$.

Galaxies detected by IRAS show little correlation between their far-infrared and blue luminosites (Soifer, 1986a). One would like to see whether the far-infrared luminosity is better correlated with the near-infrared luminosity, which is more representative of the total stellar luminosity, and less affected by internal reddening, than is the blue luminosity. Investigation of the ratio of far- to near-infrared luminosities for the minisurvey galaxies indicates that the corresponding distribution has a mean of $\log(L_{FIR}/L_{NIR}) = 0.8$ with a dispersion of $\log(L_{FIR}/L_{NIR})$ of $\sigma_o = 0.2$.

It would be useful to compare the distributions of L_{FIR}/L_{NIR} and L_{FIR}/L_B, where L_B is the blue luminosity, for the minisurvey galaxies. However, these galaxies have not yet been systematically measured at visible wavelengths. Another sample of far-infrared-bright IRAS galaxies does exist for which blue luminosities are available. This sample, the IRAS bright galaxy sample (Soifer *et al.*, 1986b), is similar to that obtained in the minisurvey in that it represents a complete, flux-limited sample of infrared selected galaxies; we assume that these galaxies will have similar properties to those in the minisurvey. The distribution of the ratio of the far-infrared to blue luminosity for the bright galaxy sample has a mean of $\log(L_{FIR}/L_B) = 0.6$ with a dispersion of $\log(L_{FIR}/L_B)$ of $\sigma_{bg} = 0.6$. Taking account of the possible differences between the two samples, the larger dispersion in L_{FIR}/L_B as compared to L_{FIR}/L_{NIR} appears to be statistically significant, indicating that far-infrared- bright galaxies have a tighter correlation between their far- and near-infrared emission than between their far-infrared and blue light. Such a tighter correlation in the far-infrared to 2.2 μm luminosity suggests that extinction by dust is indeed significantly affecting the visible luminosity of far-infrared- bright galaxies.

It has also been found that the dispersion of the distribution of $\log(L_{FIR}/L_{NIR})$ for the minisurvey galaxies increases when an attempt is made to apply beam-size corrections to the near-infrared luminosities. Such an increase in scatter indicates that the beam-size corrections are inappropriate, suggesting that the far-infrared emission in the majority of the minisurvey galaxies may have a strong nuclear component.

CONCLUSIONS

Near-infrared observations of 80 galaxies from the IRAS minisurvey have produced the following results:

1) The near-infrared colors of far-infrared-bright galaxies are similar to those of normal field spiral galaxies, but show a larger range in J-H and H-K, possibly indicating the presence of dust in far-infrared-bright galaxies. For the minisurvey sample, there is evidence for dust absorption of visual optical depths ranging up to about 5, coupled with hot dust emission.

2) The far-infrared emission of far-infrared-bright galaxies appears to be more tightly correlated with the near-infrared emission than with the visible emission. This suggests the possibility of a significant effect from dust absorption on the visible luminosity of these galaxies.

3) There is some indication that a substantial percentage of far-infrared-bright galaxies emit their infrared luminosity primarily from a strong nuclear component.

ACKNOWLEDGEMENTS

The authors extend special thanks to C. G. Wynn-Williams for helpful suggestions on a preliminary version of the manuscript. We also thank E. E. Becklin, J. N. Heasley, G. J. Hill, and C. G. Wynn-Williams of the Institute for Astronomy, University of Hawaii, for generously supplying a number of the redshifts used in this analysis, and Steve Eales, also of the Institute for Astronomy, University of Hawaii, for providing radio positions to clear up several positional ambiguities. The research presented in this paper was supported in part by the National Science Foundation grant AST 83-12699.

REFERENCES

Aaronson, J. 1977, Ph.D. thesis, Harvard University.
Beichman, C., *et al.* 1985, *Ap.J.*, **293**, 148.
Burstein, D., and Heiles, C. 1982, *A.J.*, **87**, 1165.
Carico, *et al.* 1986, in preparation.
Cohen, J. G., Frogel, J. A., Persson, S. E., and Elias, J. H. 1981, *Ap.J.*, **249**, 481.
Frogel, J. A., Persson, S. E., Aaronson, M., and Matthews, K. 1978, *Ap.J.*, **220**, 75.
Glass, I. S. 1981, *M.N.R.A.S.*, **194**, 795.
Infrared Astronomical Satellite (IRAS) Catalogs and Atlases: The Point Source Catalog. 1985, (Washington: US Government Printing Office).
Neugebauer, G., Matthews, K., Soifer, B. T., and Elias, J. H. 1985, *Ap.J.*, **298**, 275.
Oke, J. B., and Gunn, J. E. 1982, *Pub.A.S.P.*, **94**, 586.
Rowan-Robinson, M., *et al.* 1984, *Ap.J.(Letters)* **278** L7.
Soifer, B. T.,*et al.* 1986a, in preparation.
Soifer, B. T.,*et al.* 1986b, *Ap. J. (Letters)*, **303**, L41.
Soifer, B. T., *et al.* 1984, *Ap.J.(Letters)*, **278**, L71.
Zwicky, F., and Herzog, E. 1963-1968, *Catalog of Galaxies and Clusters of Galaxies* , Vol. 2 (1963), Vol. 3 (1966), and Vol. 4 (1968) (Pasadena: California Institute of Technology Press).
Zwicky, F., Herzog, E., and Wild, P. 1961, *Catalog of Galaxies and Clusters of Galaxies* , Vol. 1 (Pasadena: California Institute of Technology Press).
Zwicky, F., Karpowicz, M., and Kowal, C. T. 1965. *Catalog of Galaxies and Clusters of Galaxies* , Vol. 5 (Pasadena: California Institute of Technology Press).
Zwicky, F., and Kowal, C. T. 1968, *Catalog of Galaxies and Clusters of Galaxies* , Vol. 6 (Pasadena: California Institute of Technology Press).

GROUND-BASED FOLLOW UP OF IRAS GALAXIES

M. DENNEFELD* - H. KAROJI
Institut d'Astrophysique, Paris

P. BOUCHET
ESO, Chile

L. BOTTINELLI - L. GOUGUENHEIM
Observatoire de Meudon, France

We have undertaken optical, near-infrared, radio-continuum and HI observations of the galaxies identified with IRAS sources in a few fields roughly of the size of a sky survey plate. We present here results from two fields at galactic latitude $+27^{\circ}$ and $+43^{\circ}$ over a total area of 100 square degrees (see also Dennefeld et al. 1986).These regions contained 115 IRAS point sources, out of which 26 were identified with stars and 81 with faint galaxies, 10 of which were difficult to recognize on the Schmidt plates. A further 8 sources could not be identified with any object down to the limit of the Palomar or ESO Sky Survey Plates. As judged from the Cirrus Flags, at most 3 could be spurious sources. The surface density of galaxies lies between 0.6 and 0.9 galaxies per square degree, in accordance with other determinations (Helou, 1986). Our value is however of little statistical significance, especially because the field at $b = +27^{\circ}$ seems to contain a group of faint galaxies.

Spectroscopy was obtained with the ESO telescopes at a resolution of about 10Å. The vast majority of galaxies have low excitation spectra dominated by low-ionization lines. These spectra are typical of HII-region type galaxies, however of much lower excitation (typically $[OIII]/H\beta < 1$) than other starburst galaxies such as those described by Balzano 1983). Similar results have been found independently by Allen, Roche and Norris (1985) and Elston, Cornell and Lebofsky (1985). We stress here the importance of the reddening as determined from the $H\alpha/H\beta$ ratio: the visual absorption A_V ranges from 2 to 6 magnitudes and as a consequence the corrected L_{IR}/L_B ratios are considerably reduced if those reddenings apply to the whole galaxy. Indeed J-H, H-K colours can be reconcilied with those of "normal" galaxies when such reddening corrections are applied. In some cases, a substantial K-L excess remains, indicating a dust contribution even at short wavelengths. The strong Na absorption line seen in some spectra is also partly attributed to dust, in absence of any other late-type stellar feature.

Velocities up to 60000 km/s, resulting in large infrared luminosities, have been found. Several objects have L_{IR} of a few 10^{12} solar luminosities, similar to the ones of Arp 220 or NGC 6240, which are thus not exceptional anymore. If our numbers are representative, more than a thousand of such objects should exist all over the sky. Star formation activity is believed to be the source for this enormous IR emission. Evidence for this comes from the correlation between IR and Hα luminosities (Dennefeld et al. 1986) or from the strong Balmer absorption lines seen in the spectra. Radio-continuum observations of these extreme objects (Karoji et al. 1986) show that the star-formation activity is located in

---

* Visiting Astronomer, European Southern Observatory, Chile.

Carol J. Lonsdale Persson (Editor)
Star Formation in Galaxies

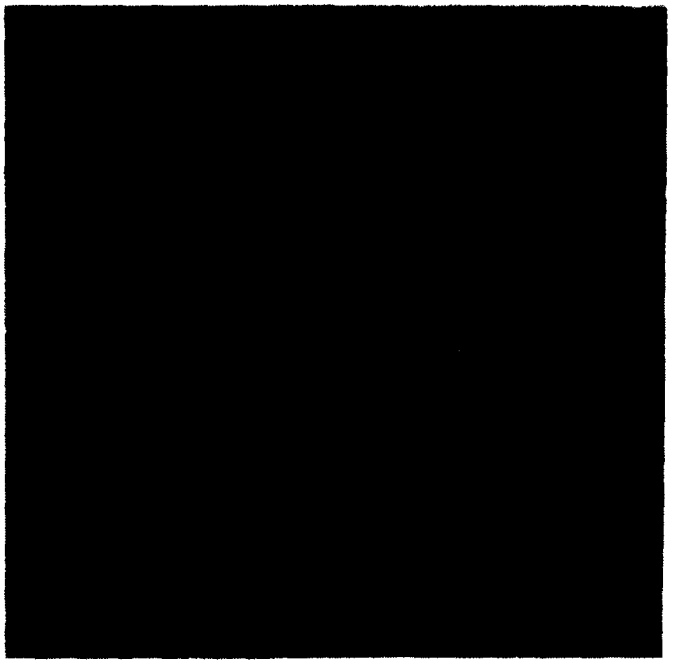

Figure 1a - A CCD picture in r (Gunn) of A 09111-1007 obtained at ESO. The eastern galaxy with two companions is not the IRAS source.

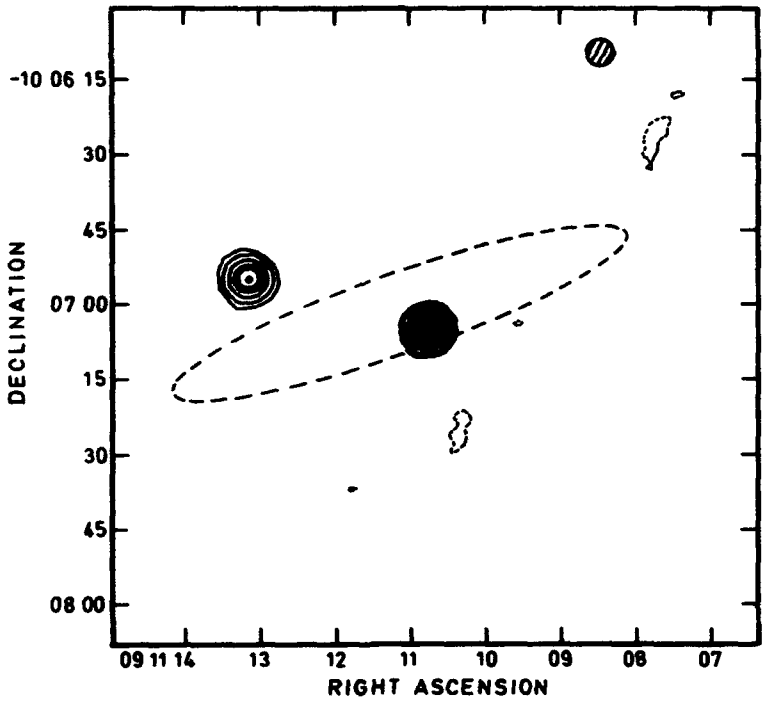

Figure 1b - A VLA map of A 09111-1007 at 20 cm. Peak brightness is 22 mJy/beam. This figure is taken from Karoji et al. (1986).

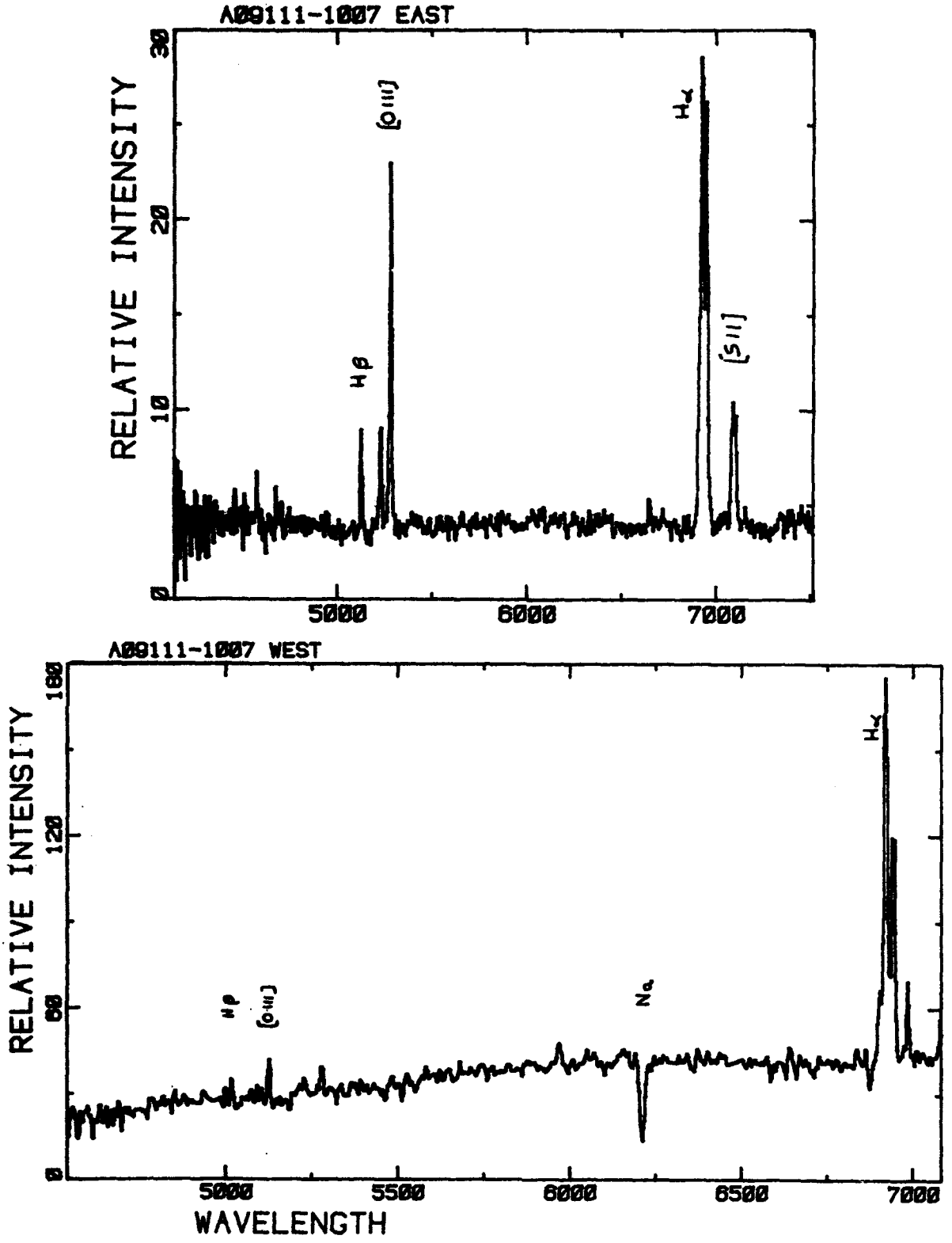

Figure 1c - Spectra obtained at ESO for the two galaxies seen in fig. 1a. The high-excitation eastern galaxy (Sey2) is not an IRAS source. The western one has a typical spectrum of IRAS galaxies with low excitation, high reddening and interstellar absorption lines

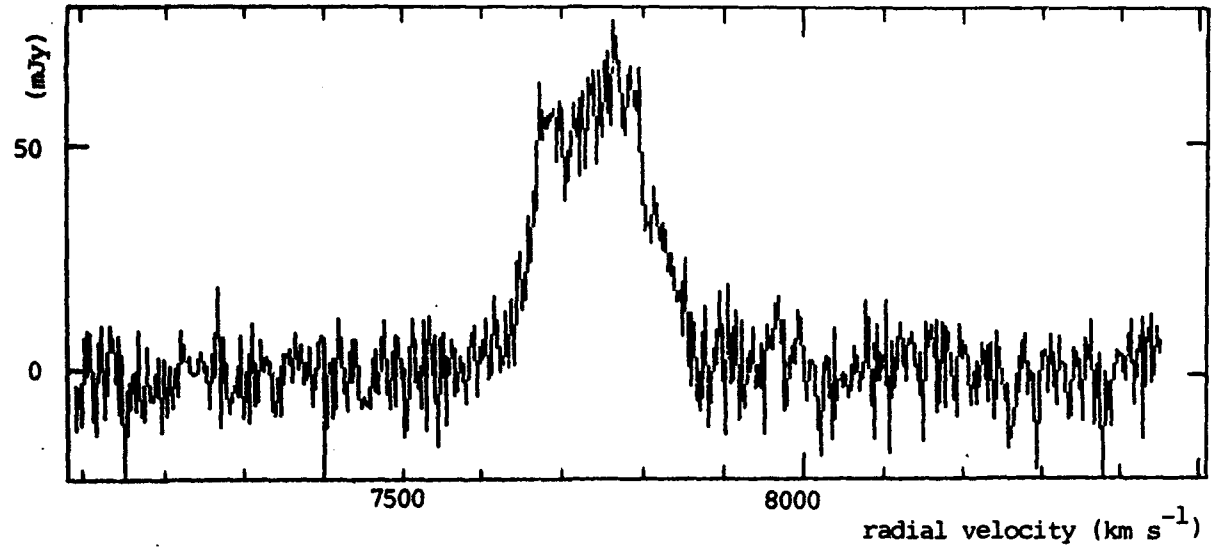

HI LINE PROFILE WITH A VELOCITY RESOLUTION OF 2.6 KM S^{-1}. RADIAL VELOCITIES ARE GIVEN IN TERMS OF HELIOCENTRIC OPTICAL REDSHIFT $C\Delta\lambda/\lambda_o$.

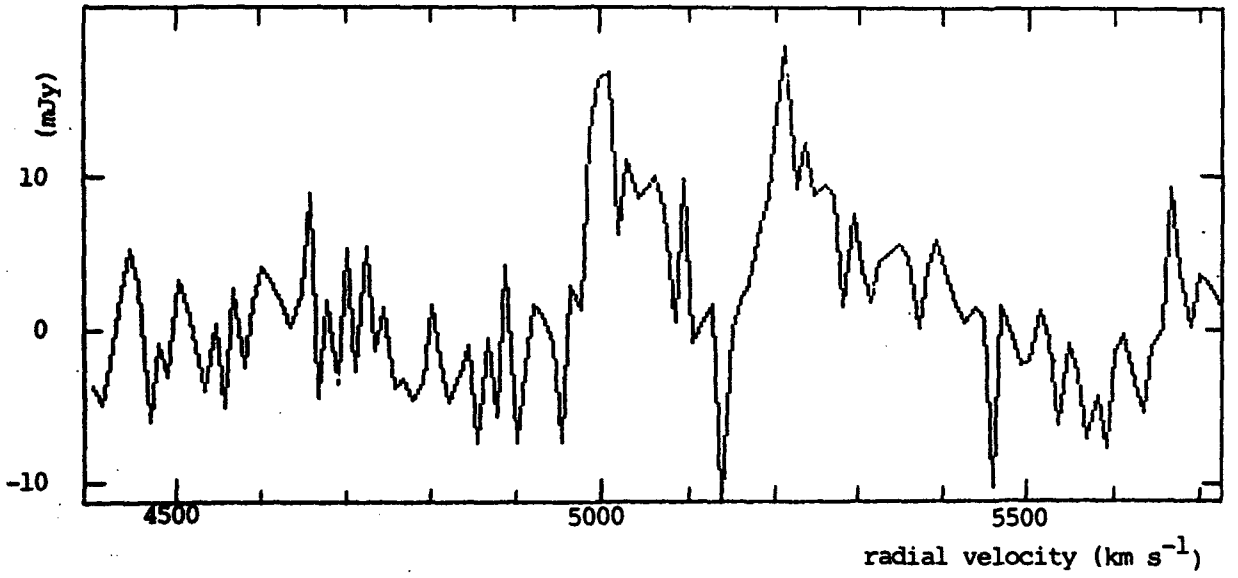

HI LINE PROFILE WITH A VELOCITY RESOLUTION OF 10.6 KM S^{-1}. RADIAL VELOCITIES ARE GIVEN IN TERMS OF HELIOCENTRIC OPTICAL REDSHIFT $C\Delta\lambda/\lambda_o$.
NOTE THE ABSORPTION FEATURE AT ABOUT 5140 KM S^{-1}.

Figure 2 - HI profiles of IRAS galaxies obtained at Nançay
Upper image is A12488-2051, lower one is A09234-1146

the central regions (unresolved at 6 kpc diameter for our far-outlying galaxies) and that the radio/IR flux density ratio is typical of star-burst activity rather than Seyfert 1 Indeed, very few Seyfert galaxies or Liners have been found in our survey (see fig.1 for an illustration). It has been suggested that interactions between galaxies are more frequent within IRAS galaxies than elsewhere (Lonsdale et al. 1984) and that this could represent the triggering mechanism for star formation. About 25% of our galaxies have neighbours within 2' but we still need more analysis (velocities and imaging) to distinguish interactions from simple clustering. At least the fuel for star formation is available: about half the objects have been detected in HI and have hydrogen masses in the range 10^9-10^{10} $M_\odot$. Large central column densities are sometimes present (see fig.2) as expected for these highly reddened objects. But it should be stressed that high star formation rates are required (larger than 100 $M_\odot$ per year) to explain the large IR luminosities unless truncated mass functions are assumed (see the accompanying paper by Belfort, Mochkovitch and Dennefeld, this volume).

It seems therefore that the overall characteristics of faint IRAS galaxies are now well established from the spectral point of view. Enough so to distinguish from spectra alone an IRAS candidate from another (see fig.1) One particularity is the high reddening which no doubt explains why these fairly numerous objects with strong Hα emission line were not discovered in the objective prism surveys mostly conducted in the blue !

REFERENCES

Allen, D.A., Roche, P.F. and Norris, R.P. 1985, M.N.R.A.S. 213, 67P.
Balzano, V.A. 1983, Ap.J 268, 602.
Belfort, P., Mochkovitch, R. and Dennefeld, M. 1986, this volume.
Dennefeld, M., Karoji, H. and Belfort, P. 1986 in "Star forming dwarf galaxies", D. Kunth, T.X. Thuan and J. Tran Thanh Van, editors, Editions Frontières, France, p.351.
Elston, R., Cornell, M.E. and Lebofsky, M.J. 1985, Ap.J. 296, 106.
Helou, G. 1986 in "Light on dark matter", F. Israël editor, 405.
Karoji, H., Dennefeld, M. and Ukita, N. 1986, Astron. Astrophys. 155, L3.
Lonsdale, C.J., Persson, S.E. and Matthews, K. 1984, Ap.J. 287, 95.

NUCLEAR INFRARED EMISSION AND THE COLORS OF IRAS GALAXIES

Gary J. Hill[1]
University of Hawaii, Institute for Astronomy
Honolulu, Hawaii 96822

ABSTRACT. J, H, K, L', and N observations of galaxies detected at 12 μm by IRAS are combined with IRAS flux densities to investigate the relationship between the infrared sizes and colors of galaxian infrared sources. It is found that typical IRAS galaxies have 10 μm radii of 0.5-2.0 kpc, while active galaxies and galaxies with higher 25-60 μm color temperatures are smaller. One unusual object, 23060+0505, is at high redshift and has an infrared luminosity of 1.5×10^{12} $L_\odot$. Its 1-100 μm energy distribution resembles that of a Seyfert 1 galaxy, but it shows very little sign of broad-line emission in the visible. Its properties suggest that it may be a prototype for a class of highly obscured active galaxy.

1. INTRODUCTION

As part of an IRAS follow-up program, the group at the University of Hawaii has been systematically obtaining redshifts, CCD imagery, and infrared photometry of a sample of IRAS point sources identified with galaxies. This paper presents some preliminary results from this large data base. In particular, a number of detections at N (10.1 μm) allow us to investigate the 10 μm size of many galaxies for comparison with other properties.

Three samples are considered. Galaxies in the first sample are drawn mainly from the preliminary P04 and P06 IRAS lists and constitute what we believe to be a "representative" sample of IRAS galaxies. Those in the second sample are from lists P11 and P16 and have "hot" ($S_{25\mu m}/S_{60\mu m} > 0.3$) far-infrared energy distributions (some of these sources are from de Grijp et al. 1985). The third sample comprises those X-ray-selected active galactic nuclei (AGN) in the sample of McAlary et al. (1983) that have both published ground-based small-aperture N observations and IRAS detections at 12 μm.

2. OBSERVATIONS

Details of the observations will be reported elsewhere. The redshifts were obtained at the University of Hawaii 2.2 m telescope on Mauna Kea using a grism spectrograph or the Faint Object Spectrograph. The spectrographs and the Galileo/Institute for Astronomy 500 x 500 TI CCD were mounted at the Cassegrain focus, giving resolutions from 8 to 16 Å.

---

[1]Visiting Astronomer, Infrared Telescope Facility, which is operated by the University of Hawaii, under contract with the National Aeronautics and Space Administration.

Carol J. Lonsdale Persson (Editor)
Star Formation in Galaxies

J, H, K, L', and N photometry was obtained at the NASA Infrared Telescope Facility (IRTF) on Mauna Kea. Often the identification of the IRAS source was made or confirmed by the presence of strong infrared emission detected at the IRTF. These data were combined with flux densities either from the IRAS Point Source Catalog (IRAS Explanatory Supplement), or for fainter sources, from coadded IRAS scans processed at IPAC.

3. 10 μm SOURCE SIZE

The sizes of the 10 μm sources in these galaxies are characterized by a "compactness" parameter. This is the ratio of the small-beam, ground-based 10 μm flux density to that measured by IRAS at 12 μm and color corrected to 10 μm. The color correction is obtained simply by extrapolating the 25/12 μm flux density ratio down to 10 μm. Since this procedure could have systematic biases for individual sources, two standard corrections, a factor of 0.71 for the steeper "representative" IRAS galaxy sample and 0.76 for the "AGN" and "hot" IRAS galaxies, were adopted. These are based on the averages of the individual galaxy corrections within each group.

Figure 1 shows the compactness as a function of distance (H_o = 75 km s^{-1} Mpc^{-1} assumed throughout). Also plotted is a simple-minded model in which the surface brightness of the infrared emission drops off exponentially with radius, with a characteristic scale length of r_o. A comparison with the observations can be made by synthesizing the compactness parameter for a series of characteristic sizes over the range of distances observed here.

It is evident that there is a separation between the "representative" IRAS galaxies and the AGN, with those IRAS galaxies having "hotter" far-infrared energy distributions falling among the AGN. The characteristic size of the "representative" IRAS galaxies is between r_o = 0.5 and 2 kpc, while the AGN and "hot" IRAS galaxies are generally <0.5 kpc. The smaller size of these sources can be understood as a greater domination of the 10 μm emission by a point nuclear source, as would be expected in the presence of an active nucleus. This interpretation is confirmed for the "hot" objects by visible spectra that show line ratios characteristic of nuclear activity (see also de Grijp et al. 1985).

3.1. Source Compactness and Color

We can also investigate the effect of size on the J, H, K, and L colors of galaxies. The galaxies are divided into two groups--those smaller than and those larger than 0.5 kpc. The J-L color characterizes the shape of the near-infrared continuum, and the 25/60 μm flux density ratio, the far-infrared. Figure 2 shows that the smaller sources have larger values of J-L (proportionately more energy output at L) and, as would be expected from Figure 1, larger 25/60 μm flux density ratios (i.e., they are hotter). The probability of these correlations arising by chance are 0.025 and <<0.001, respectively. It is thus very likely that there is an additional mid-IR (3-30 μm) continuum component in the galaxies with smaller characteristic infrared size, and this component is associated with the nuclear emission in these objects.

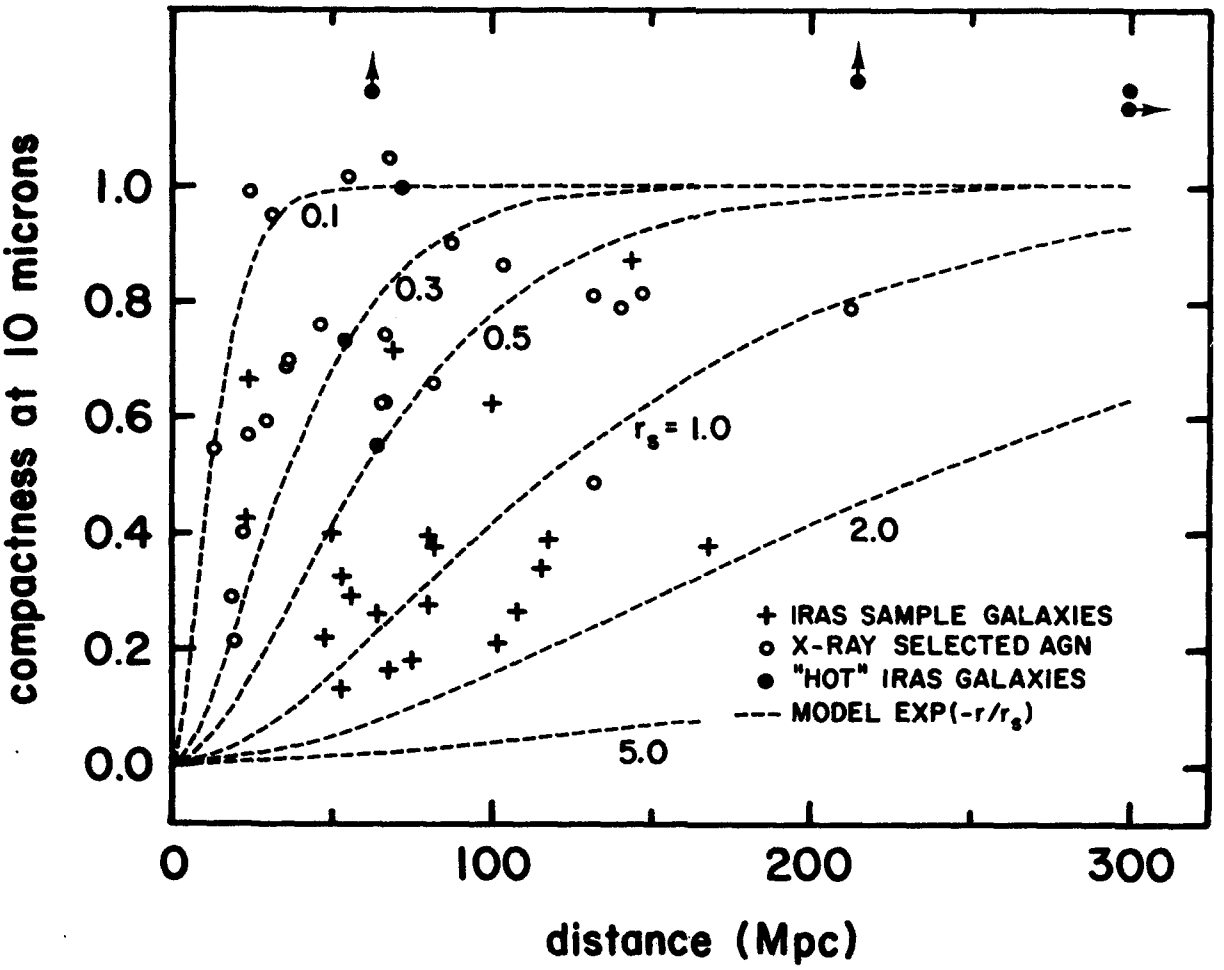

Figure 1. The 10 μm "compactness" (see text) of IRAS sources plotted against their distance in megaparsecs. The dashed lines represent a model in which the surface brightness drops as $\exp(-r/r_o)$ for a series of characteristic radii r_o in kpc. Data for the main sample of "representative" and "hot" IRAS galaxies were obtained at the IRTF with a 5.5" aperture. Data on the X-ray-selected AGN are taken from McAlary et al. (1983), with apertures ranging from 5" to 9".

4. IRAS 23060+0505P16: A HIGHLY OBSCURED 1.5 x 10^{12} $L_\odot$ AGN?

A particularly interesting source, discovered to have distinctive properties among the "hot" IRAS galaxy sample, is 23060+0505. At a redshift of z = 0.174, its luminosity is 1.5 x 10^{12} $L_\odot$, and its J-L' color is the largest (5.12) of all the galaxies in this study. This gives it one of the steepest near-infrared continua known (index α = 2.8, where $S_\nu \propto \nu^{-\alpha}$). Although its energy distribution most resembles that of a Seyfert 1 galaxy, its visible spectrum shows only weak evidence for the large broad permitted line flux expected from such objects. It does, however, show a large O III λ5007/Hβ line ratio characteristic of active galaxies, and it has a steep Balmer decrement. The radio luminosity from unpublished VLA "A" array observations is log P = 22.5 W Hz^{-1} $ster^{-1}$ at 6 cm, a value typical of Seyfert galaxies or radio quiet

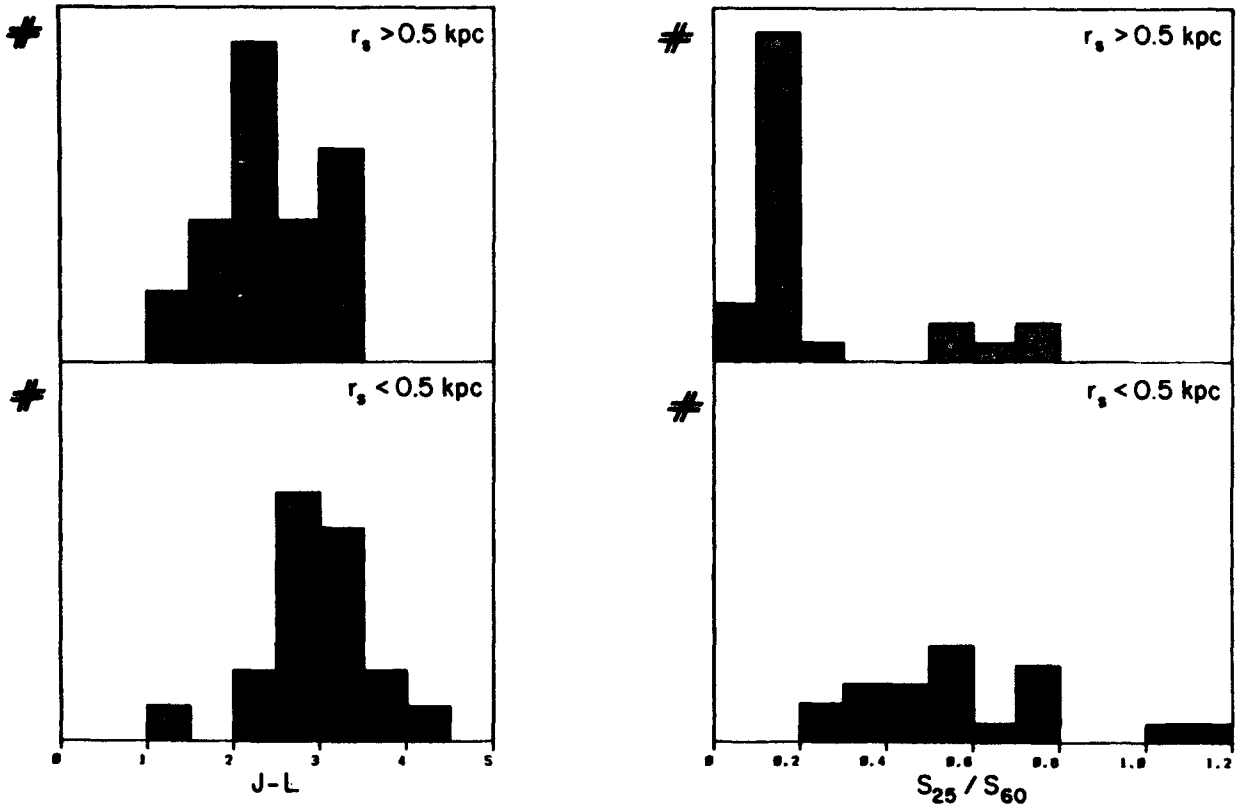

Figure 2. The distributions in J-L and 25-60 μm flux density ratio ($S_{25\mu m}/S_{60\mu m}$) for sources with characteristic 10 μm radii r_o >0.5 kpc and <0.5 kpc (sources for which there are only L' rather than L measurements have been corrected).

QSOs (Ulvestad and Wilson 1984).[2] Important clues to the nature of this object can be found in a comparison between its 1-100 μm energy distribution and those of different classes of extragalactic object (Figure 3).

4.1. The Energy Distribution

Figure 3a shows the energy distribution of 23060+0505 compared with the range observed for typical starburst and interacting galaxies (Joseph et al. 1984; Balzano 1983), and Figure 3b gives a comparison to Seyfert 2 galaxies (Rieke 1978). Both classes of galaxy are dominated at J, H, and K by the photospheric emission from late-type stars, which causes a characteristic inflexion in the energy distribution between 2 and 3 μm. This feature is not seen in 23060+0505, and it is evident that any stellar photospheric contribution to the near-infrared emission from this object is negligible compared to that observed in star-forming or Seyfert 2 galaxies and that the energy source is probably different.

---

[2]The National Radio Astronomy Observatory is operated by Associated Universities, Inc., under contract with the National Science Foundation.

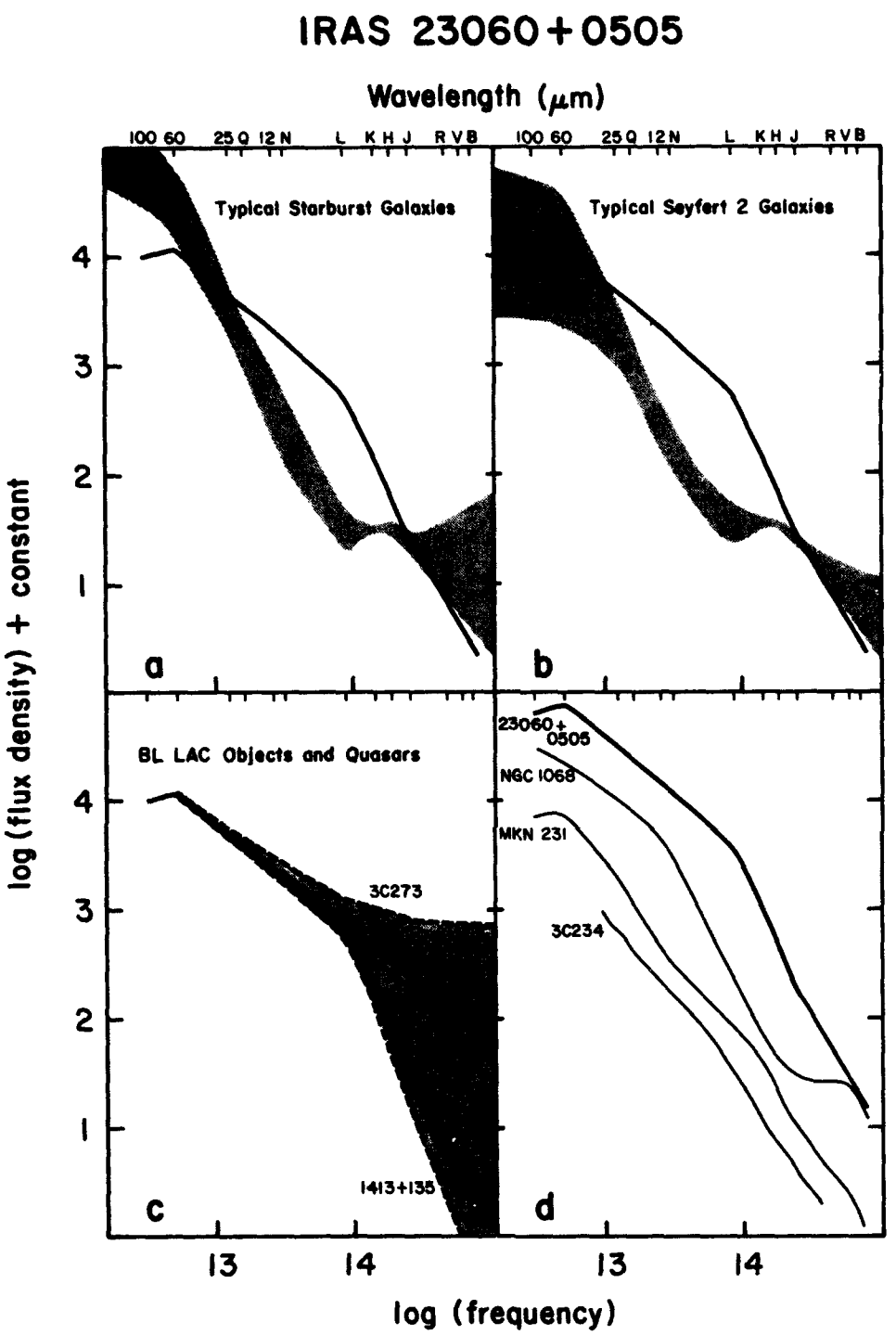

Figure 3. A comparison between the 1-100 μm energy distributions of IRAS 23060+0505 and those of other representative objects. Hatching denotes the range of values encountered for (a) starburst and interacting galaxies; (b) Seyfert 2 galaxies; and (c) Seyfert 1 galaxies, quasars, and BL Lac objects. Figure 3(d) shows 23060+0505 compared to the well-known active galaxies 3C234, NGC 1068, and Mkn 231.

A comparison to Seyfert 1 galaxies, QSOs, and BL Lac objects (Neugebauer et al. 1979; Impey et al. 1982) is made in Figure 3c. It is striking that the energy distribution bears a marked resemblance to that of the BL Lac object with the steepest energy distribution, 1413+135 (Beichman et al. 1981). However, the weakness of its radio emission is inconsistent with 23060+0505 being a BL Lac object. The result of the comparison between 1-100 μm energy distributions is that 23060+0505 most resembles a Seyfert 1 active galaxy.

4.2. Interpretation

Infrared evidence points to 23060+0505 containing a hidden AGN. Higher-quality spectra obtained with the Faint Object Spectrograph reveal only weak evidence for a broad wing to the Hα line, not the strong broad permitted lines characteristic of Seyfert 1 galaxies. This may be interpreted as being due to dust obscuration. An image obtained through the Faint Object Spectrograph shows a very compact morphology dominated by an unresolved nucleus.

An estimate of the reddening toward the region of line formation may be obtained from the Hα/Hβ line ratio, assuming an intrinsic case-B ratio of 2.8 (Osterbrock 1974). The observed ratio of >10 yields a visible reddening in excess of 4 magnitudes, indicating that the absence of strong broad lines, and probably the steepness of the visible to 4 μm continuum, is due to dust obscuration. Here a comparison to other broad-line AGN where large extinctions have been measured through observations of infrared recombination lines is enlightening (Figure 3d). The broad-line radio galaxy 3C 234 shows a strong Paschen-α line consistent with large reddening (Carleton et al. 1984), and it has a steep infrared continuum similar to 23060+0505 (Elvis et al. 1984). The highly luminous reddened broad-line AGN Markarian 231 (Rieke 1978; Lacy et al. 1982) most resembles 23060+0505 with its steep continuum and reddened hydrogen recombination lines.

The fact that this object was discovered in a survey of a relatively small number of candidates ($\approx$20) argues that it may be a prototype of a significant, previously undetected, population of highly obscured AGN with luminosities approaching those of quasars. The selection effects against even slightly reddened AGN in optical and UV surveys are well documented (see Keel 1980 and Lawrence and Elvis 1982 for example), and it has been shown that there exists a significant population of active galaxies, mainly Seyfert 2, missed by other surveys but detected in the infrared by IRAS (de Grijp et al. 1985). It is possible that some of these galaxies, classified as Seyfert 2 on the basis of optical spectroscopy, are similar to IRAS 23060+0505 and contain hidden Seyfert 1 nuclei. It has been demonstrated here that near-infrared colors are a very useful and efficient way to identify such objects.

5. ACKNOWLEDGMENTS

This work was undertaken in collaboration with Gareth Wynn-Williams, Eric Becklin, and Jim Heasley. The author thanks Gerald Cecil for help with some of the observations reported here, John MacKenty for the use of computer programs, and Walter Rice for help with IPAC reductions. This research is supported by NSF grant AST 84-18197.

REFERENCES

Balzano, V. A. 1983, Ap. J., 268, 602.
Beichman, C. A., Neugebauer, G., Soifer, B. T., Wooten, H. A., Roellig, T., and Harvey, P. M. 1981, Nature, 293, 711.
Carleton, N. P., Willner, S. P., Rudy, R. J., and Tokunaga, A. T. 1984, Ap. J., 284, 523.
de Grijp, M. H. K., Miley, G. K., Lub, J., and de Jong, T. 1985, Nature, 314, 240.
Elvis, M., Willner, S. P., Fabbiano, G., Carleton, N. P., Lawrence, A., and Ward, M. 1984, Ap. J., 280, 574.
IRAS Catalog and Atlases, Explanatory Supplement. 1985, ed. C. A. Beichman, G. Neugebauer, H. J. Habing, P. E. Clegg, and T. J. Chester (Washington, D.C.: U.S. Government Printing Office).
Impey, C. D., Brand, P. W. J. L., Wolstencroft, R. D., and Williams, P. M. 1982, M.N.R.A.S., 200, 19.
Joseph, R. D., Meikle, W. P. S., Robertson, N. A., and Wright, G. S. 1984, M.N.R.A.S., 209, 111.
Keel, W. C. 1980, A.J., 85, 198.
Lacy, J. H., Soifer, B. T., Neugebauer, G., Matthews, K., Malkan, M., Becklin, E. E., Wu, C.-C., Boggess, A., and Gull, T. R. 1982, Ap. J., 256, 75.
Lawrence, A., and Elvis, M. 1982, Ap. J., 256, 410.
McAlary, C. W., McLaren, R. A., McGonegal, R. J., and Maza, J. 1983, Ap. J. Suppl., 52, 341.
Neugebauer, G., Oke, J. B., Becklin, E. E., and Matthews, K. 1979, Ap. J., 230, 79.
Osterbrock, D. E. 1974, Astrophysics of Gaseous Nebulae (San Francisco: W. H. Freeman), p. 65.
Rieke, G. H. 1978, Ap. J., 226, 550.
Ulvestad, J. E., and Wilson, A. S. 1984, Ap. J., 278, 544.

ENHANCED STAR FORMATION - THE IMPORTANCE OF BARS IN SPIRAL GALAXIES

P. J. Puxley[1] T. G. Hawarden[2], C. M. Mountain[2] and S. K. Leggett[1]

[1]Department of Astronomy, University of Edinburgh, Blackford Hill, Edinburgh EH9 3HJ.
[2]Royal Observatory, Blackford Hill, Edinburgh EH9 3HJ.

1. ABSTRACT

We have found that amongst an IR-luminous subset of nearby spiral galaxies, nearly all of the systems with IRAS colours and luminosities indicative of enhanced star formation are barred. Radio continuum and IR-spectroscopic results support the hypothesis that this emission originates within the central 2kpc; possibly in a circumnuclear ring. We also find that outer rings are over-represented amongst these barred systems and suggest possible reasons for this phenomena.

Our recent investigation (Hawarden *et al* 1986) of the IRAS database for a large sample of 186 spiral galaxies indicates that nearly all of the systems with excess 25μm flux are barred. The sample includes all of the spirals in the Revised Shapley Ames Catalogue (Sandage & Tammann 1981, 'RSA') between SO/a and Scd (inclusive) and which were detected by IRAS in all four bands. We have excluded from our main sample those galaxies which are extended at 100μm or with Seyfert 1,2 or LINER spectra.

Figs. 1(a), (b) and (c) show the distributions of the ratios $f_\nu 25/f_\nu 12$ vs $f_\nu 100/f_\nu 25$, for barred (SB), unbarred (SA) and mixed-type (SAB) galaxies in our sample. Approximately one third of all the barred/mixed systems have large 25μm/12μm and relatively small 100μm/25μm ratios which are indicative of emission from the warm dust commonly found in starforming regions. Furthermore, these "25μm-excess" barred galaxies (hereafter referred to by using the prefix 'h') are considerably more luminous (typically 4.5 x 10^{10} Lo, with Ho = 75 kms^{-1} Mpc^{-1}) than the other barred and unbarred systems (hereafter prefixed by 'l') which have typical IR luminosities of 2 x 10^{10} Lo.

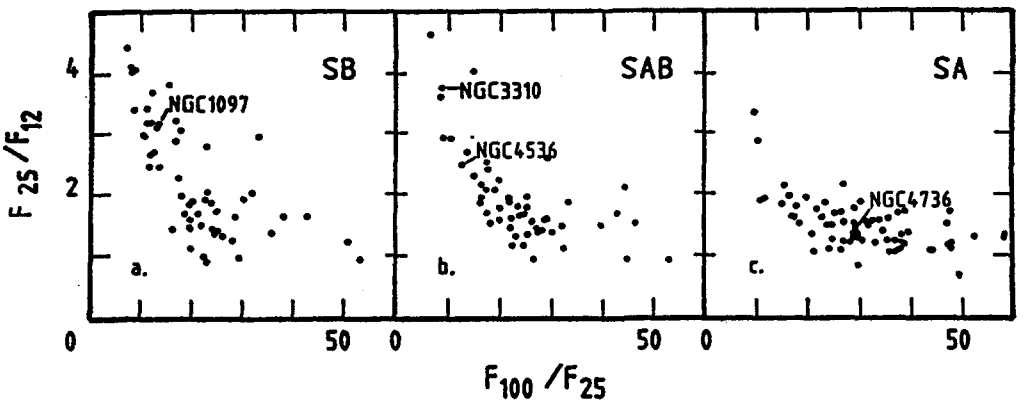

Figure 1(a), (b) & (c)

The distribution of SB, SAB and SA galaxies in the IRAS 2-colour diagram, $f_\nu 25/f_\nu 12$ against $f_\nu 100/f_\nu 25$.

Carol J. Lonsdale Persson (Editor)
Star Formation in Galaxies

To support our conjecture that the extra IR emission is due to enhanced star formation we have constructed simple models using the average IRAS fluxes of a group of unresolved HII regions in Cygnus. Addition of about 10^5 such objects to a mean 'l' galaxy accurately reproduces the spectral shape and luminosity of an 'h' system. Only the 12μm emission is underestimated but our models so far omit the extended 12μm flux which is seen throughout the Cygnus region and which has been attributed to emission from small grains (eg Wynn-Williams & Becklin 1985).

The resolution provided by IRAS was too coarse (1-2 arcmin) to enable us to determine the exact location of the source of the extra IR emission in our barred galaxies. However, recent radio continuum results (Puxley *et al*, in preparation), together with those of Hummel (1980), show that all of the barred galaxies with enhanced star formation are centrally concentrated (less than 20 arcsec) at 20cm. The distribution of radio properties as a function of morphology is shown in Table 1. We have adopted the classification scheme of Hummel such that 'C' refers to galaxies with the unresolved central component, 'E' to those with extended (ie disk) emission and 'ND' refers to non-detections. Less than one third of 'l' spirals have centrally concentrated radio emission.

Table 1

Distribution of radio classifications with morphological type

Galaxy type	C or CE	E	ND
hSB & hSAB	20 (100%)	0 (0%)	0 (0%)
lSB & lSAB	14 (45%)	13 (42%)	4 (13%)
lSA	11 (26%)	19 (44%)	13 (30%)

We have also obtained 2.1μm-2.2μm spectra of a small number of galaxies in our sample. The aperture (20 arcsec) was chosen so as to include any nuclear ring. Preliminary reduction of the spectra indicates that Brackett gamma was detected in the hSAB galaxies NGC4536 and in NGC3310 (whose positions are shown in Fig.1) but not in the lSA system NGC4736. As NGC4536 and NGC4736 have similar continuum flux densities ~3.5 Jy at 25μm) we interpret the Brackett gamma line emission in NGC4536 as arising from star formation which dominates the IRAS fluxes of this galaxy.

The positions of the two well-studied systems NGC1097 and NGC3310 are also indicated in Figs. 1(a) and 1(b). Both of these galaxies have been mapped at 10μm by Telesco and Gatley (1981, 1984) who find that the extra IR emission originates in a ring (diameter about 2kpc) of HII regions around the nucleus. Observations of HI (Sancisi, Allen & Sullivan 1979) and optical spectroscopy (Pence & Blackman 1984) implies that, in barred systems, there is an inflow of gas/dust due to the non-axisymmetric bar potential. Numerical models (eg Combes & Gerin 1985) suggest that the "circumnuclear" rings are situated near one of the inner Lindblad resonances where material swept inwards would be expected to accumulate. In addition, Fig.1(a) exhibits a noticeable "split" at $f_\nu 25/f_\nu 12$ ~2 which we speculate arises due to 'switching-on', of the enhanced star formation once some critical density of the ISM is exceeded.

We have also found a strong correlation (see Table 2) between the occurrence of outer rings (classified R.. or P.. in RSA) and enhanced star formation for our complete sample (ie including 33 Seyfert's and LINER's) of 219 galaxies. Table 2 shows that,

Table 2 Incidence of outer rings with morphological type

Galaxy type	No. of galaxies in sample	No. with outer rings
SB/SAB with vigorous star formation	59	9 (15%)
SB/SAB without vigorous star formation	72	1 (1%)
SA with vigorous star formation	2	0 (0%)
SA without vigorous star formation	86	10 (12%)

amongst barred systems, those with outer rings also have IRAS colours which we have attributed to a vigorous burst of star formation. Numerical models of barred spirals (eg Schwarz 1984) indicate that outer rings form near the outer Lindblad resonance due to the outward transport of disk material by a spiral density wave exterior to corotation. The existence of outer rings in these systems suggests that there is much interstellar material available for transport. Interior to corotation, any gas and dust may be fed inwards towards the centre by the bar-like density wave where it can form a circumnuclear ring. Table 2 also shows that outer rings are also found in unbarred galaxies and we expect a similar process to occur in these systems (with the inflow/outflow being driven by the spiral density wave) except that the lack of a bar may result in a less efficient flow, and hence we do not see vigorous star formation. This model is similar to that proposed by Simkin, Su & Schwarz (1980) who found that outer rings are a feature of many Seyfert galaxies.

In Fig. 2 we show the 2-colour diagram for the Seyfert galaxies which exhibit a remarkably similar distribution to that of the normal spirals in Fig. 1. In agreement with our assertion what the distribution in Fig. 1 is the result of circumnuclear star formation, Rodriguez Espinosa, Rudy & Jones (1986) find that the mid- and far-IR emission from Seyferts is extended and suggest that this is due to a vigorous burst of star formation around the active nucleus.

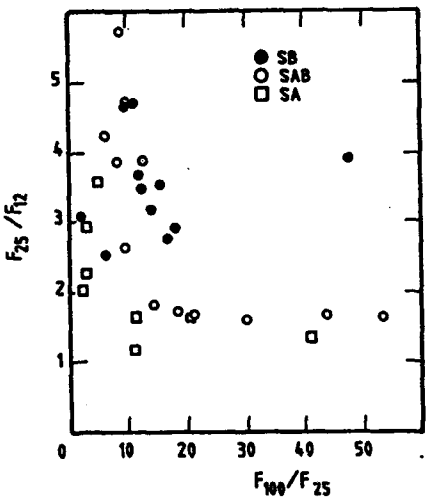

Figure 2

As for Fig. 1 but showing the galaxies whose spectra show Seyfert 1,2 or LINER features.

REFERENCES

Combes, F. & Gerin, M., 1985. *Astr. Astrophys.*, 150, 327.
de Vaucouleurs, G., de Vaucouleurs, A. & Corwin, H.C., 1976. *Second Reference Catalogue of Bright Galaxies*, University of Texas Press, Austin.
Hawarden, T.G., Mountain, C.M., Leggett, S.K. & Puxley, P.J., 1986. Mon. Not. R. Astr. Soc., 221, 41P.
Hummel, E. 1980. *Astr. Astrophys. Suppl. Ser.*, 41, 151.
Pence, W.D. & Blackman, C.P., 1984. *Mon. Not. R. astr. Soc.*, 210, 547.
Rodriguez Espinosa, J.M., Rudy, R.J. & Jones, B., 1986. *Preprint.*
Sancisi, R., Allen, R.J. & Sullivan, W.T., 1979. *Astr. Astrophys.*, 78, 217.
Sandage, A. & Tammann, G.A., 1981. *A Revised Shapley Ames Catalogue of Bright Galaxies*, Carnegie Institution of Washington Publication No. 635.
Schwarz, M.P., 1984. *Mon. Not. R. astr. Soc.*, 209, 93.
Simkin, S.M., Su, H.J. & Schwarz, M.P., 1980. *Astrophys. J.*, 237, 404.
Telesco, C.M. & Gatley, I., 1981. *Astrophys. J.*, 247, L11.
Telesco, C.M. & Gatley, I., 1984. *Astrophys. J.*, 284, 557.
Wynn-Williams, C.G. & Becklin, E.E., 1985. *Astrophys. J.*, 290, 108.

THE PROPERTIES OF HIGHLY LUMINOUS IRAS GALAXIES

R.D. Wolstencroft[1], P.J. Puxley[2], J.N. Heasley[3],
S.K. Leggett[2], A. Savage[1], H.T. MacGillivray[1],
and R.G. Clowes[1]
[1]Royal Observatory Edinburgh [2]University of Edinburgh [3]University of Hawaii

ABSTRACT

From a complete sample of 154 galaxies identified with IRAS sources in a 304 deg^2 area centered on the South Galactic Pole, a sub-sample of 58 galaxies with $L_{IR}/L_B > 3$ has been chosen. Low resolution spectra have been obtained for 30% of the sub-sample and redshifts and relative emission-line intensities have been derived. As a class these galaxies are very luminous with $\langle L_{IR} \rangle = 2.9 \times 10^{11}$ $L_\odot$ and (L_{IR}) max $= 1.3 \times 10^{12}$ $L_\odot$. CCD images and JHK photometry have been obtained for many of the sub-sample. The galaxies are for the most part newly identified and are optically faint ($16 < B < 21$), with a majority showing evidence of a recent interaction. Radio continuum observations of all galaxies of the sub-sample have recently been obtained at 20 cm (VLA) with about 75% being detected in a typical integration time of about 10 minutes.

I INTRODUCTION

We are engaged in a systematic, large-scale program of optical identification of IRAS sources (see Savage et al., 1986, and Wolstencroft et al, 1986), one of whose principal motivations is to establish a large and complete infrared selected sample of galaxies detected by IRAS (so-called IRAS galaxies). With such a sample we can carry out unbiassed studies designed to elucidate the origin of the high infrared luminosity ($L_{IR} \gtrsim 10^{11} L_\odot$) found in many of these galaxies. We have recently begun a study of such a sample that comprises 154 IRAS galaxies identified in a 304 deg^2 area centred on the South Galactic Pole (Wolstencroft et al., 1986), and this paper describes current progress.

In the first stage of this study we have selected a sub-sample of galaxies likely to contain a high proportion of the most infrared luminous galaxies in the complete sample. For an infrared selected sample, L_{IR}/L_B is correlated with L_{IR} but not with L_B (Soifer et al., 1986), which implies that much of the variation seen in L_{IR}/L_B in such a sample (0.2 to 200 in our case) is due to changes in L_{IR}. Our sub-sample comprises 58 galaxies with $L_{IR}/L_B > 3$: the L_{IR}/L_B histogram is shown in figure 1. In this paper we give some preliminary results of follow-up studies in progress, which include low dispersion spectroscopy, CCD imaging, near infrared photometry and radio continuum mapping.

II FOLLOW-UP STUDIES

Redshifts have been obtained so far for 30% of the sub-sample, using either the grism/CCD combination on the 2.2m University of Hawaii telescope (5000 to 6900Å, 4Å resolution) in long slit mode, or the low dispersion spectrograph and reticon detector on the 1.9m SAAO telescope (3500 to 7500Å, 6Å resolution). For this limited sample the infrared

Carol J. Lonsdale Persson (Editor)
Star Formation in Galaxies

luminosity falls in the range 3.8 x 10^{10} $L_\odot$ to 1.1 x 10^{12} $L_\odot$ with $\langle L_{IR} \rangle$ = 2.9 x 10^{11} $L_\odot$: the L_{IR} histogram is shown in fig 2. The properties of a few selected galaxies are given in Table 1.

Table 1

Properties of Selected Galaxies

IRAS Name	z	$L_{IR}/L_\odot$	L_{IR}/L_B	B	K	J-K	H-K	B-K
00308-2238	0.0378	2.0 x 10^{11}	25	17.0	12.71	1.43	0.51	4.3
00335-2732	0.0670	1.1 x 10^{12}	46	17.2	14.16	0.65	0.08	3.0
00402-2350	0.0229	3.3 x 10^{11}	13	14.5	10.22	1.29	0.37	4
01050-3305	0.0347	2.5 x 10^{11}	35	17.0	11.72	1.32	0.42	

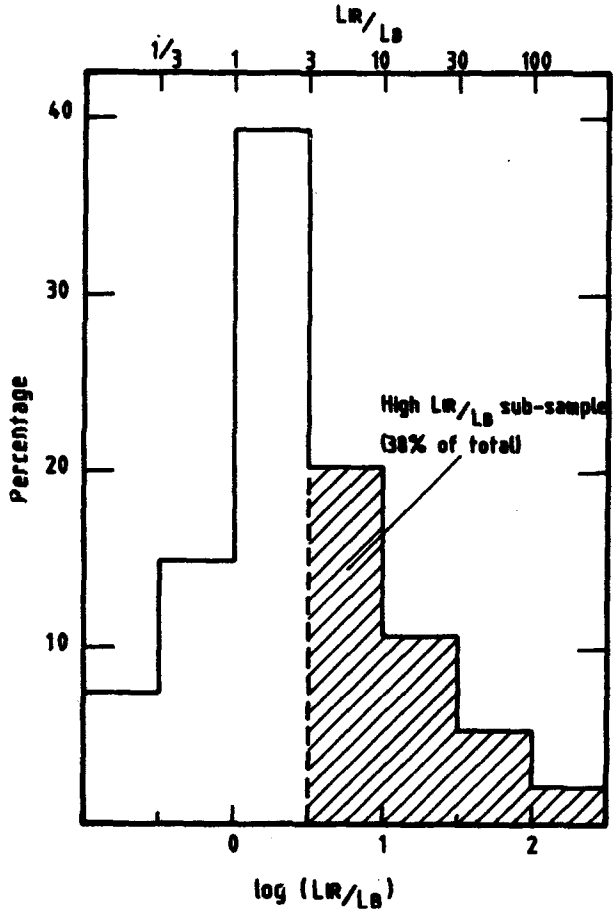

Figure 1. Histogram of L_{IR}/L_B for the complete sample of 154 IRAS galaxies in the SGP field, and for the sub-sample (L_{IR}/L_B > 3).

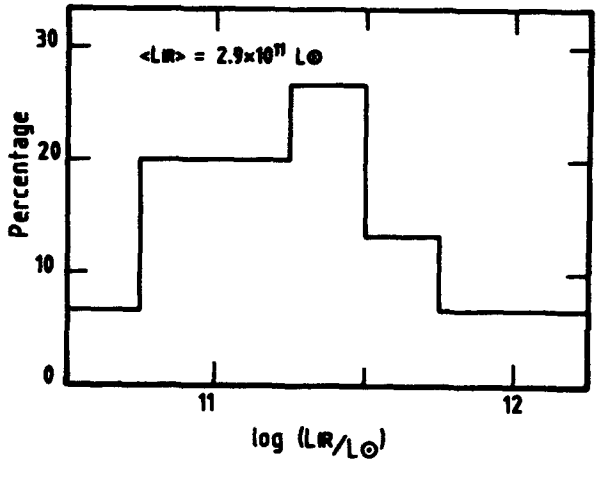

Figure 2. Histogram of L_{IR} for the sub-sample.

From visual inspection of the images on the UKST plates (see Plate 1 of Wolstencroft et al., 1986) it is clear that at least half of the galaxies in the sub-sample are 'interacting', based either on the presence of bridges, tails, double nuclei or other signs of disturbance, or on the presence of a galaxy of comparable brightness that is very close on the sky.

Broad based CCD images and low resolution spectra have been obtained, for about 30% of the sample, and these will allow a more quantitative test of this suspicion. A particularly interesting source is IRAS 00335 - 2732, which is identified with the most luminous galaxy in the sub-sample with $L_{IR} = 1.1 \times 10^{12} L_{\odot}$. There are two galaxies 6 arc sec apart at the position of the IRAS source, with diffuse emission extending between the two galaxies and also north of the fainter galaxy (see fig 3). The redshift of the brighter (B = 17.2) of the two galaxies is z = 0.0670, corresponding to a separation of 8Kpc between the galaxies (H_0 = 75 km sec^{-1} Mpc^{-1}) if they are truly interacting. The correlation between log (L_{IR}/L_B) and log (F_{100}/F_{60}) for the complete sample (Wolstencroft et al., 1986) may be interpreted (de Jong et al., 1984), in its simplest terms, as a combination of two components : (1) contributions by warm dust (T~60K) heated by young stars, and (2) cooler dust heated by the general interstellar radiation field (i.e. cirrus). In the case of IRAS 00335 - 2732, which has the most extreme temperature of the sample (F_{60}/F_{100} = 1.44), the warm dust completely dominates the far infrared emission.

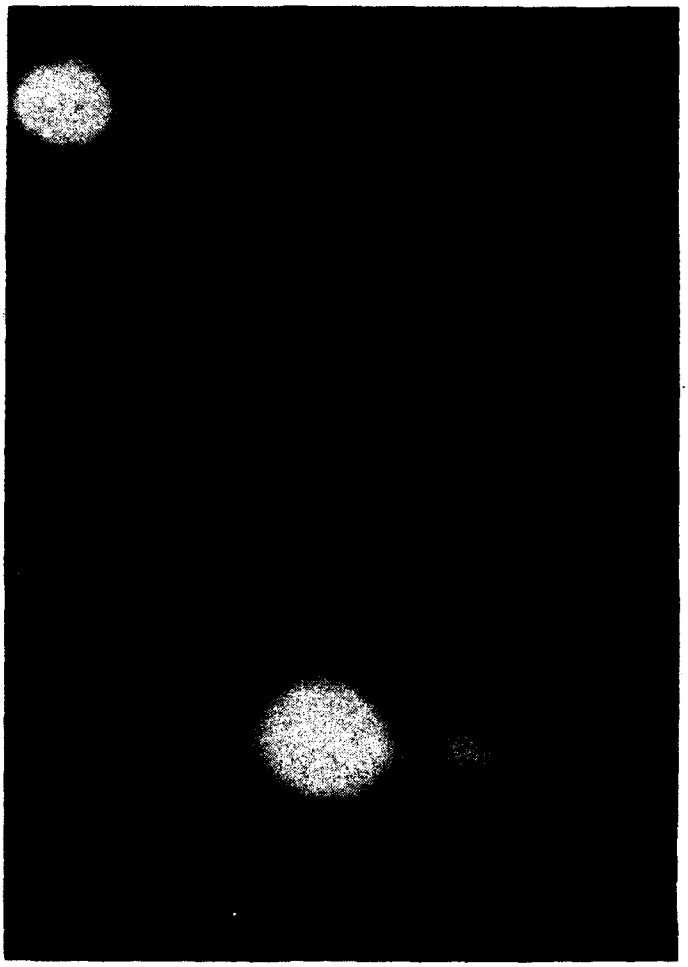

Figure 3. CCD image of IRAS 00335-2732 taken in the R band and with the Galileo CCD camera at the Cassegrain focus of the 2.2m University of Hawaii telescope. North is up and East is to the right. The faint galaxy 6 arc sec due east appears to be interacting with the brighter compact galaxy.

Near infrared colours (J-K, H-K) of a few of these galaxies have been measured on UKIRT with a 20 arc sec aperture. Some typical results are shown in fig 4. For comparison we show the range of colours found by Wolstencroft and Davies (in preparation) for an optically selected sample of normal Sbc galaxies (defined by the dashed rectangle). There is a wide spread in colours, with the extreme cases ranging from the most luminous galaxy IRAS 00335 - 2732 (J-K = 0.65, H-K = 0.08), which has very blue colours, to two galaxies with unusually red H-K colours, IRAS 01358-3300 and 01199-2307. Although all three galaxies show very clear signs of interaction, so also do the sources contained in or close to the normal galaxy sequence (galaxies in the latter sequence have colours that may perhaps be explained primarily as a mixing of bulge and point nucleus colours). If interactions have any significant influence on these near infrared colours it is most likely to occur near the peak of a burst of star formation when the maximum blueing takes place. Clearer discrimination between galaxy types using near infrared colours should be possible for those galaxies bright enough for L' measurements to be made.

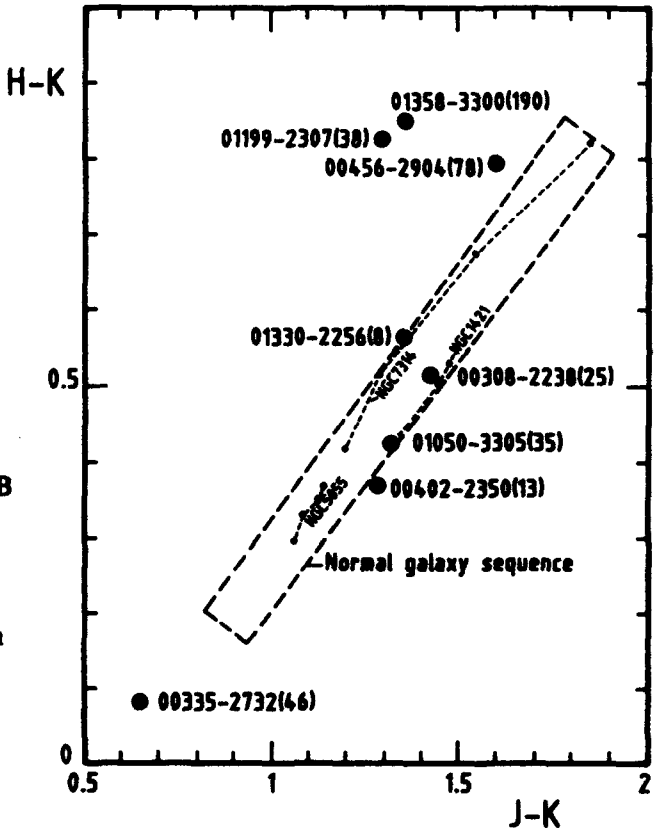

Figure 4. Near infrared colours (H-K, J-K) measured in a 20 arc sec aperture of selected galaxies with $L_{IR}/L_B > 3$. The values of L_{IR}/L_B are shown in brackets after the IRAS name. For comparison the range of colours are shown (dashed rectangle) for an optically selected sample of normal Sbc galaxies (with $0.1 < L_{IR}/L_B < 1.6$) measured with concentric apertures between 5 and 20 arc sec (Wolstencroft and Davies, in preparation). The aperture dependence for three normal galaxies are indicated.

Radio continuum mapping of all galaxies of the sub-sample has been completed recently but analysis is still at a very preliminary stage. With exposures typically of 10 minutes with the A/B array of the VLA (3 arc sec resolution) about 75% of the sample are detected above a limit of about 1 mJy at 20 cm. It will of great interest to see whether the correlation between radio continuum and far infrared emission (see e.g. Helou et al., 1985) holds for our sample of high infrared luminous galaxies.

REFERENCES

de Jong, T., et al., 1984. Astrophys. J. 278, L67.

Helou, G., Soifer, B.T., and Rowan-Robinson, M., 1985. Astrophys. J.298, L7.

Savage, A., Clowes, R.G., MacGillivray, H.T., Wolstencroft, R.D., Leggett, S.K., and Puxley, P.J. 1986. 'Systematic Identifications of IRAS Point Sources', paper presented at this conference.

Soifer, B.T., Sanders, D.B., Neugebauer, G., Danielson, G.E., Persson, C.J., Madore, B., and Persson, S.E. 1986. 'The Luminosity Function and Space Density of the IRAS Bright Galaxy Sample', paper presented at this conference.

Wolstencroft, R.D., Savage, A., Clowes, R.G., MacGillivray, H.T., Leggett, S.K. and Kalafi,M. 1986, M.N.R.A.S. (In press).

Using SIRTF to Study Extragalactic Star Formation

Edward L. Wright
UCLA Department of Astronomy
Los Angeles, CA 90024

SIRTF, the Space Infrared Telescope Facility, is a NASA mission to provide a long lifetime, sensitive and flexible infrared observatory in space. SIRTF will be able to study selected objects with a sensitivity over 5,000 times better than the IRAS survey limits, and will provide photometric and low to medium resolution spectroscopic data over almost nine octaves from 1.8 to 700 μm wavelength.

The baseline SIRTF design has an 85 cm telescope with optics and control system designed for diffraction limited operation at 4 μm and longer wavelengths. For wavelengths shorter than 4 μm, the beam size should equal the 4 μm diffraction limit, so 1" (FWHM) imaging will be possible at 2.5 μm. SIRTF will use a 28° inclination 900 km altitude orbit, and a superfluid helium dewar will cool the optics to 3 K and the baffles to about 10 K, allowing natural background limited operations at 5-135 μm at all times, and at 200 μm for 25 percent of the time.

SIRTF will be able to measure important cooling lines from neutral regions, such as the 157 μm [C II] line, and lines from H II regions such as the 88 μm [O III] line. The SIRTF spectrometer will be able to measure the [C II] line in 100 seconds from spiral galaxies 50 times fainter than the IRAS survey limit.

SIRTF will be able to survey small areas of the sky to the confusion limit in the 3-700 μm region. At 60 μm such a survey can reach a density of 10,000 sources per square degree by using a small degree of super-resolution. This count limit should be reached at a flux of 50-100 μJy, while the super starbust galaxy Arp 220 at a redshift $z = 1.4$ in a critical density Universe would have an easily detectable flux of ~300 μJy. At 4 μm a SIRTF survey will reach 500,000 sources per square degree at a flux of 0.7 μJy, while Arp 220 at $z = 1.4$ would have a flux > 14 μJy. Because the redshift is moving the peak of the starlight into the 4 μm passband, most sources in this survey will be high redshift, nearly normal galaxies. Spectral synthesis studies by Chokshi (1986) have shown that for $z < 1$ the [2]-[4] μm color of normal galaxies depends mainly on z, but for $z > 1$ the color depends on the star formation history of the galaxy. The 60 μm survey, on the other hand, will be an efficient way to pick out galaxies with very active star formation, because the peak wavelength of the far infrared emission from normal galaxies is longer than 60 μm, and is made even longer by the redshift, while starburst galaxies such as M82 and Arp 220 have substantial emission at shorter rest wavelengths.

ACKNOWLEDGEMENTS: This paper summarizes the work of the SIRTF Science Working Group and the members of the instrument teams. ELW is supprted in part by grant number NAG2-315 from the NASA Ames Research Center.

REFERENCES

Chokshi, A. 1986, Ph.D. Thesis, UCLA.

E. ACTIVE GALACTIC NUCELI

ORAL PRESENTATIONS

THE RELATION BETWEEN STAR FORMATION AND ACTIVE NUCLEI

G. H. Rieke
Steward Observatory
University of Arizona
Tucson, Arizona 85721

ABSTRACT

Three questions relevant to the relation between an active nucleus and surrounding star formation are discussed. The infrared stellar CO absorption bands can be used to identify galaxies with large populations of young, massive stars and thus can identify strong starbursts unambiguously, such as in NGC 6240, and can help identify composite active/starburst systems such as Arp 220. An active nucleus is probably not required for LINER spectral characteristics; dusty starburst galaxies, particularly if they are nearly edge-on, can produce LINER spectra through the shock heating of their interstellar media by supernovae combined with the obscuration of their nuclei in the optical. The Galactic Center would be an ideal laboratory for studying the interaction of starbursts and active nuclei, if both could be demonstrated to occur there. Failure to detect a cusp in the stellar distribution raises questions about the presence of an active nucleus, which should be answered by additional observations in the near future.

INTRODUCTION

The interaction between classic galaxy activity — the presence of a nonthermal source that dominates the energetics of the galaxy nucleus — and star formation in the galaxy is a topic on which there is a certain amount of speculation but relatively little relevant observation. IRAS should bring insights to this interdependence because much of the luminosity of both active nuclei and starbursts emerges in the infrared. However, obscuration by the interstellar dust associated with a starburst can hide the galactic nucleus in the visible and ultraviolet, making it necessary to develop new tools to distinguish and study these processes. This talk deals with three issues in this area: the use of stellar CO bands to identify powerful starbursts, the generation of LINER (Low Ionization Nuclear Emission Region) spectra by starbursts, and the possibility of observing the interaction of an active nucleus and a starburst in intimate detail in the Galactic Center.

USE OF CO BANDS TO IDENTIFY STARBURSTS

Traditionally, the presence of a large population of young, massive stars in a galaxy has been identified through observations in the blue or ultraviolet, such as an ultraviolet excess or the presence of Balmer lines in absorption. However, in powerful infrared starburst galaxies, the optical depths in interstellar extinction in the blue can be immense, so these indicators are inadequate. One example is the historical difficulty in identifying the type of activity in the prototype infrared starburst galaxy, M82.

Virtually all types of cool stars have CO absorption bands in their spectra between 2.3 and 2.5um, where they can be readily observed. The depth

Carol J. Lonsdale Persson (Editor)
Star Formation in Galaxies

of these bands depends on the stellar luminosity and metallicity (e.g., Frogel et al. 1978; Frogel, Cohen, and Persson 1983). Luminous galaxies without recent star formation have nearly identical CO band strengths (Frogel 1985 and references therein), indicating that the the infrared outputs are dominated by stellar populations with red giants of comparable mass and metallicity from galaxy to galaxy, corresponding to a main sequence turnoff slightly above one solar mass.

A starburst adds to this quiescent stellar population an additional population of much more massive stars. As soon as these stars evolve to the red supergiant phase, they will tend to produce abnormally deep CO absorption in the galaxy spectrum. If the starburst luminosity is large enough compared with that of the pre-existing quiescent stellar population, this deepening should be detectable. In fact, such deepening has been observed in M82, NGC 253, and NGC 6240, requiring that their near infrared spectra be dominated by the young, massive stars produced in starbursts.

There is evidence for very strong reddening in all three of these galaxies. However, all of them have H - K colors that are too red compared with their J - H colors for any reasonable stellar population plus foreground reddening. For NGC 253 and NGC 6240, it has been suggested that this red color arises from a normal quiescent stellar population, plus an infrared excess at 2um contributed by a nonthermal nuclear source or by thermal reradiation by dust(Scoville et al. 1985, DePoy, Becklin, and Wynn-Williams 1986). Such an excess could only dilute the CO band strength; the observed strengths require that the 2um emission be dominated by starlight from massive stars. The red H - K colors can be explained if the interstellar dust is mixed with the stars in the galaxy, so there are optical depth effects in the source, or if the extinction varies over the extended source region. J, H, K images of the three galaxies show strong color variations, which are almost certainly due to extinction variations over the sources. These data are illustrated in Figures

Figure 1. Images of M82 at J, H, and K (left to right). The frames are 27 arcsec on a side and the pixels are 0.85"; the data have been smoothed to a final resolution of 1.7". At K, the image shows a reasonably symmetric, smooth distribution of stars that suggests an edge-on disk around a brighter nucleus. Note the strong distortions from interstellar extinction as the wavelength becomes shorter.

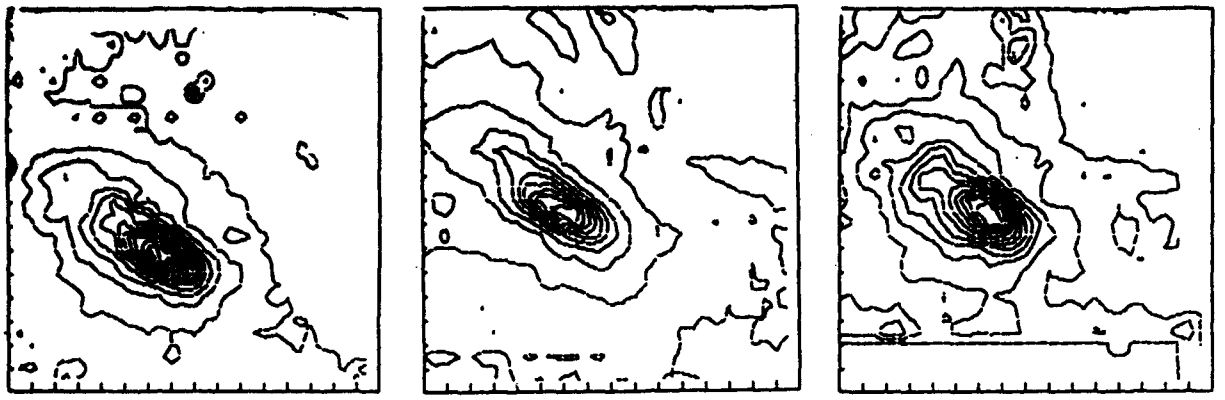

Figure 2. H and K Images of NGC 253 and Their Ratio (left to right). The frames are 27 arcsec on a side and the pixels 0.85". In the ratio K/H, there is an extended peak centered on the galaxy nucleus, indicating it is bluer than the surrounding regions.

1 - 3. At least from these examples, the strong infrared excesses typical in starburst galaxies appear to be a minor part of their emission at wavelengths as short as the 2um CO bands.

M82, NGC 253, and NGC 6240 have luminosities from red supergiants respectively of 2.5 X 10^{10} L_o (Rieke et al. 1980), 1.3 X 10^{10} L_o (Rieke et al. op. cit.) and 2 X 10^{11} L_o (Rieke et al. 1985, but with A_v set to 7, from the H - K excess), compared with far infrared luminosities of 3 X 10^{10} L_o, 3 X 10^{10} L_o, and 5 X 10^{11} L_o. Thus, the stellar luminosities deduced directly from the near infrared can account for 30 to 40% of the total infrared luminosity of the galaxy. This result arises because a coeval population of massive stars evolves in a few million years to emit a substantial fraction of its luminosity from red supergiants.

In contrast to starburst galaxies, the near infrared continua of Seyfert galaxies seem to be dominated by featureless continua; the CO bands when present are diluted substantially compared with those in galaxies with quiescent stellar populations (e.g., Cutri et al. 1981). Where relatively strong CO bands are detected along with indications of an active nucleus, the system is likely to be a composite. Arp 220 is an example; despite spectroscopic exidence for a Seyfert nucleus, its CO bands are stronger than those of quiescent galaxies (Rieke et al. 1985). Assuming A_v = 7 (corresponding to the H - K excess), a stellar luminosity of 6 X 10^{10} L_o is detected directly in the near infrared. Assuming a ratio of red giant and supergiant to total stellar luminosity similar to those in M82, NGC 253,and NGC 6240, the starburst accounts for 15 to 20% of the total luminosity of Arp 220.

LINER SPECTRA IN LATE TYPE GALAXIES

LINER spectra were originally thought to arise by shock heating, but it has recently become popular to ascribe them to the presence of a weak, powerlaw excitation spectrum produced by an active nucleus. Most of the evidence for this interpretation comes from observations of early type

galaxies. However, similar spectra are observed in late type galaxies where there are many indications of starburst activity. These galaxies raise the question of whether starbursts can produce a LINER spectrum.

We have considered this question in detail for NGC 253 (Rieke, Lebofsky, and Walker 1986). The high supernova rate in the nucleus of this galaxy repeatedly shocks the low density interstelar medium with supernova blast waves that produce the starburst wind seen in the x-ray (Fabbiano and Trinchieri 1984) and discussed by Chevalier and Clegg (1985). The molecular clouds in the nucleus are immersed in this medium, while extranuclear clouds surround it. The nuclear starburst region is heavily obscured by these clouds -- in the case of NGC 253, there is an average A_V of about 12. The radius of the Stromgren sphere for the nucleus does not extend beyond the region of heavy obscuration except where the interstellar medium is of low density. However, the low density ISM is dominated by supernova driven shocks. Thus, optical spectra do not probe the region of HII type excitation; they reflect conditions in a part of the ISM where a LINER spectrum might be expected. Heckman (this conference) reports that the filaments out of the plane of M82 also have a LINER-like spectrum, as would be expected from these arguments.

Because the extinction will tend to be concentrated in the galactic plane, a situation similar to that in NGC 253 could be expected to hold in other nearly edge on, late type, starburst galaxies with LINER spectra, such as NGC 660 and NGC 3079. In face-on galaxies, a LINER specrum can still result whenever the HII region lies behind heavy obscuration. NGC 6240 is probably a good example; from the H - K color, the strong CO bands, and the extremely red color of the dominant nuclear component in Figure 3, most of its red supergiant population and presumably much of the other starburst activity lie behind extinction of approximately $A_V \approx 7$.

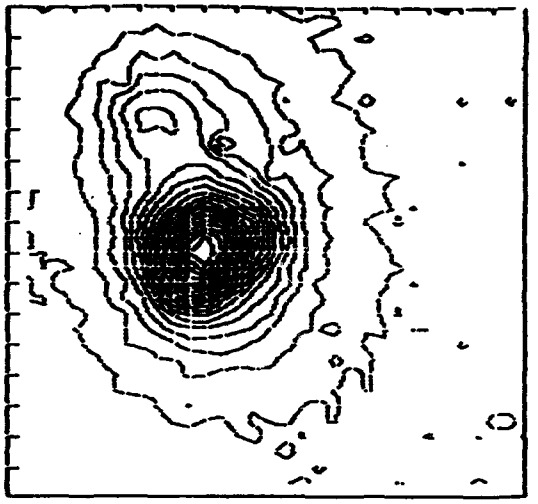

Figure 3. Image of NGC 6240 at H. The frame is 8 arcsec on a side and the pixels are 0.25". Comparison with the I image published by Fried and Schulz (1983) shows that the southern nuclear component is much redder in I - H than the northern one.

THE GALACTIC CENTER

The Galactic Center could be an ideal place to observe the interaction between an active nucleus and a starburst. Unfortunately, the presence there of either a starburst or an active nucleus has been extremely controversial. The strongest evidence for a starburst is the spectroscopic and photometric classification of a number of stars within 40 arcsec (2 parsecs) of the Galactic Center as red supergiants (Lebofsky, Rieke, and Tokunaga 1982). We have made images at *H* and *K* of 24 square arcmin centered on this region and find many additional bright red stars that are likely to be red supergiants, although spectroscopic confirmation is not yet available (Lebofsky 1986).

The evidence for a black hole (and hence an active nucleus, even if a dormant one) rests largely on the velocities of the NeII clouds (Serabyn and Lacy 1985). Given the short lifetimes of the low density gas clouds seen in neon emission, it is not certain that their motions are in equilibrium with the gravitational field; confirming evidence for the black hole is therefore desirable.

The cusp in the stellar distribution reported by Allen, Hyland, and Jones (1983) would tend to support arguments from the velocity field for the presence of a black hole. However, the image of the much larger field mentioned above confirms the presence of large nonuniformities in the extinction in this region, as suggested previously by Rieke, Telesco, and Harper (1978), and Lebofsky (1979). The central parsec of the galaxy happens to lie in a minimum of the extinction and furthermore has a number of 2um sources that are not part of the general red giant and supergiant population (Rieke and Lebofsky 1986). These two circumstances can lead to an artificial appearance of a cusp. Moreover, Allen and Sanders (1986) suggest that the compact radio source does not coincide with any sufficiently bright near infrared source to be identified with the core of a stellar cusp. However, this argument depends very strongly on the precise location of the compact radio source relative to the infrared maps. Various determinations of this location are plotted on a new, high resolution image of source 16 in Figure 4; the possibility still remains that the source coincides with a faint peak in the infrared emission.

An alternate way to look for a cusp is to measure the surface brightness between the bright stars. Assuming a central density of about 4×10^5 stars pc^{-3} (Bailey, 1980), there should be about 4000 stars per square arcsec. Most of these stars will contribute a diffuse, unresolvable background which should be an extremely accurate reflection of the distribution of stellar mass in the region. Searches for a cusp in this diffuse component will also be insensitive to the precise registration of the infrared maps relative to the position of the radio compact source.

By chance, there is a "valley" in the source distribution that comes within about 2 arcsec of the compact radio source (see Figure 4). The minimum in this valley has been compared with the minima on 32 X 32 camera frames centered on the compact source but with different pixel scales — 0.25" (Fig. 4), 0.85", and 1.3". The lowest surface brightness on these frames lies in a small region of very high extinction first noted by Lebofsky (1979) about 20" west of the central source complex. If this region is set to zero and the bottom of the valley set to 100%, most of the remaining region between bright

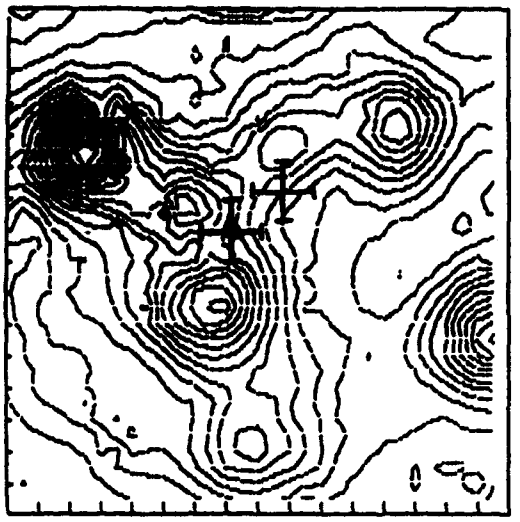

Figure 4. Image of Source 16 in the Galactic Center at K. The frame is 8 arcsec on a side and the pixels are 0.25". The cross with a dot is the location of the compact radio source according to Henry, DePoy, and Becklin (1984), while that without a dot is according to Forrest, Pipher, and Stein (1986). The "valley" referred to in the text extends from the middle of the western edge of the frame toward the southeast, ending about 2 arcsec west of the compact radio source.

sources is at a surface brightness of 50 to 75% (see Figure 5). Because the valley appears to be affected by source crowding, the true diffuse brightness there may be have been overestimated; it is also likely that the surface brightness in the zero reference region is actually larger than zero. Both of these effects will tend to reduce the true contrast between the valley floor and the surrounding regions compared with our estimate. Thus, there is an upper limit of about 1.5 to the increase in surface brightness between a distance of 1 pc and one of 0.1 pc from the compact radio source.

The apparent absence of a strong cusp in the stellar distribution leaves the question of "activity" in the Galactic Center open, but an answer should be possible soon. An improved understanding of the stellar distribution will be possible as soon as the extinction has been mapped; infrared camera images such as those described here and by Lebofsky (1986) should be capable of doing so, although the large region of extremely high extinction to the east will require images of signficantly greater sensitivity than are now available. The velocity field can be measured from spectral features in individual stars. In the 24 square arcmin field already imaged but outside the central 40 arcsec, there are 81 stars brighter than K = 9.5. Improvements in near infrared spectroscopy should soon allow velocity measurements for these stars and remove the uncertainties in the velocity field that arise because of the short lifetimes of the gas clouds measured in Ne II.

Since the Galactic Center is 1000 times closer than any classical active galaxy, even the presence of a very weak active nucleus there would help immensely in determining the interaction of such an object with the immediately surrounding galaxy.

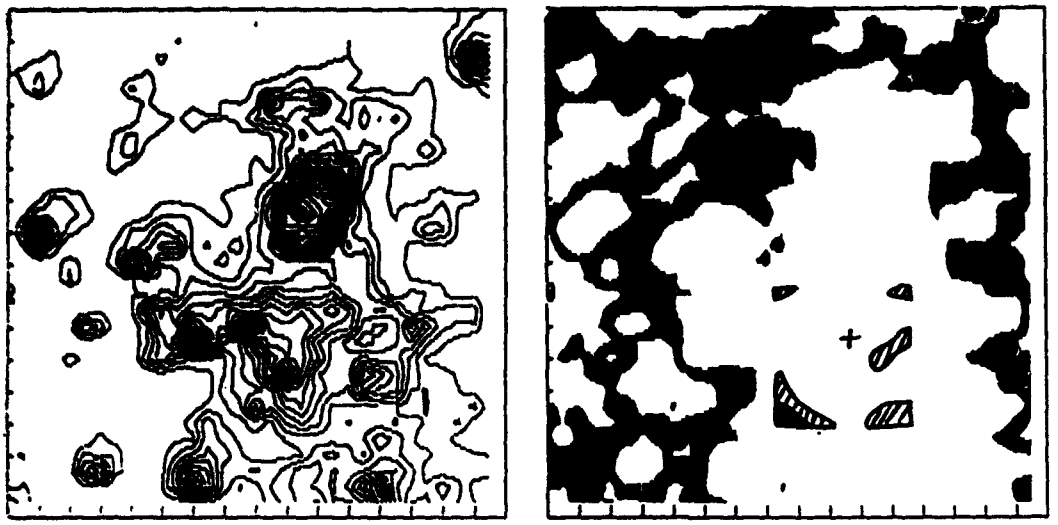

Figure 5. Image of the Galactic Center at K. The frames are 27 arcsec on a side and the pixels are 0.85". The left frame shows the sources in this region; the brightest just to the northwest of the center is source 7. In the right frame, the diffuse background between the sources is displayed, with the source 16 frame (Fig. 4) superposed. Regions where the diffuse background is 75 to 100% the surface brightness in the valley in Fig. 4 are indicated hatched. Regions where the surface brightness 50 to 75% that in the valley are shown solid.

ACKNOWLEDGMENTS

The infrared images reported here were made with a camera constructed by M. J. Lebofsky and E. F. Montgomery and were obtained and reduced with the assistance of M. J. Lebofsky. This work was supported by the National Science Foundation.

REFERENCES

Allen, D. A., Hyland, A. R., and Jones, T. J. 1983, MNRAS, 204, 1145.
Allen, D. A., and Sanders, R. H. 1986, Nature, 319, 191.
Bailey, M. E. 1980, MNRAS, 190, 217.
Chevalier, R. A., and Clegg, A. W. 1985, Nature, 317, 44.
Cutri, R. M., et al. 1981, ApJ, 245, 818.
DePoy, D. L., Becklin, E. E., and Wynn-Williams, C. G. 1986, ApJ, 307, 116.
Fabbiano, G., and Trinchieri, G. 1984, ApJ, 286, 491.
Forrest, W. J., Pipher, J. L., and Stein, W. A. 1986, ApJ (Letters), 301, L49.
Fried, J. W., and Schulz, H. 1983, Ast. and Astrophys., 118, 166.
Frogel, J. A. 1985, ApJ, 298, 528.
Frogel, J. A., Persson, S. E., Aaronson, M., and Matthews, K. 1978, ApJ, 220, 75.
Frogel, J. A., Cohen, J. G., and Persson, S. E. 1983, ApJ, 275, 773.
Henry, J. P., DePoy, D. L., and Becklin, E. E. 1984, ApJ (Letters), 285, L27.
Lebofsky, M. J. 1979, A. J., 84, 324.
Lebofsky, M. J. 1986, proceedings of the Santa Cruz Workshop on Nearly Normal Galaxies, 1986.

Lebofsky, M. J., Rieke, G. H., and Tokunaga, A. T. 1982, ApJ, 263, 736.
Rieke, G. H., Telesco, C. M., and Harper, D. A. 1978, ApJ, 220, 556.
Rieke, G. H., Cutri, R. M., Black, J. H., Kailey, W. F., McAlary, C. W., Lebofsky, M. J., and Elston R. 1985, Ap, 290, 116.
Rieke, G. H., Lebofsky, M. J., Thompson, R. I., Low, F. J., and Tokunaga, A. T. 1980, ApJ, 238, 24.
Rieke, G. H., Lebofsky, . J., and Walker, C. E. 1986, submitted to ApJ.
Rieke, G. H., and Lebofsky, M. J. 1986, to be submitted to ApJ.
Scoville, N. Z., Soifer, B. T., Neugebauer, G., Young, J. S., Matthews, K., and Yerka, J. 1985, ApJ, 289, 129.
Serabyn, E., and Lacy, J. H. 1985, ApJ, 293, 445.

QUESTIONS

T. J. Jones: One of the reasons not everbody has picked up on the interpretation of the 2um sources near the galactic center as M supergiants is because not everyone believes they are true supergiants. I believe they are mostly upper AGB stars (M_{bol} = -6 to -7) with main sequence progenitors from 3 - 7 M_o.

Answer: The spectra show a range of spectral types. Source 7, Kobayashi 9, and probably source 12 appear to be very luminous and massive supergiants and are inconsistent with your interpretation. The other stars with spectra are of lower mass and could have 3 to 7 M_o progenitors. However, all of the brighter objects appear to be massive enough that their progenitors must be relatively young ($\leq 3 \times 10^8$ years), indicating that the 2um sources formed in an extended period of recent star formation.

M. Shull: Your limits on a possible black hole in the Galactic Center depend on an equilibrium stellar cusp. If the stellar density is not sufficient, the stellar relaxation time is too long for this cusp tc be established, so you might still be able to have a massive compact object.

Answer: It seems likely that the two-body relaxation time for the galactic center is too long for a fully developed cusp (i.e., stellar density as radius to the -1.75). Nonetheless, a slightly more shallow cusp would be expected (P. J. Young 1977, Ap.J., 217,287).

J. Frogel: 1.) Galactic star clusters of near solar metallicity are all extremely star poor so that the brightest giants you can see in them are about 2 magnitudes fainter than the brightest stars you would expect to see in a large population; 2.) In Baade's window at b = -3.9^o there are M6-9 giants as bright as K = +6. These have M_{bol} of about -4.5 and, in a super metal rich environment, can still have an age of 10^{10} years.

Answer: Stars like the brightest in Baade's window will account for the fainter objects in the Galactic Center images. Taking an extinction of A_v = 30, they will have an apparent magnitude of $K \geq 9.4$; since the extinction for most of the Galactic Center region is higher, over most of the area they will be even fainter. Six of the seven stars with spectra have $K \leq 8.1$, and three of these six are of spectral types M1 to M4, where the Baade's window stars are fainter still.

Frogel: Stars with age a few Gyr can have very strong CO indices. These are AGB stars with M_{bol} on the order of -6. Such stars are found in large numbers in the Magellanic Clouds. Although in the Magellanic Clouds many of these are C stars, in a more nearly solar metallicity environment they would be M stars.

Answer: I don't believe the existence of these stars affects the arguments that the strong CO bands arise from a difference in stellar population that is most plausibly connected with a recent powerful episode of star formation. In determining the CO band strengths, comparison is made to galaxies with similar luminosities and metallicities, so some other difference must exist in the stellar populations.

P. G. Mezger: There is an HII region, Sgr A West, surrounding IRS 16. What, in your opinion, provides the ionization for this HII region?

Answer: The ultraviolet flux from the hot stars that should accompany the red supergiants appears to be adequate to ionize all the gas in this region. Some more exotic ionizing source may also contribute, but if such an object accounts for all the luminosity of the region, it is surprising how difficult it is proving to be to establish its existence for sure.

E. E. Becklin: Is it not a problem to assume a normal IMF in a region like the Galactic Center - especially the very central region?

Answer: Of course, the process of star formation should be modified by conditions in these regions. There is evidence, for example, that low mass stars form in much lower relative numbers in starbursts than in the solar neighborhood. One would expect that the modifications would get larger as one approached the nucleus; yet, in NGC 253 most of the starburst appears to lie within 20 parsecs of the nucleus, so there is no evidence for a cutoff in the process of massive star formation.

M. Harwit: Have you looked at the time scale over which a dust shroud surrounding a concentrated, higly luminous (10^{11} $L_{\odot}$) group of stars would become disrupted by the strong radiation pressure which should dominate gravitational attraction?

Answer: No. I suppose it would depend on some parameters that we don't have good estimates of, such as the magnetic field. Perhaps with more work on the timescales for the starbursts in NGC 6240 and similar galaxies, we could make some progress in this area.

GROUND-BASED 1- TO 32-μm OBSERVATIONS OF ARP 220: EVIDENCE FOR A DUST-EMBEDDED "AGN"?

E. E. Becklin and C. G. Wynn-Williams
University of Hawaii, Institute for Astronomy
Honolulu, Hawaii 96822 USA

ABSTRACT. New observations of the 10- and 20-μm size of the emission region in Arp 220 are presented. We also give ground-based photometry from 1-32 μm including measurements of the strength of the silicate feature at 10 μm. The results show that the 20-μm size of Arp 220 is smaller than 1.5 arcsec (500 pc); comparison of IRAS and ground-based observations show that IRAS 12-μm flux measured with a large arcmin beam is the same as that seen from the ground with a 3-arcsec aperture. At 10 μm a deep silicate absorption feature is seen that corresponds to a visual extinction of about 50 mag.

These results suggest that a very significant portion of the 10^{12} $L_\odot$ infrared luminosity from Arp 220 comes from a region less than or of the order of 500 pc in diameter. When these results are combined with recent measurement of a broad Brackett-α line by DePoy and an unresolved 2.2-μm source by Neugebauer, Matthews and Scoville, a very attractive possibility for the primary luminosity source Arp 220 is a dust-embedded compact Seyfert-type nucleus.

INTRODUCTION

Arp 220 (IC 4553) is a relatively nearby galaxy that IRAS found to be extremely luminous at infrared wavelengths (Soifer et al. 1984). It has a total luminosity of 10^{12} $L_\odot$ at a distance of 70 Mpc (H_o = 75 km/sec/Mpc). It emits 50 to 100 times more luminosity at infrared than visible wavelengths. Optically the galaxy appears highly disturbed and has been classified as a merger (Joseph and Wright 1985). It contains several compact radio sources (Norris 1985) and at visual wavelengths shows a thick dust lane across its center (Schild 1985).

Arp 220 appears to be one of a number of galaxies discovered by IRAS that have a total luminosity > 10^{12} $L_\odot$. The space density of these galaxies is as high or higher than optical, radio, or x-ray selected galaxies or QSOs (Soifer et al. 1986). A critical question to be answered is the dominant source of energy in Arp 220. A number of suggestions have been made such as (1) a burst of star formation (Rieke et al. 1985; Joseph and Wright 1985), (2) a dust-embedded active galactic nucleus "AGN" (Soifer et al. 1984; Norris 1985), and (3) mechanical energy from a collision of two galaxies (Harwit et al. 1986). In this paper we present new observations that suggest that a dust-embedded "AGN" is the most likely explanation for the luminosity in Arp 220.

OBSERVATIONAL RESULTS

We present previously unpublished results on the size of the emission region at 10 μm (N) and 20 μm (Q). The data were obtained on the IRTF in March 1985 and 1986 using the facility photometer with a Ga:Ge bolometer and standard interference filters.

Carol J. Lonsdale Persson (Editor)
Star Formation in Galaxies

Figure 1 shows a 20-μm profile of Arp 220 along a north-south line made with a 3-arcsec aperture. The data have been folded about the central point. Also shown is the profile of a star. Similar data also exist in the east-west direction. These data show that the galaxy and stellar profiles are similar; in other words Arp 220 is unresolved. Assuming that the two profiles are Gaussian in shape, the Arp 220 source has a characteristic size (FWHM) which is less than 1.5 arcsec. This corresponds to <500 pc at the distance of Arp 220.

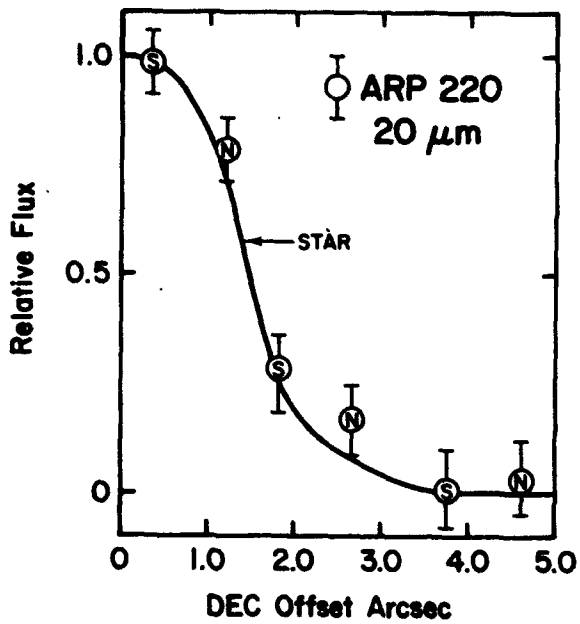

Figure 1: North-south profile at 20 μm taken with a 3-arcsec beam.

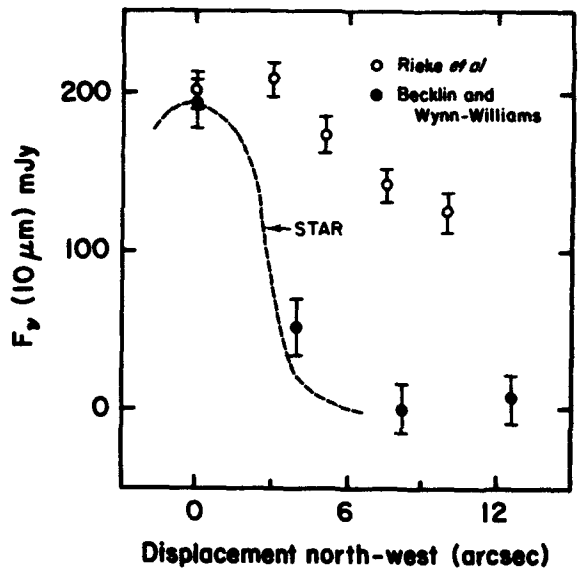

Figure 2: North-west profile at 10 μm taken with a 5.5 arcsec beam.

A 10-μm profile with 5.5-arcsec resolution along a north-west direction is shown in Figure 2 along with the profile of a star; again Arp 220 is unresolved. These data disagree with the results of Rieke et al. (1985) whose data are also shown in Figure 2. Both observations were made with the same system on the IRTF; we do not understand the discrepancy. The 20-μm profile and the 12.5-μm aperture growth curves discussed below would suggest that the present results, which show that the source is unresolved at 10 μm, are correct.

Figure 3 is an aperture growth curve at 12.5 μm, i.e., flux versus aperture size. It includes ground-based observations with beam diameters of 3.0, 5.5, and 7.0 arcsec and the IRAS data with a beam >1 arcmin in diameter. The IRAS point has been corrected for the different filter responses using the energy distribution for Arp 220 given below. The result is that >90% of the 12.5-μm flux measured by IRAS is observed in a 3-arcsec-diameter aperture.

In Figure 4 we present the energy distribution of Arp 220 from 7.8- to 12.5-μm observed with a 5.5-arcsec aperture and standard IRTF filters with $\Delta\lambda/\lambda \sim 0.1$. There is an obvious deep absorption feature at 10 μm. The shape of the feature agrees with that seen in other galactic and extragalactic sources and is ascribed to silicate dust (Roche et al. 1986). The shape of the spectrum indicates an absorption optical depth of $\tau \sim 3$, implying a visual dust extinction of $A_V \sim 50$ mag.

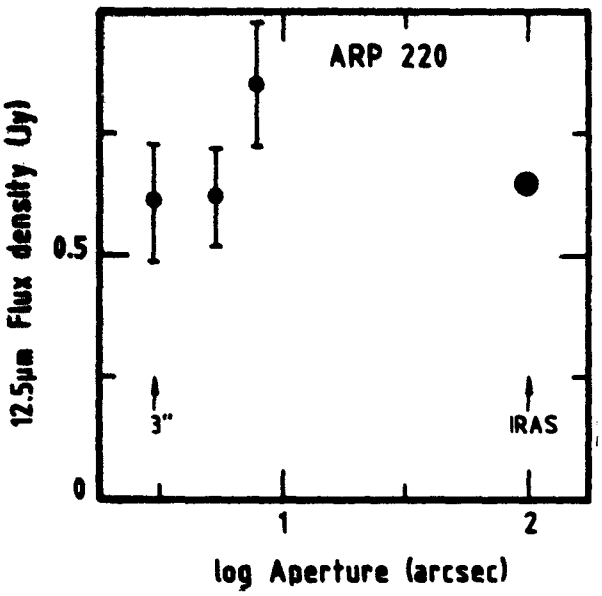

Figure 3:
Aperture growth curve at 12.5 μm.

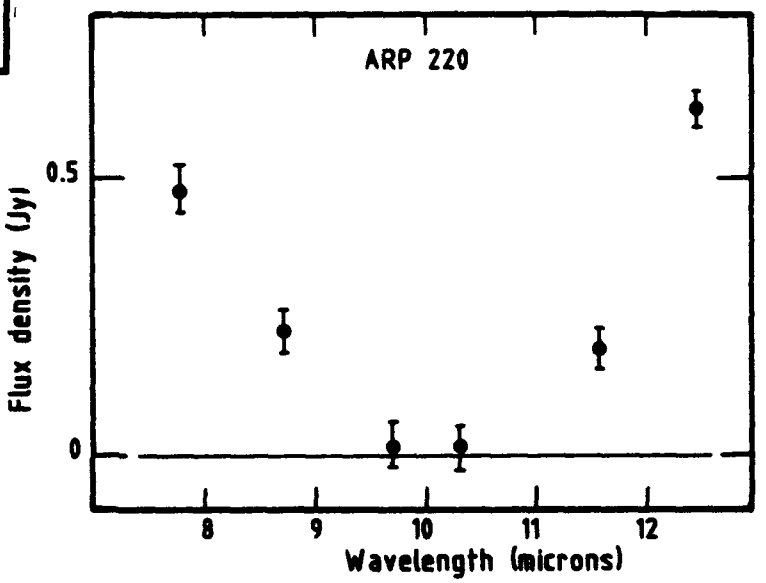

Figure 4:
Energy distribution
from 7.8 to 12.5 μm.

Figure 5 shows the complete spectrum of Arp 220 from 1 μm to 350 μm plotted as log νS_ν vs log ν; both IRAS and ground-based data are shown. The 1.65-, 2.2-, and 3.8-μm points are unpublished University of Hawaii measurements in a 4-arcsec aperture that have had an estimated stellar contribution subtracted. All of the points from 7.8 to 32 μm were made with a 5.5-arcsec aperture on the IRTF. The 350-μm point is from Emerson et al. (1984). The energy distribution shows that:

1) The energy peaks at about 50 μm; the distribution corresponds to a blackbody at a temperature of 62 K (Soifer et al. 1984).

2) Silicate absorption is a dominant feature.

3) The IRAS fluxes at 25 and 60 μm are consistent with the observed ground-based fluxes at 20 and 32 μm measured with a 5.5-arcsec aperture.

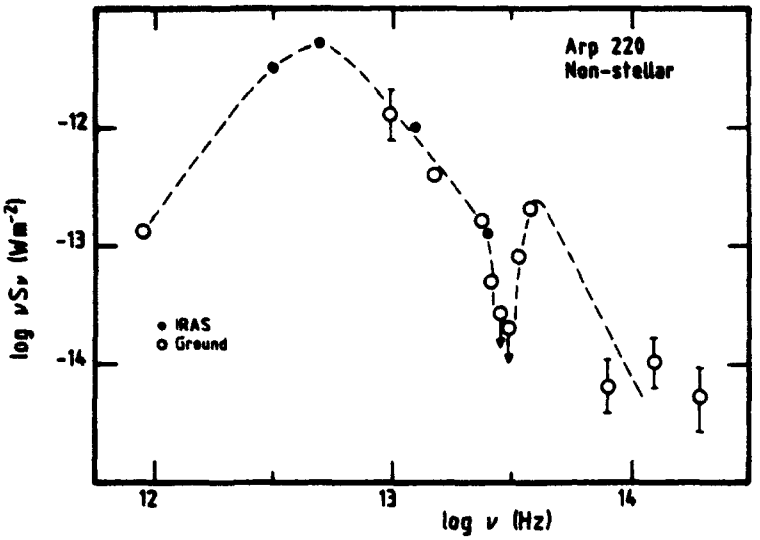

Figure 5: Energy distribution from 1 to 350 μm.

A 6-cm VLA map with 0.4-arcsec resolution is shown in Figure 6. It shows two slightly resolved sources ($\theta \sim 0.2$ arcsec) separated by about 1 arcsec in right ascension. The structure we see at 6 cm differs significantly from the triplet morphology found by Norris (1985) using the MERLIN array at 18 cm. We have not yet established whether this difference is attributable to time variability, spectral index variations, or to differences in the data reduction procedure. The compact 10- and 20-μm source lies within 1 arcsec of the midpoint of the radio peaks; this has been determined by offsetting the IRTF from nearby AGK_3 stars.

Figure 6: VLA 6-cm map.

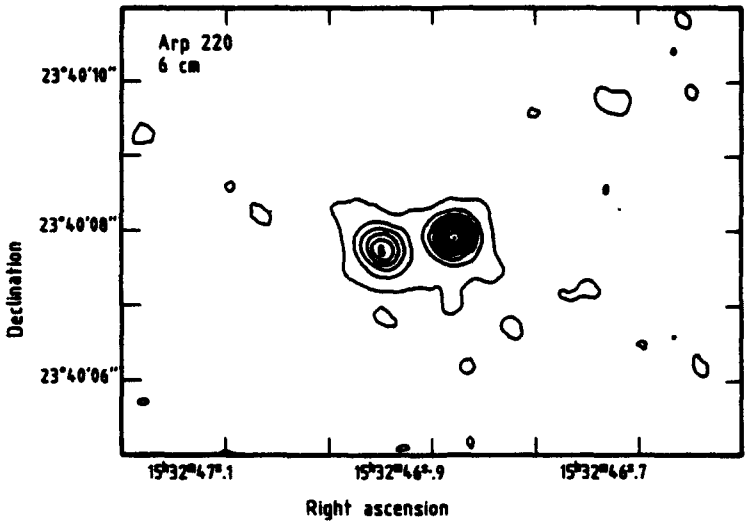

NEW OBSERVATIONS BY OTHERS

A student of ours at the Institute for Astronomy (D. DePoy) has measured the Brackett-α line at 4.1 μm on the UKIRT using CGS2 with a 5.5-arcsec beam. From his results, presented at this conference (DePoy 1986), he finds that the line is broad (~1300 km/sec FWHM). The line strength implies an infrared excess $[L_{bol}/L_{Ly\alpha} - 1] \sim 300$. Correction for the reddening based on the sili-

cate absorption depth would reduce the excess to about 100. Because the 32-μm flux originates from a region (Figure 5) with the same angular diameter as the beam used for the B_α measurements, no correction for aperture size is necessary.

The Palomar infrared group has made slit scans of Arp 220 at 2.2 μm using the 200-inch telescope (Neugebauer, Matthews, and Scoville 1986). These data are shown in Figure 7 along with a scan of a star; the slit width was ~1.0 arcsec. Model fits with Gaussian profiles indicate that there is an unresolved source at the center with a limit to the full width at half maximum of 0.2 arcsec and a 2.2-μm flux of 8 mJy. Correcting for the reddening discussed above implies an intrinsic 2.2 μm-flux of 500-1000 mJy.

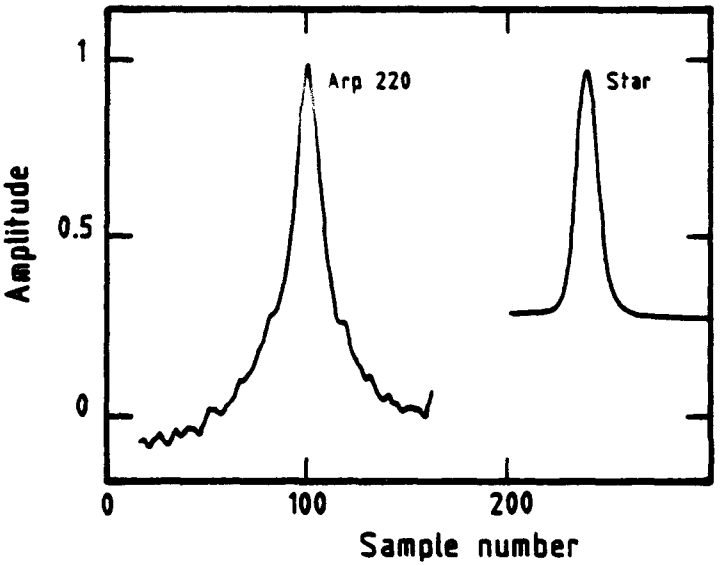

Figure 7: Slit scan at 2.2 μm from the 200-inch (Neugebauer, Matthews and Scoville 1986).

DISCUSSION

A. Thermal Infrared Component

The energy distribution shown in Figure 5 suggests that the emission mechanism in Arp 220 is thermal emission from dust (Soifer et al. 1984). If half of the 20-μm flux observed in the 3-arcsec beam is coming from a region whose diameter is equal to or less than 1.5 arcsec, then the brightness temperature at 20 μm is greater than or equal to 60 K. From the spectrum the color temperature is about 62 K (Soifer et al. 1984). Thus the optical depth in emission at 20 μm is close to one. This agrees well with the depth of the silicate absorption feature at 10 μm if $\tau_{9.7} \sim 2\ \tau_{18}$; such a relationship is observed in galactic sources (Forrest et al. 1979).

Because the source is thick at 20 μm and emits approximately like a blackbody at its 20-μm brightness temperature, it is very probable that much of the longer wavelength emission near the peak of the energy distribution is coming from a region $\theta \sim 1.5$ arcsec (~500 pc in diameter). Although radiative transfer effects could make the emission region at 50 μm somewhat larger than at 20 μm, it should be noted that this size is consistent with a 50-μm upper limit to the size of 8 arcsec measured by Joy et al. (1986) from the KAO and our 32-μm measurement with a 5.5-arcsec beam (Figure 4). The infrared radiation from

Arp 220 appears highly concentrated toward the center.

B. 1- to 3-μm Infrared Component

Both the 2.2-μm scan on the 200-inch telescope and our unpublished aperture studies from the IRTF, show that there is a component in the 1.65- to 3.8-μm range which may not be stellar; it is observed to be about 10 mJy at 2.2 μm or 500 mJy when corrected for reddening. If this component has a spectrum similar to the QSO 3C273, then its total luminosity would be of the order of 10^{12} $L_{\odot}$.

C. Collisional Energy

The present observations can be used to test the various luminosity sources in Arp 220 that have been suggested to date.

The model of Harwit et al. (1986) which predicts the amount of mechanical energy converted into infrared luminosity when two galaxies merge does not give a size for the emission region. Such a mechanism would not appear to naturally explain the emission size that we observe.

D. Star Formation

The hypotheses that a burst of star formation is the primary energy source in Arp 220 has a number of problems in light of the present set of observations.

One of the strongest arguments used to support star formation has been extended 10-μm emission (Rieke et al. 1985; Joseph and Wright 1985). The observation of extended 10-μm emission in Arp 220 appears to be in error. The surface density of star formation that is required in Arp 220 is 25 times larger than in M82; prior to IRAS, M82 had one of the highest densities of nuclear star formation. Is it reasonable to have such a rate of star formation in such a limited volume? Also a region of star formation in the central 500 pc of Arp 220 should have a corresponding 500-pc diameter radio source, but only two sources <50 pc diameter are seen at 6 cm.

Several parameters that are used to determine the amount of star formation have also been measured in Arp 220. These include the Brackett-α line strength which gives the number of ionizing photons (DePoy 1986), the CO line strength which gives an estimate of the interstellar material (Sanders and Mirabel 1985), and the 2.2-μm continuum which gives a limit on the number of M supergiants. In each case, if one scales from M82 using the total luminosity, one finds that the star formation indicators are a factor of 10 less than expected. There appears to be very little evidence for star formation producing more than 10% of the observed luminosity in Arp 220.

E. An Active Nucleus

There does appear to be a number of observations that suggest that a compact active nucleus is the primary luminosity source in Arp 220. It is the easiest and most natural way to explain the compact infrared morphology. This includes both the direct size measurement and the deep silicate absorption feature. It is also the easiest way to explain the compact radio sources, the

broad Brackett-α line, and the presence a point-like 2-μm source. The latter source, in fact, could contain enough energy to produce the observed infrared luminosity, if it is a power law source in the uv and x-ray region.

In summary, the present observations are consistent with the idea that more than 90% of the luminosity in Arp 220 originates from a radio quiet active nucleus.

SPECULATION

Based on Arp 220, MKN 231, NGC 6240, and NGC 1068 it appears that both a burst of star formation and an active nucleus are present in luminous IRAS galaxies. A burst of star formation produces $L \sim$ few x 10^{11} $L_\odot$. If $L \sim 10^{12}$ $L_\odot$, the dominant source of luminosity is a radio quiet active nucleus. Since interstellar material certainly feeds the star formation, it is natural to speculate that it also feeds the active nucleus.

ACKNOWLEDGMENTS

We thank D. DePoy, G. Neugebauer, K. Matthews, and N. Scoville for providing us with their unpublished data and N. Devereux and G. Hill for useful discussions. This work was supported under NSF grant AST 84-18197.

REFERENCES

DePoy, D. 1986, this conference.
Emerson, J. P., Clegg, P. E., Gee, G., Cunningham, C. T., Griffin, M. J., Brown, L. M. J., Robson, E. I., and Longmore, A. J. 1984, Nature, 311, 237.
Forrest, W. J., McCarthy, J. F., and Houck, J. R. 1979, Ap. J., 233, 611.
Harwit, M. O., Houck, J. R., Soifer, B. T., Palumbo, G. G. C. 1986, preprint and this conference.
Joseph, R. D. and Wright, G. S. 1985, M.N.R.A.S, 214, 87.
Joy, M., Lester, D. F., Harvey, P. M., Frueh, M. 1986, Ap. J., 307, 110.
Neugebauer, G., Matthews, K., and Scoville, N. 1986, private communication.
Norris, R. P. 1985, M.N.R.A.S., 216, 701.
Rieke, G. H., Cutri, R. M., Black, J. H., Kailey, W. F., McAlary, C. W., Lebofsky, M. J., and Elston, R. 1985, Ap. J., 290, 116.
Roche, P. F., Aitken, D. K., Smith, C. H., James, S. D. 1986, M.N.R.A.S., 218, 19P.
Schild, R. E. 1985, Sky and Telescope, 69, 24.
Sanders, D. B., and Mirabel, I. F. 1985, Ap. J. (Letters), 298, L31.
Soifer, B. T., et al. 1984, Ap. J., (Letters), 283, L1.
Soifer, B. T., Sanders, D. B., Neugebauer, G., Danielson, G. E., Lonsdale, C. J., Madore, B. F., and Persson, S. E. 1986, Ap. J. (Letters), 303, L41.

DISCUSSION

HARWIT:

The small size of Arp 220 is impressive. In the model we presented yesterday, we took 2 kpc diameter x 0.1 kpc thick disks colliding with each other in order to accommodate 10^{10} $M_\odot$ of H_2 at a normal molecular density of $n \sim 10^3 cm^{-3}$. We know that Arp 220 has that much gas from CO observations. Its compactness simply says densities are higher; but that does not affect the way such a model works. Higher densities tend to lead to higher luminosities for a given size source.

BECKLIN:

That is the nice thing about a theoretical model, it can always be fixed up to agree with observations.

UNGER:

The radio continuum emission at 18cm has an extent of about 1.5 arcsec, rather larger than at 6cm. You give an upper limit to the angular extent at 20μm of 1.5 arcsec - can you push this upper limit any further to say that the radio and 20μm emission aren't coincident?

BECKLIN:

That is unlikely, since if the source is thermal, it cannot be made smaller than 1.5 arcsec.

ELIAS:

Since you know the approximate size of the 20 micron source, and also that it has an optical depth of at least 1, what is the minimum amount of dust required?

BECKLIN:

About 10^7 $M_\odot$ in dust. If the dust to gas ratio is 0.01 by mass, this corresponds to 10^9 $M_\odot$ in gas, not too different from the amount estimated from the CO.

YOUNG:

Could you please elaborate on the point that the CO is too low by a factor of 5. Given the $M(H_2)$ and the dust temperature in Arp 220, the $L_{IR}/M(H_2)$ ratio is precisely what you expect for a galaxy with Arp 220's S_{60}/S_{100} ratio.

BECKLIN:

For a 'typical' star forming region there is a 'standard' $L_{IR}/M(H_2)$ ratio. If $L_{IR}/M(H_2)$ is larger than this ratio, physics demands that the dust temperature increase (unless $M_{dust}/M(H_2)$ were also larger). As pointed out by Phil Solomon, your relationship has physical significance, but not astrophysical significance. Astrophysically, Arp 220 has a larger $L_{IR}/M(H_2)$ ratio than 'standard' star forming galaxies.

TELESCO:

As you know, in NGC 1068 the 10μm emission comes from a very compact region, whereas the far-infrared luminosity originates from a much larger region. So you have to be careful in concluding that all the luminosity of Arp 220 comes from a region 500 pc in size.

BECKLIN:

I know very well that we have not proven a thing. However, unlike NGC 1068, Arp 220, from its spectrum, appears to have only one component, which is thick at 20μm.

SPATIAL DECONVOLUTION OF IRAS GALAXIES AT 60 UM

Frank J. Low
Steward Observatory
University of Arizona
Tucson, Arizona 85721

ABSTRACT

Using IRAS in a "slow scan" observing mode to increase the spatial sampling rate and a deconvolution analysis to increase the spatial resolution, several bright galaxies have been resolved at 60 um. Preliminary results for M 82, NGC 1068, NGC 3079 and NGC 2623 show partially resolved nuclei in the range 10 to 26 arcsec., full width at half maximum, and extended emission from 30 to 90 arcsec. from the center. In addition, the interacting system, Arp 82, along with Mark. 231 and Arp 220 were studied using the program "ADDSCAN" to average all available survey mode observations. The Arp 82 system is well resolved after deconvolution and its brighter component is extended; the two most luminous objects are not resolved with an upper limit of 15 arcsec. for Arp 220.

INTRODUCTION

In the design of the IRAS survey array the requirement for the highest possible spatial resolution was sacrificed in order to achieve wavelength and area coverage. However, a special observing mode was devised to utilize the best detector in each band coupled with the excellent pointing performance of the space craft to recover some of the lost resolution for bright sources. Unfortunately, only a few observations were obtained this way but most of those results are now available in preliminary form and are reported here since they provide important information on the size, structure and surface brightness of several bright infrared galaxies. It is also shown that many more results on the sizes and structures of extragalactic systems, especially those that are interacting, may be obtained by using a special method of processing for the survey data. After properly combining all available survey mode scans, each of which is under sampled, it is possible to recover enough information to construct a properly sampled scan of an object so that the powerful techniques of spatial deconvolution may be applied. This report includes very preliminary but interesting data obtained by this method and suggests that it should be applied to a much larger sample of galaxies.

THE "SLOW SCAN" PROGRAM

In order to deconvolve scans of bright objects to produce one dimensional images with resolution near the ultimate limit of the telescope system, three conditions must be met. First, the stability and reproducibility of the modulation transfer function, MTF, must be assured and it must be accurately measured using known point sources. Obviously, the MTF, or the point spread function, PSF, as it is often termed, should be fully optimized but this was not the case with IRAS for reasons explained above. Even though the IRAS detectors were too broad for best performance, if the second requirement of adequate sampling in the spatial domain were met, it should be possible to perform the deconvolution with success. This was accomplished for a limited set of observations by slowing the scan rate to one eighth of the normal survey rate, hence the name "slow scan". It was not possible to alter the set sampling rate

Carol J. Lonsdale Persson (Editor)
Star Formation in Galaxies

in the time domain. Fortunately, the redundant observations which make up the vast body of survey mode data offer another viable solution to this under sampling problem and that approach will be discussed below. The third requirement for successful deconvolution is that of high signal/noise, thus, only bright sources were included.

TABLE 1. SLOW SCAN PROGRAM OBJECTS

GALAXIES		STARS	POINT SOURCES
M 82	STAR BURST	alpha Lyr	alpha Boo
N 1068	SEYFERT	alpha PsA	beta Gru
N 2623	INTERACTING	beta Pic	Hygia
N 2992	INTERACTING		
N 3079	INTERACTING		

Table 1 lists the complete set of "slow scan" sources and Table 2 summarizes the relevant parameters of IRAS. The choice of extragalactic objects for this program was dictated by an interest in the size and structural features of the brightest infrared galaxies and by the idea that it should be possible to resolve a number of interacting systems and, thereby, shed light on the mechanism of the interaction as it promotes excess infrared emission. During the mission the Vega phenomenon was discovered, Aumann et al (1984), and Fred Gillett wisely included the brightest objects of that class in this program. At this time only the 60 um observations of galaxies will be discussed in more detail.

TABLE 2. IRAS PARAMETERS FOR DIFFERENT MODES OF OBSERVATION

L	L/D	DET. WIDTH	SAMPLING INTERVAL			
			SURVEY	STD. AO	SPE. AO	SLOW SCAN
(um)	(sec)	(sec)	(sec)	(sec)	(sec)	(sec)
12	4.3	45	14.4	7.2	3.6	1.8
25	8.9	45	14.4	7.2	3.6	1.8
60	21	90	29	14.4	7.3	3.6
100	35	180	58	29	14.4	7.3

Note: Detector lengths vary from 4.5 to 5 arcmin.

These observations consist of scans a few arcmin. in length which were repeated either 6 or 9 times by reversing the satellites' motion. In each band the best behaved detector in that band was used. It was found that non-linear and time dependent effects were present in the IRAS detectors which limited their performance in this application by more than the usual problem of signal/noise. For example, there are asymmetries in the scans which depend on the scan direction. By averaging the scans in both directions these effects largely cancel. It also is likely that "hysteresis" effects are present to some degree and serve as a degradation in the reproducibility of the MTF. The PSF also varies from detector to detector and as a function of cross-scan position for each detector. Normally each observation set was repeated at least once, providing both an opportunity to check for reproducibility and a second set of

data to average. Thus the minimum number of scans averaged for a single object was 6 and the maximum was 12. The raw data were position reconstructed at JPL by a process which effectively gives 1 arcsec pointing accuracy for these measurements, and they were then uniformly re-sampled at 2 arcsec. intervals. After baseline subtraction the scans were normalized to their peak values and they were aligned for coadding using the midpoints between their half amplitudes. After averaging all the scans from an observation, they were resampled at 6 arcsec. intervals before further analysis.

DECONVOLUTION TECHNIQUES

When the 60 um IRAS detector, of dimensions 1.5 arcmin by 4.7 arcmin, was scanned across a small area source, the measured profile or "measured source function", MSF, was expected to be a linear convolution of the "true source function", TSF, with the PSF. Thus the MSF may be expressed as:

$$MSF = PSF ** TSF$$

where the double asterisk stands for execution of the convolution integral. Then, in order to recover the TSF from this instrumental convolution there must be an inversion of the convolution, a procedure which may be symbolized as:

$$TSF = MSF // PSF.$$

In those cases where the diameter of the TSF is less than the diffraction limited width of the PSF, as is true for most of our objects here, it is necessary to invert the convolution integral by an iterative process of successive approximations. The result of a deconvolution, the TSF, is tested by comparing the actual MSF with the calculated convolution of that TSF with the PSF. The two deconvolution procedures used here are one-dimensional versions of the Richardson-Lucy algorithm, R-L, discussed by Heasley (1984) and the "maximum entropy method", MEM, of Frieden (1972) as described by Gull and Daniell (1978). As discussed in Appendix A, the R-L algorithm is simple and fast to execute on a small computer (IBM AT) and was modified from a program in Basic written by George Aumann at IPAC. The MEM algorithm was written in Fortran by Mike Cobb at Steward observatory and is run on a Data General MV 10000. Quite comparable results were obtained with both techniques. For these simple cases other methods may work as well.

An important check on the entire procedure is presented in Figure 1 where the four observations of two point sources, alpha Boo and beta Gru, which had been averaged together to make up the PSF, were individually deconvolved by running 1000 iterations of the R-L algorithm. The excellent agreement between these four independent observations is an indication that the technique gives highly reproducible results on bright sources and that results for the FWHM down to 9 arcsec are to be regarded with some degree of significance. This is about 0.3 of the " diffraction limit". In this sense IRAS has demonstrated the power of "super resolution" as a practical way of increasing the angular resolution of infrared telescopes. The reason that the observations of Hygia are not combined with the two stars is that it was observed with a different detector and is used here as the point source for the observations of NGC 1068.

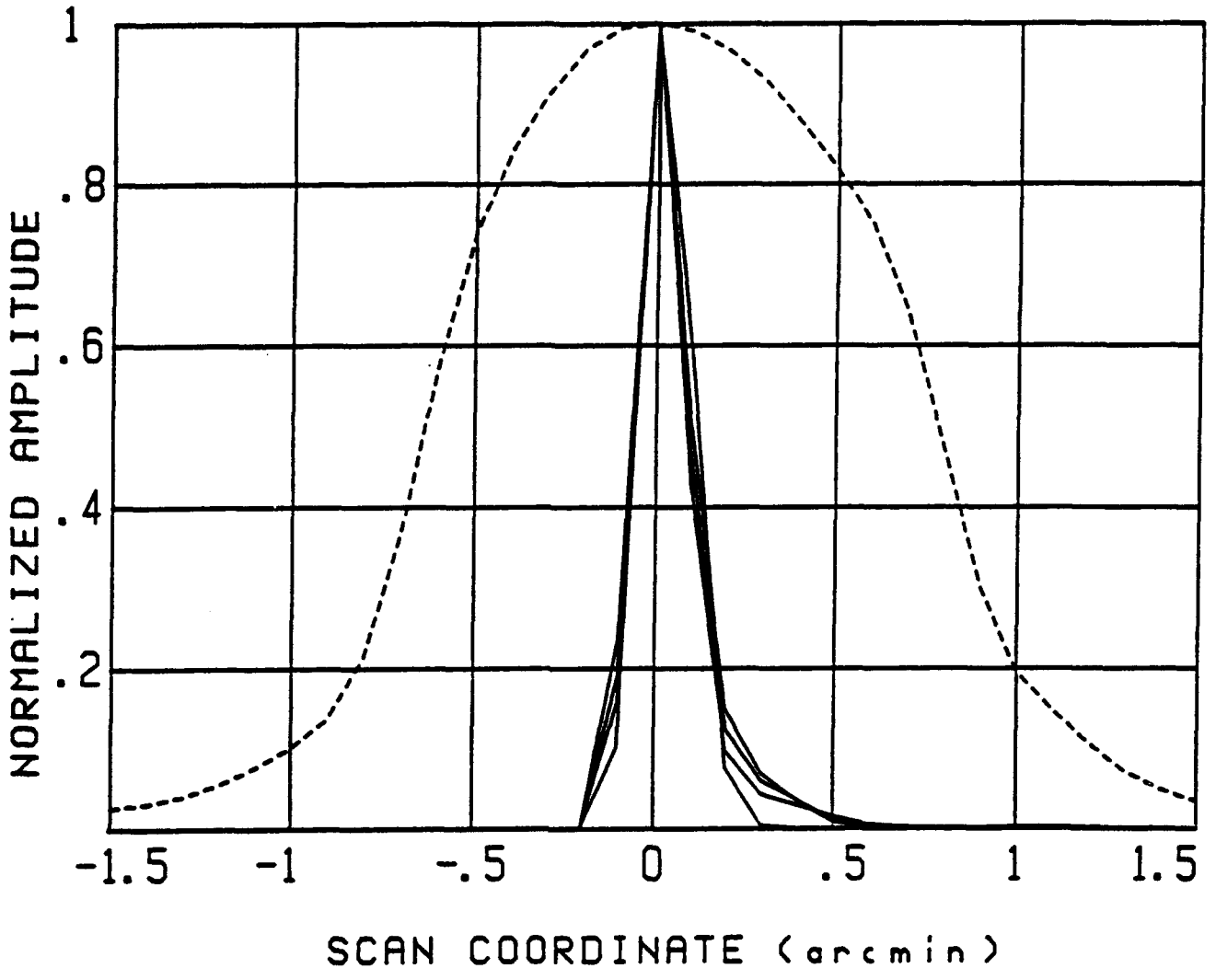

Figure 1. The dashed line represents the 60 micron PSF. The four solid lines represent the four independent observations of the two stars, alpha Boo and beta Gru, deconvolved individually with the PSF. North is to the left.

RESULTS FOR THE "SLOW SCAN" GALAXIES

Figure 2 shows the slow scan PSF, which is the unweighted average of the two point sources, and the MSF curve for M 82 obtained from the two independent observations. When reduced independently there is quite excellent agreement between the two M82 observations. Close examination of Figure 2 reveals the characteristic differences that exist between the point source and the extended source, with the MSF narrower at the top and wider at the base than the PSF. The FWHM for the PSF is 85 arcsec., slightly less than the geometrical width of the detector, as designed and built, of 90 arcsec. The two M 82 observations were taken on successive days and the scan direction was essentially perpendicular to the major axis of the galaxy. As discussed above the obvious asymmetries in these data are not fully understood and it is not yet clear why the extension on the north side of the galaxy appears greater than on the opposite side. Indeed,

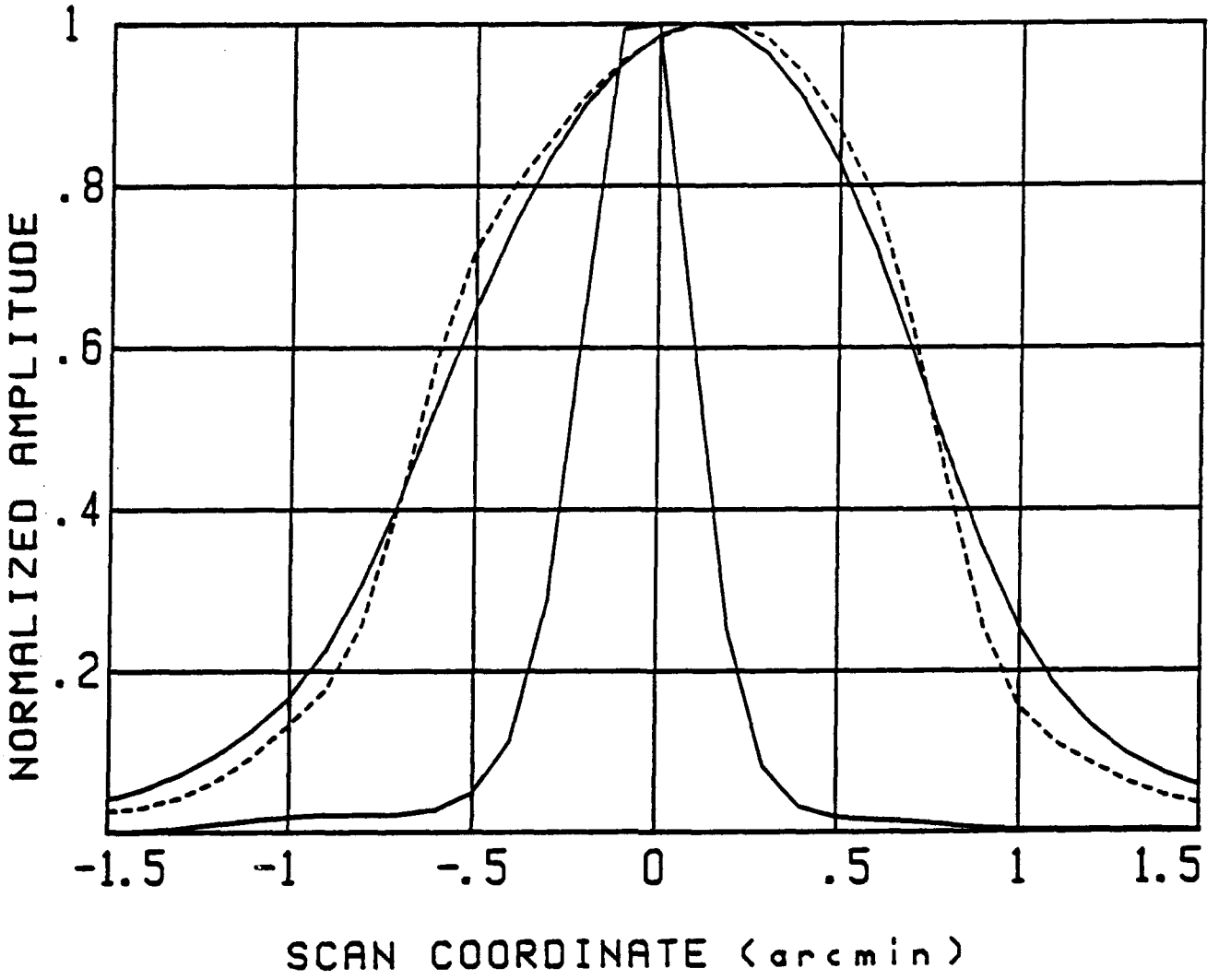

Figure 2. The dashed line represents the 60 micron PSF. The two solid lines represent the MSF and TSF for M 82. North is to the right.

further analysis is needed to determine whether the extended emission, more than one arcmin. from the nucleus, is a real property of the galaxy or a result of instrumental effects. Perhaps these effects are produced by the detector's non-linear behavior, although no satisfactory model has been found to explain this in detail. The measured FWHM is listed in Table 3. Although it is difficult to assess with certainty, the accuracy here would appear to be +/- 1 or 2 arcsec. These IRAS results, in so far as they can be directly compared, are consistent with published airborne measurements of Telesco and Harper (1980).

Figure 3 again shows the PSF for reference and includes the TSF results for NGC 2623, NGC 1068 and NGC 3079, in order of size. NGC 2623 is not clearly resolved but appears to be slightly larger than the PSF. NGC 1068, which was observed with a different detector, was deconvolved using Hygia as the point source; it too shows an asymmetry which is not yet understood from an observational point of view. NGC 1068 is the second brightest source observed

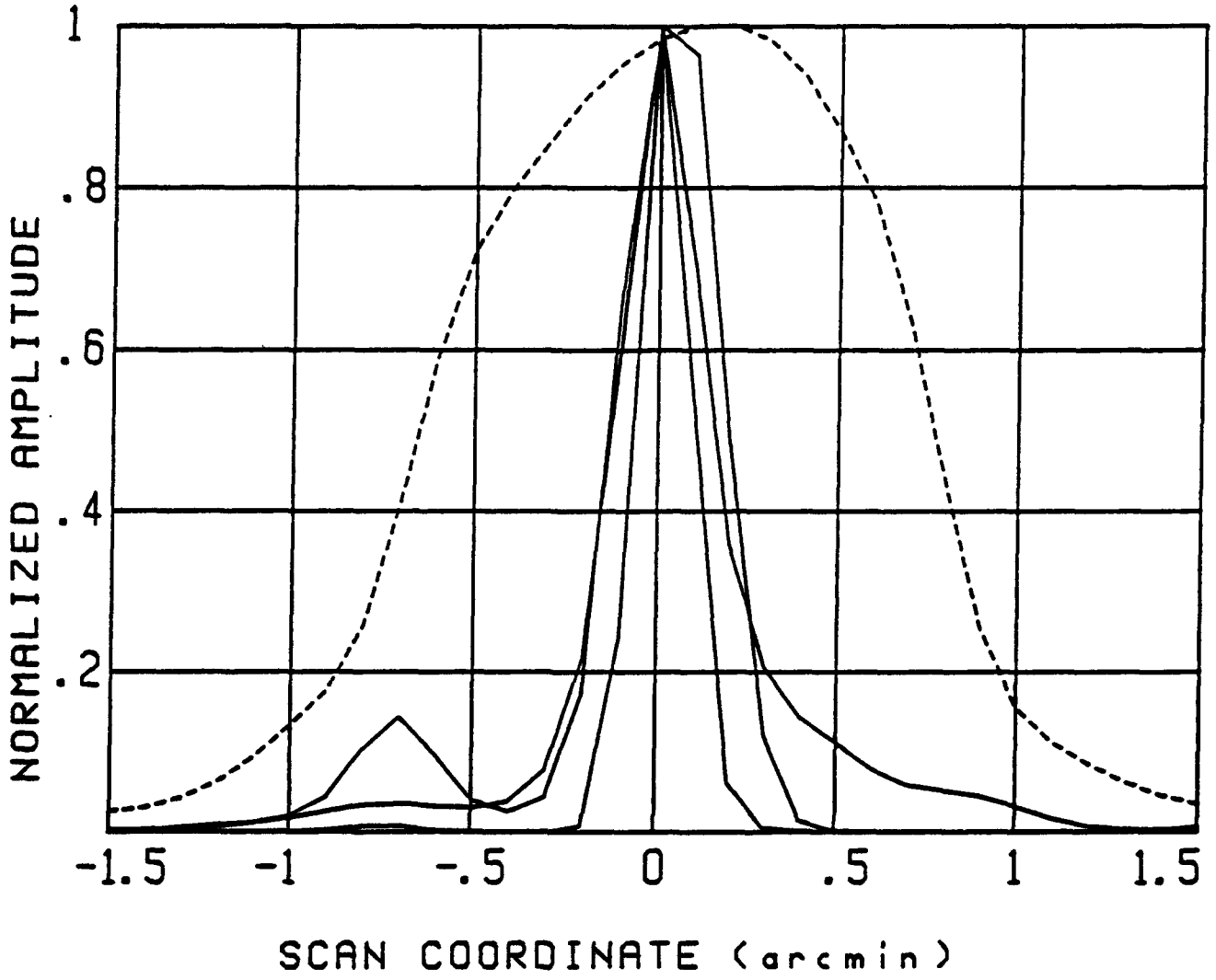

Figure 3. The dashed line represents the 60 micron PSF. The three solid lines represent the TSF for, starting with the smallest source, NGC 2623, NGC 1068 and NGC 3079, respectively. Note that NGC 1068 was deconvolved using Hygia as the PSF and only 500 iterations of R-L were used. North is to the right.

but Hygia is only slightly fainter and does not show any significant differences from the weaker point sources. At this stage of the analysis it is possible that these two galaxies, M 82 and NGC 1068, both have 60 um emission extending outward from their nuclei in an asymmetric fashion and in directions perpendicular to their major axes. Further analysis of these data and study of other IRAS observations are needed to confirm or deny this result. Fortunately, M 82 is so bright that it should be possible to use the Kuiper Airborne Observatory to test this unexplained result.

Finally, the well resolved TSF for NGC 3079 is a classic example of the "core-halo" structure with strong evidence for a second core only 40 arcsec from the brighter core. In this system the enhanced IR activity is spread over very large distances even though most of the infrared emission is, like that of other luminous infrared galaxies, concentrated near the bright nucleus. It

appears that we have an opportunity here to study both members of a strongly interacting pair of galaxies.

ADDSCAN OBSERVATIONS

As mentioned above, it is possible to combine the 8 or more redundant survey scans of a given source to construct a well sampled MSF despite the fact that each scan is badly under sampled. It can be seen in Table 2 that the interval between samples is 29 arcsec., almost 3 times the minimum requirement of 10.5 arcsec. to satisfy the Nyquist condition. The computer program used for this work was developed at IPAC and carries the name ADDSCAN. When the position reconstruction is carried out on a series of scans, the signal for each sample is placed in bins only 6 arcsec. apart. Because each scan samples at different locations on the sky, a median average of the 8 or more survey scans effectively fills the gaps by randomly distributing the information in the 6 arcsec. bins.

Using the same stars, alpha Boo and beta Gru, a PSF was constructed from ADDSCAN data and compared to the PSF from the slow scan observations. A slight degradation in the width and shape of the function is apparent but it still contains most of the spatial frequencies present in the slow scan PSF.

Using this new PSF and the MEM algorithm, three galaxies of interest were deconvolved and the results are shown in Figure 4 and in Table 3. The two most luminous objects, Mk 231 and Arp 220 are not resolved and the upper limits are listed in Table 3. The interacting pair, Arp 82, is well resolved, as shown in Figure 4, where it can also be seen that the brighter of these two galaxies is extended. Fortuitously, the scan direction is favorably placed, nearly along the direction of separation, and the measured separation in the IR is within 2 arcsec. of the optical separation. Again it is possible to resolve the two components of a strongly interacting system. The flux density of the brighter component is only 3 Jy. This means that a rather large number of galaxies, of order 2000, can be studied by this technique; of course only a fraction of the total sample will be resolved but this should add extensively to our knowledge of the size and surface brightness of IRAS galaxies.

Table 3. SUMMARY OF RESULTS

GALAXY	DISTANCE (Mpc)	DIAMETER (arcs.)	DIAMETER (Kpc)	EXTENT (arcs.)	EXTENT (Kpc)	FLUX DENSITY (Jy)	SCAN ANGLE (deg.)
M 82	3	24	0.35	150	2.2	1170	-37
N 1068	12	20	1.16	60	3.5	185	18
N 2623	53	<11	<3	--	--	31	-16
N 3079	18	18	1.6	>120	>10	35	-35
Arp 82	44	40	8.5	180	35	3	--
Arp 220	60	<15	<4.5	--	--	104	--
Mk 231	120	<26	<15	--	--	33	--

Note: DIAMETER = FWHM; EXTENT = the maximum extent of the TSF. Ho = 1 E 2 km/s/Mpc. Scan angle = position angle measured north of south in the clockwise direction.

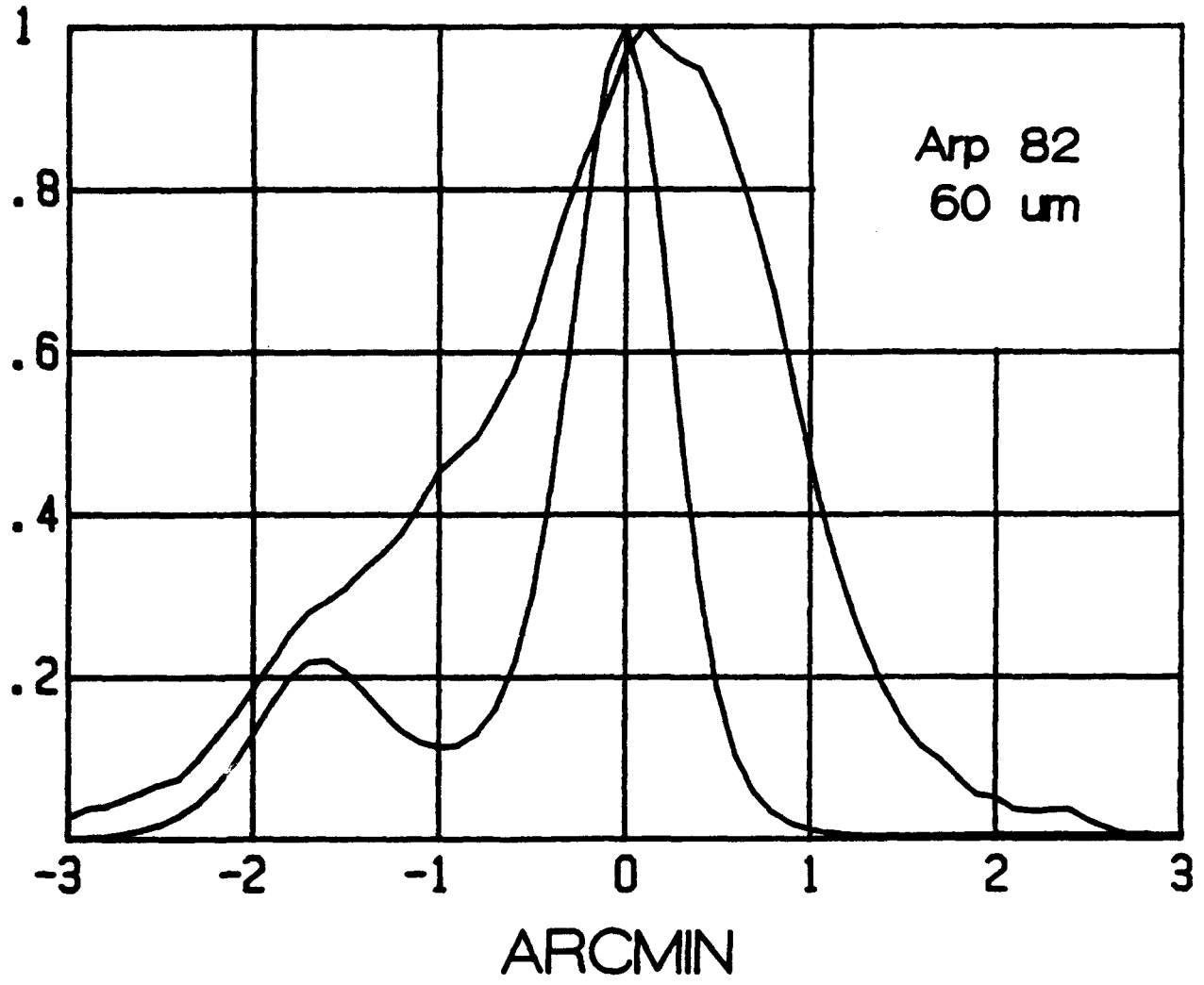

Figure 4. The result of combining all 60 micron survey scans of Arp 82 using "ADDSCAN" and the resulting deconvolution with a 60 micron PSF based on ADDSCAN observations of point sources.

APPENDIX A: The R-L Algorithm

The task of deconvolution is best accomplished by use of a so-called "nonlinear" method of successive approximations. As a practical matter the R-L algorithm offers a number of advantages including simplicity, speed of execution and predictability. Its use here is very much like that of Heasley (1984) except that it is limited to one dimension and the number of iterations used is very much larger. The following brief explanation may serve to remove any ambiguities about the method used, with the largest unsettled question the establishment of an objective criterion for determining the "proper" number of iterations.

Let:

PSF = P(x)
MSF = M(x)
TSF = T(x).

Then:

$$T(x)k = T(x)k\text{-}1[(M(x)/(T(x)k\text{-}1 \;**\; P(x)) \;**\; P(x)]$$

Where:

$$T(X)1 = M(x)[(M(x)/(M(x) \;**\; P(x)) \;**\; P(x)].$$

The data arrays, P(x) and M(x), must be carefully aligned or "phased" and the first iteration simply begins with M(x) as the initial "guess" at T(x); neither array can have zero or negative values. In executing each iteration the convolution integral, which consists of only eight lines of code in Basic, is used twice, first to form the quotient, T ** P, and then to smooth the ratio, M/(T ** P). Progress is rapid for the first few iterations and can be monitored by summing the absolute values of the differences between successive approximations. When tested on perfect data sets, such as the inversion of convolutions of simple functions, there is no tendency to oscillate or to overshoot and 1000 iterations are both productive and practical in terms of run time. The effects of various types of noise and/or distortion and of different degrees of oversampling are relevant to the results given here but are beyond the scope of this brief report.

ACKNOWLEDGMENTS

The author has benefited from many discussions with F. Gillett, G. Aumann and G. Neugebauer and he appreciates J. Good's expertise and help in extracting the data from the files at IPAC. This research was supported by the NASA IRAS Extended Mission at the Infrared Processing and Analysis Center (IPAC).

REFERENCES

Aumann, H. H., et al 1984, Ap. J. (Letters), 278, L23.
Gull, S. F., and Daniell, G. J. 1978, Nature, 272, 686.
Heasley, J. N. 1984, Pub. A. S. P., 96, 767.
Frieden, B. R. 1972, J. Opt. Soc. Am., 62, 511.
Telesco, C. M., Harper, D. A. 1980, Ap. J., 235, 392.

DISCUSSION

GEZARI:

What is the uncertainty in the deconvolved source diameters you presented?

LOW:

I believe the error is about ±2 arcsec on the diameter for the bright 'slow scan' observation at 60μm.

JOY:

On the 60μm graph of M82, you show that the point source profile is broader than the M82 profile over the central arcmin or so. How can it be concluded that M82 is resolved on any scale?

LOW:

The simplest way to assure yourself that the effect you mention is real is to consider the case of two step functions, each of width w, convolved together. The result in a triangle of base 2w and half width of w. Clearly, the upper half of the triangle is of width $< w$.

TELESCO:

M82 and NGC 1068 have already been resolved in the far-infrared on the Kuiper Airborne Observatory and these results are already in the literature. Are your requests consistent with those observations?

LOW:

At present, I believe the IRAS results and the KAO results are in agreement with respect to the sizes of the cores in M82 and NGC 1068. Because the KAO systems use chopping to subtract the background, I do not expect they will agree on the 'wings' of sources.

Star Formation Around Active Galactic Nuclei

William C. Keel
Sterrewacht Leiden
Leiden, The Netherlands

Emission-line images and high-dispersion optical spectra have been used to investigate star-forming regions in the vicinity of active galactic nuclei, including objects covering a wide range in luminosity of the central source. Rings of HII regions around the nucleus on 100-500 pc scales occur preferentially in galaxies with active nuclei, perhaps indicating a common response to gas flow in certain potential shapes. Multiaperture spectra of nearby HII-region nuclei shows many to have centrally condensed LINER-like components, suggesting that such configuration may be quite common.

The stellar population, and its history, may be probed in some of the most favorable cases. Observed stellar absorption features and crude starburst models imply ages $\sim 10^8$ years and $< 3\times10^7$ years for the starbursts around the nuclei of NGC 1068 and 7469, respectively. These are in rough concordance with lifetimes of the nuclear activity based on radio structures; if a direct link between nuclear activity and surrounding starbursts can be demonstrated, this could become an important way to study the history of individual objects. A somewhat different situation is found in Mkn 231, where the whole galaxy (merger?) exhibits optical colors and spectra suggesting either an IMF deficient in OB stars or a sudden turnoff of star formation, on scales so large that it is unlikely the nucleus is directly responsible. There thus appears to be evidence of at least two kinds of links between AGN and star formation.

Active galactic nuclei (Seyfert nuclei and their relatives, in which nonstellar sources of energy are important) and intense star formation can both deliver substantial amounts of energy to the vicinity of a galactic nucleus. Many luminous nuclei have energetics dominated by one of these mechanisms, but detailed observations show that some have a mixture. Seeing both phenomena at once raises several interesting questions:
1) Is this a general property of some kinds of nuclei? How many AGNs have surrounding starbursts, and vice versa?
2) As in 1), how many undiscovered AGNs or starbursts are hidden by a more luminous instance of the other?
3) Does one cause the other, and by what means, or do both reflect common influences such as potential-well shape or level of gas flow?
4) Can surrounding star formation tell us anything about the central active nuclei, such as lifetimes, kinetic energy output, or mechanical disturbance of the ISM?

These are important, and perhaps crucial, points in our understanding of activity and star formation in galactic nuclei. Unfortunately, the

Carol J. Lonsdale Persson (Editor)
Star Formation in Galaxies

observational ways of addressing them are as yet not well formulated. I report here some preliminary studies aimed at clarifying at least the issues involved in study of the relationships between stellar and nonstellar excitement in galactic nuclei.

HII Rings and Active Nuclei

Many spirals, particularly of intermediate Hubble type, show substructures in the nuclear region often termed "hot spots" (e.g. Sersic and Pastoriza 1967). A large fraction of these show a very regular morphology upon more detailed study: a nucleus with late-type (old) stellar population and Seyfert or LINER emission spectrum, surrounded by an elliptical ring of luminous giant HII regions. Such rings may be associated with inner resonances in the stellar orbits (see, for example, Sanders and Huntley 1976, Sanders and Tubbs 1980). Relatively few such objects are known; at the redshifts of even most Markarian Seyferts, they would be blended with the nucleus in ground-based observations. Galaxies in which this morphology is well-established are listed in Table 1 (after Hummel, van der Hulst, and Keel 1986). Note that only one of these (NGC 5427) does not appear in the lists of Sersic and Pastoriza. Typical appearances of these are illustrated in Figure 1, by an Hα image of the nucleus of NGC 5248 (from the KPNO 2.1-m with TI CCD).

TABLE 1

Galactic Nuclei with HII Rings

NGC	Ring Diameter (kpc)	Nucleus	Hubble Type
1097	1.1	LINER/Sy2	SBb
2297	0.4	LINER?	SABc
3351	0.4	LINER	SBb
4303	0.3	LINER/Sy2	SABbc
4321	1.4	LINER/Sy2	SABbc
5236	0.3	HII	SABc
5248	0.7	LINER	SABbc
5427	1.9	Sy2	Sc

From the data summarized in Table 1, it appears that galaxies with nuclear rings of HII regions are more likely to have indicators of nuclear activity (Seyfert or LINER spectra) than the norm for the Hubble types involved.[1] Particularly noteworthy is the presence of such activity even in

[1]The LINERS here are not the "blue LINERS" that are often associated with starbursts (Rieke, these proceedings); the nuclei here (except the HII nucleus of M83) show no real evidence of current star formation inside the HII rings.

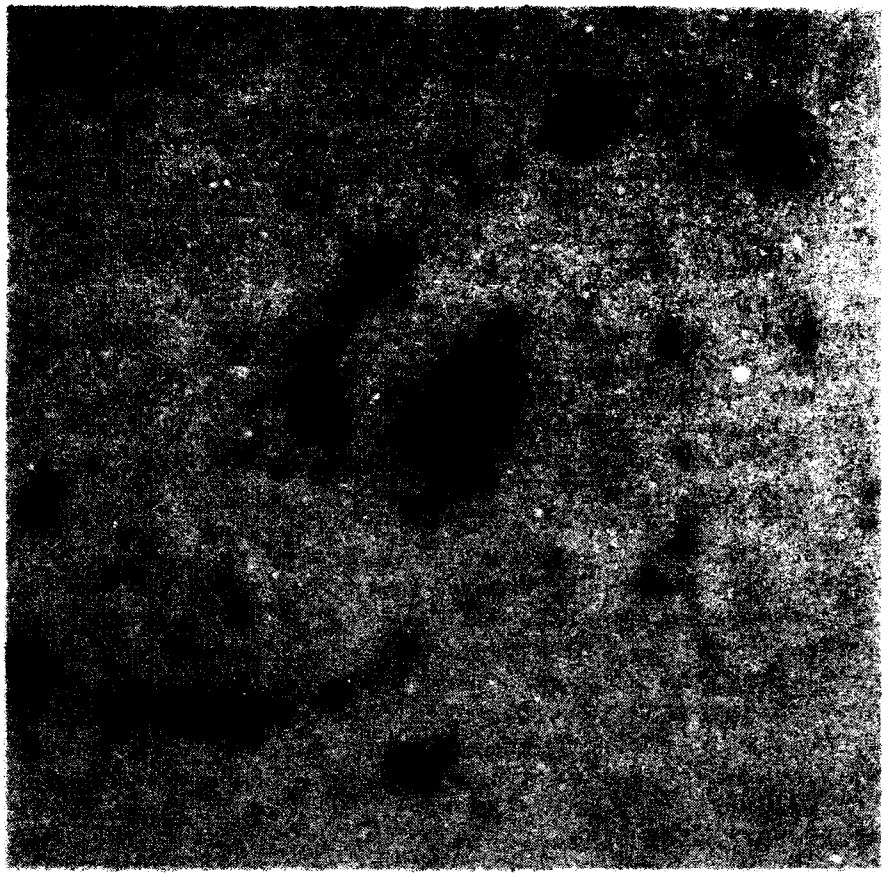

Figure 1. Continuum-subtracted Hα + [NII] image of the nuclear region of NGC 5248. The ring of HII regions around the actual nucleus is evident. The field is 160" square, with north at the top.

Sc galaxies, in which it is rare among magnitude-limited samples (e.g. Keel 1983). The available sample clearly points to some kind of connection between HII rings and nuclear activity, both perhaps formed by certain kinds of potential shapes that induce radial gas motion. Complete surveys of the incidence of such rings and properties of the associated nuclei will be important, but can be complicated by several effects. The resolution effect mentioned above means that present data would have difficulty finding such configurations at the distances characteristic of very luminous Seyferts; in such cases, spectroscopic identification of an HII-region component or use of IR colors to infer a star forming region might be possible, but difficult due to to the great luminosity of the nucleus. Second, in such very active objects, some of the signatures of HII rings can be lost. In the type 2 Seyfert NGC 5728 (M. M. Phillips et al., private communication) there is dynamical evidence of a gas ring, but its ionization is dominated by radiation from the nucleus. Very detailed study is needed for such objects; more HII rings will likely emerge from detailed studies of individual active nuclei.

Histories of Star-Forming Regions around Seyfert Nuclei

The presence of "starburst disks" - regions of intense star formation on scales of a few kiloparsecs is well established for a few nearby Seyferts. They may be recognized from emission-line properties (Morris et al. 1985, Alloin et al. 1983), infrared mapping (Cutri et al. 1984), and radio-source morphology (A. S. Wilson, these proceedings). The properties of these regions are of interest as possible probes of the history of the AGN itself, if it can be established that the onset of extensive star formation and the turn-on of the nucleus are roughly contemporaneous (admittedly a tall order, and a large question for the future). To explore the possibilities of learning the age and history of these "starburst disks", spectra of ~1Å resolution have been obtained for the Hα, Hβ, [OIII] λ5007 regions in nuclei showing a range of activity and some evidence for surrounding star formation. The observations used the IPCS at the 2.5-m Isaac Newton Telescope on La Palma and CCDs at the INT and the Kitt Peak 4-m.

Figure 2 shows the Hβ-λ5007 regions approximately 16" SW of the nucleus of NGC 1068. This region has been studied in the UV by Weedman and Huenemoerder (1985), and shows HII-region emission in the images by Balick and Heckman (1985); a discrete near-IR source here also suggests a local clump of star formation (Telesco et al. 1984). The present data shows, in addition to narrow Hβ emission from the HII region and broad [OIII] associated with the nucleus (see the kinematic analysis by Alloin et al. 1983), stellar absorption features of Hβ, MgI, Hγ, and the G-band. These features, and the Balmer emission diagnostic of the stellar Lyman continuum, have very different weightings with stellar age in an aging burst, and for a given burst model can serve as age or history diagnostics.

To illustrate this approach, consider a simple model of star formation with a Salpeter IMF turning on at some time and retaining a constant star-formation rate thereafter. INT blue spectra of the circumnuclear regions of NGC 1068 and 7469 may be roughly compared with such a model. In NGC 1068, Hβ and MgI ~ λ5175 are seen with equivalent widths of 7 and 3 Å, while neither is detected in NGC 7469 at a level ~2 Å. These data imply ages of $\sim 10^8$ and $< 10^7$ years, respectively. These are at least consistent with timescales needed to produce the extended ratio excess in each case (following de Bruyn and Wilson 1978). More detailed work, including more objects, emission-line results, and varying star forming histories, is in progress.

Star Formation in Markarian 231

The nucleus of Mkn 231 shows a number of unusual properties, including broad, blueshifted absorption, strong continuum reddening, and very strong IR emission (Adams 1972, Boksenberg et al. 1977, Rieke and Low 1972). The surrounding galaxy is also peculiar in morphology and spectroscopic properties and may be a nearby example of the conditions seen in, for example, 3C 48 (Boroson and Oke 1982). This section describes a study of the host galaxy of Mkn 231, conducted in collaboration with D. Hamilton (CTIO).

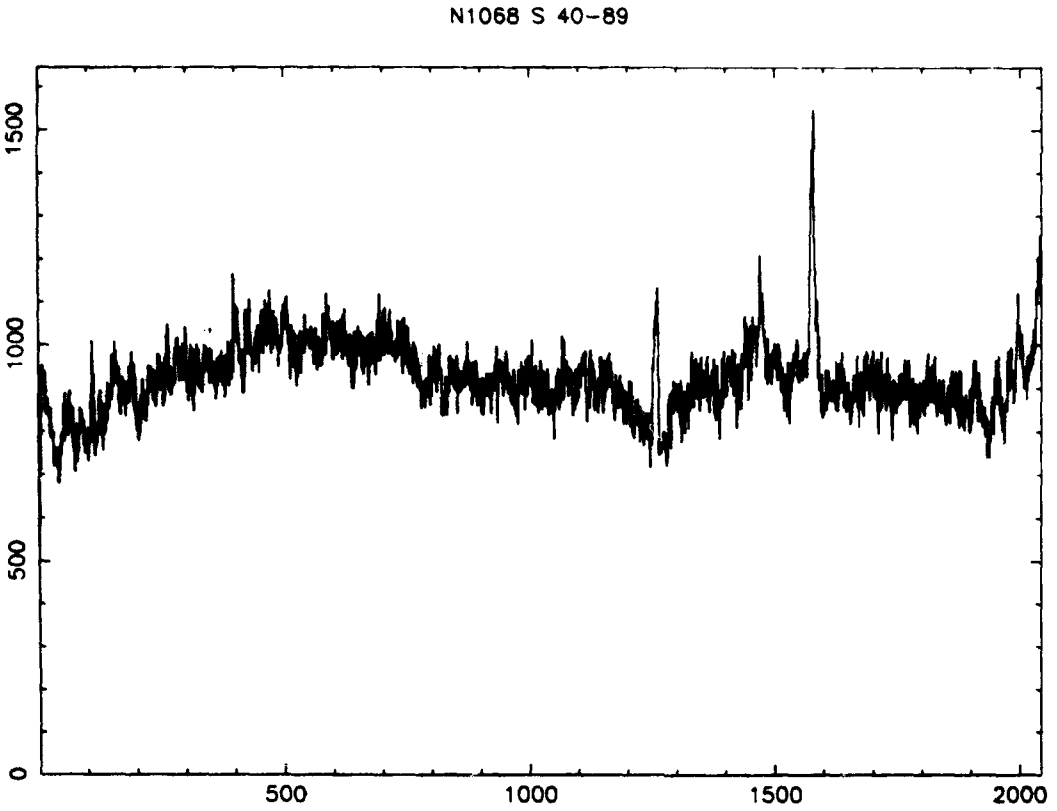

Figure 2. INT + IPCS spectrum in the 4300-5200 Å range, for the "starburst disk" of NGC 1068 16" SW of the nucleus. Stellar absorption of Hβ (a broad feature underlying the narrow emission line) is strong; other identifiable absorption lines include MgI, Hγ, and the G-band. [OIII] emission redward (to the right) of Hβ, is mostly due to the effects of the Seyfert nucleus.

Multi-color imaging shows the galaxy to be very asymmetric, with smooth amorphous condensations and, at very faint levels, a pair of probable tidal tails. A large region of nearly constant surface brightness west of the nucleus offers a good opportunity to study the stellar population. A low-resolution spectrum of this region was obtained with the Cryogenic Camera at the KPNO 4-m, and shows relatively strong Hβ as well as MgI and MgH absorption, indicating a large contribution from stars of types A and F. In itself, this indicates active star formation within the last ~5 x 10^8 years. However, the current star formation rate must be much smaller, as deduced from the lack of Hα attributable to HII regions in the disk and lack of direct observation of such regions in Hα images. Using the precepts of Kennicutt (1983), the SFR has dropped more than fourfold in this period.

It would be remarkable for a whole galaxy (of extent > 30 kpc) to turn off star formation everywhere in this time. The alternative is equally

remarkable, an IMF deficient in high mass stars. This is just the opposite of the case usually inferred for starburst galaxies. The stellar population here does appear similar to those in a few other active galaxies such as 3C 48 and 3C 459 (Miller 1981). The physics of star formation during galaxy mergers could provide important clues to what is seen here; Mkn 231 shows a pair of tails, and most giant radio galaxies, including 3C 459, show morphological or kinematic evidence of being merger products (Heckman et al. 1986). Mkn 231, at least, raises the possibility that conditions in some merging galaxies may favor formation of low-mass stars. If so, some interpretation of observations of many interacting and post-interaction systems would be much more complicated than previously thought.

Future Directions

The most pressing needs in understanding star formation around active nuclei are solid indications of how often, and at what levels, it occurs, and a detailed study of representative objects that could provide clues to the physical operation there. Schemes exist that could have a link between the phenomena going in either direction, or with both as a result of host galaxy properties. Weedman (1983) has considered the fate of condensed stellar remnants from a starburst; if they can reach a compact enough configuration, relativistic effects (Shapiro and Teukolsky 1985) could rapidly produce a single massive central object. Weedman notes that the process might be so rapid that both would be seen simultaneously.

In the other direction, active nuclei could induce surrounding star formations through shocks, perhaps via jets. There is clear evidence of jet-induced star formation on larger scales, in Cen A and Minkowski's Object (van Breugel et al. 1985, Brodie, Bowyer and McCarthy 1985, Graham and Price 1981). Finally as discussed for HII regions above, some kinds of potential might efficiently funnel gas both into kiloparsec and parsec scales, fuelling star formation and nuclear activity at the same time.

Surveys for extranuclear star formations might take several forms. IR colors (Rodriguez-Espinosa et al., these proceedings) are relatively unbiased and reddening-free, but from the IRAS database it is not clear that the star formation is on a small enough scale to be connected with the nuclei. Hα studies (imaging or slit spectroscopy) complement IR studies in spatial resolution, but can be of limited use when the nucleus is so luminous as to dominate the gas ionization at relevent distances within the disks. Finally, the work of Wilson et al. (these proceedings) suggests that radio morphology may be an additional useful diagnostic. All these kinds of surveys should be pursued.

More detailed studies of individual objects are in part available, and will continue as byproducts of studies of active nuclei.

Observations described here have been obtained at the Isaac Newton Telescope, now happily ensconced on the island of La Palma, and at Kitt Peak National Observatory and Cerro Tololo InterAmerican Observatory, National

Optical Astronomy Observatories, operated by A.U.R.A. under contract with the National Science Foundation. I am especially grateful to Susan Davidson for helping produce this manuscript on time.

REFERENCES

Adams, T. F. 1972, Ap. J. (Lett.) **176**, L1.
Alloin, D., Pelat, D., Boksenberg, A., and Sargent, W. L. W. 1983, Ap. J. **275**, 493.
Balick, B. and Heckman, T. 1985, Astr. J. **90**, 197.
Boksenberg, A., Carswell, R. F., Allen, D. A., Fosbury, R. A. E., Penston, M. V. and Sargent, W. L. W. 1977, M.N.R.A.S., **178**, 451.
Boroson, T. A. and Oke, J. B. 1982, Nature, **296**, 397.
Brodie, J. P., Bowyer, S. and McCarthy, P. 1985, Ap. J. (Lett.) **293**, L59.
Cutri, R. M., Rudy, R. J., Rieke, G. H., Tokanuga, A. T. and Willner, S. P. 1984, Ap. J., **280**, 521.
de Bruyn, A. G. and Wilson, A. J. 1978, Astr. Ap., **64**, 433.
Graham, J. A. and Price, R. M. 1981, Ap. J., **247**, 813.
Heckman, T. M., Smith, E. P., Baum, S. A., van Breugel, W. J. M., Miley, G. K., Illingworth, G. D., Bothun, G. D., and Balick, B. 1986, Ap. J. (in press).
Hummel, G., van der Hulst, J. M., and Keel, W. C. 1986, Astr. Ap. (submitted).
Keel, W. C. 1983, Ap. J. Suppl. **52**, 229.
Kennicutt, R. C., Jr., 1983, Ap. J., **272**, 54.
Miller, J. S. 1981, P.A.S.P., **93**, 681.
Morris, S., Ward, M., Whittle, M., Wilson, A. S., and Taylor, K. 1985, M.N.R.A.S., **216**, 193.
Rieke, G. H. and Low, F. J. 1972, Ap. J. (Lett.), **176**, L95.
Sanders, R. H. and Huntley, J. M. 1976, Ap. J., **209**, 53.
Sanders, R. H. and Tubbs, A. D. 1980, Ap. J., **235**, 803.
Sersic, J. L. and Pastoriza, M. 1967, P.A.S.P., **79**, 152.
Shapiro, S. L. and Teukolsky, S. A. 1985, Ap. J., **298**, 58.
Telesco, C. M., Becklin, E. E., Wynn-Williams, C. G. and Harper, D. A. 1984, Ap. J., **282**, 427.
van Breugel, W., Filippenko, A. V., Heckman, T. and Miley, G. 1985, Ap. J., **293**, 83.
Weedman, D. W. 1983, Ap. J., **266**, 479.
Weedman, D. W. and Huenemoerder, D. P. 1985, Ap. J., **291**, 72.

DISCUSSION

WILSON:

In our study of the circum-nuclear starburst in NGC 7469 (to be published in *Ap. J.* Nov. 1986), we do find evidence of Hβ absorption in some locations. Presumably, this would make the starburst somewhat older than you estimated.

KEEL:

This emphasizes an important issue in the study of these systems - spatial resolution and averaging. My data so far pertain only to limited slices through the circum-nuclear regions; since present star formation is obviously patchy, stars too young to have completely diffused will also have more or less 'lumpy' distributions. A more proper observational approach would involve mapping absorption features at many positions around the nuclei.

STAR FORMATION IN SEYFERT GALAXIES

J.M. Rodriguez Espinosa
European Southern Observatory,
Garching bei München, F.R.G.

Richard J. Rudy
Space Science Laboratory,
The Aerospace Corporation, Los Angeles

and

Barbara Jones
Center for Astrophysics and Space Science,
University of California, San Diego

An analysis of the IRAS data for a sample of classical (optically selected) Seyfert galaxies is presented. The IRAS fluxes at 25 μm, 60 μm, and 100 μm are found to be uncorrelated or only very weakly correlated with the UV/Optical continuum flux and the near and mid IR flux at 3.5 and 10 μm. To investigate the possibility that star formation accounts for the far IR flux, the IRAS measurements for the Seyfert galaxies are compared to IRAS observations of a sample of normal spiral galaxies, and a sample of Starburst galaxies. It is shown that the far IR luminosities and far IR colors of Seyfert galaxies are indistinguishable from those of the Starburst galaxies. Besides, normal galaxies are an order of magnitude less luminous than both the Seyfert and the Starburst galaxies. This indicates that star formation produces the bulk of the far-infrared emission in Seyfert galaxies.

1. INTRODUCTION

For quite a few years now, it has been known that Seyfert galaxies are strong near and far-IR sources (Rieke 1978). In this classical paper, Rieke also inferred that Seyfert galaxies might also be strong far-IR sources, and moreover, that a large fraction of their total luminosities is emitted in the infrared at wavelengths longer than ~30 μm. However direct ground-based observations of the far-IR output of these sources was not feasible due to the opacity of the atmosphere. In some instances balloon and aircraft observations of a few bright objects were carried out. That is the case for NGC 1068 (Telesco, Harper and Loewenstein 1976; Telesco and Harper 1980), NGC 4151 (Rieke and Lebofsky 1979) and NGC 4051 (Smith et al. 1983). It is interesting that in all these cases the far-IR output was interpreted as arising from emission by warm dust heated in regions of star formation. However it is only in the post-IRAS era that the far-IR emission from larger samples of objects can be studied.

Concerning Seyfert galaxies the first question to be asked is: what is the role of the active nucleus in the far-IR? It is well known that the nucleus is responsible for most of the properties of Seyfert galaxies. However, very

Carol J. Lonsdale Persson (Editor)
Star Formation in Galaxies

recently we (Rodriguez Espinosa et al. 1986; Paper I) have concluded that the far-IR emission from the active nucleus does not account for the bulk of the emission from Seyfert galaxies observed by IRAS. Our claim was based on two main points:

i) the far-IR emission originates in an extended region.

ii) in most Seyfert galaxies the non-thermal UV-optical continuum luminosity is not large enough to account for the far-IR emission via dust-reradiation of the UV-optical continuum.

Here we would like to explore further the relationship between the nucleus and the far-IR properties of Seyfert galaxies.

2. THE DATA

For our study we have considered a sample of optically selected Seyferts consisting primarily of those galaxies in Rieke (1978) and Yee (1980), most of which are overlapping. The 3.5 μm and 10 μm data are from Rieke while the UV data are from Yee. We have increased the sample with objects measured in the IR by Rudy et al. (1982) and Rudy and Rodriguez Espinosa (1985). In total there are 96 objects in the sample. Of these, 58 were detected by IRAS, and 2 objects (Mrk 304 and NGC 4151) were not observed. As for the objects not detected most of them are at redshifts such that more likely their IR emission is below the IRAS sensitivity limits.

3. RESULTS

Correlation analysis has been used to explore possible relationships of the far-IR emission of Seyfert galaxies with the active nucleus. The active nucleus is considered responsible for the UV-optical continuum emission (Weedman 1977) and for the near (3.5 μm) and mid-infrared (10 μm) emission (Rieke 1978; McAlary, McLaren and Crabtree 1979). These have been correlated with the IRAS data at 25, 60 and 100 μm with the following results:

i) Only the 25 μm emission correlates to a high degree of confidence with the 3.5 μm and 10 μm emission, indicating that whatever mechanism powers the near and mid-IR emission is also responsible for a large part of the emission from these objects at 25 μm.

ii) The UV-optical continuum emission from Seyfert galaxies does not correlate with the far-IR emission detected by IRAS.

iii) The 60 and 100 μm IRAS emission from Seyfert galaxies is uncorrelated or only weakly correlated with the 3.5 μm and 10 μm infrared emission from these sources, suggesting a weak or, at most, indirect relation between the mechanism producing the near and mid-IR emission and that responsible for the far-IR fluxes detected by IRAS.

These results underscore the idea proposed in Paper I that a large fraction of the far-IR emission from Seyfert galaxies originates in a source other than the active nucleus (see also Neugebauer, Soifer and Miley 1985).

4. STARBURSTS IN SEYFERT GALAXIES

To investigate the possibility that star formation accounts for a large fraction of the far-IR output from Seyfert galaxies, we have compared the IRAS

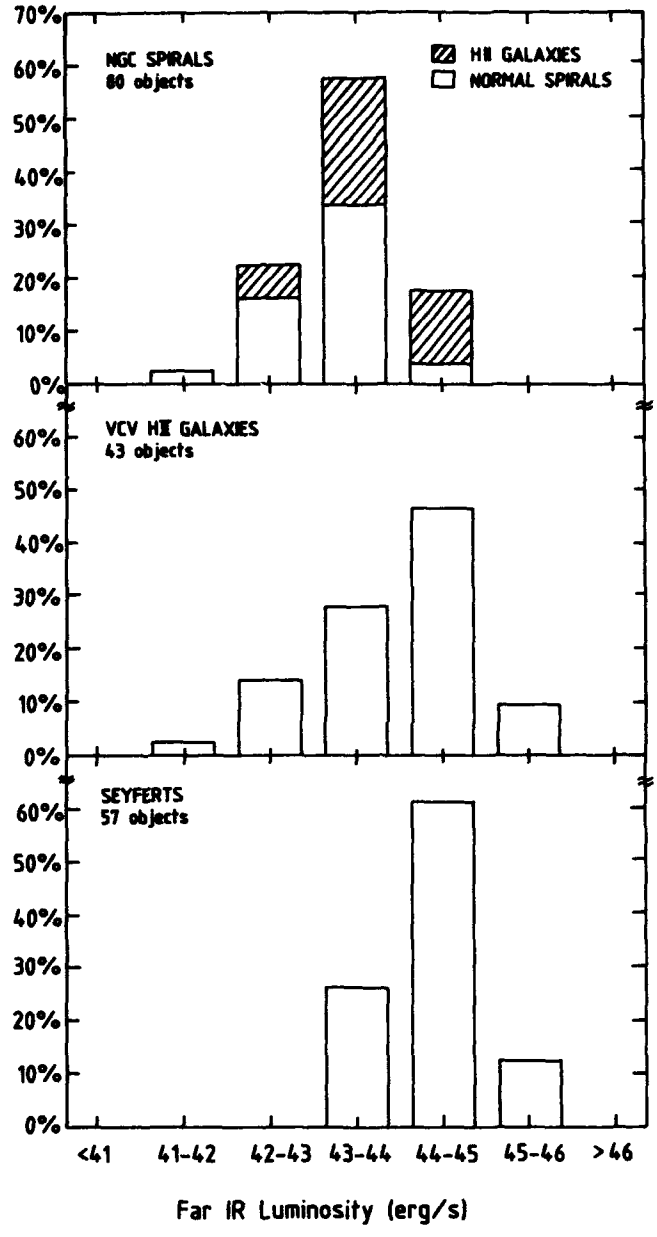

Fig. 1. The far-IR luminosity distribution of NGC spiral galaxies (top), Starburst galaxies (Véron-Cetty and Véron HII galaxies; middle), and Seyfert galaxies (bottom). In the top histogram those NGC spirals undergoing starbursts are represented by the shaded area. Note that the Seyfert galaxies are, on the average, an order of magnitude brighter than normal NGC spirals, and comparable in far-IR luminosity to the starburst galaxies.

measurements of these objects to the IRAS observations of both a sample of normal spiral galaxies and a sample of HII region galaxies. The samples of spiral galaxies and HII galaxies are those of Keel (1983) and Véron-Cetty and Véron (1984). An examination of the far-IR (IRAS) luminosity distribution of the spiral galaxies shows that on average, in the far-IR, spiral galaxies are an order of magnitude less luminous than Seyfert galaxies (Fig. 1). Moreover, the majority of the spiral galaxies whose far-IR luminosity is comparable to the far-IR luminosity of the Seyfert galaxies are what Keel (1983) described as galaxies having HII region-like spectra.

The central diagram of Figure 1 shows the luminosity distribution of the Véron-Cetty and Véron (1984) HII region galaxies. Note the striking similarity with the far-IR luminosity distribution of the Seyfert galaxies (Fig. 1, bottom).

The far-IR spectral indices for the Seyfert and the Starburst (HII) galaxies have also been examined. Figures 2 and 3 show the 60 through 100 μm,

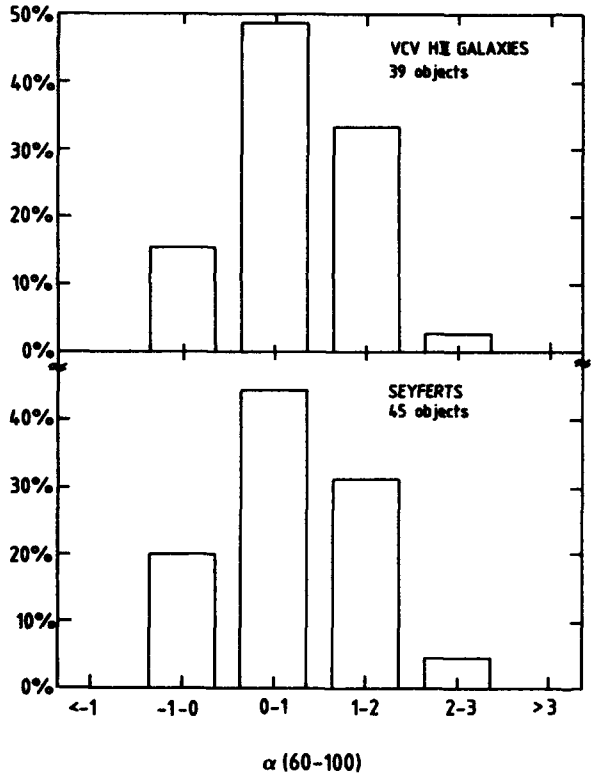

Fig. 2. The 60 through 100 μm spectral index distribution for the starburst objects (top) and the Seyfert galaxies (bottom). Note again the very clear similarity of these two distributions.

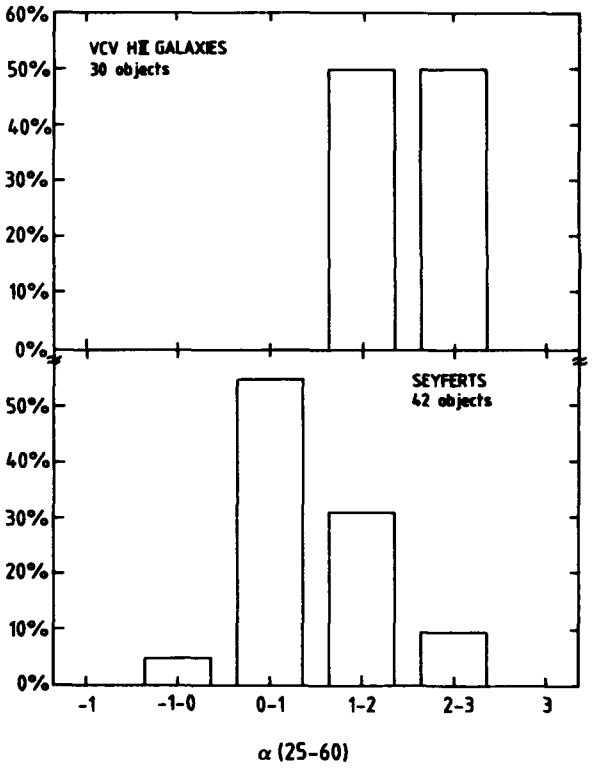

Fig. 3. The 25 through 60 μm spectral index distribution for the starburst objects (top) and the Seyfert galaxies (bottom). The Seyfert galaxies show much bluer spectral indices due to the emission from the active nucleus at the shorter wavelength.

α(60-100), and the 25 through 60 μm, α(25-60), spectral index distributions for the two types of galaxies. Note the great similarity between the α(60-100) spectral indices (Fig. 2) of both the Seyfert and the Starburst galaxies. Note at the same time the large dispersion in the values of α(60-100) for both the Seyfert and the Starburst galaxies. This dispersion can be explained by assuming that most of the 60 and 100 μm emission is due to radiation by warm dust at temperatures ranging from about 35 to 75°K (λ^{-1} emissivity). Furthermore, these temperatures are typical of dust heated by young stars in regions of star formation (e.g. Harper 1974).

Coming now to the 25 through 60 μm spectral indices we find much bluer indices in the Seyfert galaxies than in the Starburst galaxies. But this is not surprising since we would expect the strong emission from the active nucleus to reveal its presence at the shorter (25 μm) wavelength. The Starburst galaxies on the contrary show a very steep rise at the short wavelength (Fig. 3). The large dispersion seen in the α(25-60) spectral indices of the Seyfert galaxies is probably related to variations in the relative contributions of the active nucleus and the Starburst component at these two IRAS bands.

5. CONCLUSION

From the high similarity between the far-IR properties (luminosity and spectral index) of Seyfert and Starburst galaxies we conclude that a large fraction of the emission at far-IR wavelengths of Seyfert galaxies is produced by star formation episodes in regions around the active nucleus. Besides, the high incidence of large far-IR output among the Seyfert population suggests the existence of a causal link between the active nucleus and the presence of bursts of star formation.

REFERENCES

Harper, D.A. 1974, Ap.J., 192, 557.
Keel, W.C. 1983, Ap.J. Suppl., 52, 229.
McAlary, C.W., McLaren, R.A., and Crabtree, D.R. 1979, Ap.J., 234, 471.
Neugebauer, G., Soifer, B.T., and Miley, G.K. 1985, Ap.J. (Letters), 295, L27.
Rieke, G.H. 1978, Ap.J., 226, 550.
Rieke, G.H., and Lebofsky, M.J. 1979, Ann. Rev. Astr. Ap., 17, 477.
Rodriguez Espinosa, J.M., Rudy, R.J., and Jones, B. 1986, Ap.J., 309, in press. Paper I.
Rudy, R.J., LeVan, P.D., and Rodriguez Espinosa, J.M. 1982, A.J., 87, 598.
Rudy, R.J., and Rodriguez Espinosa, J.M. 1985, Ap.J., 298, 614.
Smith et al. 1983, Ap.J., 274, 571.
Telesco, C.M., and Harper, D.A. 1980, Ap.J., 235, 392.
Telesco, C.M., Harper, D.A., and Loewenstein, R.F. 1976, Ap.J. (Letters), 203, L53.
Véron-Cetty, M.P., and Véron, P. 1984, 'A Catalog of QSO's and Active Nuclei'. ESO Scientific Report No. 1.
Weedman, D.W., 1977, Ann.Rev.Astron.&Astrophys., 15, 69.
Yee, H.K.C. 1980, Ap.J., 241, 894.

DISCUSSION

EDELSON:

Your sample is both optically and infrared selected (only approx. 60% IRAS detections), so dusty objects will be over-represented compared to a true optically selected sample. Also, you study generally nearby low nuclear luminosity AGNs because of your stringent IRAS limit. You find larger values of $S_{12\mu m}/S_{10\mu m}$ than other AGN samples because the ratio of nuclear/galaxy luminosity is unusually low. The relatively steep 60-100μm IRAS spectra seen are caused by a mixture of the steep spectrum emission from the underlying galaxy mixing with the flat nuclear component. These is no evidence for starbursts in most high luminosity AGNs.

RODRIGUEZ ESPINOSA:

I think that the sample is really optically selected. It consists mainly of Markarian Seyferts, which by definition are not dusty objects, and a few classical NGC Seyferts. Your question is nevertheless very relevant. I agree that in very high luminosity objects it is difficult to find evidence of starbursts, but is it because they are not there or because we do not see them? It may well be that you can see starbursts only in a certain luminosity range, in the same way that it is difficult to observe the galaxy envelope in high redshift QSOs.

DEVEREUX:

What evidence do you have that the star formation is near the nucleus? Be wary when using IRAS colors because they reflect the nucleus/disk contrast and so you need spatial resolution to separate the nucleus and disk emission.

RODRIGUEZ ESPINOSA:

Presently, no high spatial resolution far-infrared data are available and hence the only information we have is from optical, near and mid-infrared photometry and radio work for a small set of well known sources (NGC 1068, NGC 7469...)

Concerning the far-infrared contribution of the galaxy disk we have shown that 'normal' galaxy disks are on the average one order of magnitude less luminous than either Seyfert or starburst galaxies.

BEGELMAN:

Based on the spectropolarimetry of Antonucci and Miller, one can make a strong case that NGC 1068 contains a normal type 1 Seyfert nucleus, which is obscured by a ring of gas which is so optically thick that it may well be molecular. If Seyfert 2's differ from Seyfert 1's in the presence of absence of a thick molecular disk, one might expect starbursts to be associated preferentially with Seyfert 2's.

RODRIGUEZ ESPINOSA:

That is an interesting point, although I do not think that the difference between type 1 and type 2 Seyferts is as simple as that.

DENNEFELD:

One should be careful in using the 'HII region galaxies' from the VCV catalogue as a comparison sample because it contains only the few objects which have at some time been considered as AGN and disregarded later. They might well have some peculiarity (faint or hidden active nucleus, hotter gas, ...). The luminosity or $\alpha(60,100)$ histograms of 'normal' galaxies are much broader: the fact that your histograms for HII region type or active galaxies from the VCV catalog coincide might just be a selection effect.

RODRIGUEZ ESPINOSA:

An important consideration that went into choosing the VCV HII region galaxy sample is that their redshifts are comparable to the redshifts of the optically selected Seyferts and therefore one avoids the problems associated with beam size effects. You are right, however, in that one should be cautious when using the VCV sample of HII regions. I shall look into that....

CIRCUMNUCLEAR "STARBURSTS" IN SEYFERT GALAXIES

Andrew S. Wilson
Astronomy Program, University of Maryland
College Park, MD 20742

ABSTRACT. Observational diagnostics for the recognition of circumnuclear star formation in Seyfert galaxies are described and illustrated. These methods include: a) spatially resolved optical spectroscopy, which allows the emission lines from HII regions to be separated from those originating in gas ionized by the Seyfert nucleus, b) radio continuum mapping, where the "linear" radio sources characteristic of the nuclear activity may be distinguished from the "diffuse" morphology of multiple supernova remnants generated in a starburst, c) infrared spectroscopic searches for emission features of dust, which are seen in starbursts but not in Seyfert nuclei, and d) the shape of the IRAS spectrum. These various diagnostics agree well as to the presence or absence of ongoing star formation. The IRAS spectra of a significant fraction of Seyferts are dominated by emission from dust heated by stars, not the Seyfert nucleus itself. In these cases, the spectrum is curved, being steep between 25 and 60μm and flatter between 60 and 100μm. When the Seyfert nucleus dominates, the 25-100μm spectrum is much flatter ($\alpha > -1$). It is suggested that the location of a Seyfert galaxy in the IRAS color-color diagram [$\alpha(60,25)$ vs $\alpha(100,60)$] reflects primarily the relative contributions of the active nucleus and dust heated by stars (circumnuclear or disk) to the infrared fluxes.

1. INTRODUCTION

The topic of star formation in active galaxies is of interest for two main reasons. First, it has been suggested that much of the far infrared emission observed by IRAS from Seyfert galaxies may result from an extended, non-nuclear component, perhaps dust heated by hot stars (e.g. Rodriguez-Espinosa, Rudy and Jones 1986). Much of the continuing controversy about the origin of luminous infrared emission focusses on the separation of nuclear and extended components, and on the emission mechanism of the nuclear component itself (thermal vs. non-thermal). Second, there are hints that the nuclear activity seen in objects like Seyfert galaxies and quasars may somehow be connected with enhanced star formation in the circumnuclear or galaxy-scale environment. No clear view of this possible relation exists, but discussions favoring it have fallen into one of two categories. In the first, the entire active nucleus phenomenon is attributed to star formation and its consequences (stellar winds, supernovae, supernova remnants, compact stellar remnants etc.). While few would argue that all the properties of Seyfert type 1 galaxies and quasars can be so explained, the idea that stars provide the ionizing radiation in Seyfert 2 galaxies has been widely discussed (e.g. Adams and Weedman 1975; Harwit and Pacini 1975). Pronik (1973) suggested that a mixture of the central stars of planetary nebulae and normal hot main sequence stars is the ionizing source, while Terlevich and Melnick (1985) have recently argued that the presence of massive stars with effective temperatures of more than 100,000 K (extreme Wolf-

Carol J. Lonsdale Persson (Editor)
Star Formation in Galaxies

Rayet stars) can result in emission line spectra which resemble Seyfert 2's or LINER's. Another, more speculative, suggestion is that starbursts may evolve into Seyfert galaxies if the compact stellar remnants resulting from the former settle into nuclear regions of radii ~ 1 pc, and then act as the accretors of a "conventional" active nucleus (Weedman 1983). In this view, a single massive black hole is not required, although the multiple accretors may mimic one in terms of many observational manifestations. In the second category of models, the active nucleus really does contain a "classical" supermassive black hole, but the black hole activity is triggered by, or triggers, a surrounding starburst. For example (see paper presented by C.A. Norman at this meeting), the starburst may facilitate dissipation of the angular momentum of interstellar gas, leading to enhanced accretion onto the black hole. Alternatively, the impact of high velocity nuclear ejecta, such as emission line clouds, winds or jets, on dense molecular gas could trigger a starburst.

As emphasised above, the properties of the putative nuclear starburst in the first category of models must be very different from those of "normal" star forming regions. Possible reasons include a high stellar and gaseous density in the nucleus which may, for example, lead to overlapping stellar winds and supernova remnants, and other unfamiliar phenomena. Yet in the outskirts of such a starburst, there must surely be relatively normal HII regions. Similarly, in the second category of models, when an evolutionary sequence from starburst to black hole activity (or vice versa) occurs, careful observations should reveal "composite" nuclei, unless the first form of activity completely disappears before the second one begins. Thus both categories of models predict an excess of circumnuclear star formation in comparison with non-active galaxies of similar morphological type, luminosity, etc. The key test of all of the above conjectures involves an observational check of this prediction.

In this paper, I should like to review a number of methods by which intense circumnuclear star formation may be diagnosed in Seyfert galaxies. The results of these different methods generally turn out to be in excellent agreement. In particular, I shall emphasize how the high spatial resolutions available at radio and optical wavelengths allow a clear separation of the effects of the nuclear activity proper from star formation going on around it.

2. MANIFESTATIONS OF STAR FORMATION IN SEYFERT GALAXIES

2.1 Optical Emission Line Studies

The ideal method of investigating the presence of hot young stars is to observe emission lines from their HII regions. A wide body of both low (e.g. Osterbrock 1977; Koski 1978) and high (e.g. Heckman et al. 1981; Whittle 1985) dispersion spectra exist on the nuclei of Seyfert galaxies. These data are unsuitable for detection of circumnuclear starbursts, because emission from the HII regions are usually swamped by the Seyfert nucleus. Although Véron et al. (1981) were able to deduce the presence of HII regions in the nuclei of the Seyfert galaxies NGC 7496 and NGC 7582 by noting that Hβ is narrower than [OIII]λ5007, spatially resolved spectra are usually needed. Separation of the emission lines of the HII regions from those of gas ionized by the Seyfert nucleus can then be achieved in two ways. First, the line ratios, as determined through low dispersion optical spectra, are quite different in the two types of nebulosity (e.g. Baldwin, Phillips and Terlevich 1981). Second,

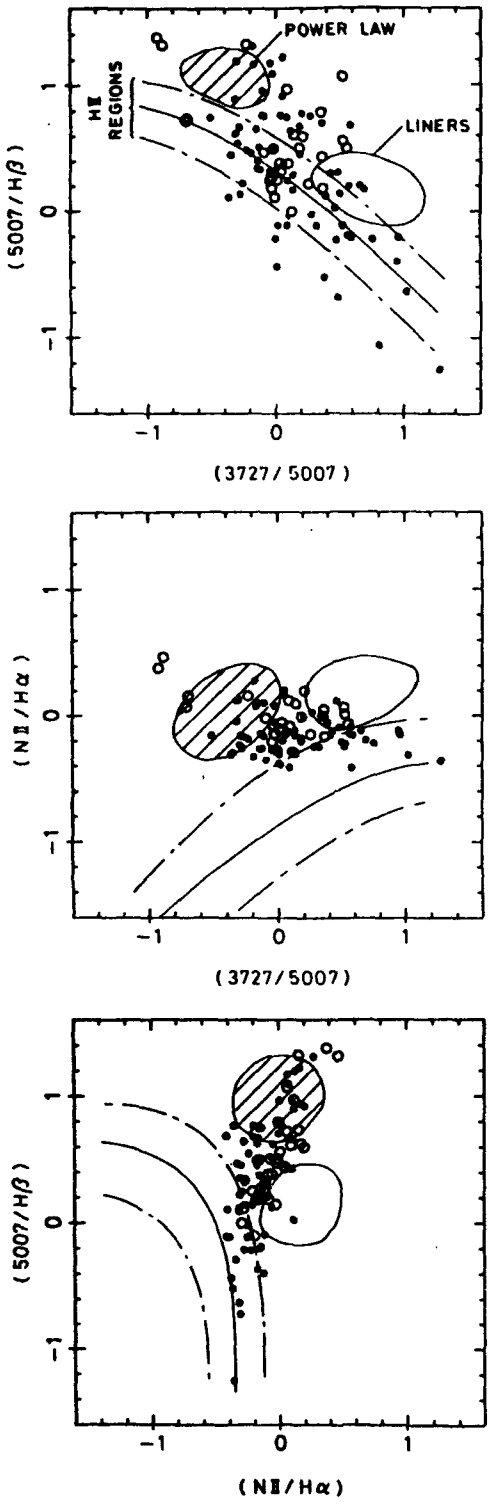

Figure 1 - Ionization diagrams showing logarithms of intensity ratios at different locations over NGC 1068, along with regions found by Baldwin, Phillips and Terlevich (1981) to be the domains of various ionization mechanisms. From Baldwin, Wilson and Whittle (1986).

the HII regions generally lie in a rotating disk or flattened distribution which is coplanar with the stellar disk further out, while the kinematics of the Seyfert excited gas ("narrow line region") are dominated by radial (inflow or outflow) motions (e.g. Heckman et al. 1981). In the following, I describe examples of the separation of Seyfert and starburst excited gas with each of these two methods.

2.1.1. Emission line Ratios. Recently, Baldwin, Wilson and Whittle (1986) have performed an extensive study of NGC 1068 by means of long slit spectra at about 30 locations over the face of the galaxy. The resulting ≈ 1500 spectra have been used to study the kinematics and ionization structure of the gas. Some of the results are illustrated in Fig. 1, which gives plots of ratios of emission lines ([OIII]λ5007/Hβ vs [OII]λ3727/[OIII]λ5007; [NII]λ6584/Hα vs [OII]λ3727/[OIII]λ5007; [OIII]λ5007/Hβ vs [NII]λ6584/Hα) which are useful for diagnosing the ionization mechanism. Each plotted point represents the line ratios at one location in the galaxy. The line ratios have been corrected for reddening assuming an intrinsic Hα/Hβ ratio of 2.86 (Brocklehurst 1971) and the reddening law of Whitford (1958). The regions of the diagrams occupied by normal HII regions, power law ionized gas and LINER's are indicated by the bands and oval shaped regions. As may be seen, the points range between the region occupied by HII regions and that which is characteristic of power law photoionized gas. Baldwin, Wilson and Whittle (1986) discuss the possibility that some of the gas is shock ionized, but prefer the idea that we are observing two components projected on top of each other. One gaseous component is ionized by the Seyfert nucleus and the other by hot stars in the starburst disk of NGC 1068; the exact location of a point in Fig. 1 then reflects the relative contributions of the two components along any given line of sight. There are other pieces of evidence supporting this view, including an early stellar population in the low excitation regions, differences in velocity field and line profiles between Hβ and [OIII]λ5007, and differences between the spatial distributions of the gases emitting these two lines.

2.1.2. Emission Line Kinematics. A recent investigation (Wilson et al. 1986) of the circumnuclear region of the type 1 Seyfert galaxy NGC 7469 illustrates the different kinematics of the nuclear starburst and the high excitation narrow line region. From long slit, high dispersion mapping of the emission lines Hβ, [OIII]λλ4959, 5007, Hα and [NII]λλ6548, 6584, we reached the following conclusions:

a) In addition to the spatially unresolved broad line region, two blended components of extended emission line gas are found. The first component is of high excitation ([OIII]λ5007/Hβ >> 1, [NII]λ6584/Hα ~ 1) and is presumably photoionized by the Seyfert nucleus, while the second is of low excitation and appears to arise in circumnuclear HII regions.

b) The high excitation component dominates the [OIII] lines, which are broad, show strong, blueward-slanting profile asymmetries and have a velocity field with a minimum near the nucleus. The kinematics of this component are thus dominated by radial motions. The low excitation component, as seen in Hα, Hβ and [NII] outside the immediate vicinity of the nucleus, emits much narrower lines and follows rotational motion in or parallel to the plane of the stellar disk of the galaxy. The difference between the line profiles of Hβ and [OIII]λ5007 may be seen in Figs. 2a and b, which shows their distribution over the circumnuclear region.

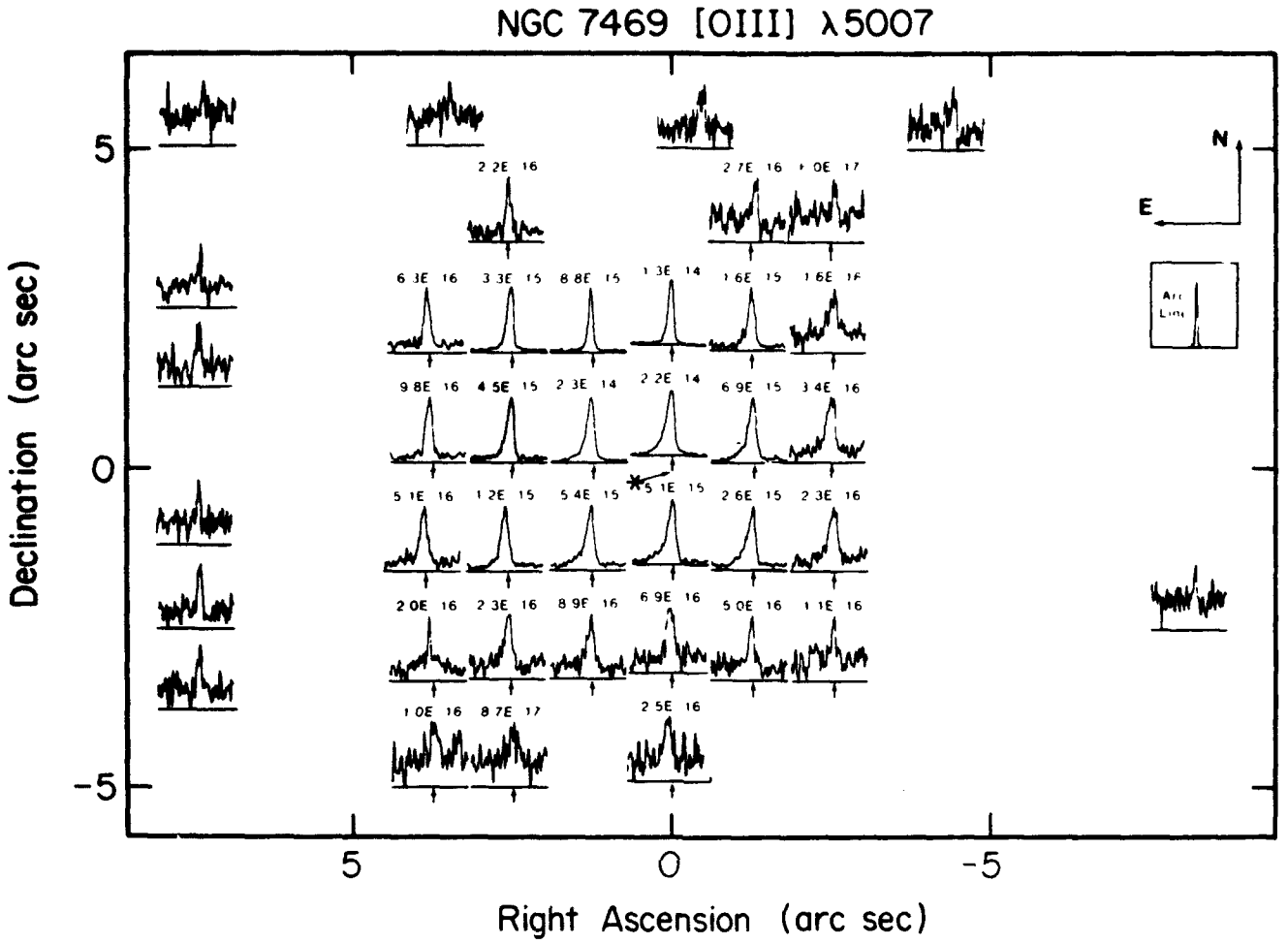

Figure 2a - Profiles of [OIII]λ5007 in NGC 7469. Each profile is normalized so that the difference between the maximum and minimum monochromatic fluxes over the range of wavelengths plotted is the same physical height. The total range of velocity plotted is 3400 km s^{-1}. The nominal position of the nucleus is indicated by the asterisk and the arc line shows the instrumental response.

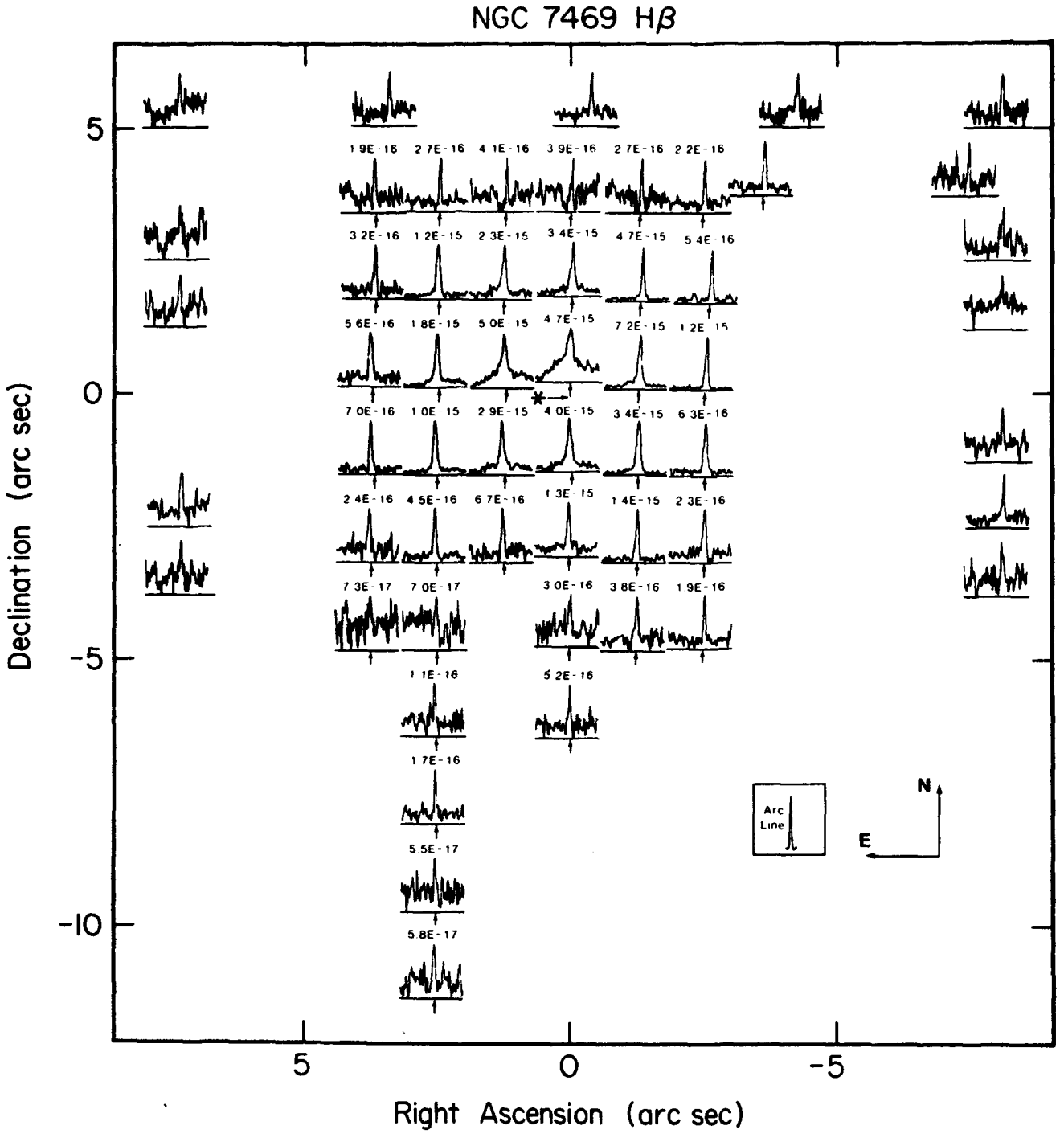

Figure 2b - Profiles of Hβ in NGC 7469; see caption to Fig. 2a and Wilson et al. (1986) for further details.

c) The observed excitation ratio [OIII]λ5007/Hβ decreases from 7.5 at the nucleus to < 1 at the edge of the nebulosity, indicating an increasing relative contribution from the HII regions towards larger radii.

d) The recession velocity of the lines at the nucleus tends to be below systemic, as defined by the mean of the flat portions of the rotation curve or the HI 21 cm single dish line profile. Both this blueshift and the nuclear linewidth are higher for [OIII] than for [NII], and higher for [NII] than for Hα. This asymmetric location of the nucleus in the velocity curve and the different nuclear linewidths of the different species reflect a mixture of the high excitation, broad blueshifted component and the low excitation, narrow rotating component, the relative contributions of each component varying from line to line.

e) The total luminosity of hot stars has been estimated from the Balmer line emission of the low excitation component, and may approach the luminosity of the mid/far infrared emission of NGC 7469, as measured by IRAS. The spectral shape of this infrared emission is typical of galaxies with nuclear HII regions (see Section 2.4), and differs from most Seyferts, supporting the idea that it represents emission from dust heated by the hot stars. In NGC 7469, then, we have a case in which the infrared luminosity of the starburst overwhelms the infrared luminosity of the type 1 Seyfert nucleus.

Fig. 3 shows part of a long slit spectrum of Mark 315, another galaxy with two components of extended emission line gas. The different structures of Hβ and [OIII]λλ4959, 5007 are clearly apparent. Other Seyferts known to have composite circumnuclear spectra include NGC 1365 (Phillips et al. 1983a), NGC 7582 (Morris et al. 1985), and Mark 509 (Phillips et al. 1983b).

2.2 Radio Continuum Morphology

Ulvestad and Wilson (1984a, b) have mapped two samples of Seyfert galaxies with the VLA at 6 and/or 20 cm. The spatially well resolved sources may be classified as either "linear" (L) or "diffuse" (D). The L class sources, which are in the majority, comprise doubles straddling the optical continuum nucleus, triples or jet-like morphologies and are considered to be fuelled by the nonthermal active nucleus in a low power version of the radio galaxy phenomenon. These linear radio sources are morphologically associated with the high ionization narrow line region (e.g. Wilson 1986; Whittle et al. 1986) and are presumably unrelated to processes of star formation. The D class objects, of which only a handful are known, exhibit a "blob-like" radio morphology which appears not to be directly related to the nuclear activity itself. Figure 4 shows a comparison of isophotes in low excitation emission lines and radio continuum radiation for four of these D class objects. Each pair of maps of a given galaxy is reproduced to the same scale. The similarities in scale and morphology of the thermal and synchrotron emitting gases are striking. In all of these objects, the off-nuclear optical emission lines exhibit the two component structure noted above - a low excitation, rotating disk with narrow lines is seen superposed on a high excitation component in radial motion and showing broad lines. The D class radio sources are thus associated with the starburst, presumably representing the integrated effects of multiple supernovae and supernova remnants (e.g. Condon et al. 1982; Ulvestad 1982). It is important to bear in mind that some of the D class sources may also contain more compact radio emission which is fuelled by the Seyfert nucleus. The

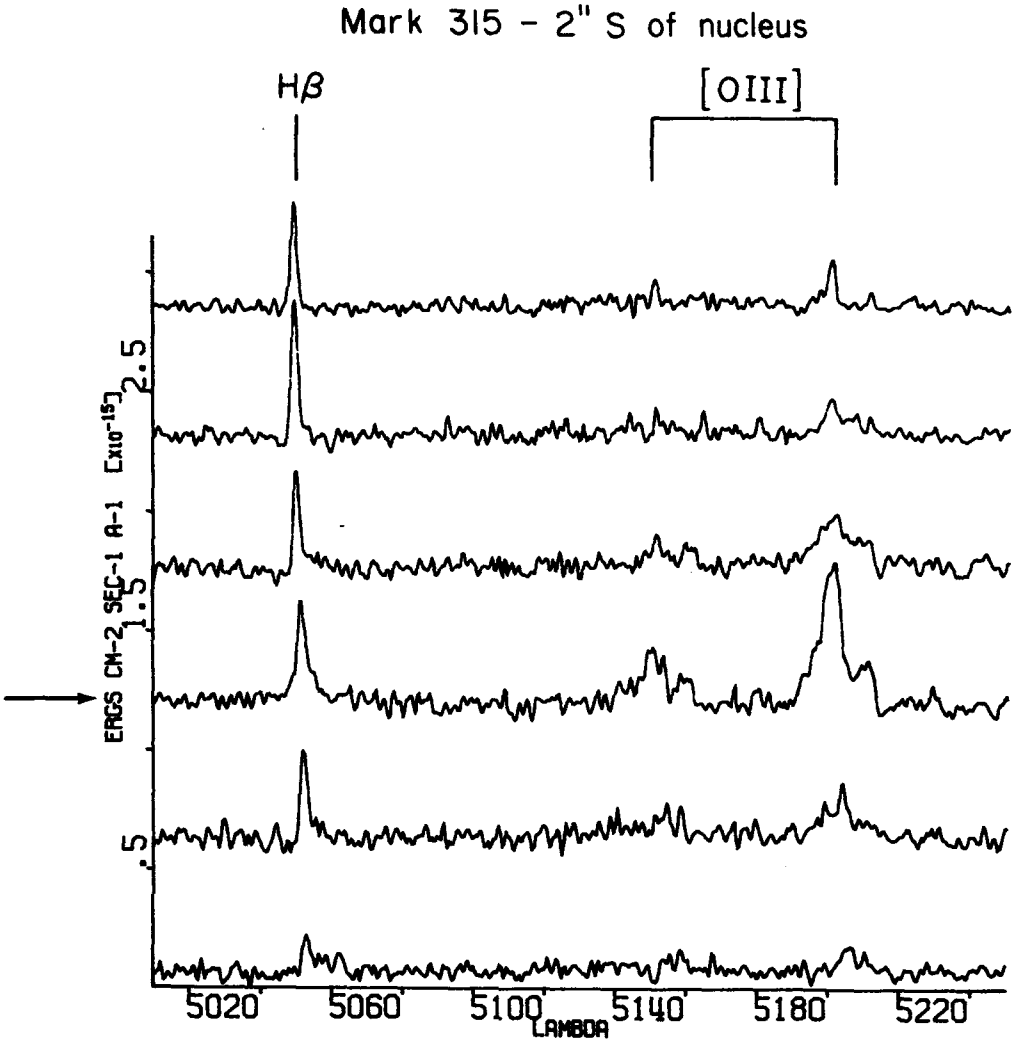

Figure 3 - Part of a long slit spectrum of Mark 315. The slit was oriented east-west and displaced 2" south of the nucleus. The individual spectra shown are separated by 1".65 along the slit and the spectrum which is closest to the nucleus is indicated by the horizontal arrow on the left (from A.S. Wilson and J.A. Baldwin, in preparation).

classic galaxy with both L and D class radio sources is NGC 1068, in which a 13" jet-like source is projected inside a starburst disk (Wilson and Ulvestad 1982, 1983; Wynn-Williams, Becklin and Scoville 1985). Also NGC 7469 and NGC 7582 show unresolved radio sources which are coincident with the optical nucleus and are probably associated with the nuclear activity proper.

2.3. Dust Emission Features

Aitken and Roche (1985) have pointed out the existence of prominent emission features due to gas and dust in the 8-13 μm spectra of starburst nuclei and the general lack of these features in the nuclei of active galaxies. It is noteworthy, however, that several of the Seyferts deduced above to possess circumnuclear starbursts do show dust emission features.

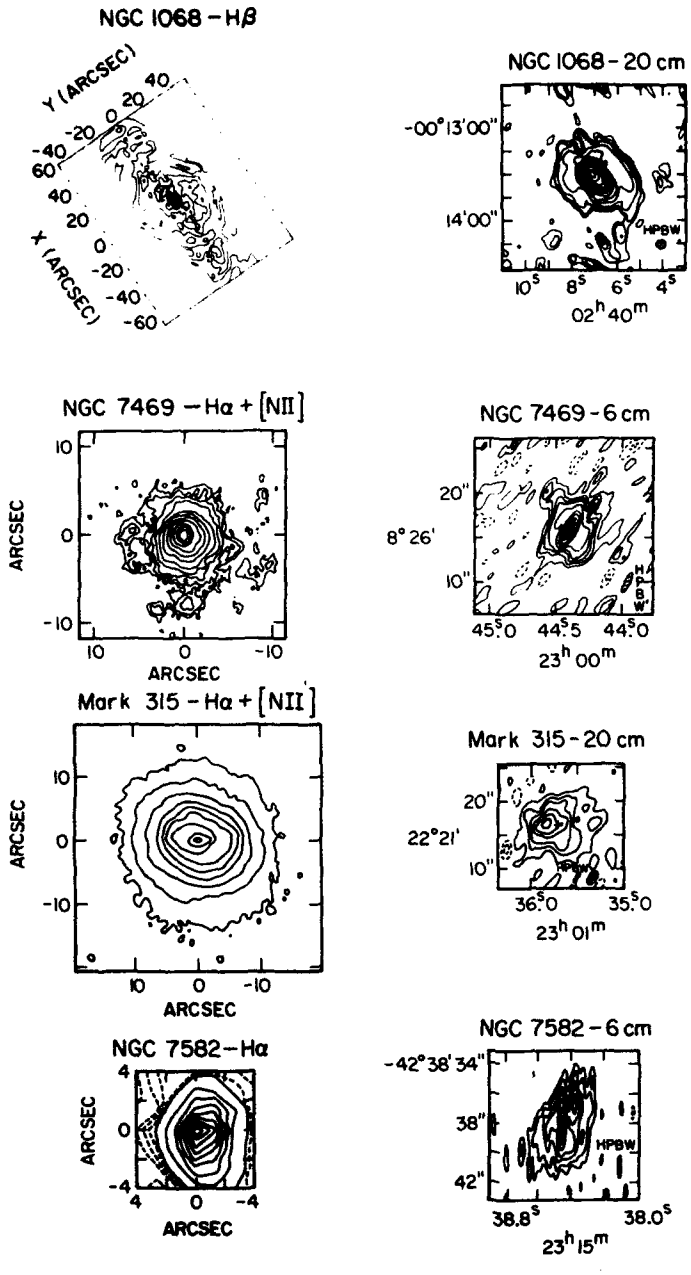

Figure 4 - Seyfert galaxies with circumnuclear starbursts. The left column shows the continuum subtracted isophotes of either Hβ, Hα or Hα + [NII]λλ6548, 6584. On the right is given contours of nonthermal radio emission at either 6 or 20 cm. Each pair of diagrams of a given galaxy is drawn to the same scale. A close morphological similarity between the two types of emission is evident. NGC 1068 (Seyfert type 2) - Hβ isophotes from Baldwin, Wilson and Whittle (1986), 20 cm isophotes from Wynn-Williams, Becklin and Scoville (1985); NGC 7469 (Seyfert type 1) - Hα + [NII] isophotes from Heckman et al. (1986), 6 cm isophotes from Ulvestad, Wilson and Sramek (1981); Mark 315 (Seyfert type 1) - Hα + [NII] isophotes from MacKenty (1986), 20 cm isophotes from Ulvestad, Wilson and Sramek (1981); NGC 7582 (Seyfert type 2) - Hα and 6 cm isophotes from Morris et al. (1985). These references should be consulted for the contour levels.

These galaxies include NGC 1365 (Aitken and Roche 1985), NGC 7469 (Aitken, Roche and Phillips 1981; Rudy et al. 1982; Cutri et al. 1984) and NGC 7582 (Roche et al. 1984). In at least NGC 1365 and NGC 7469, the dust emission features are spatially extended on the scale of the starburst, as determined from the distributions of radio continuum and low excitation optical emission lines. These dust emission features then clearly result from dust heated by hot stars, not from the active nucleus.

2.4. Far Infrared Spectra

Miley, Neugebauer and Soifer (1985) have investigated the far infrared (IRAS) colors of Seyferts by plotting the spectral index between 60 and 25μm against that between 100 and 60μm (Fig. 5a; spectral index α defined by $S \propto \nu^{\alpha}$). They find that, although Seyfert galaxies scatter widely in this plot, they have spectra which are much flatter (bluer), particularly between 60 and 25μm, than those of non-active spirals. Different species of emission line galaxy are found to have different spectral characteristics. Seyfert 1 galaxies are distributed widely in Fig. 5a, but the lower right (steeper spectrum between 60 and 25μm than between 100 and 60μm is populated mainly by objects with Seyfert 2 and nuclear HII region spectra. In histograms of the spectral curvature parameter, $\alpha(60,25) - \alpha(100,60)$, the Seyfert 1's distribute evenly about zero, while the Seyfert 2 distribution shows a preference for negative values, and the nuclear HII region spectra are even more curved (see Fig. 5a). Miley, Neugebauer and Soifer (1985) discussed these trends in terms of a mixture of three components - (i) a cold (~ 30K) disk component having spectral indices similar to those of "normal" spirals, (ii) a nonthermal nuclear component with a power law spectrum, and (iii) a mid infrared nuclear component which is probably thermal in origin and is located within the central hundred parsecs of the nucleus. If this last component does represent heated dust, the heating source could be either the nonthermal nuclear continuum or hot young stars. The segregation, albeit with a good deal of overlap, between the Seyfert 2's and the nuclear HII regions, implies a different distribution of dust temperatures between these two classes. Examination of Fig. 5a suggests the infrared spectra of nuclear HII regions lie within the zone $\alpha(60,25) < -1.5$ and $\alpha(100,60) > -1.1$. It is then of interest to ask whether the Seyfert galaxies in or near this zone also possess circumnuclear HII regions with hot star-heated dust contributing to or dominating the infrared emission.

Figure 5b shows a similar diagram in which only Seyfert galaxies known to possess off-nuclear HII regions are plotted. It should be emphasized that no attempt was made to select any particular spatial scale; the HII regions may be circumnuclear or in the galaxy disk. Also the study has not been made to any particular line flux level, nor were the galaxies selected in any well defined manner. The points in Fig. 5b show a considerable amount of scatter which presumably reflects differing ratios of nonthermally generated nuclear radiation (synchrotron radiation or dust heated by it) to that from dust heated by hot stars, either in the disk of the galaxy or in a circumnuclear starburst. It seems likely that the exact location of a Seyfert galaxy in this diagram is simply a function of the relative strengths of these two processes, the points lying along a "mixture band" joining the Seyfert nucleus and star-heated dust regimes. High spatial resolution infrared mapping is needed to confirm this hypothesis. The diagram confirms the dominance of a nuclear starburst in generating the far infrared emission of such objects as

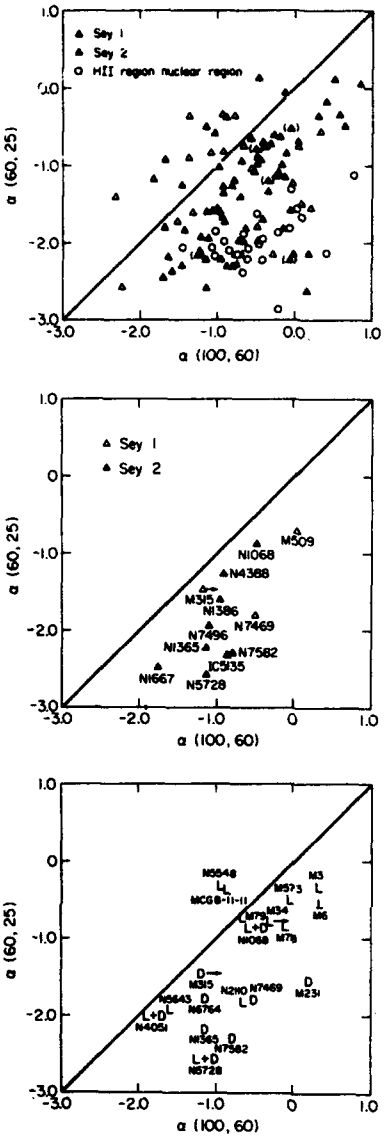

Figure 5 - Plots of the spectral index between 60 and 25μm [α(60,25)] vs. that between 100 and 60μm [α(100,60)] for Seyfert galaxies and nuclear HII regions following Miley, Neugebauer and Soifer (1985). a) Seyfert galaxies and nuclear HII regions listed in "Cataloged Galaxies and Quasars Observed in the IRAS Survey (1985)." b) Seyfert galaxies which are known to have circumnuclear HII regions. The references for the existence of HII regions are given in Section 2.1, when published. Unpublished long slit spectroscopy of Hβ and [OIII]λλ4959, 5007 by Wilson and Baldwin has also been used. c) Seyfert galaxies with known radio structural class. The symbol L refers to "linear" structure, the symbol D to "diffuse" structure and the symbol L+D is used for galaxies with both linear and diffuse components. Most structures are from our series of Ap. J. papers on radio properties of Seyfert galaxies (Ulvestad and Wilson 1984b being the most recent), plus Ulvestad and Wilson (1986, for MCG 8-11-11), Morris et al. (1985, for NGC 5643), Sandqvist, Jorsäter and Lindblad (1982, for NGC 1365) and Phillips, Wilson and Baldwin (unpublished, for NGC 5728).

NGC 7469 (a type 1 Seyfert) and NGC 7582 (a type 2).

In Figure 5c I plot the far infrared color-color diagram for Seyferts with established radio morphology. By and large, the infrared spectral properties correlate well with the radio morphology. The objects with both $\alpha(60,25)$ and $\alpha(100,60)$ greater than -1 tend to contain linear radio sources and their infrared emission seems to be dominated by nuclear activity. Several of them (e.g. Mkn 3, 78) have spatially very extended optical emission lines of high excitation, reflecting ionization by a central nonthermal source. If the far infrared emission were shown to be spatially extended in these objects, the most likely origin would involve dust coexistent with this extended narrow line region and heated directly or indirectly by the central nonthermal source. Alternatively, very compact infrared emission would likely be of synchrotron origin. Only 1 out of the 9 objects with $\alpha(60,25) > -1$ - NGC 1068 - shows evidence for a starburst. As already noted, the radio emission of NGC 1068 exhibits both a "linear" jet-like source and a "diffuse" galaxy-wide disk component.

In contrast to the flat infrared spectra of the "linear" sources, 8 out of the 10 galaxies with $\alpha(60,25) < -1.4$ show a "diffuse" radio component. Although 4 out of these 10 contain "linear" radio sources, I conclude that their infrared emission is likely radiated by dust heated by the hot stars, and is not directly related to the nonthermal active nucleus. A Wilcoxon rank-sum test indicates that $\alpha(60,25)$ is larger (60-25μm spectrum flatter) for L than for D type sources at the 99.8% confidence level, if the L+D's are included with the D's, or at the 96% confidence level, if the L+D's are included with the L's. The trend for the L's to have flatter 100-60μm spectra than the D's is much less significant. This infrared spectral distinction between L and D class objects is not related in a simple way to Seyfert type; both radio morphology classes contain both types 1 and 2.

The IRAS detectors were larger at longer wavelengths, with typical sizes of 0.'76x4.'5 at 12 and 25μm, 1.'5x4.'75 at 60μm and 3'x5' at 100μm. If the significant infrared emission is spread over scales larger than the smallest aperture, the spectra obtained will be too steep because of the extra emission in the long wavelength aperture. It is, therefore, important to check that the distribution of points in Fig. 5c is not strongly influenced by this effect. The mean redshift for the flat spectrum group ($\alpha(60,25) > -1.0$) in Fig. 5c is 6695 ± 3925 km s^{-1} (population standard deviation, not standard deviation of mean), while that for the steep spectrum group ($\alpha(60,25) < -1.4$) is 4134 ± 4072 km s^{-1}. Thus the difference in mean distances is such that the nearer objects have steeper spectra, in the expected sense for the resolution effect. The mean apparent spectral index for the flat spectrum group is $\alpha(60,25) = -0.60 \pm 0.20$ and that for the steep spectrum group $\alpha(60,25) = -1.95 \pm 0.32$, with the quoted errors again being the population standard deviation. Attribution of this difference of mean indices completely to a resolution effect would require ≈ 68% of the observed flux of the steep spectrum objects at 60μ, to originate from scales intermediate between the 25 and 60μm apertures, if the flat spectrum objects are spatially unresolved at both wavelengths. If the flat spectrum objects are also partially resolved at 25μm, this percentage becomes larger. While we have little direct information on the true spatial extent at these wavelengths, the mean difference in distances of the two groups is probably not large enough to ascribe their different infrared colors to resolution effects.

3. CONCLUSIONS

I have shown that star formation - either circumnuclear or in the galaxy disk - in Seyfert galaxies can be diagnosed through a number of observations. First, spatially resolved optical spectroscopic studies can distinguish the narrow, low excitation emission lines of HII regions from the broad, high excitation emission of the Seyfert nucleus. Either the line ratios or the kinematic properties of the gas may be used to separate the two components, the latter method relying on the result that the HII regions generally lie in a rotating, flattened system, while the gas ionized by the Seyfert nucleus follows radial motion (inflow or outflow). Second, an extended, "diffuse" or "blob-like," nonthermal radio source is observed in a minority of Seyfert galaxies and probably represents the integrated radiation of multiple supernova remnants generated by the starburst. This morphology may be contrasted with the "linear" (double, triple or jet-like) radio structure associated with the nuclear activity proper. Third, regions of star formation generally exhibit emission features of gas and dust in the 8-13μm spectral range, while these features tend to be absent in Seyfert nuclei (Aitken and Roche 1985). Seyfert galaxies which do show these features contain circumnuclear starbursts. Fourth, the IRAS band colors of Seyfert galaxies seem to correlate with the presence or absence of star formation. Seyferts with prominent disk or circumnuclear star formation show steep spectra between 25 and 60μm ($\alpha(60,25) < -1.4$) and flatter spectra between 60 and 100μm. The far infrared emission of Seyferts without significant star formation is dominated by the active nucleus and may represent direct incoherent synchrotron radiation or dust heated by it. Such galaxies show flat spectra ($\alpha > -1$) over the 25-60-100μm band. It seems likely that the far infrared colors of any given Seyfert galaxy are primarily a function of the relative strengths of the hot-star and nuclear-powered components.

It is notable that $\leq$ 20% of well resolved, circumnuclear radio sources in Seyfert galaxies are dominated by the "diffuse" component. This result provides a crude limit on the occurrence of very intense circumnuclear star formation. A similar statement cannot be made for the disk component, because our radio measurements were made mainly in the 'A' configuration of the VLA and are relatively insensitive to very extended radio emission. Our result is, however, entirely consistent with the conclusion of Roche and Aitken (private communication) who find that < 10% of Seyferts show dust emission features.

In order to assess whether star formation is more prevalent in Seyfert galaxies than in otherwise similar, non-active galaxies, we need to construct a luminosity function of some measure of the star formation in both Seyferts and a comparison sample. Such a luminosity function was shown at this meeting by Rieke, who assumed that excess infrared emission seen by the low resolution IRAS detectors, in comparison with ground-based photometry through a small aperture, was indicative of star formation. If it is true that the effects of the active nucleus are entirely confined within the few arc sec apertures typical of ground-based infrared observations, Rieke's luminosity function indicates an excess of star formation in Seyferts over normal spirals. This conclusion should be checked using some of the other indicators of star formation that I have described.

ACKNOWLEDGEMENTS

I am grateful to the Infrared Processing and Analysis Center for financial support which allowed me to attend this conference.

REFERENCES

Adams, T.F., and Weedman, D.W. 1975, Ap. J., 199, 19.

Aitken, D.K., Roche, P.F., and Phillips, M.M. 1981, M.N.R.A.S., 196, 101P.

Aitken, D.K., and Roche, P.F. 1985, M.N.R.A.S., 213, 777.

Baldwin, J.A., Phillips, M.M., and Terlevich, R. 1981, Pub. A.S.P. 93, 5.

Baldwin, J.A., Wilson, A.S., and Whittle, M. 1986, to be submitted to Ap. J.

Brocklehurst, M. 1971, M.N.R.A.S., 153, 471.

Condon, J.J., Condon, M.A., Gisler, G., and Puschell, J.J. 1982, Ap. J., 252, 102.

Cutri, R.M., Rudy, R.J., Rieke, G.H., Tokunaga, A.T., and Willner, S.P. 1984, Ap. J., 280, 521.

Harwit, M., and Pacini, F. 1975, Ap. J., 200, L127.

Heckman, T.M., Miley, G.K., van Breugel, W.J.M., and Butcher, H.R. 1981, Ap. J., 247, 403.

Heckman, T.M., Beckwith, S., Blitz, L., Skrutskie, M., and Wilson, A.S. 1986, Ap. J., 305, 157.

Koski, A.T. 1978, Ap. J., 223, 56.

MacKenty, J.W. 1986, Ap. J. (in press).

Miley, G.K., Neugebauer, G., and Soifer, B.T. 1985, Ap. J., 293, L11.

Morris, S.L., Ward, M.J., Whittle, M., Wilson, A.S., and Taylor, K. 1985, M.N.R.A.S., 216, 193.

Osterbrock, D.E. 1977, Ap. J., 215, 733.

Phillips, M.M., Turtle, A.J., Edmunds, M.G., and Pagel, B.E.J. 1983a, M.N.R.A.S. 203, 759.

Phillips, M.M., Baldwin, J.A., Atwood, B., and Carswell, R.F. 1983b, Ap. J., 274, 558.

Pronik, I.I. 1973, Soviet Astr., 16, 628.

Roche, P.F., Aitken, D.K., Phillips, M.M., and Whitmore, B. 1984, M.N.R.A.S., 207, 35.

Rodriguez-Espinosa, J.M., Rudy, R.J., and Jones, B. 1986, Ap. J. (in press).

Rudy, R.J., Jones, B., LeVan, P.D., Puetter, R.C., Smith, H.E., Willner, S.P., and Tokunaga, A.T. 1982, Ap. J., 257, 570.

Sandqvist, A., Jorsäter, S., and Lindblad, P.O. 1982, Astr. Ap., 110, 336.

Terlevich, R., and Melnick, J. 1985, M.N.R.A.S., 213, 841.

Ulvestad, J.S. 1982, Ap. J., 259, 96.

Ulvestad, J.S., Wilson, A.S., and Sramek, R.A. 1981, Ap. J. 247, 419.

Ulvestad, J.S., and Wilson, A.S. 1984a, Ap. J., 278, 544.

Ulvestad, J.S., and Wilson, A.S. 1984b, Ap. J., 285, 439.

Ulvestad, J.S., and Wilson, A.S. 1986, M.N.R.A.S., 218, 711.

Véron, P., Véron, M.P., Bergeron, J., and Zuidervijk, E.J. 1981, Astr. Ap., 97, 71.

Weedman, D.W. 1983, Ap. J., 266, 479.

Whitford, A.E. 1958, A. J., 63, 201.

Whittle, M. 1985, M.N.R.A.S., 213, 1.

Whittle, M., Haniff, C.A., Ward, M.J., Meurs, E.J.A., Pedlar, A., Unger, S.W., Axon, D.J., and Harrison, B.A. 1986, M.N.R.A.S. (in press).

Wilson, A.S. 1986, In IAU Symposium 121, Observational Evidences of Activity in Galaxies, in press (Reidel, Dordrecht).

Wilson, A.S., and Ulvestad, J.S. 1982, Ap. J., 263, 576.

Wilson, A.S., and Ulvestad, J.S. 1983, Ap. J., 275, 8.

Wilson, A.S., Baldwin, J.A., Sun Sze-dung, and Wright, A.E. 1986, Ap. J. (in press for Nov. 1, 1986 issue).

Wynn-Williams, C.G., Becklin, E.E., and Scoville, N.Z. 1985, Ap. J., 297, 607.

DISCUSSION

EDELSON:

Two comments:

1) The Miley, Neugebauer and Soifer result you quote, that Seyfert 1s, Seyfert 2s, and HII regions lie in different regions of color-color diagrams, becomes even clearer when optically selected AGNs are used.

There is a strong tendency for objects along the sequence quasar–SY1–SY2–HII regions to have increasingly steep slopes, presumably due to a larger ratio of thermal/non-thermal luminosity.

2) Our studies of optically selected Seyferts show a tight correlation (at the 99.99% confidence level) between L_{IR} and L_{RAD} for Seyfert 1s, and a weaker one (99.95% confidence level) for Seyfert 2s. These results confirm the hypothesis that the far-infrared emission from most quasars and low-reddening Seyfert 1s is primarily non-thermal in origin, while that from Seyfert 2s and other AGNs with high dust indicators is primarily thermal.

WILSON:

1) The Miley, Neugebauer and Soifer result is for optically selected AGN's.

2) We still don't have a convincing explanation for this well known correlation in Seyfert galaxies. It is very dangerous to assume that the 60 and 100μm IRAS observations of Seyferts are dominated by the nucleus. As I have tried to show, the far-infrared emission from circum-nuclear or extra-nuclear star forming regions overwhelms the emission from the nucleus in a significant fraction of Seyfert galaxies. The IRAS flux can be either be nuclear dominated or disk/starburst dominated, the exact ratio varying from galaxy to galaxy. This effect must first be sorted out before the IRAS data can be used to study the emission mechanism of the nucleus.

CUTRI:

Based on your kinematical studies, can you determine whether the extended HII regions are physically distinct from the narrow-line emitting region, or could there be a transition region which might imply that the two share common material?

WILSON:

Generally speaking, we can account for the kinematic and ionization properties in terms of a mixture of a Seyfert-like component and a normal HII region component, the relative proportions of the mix varying from place to place. It's very difficult to pick out gas which has a true intermediate spectrum. There is, however, a hint that the sources of gas in the two components may be related since the high-excitation and low-excitation morphologies are sometimes similar.

SARGENT:

There is a further diagnostic for circum-nuclear starbursts in Seyferts. High resolution (6") CO observations of NGC7469 made with the Owens Valley Millimeter Wave Interferometer show that the molecular gas is offset from the nucleus and is more or less coincident with the narrow emission line region.

WILSON:

High-resolution interferometric CO maps will, indeed, be a most valuable technique for identifying circum-nuclear starbursts. I look forward to seeing more of these fascinating results and their relation to the other diagnostics I mentioned.

BEGELMAN:

In NGC 1068, there is a compact thermal IR source which probably results from reradiation of the non-thermal continuum, in addition to a larger component, associated with the starburst. What are the prospects for distinguishing between these two components in other objects?

WILSON:

Quite good, I think. In NGC 1068, the compact (arc sec) nuclear component is the hotter one and the extended, cooler component is associated with the 'starburst' disk (Telesco *et al.* 1984, *Ap.J.*, 282, 427). Comparison of ground based measurements at 10μm and 20μm made with a small aperture with the large

aperture IRAS measurements at 12μm and 25μm can separate nuclear and disk components in other galaxies. I have shown how a disk or circum-nuclear 'starburst' component of the IRAS fluxes in Seyfert galaxies can be identified via optical line studies, radio continuum mapping, infrared spectroscopy near 10μm and the IRAS spectral shape itself. All of these methods can be used to separate nuclear from non-nuclear components in active galaxies.

IRAS OBSERVATIONS OF AGN CANDIDATES AT LOW FLUX LEVELS

Marinus H.K. de Grijp
William C. Keel

Sterrewacht Leiden, Postbus 9513 RA LEIDEN, The Netherlands

George K. Miley

Space Telescope Science Institute, Baltimore MD 21218, U.S.A.
Affiliated to the Astrophysics Divisions, Space Science Department of ESA; on leave from Sterrewacht Leiden.

ABSTRACT. IRAS Additional Observations have been used to obtain a sample of point sources at much fainter flux levels than hitherto available through the IRAS Point Source Catalog (hereafter PSC). This sample is being used to compile an incomplete but representative catalog of faint IRAS candidate AGN's and to study the evolution of the infrared bright galaxies. Ground based follow up observations (optical spectroscopy) are mainly hampered by identification confusion.

1. INTRODUCTION

We have previously shown that IRAS colours are a remarkably efficient predictor of nuclear Seyfert activity (de Grijp et al. 1985). By investigating the properties of sources in the IRAS Point Source Catalog (PSC) which have similar "warm" IR spectra to those of known AGN's, we compiled a catalog of 563 IRAS AGN candidates. Optical spectroscopy has now been carried out on several hundred of these objects, of which 69% have Seyfert spectra, most of them previously unknown.

It is clearly of great cosmological interest to extend this study to lower flux levels. We have begun to do this by examining serendipitous sources in the IRAS Additional Observations (AOs). These AOs reach sensitivities of between ~5 and ~15 deeper than the PSC. The median redshift of 0.03, and highest of 0.9 obtained for the "strong" IR Seyferts from the PSC, extrapolate to redshifts of 0.12 and 2.0 respectively for intrinsically similar objects observed to be a factor 15 fainter. It is hoped that this will bring us into realms where cosmological evolution is important.

2. AO-GRIDS AND DATA REDUCTION

To extend our survey to weaker sources we considered all AO observations carried out in the "DPS" observational mode. Each of these observations was made using a raster scan resulting in a map of a region typically 0.5 by 1.5 degrees around an object for which deep IRAS observations were deemed desirable. In addition to the source under study, each of these fields usually contained as "bonus" a few serendipitous sources. It is these sources in which we are interested here.

Many fields were observed more than once; overlapping grids were added to

obtain maximum signal/noise. Up to 11 grids of the same field were added; at this level the maps started to become confusion limited. The standard IRAS source extraction program (which was originally derived from the Leiden-Westerbork image processing system) was used on the IBM 3700 computer at Leiden to extract point-source data from the 4 bands and a band merging algorithm developed by D. Gregorich was used to compile a list of sources observed in at least 2 of the 3 longest wavelength IRAS bands (25, 60 and 100 microns).These longer wavelengths are most sensitive to galaxies.

Data covering 1040 fields were considered in this study. These fields were distributed throughout the sky and comprised all available data except for fields at low galactic latitude ($|b|<20°$) where contamination by galactic sources is significant. The outer 2 arcminutes of each field was omitted from consideration because of edge effects. To minimize problems with cirrus, grids containing more than 20 sources at 100 microns were ignored.

All sources that passed the above selection criteria were flux-calibrated as described by Young et al. (1986) and manually checked for confusion and reliability; cases where the source extraction algorithm was confused by nearby sources or cirrus were omitted. Figure 2c shows a colour-colour distribution for the 900 resultant sources detected in all 3 bands.

3. COMPARISON OF PSC AND AO SOURCES

Whereas the PSC encompasses ~95% of the sky above 20° galactic latitude (~27000 square degrees), the AO grids have a total extent of ~800 square degrees. However, because the AO grids are on average ~10 times deeper than the PSC (fig. 1), both datasets include a comparable volume of space.

Fig 1: Noise statistics of AO grids

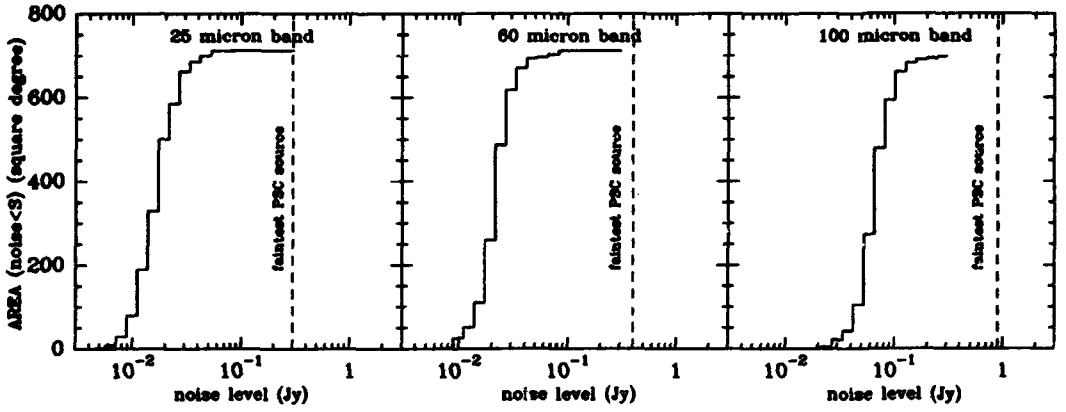

Figure 1: Each AO grid has different noise levels and size. This figure gives an overview of the total area covered at different noise levels. The lowest noise figures are reached for grids that are averages of up to 11 originals grids.

The colour-colour distribution (fig. 2a and 2c) of PSC and AO sources is virtually identical (see also next section); the major difference between them is an excess at $\alpha(25,60)=-4$, $\alpha(60,100)=-3$. These very cold sources are probably due to cirrus.

Fig 2: Colour – colour distribution of sources

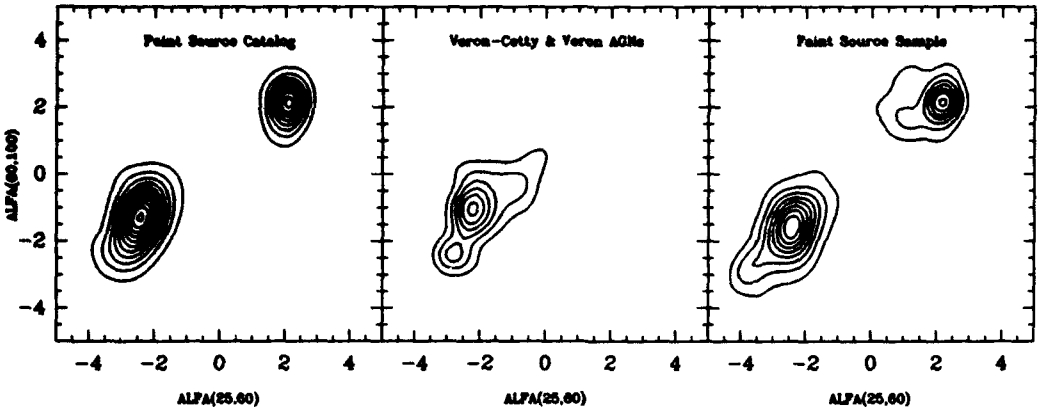

Figure 2: Source density distributions in the 25 - 60 - 100 micron colour-colour diagram. This figure shows that AGN's have flatter spectra than normal galaxies, and that faint source counts are similar to counts for bright sources. A contour representation of binned data was chosen rather than a scatter diagram to assist in a quantitative analysis of source counts. The source density units are sources per square degree per unit colour bin; the spectral index α is defined as $S_\nu \propto \nu^\alpha$. The counts in fig. 2c are weighted with a factor (flux limit P.S.C./Flux limit A0)$^{-1.5}$; so that if the counts are from a non-evolving population, they should be the same. Furthermore, the source counts are corrected to a uniform sensitivity at 60 microns; the other bands do not limit the sensitivity in this diagram.

a - Point Source Catalog sources above $|b|=20$ degrees; stars are concentrated at $\alpha(25,60)=2.0$, $\alpha(60,100)=2.0$ (Rayleigh-Jeans limit); galaxies cluster around $\alpha(25,60)=-2.5$, $\alpha(60,100)=-1.5$. The contour levels are linear increments of 0.02.

b - Point Source Catalog sources that were identified with AGN's (Veron-Cetty & Veron, 1985). Note that they extend to much flatter spectra than normal galaxies. Contour levels are linear increments of 0.001.

c - A0 sources. The similarity with fig. 2a is obvious; differences are a number of stars with IR excess (probably due to mass loss), and an excess of very cold sources, which is probably due to cirrus. Contour levels are as in fig. 2a.

The galaxy counts in fig. 2a and 2c are consistent with a non-evolving population with $N \propto S^{-1.5}$

4. SOURCE COUNTS; EVOLUTION

A detailed examination of fig. 2 can be used to assess the amount of evolution as revealed in the source counts. As shall be discussed in the next section, redshifts for most of the sources under consideration are so low that K-corrections are still unimportant. Therefore it is possible to directly compare figures 2a and 2c: a spot in the colour-colour diagrams refers to sources with the same intrinsic spectral shape, but at different flux levels. Overlaying these figures reveals no significant differences between them other than an

excess of very cold AO sources discussed in section 3. This comparison is not meaningful for stars, of course, since at the galactic latitudes concerned distant stars are not as numerous.

As a whole these source counts do not show evidence of evolution. In the next section we will investigate the redshifts probed, and thus the level up to which evolution does not seem to play an important role.

5. OPTICAL FOLLOWUP

Our original AGN detection criterion implemented on the PSC was based on the spectral indices between 25 and 60 microns of $-1.5<\alpha(25,60)<0.0$ (de Grijp and Miley 1986). From the AOs we have compiled a source list of more than 100 sources which have the same colours and we are simultaneously carrying out a program of follow up optical spectroscopy.

Spectra for a number of the discussed sources have been obtained at the European Southern Observatory (3.6 m telescope + EFOSC) and at Roque de los Muchachos Observatory (2.5-m Isaac Newton Telescope + faint-object spectrograph).

Fig 3: Spectrum of Seyfert 1 galaxy IRAS0622-645, ESO 3.6M + EFOSC

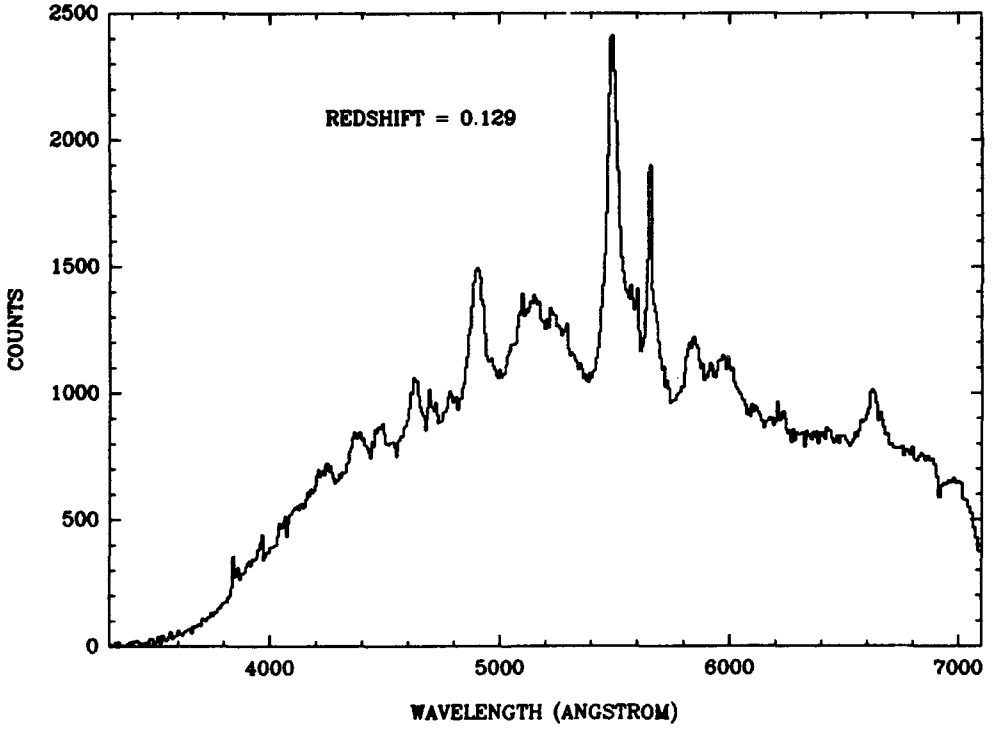

Figure 3: Spectrum of a previously unknown Seyfert 1 galaxy obtained at ESO. This elliptical galaxy was identified by taking a slitless spectrogram for a 2 x 3 arcmin field around the IRAS position. This emission line object was less than 20" from the IRAS position.

Uncertainties in the IRAS positions have so far proved to be the major difficulty in identifying optical counterparts. Since experience with the PSC showed that 90% of all objects with $-1.5<\alpha(25,60)<0.0$ are emission-line objects, this can in principle be used as a secondary identification criterion. Slitless spectroscopy with EFOSC proved to be a boon in this respect.

Although the sample observed is by no means statistically complete, the redshifts found are on average 3 times higher than for objects in the PSC, and AGNs cluster in the same part of the colour-colour diagram. As 20% of them have redshifts above $z=0.2$, careful selection of the sources in the deepest grids may yield a luminosity function for Seyferts at redshifts of ~0.3. Also a number of sources at redshifts of 1 to 2 can be expected.

We conclude that although uncertainties in the IRAS positions is a major limitation in identifying optical counterparts, high redshift objects obtained from the AO data may prove to be important for investigating cosmological evolution of AGNs.

6. ACKNOWLEDGEMENTS

The optical observations discussed here were carried out at the ESO observatory in Chile and at Roque de los Muchachos observatory on La Palma. We thank their staffs for support at the telescope. We thank H. van der Laan for useful discussions.

7. REFERENCES

de Grijp, M.H.K., Miley, G.K., Lub, J. and de Jong, T. 1985, Nature, 314, 240

IRAS Catalogs and Atlases, Explanatory Supplement, 1985 ed. Beichman, C.A., Neugebauer, G., Habing, H.J., Clegg, P.E. and Chester, T.J. (Washington DC: US Government Printing Office)

IRAS Point Source Catalog, 1985, Joint IRAS Science Working Group. (Washington DC: US Government Printing Office)

de Jong, T., Clegg, P.E., Soifer, B.T., Rowan Robinson, M., Habing, H.J., Houck, J.R., Aumann, H.H. and Raimond, E. 1984, Ap. J. (Letters) 278, L67

Miley, G.K., Neugebauer, G. and Soifer, B.T. 1985, Ap. J. (Letters) 293, L11

Neugebauer, G. et al. 1984, Ap. J. (Letters), 278, L1

Veron-Cetty, M.P. and Veron, P. 1985, A Catalog of Quasars and Active Nuclei (Munich: European Southern Observatory), Scientific Report No.4.

Young, E.T., Neugebauer, G., Kopan, E.L., Benson, R.D., Conrow, T.P., Rice, W.L. and Gregorich, D.T. 1986, A User's Guide to IRAS Pointed Observation Products (Washington DC: US Government Printing Office)

8. DISCUSSION

MALKAN: To find a reasonable number of AGN's you adopt quite restrictive IRAS colour criteria. Our work on an unbiased sample of Seyfert galaxies shows that you exclude about 80% of all AGN's. How, then, is it possible for you to construct a meaningful AGN luminosity function?

DE GRIJP:You are correct that we can only construct a luminosity function for AGNs whose IR spectra are consistent with our colour-criteria. This is about 70% of all Seyfert-like AGNs. Comparison with optical/UV-selected samples of AGN's (Neugebauer et al. 1984, Miley et al. 1985) shows that we miss 25-30%, mainly at the steep spectrum side of the adopted colour range. Presumably these steep spectrum AGN's are dominated by cold disk emission, in other words their nuclei are relatively faint. So we expect that a luminosity function constructed on the basis of our colour criterion might be underestimated at the low luminosity end, but essentially complete at high luminosities.

WINDHORST: You mentioned in your talk that your AO source counts do not support (cosmological) evolution. Hacking yesterday claimed from somewhat deeper 60 micron counts evidence for evolution. Do your and his counts agree in amplitude and slope?

DE GRIJP: I have not yet been able to compare Hacking's figures with mine in detail. From what I understood about his talk, it is not the source counts as such that are high, but the prediction of the number of faint sources that is low. This is because for his model Hacking used a luminosity function of Rowan Robinson that is low by a factor of 2 (Weedman, private communication) as compared to more recent results. (Editor's note: Hacking in fact used the local luminosity function of Soifer et al. (these proceedings)).

WINDHORST: What fraction of your 60 micron galaxies is at cosmological distances ($z \gg 0.1$)? Namely, if this fraction is considerable, even a Euclidean slope of -1.5 would be indicative of a non-uniform source distribution in a relativistic universe.

DE GRIJP: Some 20% have redshifts over 0.2, and a (small) number should have redshifts over 1.0 (based on extrapolation from the Point Source Catalog). So although there is a fraction of sources at high redshifts, I don't think that source counts alone will be enough to make a hard claim of evolution because of the low numbers involved.

POSTER PRESENTATIONS

SPECTROPHOTOMETRY OF BRACKETT LINES IN VERY LUMINOUS IRAS GALAXIES

D. L. DePoy
University of Hawaii, Institute for Astronomy
Honolulu, Hawaii 96822 USA

ABSTRACT. Observation of the Brackett-α and Brackett-γ hydrogen recombination lines have been made in a sample of galaxies chosen from the IRAS catalog to have high luminosities at infrared wavelengths. Most have strong Brackett line emission indicating large numbers of high mass stars; the formation of these stars may hence be the underlying source for the galaxies' luminosities. However, there are at least two exceptions that may not be explained in this manner: NGC 6240 and Arp 220. Additional evidence indicates that each of these exceptions may be more closely related to Seyfert-type galaxies or other active galactic nuclei.

INTRODUCTION

IRAS has shown that there are many galaxies that have high luminosities at wavelengths around 80 μm. This luminosity can be extremely high, sometimes greater than 10^{12} $L_\odot$, which is similar to that of Seyfert galaxies and other active galactic nuclei (AGN).

The cause of this luminosity is subject to debate. One possibility is that very intense episodes of star formation are producing large amounts of ultraviolet radiation from high-mass stars that subsequently is absorbed and reradiated at longer wavelengths by dust associated with the star formation sites (Rieke et al. 1985; Joseph et al. 1985). Another is that an AGN underlies the galaxy and whatever powers an AGN is powering the infrared emission (see DePoy, Becklin, and Wynn-Williams 1986). Other causes have been postulated (e.g., Harwit in these proceedings).

If high-mass stars are the source of the luminosity, then observations similar to those made in galactic star formation regions should reveal their presence. These can include observations from X-ray to radio wavelengths. However, severe limitations hamper many techniques. For example, X-ray observations are curtailed by the lack of a satellite, radio studies are complicated by nonthermal processes, and submillimeter data are limited by beam sizes that require stringent assumptions about filling factors. Observations of hydrogen recombination lines are useful in quantitatively measuring the number of hydrogen ionizing photons, but optical lines are obscured by dust and, until recently, infrared lines have been difficult to detect.

Advances in infrared instrumentation have been made, however, that allow the infrared lines to be more easily detected. The Brγ ($n = 7$ to 4) and the Brα ($n = 5$ to 4) lines offer the best observational possibilities because both are situated in unobscured portions of the atmosphere and, especially Brα, are at wavelengths long enough to be only slightly affected by dust extinction.

Carol J. Lonsdale Persson (Editor)
Star Formation in Galaxies

D. L. DEPOY

Presented here are the results of a study of Brα and Brγ line strengths in a number of galaxies specifically chosen to have high luminosities in the infrared.

SAMPLE AND OBSERVATIONS

The galaxy sample was chosen from the IRAS Point Source Catalog (IRAS Explanatory Supplement 1985). The objects from the catalog had to have been detected in the 12 μm and 25 μm bands and have the sum of the fluxes in the 60 μm and 100 μm bands greater than 35 Jy. This limit was chosen so that if the object had a ratio of 100 μm plus 60 μm flux to Brackett line strength similar to that found in M82 and NGC 253, it would be possible to detect with a signal-to-noise ratio >5 in a 1 hr integration. Each object also had to be an optically cataloged galaxy with a redshift greater than 2000 km s^{-1}. Finally, the declination limits of the sample were -40° to +60°.

There were 25 galaxies that met the above criteria. They range in luminosity from 5 x 10^{10} $L_\odot$ to 2 10^{12} $L_\odot$. Four of the sample galaxies have been detected in one or both of the Brackett lines previous to this study: NGC 1614 (Aitken, Roche, and Phillips 1981), NGC 3690 (Fischer et al. 1983), Arp 220 (Rieke et al. 1985), and NGC 6240 (DePoy, Becklin, and Wynn-Williams 1986; Rieke et al. 1985).

All of the observations have been made on the United Kingdom Infrared Telescope (UKIRT) with a seven-element cooled grating spectrometer (CGSII). A 633 lines mm^{-1} grating was used that gave a resolution of about ~550 km s^{-1} around Brα and ~1200 km s^{-1} around Brγ. The 5.5" beam was always centered on the peak of each galaxies' 2 μm continuum.

RESULTS

The data on 15 galaxies were collected during two observing runs (January and April 1986). Of the 15, 13 were detected in the Brα line and 7 in Brγ. A run in September 1986 is planned to complete the sample.

A convenient measure of the amount of star formation in a galaxy is the "Infrared Excess" (IRX), defined as

$$(L_{bol}/L_{Ly\alpha}) - 1,$$

where L_{bol} is the bolometric luminosity of the source and $L_{Ly\alpha}$ is the luminosity of the Lyα line (Jennings 1975). The bolometric luminosity of a galaxy can be estimated from the IRAS data (IRAS Explanatory Supplement 1985) and the luminosity of the Lyα line from an extinction corrected hydrogen line strength and recombination theory (see Wynn-Williams 1984).

In H II regions the IRX is typically 5-10 (Jennings 1975); in starburst galaxies such as M82 and NGC 253 the IRX is slightly higher, closer to 20 or 30 (Simon et al. 1979 and Rieke et al. 1980, respectively). In AGN, however, the IRX is usually much higher, partly because for a given amount of luminosity the much flatter UV spectrum of an AGN produces far fewer photons near the ionization energy of hydrogen (see Cutri, Rieke, and Lebofsky 1984).

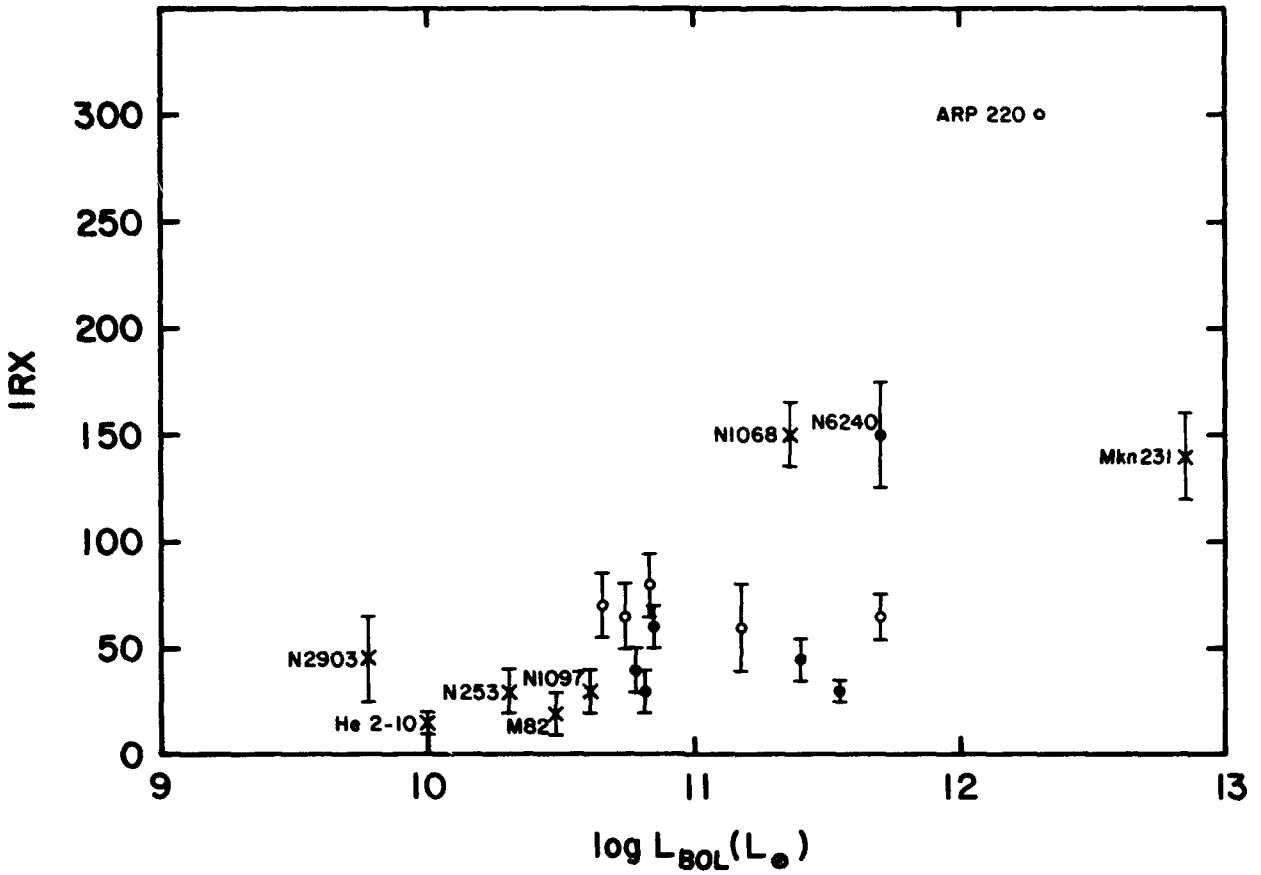

Figure 1. The infrared excess (IRX) vs. the bolometric luminosity of various objects and the sample galaxies. X's are from the literature, closed circles are program galaxies with both Brα and Brγ measured (and hence with extinction derived), and open circles are program galaxies with only the Brα measured.

Figure 1 shows the IRX of the program galaxies versus their bolometric luminosities. Also shown are the positions of some other galaxies whose Brackett lines have been reported in the literature (Beck, Beckwith, and Gatley 1984; Cutri, Rieke, and Lebofsky 1984; Hall et al. 1981; Phillips et al. 1984; Rieke et al. 1980).

Typically, the program galaxies have IRXs that are similar to or slightly higher than the starburst galaxies. In general, the galaxies with the IRXs that are slightly larger than the starburst galaxies are those with poorly determined extinctions or that are at the low redshift end of the sample. This may imply that the IRX in those cases has been overestimated, since either larger extinction or extended emission would give a larger intrinsic line strength and, hence, a lower IRX. Therefore, it appears that most of the program galaxies may be similar to starburst galaxies in their ratio of Lyman-α luminosity to bolometri luminosity. In any case, the implied hydrogen ionizing photon flux indicates a large number of high-mass stars; therefore the luminosities of the program galaxies may arise from the formation of these stars.

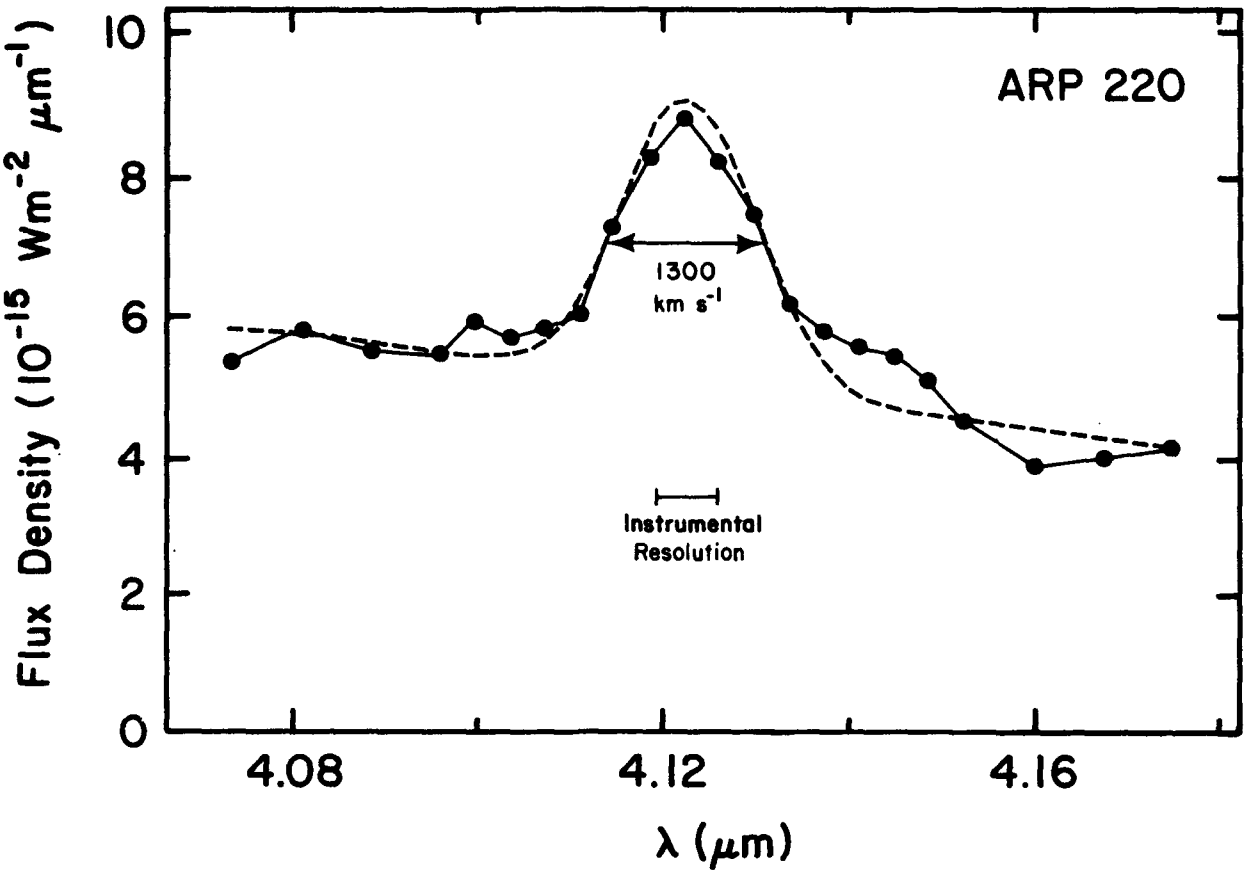

Figure 2. Brα line data on Arp 220. The dots and connecting line are the data smoothed with a three-point running mean; the dashed line is a χ^2 fit of a Gaussian and a linear continuum to the data. The Gaussian fit has a FWHM of ~1300 km s^{-1}.

There are, however, two notable exceptions, NGC 6240 and Arp 220. A thorough discussion of the data on NGC 6240 can be found in DePoy, Becklin, and Wynn-Williams (1986), in which it is argued that NGC 6240 has many properties similar to AGN. Arp 220, in addition to its very high IRX, has at least two other pieces of information that indicate that it is likely to be an AGN. First, the detected Brα in this source is very broad, about 1300 km s^{-1} FWHM (see Figure 2). Second, the 10 and 20 μm emission is unresolved spatially (see Becklin's paper in these proceedings). Therefore, Arp 220 may harbor an AGN.

CONCLUSIONS

A sample of 14 galaxies luminous in the IRAS bands have been observed for Brα and Brγ emission. The results indicate that, in general, the program galaxies have luminosities that are probably explained by the formation of high-mass stars. Two of the galaxies, however, do not fit the pattern. They may be more easily understood as AGN.

REFERENCES

Aitken, D. K., Roche, P. F., and Phillips, M. M. 1981, M.N.R.A.S., 196, 101P.
Beck, S. C., Beckwith, S., and Gatley, I. 1984, Ap. J., 279, 563.
Cutri, R. M., Rieke, G. H., and Lebofsky, M. J. 1984, Ap. J., 287, 566.
DePoy, D. L., Becklin, E. E., and Wynn-Williams, C. G. 1986, Ap. J., in press.
Fischer, J., Simon, M., Benson, J., and Solomon, P. 1983, Ap. J. (Letters), 273, L27.
Hall, D. N. B., Kleinmann, S. G., Scoville, N. Z., and Ridgway, S. T. 1981, Ap. J., 248, 898.
IRAS Catalog and Atlases, Explanatory Supplement. 1985, ed. C. A. Beichman, G. Neugebauer, H. J. Habing, P. E. Clegg, and T. J. Chester (Washington, D.C.: U.S. Government Printing Office).
Jennings, R. E. 1975, in H II Regions and Related Topics, eds. T. L. Wilson and D. Downes (Berlin: Springer-Verlag).
Joseph, R. D., and Wright, G. S. 1985, M.N.R.A.S., 214, 87.
Phillips, M. M., Aitken, D. K., and Roche, P. F. 1984, M.N.R.A.S., 207, 25.
Rieke, G. H., Lebofsky, M. J., Thompson, R. I., Low, F. J., and Tokunaga, A. T. 1980, Ap. J., 238, 24.
Rieke, G. H., Cutri, R. M., Black, J. H., Kailey, W. F., McAlary, C. W., Lebofsky, M. J., and Elston, R. 1985, Ap. J., 290, 116.
Simon, M., Simon, T, and Joyce, R. R. 1979, Ap. J., 227, 64.
Wynn-Williams, C.G. 1984, in Galactic and Extragalactic Infrared Spectroscopy: Proceedings of the XVIth ESLAB Symposium, Held in Toledo, Spain, December 6-8, 1983, ed. M. F. Kessler and J. P. Philips (Dordrecht: Reidel), p. 133.

EVIDENCE FOR EXTENDED IR EMISSION IN NGC2798 AND NGC6240

G. S. Wright[1] R. D. Joseph P. A. James and N. A. Robertson[2]
Blackett Laboratory, Imperial College,
London SW7 2BZ

(1) now at Royal Observatory, Blackford Hill, Edinburgh EH9 3HJ
(2) now at Department of Natural Philosophy, University of Glasgow, Glasgow G12 8QQ

ABSTRACT

Extended emission at 10 and 20 μm can be used to distinguish starbursts from "monsters" as the underlying energy source driving the luminous infrared emission in the central regions of galaxies. We have investigated the spatial extent of the mid-infrared emission in the interacting galaxy NCG2798 and the merger NGC6240. The 10 and 20 μm profiles of the IR source in NGC2798 are significantly wider than beam profiles measured on a standard star, supporting a starburst interpretation of its IR luminosity. For NGC6240 there is marginal evidence for an extended 10 μm source, suggesting that a significant fraction of its IR luminosity could be produced by a burst of star formation.

I. INTRODUCTION

One of the outstanding questions in extra-galactic IR astronomy is the nature of the underlying energy source powering the large IR luminosities found for many interacting galaxies.

Evidence is emerging that bursts of star formation of exceptional intensity compared to normal spirals and canonical "starburst" galaxies are responsible for the IR activity in interacting galaxies (cf. Joseph et al. 1984, Lonsdale et al. 1984, Cutri and McAlary 1985). Moreover, the subset of interacting galaxies in which a merger of the two participating galaxies has occurred are among the most luminous IR galaxies known (Joseph and Wright 1985) and it appears that the merger has resulted in a "super-starburst". However, this interpretation is open to debate because the interaction may provide the material to feed an accretion disk around a collapsed object in the nucleus. This "starbursts and monsters" debate (cf. Heckman et al. 1983) is especially controversial for the ultra-luminous merging galaxies such as NGC6240 and Arp220, although it applies to all the IRAS galaxies to some degree.

Potentially one of strongest arguments in favour of a starburst interpretation is spatially extended mid-IR emission. For a single central source heating a dust cloud, the dust can be heated sufficiently to radiate at 10 μm only if it is within a few pc of the source. So, measuring the extent of the IR emission discriminates between a compact source heating a dust cloud and luminosity sources distributed over several hundred pc, the latter being expected if the underlying energy source is a burst of star formation.

II. OBSERVATIONS

Observations of the interacting galaxy NGC2798, for which $L_{IR} \sim 6 \times 10^{10}$ Le, and the merger NGC6240 which has $L_{IR} \sim 10^{12}$ Le, were made at UKIRT in February 1986. N-S and E-W profiles of the IR sources were made by obtaining photometry on the optical

Carol J. Lonsdale Persson (Editor)
Star Formation in Galaxies

nucleus of the galaxy and then moving off the central pixel 0.75 arcsec at a time, using the UKIRT TV crosshead to obtain as accurate an offset as possible. To minimise systematic effects, such as drifts, each step out from the central pixel was made first to one side and then to the other. Observations of a nearby standard star were obtained using exactly the same method, so any residual systematic effects should be the same for both the galaxy and the star observations. A chopper throw of ~ 30 arcsec perpendicular to the offset direction was used for all the observations.

III. RESULTS

Profiles of NGC2798 in a N-S direction were obtained at both 10 and 20 μm and in an E-W direction at 10 μm. NGC6240 was observed with offsetting in a N-S direction at 10 μm. Figure 1 shows the profiles of the galaxies compared to the profiles of a nearby standard star. The position marked (0,0) is the position of the optical nucleus. The horizontal error bars are an estimate of the pointing error relative to the (0,0) position, based on the degree of consistency of the standard star profiles and the ease of guiding on the TV. The profile of the standard star has been scaled to give the best fit to the peak flux, and centred to produce the best alignment of the profiles. It is evident from these figures that the data for the galaxies indicate a wider profile than the beam profiles measured on a standard star. To estimate the significance of the difference between the galaxy profile and that of the star, we have calculated the significance with which each point lies outside the beam profile by comparing the point to profile distance with the error ellipse. The overall significance of the evidence for spatial extent is obtained by summing in quadrature the significances of each point. The significance levels of the spatial extents indicated in the galaxy profiles are given in Table I.

Table I

The significance of the difference between the galaxy and standard star profiles

NGC2798 20 μm N-S	NGC2798 10 μm N-S	NGC2798 10 μm E-W	NGC6240 10 μm N-S
4.5 σ	4.5 σ	3 σ	3 σ

We have also explored the likely size of the sources, by convolving the beam profile with a top hat function of variable width and adjusting the width of the top hat, the scaling of the profile and its alignment to obtain the best fit to the data points. This gives a source size of approximately 4 arcsec for all the profiles.

IV. DISCUSSION

For NGC2798 there is good evidence for extent at both 10 and 20 μm, and this is consistent with our multi-aperture photometry at 10 μm. We find a flux of 190 ± 18 mJy in a 5 arcsec beam and 520 ± 105 mJy in an 8 arcsec beam. The IRAS data (770 and 3130 mJy at 12 and 25 μm respectively) when compared with our 10 and 20 μm data are also consistent with a spatially extended IR source. Non-equilibrium heating of small dust grains by a compact underlying energy surce is unlikely to be producing this extended emission because there is extent at 20 μm, where such grains would radiate less effectively, on a similar scale to the 10 μm emission. The spatial extent inferred for the source, ~ 4

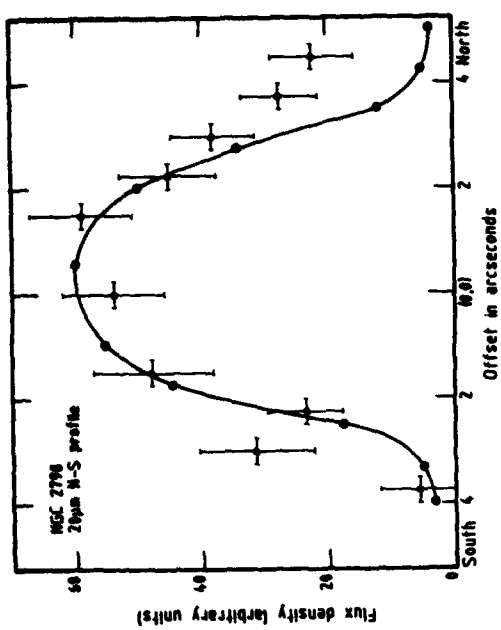

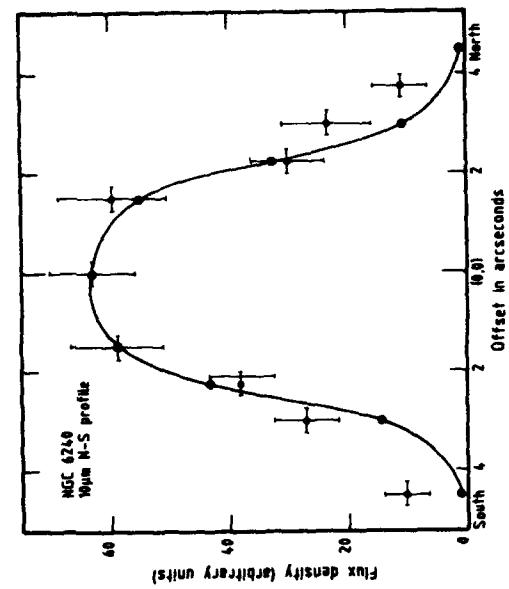

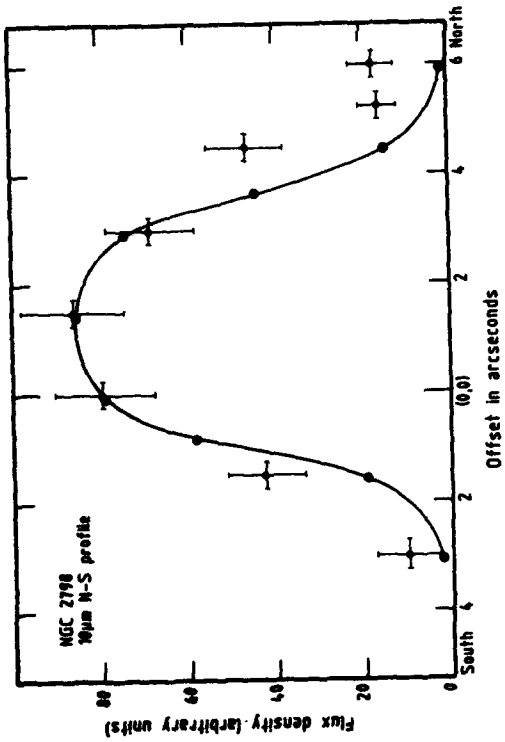

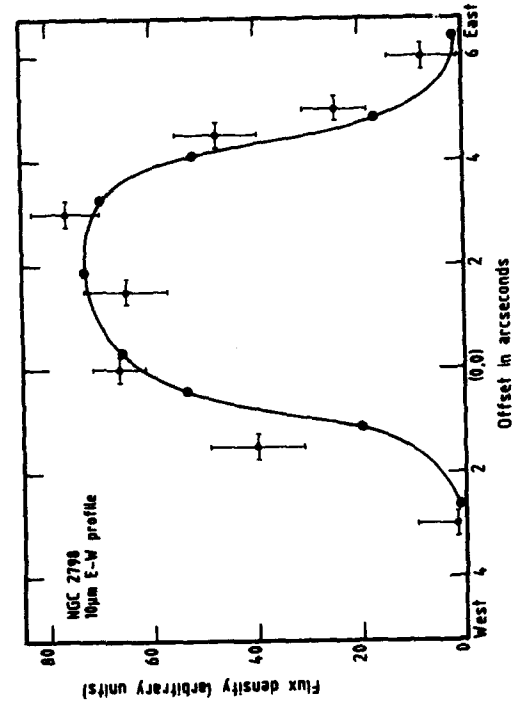

Figure 1. Profiles of the galaxies NGC2798 and NGC6240 compared with those obtained on a nearby standard star. The position marked (0,0) is the position of the optical nucleus.

arcsec, corresponds to 660 pc in NGC2798. This is much larger than the ~ 1 pc source size expected if the dust is heated by a single nuclear source. A burst of star formation is thus the most natural interpretation of the IRAS luminosity of NGC2798. The results for NGC6240 are more marginal than those for NGC2798. Nevertheless they indicate that for this ultra-luminous IR galaxy the nuclear source may be extended. This suggests that a massive burst of star formation could be the underlying energy source for a significant fraction of the enormous IR luminosity of this galaxy.

V. CONCLUSIONS

The data presented provide good evidence for spatially extended 10 and 20 μm emission in NGC2798 supporting a starburst interpretation for the 6 x 10^{10} Le IR luminosity of this interacting galaxy.

For NGC6240 there is marginal evidence (~ 3 σ) for an extended 10 μm source. This suggests that this ultra-luminous IR galaxy may indeed be the result of a super starburst, a conclusion which would be strengthened by the detection of extended 20 μm emission.

REFERENCES

Cutri, R.M. and McAlary, C.W. 1985, *Ap.J.*, 296, 90.
Heckman, T.M., van Breugel, W., Miley, G.K., and Butcher, H.R. 1983, *A.J.*, 88, 1077.
Joseph, R.D., Meikle, W.P.S., Robertson, N.A., and Wright, G.S. 1984, *M.N.R.A.S.*, 209, 111.
Joseph R.D. and Wright, G.S. 1985, *M.N.R.A.S*, 214, 87.
Lonsdale, C.J., Persson, S.E. and Matthews, K. 1984, *Ap.J*, 287, 95.

MODELS RELATING THE RADIO EMISSION AND IONISED GAS IN SEYFERT NUCLEI

A. Pedlar, S.W. Unger, D.J. Axon and J.E. Dyson
University of Manchester, England

SUMMARY

We discuss possible models in which the radio emitting components in Seyfert II nuclei can compress and accelerate the ambient nuclear medium to produce the characteristics of the narrow line region. A first order model (Pedlar, Dyson & Unger 1985), which considers only the expansion of the radio components, is briefly described. However, in many Seyfert nuclei it appears that the linear motion of the radio components is also important. This can result in shock heating of the ambient medium, and if the cooling time is long enough, can lead to a displacement between the radio component and the associated [OIII] emission lines. This effect may be present in NGC1068 (Meaburn & Pedlar 1986), and NGC5929 (Whittle et al. 1986) and by considering ram pressure balance and the cooling length it is possible to estimate lobe velocities and ambient densities.

i) INTRODUCTION

The relationship between the radio continuum and the optical forbidden line regions (FLR) was first investigated by de Bruyn and Wilson (1978) who showed that a correlation existed between the 21cm radio continuum power and the luminosity of the 5007A [OIII] line. High resolution studies using MERLIN and the VLA have confirmed that the two regions are physically associated as not only do they have similar linear extent (100-1000pc), but also there appears to be approximate pressure balance ($\sim 10^{-9}$ dynes cm-2) between the relativistic electrons/magnetic fields and the thermal electrons in the FLR gas.

Many Seyfert nuclei show elongated or double radio structure which strongly suggests that collimated ejection from the optical nucleus is taking place. By analogy with classical radio sources this has lead to the suggestion that a collimated beam is responsible for the radio emission. Hence, models involving the interaction of such beams with FLR clouds (Wilson 1983, Booler, Pedlar & Davies 1982) have been used to account for the relationship between the radio continuum emission and the FLR. There are, however, theoretical difficulties with such models, as the FLR clouds are unlikely to remain coherent entities whilst being accelerated to velocities many times their internal sound speed (Nittman et. al. 1982). Furthermore, in those cases where the [OIII] lines are well resolved (eg NGC1068 Meaburn & Pedlar 1986), there seems little evidence to support such a model.

As the very existence of such beams is in doubt, their parameters are, of course, highly uncertain. As the masses and sizes of the FLR clouds are also unknown, the combination of these two phenomena leads

Carol J. Lonsdale Persson (Editor)
Star Formation in Galaxies

to somewhat unconstrained series of models. Unlike the proposed beams, the properties of the radio emitting components are reasonably well defined (Unger et. al. 1986) and it seems much more reasonable to consider initially the interaction of these components with the nuclear environment.

ii) RADIAL EXPANSION OF THE RADIO COMPONENTS

The pressure of the relativistic gas in some of the radio emitting components appears to be greater than the thermal pressure of the ionised gas in the forbidden line region (Unger et. al. 1986). This led us to develop a simple model (Fig. 1) in which the radio components expand radially in a stationary medium, and in doing so shock heat and compress the ambient medium in the nuclear vicinity (see Pedlar, Dyson and Unger 1985). When the gas cools to ~10^4K it will be ionised by photons from the optical nucleus. This model readily explains the close physical connection between the radio emission and the FLR gas and can account for a number of global FLR properties such as linewidths, filling factors and densities. Also, as the gas is compressed by shocks rather than existing as individual clouds, it does not require a confining medium.

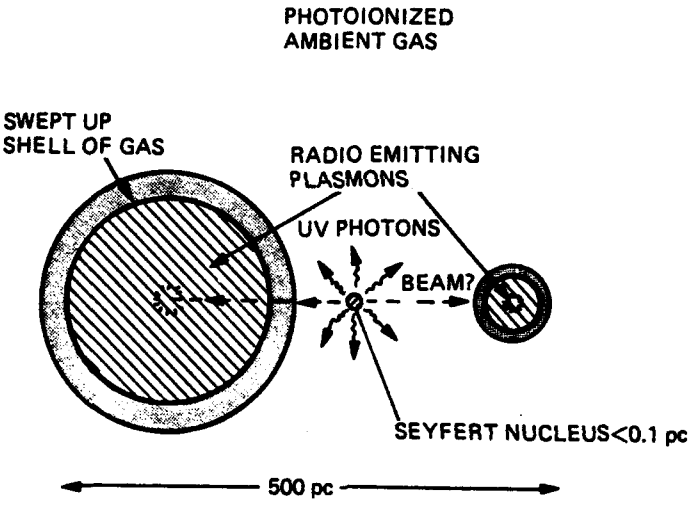

Fig. 1 Schematic diagram for the expanding radio component model. See Pedlar et. al. (1985) for a full discussion of this model.

This model predicts that much of the FLR gas will be associated with individual radio components, and that line splitting up to ~1000km/s could be observed. Unfortunately, although the radio structure is well resolved, conventional optical techniques do not have the angular resolution to determine whether the FLR components of most Seyfert II nuclei are associated with the radio components. One exception is the nucleus of NGC1068, which has an angular extent of ~8 arcsec. In this case it appears that the NE east radio component is associated with Walker's (1968) clouds I and III and exhibits line

splitting of order 1000km/s (Meaburn & Pedlar 1986). The radio structure of this component (Wilson & Ulvestad 1983), however, suggests that linear motion, as well as radial expansion is taking place which should be taken into account. We have surveyed a number of Seyfert nuclei using long slit spectroscopy and in a number of cases we have found evidence that FLR components are associated with individual radio components. The clearest example is NGC5929 (see Fig. 2) in which the FLR structure closely matches the radio double, showing two distinct velocity components.

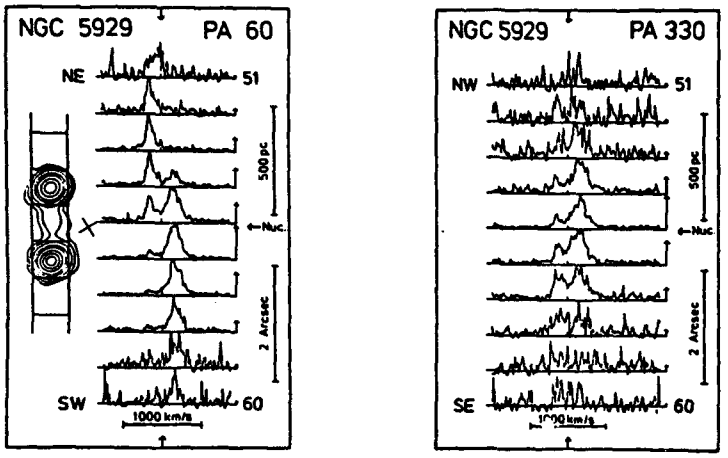

Fig. 2 [OIII] 5007A profiles along and orthogonal to the radio axis of NGC5929. See Whittle et. al. (1986) for further details.

These components lie in the same position angle as the radio components but lie slightly inside them. These observations are described in full by Whittle et. al. (1986). The linewidths of the individual FLR are relatively narrow and much smaller than would be expected to be produced by the radial expansion of stationary radio components. We suggest that the radial expansion is reduced by ram pressure due to their linear motion through the ambient gas, which, as we shall show below, can also account for the displacement between the radio and FLR components.

iii) LINEAR MOTIONS OF THE RADIO COMPONENTS

The model described by Pedlar, Dyson, and Unger assumes that the radio components expand into a stationary ambient medium. If the radio components bave been ejected from the nucleus then this approximation will only be valid after they have been braked by ram pressure of the ambient medium. Hence, in the early stages they are ram pressure confined and their linear velocity will be greater than their expansion velocity. We shall, therefore, consider the effects on the nuclear environment of linear, supersonic motions of the radio emitting components. As in the previous model we will assume that there are sufficient UV photons from the optical nucleus to ensure

that gas in the vicinity of the radio components is completely photoionised. Hence, as the emission line intensity increases as the square of the density, compression of the ambient medium due to interaction with the radio lobes will result in a local enhancement of [OIII] emission (Fig. 3).

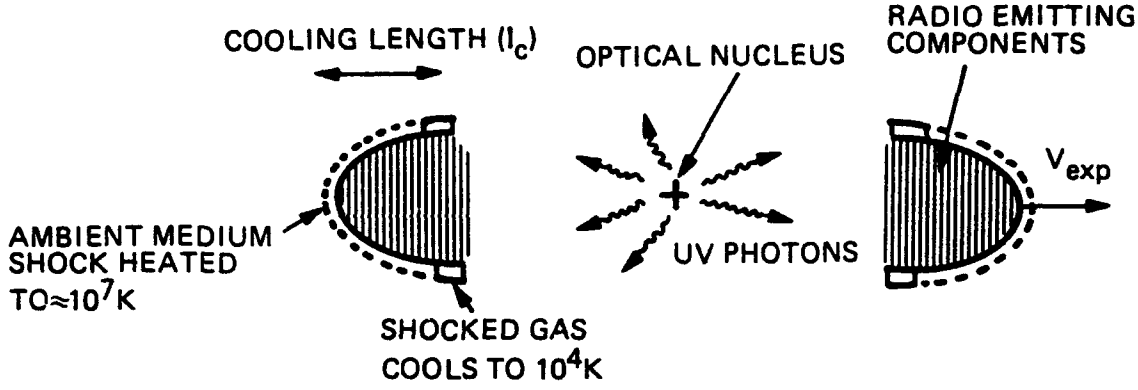

Fig. 3 Schematic diagram for the moving radio component model. The ambient medium is shock heated and compressed into a shell, and cools downstream to ~10^4 K after which it is photoionised by UV photons from the continuum nucleus.

In order to confine the radio components the pressure of the relativistic particles in the lobe (Prel) must be approximately balanced by ram pressure of the lobe moving through the ambient medium. Hence,

$$Prel=\rho v^2=1.7 \times 10^{-14} n_a V_s^{\ 2} \text{ dynes cm-2} \quad (1)$$

Where n_a is the ambient proton density in cm^{-3} and Vs is the lobe velocity in km/s. As the lobe velocity will, in most cases, be supersonic it will drive a shock into the ambient medium. This will shock heat the medium in the vicinity of the lobe to

$$T_s \sim 14\ V_s^{\ 2}\ K \quad (2)$$

with an associated cooling time

$$t_c \sim 3.2 \times 10^3\ n_s^{\ -1}\ T_s^{\ 3/2} \quad (3)$$

Where $n_s=4n_a$ is the immediate post shock density. Thus, if the lobe velocity exceeds 270km/s the gas will be shock heated to >10^6K and will have relatively long cooling times. Even in the presence of a strong UV field such gas will not emit significant optical lines until it cools. During this cooling period the radio component will move a distance ~tcVs and, consequently, there will be a linear displacement between the radio lobe and the gas which has cooled sufficiently to emit optical spectra. This cooling length will be approximately given by

$$l_c \sim t_c V_s \sim 1.4 \times 10^{-9} n_a^{\ -1} V_s^{\ 4} \text{ pc} \quad (4)$$

From the displacement between the [OIII] and radio components in NGC5929 we can estimate the cooling length to be ~50pc, and, hence, from equations 1 and 4 and the value of Prel derived from the radio continuum parameters we can estimate Vs to be ~700km/s and Na to be 7 cm-3. If we interpret the 200pc displacement between the front of the radio lobe and FLR gas in NGC1068 (Meaburn & Pedlar 1986) also as a cooling length then using Prel from Pedlar et. al. (1983) we can derive a lobe velocity of 600km/s and an ambient density of 0.7 cm-3. Note that for lobe velocities of this magnitude, even components of the interstellar medium with temperatures as high as 10^6K (ie sound speed ~150 km/s) will be compressed by a strong shock.

More detailed modeling of the ram pressure confined radio lobe and its interaction with the ambient medium are required to predict the detailed velocities and line profiles of the [OIII] emitting gas.

iv) ACKNOWLEDGEMENTS

Much of this work has been stimulated by an observing collaboration between the authors and Martin Ward, Mark Whittle, Evert Meurs, Chris Haniff and John Meaburn.

v) REFERENCES

Booler R.V., Pedlar A., & Davies R.D., 1982, MNRAS, 199, 229
deBruyn A.G. & Wilson A.S., 1978, Astron. Astrophys. 64, 433
Meaburn J.M. & Pedlar A., 1986, Astron. Astrophys. 159, 336
Nittmann J., Falle, S.A.E., & Gaskell P.H., 1982, MNRAS, 201, 833
Pedlar A., Booler, R.V., Spencer R.E. & Steward O.J., 1983, MNRAS, 202, 647
Pedlar A., Dyson J.E., & Unger S.W., 1985, MNRAS, 214, 463
Unger S.W., Pedlar A., Booler R.V. & Harrison B.A., 1986, MNRAS, 219, 387
Walker M.F., 1968, Ap. J. 151, 71
Whittle M., Haniff C.A., Ward M.J., Meurs E.J.A., Pedlar A., Unger S.W., Axon D.J. & Harrison B.A., 1986, MNRAS (in press)
Wilson A.S. & Ulvestad J.S., 1983, Ap. J. 275, 8

STRUCTURE IN THE NUCLEUS OF NGC 1068 AT 10 MICRONS

R. Tresch-Fienberg[1], G. G. Fazio[1], D. Y. Gezari[2], W. F. Hoffmann[3],
G. M. Lamb[2], P. K. Shu[2], and C. R. McCreight[4]

New 8 - 13 μm array camera images of the central kiloparsec of Seyfert 2 galaxy NGC 1068 resolve infrared source structure which is extended and asymmetric (2.1 x 0.7 arcsec FWHM), with its long axis oriented at position angle 33°. Infrared emission 1-2 arcsec to the northeast of the very center of the galaxy appears coincident with a weak, barely resolved, discrete source in the kiloparsec-scale jet detected in published radio continuum maps of the galaxy.

Very Large Array (VLA) observations show a linear, clumpy structure some 10-15 arcsec (~ 1 kpc) long, extending to the NE and SW of the nucleus. This feature is usually described as a jet (Wilson and Ulvestad 1982, 1983; Pedlar et al. 1983) though at sub-arcsec resolution the emission nearest the center of the galaxy is asymmetric in position angle (van der Hulst, Hummel, and Dickey 1982; Wilson and Ulvestad 1983). Condon et al. (1982) reject the jet hypothesis altogether, arguing instead that the radio emission arises from supernovae in regions of intense star formation.

There is clear evidence of star formation in the disk of NGC 1068. The infrared (IR) spectrum of NGC 1068 resembles thermal IR spectra seen in galactic HII regions and molecular clouds. About 98% of the galaxy's bolometric luminosity is emitted between 1.5 μm and 3 mm (Rieke and Low 1975; Telesco, Harper, and Loewenstein 1976; Hildebrand et al. 1977; Telesco and Harper 1980). A 10 μm map and far-IR aperture photometry (Telesco et al. 1984) show that about 10% of the flux density at $\lambda < 20$ μm, and virtually all of the longer wavelength IR radiation, arises principally from the galactic disk at $3 < r < 18$ arcsec, in a region where CO emission also has been detected (Rickard et al. 1977; Scoville, Young, and Lucy 1983).

The infrared images of NGC 1068 (Figure 1) were used to derive maps of the spatial distribution of 8 - 13 μm color temperature (Figure 2) and warm dust opacity (Figure 3). The results suggest that there exist two point-like luminosity sources in the central region of NGC 1068, with the brighter source at the nucleus and the fainter one some 100 parsecs to the northeast. This geometry strengthens the possibility that the 10 μm emission observed from grains in the nucleus is powered by a non-thermal source. In the context of earlier visible and radio studies, these results considerably strengthen the case for jet-induced star formation in NGC 1068.

[1]Harvard-Smithsonian Center for Astrophysics
[2]NASA Goddard Space Flight Center
[3]Steward Observatory, University of Arizona
[4]NASA Ames Research Center

Carol J. Lonsdale Persson (Editor)
Star Formation in Galaxies

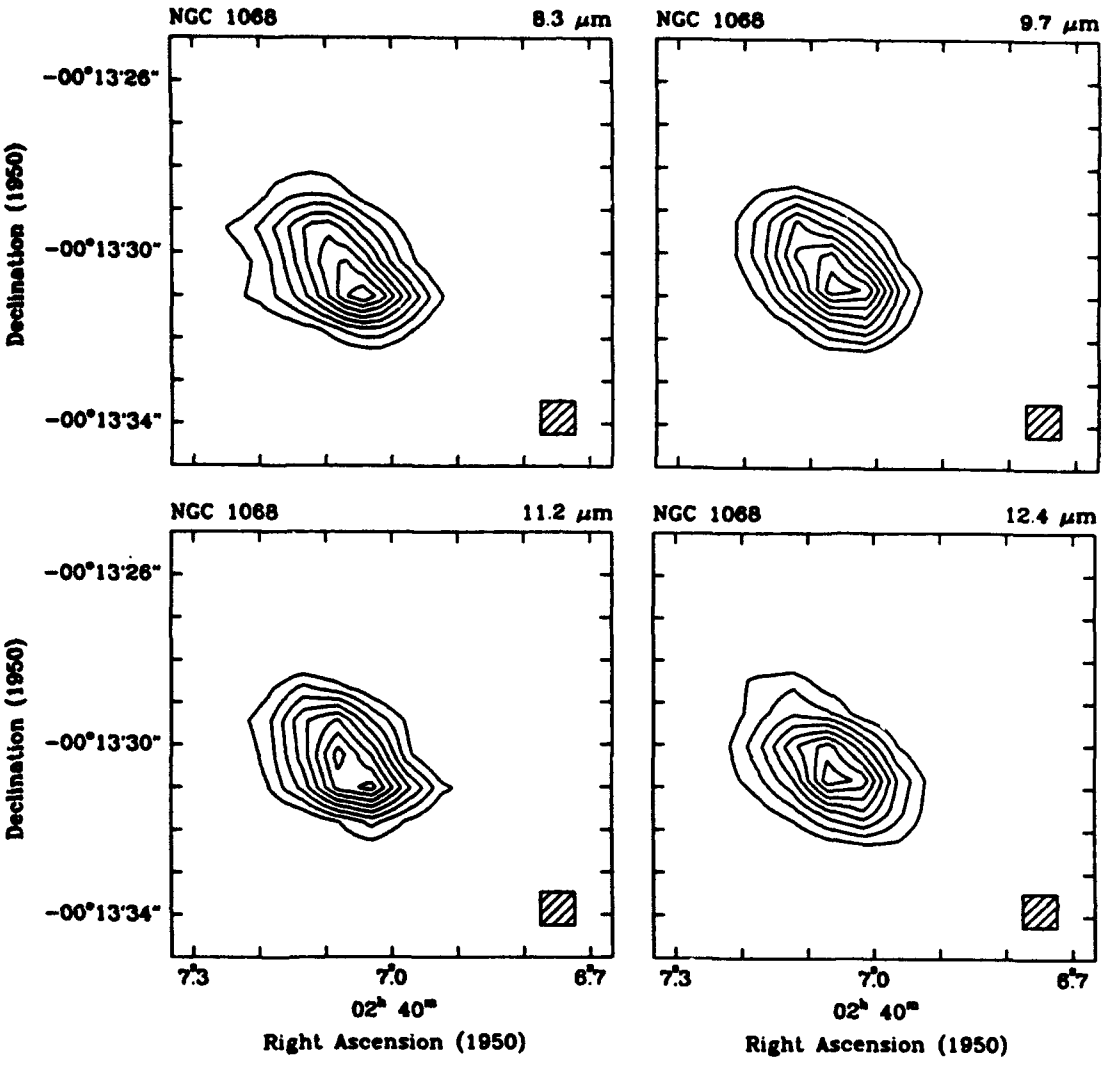

Figure 1—Calibrated isophotes for the array camera images of NGC 1068. In each case, the lowest contour level is 3σ above the mean background intensity in the periphery of the field of view, which has been subtracted from the map. The hatched square represents one 0.78 × 0.78 arcsec IR CID pixel. The contour level spacing is 1.5σ at all wavelengths: 8.3 μm (upper left), 9.8×10^9 Jy ster^{-1}; 9.7 μm (upper right), 9.1×10^9 Jy ster^{-1}; 11.2 μm (lower left), 1.3×10^{10} Jy ster^{-1}; and 12.4 μm (lower right), 1.6×10^{10} Jy ster^{-1}.

The imaging observations of NGC 1068 were made at the Infrared Telescope Facility (IRTF) on Mauna Kea, Hawaii, on 1983 August 16 using the Goddard infrared array camera system, which is based on a 16 x 16 pixel Si:Bi charge injection device (CID) array (Lamb et al. 1984; Gezari et al. 1985; Tresch-Fienberg 1985). The images were obtained in four bandpasses, with effective wavelengths of 8.3, 9.7, 11.2, and 12.4 μm and bandwidths of about 10% (Figure 1). The field of view of the array for these observations was 12.5 x 12.5 arcsec, corresponding to approximately 0.9 x 0.9 kpc.

Atmospheric conditions during the observations were very favorable; visual seeing was better than 1 arcsec. At the IRTF, the optical plate scale at the detector is 0.78 arcsec/pixel, and the diffraction-limited FWHM instrumental profile of a point source ranges from 0.9 to 1.1 arcsec between 8.3 and 12.4 μm (compared with $\lambda/D = 0.7$ arcsec at 10 μm). The actual spatial resolution of the camera system, determined from the size (FWHM) of point source calibration images, was 2.3 arcsec in R.A. and 1.3 arcsec in Dec. at all wavelengths.

The presence of a distinct IR source NE of the nucleus was tested by subtracting an instrumental point spread function (obtained from images of the reference star β Peg, c.f. Figure 5) from the array camera images and examining the remaining emission. This is appropriate because the galaxy is known to contain a compact source at its very center, based on speckle interferometry (Meaburn et al. 1982, McCarthy et al. 1982) and radio mapping (van der Hulst, Hummel, and Dickey 1982; Wilson and Ulvestad 1983).

All the images of NGC 1068 show substantial residual emission following the subtraction of a point source from the nucleus. This emission is concentrated in a small region 1.7 ± 0.4 arcsec to the NE of the nucleus at position angle 39° ± 3°. Within the uncertainties of measurement, this region coincides with the apparent extranuclear color temperature peak; it appears to be the IR counterpart of the weak radio feature described above. This new IR source emits 35% ± 10% of the total 10 μm flux density within the central 7 arcsec of the galaxy, or 7.3 ± 2.1 Jy. This demonstrates that a substantial fraction of the 10 μm emission from the central region of NGC 1068 is associated wih the radio jet outside the galaxy's core.

Close inspection of the 6 cm maps of Condon et al. (1982) and Wilson and Ulvestad (1983), as well as the 18 cm map of Pedlar et al. (1983), reveals a weak but clearly present peak in the radio continuum jet, 1.4 ± 0.2 arcsec NE of the nucleus at position angle 41° ± 9°. The 10 μm emission NE of the nucleus extends to the position of this faint radio peak, and the new color temperature and dust density maps described above indicate that there is a luminosity source there.

The existence of the NE source may be further confirmed by comparing the 8 - 13 μm appearance of the nuclear region of NGC 1068 with a simple model. Figure 4 shows a contour diagram of an IR array camera image that could result at the IRTF when observing two point sources separated by 1.6 arcsec at a position angle of 35°, with the NE source 54% as luminous as the primary source. Comparison of the real and synthetic galaxy images shows that the 10 μm morphology is reproduced quite well by this model.

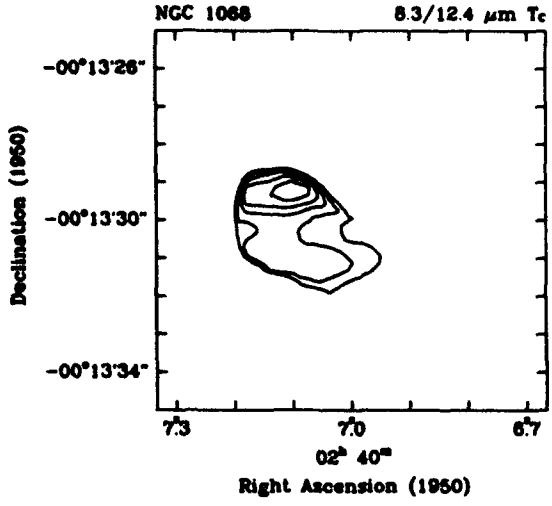

Figure 2—Map of the mid-IR color temperature near the nucleus of NGC 1068, derived from the 8.3 and 12.4 μm array camera images. Contours are plotted at 25K intervals between 300 and 425K, with the peak temperature in the NE of the map.

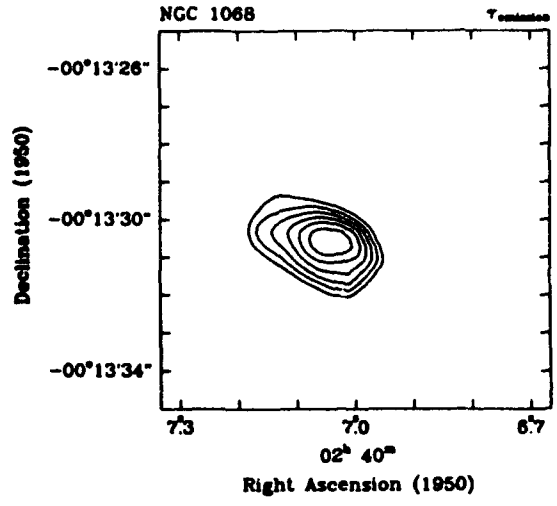

Figure 3—Map of the emission optical depth (and, by inference, the relative dust density) near the nucleus of NGC 1068, derived from the 8.3 μm intensity map and the color temperature map. Contours are plotted from $\tau = 6.66 \times 10^{-5}$ to 2.33×10^{-4}, with a level spacing of 3.33×10^{-5}.

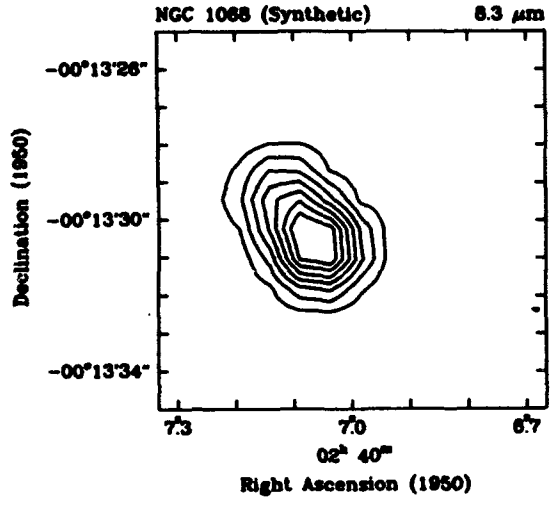

Figure 4—Contour diagram of a synthetic image generated by computing the IR array camera's response on the IRTF to a source comprised of two point-like objects separated by 1.6 arcsec at a position angle of 35°, with the NE source 54% as luminous as the primary source and spatial resolution at 10 μm of about 1.8 arcsec (the average of the 2.3 and 1.3 arcsec resolutions in R.A. and Dec. actually achieved during the observations of NGC 1068 in August 1983). The position of the primary source on the array corresponds to the assumed position of the galaxy's nucleus in the 8.3 μm array camera map (Figure 2).

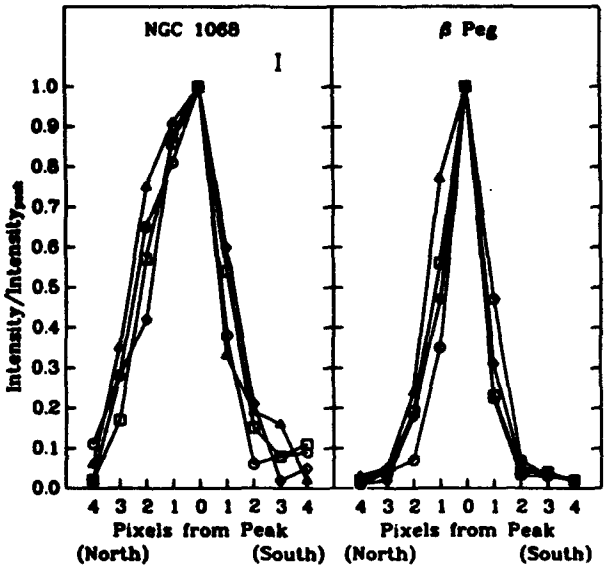

Figure 5—Intensity profiles of NGC 1068 (left) and β Peg (right) at 8.3 μm (circles), 9.7 μm (squares), 11.2 μm (triangles), and 12.4 μm (diamonds). These were generated using a 1 × 5 pixel (0.78 × 3.9 arcsec) "slit" as described in the text to simulate the declination slit scans of Bucklin *et al.* (1973). All scans have been normalized to 1.0 at the peak. A sample error bar (representing only the statistical measuring uncertainty) is shown for NGC 1068; the uncertainties for β Peg are smaller than the plotted symbols.

The principal conclusions of this work are:

1. Direct images reveal an asymmetric IR source consisting of a bright peak plus extended emission several arcsec toward the NE at position angle 33°. If the IR peak is assumed coincident with the visible/radio nucleus, then the 10 μm morphology may be interpreted as a superposition of at least two sources - one at the very center of the galaxy and another some 1.5 arcsec to the NE in the radio jet, coincident wih a weak radio continuum peak.

2. Maps of 8.3/12.4 μm color temperature and IR emission optical depth (i.e., dust density) suggest that at least two sources of luminosity are required in the central few hundred parsecs of the galaxy. The new data are consistent with the 8 - 13 μm radiation arising from thermal emission by dust grains, but a compact, non-thermal source may be responsible for some of the grain heating.

3. These results suggest that the extra-nuclear radio/IR source could be a region in which star formation has been triggered by the ejection of matter in a jet from the Seyfert nucleus.

REFERENCES

Becklin, E. E., Matthews, K., Neugebauer, G., and Wynn-Williams, C. G. 1973, Ap. J. (Letters), 186, L69.
Condon, J. J., Condon, M. A., Gisler, G., and Puschell, J. J. 1982, Ap. J., 252, 102.
Gezari, D. Y., Tresch-Fienberg, R., Fazio, G. G., Hoffmann, W. F., Gatley, I., Lamb, G., Shu, P., and McCreight, C. R. 1985, Ap. J., 299, 1007.
Hildebrand, R. H., Whitcomb, S. E., Winston, R., Stiening, R. F., Harper, D. A., and Moseley, S. H. 1977, Ap. J., 216, 698.
Lamb, G., Gezari, D., Shu, P., Tresch-Fienberg, R., Fazio, G., Hoffmann, W., and McCreight, C. 1984, Proc. S.P.I.E., 445, 113.
Meaburn, J., Morgan, B., Vine, H., Pedlar, A., and Spencer, R. 1982, Nature, 296, 331.
McCarthy, D. W., Low, F. J., Kleinmann, S. G., and Gillett, F. C. 1982, Ap. J. (Letters), 257, L7.
Pedlar, A., Booler, R. V., Spencer, R. E., and Stewart, O. J. 1983, M.N.R.A.S., 202, 647.
Rickard, L. J., Palmer, P., Morris, M., Turner, B. D., and Zuckerman, B. 1977, Ap. J., 213, 673.
Rieke, G. H. and Low, F. J. 1975, Ap. J. (Letters), 199, L13.
Scoville, N. Z., Young, J. S., and Lucy, L. B. 1983, Ap. J., 270, 443.
Telesco, C. M., Becklin, E. E., Wynn-Williams, C.G., and Harper, D. A. 1984, Ap. J., 282, 427.
Telesco, C. M. and Harper, D. A. 1980, Ap. J., 235, 392.
Telesco, C. M., Harper, D. A., and Loewenstein, R. F. 1976, Ap. J. (Letters), 203, L53.
Tresch-Fienberg, R. 1985, Ph.D. thesis, Harvard University.
van der Hulst, J. M., Hummel, E., and Dickey, J. M. 1982, Ap. J. (Letters), 261, L59.
Wilson, A. S. and Ulvestad, J. S. 1982, Ap. J., 263, 576.
Wilson, A. S. and Ulvestad, J. S. 1983, Ap. J., 275, 8.

FAR-INFRARED PROPERTIES OF OPTICALLY-SELECTED QUASARS AND SEYFERT GALAXIES

R.A. Edelson
Owens Valley Radio Observatory, California Institute of Technology

and

M.A. Malkan
Department of Astronomy, University of California, Los Angeles

Pointed IRAS observations and ground-based observations are used to determine the infrared properties of optically-selected Seyfert galaxies and quasars. The use of complete, unbiased, optically-selected samples means that statistical tests can be applied to probe the underlying properties of active galactic nuclei (AGNs).

We have studied the near-infrared-to-millimeter spectral energy distributions (SEDs) of the CfA Seyfert galaxies, a well-defined, unbiased sample of 25 Type 1 and 23 Type 2 Seyfert galaxies selected by optical spectroscopy. Spectroscopic selection allows low-luminosity, red Seyfert 2 galaxies to be found with a much higher success rate than in ultraviolet-excess surveys such as the Markarian survey. All but one of the objects observed by IRAS were detected at 60 μm, and 70% were detected at all four IRAS frequencies. A subsample of the ten brightest of the PG/BQS quasars with $B \leq 15.00$ and $M_B \leq 23.0$ were studied at infrared and radio wavelengths. Ninety percent were detected in at least three IRAS observing bands.

These data show strong trends in the infrared SEDs. Optically-selected quasars tend to have very flat infrared spectra with $\alpha_{12\mu m-60\mu m} = -0.69 \pm 0.41$ ($F_\nu \propto \nu^\alpha$, RMS scatter for individual objects), and $\alpha_{2.2\mu m-25\mu m} = -1.09 \pm 0.16$. Seyfert 1 galaxies have relatively flat infrared spectra with $\alpha_{12\mu m-60\mu m} = -1.08 \pm 0.44$ and $\alpha_{2.2\mu m-25\mu m} = -1.15 \pm 0.29$. The infrared spectra of Seyfert 2 galaxies are much steeper, with ($\alpha_{12\mu m-60\mu m} = -1.55 \pm 0.36$ and $\alpha_{2.2\mu m-25\mu m} = -1.56 \pm 0.34$). Figure 1 is a plot of $\alpha_{2.2\mu m-25\mu m}$ versus $\alpha_{12\mu m-60\mu m}$, which shows that quasars and most Seyfert 1 galaxies occupy a different region from Seyfert 2 galaxies.

This is strong evidence that the infrared spectra of Seyfert 2 galaxies are dominated by thermal emission from warm dust, while nonthermal emission is more important in the spectra of quasars and luminous Seyfert 1 nuclei. Objects with infrared SEDs dominated by thermal dust emission (starburst galaxies, Seyfert 2 galaxies, normal galaxies, etc.) almost always have steep infrared SEDs, while objects known to be dominated by nonthermal emission (such as BL Lacertae objects and OVV quasars) usually have flat SEDs. Edelson and Malkan (1986, Ap. J., 308, in press) found that Seyfert galaxies believed to be dominated by nonthermal emission in the infrared had $\alpha_{2.2\mu m-25\mu m} > -1.25$, while those thought to be dominated by thermal dust emission usually had $\alpha_{2.2\mu m-25\mu m} < -1.25$. All the optically-selected quasars and most of the high-luminosity Seyfert 1 galaxies have $\alpha_{2.2\mu m-25\mu m} > -1.37$ and $\alpha_{12\mu m-60\mu m} > -1.25$, while all the Seyfert 2 galaxies and the highly reddened, low-luminosity Seyfert 1 galaxies have $\alpha_{2.2\mu m-25\mu m} < -1.37$. Edelson and Malkan (1986) also found a strong correlation

Carol J. Lonsdale Persson (Editor)
Star Formation in Galaxies

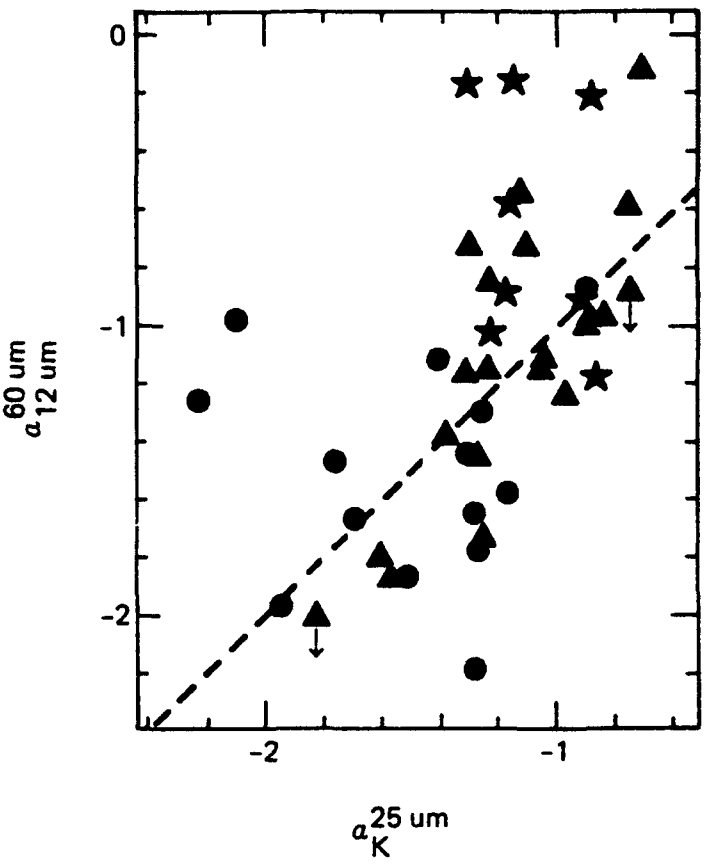

Figure 1. Color-color diagram of $\alpha 2.2\mu m/25\mu m$ versus $\alpha 12\mu m/60\,\mu m$. Quasars are denoted by stars, Seyfert 1 galaxies are denoted by triangles, and Seyfert 2 galaxies by circles. A point which lies on the dashed line has $\alpha 2.2\mu m/25\mu m = \alpha 12\mu m/60\mu m$. Quasars and Seyfert 2 galaxies occupy different regions, and most Seyfert 1 galaxies lie somewhere in between.

between reddening and infrared spectral slope. Seyfert 2 galaxies and dusty Seyfert 1 galaxies tend to have large reddenings and steep infrared SEDs, while quasars and high-luminosity Seyfert 1 galaxies have little or no detectable reddening and flat infrared SEDs.

The fact that the quasars and unreddened Seyfert 1 galaxies have straight or gently curving infrared SEDs, which extrapolate smoothly to near-infrared wavelengths, is also indicative of nonthermal emission. OVV quasars and BL Lacertae objects have infrared SEDs of this type. Dusty objects usually have infrared SEDs which curve sharply downward to higher frequencies. This is because dust cannot survive at temperatures hot enough to radiate primarily at near-infrared wavelengths.

Finally, the large 60 to 100 μm luminosities are further evidence of the dominance of nonthermal infrared emission from luminous Seyfert 1 galaxies and quasars. Assuming that the far-infrared emission from luminous quasars is thermal emission from dust, the emitting regions must be a few kpc in size. The high turnover frequencies found would imply dust high temperatures, $T_d > 70$ K. The sizes and masses are too large to be associated with the narrow-emission-line region, yet the high temperatures suggest that the dust could not lie outside the narrow-line region.

Almost one-half the Seyfert galaxies and seven of the nine quasars detected in three or more IRAS bands have far-infrared spectra which turn over between 30 and 100 μm. The nonparametric Breslow (logrank) test indicates that quasars have

higher values of the turnover frequency, ν_t, than Type 1 (or Type 2) Seyfert galaxies, at the 99.4% confidence level. Furthermore, most of the least luminous Seyfert galaxies have undetected turnovers (i.e., $\nu_t < 3$ THz). A simple explanation is that both Seyfert 1 galaxies and quasars have relatively high turnover frequencies, but that cold dust emission from the disk of the underlying galaxy masks or shifts it to lower frequencies in lower-luminosity Seyfert galaxies.

The turnover can be used to determine source parameters, depending on the emission mechanism assumed. Under the assumption that the far-infrared spectra are dominated by emission from a synchrotron self-absorbed source, with $T_B \sim 10^{11-12}$ K (as appears to be the case with quasars and luminous Seyfert galaxies) source sizes of the order of a light day are derived for quasars and luminous Seyfert 1 galaxies. These sources are typically 100 to 1000 Schwarzschild radii across, similar to the size of the hypothesized accretion disk.

For the Seyfert 2 galaxies and other dusty objects, the turnover can be used to determine minimum dust sizes and masses. This calculation yields minimum dust temperatures of 35 to 70 K. This is significantly warmer than dust in normal galaxies. Minimum source sizes of order 100 pc are derived. This suggests that the infrared emission from Seyfert 2 galaxies and dusty Seyfert galaxies arises in the narrow-line region.

INFRARED-ULTRAVIOLET SPECTRA OF ACTIVE GALACTIC NUCLEI

M.A. Malkan
Department of Astronomy, University of California, Los Angeles

and

R.A. Edelson
Owens Valley Radio Observatory, California Institute of Technology

Data from IRAS and IUE were combined with ground-based optical and infrared spectrophotometry to derive emission-line-free spectral energy distributions (SEDs) for 29 active galactic nuclei (AGNs) between 0.1 and 100 μm. The IRAS data were scaled down to account for extended emission. These correction factors, determined by comparing small-aperture ground-based 10.6 μm data with large-aperture IRAS 12 μm fluxes, were usually less than 25%. These corrected SEDs are shown in Figure 1.

Although the contaminating effects of reddening and emission from stars and dust in the underlying galaxy are significant in some SEDs, they usually can be corrected adequately. Several good indicators of nuclear dust in AGNs are identified, all of which are well correlated: 1) Steepness of infrared spectral index; 2) Reddening derived from the shape of the ultraviolet continuum; 3) Strength of the 2200 Å dust absorption feature; 4) Line ratios, such as Hα/Hβ and Lyα/Hβ; and 5) Line-free continuum colors, such as f_{4220}/f_{1770} and f_{4220}/f_{1450}.

Dust does not play a major role in many of the Seyfert 1 galaxies and quasars in this sample. The SEDs of these objects are generally well described by a simple model consisting of four spectral components, each of which dominates over a different wavelength region. Figure 2 is a plot of the model fits to three AGNs, decomposed to show the individual components. The first, which usually contains most of the total luminosity between 0.1 and 100 μm, is a power-law with $\overline{\alpha_{pl}} = -1.36 \pm 0.21$ (RMS scatter for individual objects). This power-law often has a sharp low-frequency cut-off between 40 and 100 μm, and in most of the remaining objects, the SEDs are constrained to turn over by ~ 300 μm. The simplest explanation is that the infrared luminosity is dominated by synchrotron emission from a self-absorbed source a few hundred Schwarzschild radii across, about the size of the hypothesized accretion disk. There is a strong correlation between the luminosity from this power-law at 5450 Å and the 2 keV X-ray luminosity, which suggests that the power-law may extend at least from X-ray to far-infrared wavelengths (5 1/2 decades of frequency).

The second component, which was detected in over one-half the SEDs, was a broad near-infrared excess, described by a parabola centered at 5.2 μm, with a FWHM of 3.3 frequency octaves. Although it contains less total energy than the Balmer continuum, it can account for up to 40% of the total luminosity between 2.5 and 10 μm. Its strength is well correlated with total luminosity and Hβ/[O III] ratio.

The far-ultraviolet emission is dominated by a component which was described as a blackbody with T ~ 26,000 ± 4,000 K (individual scatter). The fitted Balmer

Carol J. Lonsdale Persson (Editor)
Star Formation in Galaxies

Figure 1 (a-d)

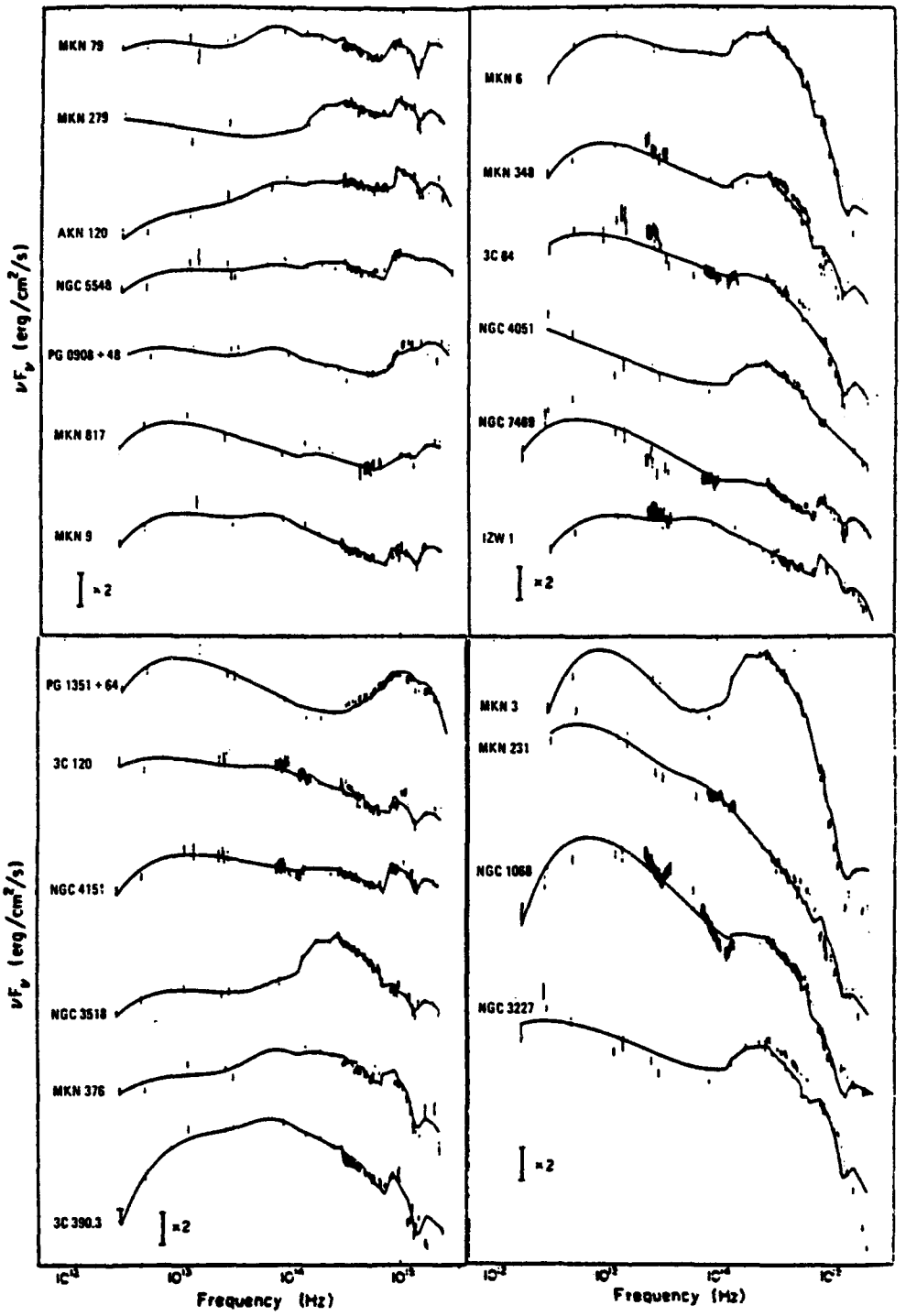

Figure 1. Fits to the infrared/optical/ultraviolet SEDs of 29 AGNs are presented in Figure 1. Observed binned continuum fluxes are shown with vertical error bars. The lines show the best-fitting models with a power law, near-infrared bump, and ultraviolet blackbody (including corrections for reddening, starlight and recombination radiation). Vertical scale is logarithm of νF_ν, so that a power-law of slope -1 (with equal power per decade) would appear as a horizontal line. The large vertical bar shows a factor of 2 in flux.

Figure 1 (e)

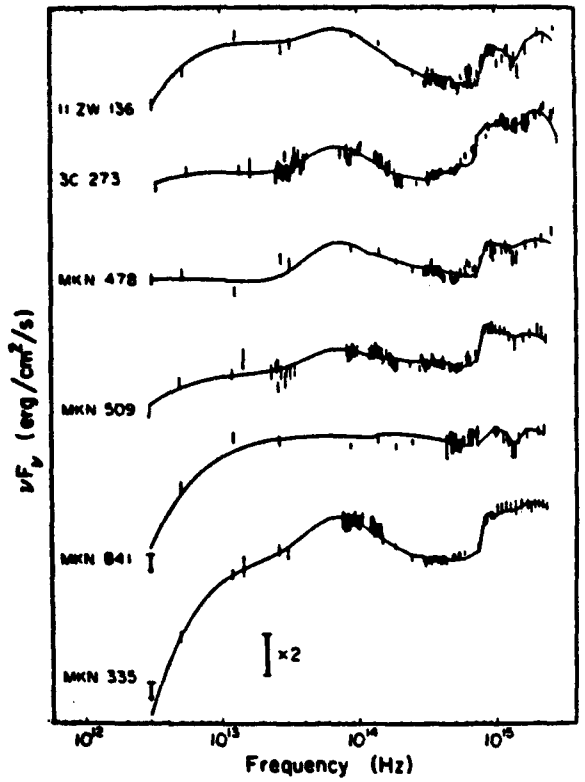

Figure 2

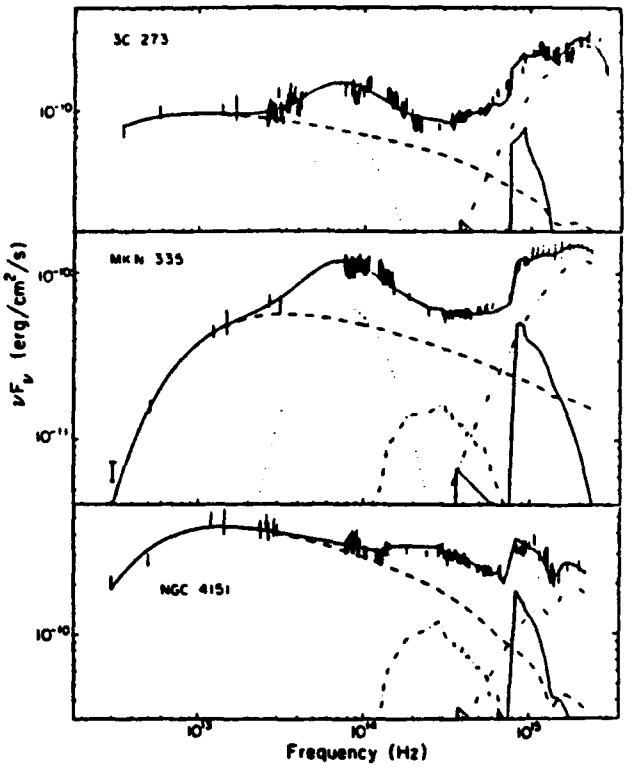

Figure 2. Detail of model fits to SEDs of 3C 273, Mkn 335, and NGC 4151. The individual components shown are the infrared power law (dashed line, which dominates the far-infrared), the near-infrared bump (dotted line; not detected in NGC 4151), the galactic starlight (dot-dash line, not detectable in 3C 273), the recombination continuum (solid line--only the Balmer continuum and a little of the Paschen continuum are strong enough to show in the figures), and the ultraviolet blackbody (dot-dot-dash line). All components have been reddened by galactic and internal reddening. The sum of these components equals the fitted model, shown by the upper solid line.

continuum/Hα ratio for the Seyfert 1 galaxies is 2.1 ± 0.6, under the assumption that the emission is optically thin with T_e = 13,000 K. This ratio is significantly greater than the prediction of Case B recombination, and shows no correlations with other AGN properties. Seyfert 2 galaxies have a lower Balmer continuum/Hα ratio than Seyfert 1 galaxies.

Although the power-law model fitted the relatively dust-free objects well, it failed to reproduce the SEDs of Seyfert 2 galaxies and Seyfert 1 galaxies with large reddenings and other strong dust indicators (i.e., NGC 3227, NGC 7469, and Mkn 231) because their fluxes beyond 10 μm are significantly contaminated by thermal emission from dust. They have minimum dust temperatures of 35-60 K, which is warmer than in normal spiral galaxies. The thermal emission appears to arise from ~ 100 $M_\odot$ of dust in a volume similar to that of the narrow line region. Low-luminosity active galaxies with 100 μm fluxes dominated by dust emission from the underlying galactic disk showed large differences between small-aperture ground-based 10-μm and large-aperture IRAS 12-μm fluxes, and steep spectral indices between 60 and 100 μm.

IRAS Observations of BL Lac Objects

C. Impey and G. Neugebauer
Palomar Observatory
Califoria Institute of Technology
Pasadena, California 91125

G. Miley
Space Telescope Science Institute
Homewood Campus
Baltimore, Maryland 21218

Abstract

IRAS data has been analyzed for 35 BL Lac objects selected from a complete 5GHz radio sample, using the coadded survey database. The detection rate is 50 % with more than 40 % detected in more than one band. This compares with only 15 % of these sources that are included in the IRAS Point Source Catalog. High luminosity BL Lac objects generally have smooth energy spectra over four or five decades in frequency, consistent with incoherent synchrotron emission from 1 cm to 1 μm. However, many low luminosity BL Lac objects have discontinuous spectra, with a large range in the spectral index at IRAS wavelengths. For BL Lacs with a total luminosity of less than 10^{44} ergs s^{-1}, most of the far infrared energy probably originates from dust heated near the galaxy nucleus. The energy budget shows that the majority of the power per unit bandwidth (νS_ν) emerges in the infrared ($1 - 100$ μm).

Introduction

BL Lac objects are compact radio sources that are distinguished by their rapid variability and high linear polarization at optical and infrared wavelengths. They are among the most energetic radiators in the universe, and apparently provide the most direct and unobscured view onto the compact engine that powers many types of active galactic nuclei. A variety of evidence indicates that relativistic motion is affecting the observed properties of the most luminous BL Lac objects. For the purposes of this study, we have included highly polarized quasars, since they share with BL Lac objects the same continuum properties of a polarized, variable core.

Methods

Few extragalactic radio sources are strong enough to be included in the IRAS Point Source Catalog (PSC), and there are two ways of reaching fainter detection limits. Approximately 40 % of the mission was devoted to pointed additional observations (AOs)

Carol J. Lonsdale Persson (Editor)
Star Formation in Galaxies

which achieved a sensitivity gain of three to eight. However, the coverage of pointed observations in this sample is very patchy. In addition, the high completeness of the survey can be traded for additional sensitivity by coadding the survey database, giving a typical sensitivity gain of a factor of three. The typical limiting sensitivities (1 σ) using survey coadds are : 12 μm – 25 mJy, 25 μm – 35 mJy, 60 μm – 35 mJy, 100 μm – 90 mJy.

The absolute calibration of flux density is based on asteroids and a set of fundamental reference stars with high quality ground-based data and good photospheric models. The following bandwidths were assumed to convert instrumental fluxes to flux densities (mJy) : 12 μm – 13.48×10^{12} Hz, 25 μm – 5.16×10^{12} Hz, 60 μm – 2.58×10^{12} Hz, 100 μm – 1.00×10^{12} Hz. These factors apply to sources with energy distributions $S_\nu \propto \nu^{-1}$, for other continuum shapes a color correction has been applied. Several nonlinear correction factors have been included, along with a correction based on the positional and sampling uncertainties from the coaddition of separate flux grids. The absolute calibration is good to 2 %, 5 %, 5 % and 10 % at 12 μm, 25 μm, 60 μm and 100 μm, but a reasonable estimate of the final uncertainty in the survey coadded fluxes is 15 %. However, many of the uncertainties in IRAS data are not normally distributed, so the contour plots and source extractions for each source have been carefully checked for anomalies, such as nearby strong sources, tracks due to bad detectors, cirrus sources at 60 μm and 100 μm, unusual source shapes, poor correlation coefficients for the template flux, and large differences between the median and local signal-to-noise in the field.

The absolute accuracy of the IRAS positions, established by a grid of $\sim$ 10,000 SAO stars, is 2.8 arcsec in-scan and 15.6 arcsec cross-scan. The mean differences between the IRAS positions and radio positions (accurate to 1 arcsec) for the detected sources are : 12 μm – 22 arcsec, 25 μm – 35 arcsec, 60 μm – 25 arcsec and 100 μm – 58 arcsec. These differences are no more than a single beam width in each waveband. The surface density of point sources down to the faint limit of the detections ($\sim$ 35 mJy at 60 μm) is roughly 54 per square degree. This assumes a surface density of 0.6 sources per square degree with S(60 μm)/S(25 μm) > 1 at a galactic latitude greater than 30°, and uses the observed Euclidean source counts of log N $\propto$ 1.5 log S. The probability of a chance coincidence between an unassociated source and the radio source position is less than 0.01 %. Therefore, the misidentification rate in this sample of 35 will be small.

Discussion

No complete sample of BL Lac objects exists, but we can get a representative idea of the properties by studying the energy distributions of BL Lacs selected from a complete radio sample. About 40 % of a sample of strong, compact radio sources show the strong optical polarization characteristic of BL Lac objects; the rest are identified with quasars and radio galaxies. The energy distributions divide easily into two classes on the basis of the *morphology of the radio/infrared energy distributions. In one set of sources* the infrared emission joins smoothly onto the compact radio emission, in the sense of a smooth and monotonic change of the spectral index α, where α = dlog S_ν/dlog ν. These sources generally include the high luminosity BL Lac objects or blazars (Figure 1a). The other

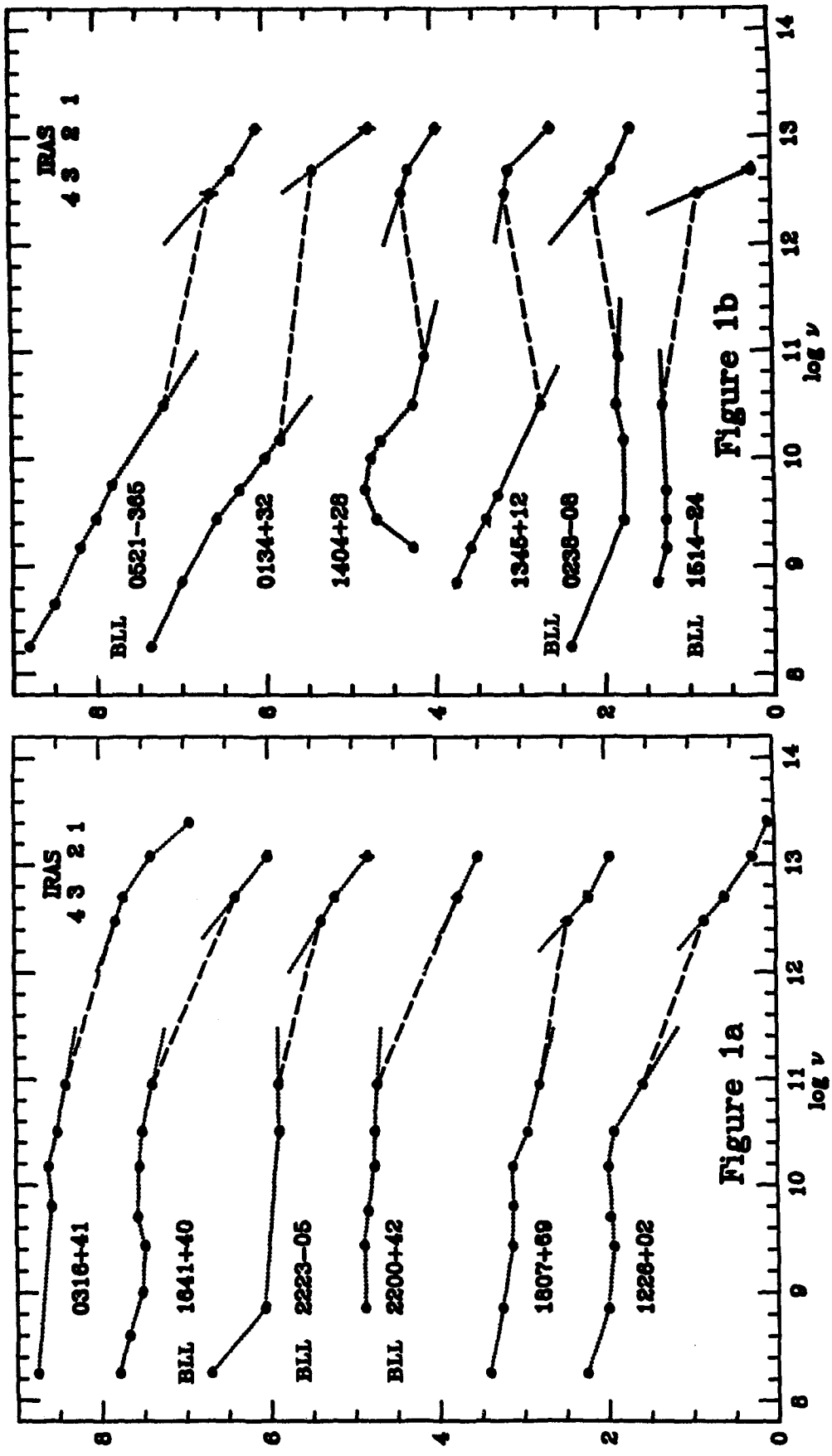
IRAS
43 21
0316+41
BLL 1041+40
BLL 2223-05
BLL 2200+42
1807+69
1228+02
log S$_\nu$ + C
log ν
Figure 1a
IRAS
43 21
BLL 0521-365
0134+32
1404+28
BLL 1345+12
BLL 0238-08
BLL 1514-24
log ν
Figure 1b

group of sources show a discontinuity between the radio and infrared emission, in the sense that the (generally steep spectrum) radio emission projects to a flux density well below the level of the IRAS data. Therefore, the spectral index must change sign at submillimeter wavelengths. These sources generally include the low luminosity BL Lac objects embedded in nearby elliptical galaxies (Figure 1b). The radio energy distributions in Figures 1a and 1b are taken from Kuhr *et al* (1981) or Owen *et al* (1980), with the IRAS data plotted on the high frequency side of the figure. The comparison of nonsimultaneous radio and infrared data does not prevent a discussion of the average spectral shape of a coilection of sources. Note that the IRAS data almost fills in the spectrum from 10^8 Hz to 10^{14} Hz.

The spectral energy distribution alone cannot pin down the emission mechanism for the infrared energy in BL Lac objects. The sources in Figure 1a have smooth continuous spectra between radio and infrared wavelengths, indicating a single emission process operating. These sources also show variability at both millimeter and near infrared wavelengths, and often linear polarization which points unambiguously to the synchrotron process. Some conclusions can be drawn about the synchrotron process in these high luminosity BL Lac objects. Two useful parameters can be calculated. One is the spectral index in the range $10 - 100$ μm, and the mean and rms dispersion of this slope for the luminous BL Lacs is $\alpha_{IR} = 1.02 \pm 0.19$. This is close to the canonical mean slope that has long been quoted both for quasars (Neugebauer *et al* 1979) and BL Lac objects (Cruz-Gonzales and Huchra 1984), but the dispersion is surprisingly small. For example, the range of infrared slope for the low luminosity radio galaxies is very large, $\alpha_{IR} = 1.74 \pm 0.81$. In addition, the optical spectral indices of a similar set of radio strong quasars (Neugebauer *et al* 1979) give a value $\alpha_{opt} = 1.89 \pm 0.79$, a steeper slope with much larger scatter. Second, the wavelength at which the spectrum turns down can be calculated. In the sychrotron model this would be associated with the most compact synchrotron component becoming optically thin. In some cases the energy spectra show a smooth and continuous curvature, and a polynomial or parabolic functional form is equally valid in fitting the spectra. In addition, there is a small scatter in the distribution of ν_B, the break frequency which has a mean and dispersion of $\log \nu_B = 11.73 \pm 0.71$. Therefore, there is a homogeneity in the synchrotron spectra of objects with a wide range of apparent luminosity (relativistic motion in some of these sources may reduce the range of intrinsic luminosity). Since energy loss mechanisms act to steepen the spectrum at high energies in the ultraviolet, there will be a larger scatter in the optical and UV spectral indices (some of this increased scatter is also due to the contribution of the broad UV *bump* seen in many quasars). However, at IRAS wavelengths the uniformity in α_{IR} must reflect a uniformity in the energy spectrum of the accelerated electrons. Similarly, the narrow dispersion in ν_B may reflect a uniformity in the physical conditions in the synchrotron core. Note that variability or errors in the extrapolation used to determine ν_B will increase rather than decrease the scatter. From basic synchrotron theory, even a monoenergetic electron distribution will integrate into a spectral energy distribution with a width of 3/2 decades in ν/ν_c where $\nu_c \sim \gamma^2 B$ is the critical frequency where most of the synchrotron power emerges. Therefore, *any* feature such as a turnover or kink in an electron energy spectrum will integrate into a feature at least as broad as the rms of ν_B for the luminous BL Lacs. On the other hand, if ν_B is

regulated by the opacity of the source, then this result may point to a narrow range in the value of the equipartition magnetic field in the cores of sources of very different luminosity.

The high luminosity BL Lacs have bolometric luminosities in the range $10^{45} - 10^{48}$ ergs s^{-1}, and 20 – 30 % of the luminosity is emitted in the infrared. For the low redshift BL Lacs, the energy spectra (Figure 1b) indicate a component with half power width of three decades of frequency and a peak in the range 100 μm to 1 mm. The lack of a smooth interface between the radio and infrared data is not due to variability, since these radio galaxies mostly have steep radio spectra with a small fraction of the flux in a compact variable core. Therefore it is likely that dust in the nucleus of the host galaxy is reradiating the moderate infrared power ($L_{IR} \sim 10^{43} - 10^{44}$ ergs s^{-1}) seen at IRAS wavelengths. Because of the steep infrared slope and inversion at millimeter wavelengths, a high fraction of 40 – 60 % of the radio galaxy luminosity can emerge in the infrared. The weaker correlation between radio and infrared power in radio galaxies does not rule out the existence of some galaxies where nonthermal radiation dominates at IRAS wavelengths. For instance, Heckman *et al* (1983) and Elvis *et al* (1984) have shown that radio galaxies with broad emission lines tend to have nonthermal power laws in the 1 – 20 μm. In general, there may be both thermal and nonthermal components in the infrared emission, and the energy distribution alone is insufficient to disentangle them. For example, in NGC 1052 the lack of 10 μm variability and steep infrared power law indicate a strong thermal component (Becklin *et al* 1982), while the significant 2 μm linear polarization means that there is also an embedded synchrotron source (Rieke *et al* 1982). For BL Lacs with $L_{IR} < 10^{44}$ ergs s^{-1}, the relative contributions of thermal and nonthermal radiation must be decided on an individual basis.

Acknowledgments

The extensive efforts of Helen Hanson in generating and analyzing the survey coadds is gratefully acknowledged. We thank Walter Rice, Carol Persson and Gene Kopan at IPAC for constant help and encouragement. This work was carried out under NASA/IRAS grant 97582 administered through Caltech/JPL. CDI received support from a Weingart Fellowship.

References

Becklin, E.E., Tokunaga, A.T. and Wynn-Williams, C.G. 1982, *Ap.J.*, **263**, 624.
Cruz-Gonzales, I. and Huchra, J.P. 1984, *A.J.*, **89**, 441.
Elvis, M., Willner, S., Fabbiano, G., Carleton, N., Lawrence, A. and Ward, M. 1984, *Ap.J.*, **280**, 574.
Heckman, T.M., Lebofsky, M.J., Rieke, G.H. and van Breugel, W. 1983, *Ap.J.*, **272**, 400
Kuhr, H., Witzel, A., Pauliny-Toth, I.I.K. and Nauber, U. 1981, *Astron.Ap.Suppl.*, **45**, 367.
Neugebauer, G., Oke, J.B., Becklin, E.E. and Matthews, K. 1979, *Ap.J.*, **230**, 79.
Owen, F.N., Spangler, S.R. and Cotton, W.D. 1980, *A.J.*, **85**, 351.
Rieke, G.H., Lebofsky, M.J. and Kemp, J.C. 1982, *Ap.J.Lett.*, **252**, L53.

Spectral Classification of Emission-line Galaxies

Sylvain Veilleux and Donald E. Osterbrock
Lick Observatory, University of California, Santa Cruz, CA 95064

ABSTRACT

A revised method of classification of narrow-line active galaxies and H II region-like galaxies is proposed. It involves the line ratios [O III] λ5007/Hβ, [N II] λ6583/Hα, [S II] ($\lambda\lambda$6716+6731)/ Hα, and [O I] λ6300/Hα. These line ratios take full advantage of the physical distinction between the two types of objects and minimize the effects of reddening correction and errors in the flux calibration. Large sets of internally consistent data are used including new previously unpublished measurements. Predictions of recent photoionization models by power-law spectra and by hot stars are compared with the observations. The classification is based on the observational data interpreted on the basis of these models.

I. Introduction

Possibly the best way we have to test our understanding of the different mechanisms responsible for the ionization in emission-line galaxies is to consider a large sample of these objects with well measured spectra, and try to determine which spectral features differentiate objects in which the photoionization is by hot OB stars from objects in which the photoionization is due to a "non-thermal" or "power-law continuum". We know that H II region-like galaxies can be distinguished from Seyfert 2 galaxies by the weakness of low-ionization lines like [N II] λ6583, [S II] $\lambda\lambda$6716,6731, and especially [O I] λ6300. It is the basis of the classification scheme of Baldwin, Phillips, and Terlevich (1981, BPT).

In the present discussion we propose a revised method of classification of narrow-line AGNs and H II region-like galaxies based on line ratios involving [O III] λ5007, [N II] λ6583, [S II] $\lambda\lambda$6716,6731, [O I] λ6300, and the Balmer lines. It excludes reddening-sensitive line ratios such as [O II] λ3727/[O III] λ5007 used by BPT. Since that paper appeared, large sets of data on emission-line galaxies have been published by Keel (1983) and Balzano (1983). These and other recent data will be included in our analysis. Our theoretical understanding of emission-line galaxies has also improved considerably during the past five years. Important publications of photoionization models by power-law spectra and by hot stars will be discussed as they can help discriminate between the two classes of objects.

II. Results and discussion

The reddening corrected line ratios of the objects in our sample are presented in figures 1-6. In these figures, NLRG stands for narrow-line radio-galaxy and NELG for narrow-emission-line galaxy (Shuder and Osterbrock 1981). In figures 1, 2, and 3 the four short dashed lines are H II region models of Evans and Dopita (1985) for

Carol J. Lonsdale Persson (Editor)
Star Formation in Galaxies

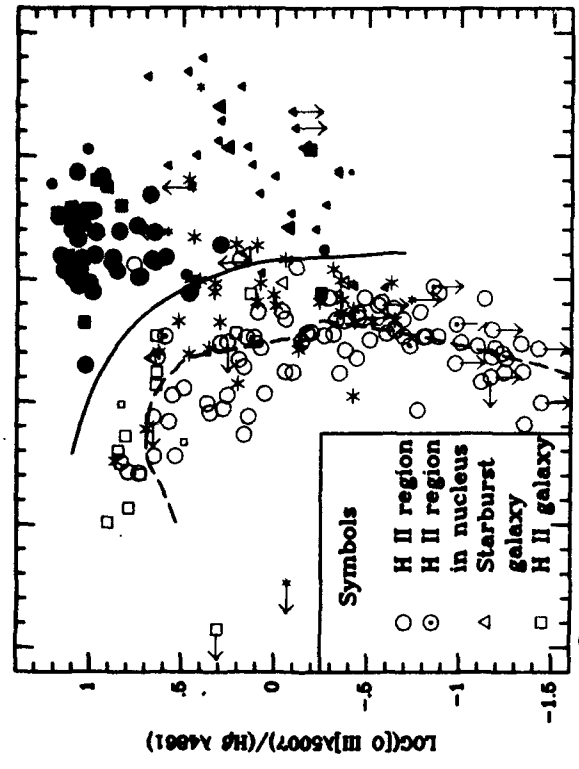

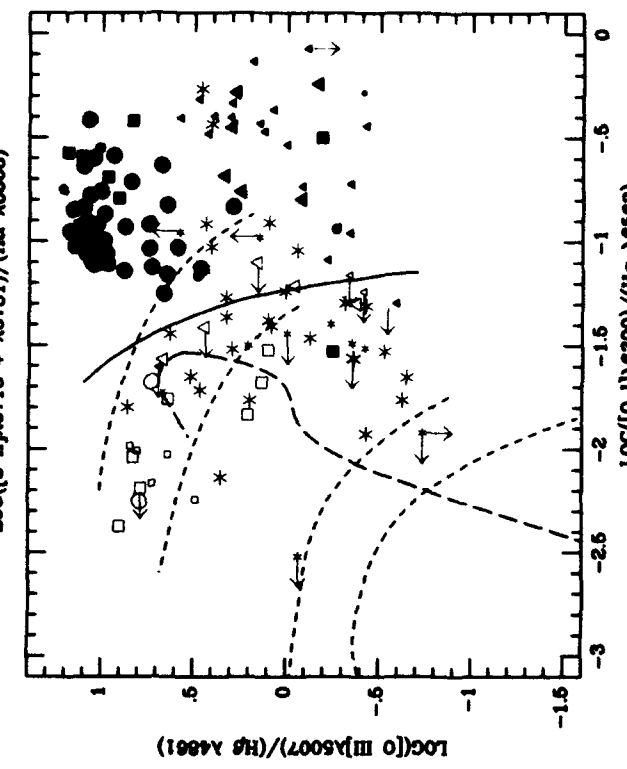

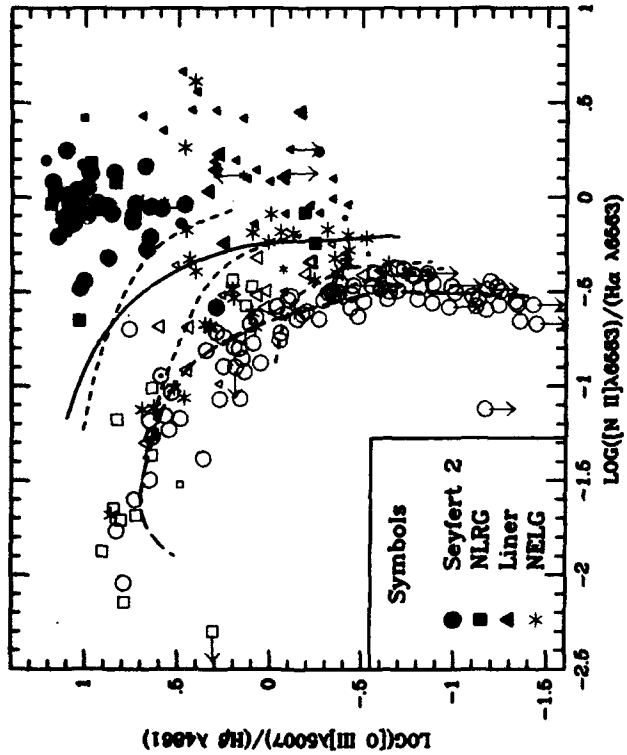

Figure 1 (above): Figure 2 (top right); Figure 3 (right)

Distribution of narrow-line active galaxies, narrow-emission-line galaxies, starburst galaxies, H II region-like galaxies and H II regions. The intensity ratios are expressed in logarithms. The size of each symbol gives an indication of its uncertainty. Arrows on data points indicate lower or upper limits. The meaning of the curves is discussed in the text.

T_e= 56 000 K, 45 000 K, 38 500 K and 37 000 K from top to bottom, respectively. The long dashed curve is the H II region model of McCall, Rybski, and Shields (1985).

In figures 4, 5, and 6 the short dashed curves are power-law models of Ferland and Netzer (1983) for solar and 0.1 solar abundances (upper and lower respectively). The ionization parameter varies along each curve from $10^{-1.5}$ to 10^{-4}. The long dashed line is the composite, two-component ($N_e = 10^2$ and 10^6 cm^{-3}) model of Stasinska (1984). The ionization parameter varies along the curve from 10^{-2} to 10^{-4}. The shock models of Shull and McKee (1979) are presented as the dot-dashed curve. Shock velocity increases along the curve from less than 80 km s^{-1} to 130 km s^{-1}.

In all six figures the solid curve divides narrow-line AGNs from H II region-like objects. A clear separation between the two classes of emission-line galaxies is apparent, especially in figures 3 and 6. The distribution of NELGs however, is not like the distribution of either class of objects. Instead some NELGs are clearly H II region galaxies while others are narrow-line AGNs.

Finally, a few objects in our sample (half-filled circles in figures 4-6) fall in the region of H II region galaxies in some diagram(s) but in the region of AGNs in some other diagram(s). Many of these objects have uncertain line ratios; others are "transition objects" where both ionization mechanisms might be operating. The "outstanding" NLRG in the first three figures was thought to be 3C 178 by Costero and Osterbrock (1977). However, a more recent accurate radio position determined by Haschick *et al.* (1980) shows that the object Costero and Osterbrock observed is not the radio galaxy 3C 178. The object they observed is an H II region galaxy that is by no means exceptional, while 3C 178 is presumably a much fainter and still unidentified quasar. This is a striking confirmation of the classification scheme.

This method of classification of emission-line galaxies is discussed in greater details in Veilleux and Osterbrock (1986).

References

Baldwin, J.A., Phillips, M.M., and Terlevich, R., 1981, *Pub. A.S.P.*, **93**, 5.
Balzano, V.A., 1983, *Ap. J.*, **268**, 602.
Costero, R. and Osterbrock, D.E. 1977, *Ap. J.*, **211**,675.
Evans, I.N., and Dopita, M.A. 1985, *Ap. J. Suppl.*, **58**, 125.
Ferland, G.J. and Netzer, H. 1983, *Ap. J.*, **264**, 105.
Haschick, A.D., Crane, P.C., Greenfield, P.E., Burke, B.F., and Baan, W.A. 1980, *Ap. J.*, **239**, 774.
Keel, W.C. 1983, *Ap. J.*, **269**, 466.
McCall, M.L., Rybski, P.M., and Shields, G.A. 1985, *Ap. J. Suppl.*, **57**, 1.
Shuder, J.M. and Osterbrock, D.E. 1981, *Ap. J.*, **250**, 55.
Shull, J.M. and McKee, C.F. 1979, *Ap. J.*, **227**, 131.
Stasinska, G. 1984, *Astr. Ap.*, **135**, 341.
Veilleux, S. and Osterbrock, D.E. 1986, *Ap. J.*, submitted.

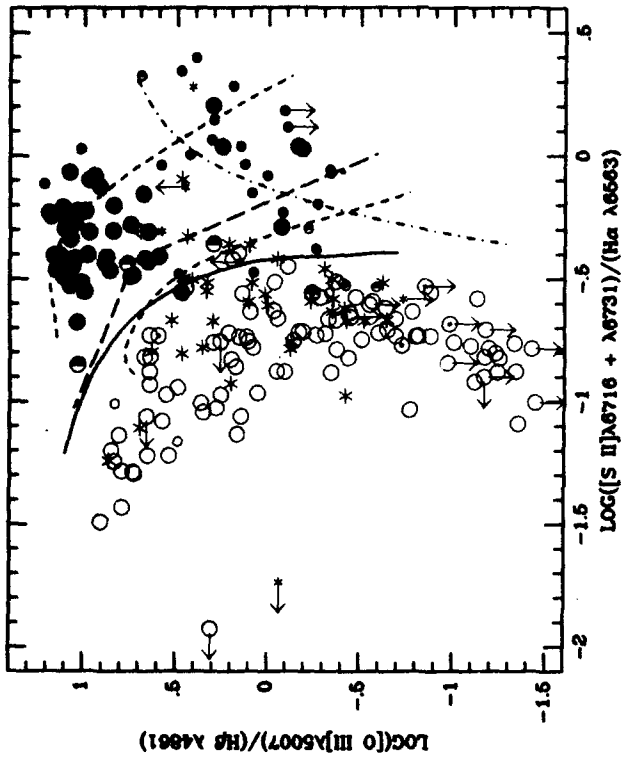

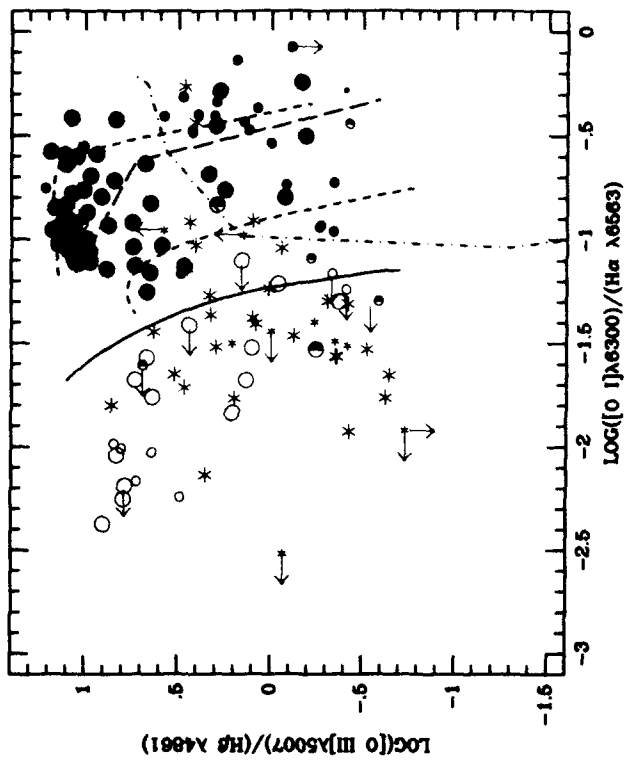

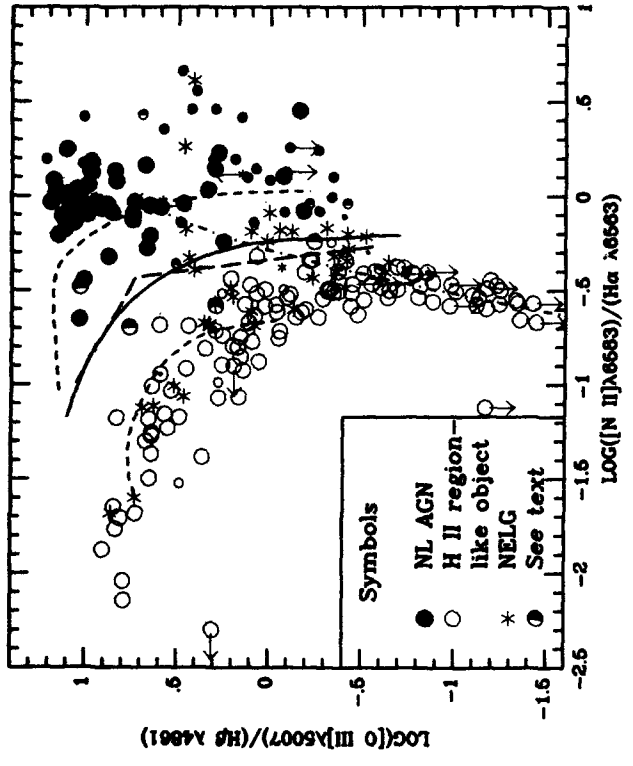

Figure 4 (above); Figure 5 (top right); Figure 6 (right)

Distribution of narrow-line active galaxies, narrow-emission-line galaxies and H II region-like objects. The intensity ratios are expressed in logarithms. The size of each symbol gives an indication of its uncertainty. Arrows on data points indicate lower or upper limits. The meaning of the curves is discussed in the text.

F. CONFERENCE SUMMARIES

SUMMARY OF SYMPOSIUM: LOW LUMINOSITY SOURCES

FRANK H. SHU
Astronomy Department, University of California, Berkeley, CA 94720

INTRODUCTION

Together with Eric Becklin I have the unenviable job of trying to summarize a very diverse and productive conference. To break the job down to more manageable proportions, we have decided that I would cover the low-luminosity sources, and Eric the high-luminosity sources. Rather than try to encapsulate the many papers presented on the former subject, I shall begin my review with a summary of some major themes and end with a few speculations on possible theoretical mechanisms.

ORIGIN OF INFRARED EXCESSES OF *IRAS* GALAXIES

One of the most basic issues addressed at this meeting is surely the question of the origin of the infrared excesses of *IRAS* galaxies with large ratios of infrared to optical luminosities. Three leading contenders were put forward as the fundamental energy source powering the phenomenon:

(a) the physical collision of two nuclear disks,

(b) a burst of star formation in the central kpc of a galaxy,

(c) reprocessing of the light from an active galactic nucleus (AGN).

In particular, Martin Harwit started his presentation of the model developed by himself and his colleagues with some strong philosophical arguments why candidate *(a)* should be favored over candidate *(b)*. Now, I personally am very susceptible to such an appeal, and am persuaded that the only viable counter to a good philosophical point is another good one. Let me therefore give what is probably the standard party line on this point, namely, the consideration of energy efficiencies.

(a) If one has a gram of matter and one wishes to generate light, dropping this matter down a galactic potential well characterized by a velocity of 300 or 500 km/s (*i.e.*, roughly 10^{-3} the speed of light) will yield a kinetic energy (which can be coverted to heat and photons in inelastic collisions) of $\sim 10^{-6}\ mc^2$.

(b) Dropping the same gram of matter onto the surface of a main-sequence star will liberate about the same potential energy as dropping it through a large galaxy, but if this (hydrogen-rich) matter later undergoes fusion reactions, the efficiency increases to about 1%. Of course, in high-mass stars, only about 10% of the entire mass is ever burned, so the overall energy release is more like $\sim 10^{-3}\ mc^2$.

(c) One can do better by dropping the same gram down a black hole. The efficiencies are not known accurately, but most estimates for swirling accretion in a disk geometry yield an energy release of about $10^{-1}\ mc^2$.

The argument now proceeds that if one wishes to explain the most energetic members of any class of phenomenon, it pays to be as efficient as possible in the use of matter to create

Carol J. Lonsdale Persson (Editor)
Star Formation in Galaxies

energy. From this point of view, when considering the most luminous of the *IRAS* galaxies, it is natural that one should first examine the AGN possibility represented by the last member of the above list. For lower and lower luminosity sources, one can perhaps safely proceed further and further back on the list. But the penalty for using one of the earlier mechanisms to explain a very high luminosity source is that the fundamental energy supply cannot last very long, and therefore the likelihood of seeing the phenomenon at any given time becomes small.

Nevertheless, I believe that ample evidence was presented at this meeting that starbursts are behind many of the less energetic examples of strong infrared-emitting galaxies. The most compelling argument concerned the spatial location and extent of the infrared emission and the associated molecular gas. Sofue, Lo, and Turner showed us beautiful maps that indicated large amounts of molecular gas, the raw material for star formation, are found in the central few hundred parsecs of candidate starburst galaxies. The total amounts of gas in these galaxies deduced from CO observations, as reported by Dave Sanders and others, is often disturbingly large – in excess of $10^{10}\ M_\odot$ in some cases. The associated far infrared emission, as detected from multi-aperture studies, is frequently spatially extended, ranging in scale from 10^{-1} kpc to 10^{1} kpc. And, as we learned from Frank Low's discussion, the *IRAS* observations themselves used in a super-resolution mode can sometimes rule out pointlike (*i.e.*, AGN) models for the source of the warm dust emission.

Equally conclusive for me were the many correlations with indicators of star formation: hydrogen recombination lines, especially the Brackett lines recommended by Paul Ho – shocked molecular hydrogen, as reported upon by Dr. Joseph and others – various spectroscopic diagnostics of young massive stars, especially the CO bandheads associated with M supergiants discussed by George Rieke – etc. The correlation with radio continuum emission was also good – in fact, inexplicably good – and I thought I heard a collective sigh of relief from the audience when Dr. Eales reported that the correlation of nonthermal radio continuum with far infrared emission may, after all, have more scatter than originally thought.

DEFINITION OF A STARBURST

Another topic which occupied much of the attention of this conference's participants seemed to be the question of the proper definition of a starburst galaxy. Dan Weedman offered a particularly sweet definition in his talk, but I gathered that most people favored a definition that would take into account some notion of a high star formation efficiency. An operationally useful measure of the rate of star formation per unit mass of raw material is the ratio

$$L_{IR}^{OB\ sf}/M_g, \tag{1}$$

where $L_{IR}^{OB\ sf}$ is the part of the (far) infrared luminosity of a galaxy which can reasonably be attributed to OB star formation and M_g is the total mass of (molecular) gas in the galaxy. Many of the papers of the conference addressed the issues of how to derive either the numerator or the denominator of the above ratio.

The best determinations of $L_{IR}^{OB\ sf}$ involved physically motivated decompositions of the infrared emission seen in the four *IRAS* bands. The models discussed by Peter Mezger, Jean-Loup Puget, and reviewed by George Helou on behalf of Michael Rowan-Robinson and Tieje de Jong, had various combinations of the following four elements in their decompositions:

$$L_\nu = L_\nu^c + L_\nu^w + L_\nu^h + L_\nu^{AGN}, \tag{2}$$

where L_ν^c is a cold or "disk" contribution which comes from H I and cold H_2 gas, L_ν^w is a warm or OB stars contribution which can be associated with a "starburst" in the extreme cases, L_ν^h is a hot or small-grain component associated with non-equilibrium heating of PAH particles, and L_ν^{AGN} is a Seyfert component associated with dust heating by a central engine. The consideration of PAHs is mostly important at 12 μm; strong emission at 25 μm may need to invoke an AGN component, but as Carol Persson has argued, the main contributors at 60 and 100 μm, where the bulk of the radiant energy is generally emitted, are the "warm" and "cold" components in most galaxies. Although the details differed somewhat, I gathered the impression that most of the workers in this field got results in reasonably good agreement with one another. For example, as a rule of thumb, roughly half each of the far infrared emission from a "normal" spiral galaxy comes from the warm and cold components. In principle, then, we now have the numerator $L_{IR}^{OB\ sf}$ as the integral of L_ν^w over frequency ν.

The determination of the denominator M_g in equation (1) turned out to be more controversial. Dr. Krugel is correct, in principle, when he says that the best method for estimating the total gas mass is from measurements of the submillimeter and millimeter luminosities. At submillimeter and millimeter wavelengths, the thermal emission from dust grains can be assumed to be optically thin, and the Planck function can be approximated accurately by its Rayleigh-Jeans limit, so that the total thermal emission is proportional to an integral of the dust temperature T_d over the mass distribution of the dust. If a single value of T_d dominates, we have

$$L_\nu \propto M_d T_d, \tag{3}$$

where M_d is the total dust mass and where the proportionality constant (essentially the dust emissivity) is a function only of the bulk optical constants of the grains and not of their sizes (if the grain radii are small in comparison to the wavelength). Since L_ν can be measured and T_d can be modeled, equation (3) allows a straightforward deduction for M_d, from which one can obtain M_g if one assumes a (standard) ratio for the gas to dust. The procedure sounds foolproof; however, one must remember that interstellar dust emissivities at submillimeter and millimeter wavelengths are not yet perfectly known; residual uncertainties of factors of 2 to 3 still exist, although this situation should improve with time as better empirical calibrations are established.

Until these calibrations are available, it would probably be wise to continue to use other methods in parallel with the one above. The CO method commonly assumes that the luminosity in the ^{12}CO line is proportional to the total amount of (molecular) gas:

$$L_{CO} = C_1 M_g, \tag{4}$$

where C_1 is a constant whose value can be obtained by calibration on nearby clouds. The question has been raised at this conference how it is valid to use optically thick radiation to estimate masses. On the face of it, this criticism sounds devastating. However, a good defense exists for the procedure; indeed, the technique did not originate with CO observers – optical astronomers use radiation from optically thick objects to estimate masses all the time! Stars like the Sun have a total optical depth of about 10^{12} through their centers, yet this does not prevent optical astronomers from gathering the integrated starlight from a galaxy to estimate its mass. What is needed, of course, is a calibration of the *mass to light ratio*, *i.e.*, the notion that in some sense one is counting stars of a common population of types. Similarly, if one is *counting clouds* of a fixed population of types, the use of equation (4) is justified. However, variations of C_1 (with gas temperature T_g, etc.) cannot be easily discounted.

Checks for the CO procedure do exist for the Milky Way. As discussed by Phil Solomon, the masses M of individual giant molecular clouds (GMCs) can be obtained both by the above conversion procedure and by application of the virial theorem. Within factors of 2 or so, the results seem in good agreement:

$$M_{CO}^{GMC} \approx M_{V.T.}^{GMC}. \tag{5}$$

In external galaxies, an indirect check exists in Judy Young's work. She finds a correlation between the total far infrared emission (not decomposed in the manner described earlier) and the CO emission of the form:

$$L_{IR} = C_2 L_{CO}^{\beta}, \tag{6}$$

where the exponent β is a pure number with a quoted range between 0.8-0.9 and C_2 is a constant for galaxies of a certain type. She also finds that the types of galaxies ("normal," "starbursts," ...) can be separated out in bands in the $\log(L_{IR})$-$\log(L_{CO})$ plane according to their dust temperatures, *i.e.*, C_2 is really a function of T_d. This conclusion, I believe, worries a number of people, for if the characteristic dust temperature T_d can vary from galaxy to galaxy, why not the characteristic gas (CO) temperature as well? In other words, is C_2 really a function of T_d, T_g, and yet other variables? How does this affect the determination of the exponent β? Despite these reservations, I believe everyone can agree that the observed systematic displacement of "starburst" galaxies from "normal" ones (as classified by other techniques) in the $\log(L_{IR})$-$\log(L_{CO})$ plane is reassuring.

The substitution of equation (4) into equation (6) yields the correlation

$$L_{IR} = C_1^{\beta} C_2 M_g^{\beta}. \tag{7}$$

The indirect check on the whole procedure arises by noting that β is close to unity, which suggests that for a given galaxy type (given C_1 and C_2), the total star formation rate ($\propto L_{IR}$) is (almost) linearly proportional to the total amount of molecular gas M_g, *i.e.*, star formation occurs (almost) independently in individual molecular clouds. The reasonableness of this conclusion speaks in favor of the CO method for determining gas masses; however, it should be noted that the argument is somewhat flawed by the result that the best fit for β is not unity and by the possible variability of C_1 and C_2. As I shall argue toward the end of my summary, in some of the more extreme starburst galaxies, the CO observations cannot be counting molecular clouds – at least not of the variety with which we are familar in the Milky Way. In any case, within the context of equation (7), the issue of enhanced star formation efficiencies manifests itself in the need for the net coefficient $C_1^{\beta} C_2$ to be a factor of 4 to 5 larger for "starburst" galaxies than for "normal" spirals. Given the uncertainties inherent in the various calibrations, I personally am unsure how seriously to take the implied interpretation that starbursts have a star formation efficiency "only" a factor of 4 to 5 larger than normal galaxies. The ratio $L_{IR}^{OB\,sf}/M_g$ could be appreciably larger than 4 to 5 if $L_{IR}^{OB\,sf}$ virtually equals the total L_{IR} in starbursts but is only half of L_{IR} in normal galaxies, and if M_g has been systematically overestimated in the former because the gas temperatures T_g are higher than in the latter.

The gas mass deduced for the central kpc of some of the most active starburst candidates is so large in some extreme cases ($\sim 10^{10}\ M_\odot$) that it should dominate the gravitational field of the region. Since the gas likely forms a rotating disk, rotation curves from resolved H I

or CO studies may yield good values for the total mass contained in the nuclear regions. It would be useful to compare such dynamically derived masses with the very large estimates for M_g that result from application of the techniques discussed above.

TRIGGERS OF OB STAR FORMATION

Another major area addressed by this conference was the discussion of mechanical triggers of OB star formation. Scoville and Kaufman talked about the effect of *spiral arms*; Devereux and Lo talked about *bars* and *oval distortions*; and a large number of speakers talked about *interacting galaxies*. In the last case, as Alar Toomre reminded us, there are a number of different levels of interactions. At the lowest level, there are gravitationally induced *orbit crashings*; at the next level, there are *thefts* of the fuel for star formation or nuclear activity; and at the most violent level, there are *mergers*. The common underlying theme in all of the proposals seems to be the idea that if one somehow gathers enough gas in a confined space, there will be enhanced OB star formation: the better this is done, the more spectacular will be the resulting starburst.

While this intuitive idea has considerable merit, and the empirical evidence for some sort of effect now seems overwhelming, a few words of caution may still not be out of place. The first caveat concerns the role of mergers in making starbursts in the central kpc of a galaxy. Alar Toomre emphasized how the dissipativeness of interstellar gas would enable it to settle deeper than the stellar component in the gravitational potential well of a merger product. However, there may be a more serious difficulty than binding energy, and that is how to get rid of the excess angular momentum in one or a few orbit crossings. Colin Norman gave a formula for angular momentum transport which indicated very short timescales, but it should be noted that his formula works best near resonances, and that his numerical estimate for the drag coefficient γ invoked the observed nuclear conditions of starburst galaxies. Getting all that gas there in the first place is the real problem. Perhaps the resolution of this problem will come from natural selection, namely, that only those mergers involving appropriate combinations of orbits and spins as to give large amounts of gaseous matter with nearly zero angular momenta will naturally produce nuclear starbursts. (With a flat rotation curve, to reach 1 kpc from 10 kpc, matter needs to have cancelled 90% of its specific angular momentum.) The other combinations may give mergers which do not yield nuclear starbursts, and it would be interesting to work out what the statistics of mergers and starbursts have to say on this possibility.

Jay Frogel in his talk likened the large-scale problem of galactic star formation to the study of a "forest." This analogy raises the caveat that it is not at all obvious how the supposed "trigger" of starbirth is supposed to work on the level of the "trees." For example, OB stars are observed to form not just anywhere in Galactic molecular clouds, but only in the densest cores where the ambient pressure in the form of density times temperature, nT, exceeds 10^7-10^8 in cgs units. Think of the Becklin-Neugebauer object, or W3 (OH), as studied by Jean Turner and Jack Welch, if you want to visualize the extreme interstellar conditions under which OB stars are born. It is the formation of these kinds of regions that one must induce if one wants to trigger OB star formation.

The final caveat begins by noting that the subject of starbursts did not begin with the *IRAS* discoveries of infrared-bright galaxies. Zwicky may well have known about the phenomenon in 1937; certainly in the early 1970s, Sargent and Searle were actively calling astronomers' attention to the problem of blue compact dwarf galaxies. Such dwarf galaxies can evidently

undergo starbursts, and as Jay Gallagher and Deidre Hunter have frequently emphasized, some of these systems seem to have none of the gravitational trigger mechanisms enthusiastically embraced at this meeting.

BIMODAL STAR FORMATION

An idea implicit to many people's discussion at this conference, but mentioned explicitly only in the talks by Scoville and Montmerle, is *bimodal star formation*. By bimodal star formation, I mean the notion first introduced by Peter Mezger and Lindsey Smith, and subsequently expanded upon by Rolf Gusten, Richard Larson, and many others, that somehow the modes of formation of low-mass stars and high-mass stars are different and take place more or less independently of each other. The idea is intrinsic to many of the papers presented here because starbursts appear to be primarily a phenomenon of enhanced *OB star formation*. Indeed, in many active regions of OB star formation, a normal initial mass function will give an untenable number of accompanying low-mass stars.

From observations of star forming regions in the Galaxy, it is known that the formation of low-mass and high-mass stars take place in morphologically different kinds of cloud cores. In regions like the Taurus or Ophiuchus molecular clouds, the small cores from which low-mass stars form have gas temperatures $T_g \sim$ 10-30 K and visual extinctions $A_V \sim 10^1$-10^2 mag. This is to be contrasted with the large dense cores in giant molecular clouds with gas temperatures $T_g \sim$ 50-100 K and visual extinctions $A_V \sim 10^2$-10^3 mag. Clearly, this morphological distinction deserves investigation as a basis for a physical theory of bimodal star formation.

Considerable evidence has now accumulated that the birth of low-mass stars is not externally triggered. A relatively complete and satisfactory theory exists, in my opinion, for how such stars form. And, as has been shown by Chas Beichman, Charlie Lada, Phil Myers, and their coworkers, there are many *IRAS* sources which look like the theoretical models for low-mass protostars. The remaining empirical question for the issue of bimodal star formation is therefore: Is the formation of high-mass stars externally triggered?

CONSTRAINTS ON STAR FORMATION TRIGGERS

One constraint on the nature of star formation triggers in the context of starburst galaxies is the need for *global simultaneity*. It does not help to make a starburst if one has a mechanism which only works on one molecular cloud at a time; one needs to make *all* (or, at least, a lot) of the molecular clouds go off more or less simultaneously. Providing global timing may be one role (perhaps the primary one) of gravitational mechanisms like spiral density waves, bars and oval distortions, and interacting galaxies, but one still needs to ensure that the relevant processes act quickly enough to produce the conditions necessary for OB starbirths. This may be a potential problem for the random agglomeration picture proposed by Struck-Marcell and Scalo. As long as they stick to one-zone models, they can get impressive bursts of star formation because in a one-zone model everything is the same everywhere and stays well synchronized. As soon as they go to multi-zone models, they encounter difficulties, as has been reported at this conference. The bursts in individual zones lose coherence, and the integrated light does not show impressive variations. Gathering clouds by fast instabilities rather than by random agglomeration may offer a solution to this problem.

There is a more subtle constraint on the nature of star formation triggers when one comes to the microscopic level of individual star-forming clouds. Historically, it was thought that

external triggers were necessary because it was thought that stars formed from H I clouds. ***H I clouds are not self-gravitating.*** Clearly, it would be very difficult to form stars out of gravitationally unbound material; therefore, something seemed needed to compress or to gather H I clouds to bring them to a self-gravitating state.

Currently, it is known that star formation occurs from H_2 clouds. ***H_2 clouds are strongly self-gravitating.*** Consequently, it is important not to be trapped by an antiquated viewpoint, to be misled by an H I perspective when we live in an H_2 world. In a sense, the original problem needs to be inverted.

The point is that the star formation efficiency in H_2 clouds is observed to be generally quite low; Nick Scoville and others quote an efficiency of $\sim 1\%$ over the free-fall time at the mean density of a giant molecular cloud. Thus, once H_2 clouds have been formed (by whatever mechanism one favors), the main theoretical problem is not how to trigger star formation, but ***how to prevent it from happening even faster.*** This is the issue, of course, of the mechanical support of molecular clouds. If we understand how this works, the enhancement of star formation efficiency amounts to the ***removal*** of the natural obstacle to rapid star formation.

SPECULATIONS ON PHYSICAL MECHANISMS

What is this obstacle to rapid starbirth? What supports molecular clouds in bulk against free-fall collapse? The last is a controversial question, but all workers, at least, are agreed on one thing: it is not thermal pressure. Thermal pressure could be important in the cores but not for the cloud as a whole. Another way of saying the same thing is that the Jeans mass M_J, at the average conditions of a molecular cloud, is much less – by a few orders of magnitude – than the cloud mass M_{cl}. This implies, of course, that Jeans mass arguments have less to do with the actual problem of star formation in molecular clouds than generally thought in many theoretical discussions on the subject.

Could the support of molecular clouds be due to turbulent pressure? Many astronomers would answer yes, but I belong to that school of thought – headed by Leon Mestel and Telemachos Mouschovias – which believes that magnetic fields play the dominant role.

Why magnetic fields? First and foremost, unlike turbulence, magnetic fields are not easy to get rid of. Because the universe lacks magnetic monopoles, magnetic fields cannot be shorted out as electric fields can be by electric charges. The longevity of magnetic fields makes them a natural candidate for a resistant obstacle to rapid star formation. The critical mass M_{cr} of conducting fluid that can be supported by a magnetic flux Φ threading it is given approximately by the well-known formula,

$$M_{cr} \approx 0.15\,\Phi/G^{1/2} \sim 10^5\,M_\odot \left(\frac{B}{30\,\mu\mathrm{G}}\right)\left(\frac{R}{20\,\mathrm{pc}}\right)^2; \qquad (8)$$

i.e., even a GMC of mass $10^5\ M_\odot$ and radius 20 pc can be supported against its self-gravity entirely magnetically if the mean field strength threading it were 30 μG. The same formula can be roughly scaled to any subclump inside it, so hereafter the subscript "cl" can refer either to "cloud" or to "clump." Equation (8) provides a second reason for believing that magnetic fields can play an important role in cloud support because tens of μG fields are now commonly measured by the Zeeman effect in the denser regions of interstellar space by Carl Heiles, Dick Crutcher, Tom Troland, and their colleagues. Finally, Fred Vrba, Steve Strom, and others have shown by mapping interstellar polarization vectors in nearby dark clouds

that magnetic fields are well ordered over the dimensions of the clouds. This provides a third reason to believe that magnetic fields are strong enough, at least in the smaller molecular clouds, to prevent bad tangling by any turbulent velocity fields that may also be present.

Magnetic fields ameliorate the problem of the rotational braking of molecular cloud cores. The acceptance of their reality also has the virtue of making supersonic (but subalfvenic) "turbulence" in molecular clouds explicable. In this picture, cloud turbulence is simply the superposition of many MHD waves with the perturbations of the fluid velocity associated with the waves generally less than or comparable to the Alfven velocity v_A. The idea is that clouds have many sources of chaotic fluid motions (stellar winds, cloud collisions, etc.) which will generate a wide spectrum of MHD waves. However, waves with superalfvenic fluid motions will generate compressive shocks that dissipate the waves rapidly. Thus, an arbitrary spectrum will quickly decay mostly to Alfven waves with fluid motions v_f that are Alfvenic or less. There is a tendency for CO observers to see the largest motions because of photon trapping (Peter Goldreich, private communication); therefore, observations tend to select for $v_f \sim v_A$. But it is easy to show from equation (8) that cloud support by magnetic fields near the critical state implies that the characteristic Alfven speeds are of the magnitude needed for virial equilibrium, *i.e.*,

$$v_A^2 \equiv \frac{B^2}{4\pi\rho} \sim v_{V.T.}^2 \equiv \frac{GM_{cl}}{R}. \tag{9}$$

Thus, $v_f \sim v_A$ implies that $v_f \sim v_{V.T.}$, *i.e.*, cloud "turbulence" automatically has a tendency to look sufficient for virial equilibrium. Pushing this line of argument further, one sees that there should even be a rough correlation $v_f \propto \rho^{-1/2}$ if the magnetic field B does not vary strongly from region to region. With B held constant, the critical state is characterized by a constant mean column density (see eq. [10]), *i.e.*, the mean volume density of clouds (outside of cores) will scale as $\rho \propto R^{-1}$. Thus might arise the correlation cited by Phil Solomon: $v_f \propto R^{1/2}$.

For the issues of more immediate concern here, once one accepts the dynamical importance of magnetic fields in cloud support, one can also immediately deduce that there are logically two regimes of interest for the problem of star formation. In the *subcritical* regime, $M_{cl} < M_{cr}$, one cannot trigger gravitational collapse (star formation) by *any* amount of increased external load (external pressure) if Φ is conserved (field freezing) because the mass-to-flux ratio M_{cl}/Φ would remain fixed and subcritical. The problem is that although one may compress the cloud, one also compresses the field B, and the restoring magnetic forces rise in tandem with the increasing gravitational attraction (assuming quasi-spherical compression). To get star formation in this situation, one strategy is obviously to decrease Φ (by ambipolar diffusion) at more or less constant M_{cl}. Ambipolar diffusion, even in a largely neutral medium like a molecular cloud, is a slow steady process, and I have suggested that this provides the mode for low-mass star formation. In this mode, the production of low-mass stars would proceed at a regulated pace virtually independent of external conditions if the condensing cloud cores are well separated from one another.

In the *supercritical* regime, $M_{cl} > M_{cr}$, the cloud's self-gravity can overwhelm the magnetic support *even if the fields were to remain frozen in the fluid.* (But, of course, ambipolar diffusion would also take place concurrently and hasten the collapse process.) Fred Adams, Susana Lizano, and I have proposed that this forms a natural scheme for getting efficient star formation and/or high-mass stars. The details are vague because the relevant calculations are not yet available, but the general idea is that a supercritical cloud would be able to generate

the large, dense, and warm cores evidently needed to produce high-mass stars. It should be noted in this regard, as mentioned earlier and as many people have commented upon before, that the condition $M_{cl} > M_{cr}$ is equivalent to the existence of a critical surface density:

$$\frac{M_{cl}}{\pi R^2} > 80 \frac{M_\odot}{\mathrm{pc}^2} \left(\frac{B}{30\,\mu\mathrm{G}} \right). \tag{10}$$

The supercritical condition corresponds to the onset of relatively rapid contraction; it gives only a lower limit on the average conditions in a cloud needed to form the dense warm cores that give rise to high-mass stars. Nevertheless, if one were to put even a healthy fraction of 80 $M_\odot$ in a square parsec into O and B stars, one might expect to get areal luminosity densities of $\sim 10^4$-10^5 $L_\odot$ pc^{-2}, which is getting close to that seen in the region of the Trapezium stars in Orion. Fred Lo and his colleagues reported limiting areal luminosity densities of $\sim 10^5$ $L_\odot$ pc^{-2} for starburst galaxies. Does this number owe its explanation to the existence of a critical surface density needed by self-gravity to overwhelm cloud magnetic fields of a plausible mean strength?

For a canonical gas to dust ratio, equation (10) is equivalent to a critical mean visual extinction:

$$A_V > 4\,\mathrm{mag} \left(\frac{B}{30\,\mu\mathrm{G}} \right). \tag{11}$$

The figure 30μG may typify the average conditions only in relatively small dark clouds; GMCs, and especially their dense cores after gravitational contraction, may well have considerably larger values. Thus, it is interesting to note the following observed progression:

(a) The Taurus molecular cloud has cores with $A_V \sim 10$ mag; it is a region of low star-formation efficiency and seems to be forming an unbound association of low-mass stars.

(b) The densest portion of the Ophiuchus molecular cloud has cores with $A_V \sim 10^2$ mag; it has a high star-formation efficiency and may be forming a bound cluster containing mostly low-mass stars but also a B star or two.

(c) Massive GMCs have large dense cores with $A_V \sim 10^3$ mag; these sites produce an abundance of OB stars.

To complete the conjecture, however, we must specify how the supercritical state is ever reached. After all, if one started initially with a distribution of clouds, some supercritical and some subcritical, one would imagine that all the supercritical ones would quickly collapse on a magnetically diluted timescale. How does one then proceed today to get clouds with $M_{cl} > M_{cr}$ from a collection whose members all have M_{cl} less than M_{cr}? The answer may be simple: the build-up of M_{cl} by agglomeration. Consider two identical clouds (either H I or H_2) suspended on parallel sets of field lines. If these two clouds collide head-on *across* their average field directions, in the aggregate, M_{cl} would have doubled and so would have Φ. Thus, there has been no gain on the critical mass-to-flux ratio. Now consider colliding two identical clouds head-on *along* mutually shared field lines; M_{cl} would again be doubled but Φ would remain the same. There has now been a gain on the critical mass-to-flux ratio. Although the examples considered are idealized, a little thought shows that even random agglomerations will tend to increase the ratio M_{cl}/Φ, and therefore, (portions of) very large aggregates are likely to become supercritical sooner or later. Is this the reason that OB stars tend preferentially to be formed from the largest GMCs?

The same train of thought reveals that the quickest route to achieving supercritical conditions is not to gather clouds randomly, but to gather them *along* field lines (perhaps by the action of instabilities triggered by the gravitational mechanisms described previously). Is this the route to trigger coherent waves of OB star formation and starbursts? Clearly, more investigation is needed. What has been put forward here does not constitute a real theory so much as a suggestion of a possible physical approach to a complex astronomical problem.

A FEW RANDOM OBSERVATIONS

Let me end my summary with a few random observations. First, if it is true that some extreme starburst galaxies have $10^{10}\ M_\odot$ in the central kpc, then the mean surface mass density must be

$$10^{10}\, M_\odot/\pi(1\,\mathrm{kpc})^2 \approx 3000\, M_\odot\,\mathrm{pc}^{-2}, \tag{12}$$

which is as dense as the densest regions of the Ophiuchus molecular cloud. Unless molecular clouds are packed several deep in the vertical direction of the nuclear disk (which is difficult to sustain mechanically), there is no room in the central regions of these galaxies to store molecular clouds of the type with which we are familar in our own galaxy. We cannot be counting ordinary molecular clouds in these extreme cases, and the use of equation (4) in its standard form (constant C_1) cannot be correct in principle.

Second, efficient star formation under the condition described by equation (12) is quite plausible if we judge from the example of Ophiuchus. If, unlike Ophichus, numerous OB stars are also formed (perhaps because of higher intrinsic gas temperatures in the cores), then feedback from vigorous star formation under very cramped quarters will undoubtedly play an important role, as has been alluded to by Tim Heckman and others at this conference. Unfortunately, rigorous consideration of all the relevant effects is likely to be quite complex – the feedbacks on star formation itself could be negative as well as positive. Solid theoretical progress will be difficult; this aspect of the field may long remain primarily an observer's domain.

Finally, we should not forget the blue compact dwarf galaxies. How do starbursts work in them? Perhaps a clue exists in their not possessing much differential rotation. According to present ideas, a body undergoing only solid-body rotation will not amplify magnetic fields via dynamo action. Could dwarf galaxies possess anomalously low magnetic fields so that they lack this natural inhibitor to rapid star formation? Or is H I gas, after all, the principal reservoir for forming stars in such galaxies? Or is the constraint of global simultaneity relaxed for dwarf galaxies because the total number of cloud complexes is small enough to allow statistical fluctuations to play more of a role? Clearly, more discussion is needed of these enigmatic objects. They may provide a clue to the problem of primordial star formation, which probably took place in a high temperature environment free of magnetic fields.

MORPHOLOGY OF LUMINOUS IRAS GALAXIES: SUMMARY TALK

E. E. Becklin
University of Hawaii, Institute for Astronomy
Honolulu, Hawaii 96822 USA

As my part of the summary I will discuss the morphology of luminous IRAS galaxies and make a few comments about where we go from here in our understanding.

MORPHOLOGY OF LUMINOUS IRAS GALAXIES

I will define a luminous IRAS galaxy as one with a luminosity of $>3 \times 10^{10}$ $L_\odot$, corresponding to the break in the galaxy luminosity function (Soifer et al. 1986). I will discuss the morphological properties of three subgroups, each separated in luminosity by about a factor of ten.

For galaxies just above the break at $L \sim 3 \times 10^{10}$ to 10^{11} $L_\odot$, there appear to be two dominant types. First, there are luminous Sc galaxies in which most of the emission is coming from the disk of the galaxy. Significant infrared emission is seen both from interstellar grains and grains in giant molecular clouds (Persson and Helou 1986; Mezger et al. 1986). For these galaxies the infrared to blue luminosity ratio is similar to galaxies of a lower luminosity. Second, there appears to be a class of optically barred galaxies (~10% of all barred galaxies) that show significant infrared emission in this luminosity range (Hawarden et al. 1986). The galaxies have been discovered by their strong 25-μm emission, but also show a blue (hot) 60- to 100-μm color. Devereux (1986) has shown that these "hot" barred galaxies appear predominantly in earlier types. Observations by Devereux (1986) and Hawarden et al. (1986) indicate that the emission is nuclear in origin and probably from a burst of star formation. The galaxies NGC 253 and M82 may be nearby examples. Very interesting results on M82 indicate a ring structure and an outflow (Sofue 1986; Lo et al.1986).

For galaxies with luminosities at $L \sim 10^{11}$ $L_\odot$ to 5×10^{11} $L_\odot$, we find that galaxy interactions and mergers become much more important (Joseph and Wright 1986; Cutri 1986; Lonsdale et al. 1984). It appears from previous work and papers presented here by Keel (1986); Rodriguez-Espinosa et al. (1986); Wilson (1986); as well as the review by Rieke (1986), that we see both nuclear star formation and an active nucleus in the form of Seyfert-type activity. Surprisingly, the amount of luminosity seen in star formation and a Seyfert-type nucleus appear almost equal. This occurs collectively in a sample of galaxies and also in many individual galaxies such as NGC 1068. At this point we do not know which phenomenon is more fundamental. Put simply, we do not know the relationship between star formation and an active compact nucleus. The results presented certainly indicate that there must in fact be an important connection. Is it as simple as the fact that both are fed by interstellar material?

Carol J. Lonsdale Persson (Editor)
Star Formation in Galaxies

At a luminosity at or greater than 10^{12} $L_\odot$ we find the following properties.

1) Infrared selected galaxies have as high or a higher space density, at a given luminosity than objects selected from optical, x-ray, or radio surveys (Soifer et al. 1986, and references therein).

2) Most or all of the galaxies have a high $L_{IR}/L_B(>10)$. These are true infrared galaxies.

3) Most or all are interacting or merging.

4) There is evidence for great amounts of interstellar material from the interstellar reddening, CO line observations (Young 1986; Sanders et al. 1986) and submillimeter continuum measurements (Emerson et al. 1984; Chini et al. 1986). Most interesting, the region of strong CO emission is, in some galaxies, very compact (Sargent et al. 1986).

5) I would speculate based on a few nearby galaxies (Becklin and Wynn-Williams 1986) that most of the infrared radiation from this class of galaxy comes from an active compact nucleus.

Finally, at a luminosity of $> 10^{13}$ $L_\odot$, we do not presently know the space density of infrared objects, although a few appear to have been found (Kleinmann and Keel 1986).

COMMENTS ON FUTURE OBSERVATIONS OF LUMINOUS IRAS GALAXIES

I would like to make some points about observations of high-luminosity infrared galaxies like Arp 220.

1) Understanding of these objects will probably be critical in solving QSO-Seyfert-energy source problem. The explanation of these phenomena may require an understanding of new physical processes (for example Harwit et al. 1986).

2) We will be better off if we study a moderate number of galaxies in great detail rather than gathering large quantities of statistics.

3) The objects will be difficult to study at optical, near infrared, and x-ray wavelengths because the optical depth in dust is too large. This was nicely pointed out by Rieke in his review.

4) We need infrared diagnostics and tools to make these studies. The primary diagnostic will be infrared spectroscopy with high angular resolution. The spectroscopy is important to understand the physical environment and to get velocity information. High quality observations will be necessary in conjunction with theoretical and laboratory studies of molecular and atomic lines.

FACILITIES FOR FUTURE OBSERVATIONS

As regards tools for these studies, ground-based, suborbital, and space-based platforms will all be important. From the ground, infrared use of the

new large telescopes like the Keck 10-meter will be extremely important. This is especially true with the use of multi-element detectors at infrared wavelengths, both for imaging and spectroscopy. Also the new submillimeter telescopes, presently under construction, will be of extreme importance in studying these galaxies in the continuum and in spectral lines. Another important tool will be the proposed 3-meter airplane telescope, SOFIA. This instrument will provide a large collecting area for spectroscopy above the earth's atmosphere and will allow high angular resolution for imaging in the far-infrared.

In space, the second generation of instruments on HST will include an instrument that extends the wavelength coverage to 2.5 μm. Because of the extreme high angular resolution possible with HST this instrument will be very important. This is particularly true for the P_α line that cannot be seen from the ground.

The reduced background of a cryogenic telescope in space increases the sensitivity of an infrared telescope many orders of magnitude. Therefore, ISO and SIRTF will be critical in studies of these galaxies. I have a political concern about where these projects are headed. ISO is approved, but is now making many critical compromises because of funding. These compromises will seriously jeopardize the science return. SIRTF does not appear to be able to get in the long NASA queue of approved projects. As an outsider, I have the following question: Is it not scientifically reasonable to bring the two projects together and create the best of both projects? It seems especially relevant to discuss this today at the scientific meeting discussing the results of the extremely successful European-USA project IRAS.

SUMMARY

A year ago Malcolm Longair reviewed the first IRAS conference and concluded that the most important new result discussed at the conference was the existence of small grains or large molecules--a discovery that, in fact, was not made by IRAS. This year I am happy to report that IRAS has brought infrared astronomy into the "big league" with respect to luminous phenomena in galaxies. It now seems clear that in the luminosity range from 10^{12} to 10^{13} $L_\odot$ there is a large density of luminous infrared galaxies. In this luminosity range, the space density of galaxies selected by their infrared emission appears larger than the corresponding objects selected on the bases of their optical, radio, or x-ray emission. More important, I personally believe that it will be the detailed studies of these infrared galaxies that will give us the answer to the energy source in all luminous objects such as Seyfert galaxies and QSOs.

REFERENCES

Becklin, E. E., and Wynn-Williams, C. G. 1986, this conference.
Cutri, R. M. 1986, this conference.
Devereux, N. 1986, this conference.
Emerson, J. P., Clegg, P. E., Gee, G., Cunningham, C. T., Griffin, M. J., Brown, L. M. J., Robson, E. I., and Longmore, A. J. 1984, Nature, 311, 237.
Harwit, M. O., Houck, J. R., Soifer, B. T., and Palumbo, G. G. C. 1986, this conference.

Hawarden, T. G., Mountain, C. M., Leggett, S. K., and Puxley, P. J. 1986, this conference.
Joseph, R. D., and Wright, G. S. 1986, M.N.R.A.S., 214, 87.
Keel, W. C. 1986, this conference.
Kleinmann, S., and Keel, W. C. 1986, late paper this conference.
Krugel, E., Chini, R., Kreysa, E., and Mezger, P. G. 1986, this conference.
Lo, K. Y., Masson, C. R., Phillips, T. G., and Scoville, N. Z. 1986, this conference.
Lonsdale, C. J., Persson, S. E., and Matthews, K. 1984, Ap. J., 287, 95.
Mezger, P. G., Cox, P., and Krugel, E. 1986, this conference.
Persson, C. G., and Helou, G. 1986, this conference.
Rieke, G. 1986, this conference.
Rodriguez-Espinosa, J. M., Rudy, R. J., and Jones, B. 1986, this conference.
Sanders, D. B., Scoville, N. Z., Soifer, B. T., Young, J. S., Schloerb, F. P., Rice, W. L., Danielson, G. E. 1986, this conference.
Sargent, A. I., Scoville, N. Z., Sanders, D. B. and Soifer, B. T. 1986, late paper this conference.
Sofue, Y. 1986, this conference.
Soifer, B. T., Sanders, D. B., Neugebauer, G., Danielson, G. E., Persson, C. J., Madore, B. F., Persson, S. E. 1986, this conference.
Wilson, A. S. 1986, this conference.
Young, J. S. 1986, this conference.

INDICES

AUTHOR INDEX

Abolins, J.A. 107
Allen, R.J. 309
Appleton, P.N. 435
Arnus, Lee 461
Axon, D.J. 711
Bally, John 267
Barrett, J.W. 37
Barsony, Mary 79
Bash, Frank N. 227
Beck, Sara C. 363
Becklin, E.E. 643,753
Beichman, C. 297,531,601
Belfort, P. 501
Bicay, M.D. 277
Bothun, G.D. 273
Bottinelli, L. 597,605
Bouchet, P. 605
Boulanger, F. 21,97,297
Brink, K. 323
Campbell, Alison W. 479
Carico, David P. 601
Caux, Emmanuel 93
Chini, R. 217
Chlewicki, G. 83,113
Clark, F.O. 83,113
Clowes, R.G. 537,623
Cohen, R.S. 67
Cox, P. 23,117
Cutri, Roc M. 409
Danielson, G.E. 411
DePoy, D.L. 701
Decher, R. 497
de Grijp, Marinus H.K. 693
Deguchi, Shuji 87
de Jong, T. 323
Dennefeld, M. 501,597,605
Devereux, Nicholas 219
Dickey, John M. 575
Dressel, Linda 579
Dwek, E. 99
Dyson, J.E. 711
Eales, S.A. 531
Edelson, R.A. 723,727
Elias, Jonathan H. 241,411,601
Eskridge, Paul B. 333
Falgarone, E. 21,97
Fazio, G.G. 717
Fich, Michel 63,103
Fowler, J.W. 71
Frogel, J.A. 161,241,517
Gallagher III, John S. 167,253,257,259
Garcia-Barreto, J. A. 483
Garwood, Robert W. 575
Gatley, I. 421
Gezari, D.Y. 717
Gillett, F. 253
Giovanelli, R. 277
Good, J.C. 3
Gouguenheim, L. 597,605
Grabelsky, D.A. 67
Graham, James R. 421,517
Guiderdoni, B. 283
Hacking, Perry 547
Handa, T. 179
Harvey, Paul M. 245,515
Harwit, Martin 387
Hauser, M.G. 99
Hawarden, T.G. 619
Hayashi, M. 179
Heasley, J.N. 623
Heckman, Timothy M. 461
Heiles, Carl 553
Helou, George 153,319,575
Hill, Gary J. 611
Hjalmarson, A. 315
Ho, Paul T.P. 363,383
Hoffmann, W.F. 717
Houck, James R. 387,547
Huchra, J.P. 565
Hummel, E. 401,589
Hunter, Deidre A. 167,253,257,259
Hyland, A.R. 245
Impey, C. 731
James, P.A. 707
Johansson, L.E.B. 315
Jones, Barbara 669
Jones, Terry Jay 245
Joseph, R.D. 421,517,707
Joy, Marshall 515
Karoji, H. 505
Kaufman, Michele 227
Keel, William C. 401,559,661, 693
Kenney, Jeffrey D. 287
Kennicutt, R.C. Jr. 235,401
Kerr, F.J. 99
Kester, D 83
Klein, U. 83,589
Kleinmann, S.G. 559,565

Kreysa, E. 217
Krugel, E. 217
Kuiper, T.B.H. 71
Lamb, G.M. 717
Lamb, S.A. 259
Laureijs, R.J. 83,113
Le Squeren, A.M. 597
Leene, A. 117
Leggett, S.G. 497
Leggett, S.K. 537,619,623
Leisawitz, D. 75
Lo, K.Y. 367
Lonsdale Persson, Carol J. 153,273,297,411, 523,601
Lord, S.D. 303
Low, Frank J. 565,651
MacGillivray, H.T. 537,623
Madore, B.F. 411,523
Malkan, M.A. 723,727
Maloney, Philip 343
Martin, J.M. 597
Martin, Robert N. 383
Matthews, K. 411,601
McCarthy, Patrick J. 461,553
McCreight, C.R. 717
Meikle, W.P.S. 517
Mezger, P.G. 23,217
Miley, George K. 461,693,731
Mochkovitch, R. 501
Mooney, T.J. 37
Morrison, Philip 485
Mountain, C.M. 619
Nakai, N. 179
Neugebauer, G. 411,523,601,731
Norman, Colin A. 395
Osterbrock, Donald E. 737
Palumbo, Giorgio G.C. 387
Paturel, G 597
Pedlar, A. 711
Perault, M. 21,97
Persson, S.E. 411,523,601
Phillips, M.M. 517
Pismis, P. 483
Pogge, Richard W. 333
Prestwich, A.H. 421
Puget, J.L. 21,97
Puxley, P.J. 537,619,623
Ramsey, B.D. 497
Reach, William 553
Rice, W.L. 107,253,273,297,523
Rieke, G.H. 633
Rivolo, A.R. 37
Robertson, N.A. 707
Rodriguez Espinosa, J.M. 669
Roettiger, K.A. 401
Rohan, Michael 485
Romanishin, W. 293
Rowan-Robinson, M. 133
Rudy, Richard J. 669
Rydbeck, Gustaf 315,331
Rydbeck, O.E.H. 315
Sadun, Alberto 485
Sage, L.J. 37
Sanders, D.B. 411,471,523
Sargent, A.I. 471
Savage, A. 537,623
Scalo, John M. 435
Scoville, N.Z. 3,411,471
Sekiguchi, Kazuhiro 507
Serra, Guy 93
Shu, Frank H. 743
Shu, P.K. 717
Silk, J. 339
Simon, M. 569
Skillman, Evan D. 263
Smith, Beverly J. 565
Sodroski, T.J. 99
Sofue, Y. 179
Soifer, B. Thomas 387,411,471,523,601
Solomon, P.M. 37
Strauss, Michael A. 553
Strom, S.E. 303
Struck-Marcell, Curtis 435
Tacconi-Garman, L. J. 491
Telesco, C.M. 497
Terebey, Susan 63,103
Thaddeus, P. 67
Thronson, Harley A. 267
Tilanus, R.P.J. 309
Tresch-Fienberg, R. 717
Turner, Jean L. 363,383
Unger, S.W. 711
Ungerer, V. 247
Vader, J. Patricia 569
van Breugel, Wil 461
van Oosterom, W. 83
van der Hulst, J.M. 235,401
Veilleux, Sylvain 737

Viallefond, F. 247
Wade, R. 421
Watson, William D. 87
Weedman, Daniel W. 351
Wesselius, P.R. 113
Whiteoak, J.B. 71
Wielebinski, R. 589
Wiklind, Tommy 315,331
Wilson, Andrew S. 675
Wolstencroft, R.D. 497,537,623
Wright, Edward L. 629
Wright, G.S. 421,517,707
Wunderlich, E. 583,589
Wynn-Williams, C.G. 125,531,643
Wyse, R.F.G. 339
Young, Judith, S. 197,287,303,491
Zhang, C.Y. 83

SUBJECT INDEX

21-centimeter line - see HI
A stars 153, 158, 209, 301, 426, 601
Abell radius 281
absorption feature, silicate 246, 644
absorption lines, Balmer 605
absorption, blue-shifted 359, 643
absorption, CO 421, 633
abundance gradients 235, 263
abundance, CO 163, 182
abundance, H_2 163
abundances, heavy elements 163, 296
abundances, oxygen 247, 254, 479
acceleration, diffusive shock 228
accretion 375, 676
accretion disks 707, 725, 727, 743
active galactic nuclei - see active nuclei
active galaxies - see active nuclei
active galaxies, highly obscured 611
active nuclei 3, 127, 133, 137, 154, 228, 275, 319, 323, 359, 411, 417, 422, 429, 461, 499, 525, 531, 534, 565, 572, 576, 579, 611, 633, 643, 648, 661, 669, 675, 693, 701, 711, 725, 727, 737, 743, 753
active nuclei, infrared 427
active nuclei, low-level 125
active nuclei, quasar-like 135, 319, 430
ADDSCAN program 560, 651
Additional Observations, IRAS 83, 247, 297, 547, 651, 693
AGB - see asymptotic giant branch
age/metallicity relation 341
AGN - see active nuclei
albedo 119
Alfven velocity 750
ambipolar diffusion 750
amorphous galaxies 171, 254, 259, 262
anemic galaxies 283, 436
angular momentum transport 747
AO - see IRAS Additional Observations
aperture synthesis 128, 378, 383
aperture synthesis CO maps 471
arm-interarm contrast 5, 203, 315
Arp galaxies 136, 401
Arp ring 107
association, OB 134, 158, 259, 374
asymptotic giant branch 25, 162
atmospheres, model stellar 247, 261
atmospheric transmission windows 421
atomic gas, stripped 292
atomic hydrogen, 21 cm - see HI
atomic surface density 493
B stars 25, 70, 97, 158, 162, 209, 261, 363, 377, 422, 751
B-H color 293
B-V color - see color, optical
background, X-ray 351
ballistic particle model 227
balloon observations 23
Balmer absorption lines 605
Balmer continuum/Hα ratio 729
Balmer decrement 235, 613
Balmer emission 263, 681
Balmer lines 247, 633
bar instabilities 429
bar, molecular 303
barred galaxies 125, 127, 217, 219, 247, 307, 483, 619, 681, 753
BCDG - see blue compact dwarf galaxies
bimodal star formation 339, 748
bipolar flow 79, 83
bipolar wind, galaxies 462
BL-Lacertae objects 579, 616, 723, 731
black holes 398, 637, 676, 743
blast waves, supernova 636
blue compact dwarf galaxies 128, 583, 592, 747
blue galaxies 167, 293, 356, 583, 592, 747, 753
blue luminosity - see luminosity, blue
blue magnitudes 412, 584, 633
blue surface brightness 275
bolometric correction 527
bolometric luminosity 76, 83, 127, 169, 248, 411, 523, 703
Brackett lines 363, 422, 427, 431, 473, 620, 648, 701
broadline region 611, 678
brown dwarf 547
bulge population 296
bulge-to-disk ratio 126
bump, UV (quasars) 734
calcium triplet 164
carbon 119
carbon monoxide emission 267
carbon stars 162, 539
centimeter wave continuum 475, 575
Cepheid variables 162
CFA galaxies 353
CFA redshift survey 565
CFA Seyfert galaxies 723
CH^+ 117, 120
chemical evolution 341, 468
Chopped Photometric Channel, IRAS 83, 128
circular polarization 87
circumnuclear disks 462
circumnuclear regions 127, 475, 675
circumnuclear ring 619
circumnuclear starbursts 661, 675

circumstellar dust shells 23, 128, 135, 141, 161, 549
cirrus 21, 103, 107, 108, 109, 113, 125, 133, 148, 153, 156, 255, 301, 319, 538, 553, 605, 631, 694
cirrus, clusters 553
classification, spectral 737
cloud collision time 457
cloud collisions 8, 30, 58, 91, 316, 378, 397, 417, 435, 473, 750
cloud complexes 67, 153, 309, 438
cloud cores 6, 23, 81, 748
cloud fluid models 435
cloud parameters 3, 37, 57, 70, 77, 315, 380, 437, 444
cloud system 67, 457
cloud, supercritical 750
cloud-cloud shielding 345
cloud-star interactions 439
clouds - see also molecular clouds
clouds 67, 113, 117, 161, 164, 343, 637, 676, 745
clouds, diffuse 113
clouds, dark 346, 749
clouds, dust 71, 133, 144, 164, 485, 707
clouds, dynamics 37, 67
clouds, giant 44, 109, 227
clouds, HI 103, 134, 749
clouds, high latitude 113
clouds, identification 113
clouds, infrared 753
clouds, lifetime 457
clouds, molecular see molecular clouds
clouds, molecular, giant - see giant molecular clouds
clouds, NeII 637
clouds, quiescent 24
clouds, structure 38, 439
clouds, surface density 42
cloudy density wave model 227
clumped extinction 238
clumpy galaxies 259, 264
clumpy structure 227, 717
clusters, cirrus sources 553
clusters, galaxy 277, 283, 555, 568
clusters, globular, 161
clusters, OB star 68, 75, 77
clusters, old 67
clusters, star 76, 161
clusters, young star 67, 107, 249, 367
CNO cycle 209
CO absorption 421, 633
CO abundance 163, 182
CO bands, stellar 633
CO emission 3, 39, 46, 67, 75, 79, 84, 99, 125, 162, 179, 185, 197, 224, 241, 267, 270, 287, 292, 303, 306, 315, 331, 340, 343, 359, 367, 378, 383, 411, 414, 471, 475, 575, 648, 744, 754
CO filament 70
CO holes 197, 201, 211, 225
CO luminosity 37, 57, 197, 204, 206, 246, 267, 269, 289
CO mapping 184, 197, 224, 369, 462, 491
CO/HI ratio 200, 494
CO/H_2 ratio 345
cold dust 23, 93, 160, 323, 507, 698, 725
collapsed objects 707
collimated outflow 535
collisional energy 648
collisional rates 440
collisionally-excited lines 427
collisions, cloud - see cloud collisions
collisions, galaxies 387, 428, 457, 465, 515, 517, 643
collisions, galaxies, off-center 457
collisions, nuclear disks 387, 743
color, B-H 293
color, bulge 626
color, far infrared 63, 73, 95, 126, 155, 253, 278, 320, 328, 479, 547, 560, 611, 619, 693
color, infrared 63, 66, 278, 280, 320, 328, 479
color, near infrared 164, 293, 482, 601, 625, 634
color, optical 155, 293, 303, 401, 479, 572, 661
color, ultraviolet 479
color-color diagram 21, 64, 97, 134, 136, 319, 320, 436, 507, 675, 686, 694
color-magnitude diagrams 162, 293
column density, H_2 344, 375
compact accretors 352
compact galaxies 136, 222, 556, 579, 582, 583, 592, 747
compact galaxies, blue dwarf 128, 583, 592, 747
compact galaxies, emission-line 128
compact HII regions 65, 66, 168, 242, 384,
compact objects, emission-line 161
compact sources, infrared 163, 243, 719
compact sources, radio 367, 473, 643, 731
compactness, 10 microns 127, 612
composite nuclei 676
cool dust 63, 125, 133, 235, 319, 585, 589, 625
cool stars 164, 633
core-halo structure 656
cores, clouds 6, 81, 23, 748

cosmic-rays 42, 377, 390, 576, 583, 593
cosmology 351, 355, 358, 547, 693,
CPC - see IRAS Chopped Photo- metric Channel
critical cloud mass 442
critical density universe 629
critical surface density 751
CS 79
cusp, Galactic Center 633
cusp, M83 305
dark clouds 346, 749
dark lane 80, 183
dense clouds 23, 264, 676
density waves 227, 315, 229, 307, 438
diffuse clouds 113
diffuse emission, far infrared 21, 23, 93, 97, 99, 103
diffuse interstellar medium 75, 113, 125, 153, 273, 275
disks, accretion 707, 725, 727, 743
disks, circumnuclear 462
disks, counter-rotating 417
disks, HI 200, 228, 283, 285
disks, molecular 3, 80, 367, 462
disks, nuclear 179, 387, 743
disks, rotating 81, 678, 746
disturbed galaxies 280, 413, 643
double lobed radio sources 533
dust 97, 117, 141, 153, 168, 245, 246, 249, 267, 293, 316, 351, 411, 525, 577, 579, 633, 675, 676, 701, 727, 754
dust clouds 71, 133, 144, 164, 485, 707
dust emission features 682
dust emissivity 83, 154, 157, 279, 280, 324, 745
dust grains 23, 75, 78, 93, 104, 109, 113, 134, 254, 301, 319, 323, 557, 708, 745, 753
dust heating 301, 363, 497, 501, 583, 681
dust lane 68, 309, 499, 643
dust mass 146, 207
dust scattering 463
dust shells, circumstellar 23, 128, 135, 141, 161, 549
dust temperature 3, 12, 15, 71, 73, 83, 95, 104, 156, 197, 204, 207, 211, 289, 324, 363, 414, 583, 745
dust, cold - see cold dust
dust, cool - see cool dust
dust, graphite 24, 119
dust, high galactic latitude 33
dust, hot - see hot dust
dust, shock heated 83
dust, silicate 24, 251, 644
dust, ultraviolet-heated 84
dust, warm - see warm dust
dust-poor galaxies 326
dust-to-gas ratio 104, 253
dusty filaments 368
dusty galaxies 170, 327, 358
dusty Seyfert galaxies 725
dusty starburst galaxies 633
dwarf, brown 247
dwarf galaxies - see galaxies, dwarf
dynamics, clouds 38, 67
E galaxies - see galaxies, elliptical
E-S0 galaxies 280
early S-stars 158
early-type galaxies - see galaxies, early-type
early-type stars 66, 261
eccentricity 534
edge-on galaxies 128, 179, 186, 276, 633
EINSTEIN fluxes 357
ELD = extended low density HII regions 100
electron densities 236
electron energy spectrum 228
electron temperature 247
electrons, relativistic 126, 228, 711
ELFS = extremely luminous far infrared sources 387
elliptical galaxies 128, 136, 273, 278, 331, 333, 517, 568, 572, 734
emission features, dust 682
emission line kinematics 678
emission-line galaxies 128, 737
emission-line galaxies, compact 161
emissivity - see dust emissivity
ESO/SERC plates 113
evolution, galaxies 161, 167, 461
evolved objects 164, 242
evolved stars 336, 515
excess, infrared - see infrared excess
extended low density HII regions 100
extended molecular disks 367
extinction 63, 129, 133, 141, 156, 168, 235, 274, 296, 323, 363, 501, 515, 518, 572, 576, 579, 601, 616, 633, 643
extinction curve 115, 251
extinction, clumped 238
extinction, Hα 153
extinction, very high 637
extragalactic HII regions 263, 436
extragalactic HII regions, giant 261
extreme ultraviolet 387
extremely luminous far infrared sources (ELFs) 387
Faber-Jackson law 57
Fabry-Perot spectrometer 310

face-on galaxies 197, 345, 491, 636
faint emission-line galaxy 559
faint galaxies 357, 605, 623, 693
faint nuclei 698
far infrared aperture photometry 717
far infrared color - see color, far infrared
far infrared emission 12, 26, 75, 83, 93, 99, 153, 235, 243, 245, 246, 255, 267, 270, 276, 277, 289, 292, 293, 315, 319, 323, 387, 401, 409, 483, 501, 507, 547, 565, 575, 579, 583, 589, 629, 669, 675, 681, 731, 744
far infrared emission, diffuse 23, 93, 97, 99, 103
far infrared luminosity 3, 12, 37, 51, 57, 75, 83, 126, 153, 167, 220, 250, 267, 294, 364, 412, 463, 471, 531, 599
far infrared spectra 133, 137, 217, 297
far infrared-to-blue luminosity ratio 128, 275, 277, 321, 352, 501, 753
far ultraviolet 119, 247, 377, 727
FeII lines 421, 431
field freezing 750
FIR - see far infrared
Fisher-Tully law 57
flat spectrum radio source 473
FLR - see forbidden line region
fluorescence 115, 422
forbidden line region, optical 711
formation, galaxies 461
fossil galaxies 336
free radicals 119
free-fall collapse 4, 749
free-free emission 26, 31, 228, 235
free-free luminosity 8
fuel theft 747
fuel, star formation 224
g-band 664
G-K stars 86
G-type stars 422
galactic nuclei - see nuclei of galaxies and active nuclei
Galactic star formation 3, 37, 63, 67, 71, 79, 83, 99, 633
galaxies, active - see active nuclei
galaxies, active, highly obscured 611
galaxies, amorphous 171, 253, 259
galaxies, anemic 283, 436
galaxies, Arp 136, 401
galaxies, barred 125, 127, 217, 219, 247, 307, 483, 619, 681, 753
galaxies, blue 167, 2193, 356, 583, 592, 747, 753
galaxies, blue compact 128, 583, 592, 747
galaxies, blue irregular 259, 295
galaxies, CFA 353
galaxies, CFA Seyfert 723
galaxies, clumpy 259, 264
galaxies, clusters 277, 283, 555, 568
galaxies, CO-bright 179
galaxies, colliding - see galaxy collisions
galaxies, colliding ring 435
galaxies, compact 136, 222, 556, 579, 582, 583, 592, 747
galaxies, compact emission-line 128, 583
galaxies, compactness 222
galaxies, disks, merged 413
galaxies, distant 171, 253
galaxies, disturbed 280, 413, 643
galaxies, dust-poor 326
galaxies, dusty 170, 327, 358
galaxies, dusty Seyfert 725
galaxies, dusty starburst 633
galaxies, dwarf 110, 128, 161, 171, 245, 253, 263, 267, 331, 395, 436, 479, 583, 592, 747
galaxies, elliptical 128, 136, 273, 278, 331, 333, 517, 568, 572, 734
galaxies, E-S0 280
galaxies, early-type 124, 126, 141, 200, 219, 278, 326, 333
galaxies, edge-on 128, 179, 186, 276, 633
galaxies, emission line 128, 737
galaxies, energetic 269
galaxies, evolution 161, 167
galaxies, extreme IRAS 504
galaxies, face-on 197, 345, 491, 636
galaxies, faint 357, 559, 605, 623, 693
galaxies, fossil 336
galaxies, gas-rich 387, 399, 421, 517
galaxies, giant 171, 253, 267
galaxies, giant radio 666
galaxies, grand design spiral 227, 343
galaxies, HI-deficient 210, 278, 283, 287
galaxies, high-redshift 560, 611
galaxies, highly obscured active 611
galaxies, HII 136, 479, 482, 510
galaxies, hot 127, 753
galaxies, Im 110, 158,
galaxies, Im clumpy 259
galaxies, infrared-bright 205, 363, 651, 747
galaxies, infrared-luminous 274, 367
galaxies, infrared-selected 323, 482, 533, 589, 601, 754
galaxies, interacting 3, 37, 51, 56, 57, 175, 197, 207, 245, 277, 280, 283, 387, 401, 406, 409, 416, 421, 431, 436, 457, 471, 501, 515, 533,

572, 582, 609, 614, 625, 652, 657, 707, 747, 753
galaxies, irregular 136, 161, 167, 171, 197, 245, 253, 263, 283, 334, 387, 401, 436, 592
galaxies, irregular amorphous 171
galaxies, irregular blue 259, 295
galaxies, irregular distant 171
galaxies, irregular dwarf 171, 436
galaxies, irregular giant 171
galaxies, irregular magellanic 259
galaxies, isolated 37, 51, 56, 57, 197, 212, 401, 406, 409,
galaxies, large 269
galaxies, late-type 126, 219, 273, 275, 406, 569, 572
galaxies, lenticular 128, 136, 273, 274, 278, 283, 333, 335, 336, 568, 572, 580, 619
galaxies, long-tailed 515
galaxies, low luminosity 125, 200, 351
galaxies, low mass 568
galaxies, low surface brightness 436
galaxies, low metallicity 294
galaxies, luminous 167, 172, 197, 200, 292, 531, 623, 634, 701, 754
galaxies, magellanic irregular 259
galaxies, Markarian 125, 351, 353, 527, 579, 662
galaxies, Markarian non-Seyfert 527
galaxies, Markarian Seyfert 662
galaxies, Markarian, blue 579
galaxies, merger remnants 436
galaxies, merging 54, 58, 197, 207, 212, 378, 413, 421, 431, 457, 465, 515, 517, 643, 648, 661, 707, 753
galaxies, merging, luminous 515
galaxies, metal poor 254, 586
galaxies, N 539
galaxies, narrow line 737
galaxies, nearby 198, 356, 383, 565
galaxies, normal 125, 134, 153, 252, 253, 273, 387, 501, 527, 534, 560, 575, 579, 583, 602, 605, 626, 629, 707, 723
galaxies, obscured, active 611
galaxies, optically-faint 465, 569, 623
galaxies, optically-selected 273, 525, 533, 723
galaxies, optically-thick 273
galaxies, peculiar 186, 217, 274, 280, 327, 499, 579, 664
galaxies, primordial 351, 358
galaxies, quiescent 135
galaxies, radio 666, 737
galaxies, ring 450, 456, 515
galaxies, Sa-Sm 30, 126, 158, 179, 182, 197, 199, 217, 219, 225, 235, 274, 280, 283, 287, 335, 395, 498, 500, 580, 583, 592, 619, 626, 753
galaxies, S0 - see galaxies, lenticular
galaxies, Seyfert 154, 219, 223, 351, 389, 412, 421, 429, 431, 523, 527, 534, 579, 602, 609, 619, 643, 652, 661, 669, 675, 693, 701, 723, 753
galaxies, Seyfert-1 135, 136, 510, 568, 611, 675, 723, 727
galaxies, Seyfert-2 136, 510, 568, 608, 614, 676, 717, 737
galaxies, Shapley-Ames 323
galaxies, spiral 75, 125, 153, 161, 182, 198, 200, 219, 235, 253, 281, 283, 287, 297, 326, 333, 336, 343, 376, 383, 401, 510, 515, 567, 575, 579, 583, 619, 662, 707
galaxies, starburst 125, 136, 223, 327, 351, 356, 399, 427, 431, 435, 485, 501, 507, 523, 527, 534, 571, 579, 605, 614, 633, 652, 669, 675, 703, 707, 723, 737, 744, 751
galaxies, stripped 210, 277, 283, 287
galaxies, superstarburst 517, 707
galaxies, UGC 273
galaxies, ultraluminous 411, 415, 471, 517
galaxies, Virgo 126, 210, 225, 525
galaxies, Vorontsov-Velyaminov 136
galaxies, Zwicky 136, 436, 747
Galaxy, diffuse emission 23, 93, 97, 99, 103,
galaxy clusters 227, 283, 550, 568
galaxy collisions 387, 428, 457, 465, 515, 517, 643
galaxy evolution 161, 167, 461
galaxy formation 461
galaxy nuclei, 129, 211, 343, 421, 498, 643
gamma-rays 41, 391
gas compression 8, 227, 246
gas depletion 449
gas depletion timescales 209, 305, 333, 336
gas dynamics 79, 267, 376, 435
gas flows 225, 661
gas infall 344, 447
gas inflow 395
gas mass 23, 217, 254, 287, 745
gas mass density 452
gas surface density 303
gas temperature 289, 374
gas, ionized 67, 75, 259, 309, 311, 316, 364, 383, 390, 678, 711
gas, molecular - see molecular gas
gas, optical emission-line 463
gas, X-ray emitting 465

gas-rich galaxies 387, 399, 421, 517
gas-to-dust ratio 24, 72, 101, 109, 163, 207, 211, 751
giant cloud complexes 67, 153, 309, 438
giant clouds 44, 109, 227
giant galaxies 171, 253, 267
giant HII regions 227, 239, 241, 252, 261, 298, 662
giant irregular galaxies 171
giant molecular clouds 3, 21, 24, 55, 57, 67, 70, 97, 153, 162, 289, 359, 367, 385, 746, 753
giant radio galaxies 666
giant stars, late-type 23, 164
globular clusters 161
GMC - see giant molecular clouds
grain mantles 116
grains, dust - see dust grains
grains, dust, heated 319, 301
grains, graphite 24, 115, 119
grains, silicate 24, 251, 644
grains, small 117, 620, 708, 755
grains, very small 23, 120
grand design spiral galaxies 227, 343
graphite grains 24, 115, 119
Hα 125, 153, 167, 172, 197, 201, 210, 211, 227, 253, 292, 303, 310, 321, 333, 401, 414, 491, 501, 569, 575, 616, 737
Hα emission line star 80
Hα extinction 153
Hα images 263, 306, 465, 662
Hα intensity contours 303
Hα luminosity 246, 605
Hα spectrophotometry 125
Hα surface photometry 235
Hα/CO ratio 197
Hα/Hβ line ratio 616, 678, 727
Hβ 560, 664, 676, 616
Hγ 560, 664
H_2 3, 37, 99, 162, 186, 291, 471, 491, 745
H_2 abundance 163
H_2 column density 344, 346
H_2 emission 388, 427
H_2 lines 422, 431
H_2 mass 29, 205, 211, 289, 315, 414
H_2 surface densities 198, 200, 492
H_2/CO ratio 163
H_2O indices 164
H_2O masers 246
halo population 161
halos, gamma-ray 391
halos, radio 391
halos, X-ray 391
He ionization 247
He^+/H^+ abundance ratio 247
heating, dust 83, 301, 363, 497, 501, 583, 681
heating, radiative 84
heating, ultraviolet 170
heavy elements 357
HI 3, 5, 26, 50, 75, 79, 99, 100, 103, 109, 119, 128, 164, 198, 200, 210, 227, 241, 245, 246, 263, 287, 230, 292, 309, 331, 333, 334, 383, 390, 421, 492, 494, 498, 553, 575, 605, 620
HI absorption lines 597
HI arms 230
HI bridge 109
HI clouds 103, 134, 749
HI deficiency 210, 278, 283, 287
HI disks 200, 228, 283, 285
HI distribution 109, 200, 242, 344
HI holes 5, 200
HI line width 293
HI mass 197, 575
HI/optical diameter ratio 285
HI regions 201
HI rich 336
HI ring 230
HI stripping - see HI deficiency
HI supershells 374
HI surface density 197, 263, 283, 305
HI, Outer Galaxy 103
high velocity outflow 463
high-redshift galaxies 560, 611
HII complexes 21, 309, 388
HII galaxies 136, 479, 482, 510
HII regions 3, 23, 38, 58, 63, 64, 67, 75, 79, 95, 97, 99, 128, 153, 162, 163, 168, 172, 235, 241, 245, 247, 259, 263, 298, 311, 320, 321, 333, 336, 364, 384, 388, 412, 414, 427, 436, 465, 510, 543, 569, 577, 585, 605, 620, 661, 666, 675, 717, 737
HII regions, bright 72
HII regions, compact 65, 66, 168, 242, 384
HII regions, distribution 334
HII regions, extended low density 100
HII regions, giant 241, 252, 261, 298, 662
HII regions, giant radio 227, 231
HII regions, radio 3, 241
HII rings 662
hot cirrus 301
hot dust 23, 63, 319, 323, 351, 414, 482, 518, 589, 601
hot galaxies 127, 753
hot gas 352
hot molecular cloud 6, 79, 383
hot spot nuclei 225, 483, 518

hot stars 133, 168, 259, 309, 351, 364, 589, 675, 737
HRI = high resolution imager 487
hydrocarbon masses 25
hydrodynamic density wave model 227, 307
i-band 227, 231, 491
ice mantles 24
ICR - see intracluster medium
Im galaxies 110, 158
Im galaxies, clumpy 259
IMF - see initial masss function
infrared - see also near/mid/far infrared
infrared activity, nuclear 427
infrared color - see color, infrared
infrared emission 11, 12, 21, 46, 97, 103, 113, 117, 125, 133, 163, 183, 206, 245, 247, 275, 319, 352, 359, 363, 383, 411, 431, 499, 556, 560, 561, 571, 579, 611, 616, 646, 652, 669, 675, 701
infrared emission, diffuse 21, 23, 93, 97, 99, 103
infrared emission, extended 83
infrared emission, spatial distribution, galaxies 128, 219, 241, 297, 497, 515, 611, 643, 651, 707, 717
infrared excess 62, 84, 99, 117, 155, 247, 250, 278, 301, 507, 652, 702, 743
infrared galaxy luminosity function 125, 358, 569
infrared luminosity 83, 100, 167, 197, 204, 206, 211, 219, 321, 364, 409, 498, 499, 597, 605, 619,
infrared mapping 497, 664
infrared reddening 246
infrared sources, compact 163, 243, 719
infrared spectra 142, 793, 717, 723
infrared spectral index 507, 727
infrared spectroscopy 129, 363, 421, 619, 675, 754
infrared spectrum 693, 717
infrared structure 107
infrared, circular isophotes 113
infrared, excess 84
infrared-bright galaxies 205, 363
infrared-emitting galaxies 138
infrared-loud quasar 418
infrared-luminous galaxies 245, 274, 351, 367
infrared-normal galaxies 277
infrared-selected galaxies 323, 482, 533, 589, 601, 754
infrared-to-blue luminosity ratio 128, 275, 277, 321, 352, 523, 753
infrared-to-radio flux 356
initial mass function 31, 101, 163, 168, 245, 249, 250, 259, 261, 303, 324, 344, 363, 479, 501, 664
instability 438, 748
instability, bar 429
inter-arm regions 5, 211
interacting galaxies - see galaxies, interacting
interaction-induced spiral waves 457
intercloud medium 438
interferometric observations 368, 471, 491
intergalactic medium 468
intermediate age stars 162
intermediate mass stars 163
interstellar extinction curve 115, 251
interstellar gas - see gas
interstellar medium 23, 75, 99, 104, 113, 125, 162, 164, 260, 287, 305, 309, 323, 367, 468, 491, 633, 648, 753
interstellar medium cycling 491
interstellar medium, dense 359
interstellar medium, diffuse 273, 275
interstellar medium, neutral - see HI
interstellar polarization vectors 749
interstellar radiation field 21, 23, 104, 134, 141, 153, 235, 247, 273, 275, 301, 320, 323, 585, 589, 625
interstellar reddening - see reddening
intracluster medium 210, 277, 283, 287, 399
ionization 67, 99, 250, 352, 678, 739
ionized gas 67, 75, 259, 309, 311, 316, 364, 383, 390, 678, 711
ionized stellar wind 79
ionizing radiation 70, 163, 235, 243, 363, 648, 675
IR/B luminosity ratio 128, 275, 277, 321, 352, 501, 523, 753
IRAS - see also far infrared, infrared
IRAS Additional Observations 83, 247, 297, 547, 651, 693
IRAS Chopped Photometric Channel 83, 128
IRAS extended mission mapping 107
IRAS minisurvey 141, 147, 323, 482, 531, 589, 601
IRAS Point Source Catalog 135, 319, 523, 547, 559, 565
IRAS Pointed Observations - see IRAS Additional Observations
IRAS Sky Brightness Images 63
IRAS Small Extended Sources - see IRAS Small Scale Structures
IRAS Small Scale Structures Catalog 523, 565
IRAS Small Scale Structures 135
IRAS spectral synthesis 133, 319, 323

IRE - see infrared excess
IRR - see galaxies, irregular
irregular galaxies - see galaxies, irregular
IRX - see infrared excess
ISM - see interstellar medium
ISO telescope 755
isolated galaxies 37, 51, 56, 57, 197, 212, 401, 406, 409
ISRF - see interstellar radiation field
IUE 259
J-F - see optical color
J-H - see near infrared color
jet-induced star formation 395, 666
jets 384, 398, 465, 666, 676, 681, 717
JHK - see near infrared
Karachentseva catalog 208
Keck 10-meter telescope 755
kinetic energy 428, 743
L(FIR) - see far infrared luminosity
late-type galaxies 126, 219, 273, 275, 406, 569, 572
late-type giants 23, 164
late-type stars 135, 153, 162, 164, 261, 541, 614
lenticular galaxies - see galaxies, lenticular
Lindblad resonance 230, 620
LINER 412, 417, 461, 609, 633, 661, 662, 676, 678
LINERs, blue 662
local supercluster 525
local universe 411, 418, 523
lock-up rate 32
long-tailed galaxies 515
low luminosity galaxies 125, 200, 351
low mass galaxies 568
low mass stars 343, 501, 748
low mass young stars 10
low metallicity galaxies 294
low redshift quasar 539
low surface brightness galaxies 436
luminosity functions 125, 162, 236, 352, 358, 523, 547, 565, 569
luminosity, blue 133, 141, 225, 560
luminosity, bolometric 76, 83, 127, 169, 248, 411, 523, 703
luminosity, cluster 37, 78, 197, 204, 206, 267
luminosity, CO 37, 57, 197, 204, 206, 246, 267, 269, 289
luminosity, far infrared see far infrared luminosity
luminosity, free-free 8
luminosity, Hα 246, 605
luminosity, infrared 23, 83, 167, 197, 204, 206, 211, 219, 559, 597, 605, 619
luminosity, infrared, large 515
luminosity, Lymanα 155
luminosity, Lyman continuum 168
luminosity, millimeter 745
luminosity, OB star 75, 364
luminosity, OH 597
luminosity, optical 133, 575, 601
luminosity, radio 168, 531, 575
luminosity, stellar 23, 31, 197, 363, 601, 634
luminous galaxies 167, 172, 197, 200, 292, 531, 623, 634, 701, 754
luminous galaxies, ultra 411, 517
luminous stars 164
Lyc - see Lyman continuum
Lyman bands 422
Lymanα 248, 363, 387, 727
Lymanα absorption 248
Lymanα luminosity 100, 155
Lymanα/Hβ ratios 727
Lyman continuum 31, 168, 246, 363, 430, 501, 519, 571
Lyman continuum luminosities 168
Lyman-line radiation 388
M giant stars 23
M stars 162
M stars, extreme 539
M supergiant stars 648, 744
magellanic irregular galaxies 259
magnetic bubble 86
magnetic fields 87, 107, 126, 228, 439, 582, 711, 749, 750
magnetohydrodynamic waves 750
main sequence stars 260, 675, 743
main sequence turnoff 634
mapping, CO 184, 197, 224, 369, 462, 491
mapping, HI 385
mapping, infrared 497, 664
mapping, millimeter 79
mapping, radio 367, 675, 717, 719
maps, temperature 15, 74, 103
Markarian galaxies 128, 351, 353, 527, 579, 662
Markarian galaxies, non-Seyfert 527
Markarian Seyfert galaxies 662
masers 87
masers, H_2O 246
masers, mega- 321, 597
masers, OH 87, 246
mass inflow 395
mass outflows 397, 428, 461, 462
mass, dust 146, 207

mass, gas 23, 217, 254, 287, 745
mass, HI 197, 575
mass, molecular gas 12, 51, 78, 186, 207, 471
mass-to-light ratio 174, 479, 745
massive cloud lifetime 457
massive molecular clouds 289
massive star formation rate 303, 491
massive stars 63, 75, 77, 137, 161, 259, 323, 343, 351, 367, 479, 501, 507, 577, 675
massive young stars 57, 267, 319, 633, 744
megamasers 321, 597
merger remnants 413, 436
merging galaxies - see galaxies, merging
metal abundances 163, 296
metal-poor galaxies 254, 586
metal-poor stars 161
metallicity 162, 247, 254, 294, 341, 399, 568, 634
metallicity gradient 235, 263
MgI 664
mid infrared - see also infrared
mid infrared emission 245, 319, 409, 497, 669, 681, 707
millimeter luminosities 745
millimeter-wave observations 79, 411, 723, 734
minisurvey galaxies - see IRAS minisurvey
Mira variables 539, 541
model stellar atmospheres 247, 261
molecular abundances, low 162
molecular annulus 199
molecular bar 183, 303
molecular cloud complex 58, 67, 100, 153
molecular cloud cores, warm 38
molecular cloud formation 211, 270, 494
molecular cloud population 303
molecular cloud, hot 79
molecular cloud, mass spectrum 37
molecular clouds 3, 11, 12, 37, 57, 71, 75, 79, 95, 97, 99, 103, 113, 119, 134, 149, 197, 203, 206, 211, 243, 320, 323, 343, 390, 417, 491, 501, 717, 746, 749
molecular clouds, dense 23
molecular clouds, dynamics 37
molecular clouds, giant - see giant molecular clouds
molecular clouds, luminosities 37
molecular clouds, mass spectrum 44
molecular clouds, masses 37
molecular clouds, quiescent 24
molecular clouds, warm 51
molecular density 305
molecular disks 3, 80, 367, 462
molecular emission 303
molecular gas 4, 6, 8, 67, 79, 141, 179, 198, 241, 287, 292, 331, 336, 367, 368, 384, 411, 744
molecular gas distribution 344
molecular gas mass 12, 51, 78, 186, 207, 471
molecular gas phase, lifetime 287
molecular gas tracer 289
molecular gas, compression 4
molecular gas, dense 676
molecular hydrogen - see also H_2
molecular hydrogen 3, 26, 37, 42, 99, 162, 182, 186, 230, 246, 291, 388, 421, 471, 491, 745
molecular hydrogen surface density 198, 200, 492
molecular lines 80, 754
molecular ring 5, 12, 21, 42, 97
molecular spiral patterns 203
molecular surface density 493
molecular-to-atomic ratio 200
molecules, large 755
monsters 707
N galaxies 539
N-body simulations 227, 444
Na absorption line 605
narrow line galaxies 737
narrow emission lines 479, 725
narrow line galaxies 737
narrow-line region 133
near infrared emission 164, 293, 409, 413, 421, 431, 482, 515, 601, 605, 613, 623, 669, 725, 734
near infrared colors - see color, near infrared
near infrared emission 164, 409, 431, 482, 515, 601, 605, 623, 669
near infrared energy distributions 243, 297, 723
near infrared mapping 515
nearby galaxies 198, 356, 383, 565
nebula, bipolar optical 80
nebulae, dark 253
nebulae, emission-line 67, 247, 461
nebulae, reflection 80
nebulae, planetary 65, 135, 675
nebulae, X-ray 462
nebulae, young planetary 135
nebulosity, blue reflection 119
NeII clouds 637
NELG - see narrow line galaxies
neutral atomic hydrogen - see HI
neutral disks 319
neutral gas 81, 375, 383
neutral gas, dense 79
neutral phase 99
NIR - see near infrared

NLRG - see narrow line galaxies
NLTE stellar atmosphere 247
non-Seyfert Markarian galaxies 527
nonthermal emission 126, 235, 383, 583, 723, 737
nonthermal emission ridge 228
nonthermal processes 471
nonthermal radio arms 227, 228, 232
nonthermal radio components 287, 383, 744
nonthermal sources 311, 351, 411, 417, 497, 589, 633, 681
nonthermal UV/optical continuum 670
normal galaxies 125, 134, 153, 252, 253, 273, 387, 501, 527, 534, 560, 575, 579, 583, 602, 605, 626, 629, 707, 723
North Ecliptic Pole 547
North Galactic Pole 549
nuclear activity - see active nuclei
nuclear bulge 201
nuclear disk 179, 387, 743
nuclear disks, collisions 387, 743
nuclear ejecta 676
nuclear emission 333, 463, 753
nuclear regions 26, 364, 517, 676, 747
nuclear sources, nonthermal 634
nuclear star formation 383, 401
nuclear starburst 154, 223, 336, 395, 411, 678
nuclei - see also active nuclei
nuclei of galaxies 3, 129, 211, 343, 359, 383, 385, 421, 498, 643, 661
nuclei, composite 676
nuclei, double 625
nuclei, faint 698
nuclei, hot spot 225, 483, 518
nuclei, quasar-like 135, 319, 430
nuclei, radio 721
nuclei, Seyfert - see galaxies, Seyfert and active nuclei
nuclei, starburst - see galaxies, starburst and starburst nuclei
nuclei, structure 717
nucleon 292
O stars 25, 63, 97, 172, 209, 246, 261, 363, 374, 479, 751
OB associations 134, 158, 259, 374
OB star clusters 68, 75, 77
OB star luminosity 75, 364
OB stars 3, 23, 26, 75, 101, 153, 162, 168, 324, 363, 383, 395, 399, 571, 585, 661, 737, 744, 747
OB-star formation 6, 23, 744
objective prism observations 354
obscuration 80, 515, 611, 616, 633
OH luminosity 597
OH masers 87, 246
OH megamasers 597
OH stars 23
OH/IR stars 135, 164
OIII emission lines 711
old clusters 67
old disk population 153
old stars 156, 161, 231, 289, 498, 518
old stellar population 517, 662
optical colors - see color, optical
optical continuum 352, 413, 669, 681
optical depth 71, 169, 175, 255, 319, 320, 488, 754
optical emission 107, 183, 235, 328, 351, 383, 401, 409, 515, 556, 569, 579, 605
optical forbidden line regions 711
optical identifications 164, 243, 601, 623, 697
optical luminosity 133, 575
optical luminosity functions 569
optical nebula, bipolar 80
optical nebulosity 117, 120, 538
optical spectra 164, 223, 259, 325, 359, 414, 417, 461, 501, 553, 620, 661, 675, 681, 723
optical spectrum, peculiar 553
optical surface brightness 255
optical thickness 289, 324, 364, 597, 745
optical thiness 384, 745
optically thick disks 18
optically thick emission 331
optically thick galaxy disks 273
optically violent variables 723
optically-faint sources 465, 569, 623
optically-selected galaxies 273, 525, 533, 723
optically-selected quasars 411, 723
orbit crashings 747
orbit crowding 3
orbit damping 457
Outer Galaxy 103
outflow, high velocity 463
outflows 395, 397, 428, 461, 753
OVV - see optically violent variables
oxygen abundance 247, 254, 479
oxygen-rich dust envelope 540
PAH - see polycyclic aromatic hydrocarbons
Palomar Observatory Sky Survey 547, 601
Palomar-Green QSOs 418, 723
particles - see also grains
particles, graphite 119
particles, Platt 119
particles, relativistic 126
Paschen lines 430, 744, 755

peculiar galaxies 186, 217, 274, 280, 327, 499, 579, 664
peculiar optical spectrum 553
percolation process 4
perigalactic passages 457
perturbation, spiral gravitational 227
photoionization models 737
photometry - see entries under specific wavelength bands
photons, ionizing 65, 163, 701
photons, Lyman continuum 168
photons, ultraviolet 422, 713
photospheric emission 128, 614
Planck function 65, 83, 157, 297, 524, 745
planetary nebulae 65, 135, 675
plasma 245, 534
Platt particles 119
Point Source Catalog - see IRAS Point Source Catalog
point spread function 651
Pointed Observations - see IRAS Additional Observations
polarization, OH masers 87
polarization, quasars/BL Lacs 731
polycyclic aromatic hydrocarbons 23, 116, 148, 301, 320, 745
position/velocity maps 315
POSS - see Palomar Observatory Sky Survey
power law 133, 140, 525, 557, 565, 649, 737
power law ionized gas 678
power law spectral indices 507
pre-main sequence objects 63, 243
primordial galaxies 351, 358
primordial star formation 752
progenitors, supernova 582
protostars 134, 246, 748
protostellar objects 163
PSC - see IRAS Point Source Catalog
Q-branch spectrum, H_2 426
QSO - see quasar
quadrupole vibration/rotation lines, H_2 422
quasar-like nuclei 135, 319, 430
quasar nucleus 417
quasars 142, 144, 351, 357, 389, 507, 616, 675, 723, 727
quasars, infrared-loud 418
quasars, low redshift 539
quasars, optically selected 411
quasars, OVV 723
quasars, Palomar-Green 418, 723
quasars, polarized 731
quasars, radio quiet 613
quasars, radio strong 734
quiescent molecular clouds 24
quiescent galaxies 135
radial gas distributions 200, 343
radial motion 663, 681
radiation pressure 418, 428
radiative heating 84, 113
radio HII regions 3
radio components, compact 473
radio continuum 63, 99, 107, 126, 183, 197, 201, 227, 235, 247, 289, 292, 311, 352, 383, 388, 409, 413, 437, 463, 473, 483, 491, 499, 575, 579, 583, 589, 597, 605, 619, 623, 711, 744
radio continuum arms 227
radio emission thermal 168, 235, 243, 321, 363, 592
radio emission, excess 364
radio galaxies 737
radio galaxies, giant 666
radio HII regions 3, 227, 231, 241
radio loud objects 525
radio luminosity 168, 531, 575
radio mapping 367, 675, 717, 719
radio nonthermal sources 525, 576
radio nuclei 721
radio quiet active nuclei 613, 649
radio source morphology 664
radio source, flat-spectrum 473
radio sources 351, 661, 681
radio sources, compact 462, 731
radio sources, double lobed 533
radio sources, time-variable 462
radio spectral line surveys 71
radio strong quasars 734
radio supernova remnants 371
radio surface brightness 534
radio-to-optical luminosity 580
radio/infrared relation 125, 531, 575, 579, 583, 589
radius, Abell 281
ram pressure 283, 711
RDD0 anemics 283
red continuum 236, 402
red giant stars 634
red stars 540
red stars, old 518
red supergiant stars 634
reddening 246, 253, 413, 430, 605, 616, 634, 646, 664, 678, 725, 727, 754
redshift 353, 358, 401, 412, 547, 560, 565, 601, 611, 623, 629, 697
reflection nebulae 80, 108, 119
relativistic effects 666

relativistic electrons 126, 228, 711
relativistic gas 126, 712
relativistic universe 698
relaxation time 457
relaxation, violent 518
remnants, merger 413, 436
remnants, stellar 32, 343, 666, 676
ring galaxies 450, 456, 515
ring, molecular 5, 12, 21, 42, 97
rings, circumnuclear 619
rings, HII 662
rotating disk 81, 678, 746
rotation curve 179, 181, 519, 746
rotational braking 750
RR-Lyrae stars 161
RSA - see Shapley Ames
S stars 158
S0 galaxies - see lenticular galaxies
Sa-Sm galaxies - see galaxies, Sa-Sm and galaxies, spiral
SB galaxies - see galaxies, barred
Salpeter initial mass function 324, 664
scattering, cloud 486
scattering, dust 463
scattering, X-ray 486
Schechter function 525, 567
Schmidt law 436
Schwarzschild radius 725
serendipitous sources 693
SES - see Small Scale Structures
Seyfert activity - see active nuclei and Seyfert nuclei
Seyfert galaxies - see galaxies, Seyfert
Seyfert galaxies, dusty 725
Seyfert galaxies, Markarian 662
Seyfert nuclei 133, 154, 223, 319, 429, 499, 525, 579, 661, 675, 711
Seyfert nuclei, mini 228
SFE - see star formation efficiency
SFR - see star formation rate
Shapley-Ames galaxies 323
shells 8, 70, 164
shells, circumstellar 23, 128, 135, 141, 161, 549
shock diagnostics 427
shock emission 449
shock excitation 422
shock focusing 307
shock heating 83, 461, 633, 711
shock ionization 678
shock region 311
shock velocity 84, 228, 427, 739
shocked gas 309, 744
shocks 4, 83, 422, 431, 577, 666
shocks, spiral density wave 228
Si IV 260
SII lines 571
silicate absorption feature 246, 643
silicate grains 24, 251, 644
SIRTF 629, 755
Sky Brightness Images (IRAS) 63
Small Extended Source Catalog (IRAS) - see Small Scale Structures Catalog
Small Extended Sources (IRAS) - see Small Scale Structures
small galaxies 267, 402
small grains 23, 117, 120, 620, 708, 755
Small Scale Structures (IRAS) 135, 236
Small Scale Structures Catalog (IRAS) 523, 565
SNR - see supernova remnants
Sofia 754
solar neighborhood 76, 97, 157, 479
solid-body rotation 343
source counts 351, 355, 547
South Ecliptic Pole 547
South Galactic Pole 623
space densities (galaxies) 353
spectra, cirrus 321
spectra, cloud mass 444
spectra, discontinuous (BL Lacs) 731
spectra, electron energy 228
spectra, emission line 259, 619, 676
spectra, line 619
spectra, LINER 414
spectra, low excitation 605
spectra, optical, peculiar 553
spectra, power law 140,
spectra, Q-branch 426
spectra, steep 675, 723, 734
spectra, stellar 261, 364
spectra, very red 540
spectra, X-ray 351, 357
spectral index 228, 384, 429, 507, 583, 592, 671, 727, 734
spectral synthesis, IRAS 133, 319, 323
spectrophotometry, Hα 125
spectroscopy 57, 247, 462, 579, 605, 629, 693
spectroscopy, far infrared 133, 137, 217, 297
spectroscopy, infrared 129, 142, 363, 421, 619, 675, 693, 717, 723, 727, 754
spectroscopy, long slit 678, 713
spectroscopy, low dispersion 623
spectroscopy, millimeterwave 723
spectroscopy, multiaperture 428, 661
spectroscopy, near infrared 297, 515, 723
spectroscopy, optical 164, 223, 259, 325, 359, 414, 417, 461, 501, 553, 620, 661, 681, 723

spectroscopy, slit 666
spectroscopy, slitless 697
spiral arms 3, 38, 95, 100, 181, 203, 230, 235, 303, 309, 315, 747
spiral density wave shocks 228
spiral density waves 263, 303, 309, 343, 429, 431, 438, 748,
spiral galaxies - see galaxies, spiral
spiral galaxies, active - see active nuclei
spiral galaxies, barred - see galaxies, barred
spiral galaxies, fossil 336
spiral galaxies, grand design 227, 343
spiral galaxies, normal - see galaxies, normal
spiral galaxy nuclei - see nuclei of galaxies
spiral gravitational perturbation 227
spiral shocks 227, 231, 267
spiral waves, interaction-induced 457
spontaneous star formation 31
star clusters 76, 161
star clusters, OB 68, 75, 77
star clusters, young 67, 107, 249, 367
star formation 31, 37, 67, 87, 99, 110, 125, 161, 217, 219, 227, 245, 263, 277, 283, 287, 303, 319, 323, 333, 336, 363, 367, 395, 401, 409, 435, 436, 461, 501, 515, 517, 527, 531, 534, 572, 589, 597, 605, 633, 661, 669, 701, 743
star formation burst - see also starburst 173, 473, 479, 579
star formation disks 225
star formation efficiency 70, 197, 204, 211, 267, 303, 344, 436, 471, 494
star formation fuel 224
star formation rate 23, 167, 197, 250, 255, 274, 293, 305, 323, 333, 336, 402, 409, 436, 499, 501, 534, 575
star formation rate, massive 303, 491
star formation trigger 8, 227, 263, 395, 401, 407, 517, 666, 747
star formation, active 320
star formation, bimodal 339, 748
star formation, enhanced 197, 457, 619
star formation, Galactic 3, 37, 63, 67, 71, 79, 83, 99, 633
star formation, global 284
star formation, high mass 3, 235, 259
star formation, induced 31
star formation, intense 127, 717
star formation, nuclear 383
star formation, OB 6, 23, 744
star formation, primordial 752
star formation, rapid 364
star formation, recent 583
star formation, recent violent 586
star formation, runaway 58, 368
star formation, spontaneous 31
star formation, suppression 457
star formation, vigorous 253
star formation, violent 586
starbirth 747
starburst activity, intense 534
starburst component 133, 145
starburst galaxies - see galaxies, starburst
starburst galaxies, dusty 633
starburst mechanisms 445
starburst models 661
starburst nuclei 154, 223, 336, 395, 411, 678
starburst, super 517
starbursts 32, 161, 167, 274, 275, 336, 363, 367, 378, 383, 397, 417, 421, 429, 435, 461, 633, 643, 707
stars, A 153, 158, 209, 301, 426, 601
stars, B 25, 70, 97, 158, 162, 209, 261, 363, 377, 422, 751
stars, blue 29, 331, 540
stars, bright 164, 637
stars, carbon 162, 539
stars, cool 164, 633
stars, early-type 66, 261
stars, evolved 336, 515
stars, extreme spheroid 341
stars, field 164
stars, G-K 86, 422
stars, giant 23, 164
stars, Hα emission-line 80
stars, hot 133, 168, 259, 309, 351, 364, 589, 675, 737
stars, hot young 364, 589, 676
stars, intermediate age 162
stars, late-type 23, 135, 153, 162, 164, 261, 541, 614
stars, low mass 343, 501, 748
stars, luminous 164
stars, M 162, 744
stars, M giant 23
stars, M, extreme 539
stars, main sequence 260, 675, 743
stars, massive 75, 77, 161, 323, 343, 351, 367, 479, 501, 507, 577, 675, 701, 743, 748
stars, massive luminous 390
stars, massive young 57, 267, 319, 633, 744
stars, metal-poor 161
stars, Mira 541
stars, O 25, 63, 97, 172, 209, 246, 261, 363, 374, 479, 751

stars, OB 3, 23, 26, 75, 101, 153, 162, 168, 324, 363, 364, 383, 395, 399, 571, 585, 661, 737, 744, 747
stars, OH/IR 135, 164
stars, old 161, 231, 289, 498
stars, old disk 156
stars, old red 518
stars, red 540
stars, red giant 634
stars, RR-Lyrae 161
stars, supergiant 162, 164, 260, 634, 648, 744
stars, thin disk 341
stars, variable 161, 539, 541
stars, very hot 261
stars, Wolf-Rayet 261
stars, young 10, 83, 323, 343, 351, 363, 383, 497, 626
stars, young massive 57, 267, 319, 723, 744
steep infrared continuum 616, 723
steep spectrum 675, 734
stellar absorption 169, 421, 633, 661
stellar associations 134, 158, 162, 259, 374
stellar atmosphere model 247, 261
stellar bar 219, 367
stellar CO 421, 633
stellar emission-line objects 164
stellar lifetime 168
stellar luminosity 23, 31, 75, 197, 363, 601, 634
stellar mass 70, 168
stellar mass distribution 482
stellar objects, young 79
stellar populations 38, 153, 167, 296, 363, 501, 572, 661, 678
stellar remnants 32, 343, 666, 676
stellar spectra 261, 364
stellar wind, ionized 79
stellar winds 70, 367, 418, 675, 750
Stokes components 87
stripping 210, 277, 283, 287
structure, clouds 38, 439
structure, nuclei 717
submillimeter emission 4, 93, 154, 217, 325, 734
submillimeter emission, diffuse 23
submillimeter luminosities 745
Supercluster, local 525
supercritical cloud 750
supergiant M stars 648, 744
supergiant stars 164, 260
supergiant stars, red 634
supernova blast waves 636
supernova explosions 418
supernova progenitors 582
supernova rate 126, 431, 579
supernova remnants 4, 126, 236, 247, 352, 367, 371, 431, 463, 534, 540, 548, 577, 675
supernova-driven wind 164, 517
supernovae 191, 246, 367, 395, 399, 461, 519, 534, 577, 633, 717
supershells, molecular 372
superstarburst galaxies 517, 707
superwinds 461
surface brightness 108, 117, 255, 275, 436, 533, 637
surface density, atomic 493
surface density, critical 751
surface density, HI 263, 283, 305
surface density, H_2 57, 198, 200, 492
surface photometry, Hα 235
synchrotron emission 126, 228, 364, 383, 589, 681, 727, 731
synchrotron mechanism 589, 734
synchrotron power 579, 582
synchrotron self-absorbed source 725
temperature fluctuations 97
temperature, dust 3, 12, 15, 71, 73, 83, 95, 104, 156, 197, 204, 207, 211, 289, 324, 363, 414, 583, 745
temperature, far infrared color - see color, far infrared
temperature, gas 289, 374
thermal electrons 711
thermal free-free emission 235
thermal radio emission 168, 235, 243, 321, 363, 592
threshold star formation 284, 444
tidal distortion 231
tidal interactions 191, 364, 375, 401, 456, 515, 582
tidal tails 413, 665
tidally-induced disruption 280
timescales, cloud collision 457
timescales, gas depletion 209, 305, 333, 336
Tio bands 164
tracers, star formation 292
trigger, star formation 8, 227, 263, 395, 401, 407, 517, 666, 747
turbulence 438, 750
UBV photometry - see color, optical and optical emission
UGC galaxies 273
ultraluminous galaxies 411, 415, 471, 517
ultraluminous infrared source 428
ultraviolet bump (quasars) 734
ultraviolet colors 479

ultraviolet emission 8, 16, 75, 117, 120, 163, 183, 352, 364, 377, 582, 664, 669, 698, 701
ultraviolet excess 633, 723
ultraviolet fluorescence 422
ultraviolet heating 84, 170
ultraviolet lines 427
ultraviolet obscuration 633
ultraviolet photons 363, 422, 713
ultraviolet region 649
ultraviolet selection 527
ultraviolet spectra 259, 702
ultraviolet surveys 579, 616
ultraviolet, extreme 387
ultraviolet, shock-produced 84
universe, critical density 629
Universe, local 523
universe, nonevolving 547
universe, relativistic 698
unresolved radio source 682
upper mass cut-off 261
variability, rapid 731
variable stars 161, 539, 541
very small grains 23, 120
violent relaxation 518
Virgo galaxies 126, 210, 225, 525
virial equilibrium 57, 750
virial mass 9, 37, 57, 68
virial theorem 746
virialized clouds 345
VLA objects 63
VLA survey 531
Vorontsov-Velyaminov galaxies 136
warm dust 23, 75, 235, 267, 323, 497, 585, 626, 717, 723, 744
warm galactic cirrus 301
Weaver-Williams HI survey 103
Werner bands 422
wind 399, 461, 676
wind, bipolar, galaxies 462
wind, stellar 70, 367, 395, 418, 750
wind, stellar, ionized 79
wind-driven bubble 70
windows, atmospheric transmission 421
winds, supernova-driven 164
Wolf-Rayet stars 261
X-ray background 351
X-ray halo 391
X-ray images 485
X-ray luminosity 133
X-ray nebulae 462
X-ray observations 183
X-ray properties 351
X-ray region 649
X-ray scattering 486
X-ray sources 358
X-ray spectra 351, 357
X-ray-emitting gas 465
X-ray-selected active galactic nuclei 611
young massive stars 57, 633
young planetary nebulae 135
young star clusters 67, 107, 249, 367
young stars 10, 83, 323, 343, 351, 363, 383, 497, 626
young stars, massive 57, 267, 319, 633, 744
young stellar objects 79
ZAS = zero age sequence 480
zodiacal background 103
zodiacal dust 24
zodiacal emission 46, 97, 99, 113, 297
Zwicky catalog 566
Zwicky galaxies 136, 436, 747

OBJECT INDEX

0134+32 733
0238-08 733
0316+41 733
0521-385 733
1226+02 733
13454+12 733
1404+28 733
1413+135 616
1514-24 733
1641+40 733
1807+69 733
2200+42 733
2223-05 733
3kpc ring, NGC 1068 146
17 Tauri 118
20 Tauri 118
23 Tauri (Merope) 118
30 Doradus 241,263
3C 48 664
3C 84 728
3C 120 728
3C 234 615
3C 273 137,729
3C 390.3 728
3C 459 666
A 1510 598
A 1720 598
A 09111-1007 606
A 09234-1146 608
A 12488-2051 608
Abell 262 277
Abell 1367 277
Abell 1656 (Coma) 277,565,568
Abell 2147 277
Abell 2151 (Herc.) 277
Abell 2232 555
Alpha Boo 652
Alpha Lyrae 652
Alpha PsA 652
Arakelian 120 728
Arp Ring 107
Arp 55 416
Arp 82 651
Arp 148 515,597
Arp 220 (IC 4553) 54,145,206,212, 354,359,363,376, 377,397,412,421, 461,465,471,473, 577,592,597,605, 629,633,643,651, 701,707
Arp 299 55
Beta Gru 652
Beta Pic 652
Cancer Cluster 277
Carina arm 68
Carina OB1 67
Cartwheel Galaxy 450
Centaurus A 398,666
Chamaeleon cloud 113
Coma Cluster 277,565,568
CPG 330 268
Cr 228 67
Cygnus region 620
Cygnus clouds 50
DDO 50 262
DDO 66 108
DDO 75 (Sextans A) 264
DDO 154 268
DDO 216 (Pegasus) 264
Draco 547
η Carinae 67
Haro 1 592
Haro 2 268,592
Haro 3 268
Haro 15 592
Haro 28 592
Hercules Cluster 277
Hygia 652
IC 10 268
IC 135 685
IC 342 128,179,187,188,199, 376 377,383,385,416
IC 410/S236 76
IC 443 431
IC 694 416,421,471
IC 1613 264
IC 1848 76
IC 2581 67
IC 4329a 140
IC 4553 - see Arp 220
IR 298.2-0.4 74
IR 298.2-0.8 74
IR 298.9-0.4 74
IRAS 00193-4033 539
IRAS 00300-2234 626
IRAS 00335-2732 625
IRAS 00344-334 140
IRAS 00402-2350 626
IRAS 00456-2904 626
IRAS 01050-3305 626

IRAS 01091-382 140
IRAS 01199-2307 626
IRAS 01228-7324 242
IRAS 01330-2256 626
IRAS 01358-3300 626
IRAS 02069-233 140
IRAS 0402+212 532
IRAS 0404+101 504
IRAS 0409+054 532
IRAS 0413+081 327
IRAS 0413+122 504
IRAS 04139+0238 577
IRAS 0414+001 327
IRAS 0421+040 533,602
IRAS 0518-25 412,523
IRAS 05216-6753 242
IRAS 0622-645 696
IRAS 08171-250 140
IRAS 08341-261 140
IRAS 0857+38 418
IRAS 0857+39 412
IRAS 09104+4109 559
IRAS 0917+69 556
IRAS 10299-2803 538
IRAS 1148+58 556
IRAS 1149+61 556
IRAS 1150-09 556
IRAS 1211+03 412
IRAS 1231-05 556
IRAS 13197-162 140
IRAS 1324+16 556
IRAS 1325+16 556
IRAS 1334+24 418
IRAS 1434-14 412
IRAS 1510+0724 597
IRAS 15194-5115 540
IRAS 1525+36 412
IRAS 1645+37 556
IRAS 1713+53 416
IRAS 17208-0014 597
IRAS 1752+329 532
IRAS 20243-022 140
IRAS 20481-571 140
IRAS 20551-425 140
IRAS 2249-18 412
IRAS 23060+0505 611,613
IRAS 23128-591 140
IRAS 23260-413 140
Jupiter 94
Kleinman-Low nebula 180
L 1542 115
L 1551 83
L 1780 113,115
Large Mag. Cloud 161,215,241, 245 247,555,591
Lk Hα 101 79
Lindsey-Shapley Ring 450
M6 685
M8 363,384
M16 15
M17 15
M17B 48
M31 128,135,148,200,206,331,374 534,555
M33 128,147,199,206,236
M34 685
M51 6,129,179,197,199,203,235, 303,309,315,383,416,534
M78 685
M79 685
M81 107,148,227,375,485,534
M81, disk 108
M82 108,126,174,179,189,259, 367,377, 383,416,421,447,462,471 485,503,534,572, 633,651,702,753
M83 6,179,181,199,303,309,377, 385,498,662
M87 287
M101 199,297,416,534
M185 332
Maffei 2 363,384
Magellanic Clouds 161,241,245,247, 555,591
Markarian 3 144,728
Markarian 6 685,728
Markarian 9 728
Markarian 34 685
Markarian 59 592
Markarian 71 592
Markarian 78 685
Markarian 79 685,728
Markarian 86 268,592
Markarian 158 148
Markarian 169 592
Markarian 171 354
Markarian 207 592
Markarian 231 54,144,354,412,359, 597,615,651,661,664,685

Markarian 273 412,597
Markarian 279 728
Markarian 304 670
Markarian 313 592
Markarian 314 592
Markarian 315 681,682,683,685
Markarian 319 581
Markarian 321 581
Markarian 323 581
Markarian 325 581
Markarian 326 581
Markarian 331 416
Markarian 335 729
Markarian 348 728
Markarian 363 581
Markarian 370 592
Markarian 376 728
Markarian 404 581
Markarian 418 581
Markarian 432 581
Markarian 463 142
Markarian 478 418,729
Markarian 479 581
Markarian 509 143,681,685,729
Markarian 527 268,592
Markarian 531 581
Markarian 534 581
Markarian 545 581
Markarian 573 685
Markarian 578 581
Markarian 817 728
Markarian 841 729
Markarian 1002 581
Markarian 1027 581
Markarian 1088 581
Markarian 1183 581
Markarian 1194 581
Markarian 1233 581
Markarian 1304 581
Markarian 1466 581
MCG 8-11-11 685
Merope 118
Milky Way 3,6,37,161,179, 197,199, 245,320,377,416,534,746
Minkowski's object 398,666
NGC 23 416
NGC 44 247
NGC 88a 242
NGC 91 247
NGC 105 249
NGC 106 143
NGC 159 163
NGC 185 268,331
NGC 205 268
NGC 214c 249
NGC 224 - see M31
NGC 253 179,206,375,377 383,384, 416,426,428,429,461,463, 702,753
NGC 281 76
NGC 335 662
NGC 473 335
NGC 520 206,363,416
NGC 598 - see M33
NGC 613 483
NGC 660 363,636
NGC 680 335
NGC 694 334,335
NGC 695 416
NGC 746 661
NGC 828 416
NGC 834 416
NGC 841 416
NGC 891 128,179,180,181, 193,200,555
NGC 936 335
NGC 992 416
NGC 1023 335
NGC 1068 137,146,201,352, 376,377, 416,421,474,615,651,661,669,683,685, 711,717,728
NGC 1068, 3kpc ring 146
NGC 1097 620,662
NGC 1140 259,260,261,262
NGC 1275 140,143,144
NGC 1300 483
NGC 1365 143,681,684,685
NGC 1377 140
NGC 1386 143,144,685
NGC 1530 224,416
NGC 1569 156,207,212,268
NGC 1614 140,363,424,429,503,702
NGC 1620 416
NGC 1624 76
NGC 1667 685
NGC 1705 259,262
NGC 1800 259,262
NCG 1808 498,499

NGC 1893 76
NGC 2076 140
NGC 2110 685
NGC 2146 327,416
NGC 2175 76
NGC 2276 416
NGC 2297 662
NGC 2339 416
NGC 2388 55
NGC 2403 199
NGC 2445 503
NGC 2623 416,503,515,651
NGC 2633 416
NGC 2683 592
NGC 2782 143,503
NGC 2798 429,707
NGC 2814 268
NGC 2841 200,201
NGC 2903 129,377
NGC 2976 268
NGC 2992 652
NGC 3031 - see M81
NGC 3034 - see M82
NGC 3077 55,109,206
NGC 3079 359,363,416,651
NGC 3090 702
NGC 3147 416
NGC 3221 416
NGC 3227 416,429,728,729
NGC 3239 264
NGC 3256 517
NGC 3274 268
NGC 3293 67
NGC 3310 129,206,207,416,620
NGC 3324 67
NGC 3372 (η Car.) 67
NGC 3504 143,416,503
NGC 3516 728
NGC 3690 359,363,416,421,425, 471,507,597
NGC 3709 636
NGC 3738 268
NGC 3783 143,144
NGC 3893 416
NGC 3938 592
NGC 4047 140
NGC 4051 669,685,728
NGC 4138 335
NGC 4151 421,669,728,729
NGC 4214 264
NGC 4238 334
NGC 4303 662
NGC 4314 483
NGC 4321 662
NGC 4385 335,336
NGC 4388 685
NGC 4418 140,144,145,206
NGC 4449 156,158,259,260,261, 262,264,268
NGC 4507 143
NGC 4527 498,499,500
NGC 4536 499,500,620
NGC 4548 303
NGC 4605 268
NGC 4666 502
NGC 4670 334,335
NGC 4736 158,200,384,416,620
NGC 4750 140
NGC 4826 416
NGC 5055 416
NGC 5078 140
NGC 5194 - see M51
NGC 5195 363
NGC 5236 - see M83
NGC 5248 662
NGC 5253 140,143,144
NGC 5256 416
NGC 5363 416
NGC 5371 592
NGC 5383 483
NGC 5427 662
NGC 5437 662
NGC 5447 299
NGC 5455 299
NGC 5457 - see M101
NGC 5461 299
NGC 5462 299
NGC 5471 299
NGC 5506 268
NGC 5530 140
NGC 5548 685,728
NGC 5631 335
NGC 5643 685
NGC 5656 140
NGC 5728 685
NGC 5929 711
NGC 5936 416
NGC 6090 416

NGC 6223 555
NGC 6225 555
NGC 6226 555
NGC 6238 555
NGC 6240 55,142,143,147,206, 376,377,416, 421,423,429,467,471 507,577,605, 633,701,702,707
NGC 6244 555
NGC 6249 427
NGC 6286 416
NGC 6501 335
NGC 6543 135,548
NGC 6552 140
NGC 6574 416,502
NGC 6643 416
NGC 6701 416
NGC 6764 144,685
NGC 6822 264
NGC 6921 416
NGC 6946 128,179,197,199, 201,202,206,211,303,343,363,376, 383,416,534
NGC 7013 334,335,336
NGC 7180 335
NGC 7280 335
NGC 7331 200,201
NGC 7380 76
NGC 7469 55,143,144,354, 416,471,683,685,728,729
NGC 7479 416
NGC 7496 676,685
NGC 7541 416
NGC 7552 143
NGC 7582 676,681,683,685
NGC 7624 140
NGC 7625 416
NGC 7674 416
NGC 7714 363
NGC 7742 335,336
NGC 7743 334,335
NGC 7771 416
NGC 7800 268
NGC 7817 140
Ophiuchus Complex 141,149, 555,748
Orion Region 367,428,479,519,555 751
Orion Mol. Cloud 42
Orion A 179,182
Orion, KL nebula 180
Pegasus Galaxy 264
Pegasus Cluster 277
Perseus Region 555
PG 0906+48 728
PG 1351+64 728
Pleiades 117
PSC 09104+4109 559
Red Rectangle 116
S 87 79
S 106 79
S 142 76
S 184 76
S 187 63
S 199 76
S 212 76
S 236 76
S 252 76
Sagittarius arm 8,51
Small Mag. Cloud 161,241
Scutum arm 8,51
Sextans A 264
Taurus Mol. Cloud 748
TON 1542 418
Tr 14 67
Tr 16 67
Trapezium 367
Trapezium stars 751
UGC 3426 140
UGC 4203 140
UGC 5101 412
UGC 8058 140
UGC 8335 140
UGC 8850 140
UGC 9412 140
UGC 12713 334,335
Vega 652
Vela ring 450
Venus 94
Virgo Cluster 126,198,283,285,287, 294,402,538,577
Virgo galaxies 205,210,225,285,525
W5/S199 76
Z355.3+1826 577
Zw 1510+0724 597
I Zw 1 142,418,728
I Zw 18 586,592
I Zw 33 268
I Zw 89 268

II Zw 40 128,173,175,268,586
II Zw 70 592
II Zw 136 418,729
III Zw 35 597
III Zw 102 268
VII Zw 506 147

NASA
National Aeronautics and Space Administration

Report Documentation Page

1. Report No.	2. Government Accession No.	3. Recipient's Catalog No.
NASA CP-2466		

4. Title and Subtitle	5. Report Date
Star Formation in Galaxies	May 1987
	6. Performing Organization Code: EZB

7. Author(s)	8. Performing Organization Report No.
	10. Work Unit No.

9. Performing Organization Name and Address	11. Contract or Grant No.
Astrophysics Division NASA Office of Space Science and Applications	

12. Sponsoring Agency Name and Address	13. Type of Report and Period Covered
National Aeronautics and Space Administration Washington, DC 20546	Conference Publication
	14. Sponsoring Agency Code

15. Supplementary Notes

16. Abstract

This document contains the proceedings of a conference held at the California Institute of Technology, Pasadena, California, June 16-19, 1986. The topic was star formation in normal, starburst, and active galaxies. On the observational side, there was particular emphasis on the comparison of radio continuum and CO data with the IRAS data, and the nature of the energy source(s) of the most infrared-luminous extragalactic objects. Other topics covered ranged from the diffuse far-infrared emission in the galaxy, through the detailed processes and triggers of star formation in disks and starburst nuclei, to the interrelationship between an active nucleus and a surrounding starburst.

17. Key Words (Suggested by Author(s))	18. Distribution Statement
star formation galaxy IRAS infrared emissions	Unclassified - Unlimited Subject Category 89

19. Security Classif. (of this report)	20. Security Classif. (of this page)	21. No. of pages	22. Price
Unclassified	Unclassified	650	A99

NASA-Langley, 1987